

Imaging in Neonates

Michael Riccabona
Editor



Imaging in Neonates

Michael Riccabona
Editor

Imaging in Neonates

 Springer

Editor

Michael Riccabona
Division of Pediatric Radiology
Medical University Graz
A – 8036 Graz, Steiermark, Austria

ISBN 978-3-031-15728-8 ISBN 978-3-031-15729-5 (eBook)
<https://doi.org/10.1007/978-3-031-15729-5>

© The Editor(s) (if applicable) and The Author(s), under exclusive license to Springer Nature Switzerland AG 2023

This work is subject to copyright. All rights are solely and exclusively licensed by the Publisher, whether the whole or part of the material is concerned, specifically the rights of translation, reprinting, reuse of illustrations, recitation, broadcasting, reproduction on microfilms or in any other physical way, and transmission or information storage and retrieval, electronic adaptation, computer software, or by similar or dissimilar methodology now known or hereafter developed. The use of general descriptive names, registered names, trademarks, service marks, etc. in this publication does not imply, even in the absence of a specific statement, that such names are exempt from the relevant protective laws and regulations and therefore free for general use.

The publisher, the authors, and the editors are safe to assume that the advice and information in this book are believed to be true and accurate at the date of publication. Neither the publisher nor the authors or the editors give a warranty, expressed or implied, with respect to the material contained herein or for any errors or omissions that may have been made. The publisher remains neutral with regard to jurisdictional claims in published maps and institutional affiliations.

This Springer imprint is published by the registered company Springer Nature Switzerland AG
The registered company address is: Gewerbestrasse 11, 6330 Cham, Switzerland

Preface

Neonates are something special—everybody realises as soon as one can hold a baby in his/her arms. They deserve special care and our attention for their well-being as they cannot articulate their feelings and needs and rely on us—which also applies to health care and medical imaging. We also depend on them, as they are the base of mankind's future. All this should be strong motivation to engage in enabling dedicated care and imaging of this special, very vulnerable patient group with quite different conditions, needs and restrictions than older children or adults—which I learned already when specialising in paediatrics in the early years of my professional career. Before becoming a (paediatric) radiologist I was a paediatrician, very much involved with neonatology and neonatal intensive care; I also was a member of the paediatric ECMO team. As such I have been searching for information on how to properly image neonates, particularly those who were critically ill, and learn about imaging options as well as restrictions.

After becoming a paediatric radiologist, I have often been asked by my clinical colleagues about imaging in neonates and where they can find information. I could suggest various book chapters or booklets on one or another subtopic but could not find a book that would give a comprehensive overview on this subspecialised topic in paediatric imaging. So, I approached various publishing companies, and eventually Springer agreed to enable this project, for which I am very grateful. This effort may provide extra value, as increasingly neonatologists are performing and reading studies themselves—similar to the situation 30–40 years ago when I as the neonatologist had to read the films, perform fluoroscopy and do the ultrasound, as no specialised (paediatric) radiologist was available; this at that time additionally motivated me to eventually become a paediatric radiologist. Today, there is also a decreased interest of young radiologists in doing these basic studies—they often prefer to read the fancy MRIs or CTs but are more reluctant to perform basic ultrasound (US) studies or fluoroscopy particularly in these tiny babies, where these studies can be time consuming and cumbersome. They also claim that there is no proper textbook where one could learn about these conditions, and in fact, there are few who have focused on imaging of neonates with all the respective implications—another additional motivation to take on this task and write/edit such a book.

Times are changing, not only has insight into some of the typical neonatal conditions grown, but also terminology and management have changed, such as new and different respiratory therapies, ECMO has decreased, and new

drugs are on the market (although many are not registered for paediatric or neonatal use, but indispensable for treating some of those very ill babies, for example, with pulmonary hypertension or oncologic and cardiac conditions, or infections with resistant bacteria or fungus). New laboratory tests and markers have been introduced and developed, but the restrictions in taking blood samples in these increasingly small and vulnerable preterm infants for repeated laboratory testing for diagnosis and follow-up (that can lead to iatrogenic anaemia) makes imaging even more important for these patients' care.

Finally, having seven grandchildren, I personally experienced the need for good imaging in certain neonatal situations and queries, particularly the need for imaging suggestions and algorithms—to avoid diagnostic overkill (which may also lead to overtreatment) but without missing important conditions with short-term and long-term sequelae. Thus, I want to dedicate this book to my grandchildren and children. I want to thank Springer for enabling this book, and my wife Barbara for her patience while preparing the book. And of course, I need to thank also all my authors and co-authors. I also want to acknowledge the support from many colleagues both in my institution and abroad by providing images, giving hints and comments on how to improve, or by editing several sections for language and content. Finally, I would like to thank everybody for their special efforts making this book possible in these crazy times with COVID and all the respective workload and illness implications—all this and all their input eventually made the book possible.

I hope you will enjoy reading this book, find the information you need, and will find the book useful to optimise imaging in these little patients entrusted to you.

Graz, Austria
December 2021

Michael Riccabona

Acknowledgement

I sincerely want to thank Dr. Brian Coley (Cincinnati, Ohio/USA) for all his efforts and support by editing many chapters of this book for language and content.

Contents

1 Introduction	1
Michael Riccabona	
2 Clinical Basics and Remarks: Why and When Do Neonatologists Need Imaging	5
Bernhard Resch	
3 General Remarks, Rules, and Considerations	19
Michael Riccabona and Hans-Joachim Mentzel	
4 Prenatal Imaging: What a Paediatric Radiologist or Neonatologist Should Know?	37
Françoise Rypens, Juliette Garel, and Chantale Lapierre	
5 Postnatal Imaging in Babies with Prenatal Diagnosed Malformations or Conditions	91
Michael Riccabona	
6 Pre-, Peri-, and Post-Operative Imaging in Neonates	103
Michael Riccabona and Holger Till	
7 Image-Guided Interventions in Newborns	121
Brian D. Coley	
8 Neonatal Neuroimaging: Ultrasound of the Neonatal Brain and Spine, with Some Remarks on Plain Film and CT	139
Michael Riccabona	
9 Neonatal Neuroimaging: Neuro MRI in Neonates	171
Gregor Kasprian	
10 Chest and Lung Imaging in Preterms and Neonates	191
Panruethai Trinavarat and Michael Riccabona	
11 Imaging the Neonatal Heart and Large Vessels	253
Erich Sorantin, M. Koestenberger, and S. Tschauer	
12 Imaging the Neonatal Urogenital Tract	281
Michael Riccabona	

-
- 13 Imaging the Neonatal GI Tract, Also Including Liver, Spleen, Pancreas, Retroperitoneum and Mesentery** 327
Maria Luisa Lobo, Samuel Stafrace, and Michael Riccabona
- 14 Imaging of the Neonatal Musculoskeletal Tract** 383
Janina M. Patsch
- 15 Imaging the Neonatal (and Paediatric) Hip** 401
Gerolf Schweintzger and Michael Riccabona
- 16 Neonatal Imaging in Thyroid Disease, Inherited Disease, Syndromes, and Oncology** 427
Janina M. Patsch
- 17 Imaging After Birth Trauma and in Suspected Non-accidental or Inflicted Injury** 453
Sebastian Tschauner and Erich Sorantin



Introduction

1

Michael Riccabona

Neonates are a very cute but also very special group. Not only are they the base for the future of mankind; they also come with specific conditions, diseases and challenges for imaging. As such, the “normal” rules for imaging (and treatment) as usually applied to adults do not fit to their needs and demands as well as their physiologically immature bodies and organ function. Additionally, prenatally detected malformations or conditions or the consequences of perinatal events often need to be addressed and may require imaging and reveal results unique to this specific cohort of patients. A very important aspect not present in imaging adults is that the paediatric and particularly the neonatal organs and structures need to be able to grow and mature, and this growth potential must be maintained unhindered to eventually enable a healthy and unimpaired adult.

Luckily, most neonates are healthy and as such do not need imaging except for some screening programmes (e.g. hip ultrasound, some places perform screening for urinary tract dilatation, or selected screening in patients at higher risks such as even serial brain ultrasound in preterm neonates, etc.). But those who present with symptoms and conditions often need even more imaging than older patient groups, as the history and clinical examination is often less decisive. Furthermore,

anxious parents and relatives urge physicians to “rule out” any possible condition as early as possible. In this setting neonatologists and paediatricians, paediatric surgeons and other surgical subspecialists as well as (paediatric) radiologists are challenged to decide if an examination is necessary and medically justified. They then have to select the most appropriate imaging tests, decide on the best timing of these examinations avoiding over-diagnosis as well as missing a diagnosis and prevent over-treatment (which is a burden not only to the health system but also to the small patients).

As neonates have a much higher sensitivity towards radiation-induced damage than older patients, radiation protection is of utmost importance. Therefore, ultrasonography (US) is the most commonly applied method for many queries, also owing to the fact that neonates pose optimal conditions for US (e.g. high water content and little fat content of the tissues, small sizes with excellent applicability of high-resolution transducers, access to areas that cannot be sonographically investigated in older patients, e.g. due to less ossification such as the hip or the brain). The other important method is radiography, sometimes supplementing or supplemented by US—particularly in the chest, sometimes of the abdomen and the extremities. A few other, mostly gastrointestinal and genitourinary conditions need fluoroscopy. CT is a rare examination in neonates, particularly as MRI can often not only solve the problem less invasively (using a feed-and-wrap approach and avoiding anaesthe-

M. Riccabona (✉)
Medical University Graz, Graz, Austria
e-mail: michael.riccabona@medunigraz.at

sia), but also offers far more information owing to its superb tissue differentiation capabilities, for example in the neonatal brain.

In order to properly select the imaging method and decide on the best timing of the examination as well as to come up with a reasonable diagnosis without over-imaging, not only knowledge about imaging itself but also of neonatal pathophysiology and conditions as well as their respective appearance is important.


The impact on treatment or management and prognosis needs to be taken into account when deciding about an imaging examination considering both efficacy and the ALARA (*As Low As Reasonably Achievable*) principle. Therefore, a close cooperation and communication with the neonatologist and the paediatric surgeon is particularly important, which is reflected in this book by chapters that are written by or together with clinical colleagues. As quite a number of neonates present for imaging because of a foetally recognised condition, an orienting chapter presenting the basics of foetal imaging is included. This as well as many specific neonatal diseases that originate in disturbances in the transition from intra-uterine to extra-uterine life also mean that knowledge of embryology and physiology is necessary to properly understand and recognise findings in neonates—not only to interpret obvious findings correctly, but also to find pathology, as one often only finds something one is searching for and knowledgeable about. It's a bit like looking for mushrooms—you need to know when and where they grow and what they look like, to then come back with a healthy and rich, satisfying harvest. However, I want to point out that conditions which do not imply imaging or imaging approaches that differ from what one would suggest in older children (such as for example ear infections or tonsillitis) will not be addressed.

Since imaging's potential as well as imaging methods are rapidly evolving and changing, with multiple innovations coming up again and again, this book can only present the current situation; some aspects might need an update possibly already at the time this book is released and published. Also, the wide variations throughout the world cannot all be addressed—adaptations to

local needs and equipment are necessary. This applies in particular to countries with restricted resources, such as where conventional plain films are still taken and digital radiography is not available (impacting the technical aspects and also the respective results). MRI may not be available, US devices may be older and have a restricted transducer choice, and CT is done with older devices that possibly do not allow for (fast) helical acquisitions and still have old detectors with poor radio-sensitivity implying a much higher patient dose. And even with modern equipment—there are many different techniques and vendors, and as such there is no universal protocol for all imaging applications in neonates and no universal imaging algorithm that can be applied unchanged to all places.

Therefore, the book aims at listing the respective conditions, illustrating the typical findings in this age group, discussing the imaging approaches, but most of all creating an understanding for the needs and conditions in neonates based on their vulnerability, the pathophysiology of the diseases during this very unique period in life, and the clinical impact of imaging that allows tailoring these examinations according to the local possibilities and the individual need. Not all entities are addressed in a dedicated chapter such as the rare neonatal or even congenital tumours (which are now increasingly detected by prenatal screening): some of them are listed in the respective organ system chapter, others such as systemic diseases are discussed in a dedicated chapter—without being able to elaborate on (patho-)physiology and the new challenges in management and treatment in detail. Nevertheless, all these tasks and particularly treatment aspects require in depth knowledge of neonatal biology (i.e. how the immature organism can handle drugs with its increased potential for toxicity) and consideration of the impact of treatment or contrast media and radiation on organ function and growth with respective long-term morbidity. Also note that in neonates even the various organs appear different from the respective adult appearance or from what we know from older children, both during normal maturation or in various diseases; e.g. the neonatal kidney looks like a severely diseased adult

kidney, and if a neonatal kidney looks like an adult kidney, it has a severe problem (Fig. 1.1). Finally, remember—not all that can be imaged needs to be imaged: always consider the burden on the patient, the impact on treatment and the costs or capacity implications on the medical system.

 Never read or interpret an image without respective relevant patient information (e.g., age and gender, clinical symptoms, biochemistry etc.) to avoid misjudgement.

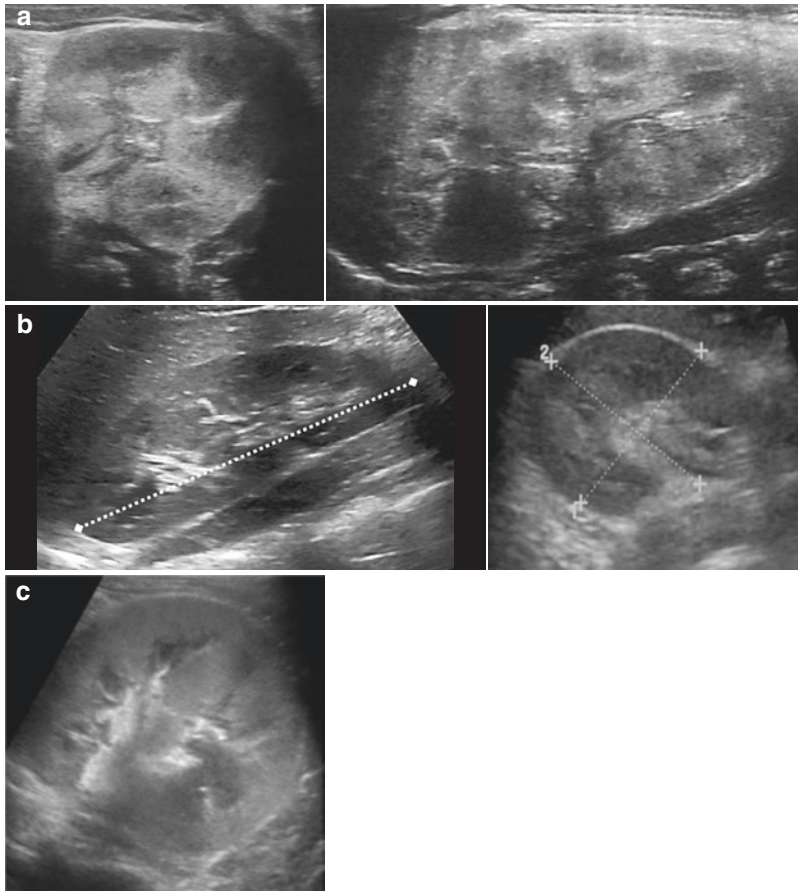


Fig. 1.1 US appearance of a normal neonatal (a) versus a normal adult (b) kidney. (a) Neonatal left kidney, axial and longitudinal (coronal) US section, flank view: physiologically the neonatal kidney is more spherical, and exhibits higher echogenicity of the cortex, with more pronounced cortico-medullary differentiation and transient physiological echogenic deposits in the distal medulla. (b) Adolescent right kidney, axial and longitudinal (coronal)

US section, flank view: normal image of a kidney in an adolescent with respective standardised measurements. Notice the decreased cortical echogenicity and less pronounced cortico-medullary differentiation compared to the neonate. (c) School age child, left kidney, axial US section: this child with glomerulonephritis exhibits a kidney, which looks very similar to a normal neonatal kidney, although this kidney is severely sick

Clinical Basics and Remarks: Why and When Do Neonatologists Need Imaging

Bernhard Resch

2.1 Introduction

Neonatology is the medicine of the neonate and the neonatal time span including the first 28 days of life. Thus, the time span increases by decreasing gestational age. Until a preterm infant reaches the calculated birth date, its age is given as post-menstrual age in weeks and days, thereafter as corrected for prematurity age. Some hallmarks of important basic definitions are given in Tables 2.1 and 2.2. Growth restriction during pregnancy (intrauterine growth restriction—IUGR) is the crossing of the percentiles that is not necessarily but very often associated with SGA. The differentiation between IUGR and SGA is mandatory with regard to IUGR as a potential factor associated with neurodevelopmental impairment.

Some other important neonatal parameters shortly discussed include blood volume, blood pressure, normal haematocrit and haemoglobin levels, transfusion volumes, and growth parameters.

- The blood volume is calculated as 80–100 mL/kg body weight. It is obvious that due to the small patient size and overall blood volume in very low birthweight (VLBW) infants tapping of only micro blood volumes for laboratory examinations is essential to avoid anaemia.

B. Resch (✉)
Division of Neonatology, Department of Pediatrics
and Adolescent Medicine, Medical University of
Graz, Graz, Austria
e-mail: Bernhard.resch@medunigraz.at

Table 2.1 Classification of neonates according to gestational age

Weeks of gestation	General terms	Definitions
<28	Limit of viability 22–25 weeks Preterm infant	Extremely low gestational age newborn (ELGAN)
28–31	Prematurity	Very preterm infant
32–33		Moderate preterm infant
34–36		Late preterm infant
37–38	Term infant	Near term infant
39–41		Term infant
≥42		Post-term infant

Abbreviations are self-explained by the tables' content

- Normal haematocrit levels lay in between 40% and 60%.
 - Polyglobulia or hyperviscosity syndrome is characterised by values of $\geq 70\%$.
 - Anaemia is characterised by either a haematocrit level below 40% or a haemoglobin value less than 12 mg/dL.
 - In healthy term infants, the cut-off value indicating the need for red cell package transfusion is either a haematocrit $< 25\%$ or a haemoglobin value < 8 g/dL.
 - The more premature a neonate is and the more intensive care medicine is necessary, the higher become the cut-off values for transfusion of red cell packages. In case of blood transfusions, the usual volumes are 10–15 mL/kg body weight, and red cell packages must always be leukocyte filtered and radiated.

Table 2.2 Classification of neonates according to birthweight

Birthweight in grams	Abbreviation	Definitions (estimated percentages of all neonates)
<1000	ELBW	Extremely low birthweight infant (0.5)
<1500	VLBW	Very low birthweight infant (1)
<2500	LBW	Low birthweight infant (5–15)
According to percentile		Definitions
<10	SGA/SFD	Small for gestational age/small for date
10–90	AGA/AFD	Appropriate for gestational age/appropriate for date
>90	LGA/LFD	Large for gestational age/large for date

Abbreviations are self-explained by the tables' content

- The lower limits of mean arterial blood pressure correspond to the gestational age in weeks.
- In the immediate post-discharge period, weight gain is about 25–50 g/day, length increases by 1 cm, and the head circumference increases >0.5 cm/week.

Radiologic examinations of the preterm and term infant are an important part of neonatal medicine. On the one side, there are increasing indications for ultrasound (US) examinations of the neonate as one part of the neonatologist's work at the neonatal intensive care unit (NICU). On the other side, there still is the need for the classical radiograph due to dominant respiratory morbidities in the neonatal period (e.g. respiratory distress, wet lung, delayed respiratory adaptation). Neonatal radiology is a highly sophisticated diagnostic sub-discipline of general and paediatric radiology dealing with a very vulnerable population at increased radiation risk. Hence, irradiation must be reduced to a minimum and the need of each examination should be carefully evaluated.

The typical first radiological examination in the life of a preterm infant or an ill term neonate is the radiograph of the lungs in case of problems, e.g. adapting to extra-uterine life or need for ventilator support. The main diagnoses in the chest include respiratory distress syndrome (RDS), transient tachypnea of the neonate (TTN) or wet lung, pneumonia, pleural effusions, (spontaneous) pneumothorax, meco-

nium aspiration syndrome, or rarely malformations including diaphragmatic hernia (CDH), atresia of the oesophagus with or without a tracheal fistula, or congenital pulmonary airway malformation (CPAM)—not to forget cardiac malformations.

2.2 Respiratory Tract

2.2.1 The Developing Lung

Extremely preterm infants are at the end of the canalicular stage (16–26 weeks post conception = 18–28 weeks gestational age) in transition to the saccular stage (24–38 weeks after conception = 26–40 weeks gestational age) of lung development. The alveolar stage starts late at 36 weeks of gestation becoming finalised at the age of approximately 8 years. The canalicular stage (mid lung development) is dominated by growth of the respiratory epithelium and the formation of respiratory bronchioles. Only at the end of the canalicular period of lung development, the foetus is able to survive. It is the rapid growth of the associated vascular bed, which supports the gas exchange of the foetus. Another important step is the differentiation from the cuboidal type 2 to the squamous type 1 cells called pneumocytes type 1 and 2. Type 2 cells are responsible for surfactant production and type 1 cells build the thin cellular layer that aids in gas exchange again. At 24 weeks of gestational age, the lungs get their alveolar appearance. At birth,

about 20–50 million alveoli have been estimated reaching 300 million at adulthood. During the canalicular stage, lung hypoplasia can occur. All lung malformations start earlier in the embryonic phase of development. Preterm birth occurring during the canalicular stage is often associated with severe respiratory distress because of poorly developed peripheral airways and immaturity of pneumocytes type 2 resulting in poor surfactant production and inadequate antioxidant responses to increased environmental oxygen. Poor development of the alveolar–capillary interface during the sacular phase may result in alveolar–capillary dysplasia and other abnormalities during this period including again pulmonary hypoplasia, acinar dysplasia, and respiratory distress syndrome if the foetus is delivered after preterm labour.

2.2.2 Surfactant Replacement Therapy

Pneumocytes type 2 secrete lipids and proteins into the foetal airways that can be measured in the amniotic fluid. The most commonly used ones are the lecithin-sphingomyelin (L/S) ratio and the surfactant proteins A and B; these are used as predictors of lung maturation. The surfactant film, consisting of multilayers of sheets of lipids and proteins, forms a hydrophobic interface capable of reducing surface tension. It prevents alveolar collapse. In the absence of surfactant, the lungs collapse, in the most severe manifestation contain no air and then present radiologically completely white—without differentiation of the heart and without aeration of the bronchi, particularly in extremely and very preterm infants. Pulmonary haemorrhage, oedema, meconium aspiration syndrome, and sepsis can lead to inactivation or loss of surfactant also resulting in severe respiratory distress.

Exogenous surfactant replacement (bovine or porcine natural and synthetic surfactant) therapy started in the 1990s and became a therapeutic milestone in neonatal intensive care

medicine. Three decades later, neonatologists use different application techniques for surfactant administration:

- The InSurE manoeuvre (intubation-surfactant-extubation procedure) uses the intubation technique with a surfactant bolus for optimally spreading the substance into both lobes of the lungs.
- Surfactant will be slowly inflated by the LISA or MIST manoeuvre (“less invasive surfactant administration” or “minimally invasive surfactant technique”, respectively) to the spontaneous breathing preterm infant via a feeding tube. The latter method is preferred in ELGAN.

Following the first radiograph that demonstrates marked RDS signs and the first surfactant administration, the second radiograph will be done to check for asymmetric distribution of surfactant or airway obstruction with atelectasis. Alternatively, bedside lung US (LUS) will increasingly help to reduce the number of radiographic examinations.

2.2.3 Pulmonary Function and Mechanisms of Lung Injury

Relative to lung volume, airway size is larger in infancy than in older children. Dysanapsis is a term describing the physiologically but disproportionate normal lung growth relative to the airways. It is a feature of all stages of postnatal lung development, as is the increased growth of the central airways in relation to the peripheral airways. Factors known to affect lung mechanics after birth include maternal smoking, nutritional deprivation and intrauterine growth restriction, infection/inflammation, and maternal glucocorticoids [1]. This might result in impaired development of the small airways and reduced numbers of alveoli, as well as thickened septal walls and basement membranes.

2.2.4 Bronchopulmonary Dysplasia

Bronchopulmonary dysplasia (BPD) or chronic lung disease (CLD) of the preterm infant is the most frequent chronic lung disease of infancy and presently defined as oxygen dependency at 36 weeks postmenstrual age. Mild and moderate disease is associated with supplemental oxygen delivery below a fraction of inspired oxygen (FiO_2) of 0.3; severe forms need non-invasive ventilation by nasal continuous positive pressure ventilation (N-CPAP), a high-flow nasal cannula (HFNC) or an increased FiO_2 above 0.3. In most cases, BPD is limited to the infants at 27 weeks and younger (ELGAN) with increasing rates by decreasing gestational age. At our centre we observed a 11.3% rate of BPD which was associated with neonatal pneumonia, longer duration of total parenteral nutrition, longer duration of mechanical ventilation, higher rates of pulmonary hypertension, and more severe retinopathy of prematurity [2].



Non-invasive ventilation and the LISA manoeuvre are crucial in reducing rates of mortality and BPD in extremely preterm infants.

2.3 Special Considerations According to the Vulnerable Term and Preterm Infant

2.3.1 Physiologic Changes During Adaption to Extra-Uterine Environment–Asphyxia

The physiologic changes from the placenta to the neonatal circulation and lungs are maintained by three mechanisms: First, the onset of breathing, that results in lung expansion followed by a decrease of pulmonary vascular resistance and an increase of pulmonary blood flow. Second, the increase of arterial oxygen pressure further decreases pulmonary vascular resistance and third, the placental circulation

stops leading to an increase in systemic vascular resistance and closure of the physiologic embryonal cardiovascular shunts, thus establishing the neonatal circulation. Monitoring of oxygen saturation by pulse-oximetry (SpO_2) during the first 15 min of life differs significantly between preterm and term infants. At 5 min, SpO_2 is about 80% versus 85% and at 10 min 90% versus 95% comparing preterm with term infants, respectively. In case of incomplete closure of these shunts, the main problem for very preterm infants is a persisting ductus arteriosus Botalli (PDA). A PDA can lead to fluid overload in the lungs and renal failure mainly in extremely preterm infants.

Disruption of the adaption from intra- to extra-uterine life occurs in neonatal diseases including wet lung or transient tachypnea of the newborn (TTN) and respiratory distress syndrome (RDS) as well as hyaline membrane disease (HMD). Several factors are associated with a wet lung including fluid reabsorption (by Starling forces, which move fluids between the vasculature and interstitial spaces determined by the balance of hydrostatic and osmotic pressure gradients), lymphatic uptake, and thoracic compression by vaginal delivery. This is the reason for the increased risk of TTN in term and late preterm infants following Caesarean section and especially following elective sections.

Other reasons for maladaptation include asphyxia, meconium aspiration syndrome, congenital diaphragmatic hernia, severe sepsis or pneumonia and rare malformations like Jeune syndrome (asphyxiating thorax dysplasia), congenital chylothorax, and other rare entities. Clinically, the Apgar score judges the newborn's well-being, routinely taken at 1, 5, and 10 min during the adaption phase to extra-uterine life. Ten points correspond to perfect adaption (see Table 2.3).

Asphyxia is a life-threatening complication during birth possibly leading to hypoxic-ischaemic encephalopathy (HIE) or multi-organ failure. Severe asphyxia is defined as a 1-min Apgar score of ≤ 3 points, but a low 5-min score might be more reliable regarding prognosis of long-term neurodevelopmental outcome.

Table 2.3 Apgar score that documents adaptation to extra-uterine life [3]

Item	Apgar acronym	0 Points	1 Point	2 Points
Skin colour	Appearance	Blue or pale all over	Blue at extremities, body pink (acrocyanosis)	No cyanosis body and extremities pink
Pulse rate	Pulse	Absent	<100 beats/min	≥100 beats/min
Reflex irritability grimace	Grimace	No response to stimulation	Grimace on suction or aggressive stimulation	Cry on stimulation
Muscle tone	Activity	None	Some flexion	Flexed arms and legs that resist extension
Respiratory effort	Respiration	Absent	Weak, irregular, gasping	Strong, robust cry

The Apgar score is defined by 5 items investigated at 1, 5, and 10 min of life. Maximum score at each time point is 10 points (perfect adaption)

Abbreviation: *min* minute

Cranial US may identify brain oedema that might correlate with diffuse neuronal necrosis, parasagittal necrosis, or thalamic lesions, which are important findings with respect to prognosis of the neonate. In preterm infants, development of periventricular cysts and their respective size has been found to have high sensitivity in the prediction of cerebral palsy; in case of periventricular echodensities (PVE), the duration (>7 days of life) and the distribution are prognostically superior to the grading of the echodensities [4].

In addition, cerebral function monitoring (CFM) might be helpful in the prediction of outcome of the newborn as is the clinical staging of HIE according to Sarnat and Sarnat—thus CFM has been established in many places as a routine measure at NICUs.

As pH, base excess and lactate levels are poor predictors for an adverse neonatal outcome, and US may be falsely negative or inconclusive, MRI serves as the reference imaging method particularly in severely asphyxiated cases, e.g. when one needs to decide on discontinuing intensive care based on a very poor prognosis. However, these studies have to be timed accurately and sometimes are difficult to perform particularly in severely ill patients undergoing cooling at the best time for early detection of brain damage.



Asphyxia can lead to typical damage of the grey matter in term infants and of the white matter (periventricular leukomalacia) in preterm infants.

2.3.2 Importance of Water and Heat Exchange to the Skin and the Environment

The neonate is extremely endangered by heat loss especially shortly following birth and in case of prematurity. Therefore, delivery room temperature should be above 25 °C, additional measures are recommended and include infant warmers, exothermic mattress, woollen caps, plastic wraps in case of extremely preterm infants, and humidified and heated gases in case of ventilator support. In preterm infants, high evaporative losses of heat decrease by increasing gestational age. Hypothermia defined as core temperature <36.0 °C increases the risk for mortality and morbidities like intracranial haemorrhage, necrotizing enterocolitis (NEC), and late-onset sepsis. Skin-to-skin contact (the so-called kangaroo method) is an important preventive measure for all neonates and especially in low-resource countries.




Hypothermia is a risk factor for mortality especially in preterm infants.

2.3.3 The Open Ductus Arteriosus and Its Mechanism of Closure

In term infants, the ductus is closed by muscle contraction within hours after birth, loss of responsiveness to prostaglandin E2 (PGE2), and occlusion of the lumen over the next days.

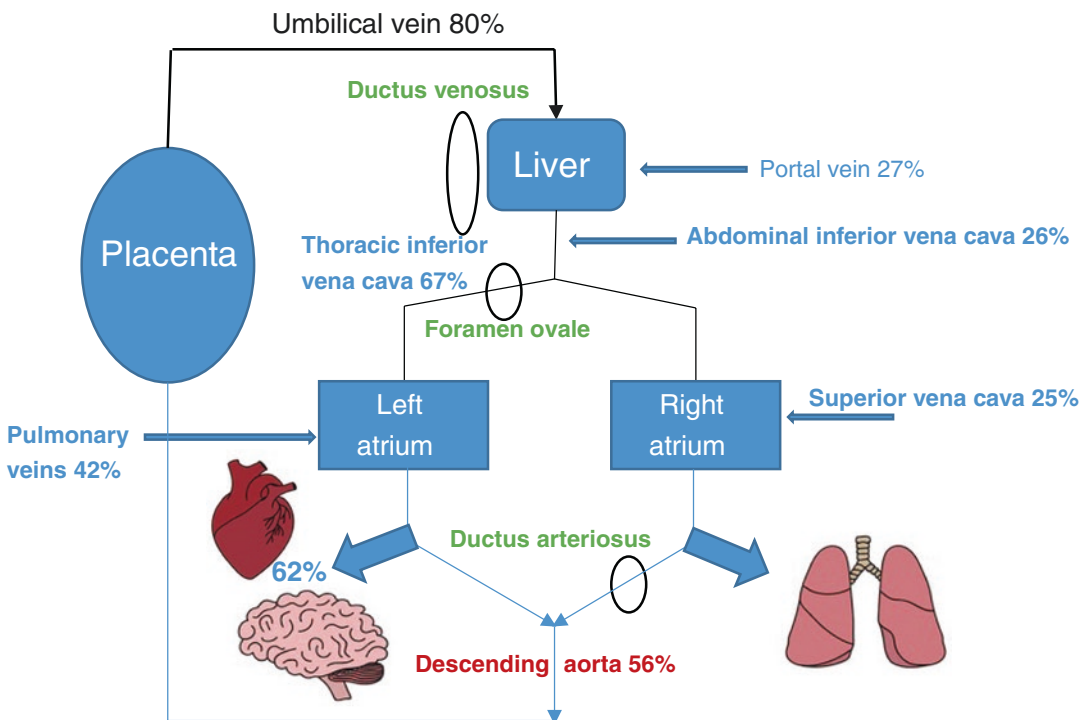
Patency of the foetal ductus arteriosus is regulated by both dilating and contracting factors. An increased pulmonary pressure keeps the ductus open, and the ductus itself produces the vasodilator Prostaglandin E2 (PGE2). The ductus has an intrinsic affinity and sensitivity to PGE2 that is synthesised by cyclooxygenase (COX) 1 and COX 2. COX-inhibitors like indomethacin or ibuprofen constrict the ductus, nitric oxide (NO) maintains the ductus open and is again produced by the ductus endothelium. Additionally, prenatal steroids reduce the risk of a patent ductus arteriosus (PDA) as do postnatal glucocorticoids, but their use in preterm infants early (first week) or late after birth (after 3 weeks) might be associated with higher rates of neurodevelopmental impairment, only the moderate early dosage after the first week of life is recommended.

In preterm infants, the diagnosis of a PDA requires treatment with COX-inhibitors due to pulmonary fluid overload that is associated with the development of BPD. Another side effect of a haemodynamically significant PDA is the reduced perfusion of the kidneys potentially leading to renal impairment.

 A PDA often deteriorates lung function in extremely preterm infants and remains to be a risk factor for BPD.

2.3.4 Foetal and Umbilico-Placental Circulation

A simplified scheme of the foetal circulation is given in Fig. 2.1. The umbilical arteries arise



Adapted from epomedicine (<https://epomedicine.com/medical-students/fetal-circulation-made-easy/>)

Fig. 2.1 Scheme of the foetal circulation and oxygenation. From the placenta, the oxygen enriched blood runs to the right heart and most of its volume bypasses the lungs via PDA and foramen ovale. During adaptation to extra-uterine life normally PDA and ductus venosus

close and by the first breaths the lung get aerated and fully accessed via the pulmonary arteries. (Adapted from epomedicine: <https://epomedicine.com/medical-students/fetal-circulation-made-easy/>)

from the internal iliac arteries and form a spiral around the umbilical vein. Blood from the umbilical vein enters the liver after passing the placenta and via the ductus venosus, and runs through the inferior vena cava to the right atrium. One part of the foetal blood goes via the pulmonary arteries to the left heart, but the majority of blood volume runs via the foramen ovale and the PDA into the arterial circulation to the head and the body. The vessels of the utero-placental circulation are maximum dilated, thus, the foetal heart ejects a maximum amount of blood. If a further increase of the cardiac output seems necessary, the foetus is capable to reduce the flow resistance or increase the driving pressure. The umbilical flow is relatively constant and increases by increasing vascular resistance. The flow can also be reduced and thus be associated with intrauterine growth restriction (IUGR).

2.3.5 Gastrointestinal Tract and Motility

The gastrointestinal tract develops from the enteroderm, the inner layer of the embryoblast. From the enteroderm epithelia of oesophagus, duodenum, jejunum, ileum, and the colon develop including its glands, the liver, pancreas, the respiratory tract, and parts of the urinary tract, thyroid, parathyroid glands, and the thymus. Following formation of the intestine, the mucosa grows rapidly and villi develop. This developmental process starts from cranial to caudal and proximal to distal. Rotation of the intestine normally is counter clockwise. A major problem is malrotation with the thread of a volvulus; one and up to two thirds of neonates have associated malformations (such as congenital diaphragmatic hernia, omphalocele, or congenital heart disease).

Digestive functions develop earlier in the foetal period than motility. Neuronal tracks are detectable at 24 weeks but reach the adult level at birth date. IUGR is a major factor associated with disturbances of gastrointestinal motility and a risk factor associated with NEC. Early feeding of very preterm infants (gut priming) has positive effects on the gut and the neonate, and breast

milk or human milk is mandatory for preterm infants during progression to full diet over the first 2–3 weeks of life.



The digestive function of the preterm gut is well established at the limit of viability; this is not the case regarding gut motility that possibly results in meconium obstruction syndrome of prematurity.

2.3.6 Inflammatory Response in the Preterm Neonate

A growing body of evidence correlates intrauterine infection or inflammation with spontaneous preterm birth. The association is stronger the more preterm the delivery is. Foetal inflammatory response syndrome, the neonatal counterpart to systemic inflammatory response syndrome, is defined as an interleukin-6 value of more than 11 pg/mL from the umbilical vessels. Own data showed that FIRS was significantly associated with adverse neonatal outcome and with the single outcome parameters intraventricular haemorrhage (IVH) and early-onset sepsis. In the bivariate analysis, FIRS was associated with death and bronchopulmonary dysplasia. Findings were markedly more common in preterm infants <32 weeks of gestational age [5]. Figure 2.2 shows the correlation between foetal inflammation/FIRS and short- and long-term sequelae.



FIRS is associated with high risk for adverse long-term outcome.

2.3.7 Miscellaneous Other Aspects

There are many more aspects, which need to be considered when dealing with neonates and preterm babies, particularly when they are very ill and at the NICU. One important aspect that needs to be specifically mentioned is that the immature organism cannot handle drugs and medication

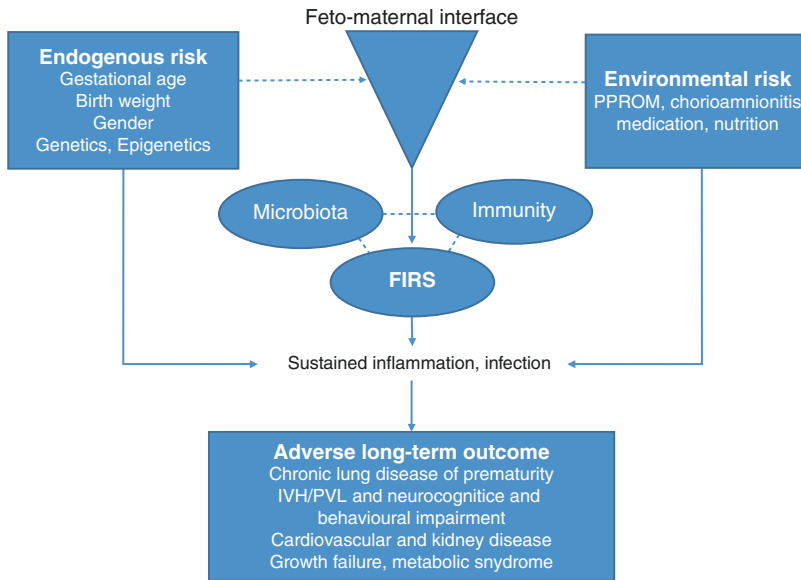


Fig. 2.2 The influence of inflammation and infection on neurodevelopmental outcome and long-term sequelae of preterm birth. The feto-maternal interface plays a certain role regarding local microbiota and immunity. By additional stimuli of endogenous and environmental origin (see left and right sided endogenous risk and environmental risk factors), a foetal inflammatory response supports

the ongoing inflammation and/or infection. All together can lead to adverse long-term outcome as stated above. Abbreviations: *FIRS* foetal inflammatory response syndrome, *PPROM* preterm premature rupture of the membranes, *IVH* intraventricular haemorrhage, *PVL* periventricular leukomalacia. (Adapted from McAdams and Juul [6] and Humberg et al. [7])

like older kids. There is an increased risk of drug toxicity—in part also explainable by the prolonged excretion and elimination time due to yet restricted renal and hepatic function. This makes a reliable and accurate diagnosis even more important—to prevent unnecessary long-term morbidity and growth- or function impairment. Furthermore, there are only a few drugs approved for use in neonates and even less for preterm infants—nevertheless, that a drug is not approved does not mean that it is forbidden. Neonatologists have to use these drugs off-label to be able to treat neonates. This, however, may imply the need for an informed consent and possibly a follow-up in terms of systemic or long-term effects; especially if specific side effects have to be considered when such

particular risks are known as a possible complication in adults.

2.4 Point-of-Care Ultrasound (POCUS)

2.4.1 POCUS of the Neonatal Brain

The neonatal brain is the most vulnerable region of a preterm infant. In that scenario, US examinations of the brain via the anterior fontanel are routinely done at days 1, 3, and 5 and thereafter once a week in case of pathologic findings. If one depicted periventricular echodensities, repeated US scans are necessary after 7 days to prove whether periventricular leukomalacia (PVL) is

developing and to grade the severity (grade I to IV). Other acoustic windows that should be used for a detailed study particularly in preterm infants include the posterior fontanelle, mastoid fontanelle, and the temporal window.

Over the last decade, main complications of neonatal intensive care medicine have worldwide declined. The reason for this decline of IVH and PVL remains partly unclear and is rather associated with improved perinatal management of the neonate and those at the limit of viability (22–25 weeks of gestation) than with single measures. Obstetrical interventions on the one hand, including antenatal corticosteroids, maternal rather than infant transport, and possibly elective caesarean delivery in extremely preterm infants—all these measures have been associated with a decreased risk of IVH. On the other hand, neonatal interventions in the delivery room including delayed cord clamping or umbilical cord milking, maintaining normothermia, avoiding fluctuations in cerebral blood flow, and optimal ventilation management all contributed to a decreased risk of IVH.

Cranial US is a relatively inexpensive, non-invasive, bedside neuroimaging method available in nearly every hospital. In preterm infants, the last US examination of the head is done at the postmenstrual age of 36–40 weeks, and in case of pathologies or for research reasons (short-term outcome), a magnetic resonance tomography (MRT, preferably in a feed-and-wrap technique, without anaesthesia) is performed.

Main indications for cranial US include:

- Antenatal indications, e.g. intrauterine detected anomalies (beyond the scope of this chapter).
- Perinatal indications like need for prolonged resuscitation, hypoxic-ischaemic encephalopathy, prematurity, very low birthweight, small for gestational age, microcephaly and macrocephaly, suspected (genetic) syndrome.
- Postnatal indications like seizures, central apnoea, encephalopathy, sepsis/meningitis/encephalitis, unexplained clinical deteriora-

tion, unexplained drop in haemoglobin levels, symptomatic hypoglycaemia, inborn errors of metabolism, preterm kernicterus, abnormal movements or tone, severe arterial hypotension or hypertension, congenital heart disease, need for surgery, extracorporeal membrane oxygenation, or work-up of malformation syndromes.

Timing of cranial US:

- The first cranial US after admission has to rule out ante- or perinatal brain injury and congenital malformations.
- The scans during the first week of life aim to detect germinal matrix intraventricular haemorrhage (IVH) grade I–III (IVH grade I = subependymal bleeding = SEB = germinal matrix haemorrhage = GMH), periventricular haemorrhagic infarction, and cerebellar haemorrhage. In at least 50% of the affected infants, the onset of GMH is on the first day of life, and by 72 h approximately 90% of the lesions are identified.
- The scans between weeks 2 and 6 help to identify post-haemorrhagic ventricular dilatation, white matter injury, focal arterial infarction, sequelae of brain infection, cystic transformation or developing atrophy, and rare cases of late IVH.
- Cystic white matter injury (periventricular leukomalacia = PVL grade I–IV) may become apparent within 14 days after the insult, although occasionally small cysts may develop up to 6 weeks after birth.
- Brain swelling and impaired perfusion most often are seen at an early stage of hypoxic-ischaemic encephalopathy of the term or near-term infant.
 - Hyperechogenicity in the basal ganglia and thalami will not evolve until approximately 2–3 days. Cortical and subcortical changes may need 5–7 days before a lesion becomes apparent.

2.4.2 Basic Echocardiography

POCUS or functional US is increasingly used to address clinical questions or to support decision-making at the NICU. POCUS answers questions on cardiovascular performance and haemodynamics; due to its non-invasive technique, rapidity of information, and the possibility to perform longitudinal functional assessments it is perfectly suited for (emergency) bedside imaging at the NICU. Clinical criteria like heart rate, blood pressure, or capillary refill time are still very important, but provide only limited insights into the adequacy of neonatal haemodynamic state. Thus, POCUS is directive and focused on a specific clinical problem. It was calculated that the management of 30% of patients treated at the (N) ICU changed due to the results of functional US and in 10% former unknown morbidities were detected. Therapeutic decision-making based on clinical evaluation remains a challenge in neonates and tiny little preterm infants. Hence, routine use of functional US allows to early identify haemodynamic compromise and therefore improves short-term outcomes [8]. Therefore, neonatologists routinely perform this basic echocardiography for functional examination of the heart (cardiac output, venous backflow and myocardial function, presence of PDA, and shunt flow direction). Indications are cardiac compromise during the first days of life, additional presence of sepsis, arterial hypotension, and signs or symptoms associated with a PDA. In case of BPD, regular echocardiography examinations are mandatory for evaluation of presence of pulmonary hypertension. More complex queries will have to be answered by paediatric cardiologists and may sometimes require additional imaging, e.g. in neonates with heart malformations.

2.4.3 Other Applications

Indications for POCUS examinations can be expanded to manoeuvres like placement of umbilical vein catheters, detection of intravascu-

lar thrombi in case of umbilical artery catheter, or the work-up for suspected NEC by depicting intra-abdominal fluid, presence of intramural gas (intestinal pneumatosis—though not specific for NEC) and gas in the portal and hepatic veins, assessing bowel wall perfusion and thickness. In many situations, US is superior to radiographs. It becomes more and more accepted that neonatologists increasingly perform basic functional echocardiography and POCUS—however, what is still lacking are standardised training and accreditation programmes.



POCUS is a bedside US examination that becomes increasingly used for guiding neonatal intensive care and treatment and/or different vascular accesses or drainages.

2.5 What Are the Main Indications for Radiologic Examinations at the NICU?

In the critically ill term and the small preterm infant, most of the radiographic examinations are done at bedside. This is the domain of the radiology technician to make high-quality radiographs of the chest or the abdomen in a clinical setting very different from the well-known environment of the radiology department. Both the radiologist and neonatologist perform and evaluate bedside US and radiologic examinations. These overlapping diagnostic skills of two differently specialised groups of physician resemble the particularity of neonatology. An overview of indications in neonatal imaging is given in Table 2.4.

Note: Doppler sonography is an add-on to many applications though less often performed during POCUS, but mostly as part of a more detailed US study—to assess perfusion of the brain or other organs (e.g. in NEC, renal vein thrombosis...) or e.g. shunt direction and sequelae in case of a PDA.

Table 2.4 Indications for the most common investigations in neonates

Location	Clinical indication	Common diagnoses
Cranial US	Preterm infant, seizures, asphyxia, lethargy, very ill or compromised neonate	Haemorrhages, infarction, PVL, hydrocephalus, malformations
Lung US	Respiratory insufficiency, respiratory distress	Pneumothorax, atelectasis, infiltration, hyaline membrane disease, pleural effusion
Abdominal US	Vomiting, meconium obstruction syndrome of prematurity, distended abdomen, bloody stools, ileus	Organomegaly, evaluation of the intestine, pneumatosis intestine (NEC), ileus, malrotation, hypertrophic pyloric stenosis, gastro-oesophageal reflux
Urinary tract US	Late-onset sepsis, pyelonephritis, foetal urinary tract dilatation (screening), suspected anomalies, fever of unknown origin	Obstructive uropathy, polycystic and multicystic kidney disease, urogenital anomalies, urinary tract dilatation
Radiographs of the chest	Respiratory distress, RDS of prematurity, position of lines and tubes	RDS, meconium aspiration syndrome, pleural effusion, pneumothorax, congenital diaphragmatic hernia, pneumonia, malformations
Radiographs of the abdomen	Ileus, bloody stools, distended abdomen, shock, position of lines and catheters	Meconium obstruction syndrome of prematurity, ileus, volvulus, malrotation, NEC, perforation
Echocardiography	Systolic or diastolic murmur, suspected PDA, functional examination to evaluate myocardial function, suspected congenital heart disease or cardiomyopathy	Congenital heart disease, PDA, arterial hypotension, low cardiac output syndrome, pulmonary hypertension (diaphragmatic hernia, BPD)
Magnetic resonance tomography (MRT) or Magnetic Resonance Imaging (MRI)	Brain	Anomalies of the brain, white matter lesions (PVL in preterm infants), infarction, hypoxic- ischaemic encephalopathy
Computed tomography (CT)	Suspected lung anomalies or interstitial lung disease—rarely indicated	Chronic lung disease

This table provides an overview on the most common investigations and its indications and diagnoses. Small parts ultrasonography like inguinal region or thyroid glands do not have priority compared to the shown regions. Abbreviations: *NEC* necrotizing enterocolitis, *PDA* persistent ductus arteriosus, *PVL* periventricular leukomalacia, *RDS* respiratory distress syndrome, *US* ultrasound

2.6 Screening

2.6.1 Screening in Neonates

Within 72 h of age, every baby is offered a thorough physical examination soon after birth to check their eyes, heart, hips and, in boys, testicles to identify babies who may have conditions that need further testing or treatment. The examination is repeated at 4–7 weeks of age, as some conditions can take a while to develop (mother child prevention programme in Austria founded 1974 and called “Mutter-Kind-Pass”). The neo-

natal hearing test is done soon after birth in term neonates. If the test is negative, repetition is necessary and connate cytomegalovirus infection has to be ruled out. The neonatal blood spot test involves taking a small sample of the baby’s blood to check it for rare but serious inborn metabolic diseases at the age of at least 36 h of age (up to day 5 of life). The reference centrum for diagnosis of inborn metabolic diseases is located in Vienna (for Austria). Additionally, Austria still has a screening programme for congenital toxoplasmosis and for developmental dysplasia of the hips (DDH).

2.6.2 Screening by US

Two major organs/systems are commonly addressed by US screening, the hip (screening for developmental dysplasia of the hip = DDH), and the urinary tract (screening for urinary tract/pelvic calyx dilatation = UTD/PCD)

Hip: There are different approaches to screen the neonatal hip by US; in Austria (and large parts of Europe) the standardised hip US according to Graf is established and successfully introduced in the mother child prevention programme (see above). There are two time-points for hip US—one in the first week of life (particularly in risk patients) and the second general screening test between 4 and 7 weeks of age. The latter should prove maturation of hips and confirm the first evaluation. In case of prematurity, interpretation of findings is correlated to the corrected age for prematurity. A review on DDH identified one diagnostic accuracy US study documenting high sensitivity (88.5%) and specificity (96.7%). The positive predictive value of was 61.6%, but the negative predictive value was nearly 100%. Ten studies of this review evaluated the impact of US in screening for DDH had various methodological weaknesses, thus limited robustness of the findings. Compared with clinical screening, general US screening in neonates may increase overall treatment rates (i.e. cause “over treatment”), but US screening seems to be associated with shorter and less intrusive treatment in those with pathology or severe hip immaturity at risk for deterioration [9]. At present, clear evidence is lacking either for or against general US screening of neonates for DDH that is still discussed controversially in some countries. Some countries proceed (also in part for economic reasons) towards a “selective screening” based on clinical examinations and risk criteria such as breach presentation—particularly in regions with a lower epidemiologic risk (see respective chapter).

Urinary tract: At least some dilatation of the foetal urinary tract or renal pelvicalyceal system is a common finding on prenatal US and is seen as an indicator for possible congenital uropathies endangering renal well-being and growth. Thus, the foetal “*Hydronephrosis*” screening pro-

gramme was established; this term is today outdated and in order to avoid misunderstandings replaced by the terms urinary tract dilatation (UTD—mostly used in North America) or pelvicalyceal distention (PCD—recommended by the ESPR in Europe). Nevertheless, the majority of cases of foetal UTD are not clinically significant, and therefore excessive concern may lead to unnecessary testing of the neonate and anxiety for parents and health care providers. The goal of prenatal management is to detect those cases of foetal UTD that might have a detrimental effect on the health and growth of the infant. This fact requires antenatal and postnatal evaluation, timely referral to a specialist, and possible interventions to minimise adverse outcomes. A postnatal screening in healthy term infants has been found not being cost-effective, in preterm infants the scans according to the obstetric US timings should be taken into consideration.



Hip sonography screening and screening of urinary tract dilatation (former “hydronephrosis”) are established in many countries despite different economic views on these screening methods.

2.7 Summary

In summary, there are certain conditions that are very specific or unique in neonates including disturbances during adaptation to extra-uterine life, persisting shunts like PDA, and chronic lung disease in ELGAN. This chapter provides the most significant physiological and pathophysiological basics to enable a deeper understanding of imaging needs and findings. Bedside US is common at the NICU needing special skills to gain adequate US quality when handling the probe within the incubator. US might further serve as a prognostic tool regarding asphyxia of term infants and periventricular leukomalacia in preterm infants. Functional US (POCUS) is increasingly common at the NICU focusing on the brain and the heart, and US screening for

developmental dysplasia of the hips and urinary tract dilation are established. Radiographs still play a major role in neonatal imaging—they should be performed with care and technical expertise; indications should be restricted according to the ALARA (As Low As Reasonably Achievable) principle in terms of radiation protection. Nevertheless, as neonates often present with unspecific symptoms and cannot express their complaints, the clinical diagnosis can be quite challenging. Laboratory test can also only be used with restrictions—some deliver unspecific results, and the number of tests is limited by the small blood volume that hinders large and repeated sampling or tapping to avoid anaemia and reduce the number of subsequent red cell package transfusion. Therefore, imaging is and will stay an important diagnostic measure for diagnosis and follow-up of many neonatal conditions, and has to be made available for all in need 24 h and 7 days a week with adequate quality.

References

- Robinson PD, Pillow JJ. The respiratory system—mechanics of the lung, airways, and the chest wall. In: Riemensberger PC, editor. *Pediatric and neonatal mechanical ventilation*. Berlin: Springer; 2015. p. 68–85.
- Reiterer F, Scheuchenegger A, Resch B, et al. Outcomes of very preterm infants with and without BPD followed to preschool age. *Pediatr Int*. 2019;61:381–7.
- Apgar V. A proposal for a new method of evaluation of the newborn infant. *Curr Res Anesth Analg*. 1953;32(4):260–7.
- Resch B, Vollaard E, Maurer U, Haas J, Rosegger H, Muller W. Risk factors and determinants of neurodevelopmental outcome in cystic periventricular leukomalacia. *Eur J Pediatr*. 2000;159:663–70.
- Hofer N, Kothari R, Morris N, et al. The fetal inflammatory response syndrome is a risk factor for morbidity in preterm neonates. *Am J Obstet Gynecol*. 2013;209(542):e1–11.
- McAdams RM, Juul SE. The role of cytokines and inflammatory cells in perinatal brain injury. *Neurol Res Int*. 2012;2012:561494. <https://doi.org/10.1155/2012/561494>.
- Humberg A, Fortmann I, Siller B, et al. Preterm birth and sustained inflammation: consequences for the neonate. *Semin Immunopathol*. 2020;42:451–68.
- El-Khuffash A, McNamara PJ. Neonatologist-performed functional echocardiography in the neonatal intensive care unit. *Semin Fetal Neonat Med*. 2011;16:50–60.
- Woolacott NF, Puhan MA, Steurer J, Kleijnen J. Ultrasonography in screening for developmental dysplasia of the hip in newborns: systematic review. *BMJ*. 2005;330(7505):1413. <https://doi.org/10.1136/bmj.38450.646088.E0>.

Further Reading

- Adamson SL, Myatt L, BMP B. Regulation of umbilical blood flow. In: Polin RA, Fox WW, Abman SH, editors. *Fetal and neonatal physiology*. 3rd ed. Philadelphia, PA: Saunders Elsevier Inc.; 2004. p. 748–58.
- Alvaro RE, Rigatto H. Cardiorespiratory adjustments at birth. In: MacDonald MG, Seshia MMK, Mullett MD, editors. *Avery's neonatology. Pathophysiology and management of the newborn*. 6th ed. Philadelphia, PA: Lippincott Williams & Wilkins; 2005. p. 284–303.
- Bancalari E. *The newborn lung: neonatology questions and controversies*. 1st ed. Philadelphia, PA: Saunders Elsevier Inc.; 2008. ISBN: 978-1-4160-3166-6.
- Baskin LS. Overview on fetal hydronephrosis. Uptodate Jul 2021.
- Buonocore G, Bracci R, Weindling M, editors. *Neonatology: a practical approach to neonatal diseases*. 2nd ed. Cham: Springer Nature; 2018. ISBN: 978-3-319-29487-2.
- Clyman RI. Mechanisms regulating closure of the ductus arteriosus. In: Polin RA, Fox WW, Abman SH, editors. *Fetal and neonatal physiology*. 3rd ed. Philadelphia, PA: Saunders Elsevier Inc.; 2004. p. 743–8.
- Dawson JA, Kamlin CO, Vento M, Wong C, Cole TJ, Donath SM, Davis PG, Morley CJ. Defining the reference range for oxygen saturation for infants after birth. *Pediatrics*. 2010;125(6):e1340–7.
- Doyle LW, Cheong JL, Ehrenkranz RA, Halliday HL. Late (>7 days) systemic postnatal corticosteroids for prevention of bronchopulmonary dysplasia in preterm infants. *Cochrane Database Syst Rev*. 2017;10(10):CD001145.
- Dudink J, Jeanne Steggerda S, Horsch S, et al. State-of-the-art neonatal cerebral ultrasound: technique and reporting. *Pediatr Res*. 2020;87:3–12.
- Gleason CA, Juul SE. *Avery's diseases of the newborn*. 10th ed. Philadelphia, PA: Elsevier; 2018. ISBN: 9780323401395.
- Graf R. The diagnosis of hip dislocation by the ultrasonic compound treatment. *Arch Orthop Traumat Surg*. 1980;97:117–33.
- Graf R, Baumgartner F, Lercher K. *Sonografie der Säuglingshüfte*. 2. Auflage ed. Heidelberg: Springer; 2011. ISBN: 978-3-642-22033-3.
- Halliday HL, Ehrenkranz RA, Doyle LW. Early postnatal (<96 hours) corticosteroids for preventing chronic lung disease in preterm infants. *Cochrane Database Syst Rev*. 2003;(1):CD001146.

- Halliday HL, Ehrenkranz RA, Doyle LW. Delayed (>3 weeks) postnatal corticosteroids for chronic lung disease in preterm infants. *Cochrane Database Syst Rev*. 2003;(1):CD001145.
- Halliday HL, Ehrenkranz RA, Doyle LW. Early (< 8 days) postnatal corticosteroids for preventing chronic lung disease in preterm infants. *Cochrane Database Syst Rev*. 2009;(1):CD001146.
- Jobe AH. The new bronchopulmonary dysplasia. *Curr Opin Pediatr*. 2011;23:167–72.
- Kotecha S. Lung growth: implications for the newborn infant. *Arch Dis Child Fetal Neonatal Ed*. 2000;82:F69–74.
- Lim J, Hagen E. Reducing germinal matrix-intraventricular hemorrhage: perinatal and delivery room factors. *Neoreviews*. 2019;20:e452–63.
- Niemark HJ, Hütten MC, Kramer BW. Surfactant for respiratory distress syndrome: new ideas on a familiar drug with innovative applications. *Neonatology*. 2017;111:408–14.
- Polin R, Abman S, Rowitch D, Benitz W. *Fetal and neonatal physiology*. 6th ed. Philadelphia, PA: Saunders Elsevier Inc.; 2021. ISBN: 9780323712842.
- Ramachandrappa A, Jain L. Elective cesarean section: its impact on neonatal respiratory outcome. *Clin Perinatol*. 2008;35:373–93.
- Resch B. Physiologie bei Früh und Reifgeborenen [German]. In: Mayr J, Fasching G, editors. *Akutes Abdomen im Kindes- und Jugendalter*. Berlin: Springer; 2018. p. 1–17.
- Resch B, Resch E, Maurer U, Mueller W. Periventricular leukomalacia and neurodevelopmental outcome. *J Pediatr*. 2011;159:1049–50.
- Riccabona M. *Pediatric ultrasound: requisites and applications*. Cham: Springer; 2020. ISBN: 978-3-030-47910-7.
- Romero R, Gómez R, Chaiworapongsa T, et al. The role of infection in preterm labour and delivery. *Pediatr Perinat Epidemiol*. 2001;15:41–56.
- Thébaud B, Lacaze-Mazmonteil T. Patent ductus arteriosus in premature infants: a never-closing act. *Paediatr Child Health*. 2010;15:267–70.
- Trevisanuto D, Sedin G. Physical environment for newborns: the thermal environment. In: Buonocore G, Bracci R, Weindling M, editors. *Neonatology*. 2nd ed. Cham: Springer; 2018. p. 323–46.
- Turner DA, Cheifetz IM. Basics of gas exchange. In: Riemensberger PC, editor. *Pediatric and neonatal mechanical ventilation*. Berlin: Springer Verlag; 2015. p. 43–54.
- van Haastert IC, Groenendaal F, Uiterwaal CS, Termote JU, van der Heide-Jalving M, Eijssermans MJ, Gorter JW, Helders PJ, Jongmans MJ, de Vries LS. Decreasing incidence and severity of cerebral palsy in prematurely born children. *J Pediatr*. 2011;159:86–91.e1.
- von Beckerath A-K, Kollmann M, Rotky-Fast C, et al. Perinatal complications and long-term neurodevelopmental outcome of infants with intrauterine growth restriction. *Am J Obstet Gynecol*. 2013;208(130):e1–6.



General Remarks, Rules, and Considerations

3

Michael Riccabona and Hans-Joachim Mentzel

3.1 General Remarks and Considerations

Neonates are not small adults nor small children—they differ considerably. Aspects that impact imaging in neonates are:

- Neonates are much smaller than children or adults.
- Neonates additionally have a different body composition and proportion. Organs are small in size and closely spaced. The tissue contains more water and less fibrous or fat components, significantly impacting their imaging appearance and influencing imaging options.
- Neonatal structures are more flexible and moveable and sometimes in a different anatomic position (e.g. liver, spleen, and kidneys not covered and protected by the ribs and the costal cage, the ovaries can be anywhere in the abdominal cavity...).
- Neonates have a faster breathing and heart rate thus necessitating a higher temporal resolution when imaging the lung, the heart, the dia-

phragm, or blood flow/vessels. Any imaging equipment must be able to offer high spatial and high temporal resolution.

- Ossification is different with many structures still cartilaginous (e.g. epiphyses, non-ossified fontanel....) that can impact imaging. Sometimes it is an advantage as these structures can be imaged by ultrasound (US) or allow access to structures behind (e.g. hip US, brain US, US of the spinal cord). On the other hand, these structures do not show up on radiographs or CT and thus cannot be imaged in the same way as in adults.
- Neonates are much more radiosensitive than children or adults; furthermore, they have a much longer lifespan where possible radiation induced tumours can manifest. Therefore, radiation protection is of outmost importance and dedicated neonatal exposure settings or (if necessary at all) CT protocols are essential. Best of all is to avoid radiation-based imaging and replace the examination by other options such as US or MRI. Especially in (very) premature babies, radiation protection and various aspects of development potential must be taken into account even more than in older infants.
- Neonates also have a higher circulating blood volume in relation to their body weight that impacts imaging protocols, for example, the relative volumes of intravascular contrast is higher and adult-based rules cannot be applied.

M. Riccabona (✉)
Medical University Graz, Graz, Austria
e-mail: michael.riccabona@medunigraz.at

H.-J. Mentzel
Section of Pediatric Radiology,
Department of Radiology,
University Hospital, Jena, Germany

- Furthermore, the physiologically immature kidney and liver means a relatively delayed contrast elimination from the body, again posing specific challenges in imaging these infants with a relatively high necessary contrast dose that may compromise other physiologic functions (e.g. suppressed thyroid function after intravenous application of iodinated contrast agents....).

Finally, it is a specific challenge to properly handle neonates for imaging, as they cannot comply with commands such as “hold your breath” or “don’t move”. The inability to verbally communicate must be compensated by creative individualised handling, both in terms of how the examination is conducted and how much immobilisation is needed and how this can or must be achieved (from cloths to restraints and tapes, to sedation or even anaesthesia that may become necessary). In order to have a cooperative baby, the environment must be adapted to their needs as much as possible:

- Avoid bright light, loud noise, or uncomfortable positions (also for the examiner).
- A heater should be readily available because babies become cold quite quickly.
- Ultrasound gel should be pre-warmed, which also applies to contrast agents (CA).
- Tissues and cloth should be at room temperature.
- Pacifiers should be at hand as well as swaddling facilities.
- Additional means that help pacify babies are glucose drops, toys with music, and possibly some soft and tender helping hands from parents, nurses, and child life specialists.

Investigating these babies gently does not mean you cannot perform required manoeuvres (for example, graded compression during US), only that you must do it gradually and kindly—(like massaging the tummy and you will be surprised how well babies tolerate these manoeuvres). Some babies also love it when you talk to them, make funny noises, or sing a song

while performing an examination. Most important is that you yourself are comfortable and calm, too, not frightened or anxious, and perform—(particularly for US examinations) constant slow movements, with a continuous touch/contact of the probe to the skin, avoiding sudden and hectic motions. Sometimes it is also helpful to feed the baby during the study.

For some investigations (such as US), one may consider imaging the baby in the mother’s arms. However, this should not become a general rule as it may be more difficult to position the baby appropriately, may subject the caregiver to radiation exposure, and often puts more stress and strain on the examiner. Sometimes, positioning manoeuvres may become necessary—again, do them gently and calmly, but do it if needed to get the optimal yield from an examination. However, in general, one should accept that not all examinations will be optimal. You need and should take more time for the imaging procedure than with more compliant children. If you stay calm, patient, and relaxed during an examination (e.g. while doing an US) and in the best case, the baby will eventually fall asleep.

3.2 Which Are the Methods That Can Be Applied and Are Used for Imaging Neonates?

All imaging methods should be available for neonates. The mainstay in inpatient care for newborns definitely is radiography and US—mostly of the chest/lung and the abdomen. Radiography is often performed at the bedside in the neonatal intensive care unit (NICU). Technically perfect exposures are essential, particularly as these patients often receive a number of radiographs during their intensive care time which can add up to a considerable radiation dose and may affect radiosensitive tissues (i.e. breast and genitalia, thyroid gland, and red bone marrow).

Ultrasound has become a major modality in neonatology and is increasingly used throughout the body—from the brain to the toe, particularly with the new advances of chest and lung

US. However, adequate equipment and transducers as well as training are mandatory and one needs to remember that even if its “only US” is still a medical investigation that must have a justifying indication, must be performed properly to lead to a reliable diagnosis, and should include proper standardised and accessible documentation for follow-up comparison and medico-legal issues.

The third important method in clinical routine used in neonates is fluoroscopy—mostly for bowel and urogenital queries. Here the skillful use of (manual) collimation with a low intermittent pulse rate is essential—besides optimised dose settings and adequate filtration (e.g. remove scatter grids...) to keep examination time short and to minimise radiation dose.

MRI is used mainly for neuroimaging—details are discussed in the respective chapter. Remember that many investigations can be performed as a “feed and wrap” approach when the baby is sleeping after being fed thus avoiding the need for sedation; otherwise, deep sedation or anaesthesia (particularly if the examination time is longer than approximately 30 min) with a secured airway will become necessary.

Computed tomography (CT) is reserved for emergency examinations, complicated pulmonary pathologies, or complex malformations (e.g. cardiovascular anomalies) and requires protocols adapted for age and weight as well as the region/query.

The aim of all imaging is to provide images and diagnoses at the lowest possible burden to the patient, and to avoid poor quality images with low diagnostic yield with unjustified high burden (Fig. 3.1).

3.2.1 Ultrasound

Ultrasound has matured from an orienting imaging tool to one of the mainstays in neonatal imaging. Initially, only the brain, the kidneys, and the heart were imaged by US; today nearly all body compartments (including also the musculoskeletal system as well as the lung and chest) can be



Fig. 3.1 Images you want to avoid. Radiograph of the lower leg: as the image is not properly collimated, one can see the hands of the person positioning the leg indicating that either the field is too large (and hands even not covered by protective gloves) and therefore unnecessary radiation has been applied, or potential pathology of the lower femur may be obscured. This kind of low quality of radiograph should be avoided, particularly in very radiosensitive neonates

addressed and many conditions can reliably be diagnosed without the need for other imaging tools. Portable high-end US devices are very helpful (possibly with a battery and short start-up time when changing from one incubator to another), and proper documentation must be provided—even if it takes some effort and time to then export the images to a hospital-wide PACS system to make the images available for follow-up etc., not only for medico-legal reasons. The commonly used prints archived in the individual patient file are a suboptimal solution.

Other prerequisites are pre-warmed US gel and adequate selection of transducers—at least a high-frequency sector/vector and a high-resolution high-frequency linear (or micro-curved) transducer are mandatory. So-called

hockey stick probes have proven useful for monitoring the insertion and positioning of catheters as well as for therapeutic interventions. In premature babies in particular, the hygienic standard for US examinations is particularly high (comparable to the use of US in the surgical theatre or on the transplant ward). Options to darken the room are very helpful; a “bi-colour mode” with tinting of the grey-scale image can be very useful if the room cannot be darkened sufficiently.

Even if US is radiation free, there are possible effects of the sound beam energy heating and mechanical effects on tissues. The risk of the applied energy is indicated by the thermal index (TI) and mechanical index (MI) which must be displayed on the US screen constantly and are updated during the investigation as soon as settings are changed. The most powerful option to keep MI and TI low (particularly important for lung and brain as well as genital US) is to reduce output gain; other factors that significantly affect sound energy are frequency at a given depth, harmonic imaging, the use of multiple focal zones, and Doppler techniques. Particular care should be taken when using innovative techniques such as US elastography or intravenous (off-label) use of US contrast agents (UCA). In part because of these aspects, every US examination needs a justifying indication and a well-defined question that can at least potentially be answered by US.

There are different ways to use US:

1. To perform a meticulous and detailed study addressing a specific query (e.g. necrotising enterocolitis and intestinal/porto-venous pneumatosis with its differential diagnosis) and then often complemented by an overview of neighbouring structures and organs, which will take time and special competence.
2. For guiding catheter placement/interventions and checking line position.
3. As a “sonoscope” (point of care US = POCUS)—for quick clinical orientation and to answer a single specific dedicated clinical question (see also below).
4. For follow-up of conditions for therapy or prognosis, particularly in order to reduce radiating imaging (such as abdominal or chest radiographs) provided US can deliver the necessary information.
5. Another application of US is screening—best known from hip US (for developmental dysplasia of the hip). Some also perform screening of the urinary tract or the brain, at least in selected patient populations. To a certain extent also follow-up of foetally suspected but equivocal findings (e.g. mild dilatation of the urinary tract) in term infants is performed.

A sonoscope is an orienting application of the POCUS approach that aims at answering a basic question and is more or less an extension of the (initial) clinical examination. Typical queries in the neonate and at the NICU/during neonatal resuscitation are: pneumothorax? lung pathology? effusions? gross heart malformation and cardiac function or pericardial effusion? hydrocephalus or brain haemorrhage/brain oedema? dilated collecting system of the urinary tract? dilated or collapsed bowel—with what kind of content?

Or, usually in slightly older babies, an orienting scan of small parts and soft tissue conditions such as in some lumps and bumps may be requested (e.g. cystic or solid? simple or complex? well defined? penetrating to/arising from deeper compartments?...) to then help defining the further diagnostic and therapeutic management. Note that though these sonoscopes usually are short and limited examinations, proper equipment as well as skill, practice, respective knowledge and education is essential to provide a good result at lowest burden to the patient and to avoid creating greater confusion and demand for more invasive imaging. The more experienced the investigator is, the better the result and the shorter the examination will be, avoiding other additional unnecessary examinations.

3.2.2 Radiographs

The most common targeted body area for radiographs is the chest followed by the abdomen, where the standard anterior-posterior projection can be supplemented by a cross table lateral projection (e.g. for depiction of free peritoneal air or gas-fluid levels) to avoid repositioning severely sick babies (Fig. 3.2). In neonates, a chest radiograph is only taken in anterior-posterior (or rarely pa.) direction, hardly ever a lateral exposure is necessary or even useful. The use of lateral projection for the detection of ventral pneumothorax should be avoided because of the necessary additional radiation, and consider that US is an excellent alternative to detect a ventral pneumothorax in preterm babies—with high sensitivity.

Sometimes imaging of skeletal structures (such as in syndromes or trauma) becomes necessary and indicated (see Figs. 3.1 and 3.10). The question of child abuse (non-accidental injury, NAI, inflicted injury) is an exceptional situation in neonates. In these (rare) cases, the child protection guidelines must be followed (see respective chapter).

In most places, digital radiography has been implemented and conventional films are out-



Fig. 3.2 Neonatal perforation—cross-table view in lateral decubitus position. In order to minimise patient burden by moving the vulnerable baby, the radiograph is taken in the incubator in a lateral decubitus position with a cross-table view, proving free peritoneal air in a preterm with NEC and bowel perforation (also note the intestinal pneumatosis) and patchy intra-abdominal calcifications, probably from an intra-uterine meconium peritonitis

dated—film-screen systems are still used in some places with restricted resources or for mobile examinations. Whichever technique is available, adequate mobile equipment for the NICU suitable for incubators with adequate resolution (at least 3–4 line pairs/mm), adapted exposure parameters, if applicable proper age adapted electronic filtering as well as data processing and image calculation/reconstruction software adapted to the body composition of the babies need to be available in order to have a reasonably low dose at sufficient and diagnostic image quality. If one observes the cumulative histogram of a chest film, there is a big difference between an adult/adolescent, a toddler, or an infant, and even far more in a preterm neonate. This must be addressed by the image reconstruction algorithms and the image processing programmes and software, also considering the signal to noise ratio (e.g. in direct detectors) with the respective pixel size per kernel. Post-processing algorithms are helpful to identify catheters or tubes making the use of contrast agents (CA) for catheter positioning unnecessary. Eventually, the radiographs have to be viewed on a proper monitor with sufficient resolution (graphic systems with more than 8 bit depth). It is very helpful to have a proper viewing area directly at the mobile device (allowing immediate inspection of the image) or easy access to the hospitals' network (to quickly enable proper reading by the paediatric radiology specialist if needed in some urgent situations). Nevertheless, the most crucial point for proper and diagnostic images at lowest possible radiation is the radiographer's technique and handling, using state of the art technical equipment.

Particularly in preterm babies, all structures between the body and the film or the cassette should be avoided, as these degrade image quality and increase the dose necessary for the exam (e.g. do not place films or cassettes in a drawer of the incubator but immediately below the baby, avoid too much cloth, tissues, or diapers for covering, possibly open the plastic top of the incubator—this will result in approx.



Fig. 3.3 (a–d) NICU radiograph in the incubator. How to optimally take a radiograph at the NICU in the incubator, even if there is little space (a). After wrapping the cassette, it is put gently below the baby or under the mattress avoiding the cassette drawer (which would increase dose and decrease image quality; however, note that this wrapping cloth can create structures on the radiograph in tiny and premature babies that should not be misread as

pathology) (b). Thereafter, the top of the incubator is removed (to avoid unnecessary radiation) and the image field is collimated using light markers (c). Remove or displace all external interfering cables and devices if possible, and assure the use of radiolucent electrodes (d)—to avoid diagnostic inaccuracies for example a pleural effusion which is difficult to evaluate because of electrodes positioned exactly at the lateral cardiophrenic angles

40% dose reduction) (Fig. 3.3). Only sometimes, in the case of instable, extremely preterm infants who should not be moved at all, it is necessary to use the incubator slot for the detector. This has to be decided on an individual base—outweighing the risk of manipulation versus the risks from (particularly) repeated exposures with the cassette in the drawer; these aspects (e.g. can the lid of the incubator be easily opened without affecting support devices?) should also be discussed with the neonatologists when they decide on purchasing new equipment. Use proper collimation guided by a light or laser cross beam to manually cone down the real image size to the questioned area, and only use the electronic shutters retrospec-

tively in selected occasions (Fig. 3.4). Babygrams should be avoided, although time and again so-called torsograms (chest and upper abdomen on one image) are required (e.g. umbilical line position, overview of adjacent pathology of the abdomen and chest such as in oesophageal atresia or diaphragmatic hernia) (Fig. 3.5). The most important single aspect of the ALARA principle (as low as reasonably achievable) in terms of dose reduction is the correct collimation. Every extra centimetre that is included on the image means considerable unnecessary additional radiation exposure for these (premature) babies.

Outside of the NICU, proper positioning and stabilisation of neonates during the exposure are

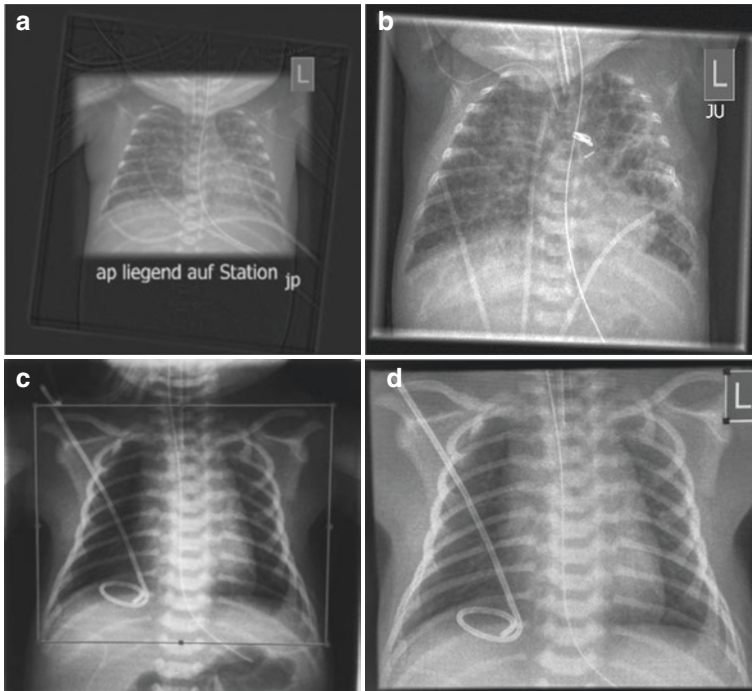


Fig. 3.4 Digital collimation versus proper prospective collimation. (a) Neonatal chest radiograph coned by post-processing software after image acquisition in a preterm infant with endotracheal and gastric tube and peripherally inserted central line—note that the exposure field is much larger than the cropped field and thus an unnecessary high radiation dose was applied (dose increase exponential!). (b) Proper collimated chest radiograph during image

acquisition—one can see the “silver shining” at the margins of the image (preterm infant after PDA ligation with endotracheal and gastric tube and peripherally inserted central line). (c, d) Uncropped original image and final image after applying digital collimation. The dose in (c) is nearly double the dose if the image would have been initially collimated like seen in image (d)

essential. Use very short exposure times, and try to immobilise the baby either placed on the respective table or using restraining devices (Fig. 3.6.).

Some European guidelines are available regarding dose, dose-area product, entrance dose, diagnostic reference level, etc. for this age group. But these need to be individually adapted with respect to the available device and technique as well as the patient situation and request. Note that in neonates and portable units rather low voltage at around 60 kVp is generally used, opposite to the high-voltage approach often used in

adults and older children. Exposure time should be short to avoid breathing and motion artefacts. Even in severely sick neonates, proper projection and placement with strong collimation is essential for diagnostically useful radiographs and efforts have to be undertaken to grant such images by properly positioning the patient, removing external devices whenever possible, etc.! This can in part be achieved not only by training and motivation (especially of NICU nurses and respiratory therapists), but by a regular (e.g. weekly) audit of respective image samples as a standardised quality control management measure.

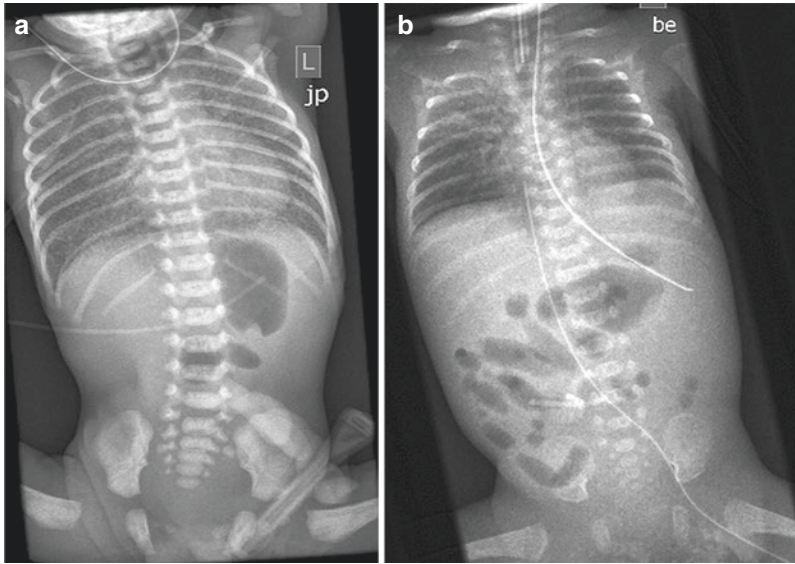


Fig. 3.5 “Torsogram” (radiograph of chest and abdomen). (a) Torsogram in a neonate with oesophageal atresia shows delineation of the upper oesophagus using air instilled by the high ending gastric tube as CA. Note the entire view of chest and abdomen enables a good over-

view, with air in the stomach indicating that there must be an associated trachea-esophageal fistula. (b) Torsogram to check the path and position of a peripherally inserted central line, running from the left leg to the right atrium. Also note tracheal and gastric tube



Fig. 3.6 Neonatal chest radiographs—positioning and immobilisation. There are many ways of properly positioning and immobilising neonates for radiographs: (a) plastic tubes (“Babix”), (b) other fixation devices supported by mother holding the baby, (c, d) mother holding

baby sitting on a chair in front of the digital panel detector, (e) example for positioning device for panel detector radiographs, and (f) positioning with immobilisation for head radiographs

3.2.3 Fluoroscopy

Fluoroscopy can be applied to neonates, often for pre- or postsurgical conditions, and the query of bowel anatomy or patency or lower urinary tract obstruction/vesicoureteral reflux. However, some of these queries can be addressed by US which avoids radiation, such as contrast-enhanced voiding urosonography (ce-VUS) for vesicoureteral reflux, and sonographic enema (=US while filling and distending the colon with a rectal saline enema also called “hydrocolon”). As these US studies can be performed in the safe environment at the bedside (e.g. for query “small unused left colon”, “meconium ileus”...), this reduces the stress and strain on these smallest of patients. This approach can even be used therapeutically, e.g. for treatment and reduction of meconium ileus.

Fluoroscopy is a stressful investigation for the newborn (and the parents, sometimes even the radiologist and the technologist). To reduce the child’s stress level, the examination room should be designed in a calm atmosphere. The use of heaters to warm the room/the baby is essential.

Additional aspects on how to optimally perform a fluoroscopic study in neonates are:

- Clothing should be removed for every examination as these not only disturb the image processing, but also sometimes lead to a higher radiation dose.
- Appropriate immobilisation of the newborn is necessary for every examination—in addition to wrapping techniques, there are special devices that can be attached to the table (Fig. 3.7). An overhead tube is recommended—possibly with remote control from a separate console.
- For neonates only a pulsed technique is acceptable, and a grid-controlled fluoroscope is recommended. Note that in neonates no detector grid for reducing scattered radiation is necessary for image quality, and only serves to unnecessarily increase the radiation dose.
- The pulse length should be reduced (2–10 ms) and low pulse rates are usually sufficient - these may vary with query and application.
- Size and weight adapted protocols with special kV/mA curves for neonates should be generated and applied.
- Remember radiation protection and the ALARA principle—spot-film exposures are rarely necessary and most queries can be answered by fluoroscopic observation with last image hold from a low pulse intermittent fluoroscopy examination, possibly using stored cine clips.
- In order to minimise dose, the field should be coned to the respective area using light or laser beams for targeting—to adapt the collimators accordingly before activating the fluoroscope.
- As a general rule for radiation protection, one should always ask oneself if the result can be

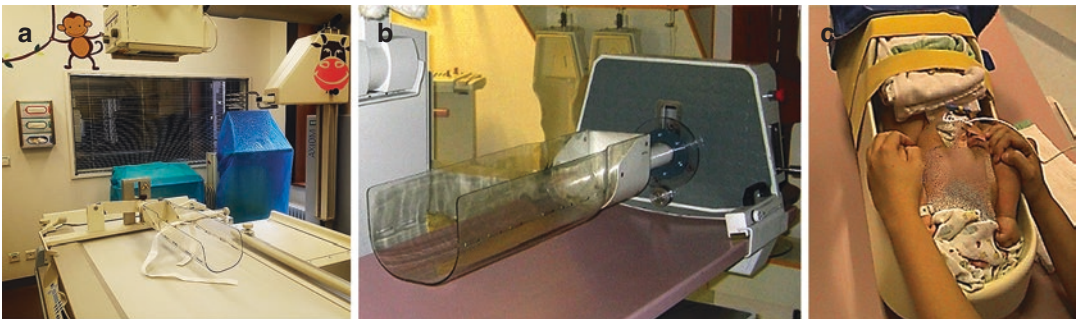


Fig. 3.7 Helping devices for positioning and immobilisation in fluoroscopy. (a) A view of a fluoroscopy suite trying to create child-friendly environment. (b) Plastic tray to position and immobilise the patient—it can be turned in

either direction from the instrumentation desk in the separate room. (c) A neonate properly and comfortably placed in the positioning cradle

achieved with another less burdening or even radiation-free investigation.

- If intraluminal CA are used, avoid too high iodine concentrations—usually a 100–150 mg I/mL is sufficient, sometimes even less.

Even rarer, fluoroscopy may become necessary for an intervention such as intravenous line/catheter placement, retrograde reduction of bowel obstruction, percutaneous nephrostomy, or other drainages.

Specific rules concerning the amount and kind of CA to use in specific cases will be addressed in the respective chapters. Contrast agents are of particular importance for fluoroscopy but can be quite cumbersome in this age group, as only a few radiopaque CA are approved for neonatal use. Additionally, neonates pose a challenge for CA application because, for example, of the immature kidneys or the possible effect on thyroid function. Nevertheless, due to little intrinsic density differences of neonatal tissues (high water content, little fat...), CA more often become necessary than in older patients. Still, the need for radiopaque CA should be questioned; sometimes air can be used as negative CA in the gastrointestinal tract helping to avoid oral or rectal CA application (see Fig. 3.2). Also remember, that these iodinated CA given orally or rectally can at least be in part absorbed and thus will have a systemic effect (see respective entry on intravenously applied CA).

3.2.4 What About CT and MRI in Neonates?

These imaging tools usually complement other exams, are rarely necessary as a first imaging exam, and can be cumbersome and difficult to apply in neonates.

- Performing a CT in a neonate is uncommon, practically only used in rare acute and severe trauma queries, or some chest/lung conditions as well as rare tumour conditions or cardiovas-

cular queries—the details of these CT protocols and measures are discussed in the respective chapters.

- If one needs to perform a CT in a neonate several general aspects need to be remembered and considered: there is a significantly shorter delay time for the various phases (arterial or venous or post-bolus) because of the intrinsically shorter distances but also the much faster heart rate, which in (preterm) neonates is around 125 (90–160) beats/min; special protocols have been developed to address this challenge (e.g. split bolus technique). As neonates have little fat and based on the high water content of all tissues with a lower intrinsic tissue contrast, intravenous CA are more often necessary along with enteric opacification. Scanning at low (80) kV is feasible in these small patients and thus one can achieve a better contrast image with lower overall radiation dose. The use of volume mode (if available) is recommended because the helical mode usually requires more radiation.
- MRI is increasingly utilised in neonates—particularly in neuroimaging, although the immature brain with minimal myelination can cause difficulty in interpretation. Therefore, in some queries, the investigation might be postponed until there is sufficient myelination for a proper diagnosis. This and the relevant indications for neonatal brain or spinal MRI will be discussed in the respective chapter.
- In the other body areas, there is very little need for MRI—particularly as handling is cumbersome due to the fast breathing rate and as one wants to avoid gadolinium due to the physiological renal immaturity. Nevertheless, some rare queries such as complex urogenital or chest/cardiac malformations and suspected tumour conditions may come up.
- Remember that MRI examinations are a great challenge in the neonatal period. It requires adequate equipment and personnel resources. Transport to the MRI unit is usually necessary and may be cumbersome, also the monitoring

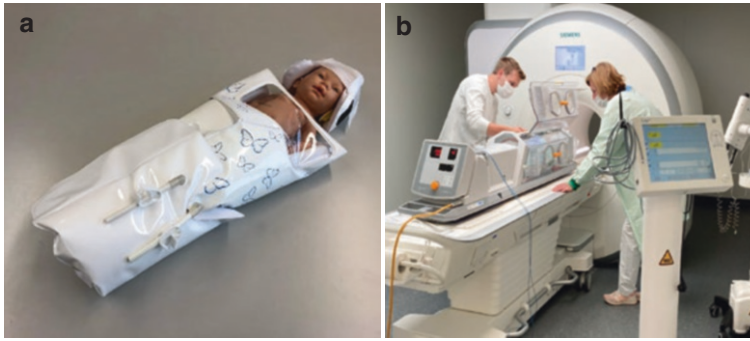


Fig. 3.8 MRI immobilisation devices and MRI compatible incubator. There are devices on the market to either immobilise the baby, e.g. for an MRI scan (Baby Cocoon, Pearltec) (a), or one can use the commercially available MRI compatible incubators which come with monitoring

devices (b) and the respective head, body, and spine coils available from several companies (e.g. Sree Medical Systems, Sanova Pharma GesmbH, Lammers Medical Technology, LMT Medical Systems GmbH)

options are often restricted. Ideally, an MRI incubator in which the baby can be moved from the NICU to the MRI and examined therein is available (Fig. 3.8). There are small-bore NICU MR units available that allow examining newborns directly on the NICU—although with some intrinsic limitations and risks; however, this development may offer new options but also creates new challenges and possibly opens up turf battles (who is doing and reading these examinations at the NICU?).

- Then (wherever and whoever does these exams) one needs to adapt the MR protocols individually, consider examination time versus spatial resolution issues with respect to the small patient size and thus little signal, try to use non-enhanced sequences for further characterisation (e.g. arterial spin labelling, diffusion weighted imaging), and consider the reduced fatty content making interpretation more difficult. As a rule of the thumb, one often needs to sacrifice some spatial resolution for reasonable speed and sufficient signal. Try to use intrinsic contrast (e.g. T2 weighted imaging without fat saturation), think of phase and frequency direction and possible folding

artefacts from arms (as these often need to be included in the field).

3.3 Indications for Imaging Neonates

First of all: many things can be imaged even in neonates, but not all that can be imaged needs to be or should be imaged. Imaging should primarily serve the patients; sometimes medico-legal issues may necessitate a study.

The other option is screening, usually by US. However, this should only be done under established protocols and must have been validated in terms of cost and benefit. The only generally accepted screening investigations at present are foetal US screening and in some countries hip US screening for developmental dysplasia of the hip (in other countries with a lower incidence this recently is changing towards a selected screening of a defined subpopulation at risk). Selected screening is also performed in preterm infants for urinary tract dilatation (in correspondence to the usual prenatal US screening) and of the brain.

Imaging should not be misused to calm and pacify parents or relatives! Imaging should have

an impact on patient management (or prognosis) in terms of efficacy, and the choice of the imaging technique is particularly essential in this vulnerable and highly radiation sensitive patient group. Every medical imaging investigation needs a justifying indication, even US, also to avoid non-justified radiation or sedation. We not only want to avoid unnecessary burden to the patient, but there are also economic and workflow reasons. Even US is cost-intensive; not so much in terms of equipment investment but in terms of working time, as medical staff is one of the major expenditures in a hospital and US is time-intensive for the ones performing the examination.

Clinically, there are many situations where imaging may be necessary and indicated:

- Confirmation, reassessment, and further definition of prenatally recognised relevant conditions.
- Perinatal events such as asphyxia or birth trauma that will need early postnatal assessment and follow-up.
- Postnatal acute conditions definitely rely on imaging in the differential diagnosis and follow-up, including the monitoring of treatment and location of devices, lines, and tubes (Fig. 3.9).
- Pre-and postoperative imaging, particularly in case of complications.
- Various diseases or conditions that are only recognised neonatally or manifest after birth such as inflammation (e.g. urinary tract infection, respiratory tract infection...), metabolic

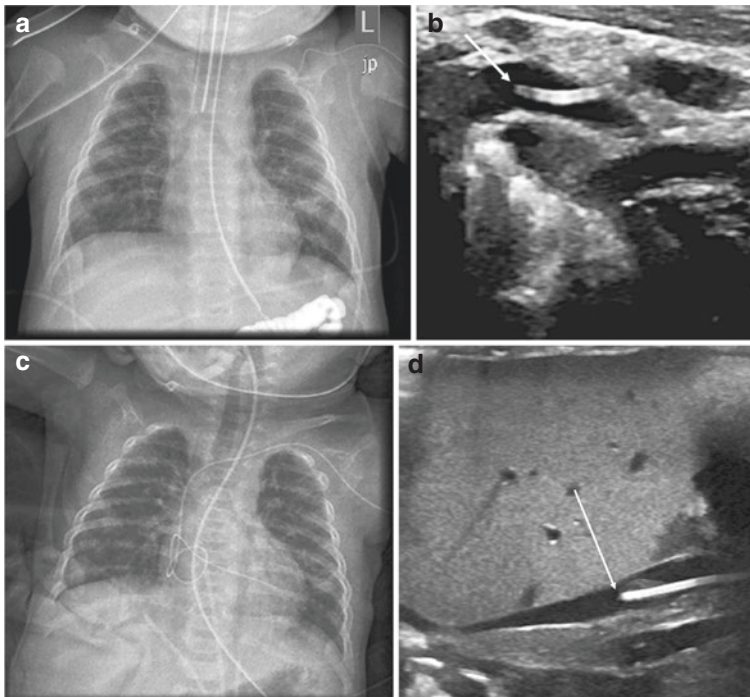


Fig. 3.9 Imaging for checking tubes and catheters. (a) Chest radiograph demonstrating the peripherally inserted line with the tip in the left subclavian vein, thus not really properly central. (b) This can also be checked by US helping to reduce radiation burden (arrow = line tip). (c)

Malposition of a central line which has been pushed in too far forming a tangle in the heart—a condition best visualised by radiographs. (d) US of the upper abdomen (mid-line sagittal section) showing the tip of a catheter in the inferior vena cava (arrow)

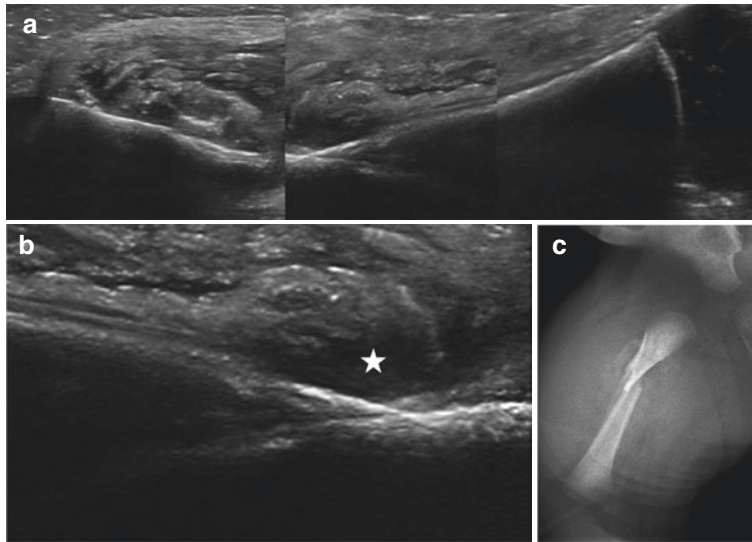


Fig. 3.10 Imaging in suspected fractures. (a) US performed because of a painful swollen leg in a 5 days old neonate revealed a fracture with already beginning callus formation, indicating a subacute fracture (probably a birth injury). (b) Un-composed US image better demonstrating

the site of the fracture with the respective periosteal haematoma (asterisk). (c) The finding was then confirmed by a radiograph that also allows better evaluation of fracture alignment

or hormonal disorders, or even fractures (Fig. 3.10).

Established imaging algorithms with standardised, individually adaptable imaging parameters and standards will help to streamline imaging avoiding unnecessary investigations and trying to reduce patient burden or radiation exposure.

3.4 Contrast Agent Applications in Neonates

Another important aspect is the use of CA in neonates, either intra-cavitarily (e.g. intravesical, or oral/rectal) or intravascular. There are different CA for US, fluoroscopy and radiographs or CT, and MRI; only a few agents are explicitly approved and registered for neonatal use which vary between countries.

3.4.1 Ultrasound Contrast Agents (UCA)

The only widely available UCA that has been approved for intravesical use is SonoVue® (or Lumason® as named in the USA) (Bracco, Italy) and in the USA is also for intravenous applications in childhood (i.e. liver imaging). Other UCA that are on the market such as Sonazoid® (excellent post-vascular phase enhancement as taken up by Kupffer cells, GE-Healthcare/USA) or Optison® (GE Healthcare/USA, mostly used in cardiac applications) and Definity® (Lantheus/USA) are not approved for paediatric use. However, even if not approved (mostly for economic reasons) numerous reports exist on the use of UCA in childhood and in neonates, intravesically or intravenously (iv). They are important as contrast-enhanced US (ce-US) allows for non-irradiating bedside imaging and may help to obviate radiation exposure: e.g. VUR detection

can be reliably achieved by contrast-enhanced voiding urosonography (ce-VUS) and thus a conventional fluoroscopic voiding cystourethrography (VCUG) using radiopaque CA may not be necessary. All UCA are based on some strong reflecting agent (usually a gas) encapsulated by a lipid, galactose, or protein shell and stabilised by palmitic acid or similar substances. These agents increase the reflected US signal by approximately 25 dB and deliver a specific harmonic signal response that can be depicted using harmonic imaging or other contrast sensitive techniques (proper US equipment and transducers capable of performing ce-US is necessary) to exquisitely depict the UCA and allow for real time observation. In iv applications, the vascular contrast dynamics of lesions, for example, an unclear solid mass in the liver, allows for improved lesion detection and characterisation similar to ce-CT or ce-MRI. The main difference to radiopaque CA is that UCA are purely intravascular agents that are not eliminated by the kidney (thus an impaired renal function does not contradict the use of UCA); the gaseous components are exhaled and the shell is metabolised in the liver. Unlike iodinated CA it does not affect the thyroid gland, and unlike gadolinium CA it is not deposited in other tissues such the brain, further increasing the safety profile. The only though relevant side effect is the very rare allergoid reaction. But UCA use increases the risk of cavitation bioeffects. While most modern flow-sensitive US techniques can answer most treatment relevant queries, if UCA is needed, be careful and reduce the acoustic power to the lowest possible limit in sensitive tissues such as the brain, the testis, the eye, or the aerated lung.

Only sparse dose recommendations for UCA exist for neonates (for SonoVue/Lumason). Intraluminal or intravesical, use a NaCl solution of approximately 1% (0.5–10%) of the filling volume (also depending on transducer, frequency and equipment, depth of the targeted area); for ce-VUS; the company's suggestion is 1 mL/bladder filling. This however has been tested for paediatric use and often is too much for the small bladder capacity of

a neonate and may cause shadowing that obscures deeper pelvic structures (such as the distal ureters). For neonatal intravenous applications, a dose of 0.1–0.15 mL/kg is recommended.

3.4.2 Radiopaque Contrast Agents

Again, there is a difference if one uses them intravenously or for opacifying a hollow organ such as the intestines or the urinary bladder. For enteric intraluminal applications, the CA may be barium or iodine based—however, consider that sometimes (particularly for the gastrointestinal tract) air can be used as an effective negative contrast agent delineating all the necessary structures to allow for a diagnosis, thus obviating the need for radiopaque CA (see Fig. 3.5). Also remember that iodinated CA can be resorbed in the GI tract and thus may cause sequelae even if administered orally or rectally. Barium is only used in otherwise healthy newborns for GI tract opacification as long as there is no existing or risk of perforation and aspiration. Otherwise, low- or iso-osmolar, often non-ionic iodinated CA with a concentration of 100–300 mg I/mL are advisable (Table 3.1).

For iv applications, it is important to consider the renal immaturity in this age group. Very ill (preterm) babies may be poorly hydrated, need a number of drugs for treatment, may have blood pressure problems and thus impaired renal perfusion (possibly exacerbated by a persistent ductus arteriosus). Therefore, the risk of CA effects on the kidney needs to be considered—even if the importance of contrast-induced nephropathy in adults has diminished. As neonates have little muscles, the normal creatinine values and glomerular filtration rate (GFR) are different from adults and need to be considered when deciding if a CA application is safe using the respective normal values (Table 3.2) and the paediatric adapted Schwarz formula for calculating paediatric GFR values. Of course, other risks for intravenous CA application such as dehydration, nephrotoxic drugs, septicaemia, or acido-

Table 3.1 Examples for intraluminal radiopaque CA registered for neonatal use

Barium	Prontobario (Bracco)	For GI tract only
	Micropaque (Guerbet)	For GI tract only
Iodine	Gastromiro (Bracco)	For GI tract only, non-ionic (Iopamidol)
	Iomeron and Jopamiro (Bracco)	For GI and GU tract
	– Different concentrations available	
	– Both are not explicitly registered for neonatal, just “paediatric” use	
	Ultravist (Bayer)	For GI and GU tract
	– Different concentrations available	

Common CA used for intraluminal opacification in the GI or GU tract and vendors (based on the present situation in Austria/Europe). The iodine-based iso-osmolar CA can also be used for other compartments, e.g. in interventional radiology, although there mostly the typical CA registered for iv use are applied. Others exist, but not all are registered for neonatal use (e.g. Imagopaque/Nycomed Imaging AS, Melitrast/Dr. Franz Köhler Chemie GmbH, Omnipaque/GE-Healthcare, Scanlux/Sanochemia Pharmazeutika GmbH, Xenetix/Guerbet), and there are differences between the various countries. The concentrations used in the GI- and particularly GU tract (e.g. VCUG) usually range from 100 to 150 (200) mg/mL; sometimes the iv CA is only available and in a higher concentration and then needs to be diluted as desired before being installed into various cavities. Gastrografin (Bayer) is ionic and hyperosmolar (Natriumamidotrizoat, Megluminamidotrizoat) that may cause electrolyte and fluid shifts with severe systemic reactions; therefore, it is not approved for neonates in some countries (if one needs to use it, e.g. for therapeutic measures such as to reduce meconium ileus, only use in a 1:3 or 1:4 solution with 0.9% NaCl and with caution and monitoring)

Abbreviations: CA contrast agent, GI tract gastrointestinal tract, GU tract genito-urinary tract, mg milligram, mL millilitre, NaCl natrium chloride = saline, VCUG voiding cystourethrography

sis need to be considered as usual. Also remember that iodinated CA may suppress thyroid function in newborns, particularly if high CA doses are administered (see also below).

Table 3.2 Mean creatinine values in neonates with respect to postnatal age and body weight

	1–2 d	1 w	2 w	3 w
Preterm 1–1.5 kg	1.10	0.72	0.55	0.40
Preterm 1.5–2 kg	1.00	0.65	0.56	0.34
Preterm 2–2.5 kg	0.94	0.53	0.43	0.34
Full term	0.75	0.45	0.34	0.31

Serum creatinine values (mg/dL) of neonates differ from older children and adults

Abbreviations: w week, d day, kg kilogram bodyweight
Adapted from Bueva and Guignard [1]

For estimating CA dose in iv applications, the different/higher relative circulating blood volume (approx. 90 mL/kg in newborns versus 60 mL/kg in adults) needs to be considered to produce sufficient contrast opacification. Therefore, the dose must be relatively higher (approx. 2–2.5 mL/kg, to a maximum of 3 mL/kg), also as usually only low to medium iodine concentrations of 100–200 mg I/mL (maximum 300 mg I/mL) can be applied. This nevertheless also increases the risk of side effects such as impairment of renal function or hypothyreosis (the latter even in neonates with a normal global thyroid function). The commonly intravenously applied CA in neonates are similar as the iodinated intraluminal CA, except for Gastromiro®: usually a 150–200 (250) mg I/mL concentration is applied in neonates. Again, agents and availability and respective dedicated approval for neonates vary with countries (Table 3.3).

3.4.3 Gadolinium-Based Contrast Agents

MRI less often needs CA due to the better signal resolution of differently composed tissues; additionally, natural agents such as water, saline, urine, or even (diluted) blueberry juice can be used as CA.

If a CA is used, the same consideration as for radiopaque iv CA hold true: consider renal function & hydration, correct acidosis, and additionally remember that even in healthy children with normal renal function Gd-chelates may be depos-

Table 3.3 Radiopaque CA approved for neonatal CT (in Austria, concentrations available and approved for neonatal use will vary throughout countries)

Accupaque (Iohexol)	GE Healthcare (only the 300 mg concentration is available and approved for neonatal use in Austria).
Iopamiro (Iopamidol)	Bracco (different concentrations available and approved, commonly 240 or 300 mg/I/mL are used).
Iomeron (Iomeprol)	Bracco (only the 300 mg concentration is available and approved for neonatal use in Austria).
Omnipaque (Iohexol)	GE Healthcare (the 240/300/350 mg concentrations are available in Austria for neonatal use).
Optiray (Ioversol)	Guerbet (only the 240/300 mg concentrations are available and approved for neonatal use in Austria).
Ultravist (Iopromide)	Bayer (different concentrations available and approved).
Visipaque (Iodixanol)	GE Healthcare (iso-osmolar non-ionic dimer; only the 320 mg concentration is available and approved for neonatal use in Austria).
Xenetix (Iobitridol)	Guerbet (only the 350 mg concentration is available and approved for neonatal use in Austria).

Concentration available and approval for neonatal use varies throughout countries, the given values are for Austria only: these CA are mostly non-ionic low-osmolar, and may need to be diluted with 0,9% NaCl if this concentration is deemed too high

ited and stored in various tissues such as the brain, the liver, the bone marrow, etc. Thus there is more than just the risk of nephrogenic systemic fibrosis (NSF) in patients with renal insufficiency (GFR <30 mL/min) or liver transplantation/disease (GFR <40 mL/min) which rarely would apply to neonates! Iron-based CA are not approved for neonates, so only gadolinium-based CA can be used. From this group of agents, only the more stable cyclic compounds are allowed for paediatric and particularly neonatal use (Table 3.4). As always, consider alternatives for CA application in this age group, and obtain and informed consent from the parents. Try to lower the dose, and allow for sufficient time (e.g. 1–3 days) before a possible

Table 3.4 Gadolinium-based MR-CA approved for neonatal use in (Austria/Europe)

Gadobutrol (Gadovist, Bayer)
Gadoteric acid (Dotarem, Guerbet)—not approved for MRA.
Clariscan (GE), Cyclolux (Sanochemia)—approved in newborns only for central nervous system.
Gadoxetate (Primovist, Bayer) is a linear compound (off label use for some dedicated liver applications rarely ever applicable to neonates, but used in some countries where others are not available at the individual institution).

Note: At present, only two CA are approved by the European Medical Agency for use in neonates! As a general rule, the normal dose is 0.1 mmol/kg or less; a double dose should be avoided (even if some use 0.2 mmol/kg for MRA and cardiac MRI). Gadoxetate (Prohance, Bracco) and Gadobentetate (Multihance, Bracco) are—in childhood—only approved for imaging the central nervous system and in infants (older than 0.5 and 2 years, respectively) or for dedicated applications such as liver imaging. In some countries, there are national regulations which explicitly state that Gd should not be used in newborn and neonates (e.g. Italy, 2018)

second CA application so that the gadolinium can be excreted to the greatest possible extent by the immature newborn kidneys. Double dose examinations should be avoided. Nevertheless—in spite of these considerations and precautions—never deny a baby an examination necessary for acute treatment decisions that are essential and unreplacable for further management.

3.5 Miscellaneous Other Aspects to Consider When Imaging Neonates

The challenges of the clinical exam and laboratory testing in neonates impact the decisions about imaging. The neonate is much more difficult to examine clinically, the symptoms are much less specific (e.g. seizures may be very discrete and not as impressive as in older children, fever is not mandatory in inflammatory conditions such as a septicemia, the clinical examina-

tion often reveals only general symptoms such as respiratory symptoms which may be due to a cardiac, a respiratory, or a systemic condition), verbal communication is not possible, and pain cannot be properly expressed and often is more generalised than in children. Laboratory findings may also be different in neonates, and repeated extensive blood sampling is problematic due to the small amount of circulating blood especially in preterm infants which hinder the generous use of laboratory tests (sometimes they may even need a red cell transfusion after such procedures). This may increase the dependency and need of non-invasive repeated imaging for establishing a diagnosis, the differential diagnostic work-up, or for follow-up. On the other hand, knowledge of these specific neonatal conditions and findings will help to properly read neonatal imaging stud-

ies, and improve discussions with clinicians on the optimal use of imaging in this vulnerable patient group.

Essential for understanding neonatal findings and physiology is a good knowledge of embryology, as this may help to explain various findings and appearances; for example, the immature lung with less fibrous interstitium but more perivascular tissue tends to more easily collapse and cause atelectasis and are prone to an interstitial emphysema/oedema. These and other findings and entities should be known and not be misread as other pathologic consolidations. Some important embryologic steps in the development of relevant organs and systems are schematically outlined in Fig. 3.11 as well as in the respective chapters; for more detailed information, please refer to dedicated embryology textbooks.

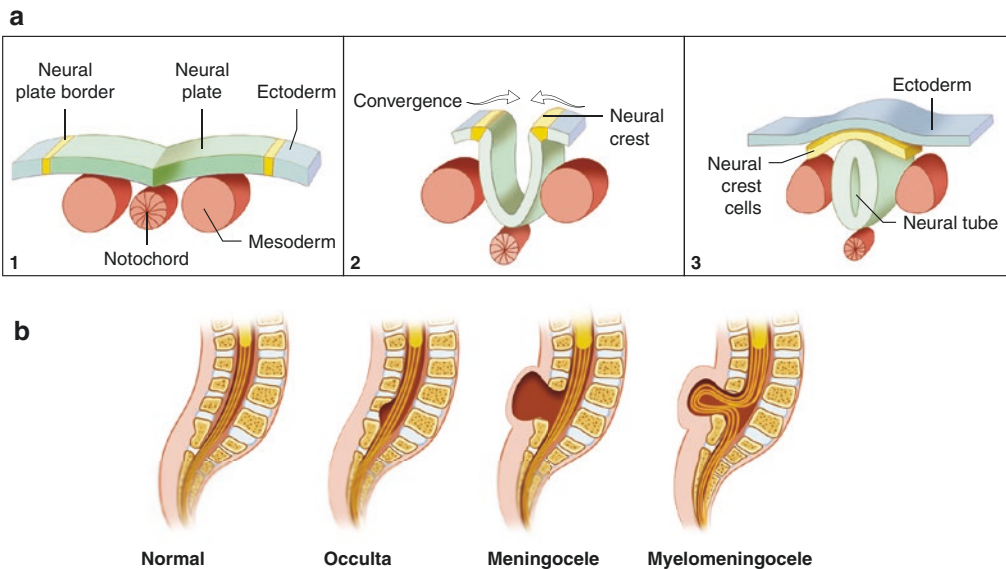


Fig. 3.11 Embryology example. (a) (1–3) Schematic drawing of the stepwise development of the neural tube called “neurulation”, which is the formation of the neural tube from neuroectoderm—this knowledge allows to understand cord pathology and dysraphism/spina bifida

such as myelomeningocele or tethered cord, diastematomyelia, dorsal spinal sinus tract, etc. (b). (Adapted from “Development of the central nervous system/neurulation”, <https://teachmeanatomy.info/the-basics/embryology/central-nervous-system/>, last accessed Dec 2021)

3.6 Summary and Conclusion

Neonates are not small adults, and not even just small children—they are special. Imaging neonates is a challenge. This particular and vulnerable patient group deserves special attention. In order to address their needs, one must have a deep understanding of embryology and the transition from foetal to postnatal life, an in-depth knowledge of the specific diseases and conditions of (preterm) neonates, knowledge and understanding about the causes of their vulnerability, and how to address each situation. One needs to know about the image appearance and the imaging approach as well as how to properly perform imaging—a skill often not present in general radiologists and technologists who have not specifically been trained for this task. Dedicated imaging protocols, patient handling, algorithms, and optimised exposure settings should be applied to obtain optimal results at lowest achievable burden to allow paediatric radiologists to map anatomy, physiology, growth, and suspected pathology. There are no universal protocols to apply to different imaging devices, so there is more operator dependency in daily routine practice heavily influencing both results and (radiation) burden. Having the most modern equipment does not automatically grant best performance, just like having the newest and biggest car does not compensate for a bad driver (and, in fact, may even make a bad situation worse). Understanding of these respective implications, restrictions, and pathophysiology is essential to optimally care for these small patients who are the future of mankind.

Acknowledgement I am tremendously grateful to Dr. Brain Coley (Cincinnati/Ohio/USA) for editing this chapter.

Reference

1. Bueva A, Guignard J. Renal function in preterm neonate. *Pediatr Res.* 1994;36:572–7. <https://doi.org/10.1203/00006450-199411000-00005>.

Further Reading

- Kjucevsek D, Riccabona M, Petit P, Avni EF, Bruno C, Damasio MB, Darge K, Littooij A, Lobo ML, Mentzel JH, Napolitano M, Wozniak M, Ording Müller LS. Intracavitary contrast-enhanced ultrasound in children: a review, with clinical applications and procedural recommendations from the ESPR Abdominal Task Force Group. *Pediatr Radiol.* 2020;50:596–606.
- Nagy E, Tschauner S, Marterer R, Riedl R, Sorantin E. Chest CTA in children younger than two years—a retrospective comparison of three contrast injection protocols. *Sci Rep.* 2019;9:18109. <https://doi.org/10.1038/s41598-019-54498-z>.
- Ntoulia A, Back SJ, Darge K. (editors) Special issue: Contrast-enhanced ultrasound (CEUS) in children. *Pediatr Radiol.* 2021;51
- Oppelt B, Gruber O, Melcher J, Melcher V, Pfandl S. *Pädiatrische Radiologie für MTRA/RT.* Edition Radiopraxis. Stuttgart: Thieme; 2010. ISBN: 9783131608512.
- Riccabona M, Mentzel HJ. Contrast enhanced US in childhood. In: Riccabona M, editor. *Pediatric ultrasound: requisites and applications.* 2nd ed. Cham: Springer; 2020. p. 59–72. ISBN: 978-3-030-47909-1.
- Riccabona M, Hirsch WF, Paertan G, Sorantin E. Special imaging issues in children. In: Riccabona M, editor. *Pediatric imaging essentials.* Stuttgart: Thieme; 2010. p. 1–36. ISBN: 978-3-13-166191-3.
- Riccabona M. Chapter 17: Contrast media use in pediatrics: safety issues. In: Thomson HS, Webb AW, editors. *Contrast media: safety issues and ESUR guidelines.* 3rd ed. Berlin: Springer; 2014. p. 245–51. ISBN: 978-3-642-36723-6.
- Schneider KO, Seidenbusch MC. Technische Anforderungen. In: Riccabona M, Beer M, Mentzel HJ, editors. *Bildgebung des Thorax bei Neugeborenen und Kleinkindern.* Berlin: Springer; 2019. p. 17–30. ISBN: 978-3-13-166191-3.
- Sorantin E. Soft-copy display and reading: what the radiologist should know in the digital era. *Pediatr Radiol.* 2008;38:1276–84.
- Sorantin E, Weissensteiner S, Oppelt B, Neumann O. Plain film and digital radiography: challenges in pediatric imaging. *ESPR 2015 Graz.* *Pediatr Radiol.* 2015;45:S247–368.



Prenatal Imaging: What a Paediatric Radiologist or Neonatologist Should Know?

Françoise Rypens, Juliette Garel,
and Chantale Lapierre

4.1 Introduction

Antenatal imaging relies essentially upon ultrasonography. Accurate prenatal diagnosis allows timely realisation of complementary examinations, evaluation, discussion of prognosis, and optimisation of prenatal, perinatal, and postnatal managements. Complex cases are best managed by interdisciplinary teams. Imaging is only a part of the prenatal work-up. Imaging techniques are now theoretically able to detect most major congenital malformations. However, even in the best conditions, some anomalies still escape to prenatal diagnosis, or are only partially assessed by it. This challenges adequate perinatal management. Also, ignoring prenatal observations in a neonate or infant with a presumed congenital anomaly may lead to inadequate decisions.

This chapter describes selected circumstances that impact perinatal and early postnatal management.

4.2 Techniques/Requisites

In most countries, prenatal imaging screening is based on first and second trimesters ultrasonographic (US) evaluations. In some countries,

F. Rypens (✉) · J. Garel · C. Lapierre
Department of Medical Imaging, CHU Sainte-Justine
Mother and Child University Hospital Center,
Montréal, QC, Canada
e-mail: francoise.rypens.med@sss.gouv.qc.ca

third trimester US is offered as part of a systematic prenatal screening. However, up to now, third trimester US exam isn't systematically performed everywhere; third trimester US being then performed because of a clinical indication or after an abnormal second trimester US.

In case of abnormal US findings or high-risk situations, the patient can be referred to a tertiary centre to obtain a detailed US exam performed by foetal specialists and to have access to a multidisciplinary team. Depending on the circumstances and anomalies, complementary imaging examinations can be realised such as Doppler US, magnetic resonance imaging (MRI), and rarely computed tomography (CT) scan.

After multidisciplinary team discussion, an honest parental counselling can be done. According to the parental decision, an adapted treatment plan is proposed, including follow-up and perinatal management. In all cases, results of the prenatal investigations must be transmitted to the teams that will take care of the neonates.

4.2.1 Ultrasound (US)

Conventional or bidimensional mode (2D) US is the base of screening and diagnostic exams. Guidelines for standards of practice are published by main professional bodies ([1], [2], GFMER).

Performance of prenatal imaging depends on screening and diagnostic politics, team expertise,

and varies locally (EUROCAT). From a societal perspective, foetal US screening has been proven to improve pregnancy datation (which may result in fewer inductions for “post-term” pregnancies), detection of multiple pregnancies, determination of chorionicity and amnionicity, cardiac activity, and detection of major malformations [3]. From an individual perspective, US screening improves management and prognosis of numerous anomalies, the best example being transposition of great arteries [4, 5]. Performances of US are decreased in case of maternal overweight, abdominal scars, myomas, polyhydramnios, oligohydramnios, and may be limited by foetal position.

As low as reasonably achievable (ALARA) principles apply to foetal US. Specific obstetrical settings with low thermic and mechanical indexes are used to decrease energy delivered to the foetus. Duration of the examination, the use of pulsed and colour Doppler, and use of 3-dimensional (3D) US are limited to clinical indications.

3D US (3D acquisition of a data volume with post-processing work-up) is a complementary US examination technique allowing image reconstructions in various planes, tomographic analysis, reconstructions with surface or bone rendering, thick cut analysis, and volume calculations. Advantages include obtention of inaccessible planes, a posteriori analysis of recorded data, and better comprehension of some malformations and dysmorphisms (Fig. 4.1). This examination has the same limitations as 2D US, is sensitive to motion artefacts, and necessitates post-processing time. The most accepted indications include facial dysmorphisms, brain malformations, and skeletal disorders.

Four-dimensional (4D) US (3D US with real time observation, with time being the fourth dimension) has few real clinical indications and increases imaging time.

Doppler allows real time analysis of blood flow using different modalities sensible or not to blood flow direction. Pulsed and colour Doppler deliver more energy to foetus than 2D US. Their use is thus restricted to a relevant justifying clinical indication.

Classical indications for Doppler analysis are evaluation of foetal growth restriction, foetal hydrops, cardiac malformations, suspected vascular anomalies, characterisation of masses and foetal tumours, and search for foetal anaemia. Pulsed Doppler analysis of the umbilical artery, middle cerebral artery, uterine arteries, and the ductus venosus is systematically performed in case of intra-uterine growth restriction, allowing detection of possible uteroplacental vascular insufficiency. These analyses are also indicated in cases of cardiac malformation, foetal hydrops, or vascular malformation allowing evaluation of the cardiac function and monitoring foetal well-being. Monitoring of the flow velocity in foetal middle cerebral artery allows detection of foetal anaemia (for example after parvovirus infection or in some complicated monochorionic pregnancies) or polycythaemia (such as in twin anaemia polycythaemia sequence).

4.2.1.1 First Trimester US

Early first trimester US, from 6 to 10 weeks of gestation (wg), precises gestational age, verifies viability, determines number of foetuses and type of multiple pregnancy (chorionicity and amnionicity).

Between 11 and 13 + 6 wg, measurement of the nuchal translucency and early anatomical survey allow detection of foetuses at risk for aneuploidies and/or malformations. Some malformations can already be detected at this age, particularly in population at risk or if abnormalities are multiple [6] (Fig. 4.2).

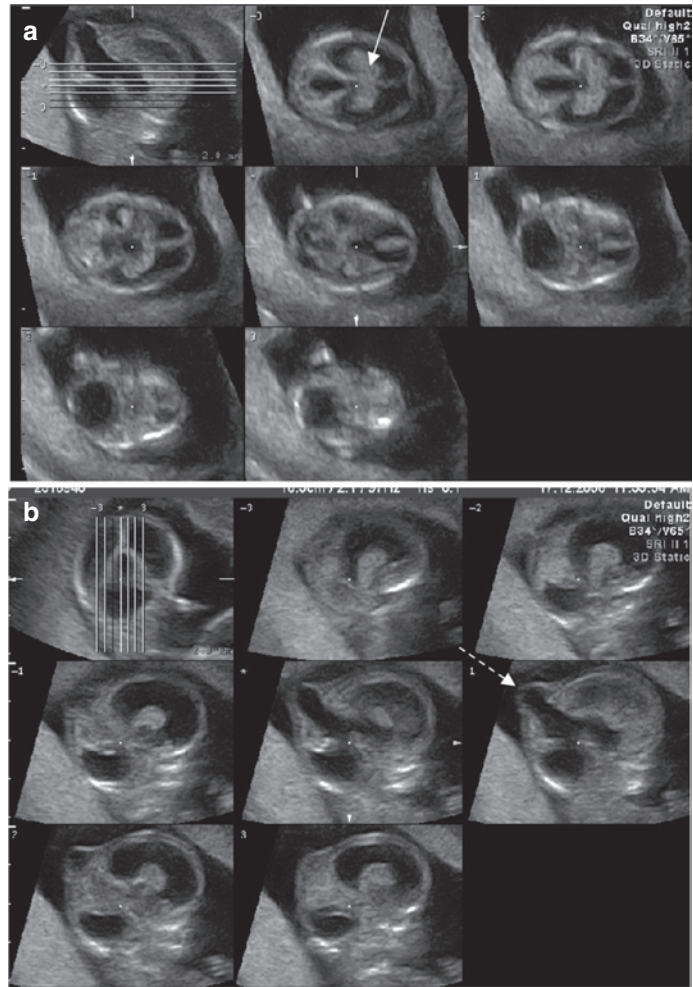
In overweight patients, this period may be the only opportunity to have relatively adequate visualisation of the foetus, combining abdominal and endovaginal approaches.

Yet, even in the best circumstances, first trimester US doesn't replace second trimester US.

4.2.1.2 Second Trimester US

Second trimester US is the corner stone of prenatal imaging. Screening is usually performed between 18 and 22 wg. The examination includes

Fig. 4.1 First trimester US at 12 wg with 3D axial (a) and sagittal (b) reconstructions demonstrates a syntelencephaly (arrow) associated with a posterior cyst and a cephalocele (dotted arrow), and abnormal posterior fossa



assessment of foetal anatomy, biometry and well-being, evaluation of amniotic fluid volume, placenta, and uterus.

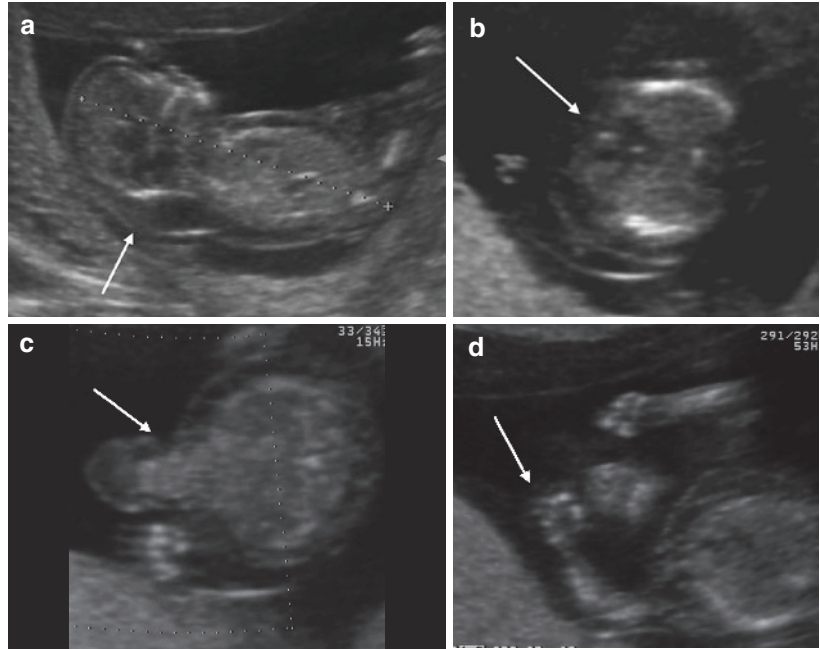
Performances of second trimester US vary depending on the sonographer experience and criteria included in the screening. The best example is the cardiac examination: adding a study of ventricular ejection chambers and the three-vessel trachea view to the classical four-chamber view, significantly improves detection of cardiac malformations, including conotruncal anomalies. Looking carefully at limbs up to the toes increase detection of limb malformations and helps for the differential diagnosis of various congenital anomalies [7].

Performances of US screening remain low for limb malformations, anomalies not covered by standards such as ears and some facial dysmorphisms, anal imperforation, and anomalies occurring later during pregnancy. Even in the best circumstances, second trimester US will miss up to 20–40% of congenital anomalies.

4.2.1.3 Third Trimester US

Third trimester US has clear indications for evaluation of foetal growth and follow-up of cardiac, renal, bowel abnormalities, and brain morphology. It is the last prenatal opportunity to detect cardiac or renal malformations necessitating specific perinatal management. By example, foe-

Fig. 4.2 First trimester US at 12 wg in a foetus with thickened nuchal translucency and hydrops (arrow in **a**) shows the presence of an atrioventricular malformation (arrow in **b**), an atypical omphalocele (arrow in **c**) and clenched hands (arrow in **d**) in a case of trisomy 18



tal renal function increases from 10 to 12 times from 20 to 40 wg, allowing better detection of urological diseases during the third trimester, and explaining the better predictive value of third trimester US compared to second trimester US for significant urological anomalies.

However, even with routine third trimester US, some congenital anomalies manifesting later during pregnancy will escape to prenatal detection (e.g. clastic lesions, some microcephalies). Performing a late third trimester US evaluation after 34 wg improves detection of foetal growth restriction compared with the traditional third trimester US performed around 30–32 wg.

4.2.2 Foetal Magnetic Resonance Imaging (MRI)

MRI is a useful complementary examination for specific anomalies during the third and second trimesters of gestation [8]. It is performed by (paediatric) radiologists with specific experience in foetal imaging. MRI using high magnetic field and acoustic waves exposes the foetus to potential magnetic, acoustic, and thermal

effects. Adapted fast sequences with low specific absorption rate (less than 4 W/kg) are used. Up to now, no significant biological effects have been described in clinical use. There is no foetal indication for gadolinium-based intravenous contrast agents. These contrast media cross the placenta and are only rarely used for selected maternal indications (Guidelines of the American College of Obstetricians and Gynecologists).

T2 sequences are used for assessment of foetal anatomy and biometry. T1 sequences with lower spatial resolution help to characterise tissue, showing normal hyperintense signal of the myelin, the hypophysis, the thyroid gland, the meconium, and the subcutaneous fat. Some blood products, brain tubers, and high-flow vascular malformations appear also hyperintense in selected T1 sequences (Fig. 4.3). Other types of sequences, such as diffusion imaging and echo-planar sequences, are used depending on indications (Fig. 4.4).

Advantages of MRI include good contrast resolution, large field of view (interesting for voluminous malformations), absence of bone artefacts, and 3D possibilities. Disadvantages include lower spatial resolution than US, suscep-

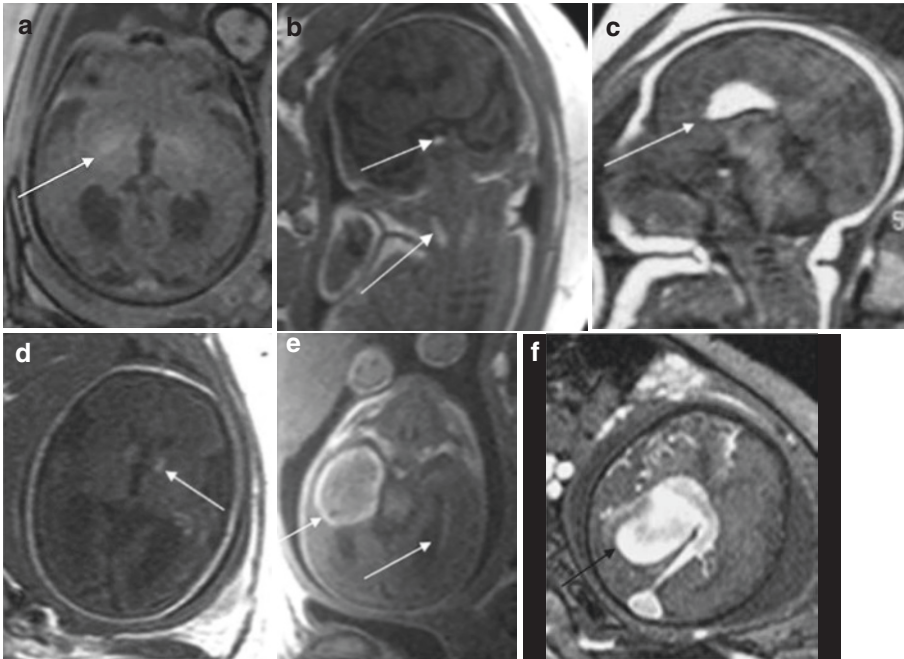


Fig. 4.3 Foetal cerebral MRI. T1 sequences in different foetuses showing the normal hyperintense signal of myelin (a), the hypophysis and thyroid gland (b), the abnormal hyperintense signal of a pericallosal lipoma (c),

a subependymal hamartoma (d), a parenchymal and intraventricular haemorrhage (e), and a vein of Galen malformation (f) (arrows point to the hypersignal)

tibility to motion artefacts, few obtainable dynamic information, maternal discomfort in case of a long examination duration, and maternal contraindications to high magnetic field exposure.

Classical indications for foetal MRI include better characterisation of brain anomalies, complementary evaluation of spinal dysraphisms potentially amenable to prenatal surgery, delineation of the upper airways in cervicofacial anomalies, characterisation of diaphragmatic hernias, evaluation of abdominal malformations and/or large malformations. It is also indicated in complicated monochorionic multiple pregnancies (detection of clastic brain lesions), in congenital infections and with some previous history (such as migration disorders) (Table 4.1).

US remains the best choice for first trimester examinations, the study of foetal heart and for fine structures such as the spinal cord and the extremities.

4.2.3 Foetal Computed Tomography (CT)

Foetal CT scan replaces uterine X-rays. With the improvement of the apparatus and software, foetal CT has now a better spatial resolution, necessitates lower acquisition time, and delivers lower foetal irradiation. However, this examination **must** be performed by a specialised team. The protocol depends on patient morphology, and the specific machine used. In all cases, delivered radiation dose must be restricted to the minimum (usually with a CTDI of less than 3 mGy corresponding to an effective dose of 2.2–5 mSv), which is comparable to natural irradiation (reaching up to 3.6 mSv, depending on the location). Most examinations are performed after 26 wg. Before this age, 3D US is more useful.

Advantages of CT compared to US include no bone shadowing, better analysis of metaphyses, pelvis, and vertebrae, and possible post-acquisition

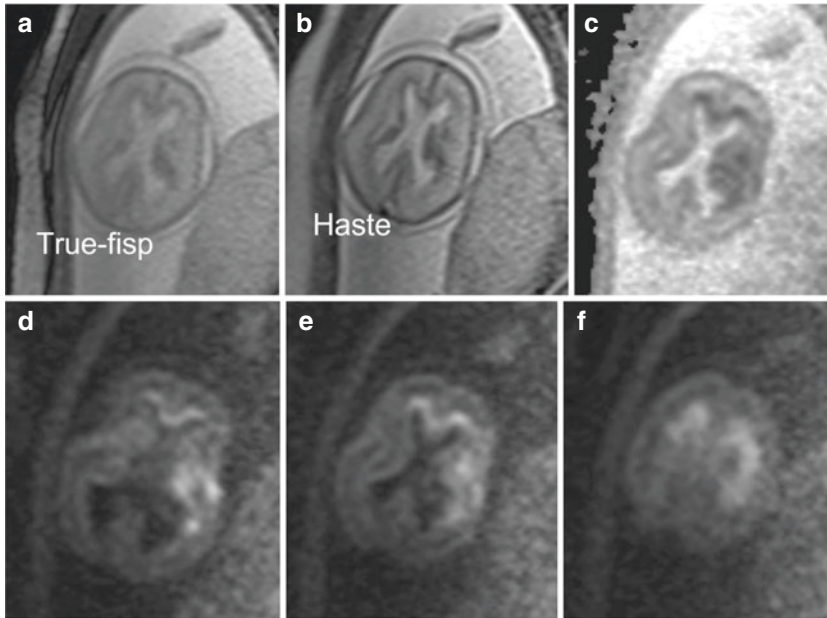


Fig. 4.4 21-wg foetus with hydrops in a case of parvovirus B19 infection. True FISP (a) and HASTE (b) sequences show discrete anomalies. More extensive lesions are better demonstrated by diffusion sequences (c–f)

Table 4.1 Classical indications for foetal MRI—always consider if it affects management

Central nervous system	<ul style="list-style-type: none"> • Ventriculomegaly • Midline anomalies (e.g. corpus callosum, absence of septum pellucidum) • Posterior fossa anomaly • Microcephaly • Vascular anomaly • Clastic anomaly (e.g. schizencephaly, complicated monochorionic twin pregnancy) • Suspected gyration anomaly • Mass and tumours • Cardiac rhabdomyoma • Infection • Previous gyration anomaly, history of other malformations
Face and neck	<ul style="list-style-type: none"> • Significant micrognathia • Tumours and vascular malformations • Oesophageal atresia (if it affects management)
Chest	<ul style="list-style-type: none"> • Diaphragmatic hernia • Parenchymal lung malformation (if it affects management) • Mediastinal tumours • Complex malformations
Abdomen	<ul style="list-style-type: none"> • Large omphalocele • Masses and tumours • Complex digestive anomalies (if it affects management) • Complex genitourinary malformations (if it affects management)
Spine	<ul style="list-style-type: none"> • Complex malformations • Discordance between intracranial and spinal US observations • Before foetal surgery

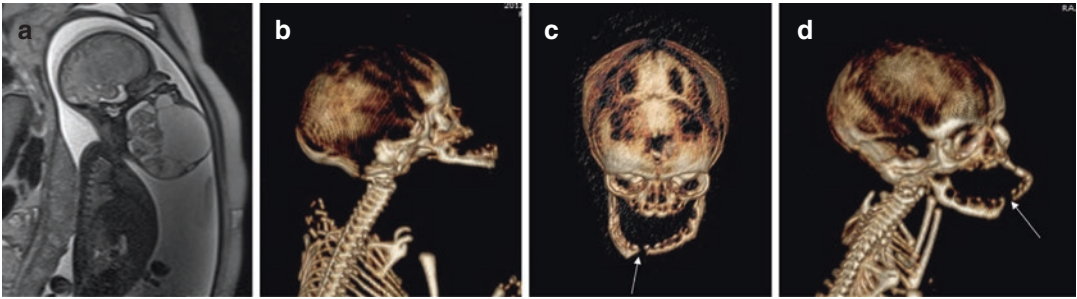


Fig. 4.5 Cervicofacial teratoma. MRI at 32 wg shows the cervical extension (a). The volume rendering CT scan (b–d) at 32 wg demonstrates prognathism and diastasis of the mandible (arrows in c, d)

analysis of recorded data. However, cartilaginous structures, extremities during second trimester of gestation and thin structures such as calvaria and nasal bones are less visible. Post-processing of the acquired data takes time, and interpretation may be limited by gestational age, motion artefacts, and maternal obesity. Evaluation of foetal mineralisation remains challenging [9, 10].

Indications for foetal CT scans are rare. They include suspected severe skeletal dysplasias with incomplete US characterisation, and exceptional focal anomalies (Fig. 4.5).

4.3 Anomalies Implying Significant Modification of Perinatal Management

4.3.1 Cervicofacial Anomalies with Possible Airway/Respiratory Challenge and Soft-Tissue Masses

All cervicofacial masses or malformations can obstruct airways and the upper digestive tract. Characterisation of these lesions relies on US and Doppler, and evaluation of the extension and airways relies on MRI.

4.3.1.1 Micro and Retrognathia

Differentiation between micrognathia and retrognathia is difficult in utero, both coexisting frequently. Detection of micro-retrognathia can be done during

the first trimester US in the most serious cases. Diagnosis relies on prominent appearance of the upper lip and receding chin on a mid-sagittal view of the face. Follow-up is indicated since the anomaly may be more evident with time.

Evaluation of prognosis relies on detection of the frequent associated anomalies (e.g. Treacher-Collins syndrome). Micrognathia associated with a palatine cleft and a glossoptosis indicates Pierre-Robin sequence. Significant glossoptosis will manifest with a polyhydramnios after 25 wg. On the other hand, absence of a polyhydramnios during the third trimester suggests relatively good swallowing, and probably good neonatal adaptation.

3D US is useful to precise facial dysmorphism and to detect an isolated posterior palatine cleft. Foetal MRI allows for analysis of the palate but is mainly indicated for detection of intracranial anomalies (Fig. 4.6).

4.3.1.2 Soft-Tissue and Cervicofacial Masses

Foetal cervicofacial masses are rare. Main diagnoses include tumours (teratoma and vascular tumours), vascular malformations (lymphatic, venous, and mixed malformations), and some rarer lesions (goitre, epulis, branchial cyst, ranula cyst). Main concerns are airway compromise, cardiac insufficiency, functional impairment, and disfigurement.

Diagnosis relies on the US appearance, its vascularity (Doppler), and the location. MRI bet-

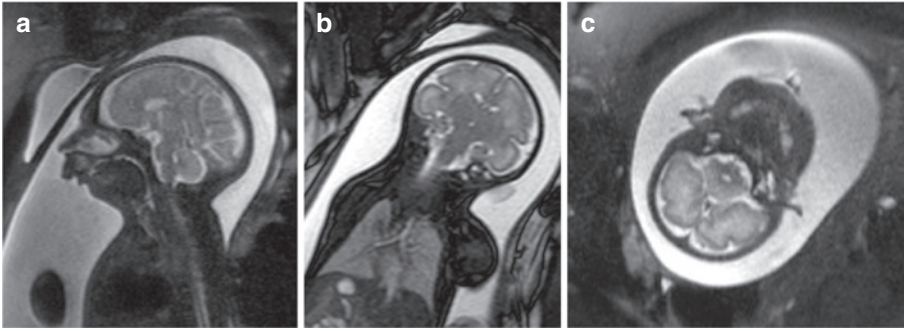


Fig. 4.6 MRI performed at 34 wg in a foetus with severe micrognathia (a), polyhydramnios and microcephaly, shows microencephaly (a, b) with simplified gyration and an abnormal small cerebellum (c) (autopsy denied)

ter precises the entire extent of the malformation and the impact on the airways.

- Purely or almost purely cystic lesions correspond usually to *macrocytic lymphatic malformations* (LMs). LMs can be located anywhere but have a predilection for cervico-mediastinal and axillary locations. The appearance of LMs depends on the size of the abnormal lymphatics. Macrocytic LMs have a typical aspect on US: large soft cystic lesion with floating septa (Fig. 4.7). Microcystic LMs appear as ill-defined hyperechoic solid masses. Mixed LMs have both components (cysts and ill-defined hyperechoic areas). US underestimates the microcystic extent of the malformation, which is better demonstrated with MRI (Fig. 4.8). Definite indications for MRI are evaluation of the microcystic part and extension of LMs.
- The differential diagnosis of a cystic lesion depends also on its location (Table 4.2). Rarely, a teratoma may initially look almost purely cystic but solid components and vessels will become more evident with growth of the lesion.
- A mixed appearance (cystic and solid components) is not specific and is observed in most significant cervicofacial masses including vascular malformations, vascular tumours, and teratomas. Presence of calcifications is not specific and can be detected in teratomas, congenital haemangiomas, and other tumours.
- *Venous malformations* (VMs) have variable aspects at US. They appear as compressible hypoechoic cavitory lesions with slow flow. Phleboliths, typical of this diagnosis, can only be demonstrated after birth. The low-velocity flow is difficult to detect in utero. Compressed abnormal veins escape US detection. US and Doppler US underestimate extent of slow-flow lesions, and extension is much better demonstrated by MRI (Fig. 4.9).
 - *Congenital haemangiomas* are high-flow vascular soft-tissue tumours that have a predilection for locations such as the head and neck and the limbs close to the articulation. In opposite to infantile haemangiomas appearing after birth, the endothelial cells of congenital haemangioma don't express GLUT-1. Congenital haemangiomas appear as a mixed or solid soft tumour on US and are hypervascular at colour Doppler US. Pulsed Doppler shows low resistive arteries, arteriovenous shunting, and prominent veins. Calcifications can be present. At MRI, they appear as a heterogeneous and well-delimited soft-tissue mass. Their signal is intermediate on T1 sequences and hyperintense on T2 sequences. Most of these tumours are detected during the third trimester and correspond to rapidly involuting congenital haemangiomas (RICH) or partially involuting congenital haemangiomas (PICH) (Fig. 4.10). They are at risk of haemorrhage. Some other vascular tumours (haemangioendothelioma) are associated with platelet consumption (Kasabach-Merritt phenomenon).

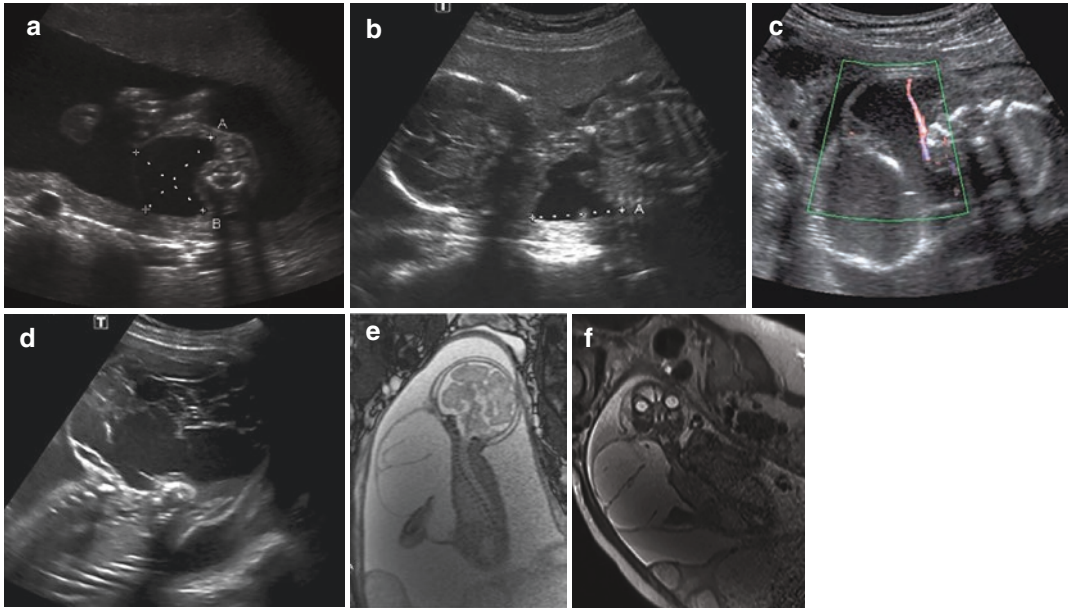


Fig. 4.7 Evolution of a macrocystic LM. At 20 wg (a, b), the cystic lesion is simple and measures 3 cm. At 22 wg (c), the lesion increases in size reaching up to 5 cm with a more echogenic content and presence of vessels in septa. At 24 wg (d), the size of the lesion is now at 10 cm and a

fluid-fluid level secondary to sediment is visualised. True FISP MR sequences obtained at 30 wg (e, f) show the extent of the lesion and the preservation of airways. The neonate was delivered normally without EXIT (ex-utero intrapartum treatment)

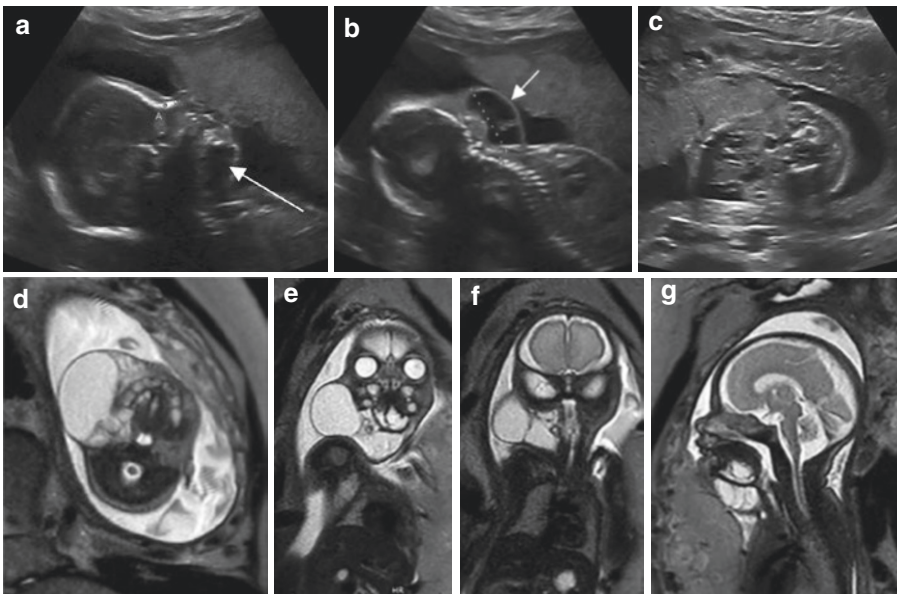


Fig. 4.8 Mixed LM. US exam (a–c) at 22 wg detects the macrocystic part of the malformation (arrows). The extent of the suspected microcystic part is difficult to delineate.

True FISP MR sequences (d–g) at 29 wg demonstrate better the profound microcystic part of the lingual invasion and the airway permeability

Table 4.2 Differential diagnosis of cystic cervicofacial lesion according to its location

Diagnosis	Location
Lymphatic malformation	Everywhere
Cephalocele	Intracranial extension
Ranula cyst	Submandibular space
Dermoid cyst	Medial, below the tongue in the oral floor
Thyroglossal cyst	Medial, along the thyroglossal tract
Branchial cyst	Lateral

- *Teratomas* can be located almost anywhere (the most frequent location in utero is sacro-coccygeal). They are often heterogeneous with solid and cystic components, frequent calcifications, and variable vascularisation. Their growth in utero is variable and unpredictable at time of diagnosis. This tumour is frequently highly vascularised, and significant vascular steal can cause cardiac insufficiency, hydrops, and death. Teratomas have a stiff consistency and may be aggressive tumours

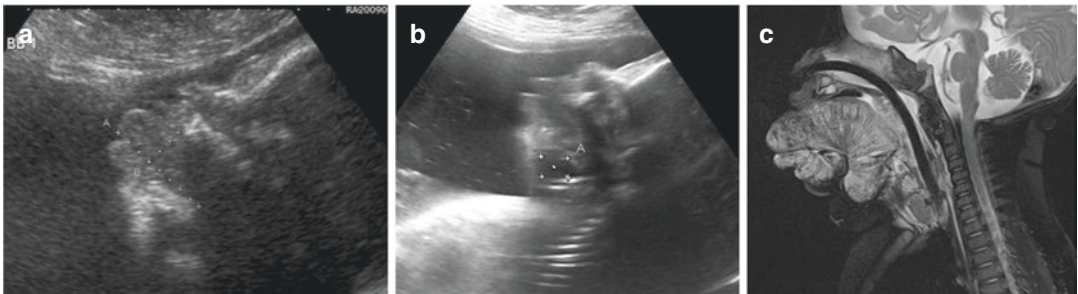
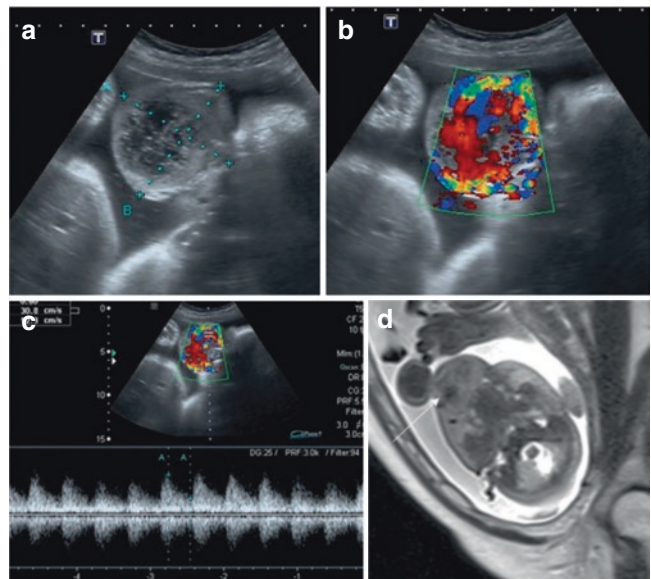


Fig. 4.9 Macroglossia detected at 36 wg. US shows also a cystic lesion, apparently not vascularised, in the submaxillary region (a, b: between crosses). Foetal MRI couldn't be performed due to morbid maternal obesity.

Postnatal sagittal T2 MR sequence image demonstrates an extensive venous malformation, completely underestimated in utero (c)

Fig. 4.10 RICH at 36 wg. Heterogeneous subcutaneous facial lesion (a). Colour and pulsed Doppler images show a hypervascular soft-tissue lesion (b, c). Axial true FISP MR sequence image demonstrates the corresponding flow voids in the mass (arrow) (d)



that compress and invade adjacent structures (Fig. 4.11). Follow-up US with Doppler and haemodynamic evaluation of the foetus is necessary. MRI is clearly indispensable, better demonstrating the tumoural extent and its repercussions on the airways (Fig. 4.12). It may be useful to repeat it close to delivery. The same follow-up is proposed for the most common sacrococcygeal tumours.

- Purely solid lesions are rare. Various tumours may present with an initial solid appearance (Fig. 4.13).

Significant cervicofacial masses must be assessed by a multidisciplinary team. After diagnosis, characterisation and evaluation by imaging, and counselling, a monitoring plan must be established. It must be adapted to the type of lesion, its size, location, and growth pattern, with closer follow-up for high-flow lesions. Choice of delivery and decision to perform an EXIT (ex-utero intrapartum treatment procedure) rely on airway repercussions and not on the size of the lesion (Figs. 4.7, 4.8, and 4.12). Postnatal embolisation is indicated in neonates with high-flow

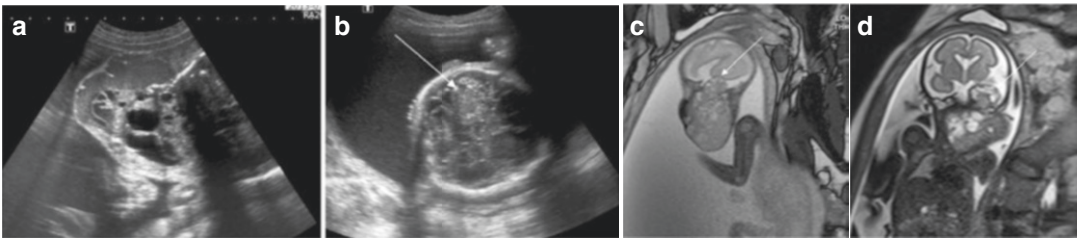


Fig. 4.11 Cervical teratoma. US (a, b) and MRI (c, d) at 27 wg: US images show a heterogeneous cervical tumour. Intracranial invasion suspected at US is better demonstrated by MRI (arrows)

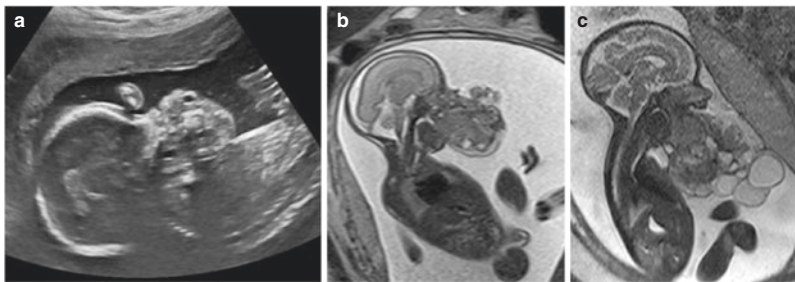


Fig. 4.12 Epignathus teratoma originating from the hard palate with extrabuccal extension. US evaluation at 23 wg (a). MRI performed at 23 wg (b) and 30 wg (c) shows

growth of the tumour and airways preservation. EXIT was successfully performed

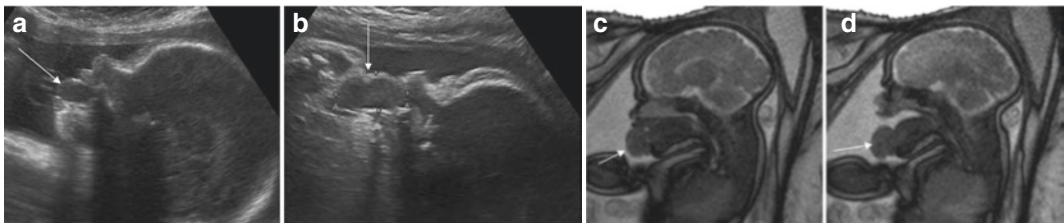



Fig. 4.13 Epulis. US (a, b) and MR (c, d) evaluation at 30 wg show a solid lesion independent from the tongue (arrow) and originating from the inferior maxillary gingiva

lesions, heart failure, airway compression, and who are at risk of bleeding.

 Colour and pulsed Doppler must always be performed in case of a soft-tissue mass. It allows for differentiation between high-flow (teratoma, congenital haemangioma) and low-flow (VM, LM) lesions. High-flow lesions are at risk of cardiac failure, intra-uterine growth retardation, pre-term labour, and haemorrhage after birth. Close monitoring with cardiac US and Doppler is mandatory for high-flow lesions.

Location of the mass can sometimes help to narrow down the differential diagnosis, such as the typical anatomical locations of goitre, ranula cyst, branchial cyst, and epulis (Fig. 4.14). Location doesn't help for the other tumours and malformations which can be found anywhere in the body.

MRI precises the extent of slow-flow lesions and the impact on airways.

4.3.2 Thoracic Malformations at Risk for Respiratory Distress

Most significant thoracic malformations are detected owing to mediastinal shift and/or abnormal lung echogenicity.

After exclusion of an abnormal situs and a cardiac malformation, mediastinal deviation is usually secondary to a mass effect from one hemithorax (e.g. diaphragmatic hernia, parenchymal lung malformation, pleural effusion), or more rarely due to unilateral lung hypoplasia or aplasia (Fig. 4.15 and Table 4.3).

Goals of prenatal imaging are to diagnose the type of malformation and to precise its prognosis.

The differential diagnosis relies on careful analysis of both lungs, upper abdomen content, and diaphragmatic continuity by US and Doppler (Table 4.4).

4.3.2.1 Congenital Diaphragmatic Hernia (DH)

Congenital DH has a high mortality and morbidity. A Bochdalek hernia characterised by a posteromedial diaphragmatic defect is the most

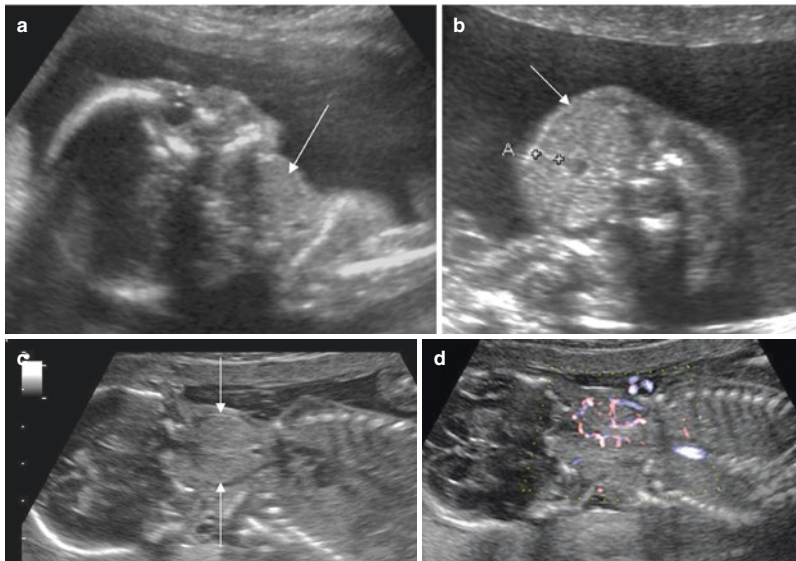


Fig. 4.14 Goitrous hypothyroidism, secondary to dys-hormonogenesis, detected at 19 wg. US shows an anterior bilobar cervical mass (arrows), with foetal cervical hyperextension, and polyhydramnios (a–c). Doppler (d)

shows peripheral hypervascularity typical of hypothyroidism. Two intra-amniotic thyroxin injections allowed normalisation of the size of the thyroid gland and amniotic fluid

Fig. 4.15 Right lung aplasia. Axial thoracic (a) and abdominal (b) US slices performed at 20 wg show right displacement of the mediastinum (arrow) in a case of right lung aplasia (dotted arrow points to normal position of the stomach on the left side)

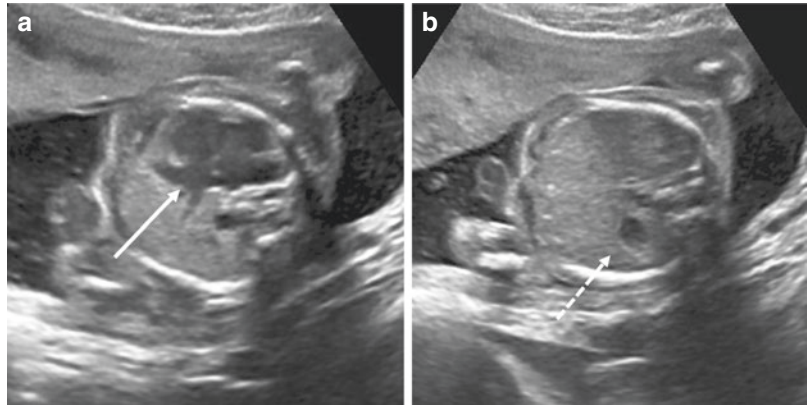


Table 4.3 Causes of abnormal mediastinal orientation or position

Displacement of the mediastinum due to mass effects (e.g. diaphragmatic hernia, pulmonary malformation, pleural effusion)
Displacement of the mediastinum due to unilateral lung hypoplasia or aplasia
Abnormal visceral-atrial situs
Cardiac malformations
Cardiac axial deviation due to significant abdominal malformations (e.g. abdominal mass, large omphalocele)

Table 4.4 Differential diagnosis between diaphragmatic hernia and lung malformation

	Diaphragmatic hernia	Lung malformation
Mass	++	++
Diaphragmatic defect	+	-
Abdominal US	Abnormal	Normal
Herniated organs	+	-
Paradoxical diaphragmatic motion (third trimester)	+	-
Intrathoracic peristalsis	+	-

frequent cause of DH in foetuses. Hiatal and retrosternal hernias are exceptional (Fig. 4.16). Most DH are left-sided (85%), less frequently right-sided (13%) or bilateral (2%).

Most cases of DH are detected during the second trimester, but some will manifest later during the third trimester or even after birth aspect HD (Table 4.5). Several pitfalls explain sometimes difficult diagnosis of DH. In most cases of left DH, the intrathoracic position of the stomach is easily recognised (sometimes as early as 12 wg) and then the diagnosis is obvious (Fig. 4.17). If the stomach remains in the abdomen, the diagnosis depends on the recognition of bowel loops inside the left hemithorax. A right DH is difficult to detect due to the foetally similar echogenicity of the liver and the lung (Fig. 4.18). Therefore, a right DH must always remain in the differential diagnosis of a left mediastinal shift. Doppler is essential to make the diagnosis, demonstrating the abnormal route of the hepatic vessels and the portal vein. Bilateral DH is a tricky diagnosis,

because there can be no significant lateral mediastinal deviation or because one side of the herniations is underestimated (Fig. 4.19).

Detailed US analysis, cardiac US, and genetic counselling are essential (Russo et al. 2018). Thirty percent of foetal cases are associated with malformations and/or genetic anomalies that worsen the prognosis.

The prognostic evaluation in isolated forms is based on the lung volume and the liver position. By US, the lung volume is estimated by the lung to head ratio (LHR) which is the ratio of the area of the lung contralateral to the hernia defect to the head circumference [11]. Various programmes available on internet allow calculation of the more useful “observed to expected LHR” (o/e LHR) corresponding to the measured LHR divided by the expected LHR at the same gestational age. LHR measurement is more reliably performed at 22 and 32 wg. Posterior displacement of the stomach in left DH, and

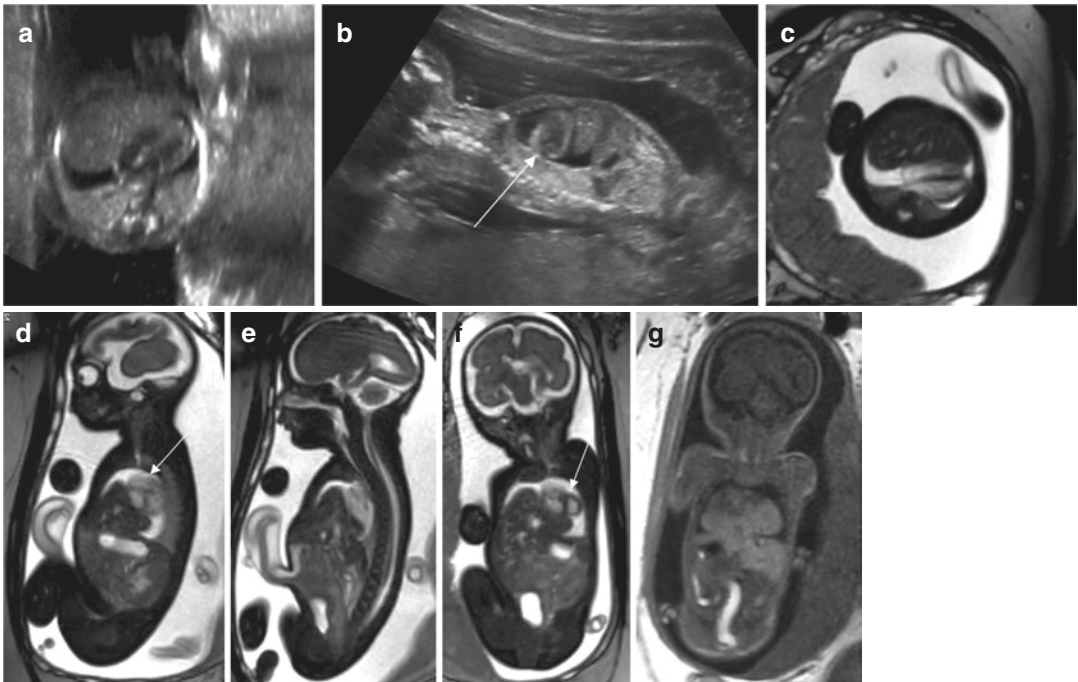


Fig. 4.16 Retrosternal diaphragmatic hernia. US evaluation at 16 wg (a, b) and T2 (c–f) and T1 MRI slices (g) at 28 wg

show liver herniation in the pericardium surrounded by fluid with upward and backward displacement of the heart (arrow)

Table 4.5 Sonographic diagnostic criteria for left or right diaphragmatic hernia (DH)

Left DH	Right mediastinal shift
	Left heterogeneous hemithorax
	Left deviation of the umbilical vein
	Intrathoracic bowel, stomach, part of liver
	Left abnormal diaphragm
Right DH	Left mediastinal shift
	Abnormal right hemithorax
	Abnormal position of gallbladder
	Abnormal position of portal, umbilical, and hepatic veins
	Liver ascension

Doppler help to detect liver herniation such as abnormal route of the portal vein and abnormal position of hepatic vein at Doppler US (Fig. 4.17).

MRI should be performed in each suspected DH. It allows a more accurate measurement of the total lung volume (TLV) [12]. As for the LHR, the observed TLV is divided by the expected TLV for the gestational age to obtain the observed to expected LV (o/e TLV). The best

moment to perform the MRI is around 30 wg. The prognostic value of the o/e TLV is not superior to the o/e LHR obtained with US. However, MRI offers a better evaluation of the liver herniation and the size of the diaphragmatic defect (Figs. 4.16, 4.17, 4.18, and 4.19).

After a complete work-up, an honest and careful counselling about therapeutic options, complications, and prognosis is ideally performed by a multidisciplinary team including an obstetrician, a neonatologist, and a paediatric surgeon. Expectation and postnatal treatment are proposed for mild forms. In selected institutions, FETO (Fetoscopic Endoluminal Tracheal Occlusion) performed at 27–29 wg can be proposed for severe forms. The FETO trial has proven significant benefit on survival over expectant care for severe isolated DH, but at the price of increased risk of prelabour rupture of membranes and preterm birth (Deprest et al. 2021a, b). Most neonates still have pulmonary hypertension and bronchopulmonary dysplasia.

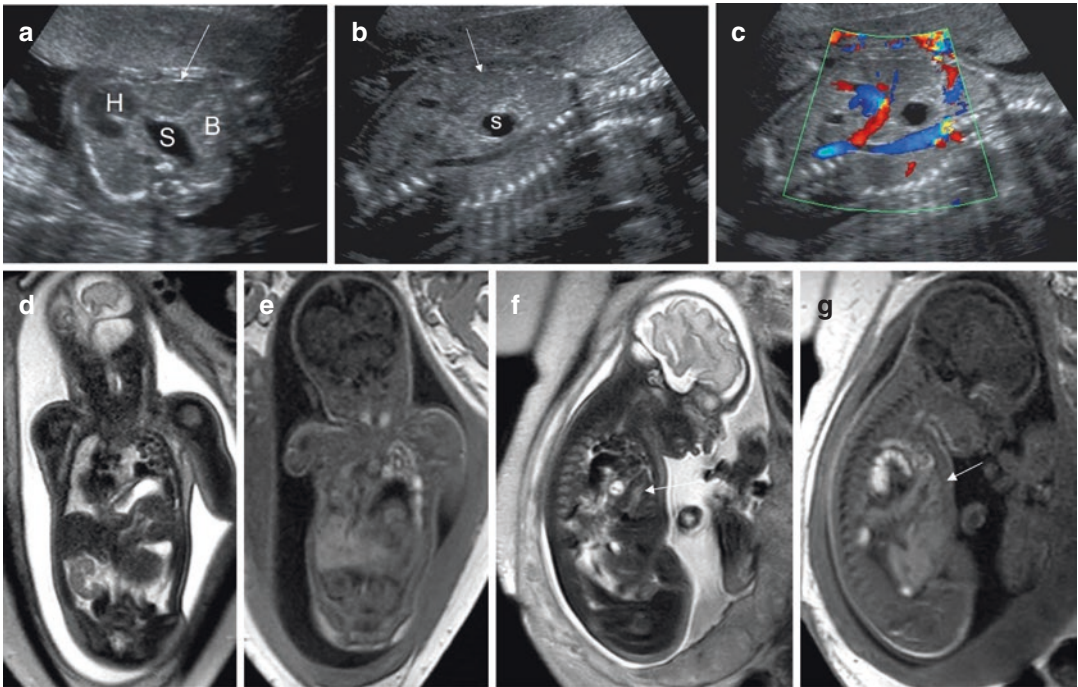


Fig. 4.17 Left diaphragmatic hernia (DH). US at 20 wg shows right displacement of the heart (H) by a left DH containing the liver (arrow), stomach (S), and bowel (B) (a, b). Doppler US examination shows portal branches in the herniated left liver lobe (c). MRI performed at 31 wg

shows the content of the hernia in coronal (d, e) and sagittal T2 (True FISP) and T1 slices (f, g): stomach, small and large bowel and part of the liver (arrow points to the liver). o/e TLV measured by MRI was 22%

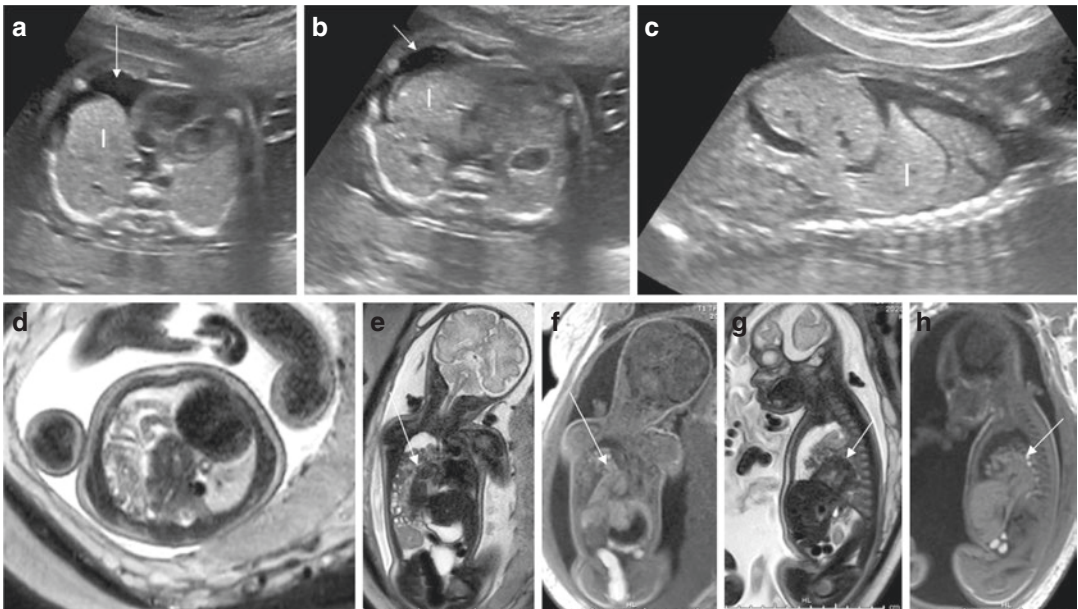


Fig. 4.18 Right diaphragmatic hernia (DH). Axial US (a, b) at 23 wg shows slight left displacement of the mediastinum. There is a pleural effusion (arrow). The herniated liver (l) is difficult to differentiate from the right lung and is bet-

ter demonstrated in the sagittal slice (c). MRI performed at 33 wg. Axial (d), coronal (e, f), and sagittal (g, h) T2 and T1 slices better demonstrate the hernia content (small bowel and liver) (arrow: liver). o/e TLV is estimated to 17%

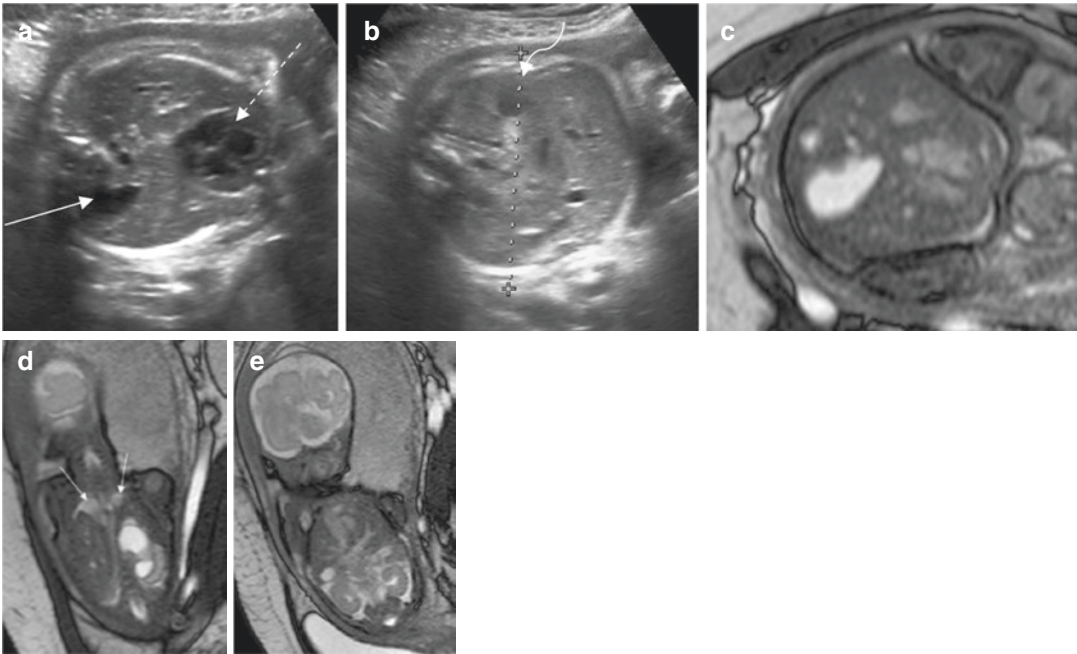


Fig. 4.19 Bilateral diaphragmatic hernia (DH). Patient referred for oligohydramnios at 31 wg. US evaluation shows the normal position of the mediastinum (dotted arrow in **a**), apparent normal position of the stomach

(curved arrow in **b**), and a fluid structure in the hemithorax (arrow in **a**). T2 weighted MRI (**c-e**) demonstrates bilateral DH (liver and stomach herniated) with very small lungs (arrows)

Pulmonary hypertension, one major complication of DH, remains impossible to predict accurately with prenatal imaging.



The diagnosis of congenital DH relies on detection of variable mediastinal shift secondary to the presence of abdominal viscera in intrathoracic location. Associated malformations and/or genetic anomalies are present in 30% of cases and reduce the outcome. In isolated forms, the prognosis depends on the lung volume and the liver position. However, the individual prognosis remains difficult to determine and the risk of pulmonary hypertension is still impossible to predict.

4.3.2.2 Congenital Lung Malformation

Congenital lung malformation (CLM) is used as an umbrella term and includes congenital pulmo-

nary airway malformation (CPAM), sequestration (S), hyperinflation (H, formerly known as congenital lobar emphysema), bronchial atresia (BA), and bronchogenic cyst (BC). It is suggested that CLM results from abnormal lung development that can affect (with various degrees) airways, alveoli, mesenchyme, and lung vessels. The different types of malformations depend on the predominant anomaly [13]. In fact, most malformations are mixed at histopathologic examination and hyperinflation is more frequent than usually thought.

Even if lung malformations can rarely be associated with diaphragmatic hernia, most are isolated findings. Lung malformations have usually an excellent prognosis and must be differentiated from diaphragmatic hernia (Table 4.4).

Since generalised use of prenatal US screening, the prevalence of lung malformations has increased. Nowadays, most parenchymal lung malformations are detected before birth. In opposition to what was

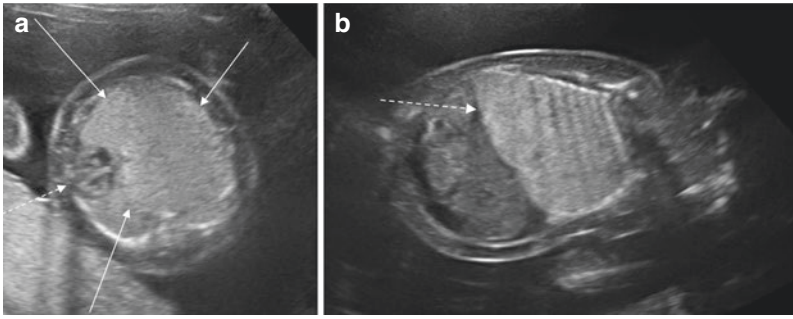


Fig. 4.20 Pulmonary malformation and hydrops. Axial (a) and coronal (b) US images performed at 20 wg show a large hyperechoic malformation (arrows) displacing the

mediastinum (dotted arrow), inverting the diaphragm (dotted arrow), associated with ascites, subcutaneous oedema, and polyhydramnios

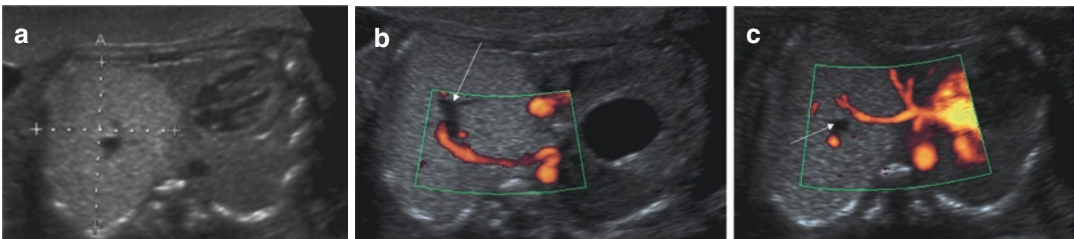


Fig. 4.21 Intralobar sequestration. Axial slices and Doppler performed at 21 wg. The hyperechoic malformation (between crosses, a) located in the right lower lobe displaces the mediastinum. The arterial systemic artery

originating from the descending aorta and the normal pulmonary venous return are demonstrated by power Doppler (b, c). A bronchocele is located centrally (arrow, b, c)

described in historical clinical series, most lung malformations detected before birth have a good prognosis, the majority being asymptomatic after birth [14]. Exceptionally, some large malformations can induce hydrops and foetal death if not treated (Fig. 4.20). In the minority of prenatal cases, some large malformations can also be responsible for neonatal distress (due to mass effect and progressive postnatal hyperinflation) or cardiac decompensation in case of a significant vascular shunt. Appearance during the third trimester helps to precise the postnatal risk for such a pejorative evolution and to propose an adequately adapted perinatal setting.

Careful analysis of US appearance, location, and type of vascularisation helps to characterise the malformation and propose a presumptive diagnosis. Foetal MRI is helpful during the third trimester to precise the localisation of the malformation and its extension. However, MRI is not

indicated if it doesn't modify the peri- or postnatal work-up.

Hyperechoic homogeneous lung lesions correspond to hyperinflation or sequestration. Type 3 CPAM is in fact exceptional (case reports). Doppler US allows for detection of an abnormal systemic arterial supply that signs sequestration.

- *Sequestration (S)* corresponds to an unfunctional lung parenchyma vascularised by a systemic arterial supply (Fig. 4.21). Extra- and intralobar sequesters can be detected in utero. Extralobar S lacks normal communication with the bronchial tree and is usually not aerated after birth (except if there is an oesophageal bronchus). Extralobar S has its own pleura, often has a systemic venous return, and can be infradiaphragmatic. Intralobar S is always intrathoracic and usually located in the inferior pulmonary lobes (Fig. 4.23). It can be

associated with a bronchocele. Venous return is usually pulmonary. During the second trimester, S appears typically as a more echoic homogeneous lung part. With time, the difference of echogenicity between S and normal lung diminishes until often “disappearance” during third trimester. However, the S is still present and postnatal imaging by CT (and US) remains essential. Arterial supply, usually from the thoracic descending or upper abdominal aorta, is more easily detected with Doppler US than with foetal MRI, which is used for delineation of lung malformations by some teams. Systemic arterial supply is sometimes not detected in utero and even after birth, due to the small size of systemic arteries. Rarely, a S can be associated with pleural effusion or DH; in these rare cases, prognosis depends on the extent of the DH. The majority of neonates with S will be asymptomatic after birth. Exceptionally, a large arteriovenous shunt will necessitate postnatal endovascular occlusion.

- When no systemic vascularisation is detected, *overinflation* must be suspected in case of a

hyperechoic homogeneous lung (Fig. 4.22). Overinflation is due to airway obstruction (complete in case of bronchial atresia or partial in case of bronchial stenosis such as in case of the “congenital lobar emphysema”). The typical appearance of overinflation is a territory of hyperechogenic lung with normal or stretched pulmonary vessels. No cyst is visible but a bronchocele may be detected in case of bronchial atresia. The bronchocele appears as a tubular fluid filled structure centrally located or next to the hilum. On MRI, the affected lung appears hyperintense on the T2 sequence. Overinflation is more frequent in the upper lobes and the middle lobe but can be found everywhere and even be segmental. The detection of a hilar bronchogenic cyst is difficult, but can be the clue for diagnosing a lobar emphysema. In some cases of overinflation, tiny peripheral cysts can be observed. This aspect doesn't sign the presence of an associated CPAM. Rarely, overinflation can spontaneously disappear after birth with no cause or abnormality detected after birth. These cases are thought to be sec-

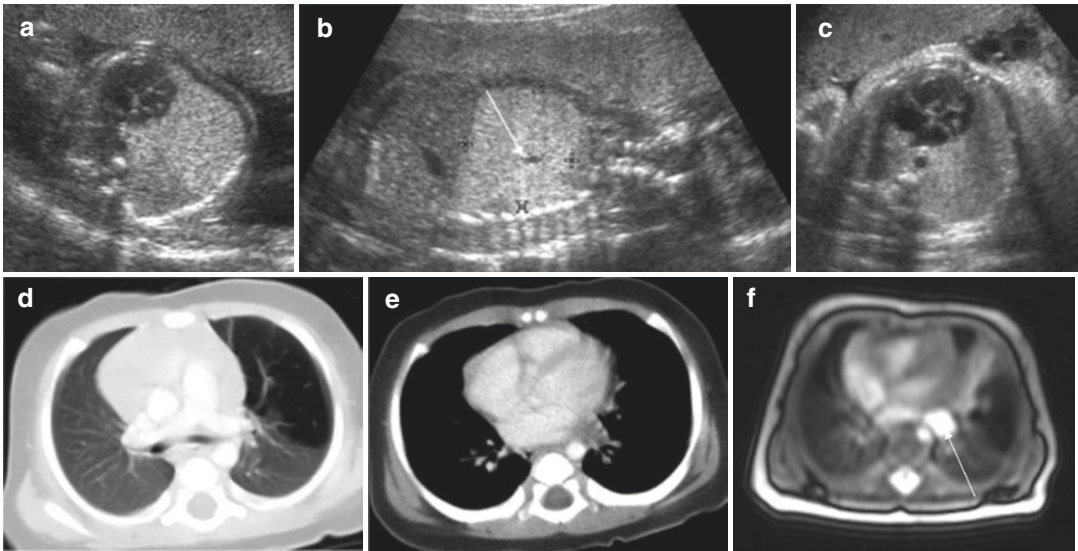


Fig. 4.22 Hyperinflation secondary to a bronchogenic cyst. Prenatal evaluation. US evaluation at 19 wg (a, b) shows a hyperechoic pulmonary malformation containing a bronchocele (arrow) and displacing the mediastinum towards the right side. At 32 wg (c), the malformation is

difficult to differentiate from the adjacent lung and there is less mediastinal shift. CT scan (d, e) and MRI (f) performed at 6 months of age show the upper left lobe hyperinflation secondary to a hilar bronchogenic cyst that was only detected by postnatal MRI (arrow, f)

ondary to spontaneous resolution of a transitory bronchial obstruction.

Lung cysts associated with a hyperechoic lung parenchyma suggest *CPAM* or *mixed malformation*, and rarely a bronchial cyst (surrounded by normal compressed hyperechoic lung).

- CPAMs are differentiated in five histologic types according to Stocker. Types 1 and 2 are the forms of CPAM detected in utero. In Type 1, large cysts coexist with smaller cysts. Type 2 is more frequent and characterised by multiple small cysts. Type 3 with invisible tiny cysts and appearing “solid” is almost never found in utero. In fact, virtually all hyperechoic homogeneous lesions found in utero correspond to overinflation and/or sequestration (see above). At US, CPAMs appear as heterogeneous lesions with cysts of various size. Adjacent lung parenchyma appears often hyperechoic, corresponding to malformed lung or compressed normal adjacent lung. CPAMs are vascularised by normal pulmonary vessels and can occur anywhere. They are usually unilobar, rarely multilobar or bilateral (Fig. 4.23).

CPAMs are detected during the second trimester. In most cases, their size increases until 25 wg, then remains stable or even decreases relatively to the foetus size after 29 wg [15]. With time, lesions are less visible during the third trimester due to normal variation of echogenicity of foetal lung, but these malformations are still present. Large CPAMs can exceptionally be responsible for hydrops and various criteria have been used to detect foetuses with risk for hydrops or neonatal distress and foetuses that could benefit from foetal intervention. Doppler US is mandatory. Detection of systemic arterial supply implies the presence of a mixed malformation, usually located in the inferior pulmonary lobes (Fig. 4.23). Treatment remains under discussion in asymptomatic cases.

The differential diagnosis of lung malformation includes diaphragmatic hernia, and exceptionally lung tumours (see above for diaphragmatic hernia). Lung tumours must be evoked when no anomaly is noted during a second trimester US or when an unusual soft-tissue mass is observed in a “pulmonary malformation” during a third trimester US.

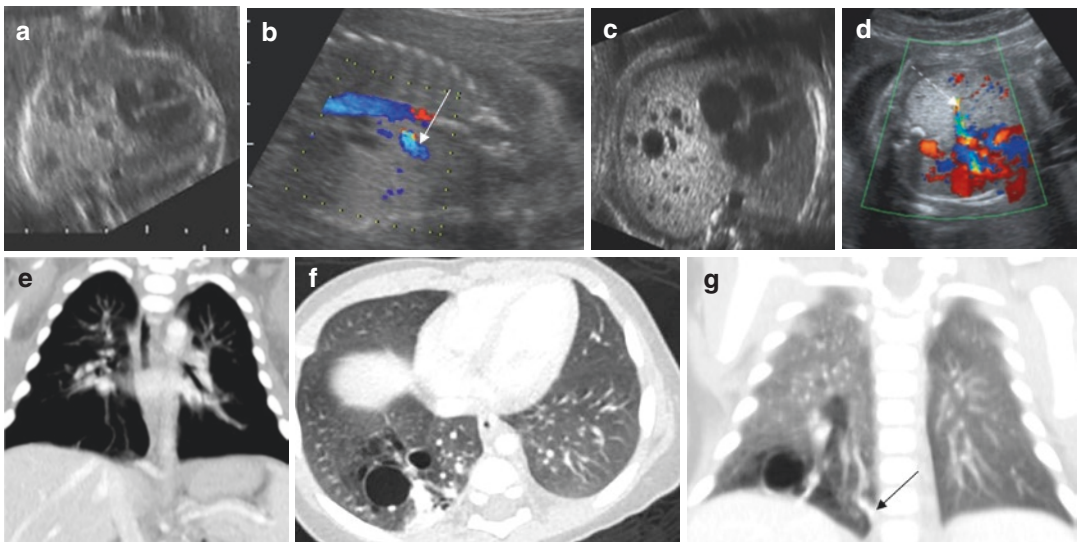


Fig. 4.23 Mixed pulmonary malformation with CPAM and intralobar sequestration. US at 22 wg (a, b) and 25 wg (c, d) shows a hyperechoic right lower mass containing cysts of various sizes, a systemic arterial supply (arrow)

and a normal pulmonary venous drainage (dotted arrow). The corresponding CT scan performed at 3 months of age confirms the findings (e–g)

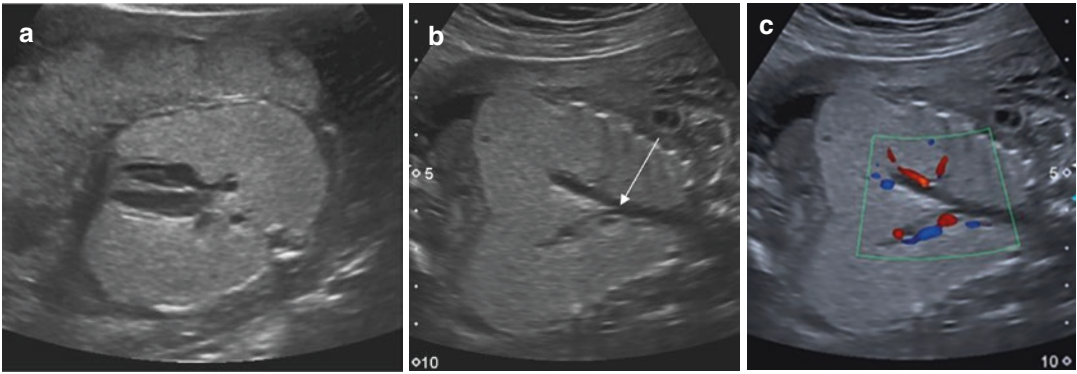


Fig. 4.24 CHAOS. Axial (a) and coronal (b) US images at 22 wg show huge lungs compressing the mediastinum and inverting the diaphragm. The trachea and main bron-

chi are distended (arrow). Colour Doppler helps to differentiate the bronchi from vessels (c)

Bilateral lung hyperechogenicity suggests usually a more pejorative disease. CPAMs can rarely be bilateral. However, large hyperechoic lungs inverting the diaphragm, associated with an enlarged trachea and main bronchi, usually indicate a congenital high airway obstruction syndrome (CHAOS) which has a poor prognosis (usually lethal). Most cases are detected during second trimester US and are already commonly associated with hydrops (Fig. 4.24). Half of the cases are associated with other congenital anomalies, the most common being Fraser syndrome.

In all cases of pulmonary malformations, a detailed postnatal work-up is necessary, even if no anomaly is seen during the third trimester. Standard X-ray and abdominal US (if the lesions were in lower thoracic or abdominal location) can be performed early after birth. In asymptomatic neonates, a thoracic CT with contrast is recommended 3–6 months after birth to define lung anatomy, precise the diagnosis and propose adequate treatment and follow-up.



Prevalence of pulmonary malformations has significantly increased since the systematic use of prenatal US screening. It's not all of these malformations that are CPAM or S and overinflation is more fre-

quent than usually thought. In fact, most of these malformations are mixed at histologic-pathologic examination. An adequate analysis of the US appearance and use of an adequate descriptive terminology allow more precise diagnosis and thus more precise counselling. Most parenchymal lung malformations detected in utero have a good prognosis. The definite treatment remains controversial for asymptomatic lesions.

4.3.3 Congenital Heart Defects (CHDs)

CHDs affect around 1% of life births. Some parental and foetal factors increase the risk for CHDs. Most cases of CHDs occur however in low-risk pregnancies, which emphasises the role of prenatal US screening [16].

Thickening of nuchal translucency (above 3.5 mm or above the 99th percentile) during a first trimester US increases the risk for aneuploidies and foetal malformations, particularly for CHDs. Increased nuchal translucency is a formal indication for genetic counselling, detailed second trimester US, and foetal echocardiography. In good circumstances, some CHDs can already be detected at this young gestational age.

Most CHDs will be detected during second trimester US screening. The standard examination of the foetal heart during second trimester US includes five axial slices: a superior abdominal axial slice, a four-chamber view, left and right outflow tract views, and the three-vessel trachea view [1]. The abdominal view and identification of foetal left and right sides are important for recognition of the visceral/abdominal situs. The four-chamber view allows the detection of significant CHD which include for example an atrioventricular canal defect, hypoplastic left or right heart syndromes, Ebstein's anomaly, and atrioventricular valve stenosis or atresia. The study of the outflow tracts is essential for detection of conotruncal anomalies (truncus arteriosus, double outlet right ventricle, D-transposition of great arteries (D-TGA), tetralogy of Fallot (TOF)), as well as aortic and pulmonary anomalies. These CHD would be completely missed if only a four-chamber view was done.

The impact of third trimester US is clear for the foetal heart. Third trimester US allows

detection of some CHD with late manifestations. In the third trimester, foetal cardiac flow increases significantly. So, haemodynamic repercussions on abnormal cardiac valves and chambers are often more evident (e.g. hypoplastic left heart syndrome, Ebstein's anomaly, isolated pulmonary or aortic valvular stenosis, cardiomyopathies). Also, cardiac tumours (rhabdomyoma, fibroma) are usually diagnosed in this period (Fig. 4.25). Finally, third trimester US is a last chance for detecting a CHD that will require an appropriate delivery setting. However, visualisation of all cardiac structures may be limited by foetal position and bone shadowing.

All anomalies or suspected anomalies during first, second, or third trimester US imply reference for a detailed foetal echocardiography and genetic counselling. This enables a precise diagnosis, adequate specialised counselling about management and prognosis, an adapted follow-up, and a delivery management in the best possible conditions.

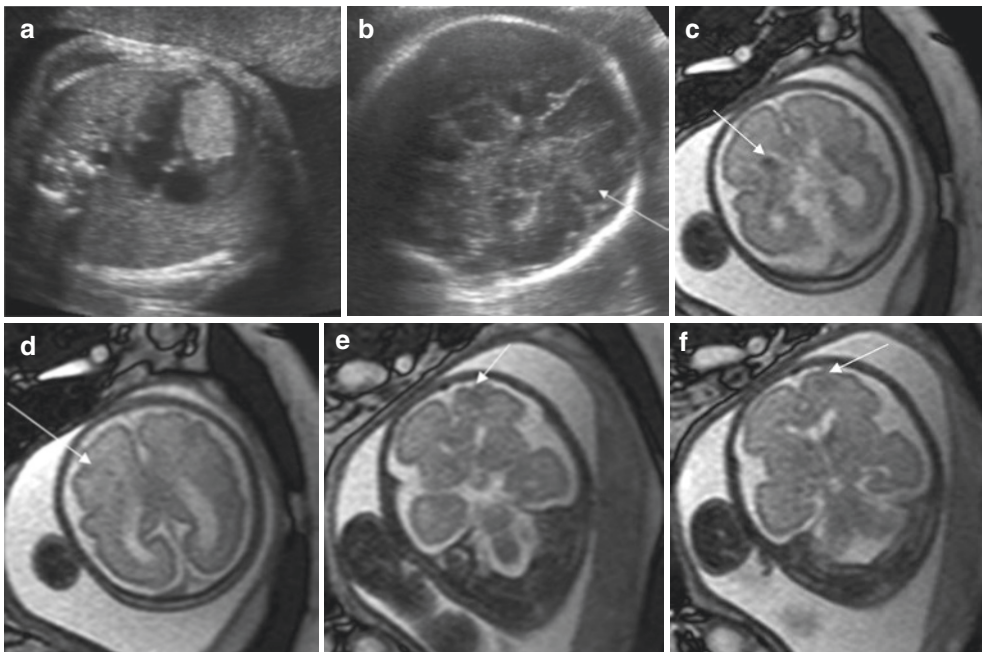


Fig. 4.25 Tuberous sclerosis. US shows a large rhabdomyoma in the right ventricle (a) and possible frontal cortical tuber (arrow in b) in a 28-wg foetus. MRI performed

at the same time demonstrates multiple hamartomatous brain lesions in T2 weighted sequences (arrows, c-f)

Foetal MRI has only one clinical indication in CHD: the search for typical brain lesions of tuberous sclerosis, in case of detection of a cardiac tumour (Fig. 4.25). Foetal volumetric brain MRI is performed for research purposes in case of significant CHD.

Inconstant prenatal CHD detection maintains neonatologists in uncomfortable situations. D-transposition of great arteries (D-TGA), right and left obstructive CHDs are ductal dependent and remain a challenge for perinatal management.

- In simple *TGA*, there is atrioventricular concordance but ventriculoarterial discordance. Detection mainly relies on the three-vessel view. Anatomically, classic findings are a right anterior location of ascending aorta and a left posterior location of main pulmonary artery. Due to the parallel course of great vessels, this cardiopathy can be suspected on the three-vessel view when only two vessels are identified (Fig. 4.26). Foetuses with D-TGA are stable in utero but can quickly become cyanotic after birth. They may require urgent balloon atrial septostomy (Rashkind procedure) if there is no significant shunt between right and left cavities. Delivery should occur in third level facilities with available interventional cardiologists.
- *TOF*, the most common cyanotic CHD, is another example of malformation of which diagnosis relies on careful analysis of out-

flow tracts. TOF is characterised by association of right ventricular outflow tract obstruction, ventricular septal defect, and overriding aorta. A right-sided aortic arch is present in 25% of cases. The degree of pulmonary hypoplasia or atresia impacts prognosis. In classical TOF, the four-chamber view is almost normal. Detection relies on abnormal three-vessel view: ascending aorta appears larger than main pulmonary artery (Fig. 4.27). The discrepancy of size increases with the severity of pulmonary hypoplasia. In severe cases, the main pulmonary artery is very small, almost invisible. In TOF with absent pulmonary valve, perinatal management is furthermore complicated by significant ventilatory problems due to airway compression by dilated pulmonary arteries. Impact of dilated pulmonary arteries on the airways can sometimes already be detected in utero, with heterogeneous lung parenchyma (Fig. 4.28).

- Neonates with *aortic coarctation* may present with acute decompensation when the arterial duct closes. Aortic coarctation remains a challenging diagnosis even for foetal cardiologists. Prenatal suspicion of aortic coarctation is characterised by low sensitivity and high false positive diagnosis. Detection of aortic coarctation relies on abnormal right ventricular preponderance and bigger great arteries asymmetry than usual (pulmonary artery > aorta) [17]. In normal foetuses, left and right ventricles have a

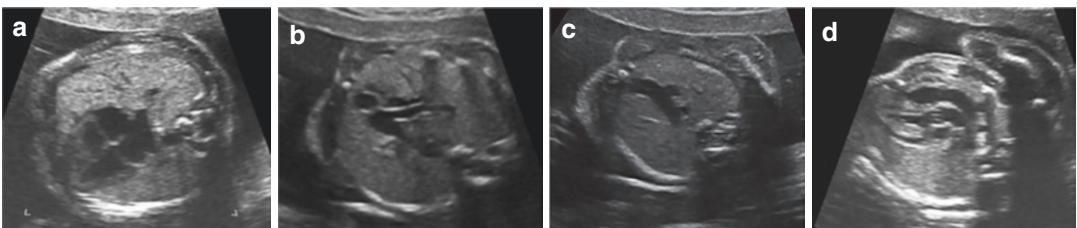


Fig. 4.26 d-TGA at 22 wg. The four-chamber view appears almost normal except for a slight leftward cardiac axis deviation (a). On the three-vessel view, pulmonary artery is located posteriorly to the ascending aorta (b). On

the three-vessel view and trachea view, only two vessels are detected and the anterior location of the aorta is confirmed (c). Oblique slice shows parallel course of great vessels (d)

similar size during second trimester. During third trimester, a normal slight right ventricular preponderance exists, and pulmonary artery is normally slightly larger than ascending aorta. By opposition, right ventricular preponderance during second trimester is clearly abnormal. Identification of abnormal right ventricle preponderance during the third trimester is more difficult and relies on measurements of right/left ventricular cavities and arteries [18]. More specific but less sensitive signs include posterior deformation of the cardiac arch, hypoplasia of the transverse arch, and elongation of the distal aortic arch. Even after birth, diagnosis can remain difficult with a patent ductus arteriosus.

- *Total anomalous pulmonary venous connection (TAPVC)* manifests with significant cyanosis and hypoxemia after birth. Most venous abnormal collectors have a supradiaphragmatic

venous unrestricted drainage whereas infradiaphragmatic collectors are usually restrictive. Restrictive drainage will be associated with severe postnatal pulmonary oedema requiring urgent surgical correction. Prenatal detection of TAPVC remains difficult and relies exquisitely on the four-chamber view. Clear visualisation of at least one pulmonary vein draining into the left atrium during a second trimester US excludes TAPVC. In TAPVC, the left auricular posterior wall appears abnormally convex, and no pulmonary vein draining in the left auricle is identified with US and Doppler US (Fig. 4.29). In most cases of TAPVC, a common venous collector courses vertically behind the left auricle. The presence of this collector can mimic normal pulmonary veins on US. Doppler US is necessary to detect the abnormal flow in the common duct, absence of normal pulmonary veins draining into the

Fig. 4.27 TOF. Axial US at 24 wg shows a small main pulmonary artery on the three-vessel view (arrow in **a**), and a large septal defect on four-chamber view (**b**)

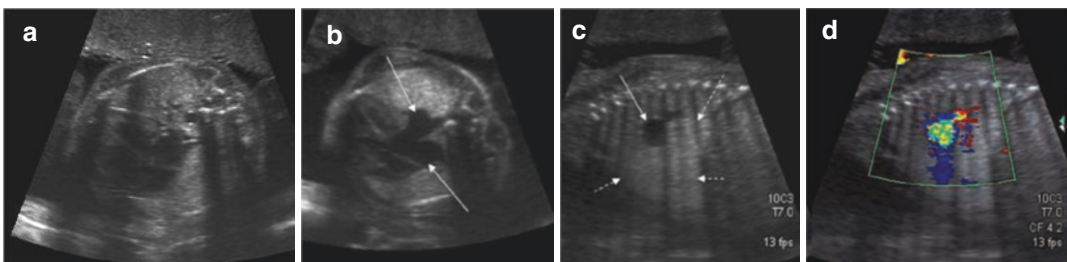
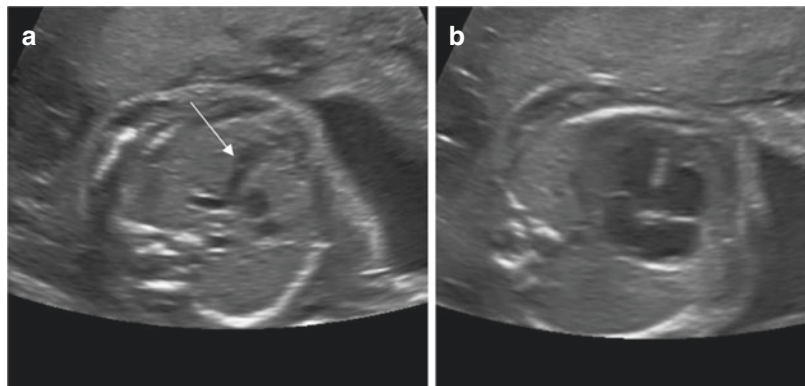
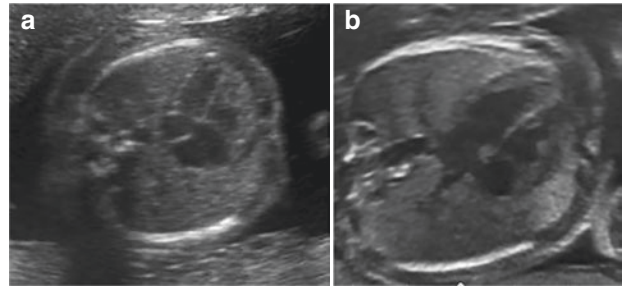



Fig. 4.28 TOF with absent pulmonary valve. US evaluation at 24 wg shows slight deviation of the axis of the heart (**a**) and massive dilated pulmonary artery branches (arrows

in **b**, **c**) associated with heterogeneous lung parenchyma (dotted arrows in **c**) secondary to compressed bronchi. Colour Doppler in (**d**) shows a huge pulmonary artery

Fig. 4.29 TAPVC. (a) The left auricle is small with a convex posterior wall. There is no pulmonary vein draining in the left auricle. There is a slight asymmetrical size of cardiac chambers. (b) Shows the normal configuration for comparison



left auricle, and to detect abnormal drainage in unusual veins such as vertical vein, portal vein, or ductus venosus.

 Even if the detection of cardiac anomalies has been improved with the routine analysis of the cardiac anatomy with five systematic different slices, some critical malformations that require a rapid neonatal treatment, such as aortic coarctation or total obstructive pulmonary venous return anomaly, remain difficult to diagnose prenatally and can escape to careful prenatal screening.

4.3.4 Abdominal Wall Defects

Abdominal wall defects include omphalocele, gastroschisis, bladder exstrophy, and more complex anomalies (cloacal exstrophy and exstrophy-epispadias complex (EEC) up to omphalocele-exstrophy-imperforate anus and spinal defects (OEIS complex).

Most of these conditions can be detected during a late first trimester US and are evident during the second trimester exam.

A classical pitfall during the first trimester is the physiological umbilical hernia. A physiological hernia contains only bowel, is located at the level of the umbilical cord, has a small size (usually less than 7 mm), and disappears after 12 wg. All other abdominal defects are abnormal.

4.3.4.1 Omphalocele

An omphalocele is a hernia located at the base of the umbilical cord. The mass is centrally located and covered by skin (in the exceptional case of rupture, there will be no membrane surrounding the hernia). The umbilical cord inserts on the hernia, but not necessarily centrally (Figs. 4.2 and 4.30). Oedema of the wall of the omphalocele and the umbilical cord can be observed but has no prognostic significance.

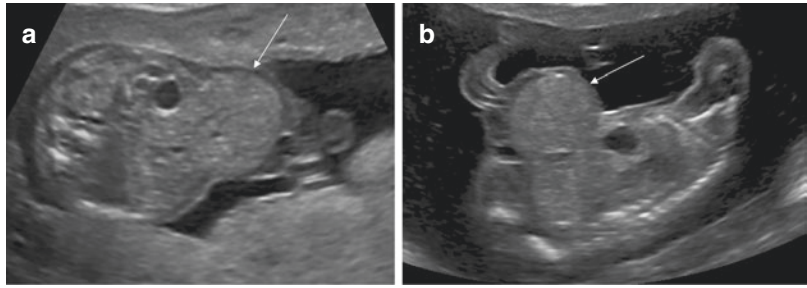
The defect is classified according to its content and size. A typical omphalocele contains some part of the liver and sometimes stomach and bowel. An atypical omphalocele contains only bowel, is usually smaller, and is more frequently associated with aneuploidies (Fig. 4.2). Omphalocele is considered as giant if it contains at least 80% of the liver volume, if its diameter is equal or larger than the abdominal diameter and/or if the size of the collar is more than 5 cm. The perinatal and postnatal management of giant omphaloceles is trickier, with frequent respiratory problems and sometimes need for long-term parenteral nutrition.

Omphaloceles are frequently associated with other malformations, genetic anomalies, and syndromes (e.g. Beckwith-Wiedemann syndrome) which impact prognosis.

A detailed US, genetic counselling, MRI in case of giant form, and foetal growth follow-up are indicated. Note that in omphaloceles, evaluation of the foetal weight is underestimated by US.

The differential diagnosis includes gastroschisis and more complex anomalies such as pentalogy of Cantrell (upper celosomy charac-

Fig. 4.30 Omphalocele. Axial (a) and sagittal (b) US slices at 19 wg show a typical omphalocele containing part of the liver (arrow). There is slight oedema of the wall of the omphalocele



terised by a combination of midline supra-umbilical wall defect, lower sternal cleft, diaphragmatic pericardial defect, anterior diaphragmatic defect, and various cardiac malformations).



It is cautious to control unusual appearance of the foetal abdominal wall after 12 wg in order to differentiate the transitory physiological hernia from a pathological omphalocele. An omphalocele is a hernia located at the base of the umbilical cord. It is frequently associated with other malformations, syndromes, or genetic anomalies that worsen the prognosis. Small atypical omphaloceles containing only bowel are more frequently associated with aneuploidies than typical omphaloceles containing part of the liver.

4.3.4.2 Gastroschisis

Gastroschisis results from a vascular insult. The umbilical cord inserts normally. There is a right paraumbilical defect out of which intra-abdominal content herniates (mostly bowel, rarely other organs). Bowel loops float inside the amniotic cavity without a covering membrane, taking a cauliflower appearance (Fig. 4.31). This malformation is frequently associated with intra-uterine growth retardation but not with an increased risk of aneuploidies. Prognosis relies mainly on bowel consequences (bowel atresia, bowel dystonia, short bowel syndrome).



Fig. 4.31 Gastroschisis at 22 wg. This axial US slice shows herniation of the bowel through a right paraumbilical defect (between crosses). The arrow points at the umbilical cord

The differential diagnosis includes conditions with a worse prognosis: short umbilical cord syndrome, limb body wall syndrome, amniotic band sequence. These diagnoses must be suspected in presence of a large abdominal wall defect, with multiple organs herniated, and when other anomalies such as a scoliosis and abnormal adherent membranes are detected (Fig. 4.32).

The diagnosis of gastroschisis by US is easy but evaluation of its individual prognosis is difficult. Complications are more frequent in case of a narrow wall defect (less than 10 mm), intra-abdominal echogenic dilated bowel loops (EDBL), intra-abdominal bowel loop dilatation, agglutination of collapsed herniated loops, bowel wall thickening of herniated loops (more than 3 mm), in case of mesenteric oedema or when sudden modification of appearance is detected (such as increased peristalsis or sudden disparities of peri-

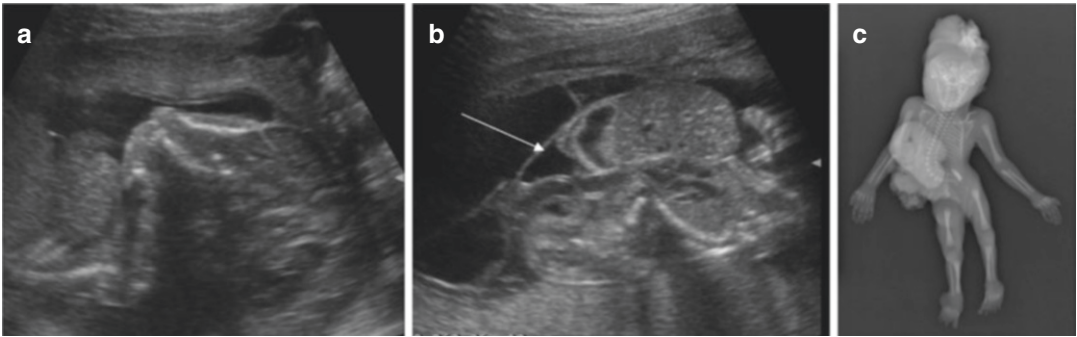


Fig. 4.32 Amniotic band sequence. (a, b) US shows a large abdominal defect with herniation of the liver, stomach, bowel, associated with severe scoliosis, acrania, and

thick membranes (arrows) at 19 wg. (c) Shows a postmortem radiograph of the foetus

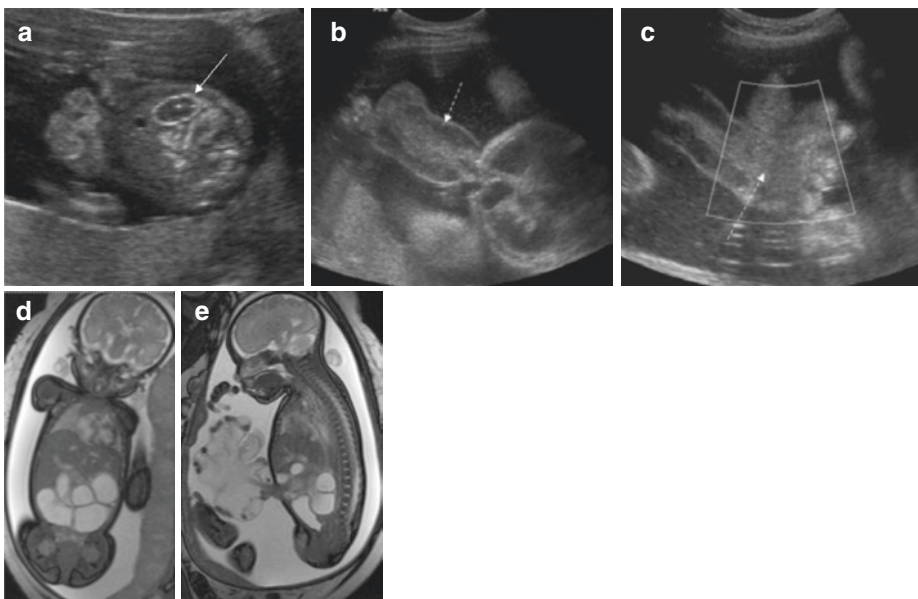



Fig. 4.33 Complicated gastroschisis. US at 17 wg (a) shows EDBL (arrow in a). At 32 wg (b, c), herniated bowel loops appear collapsed. There is mesenteric oedema without detectable flow (dotted arrows in b, c). Dilatation of intra-abdominal bowel has increased. MRI performed

the same day in coronal (d) and sagittal (e) T2-weighted slices shows the same findings. The herniated bowel was necrotic and the dilated intra-abdominal bowel loops corresponded only to duodenum

stasis of intra-abdominal dilated bowel loops) [19] (Fig. 4.33). Mesenteric flow to the herniated bowel can be evaluated with Doppler but prognosis value of this sign is still unknown. MRI is rarely indicated in case of suspected complications (Fig. 4.33).

Close follow-up is proposed until delivery. There is an increased risk of unexplained third trimester death. Therefore, most teams propose an individually tailored approach with delivery around 37 wg or earlier in case of abrupt modification of appearance.

 In opposition to omphalocele, gastroschisis corresponds to uncovered hernia from a right paraumbilical abdominal wall defect. Gastroschisis isn't associated with increased risk of aneuploidy but rather with intra-uterine growth retardation, bowel compromise, and third trimester intra-uterine demise. The prognosis mainly relies on the viability of the herniated bowel.

4.3.5 Abnormal Appearance of the Digestive Tract

4.3.5.1 Absence of Visualisation of the Stomach

Absence of visualisation of the stomach can be secondary to an oesophageal atresia but can also be observed in other circumstances (Table 4.6).

4.3.5.2 Oesophageal Atresia

Classical signs of an oesophageal atresia include repeated absence of visualisation of foetal stomach, progressive development of a polyhydramnios, and sometimes visualisation of a proximal dilated oesophageal pouch. If a tracheoesophageal fistula is present, a small and sometimes a normal stomach is visible. The presence of a fistula and the absence of a systematic third trimester US examination explain why some oesophageal atresia escape prenatal detection. A detailed US is necessary to detect associated anomalies (e.g. VACTER association). Genetic counselling and follow-up are necessary.

MRI has a better accuracy for detection of oesophageal atresia, showing tracheal bowing and proximal dilated oesophageal pouch on thick slices and dynamic sequences (Fig. 4.34). MRI findings can also have a prognostic significance. Absence of visualisation of the proximal jejunal loops on T2 sequences and presence of a small not so hyperintense microcolon on T1 sequence

Table 4.6 Causes of absence of visualisation or small foetal stomach at US

Physiologic and normal (stomach will be seen later during or in another examination)
Mechanical obstruction of foetal oesophagus
– Oesophageal atresia
– Goitre
– Mediastinal tumours
Abnormal foetal swallowing (neurogenic disorders)
Anamnios (no liquid to swallow)

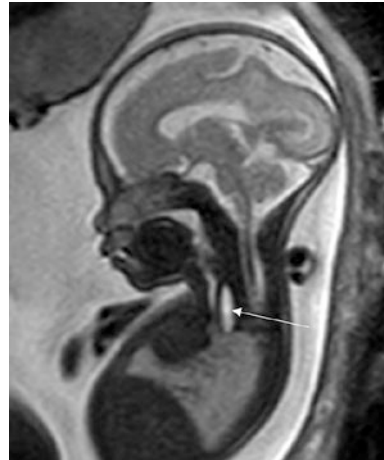


Fig. 4.34 Oesophageal atresia. A dynamic thick slab MRI sequence shows a dilated proximal oesophagus (arrow) in a 28-wg-old foetus

can suggest a long gap atresia. In opposition, visualisation of the lower oesophageal lumen and of proximal jejunal loops without a microcolon suggests the presence of a fistula.

4.3.5.3 Proximal (Gastric/Duodenal) Digestive Obstruction

Detection of a dilated stomach can suggest a proximal bowel obstruction. A dilated stomach is rarely isolated because pyloric atresia is exceptional. The association of a dilated stomach and proximal duodenum gives a typical “double bubble appearance” (Fig. 4.35). This sign is often not present during early second trimester and will be evident later, associated with a polyhydramnios. Any cause of duodenal obstruction (duodenal atresia, web, annular pancreas) can cause a dou-

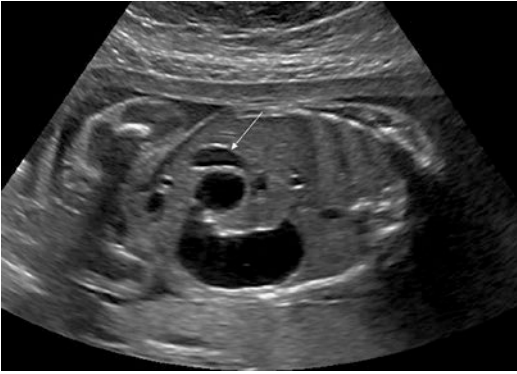


Fig. 4.35 Duodenal atresia at 24 wg. US shows the typical double bubble appearance corresponding to a dilated duodenum communicating with the stomach by the pylorus (arrow: gallbladder)

ble bubble sign. The presence of a duodenal atresia significantly increases the risk for trisomy 21. A detailed US and genetic counselling are thus mandatory.

The double bubble appearance (where the two “cysts” communicate by the pylorus) must be differentiated from other cystic structures located in the mid abdomen, in which there is no connection with the stomach lumen. Examples are duodenal duplication cyst, omental/peritoneal cyst, hepatic cyst, mesenchymal hamartoma, and choledochal cyst. Also, biliary atresia must always be kept in mind when a right upper abdominal quadrant cyst is discovered in a foetus. In rare situation, some forms of biliary atresia can present with hepatic hilar cyst (Fig. 4.36). Adequate examinations must be performed after birth to exclude biliary atresia.

4.3.5.4 Small and Large Bowels Obstruction

Normally, small and large bowels are collapsed whereas the rectum is visible during the second trimester. The distinction between small and large bowels becomes evident only later in pregnancy. The lumen of the small bowel is normally less than 3–3.5 mm during the second trimester and less than 7 mm during the third trimester [20]. The large bowel has a much more variable size, and its lumen can reach up to 23 mm during the third trimester [21].

Dilated bowel loops, hyperechoic intestinal content, increased echogenicity of bowel wall, or ascites suggest a mechanical or functional obstruction. Location and appearance of the abnormal bowel, gestational age at diagnosis, and evolution at follow-up help for diagnosis. Attention should be paid to the gallbladder. Absence of visibility of the foetal gallbladder during the second trimester US raises the possibility of cystic fibrosis or biliary atresia. Appearance of the gallbladder during the third trimester is more variable and has usually no signification.

It is difficult to precise the cause and the level of the bowel obstruction in utero. Most cases of foetal bowel dilatation concern the small bowel. It is exceptional to detect colonic dilatation in utero even in case of distal occlusion or Hirschsprung disease. The only exceptions are complex urorectal malformations where a pelvic dilated distal loop can be detected since the first trimester, and in case of chloride diarrhoea.

As a rule of thumb, early polyhydramnios and a dilated bowel loop suggest a proximal obstruction. The greater compliance of the jejunum explains the larger dilatation and lesser risk of perforation in jejunal obstruction than in ileal obstruction. A meconium peritonitis is more frequent in ileal occlusion with secondary perforation. Multiple dilated bowel loops suggest a more distal obstacle (jejuno-ileal or ileal), functional obstruction, or chloride diarrhoea. Increased peristalsis suggests a mechanical occlusion.

Bowel atresia is the most frequent cause of small bowel dilatation. In most cases, the atresia is single. However, absence of visibility of small bowel loops distally to the obstruction on US and MRI suggests the presence of multiple atresias or an apple peel syndrome.

Another presentation of multiple intestinal atresias is the presence of multiple dilated bowel loops associated with enteroliths located in adjacent collapsed loops (Fig. 4.37).

Enteroliths (corresponding to calcified meconium) can be detected in foetuses with bowel dilatation and has a poor prognostic value. Enteroliths are usually discovered in complex

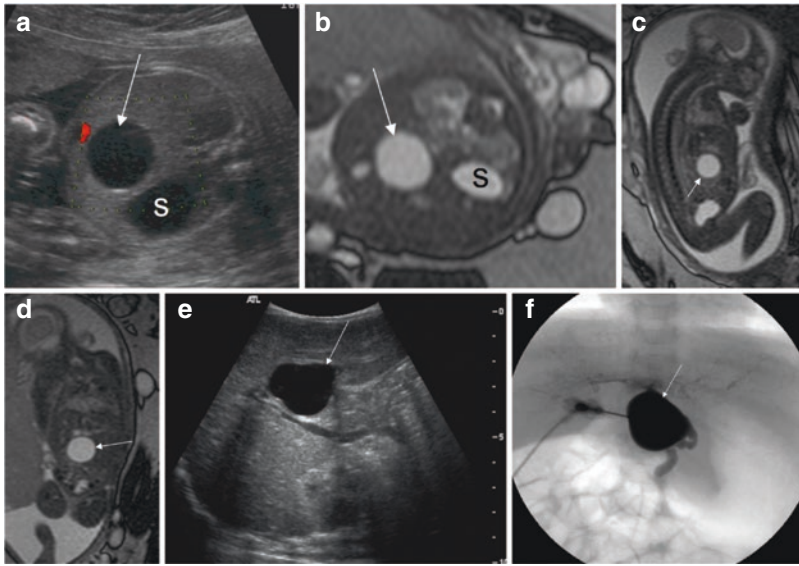
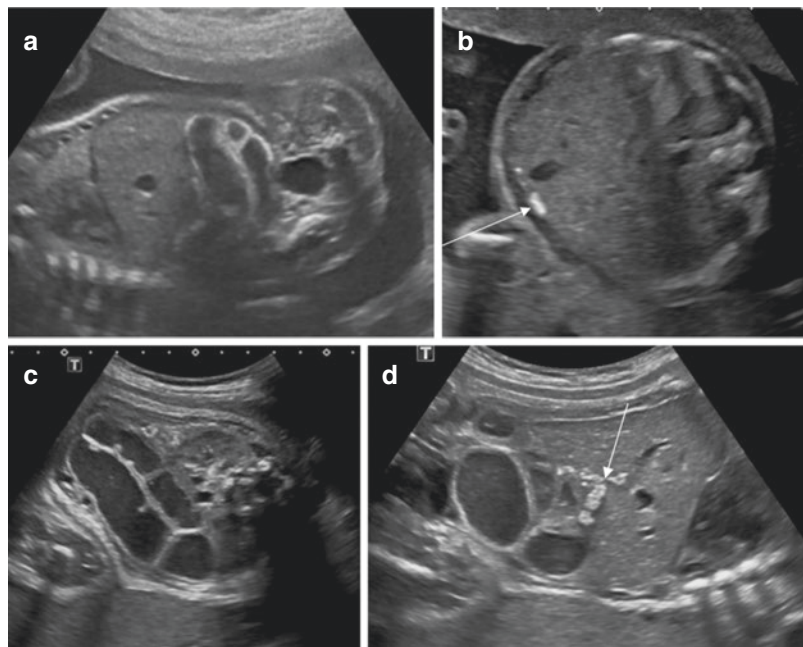


Fig. 4.36 Biliary atresia with a hilar cyst (arrow) demonstrated with US (a) and MRI (b–d) at 28 wg. The stomach (S) and the cystic structure (arrow) aren’t connected (a–d). The corresponding postnatal US (e) and percutaneous cholangiography in the neonate (f) confirm the biliary atresia (arrow points to the cyst)

Fig. 4.37 Multiple intestinal atresias. US at 22 wg (a, b) shows EDBL and peritoneal calcifications (arrow, b). At 32 wg (c, d) enteroliths (arrow in d) are seen in collapsed loops near dilated bowel loops



urorectal malformations such as cloacal malformation or urorectal septum. They are then thought to result from mixing of urine and meconium in abnormal urodigestive communications. Such complex malformations are usu-

ally detected early during first or second trimester by visualisation of a dilated pelvic bowel loop sometimes containing enteroliths (Fig. 4.38). Enteroliths can also rarely be observed in collapsed loops adjacent to dilated

bowel loops. In these circumstances, they are usually detected during late second or third trimester and suggest three possible diagnoses: a complicated meconial ileus, multiple intestinal atresias, or an extensive aganglionosis (Figs. 4.37 and 4.39). These infants have a much more complicated postnatal course, with sometimes intractable diseases such as in hereditary multiple intestinal atresias.



Fig. 4.38 Enteroliths in a dilated pelvic bowel loop (arrow) in a case of cloacal malformation at 15 wg

An arciform appearance of a dilated loop eventually associated with a fluid-fluid level suggests a closed loop or a volvulus (Fig. 4.40). Wrapping of loops around an axis suggest a mid-gut volvulus. The whirlpool sign can be demonstrated with colour Doppler US as after birth.

4.3.5.5 Echogenic Dilated Bowel Loops (EDBL)

In EDBL, the bowel wall is as echogenic as foetal bone. With improvement of equipment, it became even more important to adjust some US parameters in order to confirm the diagnosis such as taking away harmonic imaging or scanning with lower frequency. The hyperechogenicity of the bowel must persist after these adjustments to be considered as abnormal. Most cases of EDBL are isolated, transitory and without consequences.

However, the presence of EDBL implies complementary examinations since they can rarely be associated with cystic fibrosis, trisomy 21, infections, ischaemic bowel lesion, later IUGR, and complicated gastroschisis

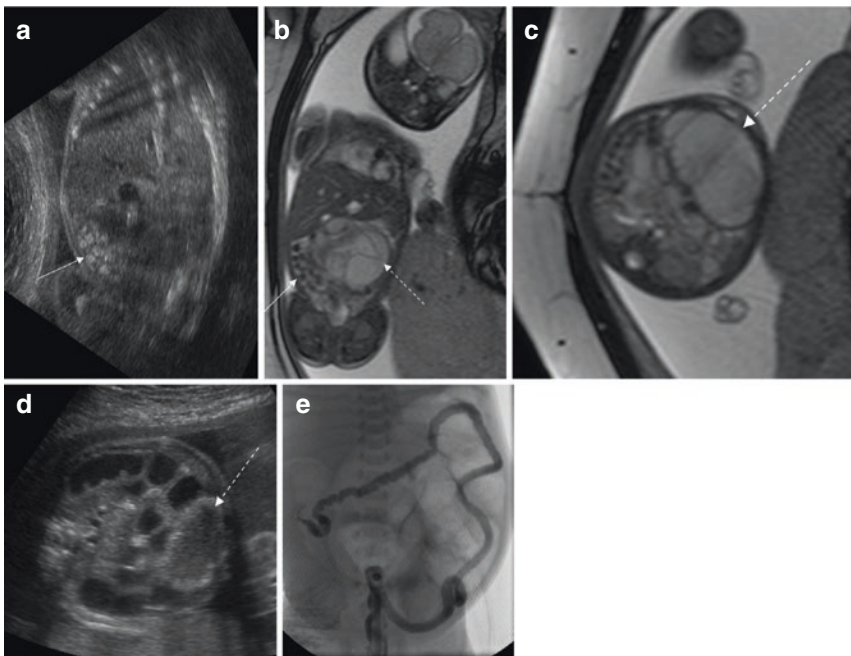
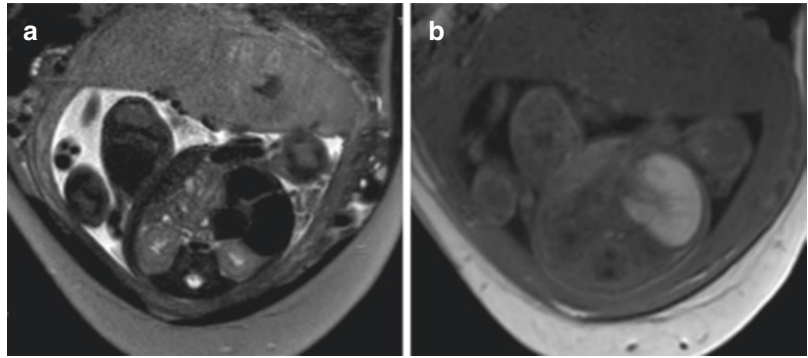


Fig. 4.39 Complicated meconium ileus. US (a, d) and MRI (b, c) show hyperechoic content (hypointense on T2 MRI) in collapsed bowel loops (arrow), and a meconium pseudocyst (dotted arrow in b–d) and dilatation of proxi-

mal intestinal loops at 28 wg (d). Enema performed after birth (e) shows a microcolon and dilated proximal small bowel without contrast reflux in the dilated intestinal loop. At surgery, an atretic jejunal segment was diagnosed

Fig. 4.40 Segmental volvulus. Axial MRI shows a closed dilated loop with hypointense T2 (HASTE) (a) and hyperintense T1 signal content (b)



(Figs. 4.33 and 4.37). In case of isolated EDBL, follow-up US after 28 wg is necessary to detect bowel atresia and IUGR. A normal third trimester US associated with normal results of complementary examinations is reassuring and no postnatal examinations are then necessary.

4.3.5.6 Meconium Peritonitis

Any causes of bowel perforation can cause chemical peritoneal irritation and meconium peritonitis. Aetiology is unknown in most cases of meconium peritonitis, and the only US findings are peritoneal calcifications. In an acute setting, sometimes echogenic and complex ascites are observed associated with dilated loops. The bowel perforation can heal without sequel, leaving only scattered peritoneal calcifications, or can be complicated by a residual stenosis or an (even pre-existing) atresia (Fig. 4.37). With time, ascites loculation may lead to a peritoneal pseudocyst which is heterogeneous with often peripheral calcifications (Fig. 4.41). The prognosis relies on results of complementary examinations (search for cystic fibrosis, infection), and follow-up. When only scattered calcifications are detected, the infant outcome is favourable and then often the only postnatal finding are peritoneal calcifications visible on radiographs or abdominal US. The presence of ascites, a pseudocyst, bowel dilatation, and a polyhydramnios suggests a persisting underlying cause (e.g. atresia, volvulus, cystic fibrosis) and most of these neonates will need postnatal surgery (Figs. 4.37, 4.39, and 4.40).

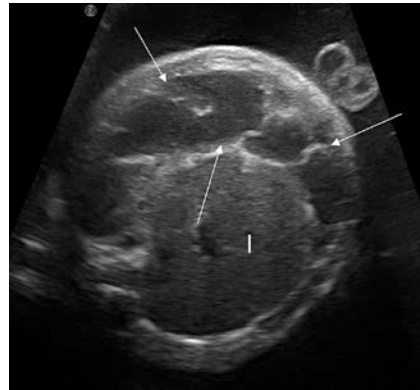


Fig. 4.41 Meconium peritonitis. US shows septated ascites (arrows) with peripheral calcifications evolving towards pseudocysts surrounding the liver (l)

MRI can be useful in selected cases with bowel dilatation. MRI differentiates easily normal small and large bowel by their respective appearance on T2 and T1 sequences. Normal proximal small bowel has an hyperintense T2 content and hypointense T1 content. The meconium is normally present in the distal small bowel and in the large bowel and is hyperintense on T1 sequences and hypointense on T2 sequences. In a bowel obstruction, hyperintense content on a T1 sequence usually corresponds to the presence of blood products in a proximal small bowel loop and doesn't imply that it is a large bowel containing meconium (Fig. 4.39). MRI can be useful to precise the level or the cause of obstruction. MRI is more useful for evaluation of the digestive loops distal to the obstruction (e.g. in a suspected volvulus or multiple atresias) and the size of the colon (e.g.

search for a microcolon). However, determining the length of the presumed viable bowel remains difficult (Fig. 4.33).



Proximal bowel obstruction manifests by significant bowel dilatation and early polyhydramnios. Ileal obstruction is more prone to perforation, meconial peritonitis, and later multiple bowel loop dilatation. Distal bowel obstruction can have no amniotic fluid volume repercussion, and no prenatal bowel anomaly.

Enteroliths detected in dilated or collapsed bowel loops are associated with serious diseases necessitating neonatal surgery.

EDBL is a transitory observation that can be related to multiple circumstances implying possible digestive impact. EDBL necessitates complete foetal US, complementary examinations, and follow-up. Disappearance during follow-up and normal results of complementary exams are usually associated with good prognosis.

Meconial peritonitis reflects digestive perforation. Peritoneal calcifications can be the only sign of meconial peritonitis and when isolated, this observation usually has a good prognosis. In opposition, persistence of bowel dilatation, or presence of a peritoneal pseudocyst at follow-up, will often require neonatal surgery to release intestinal obstruction.

4.3.6 Anomalies with Possible Renal Insufficiency

Urinary tract malformations are among the most common causes of congenital anomalies.

Foetal kidneys can be detected as early as 11–12 wg. Foetal kidneys have a normal hyperechogenic appearance during the first half of pregnancy. Renal echogenicity compared with the adjacent liver then progressively decreases during gestation.

The corticomedullary differentiation appears progressively and is normally visible after 18 wg in good US conditions. Bipolar diameter is correlated with gestational age (renal length in mm = $1.1 \times$ gestational age in weeks) and nomograms of renal size are published. Deviation of more than two standard deviations is considered abnormal.

Normal antero-posterior intrarenal pelvic diameter is less than 4 mm between 16 and 27 wg, less than 7 mm between 28 wg and birth (Nguyen et al. 2014). As after birth, the degree of hydration, the bladder filling volume, foetal position, and male sex can explain a physiological pelvi-ectasia during US. Normal calices and ureters are usually not visible.

The foetal bladder can be detected as early as 9–10 wg and must be seen in all foetuses after 15 wg; its size increases with gestational age.

The amniotic fluid volume reflects foetal urinary output after 15 wg. It is evaluated subjectively, by a single pocket evaluation (normal between 2 and 8 cm) or using the amniotic fluid index (normal from 80 to 240). Normal foetal diuresis increases 10–12 times between the second and third trimesters.

4.3.6.1 Bladder Anomalies

- *Non-visualisation of the foetal bladder.* Absence of visualisation of the bladder in a foetus is always abnormal after 15 wg. It is an ominous sign for absent renal diuresis (when associated with oligohydramnios) or a bladder malformation.

In case of normal appearing foetal kidneys and normal amniotic fluid volume, the repeated absence of visualisation of the bladder suggests a bladder exstrophy or a more complex malformation.

In case of bladder exstrophy, no bladder (or rarely a tiny bladder) is visible, the umbilical cord inserts unusually low and inferior, and the abdominal wall may have an irregular aspect (Fig. 4.42). A peculiar study of the genitalia, the anal canal, and the spine must be performed to detect more complex malformations such as cloacal exstrophy, exstrophy-epispadias complex (EEC) or

Fig. 4.42 Bladder exstrophy. Axial (a) and sagittal (b) US at 22 wg show absence of bladder and irregular appearance of the infraumbilical abdominal wall (arrow, b) corresponding to the exposed bladder

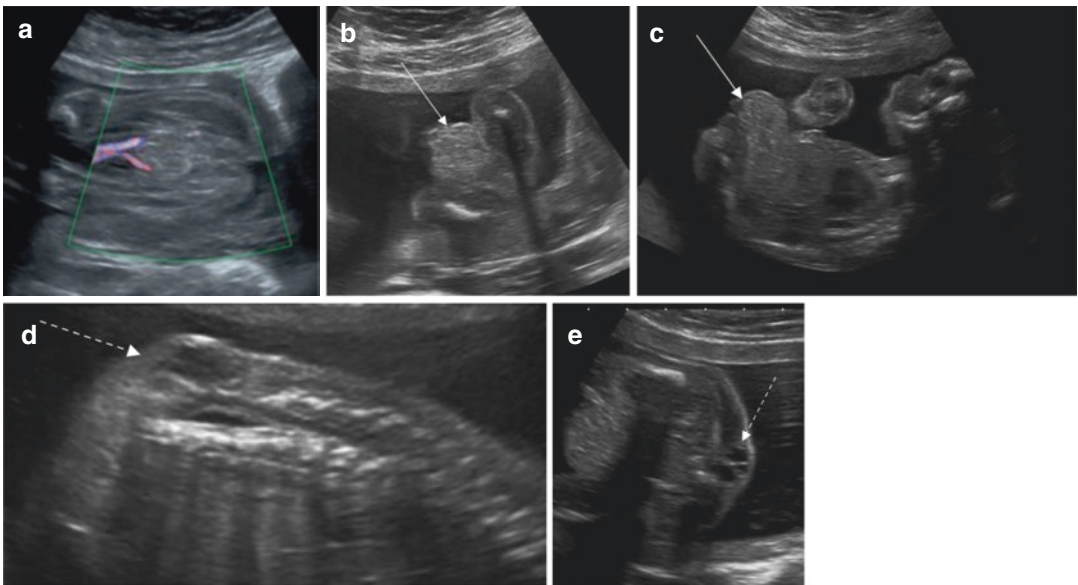
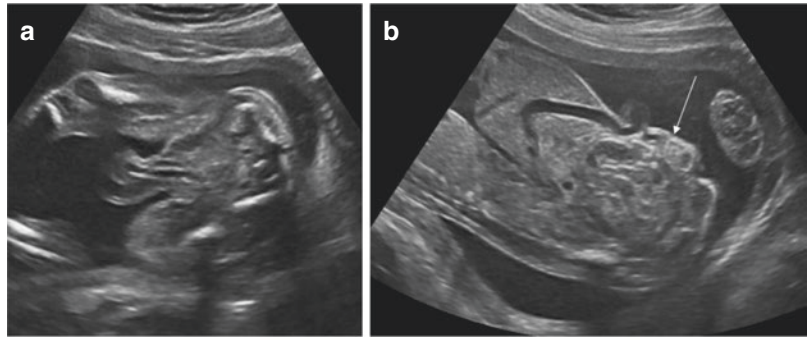


Fig. 4.43 OEIS. US performed at 21 wg. No bladder is visible between umbilical arteries (a). There is a cloacal exstrophy (arrows point to the inferior celosomy and clo-

cal exstrophy) (b, c) associated with a lipomyelomeningocele (dotted arrow, d, e)

omphalocele-exstrophy-imperforate anus-spinal defect (OEIS) complex (Fig. 4.43). Foetal MRI can help to demonstrate associated anomalies. Management of complex anomalies associated with bladder exstrophy is difficult and requires a multidisciplinary team.

- *Enlarged bladder or megacystis*

The aetiology of a megacystis varies according to the sex and gestational age at diagnosis.

During the first trimester, megacystis is defined as a bladder bigger than 7 mm. Megacystis can be a sign of aneuploidies (trisomy 13, 18) regardless of bladder diameter [22]. Karyotyping is therefore recommended.

Most isolated moderate megacystis (less than 12.5 mm) resolve spontaneously. Megacystis can also be a sign of a distal obstructive uropathy, especially when severe (more than 15 mm) and when it does not resolve. Very large bladders during the first trimester are usually due to urethral stenosis, posterior urethral valves, or even urethral atresia.

The definition of megacystis after the first trimester is variable in the literature.

Megacystis is often defined as a bladder bigger than 30 mm during the second trimester or bigger than 50 mm (60 mm for female fetuses) during the third trimester [23]. Another definition uses a sagittal diameter (in

mm) greater than the gestational age (in weeks) + 12. Some authors consider an enlarged bladder with failure to empty over a period of at least 45 min abnormal [24]. A megacystis can be a sign of obstruction as in posterior urethral valve, can be secondary to vesicoureteral reflux (VUR) or be seen in syndromes, such as megacystis-microcolon-intestinal hypoperistalsis syndrome (MMIHS) or Prune Belly syndrome. When the bladder is significantly enlarged, its abdominal part is bigger than its intrapelvic part, which gives a pseudo-keyhole appearance (which, however, is not specific of a disease). The differential diagnosis of a megacystis relies on the appearance of the foetal bladder wall, the posterior urethra, the large bowel, and the genitalia.

- *Posterior urethral valve (PUV)* is a classical cause of megacystis in male foetuses. The bladder size can be increased, and the bladder wall is

often thickened. Diagnosis relies on a sagittal perineal view of the posterior urethra [25]. In PUV, the posterior urethra is dilated. In most cases, pyelocaliceal and ureteral dilatations are present (Fig. 4.44). Evolution of PUV is unpredictable. Pejorative signs include a precocious detection, oligohydramnios, and renal parenchymal anomalies. The presence of an urinoma has no negative prognostic value; this could even protect the renal parenchyma and/or the other kidney from increased pressure (Fig. 4.45).

- *Gross vesicoureteral reflux (VUR)* is another frequent cause of megacystis in foetuses. The bladder wall is usually thin and coexists with other signs of reflux. The posterior urethra is normal.
- *Prune Belly syndrome* is a rare cause of megacystis. A large bladder with thickened wall is detected usually early during pregnancy. A flabby appearance of the foetal abdomen may

Fig. 4.44 Posterior urethral valve. Coronal US at 21 wg shows bilateral urinary dilatation (a). Sagittal US shows the dilated bladder (b) associated with dilatation of the posterior urethra (arrow in b)

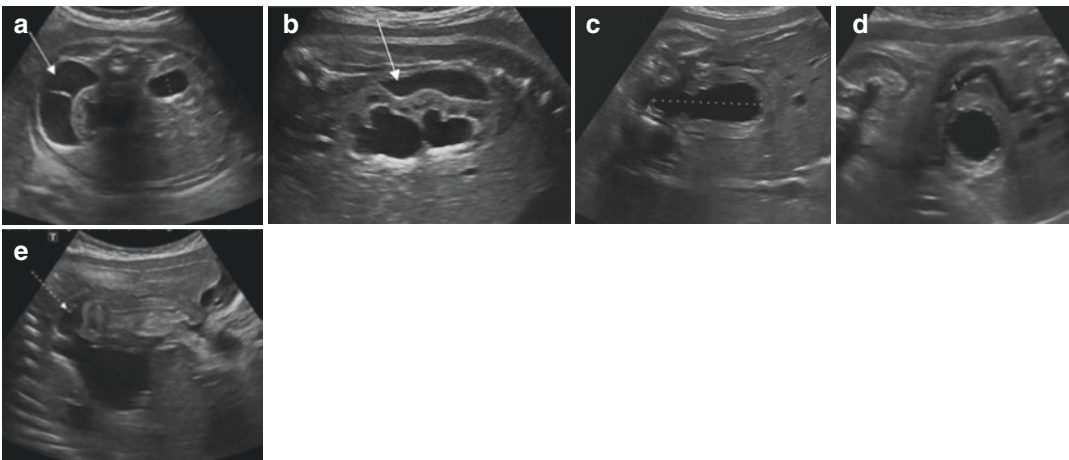
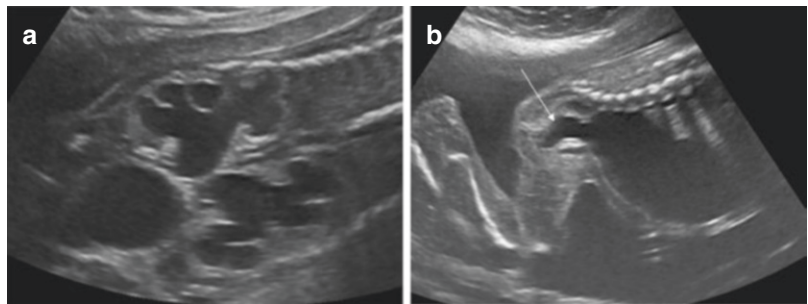


Fig. 4.45 Posterior urethral valve. US at 21 wg (a, b) shows bilateral pelvicalyceal dilatation with unilateral urinoma (arrow). US at 36 wg better shows the thickened

bladder wall (c, d), and a dilated ureter (A between crosses) (d). The perineal view at 36 wg demonstrates clearly the dilated posterior urethra (dotted arrow) (e)

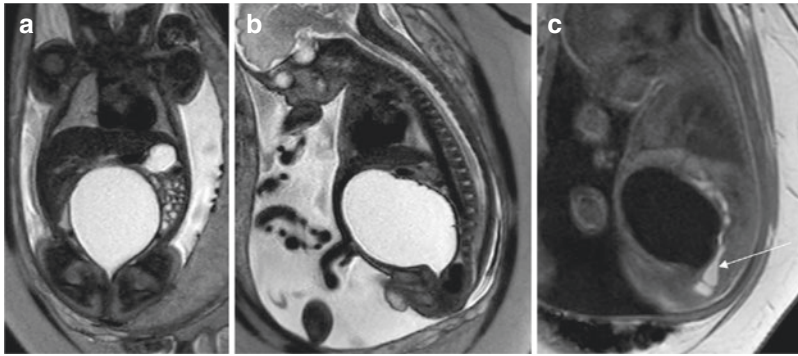


Fig. 4.46 Prune Belly syndrome. US detected a megacystis. Coronal T2 (a), sagittal T2 (b), and sagittal T1 (c) MRI slices show a megacystis in a male foetus at 32 wg.

The T1 sequence shows a normal size of the large bowel (arrow, c). Testes are not in the scrotal position

be observed. This malformation mostly affects male foetuses. Posterior urethral dilatation with oligohydramnios and megalourethra can coexist (Fig. 4.46). The typical cryptorchidism can be detected during the third trimester.


- Lastly, *megacystis-microcolon-intestinal hypoperistalsis syndrome* (MMIHS) must be included in the differential diagnosis when an enlarged bladder is confirmed. This syndrome affects females more than males and is characterised by abnormal innervation of the bladder and bowel muscles. The bladder wall is thin, amniotic fluid is normal, and dilatation of the renal cavities is frequent. Diagnosis relies on detection of a small colon that will be better demonstrated with MRI. The prognosis is poor.

4.3.6.2 Foetal Pelvicalyceal Dilatation

Pelvic or pelvicalyceal dilatation detected during second trimester US has variable significance. It can be physiological and transitory or sign of a significant foetal uropathy (obstruction, VUR) or aneuploidy (such as trisomy 21). As with all foetal anomalies, a detailed foetal US must be performed to search for associated anomalies.

The risk for a significant uropathy depends on the degree and intra-uterine progression of the pelvicalyceal dilatation, the presence of renal parenchymal anomalies, and abnormal amniotic fluid volume. The positive predictive value of dilatation for a significant uropathy is higher during the third trimester US than during the second trimester US (Nguyen et al. 2014).

Various classifications of renal collecting system dilatations have been used. Consensus between urological and radiological societies in North America has now led to a unified classification of urinary dilatation for prenatal (and postnatal) care: the urinary tract dilatation (UTD) classification. In Europe, the pelvicalyceal system (PCD) grading as introduced by the ESPR abdominal imaging task force is used for postnatal classification, whereas obstetricians still use the Fernbach classification for intra-uterine grading (SFU) (see Chap. 4). The UTD system uses six US findings to describe the urinary tract: anterior-posterior renal pelvic diameter, caliceal dilatation (with postnatal distinction between central and peripheral calices), renal parenchy-

 The absence of visibility of the bladder after 15 wg is highly suspicious of bladder exstrophy or related malformation.

An enlarged bladder may be observed in various circumstances depending on the gestational age and the foetal sex. The differential diagnosis relies on careful analysis of the posterior urethra, the bladder wall, the size of the large bowel, and the genitalia.

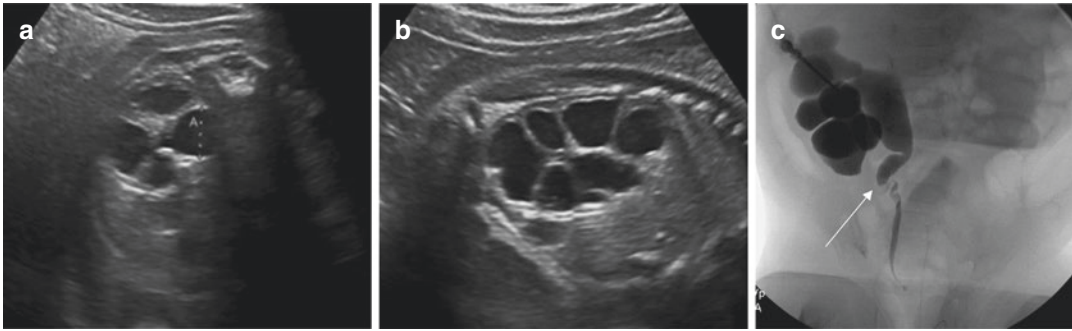


Fig. 4.47 Pelvi-ureteral junction syndrome/obstruction. The pelvis size was 6 mm at 24 wg. It has increased to 15 mm at 34 wg (a, b). Percutaneous nephrostomy per-

formed at 2 months of life at the time of surgery demonstrates the upper junction syndrome (arrow, c)

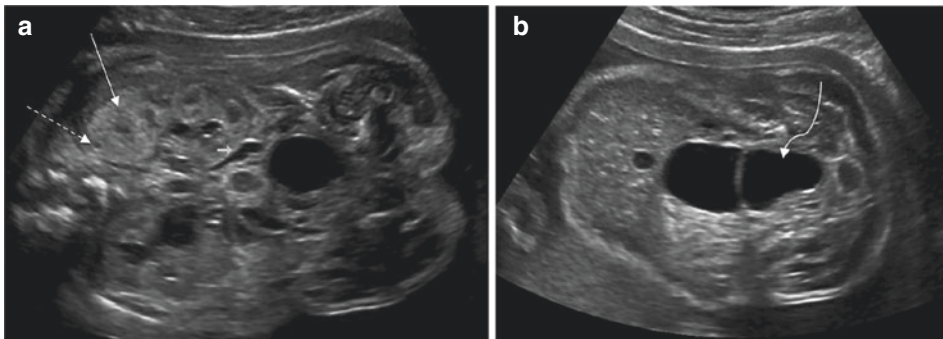


Fig. 4.48 Complicated duplex system. The parenchyma of the upper moiety of the duplex kidney is hyperechoic, without corticomedullary differentiation (arrow in a). A

tiny cyst is present (dotted arrow). It is associated with a megaureter (small arrow) and a large ureterocele (curved arrow in b)


mal thickness and appearance, bladder appearance, and ureteral appearance. Even if not perfect, this classification recommends items that must be studied and described during US, is correlated with the risk of postnatal uropathies, and suggests adapted and standardised follow-up depending on the grade of dilatation.

Upper junction (or pelvi-ureteral junction) syndrome (or obstruction) is one of the most common causes of pelvic dilatation detected in utero. Pelvis and calices are variably dilated, the ureter is not visible, and the bladder is normal (Fig. 4.47). It is usually sporadic and unilateral. The prognosis depends on the uni- or bilaterality of the anomaly, and on the appearance of the renal parenchyma. Thinning and hyperechogenicity of the parenchyma, loss of corticomedullary differentiation, and depiction of

parenchymal cysts are poor prognosis factors for the renal function of the affected kidney whereas bilateral anomalies can affect the global renal function.

VUR can be difficult to differentiate from obstruction in utero. Changes of pelvic diameter during the US exam, transitory visualisation of the ureters, pelvic urothelial thickening, and a large bladder can suggest this diagnosis.

A complicated kidney duplication classically associates obstruction of the upper system, and VUR into the inferior moiety. Upper pole dilatation is often associated with an ureterocele that can sometimes obstruct the other kidney or the bladder outlet (Fig. 4.48). By opposition, discovery of a simple duplex kidney without dilatation doesn't require any complementary examination.

 Pelvicalyceal dilatations detected during second trimester of gestation can be physiological and transitory or the sign of an uropathy or associated with aneuploidy. The risk of significant uropathy depends on the degree and intra-uterine progression of the dilatation, the presence of renal parenchymal repercussions (hyperechogenicity, loss of corticomedullary differentiation, parenchymal thinning and cysts), and oligohydramnios. A dilatation persisting during the third trimester US has higher positive predictive value for a significant uropathy.

4.3.6.3 Foetal Nephropathies

Abnormal renal echogenicity or size, the presence of cysts and of oligohydramnios suggest a nephropathy. Abnormal kidney appearance can be isolated, secondary to an obstruction, an infection (e.g. CMV), or associated with multiple syndromes and genetic anomalies.

Detection and characterisation rely essentially on US. Foetal MRI is mandatory in case of suspected ciliopathy, searching for specific brain anomalies (e.g. Joubert syndrome and related anomalies). Another reason to perform MRI is that US may miss small renal remnants which might be picked up by foetal MRI using diffusion weighted sequences. This may sometimes impact prognosis and further management.

US diagnosis relies on detailed renal analysis including measurement of renal length, analysis of renal echogenicity, evaluation of corticomedullary differentiation, presence of renal cysts (number, size, and location), and detection of pelvicalyceal dilatation. A careful and meticulous search for associated anomalies (particularly of the central nervous system and the search for polydactyly) must be performed. The timing of detection of the renal anomaly and the amount of amniotic fluid add prognostic information. In all cases, early oligohydramnios raises the possibility of significant pulmonary hypoplasia and is a poor prognostic sign. US examination of the parents and familial inquiry are indispensable. In

case of a known familial history of renal (cystic) disease or syndrome, or of a previous affected sibling, recurrence of the same disease must be suspected. Additionally, renal size and the gestational age at diagnosis help to differentiate between different diseases.

- Detection of massively enlarged hyperechoic kidneys during the first trimester or early second trimester suggests *Meckel-Gruber* syndrome. Enlarged medulla and multiple renal cysts are typical. A careful search for polydactyly and brain malformations (e.g. cephalocele and posterior fossa anomaly) will confirm the diagnosis (Fig. 4.49).
- Detection of massively enlarged kidneys during the second or third trimester suggests two other ciliopathies: *autosomal recessive polycystic kidney disease* (ARPKD), or *Bardet-Biedl syndrome* (BBS).

Autosomal recessive polycystic kidney disease (ARPKD) due to PKHD1 mutation is pathologically characterised by the abnormal dilatation of collector tubules and distal tubular ducts, and hepatic fibrosis. Typical features on prenatal US include very large kidneys (more than four to eight standard deviations) without corticomedullary differentiation (Fig. 4.50). There is oligohydramnios, pulmonary hypoplasia and a “Potter sequence”. Another characteristic appearance is large hyperechoic kidneys with corticomedullary inversion and medullary cysts (Fig. 4.51). Progressive modification of the renal aspect with enlarging kidneys during pregnancy is typical of the disease (Fig. 4.50). Rare observation of a liver hilar cyst is the only prenatal sign of the coexisting hepatic fibrosis which is always present with variable degree in this disease. Expressivity is extremely variable even in the same family. This explains multiple possible appearances in utero and after birth. Some children will present with renal insufficiency and others with congenital hepatic fibrosis and limited renal disease. The phenotype of renal and liver anomalies classically varies in inverse proportions.

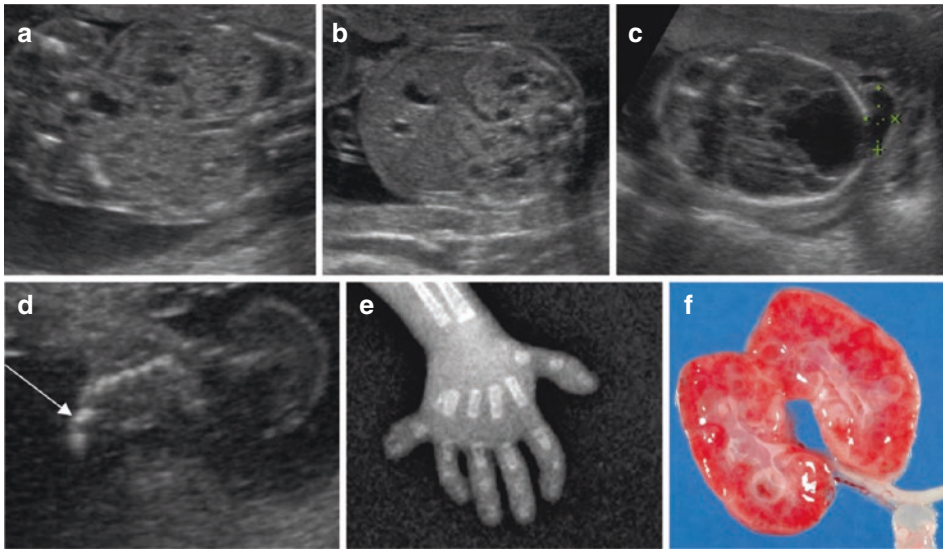
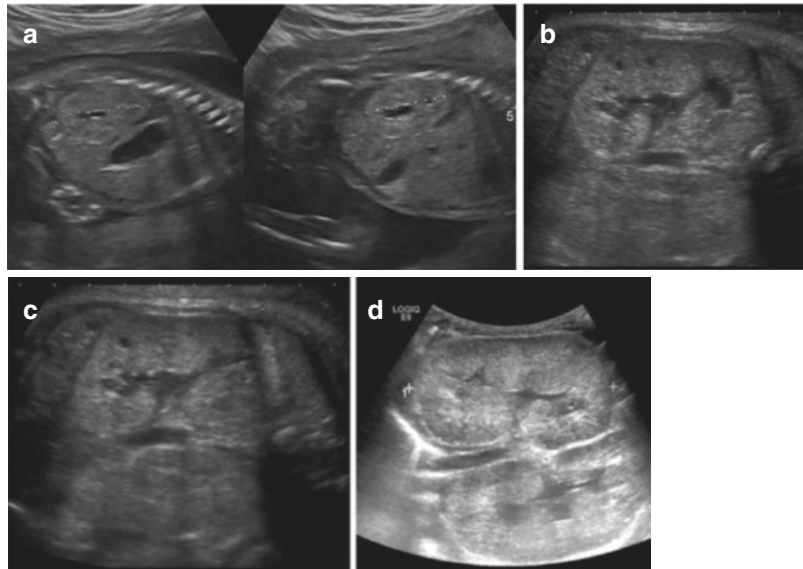


Fig. 4.49 Meckel-Gruber syndrome. US at 17 wg shows large hyperechoic kidneys with medullary cysts (**a**: coronal view, **b**: axial view), an occipital meningocele (between crosses, **c**) and polydactyly (arrow, **d**). (**e**) shows

the corresponding radiograph of the hand and (**f**) shows corresponding macroscopic appearance of the kidney at pathology

Fig. 4.50 ARPKD. At 22 wg (**a**, dual split image), the amniotic fluid volume is normal but US shows hyperechoic kidneys, with a size at the upper limit of normal. At 31 wg (**b**, **c**), there is an oligohydramnios, and the kidneys are large, hyperechoic, and undifferentiated with small cysts. US exam performed at first day of life shows huge hyperechoic kidneys without corticomedullary differentiation (**d**)



Detection of postaxial polydactyly associated with hyperechoic kidneys suggests other ciliopathies: Bardet-Biedl syndrome or related ciliopathies, depending on the causal gene (Fig. 4.52). Prenatal diagnosis of BBS can be tricky because polydactyly is

difficult to detect. Renal cysts and other manifestations of BBS will usually appear after birth. Corticomedullary differentiation helps for the differential diagnosis. It can be increased, decreased, or even inverted (Table 4.7).

Fig. 4.51 ARPKD. US (axial (a) and coronal (b) slices) in another patient at 34 wg with oligohydramnios, shows very large kidneys occupying almost all the foetal abdomen, with typical corticomedullary inversion

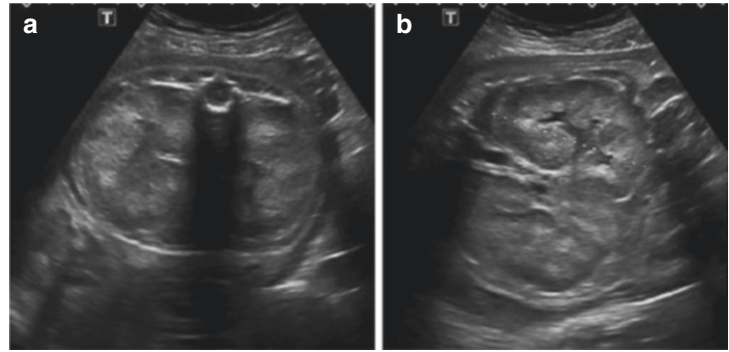


Fig. 4.52 Bardet-Biedl syndrome. US at 28 wg shows hyperechoic undifferentiated kidneys (a, b) associated with post-axial polydactyly of the four limbs (c, d) (arrow)

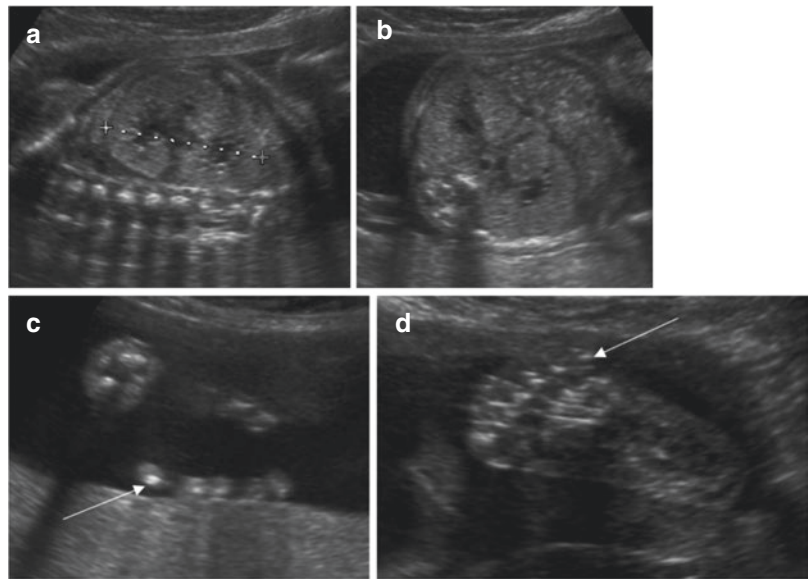


Table 4.7 Abnormal renal corticomedullary differentiation

Increased differentiation	Reduced/absent differentiation	Inversed differentiation
Dominant polycystic renal disease	Dysplasias	Autosomal recessive polycystic disease
HNF 1 beta	Cystic diseases	
CMV	HNF-1 beta	
Ischaemia		
Nephrotic syndrome		
Normal variant		

- Increased corticomedullary differentiation can be observed as a normal variant in an echogenic mother but can also be the first sign for another ciliopathy: *autosomal dominant polycystic kidney disease* (ADPKD).

Autosomal dominant polycystic kidney disease (ADPKD) due to mutation of PKD1 or PKD2 is more prevalent than ARPKD. 10%

occur as de novo mutations. Cysts of variable sizes can occur throughout the nephron. Most affected foetuses will have a normal US. Suggestive prenatal findings include foetal kidneys with cortical hyperechogenicity and normal size or slightly increased size, increased corticomedullary differentiation, and rarely cysts (Fig. 4.53). Amniotic fluid

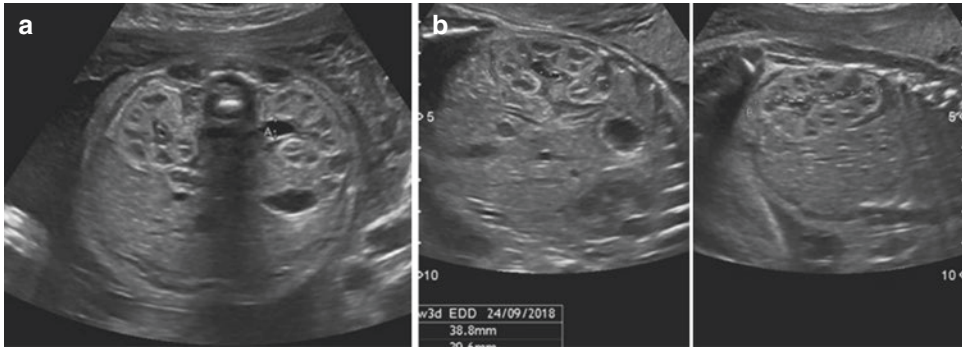


Fig. 4.53 ADPKD. US at 25 wg shows kidneys of normal size but with a hyperechoic cortex and increased corticomedullary differentiation (a: axial, b: parasagittal

slices). US performed in parents detected unknown multiple renal cysts in the father

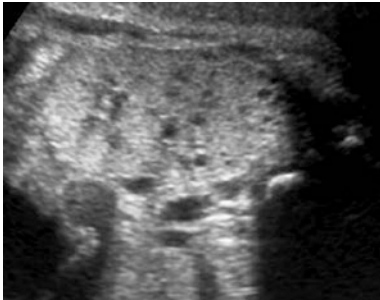


Fig. 4.54 Glomerulocystic form of ADPKD. US at 31 wg shows undifferentiated hyperechoic kidneys with tiny mostly peripheral cysts

volume is usually normal. An isolated cyst can rarely be the first sign of ADPKD detected in utero (usually the cysts will appear later during life). In the rare glomerulocystic form, kidneys are enlarged, without corticomedullary differentiation, and with tiny subcapsular cysts (Fig. 4.54). Performing a kidney US of the parents and grandparents (if the parents are young) is helpful to confirm the diagnosis in the familial forms (sometimes unknown by the parents themselves).

- Transcription Factor 2 mutation (TCF2)/Hepatocyte nuclear factor-1 beta (HNF-1 beta) mutations must always be searched when facing a nephropathy or uropathy. The diagnosis relies on genetic analysis. *HNF-1 beta* mutation is the most common monogenic cause of kidney disease. A wide spectrum of

renal anomalies can be observed in HNF-1 beta mutations such as hyperechoic kidneys, loss of corticomedullary differentiation, subcapsular cysts, renal agenesis or hypoplasia, dysplasia, isolated cyst, dilatation, and multicystic dysplastic kidney (MCDK) (Fig. 4.55). A familial history of diabetes mellitus is frequent. Evocative subcapsular cysts are usually detected after birth. Postnatal US must search for pancreatic and genital anomalies (with this gene being implicated in maturity-onset diabetes of the young—MODY).

- Multiple, sometimes large renal cysts are another sign for nephropathy. Gestational age at detection, number, size, and location of cysts help to precise diagnosis. The most frequent diagnosis is *multicystic dysplastic kidney* (MCDK). Large cysts (more than 10 mm) are rare and suggest possible *tuberous sclerosis*, HNF-1 beta mutation, or rarely ADPKD.

MCDK is one of the most common nephropathies detected in utero [26]. Abnormal interaction between the ureteral bud and the nephrogenic blastema is thought to be responsible for this unfunctional kidney parenchyma. Typically, the diagnosis relies on the detection of cysts of variable sizes without connection between them, without recognisable normal parenchyma and without a central renal pelvis (Fig. 4.56). The

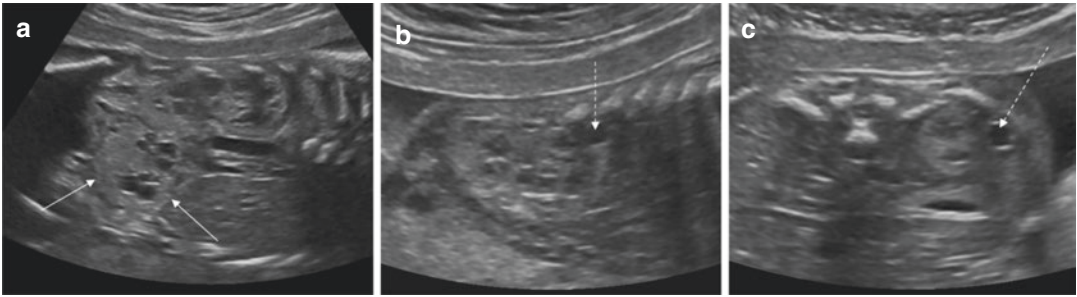
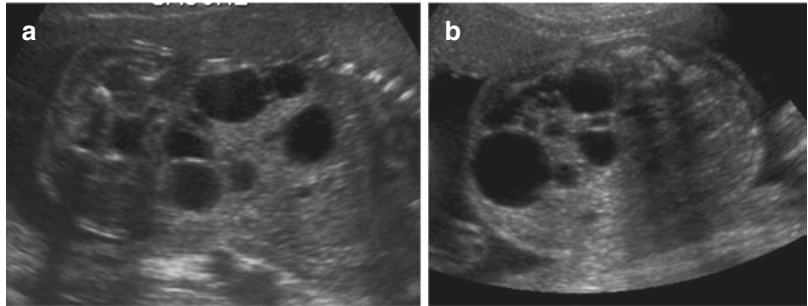


Fig. 4.55 HNF-1 beta mutation. US at 21 wg shows a right ectopic pelvic dysplastic kidney (arrows) (a). The left kidney (b, c) is hyperechoic with a cortical cyst (dotted arrow)

Fig. 4.56 MCDK. US at 22 wg shows a large left MCDK with peripheral not connecting cysts and absence of normal parenchyma (a: coronal slice, b: axial slice). The right kidney and the amniotic fluid were normal



prognosis depends on the contralateral kidney. This malformation can be unilateral, bilateral, or segmental. Bilateral MCDK is invariably associated with end stage renal failure and early oligohydramnios. In 30–40% of unilateral cases, contralateral renal hypertrophy is observed (and thought to be a good prognosis sign). Third trimester follow-up and postnatal work-up including US are recommended in order to detect contralateral anomalies that can be found in up to 30% of cases. MCDK can sometimes reach large proportions. Most MCDK will progressively decrease in size, prenatally or more frequently postnatally. Rarely, some MCDK will continue to grow and resection is then suggested.

The differential diagnosis must be made with an obstructive cystic renal dysplasia, characterised by a hyperechogenic parenchyma eventually associated with cysts, for example in upper pelvic-ureteric junction obstruction or in PUV as well as gross VUR [26].



Nephropathies, detected by abnormal kidney size or appearance (hyperechogenicity, cysts, loss of corticomedullary differentiation), can be isolated, secondary to severe uropathies, or associated with various genetic diseases (the most frequent being ciliopathies and HNF-1 beta mutation). The diagnosis relies on the gestational age, the renal size, the kidney appearance, and the presence or absence of associated anomalies. The prognosis relies on the presumed diagnosis, and amniotic fluid volume.

Most foetuses with ADPKD have normal appearing kidneys on foetal US.

4.3.7 Spinal Cord Anomalies

Detection and characterisation of spinal cord anomalies rely on US. The spinal cord and the conus medullaris are easily depicted by US. Normally, the conus medullaris ends between

L2 and L3 before 24 wg and above L2/3 at the end of gestation. The most useful anatomic landmark to determine the position of the conus medullaris is the first sacral vertebra, which has a posterior angulation on a sagittal scan. Another marker is to look at the last rib, assuming that 12 ribs are present in the foetus.

Due to its lower spatial resolution, MRI is less useful for dysraphisms in utero, except for exploration of foetal brain, in rare circumstances of discordant cranial and spinal US findings, or when foetal surgery is considered.

4.3.7.1 Open Spinal Dysraphisms

These are neonatal surgical emergencies that are easily detected by prenatal screening. Absence of skin covering in open dysraphisms explains the increased level of alpha foetoprotein and acetylcholinesterase in the amniotic fluid. Detection of open dysraphisms relies on cranial and cerebral anomalies. A small posterior fossa, loss of visibility of the cisterna magna, deformation of the cerebellum with posterior convexity (the “banana sign”), and herniation of cerebellar tonsils (Chiari II) are characteristic. Affected foetuses present also with a typical flattening of the frontal bones during second trimester (the “lemon sign”). This sign is absent after birth. Callosal dysgenesis is frequent in open dysraphisms but doesn’t modify prognosis [27]. Prognosis depends on the level of the dysraphism (the lower the better). Ventriculomegaly, malposition of the lower limbs, and amyotrophy are poor prognostic factors [28].

- In myelomeningoceles (MMC), the spinal cord (without recognisable conus medullaris) ends into a meningeal hernia, covered by a thin membrane. The posterior vertebral arches are abnormally oriented (posteriorly everted or parallel) and nerve roots are visible in the meningeal sac (Fig. 4.57).
- In myeloceles (MC), there is no meningeal sac, the neural placode is seen without any skin coverage. Diagnosis relies on axial and sagittal slices showing abnormal orientation of posterior vertebral arches and absence of normal skin (Fig. 4.58).

4.3.7.2 Closed Spinal Dysraphism

By opposition to open spinal dysraphisms, most closed spinal dysraphisms escape prenatal detection: brain and skull are usually normal and the spinal cord is not included in most US screening programmes. In closed spinal dysraphism, there is no Chiari II deformation, and thus the diagnosis relies directly on detection of the spinal malformation. Meningocele, lipomyelomeningocele, or limited dorsal myeloschisis are examples of closed spinal dysraphisms.

- A *meningocele* corresponds to a meningeal hernia, with a liquid content and covered by normal skin. Most cases are thoracic. The spinal cord is normal but can be tethered in a low position. There is no stalk connecting the medulla to the defect (Fig. 4.59).

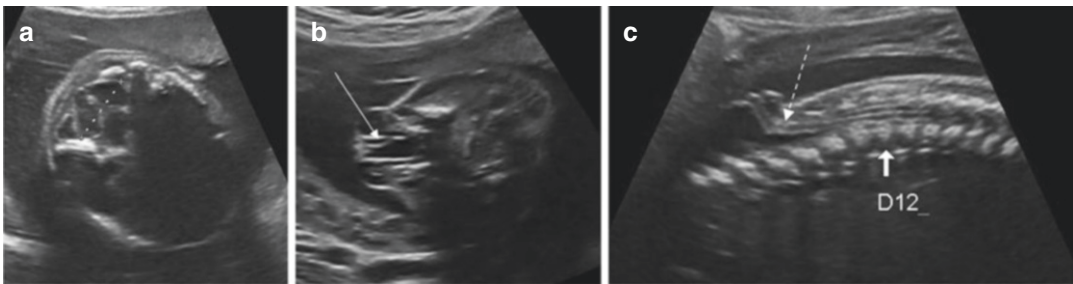


Fig. 4.57 Myelomeningocele. Axial posterior fossa US at 22 wg (a) shows a Chiari II malformation with a small posterior fossa and deformation of the cerebellum (between crosses). Axial (b) and sagittal (c) US spinal

slices demonstrate the open spinal defect. The spinal cord (dotted arrow) ends into a meningeal hernia covered with a thin membrane and containing nervous roots (arrow)



Fig. 4.58 Myelocele. US at 22 wg in a monochorionic twin pregnancy shows a Chiari II malformation (a), a sacral myelocele with the spinal cord opening at the skin, without a meningocele (dotted arrow) (b) and cervicothoracic hydromyelia (arrow in c)

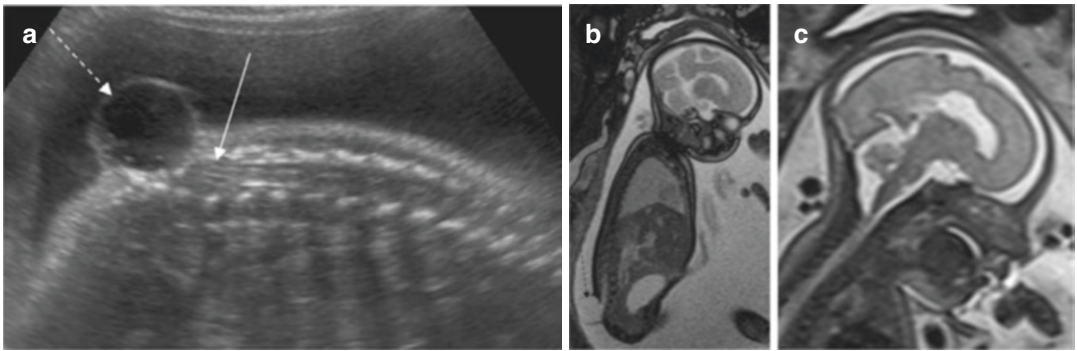


Fig. 4.59 Sacral meningocele. US (a) and MRI (b, c) at 28 wg show a sacral meningocele (dotted arrows) with low lying spinal cord (arrow) but without a Chiari II malformation

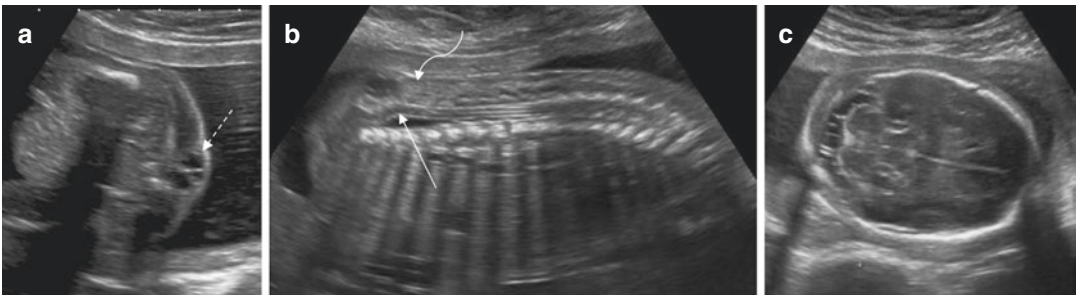



Fig. 4.60 Lipomyelomeningocele. US at 21 wg in a patient with an OEIS sequence (same patient as Fig. 4.43) shows a lumbosacral closed defect with a meningeal sac (a: dotted arrow) and a lipomatous mass (b: curved arrow). The spinal cord is abnormally low without conus medullaris differentiation, and takes an abnormal posterior curve (arrow) (b). The posterior fossa is normal: there is no Chiari II malformation (c)

- Lipomyeloceles and lipomyelomeningoceles are the most frequent closed dysraphisms. These malformations are characterised by a low spinal cord in contact with an intra- and extramedullary lipoma with or without a meningocele (Fig. 4.60). The presence of a subcutaneous heterogenous mass helps the prenatal detection. In opposite to the typical postnatal appearance, most lipomatous contents are not hyperechoic on US before the third trimester. Absence of high signal on T1 weighted sequences is also usually observed on foetal MRI. Detailed US is mandatory to detect

possible associated urogenital malformations and sacral anomalies.

- Limited dorsal myeloschisis (LDM) is a peculiar form of “closed” dysraphism that has been recently defined (Pang et al. 2013; Friszer et al. 2017). It is characterised by the presence of a focal “closed” midline skin defect associated with one fibro-neural stalk that links the skin lesion to the underlying cord. Posterior vertebral arches have usually a normal obliquity in axial US scans. When a posterior spinal mass is observed, there is a relatively thick peripheral lining in continuity with the adjacent normal skin (in myelomeningocele, the peripheral lining is thin). The spinal cord remains in the spinal canal and is visible below the dysraphism (except in sacral malformations), but may look backwardly displaced at the level of the fibro-neural stalk (Fig. 4.61). Usually, there is no Chiari II deformation in LDM, whereas Chiari II is almost always present in MMC or MC. There seems to be no correlation between the level of the LDM and the degree of sensorimotor anomalies. Prognosis is much better than for open dysraphisms.

 Open spinal cord defects are easily detected in utero thanks to the presence of Chiari II anomaly characterised by a small posterior fossa, herniated cerebellar tonsils, and frontal bone flattening in utero (this last sign is not present after birth). The prognosis depends on the level of the defect and the presence of associated anomalies (with the exception of callosal anomalies, frequent and that don't modify the prognosis).

The detection of closed spinal dysraphisms relies on detailed examination of the spinal cord. Since there is no Chiari II malformation, most closed spinal dysraphisms escape prenatal detection.

4.3.8 Musculoskeletal Anomalies with Perinatal Implications

It is beyond the scope of this chapter to describe all dysostosis and bone dysplasias. Readers are referred to more detailed articles and textbooks. This chapter will concentrate on some musculoskeletal anomalies that can be difficult to detect, tricky to manage, or be a sign for a more complex anomaly.

Diagnosis relies on US. MRI is indicated to search for associated anomalies such as brain malformations. CT can rarely be indicated after a multidisciplinary discussion. It can be useful in some cases of complex dysplasia not sufficiently characterisable by US or in some exceptional situations.

4.3.8.1 Segmental Vertebral Anomalies

Three vertebral ossification centers are normally present per vertebra except for atlas and the sacral vertebrae. Ossification of S1 is visible at 15 wg, of S4 at 21 wg and usually five sacral ossified vertebral centres are visible after 26 wg. The coccyx ossifies after birth. Normal ossifications centres have a regular appearance and follow a smooth alignment. The only normal fixed curvature in a foetus is the sacral lordosis. Irregular vertebral ossification centres and other fixed spinal curves are abnormal.

Diagnosis relies on US. Segmental vertebral anomalies can be isolated, associated with spinal dysraphism or VACTERL association, and rarely with some dysplasias (Fig. 4.62).

Detailed US is mandatory to precise the type and extent of the vertebral anomaly, and the presence of associated medullary or spine malformation (dysraphism, diastematomyelia). The prognosis depends on the type and extent of the anomaly, on the degree of spinal deformation and presence of dysraphism or associated anomalies. The presence of spinal dysraphism will then dictate prognosis (see above).

- The VACTERL association includes vertebral, anorectal, cardiac, tracheoesophageal, renal, and limb malformations. An isolated segmental vertebral anomaly can be the emerged part of the iceberg. Anal imperforation, some forms of oesophageal atresia and some cardiac malfor-

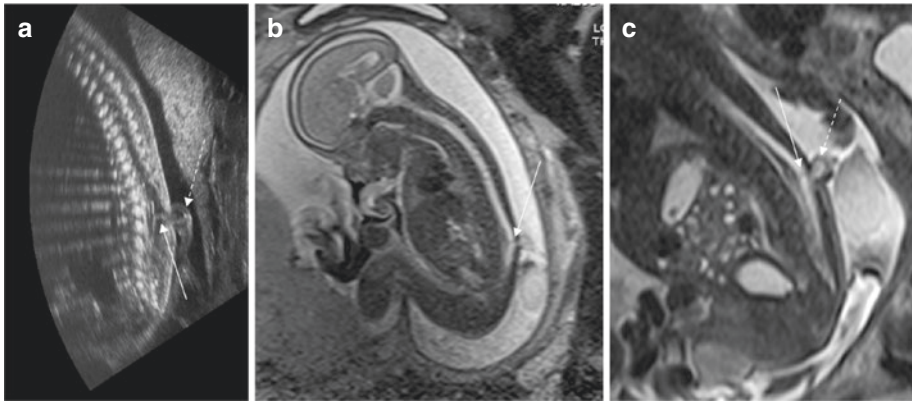
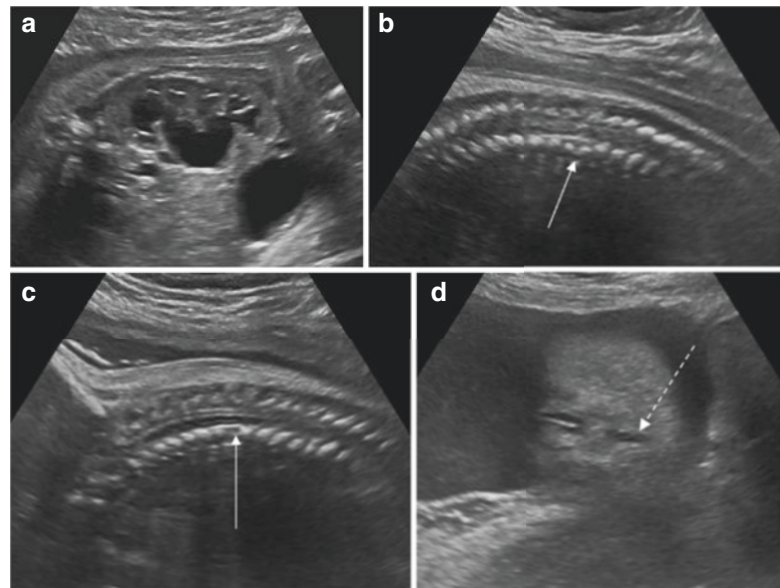


Fig. 4.61 LDM. Sagittal US and T2 MRI at 24 wg (a, b) and sagittal T2 MRI at 31 wg (c) show a closed spinal defect with a midline skin defect (dotted arrow) associ-

ated with a thick fibro-neural stalk (arrow). The spinal cord is visible below the dysraphism and there is no Chiari II malformation

Fig. 4.62 VACTERL association. US at 31 wg shows pyelocaliceal dilatation (a). Discrete segmental vertebral anomalies are detected in the upper and lower thoracic spine (arrows in b and c). There is no visualisation of the anal sphincter suggesting an anal imperforation (confirmed after birth) (dotted arrow in d)



mation can be too subtle to detect but will impact prognosis and perinatal management.

Thus the detection of segmental vertebral anomalies implies to promptly perform a detailed US study, a foetal echocardiography, genetic counselling, and sometimes a multi-disciplinary support.

4.3.8.2 Skeletal Dysplasias

Skeletal dysplasias are a complex heterogeneous group of more than 400 different cartilage and bone growth diseases. Most severe bone dysplasias are detected during second trimester US

screening. Specific prenatal diagnosis is possible in 40–60% of cases with prenatal imaging and genetic analysis. In most series, the four most frequent prenatal diagnoses correspond to three lethal diseases (type 2 osteogenesis imperfecta, thanatophoric dysplasia, achondrogenesis) and achondroplasia. This last disease is not lethal, and usually detected after the second trimester of gestation. Detailed US analysis and sometimes prenatal CT scan precise the differential diagnosis to some categories and allow a more specific genetic analysis. A definite diagnosis is sometimes only possible after birth.

Prenatal imaging is excellent for evaluation of disease severity. Lethality is usually due to lung hypoplasia. More than 80% of bone dysplasia detected during first trimester US are lethal if an increased nuchal translucency is detected. At least 50% of bone dysplasias detected during second trimester US screening are lethal due to the associated lung hypoplasia. Less severe diseases completely escape second trimester US detection.

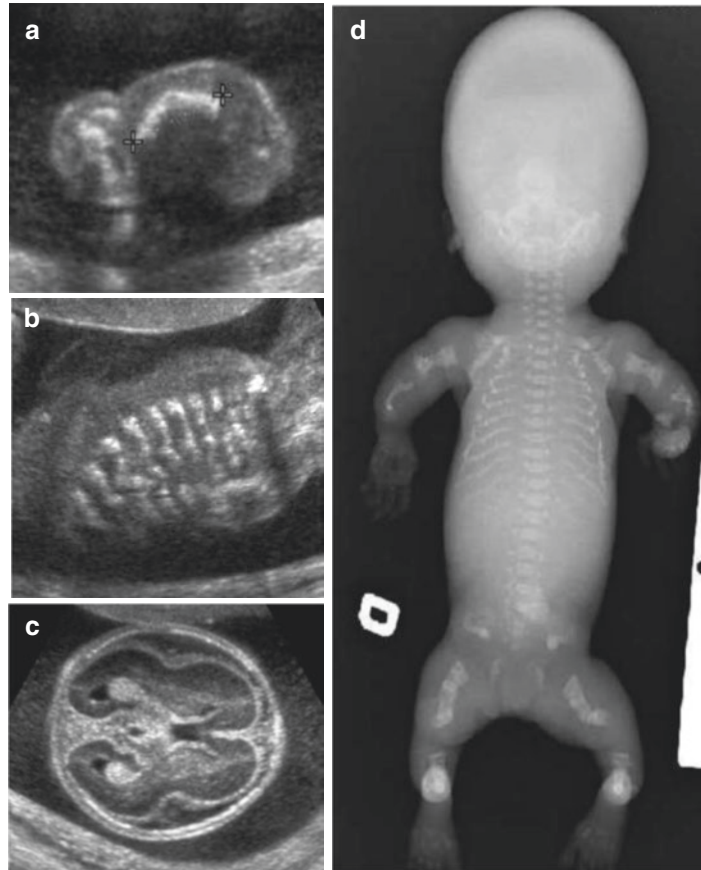
- *Osteogenesis imperfecta (OI)*

This is a heterogeneous group of bone diseases characterised by abnormal collagen formation. Different genes are implicated in this group of diseases. Phenotype is variable, depending on the gene affected and bone fragility. Severe cases of OI are lethal due to lung hypoplasia associated with multiple ribs fractures. Prenatal diagnosis allows detection of the most severe cases presenting with bone demineralisation and fractures

(Fig. 4.63). Prognosis is more difficult to establish in intermediate cases presenting with long bones fractures but no apparent ribs fractures.

- *Achondroplasia and hypochondroplasia* are among the most prevalent living bone dysplasias. Achondroplasia is inherited as an autosomal dominant trait; nevertheless, most cases occur after spontaneous neomutation. Second trimester US is usually completely normal and diagnosis will be performed later. Characteristic rhizomelic micromelia can be detected at the end of the second trimester or more frequently during the third trimester US. Femoral length growth is always abnormal after 27 wg. Abnormal morphology of the proximal femur (abnormal metaphysis and increased metaphyseal-diaphyseal angle), macrocephaly with frontal bossing, accentuation of a saddle nose, trident hands (separation of third and fourth digits), platyspondyly, and

Fig. 4.63 Osteogenesis imperfecta type 2a. US at 22 wg detects short multiple fractured and angulated bones (femur in **a**), multiple ribs fractures (**b**) and abnormal increased visibility of the foetal brain due to skull undermineralisation (**c**). X-ray of the foetus shows demineralisation and multiple fractures (**d**)



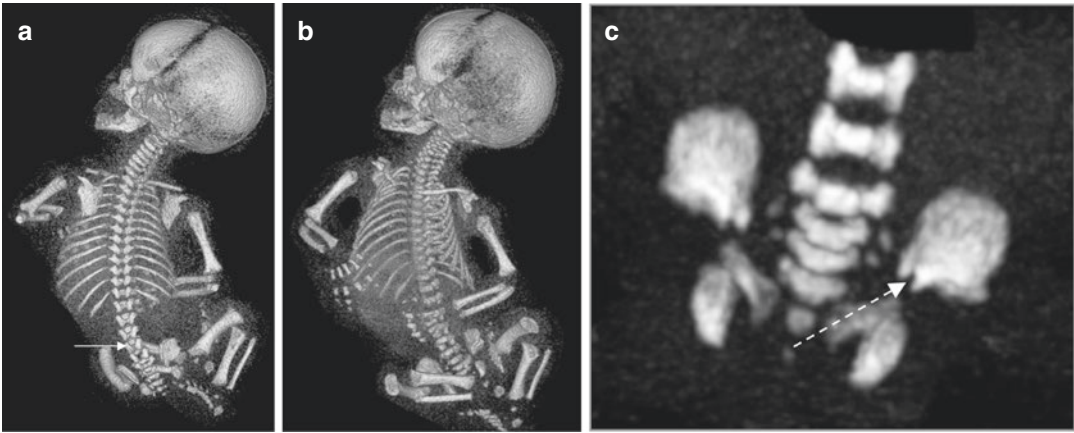



Fig. 4.64 Achondroplasia. CT scan performed at 32 wg shows frontal bossing (**a, b**), progressive diminution of the interpedicular distance in the lumbar spine (arrow in **a**), and sciatic notches (dotted arrow in **c**)

an abnormal pelvis with squared iliac wings and small ischiatic notches are typical signs of achondroplasia. Prenatal diagnosis is easy during third trimester due to typical US findings. In some cases, CT scan can allow confirmation of the diagnosis (Fig. 4.64).

Prenatal diagnosis of hypochondroplasia relies on subtler signs and is more difficult.

 The presence of segmental vertebral anomalies can be the emerged part of a serious disease such as VACTERL association, and implies a detailed US foetal examination.

Skeletal dysplasias represent a large heterogeneous group of multiple diseases with variable prognosis. The most severe diseases are detected during the first and second trimesters of gestation. Prenatal imaging excels for evaluation of disease severity but is less performant for precise diagnosis in non-lethal diseases. Achondroplasia, one of the most frequent skeletal dysplasia, is usually missed during second trimester US. Achondroplasia is usually detected after 27 wg when the shortening of the femur and associated findings are evident.

4.3.9 Brain Anomalies: Limitations of Prenatal Imaging

US and MRI are complementary modalities for foetal brain imaging. US has better spatial resolution while MRI has better contrast resolution. Advantages of US are depiction of hydrocephaly, of calcifications, and a better corpus callosum analysis. MRI allows a complete evaluation of the entire cerebral parenchyma (absence of cranial vault shadowing as present on US), enables a proper evaluation of the cortex (greater contrast resolution), and provides a better analysis of several structures such as the olfactive and optic tracts, the pituitary, the internal ear, and the brainstem. The clinical impact of MRI depends on the quality of the previous neuro-US and on the gestational age; generally speaking, foetal MRI provides more important information during the third trimester in relation to the brain maturation.

Indications for foetal MRI include the confirmation of an equivocal US finding, the search for a precise diagnosis, the determination of the prognosis of brain anomalies, and the routine evaluation of the brain in the presence of risk factors (see Table 4.1). Nevertheless, this always has to be seen with respect to prognostic or management implications.

The goal of this chapter is not to review exhaustively the semiology of all brain anomalies, but to expose some limitations of prena-

tal imaging for the depiction of certain brain anomalies. Discordance between pre- and postnatal imaging with a significant prognostic impact has been observed in about 9% of cases [29].

4.3.9.1 Midline Anomalies

- The diagnosis of *corpus callosum (CC) dysgenesis* is based on direct (i.e. non-visualisation of the CC) and indirect signs (i.e. an abnormal cavum septum pellucidum, parallel lateral ventricles, a large inter hemispheric fissure, an abnormal pericallosal artery, and a radial pattern of the sulci of the internal aspect of the hemispheres). It is difficult prenatally to distinguish between a complete CC agenesis and a partial/near complete CC agenesis. The final diagnosis is often made postnatally.

When facing a CC dysgenesis, the role of imaging, particularly MRI, is to identify associated cerebral anomalies indicating that the anomaly is probably part of a genetic, metabolic, or infectious process, with a usually poor outcome (Fig. 4.65).

However, certain associated malformations such as *interhemispheric cysts* or the less frequent *pericallosal lipoma* have a very good prognosis, with a normal neurodevelopmental outcome [30]. The classic hyperechogenicity on US or the T1 hyperintensity on MRI seen in fatty tissue is not always seen prenatally, probably related to fat maturation within the lipoma and subse-

quently to gestational age. Accordingly, the identification of a pericallosal lipoma can be hazardous in a foetus and the absence of pericallosal T1 hypersignal should not exclude the diagnosis of such a lipoma. Note that knowledge of this limitation impacts parent counselling.

- Absence of visualisation of the septum on US suggests a possible *septal agenesis* or secondary destruction of the septum. Septal agenesis (SA) is evoked when the cavum septum pellucidum is not seen, in association with the identification of squared fused frontal horns and low-set fornix (Fig. 4.66).
- Presence of *schizencephaly* suggests a possible clastic aetiology. SA can also be isolated, or rarely be part of a syndromic frame, such as *septo-optic dysplasia (SOP)*, which has a wide phenotypic range. The prenatal recognition of SOP is challenging because optic pathways are very thin structures, difficult to evaluate properly with US or MRI. The pituitary gland and stalk are visible on MRI, but subtle anomalies can be overlooked [8]. Therefore, counselling a couple whose foetus presents with an apparently isolated SA remains difficult and it is often impossible to precise the prognosis prior to birth.

4.3.9.2 Posterior Fossa Malformations

Posterior fossa anomalies include mega cisterna magna, arachnoid cysts, Blake's pouch cysts (BPC), and Dandy-Walker malformations (DWM). It is paramount to distinguish those two

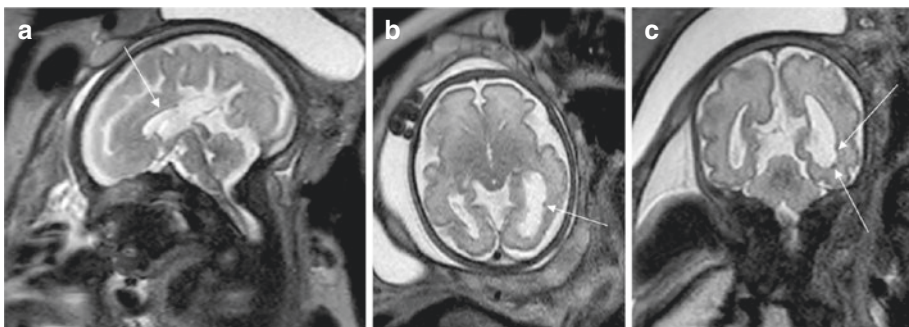


Fig. 4.65 Partial corpus callosum (CC) agenesis associated with subependymal heterotopias. MRI at 32 wg confirms a short CC in sagittal slice (arrow in **a**) and detects subependymal heterotopia (arrows in **b** and **c**)

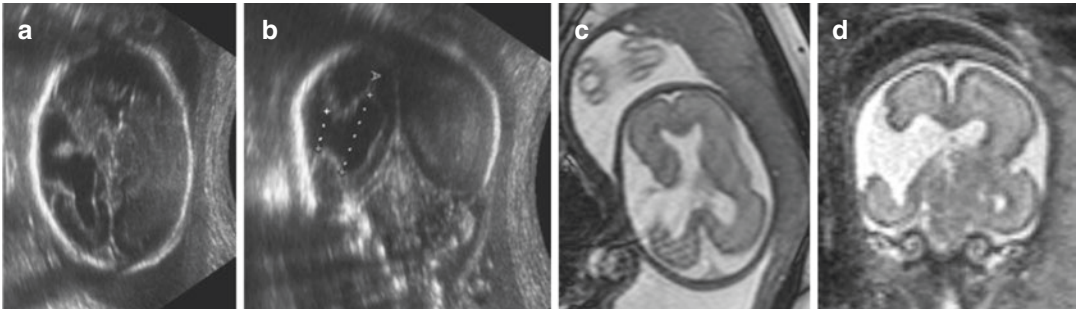


Fig. 4.66 Absence of septum pellucidum and schizencephaly. The patient was referred for ventriculomegaly at 24 wg. US detected absence of septum pellucidum and

open lip schizencephaly (**a, b**). MRI confirmed the US findings (**c, d**: correlation between US and MR findings). Autopsy was denied

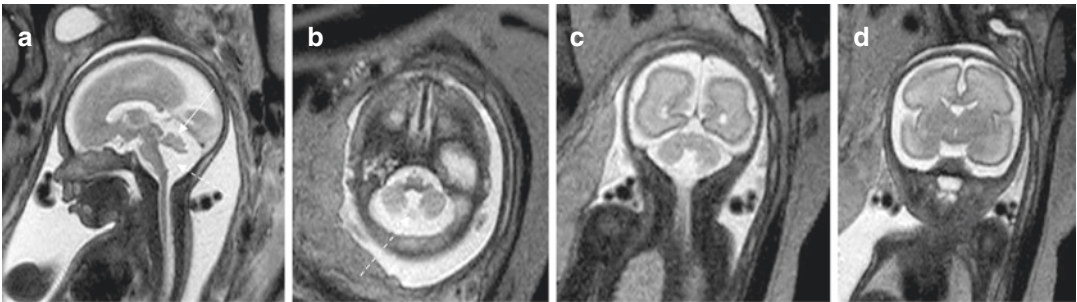


Fig. 4.67 Blake pouch cyst. MRI performed at 27 wg in a foetus with “enlarged fourth ventricle” demonstrates a shifted normal vermis (arrow in a) in enlarged fluid spaces

of the posterior fossa (dotted arrow **a, b**). There is no ventricular dilatation (**c, d**)

latter entities before birth because their prognosis is very different.

- In the BPC, the vermis is normal and the prognosis is excellent, with a high probability of resolution in utero and a normal intellectual development in almost all cases [31] (Fig. 4.67).
- In a DWM, the vermis is dysgenetic, and the prognosis more dismal, with a high risk of chromosomal and associated structural anomalies, even when the DWM appears isolated on US (D’Antonio et al. 2016) (Fig. 4.68).
- On imaging, the fourth ventricle is open and the tentorium insertion is elevated in both entities. Thus, making the correct diagnosis can be a challenge, especially when the pouch is large and the mass effect on the vermis is important. In those cases, when it is impossi-

ble to correctly analyse the vermian morphology with US and MRI, the prenatal counselling is limited [32].

4.3.9.3 Ventricular Dilatation

Ventriculomegaly is defined as a transversal diameter of the ventricular atrium larger than 10 mm. Foetally, it is graded depending on the degree of dilatation: mild (less than 12 mm), moderate (13–15 mm), or severe (more than 15 mm). Ventriculomegaly is only a sign, and prognosis depends on the severity, the cause, and the associated anomalies. Therefore, a detailed US, a search for infection and karyotypic anomalies, an MRI, and follow-up examinations are mandatory (Fig. 4.69).

A limitation can be the variability in measuring the ventricles, when the measurement technique is not standardised, especially when serial

Fig. 4.68 Dandy-Walker malformation. Sagittal (a) and coronal (b) MRI performed at 29 wg shows a small dysgenetic vermis upward displaced (arrow) in a large posterior fossa with upward displacement of the tentorium insertion (dotted arrow in a) and bilateral ventricular dilatation

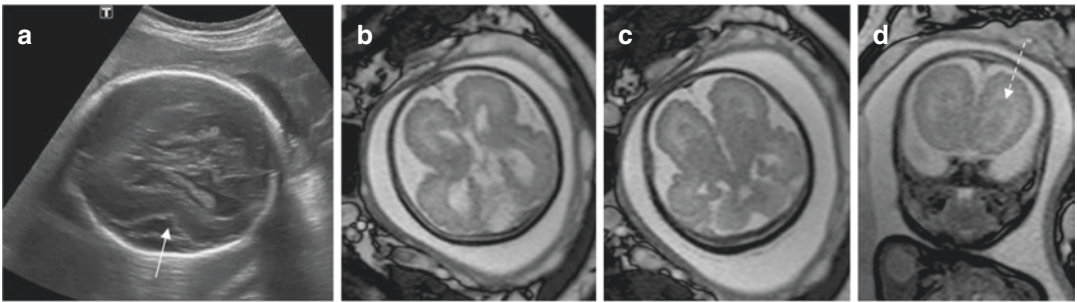
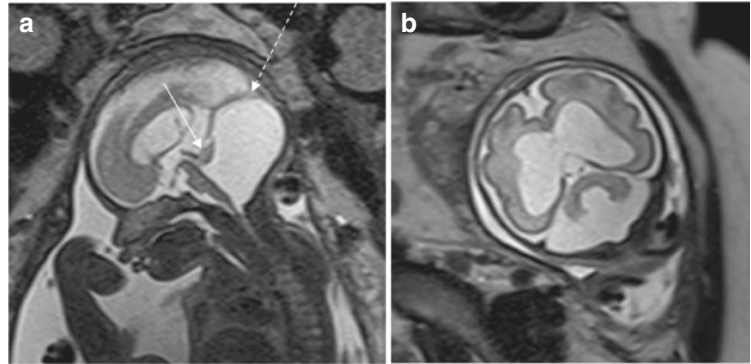


Fig. 4.69 Zellweger syndrome. A patient referred for ventriculomegaly (atria 11–12 mm) and polyhydramnios. US (a) shows abnormal Sylvian fissure (arrow). MRI (b–

d) demonstrates diffuse abnormal gyration with abnormal Sylvian fissures, diffuse polymicrogyria, thickened cortex, and laminar heterotopia (dotted arrow in d)

examinations are performed by different operators. This can lead to overdiagnosis of mild ventriculomegaly justifying invasive procedures such as foetal karyotyping and generating parental anxiety. To overcome this problem, we suggest following the method outlined by Guibaud [33].

4.3.9.4 Malformations of Cortical Development

Due to its higher contrast resolution, MRI is superior to US for cortical analysis using a thin hypointense signal on T2 sequences representing the cortical ribbon.


- Polymicrogyria (PMG), defined as abnormal arrangement and excessive folding of cerebral cortical cell layers, can be secondary to various aetiologies (ischaemic, infectious, genetic) and is displayed as a scalloped and

thick cortex at pathology. This diagnosis is easily missed on prenatal MR, due to its low spatial resolution (Fig. 4.69).

- Similarly, subependymal heterotopias are difficult to recognise in utero (Fig. 4.65). This limitation has a clinical impact, overlooking severe conditions, for example Aicardi Syndrome (agenesis of the corpus callosum, arachnoid cyst, PMG, subependymal heterotopia, microcephaly in a female foetus).

4.3.9.5 White Matter Anomalies

During the third trimester, there is a physiological high T2 signal on MRI of the subcortical white matter, particularly at the level of the temporal lobes. Therefore, making the diagnosis of a white matter anomaly prenatally is difficult, and such a diagnosis is often only possible postnatally.

 US and MRI complement one another in the imaging of the foetal brain with the better spatial resolution of US and the better contrast resolution of MRI. Foetal MRI is indicated if it can modify the diagnosis, prognosis, or the management of the pregnancy. In numerous situations (e.g. in case of midline anomalies, ventricular dilatation, microcephaly, etc.), MRI brings useful complementary information modifying the prognosis. However, the performances of prenatal imaging remain lower than what can be obtained after birth. Some brain anomalies, such as heterotopias, micropolygyria, etc., escape to prenatal diagnosis. The counselling must always take into account this limitation.

4.4 Conclusion

Prenatal imaging relies essentially on two complementary imaging modalities: US and MRI.

Today, it is possible to detect and characterise most significant congenital anomalies already in a foetus which allows for optimising pre- and perinatal management. However, limitations of prenatal imaging must be acknowledged by the team taking care of the foetus and the neonate.

References

- Carvalho JS, Allan LD, Chaoui R, et al. ISUOG practice guidelines (updated): sonographic screening examination of the fetal heart. *Ultrasound Obstet Gynecol.* 2013;41:348–59.
- Cargill Y, Morin L, et al. Content of a complete routine second trimester obstetrical ultrasound examination and report. SOGC clinical practice guideline No 223. *J Obstet Gynaecol Can.* 2009;31(3):272–5.
- Whitworth M, Bricker L, Mullan C. Ultrasound for fetal assessment in early pregnancy. *Cochrane Database Syst Rev.* 2015;(7):CD007058. <https://doi.org/10.1002/14651858.CD007058.pub3>.
- Carvalho JS. Antenatal diagnosis of critical congenital heart disease. Optimal place of delivery is where appropriate care can be delivered. *Arch Dis Child.* 2016;101(6):505–7.
- Holland BJ, Meyers JA, Woods CR Jr. Prenatal diagnosis of critical congenital heart disease reduces risk of death from cardiovascular compromise prior to planned neonatal cardiac surgery: a meta-analysis. *Ultrasound Obstet Gynecol.* 2015;45:631–8.
- Karim JN, Roberts NW, Salomon LJ, Papageorghiu AT. Systematic review of first-trimester ultrasound screening for detection of fetal structural anomalies and factors that affect screening performance. *Ultrasound Obstet Gynecol.* 2017;50(4):429–41.
- Rypens F, Dubois J, Garel L, et al. Obstetric US: watch the fetal hands. *Radiographics.* 2006;26(3):811–29.
- Blondiaux E, Garel C. Fetal cerebral imaging—ultrasound vs. MRI: an update. *Acta Radiol.* 2013;54(9):1046–54.
- Victoria T, Epelman M, Coleman BG, et al. Low-dose fetal CT in the prenatal evaluation of skeletal dysplasias and other severe skeletal abnormalities. *AJR.* 2013;200:989–1000.
- Adler-Levy Y, Yagel S, Nadjori M, et al. Use of low dose computed tomography with 3D reconstructions for the prenatal evaluation of suspected skeletal dysplasia. *Isr Med Assoc J.* 2015;17(1):42–6.
- Jani JC, Peralta CFA, Nicolaides KH. Lung-to-head ratio: a need to unify the technique. *Ultrasound Obstet Gynecol.* 2012;39:2–6.
- Rypens F, Metens T, Rocourt N, et al. Fetal lung volume: estimation at MR imaging—initial results. *Radiology.* 2001;219:236–41.
- Langston C. New concepts in the pathology of congenital lung malformations. *Semin Pediatr Surg.* 2003;12(1):17–37.
- Stanton M, Njere I, Ade-Ajayi N, et al. Systematic review and meta-analysis of the postnatal management of congenital cystic lung lesions. *J Pediatr Surg.* 2009;44(5):1027–33.
- Hellmund A, Berg C, Geipel A, et al. Prenatal diagnosis and evaluation of sonographic predictors for intervention and adverse outcome in congenital pulmonary airway malformation. *PLoS One.* 2016;11(3):e0150474. <https://doi.org/10.1371/journal.pone.0150474>.
- Sun HY. Prenatal diagnosis of congenital heart defects: echocardiography. *Transl Pediatr.* 2021;10(8):2210–24.
- Familiari A, Morlando M, Khalil A, et al. Risk factors for coarctation of the aorta on prenatal ultrasound. A systematic review and meta-analysis. *Circulation.* 2017;135:772–85.
- Fricke K, Liuba P, Weismann CG. Fetal echocardiographic dimension indices: important predictors of postnatal coarctation. *Pediatr Cardiol.* 2021;42:517–25.
- D’Antonio F, Virgone C, Rizzo G, et al. Prenatal risk factors and outcomes in gastroschisis: a meta-analysis. *Pediatrics.* 2015;136(1):e159–69.

20. Parulekar SG. Sonography of normal fetal bowel. *J Ultrasound Med.* 1991;10(4):211–20.
21. Lap CC, Voskuilen CS, Pistorius LR, et al. Reference curves for the normal fetal small bowel and colon diameters: their usefulness in fetuses with suspected dilated bowel. *J Matern Fetal Neonatal Med.* 2020;33(4):633–8.
22. Lesieur E, Barrois M, Bourdon M, et al. Megacystis in the first trimester of pregnancy: prognostic factors and perinatal outcomes. *PLoS One.* 2021;16(9):e0255890.
23. Maizels M, Alpert SA, Houston JTB, et al. Fetal bladder sagittal length: a simple monitor to assess normal and enlarged fetal bladder size and forecast clinical outcome. *J Urol.* 2004;172(5 Pt 1):1995–9.
24. McHugo J, Whittle M. Enlarged fetal bladders: etiology, management and outcome. *Prenatal Diagn.* 2001;21:958–63.
25. Garel J, Blondiaux E, Della Valle V, et al. The perineal midsagittal view in male fetuses—pivotal for assessing genitourinary disorders. *Pediatr Radiol.* 2020;50(4):575–82.
26. Meyers ML, Treece AL, Brown BP, Vemulakonda VM. Imaging of fetal cystic kidney disease: multicystic dysplastic kidney versus renal cystic dysplasia. *Pediatr Radiol.* 2020;50(13):1921–33.
27. Maurice P, et al. New insights in cerebral findings associated with fetal myelo-meningocele: a retrospective cohort study in a single tertiary centre. *BJOG.* 2021;128(2):376–83.
28. Gotha L, Pruthi V, Abbasi N, et al. Fetal spina bifida: what we tell the parents. *Prenat Diagn.* 2020;40:1499–507.
29. Dhoub A, Blondiaux E, Moutard ML, et al. Correlation between pre- and post-natal cerebral magnetic resonance imaging. *Ultrasound Obstet Gynecol.* 2011;38:170–8.
30. Garel C, Moutard ML. Main congenital cerebral anomalies; how prenatal imaging aids counselling. *Fetal Diagn Ther.* 2014;35(4):229–39.
31. Gandolfi CG, Contro E, Carletti A, et al. Prenatal diagnosis and outcome of fetal posterior fossa fluid collections. *Ultrasound Obstet Gynecol.* 2012;39(6):625–31.
32. Guibaud L, Larroque A, Ville D, et al. Prenatal diagnosis of “isolated” Dandy walker malformation: imaging findings and prenatal counselling. *Prenat Diagn.* 2012;32:185–93.
33. Guibaud L. Fetal cerebral ventricular measurement and ventriculomegaly: time for procedure standardization. *Ultrasound Obstet Gynecol.* 2009;34:127–30.
- Cassart M, Massez A, Cos T, et al. Contribution of three-dimensional computed tomography in the assessment of fetal skeletal dysplasias. *US Obstet Gynecol.* 2007;29(5):537–43.
- Chabra S, Peterson SE, Cheng EY. Development of a prenatal clinical care pathway for uncomplicated gastroschisis and literature review. *J Neonatal Perinatal Med.* 2021;14(1):75–83.
- Chougar L, Blondiaux E, Moutard ML, et al. Variability of T1-weighted signal intensity of pericallosal lipomas in the fetus. *Pediatr Radiol.* 2018;48(3):383–91.
- Cook J, Chitty LS, De Coppi P, et al. The natural history of prenatal diagnosed congenital cystic lung lesions: long-term follow-up of 119 cases. *Arch Dis Child.* 2017;102(9):798–803.
- D’Antonio F, Khalil A, Garel C, et al. Systematic review and meta-analysis of isolated posterior fossa malformations on prenatal ultrasound imaging (part 1): nomenclature, diagnostic accuracy and associated anomalies. *Ultrasound Obstet Gynecol.* 2016;47(6):690–7.
- Deprest JA, Benachi A, Gratacos E, et al. Randomized trial of fetal surgery for moderate left diaphragmatic hernia. *N Engl J Med.* 2021a;385:119–29.
- Deprest JA, Nicolaides KH, Benachi A, et al. Randomized trial of fetal surgery for severe left diaphragmatic hernia. *N Engl J Med.* 2021b;385:107–18.
- Devriendt A, Cassart M, Massez A, et al. Fetal kidneys: additional sonographic criteria of normal development. *Prenat Diagn.* 2013;33(13):1248–52.
- Dubois J, Alison M. Vascular anomalies: what a radiologist needs to know. *Pediatr Radiol.* 2010;40:318–26.
- Ethun CG, Fallon SC, Cassady CI, et al. Fetal MRI improves diagnostic accuracy in patients referred to a fetal center for suspected esophageal atresia. *J Pediatr Surg.* 2014;49(5):712–5.
- EUROCAT. European network of population-based registries for the epidemiological surveillance of congenital anomalies. 2022.
- Friszer S, Dhombres F, Morel B, et al. Limited dorsal myeloschisis: a diagnostic pitfall in the prenatal ultrasound of fetal dysraphism. *Fetal Diagn Ther.* 2017;41(2):136–44.
- GFMER. Obstetrics and gynecology guidelines/prenatal ultrasound. 2022.
- Gimpel C, Avni FE, Bergmann C, et al. Perinatal diagnosis, management, and follow-up of cystic renal diseases: a clinical practice recommendation with systematic literature review. *JAMA Pediatr.* 2018;172(1):74–86.
- American College of Obstetricians and Gynecologists. Guidelines for diagnosis imaging during pregnancy and lactation. Committee opinion N 723. *Obstet Gynecol.* 2017;130:e210–6.
- Hall JG. Arthrogryposis (multiple congenital contractures): diagnostic approach to etiology, classification, genetics, and general principles. *Eur J Med Genet.* 2014;57:464–72.
- Hall CM, Offiah AC, Forzano F, et al. Fetal and perinatal skeletal dysplasias. London: Radcliffe Publishing Ltd.; 2012.

Further Reading

AIUM practice parameter for the performance of fetal echocardiography. *J Ultrasound Med.* 2020;39(1):E5–E16. <https://doi.org/10.1002/jum.15188>.

- Hochart V, Verpillat P, Langlois C, et al. The contribution of fetal MR imaging to the assessment of esophageal atresia. *Eur Radiol.* 2015;25(2):306–14.
- Kane SC, Ancona E, Reidy K, et al. The utility of the congenital pulmonary airway malformation-volume ratio in the assessment of fetal echogenic lung lesions: a systematic review. *Fetal Diagn Ther.* 2020;47:171–81.
- Nguyen HT, Benson CB, Bromley B, et al. Multidisciplinary consensus on the classification of prenatal and postnatal urinary tract dilation (UTD classification system). *J Pediatr Urol.* 2014;10:982–99.
- Pang D, Zovickian J, Wong S-T, et al. Limited dorsal myeloschisis: a not-so-rare form of primary neurulation defect. *Childs Nerv Syst.* 2013;29:1459–84.
- Pardy C, D'Antonio F, Khalil A, et al. Prenatal detection of esophageal atresia: a systematic review and meta-analysis. *Acta Obstet Gynecol Scand.* 2019;98:689–99.
- Russo FM, Cordier A-G, De Catte L, et al. Proposal for standardized prenatal ultrasound assessment of the fetus with congenital diaphragmatic hernia by the European reference network on rare inherited and congenital anomalies (ERNICA). *Prenat Diagn.* 2018;38:629–37.
- Salomon LJ, Alfirevic Z, Bilardo CM, et al. ISUOG practice guidelines: performances of first-trimester ultrasound scan. *Ultrasound Obstet Gynecol.* 2013;41:102–13.
- Salomon LJ, Alfirevic Z, Berghella V, et al. Practice guidelines for performance of the routine mid-trimester fetal ultrasound scan. ISUOG guidelines. *Ultrasound Obstet Gynecol.* 2010; <https://doi.org/10.1002/uog.8831>.
- Tenisch E, Raboisson M-J, Rypens F, et al. Significance of lung anomalies in fetuses affected by tetralogy of Fallot with absent pulmonary valve syndrome. *Cardiol Young.* 2017;27(9):1740–7.
- Tessier A, Sarreau M, Pelluard F, et al. Fraser syndrome features suggestive of prenatal diagnosis in a review of 38 cases. *Prenat Diagn.* 2016;36(13):1270–5.
- Van Nesselrooij AEL, Teunissen AKK, Clur SA, et al. Why are congenital heart defects being missed? *Ultrasound Obstet Gynecol.* 2020;55:747–57.
- Van Velzen CL, Ket JCF, Van de Ven PM, et al. Systematic review and meta-analysis of the performance of second-trimester screening for prenatal detection of congenital heart defects. *Int J Gynecol Obstet.* 2018;140(2):137–45.



Postnatal Imaging in Babies with Prenatal Diagnosed Malformations or Conditions

5

Michael Riccabona

5.1 Introduction

The advent of prenatal imaging brought a huge change in peri- and postnatal care and outcome, but also in foetal management. One of the consequences is that pregnancies with fetuses who suffer from severe malformations that are known to be incompatible with life are recognised early and the pregnancy is terminated. Thus, some conditions are now far less frequently seen in neonatology (e.g. severe diaphragmatic hernia with too little lung parenchyma for postnatal survival, large myelomeningoceles, severe brain malformations). This also explains why many of those conditions that were diagnosed neonatally some decades ago and were part of the spectrum of what neonatologists needed to know are today hardly encountered any more by neonatologist and paediatricians and thus they are less and less knowledgeable in this field (e.g. various skeletal dysplasias and syndromes).

On the other hand, knowledge of a foetal/congenital condition influences management not only during pregnancy, but also of birth itself, and the postnatal handling and treatment.

The task of postnatal imaging in these babies is to confirm the prenatal suspicion or diagnosis, to grade the severity and assess the extent of the

condition or defect, and then to monitor treatment, possible complications and the further development. Furthermore, imaging is essential to search for possible additional associated malformations that have not been recognised prenatally. The role of paediatric radiology is to help select the proper method applicable to the request, to consider radiation protection issues in terms of the ALARA principle, and to propose the best timing for the least burdensome investigation capable of answering the therapeutically or prognostically relevant questions. And of course, to provide high quality imaging enabling a reliable imaging diagnosis and offering all necessary information for treatment and management decisions. This requires having sufficient clinical knowledge (particularly of the therapeutic implications and needs), technical expertise and adequate equipment, and a good relationship and communication with the referring clinician.

5.2 Imaging Approach in Foetally Diagnosed Malformations and Conditions: What to Do When, and Who and Why?

To properly decide on the best, most suitable, reliable and least burdensome investigation, a thorough knowledge of embryology is a prerequisite. Furthermore, foetal imaging findings should be known prior to any postnatal

M. Riccabona (✉)
Medical University Graz, Graz, Austria
e-mail: michael.riccabona@medunigraz.at

investigation; a fact that still often is a problem at birth when urgent decisions have to be taken—e.g. when the place where birth is taking place is not the hospital where the prenatal investigations have been performed, or by incompatibility of PACS or IT systems of different hospitals, departments or environments. There are three major questions: when to do the examination, which kind of investigation is necessary and is it now or later (sometimes a first necessary imaging study will have to be complemented by further studies afterwards, e.g. after stabilisation of the patient), and who is needed to perform the study to ensure a reliable and useful diagnosis that provides all necessary information for decision making, treatment and management. And remember, with some prenatally recognised findings no or at least no urgent imaging is required—particularly a burdening a study should never be done just for pacifying anxious parents, relatives, or colleagues.

5.2.1 When to Do

The decision on *when to do* the exam depends on the clinical stability of the neonate and how urgent the respective information is needed—if at all.

- Sometimes, an urgent surgery is performed just based on a radiograph and/or the clinical presentation, and the imaging work-up will then be done afterwards.
- Other conditions in clinically stable and not endangered patients will be more thoroughly assessed before imaging or treatment decisions are taken.
- One also needs to consider maturity of organs and systems—for example, assessment of a foetal urinary tract dilatation may be useless if done too early, as there is little urine production because of the physiologic renal immaturity and transition from foetal to postnatal life (and thus the renal collecting system may be collapsed in spite of an existing problem, which might be missed in such an examination on the first days of life). On the other

hand, if there is the suspicion, e.g. of a posterior urethral valve, imaging is performed in the first 24–48 h to prevent possible further renal function deterioration by securing unhindered urine drainage if necessary.

- And there are cases where the detailed imaging work-up is postponed, e.g. until immediately pre-operative—such as in a sequestration which initially is confirmed (usually by chest radiograph and US), whereas the CT(A) or MR(A) for complete assessment is done close to the planned surgery. Or in other small prenatally detected lung lesions which have been stable during foetal life and are not visible on radiographs or US at birth and the baby does not show any symptoms, a final work-up by usually a CT is delayed until 6–12 months of life.

5.2.2 What to Do: Which Kind of Imaging Is Needed?

The question *what to do* depends on the query, and on which modality is capable to sufficiently answer the clinically relevant questions; always the investigation least burdensome to the baby should be preferred. It also depends on the availability of a modality and the respective local expertise. Thus, if prenatally a malformation is depicted that will need expert peri- and postnatal management, the mother should be transferred to a dedicated centre for giving birth to ensure adequate perinatal management and also imaging and management/treatment after birth.

5.2.3 Who Should Perform the Examinations?

Imaging should be done by a knowledgeable person trained in performing and reading the examination—usually this is the paediatric radiologist or for echocardiography the paediatric cardiologist, although experienced paediatricians, paediatric surgeons and neonatologists can often also answer the acutely relevant respective questions

which often is the case in more remote locations or in after duty hours.

- Additionally, one needs to decide if a thorough investigation is needed, or, e.g. a “sonoscope” in terms of an orienting point-of-care US (POCUS) for a first impression is sufficient.

Finally—after the initial reassessment—confirmation and grading of the finding or follow-up examinations will be necessary to monitor for improvement or progression, but unless there are rapidly evolving or deteriorating conditions or a complication such as in a high-pressure hydrocephalus or severe bilateral urinary tract obstruction impairing renal function these follow-up studies are often done after the neonatal period.

5.3 Imaging in Foetally Diagnosed Malformations and Conditions: Examples

So, in the light of above detailed general considerations, let’s briefly address the most common conditions and queries individually—more details can then be found in the respective dedicated chapters. The foetal imaging (mostly by US and MRI) with its potential and restrictions is described in the chapter on foetal imaging, also addressing some suggestions of peri- and postnatal requirements.

5.3.1 Hydrocephalus and Brain Malformations

Brain US (with Doppler and transtemporal approach) is the first approach postnatally to confirm the suspicion, supplemented by MRI (usually a feed and wrap technique avoiding deep sedation is sufficient for these queries in the first months of life). Often this is postponed to a later moment (e.g. preoperatively or to allow the brain to mature and thus to be able to give a definite diagnosis) and thus not addressed here; some more considerations are discussed in Chap. 9 on neuro-MRI (Fig. 5.1).

5.3.2 Spinal (Cord) Malformations and Associated Findings

The spinal canal can be beautifully imaged by US in the first weeks (as long as good access to the spinal canal is granted before ossification hinders a diagnostically safe assessment) (Fig. 5.2); sometimes MRI is done to supplement US.

An open myelomeningocele, however, usually is imaged only after surgical closure—except for the work-up of associated findings (e.g. in the urinary tract by US, osseous spinal pathology by spine radiographs) or secondary hydrocephalus/brain malformation (usually examined also by brain US, sometimes complemented by delayed MRI).

5.3.3 Congenital Pulmonary Airway Malformation (CPAM) and Sequestration or Other Congenital Lung Conditions (e.g. Congenital Lobar Emphysema, Bronchogenic Cyst...)

Today, most or many, but not all of these conditions are picked up by prenatal imaging. Initially, mostly an early chest radiograph and an US of the chest and abdomen (“torsogram”) are performed, supplemented by MRI or CT—if unclear or preoperatively (Fig. 5.3).

5.3.4 Diaphragmatic Hernia and Oesophageal Atresia

Most of these are detected prenatally in the developed world, not so in countries with as yet poorly developed health care systems or restricted access to these services. Chest and abdominal radiographs and US of the chest and abdomen, possibly with filling the stomach via gastric tube with tea or saline (e.g. for evaluating a sliding hiatal hernia) are usually sufficient for management decisions (Fig. 5.4). Sometimes, in complex conditions (e.g. if associated with a sequestration) a CTA or MRA may become necessary (Fig. 5.4).

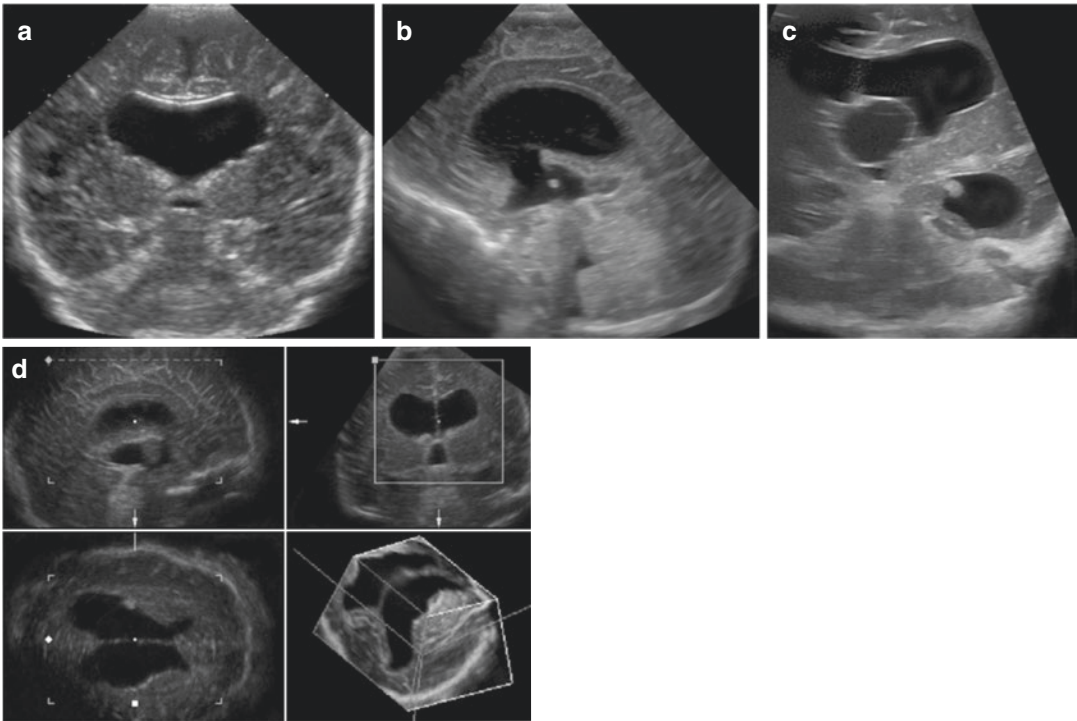


Fig. 5.1 US in congenital hydrocephalus. (a) Coronal transfontanellar view of a neonate with antenatally suspected holoprosencephaly demonstrates the dilated and atypically shaped lateral ventricles and the missing septum making it a single ventricle. (b) Sagittal section through the open fontanel in a neonatal supraventricular hydrocephalus. The dilated huge third ventricle can easily be recognised, with a disproportionately small fourth ven-

tricle. (c) Hydrocephalus due to a cystic mass compromising the foramen of Monro and causing asymmetric dilatation of the lateral ventricles. (d) Three-dimensional US can be used to conspicuously visualise the anatomy of a hydrocephalus, in this example applying a multi-axial display. The left lower box from a different neonate utilises the “box view” display

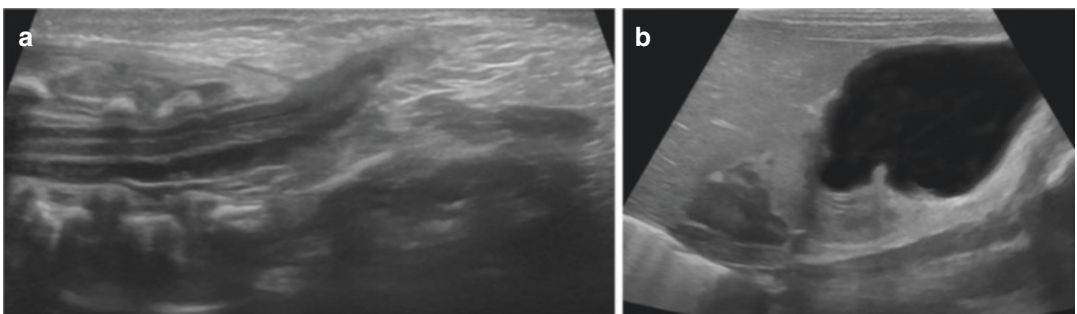


Fig. 5.2 Spinal cord pathology and associated findings. (a) Spinal cord US in a newborn with covered lipomeningocele: Note the deep ending cord attached to a small sacral lipoma causing tethering of the cord (sagittal US

from dorsal). (b) Same child—additional significant pelvic/cecal distention and a hypertrophic adrenal gland is seen

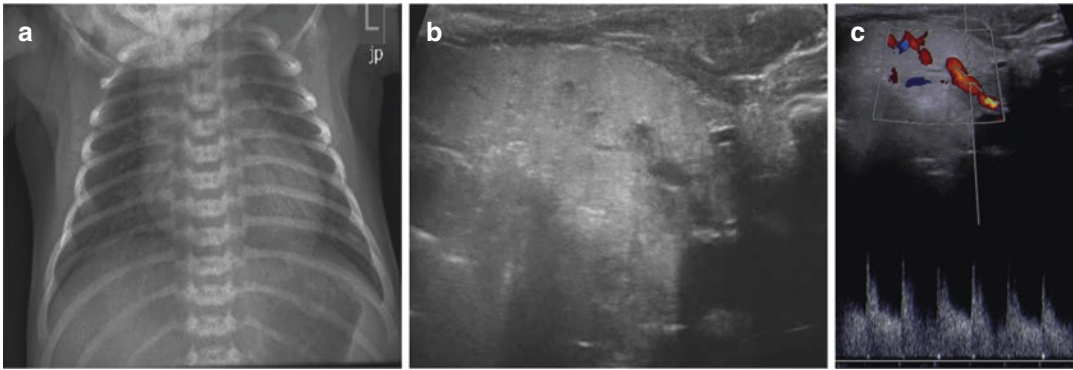


Fig. 5.3 Chest radiograph and US in pulmonary sequestration. (a) Neonatal chest radiograph: There is a subtle basal opacity on the left side adjacent to the spine. (b) Chest US using a dorsal approach (high-resolution linear transducer): an echogenic unaerated sequestration with

some cyst-like areas representing large vessels is depicted. (c) Colour Doppler sonography shows flow signals in those “cysts”, and the spectral trace confirms the arterial flow pattern of the feeding artery deriving from the thoracic aorta

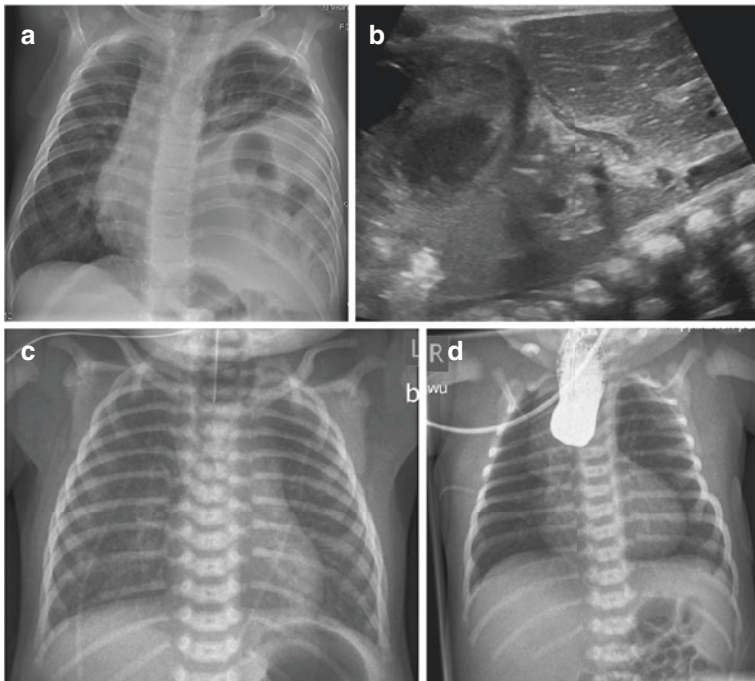


Fig. 5.4 Imaging in diaphragmatic hernia and oesophageal atresia. (a) Chest radiographs in a neonate with diaphragmatic hernia showing the deviated heart and mediastinum due to the gas filled bowel loops and abdominal organs herniated into the left hemithorax. In this slightly older baby with only few clinical symptoms, the right lung is normal and a nicely ventilated left upper lobe is seen. (b) Ultrasound (oblique sagittal-coronal section on the left side) demonstrates the diaphragmatic defect and the liver reaching up into the left hemithorax; additionally, partially collapsed bowel loops can be seen above

the remnants of the diaphragm. (c, d) Chest radiograph after birth in a neonate with foetally suspected oesophageal atresia: the gastric tube cannot be advanced and ends in the upper chest level, but air is seen in the stomach and bowel loops indicating a distal tracheo-oesophageal fistula. To better delineate the proximal oesophageal pouch and length or to confirm the diagnosis, contrast can be instilled via the gastric tube (d), however, this is only rarely necessary and implies the risk of contrast aspiration

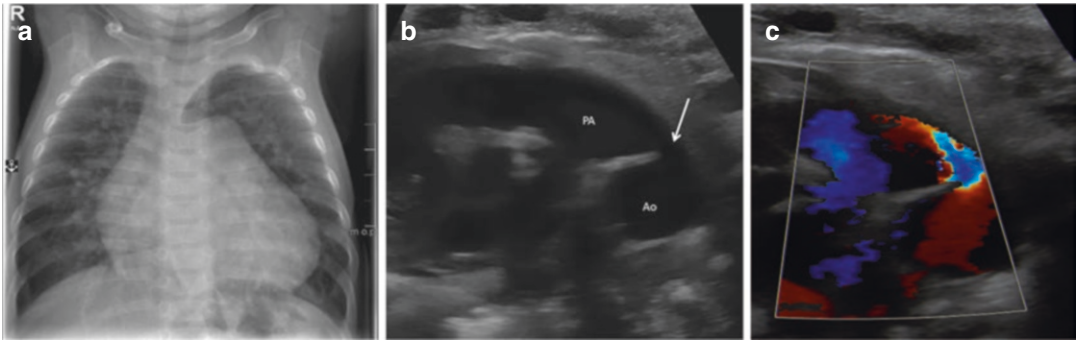


Fig. 5.5 Chest radiograph in congenital cardiac malformation. (a) Chest radiograph in a 1-month-old neonate with a decompensated large ventricular septal defect: enlarged heart with large pulmonary vessels due to pulmonary hyperperfusion because of large recirculation volume and reactive hyperinflation; also note the small and irregular

aortic shadow! (b, c) Ultrasound shows a large PDA (arrow) in a preterm neonate (b) and CDS confirms the left to right shunt with a turbulent and rapid flow pattern (c). *Abbreviations: PA pulmonary artery, Ao aorta, PDA persisting ductus arteriosus*

5.3.5 Congenital Heart Disease and Malformations

Chest radiographs and echocardiography, and if necessary (also for functional evaluation, pressure measurements, etc.) cardiac catheter angiography are done in such suspicions—although by far not all these malformations are picked up prenatally. The work-up of associated malformations or syndromic conditions usually is achieved using US, supplemented by radiographs or MRI in the individual case; in severe and complex conditions a cardiac MRI/MRA or even CT/CTA may become necessary (Fig. 5.5).

5.3.6 Urinary Tract Dilatation and Malformations

This is a very common prenatal finding, and often parents are very anxious—even in low grade dilatation of the urinary tract with low probability of a severe condition. Imaging may be seen as some kind of reassurance service after birth, particularly in mild or nearly normal findings. These leads to generous indications for postnatal (US) imaging. Several approaches have been undertaken to improve and streamline postnatal imaging making it more efficient—however, up to now these efforts have not significantly decreased the number of

rather unnecessary early studies or solved this problem, in part probably also for medico-legal issues, in part for economic reasons.

Depending on the severity of the foetal findings, an early or delayed US of the urinary tract and abdomen (possibly also the spinal canal) is performed guiding subsequent imaging by, e.g. contrast-enhanced voiding urosonography or voiding cystourethrography, or/and scintigraphy and/or MRU (usually postponed because of the initial physiologic renal immaturity). Severe and particularly bilateral foetal findings (dilatation, dysplasia or cystic disease), urinary ascites or the suspicion of a posterior urethral valve indicate an early assessment in the first 24–48 h after birth. Other conditions often do not benefit from early studies which may even cause confusion (underestimation of dilatation due to perinatal abdominal pressure emptying the collecting system and the physiologic renal immaturity as well as little urine production in the first days of life).

If associated with lung hypoplasia, chest radiographs will become necessary, as well as skeletal radiographs in case of a complex syndrome with bony involvement (e.g. bladder exstrophy, part of a systemic malformation syndrome...) (Fig. 5.6).

For foetally suspected cystic kidney disease, US will usually suffice in the neonatal age.

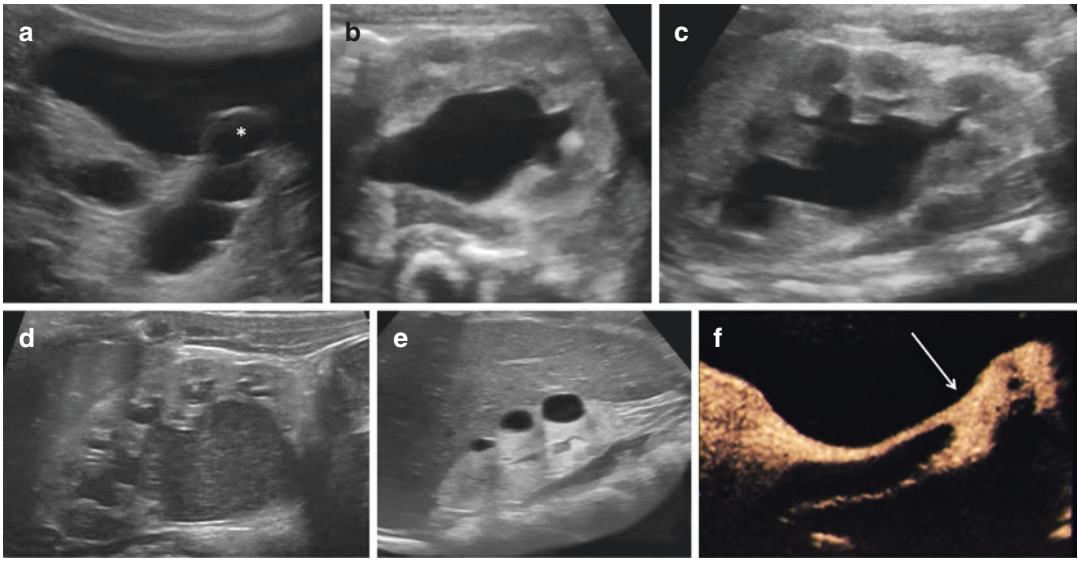


Fig. 5.6 US in congenital urinary tract dilatation (UTD) and other congenital renal abnormalities. **(a)** Ultrasound, axial view of the pelvis in a neonate with history of prenatally diagnosed megaureter: an ureterocele protruding into the urinary bladder is depicted on the left side (asterisk), with the corresponding megaureter. The other cystic retrovesical structure is the ovary with a small follicular cyst. **(b)** Axial flank US view of left kidney in a neonate with prenatally diagnosed pelvicalyceal dilatation: note the dilated central collecting system with preserved cortico-medullary differentiation of the relatively normal renal parenchyma. **(c)** Coronal flank US view of left kidney in a neonate with prenatally diagnosed pelvicalyceal dilatation: The dilated collecting system is depicted, but with still relatively normal shape of the fornices and papillae and only some minor thinning of the preserved and normal appearing renal parenchyma. **(d)** Coronal flank US

view of left kidney in a neonate with prenatally diagnosed pelvicalyceal dilatation: echoes in the dilated central collecting system are shown—this can be seen in infection, but in this case is due to clearing of the neonatally physiological deposits of the distal medullae into the collecting system. **(e)** Coronal US view of a small echogenic kidney with reduced cortico-medullary differentiation and several cortical (dysplastic) renal cysts. Prenatally this had been confused with neonatal “hydronephrosis” or a high grade obstruction may have been the reason for developing an obstructive cystic dysplasia. **(f)** Urogenital sinus (distal connection between vagina and urethra in adrenogenital syndrome/congenital adrenal hypertrophy) depicted by a perineal contrast-enhanced US (sagittal section, during voiding—arrow), with only subtle contrast reflux into the vagina

5.3.7 Atresia/Obstruction/Stenosis of the Gastrointestinal (GI) Tract

These conditions may more easily be missed prenatally—sometimes only postnatally the suspicion arises based on clinical symptoms. The urgency of imaging depends on the underlying condition—usually (as a rule of the thumb) higher atresias/stenoses are more urgent than lower abnormalities. Chest and abdominal radiographs (torsograms) as well as US (using filling techniques such as the “hydro-colon”, possibly with diluted US contrast

agents) and fluoroscopy (upper GI-studies such as barium meals, follow-through, contrast enema) may be necessary for the complete imaging work-up (Fig. 5.7).

5.3.8 Limb Deformity and Malformation or Fracture, Skeletal Dysplasias, Small Parts and Miscellaneous Other Queries

These congenital malformations may be detected prenatally—often as part of a syndrome, some isolated;

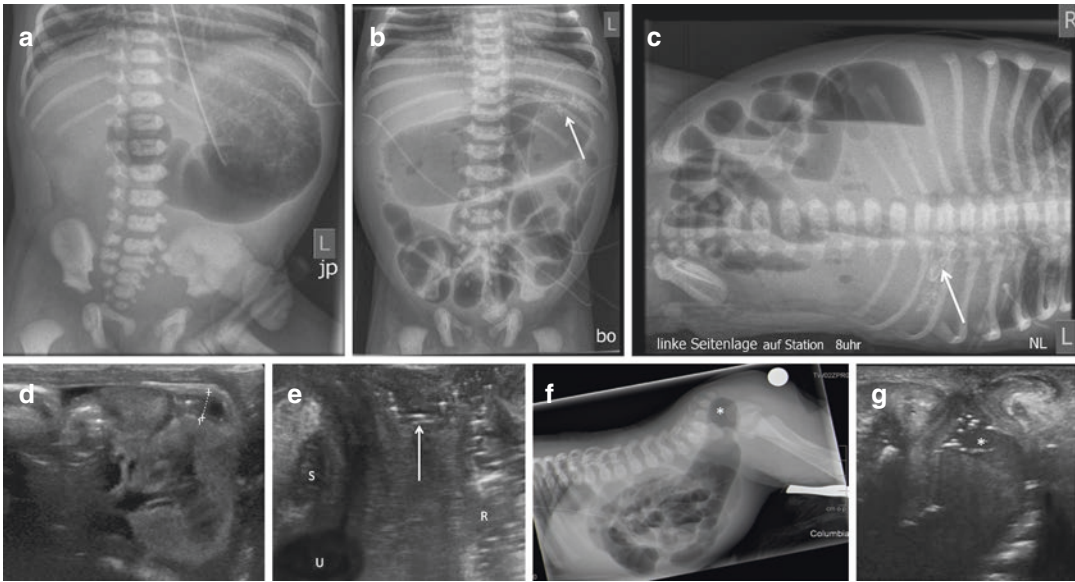


Fig. 5.7 Congenital gastrointestinal tract obstruction: radiograph, US and fluoroscopy. **(a)** Abdominal radiograph in a neonate with (foetally) suspected upper GI obstruction taken soon after birth: Double bubble in duodenal atresia. **(b, c)** Ileal atresia/high grade stenosis with intrauterine perforation and meconium peritonitis depicted by intra-abdominal calcifications (arrow). The air-fluid level in the lateral decubitus projection demonstrates the (secondary?) ileus **(c)**. **(d)** Small left colon in neonate with distal small bowel atresia after hydrocolon (saline enema under US guidance)—the non-distensible, fluid-filled small left colon is demonstrated (+...+). **(e)** Anorectal malformation: an anovaginal “vestibular” fis-

tula seen on a sagittally oriented perineal US as air bubbles connecting the vaginal vestibulum and the rectum (arrow)—the narrow appearing rectum appears patent (S = symphysis, U = urinary bladder, R = rectum). **(f)** Columbia radiograph (bottom-up cross-table view with metallic marker on anal dimple) in anal atresia: note the relatively long distance between the air-filled rectal pouch (asterisk) and the marker. **(g)** Same neonate as in **(f)**—perineal US: fluid-filled rectal pouch (asterisk) reaching much deeper than the air on the respective radiograph, making it a low anal atresia and not (as suspected on the radiograph) an intermediate or high anorectal malformation, with respective therapeutic implications

some fractures may also occur during birth. Radiographs of the affected limb, supplemented by US (e.g. for cartilaginous components) usually suffice—complemented by the respective work-up of the underlying condition or syndrome (Fig. 5.8). However, there are conditions which—though congenital—are only recognised after birth, such as neonatal Graves’ disease. Some congenital small parts pathology may be missed by prenatal diagnostics and recognised only postnatally, then initiating imaging (Fig. 5.9).

5.3.9 Congenital Tumourous Conditions

There are several such conditions (e.g. cystic masses/“lymphangioma” or teratomas anywhere

in the body) and a differential diagnosis of suspected masses. Although many of these masses are seen prenatally, the specificity of prenatal imaging is rather low except for some entities (such as a typical sacrococcygeal teratoma or a lymphatic malformation). Usually, an early US investigation is the first step—complemented by radiographs and MRI (rarely CT), particularly if doubtful or to visualise the entire extent, for staging, or preoperatively (Fig. 5.10). Note that a prenatally suspected tumour may be something else such as adrenal gland haemorrhage, a haemorrhagic ovarian cyst, a gastrointestinal duplication and not a neuroblastoma or a teratoma, or a large renal cyst/cystic tumour may turn out to be a dilated upper moiety system of a duplex kidney.

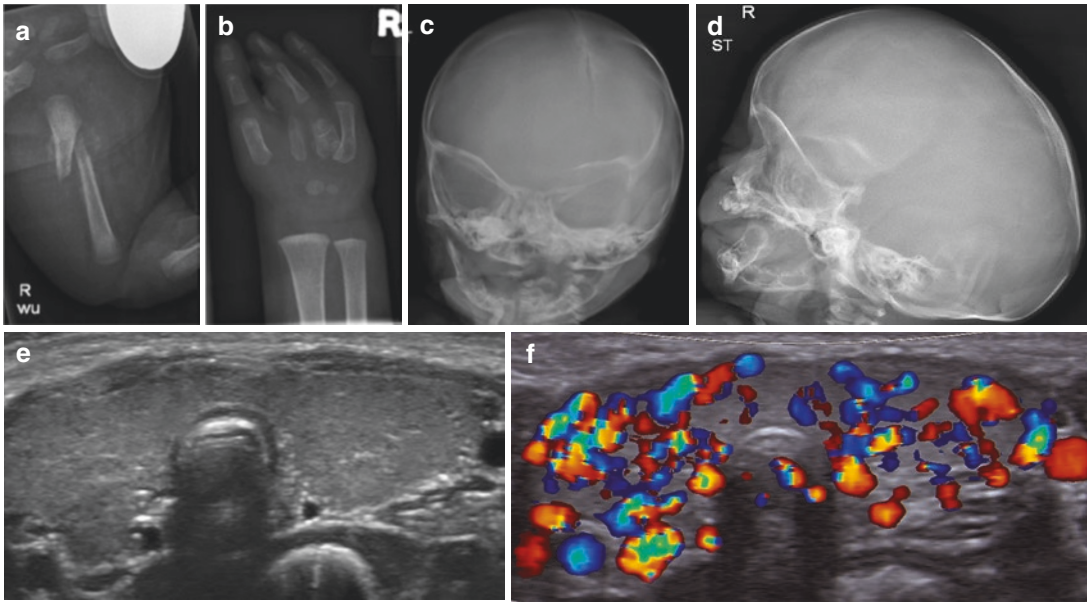


Fig. 5.8 Fracture, malformation and small parts queries: radiograph and US. (a) A neonate with a swollen leg, also avoiding leg movements: radiograph reveals a femur fracture with dislocation and shortening as well as a large, partially calcified periosteal haematoma indicating that the fracture is slightly older. (b) Prenatally suspected hand malformation (missing fingers)—the radiograph to assess the osseous structures was delayed to allow for some ossi-

fication. (c, d) Atypical shape of the head on prenatal scans—the radiographs taken on day 16 of this premature infant demonstrates premature cranial synostosis. Note the rotated projection to allow for proper visualisation of the sutures. (e, f) Neonatal congenital hyperthyroidism/Graves' disease: symmetrically and diffusely enlarged thyroid gland (e) with diffuse hypervascularity (“vascular inferno”) on CDS (f)

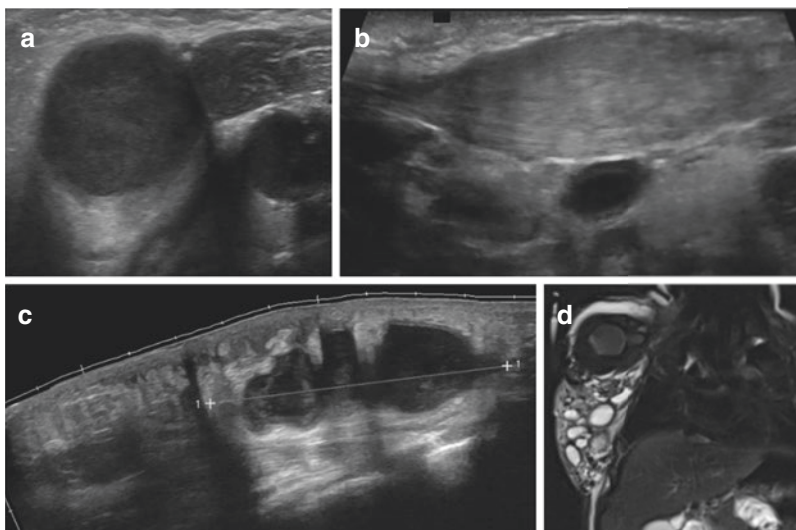


Fig. 5.9 Imaging in congenital small part conditions. (a, b) Cystic neck mass suspected on prenatal scans and obvious on clinical inspection after birth—US reveals a lateral cervical brachial cleft cyst (a). As a differential diagnosis of an asymmetric neonatal neck mass fibromatosis of the sternocleidomastoid muscle needs to be considered, with the typical clinical history, delayed manifestation and on US a muscular swelling in continuity with the muscle borders (b). (c) Coronal US of the chest wall, extended/panorama view: a large multicystic mass is depicted in the

subcutaneous soft tissue (+...+) with some internal echoes, indicating haemorrhage into this lymphatic malformation that was already known from prenatal imaging. (d) Coronal T2 weighted MRI of the chest confirming the prenatally recognised “cystic lymphangioma” of the chest wall done for better visualisation of the extent and possible penetration of the mass, much more conspicuously achieved than on the previous US study shown in (c). For more information on these and similar entities also see Chaps. 14 and 16

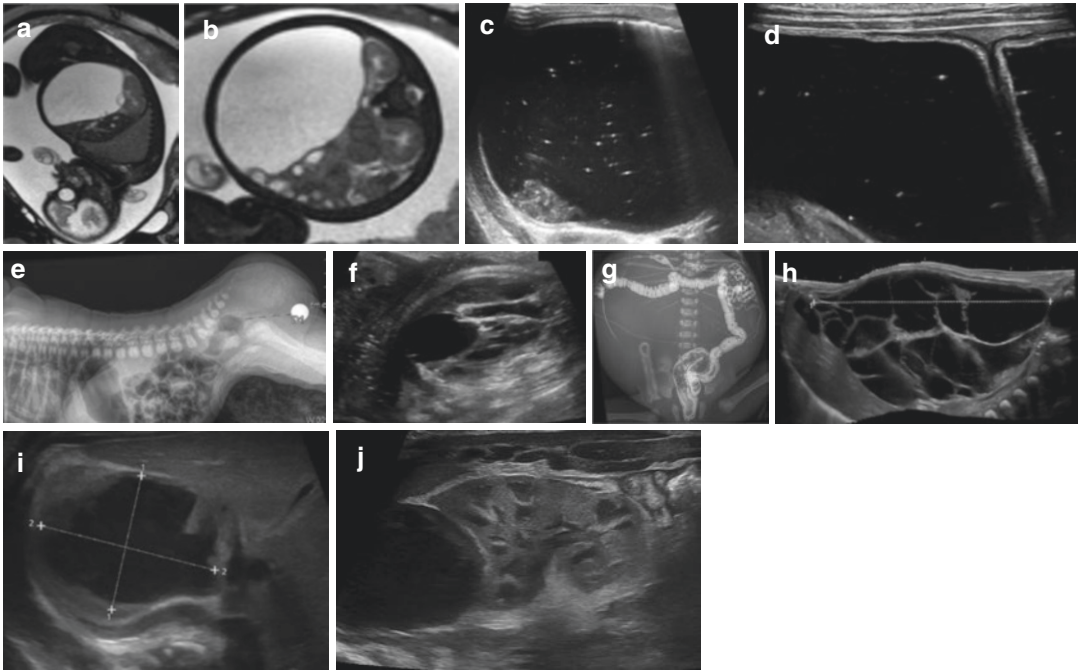


Fig. 5.10 Imaging in congenital prenatally recognised masses. (a, b) Sagittal (a) and axial (b) T2 weighted foetal MRI shows a prenatally detected huge cystic abdominal mass (courtesy ML Lobo, Lisbon/Portugal). (c, d) The postnatal US in the same baby as (a, b) demonstrates a giant, slightly complex abdominal fluid-filled cyst in the right and central quadrants with debris and air content (c), which exhibits a typical gut wall stratification (“gut signature”), (d) and peristalsis on real time US creating pseudo-septations—consistent with a large enteric duplication cyst (courtesy ML Lobo, Lisbon/Portugal). (e, f) Columbia radiograph with a metallic marker in the anal dimple area demonstrating a soft tissue mass between the coccyx and displaced anorectal structures in a neonate with foetally detected cystic pelvic mass (e); on US in a perineal view

this is a partially cystic complex tumour (f) compressing the otherwise open and continuous rectum and anal canal (sacrococcygeal teratoma). (g, h) An abdominal radiograph (g) shows a distended abdomen with contrast filled and displaced colon after contrast enema; US confirms the prenatally detected multi-cystic nature of the mass eventually proven to be a giant cystic lymphatic malformation (h, extended view US, +...+). (i, j) A foetally diagnosed cyst (+...+) at the upper pole of the right kidney shows some sedimented internal echoes on the axial flank neonatal US (i) also impressing the upper pole of the kidney on the longitudinal scan (j) thus obviously of adrenal origin—likely to be an old haemorrhage. During follow-up, the “cyst” shrunk and eventually only some remnants with beginning calcification were seen proving the aetiology (not shown)

5.4 Summary and Conclusion

In summary, postnatal imaging in prenatally recognised malformations and conditions is based on the management needs—many of those conditions are not an emergency, and sometimes postponing the imaging study is even helpful to avoid misdiagnosis or underestimation of severity, that also helps to reduce the number of necessary imaging studies. Nevertheless, there are congenital conditions that are not depicted prenatally—then postnatal imaging will reveal the diagnosis

and guide further steps. In some conditions, postnatal imaging can also alter the prenatal suspicion or redefine the condition adding essential further information (Fig. 5.11).

Imaging heavily relies on radiographs and US, supplemented by fluoroscopy and MRI, rarely a CT. Paediatric radiology’s task is to help tailoring the respective imaging algorithm individually in close cooperation with the referring/treating physician also based on and considering all available prenatal information. It is the responsibility of the paediatric radiologist to

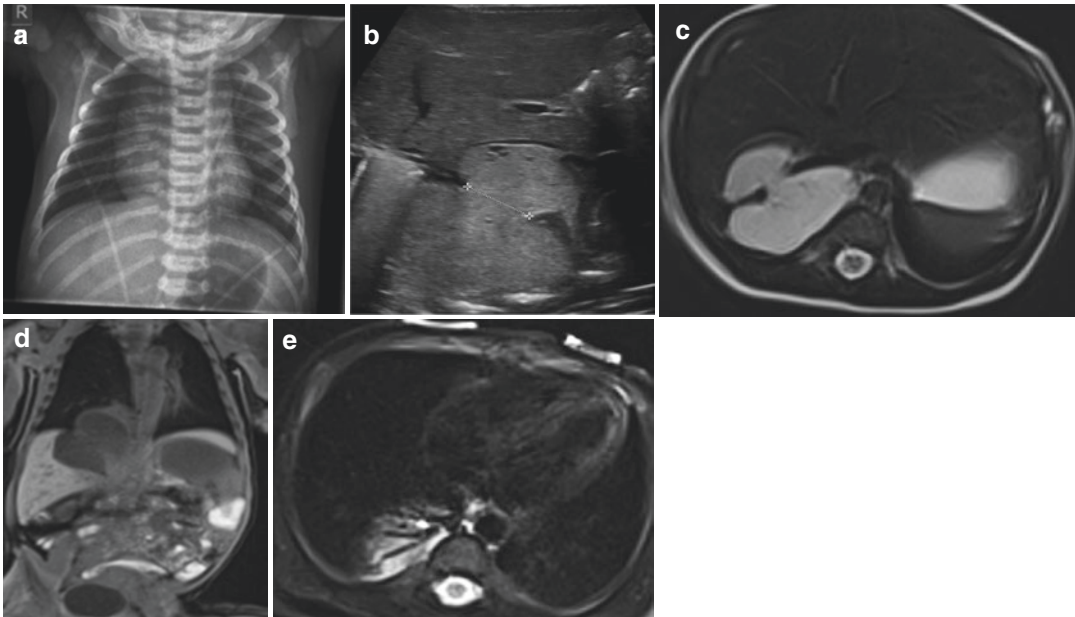


Fig. 5.11 Congenital condition with postnatal surprise on detailed imaging. (a) Foetally, a large basal pulmonary mass was suspected, probably a sequestration. On the neonatal chest radiograph not much could be appreciated. (b) Ultrasound of the right upper quadrant and basal right chest shows an echogenic homogenous mass which has a large dorso-basal intrathoracic and a smaller infra-diaphragmatic component, with an obvious defect in the

diaphragm (+...+). (c–e) An unenhanced “feed and wrap” MRI was performed to confirm the suspicion of a two-compartment sequestration with a diaphragmatic defect in a T2-weighted axial (c) and a T1-weighted coronal section (d); the respective feeding vessels can be appreciated by their flow-void on the fat suppressed T2-weighted axial view at the respective level (e)

select the least burdensome imaging method that allows a decisive diagnosis answering the therapeutically relevant question, and to decide on the most meaningful timing of the investigation. The paediatric radiologist then skillfully performs and interprets the respective investigations by granting high quality imaging adapted to the neonatal needs and options, considering the age specific requirements and restrictions, with expert knowledge of the imaging appearance of all relevant neonatal conditions and the respective differential diagnoses—to ensure a reliable diagnosis.

Further Reading

- Birkemeier KL. Imaging of solid congenital abdominal masses: a review of the literature and practical approach to image interpretation. *Pediatr Radiol.* 2020;50:1907–20.
- Eber E. Antenatal diagnosis of congenital thoracic malformations: early surgery, late surgery, or no surgery? *Semin Respir Crit Care Med.* 2007;28:355–66.
- Sadler TW. *Langman’s medical embryology*. 13th ed. Philadelphia: Wolters Kluwer; 2018. ISBN: 9781975114848.
- Wall J, Coates A. Prenatal imaging and postnatal presentation, diagnosis and management of congenital lung malformations. *Curr Opin Pediatr.* 2014;26:315–9.



Pre-, Peri-, and Post-Operative Imaging in Neonates

6

Michael Riccabona and Holger Till

6.1 Introduction

There are conditions where neonates need urgent surgery, most commonly bowel perforations or congenital anomalies causing gastrointestinal or urogenital tract obstruction. In these queries, imaging is essential to establish the correct diagnosis and to decide upon adequate therapy. Furthermore, there are some imaging needs in acute cardiac conditions that need early intervention or surgery; these are discussed in the respective chapter.

Pre-operative imaging will vary; there are some conditions that do not need much pre-operative imaging, such as an open myelomeningocele where often the imaging work-up is performed after primary closure of the defect. Other conditions are obvious clinically or are depicted on a radiograph such as in oesophageal atresia (OEA) where the gastric tube cannot be passed and the radiograph shows (particularly after instillation of air through the high ending tube) the dilated proximal oesophagus without a depictable distal oesophagus (Fig. 6.1). Even some classification can be achieved by carefully analysing the radiograph depending on the amount and location of abdominal air/gas—in the example of the OEA one can postulate a trachea-oesophageal fistula if there is air in the

stomach and/or bowel. In contrast, an OEA without a fistula the radiograph shows a gasless abdomen.

Again, OEA treatment can be performed based on this finding and potential further work-up for associated malformations (e.g. VACTERL syndrome) is continued after the initial surgery. However, some perform an orienting screening pre-operatively by performing echocardiography, taking radiographs of the abdomen and spine, and performing a sonographic abdominal survey.

Some other conditions can be obvious clinically, but may need confirmation (e.g. volvulus, with typical signs of high obstruction on an abdominal radiograph and the acute onset of the symptoms). However, with increasing medico-legal issues, imaging confirmation of the suspicion is often requested and then an US study of the mesenteric root and the course of the duodenum (e.g. after filling of the stomach with saline or diluted US contrast agent) is performed, sometimes complemented by an upper GI fluoroscopic study (for example, if the US investigation delivers equivocal results).

Finally, there are complex malformations, which will need a more thorough work-up for treatment decisions, such as anorectal malformations (ARM) including the most complex combinations like cloacal malformations. In these queries, an initial radiographic and sonographic work-up is performed, possibly supplemented by fluoroscopy to then decide on the surgical

M. Riccabona (✉) · H. Till
Medical University Graz, Graz, Austria
e-mail: Michael.riccabona@medunigraz.at

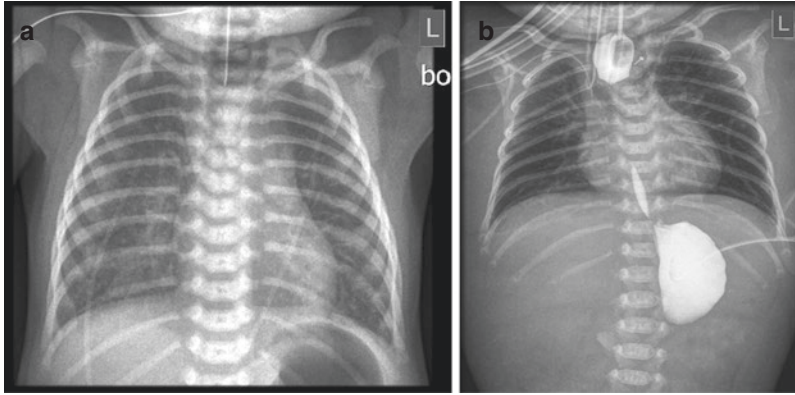


Fig. 6.1 Oesophageal atresia (OEA). (a) OEA with gastric tube that cannot be passed further down. Air given through the gastric tube delineates the short, dilated proximal part of the oesophagus. Note that there are 13 rib pairs as an associated anomaly. Air in the stomach indicates that there is a lower tracheoesophageal fistula. (b) Long distance OEA with no primary correction possible. A gas-

trostomy tube was placed and the length of the OEA outlined by filling the stomach with reflux into the distal oesophagus and the proximal oesophageal pouch with radiopaque CA. Note that the rest of the abdomen is gas-free, so there is either no lower tracheoesophageal fistula or there is a secondary gastric outlet/duodenal stenosis

approach. Even scintigraphy may sometimes become necessary such as in the work-up of a suspected biliary atresia, or for evaluating gross renal function when deciding whether to try to save a kidney or take it out.

Peri-operative imaging is very rarely necessary in this patient group—only catheter or cannula/drainage positioning may be supplemented by imaging using fluoroscopy or bedside intraoperative US.

Post-operative imaging depends on the underlying condition and the clinical course of the patient. In some cases, no further imaging is necessary as long as the patient does well (e.g. after malrotation or volvulus, after hypertrophic pyloric stenosis...). In other conditions, further development and growth need to be monitored, for example after a colostomy or ileostomy imaging may become necessary to decide on stoma closure—ensuring unhindered patency of the affected bowel segment or loop. This is then commonly performed by fluoroscopy and contrast agent instillation, alternatively by US observing the bowel after instillation of a saline solution or diluted US contrast agent.

As soon as complications arise, imaging is often necessary and mostly based on radiographs

and US, sometimes complemented by fluoroscopy. Except after neurosurgery, CT or MRI is rarely needed for post-operative evaluation in this age group. With post-operative complications, note that often not only the affected surgical area may be the target of imaging but also other or systemic complications may need imaging too—such as the chest in intubated babies after abdominal surgery, or brain US after surgery of preterm neonates or MMC-closure.

Nevertheless, there is an increasing demand for imaging partially due to its availability, partially for medico-legal issues, in part because of prenatal imaging and respective implications on postnatal management and imaging, and partially because of the change in training and education of paediatric surgeons with a trend to request as much imaging as possible. But remember, not everything that is possible and can be imaged is really needed or necessary, and investigations always pose a burden to the baby and cause delay in management. Furthermore, economic aspects, workload, and burden, as well as availability on a 24 h/7 days/365 days basis need to be considered. And, as neonates with these conditions may present after office hours, it is helpful to have a consensus-based imaging algorithm for the most

urgent and common requests available at the individual hospital to guide the necessary imaging work-up. This algorithm should be developed together with the paediatric surgeons, addressing both their needs and the considerations of the imaging department and the specific needs of the vulnerable neonates.

The following pages will try to address the most common and relevant conditions that need pre-/peri- or post-operative imaging, considering both the surgeons needs and the imaging options and restrictions.

6.2 Pre-operative Imaging

Timing of the pre-operative imaging depends on the urgency and the clinical status of the patient as well as on the respective condition. Mainstays in pre-operative imaging are radiography and US, supplemented by fluoroscopy.

6.2.1 Brain

In the *brain*, only severe acute haemorrhage (or rarely hydrocephalus) with significantly elevated intracranial pressure (such as in an epidural haematoma after forceps delivery—Fig. 6.2) may need urgent pre-operative imaging. The surgeon must know the underlying entity, possibly related pathology that may impact the surgical approach, and might like to know more details on the anatomy.

- Usually, US is the first step, complemented by MRI if necessary (or CT, if MRI is unavailable or cannot be performed for other reasons). Other conditions where urgent surgery may become necessary in the brain include obstructive high-pressure hydrocephalus (mostly already known from prenatal US or MRI). Again, the imaging approach is the same as with increased intracranial pressure secondary to haemorrhage.

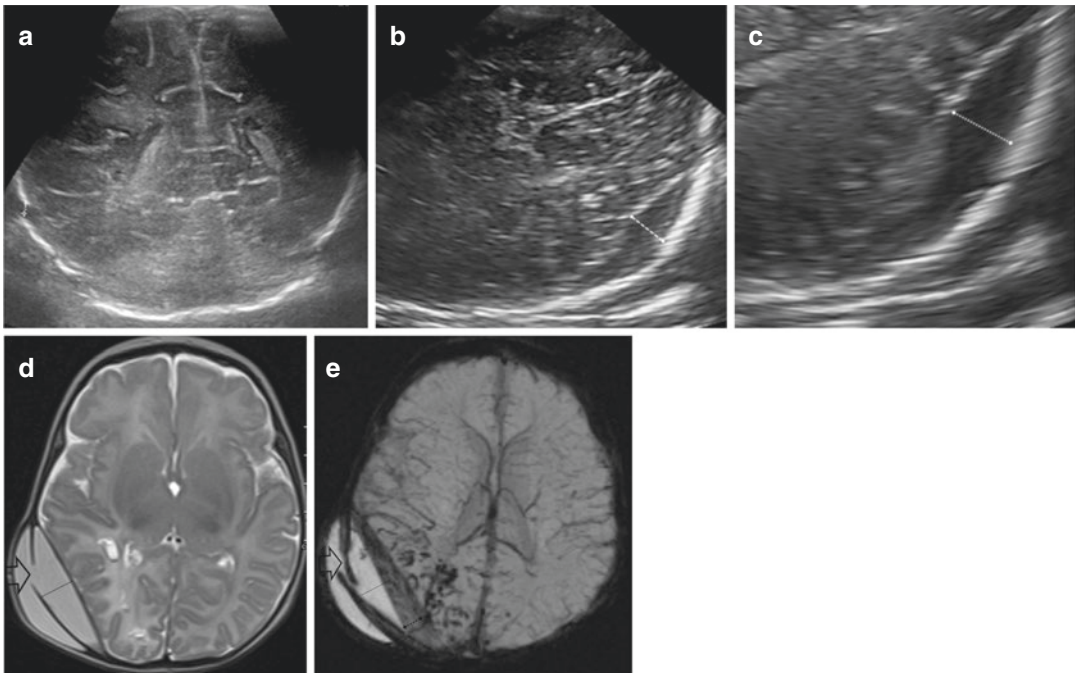


Fig. 6.2 EDH after birth trauma with need for surgical relief. (a) Transfontanelar US reveals a suspected haemorrhage involving the tentorial region and the right sided extra-axial CSF space seen as in homogeneously increased echogenicity, with suspicion of a skull fracture (+...+). (b,

c) Additional transtemporal views confirm the epidural haemorrhage. (d, e) Axial MRI confirms the haemorrhage and the fracture (arrow) on T2-weighted and susceptibility-weighted sequences

6.2.2 Chest

In the *chest*, there is hardly any condition that needs urgent surgical treatment in the neonatal period except for OEA (requiring primary ligation of the trachea-oesophageal fistula and preferably a simultaneous primary anastomosis) or congenital diaphragmatic hernia (CDH) requiring repair after cardiopulmonary stabilisation. Even in pulmonary malformations (such as sequestrations or CPAM) surgery is delayed to a later age in uncomplicated cases without cardiopulmonary symptoms and thus only the standard imaging for assuring diagnoses and grading the severity and extent are performed.

- An acute event is pneumothorax (Fig. 6.3)—however, this is usually diagnosed by radiographs (or bedside lung US) and drained by the neonatologist or anaesthesiologist; it does not require surgical intervention or dedicated imaging.
- A rare condition is a large lobar emphysema that may cause severe respiratory distress, necessitating early lobectomy (Fig. 6.4). Pre-operatively detailed information about the anatomy is absolutely essential; which lobe is affected, which arterial and vascular supply must be dealt with, which pathology must be

managed (macro- and microcystic disease), which complications already exist (mediastinal shift)? Definitive information about tracheal or bronchial anomalies are mandatory pre-operatively and not just a “nice-to-have” and can only be revealed by sectional imaging. Imaging generally is based on radiographs, supplemented by CT for demonstration of the lobar anatomy.

- Cardiac conditions are addressed in the respective chapter.



Fig. 6.4 Lobar emphysema/congenital lobar overinflation. Left lobe lobar emphysema causing mediastinal shift to the right and severe ventilation restriction, thus this condition needed urgent surgical intervention as a newborn

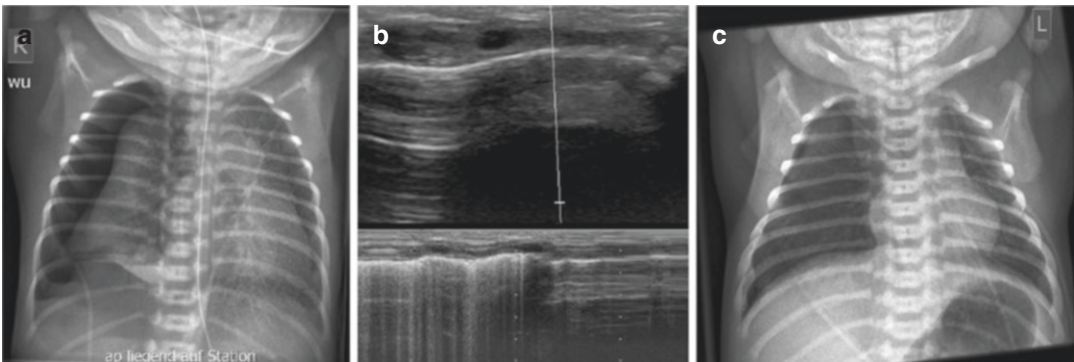


Fig. 6.3 Pneumothorax. (a) Chest radiograph with obvious right tension pneumothorax and mediastinal shift to the left. (b) Lung ultrasound: the image shows the transition of ventilated lung to pneumothorax—the m-mode trace on the bottom of the image indicates the normal lung

aeration on the left, whereas on the right the “barcode sign” documents the pneumothorax and absence of lung sliding. (c) Chest radiograph with small lateral pneumothorax—easy to be missed

6.2.3 Upper Gastrointestinal Obstruction

Upper GI obstruction and atresias represent the most common indications for early neonatal surgery. These conditions include duodenal atresia (DA) or volvulus, rarely a congenital (or early onset) hypertrophic pyloric stenosis or a gastric web may occur. Imaging is tailored towards what the surgeon needs to know. Imaging must confirm the diagnosis and possibly allow adequate preoperative classification of the malformation.

- Duodenal atresia represents a spectrum ranging from typical DA with annular pancreas (double bubble phenomenon on the radiograph, Fig. 6.5) to a central perforated web (no real double bubble, some gas/air may pass through the little hole in the web and fill more distal bowel loops on the abdominal radiograph).
- Volvulus is usually based on an inadequate embryological fixation of the midgut or hindgut causing malrotation, and is an absolute emergency. Primitive bands passing over the duodenum (Ladd bands) may cause upper GI-obstruction. Without further delay, imaging must establish the diagnosis to allow for emergency surgery.
- Adequate imaging is usually achieved by a chest radiograph including the upper abdomen with an oesophageal or stomach tube in place, possibly with additional instillation of air for better delineation of the intestinal structures.

Sometimes an US is requested, particularly if there is a suspicion of an associated duplication cyst or an annular pancreas (the latter difficult to definitely assess by US), or for volvulus (Fig. 6.6). There is no need for pre-operative fluoroscopy except for a suspected volvulus with an equivocal US finding or unclear partial obstruction (for example caused by a web).

- Hypertrophic pyloric stenosis usually manifests a little later in life, but can happen neonatally and is diagnosed by US without the need for any additional imaging (Fig. 6.7).

6.2.4 Lower Gastrointestinal obstruction

Except for anorectal malformations (ARM, see below) other (*lower*) **intestinal atresias and stenoses** usually manifest a little later in the neonatal period. They can occur anywhere in the (small) bowel and may be isolated or multiple. Clinically they present as a complete intestinal obstruction.

- Once the diagnosis has been suspected by radiographs, the location, extend and type of intestinal atresia(s) can only be established during a limited laparotomy exposing the complete intestine.
- Therefore, an abdominal radiograph and a “screening” US are commonly performed, only seldom supplemented by fluoroscopy (upper GI-study or retrograde colonography/enema).

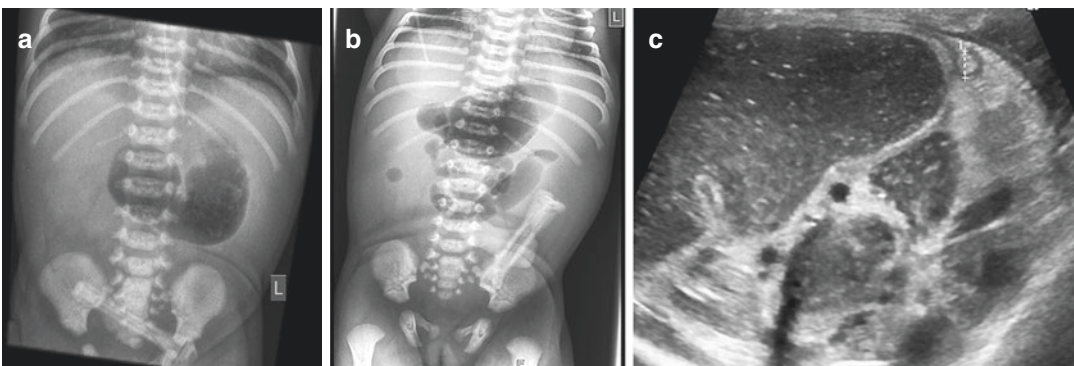


Fig. 6.5 Double bubble in duodenal atresia—with differential diagnosis. (a) Typical double bubble appearance on radiograph in a baby with duodenal atresia. (b) Small bowel atresia—there is more air in more distant small

bowel loops, but no air in the colon. (c) Confirmation of the suspicion in image (b) by US: grossly dilated small bowel loop with complex content, but an unused small left hemicolon (+...+)

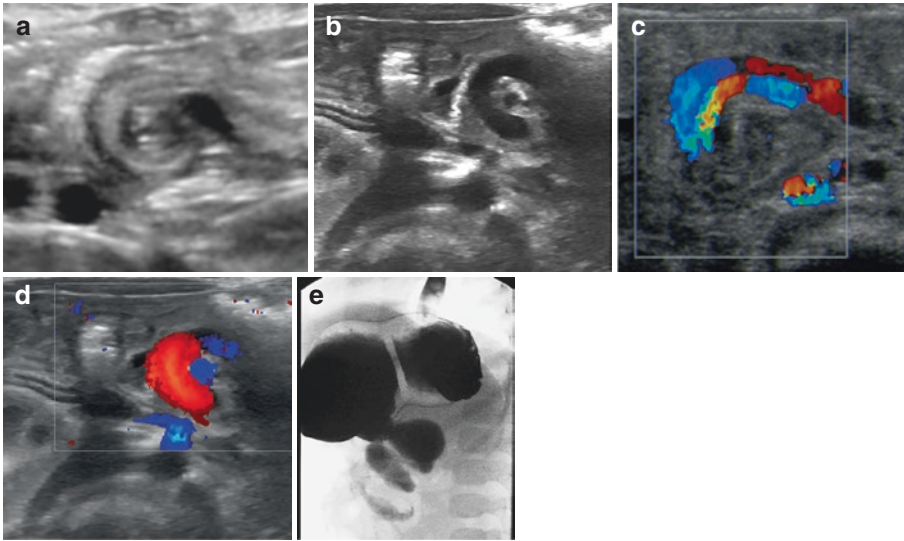


Fig. 6.6 US and fluoroscopy in volvulus. (a–d) US shows the typical mass with spiralling bowel loops (a) and/or mesenteric vessels (i.e. dilated mesenteric vein) (b) around the mesenteric root (“whirl pool sign”). The vessels are much better seen on CDS (c, d). (e) In sonographically equivocal cases with a relatively stable neonate

fluoroscopy will be the complementing imaging showing the spiralling contrast filled bowel loops (NOTE: But do not unnecessarily delay surgery to avoid long segment small bowel necrosis with resulting short bowel syndrome!)

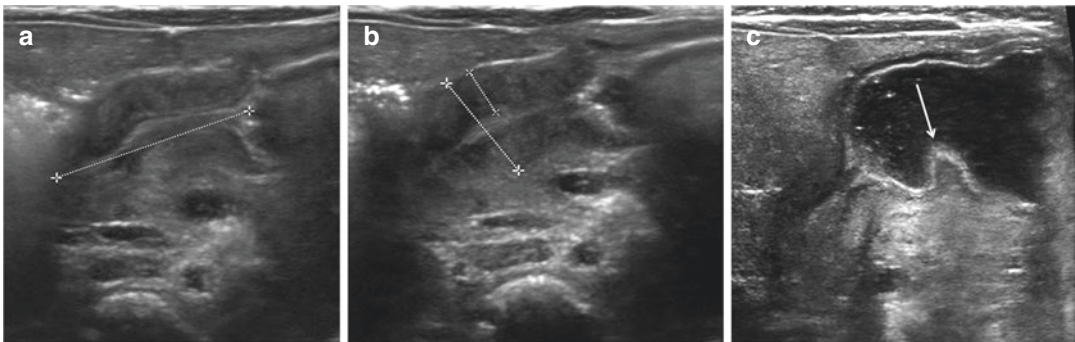


Fig. 6.7 Hypertrophic pyloric stenosis. US in a former preterm neonate (2 weeks corrected gestational age): elongated pylorus (a) with thickened wall and diameter

(b, +...+) as well as narrow pyloric canal, without passage of fluid from the stomach after drinking (c)—in spite of the strong peristaltic wave (arrow)

With the advent of new US techniques and US contrast agents, filling the bowel orally or rectally became feasible, and some of the relevant questions can now be answered also by US, helping to reduce the need for fluoroscopy (Fig. 6.8).

Bowel perforation, especially in very low birthweight (VLBW) infants, usually occurs either secondary to an obstruction or inflammation with necrosis of the bowel wall (necrotizing enterocolitis, NEC).

- Prenatally, vascular events causing local bowel ischaemia with secondary necrosis and rupture, which the typical image of calcified meconium remnants scattered throughout the abdomen visible on US and radiographs (Fig. 6.9).
- Postnatally, bowel perforation is diagnosed by either US (“curtain sign”) or radiography using a cross-table projection with the baby in a lateral decubitus position (Fig. 6.10).

Fig. 6.8 Unused left (micro-)colon. (a) Contrast enema reveals a patent, but small colon in a neonate with colonic atresia; similar findings can be seen in meconium plug or meconium ileus. (b) Sonographic “hydrocolon” (US with NaCl enema) reveals a small poorly distensible sigmoid and colon (+...+)

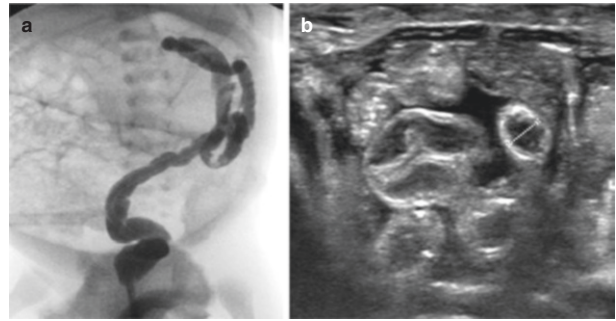


Fig. 6.9 Congenital meconium peritonitis. (a) US reveals irregular coarse and punctate calcifications on the liver surface. (b) The respective abdominal radiograph confirms the findings indicating calcified remnants after intrauterine bowel perforation and meconium peritonitis

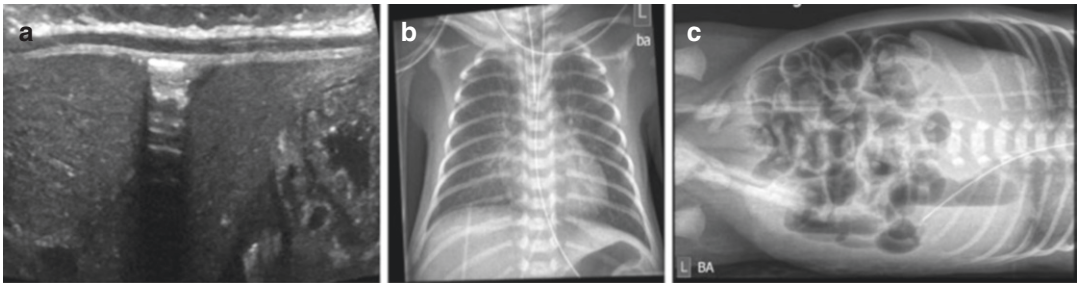
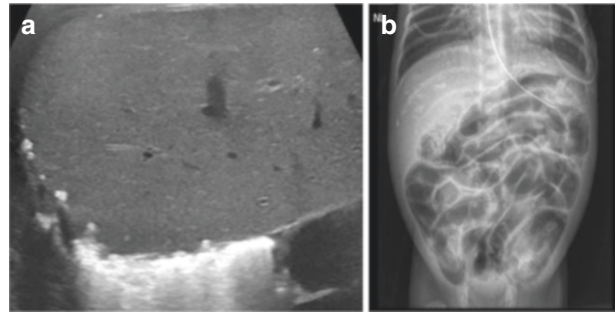


Fig. 6.10 Perforation with free air—US and radiograph. (a) US reveals peritoneal air (detectable as reverberation echoes which can be pressed away by transducer pressure = curtain phenomenon) in front of the liver. (b, c) A chest radiograph revealed the suspicion of a “football

sign” and thus free peritoneal air—the respective additional abdominal radiograph in left lateral decubitus position and a cross-table view confirms the free peritoneal air in a preterm neonate with necrotizing enterocolitis

- Note that these films are only diagnostic if there is sufficient time with the baby in this position to allow the free “air” (i.e. bowel gas) to gather in the highest compartments, and if there is air/gas in the respective perforated bowel segment at all. If the affected bowel loop contains only fluid or meconium, no free air/gas can be seen and thus the diagnosis becomes difficult, sometimes impossible. Then one needs to rely on other clinical or imaging signs of secondary complications

such as meconium balls in the free abdominal fluid or peritonitis.

6.2.5 Anorectal and or Cloacal Malformations

In *anorectal (or cloacal) malformation (ARM)*, the appropriate post-natal surgical strategy depends on the type of ARM. In the so-called low forms, there is usually a fistula to the perineum. If

the fistula is wide enough to allow for adequate passage of meconium and stool or can be sufficiently enlarged by gentle bouginage, a colostomy may not be necessary. Most other higher forms of ARM without any external fistula require colostomy diversion for adequate passage of stool and for adequate imaging later. Thus, most surgeons prefer a low colostomy.

- Perineal US will help to define the level of the atresia and allow for assessment of possible associated malformations. The abdominal radiograph is still considered an essential step with an additional Columbia view (bottom-up cross-table radiograph, with a marker placed on the anal dimple) (Fig. 6.11).
- Fluoroscopy (and sometimes and increasingly MRI) is performed mostly after initial surgery (primary pull through or colostomy) for defining the further treatment, depicting possible fistulae, or assessing associated malformations as well as the pelvic floor muscles.

Cloacal malformations are more complex, with a higher demand on imaging both in the pre- and post-operative state; these patients should be referred to and managed by a dedicated centre following international guidelines, e.g. from the ESPR abdominal imaging task force. More details on this can be found in the respective chapter.

6.2.6 Hirschsprung Disease

Hirschsprung disease (HD) represents another congenital malformation of the hindgut causing functional intestinal obstruction. The disorder is caused by aganglionosis of the large bowel starting from the rectum and extending proximally and may involve the entire colon (total colonic aganglionosis); the affected bowel segment remains contracted and narrow. Clinically, HD represents a spectrum, mostly depending in the extent of the disease. In extensive cases, a newborn may develop significant abdominal disten-

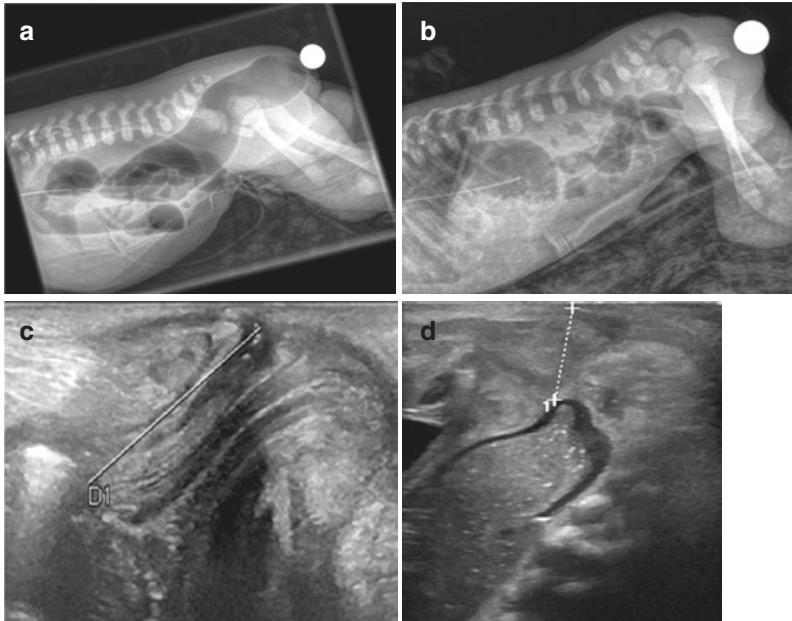


Fig. 6.11 Columbia view and perineal US in anal atresia/anorectal malformation. (a) Columbia radiograph (bottom-up prone cross-table abdominal radiograph, with a marker on the anal dimple) reveals low anal atresia—with the air-filled rectum reaching down to the marker. (b) Intermediate ARM—the distance between marker and air-

filled rectum is obvious. (c) Perineal US reveals a long distance between the anal dimple and the air-filled rectum (D1---)—but there are air echoes in the anal canal indicating a high-grade stenosis and not a complete atresia. (d) Note the obvious distance between the perineum and the occluded rectum (+...+1) in an anal atresia

sion and the inability to pass stool. Other cases with ultrashort segment HD may be completely normal initially. Besides the clinical sign of constipation, one needs to worry about evidence of systemic inflammation based on Hirschsprung associated enterocolitis (HAEC), which may be life threatening.

- The diagnosis is usually confirmed by rectal biopsies and immune-histochemical staining for ganglion cells and nerve fibres. Anorectal manometry demonstrates missing relaxations of the internal sphincter and supports the diagnosis, but is cumbersome in neonates. The extent of the aganglionosis may be revealed by defaecography or perineal and bowel US (possibly after a saline enema). However, they may miss an ultra-short segment particularly in the neonatal age, but may reveal other indirect signs. Therefore to eventually clarify the exact extent of the disease before surgery, radiography and fluoroscopy seem mandatory.

6.2.7 Secondary Bowel Obstruction

Secondary bowel obstruction as commonly observed in preterms or very low birth weight infants may result from a still immature enteric nervous system causing secondary meconium plug or bowel motility problems—with inspissated bowel content causing the obstruction.

- Especially in these delicate patients, the surgical responsibility is to perform or to delay laparotomy and enterostomy placement. Conservative and medical treatment represents the first-line approach. However, experts agree that a perforation should be avoided and that even pre-emptive prophylactic decompression could become indicated after joint decision with the neonatologist and paediatric radiologist.
- For diagnosis, to monitor the success of conservative treatment, and to detect complications that may lead to perforation, usually radiographs are performed, supplemented by US including in selected cases a sonographic hydrocolon (= US during a saline enema, e.g. for depiction of a small or unused left colon) or

fluoroscopy. Ultrasound additionally allows for visualisation of possible duplication cysts, large Meckel diverticulum or bowel wall pneumatosis (which can be observed both in severe dilated and obstructed bowel and NEC—the latter usually is differentiated by clinical findings and laboratory parameters, Fig. 6.12). Perforation is depicted by either US (“curtain sign”) or abdominal radiographs (cross-table view, football sign—see Fig. 6.9)—usually no additional or other imaging is necessary.

6.2.8 Biliary Atresia

Biliary atresia (BA) and other liver/bile conditions require early diagnosis and intervention—the earlier the diagnosis is established and treatment can be started, the better the prognosis. Basically, the aim is to differentiate between the extra- and intrahepatic forms of BA or other liver conditions.

- Liver biopsy remains essential for diagnosis and its differential, though is not always diagnostic. MRI at present plays no role in evaluating these children. Hepatobiliary scintigraphy is often performed in the work-up, although even scintigraphy may have problems in dividing the different forms and in differentiation of the various causes of impaired bile drainage.
- Ultrasound is the first screening test (with indirect criteria that rate the probability for BA as low or high) and radiographs play no role in this entity; US-guided or often intraoperative cholangiography is performed for final confirmation.
- International consensus recommendations and flow-charts exist on how to approach these neonates. Especially the extrahepatic forms may benefit from surgery (drainage of bile into the gut = Kasai procedure) which is usually performed slightly after the neonatal period.

Other liver/bile conditions that may need early imaging (and sometimes intervention) are choledochal cysts and liver tumours (particularly neonatal haemangiomatosis/haemangioendothelioma) (Fig. 6.13).

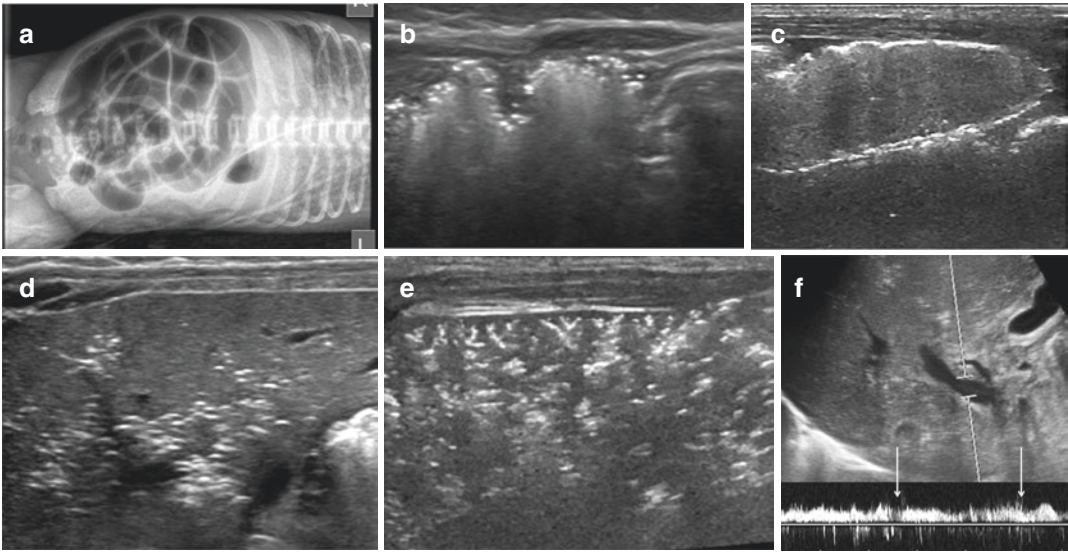


Fig. 6.12 Pneumatosis. (a) Abdominal radiograph in a preterm neonate with suspicion of necrotizing enterocolitis—the cross-table view in lateral decubitus position was done for free peritoneal air: note the obvious tiny gas bubbles in the wall of the caecum and ascending colon. (b, c) US confirms gas bubbles (seen as stippled echoes) in the bowel wall and not just the lumen (c is a different case with more fluid bowel content enabling an even bet-

ter visualisation of the bubbles in the wall). (d–f) The echogenic gas bubbles have reached the liver, with numerous gas bubbles in the small (peripheral) portal venous branches; spectral Doppler tracing from the portal vein proves the gaseous content by displaying the typical bidirectional gas spikes (arrows, indicating some of the bidirectional spikes)

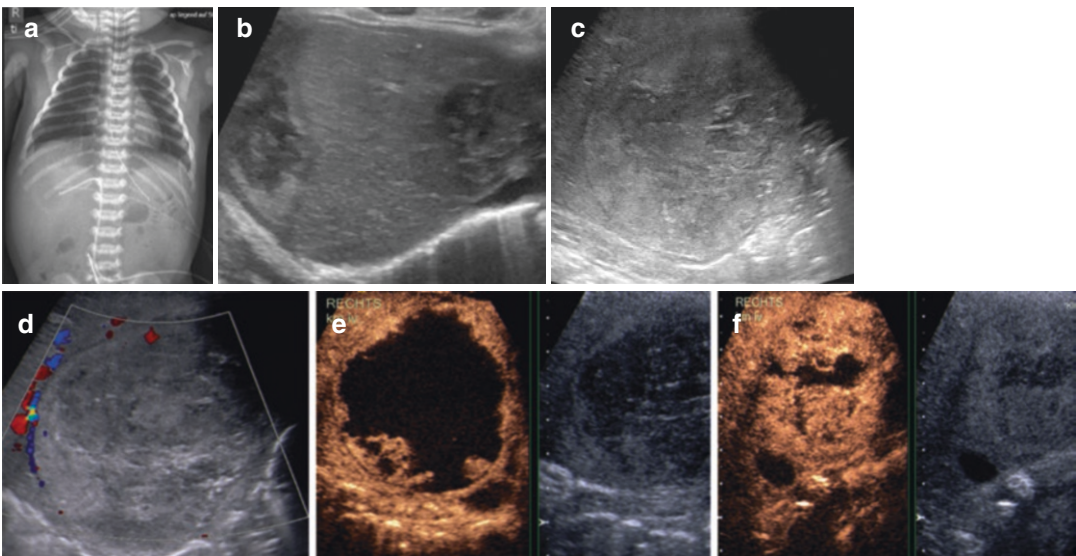


Fig. 6.13 Liver conditions. (a) A torsogram of a neonate shows malposition of an umbilical vein line in the liver (which was then removed—however, some medication had already been infused). (b) Several days later, US subsequently detected two inhomogeneous complex-fluid lesions the liver (same patient as in a), consistent with iatrogenic necrosis (and potentially abscess formation). (c,

d) US depicts a large mass in the liver of a neonate with peripheral hypervascularisation, most probably a congenital haemangioma. (e, f) Contrast-enhanced US then demonstrates the typical perfusion and enhancement pattern: early peripheral enhancement and a gradual fill-in phenomenon (Iris phenomenon) typical for haemangioma

6.2.9 Urogenital Tract

In the *urogenital tract* only severe bilateral obstruction will need early surgery—most commonly low obstruction by a posterior urethral valve (PUV); rarely bilateral severe pelvico-ureteric junction obstruction (PUJO) or infected dilated systems need emergent intervention. Most of these cases are recognised prenatally and present early after birth for reassessment/confirmation. The goal of treatment is to secure unhindered urinary drainage and to preserve as much renal function (and growth potential) as possible.

- Imaging usually starts with a meticulous US-study, supplemented by fluoroscopy (voiding cysto-urethrography = VCUG). Some perform

a contrast-enhanced voiding urosonography (ce-VUS) instead, particularly if bedside imaging is needed (as these babies often require mechanical ventilation) (Fig. 6.14). As scintigraphy is limited in the immature kidneys, it is used more reluctantly and only serves as a gross indicator of severe dysfunction—however, it sometimes is performed (after an effective drainage is secured via suprapubic catheter or percutaneous nephrostomy) if this information is crucial for deciding on the best treatment approach.

- (Pre-operative) MRI and MR-urography (MRU) may help in sorting out anatomy in very complex malformations, but as in this age (due to the immature renal function) contrast applications should be avoided, no reliable functional information can be retrieved.

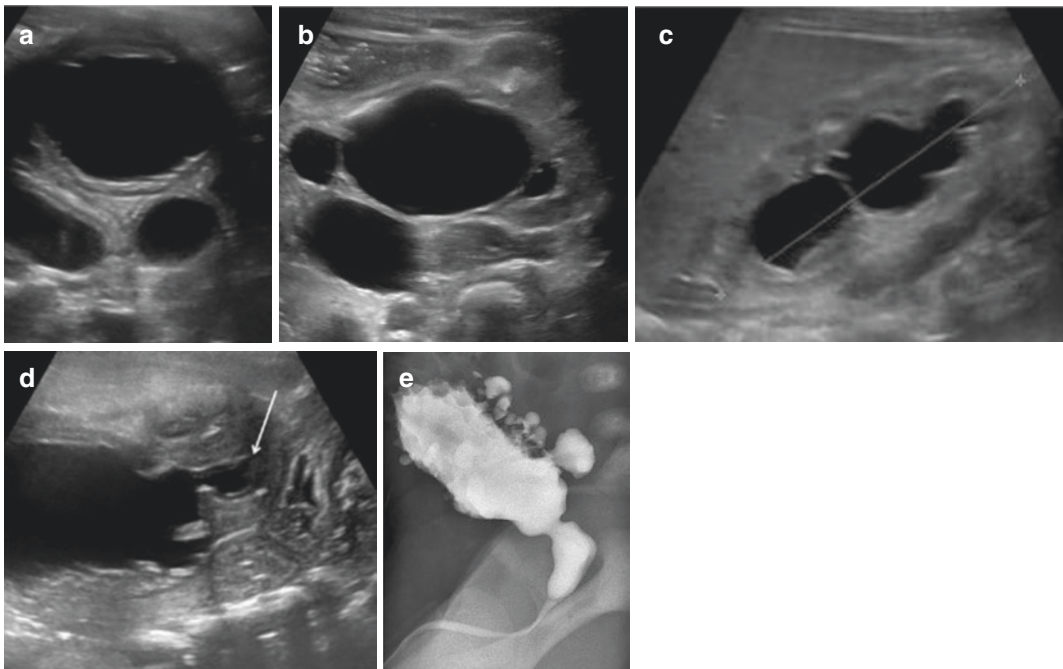


Fig. 6.14 PUV and severe urinary tract dilatation. (a) Axial US view of the lower pelvis and urinary bladder in a male neonate with lung hypoplasia and oligohydramnios reveals a well-filled thick-walled and trabeculated urinary bladder and bilaterally hugely dilated ureters behind the bladder. (b, c) Gross dilatation of the collecting system of the slightly dysplastic looking kidneys is seen. (d) Perineal

US reveals a typical valve like configuration of the posterior urethra (arrow) with open bladder neck during voiding attempts which are not very successful, consistent with a posterior urethral valve. (e) VCUG then confirms the diagnosis, and additionally nicely shows the (pseudo-) diverticula as well as a Hutch diverticulum

Many international consensus recommendations exist helping to decide on the imaging approach in these neonates.

6.2.10 Musculoskeletal Conditions

Some rare *musculoskeletal conditions* will need surgical treatment, e.g. osteomyelitis or fractures. These conditions are sometimes difficult to assess clinically in this age group, and imaging often is essential. Sometimes (e.g. fractures) the condition is diagnosed as an unsuspected incidental finding.

- Imaging again relies on US and radiographs; some conditions need an additional MRI or scintigraphy or even a CT.

Another condition is developmental dysplasia of the hips, which may be severely dislocated and then will need urgent repositioning and fixation after US diagnosis (Fig. 6.15).

Moreover, a rare small part query is an abscess formation that might need drainage (e.g. in lymph nodes—mostly cervical, with the respective differential diagnosis—see Fig. 6.16) or sometimes a neonatal breast abscess.

- Usually US is performed to evaluate for the necrotic centre, assess possible hyperaemia of the membrane by (a)CDS, and to interrogate the depth and penetration as well as the surrounding anatomic structures.

6.2.11 (Pseudo)tumours

There are rare congenital (*pseudo*-)tumours (and vascular malformations) such as sacral teratoma, neuroblastoma, mesoblastic nephroma, or lymphatic malformation. Besides detection/confirmation of the condition, classification of the entity may be necessary and poses a challenge (as contrast application

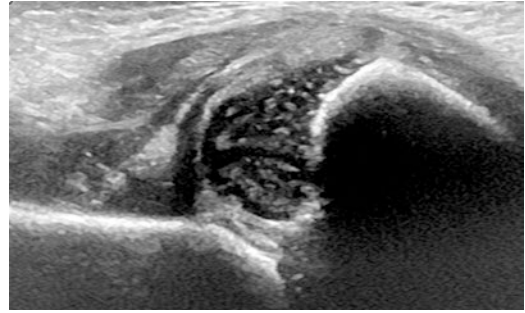


Fig. 6.15 Dislocated hip. Coronal US image of a dislocated hip (Graf type IV) due to developmental dysplasia which may need immediate repositioning and stabilisation

options are limited). Besides US, sectional imaging (preferably performed by MRI) usually becomes necessary—particularly for demonstrating the detailed anatomy (preoperatively) and for staging if a malignant tumour is suspected (Fig. 6.16). There are conditions which need early surgery such as a sacral teratoma, conditions where surgery is performed slightly delayed such as in a mesoblastic nephroma, and conditions where a watch and wait strategy is advocated such as in a low grade congenital/neonatal neuroblastoma. Imaging thus depends and varies, sometimes only (image-guided) biopsy reveals the entity, or in some conditions image-guided interventions become necessary (e.g. embolisation by catheter angiography of a large hepatic haemangioendothelioma with high shunt flow and cardio-vascular failure, instillation of sclerosing agents into lymphatic malformations if they threaten essential organs or vital functions). In the brain, the only condition that needs to be mentioned is the vein of Galen aneurysm, an arterio-vascular malformation (AVM) that will need early intervention (usually by catheter angiography with embolisation). Besides US detects the AVM, and detailed analysis is then performed by MRI (and MR-Angiography), sometimes CT-angiography is also requested pre-interventionally.

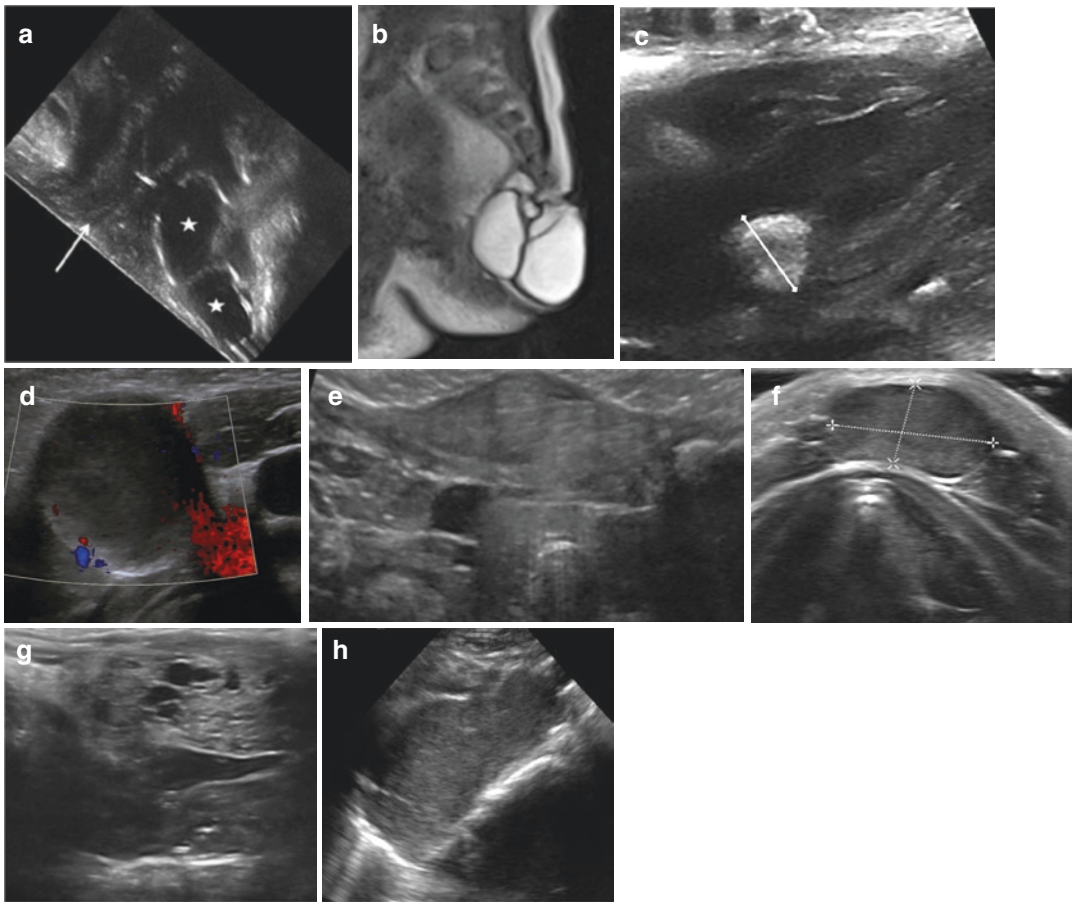


Fig. 6.16 Imaging neonatal tumours. (a) The most common neonatal (congenital) tumour—a pre-sacral sacrococcygeal teratoma. Preoperative imaging by perineal US shows the cystic intra-pelvic components (asterisk) arising from the hypoplastic sacrum dorsal to the anal canal (arrow); (b) the complementing preoperative sagittal MRI outlines the entire extent of the mass. (c) US depicts an echogenic mass in the atrium which was first believed to

be a cardiac rhabdomyoma in tuberous sclerosis, but then turned out to be an atrial thrombus after a central venous line. (d–f) US for differentiating neonatal tumourous masses in the neck: lateral brachial neck cyst (d) the image (f) is the thyroglossal cyst and (e) the fibromatosis coli, or a partially cystic lymphangioma (g). (g) The feared neuroblastoma is positioned much deeper and hardly induces visible a neck mass (h)

6.3 Peri-operative Imaging

Peri-operative imaging is rarely needed in neonates, but if needed US and fluoroscopy are used.

The most common application is placement and position check of central intravenous lines; also tube or drain position may need to be checked or documented. For fluoroscopy, some CA instillation into the small, poorly radiopaque tubes may become necessary—unless they have a

special inlay allowing for radiographic visualisation.

In some more complicated situations, an intra-operative assessment of yet undetailed anatomy may become necessary—e.g. to define the length of the distal oesophageal segment in OEA to then decide if a primary repair is possible or if a long distance obviates the primary approach, or intraoperative cholangiography to confirm biliary atresia and continue with the Kasai procedure (Fig. 6.17).

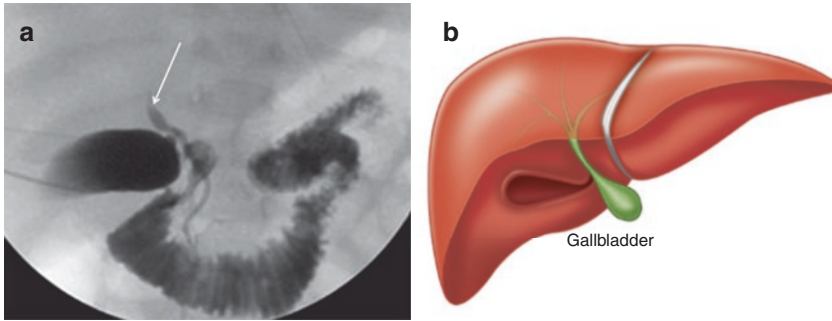


Fig. 6.17 Intraoperative cholangiography in biliary atresia. **(a)** Intraoperative cholangiogram with contrast instilled through a surprisingly large gallbladder reveals existing extrahepatic bile ducts and prompt drainage into bowel, but no contrast filled intrahepatic ducts; only a central cyst-like dilatation of the remnant of the hepatic duct

is opacified (arrow)—consistent with the type 1 biliary atresia according to the Davenport classification. **(b)** Schematic drawing of type 1 biliary classification according to Davenport. (Adapted from Davenport M. 2012; Biliary atresia: Clinical aspects. *Semin Pediatr Surg* 21:175–184)

For further details, refer to the respective chapters.

6.4 Post-operative Imaging

Timing of the post-operative imaging depends on the urgency and the clinical status of the patient as well as on the respective condition. Mainstay modalities are radiography and US, supplemented by fluoroscopy.

Of course, the normal monitoring for intensive care measures such as chest radiographs (for tubes, drainages, cannulas, and lines, as well as for the ventilated lung) and US (for evaluating the brain, effusions and collections, or abdominal queries) are performed as long as the patients need this support.

Many conditions do not need additional dedicated early postoperative imaging. Others will need imaging assessment early postoperatively to assess adequacy of the intervention—e.g. in obstructive uropathy when other parameters do not allow for judgement of the postoperative recovery, or for early detection of common complications.

Some conditions which do not need extensive post-operative imaging (maybe just a chest radiograph after intubation and line placement) will need postoperative monitoring—e.g. after abdominal closure of a gastroschisis or omphalo-

cele (query for these studies: associated malformations? compression of the inferior cava vein? bowel perfusion—particularly if the defect was large?).

However, many conditions need imaging only to monitor growth and future development, which is then usually performed after the neonatal period.

- In urogenital surgery often at least an US follow-up is requested to monitor the postoperative course, although US may be limited particularly in assessing early postoperative obstruction. For most major anomalies, the relevant medical societies have published guidelines for postoperative follow-up care.
- After bowel surgery, the surgeon must monitor adequate function. Postoperative imaging must be tailored to the underlying disease and its specific complication management, but also timed to the patient's needs.

This is most commonly addressed by fluoroscopy (loopography, enema, antegrade/retrograde colonography/colostography...), some of these questions can also be addressed by modern US using filling techniques (Fig. 6.18).

- After chest surgery, US (for effusions and collections, as well as for diaphragmatic palsy) and chest radiographs are sufficient (Fig. 6.19); only in uncommon complicated

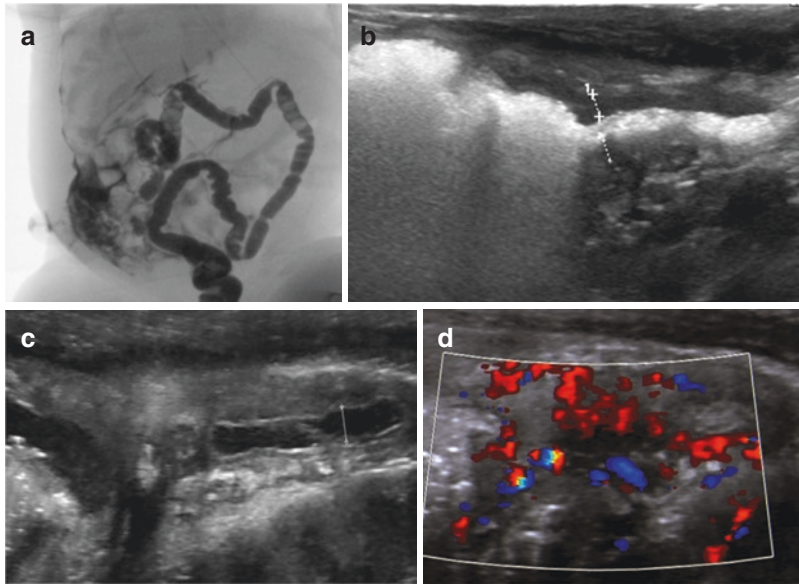


Fig. 6.18 Loopography before enterostomy closure. (a) Instillation of radiopaque CA via the aboral distal loop of an enterostomy: the colon is patent, but close to the stoma there is contrast extravasation into the abdominal cavity indicating local perforation and necrosis. (b) Another patient where US reveals a stenosis close to the stoma by

a still thickened bowel wall (+...) with a hugely distended proximal loop (the echogenic bright bowel gas serves as intrinsic contrast). (c) Saline installation confirms the narrowed and indistensible bowel segment (+...); (d) CDS depicts hypervascularity of the affected bowel wall indicating ongoing inflammation

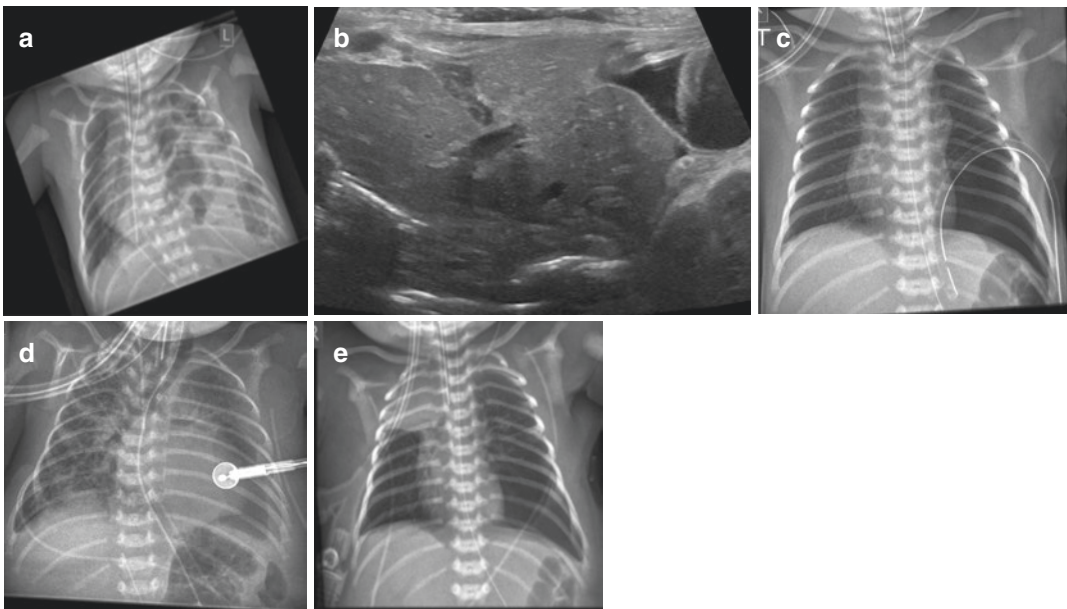


Fig. 6.19 Congenital diaphragmatic hernia. (a) Chest radiograph in diaphragmatic hernia showing mediastinal shift to the right due to air-filled intestines and the left liver lobe occupying the left hemithorax. (b) Coronal US image from left flank showing large parts of the liver her-

niated into the left hemithorax. (c, d) Chest radiographs after CDH repair: (c) shows the physiological “pneumothorax”, (d) the increasing pleural effusion filling the empty thoracic cavity, and (e) postoperative atelectasis due to a tracheal tube ending too low

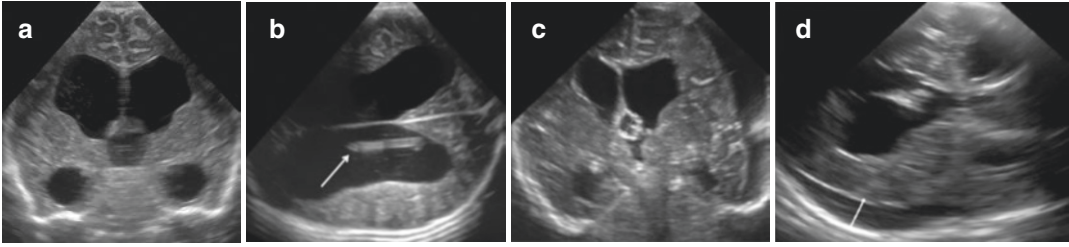


Fig. 6.20 Brain US in neonatal hydrocephalus after shunting for follow-up and depicting shunt complications. (a, b) Ultrasound in shunted supra-tentorial hydrocephalus in a neonate showing continued dilatation of the ventricles, but preserved extra-axial CSF space; the shunt drain is seen in the lateral ventricle on a transtemporal

view (arrow, b). (c, d) US in neonatal hydrocephalus after emergency shunting and fenestration of a cyst compromising the foramen of Monro (residual remnants, +...+) are seen in (c), complicated by a large left extra-axial collection confirmed by the transtemporal view (+----+) (d)

postoperative patients CT will become necessary.

- After brain surgery (mostly for hydrocephalus) follow-up is initiated to monitor the decompression and size of the ventricles and to detect signs that may indicate shunt dysfunction or elevated brain pressure (Fig. 6.20). After closure of a MMC, brain US will be needed to assess for a potential secondary hydrocephalus.
- The postoperative imaging after cardiac surgery is addressed in the respective chapter.

6.5 Summary and Take Away

There are some conditions that require surgery in the neonatal age, and thus imaging may be necessary—not only for establishing the diagnosis, but also to deliver the necessary details regarding relevant anatomy or extent of the disease. Radiological imaging in neonates with surgical diseases requires dedicated expertise and experience. In these fragile and delicate patients, the most efficient radiological work-up using targeted investigations is mandatory; any radiation in this age group carries an increased risk for developing malignancies later in life and must be limited as much as possible. Ultrasound is therefore an essential method for these surgical queries and can answer many questions sufficiently—particularly applying modern US

techniques such as CDS, perineal US, hydrocolon, or ce-US. As newborns with surgical conditions benefit from quick and efficient radiological work-up, these investigations must be made available timely and with lowest burden to the patient. Nevertheless—a necessary investigation even if requiring CA or radiation (e.g. fluoroscopy, CT, MRI) should never be denied if essential for diagnosis or treatment. And finally, care of these babies demands perfect communication and collaboration between paediatric radiologists and paediatric surgeons to take the best decisions that will make a major difference at the beginning of their lives.

Acknowledgement I want to thank Dr. Brian Coley (Cincinnati/Ohio, US) very much for editing this chapter.

Further Reading

- Avni F, Tondeur M, Priso RH. Upper urinary tract dilatation in newborns and infants, and the postnatal work-up of congenital uro-nephropathies. In: Riccabona M, editor. Paediatric urogenital radiology. 3rd ed. Cham: Springer; 2018. p. 465–80.
- Davenport M. Biliary atresia: clinical aspects. *Semin Pediatr Surg.* 2012;21:175–84.
- Gordon I, Riccabona M. Investigating the newborn kidney—update on imaging techniques. *Semin Neonatol.* 2003;8:269–78.
- Kjucevsek D, Riccabona M, Petit P, Avni EF, Bruno C, Damasio MB, Darge K, Littooij A, Lobo ML, Mentzel JH, Napolitano M, Wozniak M, Ording Müller LS. Intracavitary contrast-enhanced ultrasound in

- children: a review, with clinical applications and procedural recommendations from the ESPR Abdominal Task Force Group. *Pediatr Radiol.* 2020;50:596–606.
- Napolitano M, Franchi-Abella S, Damasio BM, Augdal TA, Avni FE, Bruno C, Darge K, Ključevšek D, Littooi AS, Lobo ML, Mentzel HJ, Riccabona M, Stafrace S, Toso S, Woźniak MM, DiLeo G, Sardanelli F, Ording Müller LS, Petit P. Practical approach to imaging diagnosis of biliary atresia, part 1: prenatal ultrasound and magnetic resonance imaging, and postnatal ultrasound. *Pediatr Radiol.* 2021a;51:314–31.
- Napolitano M, Franchi-Abella S, Damasio MB, Augdal TA, Avni FE, Bruno C, Darge K, Ključevšek D, Littooi AS, Lobo ML, Mentzel HJ, Riccabona M, Stafrace S, Toso S, Woźniak MM, Di Leo G, Sardanelli F, Ording Müller LS, Petit P. Practical approach for the diagnosis of biliary atresia on imaging: an up-date and guidelines from the ESPR. Part 2: MRCP, hepatobiliary scintigraphy, percutaneous cholecysto-cholangiography, ERCP, percutaneous liver biopsy, risk scores and decisional flow chart. *Pediatr Radiol.* 2021b;52:1545–54.
- Puri P, Höllwarth M, O'Donnell AM, editors. *Pediatric surgery. Diagnosis and management.* 2nd ed. Cham: Springer; 2021.
- Ralls M, Thompson BJ, Adler B, Ma G, Bates GHD, Kraus S, Jarboe M. *Radiology of anorectal malformations: what does the surgeon need to know?* *Semin Pediatr Surg.* 2020;29:150997.
- Riccabona M. Imaging if the neonatal genito-urinary tract. *Eur J Radiol.* 2006a;60:187–98.
- Riccabona M. (editor) *Imaging neonates. Special pediatric edition.* *Eur J Radiol.* 2006b;60.
- Riccabona M, editor. *Pediatric imaging essentials.* Stuttgart: Thieme; 2013. ISBN: 978-3-13-166191-3.
- Riccabona M, editor. *Pediatric ultrasound—requisites and applications.* 2nd revised ed. Berlin: Springer; 2020. ISBN: 978-3-642-39155-2.
- Riccabona M, Avni FE, Blickman JG, Darge K, Dacher JN, Lobo LM, Willi U. Imaging recommendations in paediatric uro-radiology: minutes of the ESPR workgroup session on urinary tract infection, foetal hydronephrosis, urinary tract ultrasonography and voiding cysto-urothography. *ESPR-Meeting, Barcelona/Spain, June 2007.* *ESUR Paediatric Guideline Subcommittee and ESPR Paediatric Uroradiology Work Group. Pediatr Radiol.* 2008;38:138–45.
- Riccabona M, Avni FE, Blickman JG, Dacher JN, Darge K, Lobo ML, Willi U. Imaging recommendations in paediatric uro-radiology, part II: urolithiasis and haematuria in children, paediatric obstructive uropathy, and postnatal work-up of foetally diagnosed high grade hydronephrosis. Minutes of a mini-symposium at the ESPR annual meeting. *Pediatr Radiol.* 2009;39(8):891–8.
- Riccabona M, Lobo ML, Ording-Muller LS, Augdal TA, Avni FE, Blickman J, Bruno C, Damasio B, Darge K, Ntoulia A, Papadopoulou F, Vivier PH. *ESPR Abdominal (GU and GI) Imaging Task Force—imaging recommendations in paediatric uro-radiology, part IX: imaging in anorectal and cloacal malformation, imaging in childhood ovarian torsion, and efforts in standardising pediatric uro-radiology terminology. Report on the mini-symposium at the ESPR meeting in Graz, June 2015.* *Pediatr Radiol.* 2017;47:1369–80.
- Riccabona M, Oswald J, Donoghue V. *Postoperative imaging and findings.* In: Riccabona M, editor. *Paediatric urogenital radiology.* 3rd ed. Cham: Springer; 2018. p. 517–35.
- Riccabona M, Beer M, Metzger HJ, editors. *Bildgebung des Thorax bei Neugeborenen und Kleinkindern.* Berlin: Springer; 2019.
- Sauer H, Kurz R, editors. *Checkliste Kinderchirurgie.* Springer; 1981. ISBN: 3-13-593201-X.
- Stafrace S, Lobo LM, Augdal TA, Avni FE, Bruno C, Damasio MB, Darge K, Franchi-Abella S, Herrmann J, Ibe D, Ključevšek D, Mentzel HJ, Napolitano M, Ntoulia A, Ording Müller LS, Perucca G, Petit Ph, Smets AM, Toso S, Woźniak MM, Riccabona M. Imaging of anorectal malformations: where are we now? *Pediatr Radiol.* 2022;52(9):1802–1809. <https://doi.org/10.1007/s00247-022-05395-7>.
- Westgarth-Taylor C, Westgarth-Taylor TL, Wood R, Levit M. Imaging in anorectal malformations: what does the surgeon need to know? *S Afr J Radiol.* 2015;19:903–13.



Image-Guided Interventions in Newborns

7

Brian D. Coley

7.1 Introduction

Interventional radiology techniques and procedures have dramatically improved the care of neonates, and image guidance has provided safer and often more effective procedures than traditional methods or open surgery. Like everything related to the care of the newborn, an understanding of their fragile physiology and the unique nature of their conditions is required in order to best care for them. This often requires a team of specialists to arrive at the best decisions about any proposed procedure. Once a decision is made to perform an intervention, attention needs to be paid to preparing the patient (and parents), sedation and anaesthesia, image guidance and equipment selection, and ensuring that the appropriate support personnel are present during and after the procedure.

usually guides the overall care plan, but there may be input from paediatric subspecialists, surgeons, anaesthetists, and of course radiologists. Ideally, the patient's family will also be involved in these discussions and decisions. The interventional radiologist must make themselves aware of the patient's condition, prior and current laboratory values and imaging results, the diagnostic or therapeutic goals, and must be experienced in the requested procedure. Whether the procedure is performed at the bedside in the NICU or in the radiology department, there must be sufficient well-trained personnel (technologists, nurses, etc.) to support both the patient and the proceduralist to achieve the best outcomes.

7.2 Requisites

7.2.1 The Team

Many neonatal conditions are complex and require the input of multiple specialists to make the best management decisions. A neonatologist

7.2.2 Image Guidance Methods

US is the main modality for image guidance in neonatal intervention. Advantages include excellent visualisation of neonatal structures, portability, and avoidance of ionising radiation. With US procedures may be performed in the NICU at the bedside for critically ill children. Anatomy can be visualised directly in multiple planes, and needles and catheters guided to their target with real-time control and accuracy. The best available US equipment should be used to provide optimal imaging. Due to the neonate's small size, high-frequency linear or curved linear array transducers can provide detailed imaging. Small-footprint transducers are needed for imaging through small

B. D. Coley (✉)
Radiology and Pediatrics, Cincinnati Children's
Hospital Medical Center, University of Cincinnati
College of Medicine, Cincinnati, OH, USA
e-mail: brian.coley@cchmc.org

acoustic windows. The system should have colour and pulsed Doppler capabilities. Most structures will be well seen, but UCA may have occasional value. Most US guidance is performed freehand, but needle guides can occasionally be useful.

If performed in radiology, fluoroscopy may be used to allow visualisation of wires and catheters (particularly if located in areas that obscure US like within the chest and cranium) and for intravascular contrast administration. Fluoroscopy settings should limit radiation exposure by optimising kVp and mAS, reducing pulse rate, and using any manufacturer dose reduction software. Physical collimation should limit visualisation to only those areas needed for the examination. Any diagnostic or interventional procedure using radiation should adhere to the ALARA principle (As Low As Reasonably Achievable).

7.2.3 Equipment

Not surprising, the equipment used to perform neonatal interventions often differs from that used in older children and adults. Shorter distances, smaller structures, and more delicate tissues require different devices and greater care in their use. The availability of smaller devices has improved but is still sometimes limited. Given the different and changing products and their availability in different countries, the following is only a general discussion. The interventional radiologist needs to be aware of what is available to them and elect those devices most suitable to their practice and experience.

- *Needles:* Every interventional procedure involves precisely guiding a needle to a target. The needs of the procedure determine the choice of needle. Simple small gauge needles (22 or 24-gauge) can be used to aspirate thin fluid collections or to inject contrast into a structure. Coaxial needles with a removable inner stylet and outer metal or plastic sheath are especially useful as the inner stylet mini-

mises tissue coring and after stylet removal can allow aspiration or passage of a guide wire for subsequent work. Small guide wires (0.018 in. and smaller) can be passed through 22 or 24-gauge angiocatheters. To minimise tissue trauma from serial dilatation and to provide greater working stability, sometimes it is preferable to use a larger gauge sheathed needle to place a larger gauge guidewire directly.

- *Wires:* The Seldinger technique starts with placing a needle into a structure followed by the passage of a guide wire to allow subsequent tract dilatation and catheter placement. Smaller wires with more floppy tips are typically used for vascular access or for initial access where use of a larger or stiffer device would be dangerous. Larger and stiffer wires are used where there is need for greater support for subsequent dilatation or the passage of larger catheters. There are a vast array of wire sizes, constructions, composition, and stiffness, many designed for very specific procedures. No matter what wire is used, the interventional radiologist must always be aware of the location of the tip of the wire and ensure that the wire does not become bent or kinked.
- *Drainage catheters:* For treating abscesses or relieving obstructions, it is often necessary to leave a drainage catheter in place. Drainage of thin liquid material may be sufficient with a very small catheter (4F–6F) whereas thicker collections may require larger catheters (8F–12F or rarely even larger). Drainage catheters often have a loop at the end with drainage holes along the inner curvature of the loop (a “pigtail”) that may have a locking thread. This design helps the catheter to remain in position and helps to prevent catheter occlusion. Once placed, proper positioning can be confirmed with gentle instillation of saline or ultrasound contrast if using US, or iodinated contrast if using fluoroscopic assistance.

After confirmation of proper placement, the catheter must be secured to the skin to help prevent dislodgement. Catheters can be

sutured directly to the skin, and adhesive retention device may be used. No matter what method is used, care must be taken with the delicate skin of the newborn. A sterile bio-occlusive dressing also helps to secure the catheter.

- *Vascular catheters:* These include catheters used during intravascular diagnostic and treatment procedures and those left in place to allow for long-term vascular access.

In neonates, it is preferable to perform angiography via a vascular access sheath to minimise blood vessel trauma. Catheters of 3F or 4F are typically used for diagnostic angiography (much less common currently with improvements in CT and MR angiography). For superselective diagnostic injections or for embolisation or sclerotherapy, small micro-catheters can be placed coaxially within a guiding 3F or 4F catheter.

The choice of indwelling catheter for vascular access depends upon the fluids to be infused, the anticipated duration of therapy, and the available access, and should be made in collaboration with the clinical team. Peripherally inserted central catheters (PICC) from 1.9F to 3F are a common choice for medium-term access needs. Larger multilumen catheters may be needed clinically, but have an increased risk of complications such as vessel stenosis and thrombosis. Tunnelled catheters are usually reserved for longer access needs and provide some protection against line infection. These may be placed by either interventional radiology or surgery teams.

- *Biopsy devices:* Specialised percutaneous biopsy needles are constructed with an inner slotted stylet and outer cutting cannula to retrieve a core of tissue. Manually operated biopsy needles allow extension of the inner slotted stylet into the target of interest and then passage of the outer cannula, semi-automated devices allow manual passage of the inner cannula and then spring-loaded “firing” of the outer cannula, and fully automated devices in which the inner stylet and outer

cannula are sequentially “fired” from a spring-loaded device. Different devices have different diameters, specimen lengths, and depth of penetration. The size and number of samples vary depending upon the tissue sampled and the diagnostic needs, but in general smallest and fewest number of samples needed for diagnosis should be obtained.

7.2.4 Patient Preparation

When preparing to perform a procedure, the paediatric interventional radiologist has at least two patients: the child and the parent. Both need attention. The parents of a sick newborn are already stressed and anxious, and the idea of their child undergoing any kind of procedure will understandably make this worse. The interventional radiologist should speak with the parents directly about the procedure and the reason for doing it, as well as any potential risks and complications.

Prior to the procedure, all relevant imaging and laboratory studies should be performed and reviewed. If appropriate for the procedure, platelet count and coagulation profiles should be checked and corrected if necessary. For abscess drainage, biliary intervention, and nephrostomy tube placement, pre-procedural antibiotics should be administered. Whether the procedure is performed at the bedside or in the interventional radiology suite, the room should be warmed and warming devices used. Neonates are very susceptible to hypothermia, which can cause severe physiologic consequences.

Proper patient and radiologist positioning is essential for a safe and effective procedure. Consider the path of the needle and what manoeuvres will be performed. Make sure that the patient is properly supported and secured. Make sure that the table height is appropriate for the interventional radiologist, that imaging screen is easily seen, and that necessary equipment is within comfortable reach (Fig. 7.1). The effort focusing on patient and radiologist posi-



Fig. 7.1 Patient positioning and preparation. Prior to beginning the procedure on this neonate, he is positioned on the interventional table at a comfortable height for the interventional radiologist, with easy access to both ultrasound and fluoroscopy if needed. The US and fluoroscopy screens are easily seen. Two other personnel are in the room for patient monitoring and safety, and to provide supplies and assist the radiologist if needed

tioning and preparing for the procedure is well worth the time and will result in a faster and safer procedure.

7.2.5 Sedation and Analgesia

Most neonates will require sedation or anaesthesia for the safe performance of many interventional procedures. The goal is to have a still and comfortable patient while maintaining the greatest level of safety. Sedation and analgesia should be provided and monitored by dedicated trained personnel, not the interventional radiologist (who should concentrate on the procedure itself, although in constant communication with those providing sedation).

Resuscitation equipment must be immediately available. The choice of sedation and anaesthesia depends upon the length and complexity of the procedure, the amount of pain expected, the physiology of the patient, and local preferences. Organ capsules, periosteum, pleura, and peritoneum are all richly innervated and produce pain when a needle passes through. Targeted local anaesthesia can greatly minimise this pain, which in turn can decrease the depth of sedation required and improve patient safety. Remember that local anaesthetics require at least 1–2 min to take effect, so be patient.

7.2.6 Post-procedural Care

The interventional radiologist's responsibility to the patient and parents does not end once the procedure is performed. Even simple procedure should be discussed with the parents after they are finished, and the radiologist should make sure that the patient is stable once back in their room. Biopsy patients should be monitored for bleeding complications. Any indwelling catheter that was placed should be monitored for proper function and care. The interventional radiologist is an important member of the clinical care team, and ongoing communication will improve procedural outcomes.



The most important requisites for image-guided interventions in neonates are consultation and shared decision making among the patient care team and family regarding the needed diagnostic information or therapeutic intervention with agreement on the care plan. First choose the best location for the procedure (at the bedside or in interventional radiology suite) taking into account procedural needs, contingencies, and patient condition.

Ultrasound is sufficient for guiding many procedures, with fluoroscopy often being helpful. If fluoroscopy is used, make sure to adapt technique and minimise exposure of the sensitive newborn to as little radiation as possible. Ensure that the proper equipment is present for the procedure before beginning. If performing the procedure at the bedside, consider bringing duplicates of each piece of equipment (in case of dropping, contamination, etc.). Ensure that the baby stays warm and is positioned as comfortably as possible. Ensure that you as the operator are positioned comfortably (e.g. sitting or standing, not having to contort in awkward positions, can see imaging screens, etc.).

If sedation or anaesthesia is used, have experience providers present to administer and monitor the patient.

Finally, being involved in the post-procedural care of the patient can lead to greater treatment success.

7.3 Clinical Applications

7.3.1 Vascular Access

Almost every patient in a NICU relies upon intravenous therapies as part of their treatment. While peripheral intravenous access is sufficient for some patients, many will need central venous access to support total parenteral nutrition (TPN) and other medications that cannot be administered peripherally. After delivery, central venous access is most commonly achieved with an umbilical venous catheter (UVC), but these cannot be safely left in place for longer than 7–10 days. Ultrasound can be used to help guide UVC placement and to confirm proper positioning near the IVC/right atrial junction, and to identify malpositioned catheters prior to use so as to avoid complications (Fig. 7.2).

If longer-duration access is required, it is important to carefully consider the likely needs of the patient, especially how long access will be required and how many lumens are needed. Ideally these decisions are made between the clinical team and a multi-disciplinary vascular access team composed of interventional radiologists, surgeons, and specially trained nurses or the neonatologists themselves. In general, the smallest line with the fewest lumens that allows appropriate patient care is the best option and leads to the fewest complications. Central venous catheters should be removed as soon as the child's condition allows to mini-

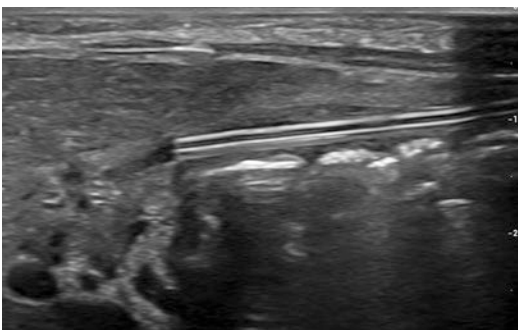


Fig. 7.2 Malpositioned UVC. Longitudinal US in a newborn with UVC malposition suspected on radiographs shows the UVC tip to be in the umbilical portion of the left portal vein within the liver

mise complications such as infection and thrombosis.

For neonates, a single or double lumen peripherally inserted central catheter (PICC) is often the best choice and provides medium-term vascular access. These are often placed at the bedside by a nurse or physician. Ultrasound guidance allows access of smaller and deeper vessels, improves procedural success, and reduces complications (Fig. 7.3). If there is difficulty in placement, the interventional radiologist may become involved. Longer term vascular access may require a tunneled catheter (the

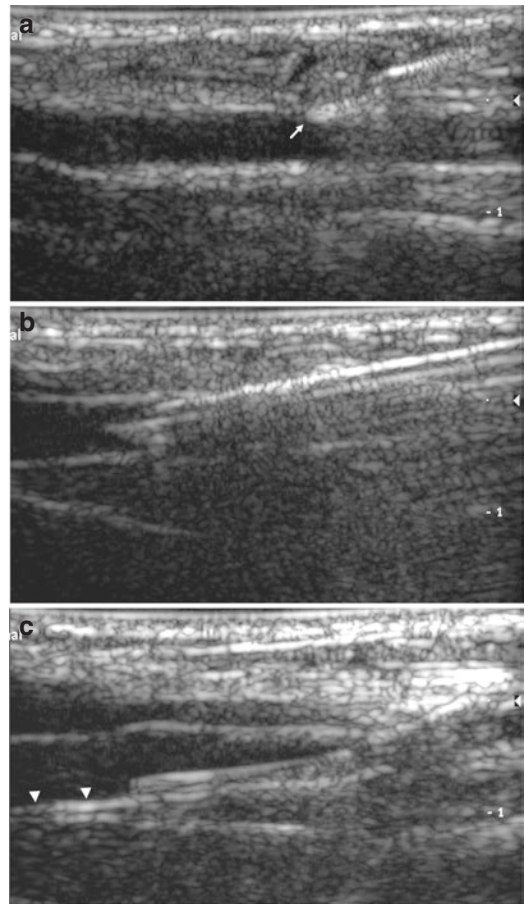



Fig. 7.3 Ultrasound-guided venous access and Seldinger technique. Longitudinal US image of a 3 mm basilic vein shows an approaching 22G needle with the point of the bevel at the anterior vein wall (arrow) (a). After advancing the needle, the bevel is clearly seen within the lumen of the vein (b). Subsequently, a guidewire is passed (arrowheads) followed by a vascular sheath allowing passage of the catheter (c)

details of specific catheters are beyond the scope of the chapter), which can be placed by either interventional radiologists or surgeons. No matter who places the catheter, it has been well-proven that using US guidance for the initial venous access results in greater success with fewer complications. If placed from the upper extremity central venous catheter tips should be positioned within the superior vena cava, and if placed from the lower extremity positioned near the inferior vena cava/right atrial junction (high position) or below the renal veins (low position). Care needs to be taken not to place upper extremity central catheters into the right atrium as these can lead to complications such as arrhythmia and cardiac perforation.

Finally, some centres use US for optimally positioning large ECMO catheters: during the procedure, the tip of the venous catheter is checked in the right atrium or proximal IVC and the arterial catheter at the aortic arch/common brachiocephalic trunk to assure bidirectional flow into the aorta without compromising flow to the coronary arteries and avoiding valve insufficiency. Once ECMO is started and ventilation is reduced, repositioning and adaptation are then checked (after the diaphragm moved up due to less respiration pressure thus usually also impacting catheter tip position) before the catheters are fixed.

 Image-guided vascular access in neonates: Umbilical venous catheters are used in the first week of life, and their position can be assessed by US.

Peripherally inserted central catheters (PICC) are the most commonly used access for medium and long-term central venous requirements. These can be placed at the bedside or in the interventional radiology suite, and US guidance improves placement success.

Central venous catheters or large arterial access catheters are usually only placed in surgical or oncology conditions, or for ECMO.

7.3.2 Enteric Access

Nutritional support is essential for the health and growth of newborns, especially the premature and those fighting other diseases or conditions. While total parenteral nutrition can be given through central venous catheters, it is preferable to feed babies enterally whenever possible. If a baby cannot properly take a bottle or obtain enough nutrition through normal feeding, then enteral support becomes necessary.

Nasogastric or orogastric tubes are the easiest method to support enteral nutrition and are placed at the bedside often with radiographic confirmation of positioning (although this can also be done with ultrasound). If gastroesophageal reflux or poor gastric motility is a problem, tubes can be advanced beyond the pylorus into the duodenum or even the proximal small bowel (Fig. 7.4). This can be done at the bedside, but the radiologist will often become involved as positioning may require the use of fluoroscopy, guidewires, and rarely guiding catheters for proper tube positioning. As with any procedure, it is important to place the proper tube, and this requires considering the patient's medical and nutritional needs as well as the size of the patient. In general, most neonatal nasoduodenal or nasojejunal tubes should be no



Fig. 7.4 Nasojejunal feeding tube placement. Completion image after placement of a 6F feeding tube in a 2-week-old boy with neonatal brain injury shows the tube in good position with its tip near the ligament of Treitz. Note that fluoroscopic last-image hold capture was used rather than a new exposure to minimise radiation dose

larger than 6F. Larger tubes may not traverse the small turns of the neonatal GI tract and there is an increased risk of bowel perforation.

In neonates with neurological dysfunction needing long-term enteric access, those with specific nutritional requirements, and those with altered oral and oesophageal anatomy, gastrostomy tube placement may be required. Gastrostomy tubes may be placed surgically, endoscopically, or by interventional radiological techniques, and the decision of what approach will vary by the needs of the patient and institutional practices. Interventional radiology placed gastrostomy tubes can be performed with either an antegrade approach (in which a needle is directed from the stomach out the abdominal wall via a transoral approach) or retrograde. In performing a retrograde percutaneous gastrostomy, the margins of the liver and spleen are determined with US, and the position of the small bowel and colon defined with fluoroscopy. A site below the left costal margin and lateral to the rectus abdominis muscle is chosen and the stomach inflated via a nasogastric tube. A needle is passed into the stomach and a gastric fastener placed to help secure the stomach to the anterior abdominal wall. Through the initial puncture or a second puncture a guidewire is passed, the tract dilated, and an appropriately sized balloon gastrostomy tube placed and secured in position. In patients with gastroesophageal reflux and at risk for aspiration, a jejunal tube can be placed coaxially through the gastrostomy tube, or a primary percutaneous gastrojejunostomy tube can be performed. In general, the retrograde technique decreases (but does not eliminate) the risk of injury to the colon, liver, and spleen compared to antegrade approaches. Complications include gastric leak and infection, most of which are treatable non-surgically.



Image-guided enteric access in neonates: Newborns in need of short-term feeding assistance can be supported by nasogastric tubes, or post-pyloric tubes that can be placed at the bedside or by radiologists. Because of the small size of the intes-

tines and risk of perforation, post-pyloric feeding tubes should not be larger than 6F unless there are special patient care needs.

Long-term enteric access via a gastrostomy can be accomplished through surgical, endoscopic, interventional radiological, and combined approaches. When using fluoroscopy, ensure that dose parameters are optimised for the patient size, do not use image magnification (unless only digital), reduce frame rate, and keep the image intensifier as close to the patient as possible to minimise radiation exposure.

7.3.3 Aspiration and Drainage

Aspiration and drainage of fluid collections and for either diagnosis or treatment are a basic part of neonatal interventional radiology practice.

7.3.3.1 Peritoneal Cavity

Intraabdominal fluid collections in neonates may be simple ascites, bile or chyle leaks, or related to infection and abscess formation from necrotising enterocolitis or surgical procedures. Paracentesis can provide diagnostic information about the nature of the fluid and can also be therapeutic in the setting of respiratory compromise, abdominal compartment syndrome, or infection. US guidance of needle placement allows targeting of even small fluid collections and ensures that adjacent organs are not inadvertently injured. After an appropriate access site is chosen and the skin sterilely prepared, local anaesthesia is injected from the skin surface to the peritoneum. For simple fluid collections, small gauge needles or angiocatheters (e.g. 22G or smaller) are sufficient (Fig. 7.5), but thicker or more complicated collections may require larger needles or catheters (e.g. 18G needles or 4F catheters). If a drainage catheter needs to be left in place in the case of abscesses, it should be positioned in the most dependent portion of the collection to ensure complete drainage. The approach is the same as for an aspiration, except that once a sample is obtained for necessary



Fig. 7.5 Paracentesis. Persistent simple ascites of unclear aetiology is sampled via US guidance with a 23G needle, with care being taken not to puncture the underlying bowel (B)

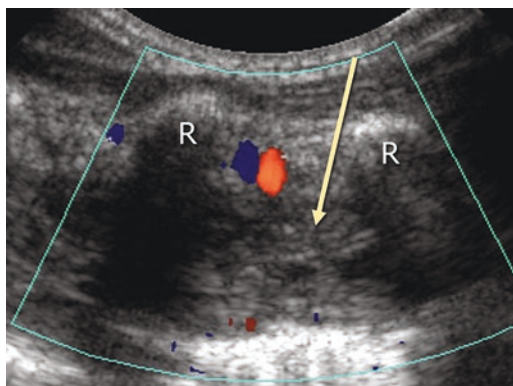


Fig. 7.6 Thoracentesis approach. Longitudinal image between two ribs (R) shows the artery and vein of the intercostal neurovascular bundle below the superior rib. The approach into the thorax should follow the arrow and pass immediately superior to the rib at the needed level

studies a guide wire is passed through the access needle or sheath, the tract dilated (if necessary), and a catheter positioned into the collection. After drain placement and abscess aspiration, US (possibly supported by UCA instillation) can determine the adequacy of drainage and the need for additional drains or drain repositioning. The catheter is then secured in position to prevent inadvertent dislodgement and left in place until drainage ceases and the patient becomes afebrile. If the patient's symptoms do not improve, follow-up imaging to evaluate for untreated collections may be necessary.

7.3.3.2 Thorax

Pleural effusions in newborns may result from chylothorax, congenital heart disease, hydrops, infection, and after surgery. After choosing a site for thoracentesis, local anaesthesia should be placed from skin surface to the parietal pleura. Needles should be directed over the top of a rib, avoiding the neurovascular bundle that is on the inferior surface of each rib (Fig. 7.6). Ultrasound guidance can assure that the needle does not puncture the underlying lung, and if the thoracentesis is meant to be therapeutic can assess completeness of fluid drainage (Fig. 7.7). For ongoing processes or infected collections (e.g. empyema), a drainage catheter should be placed in the most dependent part of the collection to allow optimal drainage. In the case of parapneumonic collections, US may disclose septations and loculations

indicating that it may be necessary to instil fibrinolytic medications (e.g. tPA, urokinase) to facilitate more complete drainage.

7.3.3.3 Liver and Biliary Tract

Percutaneous cholangiography is occasionally required in neonates with persistent hyperbilirubinaemia suspected of having biliary obstruction (e.g. biliary atresia) or malformations (e.g. choledochal cyst). If a gallbladder is present (whether normal or rudimentary), it is often easiest to access if there are not dilated intrahepatic ducts (Fig. 7.8). If one is accessing dilated bile ducts, pre-procedural antibiotics should be given to avoid cholangitis. Intrahepatic collections are uncommon in the neonate, and most are related to complications of umbilical venous catheters. If these collections become infected, they may require US-guided percutaneous aspiration for diagnosis of causative organisms and catheter drainage for treatment

7.3.3.4 Genitourinary Tract

Congenital urinary tract dilatation (UTD) is a common condition and the causes and whether there is obstruction are usually discernible with non-invasive imaging. However, some cases are less clear in which case percutaneous renal access and nephrostomy tube placement may be needed for proper diagnosis, to relieve obstruction, to assess the recoverable function of a dilated kidney, and for drainage of infection.

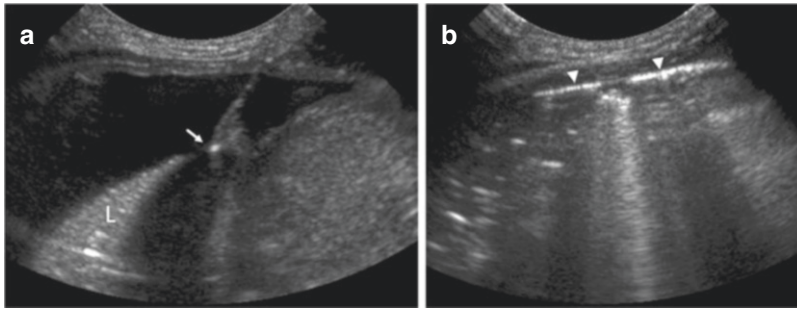


Fig. 7.7 Thoracentesis. A small angiocatheter is placed into a simple pleural effusion with care taken to avoid the tip (arrow) puncturing the underlying atelectatic lung (L)

(a). After near complete aspiration of the effusion, the echogenic catheter sheath (arrowheads) is seen with early re-expansion of the underlying lung (b)

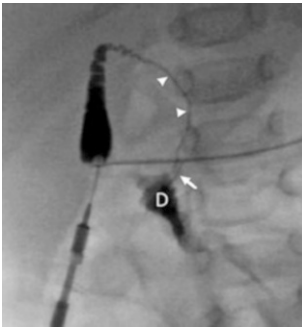


Fig. 7.8 Percutaneous cholangiogram in biliary atresia. Contrast injection after gallbladder puncture in a 3-week old with persistent jaundice shows a small gallbladder with a patent cystic duct (arrowheads) and a patent distal common bile duct (arrow) with contrast emptying into the duodenum (D). However, the common hepatic duct and intrahepatic bile ducts do not opacify. Subsequent liver biopsy and surgery confirmed biliary atresia

In cases of suspected infection, pre-procedural antibiotics should be given. After adequate sedation, the patient is placed in a prone or prone-oblique position, the skin sterilely prepared, and local anaesthesia delivered from skin to renal capsule. For routine drainage of a dilated collecting system, a subcostal approach into a lower pole calyx is usually the easiest approach (Fig. 7.9). For simple aspirations, access with a 22G needle is sufficient. If the fluid is obviously infected, then a small gauge guidewire (e.g. 0.018) with subsequent tract dilatation and catheter placement is used. Most neonatal kidneys can be adequately drained with a 5F or 6F catheter, while 8F catheters may be necessary in those with pyonephrosis or the rare renal abscess (provided it is not responding

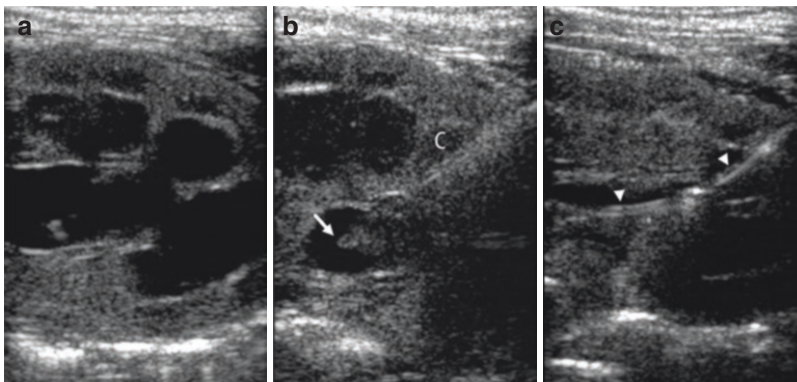



Fig. 7.9 Percutaneous nephrostomy for renal obstruction. Longitudinal sonogram shows a dilated renal pelvis and calyces with compression of the medullary pyramids (a). A 22G needle is placed into the renal pelvis (arrow)

via a lower pole calyx (C) (b). After passage of a guide-wire and 6F drainage catheter (arrowheads), there is immediate decompression of the upper collecting system (c)


to antibiotic treatment). If it is already known that a drainage catheter is to be placed, then it may be advantageous to access the kidney with a larger needle (with a stylet to prevent tissue coring) so that a larger wire providing more security can be placed primarily. This can be safely done with US guidance and by limiting wire exchanges may results in a safer procedure. The use of a combined US and fluoroscopic approach is often advantageous.

Other genitourinary interventions include percutaneous cystostomy for bladder outlet obstruction when it is not possible to pass a urethral catheter. Decompressing the bladder relieves ureteric pressure and accompanying UTD that can improve renal function. Neonatal ovarian cysts are common and usually asymptomatic but predispose to ovarian torsion if larger than 4 cm. Most resolve spontaneously, but US-guided aspiration provides a less invasive treatment option than surgery for persistent or growing cysts (Fig. 7.10).

 Image-guided aspiration and drainage in neonates: Ultrasound is typically the only guidance method needed. When performing thoracentesis, always place the needle immediately over a rib to avoid the intercostal vessels. When aspirating a collection, have the equipment ready to leave a drainage catheter if it becomes necessary. Use pre-procedural antibiotics when accessing obstructed systems or in cases of infection.

7.3.4 Lumbar Puncture

In the evaluation of the septic neonate, lumbar puncture (LP) for cerebrospinal fluid (CSF) analysis is often required. This is usually accomplished clinically, but in some cases may be unsuccessful or excess blood in a CSF sample may preclude adequate analysis. Because of the acoustic window allowed by incompletely ossified posterior elements, US can reveal post-LP complications such as extradural collections compressing the thecal sac that would make further LP attempts futile. Imaging the patient in a semi-upright position may show distention of the thecal sac and provide a target for CSF collection (Fig. 7.11). If clear CSF is seen, US-guided LP allows successful access of even small pockets of CSF and thus can allow more rapid diagnoses. It is advantageous to place the patient at a 45° upright angle over a cushion or pillow to allow the distal thecal sac to distend as much as possible from the height of the CSF column. With supportive positioning and the use of local anaesthesia, US-guided LP can be performed without sedation. A small spinal needle (22G or smaller) is then directed under direct US guidance via a mid-line or paramidline sagittal approach (Fig. 7.12).

 Image-guided lumbar puncture in neonates: Ultrasound can detect clinical LP complications and assess if there is CSF available to be sampled. Placing the patient semi-upright at 45° will enable visualisation of fluid and make LP easier.

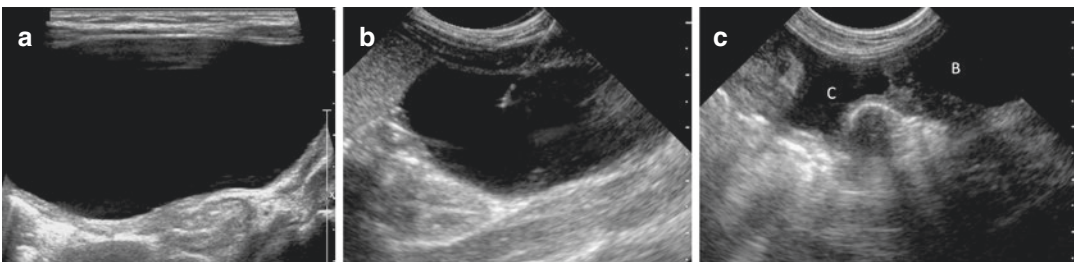


Fig. 7.10 Neonatal ovarian cyst aspiration. Initial ultrasound shows a large cyst extending from the pelvis into the upper abdomen (a). Other images showed small daughter

cysts confirming ovarian origin. A 22G needle is placed into the cyst (b). After aspiration, the cyst (C) is greatly decompressed and seen just above the urinary bladder (B) (c)

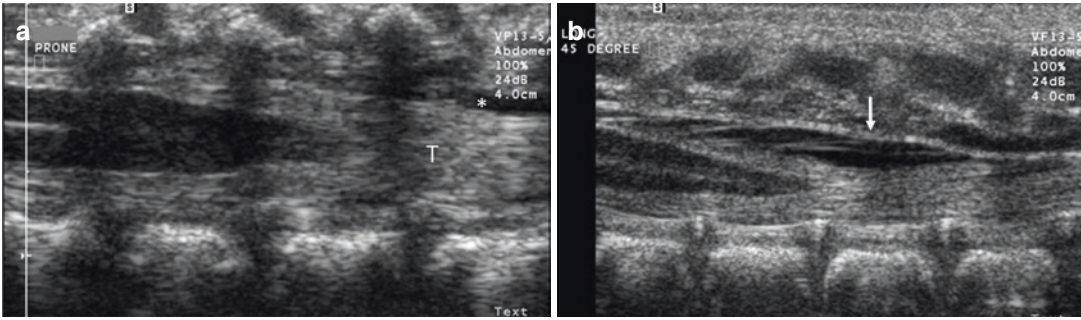


Fig. 7.11 Failed lumbar puncture. Longitudinal sonogram in a septic infant after unsuccessful clinical lumbar puncture shows collapsed nerve roots with no fluid in the thecal sac (T) and a small amount of leaked extradural

CSF or blood (asterisk) (a). After placing the baby 45° upright on a pillow for 5 minutes, clear CSF (arrow) is now seen within the thecal sac that is sufficient for image-guided lumbar puncture attempt (b)

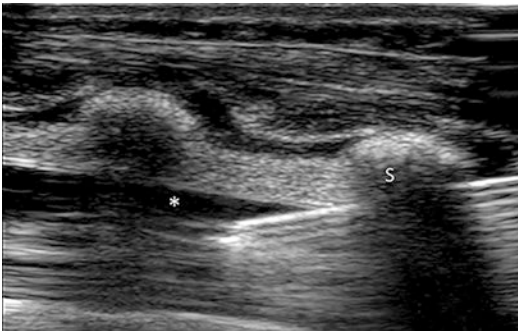


Fig. 7.12 Lumbar puncture. Longitudinal sonogram shows a 22G spinal needle taking a low-angle approach passing just below a spinous process (S) into clear CSF within the thecal sac (asterisk)



Fig. 7.13 Liver biopsy. In preparing to perform a liver biopsy, liberal local anaesthesia is placed with the needle tip (arrow) against the liver capsule

7.3.5 Biopsy

Image-guided percutaneous tissue biopsy is often preferred to open surgical biopsy in neonates. Biopsies may be targeted for diagnosis of a specific focal lesion or may involve sampling of an organ to determine overall structure and condition. Prior to the biopsy, it is essential to discuss with the pathologist what type and quantity of a sample are needed for diagnosis. Almost all abdominal and soft tissue solid lesions are localisable by US, and even chest and mediastinal masses can be localised if there is an adequate acoustic window. Ultrasound also allows the multiplanar planning of a safe biopsy approach to avoid inadvertent injury of adjacent structures. Biopsy devices may be manual, semi-automated, or completely automated (see Sect. 7.2.3).

7.3.5.1 Liver

Liver biopsy may be performed for characterisation of diffuse disease (e.g. biliary atresia) or for focal hepatic lesions (e.g. neuroblastoma metastases), and is most safely performed with US guidance. Prior to the procedure, platelet counts and coagulation profiles should be checked and corrected. Once the area of interest is localised (often the right hepatic lobe for general tissue sampling), an appropriate site below the costal margin is chosen for skin entry. Local anaesthetic should be delivered from the skin surface to the peritoneum and liver capsule to minimise pain (Fig. 7.13). If a single biopsy is to be obtained, the biopsy needle should be placed deep to the liver capsule to avoid unnecessary injury when the sample is obtained. If two or more samples are to be obtained, consider using a coaxial technique



Fig. 7.14 Liver biopsy with tract embolisation. After a coaxial technique percutaneous biopsy in a neonate with partially corrected coagulopathy, gelatin sponge (arrowheads) has been introduced through the biopsy guiding cannula (arrow) to promote haemostasis

where a larger guiding cannula is placed into the liver below the capsule and the biopsy device deployed through the cannula. The coaxial technique permits multiple samples with only one puncture of the liver capsule and allows for embolisation of the biopsy tract (e.g. with gelatin sponge) to minimise bleeding complications (Fig. 7.14).

7.3.5.2 Kidney

Renal biopsy is rarely required in neonates but may be necessary to characterise forms of dysplasia or inflammation or to identify and characterise neoplastic involvement. Ultrasound guidance is essential for safe tissue sampling and to avoid vascular and collecting system injury. Smaller biopsy needles (e.g. 18G) are usually sufficient. Even with careful technique, bleeding and arteriovenous fistula formation may be complications, but are usually self-limited and managed conservatively.



Image-guided biopsy in neonates: While small gauge samples are usually sufficient, consult with the pathologist who will be evaluating the specimen to ensure that sufficient material is acquired for diagnosis.

Organ capsules are highly innervated, so place ample local anaesthetic next to the capsule to reduce pain. The coaxial technique allows multiple biopsies with reduced trauma from needle passes and allows embolisation of the biopsy tract if needed.

7.3.6 Vascular Intervention

With modern imaging, diagnostic arteriography and venography are rarely needed. Some conditions, particularly cardiac conditions or vascular malformations, may require arteriography and endovascular treatment. The most common sites for transarterial access are the femoral artery and umbilical artery in the newborn. The small vessels of the neonate are predisposed to spasm and thrombosis that can rarely lead to vascular compromise of an extremity. The use of the smallest catheters necessary to achieve the desired diagnostic or therapeutic goals, systemic heparinisation (unless contraindicated) and pulse monitoring during the procedure, and treatment of any resulting access site occlusion can minimise local access site complications.

7.3.6.1 Vascular Tumours

Infantile haemangiomas are the most common benign vascular neoplasms in neonates and can occur anywhere in the body. The typical natural history is for them to appear in the first weeks of life, grow in the first year of life (sometimes dramatically), and then involute throughout early childhood. Most of these are asymptomatic. Cutaneous lesions may produce cosmetic disfigurement and can bleed or become secondarily infected. Visceral infantile haemangiomas most often involve the liver and may be single or multiple. When multiple and during their growth phase, intralesional arteriovenous shunting may result in cardiac overcirculation, hepatic dysfunction, and rarely consumptive coagulopathy. Most symptomatic infantile haemangiomas respond well to medical therapy (e.g. propranolol) and rarely require transcatheter embolisation.

Congenital haemangiomas are present at birth and may rapidly involute, partially involute, or not involute. These are less responsive to medical therapy and may require intervention if symptomatic or disfiguring.

Kaposiform haemangioendotheliomas are a rare tumour arising in infancy and occasionally in the neonatal period. These aggressive lesions can produce life-threatening consumptive coagulopathy; as there is no effective medical therapy, interventional radiology and surgical approaches are necessary.

Regardless of the location and histology of the vascular tumour, the goal of intervention is to identify and selectively catheterise the feeding arteries and occlude them. Microcatheters delivered through a larger guiding catheter allow selection of very small vessels which may then be occluded with particles, liquid embolic agents, or even coils. Before embolisation, angiography should ensure that there are no large arteriovenous shunts that may result in embolisation material passing into the venous circulation. In the setting of diffuse hepatic involvement, embolisation may need to be staged to ensure sufficient hepatic blood flow and to avoid exacerbating hepatic failure.

7.3.6.2 Vascular Malformations

Vascular malformations result from abnormal development of the lymphatic, venous, and/or arterial system and thus are present at birth. They may be simple (involving just one type of vascular structure) or complex (involving more than one type) and are often further grouped into low flow (lymphatic and venous malformations) and high flow lesions (arteriovenous malformations and arteriovenous fistulas).

Low flow lymphatic, venous, and venolymphatic malformations rarely require treatment in the neonatal period (and may not even be recognised until later in childhood). However, larger lesions or those impinging on important structures (e.g. head and neck lesions compromising the airway) may require treatment. Medical treatment with sirolimus has shown promise for shrinking lymphatic malformations but less so for venous and mixed malformations. Interventional sclerotherapy provides an

effective alternative or adjunct to surgery for the management of these malformations. The details and discussion of specific agents are beyond the scope of this discussion, but the common approach is to access the malformation, assess the amount of lesion filled by contrast injection (usually under fluoroscopy, but US and UCA can also be used), ensure that any outflow into normal structures is controlled (in the case of venous malformations), and instil a sclerosing agent into the structure to create endothelial injury and subsequent obliteration of the lesion. Interventional therapy may be sufficient for complete treatment or may be part of combined medical and surgical therapy.

Arteriovenous malformations (AVM) and arteriovenous fistulas (AVF) are more likely to cause problems of organ function or problems with growth and development. Peripheral AVMs may lead to growth disturbance through a combination of hypervascularity to the lesion and underperfusion of other areas due to vascular steal. While rarely presenting in neonates, intracranial AVMs carry a risk of intracranial haemorrhage. In the liver, congenital portosystemic and hepatic arteriovenous shunts can produce hepatic dysfunction, encephalopathy, and cardiac failure if the volume of left to right shunting is large.

Vein of Galen malformations are a spectrum of intracranial high flow VMs/AVFs ranging from simple or complex arteriovenous fistulae and may even include components of AVM. These may be diagnosed prenatally and patients present with congestive heart failure, cranial bruit, hydrocephalus (from compression of enlarged vascular structures on ventricular outflow) and central nervous system problems related to cerebral ischaemia from arterial steal. Endovascular treatment aims to occlude the abnormal arteriovenous communications to allow normal perfusion to the rest of the brain and subsequent normal development. Due to the complex vascular supply to these malformations and the shift in cerebral haemodynamics that result from therapy, treatment is usually staged over several sessions (Fig. 7.15).

As with the treatment of vascular tumours, treatment of AVMs begins with selective catheterisation

of feeding arteries. It is important to obliterate the vascular nidus of an AVM and not just the feeding arteries, otherwise new arteries may be recruited to supply the lesion. The presence of associated intralesional AVF or shunts must be evaluated before injecting embolic material. Arteriovenous fistulas lack an intervening nidus between the arterial and

venous systems. Treatment involves occlusion of the abnormal communication and may be approached by either the arterial or venous systems (Figs. 7.16 and 7.17). These often require the use of occluding devices and coils to slow or halt venous outflow, and coils and liquid embolic agents (e.g. glue or other polymers) to occlude arterial inflow.

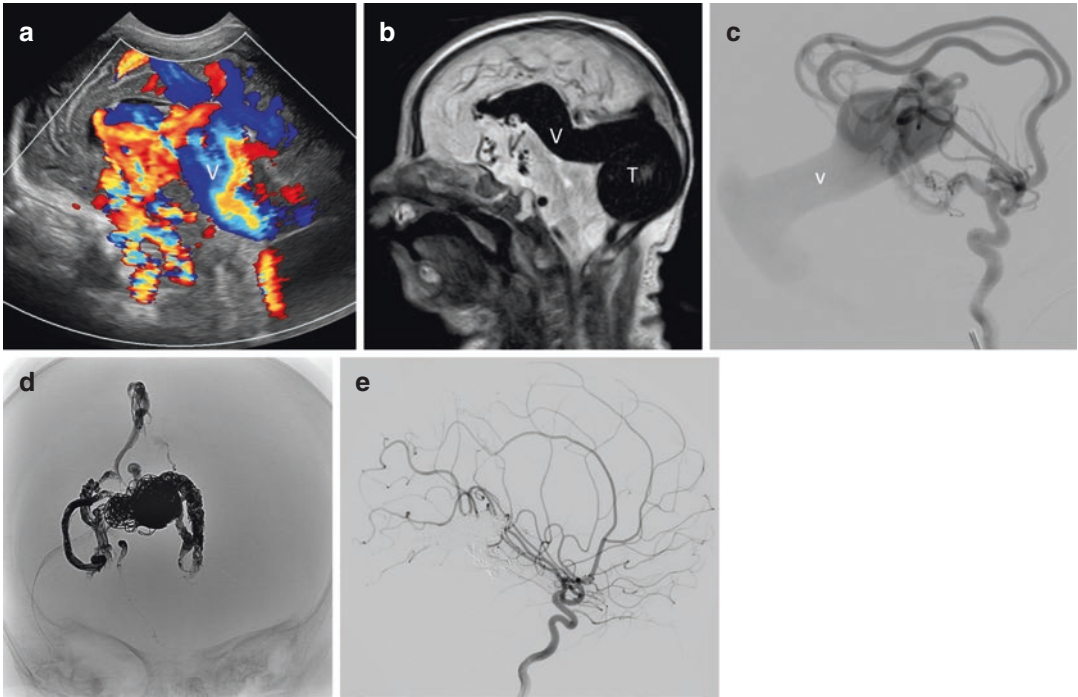


Fig. 7.15 Staged treatment of vein of Galen malformation. Sagittal midline colour Doppler US in a newborn with heart failure and a cranial bruit shows enlarged internal carotid and pericallosal arteries with turbulent flow and a dilated strait sinus and vein of Galen (V) (a). Corresponding sagittal T1-weighted MRI shows a dilated vein of Galen (V) and a massively enlarged torcular herophili (T) (b). Right internal carotid arterial injection digital

subtraction angiogram shows enlarged pericallosal arteries and middle cerebral arterial arteriovenous communications to a dilated vein of Galen (V) (c). Frontal scout view after four separate treatment sessions shows the placement of numerous coils and liquid embolic agents into the supplying arteries (d). Lateral completion digital subtraction arteriogram of the right internal carotid artery shows normal vessels and no arteriovenous shunting (e)

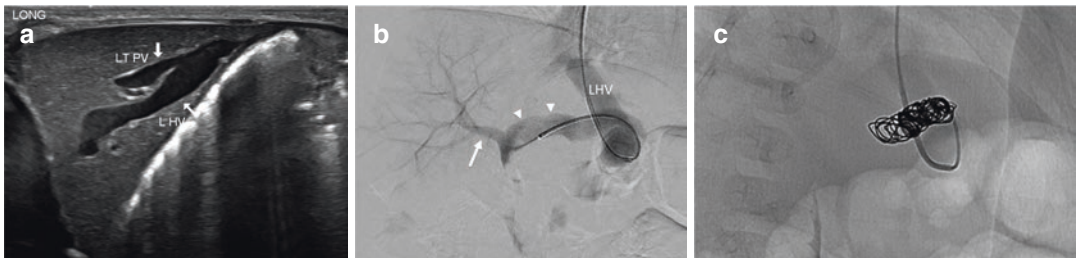


Fig. 7.16 Congenital portovenous fistula in a baby with liver dysfunction. US of the left hepatic lobe shows an abnormal communication between an enlarged left portal vein (LT PV) and an enlarged left hepatic vein (LHV) (a). The right internal jugular vein was accessed a catheter

directed retrograde into the abnormal fistulous connection (arrowheads) between the portal vein (arrow) and the left hepatic vein (LHV) (b). Multiple embolisation coils completely closed the fistula, and normal liver function returned (c)

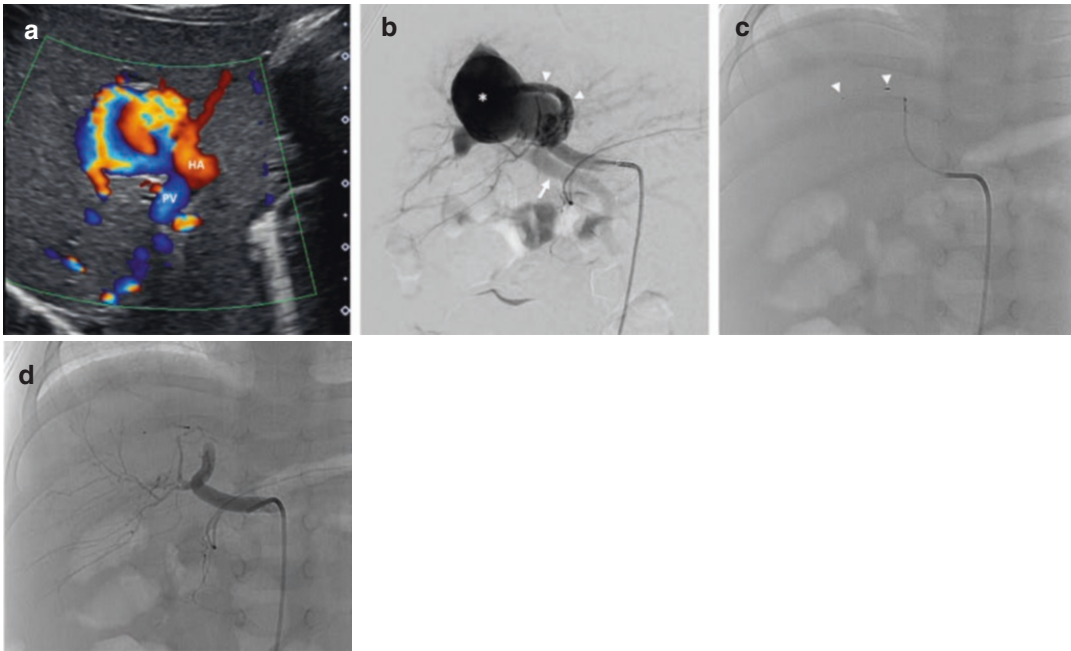



Fig. 7.17 Congenital hepatic arterioportal fistula diagnosed prenatally in a baby with liver dysfunction and portal hypertension. Colour Doppler US shows an enlarged hepatic artery (HA) feeding into an aneurysmally dilated segment of the portal vein. Notice that the flow in the main portal vein (PV) is retrograde (**a**). Selective hepatic arterial injection shows an enlarged left hepatic arterial branch

(arrowheads) feeding directly into a portal venous aneurysm (asterisk). Note the retrograde flow within the main portal vein (arrow) (**b**). A microcatheter was placed through the previous angiography catheter and a vascular occlusion device deployed (marked by arrowheads) (**c**). Completion angiogram shows that the fistula is occluded and there is preserved hepatic arterial flow to the rest of the liver (**d**)

 Image-guided vascular interventions in neonates: Advances in imaging have made diagnostic angiography largely obsolete, but there are situations where transcatheter vascular treatment is needed. Most infantile haemangiomas require no treatment or respond to medical therapy. Rarely will embolisation be needed due to congestive heart failure or liver dysfunction. Before embolising any lesion, you need to assess for arteriovenous shunting that could lead to inadvertent systemic embolisation.

Low flow venous and lymphatic malformations rarely require treatment in the neo-

natal period, but can be sclerosed with minimally invasive techniques. High flow AVMs and AVFs may cause organ malfunction and congestive heart failure due to arteriovenous shunting. AVMs are typically embolised from an arterial approach, and the entire nidus needs to be embolised to prevent recruitment of new arteries. AVFs may be approached from the arterial or venous side depending upon the anatomy and haemodynamics.

Complex malformations may require multiple staged procedures for complete treatment.

7.4 Summary

Interventional radiology techniques have dramatically improved the minimally invasive care of patients, including neonates, over the years. These methods offer safer and less physiologically stressful approaches to diagnosis and intervention. Ultrasound is sufficient for procedural guidance for most procedures and avoids exposing sensitive newborns to ionising radiation. Ultrasound guidance also allows procedures to be performed at the bedside, which often is a safer environment for the child. Absolutely essential is a team approach in deciding if an interventional procedure is warranted and what type of procedure is best for the child. Parent involvement in these decisions and discussions of expected benefits and risks is important. When performing procedures, all those present must be experienced in their assigned roles (radiologist, anaesthetist, neonatologist, nurse, etc.). Properly organised and performed, interventional radiology can provide tremendous benefits to our smallest and most fragile patients.

Further Reading

- Aria D, Vatsky S, Towbin R, Schaefer CM, Kaye R. Interventional radiology in the neonate and young infant. *Semin Ultrasound CT MR*. 2014;35:588–607.
- Bahous G, Salajegheh P, Anari AM, et al. A review of peripherally inserted central catheters and various types of vascular access in very small children and pediatric patients and their potential complications. *J Med Life*. 2021;14:298–309.
- Barnacle AM. Interventional radiology in infancy. *Early Hum Dev*. 2014;90:787–90.
- Brinjikji W, Krings T, Murad MN, Rouchaud A, Meila D. Endovascular treatment of vein of Galen malformations: a systematic review and meta-analysis. *Am J Neuroradiol*. 2017;38:2308–14.
- Cahill AM, Annam A, Baskin KM, et al. Society of Interventional Radiology quality improvement standards for percutaneous nephrostomy in the pediatric population. *J Vasc Interv Radiol*. 2021;32:146–9.
- Coley B, Shiels W II, Hogan M. Diagnostic and interventional sonography in neonatal and infant lumbar puncture. *Pediatr Radiol*. 2001;31:399–402.
- Coley BD, Hogan MJ. Image-guided interventions in neonates. *Eur J Radiol*. 2006;60:208–20.
- Connolly B, Racadio J, Towbin R. Practice of ALARA in the pediatric interventional suite. *Pediatr Radiol*. 2006;36(Suppl 2):163–7.
- Connolly B. Gastrointestinal interventions—emphasis on children. *Tech Vasc Interv Radiol*. 2003;6:182–91.
- Feola GP, Hogan MJ, Baskin KM, et al. Quality improvement standards for the treatment of pediatric empyema. *J Vasc Interv Radiol*. 2018;29:1415–22.
- Fraga MV, Stoller JZ, Glau CL, et al. Seeing is believing: ultrasound in pediatric procedural performance. *Pediatrics*. 2019;144:e20191401.
- Hawkins CM, Chewning RH. Diagnosis and management of extracranial vascular malformations in children: arteriovenous malformations, venous malformations, and lymphatic malformations. *Semin Roentgenol*. 2019;54:337–248.
- Hwang JY, Shin JH, Lee YJ, et al. Percutaneous nephrostomy placement in infants and young children. *Diagn Interv Imaging*. 2018;99:157–62.
- Laffan EE, McNamara PJ, Amaral J, et al. Review of interventional procedures in the very low birth-weight infant (<1.5 kg): complications, lessons learned and current practice. *Pediatr Radiol*. 2009;39:781–90.
- Lin W, Zhao L, Lu Y, He L, Hu X. Interventional embolization of congenital intrahepatic shunts in children. *Pediatr Radiol*. 2016;46:541–7.
- Lord DJE, Chennapraganda SM. Embolization in neonates and infants. *Tech Vasc Interv Radiol*. 2011;14:32–41.
- Lungren MP, Patel MN, Racadio JM, Johnson ND. Ultrasound-guided interventions in children. *Eur J Radiol*. 2014;83:1582–91.
- Maruani A, Tavernier E, Boccara O, et al. Sirolimus (rapamycin) for slow-flow malformations in children: the observational-phase randomized clinical PERFORMUS trial. *JAMA Dermatol*. 2021;157:1289–98.
- Morshed RA, Winkler EA, Kim H, et al. High-flow vascular malformations in children. *Semin Neurol*. 2020;40:303–14.
- Pierce DB, Shivaram G, Koo KSH, et al. Ultrasound-guided lumbar puncture in pediatric patients: technical success and safety. *Pediatr Radiol*. 2018;48:875–81.
- Riccabona M, Dacar D, Zobel G, Haim M, Urlesberger B, Maurer U, Reiterer F. Sonographically guided cannula positioning for ECMO. *Pediatr Radiol*. 1995;25:643–5.
- Riccabona M, Sorantin E, Hausegger K. Imaging guided interventional procedures in paediatric uro-radiology—a case based overview. *Eur J Radiol*. 2002;43:167–79.
- Riccabona M, Zobel G, Haim M, Dacar D, Urlesberger B, Reiterer F, Maurer U. Venous vascular lesions in ECMO: detection and follow up by color Doppler sonography. *Eur Radiol*. 1997;7:1383–6.

- Teplisky D, Tincani EU, Lipsich J, Sierre S. Congenital arteriportal fistulas: radiological treatment and color Doppler US follow-up. *Pediatr Radiol*. 2012;42:1326–32.
- Ullman AJ, Bernstein SJ, Brown E, et al. The Michigan appropriateness guide for intravenous catheters in paediatrics: miniMAGIC. *Pediatrics*. 2020;145(S3):e201934741.
- Wildgruber M, Sadick M, Muller-Wille R, Wohlgemuth WA. Vascular tumors in infants and adolescents. *Insights Imaging*. 2019;13:30.

Neonatal Neuroimaging: Ultrasound of the Neonatal Brain and Spine, with Some Remarks on Plain Film and CT

Michael Riccabona

8.1 Introduction

In preterm and term neonates, any kind of brain injury is one of the most crucial determinators of long-term outcome. Preterm neonates are particularly prone to brain injury due to the immature small vessels causing typical haemorrhages, as well as the high oxygen demand of the devolving brain, which are intrinsically and physiologically different from the mature or adult-type distribution. Monitoring and early detection, proper management, and prevention of further progression or damage are an essential part of neonatal intensive care (NIC).

Neurosonography as a non-invasive bed-side modality is ideal for this task and has become an established part of NIC. It offers a superb imaging option not available in older children or adults, as the open fontanelles and the thinner skull allow an unhindered access of sound waves into the intracranial compartments. Due to the size of (preterm) neonates, high-resolution transducers can be used allowing for good spatial resolution. Using additional unconventional acoustic windows (e.g. transcranial, mastoid, or lesser fontanelle...) nearly the entire brain can be assessed reducing the need for

other imaging and ideal for the often-necessary follow-up examinations. Also, the skull itself (e.g. for evaluating suspected fractures) or the extra-cranial soft tissues (e.g. assessing haematoma, haemangioma, cysts, or nodules) can be approached sonographically. Furthermore, ultrasonography (US) can be performed at the bedside, does not involve radiation, and usually needs no sedation.

However, to comply with all these demands and possibilities, proper equipment as well as education, knowledge, and training are mandatory. Ultrasound limitations must be considered and potential sound-induced bioeffects need to be respected when applying US in a prudent manner. It needs to be decided whether an orienting “sonoscope” is sufficient in the individual situation or a full examination including transcranial access and (colour) Doppler sonography (CDS) is necessary for diagnosis and to prevent missing important findings such as posterior fossa pathology, peripheral haemorrhage, or perfusion disturbance.

This chapter will address the requisites and needs for neonatal neurosonography, and it will list the relevant conditions, queries, and findings including the respective differential diagnoses (DDx) and the need for further imaging. It will mention the few and rarer indications (and findings) for a neonatal skull radiograph or a brain/head CT. Note that for reading US findings the same criteria as for

M. Riccabona (✉)
Medical University Graz, Graz, Austria
e-mail: michael.riccabona@medunigraz.at

CT or MRI can be applied—e.g. observe the shape of ventricles for depicting elevated brain pressure indicated by ballooning temporal and frontal horns, or depiction of remnants of periventricular leukomalacia (PVL) by regional loss of the white matter and altered shape of the ventricular border. Intrinsicly, this chapter does not intend to replace an US textbook (some given in the “further reading” list at the end of this chapter) which one needs to consult if more details on neurosonography are desired.

8.2 Requisites

There are essential requisites for performing state-of-the-art neonatal neurosonography particularly at the NIC unit (NICU):

- Adequate portable equipment offering good image quality with a sufficient dynamic range (I suggest at least 80 db or higher), capable to support a high-resolution linear (possibly with phasing for a trapezoid image) and sector/vector/micro-curved transducers.
- A battery driven system with short start-up time is helpful in daily routine when moving from incubator to incubator in the NICU.
- (Colour) Doppler sonography (CDS) option.
- Adequate range of transducers with flexible cables—at least a high one resolution linear transducer (approx. 14–5 MHz, the option to phase the image to a trapezoid mode is very helpful) and one sector/vector transducer (range 10–4 MHz); some use micro-curved transducers (range 14–5 MHz) which are useful but carry the risk of brain surface and superior sagittal sinus compression. An additional lower frequency sector/vector transducer can be helpful in older or larger babies for transcranial access and Doppler applications (range 8–3 MHz). All transducers should be able to perform (C)DS.
- Image tinting or “bi-colour” mode is helpful if one needs to work in surroundings where darkening cannot be achieved—to support perception of subtle findings such as regional oedema or grey-white matter differentiation,

as physiologically the eye can better perceive these findings in colour than in grey-scale (because of the higher number of colour receptors in retina).

- (Digital) documentation capabilities; the ability to store clips for review is very helpful. Furthermore, a standardised imaging protocol with a consistent report format is recommended.
- Three-dimensional ultrasound (3dUS) or contrast-enhanced ultrasound (ce-US) are add-on options for dedicated centres with interest in research.
- Familiarity with the topographic anatomy of the brain and its vessels.
- Finally, knowledge of the normal age dependent appearance is essential (Fig. 8.1). Typical age dependent variations are size and shape of ventricles and extra-axial CSF space (larger ventricles, large CSF spaces in preterm), amount of gyration (far less in preterm), degree of grey-white matter differentiation (as also known from MRI), and physiological structures such as cavum septi pellucidi et vergae.

Remember that the neonatal brain is vulnerable, and US deposits energy in any structure examined. US can increase temperature of a scanned tissue if performed at high output gain for a long period (particularly in poorly perfused areas) indicated by the thermal index (TI), which must be displayed on the US screen as a rule of thumb, this TI (as well as the mechanic index, MI) should be kept below 1 (or for a short time up to 1.5). As particularly (colour) Doppler sonography (CDS) uses considerably higher output gain than baseline grey-scale US, CDS should be applied with caution and only activated if there is a query or indication that justifies the use of Doppler US. US also delivers mechanic forces by the pressure of the sound wave indicated by MI (also always displaced on the US screen) which should be kept below 0.8–1 during the examination.

Cavitation effects are another possible source of US-induced damage. However, in the brain this practically only applies if US contrast agents (UCA) are used. This application at pres-

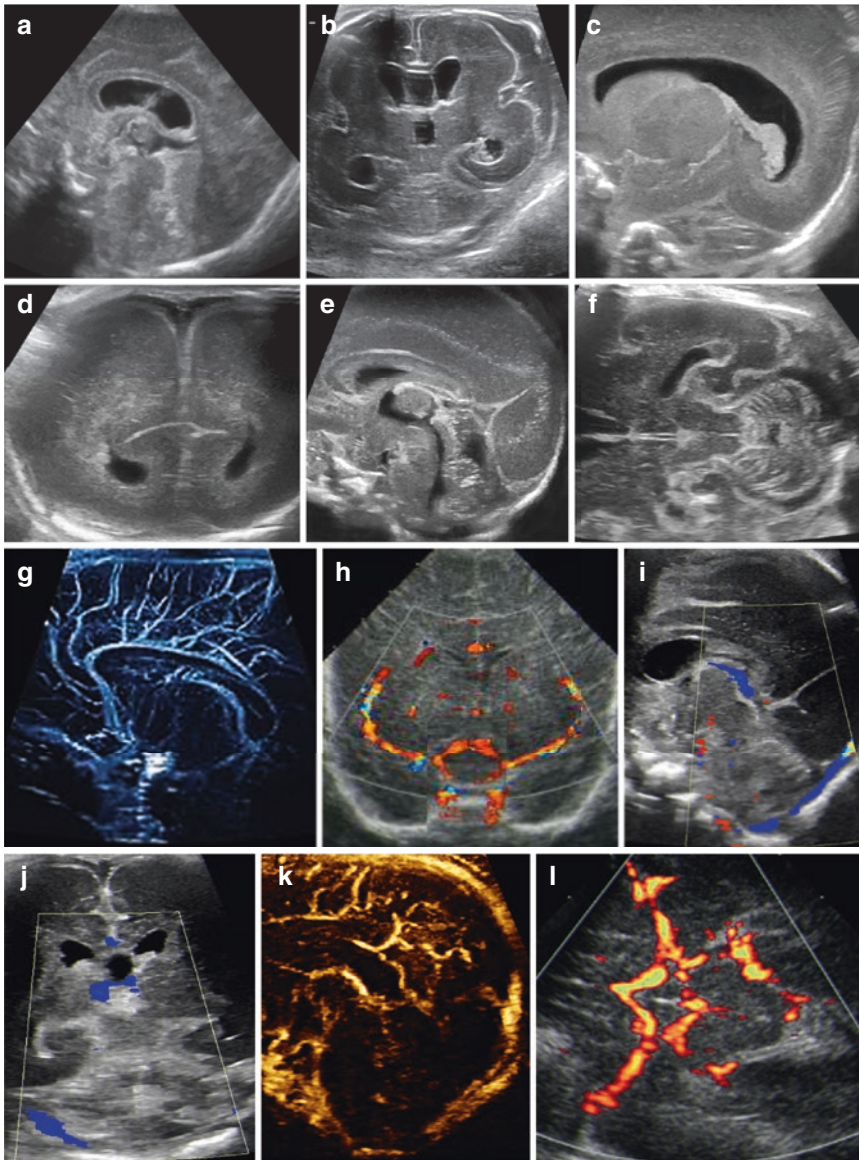


Fig. 8.1 Age dependent normal appearance of brain US, including typical physiological variations and signs of immaturity, as well as some Doppler findings. **(a)** Sagittal transfontanelle section (vector transducer): cavum septi pellucidi and vergae—typical in preterms. May also persist later as normal variation. **(b)** Coronal section with a high-resolution linear transducer—also displays these physiological cavi, additionally some distention of the lateral ventricles and reduced gyration as well as nearly “colpocephalic” configuration of the posterior horns can be appreciated in this very preterm and immature baby. **(c, d)** Parasagittal tilted **(c)** and occipital coronal **(d)** section with a linear transducer: some prominence of the lateral ventricle and reduced differentiation and gyration in a pre-term baby. **(e)** Midline sagittal transfontanelle view with a phased linear transducer displaying the posterior fossa and wide extra-axial CSF spaces—physiological in pre-

term babies. **(f)** Trans-mastoid axial view of the posterior fossa for better visualisation and detailed cerebellar anatomy and the posterior horns (phased linear transducer). **(g, h)** Visualisation of the major brain arteries in a sagittal **(g)**, superb microvascular imaging = SMI, Canon) and coronal **(h)**, CDS, composed image) view. **(i–k)** The major cerebral veins are nicely visible on CDS **(i)**, sagittal view; **j**, coronal view of the posterior fossa depicting the deep sinuses) or other flow-sensitive techniques such as “B-flow” which is less angle sensitive and this example illustrates flow in the entire superior sagittal sinus **(k)**, sagittal view, GE), but also depicts the regional arteries and does not show flow direction. **(l)** A amplitude-coded colour Doppler sonography (aCDS, also known as “power Doppler”) is particularly valuable for showing the continuity of the vessels at poor Doppler angles—such as in this transtemporal view of the circle of Willis

ent is rare, but this phenomenon needs to be respected when considering ce-US of the neonatal brain.

8.3 Brain Haemorrhage

Brain haemorrhage is an important condition with potentially severe sequelae that is ideally suited for bedside US not only in the initial diagnoses, but also for follow-up. This is a completely different approach from the imaging in older children and adults. Only the “rule out” of a particularly small haemorrhage in the periphery or extra-axial compartments is difficult or impossible with US. The depiction of blood products in long-term follow-up is another limitation of US, where MRI is far more sensitive.

8.3.1 US Appearance of Haemorrhages

The US appearance changes with the age and duration of the haemorrhage:

- Iso-echogenic to fluid in hyperacute state (maybe one can observe floating or swirling echoes).
- Echogenic in acute to subacute stage.
- Increasingly inhomogeneous with clot-like appearance and cyst-like compartments in old haemorrhages and lysis—if the haemorrhage was intraventricular then the ventricular lining may become thicker and echogenic.
- Eventually only atrophy, a porencephalic cyst or ventriculomegaly as well as choroid plexus or border irregularities may be visible as long-term remnants; sometimes there are no sonographically depictable remnants.

8.3.2 Classification of Intracranial Haemorrhages

With different patient age (based on different distribution of metabolic activity, growing neurons with immaturity, and associated dif-

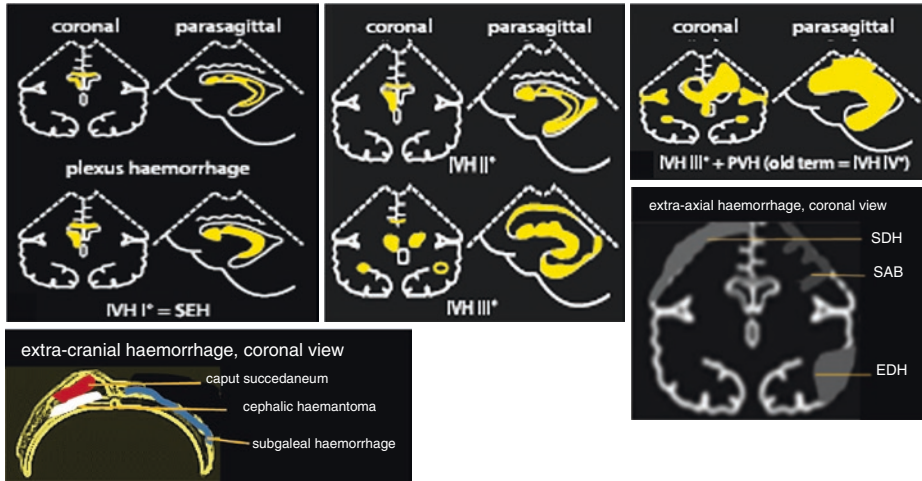
ferences in pathophysiology) the appearance and localisation of intracranial haemorrhages vary:

- **Preterm**

Brain haemorrhage is one of the most common findings, particularly in preterm infants. Haemorrhages may occur pre- or perinatally, but usually manifest during the first days in the NICU. The stages and grading of these haemorrhages have been updated a few years ago and is well established and standardised (Table 8.1). Usually, they arise from ruptured small vessels at the sub-ependymal plate at the caudothalamic groove, and why these early bleeds are called sub-ependymal haemorrhage (SEH, or sub-ependymal bleeds = SEB) which is equivalent to the older and slightly incorrect term intraventricular haemorrhage grade 1 (IVH I) (Fig. 8.2). When these bleeds deteriorate, they either stay covered by the ependymal lining causing sometimes impressive plexus haemorrhages, or rupture the ependyma with bleeding into the ventricular lumen. This intraventricular blood is usually confined to the lateral ventricle on the side of the SEH, but from there may spread into the contralateral side or the third and fourth ventricle, and eventually into the extra-axial and spinal CSF space. Depending on the amount of blood in the ventricle and presence of ventricular dilatation these are then called IVH II (little blood in ventricle, no ventricular dilatation) or IVH III (at least 50% of ventricle filled with blood, ventricular dilatation) (Fig. 8.2b). Choroid plexus haemorrhages stay within the plexus, but may become impressively large and are then difficult to differentiate from IVH II (and if they block the foramen of Monro they may also cause asymmetric ventricular dilatation).

The other cause of brain haemorrhage in preterm babies is secondary haemorrhage into a hypoxic or congested area (“venous haemorrhagic infarction”), which most commonly occurs when a large IVH compresses the draining veins running at the ventricular border

Table 8.1 Brain haemorrhages—classification with schematic drawings (according to Riccabona M, Pediatric ultrasound - requisites and applications, Springer 2020, Fig.8.37a, b p. 153)



Schematic drawing of different intra- and extracranial haemorrhages

Abbreviations: intraventricular haemorrhage (IVH), subependidymal haemorrhage (SEB), periventricular haemorrhage (PVH), subarachnoid bleed (SAB), epidural haematoma (EDH), subdural haematoma (SDH)

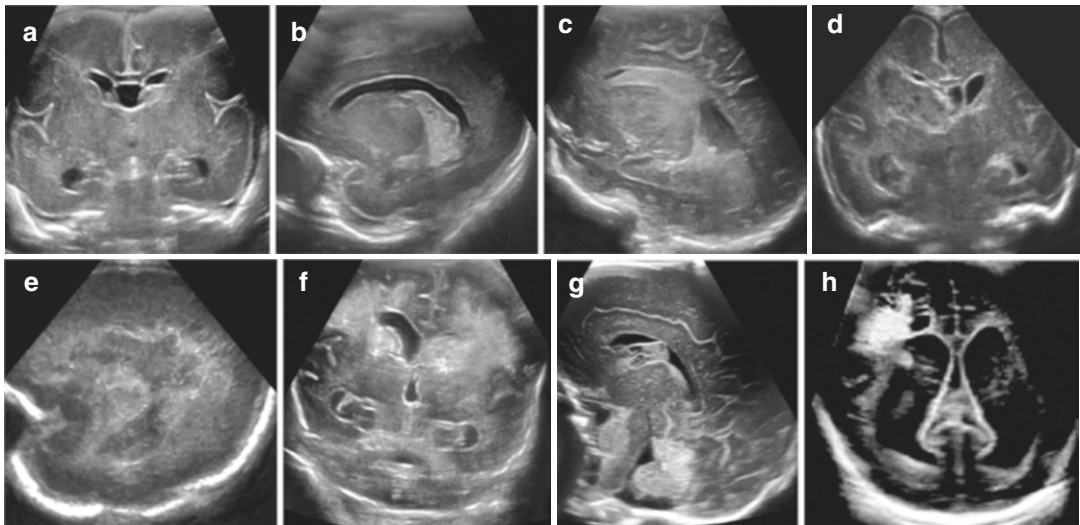


Fig. 8.2 Typical US images of haemorrhages in preterm neonates. (a) Coronal view, phased linear transducer: IVH I on the left side (arrow)—seen as an echogenic focus at the caudothalamic groove. (b) Parasagittal view, phased linear transducer: IVH II seen as large haemorrhagic echogenic plexus of the lateral ventricle—with some echoes in the posterior horn indicating blood in the non-dilated ventricle. (c) Parasagittal view, phased linear transducer: IVH III—as demonstrated by ventricular dilatation and much more blood (= echoes) in the ventricular lumen. (d, e) Coronal (d) and parasagittal (e)

view, vector transducer: IVH III + PVH (old term IVH IV)—blood filled dilated lateral ventricle with haemorrhagic infarction of the adjacent brain parenchyma. (f) Coronal view, phased linear transducer: bilateral severe PVH, on the left side obvious IVH III. (g) Sagittal view, phased linear transducer: stepwise resolution of haemorrhage—with lytic clot in the plexus. (h) Coronal view, phased linear transducer: lysis of a right sided PVH indicated by anechoic-lytic transformation of the initially echogenic haemorrhage replacing the destroyed brain parenchyma

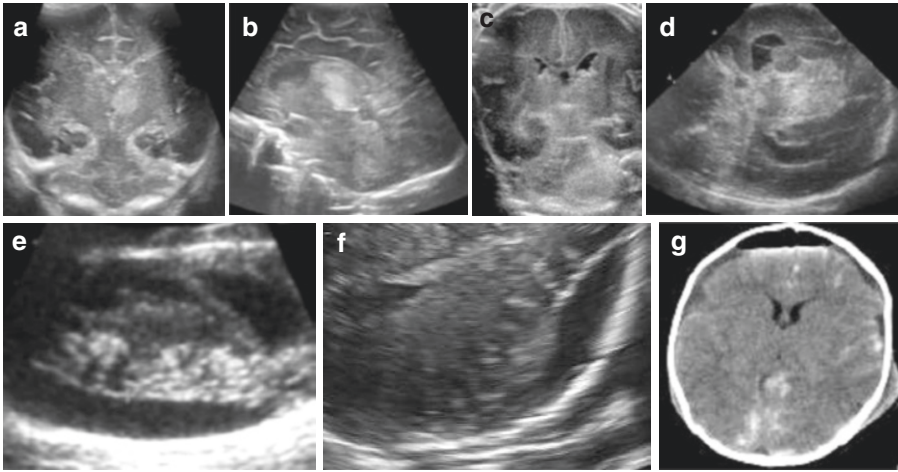


Fig. 8.3 US appearance of intracranial haemorrhage in term infants. (a, b) Basal ganglia haemorrhage in a term infant in a coronal (a) and sagittal (b) view seen as diffusely increased echogenicity on the left side (image right side) using a phased linear transducer. (c, d) Tentorial bleed after birth trauma in a preterm: coronal view using a linear transducer shows increased echogenicity and anatomic distortion of the left tentorium (c), and in a term neonate seen on a transtemporal view with a vector transducer as hazy increased echogenicity at the roof of the tentorium (d). (e) Subdural haemorrhage using a transtemporal approach and a sector transducer (+...+)

(zoomed view). (f) Epidural haemorrhage with compression and displacement of the adjacent brain imaged by a transtemporal access from the contralateral side using a sector transducer; the causative skull fracture is depictable too. (g) If US is unclear, there are mismatching clinical and anamnestic findings, no high-quality US is available, or even preoperative, additional or complementing imaging by CT and/or MRI will become necessary—as in this case with a SAB a, SDH and a skull fracture causing the pneumocephalus (which also explains why transfontanelar US was unsuccessful, as the access was obscured) after a traffic accident

(these are today named IVH III + periventricular haemorrhage = PVH, old term “IVH IV”) (Fig. 8.2) or into periventricular hypoxic areas. US can reliably detect these haemorrhages and grade them, and is used for follow-up to monitor either progression or lysis—with assessment of the sequelae such as porencephalic cystic defects or post-haemorrhagic hydrocephalus (see below) (Fig. 8.2).

- **Term neonates**

Haemorrhages in term neonates tend to occur in different parts of the brain and have different causes (e.g. coagulopathies, elevated blood pressure, birth trauma, vascular malformations). They most commonly occur in the basal ganglia, the posterior fossa (cerebellar or tentorial bleed), or, e.g. after trauma in other extra-axial locations (epidural, subdural, subarachnoid) (Fig. 8.3)—the latter far more difficult to depict by US,

as such US cannot reliably “rule out” subarachnoid haemorrhage. If this is suspected and of therapeutic consequence, an MRI (or if not available a CT) must be performed (Fig. 8.3).

- **Other haemorrhages**

Ultrasound can assess also other intra- or extra-cranial haematoma such as a cephalohaematoma or subgaleal haematoma (e.g. after a fracture or forceps delivery), but this is rarely necessary for guiding management (Fig. 8.4). Furthermore, US will visualise haematoma in the spinal canal—either from blood that has extended from an intracranial haemorrhage and forms a clot at the spinal level, or after birth trauma or lumbar puncture. Again, CT or preferably MRI is used in equivocal findings, for confirmation and assessment of the entire extent, or for medico-legal issues (Fig. 8.4).

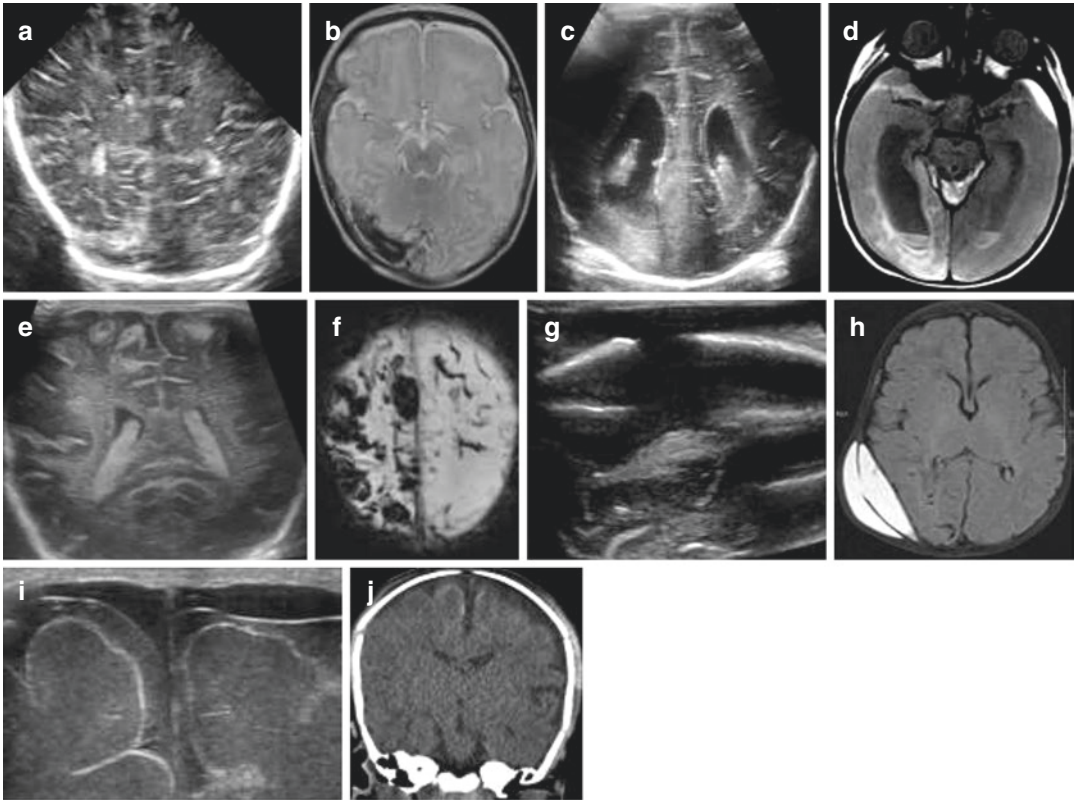


Fig. 8.4 US of other intra- or extra-cranial haemorrhages. (a) Para-tentorial extra-axial haemorrhage on a coronal transfontanellar view seen as echogenic asymmetric structure along the occipital lobe on the right side. (b) Confirmation of suspected pathology of (a) by MRI in an axial section. (c) Haemorrhagic infarction in the occipital lobe (coronal view, trapezoid view of liner transducer) also showing some blood levelling in the posterior horn of the lateral ventricles. (d) Confirmation of suspected pathology of (c) by MRI. (e, f) Subcortical contusion haemorrhage on a coronal view with a high-resolution linear transducer (e), with confirmation by MRI (f, SWI sequence), highly suspicious of an abusive head trauma (shaken baby, non-accidental/inflicted injury...). (g) Epidural haematoma after

birth trauma with a skull fracture imaged by US using a linear transducer; the fracture gap allows access to the underlying intracranial regions and shows the epidural haematoma with compression and displacement of the brain. Note the mirror artefact which may mimic an intracranial pathology. (h) MRI confirms the US findings (same patient as g). (i, j) A neonate with subarachnoid haemorrhage clearly seen on this coronal transfontanellar US (i) using a high-resolution linear transducer indicated by the widened subarachnoid space with echoes, whereas the subdural space contains clear and uncomplicated CSF—much better and more conspicuously displayed than on the corresponding CT with only subtle findings (j)

- **Follow-up**

Ultrasound is frequently used to follow-up haemorrhages. If there has been a haemorrhage into the ventricles one often can observe a thickened and echogenic ventricular wall due to the aseptic ventriculitis caused by the blood breakdown products helping to define the entity. Further details

particularly on post-haemorrhagic hydrocephalus with increased brain pressure are given below (entry “hydrocephalus”).

- **Key imaging features**

The role of US in assessing *inflicted non-accidental injuries* and findings after *birth trauma* will be discussed in more detail in the respective chapter (Fig. 8.5).

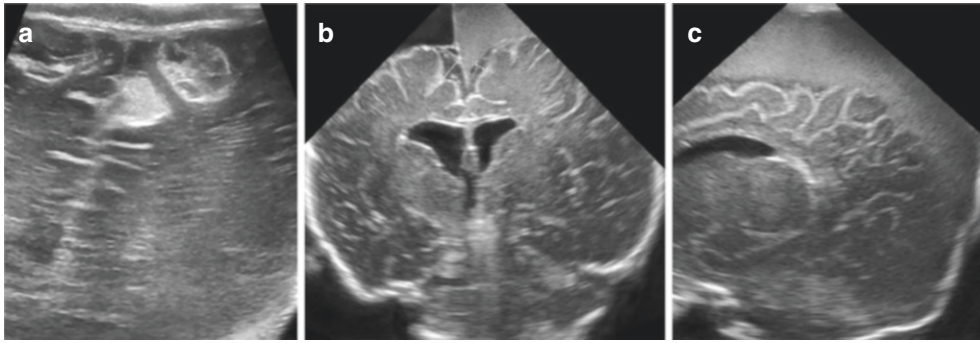



Fig. 8.5 US findings in non-accidental injury (NAI)/inflicted injuries/“battered child syndrome”. **(a)** US of the brain surface (sagittal view, high-resolution transducer) showing typical tear-drop shaped subacute inhomogeneous (sub-)cortical echogenic lesions, consistent with

haemorrhages after bridging vein rupture in NAI/shaken baby syndrome/inflicted injury. **(b, c)** Subdural haematoma in a baby suffering from inflicted injury—coronal **(b)** and parasagittal tilted view **(c)** using a vector transducer

 Acute haemorrhages appear as hyper-echoic clots in the respective location as described above. Blood in the ventricle is less echoic and looks like a complex fluid with floating echoes—turning into intermediate dense echoes layers if older. A similar appearance is seen in the extra-axial space, only the hyperacute stage the CSF space may appear still rather hypoechoic, versus rather hyperechoic echoes in the acute stage.

During resolution, the clots turn inhomogeneous and may increasingly become cystic, the blood in ventricles and other collections will become anechoic just like any other fluid.

umbilical cord strangulation); other instances such as a prolonged apnoea, shock or cardio-circulatory arrest, insufficient blood pressure and brain perfusion, or a near miss event will lead to the same phenomena. Typical clinical courses after asphyxia depend on the severity and duration of the hypoxic-ischaemic event: the less severe and the shorter, the less sequelae will occur.

Ultrasound imaging may show different patterns (Fig. 8.6):

- Initially, one often does not see any changes, as the respective findings and pathology develop during reperfusion.
- With reperfusion, (brain) oedema develops causing either regional (in areas of high oxygen demand that differ in preterm and term neonates) or diffuse brain oedema. This will occur between 12 and 48 h after the event, thereafter gradually returning to a more normal appearance depend on injury severity.
- On US this appears as focal or diffusely increased echogenicity with poor structural and grey-white matter differentiation (“bright brain”) and narrowing of the CSF spaces (particularly well depicted in the slit-like lateral ventricles).
- Eventually necrotic areas may become multicystic before atrophy may develop.

In cases of extensive damage that leads to global atrophy, the CSF spaces become enlarged, the sulci widened and the gyri flat-

8.4 Brain Hypoxia

Brain hypoxia is one of the most threatening brain injuries with potential serious long-term implications. Again, there are different forms that preferably occur at typical ages or clinical circumstances.

8.4.1 Asphyxia

The typical severe manifestation of brain hypoxia is asphyxia, usually occurring during birth and more common in term neonates (e.g.

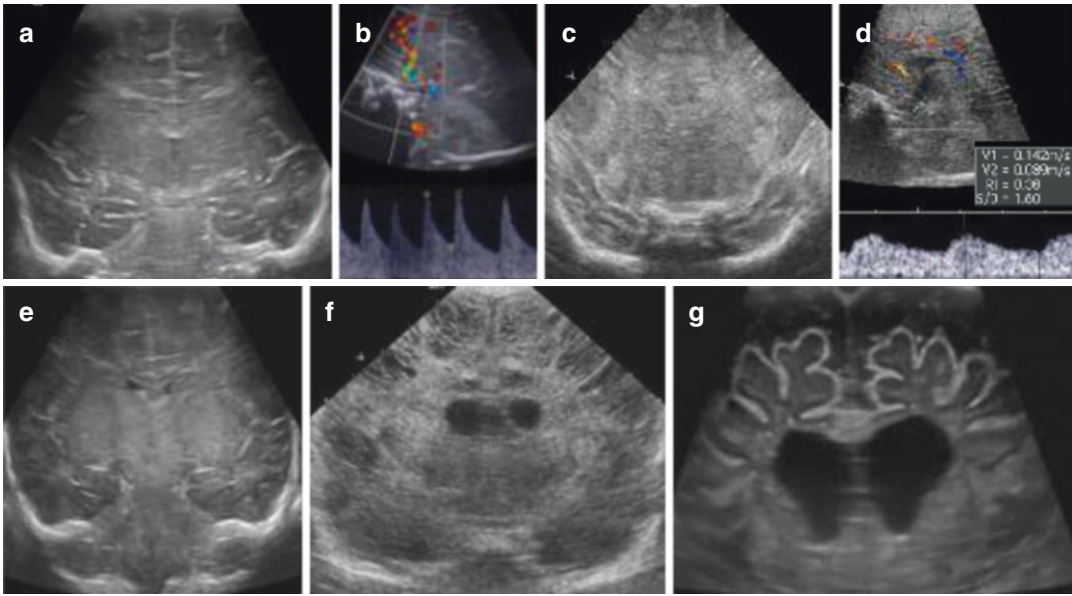


Fig. 8.6 US in asphyxia. (a) Bright brain in a coronal view with a phased linear transducer: compressed lateral ventricles with echogenic, undifferentiated parenchyma in a term neonate after asphyxia. (b) Respective Doppler findings in the same child as (a): increased diastolic velocity with decreased RI, typical for the hyperaemic phase of brain oedema. (c) More severe form of brain oedema at slightly later stage with patchy echogenicities on top of bright brain, scanned in a coronal view with a vector transducer. (d) Respective spectral Doppler (as in e) findings with very low RI and high

diastolic flow (hyperaemia). (e) More profound and deep form of asphyxia indicated by the basal ganglia predominance of brain oedema (coronal view, phased linear transducer). (f) Brain atrophy with dilated ventricles and cystic necrosis of the cortex after severe asphyxia (coronal view, vector transducer); note the different location of the cystic changes compared to PVL. (g) Atrophic brain with widened internal and external CSF spaces without increased intracranial pressure and diminished brain parenchyma (coronal view, phased linear transducer)

tened, and necrotic changes can be observed in the brain parenchyma, often exhibiting multiple confluent little cysts.

- Gliosis is far more difficult to depict on US—here MRI is helpful. MRI also serves for early definition of the global extent of the damage which may be prognostically important, e.g. for the decision to withdraw intensive care support. Details on these MRI applications can be found in the respective chapter on neonatal neuro-MRI.

As grey-scale US often is poor in and may be delayed in depicting these changes, (C)DS is an essential tool for diagnosis and follow-up of global brain asphyxia; for proper interpretation of these Doppler findings age dependent normal flow velocity values need to be considered (Table 8.2). However, these findings may be

Table 8.2 Normal flow velocities in major intracranial vessels in neonates

Flow velocities (cm/s) and resistive index (RI) in newborns			
	ACA	BA	ICA
V_{syst}	42 ± 15	41 ± 16	50 ± 15
V_{ed}	11 ± 5	11 ± 4	11 ± 4
RI	0.73 ± 0.08	0.72 ± 0.09	0.77 ± 0.08

Normal Doppler values for major cerebral arteries in term neonates. Note that these differ in preterm babies and vary with age, but are also influenced by many other (systemic) factors. As a rule of thumb one can say, that the younger the baby the lower the flow velocities and the higher the RI

Abbreviations: V_{sys} peak systolic velocity, V_{ed} end-diastolic peak velocity, ACA anterior cerebral artery, BA basilar artery, ICA internal carotid artery

Adapted from Deeg KH. *Zerebrale Dopplersonographie im Kindesalter*. Springer, 1989, and Deeg KH, Rupprecht T. *Pulsed Doppler sonographic measurement of normal values for flow velocities in the intracranial arteries of healthy newborns*. *Pediatr Radiol* 1989;19:71–78

obscured (particularly in preterm babies) by systemic influences, such as a persistent ductus arteriosus (PDA), medication, cardiac compromise, or anaemia/hypovolaemia.

The typical Doppler findings during the development and resolution of brain oedema are (Table 8.3):

- After a short (up to 24 h) period of a relatively normal flow pattern, hyperperfusion starts showing initially diastolic, then an increase in systolic and global velocities—with a respective decrease of the Resistive Index (RI) (Fig. 8.6b, d).
- With increasing intracranial pressure flow velocities decrease again—after a pseudo-normal transition phase the diastolic velocities decrease first (causing an increased RI, with

often a tent-shaped diastolic flow spectral pattern). Then the systolic velocities become diminished indicating deterioration of peripheral perfusion.

- Eventually, cessation of brain perfusion is seen as lack of any flow (also to be confirmed in cervical and major brain arteries). A spike-like undulating residual flow pattern at the skull base vessels will sometimes occur in early phase of brain death.


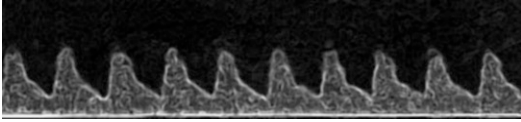
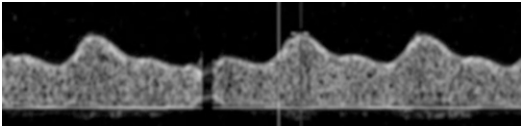
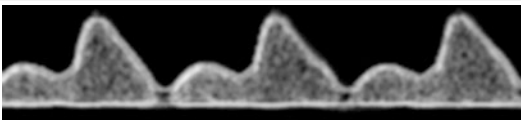
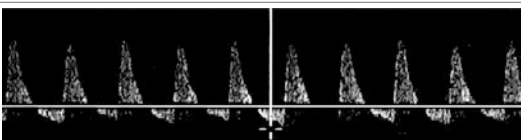
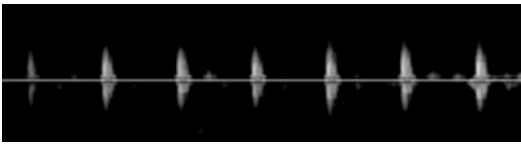
 Doppler analysis allows for proper staging and assessment of brain perfusion during the course and evolution of brain oedema.

Table 8.3 Doppler spectra in asphyxia/hypoxic-ischaemic damage and brain death

	Stage I (Pseudo)normal flow pattern and velocities
	Stage II Hyperaemia: high flow velocities in systole and diastole
	Stage III First diastolic, then global flow impairment: velocities decrease, possibly tent-shaped diastole, decreased systolic acceleration, eventually also systolic velocities diminish
	Stage IV Diastolic flow reversal, RI > 1.0. DDX: extracranial origin—e.g. cardiac?
	Brain death No flow depictable, or just spike like undulations of blood particle in basal vessels without antegrade brain perfusion

Doppler spectra and grading in developing brain oedema. The evolution of findings may stop and return to normal at any point as soon as oedema resolves, brain pressure decreases and the brain normalises

However, these flow patterns are also influenced by measures and effects of neuro-resuscitation such as (hyper-) ventilation, pCO₂, blood pressure and drugs

Adapted from M. Riccabona: *Neurosonography in neonates, infants and children*. In Riccabona M (ed) *Pediatric Ultrasound, second edition, 2020, Springer, Berlin-Heidelberg*. P 141; ISBN 978-3-642-39155-2, ISDN 978-3-030-47909-1

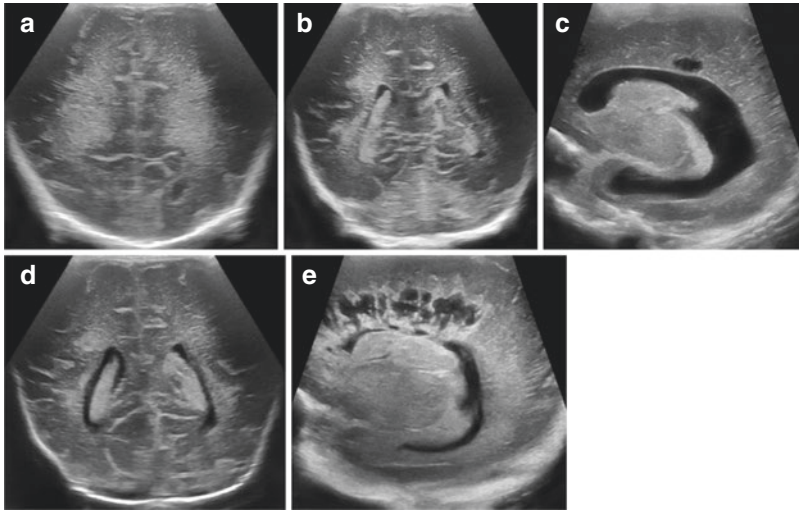



Fig. 8.7 US in periventricular leukomalacia. (a) Coronal view, phased linear transducer: bilaterally increased periventricular echogenicity with regional patchy appearance in a preterm—at that stage periventricular oedema cannot be differentiated from immaturity. (b) Coronal view, phased linear transducer: asymmetric patchy increased periventricular echogenicity, most probably an early stage of a regional PVL. (c) Parasagittal view, phased linear transducer: On follow-up the regional echogenicity turns cys-

tic—confirming the localised PVL. (d) Coronal view, phased linear transducer: on top of irregular parenchymal echogenicity of the occipital periventricular white matter, regional periventricular parenchymal thinning indicates white matter loss and probably beginning gliosis as a long-term remnant (non-cystic PVL). (e) Parasagittal view, phased linear transducer: a more severe polycystic remnant of a large PVL (grade III–IV)

8.4.2 Periventricular Leukomalacia





Hypoxia in preterm neonates (either by asphyxia or by other systemic cause for perfusion/oxygenation impairment, such as shock, repeated/prolonged apnoea, hypoventilation, or blood pressure problems) will lead to damage of the metabolically active regions of the growing brain and neurons—usually in the periventricular spaces. As physiologically these areas are yet immature and with a higher water content these naturally may appear echogenic. Therefore, oedematous changes that exhibit the same sonomorphologic pattern are difficult to differentiate. This early and unspecific finding is called periventricular echogenicity (PVE). Only an obvious asymmetry or focal patchy changes may hint towards a real hypoxic event possibly with a secondary (sometimes haemorrhagic) infarction causing the patchy echogenicity in some areas (Fig. 8.7).

- Gliotic changes and focal atrophy as a long-term sequela are more difficult to depict on US and might only be seen as thinning of the white matter (and corpus callosum) with some contour irregularity and widening of the ventricle, using the same criteria one would apply with MRI. The severity can be graded according to its extent and size (Table 8.4).

 On US only subsequent progression will eventually confirm the suspicions, when these PVEs either mature and disappear, or focal necrotic changes indicated by confluent cysts can be depicted—then called cystic periventricular leukomalacia (PVL) (Fig. 8.7c–e).

Note that in preterm neonates cerebellar (mostly hypoxic, but sometimes also haemor-

Table 8.4 Grading of PVE/PVL and schematic drawings

	Grade I: Transient periventricular echodensities persisting for >7 days.
	Grade II: Transient periventricular echodensities evolving into small, localised frontoparietal cysts.
	Grade III: Periventricular echodensities evolving into extensive periventricular cystic lesions in occipital and frontoparietal region.
	Grade IV: Large areas of increased periventricular echogenicity in deep white matter developing into extensive subcortical cysts.

Typical findings in different grades of PVL. Another grading assesses extent: uni- or bilateral (outcome much worse in the latter), or from only small frontal or occipital manifestation to more pronounced (less/more 50% of white matter) to severe long-distance extension, eventually involving entire periventricular white matter (again using grade I–IV for these four types)

rhagic) pathology occurs more often than initially thought. These can be difficult to depict on US and will need MRI, but in preterm babies the poorly ossified skull will allow a good visualisation of the cerebellum even using a linear transducer from a mastoid or transtemporal or nuchal access (see Fig. 8.1). Often, only a small cerebellar size indicates previous damage to the cerebellum.

8.4.3 Infarction/Neonatal Stroke

The third major appearance of brain hypoxia is infarction—a focal interruption of blood flow and/or oxygenation; in some instances, a “metabolic stroke” may occur. Ultrasound will show developing segmental oedema in the typical distribution (watershed areas, territorial infarcts depending on the affected brain artery, venous infarctions) often with some delay as compared to MRI (Fig. 8.8).

Grey-scale US will show (with some delay) increased echogenicity and swelling of the affected area with a hazy differentiation and

compressed adjacent CSF spaces; usually the sulcal lining is preserved. After some days the echogenicity becomes normal again making it difficult to depict by US.

CDS is less helpful unless there is a large vessel involved, even then only meticulous assessment of all vessels will enable such a diagnosis.

Only for thrombosis of major veins accessible to US (particularly the superior sagittal sinus), CDS and grey-scale US offer a reliable diagnostic option.

There is hope that ce-US may improve early diagnosis, but is as yet hindered by the limited ability of equipment and transducers for brain ce-US and fears that cavitation effects may put the already injured and still perfused penumbral brain parenchyma at risk for further damage. The same argument holds also true for the option of a better and earlier assessment of PVE/PVL by ce-US.

In this scenario MRI (even with a positive US suspicion—Fig. 8.8e, i, j) will often become indicated, and US may be then used for follow-up, eventually showing the local atrophy or cystic remnants of the affected brain.

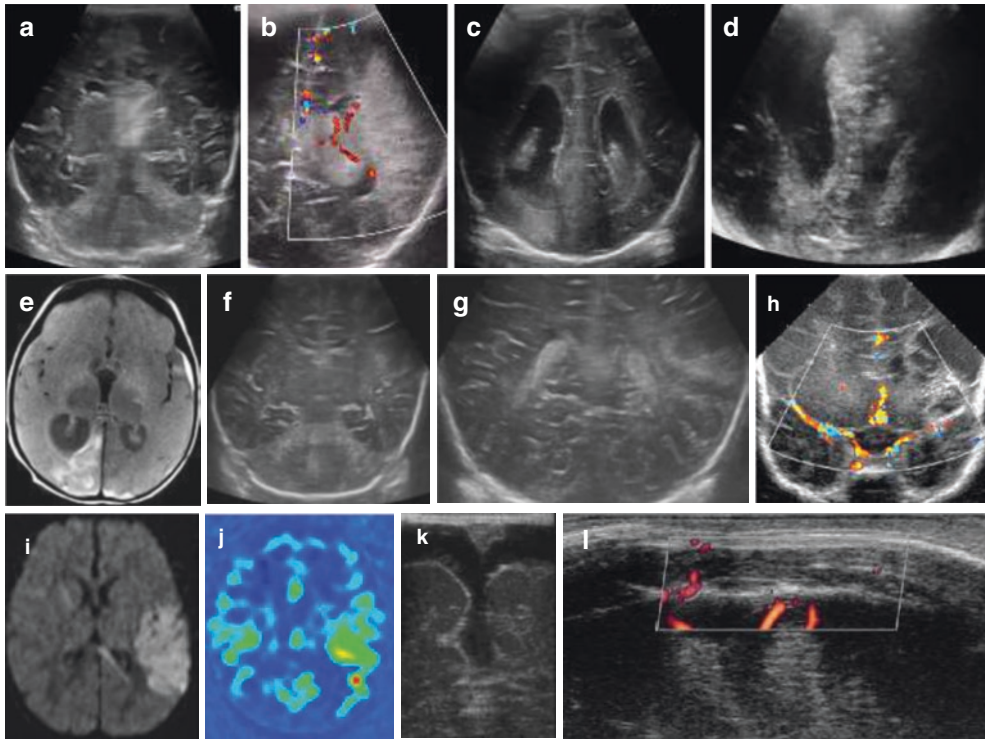


Fig. 8.8 US in neonatal stroke and its remnants. (a) Coronal view, phased linear transducer: echogenicity in the basal ganglia on the left side indicating a haemorrhagic infarction. (b) Regional increased echogenicity in the left middle cerebral artery territory in a neonatal stroke—note the regionally decreased visibility of vessels on CDS. (c) Regionally increased echogenicity in the right posterior territory on a coronal view (compared to normal parenchymal echogenicity on the left side) in a neonatal stroke; also note some blood in the adjacent posterior horn of the lateral ventricle. (d) Regionally increased oedematous brain parenchyma in the right sided posterior division imaged from a nuchal access using a phased linear transducer (also causing some artificial blurring in the near field) indicating a stroke. (e) Corresponding MRI confirming the US suspicion. (f, g) Coronal view, phased linear transducer: the

overview image shows only minor and subtle, asymmetric tissue inhomogeneities on the left side (e). After zooming in and optimising the image, the regional changes in a left middle cerebral artery stroke become more obvious (g). (h) Resolution of a left hemisphere stroke (left middle cerebral artery territory, vector transducer, coronal view with CDS): besides the multi-cystic necrotic remnants of the affected brain CDS shows the asymmetrically reduced flow in the affected left middle cerebral artery. (i, j) MRI with diffusion weighted imaging (i) and perfusion (non-enhanced techniques) imaging (j) is indicated for confirming a neonatal stroke and better definition of its extent. (k) Thrombosis of the superior sagittal sinus seen as echogenic inhomogeneous lumen of the sinus coronal view without depictable flow on aCDS (l, sagittal view) using a high-resolution linear transducer placed at/along the suture



Ultrasound is limited in diagnosing stroke/focal ischaemic injuries early - however, US may pick-up strokes by meticulous scanning and can contribute to follow-up. However, MRI with diffusion imaging will be necessary in quite many cases for early detection, confirmation and assessment of exact extent of a neonatal stroke.

8.5 Brain Malformations

Brain malformations are often known and depicted prenatally by US and confirmed by foetal MRI. There are many different forms, with different and changing classifications (Table 8.5). Postnatal US is used to confirm the suspicion, maybe redefine the diagnosis, and to monitor its development.

Neurosonography is the method of choice in neonates for bed-side assessment of the ventricular

Table 8.5 Overview on important brain malformations. (a) Malformations of the cerebrum. (b) Proliferation and migration disorders. (c) Cerebellar malformations

Anomalies of the corpus callosum	
Agenesis of the corpus callosum: total/partial	Lack of callosal and hippocampal commissures. Cingulate sulci absent. Colpocephaly (large trigones and occipital horns).
Callosal agenesis with interhemispheric cyst	Type I: Communication of cyst with ventricles. Type II: Multiple cysts without ventricular communication.
Intracranial lipoma	Location: subarachnoid space (deep interhemispheric fissure) May exhibit calcification.
Cephalocele Meningoencephalocele, meningocele, atretic cephalocele, gliocele	Skull-/dura defect, extracranial extension of intracranial structures. Occipitocervical, occipital, parietal, frontal, temporal (superior surface of petrous ridge), fronto-ethmoidal (between nasal + ethmoid bone), sphenomaxillary (through orbital fissures into pterygopalatine fossa), sphenoorbital, nasopharyngeal (through ethmoid, sphenoid, or basiocciput into nasal cavity or pharynx), lateral (along coronal or lambdoid sutures).
Holoprosencephaly (HPE)	
Alobar holoprosencephaly	Severest form. Midline facial deformities and hypotelorism. Fused thalami (no third ventricle). No interhemispheric fissure and corpus callosum. Crescent-shaped holoventricle, continuous large dorsal cyst. Deep brain structures (hypothalamus and caudate nuclei) affected.
Semilobar holoprosencephaly	Facial anomalies mild or absent. Interhemispheric fissure and falx in posterior portions; frontal lobes small and not separated. Hippocampus incompletely formed. Callosal anterior body, genu + rostrum absent. Deep grey nuclei partially separated. Dorsal cysts (when thalamic non-cleavage present).
Lobar holoprosencephaly	Third ventricle fully formed. Interhemispheric fissure extends anteriorly, most anterior portions of falx hypoplastic. Septum pellucidum absent. Small frontal lobes (and frontal horns).
Syntelencephaly (middle interhemispheric variant of HPE)	Posterior frontal and parietal convexities most severely affected. Anteroinferior frontal lobes portions and deep grey nuclei completely separated. Callosal body absent (callosal genu and splenium normal).
Septo-optic dysplasia (de Morsier)	Septum pellucidum hypo-/aplastic, optic nerves hypoplastic. Often hypothalamic-pituitary dysfunction. Possible overlap with lobar holoprosencephaly.
Chiari malformations	
Chiari I malformation	Caudal cerebellar tonsillar ectopia.
Chiari II malformation	Associated with myelomeningocele. Small posterior fossa. Cerebellum indented by tentorium and foramen magnum. Medulla oblongata and cervical spinal cord stretched inferiorly. Other abnormalities: tectum “beaking”, callosal a-/hypogenesis, large massa intermedia, falx fenestration, interdigitation of gyri, occipital stenogyria. Hydrocephalus.
Malformations of cortical development	
<i>Abnormal neuronal/glial proliferation or apoptosis</i>	
Microcephalie	Microcephaly with normal to thin cortex Microlissencephaly (extreme missencephaly with thick cortex) Microcephaly with polymicrogyria/cortical dysplasia
Megalencephalie	
<i>Abnormal proliferation</i>	
<i>Nonneoplastic</i>	
Cortical hamartomas (“tubers”) of tuberous sclerosis	Predominantly subcortical in enlarged gyrus. Neonates: T1 hyperintense, T2 hypointense. Older infants: T1 hypointense (possibly hyperintense = calcification), T2 hyperintense
Cortical dysplasia with balloon cells	Focal cortical thickening (and abnormal gyral pattern), blurred cortical white matter junction, marked T2 prolongation of underlying white matter (extending radially inward to ventricular surface).

Table 8.5 (continued)

Hemimegalencephaly	Hamartomatous overgrowth of all/part of cerebral hemisphere and neuronal migration defects (pachygyria, polymicrogyria, heterotopia), white matter gliosis in affected hemisphere. Macrocephaly. Enlarged ipsilateral ventricle with straight frontal horn.
<i>Neoplastic</i>	
DNET, Ganglioglioma, Gangliocytoma	
<i>Abnormal neuronal migration</i>	
Lissencephaly (Agyria-Pachygyria Complex)/subcortical band heterotopia spectrum	Smooth brain surface with diminished white matter. Pachygyria: thickened cortex, broad gyri, shallow sulci. Focal or diffuse.
Cobblestone complex	
Walker-Warburg syndrome	Cobblestone lissencephaly. Significant ventricular dilatation. Multiple cortical indentations into white matter.
Heterotopia	Lesions displaying a similar signal as cortex.
Subependymal	Typically ovoid masses, long axis parallel to ventricular wall, possibly exophytic; rarely smooth and linear.
Focal subcortical	Large masses; thin overlying cortex; small and distorted ipsilateral hemisphere.
<i>Abnormal cortical organisation</i>	
Polymicrogyria	Multiple small and irregular sulci, enlarged overlying subarachnoid spaces, mild ventricular dilatation.
Schizencephaly	Genetic and acquired causes. Parenchymal cleft between cerebral surface and ventricle, irregular cortex (as in polymicrogyria) lining cleft. Clefts: uni- or bilateral, fused or separated lips.
Cortical dysplasia without balloon cells	Focal cortical thinning with T2 hyperintensity and volume loss of underlying white matter.
<i>Cerebellar malformations</i>	
<i>Cerebellar hypoplasia</i>	
<i>Focal hypoplasia</i>	Isolated vermis. Hemisphere hypoplasia.
<i>Generalised hypoplasia</i>	
With enlarged fourth ventricle (“cyst”)— Dandy-Walker continuum	Dandy Walker Malformation: Enlarged posterior fossa. Elevated tentorium (above the inion). Hypo-/agenesis of cerebellar vermis. Cystic dilatation of fourth ventricle. DDx: Mega cisterna magna = enlarged cisterna magna, but normal cerebellar vermis and fourth ventricle.
Normal fourth ventricle (no “cyst”)	With normal pons. With small pons (Pontocerebellar hypoplasia of Barth, types I and II, cerebellar hypoplasia)
<i>Cerebellar dysplasia</i>	
<i>Focal dysplasia</i>	
Isolated vermian dysplasia	
Molar tooth malformations (Joubert syndrome)	Small dysplastic cerebellar vermis. Midline clefting. Triangular-shaped mid-fourth ventricle, “batwing”-shaped fourth ventricle superiorly. Superior cerebellar peduncles nearly horizontal.
Rhombencephalosynapsis	Fusion of cerebellar hemispheres, with absence/hypoplasia of cerebellar vermis and fusion of superior cerebellar peduncles.
Isolated hemispheric dysplasia	
Focal cerebellar cortical dysplasia/heterotopia	
Dysplastic cerebellar gangliocytoma	Overgrown appearing cerebellum with thickened folia (usually involvement of portion of one hemisphere). Abnormal contrast enhancement may be present.
<i>Generalised dysplasia</i>	

(continued)

Table 8.5 (continued)

Anomalies of the brain stem	
Mesencephalic clefts	Midline cleft extending from interpeduncular cistern posteriorly to aqueduct. Compressed appearance of mesencephalon.
Agenesis of the mesencephalon and metencephalon with cerebellar hypoplasia	(Nearly) complete absence of lower midbrain and pons, associated with small cerebellum.
Anomalies of the hypothalamic—pituitary axis	
Pituitary absence/hypoplasia	Absence/hypoplasia of anterior and posterior lobes and (often) pituitary stalk. Small and flat sella. Ectopic posterior pituitary gland.
Pituitary duplication	Duplication of hypothalamus and pituitary gland. Nearly always other anomalies of face and brain.
Kallmann syndrome (hypogonadotropic hypogonadism)	Hypoplasia or absence of olfactory sulci and olfactory bulbs. Small pituitary gland.
Hypothalamic dysgenesis	

List of common or important brain malformations, giving a short definition as well as a brief description of important imaging and anatomic features (not a complete list, some less important conditions missing, e.g. midbrain malformations...)

Adapted from *Simbrunner J, Riccabona M (2006) Imaging of the neonatal CNS. Eur J Radiol 60: 133–151*

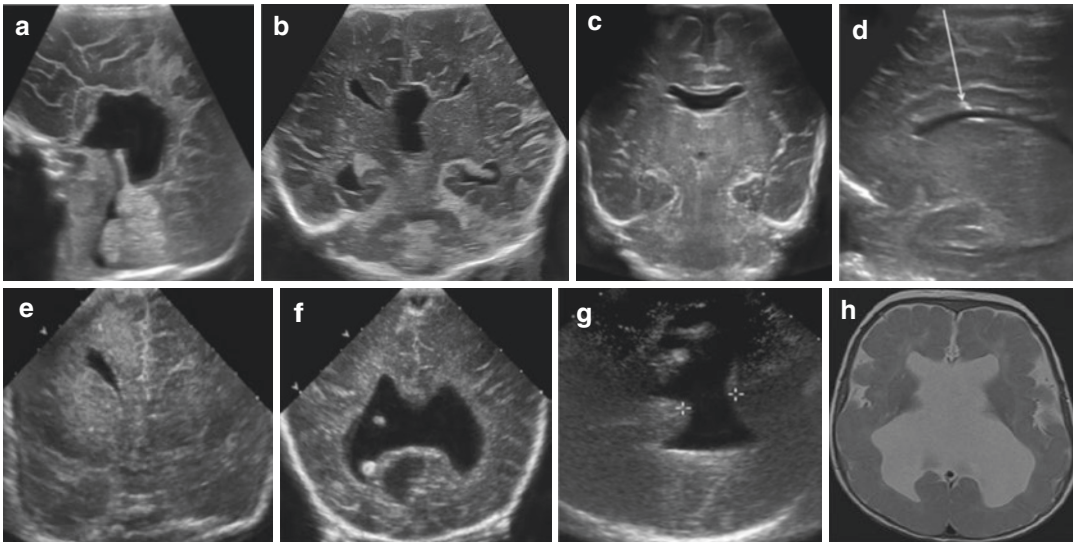


Fig. 8.9 US of brain malformations. (a, b) Agenesis of the corpus callosum: sagittal (a) and coronal (b) US view using a phased linear transducer demonstrate the absent corpus callosum, with the typical steer horn appearance of the anterior horns of the lateral ventricles and the high roof of the enlarged third ventricle. (c) Coronal section using a phased linear transducer showing septum agenesis, seen as missing demarcation between the prominent right and left lateral ventricles; also note some widening of the interhemispheric fissure and extra-axial CSF space. (d) Regional echogenic node with increased echogenicity (arrow) on a sagittal view with a phase linear transducer

in the corpus callosum—in a neonate with tuberous sclerosis. (e) Regional mass-like increased echogenicity with a misshapen frontal horn of the right lateral ventricle in hemimegalencephaly imaged with a vector transducer in a coronal view that enables easy left to right comparison. (f–h) Holoprosencephaly: a coronal US section using a vector transducer shows the communicating posterior horns (and an additional arachnoid cyst posteriorly); the transtemporal view (g) conspicuously confirms the lack of any separating structure or septum between the connected posterior horns. MRI of the same patient for confirmation (h)

system and allows visualisation of major anatomic structures such as the corpus callosum (Fig. 8.9). Meticulous investigations using all available acoustic windows and making utmost use of different

transducers, frequencies, image compounding, noise filters, or harmonic imaging will increase the yield and allow a better US classification using the same criteria as any other sectional imaging.

Limitations of US are the depiction of myelination delay, pathology of the brainstem, migration disorders, and peripheral pathology such as regional polymicrogyria. Sometimes 3dUS may enhance perception and visualisation, such as for assessment of the brain surface in polymicrogyria.

Neurosonography is supplemented by MRI which often is delayed until some brain maturation has taken place to enable a better depiction of changes such as heterotopia or migration disorders, as these are the fields where US has significant limitations.



Ultrasound is used to confirm the prenatal suspicion and may deliver most of the relevant information - however, in many of these malformations a delayed MRI will be performed to further evaluate a more complex situation.

8.6 Hydrocephalus and Cysts

Hydrocephalus and cysts are a common US indication—their prognosis and implications depend on the aetiology and origin. US often is sufficient for detection and for follow-up, supplemented by MRI if something of therapeutic relevance remains unclear. Only rarely a CT may become necessary in the acute setting of acute hydrocephalus with equivocal US findings and unavailability of (or contraindication for) MRI.

8.6.1 Hydrocephalus

Hydrocephalus is either part of a congenital malformation or secondary to another condition such as a brain haemorrhage, infection, or a space occupying lesion; rarely other causes such as overproduction of cerebrospinal fluid (CSF) may occur also in neonates. Classifications exist depending on pathophysiologic origin or affected CSF compartment (Table 8.6).

Imaging should try to define the origin/cause of a hydrocephalus, demonstrate the extent and severity, and estimate possibly existing brain/intracranial pressure - to help deciding on treat-

Table 8.6 Classification of hydrocephalus

Depending on cause: Hypersecretive, occlusive (stenotic, compression of foramina or aqueduct, after haemorrhage or inflammation), non-resorptive, part of a malformation, ex-vacuo (e.g. atrophy)

Depending on pressure: No-pressure (atrophy, dysplastic-malformative), low-pressure, or high-pressure (may need treatment/shunting/relieve by puncture) hydrocephalus

Depending on location: Supra-/infratentorial, intra-/extra-axial, global hydrocephalus

ment. For this a detailed morphological analysis, additional supplementing transcranial US access, Doppler behaviour, and other phenomena as known from CT/MRI (e.g. transependymal exudation, ballooning of temporal and frontal horns, narrowing of extra-axial CSF-spaces...) should be applied.

US can be used regardless of the underlying entity trying to assess the degree of CSF space dilatation, to check for progression, and to depict associated changes such as a malformation. However, it is most important to depict possible elevated brain pressure necessitating intervention.

How to do US for hydrocephalus?

- Besides an assessment of the entire brain with adjustment of the time gain compensation (TCG) one analyses the ventricular shape (e.g. ballooning of temporal horns? which parts of the CSF spaces are enlarged? is the extra-axial space narrowed?) and size by trying to assess standardised planes for repeatable and comparable measurements (Fig. 8.10). These should not only measure ventricular size (diameter and distances, circumference, cross-sectional area), but should also include the brain parenchyma since ratios between ventricle size and brain parenchyma may help monitoring brain development during growth. For example, with patient growth ventricles can increase but also that brain parenchyma may grow in a balanced fashion, which may be missed if the brain parenchyma is not measured.
- If there is concern for increased intracranial pressure, one should apply Doppler which may reveal reduced diastolic velocities with elevated RI values. If so, make sure these only apply to the brain and are not found in other systemic vessels—which then would suggest a systemic

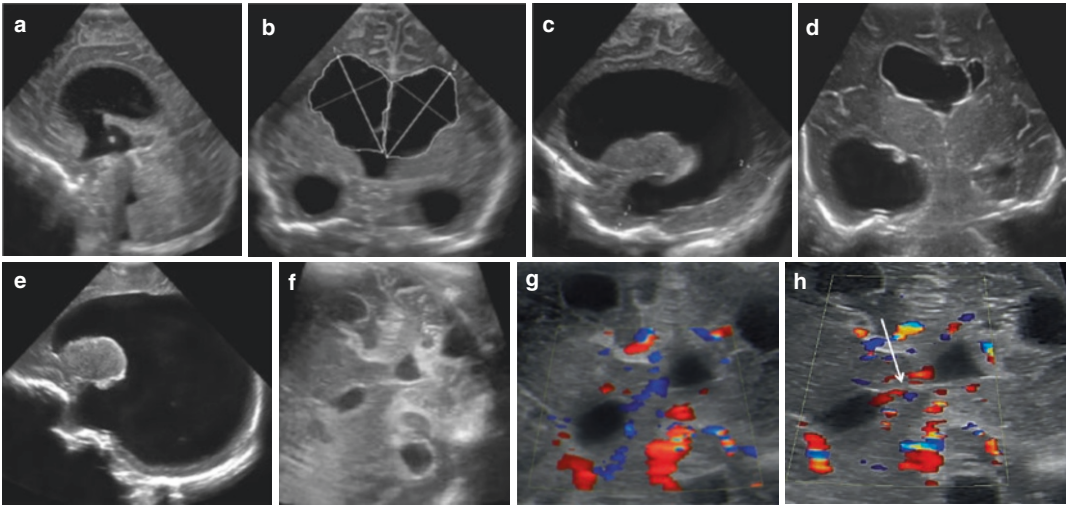


Fig. 8.10 US in hydrocephalus. (a–c) Supratentorial hydrocephalus: a midline sagittal (a), coronal (b), and parasagittal (c) view with a vector transducer demonstrates the dilated supratentorial ventricles with thinning of the brain parenchyma; (b) illustrates typical measurements of the lateral ventricle (axial, diameter, circumference, and sectional area), whereas (c) illustrates measurement of the parenchymal thickness (x...x). (d) Unilateral dilatation of the right lateral ventricle with mass effect, compressing and displacing the septum and impressing the left lateral ventricle, on a coronal view. (e) Parasagittal view with a vector transducer demonstrates gross dilatation of the lateral ventricle with significant

thinning of the occipital and temporal parenchyma and ballooning of the posterior and temporal horn—indicating increased intracranial pressure (same criteria as used for CT/MRI). (f–h) A transtemporal or trans-mastoid approach may help to assess the morphology of the aqueduct of Sylvius (f) helping to define the level of obstruction in hydrocephalus, and possibly helping to decide on therapeutic measures (e.g. a still patent aqueduct may allow for serial lumbar punctures for ventricular drainage to avoid shunting). Aqueduct flow can be visualised by CDS if the CSF contains reflecting particles and then can also demonstrate the bidirectional CSF flow within the aqueduct (g, h, white arrow)

and not an intracranial origin. In equivocal findings, the fontanelle pressure test (with an increase in RI and a decrease of diastolic flow velocity during the pressure manoeuvre in the referenced vessel, usually the middle cerebral artery accessed from transtemporal, or the pericallosal branch of the anterior cerebral artery if interrogated through the fontanelle) can be helpful (Fig. 8.11). The intra-/extra-cranial internal carotid artery systolic velocity ratio (accessed through the fontanelle without angle correction) (Table 8.7) may prove helpful. CDS may also visualise aqueduct of Sylvius flow (provided there are reflecting particles in the CSF such as proteins or blood products that enable a Doppler signal—Figs. 8.10 and 8.11) helping to decide on management (e.g. in a narrow but patent aqueduct, serial lumbar punctures may be a therapeutic option in post-haemorrhagic hydrocephalus).

- Standardised and repeatable measurements will help during follow-up.
- After ventricular shunting, US can be used to visualise the shunt catheter (particularly using a transcranial access) and its course and the changes of the CSF space (e.g. collapsed ventricle in over-shunting with secondary subdural haemorrhage by rupture of bridging veins) (Fig. 8.12).

Additionally, shunt complications such as CSF extravasation at the valve or shunt disruption or obstructing cysts at the abdominal end of the shunt can be assessed (Fig. 8.12). Intracranial pressure in shunt failure can be assessed using the same Doppler approach as described above—as long as there is an open fontanelle and pressure manoeuvres are possible. The transtemporal Doppler approach after closure of the fontanelle will reveal decreased flow only if there is a significantly increased

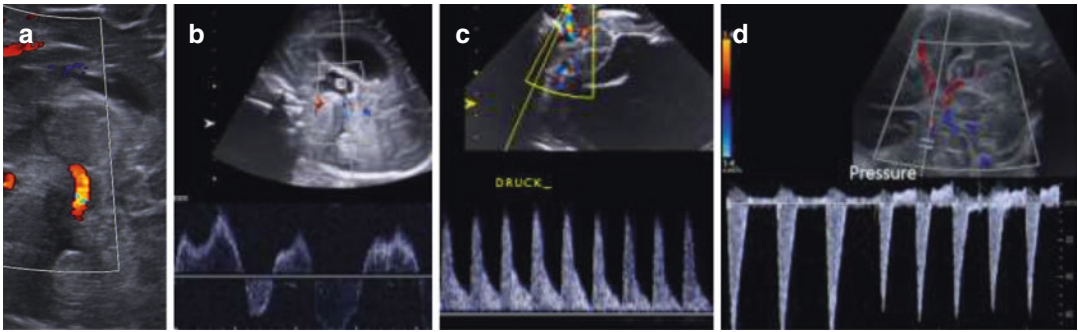


Fig. 8.11 Doppler sonography in hydrocephalus. (a) CDS sagittal midline section demonstrating flow in the aqueduct using a fontanelar view encoded in red. (b) Spectral trace and analysis of the Doppler signal in this neonate with hydrocephalus demonstrate bidirectional persisting flow in the aqueduct in spite of the rather narrow fourth ventricle. (c, d) Transtemporal US view with

CDS and spectral trace/analysis in hydrocephalus: the arterial flow of the interrogated middle cerebral artery changes when fontanelar pressure is applied (“Druck”/Pressure): note the decrease in diastolic and then also systolic flow velocities indicating elevated intracranial pressure in (c), and a reversed diastolic flow in (d)

Table 8.7 Intracranial to extra-cranial Internal Carotid Artery Index (I/E ACI ratio)


0.8(7)–1.1 = normal

>1.1 = slightly increased

<0.8(7) = severely increased (>20 cm H₂O)

Calculation: systolic peak velocity of intracranial divided by the systolic peak velocity of the extracranial portion of the internal carotid artery. According to *Deeg KH, Wolf A: Doppler ultrasonographic diagnosis of increased intracranial pressure by comparison of flow velocities in the extra- and intracranial sections of the internal carotid artery (German). Ultraschall Med 2000; 21: 259–264. <https://doi.org/10.1055/s-2000-9125>*

intracranial pressure. Alternatively, the widening of the optic nerve sheath can be visualised by trans-bulbar eye US; the cut off normal value in the first year of life measured 3 mm behind the bulb is around 4–5 mm, depending on the method used for measurement. There are no normal values for preterm neonates.

 Hydrocephalus can be congenital or aquired; US often is sufficient for diagnosing the condition and for follow-up. Doppler US is essential to assess elevated brain pressure. rarely an emergency CT is indicated or justified, whereas MRI may be an option particularly in more complex cases.

8.6.2 Brain and Intracranial Cysts

Cysts are not uncommon in the brain and their origin can sometimes be defined. They can be dysontogenetic (e.g. neuro-epithelial or choroid plexus cysts), post-haemorrhagic, post-infectious or after ischaemia, can be part of a malformation, or a variation in itself (e.g. temporal extra-axial cyst, other arachnoid cysts) (Fig. 8.13). Cysts should not be confused with physiological spaces such as cavum septi pellucidi, vergae and veli interpositi (see Fig. 8.1). Also, large vascular malformations or ectasia/aneurysm may appear as cysts. Thus, for DDx, a CDS investigation is mandatory. Findings in other parts of the brain or the body (e.g. in a systemic syndromatous disease that comes with cystic changes) may help to narrow down the DDx.

In terms of aetiology and prognosis, often only history and future development will give the definite answer; therefore, cysts are often followed-up by US to monitor for growth and evolution.

- Post-haemorrhagic (and sometimes post-inflammatory cysts) cysts tend to be inhomogeneous and appear “complicated” in early stages when clot lysis is taking place.

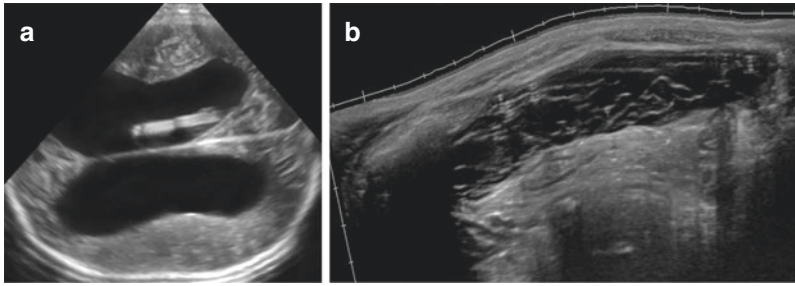


Fig. 8.12 US for follow-up of hydrocephalus after shunting. (a) Transtemporal view of a hydrocephalus with a shunt drain in the lateral ventricle. (b) Huge complicated

cyst with septae in the abdomen at the distal end of a ventriculoperitoneal shunt

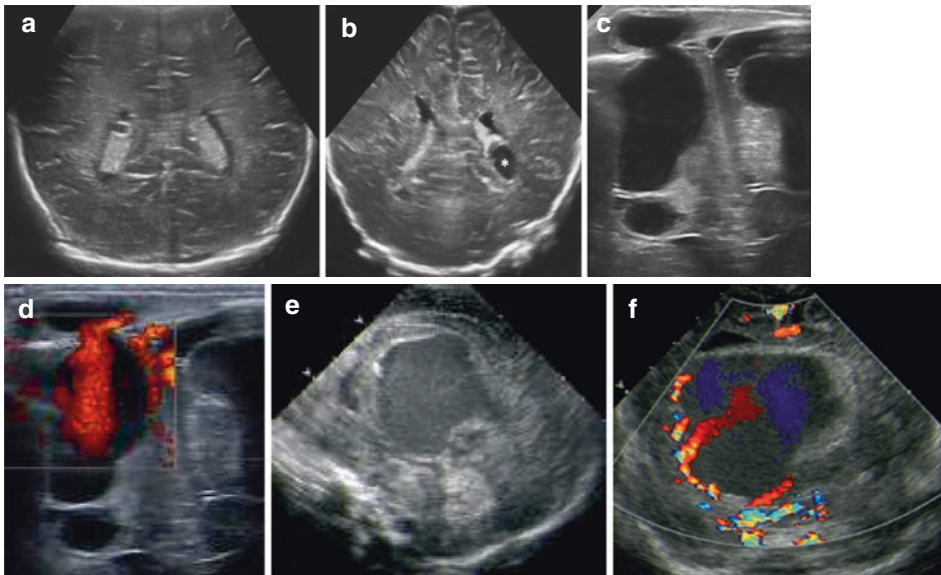


Fig. 8.13 US of intracranial/intra-cerebral cysts and respective differential diagnosis, value of Doppler US, and other Doppler applications. (a) Coronal section, phased linear transducer: small cyst in the choroid plexus of the right ventricle (+...+). (b) Coronal section, vector transducer: large, somewhat atypically shaped post-haemorrhagic plexus cyst in the posterior horn of the left lateral ventricle (asterisk). (c) Coronal section, close to fontanelle—linear transducer placed on an “elastic lump”: Huge porencephalic cyst with extra-cranial herniation of

unknown origin. (d) Same patient as in image (c)—power Doppler demonstrates flash echoes confirming the continuity between the two cystic compartments and indicating that there are particles in the fluid enabling the Doppler signal (probably old haemorrhage). (e, f) Differential diagnosis of cystic intracranial structures: a complex complicated large cystic structure with diffuse echoes in a midline sagittal scan is depicted (e). CDS reveals internal irregular flow within the “cyst” and large feeding vessels (f), establishing the diagnosis of a vein of Galen aneurysm



Note that US, thanks to the superb resolution of linear transducers, may depict tiny cysts and particularly small internal septae better than MRI, whereas MRI may help to better define the origin, e.g. by showing blood products in a cyst.

8.7 Infectious Conditions

Brain infections may occur pre- or postnatally; the picture can be quite variable—from clinically normal appearance to severe symptoms or remnants after infection (such as calcifications). Sonographic findings in the brain do not always match the clinical picture, and US cannot be used to “rule out” such an infection.

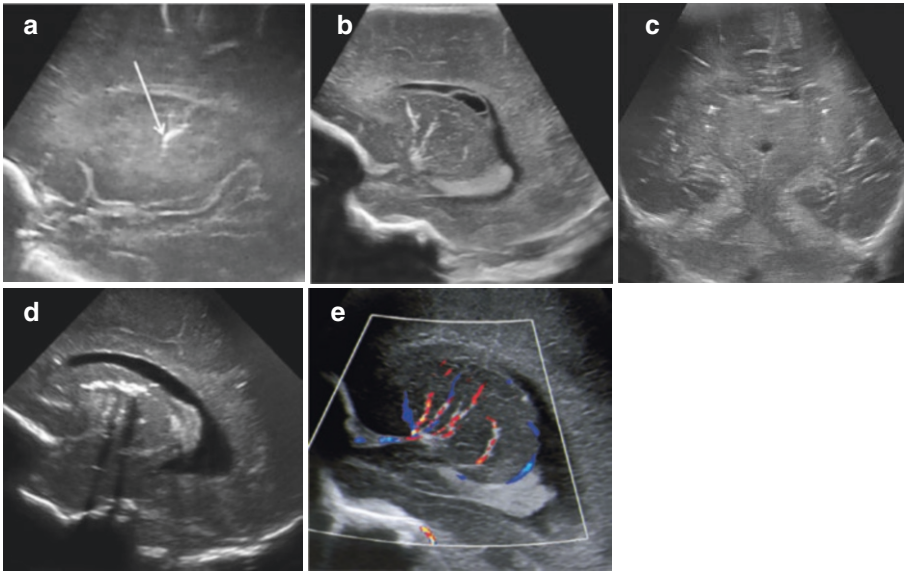


Fig. 8.14 US appearance of non-calcifying vasculopathy, brain calcifications, and brain tumours. (a, b) Parasagittal transfontanellar US reveals mild (a, arrow) and more severe (b) non-calcifying vasculopathy. In (b) also a plexus cyst and some periventricular echogenicities are seen. (c) Multiple stippled echoes in the coronal view in a neonate with conatal infection and basal ganglia cal-

cifications. (d) More severe calcifications with shadowing (rare in brain US) in this parasagittal view of the basal ganglia. (e) CDS demonstrates flow in the vicinity of the echogenic stripes indicating the respective vessels, which do not have to be occluded, and confirms that the pathology is not a thrombosis in the vessels, but affects the perivascular bed

8.7.1 Congenital/Foetal Infections

Congenital/foetal infections may be associated with postnatal central nervous system (CNS) findings and severe sequelae in the affected baby—mostly these are “TORCH” infections (Toxoplasmosis, Rubella, Cytomegaly, Herpes and others...). Many of them may leave remnants in the cerebrum such as punctuate or striate calcifications, cysts, scars, infarction and its remnants, or atrophy—these all can often be depicted by US; however, some infections may have few or no sonographically visible changes. Additional common findings are the so-called non-calcifying vasculopathy (“lenticulostriate vasculopathy”—an unspecific finding, seen in a number of conditions, Fig. 8.14) and choroid plexus or germinolytic/sub-ependymal cysts. Often an additional US of the abdomen may reveal other findings such as liver involvement or splenomegaly helping to better interpret sometimes the non-specific findings on brain US (Fig. 8.15).

The recently described Zika virus has been found to cause in utero infection and often involves the brain (“Zika virus syndrome”). In

foetal infection, it leads to severe microcephaly in which the skull has partially collapsed. In the CNS one may find (detectable in part by US, better by MRI)

- Decreased brain tissue with a specific pattern of brain damage including subcortical calcifications, atrophy and asymmetry, abnormally formed or absent brain structures, hydrocephalus, and neuronal migration disorders.
- Damage to the back of the eye, including macular scarring and focal retinal pigmentary mottling, optic nerve hypoplasia or atrophy, other retinal lesions, iris colobomas, congenital glaucoma, microphthalmia, lens subluxation, cataracts, and intraocular calcifications.

The degree of damage varies, and there are no definite or specific findings in peri- or postnatal Zika virus infections (Source: U.S. National Center on Birth Defects and Developmental Disabilities, Center for Disease Control and Prevention, <https://www.cdc.gov/pregnancy/zika/testing-follow-up/zika-syndrome-birth-defects.html>, last visited 30.3.2021).

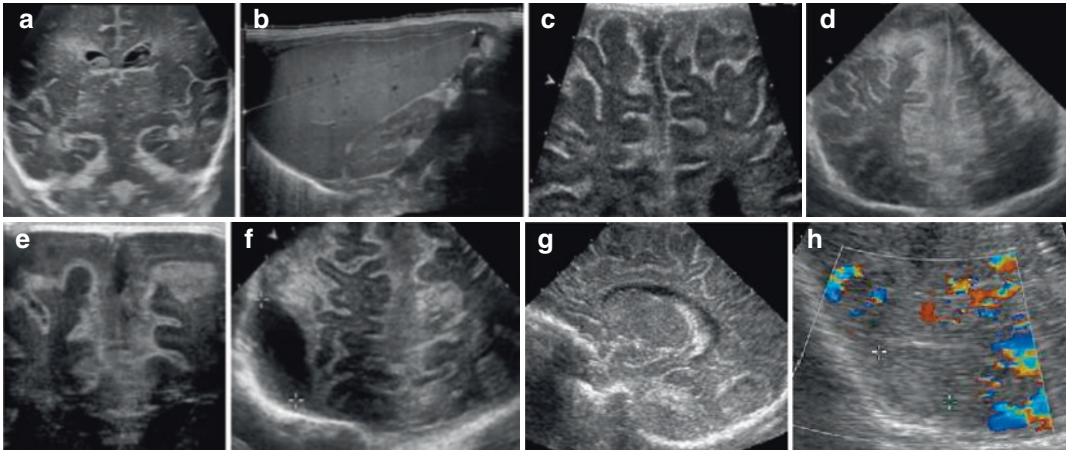


Fig. 8.15 US in brain infections. (a) Conatal CMV-infection: numerous findings such as echogenic paraventricular oedema, cysts, ventricular asymmetry, old IVH, and echogenic spots in the basal ganglia. (b) Same neonate as in a: additional abdominal US shows hepatomegaly—this demonstrates that extending the examination to the abdomen may be helpful if one thinks about a conatal infection. (c–e) Mening(oencephal)itis: echogenic thickening of the meninges outlining the sulci in a neonate with meningitis—a rather subtle finding (c). In severe bacterial meningitis, the findings may be much more prominent

(d). Using a high-resolution linear transducer, one may depict areas of affected brain tissue thus establishing the diagnosis of meningoencephalitis (e). (f) Dural empyema (+...+) is depicted as a well demarcated complex cystic lesion with sedimentation in the paramedian high frontal area using a sector transducer with a latero-frontal tilted fontanellar access. (g, h) Brain abscess seen as a local spherical defect (+...+ in h) with some mass effect and an echogenic outlining (= abscess membrane) on a parasagittal view with a vector transducer (g), without central vascularity or perfusion on CDS (h)

8.7.2 Postnatal Infections

Postnatal CNS infections are much rarer and may either affect the meninges, the brain, or both

- **Meningitis**

Meningitis may exhibit enlarged extra-axial spaces with some echogenicities—particularly with bacterial mening(oencephal-)itis—and increased echogenicity of the sulcal lining (i.e. swelling of the subarachnoid space). In severe conditions, impressive hyperaemia of the meninges can be observed by CDS (Fig. 8.15). However, often US remains non-specific or even normal, and diagnosis is made by lumbar puncture.

- **Complications in meningitis/subdural empyema**

Visualisation of a severe complication of meningitis, subdural empyema, may be difficult on US since peripheral extra-axial spaces are poorly accessible for US, although many of those can be depicted by a meticulous search and using a transtemporal access, too (Fig. 8.15). An MRI or even a CT may become

necessary showing the well-demarcated complex collection in the extra-axial space with a membrane-like outline, which may show contrast enhancement.

- **Encephalitis**

Encephalitis is often viral (e.g. herpes) and can only be seen sonographically if focal oedema, haemorrhage, necrosis, or abscess formation occur. In bacterial meningoencephalitis, these typically manifest as (sub)cortical defects, whereas herpes infections tend to affect deeper brain structures. Atypical infections such as tuberculosis are very rare in neonates and practically only occur in immunocompromised patients (e.g. congenital HIV) and developing countries with restricted health care.

The sonomorphology varies with the underlying entity and stage of the disease. Diffuse viral encephalitis is sometimes invisible to US (or even MRI), sometimes shows more (multi-)focal manifestation regional oedematous echogenic and hazy areas may be visible, or may become even more echogenic with secondary infarctions or even haemorrhage (commonly seen in herpes encephalitis).

US findings may also be inhomogeneous, e.g. if different phenomena are present or if sub-acute/older.


Meningoencephalitis displays the findings of a meningitis with additional focal brain lesions that may exhibit different features.

- **Brain abscess**

Abscess formation occurs during/after bacterial or fungal encephalitis or as an embolic spread in sepsis, often in immunocompromised, neonates with central lines or cardiac malformations, or oncology patients during/after chemotherapy.

Sonomorphologically abscesses appear as central hypoechoic or inhomogeneous cyst-like lesions due to pus and necrosis, with often an echogenic membrane (potentially with fluid levels) (Fig. 8.15). CDS only sometimes depicts the peripheral, halo-like hypervascularity, and lack of flow in the lesion itself. In unclear cases, ce-US may confirm the lack of central vascularity and the hypervascularisation of the membrane and surrounding parenchyma.

For differential diagnosis, all other focal lesions need to be considered, particularly centrally necrotic, cystic, or haemorrhagic tumours may appear sonographically similar.

 Ultrasound is unspecific in brain infections, but may show associated changes or even abscesses; sometimes a supplementing MRI is helpful.

8.8 Miscellaneous Other Conditions

There are other rare conditions and other nonspecific findings (e.g. non-calcifying vasculopathy, see Fig. 8.14).

Ultrasound will pick-up many of those findings in neonates (for vascular malformations and other vascular queries, CDS with confirmation by spectral Doppler analysis is essential—Fig. 8.16, see also Fig. 8.13). Even congenital or neonatal

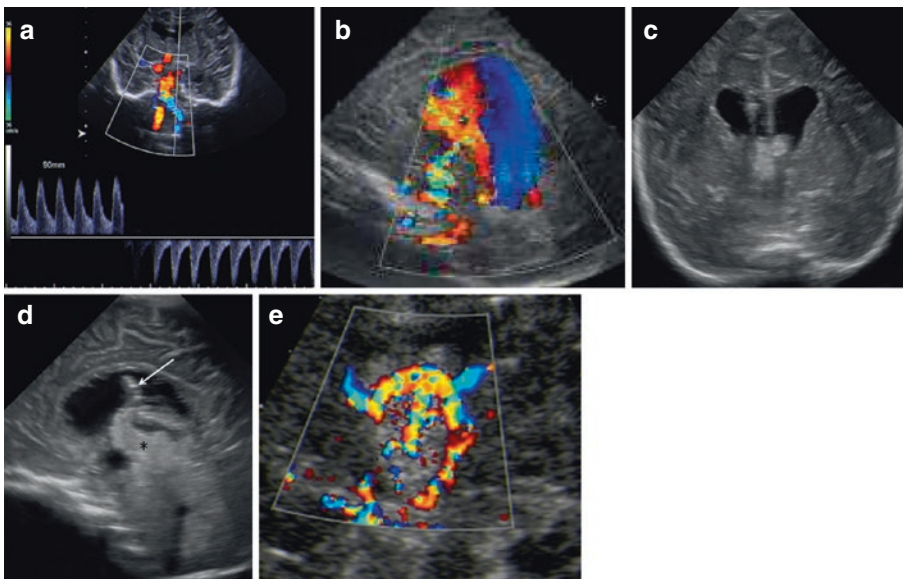


Fig. 8.16 Other brain CDS applications. (a) Doppler US for subclavian steal phenomenon: CDS shows different encoding of the left and right vertebral artery in this coronal transfontanelar view indicating a reversed flow (blue) in the left vertebral artery as collateralisation of the impaired aortic arch, confirmed by the spectral Doppler flow trace and analysis. (b) A complex cystic structure with diffuse echoes in a midline sagittal scan demonstrates internal irregular flow on CDS and a dilated drain-

ing vein—consistent with a vein of Galen malformation. (c, d) Unusual echogenic swelling of the choroid plexus at the roof of the third ventricle in a coronal (c) and sagittal view (d, black asterisk) vector transducer in a choroid plexus papilloma. Note the shunt placed for drainage of the hypersecretion hydrocephalus (arrow). (e) CDS reveals increased vascularity with vivid and turbulent flow within the echogenic tumour in the same neonate as in (c, d)

brain tumours, though rare, may occur (Fig. 8.16). With tumours and vascular queries/malformations, supplemental sectional imaging (and possibly angiography—see Fig. 8.23) will become necessary.

The essential message with respect to these entities is to keep them in mind for the DDX—particularly if an US appearance is not typical for the suspected condition, or the clinical history and context does not fit the US finding, or one needs to search for a cause for, e.g. an unusual haemorrhage or unexplainable infarction.

8.9 Spinal and Spinal Canal/Cord US

Neonates offer the unique possibility for US to visualise the spinal canal content—because of the yet non-ossified dorsal arches of the vertebrae sound can access this compartment. As such spinal cord malformations can be exquisitely investigated by US using high-resolution linear transducers; special US techniques such as “panoramic imaging” or “extended view” (different terms used by different vendors) can be helpful and allow to display long sections of the spinal

canal and its content; knowledge of normal findings is however essential (Fig. 8.17).

8.9.1 How to do Spinal Cord US

For this examination, the baby is in a prone or lateral decubitus position, and a pillow under the belly is helpful to avoid overextension then degrading US access. Plenty (pre-warmed) US gel is helpful to allow good transducer contact with the skin and to avoid painful transducer movements which can decrease patient cooperation.

Normal anatomy as well as various physiological variations need to be known and not over-called as a pathology; physiologic variations that do not equal pathology are a terminal ventricle (“fifth ventricle”), a filar cyst, or dorsally bent cartilaginous coccyges (often associated with a simple sacral dimple) (Figs. 8.17 and 8.18). This also applies to the normal lumbar and cervical intumescencia (i.e. the physiological spinal cord enlargement) and the variation in conus position with patient age.

The most common cause for an US request is the *simple sacral dimple*. This is not because of a higher incidence of associated spinal cord mal-

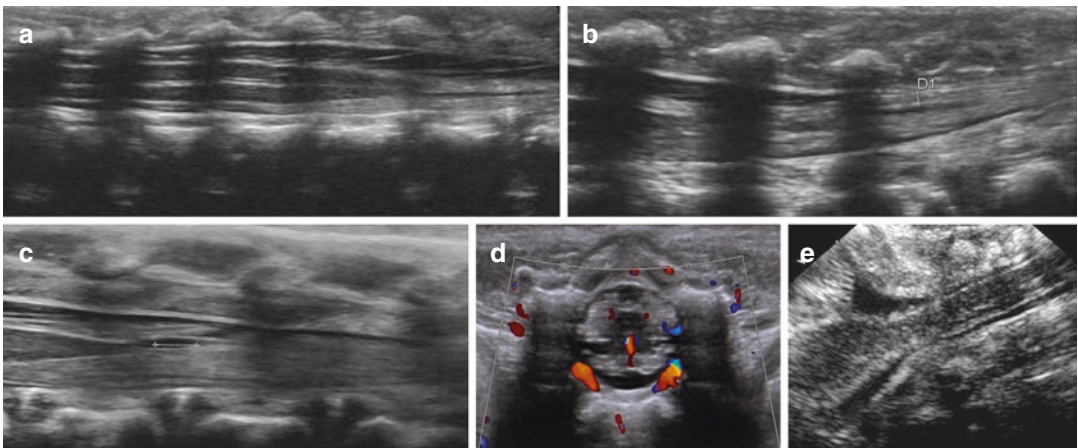


Fig. 8.17 Spine US: normal findings. (a) Dorsal sagittal midline view using a linear transducer: normal appearance of the lumbar spinal canal with the conus, typically at the level of L2. (b) The terminal filum can also be depicted (D1) and should not measure more than 2 mm diameter, best measured in the axial view. (c) A terminal fifth ventricle (“ventriculus”, +...+) is a normal variation

and should not be confused with a dilated central canal. (d) Axial view of the lumbar cord with the ligaments, the nerve roots, and the central echo complex. CDS also depicts and visualises the respective vessels. (e) Midline sagittal section from a nuchal approach using a phased linear transducer to visualise the cranio-cervical junction and proximal cervical cord

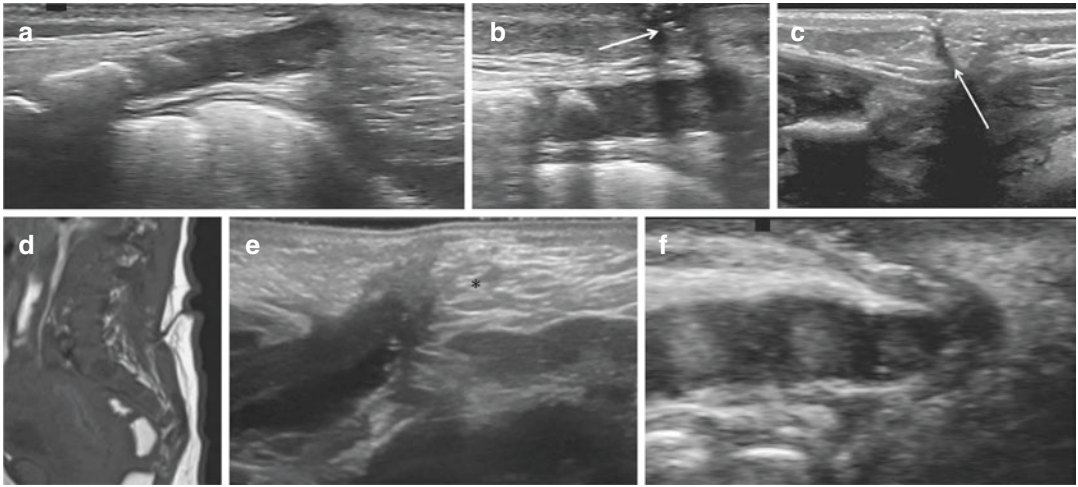


Fig. 8.18 US appearance of a sacral dimple with pilonidal sinus and DDX. (a) Dorsal sagittal acquisition of the cartilaginous coccyges showing the dorsally bent lowest coccyges—with some kind of tract coursing upwards to the skin with the simple sacral dimple. (b) Zoomed image of the pilonidal sinus with some echogenic air bubbles (arrow) indicating that there must be a lumen—however, its size is better assessed by a probe, as the weight of the attached transducer compresses the tract and obviates a correct assessment of its width. (c) Dermal sinus tract: observe the connection between skin and spinal canal usu-

ally coursing in the opposite direction as a pilonidal tract, and originating much higher in the back (arrow). (d) MRI confirmation of Fig. 8.17c. Note the somewhat unusual direction of the tract in this sagittal T1 weighted image without fat saturation. (e) A tethered cord attached at a lipoma (asterisk) at the level of the sacrum (may be also classified as a covered dysraphism in terms of a lipomyelocele). (f) The tract of a sacral dimple shows some central echoes proving a lumen of the tract, better assessed clinically than by US (as the US transducer may compress the lumen)

formations, but because of anxious colleagues and/or (grand) parents seeking relief and pacification. Sometimes also the length and the size of the connecting tract (typically coursing down caudally from the cutaneous dimple to the lowest coccygeal body which may be bent dorsally—Fig. 8.18) is inquired, and also, if there is an open lumen helping to decide on a possible excision to prevent later abscesses. However, as the pressure of the US probe may compress such a lumen, this therapeutically relevant information is better determined by trying to insert a thin metal probe. Cysts along that tract are a rarity, and these never connect to the spinal canal and should not be confused with a dorsal dermal sinus tract.

8.9.2 Spinal Canal and Cord Malformations, Dysraphism

There are many congenital spinal cord conditions that can be assessed by US.

- **Dermal sinus tracts** at higher spine levels, and usually course upwards from the dorsal cutaneous opening into the spinal canal. They (as with other spinal malformations) can be associated with other cutaneous stigmata such as hairy patches, dorsal midline haemangioma, or lipomatous swelling.

In these conditions, US will demonstrate the tract, follow it to its entrance into the spinal canal, demonstrate associated lipoma or lipomatous tissue, or associated cord pathology such as tethering or syringomyelia. As there is a possible connection to the spinal meninges, sterile handling (including sterile US gel) is recommended to prevent iatrogenic infection.

- **Open dysraphism** such as (myelo-)meningoceles are usually not investigated initially, but an US search for co-existing hydrocephalus with Arnold-Chiari Syndrome or other malformations can be performed. If necessary, the

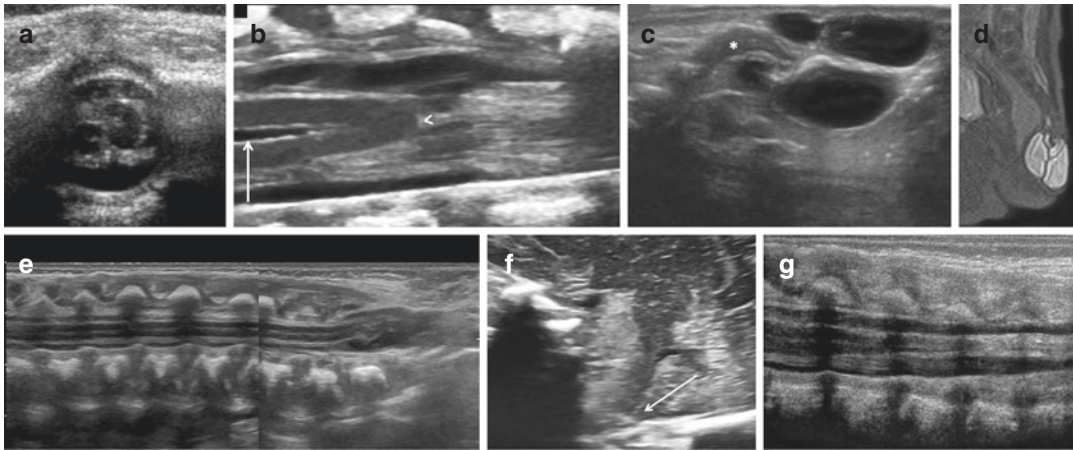


Fig. 8.19 US in various US spinal cord pathologies. (a) Two cords (arrows) visible in this axial view of the spinal canal indicating diastematomyelia. (b) Dilated central echo complex (arrow) indicating a dilated central canal in hydro-/syringomyelia. Note the slightly round shape of the conus (arrowhead) as often seen in a short cord/caudal regression syndrome. (c) US, acquired dorsally at the level of the cartilaginous coccyges (asterisk) with a linear transducer, shows the intrapelvic extent of a cystic presacral teratoma. (d) MRI (T2 weighted, fat saturation,

midline sagittal orientation, same patient as in Fig. 8.18c) confirms the US findings. (e) Covered dysraphism (dual/split screen image): skin covered myelomeningocele with associated tethered cord. (f) Sagittal transfontanelar US view of posterior fossa demonstrates associated low position of vermis (arrow) in a patient with MMC—that is why US of the brain should be performed in every patient with a spinal cord malformation. (g) Tethered cord due to a thickened, echogenic, lipomatous terminal filum—with associated deep position of the conus

spinal canal can then be examined after surgical closure to monitor further development (e.g. tethering, hydromyelia) or to assess complications such as post-surgical infection or abscess, CSF fistula, and others.

- **Closed/occult dysraphism** as well as a **tethered cord** can be seen and detected by US. The investigation is indicated either because of cutaneous stigma, swelling, neurologic symptoms suspicious for cord pathology, or as part of a sonographic work-up in more complex malformations (e.g. VACTERL...) that may be associated with spinal cord malformations. The level of the medullary conus needs to be defined—in a term baby this is usually at the height of the second (to third) lumbar vertebral body, whereas this may be a bit lower in preterm neonates. If the conus is low, US can evaluate the motility of the cord and the nervous structures including the terminal filum, and normal respiratory modulated undulations can be documented by m-mode or cine-clips. Furthermore, the cause for the tethering can be often also depicted, such as a lipoma attach-

ing the filum or a lipomatous echogenic **thickened filum** (diameter >2 mm).

- Other aspects that need to be assessed are:
 - The size of the cord—with the physiological thickening at the lumbar and the cervical level. This implies knowledge of the **normal appearance** of the spinal canal content (see Fig. 8.17).
 - The width of the central canal (usually not visible—only the central echo complex is seen) in order not to miss a **hydro-** or **syringomyelia** (Fig. 8.19).
 - The presence of a possible **intraspinial lipoma** as often associated with dysraphic malformations, on US seen as an echogenic tumorous mass that commonly attaches to the conus or the filum; additionally a sacrococcygeal teratoma may impact the appearance of the sacral spine, and cystic components of such a tumour need to be differentiated from a ventral meningocele (Fig. 8.19).
 - The cord itself: there may be a cord duplication with or without an osseous rim, then

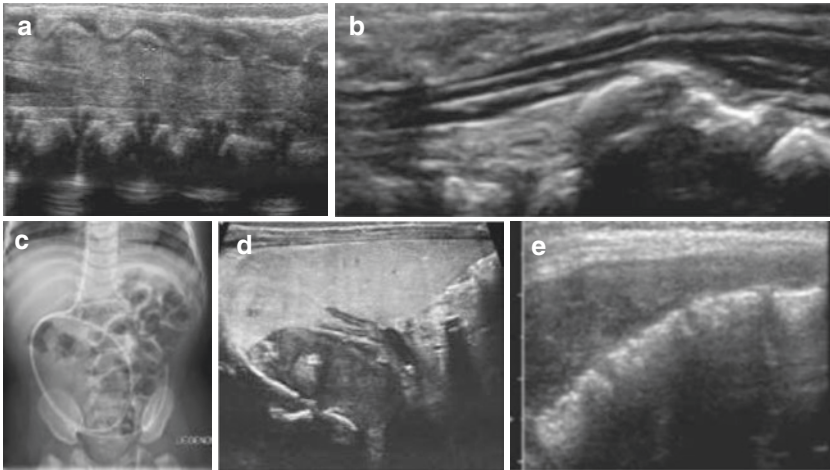


Fig. 8.20 US findings in other spine conditions. (a) Intraspinal haematoma after unsuccessful lumbar puncture (+...+). (b, c) Hemivertebrae with associated effects on cord at the level of the osseous spinal deformity (b), with the corresponding radiograph (c); note the abdominal portion of a ventriculoperitoneal shunt drain. (d, e) Intraspinous tumour

extension of a pre-/paravertebral neuroblastoma: intrusion of the neuroforamen with cord displacement in thoraco-lumbar level (d), or complete spinal canal invasion of a neuroblastoma at the lumbosacral level (e—note the low echogenicity soft tissue content of the sacral spinal canal due to the tumour masses which completely fill the sacral canal)

called *diastematomyelia or split cord malformation* (Fig. 8.19), or an interruption or injury/haematoma (e.g. after birth trauma).

- There also may be a *hypoplastic cord*, typically with a high and rounded end—as seen in caudal regression syndrome (Fig. 8.19).

8.9.3 Other Pathology of the Spinal Canal

There are other conditions that can be seen by US such as an *intraspinous haematoma* (e.g. after trauma, after lumbar puncture, but also from intracranial blood drained from the cranial CSF after a haemorrhage or after inflicted injuries).

US can also be used to define the level of a new lumbar puncture approach avoiding such a haematoma, or even guide the intervention by directly observing the needle path.

In *meningitis/myelitis*, there are no or only nonspecific findings, and US is thus not useful. Sometimes, particularly in bacterial meningitis, some echoes may be visible in the spinal CSF. Sometimes an empyema can

be detected—but this is primarily an MRI indication.

Spinal cord and spinal canal *tumours* also may occur—either of intraspinal origin, such as lipoma (then mostly associated with a dysraphism), with spine involvement such as in a congenital sacro-coccygeal teratoma (see Fig. 8.19), or secondary, such as a neuroblastoma that has invaded the spinal canal via a neuroforamen (Fig. 8.20). Therefore, particularly with such findings, the adjacent soft tissues should also be inspected.



in neonates, due to the jet poor ossification of dorsal elements, US is ideal for evaluating spinal canal and cord conditions and can be used liberally and successful in most queries

8.9.4 Spine US

The spine itself is more difficult to assess—but particularly the cartilaginous parts can be visualised. Ultrasound can demonstrate missing distal vertebrae such as in *caudal regression syndrome*

or Currarino Syndrome, with a diminished number of coccygeal and even sacral or lumbar vertebrae.

Ultrasonography may demonstrate hemivertebrae by showing asymmetry of the vertebral arches or bodies—so sometimes a missing echogenic outline of a hemivertebra will allow suggestion of a spinal osseous malformations, as does an unusual contour with possibly a step-off or a bend (Fig. 8.20). Nevertheless, a radiograph or even MRI will become necessary in many of these cases.

Ultrasonography may sometimes be helpful also in *spondylodiscitis*, but this is a rarity in neonates and not further discussed in detail; just note that US cannot “rule out” this condition. For these queries, an MRI is practically compulsory.

Remember that there may be *pre- or paraspinal extent* of spinal canal pathology (e.g. ventral meningocele). A complementing ventral access trying to visualise the ventral lining of the spine may be helpful not to miss those conditions (or even a complementing MRI may become necessary). This is of particular importance when trying to assess spondylodiscitis, as these usually arise in the ventral osseous parts and therefore cause rather ventral changes and collections, even abscesses. Nerve tumours such as neurofibroma are easily missed if only a dorsal approach is used—without evaluating the lateral and ventral regions.

8.10 Other Peripheral Neurosonographic Applications in Neonates

One can also evaluate a few peripheral nerve structures, such as neurogenic tumours (neurinoma, neurofibroma, retinoblastoma...) or eye pathology such as malformations (e.g. microphthalmia, congenital glaucoma, persistent membranes and vessels, coloboma with retinal detachment) (Fig. 8.21). Additionally, the extra-/retrobulbar intra-orbital space can be assessed (e.g. an enlarged optic nerve sheet and/or papilla swelling in (pressure) hydrocephalus), and retrobulbar tumours (mostly haemangioma or lymphangioma) can also be depicted.

Rarely also nerve injury can be assessed (e.g. of the brachial plexus after birth trauma). Ultrasonography can sometimes be helpful as a bedside investigation, possibly also for planning and tailoring other examinations—mostly an MRI.

As such, it is important to remember the potential of US to address some of these queries, although this is often tricky and challenging, and US may only partially visualise the given pathology, and an MRI may eventually become necessary.

How to perform these US investigations:

- For eye and orbit US, plenty of gel is applied to the upper closed eyelid using mostly linear high-resolution transducer (small footprint,

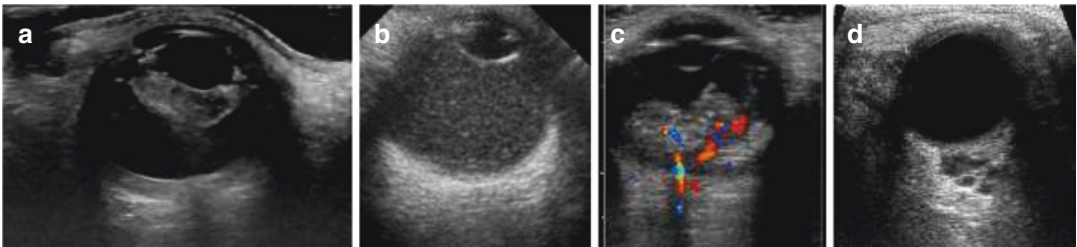


Fig. 8.21 Eye US—typical findings. (a) Distorted globe and lens with some soft tissue mass imaged using a high-resolution linear transducer and plenty of US gel—in a neonate with congenital coloboma and persistent vitreous tissue. (b) Eye US using a vector transducer shows that the globe is completely filled with echoes in a neonate with congenital glaucoma. (c)

Retinoblastoma: intraocular soft tissue tumour mass with vascularisation depictable by CDS—imaged using a high-resolution linear transducer. (d) Retro-orbital lymphatic malformation imaged using a phased linear transducer: note the cystic lesions behind the globe, with rather thick septae and some internal echoes due to previous haemorrhage

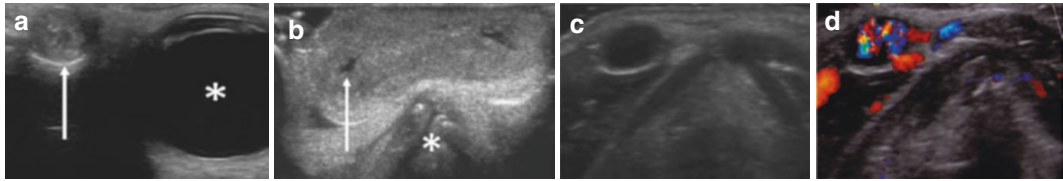


Fig. 8.22 US of forehead soft tissue masses such as dacryocystocele and respective differential diagnosis. (a) Complex cystic mass (arrow) medially to the bulb (*) in a neonate with dacryocystocele, imaged using a high-resolution linear transducer. (b) Frontal glioma sitting on the root of the nose (*), with non-differentiated brain-like

appearance and even a rudimentary central hypoechoic ventricular structure (arrow) imaged using a high-resolution linear transducer. (c, d) A little bump on the forehead near the root of the nose: US reveals a cyst-like subcutaneous structure (c) with vivid flow on CDS (d), consistent with a haemangioma/vascular malformation

possibly with phasing to trapezoid mode). As the globe easily heats due to the lack of perfusion, the lowest possible output gain should be used and the MI/TI kept well below 0.5 (or even lower). As external orientation is difficult or impossible, pictograms are important. Always assess the entire orbit not to miss parabolbar pathology such as haemangioma or lymphangioma, also a dacryocystocele can easily be imaged by US (sometimes done for DDX, e.g. vs. a tumour or an encephalocele) obviating the need for other imaging (Fig. 8.22).

- For peripheral nerves, high-resolution transducers are used with plenty of pre-warmed US gel. The most important requisite for this US application is, however, an excellent anatomic-topographic knowledge necessary for identifying and following the major nerves.

More details on these specific rare applications go beyond the scope of this book and are thus not discussed further.

8.11 Is There a Role for Radiographs, Fluoroscopy, or CT in Neonatal Neuroimaging?

8.11.1 Radiographs

Skull radiography has a significant obstacle in neonates: poor ossification. Therefore, it can be quite difficult to read these images and many

applications as known from older children or adults do not apply to neonates.

Sometimes, a medico-legally indicated radiograph is taken in a gross fracture (though then US may show the fracture as well and CT might only become necessary for evaluating a possible subdural, epidural, or subarachnoid haemorrhage, and then the fracture is visualised much better). Other indications may be syndromic conditions where head shape, size, and other skull features may help with DDX (see respective chapter).

Premature synostosis of the skull sutures is not a typical neonatal query and not addressed—increasingly US is advocated as a first imaging method, supplemented by radiography; CT is only performed pre-operatively.

Another indication for a radiograph is in neonates with spinal malformations or in conditions that may be associated with osseous spinal anomalies (see Fig. 8.20).

- Remember to adapt all parameters to the patients age and size: matrix of the detector plate, size of the individual detector, digital filters, reconstruction algorithms adapted to the different cumulative histogram at different sizes and body areas, consider radiometric and geometric resolution, signal to noise ratio and dose parameters, remove grids and collimate properly. A minimum spatial resolution is necessary to come-up with diagnostically reasonable image quality, as well as a high-resolution monitor that is able to display these subtle differences and findings.

8.11.2 Computed Tomography (CT)

CT of the neonatal brain is mainly performed in high suspicion of a cranial haemorrhage with equivocal US after some sort of significant trauma, or if MRI is unavailable/contraindicated (e.g. in hydrocephalus and brain malformations as well as for follow-up after shunting, particularly in acute suspected shunt complications and failure) (see Fig. 8.3, 8.4).

- If a CT needs to be performed, the high radiation sensitivity of the neonatal brain and skull (with yet plenty of radiation sensitive red bone marrow increasing the risk of developing leukaemia) needs to be considered as well as the different tissue composition and less skull ossification—thus the CT protocol must be adapted and optimised accordingly (i.e. lower mA and kV, adapt collimation and slice thickness—this varies with the individual vendors as well as with the age/size of the neonate too, and thus no universal protocol is available).
- Intravenous contrast agents are hardly ever needed—except for CT-angiography (CTA) in queries associated with vascular malformations or vessel injury.

8.11.3 Catheter Angiography and Fluoroscopy

In the neonatal nervous system, fluoroscopy is only used rarely—as catheter angiography (usually digital subtraction angiography) in conjunction with or as preparation for an interventional procedure such as embolisation/occlusion of a cerebral arterio-venous malformation (Fig. 8.23). For further details, see respective chapter.

MRI is addressed in dedicated chapter and not addressed here.

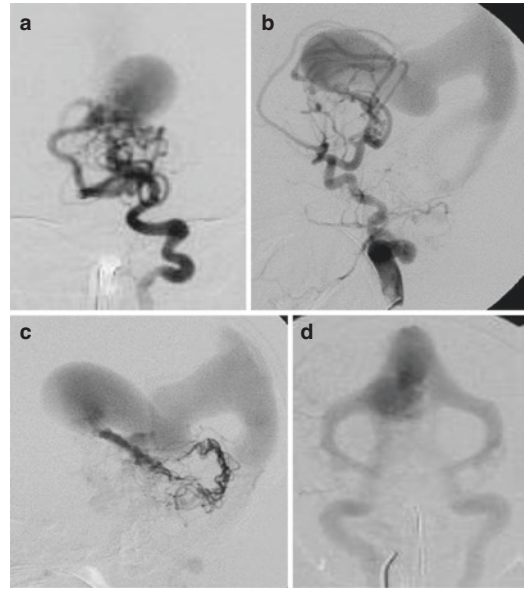


Fig. 8.23 Catheter angiography in the neonatal brain. Digital subtraction catheter angiography of a large cerebral AVM (vein of Galen malformation) performed just prior to interventional treatment in a term neonate: The first image (a) shows the arterial phase in a coronal projection, followed by early shunting into the dilated veins (b, c, in lateral projection), with rapid washout, so that soon only the enlarged and then hazily contrast filled veins and the aneurysm are still visible in the final coronal projection (d)

8.12 Summary and Conclusions: Take Away

Neonatal neurosonography is a powerful imaging tool particularly in this age group, not only as a bed-side orienting method; it allows a complete and sufficient evaluation of many conditions without the need for additional imaging or any radiation hazards. Thus, it has become one of the mainstays of neonatal neuroimaging. In the hand of skilled examiners with good equipment, it serves not only for a reliable diagnosis, but also for follow-up and monitoring, assessment of complications, as well as documentation and medico-legal issues at minimal burden to the

small patients. Particularly in the NICU, US has become an established and indispensable tool for decision making and guiding therapy and management.

The most important and frequent indications for neonatal neurosonography are suspected brain haemorrhages, hypoxic-ischaemic events, infections, hydrocephalus, as well as brain and spinal cord malformation. Proper education and sufficient experience are necessary to properly exploit the huge potential of US to the best of our small patients; then it also becomes a source for professional satisfaction and improved care with better (long-term) results and outcome.

Nevertheless, restrictions and limitations have to be acknowledged and then complementary or alternate imaging will become necessary. Skull radiographs and CT play a minor role in this age group—additional imaging is usually achieved by MRI, which is discussed in the next chapter.

Acknowledgments I am very grateful to Dr. Brian Coley (Columbus/Ohio) for editing this chapter.

Further Reading

- Coley BD, Siegel MJ. Spinal ultrasonography. In: Siegel MJ, editor. *Pediatric sonography*. 4th ed. Philadelphia, PA: Lippincott Williams & Wilkins, Wolters Kluwer Business; 2011. p. 647–74.
- Deeg KH, Wolf A. Doppler ultrasonographic diagnosis of increased intracranial pressure by comparison of flow velocities in the extra- and intracranial sections of the internal carotid artery (German). *Ultraschall Med*. 2000;21:259–64. <https://doi.org/10.1055/s-2000-9125>.
- Deeg KH. *Zerebrale Dopplersonographie im Kindesalter*. Berlin: Springer; 1989.
- Deeg KH, Rupprecht T. Pulsed Doppler sonographic measurement of normal values for the flow velocities in the intracranial arteries of healthy newborns. *Pediatr Radiol*. 1989;19:71–8.
- Govaert P, DeVries LS. *An atlas of neonatal brain sonography*. 2nd ed. London: Mac Keith Press; 2010. ISBN-10: 9781898683568.
- Helmke H, Hanson HC. Fundamentals of transorbital sonographic evaluation of optic nerve sheath expansion under intracranial hypertension II. Patient study. *Pediatr Radiol*. 1996;26:706–10.
- Janthanimi P, Dumrongpisutikul N. Pediatric optic nerve and optic nerve sheath diameter on magnetic resonance imaging. *Pediatr Radiol*. 2019;49:1071–7.
- Meijler G, Steggerda S. *Neonatal cranial ultrasonography*. Cham. ISBN: 978-3-319-77814-3: Springer; 2019. <https://doi.org/10.1007/978-3-319-77815-0>.
- Riccabona M. Neonatal neurosonography. *Eur J Radiol*. 2014;83:1495–506. <https://doi.org/10.1016/j.ejrad.2014.04.033>.
- Riccabona M, Nelson TR, Resch B, Pretorius DP. Potential of three-dimensional ultrasound in neonatal and pediatric neurosonography: a pictorial essay. *Eur Radiol*. 2003;13(9):2082–93.
- Riccabona M. Neurosonography in neonates, infants and children and ultrasound of the neonatal spinal canal and cord. In: Riccabona M, editor. *Pediatric ultrasound—requisites and applications*. 2nd rev. ed. Berlin: Springer; 2020. ISBN: 978-3-642-39155-2, ISBN: 978-3-030-47909-1.
- Resch B, Resch E, Maurer-Fellbaum U, Pichler-Stachl E, Riccabona M, Hofer N, Urlesberger B. The whole spectrum of cystic periventricular leukomalacia of the preterm infant: results from a large consecutive case series. *Childs Nerv Syst*. 2015;31:1527–32. <https://doi.org/10.1007/s00381-015-2786-3>.
- Siegel MJ. Brain. In: Siegel MJ, editor. *Pediatric sonography*. 4th ed. Philadelphia, PA: Lippincott Williams & Wilkins, Wolters Kluwer Business; 2011. p. 43–117.
- Simbrunner J, Riccabona M. Imaging of the neonatal CNS. *Eur J Radiol*. 2006;60:133–51.



Neonatal Neuroimaging: Neuro MRI in Neonates

9

Gregor Kasprian

9.1 Introduction

Due to the perfect tissue contrast and the good detail resolution, magnetic resonance imaging is a rapidly evolving highly clinically informative imaging modality, which—for certain indications—is nowadays considered the gold standard in neonatal neuroimaging. Neonatal neuro MRI requires not only knowledge of the examination strategy and technique, but also a profound knowledge of the principles of neonatal brain development and the unique contrast that arises in this context.

Of course, this chapter cannot replace a complete and detailed view on this subject—therefore the reader is referred to dedicated books in this field (for instance see [1–3]). This chapter should give an up-to-date overview of how neuro MRI examinations are planned and prepared and which classical findings are to be expected.

Due to the technical complexity and logistical challenges, neonatal neuro MRI cannot be certainly no comprehensive and easily accessible imaging modality. In most cases, a neonatal neurosonogram (see Chap. 8) is available before as an imaging reference. Moreover, in many places,

there has been extensive imaging documentation during pregnancy, which contains valuable information. Ideally, this information and data are available to the MR examiner.

In the following paragraphs, a practical and comprehensive overview of the use of MRI in the examination of the central and peripheral nervous system of the neonate should be given. In particular, requisites and investigation strategies will be emphasised, as the significance of the imaging results is strongly dependent on the setting in which it takes place.

9.2 Requisites/Imaging Strategy

9.2.1 Investigation Strategy and Preparation

An accurate and good preparation has a significant contribution to the success of the MR examination. The following aspects should be taken into account when preparing a neonatal MRI:

1. Patient's history: Gestational age at the time of birth, in case of prematurely born neonates accordingly to the *corrected* gestational age in weeks. Pregnancy/fetomaternal history. Information about abnormalities found at prenatal sonography or—if available—at prenatal MRI examinations. Information about any existing genetic finding or underlying disease. Clinical suspicion/signs of

G. Kasprian (✉)
Division of Neuroradiology, Department of
Biomedical Imaging and Image-Guided Therapy,
Medical University of Vienna, Vienna, Austria
e-mail: gregor.kasprian@meduniwien.ac.at

metabolic disease. Clinical history or evidence of perinatal infections.

2. Accurate information about the neonate's symptoms or previous ultrasound or laboratory findings is presented as detailed as possible.
3. Preparation of the neonate, outside the MR scanner—planning of breastfeeding intervals (“feed and wrap”), eventually sedation, MR-compatible clothing without metal buttons. Safety assessment of implants (children after heart surgery, shunt systems), availability of monitoring options for ECG or pulse monitoring.
4. Final steps: preparation of a “feed and wrap” setup: putting on a vacuum mattress, best before breastfeeding. Potentially also use swaddling or vacuum-pack bags to immobilise the baby. Provision of the child with appropriate ear protection. Precise safety check, if metallic objects are close to the child (MR incompatible ECG cables, etc.) or in contact with the neonate's skin, in case of using sedation, chloral hydrate 50 mg/kg is administered before the scan (for details see [2]).



Things done, *before* the neonate goes into the MRI:

1. History, prenatal imaging/lab or genetic results, exact/corrected gestational age
2. Symptoms, postnatal imaging results, exact indication for examination
3. Preparation outside MRI: planning of breastfeeding, metal-free clothing, MR compatibility of implants
4. Safety check! Ear protection, ID check

9.2.2 Performing the MRI

For neonatal head imaging, both 1.5 and 3 T MRI imaging are available. In both cases, either a multichannel adult head coil or a dedicated neonatal head coil is used for imaging. More modern sys-

tems are equipped with dedicated multichannel neonatal head coils, which are adapted to the specific anatomy of the neonatal head and can provide correspondingly high-quality images. However, systems that are not dedicated to neonatal anatomical conditions can also be used with good examination quality. Both 1.5 and 3 T MRI imaging are considered safe for neonates. As the specific absorption rates are significantly higher at 3 T, a slight (up to 0.5 °C) increase in neonatal body temperature has been a matter of concern [4], but was not observed by a recent study, measuring the core body temperatures during neonatal brain scanning of up to 55 min [5]. With adequate hearing protection, the high noise level in the examination room is usually below 99 dBA, which is not considered problematic for future hearing function or causing pain [6].

A neonatal head MRI examination should be carried out in a way that the most important imaging data is acquired at the beginning and the least important and redundant (to ultrasound) information is acquired finally. Following this strategy, the examiner can make sure that the important MRI-specific information is secured, even in cases, when there is the clinical necessity to interrupt or terminate the examination prematurely. The following sequences are part of a typical neonatal head MRI protocol and are listed to their importance and uniqueness:

9.2.3 Basic MR Sequences

9.2.3.1 Diffusion-Weighted (DWI) MRI Sequence

Diffusion sequences provide information that is not comprehensible on conventional T1-weighted or T2-weighted sequences. For example, intracellular edema is usually invisible on all other sequences and can only be captured by the diffusion sequence. The special feature of MR diffusion sequences is that this technique can quantify and measure the distribution and amount of motion of protons in a given tissue [7]. This is particularly valuable if early hypoxia-associated changes are to be detected (see Sect. 9.3). In addition to the detection of ischaemic changes,

diffusion sequences also provide valuable additional information in metabolic diseases as well as in inflammatory alterations (e.g. meningoencephalitis, Sect. 9.6). The specific physical background of DWI is so unique that the acquired imaging data cannot be collected by any other imaging modality.

The strength of diffusion weighting of an MR sequence is indicated by the “*b*-value”. The higher this parameter, the more diffusion-weighted the given sequence. Due to the high-water content of the neonatal brain, a *b*-value of 0 and 700 s/mm² is recommended for DWI in neonates. Due to its fast acquisition, diffusion sequences are usually acquired using an echo-planar readout mode. As this readout is sensitive to magnetic field distortions, introduced by iron or iron-containing tissues such as blood, *b* = 0 / mm² images also contain information regarding haemorrhages or residuals of haemorrhages. A more technical in-depth review of the technique and clinical application of DWI in neuroimaging is available elsewhere [8].

9.2.3.2 T2-Weighted Sequences

T2-weighted sequences are the anatomical reference sequences in neonatal brain MRI. Due to the high water content of the neonatal brain, T2-weighted sequences provide detailed anatomical contrast and also provide information about the degree of myelination of the immature brain. Extracellular edema leads to signal changes that are also easily detectable by T2-weighted contrast. T2-weighted sequences are acquired using a small/appropriate field of view with slice thicknesses of less than 3 mm. Either, they are acquired in all orthogonal planes separately, or they are acquired (on modern MR scanners) using an acquisition mode in 3D—which can be reconstructed in any plane. As streaming blood leads to a signal loss on T2-weighted images, flowing blood appears hypointense (dark) on T2 Turbo Spin Echo (TSE, = acquisition mode). The absence of a dark signal in the dural sinus or cerebral blood vessels—such as the cerebral arteries—on T2-weighted sequences may indicate the occlusion of the given vessel.

9.2.3.3 Susceptibility-Weighted Imaging (SWI)

This acquisition technique allows to capture small magnetic field homogeneities with high sensitivity, which are represented as extinction artefacts (black dots) in the MR image. Due to the iron content of blood, bleeding residues or blood degradation products are therefore detected with unprecedented sensitivity. SWI is thus the most sensitive imaging technique for detecting haemorrhagic residues both intraventricular and superficially on the brain surface, in the posterior fossa as well as supratentorial.

9.2.3.4 T1-Weighted Imaging

T1 TSE or T1 3-D sequences allow good anatomical visualisation of the neonatal brain. They are particularly valuable in the depiction of myelinated brain structures such as the brainstem and the cerebellum. T1-weighted sequences depict fat-containing tissues as bright or hyperintense. Thus mature (= phospholipid containing) myelin is depicted as hyperintense/bright. Also, intracortical myelin is sensitively visualised by T1, as the precentral gyrus and its cortex appear bright on T1-weighted images.

In MRI of cases after neonatal asphyxia, corresponding signal changes can be found in the subacute stage through T1-weighted imaging (see Sect. 9.3). On T1-weighted images, the posterior lobe of the pituitary gland can be seen as a bright structure (specific protein content). T1 is also ideal for the representation of fat-rich structures such as lipomas. Native T1-weighted sequences are also helpful in the detection of subacute haemorrhagic residues (containing methemoglobin) which are T1-weighted bright/hyperintense.

9.2.3.5 BTFE/CISS Sequences

In cases, where complex brain malformations or syndromic conditions are to be characterised, CISS/BTFE sequences are extremely helpful. They complement standard T2TSE sequences with slice thicknesses of up to 1 mm and an excellent resolution in visualising small structures such as cysts or cyst membranes as well as

cranial nerves or posterior fossa structures. Whenever there is a suspicion of cranial nerve agenesis or the need to characterise arachnoid cysts, CISS/BTFE sequences should be added to the standard protocol.

9.2.4 Advanced MR Techniques

9.2.4.1 MR Spectroscopy

MR spectroscopy can be used to detect certain metabolites in the neonatal brain. Most valuably, the possibility to detect lactate allows to further specify changes associated with disorders leading to anaerobic metabolic changes (glycolysis) and thus to an accumulation of lactate. This is particularly valuable when assessing cases after neonatal asphyxia [9] (see Sect. 9.3), or when characterising metabolic disorders such as mitochondriopathies (Fig. 9.1e). Generally, spectroscopy is performed using an echo time (TE) of

135 ms, which provides the most robust results. When interpreting neonatal spectroscopy results, it is important to understand the specific metabolite distribution and concentration of the neonatal brain, which essentially diverges from the spectrum of the normal adult brain tissue.

9.2.4.2 Diffusion Tensor Imaging (DTI)

DTI allows a detailed geometrical characterisation of local tissue microstructures. Its application in neonatal brain imaging is particularly useful if so-called eloquent pathways are to be visualised to inform surgeons about their course before surgery. “Eloquent” pathways are white matter pathways, which carry neural information essential for basic physical activities, such as motor, sensory, visual, or acoustic function. On the other hand, it is possible to detect and characterise abnormal trajectories of white matter pathways using DTI and specify the diagnosis of brain malformations (Fig. 9.2e, f).

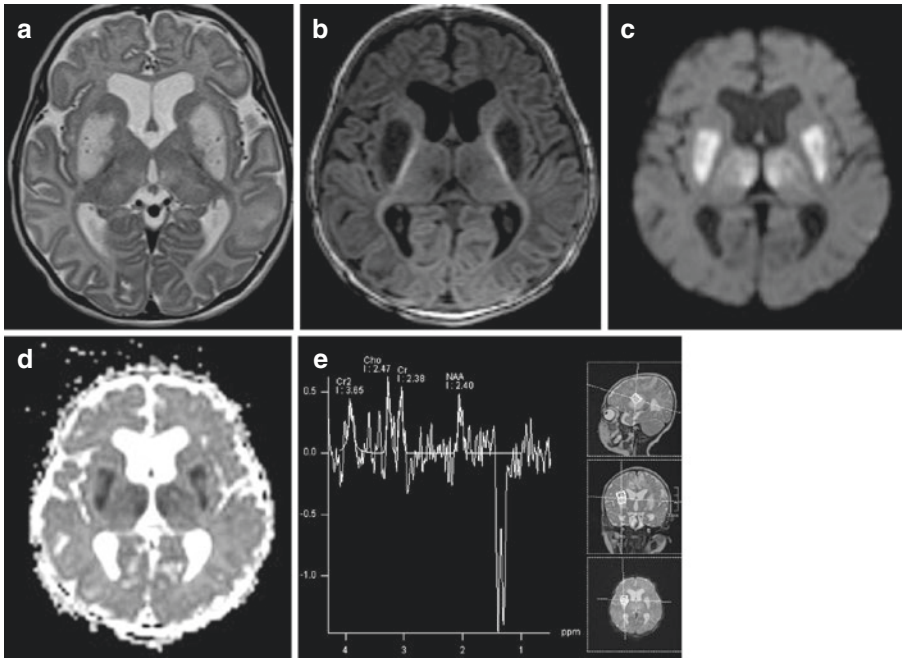


Fig. 9.1 Neonate with drug resistant epilepsy: axial T2-weighted (a), T1 weighted (b), DWI (c), apparent diffusion coefficient (ADC) (d), single voxel spectroscopy (e). Note the symmetric bilateral T2-weighted hyperin-

tense signal alterations of the lentiform nucleus with diffusion restriction and significant lactate peak (e). These features are characteristic for mitochondriopathies

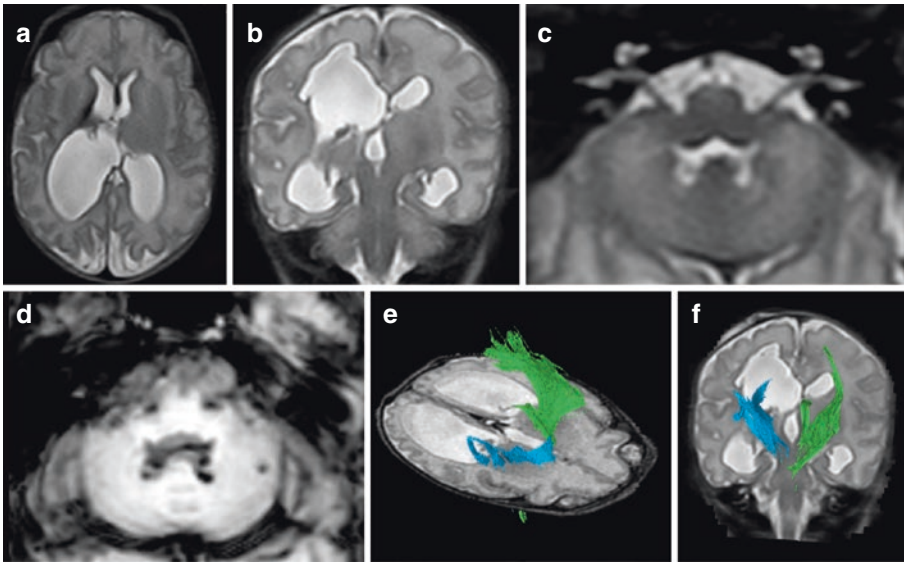


Fig. 9.2 Intraventricular haemorrhage with perihemorrhagic parenchymal lesion with white matter defect of the right ventricle (a, b). Note that conventional T2-weighted images are insufficient to identify blood breakdown prod-

ucts, which are sensitively detected by SWI (c, d). Diffusion tensor imaging and tractography enable the depiction of the corticospinal tracts bilaterally with discontinuity of the right sensory motor pathways (e, f)

9.2.4.3 Arterial Spin Labelling

Arterial spin Labelling (ASL) is based on the possibility to “magnetically” tag inflowing protons, for instance, at the level of the extracerebral carotid artery. The difference in signal between brain tissue before and after the tagged protons has arrived in the cerebral microvasculature can be measured by MRI and visualised as a colour-coded map. Using ASL areas of regional hyperperfusion or hypoperfusion can be visualised. This technique may see increasing use as a biomarker for post hypoxic hyperperfusion injury in cases of hypoxic-ischaemic injury [10].

9.2.4.4 Blood Oxygen Level Dependent (BOLD) fMRI Imaging

Using BOLD fMRI, so-called resting-state networks of the neonatal brain can be visualised [11]. Diagnostically and clinically, this is currently not relevant. In the future, however, it is to be expected that functional neonatal brain imaging and the visualisation of functional connectivity networks will allow prognostic statements.

For this purpose, it is necessary to image normal reference collectives to compare them with individual patients. The technique is based on the ability of MRI to measure the magnetic properties of oxygenized and deoxygenized blood. Signal changes occur in dependency of the local vascular autoregulation and oxygen consumption and thus reflect localised brain activity. Modern postprocessing methods allow to measure the connectivity between active areas and to generate maps of the functional connections of the neonatal brain in health and disease [11].

9.2.4.5 Synthetic MRI[©], MR Fingerprinting

Synthetic MRI imaging opens the possibility to record various MRI parameters by acquiring a single multi-echo sequence (MDMSE sequence). By comparison with a reference databank, different tissue contrasts (T1-, T2-weighted, proton density) can be generated after the acquisition of only a single MR sequence. Recently, it has been shown that this

technique is in no way inferior to standard basic MR sequences in the detection of haemorrhages [12]. In addition, this approach also makes it possible to quantify myelination and to identify delays in the context of premature birth [13]. Another modern technology that will be used in neonatal imaging in the future is called “MRI fingerprinting” [14]. Here, too, numerous parameters are measured as part of a single multi-echo sequence, which then is compared with a dictionary. In addition to calculating different MR contrasts based on a single sequence acquisition, quantification of T1 or T2-relaxation times and tissue-specific MR metrics will be possible. These are exciting approaches to make MRI more quantitative and interpretation less subjective and comparable between institutions.



The most important step, when performing neonatal head MRI is *preparation*. Essentially the diagnostic aim of the MR investigation should be known. Following that, basic (T2-weighted, DWI, T1 weighted and SWI sequences) or advanced MR techniques can be used to provide the clinically relevant information.

9.3 Hypoxic-Ischaemic Injury

In developed countries, this rare but serious condition occurs in an average of 1.5 out of 1000 live births [15]. The cause and severity of hypoxia can vary significantly and may range from mild (usually short) to severe (usually prolonged) and from umbilical cord compression to protracted birth, placental abruption, maternal eclampsia, foetal bradycardia, or meconium aspiration. Moreover, as the aetiology and the imaging appearance and their cerebrovascular physiology differ, a distinction has to be made between encephalopathy of the term-born neonate and hypoxia in premature babies [16].

Due to advances in neonatal intensive care, the clinical consequences of hypoxia and asphyxia

are less dramatic today than they were 10–20 years ago. In particular, the clinically generous and expert use of therapeutic hypothermia has led to milder long-term sequelae.

When assessing a neonatal after hypoxic injury, it is important to be aware that imaging is only one piece of the puzzle. In addition to ultrasound and MRI, clinical and laboratory chemical parameters, as well as the important AEEG, are used to evaluate the prognosis of the affected child.

Usually, only prolonged and severe forms of HIE lead to MRI changes [17]. However, MRI is the gold standard and most sensitive imaging modality in the assessment of the asphyxiated neonate, as it shows the highest sensitivity in depicting cortical and basal ganglia injury in HIE. Depending on the time point after the initial hypoxic-ischaemic event, MRI characteristics of HIE are changing in their imaging presentation. Thus, in the first 24 h, structural sequences can show hardly any changes, while still, a serious hypoxic encephalopathy is present. To prevent wrong negative or too favourable prognoses based on missed imaging findings, knowledge of the time course of brain MRI changes in HIE is of utmost importance. The right sequences and techniques need to be deployed and interpreted based on knowledge of the exact timing and aetiology of the underlying event.

9.3.1 MRI Within the First 24–96 h After HI Event

In this time frame, structural T2- and T1-weighted sequences often appear inconspicuous. The most valuable sequence in the early assessment of HIE is the diffusion-weighted sequence. Using DWI, in particular cortical diffusion restrictions as well as diffusion restrictions in the white matter—in particular in the corpus callosum as well as in the inner capsule should be searched for. Not only the diffusion-weighted $b = 700\text{--}1000\text{ s/mm}^2$ images must be examined, but also the ADC maps are evaluated in detail. A common pitfall associated with the assessment of neonatal diffusion-weighted sequences is the erroneous

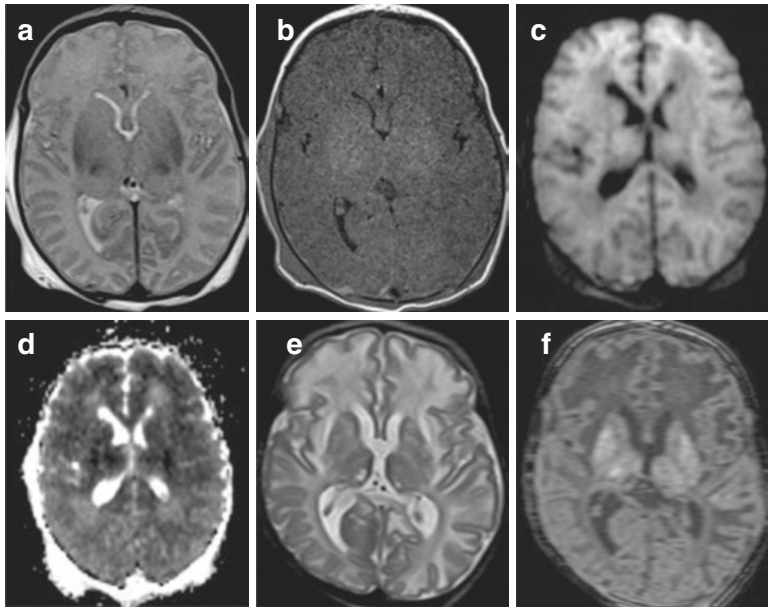


Fig. 9.3 Severe hypoxic ischaemic encephalopathy (HIE) in a neonate, imaged at day 3 (**a–d**) and week 4 (**e, f**). There is significant brain swelling and edema, visible at T2-weighted sequences (**a**). However the grade of severity may be underestimated by assessing T2-weighted and T1 weighted (**b**) sequences alone. DWI source images (**c**) may also mask the

true extent of the pathological changes, which are most accentuated and detectable at ADC maps (**d**). Follow-up at 4 weeks after injury show the severe atrophy and destructive changes (**e, f**). Moreover T1-weighted images show hyperintense signal changes of the basal ganglia, which are characteristic for late HIE associated changes (**f**)

wrong negative evaluation of diffusion source images while ignoring the ADC maps, which visualise the true extent of the injury in an unbiased fashion (Fig. 9.3a, d). DWI changes may “pseudonormalise” (= visually disappear, despite significant tissue damage) after 4–5 days in normothermic and even later (after 7 days) in hypothermia treated babies [18].

In addition to diffusion-weighted imaging, MRI spectroscopy is a helpful technique for detecting and characterising HIE within the first 18–96 h after onset [19]. Single voxel spectroscopy in the basal ganglia area with an echo time of at least 135–144 ms allows the detection of a lactate peak at 1.3 ppm (inverted doublet peak). The presence of lactate in HIE cases is one of the strongest adverse predictive parameters [9, 19, 20] in the prognostic assessment but needs to be interpreted with caution as lactate can be present in the non-HIE brain of preterm neonates. Moreover, MR spectroscopy used 1 week after

the event is less predictive of adverse outcomes compared to its use within the first 18–96 h [19].

9.3.2 MRI More Than 3 Days After HI Event

After 78 h, changes in structural T2-weighted sequences are becoming increasingly apparent. Changes associated with extracellular edema are detected, which lead to local or global swelling of brain tissue. Accordingly, edema causes T2 prolongation and thus hyperintense signal alteration of hypoxia altered brain regions. Often subtle T2-weighted signal changes are visible, whereby the inner capsule is not distinguishable from the surrounding basal ganglia and the thalamus. The physiological hypointensities of the posterolateral putamen and the ventromedial thalamus become less evident and indistinct to the adjacent grey matter.

Finally, T1-weighted signal changes in the basal ganglia and thalamus are becoming increasingly apparent (Fig. 9.3f). These are displayed as often circumscribed T1 hyperintensities in the region of the putamen and the thalamus. Accurate anatomical assessment is essential: the physiological T1-weighted hyperintensity of the posterolateral putamen should always be less pronounced than the circumscribed T1 hyperintensity of the thalamic/internal capsule [17]. In HIE, this relationship appears as inverse, with the physiological hyperintensity of the posterior limb of the internal capsule disappearing (absent posterior limb sign) [21] and hyperintensities of the posterolateral putamen and ventrolateral thalami becoming more evident and pronounced. In cases of profound (severe and abrupt, “total asphyxia”, for instance, in placental abruption) hypoxia also brainstem nuclei, most prominently and visibly in the midbrain are involved and display T1-weighted hyperintense signal alterations.

The described MRI changes can sometimes be relatively subtle, especially due to the now generously used hypothermia treatment. In the event of a clinical discrepancy between the clinical neonatology impression and the initial MRI impression, the MRI images should in any case be re-evaluated or MRI repeated within a different time window to improve the prognostic accuracy.

9.4 Neonatal Brain Haemorrhage

The vast majority of intracranial haemorrhages in the newborn occur in form of intraventricular haemorrhages (IVH) in premature neonates. Still, IVH is rarely found in term-born infants, differing in location and aetiology from preterm IVH with term-born showing IVH major predilection sites at the choroid plexus and thalamus and sinus vein thrombosis [22] or arteriovenous malformations [23] as major underlying pathologies. Neonatal MRI imaging is not the examination of the first choice, as ultrasound allows easier bedside access and examination logistics. Neonatal head ultrasound thus provides the initial diagnosis of IVH in most cases (see Chap. 8). Also, monitoring of the ventricle size to exclude a CSF circulation disorder

is carried out primarily by ultrasound. MRI imaging for IVH is primarily applied to provide an accurate prognostic assessment. However, the common classification of IVH in grades 1–4 is superficial and insufficient to generate a long-term prognostic assessment [24, 25]. Due to the complete visualisation of the neonatal brain of both the supra- and infratentorial structures by MRI, it is possible to evaluate all relevant functional compartments of the developing brain without limitations. In particular—cortical structures—which are often inaccessible due to acoustic shadowing can be well assessed by MRI. In addition, the extent of intra- and extra-ventricular bleeding residuals can sensitively be assessed using blood-sensitive MRI sequences. As there are no technical limitations in visualising posterior fossa structures, MRI also shows advantages over ultrasound in the morphological assessment of frequently associated cerebellar pathologies/haemorrhages (Fig. 9.2c, d). Using the classical transfontanellar view, ultrasound misses 80% of cerebellar haemorrhages detected by MRI. Even, when using the mastoid view, only half of the cerebellar haemorrhages visualised by MRI are seen by ultrasound [26].

9.4.1 MR Scoring of IVH

For better prognostic assessment, a recent MRI-based scoring system in cases of intraventricular haemorrhage of preterm neonates has been developed and outperforms the prognostic precision of the currently widely used ultrasound-based IVH grading scheme [25]. It is based on the assessment of functional compartments and functionally relevant brain regions such as the primary sensorimotor cortex, the visual cortex, the thalamus as an important sensory relay station and gateway to consciousness as well as the corresponding connections originating from these centres such as the pyramidal tract (Fig. 9.2e, f), the thalamic radiation, the optic radiation, and the corpus callosum. In addition, lesions or changes to the hippocampus are assessed and included in the score. Moreover, there are specific regions, where significant crossings of functionally relevant fibre systems

occur [27]. These regions have been coined as “crossroads” and can be visualised unequivocally by MRI. In that regard, the use of modern MRI techniques such as diffusion tensor imaging (DTI), which allows a non-invasive representation of these pathways in 3-D, is particularly valuable and can further improve prognostic accuracy in these cases (Fig. 9.2e, f) [28].

9.4.2 MR Characteristics of Neonatal Intracranial Haemorrhages

The typical intraventricular haemorrhage is located in the region of the caudothalamic groove (see Chap. 8). The anatomical structures are located in the vicinity—the caudate nucleus and the thalamus are often damaged by the haemorrhage. MRI imaging allows a detailed assessment of the associated parenchymal damage. Using SWI or T2* sequences, the extent of the intraventricular haemorrhagic residues can be well documented. In case of significant haemorrhagic residues in the fourth ventricle as well as in the aqueduct, there is a high chance for CSF circulation blockage. T2-weighted sequences (T2 3-D sequences)—Fig. 9.4b—are particularly suitable in these situations, as they have a high sensitivity for CSF flow signals (“flow voids”), which appear as T2-weighted dark signals in regions, where there is an accelerated CSF flow (foramen of Monro, site of a ventriculostomy or the mesence-

phalic aqueduct). The absence of these T2-weighted flow voids indicates a lack of sufficient CSF flow and helps to explain and locate the origin and site of CSF blockage in IVH cases developing hydrocephalus (Fig. 9.4a–c).

SWI/T2* is also suitable for detecting superficial cortical blood deposits in extensive intraventricular bleeding supra- and infratentorial (Fig. 9.2d). These can etiologically be causative for the occurrence of epilepsy. Particularly noteworthy is the image of a “cerebellar disruption”. The term “disruption” describes the breakdown of a structure that originally showed a normal course of development or had a normal developmental potential. Thus, without the presence of an adverse event—such as a haemorrhage—the organ or structure would have developed normally. In the case of cerebellar distribution, superficial haemosiderin deposits lead to reduced growth or even apoptosis with the consequence of the development of a structurally visible pontocerebellar hypoplasia (Fig. 9.5a–c) [29].

9.4.3 Cerebral Haemorrhages Other Than Intraventricular Haemorrhages

Neonatal cerebral haemorrhages in mature, term-born babies are far less common than classical intraventricular haemorrhages. These haemorrhages are often associated with neonatal or perinatal infections (frequently seen on Parvovirus

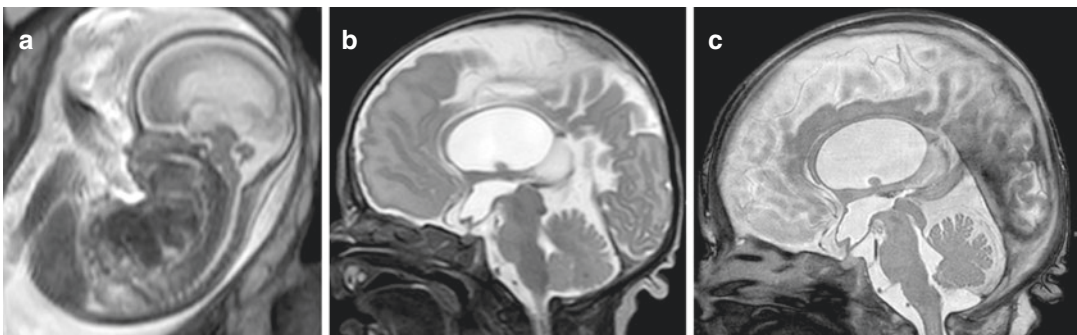


Fig. 9.4 Foetal occlusion of the mesencephalic aqueduct depicted at 25 gestational weeks by foetal MRI (T2-weighted sequence) (a). The same case, imaged postnatally, shows an occlusion of the mesencephalic aque-

duct without a characteristic flow void signal at T2-weighted 3D sequences (b). BTFE sequences (c) have a high linear resolution to visualise the patency or occlusion—as in this case—of the aqueduct

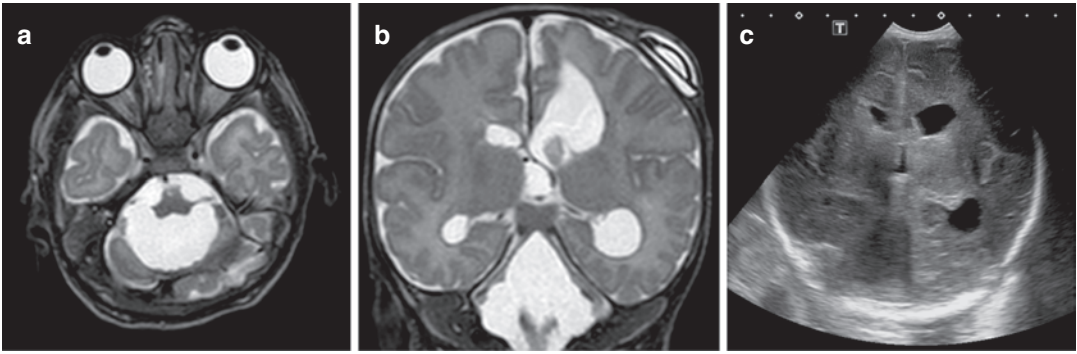


Fig. 9.5 Cerebellar disruption after severe intraventricular haemorrhage in a preterm infant (a). Please note the severe and extensive destructions of the cerebellum secondary to haemosiderin deposits without direct haemor-

rhagic lesion to the cerebellum (secondary changes) (b). On transcranial ultrasound (c) these changes could be easily missed, if the posterior fossa is not assessed thoroughly

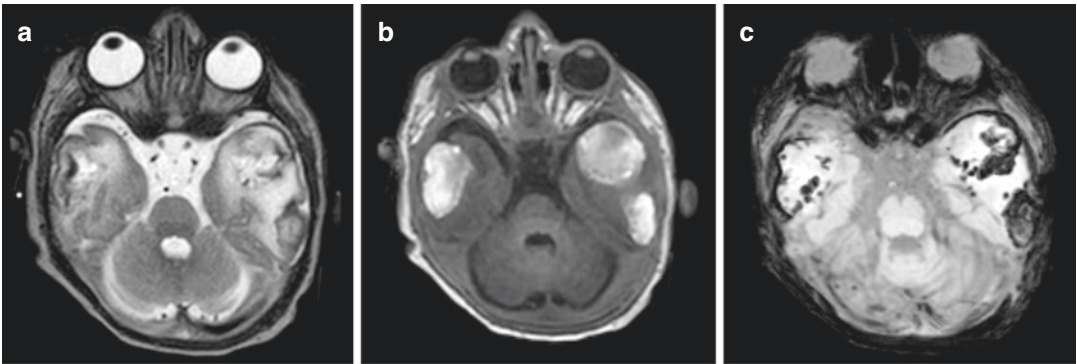


Fig. 9.6 (a–c) Case of a rather rare, but typical subpial haemorrhage in a neonate with seizures. Please note the typical pattern of haemorrhagic changes within the neonatal brain parenchyma, close to the surface of the neonatal brain

B19 or other infections) or blood clotting disorders/thrombophilia. For instance, extensive haemorrhages (intraventricular and parenchymal) can also occur as part of genetic syndromes such as the COL4A1 mutation [30].


A special case of neonatal cerebral haemorrhage is the subpial haemorrhage (Fig. 9.6a–c) [31]. This is a specific form of neonatal cerebral haemorrhage which is located just underneath the pia mater and appears as a well-circumscribed intra-axially located haemorrhage. Often these haemorrhages occur bilaterally and are located in the temporal or cerebellar regions [32]. The appearance is very typical and specific to the newborn age. Subpial haematomas are rather rare overall. So far, no direct association with a specific trigger has been found, but

there seems to be an association with acute coagulopathies [31, 33]. The prognosis of these lesions currently seems heterogeneous, whereby their outcome seems to depend mainly on the underlying disease.

Subdural haematoma in the newborn—especially if multiple, bilateral, and located in the convexity and distant to fractures, surrounding the falx or in the posterior fossa—should always raise the question of non-accidental head injury in abusive head trauma [32]. Again, SWI sequences are particularly informative in this context as they enable the depiction of the so-called tadpole sign [34]. This sign represents a small enlargement of a ruptured bridging vein, associated with a local tubular bridging vein thrombosis close to the superior sagittal sinus in

the parasagittal region, resulting in a tadpole- [34] or lollipop like [35] picture.

Subdural haematoma is not exclusively associated with abusive head trauma, as they most frequently occur in form of parturitional SDH [32], which usually resolves 4 weeks after birth. Moreover, neonatal subdural haematomas can occur in all conditions in which there is significant underdevelopment or atrophy of the neonatal brain and are not specific for non-accidental head injuries. Above all, these include glutaric aciduria type one, which is associated with large arachnoid cysts and dilated subarachnoid spaces due to significant brain atrophy. Even in children with various underlying diseases such as congenital heart defects, there is a frequently reduced brain volume and consecutive enlargement of the subarachnoid space [36]. This leads to increased mechanical tension on the bridging veins and an increased risk of subdural haematoma—even after minor head trauma. In these cases, a critical differential diagnostic discussion—involving a multidisciplinary team—is necessary to prevent wrong assumptions or decisions leading to un- or overprotected children.

 Hypoxic ischemic brain injury (HIE) and intraventricular hemorrhages (IVH) are the most frequent indications for neonatal head MRI. Knowledge about the natural timecourse in HIE determines the MR sequence, providing the essential prognostic information. Historic grading systems in IVH are limited in their prognostic information, thus newer ways to evaluate this aspects have been developed and should be applied in future.

9.5 MRI of the Brain Injury Spectrum in Premature Neonates

Brain injury in premature infants or also defined as “encephalopathy of prematurity” shows a multifactorial aetiology. Its central aspect is coined as “periventricular leukomalacia” or white matter

injury. However, prematurity affects a variety of neonatal brain compartments involving grey and white matter brain regions. To properly understand brain changes due to immaturity and premature birth, it is important not only to focus on white matter injury alone. In this aspect, MRI plays an important role, as MRI provides an excellent tissue contrast to assess grey and white matter compartments equally well. It is important to understand, that only a minority of the microscopic and profound changes to the foetal brain parenchyma can be seen by MRI or neonatal brain imaging [37]. The mainstay of changes due to immaturity and prematurity remains undetected by any currently used imaging method. Still, a thorough analysis and detection of prematurity-associated brain changes allow a better prognostication and counselling of parents.

9.5.1 Aetiology of Prematurity-Associated Neonatal Brain Changes

The central aspect in the evolution of prematurity-associated brain changes is the interplay between chronic hypoxia/ischaemia as well as inflammatory/infectious changes to the developing immature brain. Especially ischaemia is triggered and aggravated by the fact that autoregulation of the cerebrovasculature of the immature nervous system is incompetent in dealing with the unnatural requirements of haemodynamic responses, occurring outside of the maternal womb. This leads to a variety of ischaemia-triggered responses to the brain parenchyma, most profoundly to the periventricular white matter, of which some can be visualised by neonatal brain imaging. Furthermore, pre-existing infection and/or inflammation to the developing brain—as the cause or as a consequence of maternal prenatal infection or foetal inflammatory response syndrome—can aggravate the abnormal haemodynamic responses and the microstructural and cellular changes to the neonatal brain.

Ultimately, this leads to a spectrum of severity of structural imaging changes seen on ultrasound and MRI at different stages of

development. Some of these changes can be better as seen earlier—at prenatal states of development—and others can be better evaluated at the term equivalent age. The full-blown consequences combined with reactive compensatory mechanisms of the neonatal brain become fully apparent after the completion of myelination at later stages of infant development.

9.5.2 MRI Features of Prematurity-Associated Neonatal Brain Changes

9.5.2.1 Periventricular Leukomalacia (PVL)

From a neuropathological standpoint, PVL consists of two distinct components. One is *focal necrosis*, the other is *diffuse white matter injury* marked by astrogliosis and microglial activation [37]. This leads to three different levels of severity in PVL. The most extreme but fortunately rarest form is “*cystic PVL*”, a state where large regions of the periventricular white matter are necrotic and have transformed to cystic CSF-filled areas. In these regions, the white matter of the neonatal brain is destroyed and the connections running through these regions are completely lost. “*Noncystic PVL*” represents a more moderate form, which is characterised by diffuse changes of signal to the developing white matter. Under the microscope of a neuropathologist, there are multiple small foci of necrosis, which are less than 1 mm in diameter [38]. This is too little to be visualised by MRI and invisible to clinical neonatal neuroimaging [37]. However, in some cases particularly at earlier time points of imaging (earlier than 32 gestational weeks) so-called *punctate white matter lesions* can be seen on MRI [39]. These are T1-weighted hyperintense, T2-weighted hypointense, and sometimes diffusion restricted, linear, or clustered dot-like areas of signal alterations within the white matter. They are located in different regions of the cerebral white matter, in the frontal, parietal, and central regions [40]. Depending on their location and their number, they provide some information on the severity of these moderate brain changes.

However, later—particularly at term-equivalent stages—punctate white matter lesions are rare [39]. At this stage *diffuse white matter atrophy* dominates. As a consequence, the lateral ventricles appear enlarged. Diffuse non-cystic PVL can be seen on ultrasound by increased echogenicity of the white matter (see Chap. 8). In most of those cases, MRI also shows diffuse white matter signal abnormalities, whereas transcranial ultrasound detects only half of cases with extensive signal intensity abnormalities or cystic changes in the cerebral WM as shown with MR imaging at term [41]. Also in cases with normal or transient echogenicity changes on ultrasound, MRI frequently provides additional information by depicting diffuse signal changes, which are not seen to the same extreme extent by ultrasound [41].

Recently conventional neonatal brain MRI is complemented by more sensitive methods to detect neonatal white matter injury such as diffusion tensor imaging. In different study settings and clinical study cohorts, DTI has shown to be predictive in motor [42], cognitive [43], language [44], and visual [45] outcomes of neonates with PVL. Future studies will need to prove if these results can be also applied to individual cases.

9.5.2.2 Cortical and Subcortical Grey Matter Injury of Prematurity

Cortical grey matter is affected by premature birth and often results in *signal abnormalities on standard MRI sequences and/or significant atrophy of the developing cortex*. Cortical atrophy is visually seen by an enlargement of the subarachnoid space and distance between the cortical folds, or grossly as increased interhemispheric distance [46]. Pure visual inspection of atrophic changes is extremely examiner-dependent and subjective. Semiquantitative evaluation with areal measurement of basal ganglia and thalamus offers the first step towards a more quantitative and objective evaluation of grey matter loss after premature birth [46]. In the future, more objective ways of evaluating cortical atrophy in premature neonates are currently developed. For now, different scoring systems can be used in this

regard [46, 47]. Furthermore, cortical folding can show immature patterns, most prominently detected in the region of the Sylvian fissure—also coined as “opercularisation”—which is often incompletely closed and the insula not fully covered (which is typically the case at term-equivalent stages of development).

Subcortical grey matter—the basal ganglia as well as the cerebellar grey matter—is also frequently affected by prematurity. These regions play an important role in global brain function and also need to be assessed by neonatal brain imaging. Again, the evaluation of *atrophy of the basal ganglia and specifically the thalamus* require some experience in neonatal brain imaging. However, volume loss of these regions is important to be described in neonatal brain imaging reports of prematurely born babies. Sometimes signal intensity abnormalities on conventional T1- and T2-weighted sequences of the cerebellar grey matter or the basal ganglia and thalamus are seen and need to be documented.

In summary, cortical and subcortical volume reductions in neonates born prematurely are important prognostic factors, but—unfortunately—are frequently not reported in neonatal brain MR examinations [48].

9.6 Neonatal Brain Infection

The acronym “CHEAP TORCHESZ” [49]—well summarises the wide spectrum of congenital infections of the central nervous system. It stands for C—Chickenpox, and shingles; H—Hepatitis B, C, (D), E; E—Enteroviruses; A—AIDS (HIV infection); P—Parvovirus B19; T—Toxoplasmosis; O—Other (Group B Streptococcus, Listeria, Candida, Lyme disease); R—Rubella; C—Cytomegalovirus; H—Herpes simplex; E—Everything else sexually transmitted (gonorrhoea, Chlamydia infection, Ureaplasma urealyticum, human papillomavirus); S—Syphilis. More recently the Zika pandemic has been added to this group of diseases [50]. Most of these conditions are associated with a more or less specific imaging appearance on

neonatal (also see [51, 52]) and foetal (for a detailed review see [53]) brain MRI.

9.6.1 Bacterial Meningitis

Due to the high mortality of 10–15% in developed countries, group B streptococci (GBS) meningitis is still an important infection of the neonatal CNS [54]. Imaging in neonatal meningitis is certainly only an adjunct to lumbar puncture and clinical laboratory tests. In this chapter, MRI features of neonatal bacterial meningitis should be used exemplary for other bacterial neonatal brain infections (in preterm neonates, *E. coli* is more common as GBS [54]), as the profile of their complications is somewhat similar.

As the major path of infection to the neonatal CNS in bacterial meningitis is haematogenic (and “vertical”, from mother to foetus), the initial MRI changes are seen in the neonatal brain parenchyma and the ventricles leading to a characteristic triad: choroid plexus engorgement, avid contrast *enhancement of the ependyma, and intraventricular accumulation of debris* [51]. Thus, *leptomeningeal/arachnoid space contrast enhancement* (“arachnoiditis”), as seen in adult or late-onset (onset >7 days) meningoencephalitis is occurring rather late and can even be absent in neonatal sepsis/meningoencephalitis (onset usually within 48 h and <7 days). In this situation, the addition of fluid-attenuated inversion recovery (FLAIR) imaging is advisable, as it sensitively detects debris and protein-rich CSF components. In the course of infection cortical signal intensity changes on T1- (hypo-/hyperintense) and T2-weighted sequences (hyperintense) as well as often widespread areas of diffusion restriction in different cortical regions and occasionally also the white matter is seen. The differentiation and continuity between encephalitis and vasculitis/arteritis-*associated cortical infarction and laminar necrosis* are frequently fluent. The role of neonatal MR in bacterial meningitis is not to provide the initial diagnosis (this is the duty of the clinical assess-

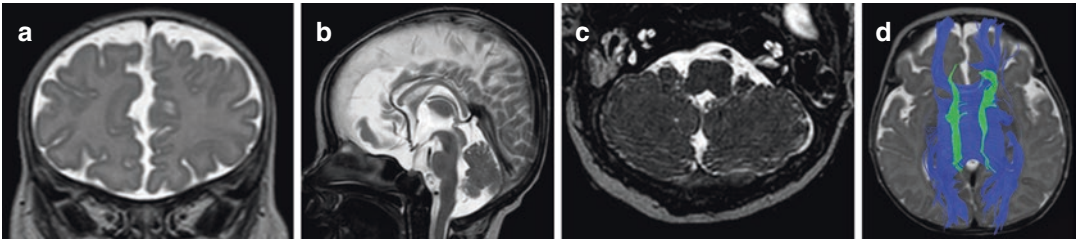


Fig. 9.7 Neuroimaging feature of a complex genetic syndromic disorder—the CHARGE Syndrome: note the absence of the olfactory bulbs (a) and the hypoplasia of the vestibular system (b) as well as the hypoplasia of the vestibulocochlear

nerves (c). Tractography (d) depicts the corpus callosum (blue fibres) and the cingulum fibres without any signs of a Probst Bundle

ment combined with lab tests), but to indicate the extent of encephalitis and confirm the clinical diagnosis of meningitis (particularly in cases, where the clinical impression is doubtful) in depicting the extent of meningeal or brain involvement as well as potential accompanying complications, which require a change in (surgical) therapy. Further, MRI can also sensitively indicate early signs of ventricular enlargement and incipient *hydrocephalus* (*communicating or obstructive*). MRI also sensitively detects neonatal *brain abscesses*—typically located in the periventricular white matter—by their central diffusion restriction (dark on ADC map, bright on DWI $b = 700\text{--}1000\text{ s/mm}^2$) and their characteristic rim-like contrast enhancement (at later stages). Moreover, bacterial meningitis is frequently associated with *sinus vein thrombosis*, which always should be excluded by neonatal MRI (Fig. 9.7a–d).

For the MR characteristics of less common specific neonatal infections (herpes simplex, enterovirus, fungal infections), the reader is referred to more in-depth descriptions (see [51, 52]).

9.7 MRI of Malformations of the Brain

Many brain malformations—which were used to be detected postnatally using neonatal brain MRI—are nowadays diagnosed prenatally by obstetric ultrasound. In countries with prenatal

screening programmes brain malformations presenting with an enlargement of the lateral ventricles—ventriculomegaly are mostly discovered before birth. Thus, in most cases with brain malformations, there is a history of foetal imaging before neonatal imaging. This requires a restructuring and reorganisation of the perinatal imaging strategies in cases of brain malformations. An essential step in that regard is establishing continuity between pre- and postnatal imaging information. This requires communication between referring neonatologists, obstetricians, and radiologists, as often existing prenatal imaging data is not linked to postnatal examinations. For instance, if a brain malformation, which is primarily asymptomatic is encountered prenatally by prenatal ultrasound and fully classified by expert foetal MRI, postnatal neonatal MRI is not necessary. On contrary, if the neonate is presenting with symptoms, which are not in line with the prenatal imaging diagnosis, postnatal neonatal MRI is essential to reveal the full extent of the pathology. This is particularly true for situations where syndromes are expected or diagnosed in the course of further prenatal or perinatal workup. Figure 9.8a–d shows a case of CHARGE syndrome, which presented prenatally by polyhydramnios and esophageal atresia, showing a characteristic pouch sign at foetal MRI. Already at foetal imaging, the anterior portion of the corpus callosum appeared shortened. Postnatal imaging confirmed callosal dysgenesis with anterior shortening of the rostrum and genu regions of the corpus callosum (Fig. 9.8b, d) and further

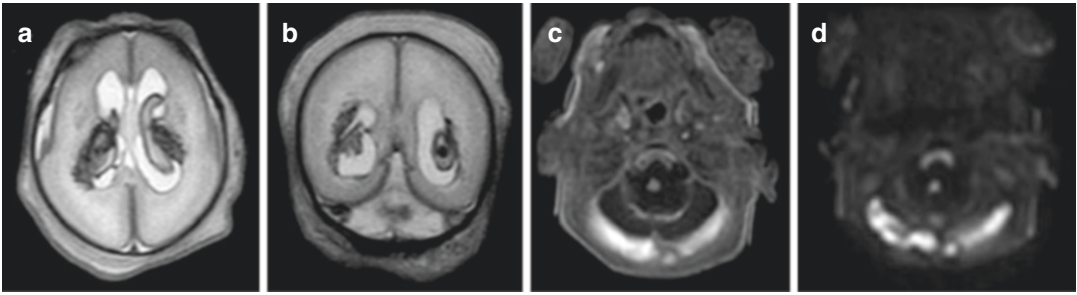


Fig. 9.8 Axial (a) and coronal (b) T2-weighted sequences of a neonate suffering from a bilateral sinus vein thrombosis—indicated by the T1 weighted hyperintense signal changes in the transverse sinus bilaterally (c). At subacute stages thrombi appear T1 weighted hyperintense (c) and

bright (= diffusion restricted) on DWI source images (d). Please also note the significant brain swelling and obliteration of external CSF spaces (a, b) due to congestion. This is a prerequisite for intraventricular haemorrhages—best seen on (a)

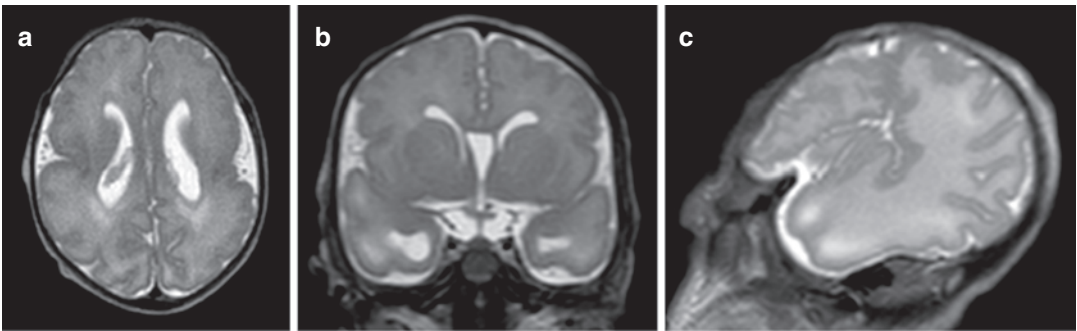


Fig. 9.9 Axial (a), coronal (b), sagittal (c) T2-weighted sequences of a neonate with congenital CMV infection. Note the bilateral perisylvian polymicrogyria as well as the cysts adjacent to the temporal horns of the lateral ventricles and the T2-weighted hyperintensities/brightness of

the anterior temporal lobes bilaterally. Further the opercularisation (covering of the insula by the frontal lobes) is incomplete. These changes are characteristic for an early CMV infection during the first or second trimester of pregnancy

specified the syndromic situation by indicating the absence of both olfactory bulbs (Fig. 9.8a) and bilateral thinning of vestibular nerves as well as hypoplasia of the vestibular system (Fig. 9.8c). This is an example of how prenatal imaging and postnatal imaging can be complimented to fully understand the complete phenotypic spectrum of the syndromic condition.

As a full comprehensive review of all brain malformations is far beyond the scope of this chapter, the most important structural signs of brain and spine malformations are listed below. These features in combination can be used to phenotype a specific syndromic condition and help to explain specific neonatal syndromes, such as seizures, which in case of brain malformations are often intractable by antiepileptic drugs.

9.7.1 Polymicrogyria

The term polymicrogyria describes a condition, where there are irregularities in the cortical ribbon forming multiple small gyri and sulci, not resembling the normal appearance of a gyrus or sulcus (Fig. 9.9a–c). Polymicrogyria can appear in form of a syndromic/genetic condition or can represent the sequela of a prenatal ischaemic or clastic/haemorrhagic event [55]. For instance, in the setting of fetofetal transfusion syndrome polymicrogyria is frequently found as the consequence of foetal ischaemia. Thus, polymicrogyria in one or both monozygotic twins is a finding, which is compatible with the underlying developmental aetiology. Furthermore, polymicrogyria is the most common abnormality found

in cases of cytomegalovirus infection, which is—due to its location on the lateral convexity of the brain—frequently underestimated or even missed by ultrasound. By further characterising the extent, appearance, location, uni- or bilaterality, MRI provides important additional information concerning the aetiology (genetic vs acquired). In the case depicted in Fig. 9.9a–c, polymicrogyria in the perisylvian regions is accompanied by bilateral cysts anterior to the temporal horns of the lateral ventricles and white matter abnormalities in the temporal pole areas—features typical for congenital cytomegalovirus infections.

9.7.2 Lissencephaly/Pachygyria

Lissencephaly describes a condition in which the number and appearance of gyri and sulci are reduced, resulting in a smooth brain. If there are too few and too broad/simplified gyri found, the term pachygyria describes this condition even better. Some specific forms of lissencephaly—those of the so-called cobblestone complex—may show a rather irregular cortical (“cobblestone”-like) appearance, but still are categorised under the term lissencephaly. Lissencephalies can be syndromes by themselves (Walker Warburg syndrome, Miller Dieker syndrome, Alpha-dystroglykanopathies, etc.), or used as a descriptive term to represent syndromic conditions like tubulinopathies.

9.7.3 Schizencephaly

A defect which (almost) reaches from the sub-arachnoid space to the ventricular surface is defined as schizencephaly or schizencephalic cleft. This condition is usually associated with a prenatal acquired event such as localised haemorrhage or ischaemia. Whenever schizencephaly is encountered, local blood breakdown residuals should be searched for, using SWI or T2* sequences. Moreover, schizencephaly should always prompt the clinical evaluation of possible etiologic factors such as congenital heart disease, fetofetal transfusion syndrome, coag-

ulation disorders, genetic conditions (such as COL41A mutations [56]), or even a thorough histologic analysis of the placenta, if available, to exclude or identify placental thrombotic vasculopathy [57].

9.7.4 Focal Cortical Dysplasia (FCD)

FCD leads to either very subtle and hardly recognisable changes (“blurring” of the grey/white matter boundary) of the neonatal cortex (T2-weighted hypointense) or a more distinct thickening of the cortex and the so-called transmantle sign—a T2-weighted hypointensity—spanning from the cortex to the lateral ventricles. The blurring between grey and white matter boundary can be detected at neonatal stages between birth and 15 months of age [58]. Afterward, these lesions enter a stage of non-visualisation by MRI. Due to the process of myelination, the signal of cortex and white matter is changing in a way that the grey/white matter boundary is less well defined and these lesions are getting less conspicuous between 15 months up to the age of 3–4 years. This should be kept in mind, whenever a case with medically refractory epilepsy is encountered after birth. Early detection may lead to early surgical treatment and overall better neurodevelopmental outcomes.

9.7.5 Cystic Posterior Fossa Malformations

There is a range of abnormalities, which can be encountered in the posterior fossa, most of them presenting as cystic posterior fossa malformations. Neonatal hypotonia during neonatal neurologic examination is an early cerebellar sign [59], which should prompt neonatal brain MRI. Due to the excellent tissue resolution and contrast of the cerebellum and the brainstem, MRI is not limited to the unequivocal visualisation of these structures. This is important to classify and understand the exact aetiology and nature of the posterior

fossa malformation. It is advisable to intentionally prevent the diagnosis of “dandy walker malformation” and instead provide a thorough descriptive statement on the cerebellum and the brainstem. Premature diagnoses of a so-called Dandy walker malformation or Blakes pouch cyst may lead to ultimately wrong morphological classifications and misleading categorisations of posterior fossa malformations. As Dandy walker malformation or Blakes pouch cysts are very specific diagnoses confined to only a portion of cystic posterior fossa malformations, the diagnosis of these conditions should be reserved to expert paediatric neuroradiologists in the field [60]. For a basic categorisation, a thorough descriptive statement on the posterior fossa abnormality is sufficient to enable to inform the treating physicians. This should always include the assessment of the size and shape of the cerebellar hemispheres, the cerebellar vermis, its position relative to the brainstem, the shape of the brainstem/pons, and the normal areal relationships of the midbrain/pons/medulla oblongata (normally showing a ratio of 1/2/1) [61].



Brain malformations are frequently suspected at prenatal stages of brain development. Neonatal imaging has the role to confirm and further characterize the malformation, overcoming limitations in resolution of fetal MRI. In cases of infections, neonatal head imaging serves to identify complications such as encephalitis and vasculitis.

9.8 Metabolic Disorders

In countries with neonatal metabolic screening programmes for metabolic diseases, the primary diagnosis of metabolic disorders is usually not provided by MRI. However, in some cases, the metabolic aberration and enzymatic defect are not included in the screening panel and thus may

not be identified right away. In those cases, neonatal brain MRI can be a very helpful diagnostic aid in the diagnosis of metabolic disorders. Again, the incredible heterogeneity and number of metabolic disorders are far beyond the scope of this chapter. The reader is referred to specific paediatric neurological textbooks. However, there are some signs and indicators, which should stress the suspicion of a metabolic disorder:

9.8.1 Bilateral Basal Ganglia Signal Abnormalities/Diffusion Restriction

Basal ganglia signal abnormalities are common and frequently found in cases of hypoxic-ischaemic encephalopathy as described above (see Sect. 9.3). In some cases—without a history of neonatal or perinatal asphyxia—presenting with neonatal seizures a mitochondrial disorder can be the cause of the disease (Fig. 9.1). Mitochondrial disorders frequently present with bilateral basal ganglia signal alterations on conventional T1- and T2-weighted sequences and prominent diffusion restriction on DWI sequences. Clinically unexplained symmetric signal alterations of the basal ganglia should always stress the presence of a mitochondriopathy. T1 hyperintense signal alterations of the basal ganglia can sometimes be explained by hyperbilirubinemia, which is usually rare nowadays, as the condition is frequently diagnosed clinically at early stages and treated accordingly. Alternative explanations for signal and/or diffusion abnormalities of the basal ganglia are other metabolic disorders (aminoaciduria), such as maple sirup urine disease or toxic (also drugs like valproate toxicity) encephalopathies.

9.8.1.1 White Matter Signal Abnormalities

Some metabolic disorders lead to the entire absence of proper myelin formation. Prototypic is the rare Pelizaeus Merzbacher disease—a disorder in which no proper myelin is formed. Suspicion should be raised if the white matter does not show signs of myelination at all [3].

Thus, the posterior limbs of the internal capsule as well as the brainstem and cerebellum should always be explored for the early presence of myelin. However, an appropriate diagnosis of these conditions would not be made too early by non-expert radiologists. For the thorough clinical and imaging descriptions of hypo- and demyelinating disorders, see more in-depth literature.

9.8.1.2 Dysmyelinating Disorders

In some cases, myelin is formed, but is not composed properly and thus appears abnormally on MRI. In these cases, there is the suspicion of a dysmyelinating metabolic disorder. Again, a wide range of dysmyelinating disorders exists, which frequently need to be separated from (more frequently appearing) post-infectious or preterm birth-associated white matter changes.



When evaluating metabolic disorders, pattern analysis is essential. However this requires a lot of experience, which is hardly available. Thus, the identification of basic patterns of metabolic disorders and their discrimination from acquired conditions or malformations is important.

9.9 Summary and Overall Conclusion

Neonatal Neuro-MRI is a logistically challenging method, which requires experience and active collaboration between neonatologists, radiologists, nurses, child care specialists and technicians. If the diagnostic aim of the examination is clearly outlined prior to the examination, MRI can provide valuable prognostic information and further phenotypic characterisation of rare neonatal neurological disorders, facilitating future therapeutic approaches.

References

1. Griffiths P, Morris J, Larroche JC, Reeves MJ. Atlas of fetal and postnatal brain MR. Philadelphia, PA: Mosby; 2009.
2. Rutherford MA. MRI of the neonatal brain. London: W.B. Saunders; 2001.
3. Valk PDJ, van der Knaap DMS. Magnetic resonance of myelin, myelination, and myelin disorders. Berlin: Springer; 1989.
4. Machata AM, Willschke H, Kabon B, Prayer D, Marhofer P. Effect of brain magnetic resonance imaging on body core temperature in sedated infants and children. *Br J Anaesth.* 2009;102:385–9.
5. Cawley P, Few K, Greenwood R, Malcolm P, Johnson G, Lally P, Thayyil S, Clarke P. Does magnetic resonance brain scanning at 3.0 Tesla pose a hyperthermic challenge to term neonates? *J Pediatr.* 2016;175:228–230.e221.
6. Tocchio S, Kline-Fath B, Kanal E, Schmithorst VJ, Panigrahy A. MRI evaluation and safety in the developing brain. *Semin Perinatol.* 2015;39:73–104.
7. Ouyang M, Dubois J, Yu Q, Mukherjee P, Huang H. Delineation of early brain development from fetuses to infants with diffusion MRI and beyond. *Neuroimage.* 2019;185:836–50.
8. Jones DK. Diffusion MRI. New York: Oxford University Press; 2010.
9. Thayyil S, Chandrasekaran M, Taylor A, Bainbridge A, Cady EB, Chong WK, Murad S, Omar RZ, Robertson NJ. Cerebral magnetic resonance biomarkers in neonatal encephalopathy: a meta-analysis. *Pediatrics.* 2010;125:e382–95.
10. Wintermark P, Hansen A, Gregas MC, Soul J, Labrecque M, Robertson RL, Warfield SK. Brain perfusion in asphyxiated newborns treated with therapeutic hypothermia. *Am J Neuroradiol.* 2011;32:2023–9.
11. Zhang H, Shen D, Lin W. Resting-state functional MRI studies on infant brains: a decade of gap-filling efforts. *Neuroimage.* 2019;185:664–84.
12. Schmidbauer V, Geisl G, Cardoso Diogo M, Jengojan S, Perepelov V, Weber M, Goeral K, Lindenlaub F, Klebermass-Schrehof K, Berger A, Prayer D, Kasprian G. Validity of SyMRI for assessment of the neonatal brain. *Clin Neuroradiol.* 2021;31:315–23.
13. Schmidbauer V, Geisl G, Diogo M, Weber M, Goeral K, Klebermass-Schrehof K, Berger A, Prayer D, Kasprian G. SyMRI detects delayed myelination in preterm neonates. *Eur Radiol.* 2019;29:7063–72.
14. Panda A, Mehta BB, Coppo S, Jiang Y, Ma D, Seiberlich N, Griswold MA, Gulani V. Magnetic resonance fingerprinting—an overview. *Curr Opin Biomed Eng.* 2017;3:56–66.
15. Kurinczuk JJ, White-Koning M, Badawi N. Epidemiology of neonatal encephalopathy and hypoxic-ischaemic encephalopathy. *Early Hum Dev.* 2010;86:329–38.

16. Barkovich AJ, Sargent SK. Profound asphyxia in the premature infant: imaging findings. *AJNR Am J Neuroradiol.* 1995;16:1837–46.
17. Ghei SK, Zan E, Nathan JE, Choudhri A, Tekes A, Huisman TAGM, Izbudak I. MR imaging of hypoxic-ischemic injury in term neonates: pearls and pitfalls. *Radiographics.* 2014;34:1047–61.
18. Bednarek N, Mathur A, Inder T, Wilkinson J, Neil J, Shimony J. Impact of therapeutic hypothermia on MRI diffusion changes in neonatal encephalopathy. *Neurology.* 2012;78:1420–7.
19. Shibasaki J, Aida N, Morisaki N, Tomiyasu M, Nishi Y, Toyoshima K. Changes in brain metabolite concentrations after neonatal hypoxic-ischemic encephalopathy. *Radiology.* 2018;288:840–8.
20. Zarifi MK, Astrakas LG, Poussaint TY, Plessis Ad A, Zurakowski D, Tzika AA. Prediction of adverse outcome with cerebral lactate level and apparent diffusion coefficient in infants with perinatal asphyxia. *Radiology.* 2002;225:859–70.
21. Rutherford MA, Pennock JM, Counsell SJ, Mercuri E, Cowan FM, Dubowitz LM, Edwards AD. Abnormal magnetic resonance signal in the internal capsule predicts poor neurodevelopmental outcome in infants with hypoxic-ischemic encephalopathy. *Pediatrics.* 1998;102:323–8.
22. Wu YW, Hamrick SEG, Miller SP, Haward MF, Lai MC, Callen PW, Barkovich AJ, Ferriero DM. Intraventricular hemorrhage in term neonates caused by sinovenous thrombosis. *Ann Neurol.* 2003;54:123–6.
23. Heck DV, Gailloud P, Cohen HL, Clatterbuck RE, Tamargo R, Avellino AM, Murphy KP. Choroid plexus arteriovenous malformation presenting with intraventricular hemorrhage. *J Pediatr.* 2002;141:710–1.
24. Brouwer A, Groenendaal F, Van Haastert I-L, Rademaker K, Hanlo P, De Vries L. Neurodevelopmental outcome of preterm infants with severe intraventricular hemorrhage and therapy for post-hemorrhagic ventricular dilatation. *J Pediatr.* 2008;152:648–54.
25. Goeral K, Kasprian G, Hüning BM, Waldhoer T, Fuiko R, Schmidbauer V, Prayer D, Felderhoff-Müser U, Berger A, Olischar M, Klebermass-Schrehof K. A novel magnetic resonance imaging-based scoring system to predict outcome in neonates born preterm with intraventricular haemorrhage. *Dev Med Child Neurol.* 2022;64:608–17.
26. Steggerda SJ, de Bruïne FT, Smits-Wintjens VEJH, Walther FJ, van Wezel-Meijler G. Ultrasound detection of posterior fossa abnormalities in full-term neonates. *Early Hum Dev.* 2012;88:233–9.
27. Judas M, Rados M, Jovanov-Milosevic N, Hrabac P, Stern-Padovan R, Kostovic I. Structural, immunocytochemical, and mr imaging properties of periventricular crossroads of growing cortical pathways in preterm infants. *AJNR Am J Neuroradiol.* 2005;26:2671–84.
28. Milos R-I, Jovanov-Milošević N, Mitter C, Bobić-Rasonja M, Pogledic I, Gruber GM, Kasprian G, Brugger PC, Weber M, Judaš M, Prayer D. Developmental dynamics of the periventricular parietal crossroads of growing cortical pathways in the fetal brain—in vivo fetal MRI with histological correlation. *Neuroimage.* 2020;210:116553.
29. Messerschmidt A, Brugger PC, Boltshauser E, Zoder G, Sterniste W, Birnbacher R, Prayer D. Disruption of cerebellar development: potential complication of extreme prematurity. *Am J Neuroradiol.* 2005;26:1659–67.
30. Jeanne M, Labelle-Dumais C, Jorgensen J, Kauffman WB, Mancini GM, Favor J, Valant V, Greenberg SM, Rosand J, Gould DB. COL4A2 mutations impair COL4A1 and COL4A2 secretion and cause hemorrhagic stroke. *Am J Hum Genet.* 2012;90:91–101.
31. Cain DW, Dingman AL, Armstrong J, Stence NV, Jensen AM, Mirsky DM. Subpial hemorrhage of the neonate. *Stroke.* 2020;51:315–8.
32. Orman G, Kralik SF, Meoded A, Desai N, Risen S, Huisman TAGM. MRI findings in pediatric abusive head trauma: a review. *J Neuroimaging.* 2020;30:15–27.
33. Assis Z, Kirton A, Pauranik A, Sherriff M, Wei XC. Idiopathic neonatal subpial hemorrhage with underlying cerebral infarct: imaging features and clinical outcome. *Am J Neuroradiol.* 2021;42:185–93.
34. Hahnemann ML, Kinner S, Schweiger B, Bajanowski T, Karger B, Pfeiffer H, Wittschieber D. Imaging of bridging vein thrombosis in infants with abusive head trauma: the “Tadpole Sign”. *Eur Radiol.* 2015;25:299–305.
35. Choudhary AK, Bradford R, Dias MS, Thamburaj K, Boal DK. Venous injury in abusive head trauma. *Pediatr Radiol.* 2015;45:1803–13.
36. Zielonka M, Braun K, Bengel A, Seitz A, Kölker S, Boy N. Severe acute subdural hemorrhage in a patient with glutaric aciduria type I after minor head trauma: a case report. *J Child Neurol.* 2015;30:1065–9.
37. Neil JJ, Volpe JJ. Chapter 16—Encephalopathy of prematurity: clinical-neurological features, diagnosis, imaging, prognosis, therapy. In: Volpe JJ, Inder TE, Darras BT, de Vries LS, du Plessis AJ, Neil JJ, Perlman JM, editors. *Volpe’s neurology of the newborn.* 6th ed. Philadelphia: Elsevier; 2018. p. 425–457.e411.
38. Pierson CR, Folkerth RD, Billiards SS, Trachtenberg FL, Drinkwater ME, Volpe JJ, Kinney HC. Gray matter injury associated with periventricular leukomalacia in the premature infant. *Acta Neuropathol.* 2007;114:619–31.
39. Dyet LE, Kennea N, Counsell SJ, Maalouf EF, Ajayi-Obe M, Duggan PJ, Harrison M, Allsop JM, Hajnal J, Herlihy AH, Edwards B, Laroche S, Cowan FM, Rutherford MA, Edwards AD. Natural history of brain lesions in extremely preterm infants studied

- with serial magnetic resonance imaging from birth and neurodevelopmental assessment. *Pediatrics*. 2006;118:536–48.
40. Guo T, Duerden EG, Adams E, Chau V, Branson HM, Chakravarty MM, Poskitt KJ, Synnes A, Grunau RE, Miller SP. Quantitative assessment of white matter injury in preterm neonates. *Neurology*. 2017;88:614–22.
 41. Inder TE, Anderson NJ, Spencer C, Wells S, Volpe JJ. White matter injury in the premature infant: a comparison between serial cranial sonographic and MR findings at term. *AJNR Am J Neuroradiol*. 2003;24:805–9.
 42. Barnett ML, Tumor N, Ball G, Chew A, Falconer S, Aljabar P, Kimpton JA, Kennea N, Rutherford M, David Edwards A, Counsell SJ. Exploring the multiple-hit hypothesis of preterm white matter damage using diffusion MRI. *Neuroimage Clin*. 2018;17:596–606.
 43. Ball G, Pazderova L, Chew A, Tumor N, Merchant N, Arichi T, Allsop JM, Cowan FM, Edwards AD, Counsell SJ. Thalamocortical connectivity predicts cognition in children born preterm. *Cereb Cortex*. 2015;25:4310–8.
 44. Salvan P, Tournier JD, Batalle D, Falconer S, Chew A, Kennea N, Aljabar P, Dehaene-Lambertz G, Arichi T, Edwards AD, Counsell SJ. Language ability in preterm children is associated with arcuate fasciculi microstructure at term. *Hum Brain Mapp*. 2017;38:3836–47.
 45. Groppo M, Ricci D, Bassi L, Merchant N, Doria V, Arichi T, Allsop JM, Ramenghi L, Fox MJ, Cowan FM, Counsell SJ, Edwards AD. Development of the optic radiations and visual function after premature birth. *Cortex*. 2014;56:30–7.
 46. Kidokoro H, Neil JJ, Inder TE. New MR imaging assessment tool to define brain abnormalities in very preterm infants at term. *Am J Neuroradiol*. 2013;34:2208–14.
 47. Woodward LJ, Anderson PJ, Austin NC, Howard K, Inder TE. Neonatal MRI to predict neurodevelopmental outcomes in preterm infants. *N Engl J Med*. 2006;355:685–94.
 48. Slaughter LA, Bonfante-Mejia E, Hintz SR, Dvorchik I, Parikh NA. Early conventional MRI for prediction of neurodevelopmental impairment in extremely-low-birth-weight infants. *Neonatology*. 2016;110:47–54.
 49. Ford-Jones EL, Kellner JD. “CHEAP TORCHES”: an acronym for congenital and perinatal infections. *Pediatr Infect Dis J*. 1995;14:638–9.
 50. de Fatima Vasco Aragao M, van der Linden V, Brainer-Lima AM, Coeli RR, Rocha MA, Sobral da Silva P, Durce Costa Gomes de Carvalho M, van der Linden A, Cesario de Holanda A, Valenca MM. Clinical features and neuroimaging (CT and MRI) findings in presumed Zika virus related congenital infection and microcephaly: retrospective case series study. *BMJ*. 2016;353:i1901.
 51. Schneider JF. Neonatal brain infections. *Pediatr Radiol*. 2011;41:143–8.
 52. Tortori-Donati P, Rossi A, Biancheri R. Infectious diseases. Berlin: Springer; 2005. p. 469–542.
 53. Prayer D, Asenbaum U, Brugger PC, Kasprian G. Acquired brain pathology. In: Prayer D, editor. *Fetal MRI*. Berlin: Springer; 2011. p. 309–27.
 54. Gaschignard J, Levy C, Romain O, Cohen R, Bingen E, Aujard Y, Boileau P. Neonatal bacterial meningitis: 444 cases in 7 years. *Pediatr Infect Dis J*. 2011;30:212–7.
 55. Leventer RJ, Jansen A, Pilz DT, Stoodley N, Marini C, Dubeau F, Malone J, Mitchell LA, Mandelstam S, Scheffer IE, Berkovic SF, Andermann F, Andermann E, Guerrini R, Dobyns WB. Clinical and imaging heterogeneity of polymicrogyria: a study of 328 patients. *Brain*. 2010;133:1415–27.
 56. Hausman-Kedem M, Ben-Sira L, Kidron D, Ben-Shachar S, Straussberg R, Marom D, Ponger P, Bar-Shira A, Malinge G, Fattal-Valevski A. Deletion in COL4A2 is associated with a three-generation variable phenotype: from fetal to adult manifestations. *Eur J Hum Genet*. 2021;29:1654.
 57. Redline RW. Disorders of placental circulation and the fetal brain. *Clin Perinatol*. 2009;36:549–59.
 58. Jain P, Whitney R, Widjaja E. Appearance of FCD type II changes with brain maturation in early childhood. *Neuropediatrics*. 2019;50:264–5.
 59. Bolduc ME, Limperopoulos C. Neurodevelopmental outcomes in children with cerebellar malformations: a systematic review. *Dev Med Child Neurol*. 2009;51:256–67.
 60. Aldinger KA, Doherty D. The genetics of cerebellar malformations. *Semin Fetal Neonatal Med*. 2016;21:321–32.
 61. Doherty D, Millen KJ, Barkovich AJ. Midbrain and hindbrain malformations: advances in clinical diagnosis, imaging, and genetics. *Lancet Neurol*. 2013;12:381–93.



Chest and Lung Imaging in Preterms and Neonates

10

Panruethai Trinavarat and Michael Riccabona

10.1 Introduction

Chest and lung disorders, particular with respiratory distress, are the most frequent indications for imaging requests both in term and preterm neonates to identify the underlying cause or to narrow the differential diagnosis. An appropriate imaging technique is vital to get diagnostic image quality; as radiation exposure is a high concern, the ALARA (as low as reasonably achievable) principle is indispensable for all imaging examinations that utilise ionising radiation particularly in this vulnerable age group.

Many chest and lung diseases are unique to this period of early life, and most are directly or indirectly related to foetal and physiologic development. Basic knowledge of bronchopulmonary foregut development is essential for understanding the diseases, its evolution, and its imaging appearance. The newborn infant

is vulnerable to a wide spectrum of chest and lung diseases, which for imaging are often grouped into pulmonary lesions, air leak, tracheal lesions, oesophageal lesions, mediastinal widening, diaphragmatic lesion, and chest wall lesions. Most of the abnormalities are from the lung and thus the mainstay of neonatal imaging is chest radiography, which will be the focus of this chapter, however, other complementing modalities such as lung ultrasound (US), CT, MRI, and fluoroscopy will be addressed too. Most common abbreviations of chest and lung diseases in this chapter are listed in Table 10.1.

Table 10.1 Common abbreviations of chest and lung diseases used in this chapter

Abbreviation	Chest and lung disease
BPD	Bronchopulmonary dysplasia
CDH	Congenital diaphragmatic hernia
CLH	Congenital lobar hyperinflation (old term = congenital lobar emphysema)
CPAM	Congenital pulmonary airway malformation
CPL	Congenital pulmonary lymphangiectasia
(I)RDS	(Idiopathic) Respiratory distress syndrome
MAS	Meconium aspiration syndrome
PDA	Patent ductus arteriosus of Botalli
PIE	Pulmonary interstitial emphysema
PPHN	Persistent pulmonary hypertension in the newborn (old term = persistent foetal circulation = PFC)
TTN	Transient tachypnea of the newborn (old term = “wet lung”)

Supplementary Information The online version contains supplementary material available at https://doi.org/10.1007/978-3-031-15729-5_10.

P. Trinavarat (✉)
Department of Radiology, Faculty of Medicine,
Chulalongkorn University, Bangkok, Thailand

M. Riccabona
Medical University Graz, Graz, Austria

10.2 Imaging Modalities for Chest and Lung Imaging in Neonates

The mainstay of imaging for evaluation of the neonatal chest and lung is chest radiography. Ultrasound, CT, and MRI provide cross-sectional images and are used for problem solving and treatment planning when indicated, as well as fluoroscopy in dedicated mostly trachea-oesophageal queries.

10.2.1 Chest Radiography

Nowadays digital radiography is used worldwide, and has almost completely replaced film-screen system.

There are essential requisites for performing digital chest radiography in neonates:

- **Knowledge of digital radiographic equipment**
 - The flat-panel detector of direct radiography (DR), either direct- or indirect-conversion DR, has advantages over the imaging plate of computed radiography (CR) in better ability to convert X-ray energy into electrical signals with less noise added during the process, and better transferring the modulation of the input signals to its output, eventually providing a better image resolution.
 - Detector size of 25 × 30 cm covers the neonatal chest, and pixel size (square shape) should be at least 200 μm. This makes the matrix size of 1250 × 1500 pixels. Spatial resolution of the 200 μm pixel size in line pairs per millimetre can be calculated by (1/1000) divided by (2 × pixel size in μm), which is 2.5 lp/mm.
 - Post-processing (involving image contrast adjustment, noise reduction, and edge enhancement) is a very important part of digital radiography to improve image quality. Even most of the CR/DR system have lower spatial resolution (2.5–3.6 lp/mm) than film-screen system (5 lp/mm), and this weakness cannot be compensated by post-processing operations, at least all adjustable settings must be adapted properly according to the anatomic region and patient's age/size and density distribution.
- Generally, the diagnostic value of CR systems is at least equivalent to film-screen system while DR system offers a better image quality and lower radiation exposure than CR system, which is perfectly suitable for neonatal imaging. However, visual grading analysis shows no significant difference of image quality in neonatal chest radiography between CR and indirect-conversion DR. To complete “the imaging chain”, a monitor with sufficient resolution and at least 12-bit depth (better higher) is essential for viewing. So do not use a normal PC monitor for reading these radiographs, because you may miss essential findings such as a subtle pneumothorax! .
- **Good imaging practice of the operators**
 - Radiographers should allocate enough time for positioning, collimation adjustment, and proper radiation exposure to neonates.
 - The patient must be placed in supine position and not rotated. Rotation can create pseudo-lucent lung on one side and may make it difficult or impossible to assess a mediastinal shift. The patient's head should be straight because the chest usually moves with the head turning. Arms are out of the field of view.
 - The X-ray tube should be in a perpendicular plane to the patient and detector. The X-ray beam is centred in the midline at nipple level, this will be about level of the seventh thoracic vertebra on the image.
 - Caution: a comfort pad between babies and detectors and/or using the build-in tray of the incubator requires a higher exposure setting. Removal of comfort pads underneath the babies (and avoiding the build-in trays) is essential to reduce radiation exposure.
 - Exposure should be attempted at full inspiration during quiet breathing. The target is

five to six anterior ribs and/or eight posterior ribs above right hemidiaphragm.

- The coverage of the chest radiograph should extend craniocaudally from cervical trachea to T12/L1 with the tolerance of 1.0 cm at each edge from the area of interest, according to the European guidelines on quality criteria for diagnostic radiographic images in paediatrics from the European Commission in 1996 [1]. A larger field size than necessary will not only increase scattered radiation that impairs image quality, but also deliver unnecessary radiation to the body outside the targeted area. In addition, it may affect the accuracy of image processing. Post-exposure electronic cropping is useful, but it may be misused to cover-up unprofessional collimations.
- Automatic exposure control (AEC) is not recommended in neonates because their small size usually not covers the AEC sensors. A manual technique is more appropriate, but requires technique charts for each size, each area being imaged, and each detector model.
- The anti-scatter grid is not necessary in neonates. The grid will be only beneficial if the body part is at least 10–12 cm of water-equivalent thickness [2] which is very unlikely in the neonatal chest. Using grid furthermore increases radiation.
- Adhering to the ALARA principle, a reasonable low dose without sacrificing confidence in image interpretation of neonatal chest radiographs requires standardised exposure protocols with preference of high kVp and low mAs technique.
- **Radiation dose**
 - Radiation exposure in preterm and term neonates is of more concern than in other older age groups because their cells are still developing (the high mitosis rate makes them very vulnerable for radiation-induced damage) and they have a longer life expectancy. Moreover, sick babies in the NICU often require repeated images for diagnosis, monitoring, checking positions of tubes and lines, and follow-up—adding up to a considerable overall radiation burden.
 - “Exposure creep” is a deep concern in digital radiography. From the wide dynamic range of digital detectors, the overexposed images look nice and the technique and dose behind the image may be overlooked. Monitoring of radiation dose and all aspects of the imaging chain (all aspects—from the image acquisition to the final reading, e.g. monitor performance) used in diagnostic radiology is therefore essential. Additionally, diagnostic reference levels should be respected and considered—according to the European Guidelines of paediatric DRL (PiDRL) revised on Jul 18, 2016, the DRL of P_{KA} (Kerma area product) in babies weighing less than 5 kg is 15 mGy cm² [3].
 - There are three important standardised terms of adequate exposure estimations in digital radiography: target exposure index (EI_T), exposure index (EI), and deviation index (DI). They are the feedback indicators to ensure the correct use of the equipment with proper radiation exposure to patients of different sizes. The EI_T is programmed in each machine to indicate the required X-ray photons reaching the receptor to get a diagnostic image. The EI defines how many photons reach the detector in an individual exposure. The DI indicates the difference of EI comparing to EI_T but in a logarithmic equation. Deviation index = 1 implies 25% over-exposure and DI = 3 implies 100% over-exposure, while DI = -1 means 20% below exposure, and DI = -3 means 50% below exposure. However, EI and DI cannot be interpreted in poorly collimated image. Wide collimation results in inclusion of extra areas of air, which will increase EI suggesting over-exposure where in fact the images are underexposed [4].
- **Essential requisites for radiologists**
 - Radiologists should know the embryology of the lung development, the radiologic appearance of the lung and chest in neo-

nates that differs from other age groups, and have all relevant clinical information when reading the images.

- Radiologists should be responsible for radiation protection of these patients. During the daily routine work, radiologists should give a feedback when detecting problems with image quality, collimation area, and unusual DI or P_{KA} values.

10.2.2 Chest Ultrasound (US)

Ultrasound is suitable for detection and assessment of chest wall lumps and bumps, suspicious abnormal mediastinal widening, elevation or lobulation and palsy of the diaphragm, pleural effusion, and consolidations (e.g. pneumonia, sequestration). There is also an increasing use of point-of-care (POC) US in the neonatal lung to diagnose the cause of respiratory distress and in the respective follow-up.

There are essential requisites for performing chest and lung US (LUS) in neonates:

- Adequate US equipment and transducers are required. High-resolution linear transducer

(7.5 MHz or higher) with small footprint is mostly used for LUS in neonates.

As the new LUS applications such use A and B lines and thus artefacts for diagnosis, all functions which reduce those artefacts need to be shut off such as Harmonic Imaging, image compounding or speckle / noise reduction filters in these applications. However, these can be used for imaging consolidations, effusions and similar entities.

- Pulmonary capillary haemorrhage is an important adverse biological effect from LUS, and has been observed in several animal models, particularly when using high output energy. Therefore, the mechanical index should be kept low during LUS examinations to diminish this adverse effect, particularly when insonating aerated lung.
- Basic knowledge of LUS and specific terminology used in POC-US are required (Table 10.2).
 - Different tissues have their unique acoustic impedance values (correlated with the resistance to the propagation of US waves through the tissue). When there is a marked difference in acoustic impedance at the interface of two tissues, such as at visceral

Table 10.2 Common signs of LUS—with background explanation and some image examples in alphabetical order (adapted from [5])

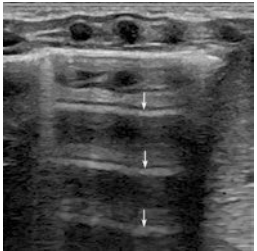

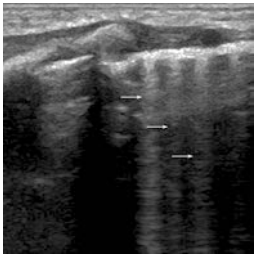

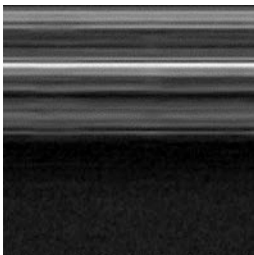

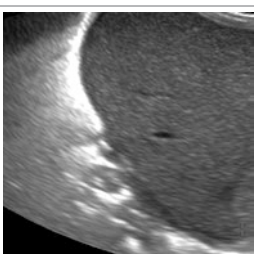
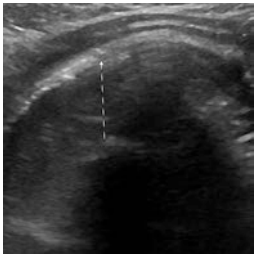
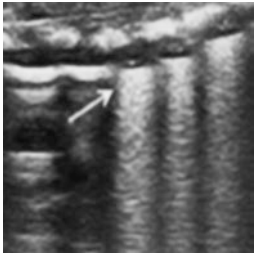
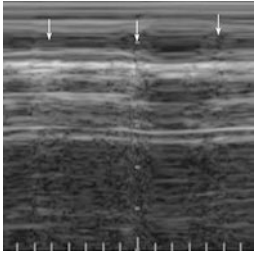
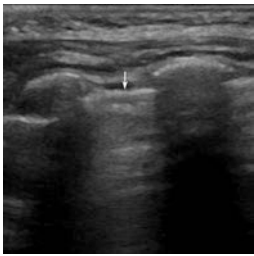
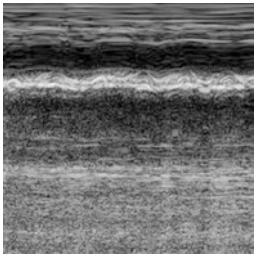
Signs of LUS	Description	Condition	Image
A-line	Horizontal lines, move with respiration	Normal finding	
Air bronchogram = Sonopneumo-bronchogram	Line-like series of echogenic dots, may undulate with respiration, represent residual air bubbles in otherwise insufficient ventilated bronchus	Typical in pneumonia May be in dystelelectasis	

Table 10.2 (continued)

Signs of LUS	Description	Condition	Image
B-line	= Lung rocket Vertical lines, arise from pleural line, spread downwards to edge of image, well-defined, erase A-lines, move with breathing	Various conditions, a few (1–3) may be normal, otherwise “alveolo-interstitial syndrome”	
	Coalesce or impact B-lines produce white lung	Neonatal (I)RDS	
Barcode sign	= Stratosphere sign	M-mode in pneumothorax	
Consolidation	Area of non-ventilated lung, with liver-like appearance (hepatisation), may contain sonopneumobronchogram. May be solitary or patchy and multifocal	Pneumonia Atelectasis Multiple areas in MAS or BPD	
	If small/irregular, subpleural	Any condition with a patchy distribution, e.g. MAS, BPD, bronchopneumonia, etc.	

(continued)

Table 10.2 (continued)

Signs of LUS	Description	Condition	Image
Lung point	Transition from ventilated lung with sliding to air without respiratory sliding in B-mode (or from seashore sign to barcode sign in M-mode)	Typically seen in pneumothorax	
	Double lung point: Transition from different lung US appearances	Typically seen in TTN	
Lung pulse	Pulsations from cardiac motion transmitted through lung to reach parietal pleura	Conditions with static pleural line, e.g. atelectasis from contralateral one lung intubation, apnea	
Lung sliding	Sliding of lung surface, best documented by video clip	Normal ventilation, but with respect Ddx and pitfalls	
Pleural line	A white line underneath chest wall, representing pleural lung interface In parasagittal scanning, pleural line and adjacent ribs creating the bat sign	Smooth thin line = normal Thick irregular line = abnormal	
Seashore sign	Lung sliding, documented by M-mode	Normal ventilation	

pleura and lung interface, US waves cannot pass through but are totally reflected back to the transducer, creating a strong echogenic line of pleural-lung interface called “**pleural line**”. Moreover, this is followed by multiple back-and-forth reflections between the transducer–skin and the pleural–lung interface, from which the transducer receives repetitive signals and the machine creates several parallel lines beneath the pleural line. This is called a reverberation artefact in physics, and named “**A-line**” in LUS.

- Normal lung parenchyma with air-filled alveoli and thin interstitium underneath the pleural–lung interface are not perceptible by US. However, in the initial 4–24 h of life, there may be physiologic foetal lung fluid that creates tiny air–fluid interfaces where sound resonance occurs—this appears on US as vertical echogenic lines from the visceral pleura downwards. This artefact is called “**B-line**” in LUS. After the foetal lung fluid is completely absorbed, there should be no or only very few B-lines detectable in a normal lung. Any other condition that causes a significantly decreased proportion of aerated alveoli in relation to the pulmonary interstitium can produce multiple “B-lines” then called “alveolo-interstitial syndrome”, e.g. pulmonary oedema. Coalescent or compact B-lines will present as “**white lung**”. In the other way, total replacement of air in alveoli with any kind of fluid will provide visualisation of lung parenchyma, eventually shown as homogeneous low to medium echogenicity called “consolidation”, also called “**lung hepatisation**”, often with shaggy border (“**shred**” sign) and internal sonographic air bronchogram. Atelectasis provides the same or a similar pattern—so it may be difficult to differentiate atelectasis from consolidation, unless having significant volume loss, which may show better-defined borders and concave angles at the lung margin and a more parallel air bronchogram.
- During respiration, the lung moves and there is sliding of the visceral pleura underneath the parietal pleura which can be observed on

real-time B-mode imaging. This is called “**lung sliding**” or “lung gliding” sign. Absence of “lung sliding” means either a pneumothorax or having no or minimal lung movement (e.g. in hyperinflation/air trapping). The transition site of the pleural free air in pneumothorax to the ventilated lung is named “**lung point**”. When the transducer is placed at this margin, one can observe absence of lung sliding on the more anterior/medial side and presence of lung sliding on the more posterior/lateral side.

- On motion-mode US (M-mode) the pleural line that has “lung sliding” and the reverberation artefact below will show a granular pattern, this is named “**seashore**” sign. In pneumothorax, M-mode will produce very sharp lines that look like a barcode and thus is called “**stratosphere**” or “**barcode**” sign.
- Pulsations from the heart can reach the parietal pleura and can be demonstrated in M-mode. The presence of this “**lung pulse**” is usually noted when scanning an atelectatic lung from contralateral one lung intubation and in normal lung during apnea.
- Point-of-care US of the lung is used in neonates to diagnose pneumothorax, RDS, TTN/wet lung with reported high sensitivity and specificity in selected populations.

10.2.3 Chest CT, MRI, and Fluoroscopy

There are essential requisites for performing chest CT, MRI, and fluoroscopy in neonates:

- Radiation dose from CT in neonates, particularly the very preterm and very small ones, is more of concern than in other age groups. A clear and justifying indication for every CT examination is required, and every effort to lower radiation dose must be attempted.
 - Consider if another modality can answer the clinical query.
 - Reconsider the need of contrast agents—sometimes an unenhanced study will suffice.
 - If you need a contrast-enhanced CT—minimise multiple scanning acquisitions by either.

Selecting the most appropriate phase for indication, or

Using a slower and more prolonged contrast injection to attain both pulmonary circulation and aortic phase in a single acquisition, or

Use a split bolus technique to acquire multi-phases of contrast enhancement in the same acquisition, however, this is very cumbersome in neonates for many reasons. Additionally, the renal immaturity obviates the use of the higher contrast amount for this application and therefore is hardly ever used. As an alternative, the “Micro-bolus technique” with automated or visual contrast tracking can be applied [6].

- Set an appropriate scan range based on indication.
- Use low-dose, weight-/size- and indication-based protocols. The lowest available kVp, 60–80 kVp according to vendors, is proper for chest and lung CT in neonates. Modern CT scanners with iterative reconstruction or deep learning allowing a lower mA setting can further decrease radiation exposure, also a tin filter as offered by some vendors allows to even further lower the dose approaching values of a digital radiograph. Another important aspect is to properly place the patient in the iso-centre of the bore—this does not only improve image quality, but also helps to lower the dose.
- As with every CT—remember that the scout is an essential part of the total radiation exposure, sometimes not even included in the CTDI calculation of some vendors—therefore reduce the scout range, do a p.a. scout, reduce the scout dose, re-think if both planes are necessary for the scout or if a scout is necessary at all.
- High-resolution CT (HRCT) is rarely used in neonates, it may be indicated in suspicion of childhood interstitial lung disease or for some rare disorders of infancy, e.g. surfactant dysfunction. The volumetric helical HRCT provides higher radiation dose than the non-contiguous HRCT, but with the advantage for multiplanar reformation and for the pulmonary lesion with irregular dis-

tribution. However, non-contiguous HRCT should be considered for the expiratory phase scanning and in follow-up of diseases with diffuse and regular distribution to lower patient overall radiation burden.

- Magnetic resonance imaging (MRI) is a radiation-free alternative for CT imaging, and it is gaining more recognition in chest and lung imaging. It mostly used for mass lesions such as a suspected mediastinal tumour or sequestrations, as well as for diaphragmatic queries. Most of these investigations can successfully be performed in a “feed and wrap” approach, thus avoiding sedation or anaesthesia.
 - The most useful standard technique for lung imaging in infants is respiration-triggered T2-weighted turbo spine-echo (TSE) sequence. This technique shows good T2-contrast of the pathologies against the dark lung, with mostly free of respiratory motion and sharp images [7].
 - Gadolinium is used only when indicated (such as for mediastinal solid lesion) and if really urgently necessary—try to postpone such a contrast-enhanced study whenever possible, because of the physiological immaturity of the kidney resulting in longer gadolinium recirculation times and slower excretion, thus increasing the risk of gadolinium deposits in the body. In order to image thoracic blood vessels, such as in pulmonary sequestration, fast dynamic MR angiography, e.g. with time-resolved angiography with stochastic trajectory (TWIST) can examine the entire lung in 2–3 s. As an alternative, non-enhanced flow-sensitive MRA-techniques can and should be used and often suffice for analysing the large vessels.
 - However, with proton-poor lesions (e.g. small lung cysts, emphysema, small calcifications, and early stage of fibrosis), CT is definitely superior, although cystic CPAM can now be depicted by new improved MR techniques, but still have blurring of their boundaries.
- Fluoroscopy may also be necessary in some chest conditions, particularly for evaluation of the oesophagus and potential trachea-oesophageal fistula.
 - Besides the necessity to reduce the dose adapted to the area imaged and the patient

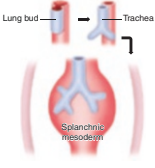
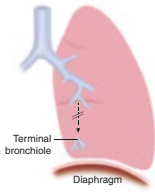
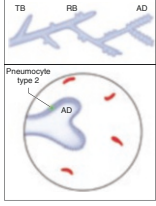
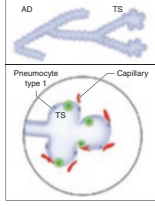
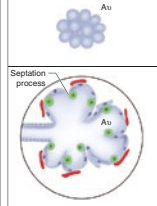
size as well as to limit the screening time, a digital equipment with amplifier and last image hold without a scatter grid should be used. Continuous screening is hardly ever necessary, low pulse rates (maximum 6 frames/s) are advisable. Also in fluoroscopy, proper collimation and use of shutters (not only the electronic retrospective shutters, define shutter size before starting the screening) are recommended, as well as a proper distance from the tube (place the patient as close to the detector as possible) and adequate centring. As in most conditions, there is a risk of aspiration in these studies in this age group,

barium is avoided as an oral contrast agent and water solvable contrast should be used.

10.3 Embryology of the Respiratory System

Basic embryonic knowledge of bronchopulmonary foregut development is essential for understanding the disease process which has a close relationship between the airway, the lung, the interstitium, and vascular structure. Stages of embryonic bronchopulmonary development are summarised in Table 10.3.

Table 10.3 Summary of bronchopulmonary development [8]

Embryonic stage 3–6 weeks GA	Pseudoglandular stage 5–17 weeks GA	Canalicular stage 16–25 weeks GA	Saccular stage 24 weeks GA- at birth	Alveolar stage Phase 1: 36 weeks GA –3 years Phase 2: Age 3–8 years
				
<ul style="list-style-type: none"> • Development of lung bud from ventral wall of foregut • Growth of lung bud in caudal direction to form trachea and separation from oesophagus • Primary, secondary, and tertiary bronchial buds to form main, lobar, and segmental bronchi, respectively • Bronchial buds growing into splanchnopleuric mesoderm • Development of visceral pleura • Extra-pulmonary arteries • Starting development of diaphragm at 4 weeks GA 	<ul style="list-style-type: none"> • Bronchial branching to the level of terminal bronchioles • Development of cartilage and smooth muscles of the airway • Development of intrapulmonary arteries from splanchnopleuric mesoderm • Complete development of diaphragm at 8–10 weeks GA • Production of foetal lung fluid by epithelial cells at 6 weeks GA 	<ul style="list-style-type: none"> • From terminal bronchioles (TB), development of respiratory bronchioles (RB), and alveolar ducts (AD) • Presence of type 2 pneumocytes and early differentiation from type 2 to type 1 pneumocytes • Extensive vascularisation surrounding the acini • Beginning of foetal breathing movement at 20 weeks GA • Lamellar bodies detected in type 2 pneumocytes at 20 weeks GA • Starting surfactant production at 22–24 weeks GA 	<ul style="list-style-type: none"> • Development of terminal sacs (TS) (primitive alveoli) • Maturation and differentiation of type 2 into type 1 pneumocytes • Increased surface for gas exchange • Formation and expansion of pulmonary capillaries • Surfactant not adequate until late preterm 	<p>Phase 1</p> <ul style="list-style-type: none"> • Increased number of alveoli (Av) by alveolar division through a septation process, with the majority occurring within the first 6 months • Increased pulmonary capillaries • Functional closure of PDA within 12–24 h after birth <p>Phase 2</p> <ul style="list-style-type: none"> • Increased number of alveoli at a slower rate • Increased size of alveoli

Development of the lung is classified into five stages, starting at the third week of gestational age and being completed by the age of 8 years. During bronchopulmonary development in each stage, there is simultaneous development of pulmonary vasculature and the diaphragm. The levels of functional maturity follow the levels of structural maturity

10.4 Normal Imaging Findings in Neonates

10.4.1 Chest Radiographs

For chest radiographs usually only an AP view of the chest is required in neonates to provide all the necessary diagnostic information; there is no diagnostic benefit from routine lateral views, which are rarely requested—if, then based on a clinical indication and an unclear AP view. The abdomen is often included in the initial chest radiograph to evaluate bowel loops and position of umbilical catheters.

There are some unique findings in normal neonatal chest radiograph as compared to older children and adults (Fig. 10.1).

- The clavicles are relatively higher to the level of about T1 and more in transverse lie.
- Normal thymus in anterior mediastinum occupies a large proportion of area in neonatal chest. There is a wide variance in size and shape of the normal thymus, with well-known “sail” or “wave” signs. The cardiothymic silhouette may obscure the true lateral borders of the heart. A small “hypo-/atrophic” thymus at birth is found when prenatal maternal corticosteroids have been prescribed.
- Transient cardiomegaly may occur within the first few hours of life during physiologic changing process of pulmonary circulation.



Fig. 10.1 Normal neonatal chest radiograph. Chest radiograph shows normal cardiothymic shadow with left thymic wave sign and the clear lung

The ductus bump from the still open ductus arteriosus may also be observed.

- Transient prominent pulmonary vasculature from residual lung fluid can be observed within the first few hours of life.
- Tracheal cartilages are soft and can be easily bending or buckling during expiration.
- The diaphragm has less curvature. The right and left hemidiaphragm can be at the same level. Lobulation of right hemidiaphragm at anteromedial part may be detected in some neonates when hyperinflation, some consider it as a normal variation while others consider a focal diaphragmatic eventration.

The imaging approach of pulmonary lesions is heavily based on chest radiographs and may start with assessment of whether there is a unilateral or bilateral involvement, an opaque or a hyperlucent lung, a presence or absence of cystic lesions, and an increased or decreased lung volume, which is helpful in narrowing the differential diagnosis (Table 10.4). Furthermore, the mediastinum (size, shape), the heart (size, shape, and position—see Chap. 11) and the pulmonary vessels/vasculature (decreased, increased, and normal) should be assessed. Finally, don't forget to look at the soft tissues and the skeleton.

10.4.2 Chest and Lung Ultrasound (US)

Lung ultrasound (LUS) is used in the emergency bedside setting (NICU, resuscitation) or POCUS-setting, or for follow-up of entities suited for LUS, or as a supplement to chest radiographs.

For chest and lung US in neonates, there are some differences from older children and adults.

- Ossification centres of the sternum are partially ossified and not yet fused, particular in the preterm, providing a large acoustic window for visualisation of the thymus and great vessels.
- The neonatal thymus is relatively prominent in size and usually has convex lateral bor-

Table 10.4 An approach to a neonatal chest radiograph—typical findings on neonatal chest radiographs

	Pulmonary density	Pulmonary volume	Pulmonary and not-pulmonary causes
Bilateral	Opaque	Decreased	<ul style="list-style-type: none"> • (IRDS (before treatment))
		Increased or normal	<ul style="list-style-type: none"> • (IRDS (during treatment)) • MAS • TTN (wet lung) • Pulmonary lymphangiectasia • Pulmonary oedema • Neonatal pneumonia • (Not lung) Bilateral pleural effusion
	Hyperlucent	Increased	<ul style="list-style-type: none"> • Bilateral CLH • Bilateral bronchial atresia • Bilateral cystic CPAM • Pulmonary interstitial emphysema • BPD • (Not lung) Bilateral pneumothorax
	Normal	Decreased	<ul style="list-style-type: none"> • Bilateral pulmonary hypoplasia
Unilateral	Hyperlucent	Increased	<ul style="list-style-type: none"> • CLH • Bronchial atresia • Partial bronchial obstruction from intrinsic or extrinsic lesion • One lung intubation • CPAM (cystic type) • Bronchogenic cyst • Localised PIE • (Not lung) Congenital diaphragmatic hernia • (Not lung) Pneumothorax
		Decreased	<ul style="list-style-type: none"> • Destroyed lung with cystic change
	Opaque	Increased or normal	<ul style="list-style-type: none"> • Neonatal pneumonia • Pulmonary sequestration, solid-type CPAM • Early fluid-filled CLH, CPAM or bronchial atresia • (Not lung) Early fluid-filled bowel loops in congenital diaphragmatic hernia • (Not lung) Pleural effusion
		Decreased	<ul style="list-style-type: none"> • Atelectasis • Pulmonary agenesis, aplasia, or hypoplasia

To approach a neonatal chest radiograph: assess if changes are uni- or bilateral, diffuse or localised, define lung opacity and the kind of pattern, the lung volume, and if there are extra-pulmonic changes such as an effusion or a pneumothorax. Eventually assess also heart (size, shape—see Chap. 11) and lung vessels and perfusion (increased, normal or decreased). Don't forget to analyse the mediastinum and skeleton (e.g. fracture of the clavicle). More details of the listed entities are described in the following sections of this chapter

ders, however, it is soft and does not compress or displace any adjacent structures in the mediastinum or crossing vessels. It can protrude to the neck, particularly during crying. The thymus shows homogeneous background echogenicity, similar or slightly lower than that of the liver, with several short linear or branching echogenic foci, producing a “starry sky” pattern. Colour Doppler sonography (CDS) of the normal thymus in

young infants reveals a few vascular structures with a low-resistant arterial waveform on spectral analysis.

- The presence of physiologic lung fluid produces “white-out” lungs (or compact B-lines) at birth, then changing to discrete B-lines which is observed within 10 min, and finally there is a gradual disappearance of B-lines within 4–24 h in most of healthy termed neonates [9].

- The lungs of the preterm neonates are more prone to atelectasis because of the immature histologic pulmonary structure, and can be perceived on LUS as focal areas of low- to medium-intensity echoes, which can mimic a consolidation.

10.4.3 Chest CT/MRI

Chest CT can be performed either in free breathing or with controlled respiration, the latter usually with alveolar recruitment. When performing under free breathing, there is a low tidal volume which produces higher attenuation value of the lung, particular at the dependent parts. The outlines of the bronchovascular marking are less sharpened from respiratory motion. Typical normal neonatal thymus has trapezoid shape with biconvex lateral contours in cross-sectional plane and has homogeneously high attenuation of about 80 HU which is higher than muscle of the chest wall and the heart, then gradually declines in density after the first year of life to about 56 HU at the age of 14 years from fatty infiltration [10]. It shows a homogeneous enhancement after intravenous contrast injection. But a CT is not indicated for the assessment of the normal thymus.

On chest MRI, the lung barely has signal in both T1- and T2-weighted images, because it has a very lower proton density. The thymus has homogeneous signal intensity that slightly higher than muscle on T1-weighted image and close to fat on T2-weighted image.

10.4.4 Chest Fluoroscopy

Fluoroscopy is used sometimes for assessing diaphragmatic movements and it shows synchronous bilateral respiratory motion, often a higher amplitude is observed on the left than on the right side—however, this application has generally been replaced by US of the diaphragm.

The other application of fluoroscopy (besides catheter angiography, which is discussed in Chap. 11) is the assessment of the tracheobron-

chial tree and the oesophagus. Here often contrast agents are used (sometimes the air can serve as an intrinsic contrast).

A normal oesophagogram in patients at any age usually shows smooth-outlined contrasted-filled oesophagus, forward propulsive oesophageal peristalsis, and a normal position of oesophago-gastric junction below the diaphragm with an acute angle of “the angle of His”. In neonates and young infants, however, oesophageal peristalsis and lower oesophageal sphincter are immature. Distal two-thirds of their oesophagus may be wider from weaker peristalsis. The “angle of His” in neonates is rather obtuse than acute and there is frequent transient relaxation of lower oesophageal sphincter, so gastro-oesophageal reflux is common, particularly the preterms, and is considered physiologic if clinically asymptomatic.

10.5 Pulmonary Abnormalities

Pulmonary abnormalities are the most common findings in chest radiographs of term and preterm neonates presenting with respiratory distress.

Radiologists also require all relevant clinical information, e.g. gestational age, result of prenatal US, prenatal and perinatal events (maternal diabetes, maternal steroid prophylaxis, premature rupture of the membrane, difficult delivery, meconium in amniotic fluid), cardiac problems (murmur, cyanosis, results of echocardiography), and treatment (surfactant, pleural tapping) for a most accurate image interpretation.

The following will address the different conditions listed according to their imaging appearance and importance. A short clinical summary is provided, too, as well as a summary of key imaging findings.

- **Bilateral pulmonary involvement with increased opacities** are the most common abnormalities detected in preterm and term neonates with respiratory distress. The major diseases in this group are TTN, RDS, preterm neonate with accelerated lung maturation, MAS, pulmonary oedema, and those in the

overlapped group such as neonatal pneumonia.

Their radiographic findings may be subcategorised in four lung patterns (Fig. 10.2):

- Clear lung
- Diffuse ground-glass or fine granular pattern
- Perihilar streak pattern
- Coarse patchy reticulonodular pattern

Note that a single disease can manifest with a variety of lung patterns; for example, TTN typically presents with perihilar streak pattern, but may also present with diffuse ground-glass opacity. On the other hand, one lung pattern can be produced by a variety of lung diseases; for example, diffuse ground-glass opacity is typical presentation of (I) RDS, but also can be found in neonatal pneumonia, TTN, pulmonary oedema, and preterm neonates with accelerated lung maturation (Table 10.5). And also note that treatment measures may also affect the radiographic appearance—for example after administration of surfactant in (I)RDS the initially diffuse bilateral pattern may become more localised and patchy, with areas of relatively normal lung and of still affected lung. As a result, there may be overlap and variance in the appearance of the individual condition, e.g. pattern and distribution of opacities or/and lung volume, also depending on severity and also during treatment.

- When there is **bilateral pulmonary involvement with hyperlucent areas**, the causes are more commonly acquired (e.g. PIE and BPD) (Fig. 10.3) than congenital (e.g. bilateral CLH, bronchial atresia, and CPAM).
- In a **unilateral hyperlucent lung with increased volume**, most of the lesions are developmental anomalies and require surgical treatment. The hyperlucent areas can be subdivided into those without and with air-filled cysts (Fig. 10.4) (Table 10.6).
 - A unilateral large lucent lung without cysts is further assessed by defining in which area air trapping occurs, whether it involves one lung, one lobe, or lung segment.
 - A unilateral large lucent lung with cysts is further assessed by characterising the cyst, e.g. whether uni- or multilocular.
- A **unilateral radiolucent lung with a decreased volume** is uncommonly present in neonates.
 - One lung can be small and normally aerated in pulmonary hypoplasia or agenesis of one lobe. The lung on the affected side may have normal density on chest radiograph or may show increased density from the ipsilateral shift of the mediastinum.
 - Cystic changes in a small-sized lung in neonates are even rarer, as it indicates destroyed lung with fibrotic and bronchiectatic changes. One possible cause is a congenital broncho-oesophageal fistula (Fig. 10.5),

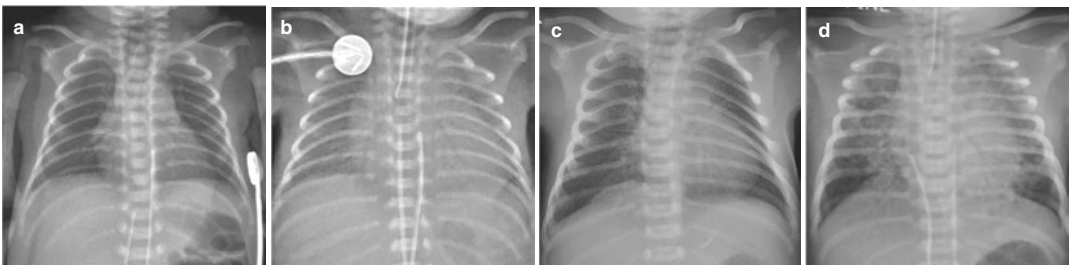


Fig. 10.2 (a–d) Four patterns of bilateral pulmonary involvement in preterm and term neonates. (a) “Clear lung” pattern in a newborn from 28 weeks’ gestation (prenatal maternal steroid prophylaxis) with structural premature lung. (b) “Diffuse ground-glass” pattern with air

bronchogram in a newborn from 27 weeks’ gestation with (I)RDS. (c) “Perihilar streak” pattern in a term newborn with TTN. (d) “Coarse patchy reticulonodular” pattern in a term newborn with meconium aspiration syndrome

Table 10.5 Radiographic patterns of bilateral pulmonary opacities in neonates and the clinical information required for differential diagnosis (adapted from [11])

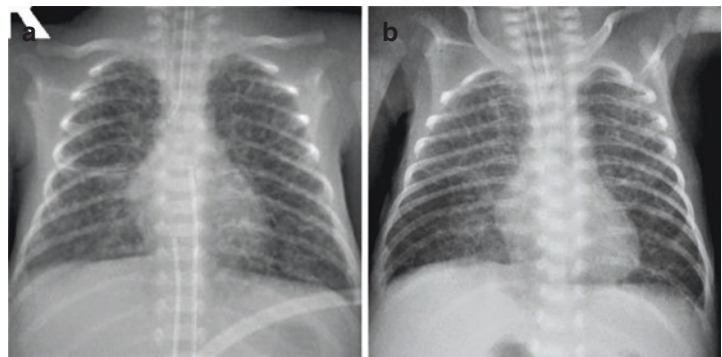
Radiographic pattern	Neonatal pulmonary conditions	Clinical and laboratory information required for the diagnosis
Clear lung	<ol style="list-style-type: none"> 1. Normal lung 2. Primary PPHN 3. Preterm with accelerated lung maturation^a 4. (Sub-radiographic) Neonatal pneumonia 5. Bilateral pulmonary hypoplasia 	<ol style="list-style-type: none"> 1. No or minimal sign or symptom 2. Cyanosis, low blood oxygen level, respiratory distress 3. Narrow superior mediastinum, low GA with history of maternal steroid prophylaxis 4. PROM, clinical sepsis, respiratory distress 5. Oligohydramnios
Diffuse ground-glass or fine granular pattern	<ol style="list-style-type: none"> 1. RDS 2. Neonatal pneumonia 3. TTN 4. Pulmonary oedema 5. Preterm with accelerated lung maturation^a 	<ol style="list-style-type: none"> 1. Low GA, or near-termed IDM 2. PROM, clinical sepsis 3. Mild symptom with progressing improvement 4. Murmur, echocardiography 5. Narrow superior mediastinum, low GA with history of maternal steroid prophylaxis, SF analysis from respiratory effluent
Perihilar streak pattern	<ol style="list-style-type: none"> 1. TTN 2. Pulmonary oedema 3. Neonatal pneumonia 4. Preterm with accelerated lung maturation^a 5. MAS 	<ol style="list-style-type: none"> 1. No labour pain 2. Murmur, echocardiography 3. PROM, clinical sepsis 4. Narrow superior mediastinum, low GA with history of maternal steroid prophylaxis 5. Meconium-stained amniotic fluid
Coarse patchy reticulonodular pattern	<ol style="list-style-type: none"> 1. MAS 2. Other-particle aspiration syndrome 3. Neonatal pneumonia 	<ol style="list-style-type: none"> 1. Meconium-stained amniotic fluid 2. Other particles in amniotic fluid 3. PROM, clinical sepsis

Overview of typical patterns with respective diseases/conditions/clinical presentation encountered on a neonatal chest radiography

Abbreviations: GA gestational age, PROM premature rupture of membrane, IDM infant of diabetic mother, SF surfactant

^a Preterm with accelerated lung maturation means structural premature lungs but with ability of surfactant production from prenatal maternal prescription of steroids or stress

Fig. 10.3 (a, b) Bilateral pulmonary lesions with multiple small cysts. (a) Pulmonary interstitial emphysema (PIE) in a 6-day-old preterm neonate with (I)RDS. (b) Bronchopulmonary dysplasia (BPD) in a 27-day-old preterm neonate with (I)RDS



particular when the ipsilateral main or lobar bronchus is not identified, and an oesophagogram is suggested to verify the diagnosis.

- **A unilateral opaque lung** may occur with either decreased, normal or increased volume.

- Assessment of lung volume helps in separating the diseases with significantly volume loss (pulmonary agenesis/atresia and atelectasis) (Fig. 10.6a) from the other conditions.
- For the group with normal or increased lung volume, analyse the opacity of its

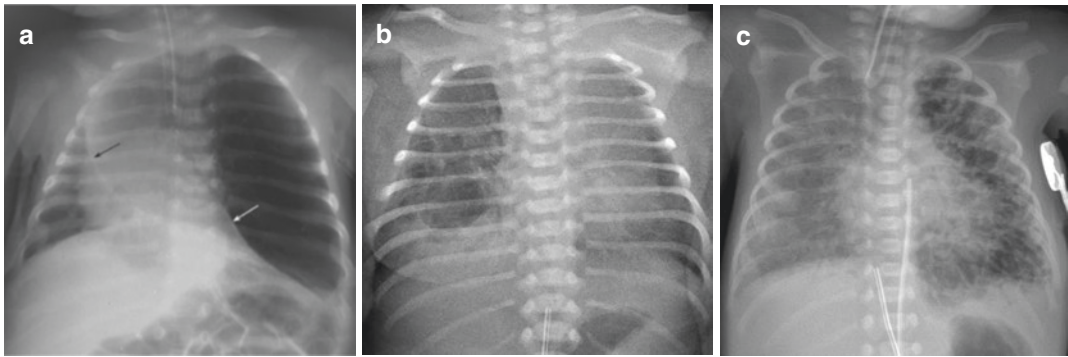


Fig. 10.4 (a–c) Unilateral hyperlucent lung in neonates (a) without cyst and (b, c) with cysts. (a) Congenital lobar hyperinflation in a 7-day-old neonate with severe respiratory distress. There is marked expansion of left upper lobe across midline (black arrow) causing atelectasis of left lower lobe (white arrow) and contralateral mediastinal

shift. (b) Congenital pulmonary airway malformation type 1 in a 1-day-old neonate. Multiple cysts are noted in right lower lobe with one cyst above 2-cm diameter. (c) Unilateral PIE in a preterm neonate of 25 weeks’ gestation. Multiple cysts develop in the entire left lung on the second day of life

Table 10.6 A list of pulmonary diseases with unilateral large hyperlucent lungs according to areas of involvement and cyst characters

Unilateral hyperlucent lung “without cyst”	
Area of involvement	Diseases
• Lung segment	• Bronchial atresia
• One lobe	• CLH
• One lung	• One lung intubation • Narrowing of main bronchus by intrinsic or extrinsic lesion • (Not lung) Pneumothorax
Unilateral hyperlucent lung “with cyst”	
Cyst character	Diseases
• Multiple cysts	• CPAM • Unilateral or localised PIE • (Not lung) Congenital diaphragmatic hernia
• Unilocular cyst	• Bronchogenic cyst • CPAM • Localised PIE

Overview for approaching imaging finding of a unilateral hyperlucent lung, consider first whether it is with or without cystic, areas of involvement and/or cyst characteristics, to match with typical diseases

location, its shape and margins, consider patient’s age at imaging, and take all available relevant clinical information into account to come up with a differential diagnosis between pneumonia, pulmonary

sequestration, fluid-filled cystic lesions, or pleural effusion (Fig. 10.6b). Further follow-up chest radiographs and/or US or CT may be required.

10.5.1 Respiratory Distress Syndrome (RDS)

Respiratory distress syndrome (RDS) is caused by having inadequate amount of surfactant in the newborn lungs, producing high surface tension and alveolar collapse at end expiration—originally it was named idiopathic RDS (IRDS) of the newborn.

- Surfactant is produced by type II pneumocytes, and firstly detected in 22–24 weeks’ gestation, but not adequate until late preterm. Preterm neonates born at 26–28 weeks have high risk, 60–80%, of developing RDS while the risk decreases to 15–30% when born at 32–36 weeks’ gestation.
- (Idiopathic)RDS is much less common in late preterm neonates after 34 weeks’ gestation, except in those born from poorly controlled diabetic mothers, because a high insulin level in the foetus can inhibit the expression of the surfactant protein-A gene. There are many

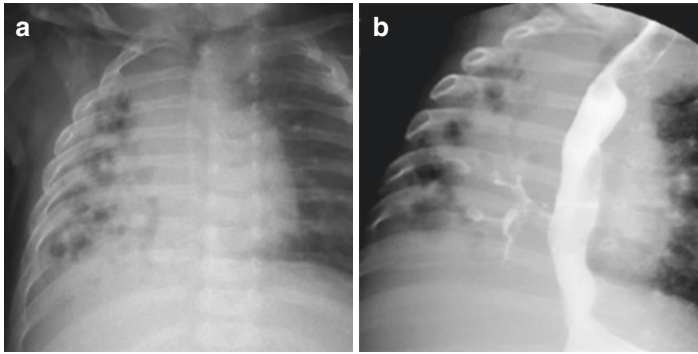


Fig. 10.5 (a, b) Bronchiectasis from oesophageal bronchus. (a) Chest radiograph of a 1-month-old infant with recurrent pneumonia reveals multiple small cysts on the background of small-sized opaque right lung, suggestive

of cystic bronchiectasis in the destroyed lung. (b) Oesophagography shows a bronchus to the right lung arising from lower half of thoracic oesophagus. There is no right main bronchus from bronchoscopy

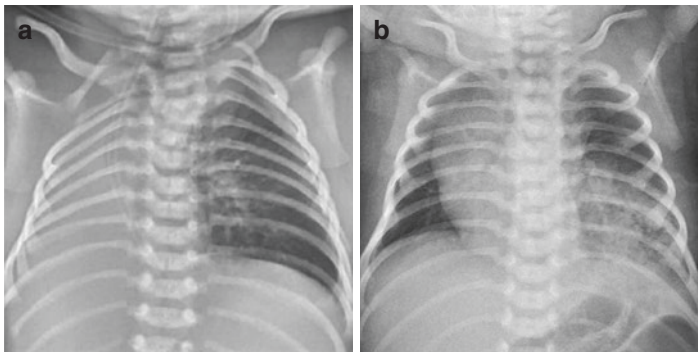


Fig. 10.6 (a, b) Unilateral opaque lung in neonates with (a) volume loss and (b) increased volume. (a) Agenesis/aplasia of the right lung. There is no aeration of the right lung with marked ipsilateral mediastinal shift. (b) Fluid-filled CPAM type 2 in left lower lobe. Prenatal US detects

cystic lung disease in left lower lobe. Early postnatal chest radiograph shows consolidation in left lower lobe with contralateral mediastinal shift. This opaque lesion is later filled with air (see Fig. 10.26)

other risk factors of (I)RDS on both the maternal (multiple pregnancy, elective caesarean section, maternal cholestasis, etc.) and the neonatal sides (male gender, familial disposition, birth asphyxia, etc.).

- Antenatal maternal administration of corticosteroids has been used to decrease the incidence of (I)RDS and serious adverse outcomes related to prematurity, but there is no obvious benefit for chronic lung disease.

Imaging has an important role in diagnosis and grading of (I)RDS.

- The **chest radiograph** is the standard imaging tool for diagnosis of (I)RDS.
 - Typical chest radiographs of untreated (I)RDS show pulmonary under-aeration, homogeneously and symmetrically increased opacities (ground-glass appearance) of both lungs and presence of air bronchogram (Fig. 10.7).
 - Under-aeration may not be regularly detected because early ventilation support usually has been assigned.
 - The degree of pulmonary opacity varies according to the degree of alveolar col-

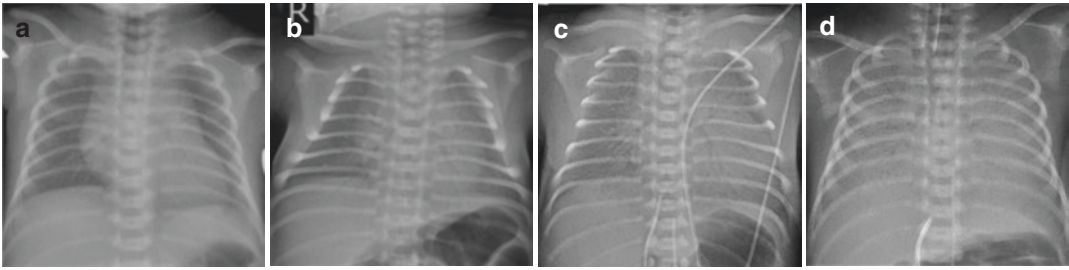
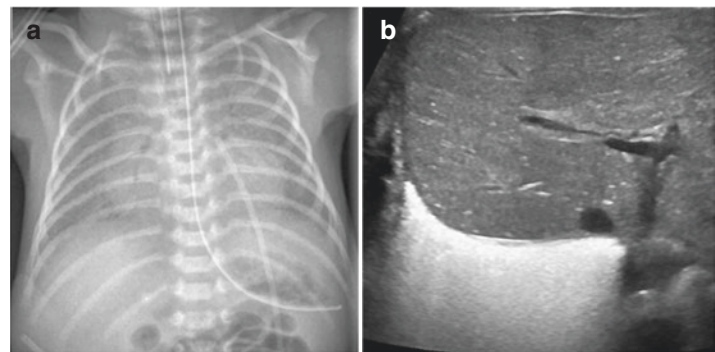


Fig. 10.7 (a–d) Chest radiograph of (I)RDS and its roentgenographic grading. (a) Grade I. A newborn from 33 weeks' gestation has diffuse fine granularity producing mild ground-glass opacity in both lungs. (b) Grade II. A newborn from 34 weeks' gestation has diffuse moderate

ground-glass opacity and air bronchogram. (c) Grade III. A newborn from 29 weeks' gestation has diffuse marked ground-glass opacity and air bronchogram. (d) Grade IV. A newborn from 30 weeks' gestation has white-out lungs obscuring mediastinal and diaphragmatic borders

Fig. 10.8 (a, b) Lung US of (I)RDS. (a) Chest radiograph shows diffuse marked ground-glass opacity and air bronchogram. (b) On LUS, white lung from impact B-lines is noted



lapse, ranging from mild ground-glass opacity with fine granularity (grade I), moderate grainy ground-glass opacity with widespread air bronchogram (grade II), further increased density to alveolar opacity with air bronchogram (grade III), and white-out lungs with obscured mediastinal and diaphragmatic borders, usually with less pronounced air bronchogram (grade IV).

- However, radiographic findings similar to the (I)RDS ground-glass pattern (although not that granular) may be also found in TTN, prematurity with accelerated lung maturity, neonatal pneumonia, diffuse pulmonary haemorrhage, and severe pulmonary venous congestion.
- Knowledge of all related clinical information is necessary for suggesting the proper diagnosis, or at least to narrow the differential diagnosis.
- On LUS, severe (I)RDS is seen as white lung (Fig. 10.8).

- Lower degree (I)RDS still shows coalescent B-lines to a lesser extent—even some US-based grading has been proposed [12], with B-lines detected only in expiration defined as grade I, B-lines during inspiration and white lung during expiration defined as grade II, and white lungs irrespective of respiratory phase as grade III.
- Evaluation and scoring of lung pattern (B-lines, coalesce B-lines, and consolidation) may be used to predict the need of surfactant administration in preterm less than 34-weeks' gestational age under continuous positive airway pressure [13].

Antenatally administered maternal corticosteroids have significantly reduced the incidence of (I)RDS. These **premature infants with accelerated lung maturity** have enough surfactant, which can be confirmed by biochemical analysis of pulmonary effluent. Their chest radiographs usually show a small thymic shadow, but the lungs may provide a variety of patterns, includ-

Fig. 10.9 (a, b) Preterm newborns with accelerated lung maturity from antenatal maternal steroid prophylaxis. (a) “Perihilar streak” pattern in a newborn from 32 weeks’ gestation. (b) “Ground-glass” pattern without obvious air bronchogram in a newborn from 29 weeks’ gestation

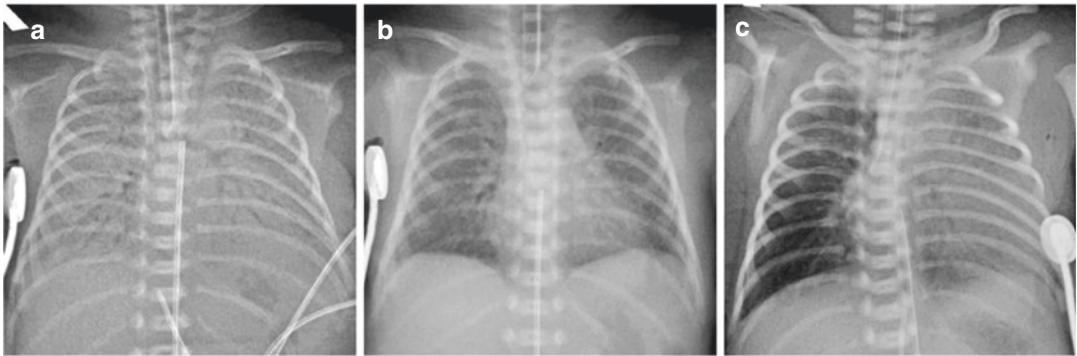
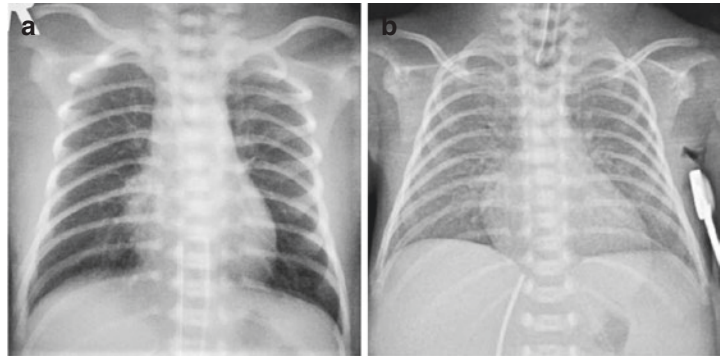


Fig. 10.10 (a–c) (Idiopathic) Respiratory distress syndrome, treated with exogenous surfactant (SF). (a) White-out lungs from (I)RDS is noted in a newborn from 26 weeks’ gestation. (b) Same patient as in (a) after receiving SF, there is uniformly decreased pulmonary

opacity. (c) Another preterm newborn from 26 weeks’ gestation with (I)RDS after receiving SF, there is non-uniform improvement with clearing only right lung. Note tip of ET tube in right main bronchus

ing clear lungs (Fig. 10.2a), streaky pattern mimicking TTN (most common pattern) (Fig. 10.9a), or diffuse fine granular pattern mimicking mild (I)RDS but without obvious air bronchogram (Fig. 10.9b). The opacities detected are from pulmonary immaturity (immature lung syndrome) with a thickened interstitium and fluid leaks.

Radiographic findings change depending on the treatment technique and the response to treatment.

- When **exogenous surfactant** is used, the ground-glass opacities typically quickly clear or uniformly decreased (Fig. 10.10a, b). However, non-uniform improvement can occur either from suboptimal techniques during surfactant administration

with inhomogeneous surfactant distribution (Fig. 10.10c) or from the pre-existing uneven pulmonary aeration before surfactant administration. Additionally, no response after the first dose of surfactant therapy may occur in 10–30% [14].

- In uncomplicated (I)RDS without receiving surfactant therapy, **conventional positive pressure ventilation** can expand the lungs and the diffuse opacities are less pronounced. No significant change or worsening of the image may be observed within the first 2 days followed by gradual clearing over days or weeks.

During the course of disease, many neonates may suffer from other co-morbid conditions,

Fig. 10.11 (a, b) Patent ductus arteriosus (PDA) presenting after improvement of (I)RDS. Same neonate as in Fig. 10.7b. (a) Resolution of ground-glass opacity on the third day of life. (b) Developed cardiomegaly and diffuse ground-glass opacity from pulmonary oedema on the fourth day of life, proven to have PDA by echocardiography

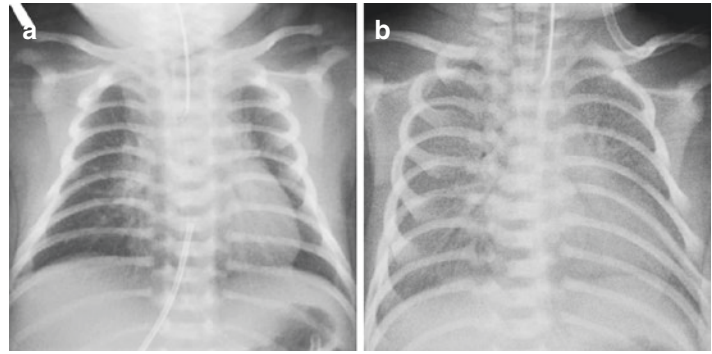
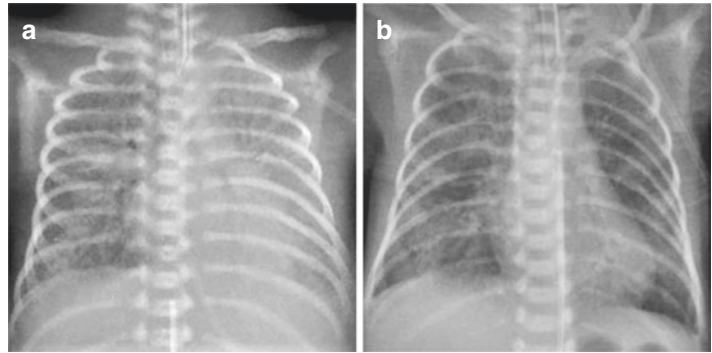


Fig. 10.12 (a, b) Pulmonary haemorrhage. (a) Diffuse pulmonary opacities are noted in both lungs with clinical evidence of pulmonary haemorrhage on the fourth day of life in a term neonate. (b) Multifocal patchy opacities are noted in right upper lobe and both lower lobes with clinical pulmonary haemorrhage on the third day of life in a preterm neonate with (I)RDS treated with surfactant



such as retention of lung fluid, neonatal pneumonia, and patent arterial duct. Or they may suffer from complications of treatment, such as air leaks or pulmonary haemorrhage. These conditions can alter imaging findings in early phase or may show as a recurrent pulmonary opacity after clearing. Image interpretation is limited without adequate clinical information of treatment and patient status.

- **Patent ductus arteriosus (PDA)** has an incidence ranging from 20% to 60% in preterm babies, and reaching 80% in those with (I)RDS [15]. The pulmonary vascular resistance decreases when (I)RDS improves, and a left-to-right shunt occurs through the PDA. The diagnosis is usually made by auscultation of murmur and confirmed by echocardiography. If there is a significant shunting, the chest X-ray may show rapidly

increased cardiac size, increased pulmonary vasculature, (centrally pronounced) pulmonary oedema, and probably a pleural effusion (Fig. 10.11).

- **Pulmonary haemorrhage** may occur in infants with severe (I)RDS who have received surfactant therapy, and usually manifests within the first week of life. It is diagnosed by clinical detection of non-traumatic blood from the endotracheal tube. Chest radiographs of acute pulmonary haemorrhage (or haemorrhagic pulmonary oedema as observed in decompensating cardiac conditions) show an increased pulmonary opacity (often pronounced centrally) which is more commonly diffuse rather than focal or patchy (Fig. 10.12), but there can be no obvious change compared to prior images.
- **Air leaks** from barotrauma include pulmonary interstitial emphysema, pneumothorax, pneu-

momediastinum, and pneumopericardium—this will be discussed below in Sect. 10.7.

10.5.2 Bronchopulmonary Dysplasia (BPD)

Late complication of (I)RDS is the development of BPD, also known as chronic lung disease of prematurity, usually a bilateral process. Development of BPD has a multifactorial aetiology. Not only barotrauma and oxygen toxicity on the premature lung, but also perinatal infection/inflammation, genetics, and NICU care are also contributing factors to growth disturbance of preterm bronchioles, acini and their vascular structure. The risk of BPD is higher in infants with smaller size and younger gestational age. The incidence is about 55% for infants born at 26–27 week's gestation [16].

- **Traditional BPD** had been described before the era of exogenous surfactant therapy when infants with (I)RDS were treated with positive pressure mechanical ventilation and high oxygen concentration, which caused alveolar overdistension, necrotizing bronchiolitis, alveolar wall fibrosis, and capillary leakage.

- The four stages of histological and radiological development of traditional BPD range from ground-glass opacity in phase I (2–3 days), white-out lung in phase II (4–10 days), small cystic change in phase III (10–20 days), and disorganised aeration with heterogeneous patterns of strands, opacities, air trapping and cystic appearance in phase IV (more than 30 days) [17].

- As today antenatal maternal corticosteroids and postnatal surfactant therapy are more commonly used, more extreme preterm neonates are surviving from advanced neonatal care, and BPD has changed in histological and radiological presentations. Because of milder and different respiratory support, there is less necrotizing bronchiolitis and less but more uniform alveolar wall fibrosis. The lungs are extremely structural immature and easily damaged by other contributing factors such as perinatal infection and the postnatal medical care.

- On chest radiographs, the **nowadays BPD** shows gradual progression from clear or almost clear lung to diffusely hazy lung, then uniform coarse interstitial opacities with diffuse hyperinflation, focal air trapping, and atelectasis. Cystic lucencies, if present, are small and more uniform (Fig. 10.13a, b) [18]. Improvement of lung

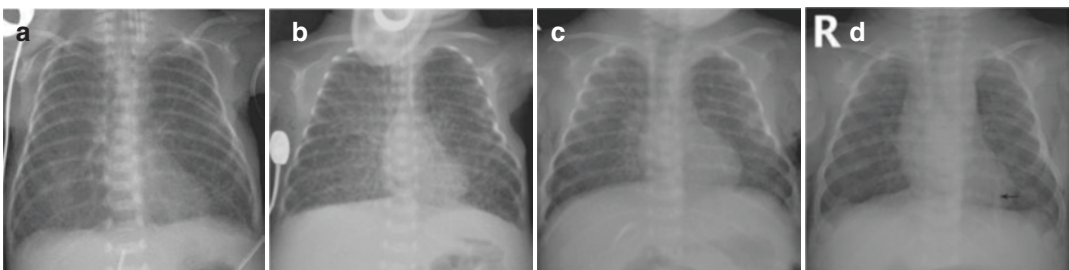


Fig. 10.13 (a–d) Bronchopulmonary dysplasia. **(a)** In a preterm neonate from 24 weeks' gestation at age of 17 days, there are pulmonary hyperinflation, diffusely thickened interstitium in both lungs and an area of ground-glass opacity in medial part right lung. These are likely from premature lung with area of fluid leak from increased permeability of pulmonary capillaries. **(b)** At age of 38 days, there is a progression to coarse reticular opacities and uniform small cysts diffusely in bilateral hyperinflated lungs. Larger areas of ground-glass opacity in

medial part of both lungs are noted, particular the right side. **(c)** At age of 62 days, there is an improvement of lung abnormalities with less pulmonary hyperinflation, resolving of small cystic lesions and the ground-glass opacities. Partially decreased but remained coarsened reticular opacities are noted. **(d)** At age of 4 months, there is further improvement with less reticular opacities. A vertical linear opacity in left lower lobe is from subsegmental atelectasis (arrow). Regrowth of the thymus is noted


changes is observed in follow-up images (Fig. 10.13c, d).

- Lung US may be used to predict the development of moderate to severe BPD by evaluation and scoring of lung aeration from the third day of life with a moderate diagnostic accuracy [19]. When BPD has developed, US shows a thickened pleural line with subpleural scattered small consolidations and prominence of B-lines.

10.5.3 Transient Tachypnea of the Newborn (TTN): Old Term “Wet Lung”

In TTN, there is a prolonged clearance of foetal lung fluid into pulmonary circulation. Normally the clearance of lung fluid occurs through the airway epithelial sodium channels (ENaC), promoted by circulating catecholamines which is rapidly increasing during labour pain. When there is a lower level of circulating catecholamines at birth, particular in babies from caesarean section without labour, the mechanism of foetal lung fluid clearance is delayed.

Transient tachypnea of the newborn mostly occurs in term and late preterm babies. However, a higher incidence of TTN is found with lower gestational age [20]. Glucocorticoids given antenatally to women at risk of preterm birth, not only benefit in reducing (I)RDS, but also can increase the activity of ENaC and then decrease the incidence of TTN.

 Babies with TTN present with mild to moderate degree of respiratory distress soon after birth. The disease is usually a clinical diagnosis by exclusion. It has a benign course with complete resolution of symptoms within 48 h in most of the cases. Supportive management is usually sufficient but more severe TTN that requires ventilator support may occur occasionally.

Imaging with chest radiograph when clinical suspecting TTN is usually required.

- Typical TTN pattern shows bilateral perihilar streakiness (Figs. 10.2c, 10.14a, and 10.15a), varying in severity from prominent vascular markings to interstitial oedema. Associated findings are pulmonary hyperinflation, small amount of pleural effusion, and mild cardiomegaly. If follow-up, most TTN babies will have normal chest radiograph within 24–48 h, in severe case not later than 72 h.
- Other lung patterns in TTN include the normal pattern and the ground-glass pattern (Fig. 10.15b). On the other hand, the perihilar streaky pattern typical for TTN can be found in neonatal pneumonia, mild aspiration syndrome, or pulmonary venous congestion, so the diagnosis cannot be made by imaging alone.
- If the abnormality persists after 72 h, diseases other than TTN must be considered, even

Fig. 10.14 (a, b) Transient tachypnea of the newborn. (a) Chest radiograph of a term neonate shows “perihilar streak” pattern. (b) Lung US shows double lung point (arrow). (Courtesy of Dr. Kanokporn Chutiwongthanaphat, Queen Sirikit National Institute of Child Health, Bangkok, Thailand)

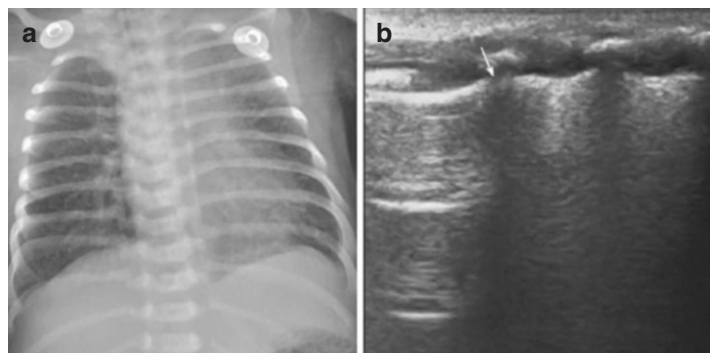
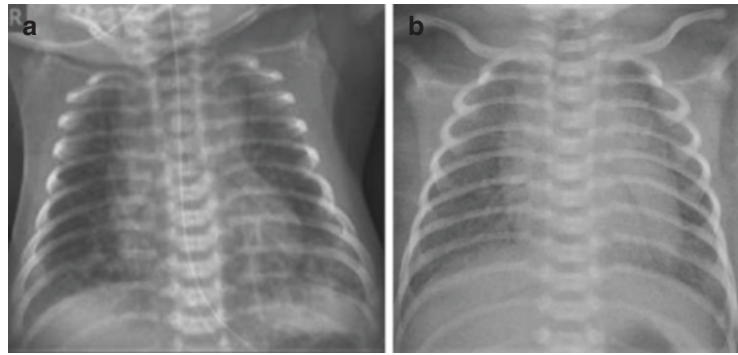


Fig. 10.15 (a, b) Transient tachypnea of the newborn. (a) Chest radiograph shows bilateral perihilar streaks and both lower lobe peribronchial opacities with patchy areas at both lung bases. (b) “Ground-glass” lung pattern is noted in a term newborn with clinical course compatible with TTN



though prolonged TTNs have also been reported.

Lung US can also be applied for this query:

- On LUS with the transducer in sagittal plane, TTN typically shows more involvement of lower than upper lung, such as having multiple B-lines or nearly normal pattern in upper lung fields, changing to compact B-lines (white lung) in the lower lung, with a sharp transitional zone called double lung point (Fig. 10.14b). Alternatively, there can be numerous B-lines without a double lung point.
- Severe TTN may show bilateral white lungs.

10.5.4 Meconium Aspiration Syndrome and Other Particle Aspiration in Neonates

Neonatal aspiration syndrome is defined as respiratory distress in neonates related to tracheobronchial aspiration of fluid or particulate material, with the most common cause from aspiration of meconium-stained amniotic fluid (MSAF).

- **Meconium aspiration syndrome (MAS)**

While MSAF is found in 10–15% in all deliveries, MAS develops only in 4–10% of infants born through MSAF [21]. Ante- or intrapartum hypoxia and acidosis in term foetus

lead to both meconium passing and foetal gassing. The thickness of meconium in amniotic fluid has a direct relationship with the severity of the lung disease.

Meconium aspiration syndrome is one of the serious diseases in neonates, as not only airway obstruction by aspirated meconium occurs, but also the development of chemical pneumonitis, surfactant dysfunction, air leak complications, and persistent pulmonary hypertension (PPHN) are present.

The typical imaging features of MAS on radiographs are bilateral pulmonary hyperinflation, areas of patchy and reticulonodular infiltrates interspersed with hyperlucent areas (Fig. 10.16), and frequent air leak complication.

- Aspirated meconium can cause partial or complete airway obstruction, particular the small airways.
 - Partial obstruction leads to focal areas of air trapping, overall pulmonary hyperinflation, and complication of air leaks.
 - The patchy and reticulonodular infiltrates could be the result of atelectasis, chemical pneumonitis, and pulmonary oedema.
 - Cardiomegaly can be found from having intrauterine asphyxia.
- Besides the classical findings mentioned above, MAS in a milder form may give the perihilar streak pattern.

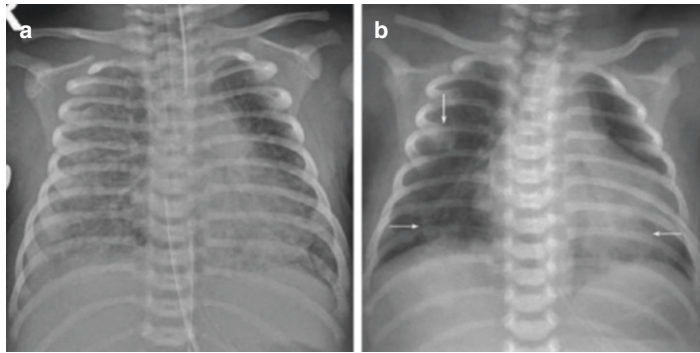



Fig. 10.16 (a, b) Meconium aspiration syndrome, different degree of pulmonary opacities in two neonates. (a) Extensive alveolar opacity in the right lung, reticulonodular opacities in both lungs, and overall hyperinflation with relative lucent area in left upper lobe. (b) In another neo-

nate, there are multifocal patchy nodular opacities in right upper lobe and both lower lobes (arrows) and hyperinflation with attenuated lung markings. Cardiomegaly is noted

- Complication of PPHN cannot be radiographically evident, so the clinical appearance can be poorer than radiographic findings.

Lung US performs poorly in MAS.

 Lung US findings in MAS are consolidations and/or atelectasis, and coalesced or sparse B-lines alternated with spared areas. The detected abnormalities are not uniform and frequently asymmetric, and vary with time. A marked difference in the findings among affected babies can be observed.

• **Other neonatal aspiration syndrome**

Perinatal aspiration of amniotic fluid that contains other particles than meconium (e.g. vernix caseosa, desquamated epithelial cells in ichthyosis) or other kinds of fluid (e.g. blood, gastric content, and water in case of underwater birth) can also cause respiratory distress in neonates.

The initial radiographic chest findings in most of them are similar as in MAS, but the course of the diseases and its complications can be different. Aspiration of vernix caseosa and in ichthyosis syndrome can be life threatening, while aspiration of maternal blood usually has a rapid improvement. There can also be just aspiration of

unstained clear amniotic fluid—hardly to be differentiated from a wet lung and usually without serious sequelae. Whether aspiration of clear amniotic fluid can cause respiratory distress or not is still controversial.

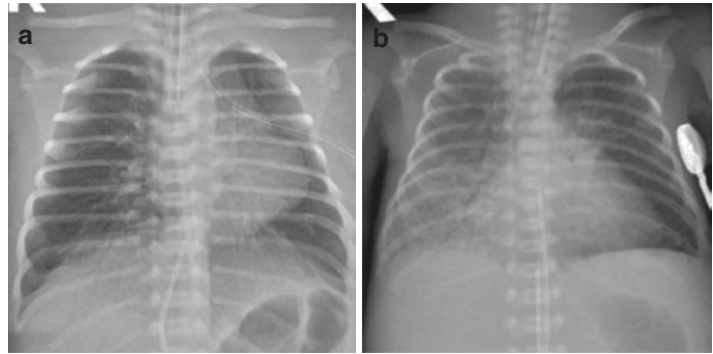
10.5.5 Neonatal Pneumonia

Neonatal pneumonia may be transmitted vertically from the mother or acquired from the peri- and postnatal environment. Many of the normal lung defense mechanisms are compromised in the foetus and neonate, leading to an increased susceptibility to infection. However, neonatal pneumonias are often difficult to identify because clinical manifestations and laboratory tests are often nonspecific. And a neonatal pneumonia may be organ manifestation of a neonatal sepsis, too.

There is a wide variety of radiographic findings.

- As there is no specific pattern of neonatal pneumonia on a chest radiograph, any abnormality on chest radiographs in babies with clinical suspicion of a neonatal pneumonia may suggest a pulmonary infection and warrants the initiation of broad-spectrum antibiotic coverage.
- Pulmonary lesions can be unilateral or bilateral and can be perihilar streak pattern, segmental or lobar consolidation, ground-glass

Fig. 10.17 (a, b)
Neonatal pneumonia.
(a) Perihilar streak pattern with marked hyperinflation in a 3-day-old term neonate with clinical diagnosis of sepsis and PPHN.
(b) Consolidation in right lower lobe in a 2-day-old neonate with *E. coli* pneumonia



pattern, focal or multifocal patchy opacities, or even a clear lung (Fig. 10.17). Clear lung in the diagnosis of pneumonia is explained by early pneumonia that not yet has become radiographically manifest, which can happen in about 15% of the cases [22].

Lung US can be used and then is quite reliable for diagnosis and for follow-up as soon as the pathology reaches either the peripheral pleura or the thymus or the diaphragm.

- In severe neonatal pneumonia, LUS may show large areas of (liver-like) consolidation with or without sonopneumobronchogram, and potentially increased vascularity on CDS.
- Additionally, the often-coexisting inflammatory pleural effusion can be seen, as well as the reduced diaphragmatic excursions.
- During the course, US may depict necrotic areas or abscess formations, but the more the lung is reventilated, the more LUS loses access and then is less valuable.

It is almost impossible to determine the causative organism by chest X-ray. Occasionally, when air space opacity is associated with pleural effusion or pneumatocele, a bacterial aetiology may be suggested, or when associated with metaphyseal bone lesions congenital syphilis may be suggested [23]. About 50% of infants who have group B beta Streptococcus pneumonia have radiographic findings indistinguishable from those of (I)RDS or TTN, and the presence of hyperinflation (before assisted ventilation), pleu-

ral effusion, and mild cardiomegaly (without cardiac anomalies) may suggest its diagnosis [24].

The transplacental route of infection (such as from TORCH, *Treponema pallidum*, *Mycobacterium tuberculosis*, *Listeria monocytogenes*) usually leads to a systemic disease with multi-organ involvement, and pneumonia may be a part of it.

- For example, neonates with an intrauterine cytomegalovirus (CMV) infection usually manifest with low birth weight, hepatosplenomegaly, and CNS involvement, but congenital CMV pneumonia is uncommon. When present, it shows diffuse reticulonodular opacities.
- *Mycobacterium tuberculosis* can be transmitted to the foetus either by transplacental route or by foetal ingestion or aspiration of infected amniotic fluid, so the primary focus may be found in the liver, the lung, or the GI-tract before systemic dissemination.
 - Pulmonary lesions are very common in congenital tuberculosis, detected in more than 90% of the cases, mainly with a miliary pattern, followed by consolidation. Other findings include multiple nodules (Fig. 10.18), bronchopneumonia, hilar adenopathy, and pleural effusion. Chest radiograph can be normal in early course of the disease.

Aspiration (see also above) is a common cause of neonatal pneumonia with a higher incidence in preterms and those with anomalies of the neurological system or the airways and/or digestive tracts.


 The radiographic findings of an aspiration pneumonia depend on the aspirated volume and chronicity, including a pulmonary oedema pattern, areas of consolidation with a gravity dependent distribution, or bronchopneumonic aspects with patchy air space opacities. Additionally, atelectasis and regional overinflation may be present.



Fig. 10.18 Congenital tuberculosis. A preterm neonate born from maternal active tuberculosis has been hospitalised and separated from her mother since birth with initial clear lungs. She then has pulmonary oedema and fever. After PDA ligation and improvement of pulmonary oedema, chest X-ray reveals extensive scattered pulmonary nodules in both lungs, proven to be pulmonary tuberculosis

10.5.6 Congenital Pulmonary Lymphangiectasia (CPL)

Congenital pulmonary lymphangiectasia is characterised by diffuse dilatation of pulmonary lymphatic channels in the subpleural, interlobar, and peribronchovascular interstitium. It may be found in isolation, associated with generalised lymphangiectasia, as a part of syndromes, or secondary to lymphatic or left-sided cardiac obstructive lesion. Most of them present shortly after birth with severe respiratory distress and cyanosis. Other cases may present with respiratory symptoms later during infancy. The gold standard for diagnosis of CPL is lung biopsy with histological and immune-histochemical studies.

Imaging modalities for CPL are chest radiography and CT or MRI, from which CT is preferred for suggesting the diagnosis. Lung US is less useful and if some pathology resembling the alveolo-interstitial syndrome is seen, rather unspecific.

- Chest X-ray usually shows hyperinflation, diffuse pulmonary opacities with coarse interstitial infiltrates, or peribronchovascular thickening—indistinguishable from interstitial pulmonary oedema also on LUS; this may change to a more perihilar interstitial pattern on follow-ups (Fig. 10.19a, b).
- Chest CT demonstrates diffuse thickening of the peribronchovascular interstitium and the

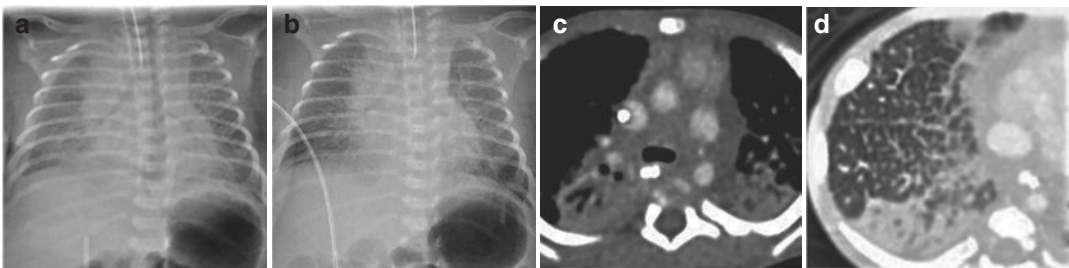


Fig. 10.19 (a–d) Congenital pulmonary lymphangiectasia. (a) Chest radiograph on the first day of life, pulmonary oedema with right pleural effusion is noted. (b) After conservative treatment, there is an improvement of pulmonary oedema within 24 h but still remained perihilar interstitial pattern. (c) Chest CT in mediastinal window

shows low-density infiltration within the mediastinum surrounding vascular structure and trachea at bifurcation level. (d) Chest CT in lung window shows thickening of interlobular septa in right basal lung. Dependent atelectasis is noted posteriorly

interlobular septa. In addition, diffuse infiltration in the mediastinum can be seen (Fig. 10.19c, d).

- Chest MRI also shows thickening of the interstitium in T1WI and high-signal material within the pulmonary interstitium in T2WI.
- Pleural effusion and atelectasis are also common findings.

The radiological findings in CPL may improve along with clinical features over time.

10.5.7 Air Space Diseases

10.5.7.1 Congenital Lobar Hyperinflation (CLH)

Congenital lobar hyperinflation, also known as congenital lobar overinflation and lobar emphysema, is defined as air trapping in a pulmonary lobe that causes pressure effects on adjacent organs or tissues. The disease can be detected antenatally by US or MRI.

The main aetiology is a defective cartilage of the bronchial wall, which then collapses during expiration. Other causes of CLH are bronchial stenosis, extrinsic bronchial compression by an aberrant vessel, a cyst, or a mass. However, the cause remains unknown (“idiopathic”) in many cases.

There is a rare disease called “polyalveolar lobe”, which is pathologically diagnosed by increased radial alveolar counts and increased alveolar numbers compared to those of age-matched patients; it can be with or without alveo-

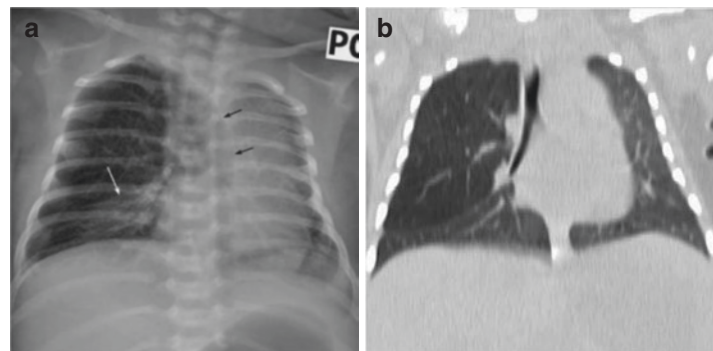
lar overdistension and provides the same radiographic findings as CLH.

About half of CLHs present within the first week of life, mostly with symptoms of respiratory distress because of progressive hyperinflation. The disease usually involves one lobe, but may be multilobar. The orders of lobar predilection with their percentages made easy to remember are left upper lobe (43%), right middle lobe (32%), right upper lobe (21%), and lower lobes (2% each) [25]. Associated findings are congenital heart disease (14–20%) and rarely pectus excavatum, hiatal hernia, diaphragmatic hernia, bronchial atresia, and tracheal bronchus.

Diagnosis can often be made from the chest radiograph and usually is confirmed by CT; LUS after birth is tricky and may only show an area with hyperinflation and reduced respiratory movement—with usually a sharp transition to the other lung surface.

- Early chest X-ray within a few hours or days of life may show focal mass-like opacity of water density from retained foetal lung fluid within the lesion, then gradually replaced by air.
- Follow-up chest radiographs or CT then show classical finding of the large hyperlucent lobe with attenuated vascular markings from reflex vasospasm (Figs. 10.4a and 10.20). The progressive lobar hyperinflation can cause atelectasis of adjacent lobes, contralateral shift of the mediastinum, and depression of ipsilateral diaphragm.
- Chest CT is usually the investigation of choice, not only to confirm the diagnosis, but

Fig. 10.20 (a, b) Congenital lobar hyperinflation. (a) Chest radiograph of a newborn shows a large hyperlucent right upper lobe herniating to the left (black arrows) with attenuated vascular markings, and causing partial atelectasis of right lower lung (white arrow). (b) Chest CT in coronal plane, air trapping in right upper lobe is confirmed without demonstrable cause of obstruction



also to detect extrinsic compression on the bronchus by a mass or cyst or aberrant vessel, other associated abnormalities, and determine the boundaries of normal lung for surgical planning.

Surgical resection is required in severe or progressive symptomatic cases. However, conservative treatment options have increased for patients with mild to moderate symptoms but require a close follow-up.

10.5.7.2 Bronchial Atresia

Bronchial atresia can be divided by the location of atresia into central and peripheral types.

- The central type, involving proximal main-stem or lobar bronchus, is rare and mostly lethal in utero or early after birth from very large size of the affected lobe with significant pressure effect on the adjacent lung and cardiovascular structure. It will not be discussed further.
- The peripheral type has atresia at segmental or subsegmental bronchus, and may be further subdivided into an isolated lesion or being a part of a combined lung malformation, particular with type 2 CPAM, pulmonary sequestration and its hybrids.
- Isolated peripheral bronchial atresia is more common in upper lobes, frequently in apico-

posterior segment of left upper lobe, usually asymptomatic and incidentally detected in young adults.

Chest radiograph may show pulmonary abnormalities, however, (peripheral) bronchial atresia is usually diagnosed by CT scan.

- Characteristic imaging findings of bronchial atresia include a hyperinflated lung segment and a mucocele in the central axis of the affected segment.
- If imaging is done early in life, the distal involved segment may be still opaque from retained lung fluid (Fig. 10.21a). Then it will be gradually filled with air within days or weeks. Air can reach the affected segment from adjacent normal segment by collateral ventilation, but is difficult to exit. Then the affected segment becomes hyperinflated and has attenuated vascular markings (from reflex vasoconstriction due to hypercapnia). The bronchus just distal to atretic site is focally dilated and may be filled with air or impacted mucous (termed mucocele) (Fig. 10.21b, c).
- The chest radiograph can be normal in neonates with isolated bronchial atresia, as hyperinflation may be mild, and the mucocele is small or still not formed. The mucocele will develop progressively in months. When bron-

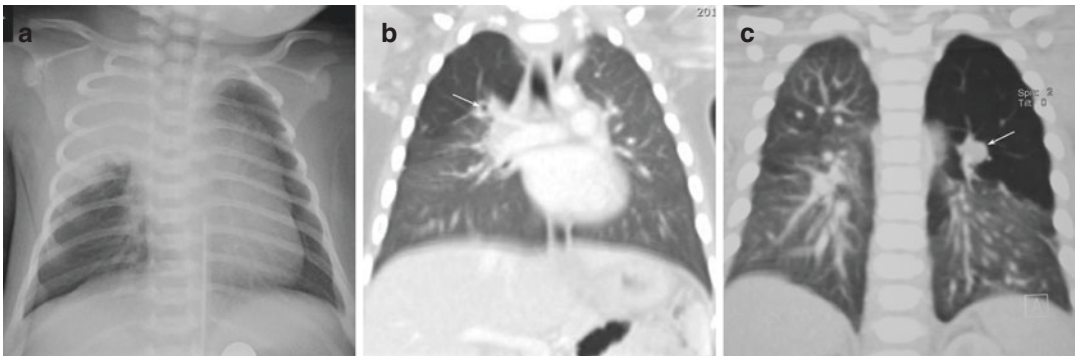


Fig. 10.21 (a–c) Bronchial atresia/occlusion. (a) A term neonate has a consolidation in right upper lobe on the first day of life. (b) Same patient as in (a), chest CT at 7-month-old shows hyperinflated apical segment of right upper lobe with attenuated lung markings and an air-filled dilated bronchus (arrow) near right superior pulmonary

artery. (c) Chest CT in another infant of 8-month-old shows hyperinflated apicoposterior segment of left upper lobe with attenuated lung markings and a mucous-filled dilated bronchus (arrow) in the central axis of the segment

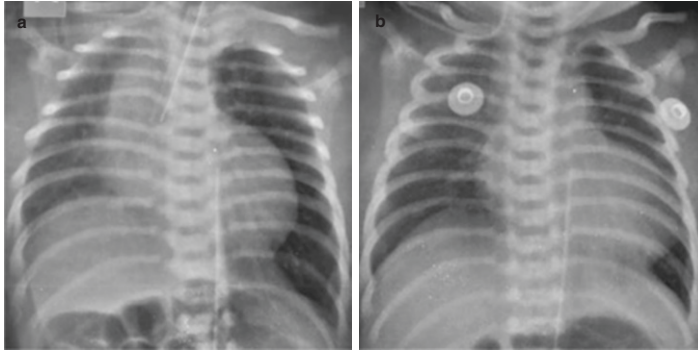


Fig. 10.22 (a, b) Air trapping in left lung from intubation in right main bronchus. A 4-day-old girl with a recent right modified Blalock-Taussig shunt. (a) The tip of ET tube is noted in right main bronchus, but relatively larger volume and hyperlucency of the left lung with mediastinal shift to the right. The findings are suggestive of air trap-

ping in the left lung—probably from partial obstruction at the origin of left main bronchus by the ET tube. (b) Same patient as in (a), after removal of ET tube on the following day, there is symmetrical inflation and density of both lungs

chial atresia is a part of a combined lung malformation, findings of bronchial atresia in chest radiographs are mostly obscured by other abnormalities.

- Chest CT is the investigation of choice for diagnosis of bronchial atresia for better depiction of the mucocele which is a non-enhanced structure with nodular or tubular or branching tubular shape at the medial side of the hyperinflated segment either in isolated case or in the combined malformation.

Treatment of bronchial atresia is still under discussion. Most physicians prefer conservative treatment unless patients become symptomatic or there is evidence of lesion progression. However, some prefer prophylactic surgical resection for preventing complications.

10.5.7.3 Other Causes of Pulmonary Hyperinflation in One Lung

The most common cause of pulmonary hyperinflation in one lung is selected (accidental) single lung intubation. The other causes are lesions that can cause check-valve obstruction at the main bronchus. There are many causes: an extrinsic mass, a cyst or an aberrant vessel in the mediastinum, a weak cartilage of the main bronchus (bronchomalacia), an endobronchial lesion such as a foreign body (mostly iatrogenic from a fragment of suction

catheter or intubation stylet or after aspiration), an endobronchial tumour (very rare, particularly in neonates), a single lung intubation on the contralateral side (Fig. 10.22), and the *acquired lobar hyperinflation* (ALH) in BPD (Fig. 10.23).

- Acquired lobar hyperinflation in BPD usually affects the right middle and/or right lower lobes, likely caused by bronchial trauma due to frequent endobronchial suction, then forming inflammatory granuloma/polyps.

10.5.8 Cystic Pulmonary Lesions

10.5.8.1 Pulmonary Bronchogenic Cyst

Bronchogenic cysts arise from aberrant bronchial budding, mostly located in middle mediastinum. About 10–20% of bronchogenic cysts are found in the lung, manifesting as an isolated air-filled thin-walled cyst with or without air-fluid level or a nodular lesion (fluid-filled cyst) on a chest radiograph.

- Except for prenatal detection by LUS, pulmonary bronchogenic cyst usually presents later in childhood or early adulthood either incidentally or from its mass effect or complications (most commonly infection).

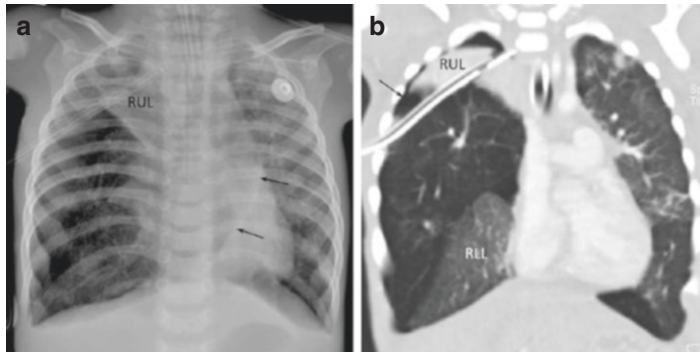


Fig. 10.23 (a, b) Acquired lobar hyperinflation of right middle lobe. An 8-month-old infant with BPD presents with a right pneumothorax, treated with ICD tube placement. (a) On chest radiograph, there are hyperinflation of right middle lobe with herniation to the left (arrows) and

complete atelectasis of right upper lobe (RUL). (b) Chest CT confirms air trapping in right middle lobe with vascular attenuation, complete atelectasis of right upper lobe, hypoinflation of right lower lobe (RLL), and small amount of right pneumothorax (arrow)

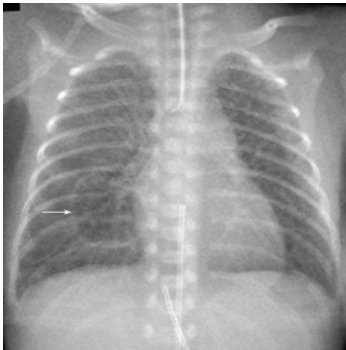


Fig. 10.24 Localised pulmonary interstitial emphysema (PIE). In a preterm neonate from 25 weeks' gestation at age of 3-day-old, a large localised thin-wall cyst of PIE develops in right lower lung (arrow), and a few small round PIE in left upper lobe

Thus, often the final diagnosis is established by CT.

10.5.8.2 Localised Pulmonary Interstitial Emphysema (PIE)

Pulmonary interstitial emphysema is an air leak phenomenon from barotrauma. It is much more common to be diffuse rather than localised.

- When PIE is localised, it can mimic CPAM or a pulmonary bronchogenic cyst (Fig. 10.24).

A review of prior chest radiographs of not having cystic pulmonary lesion (either lucent or opaque) and decrease in size on follow-up suggests the correct diagnosis of localised PIE, however, some localised PIE may persist for months.

10.5.8.3 Congenital Pulmonary Airway Malformation (CPAM) and Hybrid Lesion

Congenital pulmonary airway malformation, formerly known as congenital cystic adenomatoid malformation (CCAM), is abnormal lung tissue, mostly multicystic, probably generated by maldevelopment of the foetal airway with bronchial obstruction, atresia, or peristaltic abnormality. It is the most common congenital lung malformation, and accounts for the majority of congenital cystic lung diseases.

Most of CPAMs are now detected and diagnosed prenatally.

Congenital pulmonary airway malformation has a spectrum of clinical presentation, relating to type and size of the lesion, associated anomaly and complication.

- The most commonly used classification of CPAM is the modified pathological classifica-

tion by Stocker subdividing CPAMs into five types (type 0 to type 4) [26].

- Type 0 has bilateral acinar dysgenesis or dysplasia which has a solid appearance on radiography and gross specimen. Type 0 is incompatible with life.
- Type 1 is a large-(multi)cystic lesion, more than 2.0 cm of at least one cyst, frequently symptomatic at birth.
- Type 2 is a small-multicystic lesion, 0.5–2.0 cm range of each cyst, mostly asymptomatic at birth. The “hybrid lesion” of type 2 CPAM and pulmonary sequestration is well recognised. Type 2 CPAM is found in the spectrum related to the “bronchial atresia sequence”, ranging from classic histologic type 2 CPAM on one side to congenital lobar hyperinflation on the other side [27]. More type 2 CPAMs are detected prenatally.
- Type 3 is adenomatoid lesion, showing solid appearance on gross and imaging findings. This type is relatively rare.
- Type 4 is a large alveolar cyst that has a strong association with the cystic type of pleuropulmonary blastoma.
- Radiographic classification usually uses only type 1–3 (large cyst, small cyst, solid type). Both type 1 and type 4 usually have large cysts with overlapping size.
- Complications of CPAM are infection and development of malignancy. Besides the cystic type of the pleuropulmonary blastoma in type 4 CPAM, there is also a concern of an association with a mucinous adenocarcinoma in type 1 CPAM.

Neonates with CPAMs usually receive a chest radiograph followed by a LUS in the early postnatal setting when the cyst(s) still contain foetal lung fluid.

Follow-up depends on the initial findings and usually requires chest radiographs.

- On initial chest radiograph, cystic CPAMs may be fluid-filled and will present with a focal area of increased pulmonary opacity

(Fig. 10.6b)—these are also assessable by LUS. When fluid has been replaced by air, the follow-up chest radiograph will show hyperlucent area with multicystic appearance (Figs. 10.4b, 10.25, and 10.26). Smaller CPAMs that detected in prenatal US are frequently not well detected by chest radiographs. The symptomatic CPAMs at birth are usually large and have pressure effect on adjacent structures.

- Type 3 has solid appearance on imaging and is also suited for LUS.
- The final work-up is achieved by contrast-enhanced CT, which is the imaging of choice for CPAM and can provide detailed information to confirm the presence of the lesion, differentiate it from other congenital malformation, delineate the extent of lobar or segmental involvement, measure the size of the cyst(s), detect coexisting lesions, and evaluate its vascular supply for therapeutic management.
 - However, CT cannot differentiate between cystic pleuropulmonary blastoma and the large cyst CPAM. Even though, one may try suggesting the possibility of type 4 CPAM when finding a peripheral lung cyst larger than 7.9 cm with mediastinal shift and pneumothorax [28].
 - A review of prenatal US is helpful. As lung tumours are usually not detected by foetal US on a mid-second trimester scan, any cystic lesion detected postnatally with a negative prenatal US result should raise a concern of the cystic type of pleuropulmonary blastoma [29].
- Increasingly, also lung MRI is being advocated.

TIPP To perform CT in cases of suspected CPAM that locates in the lower lobe, there is a necessity to differentiate it from a possible hybrid lesion by identifying a systemic arterial supply which may arise from the abdominal aorta or its branch. Therefore, the lowermost end of the scan range should be extended to level of lower L2 body to include the origin of renal artery, and the

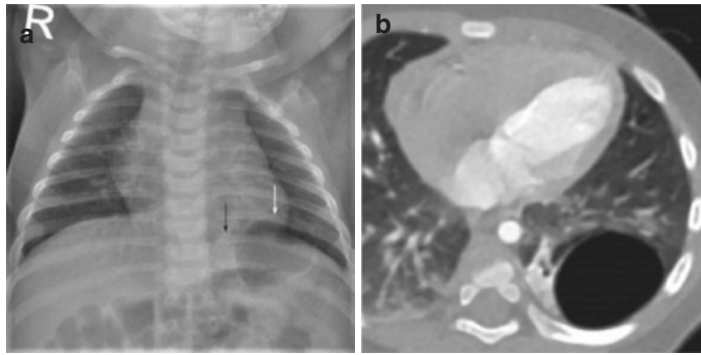


Fig. 10.25 (a, b) Congenital pulmonary airway malformation, type 1. (a) Chest radiograph of a young infant shows a 3-cm thin-walled cyst at left lung base (white arrow) with adjacent small patchy opacity (black arrow)

between the cyst and the spine. (b) Chest CT for preoperative planning is performed at age of 4 months. The study confirms lung cyst with adjacent consolidation

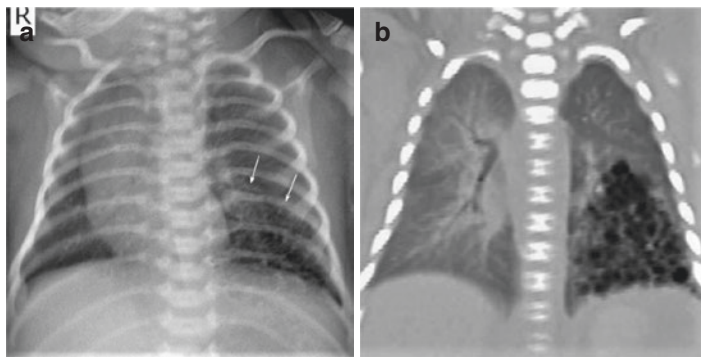


Fig. 10.26 (a, b) Congenital pulmonary airway malformation, type 2. Same patient as in Fig. 10.6b. (a) Chest radiograph at age of 7 days reveals pulmonary hyperlucency with internal several curvilinear walls of multiple

small cysts at left lower lung (arrows), and contralateral mediastinal shift. (b) Chest CT in coronal image confirms multiple small cysts about the same size in LLL

uppermost end should include the subclavian artery.

- The appropriate age to perform the first chest CT depends on severity of symptoms and treatment planning. Severely symptomatic CPAM at birth requires an emergency CT after respiratory stabilisation because the affected neonate may require an early operation.

Treatment of asymptomatic CPAM is controversial with different clinical practices,

mostly elective surgery is performed between the age of 6 months to 1 year or up to 2 years, and then the first preoperative CT examination is usually around the age of 1–6 months. There is a trend to have an earlier elective surgery for asymptomatic CPAMs, proposed at 3–6 months of age—before developing complication [30]. Thus the imaging strategy is also changing—a relatively early CT to establish the diagnosis, and another one preoperatively; no intermittent follow-CTs are then done for radiation protection.

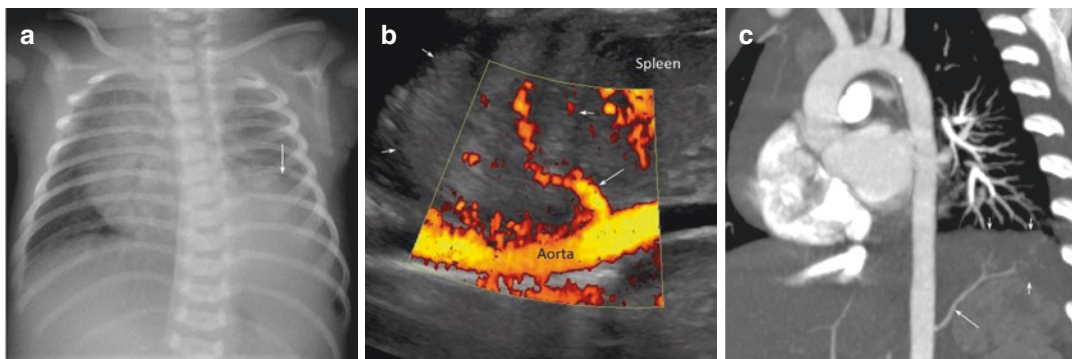
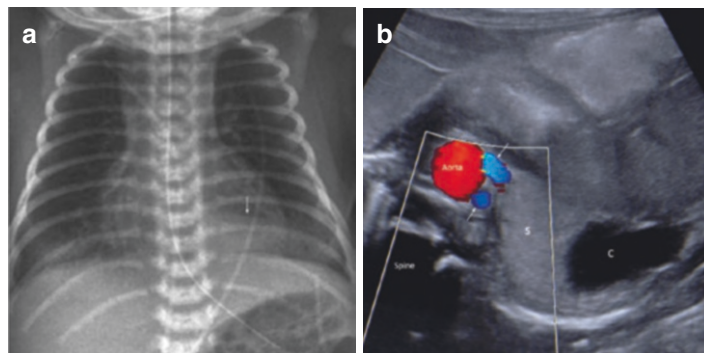


Fig. 10.28 (a–c) Extralobar pulmonary sequestration (ELS). (a) Chest radiograph of a term newborn on the first day of life, there is a large mass with a well-defined upper border (arrow) in lower half of left lung with small amount of pleural effusion. (b) Chest US on power mode reveals a (sequestered) lobar consolidation (short arrows) with-

out air bronchogram. Its feeding artery (long arrow) arises from the aorta just below the diaphragm. (c) Thoracic CTA at age of 11-month-old for preoperative planning, the thick-slab MIP demonstrates an arterial branch (long arrow) from abdominal aorta to the sequestered lung (short arrows)

Fig. 10.29 (a, b) The hybrid lesion. (a) Chest radiograph reveals a retrocardiac consolidation or mass with partially sharp upper margin (arrow). (b) Chest US in transverse plane detects the solid (s) and cystic (c) components of the mass with a pair of vessels (upper and lower arrows)



effusion may be detected and can be massive, probably caused by venous obstruction.

- Lung US shows a consolidated, medium echogenic lung, rarely with some cystic areas. CDS will reveal its arterial supply originating from the systemic circulation (Figs. 10.28b and 10.29b), and may demonstrate its (systemic) venous drainage that usually does not exhibit the flow direction of a pulmonary vein.
- Thoracic CTA with post-processing of MPR, 2D- or 3D-MIP, and 3D-volume rendering is usually required for a preoperative roadmap for surgical planning and detection of associated other malformations in the rest of the lung and the mediastinum (Fig. 10.28c).
- Thoracic MRI with MRA can be an alternative, but is not as good as CT for the detection of cystic lung lesion, if associated.

Please note that not all congenital systemic-artery-supplied lungs are considered sequestration. There can be an isolated aberrant systemic arterial branch to supply normal lung tissue which has a normal communication with the bronchial tree. Some cases of pulmonary venolobar (Scimitar) syndrome may have a systemic arterial supply, but most of them are not sequestered lungs.

Extralobar sequestration is treated with surgical resection; however, some recommend follow-up in asymptomatic patients as infection is not common. The patients' age considered appropriate for elective surgery may vary among hospitals. Timing and number(s) of preoperative CT (or MRIs) scan should be carefully planned with consensus among paediatricians, paediatric surgeons, and radiologists to lower the risk from ionising radiation; optimally the CT (or MRI) is

only performed in the preoperative phase avoiding multiple follow-up exams—provided the diagnosis is clear and US can be used to monitor the condition till surgery.

10.5.9.2 Fluid-Filled Congenital Cystic Pulmonary Lesions

During early neonatal life, cystic pulmonary lesions (e.g. CPAM) and the lung distal to proximal airway obstruction (e.g. CLH, bronchial atresia) as well as herniated bowel loops (congenital diaphragmatic hernia) may be fluid-filled and look opaque with pressure effect on initial chest X-ray (Figs. 10.6b and 10.21a). Ultrasound can be used to detect its fluid nature. Fluid will then be replaced with air in the following radiographs and provide typical patterns of those diseases.

10.5.9.3 Lung Tumours and other Solid Appearing Masses

Lung tumours in neonates and infants are rare. Primary lung tumours in this age group include the pleuropulmonary blastoma of the cystic type, the foetal interstitial lung tumour, the infantile fibrosarcoma, and the congenital peribronchial myofibroblastic tumour. Unlike congenital malformations, these lung tumours are usually not detected by US on a mid-second trimester scan which is an important suggestive clue when detected postnatally [29]. Among the solid lung tumours, the foetal interstitial lung tumour has characteristic uniformly low density on CT [33], and the congenital peribronchial myofibroblastic tumour has a peribronchial distribution [34]. Pulmonary metastasis is rare in the neonatal period but may occur in neonates with congenital solid malignancies (e.g. neuroblastoma).

Other differential diagnoses of a pulmonary solid-appearing mass in neonates include CPAM type 3, an infection, and vascular malformations. Chest radiographs of fungal infection, particular invasive aspergillosis in chronic granulomatous disease, can present with mass-like lung lesions in the first few months of life. Pulmonary arteriovenous malformations may be detected incidentally in early life, but usually produces symptoms in older children or adults.

10.5.10 Pulmonary Agenesis/Aplasia Hypoplasia and Related/Similar Conditions

10.5.10.1 Pulmonary Agenesis/Aplasia

Pulmonary agenesis and aplasia result from a developmental arrest of the primitive lung which is more common unilateral or unilobar, and rarely bilateral (then is incompatible with extrauterine life). Complete absence of the lung tissue, vascular supply, and bronchial tree are the characters of pulmonary agenesis, while pulmonary aplasia shows the same findings except for the presence of a rudimentary bronchus. Unilateral pulmonary agenesis or aplasia is frequently (about 75%) associated with other bronchopulmonary foregut malformations (such as tracheal stenosis, oesophageal atresia with/without fistula, bronchogenic cyst), and malformations of the cardiovascular, genitourinary, and musculoskeletal systems.



In the chest radiograph of a unilateral pulmonary agenesis or aplasia, the affected hemithorax is opaque and occupied by the shifted heart and mediastinum with narrowed rib spacing (Fig. 10.6a). The contralateral lung is enlarged and herniated to the empty lung side.

- Further imaging studies, with US or CT or MRI, can be used to differentiate between atelectasis and pulmonary absence by identifying the collapsed lung parenchyma and presence of the ipsilateral pulmonary artery.
- Chest CT/MRI can also differentiate pulmonary aplasia from agenesis by demonstration of a rudimentary bronchus (Fig. 10.30); however, this does not affect the treatment or the prognosis.

10.5.10.2 Pulmonary Hypoplasia

Pulmonary hypoplasia is characterised by a decrease in number of alveoli and distal bronchi.

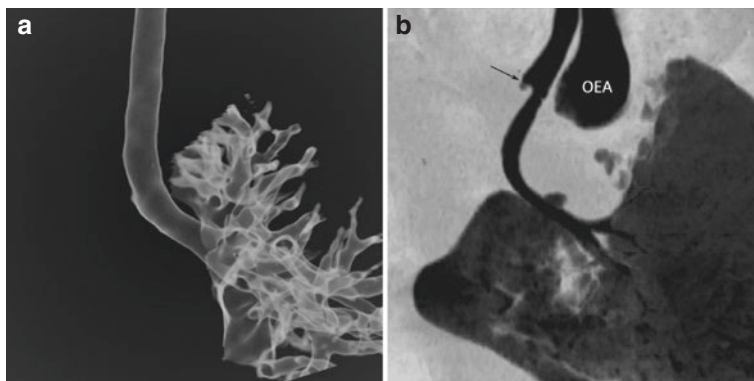


Fig. 10.30 (a, b) Pulmonary agenesis/aplasia. (a) Pulmonary agenesis. CT virtual bronchography reveals completely absence of the right main bronchus. (b) Pulmonary aplasia.

Minimal intensity projection shows rudimentary right main bronchus (arrow) of pulmonary aplasia and dilated blind pouch of oesophageal atresia (OEA)

In addition, the pulmonary artery and bronchi are smaller on the affected side. The aetiology of pulmonary hypoplasia is suggested to be from the imbalance of foetal lung fluid and amniotic fluid volume. Most cases of pulmonary hypoplasia are secondary to inadequate thoracic space for foetal lung expansion (such as congenital diaphragmatic hernia, skeletal dysplasia with a narrow thoracic cage, severe renal disease with oligohydramnios, or PROM at 15–28 weeks' gestation), while only few cases are primary (or isolated) conditions.

Foetal US or MRI are able to diagnose and assess the degree of lung hypoplasia. One or both lung(s) may be affected. When pulmonary hypoplasia is bilateral and severe, respiratory distress is marked at birth, whereas neonates with primary unilateral lung hypoplasia may be asymptomatic.

The chest radiographic findings of pulmonary hypoplasia depend on the underlying cause and the degree of hypoplasia.

- Typically, unilateral pulmonary hypoplasia shows asymmetrical small lung volume with normal or increased opacity on the affected side with ipsilateral shift of the heart, mediastinum, and the diaphragm (Figs. 10.31 and 10.32). The apparently increased opacity of pulmonary hypoplasia is explained by summation of soft tissue density from ipsilateral mediastinal shift.



Fig. 10.31 Pulmonary hypoplasia secondary to congenital diaphragmatic hernia. Several months after surgical repair of left Bochdalek hernia, there is relatively small size of the left lung and left pulmonary vessels

- Pulmonary vascularity in the hypoplastic lung is decreased.
- Bilateral pulmonary hypoplasia will show bilateral small lung volume; however, this is more difficult to diagnose because it may mimic an expiratory exposure.

Known complications of pulmonary hypoplasia are pneumothorax and pulmonary hypertension.

10.5.10.3 Scimitar Syndrome or Pulmonary Venolobar Syndrome

When a scimitar sign is detected in a chest radiograph that shows unilateral pulmonary

hypoplasia, usually on the right side, scimitar syndrome (pulmonary venolobar syndrome) is considered.

- The “scimitar sign” is the curve shadow of the partial anomalous pulmonary vein parallel to the heart in a downward direction to drain into the inferior vena cava (less common to right atrium, hepatic vein, or portal vein) giving a picture of a Turkish sword (a “scimitar”) in the right lower median lung.
- Ultrasound may show the aberrant vein, but CT or MRI is commonly used to confirm the diagnosis (Fig. 10.32b) and for surgical planning in symptomatic patient (suffering from significant left-to-right shunt).

As most of the patients with a scimitar syndrome are asymptomatic, the syndrome is usually not reported in infants, unless incidentally detected, e.g. during investigating clinically significant other anomalies.


- Associated anomalies in Scimitar syndrome are congenital heart disease, an accessory diaphragm, eventration of the diaphragm, a horseshoe lung, the systemic arterial supply to the hypoplastic lung with or without pulmo-

nary sequestration, and the absence of one pulmonary artery.

10.5.10.4 Atelectasis

Atelectasis is detected on chest radiograph as area of homogeneous opacity.

- Significant volume loss can be demonstrated when there is a collapse of pulmonary lobe(s), but not seen in segmental or subsegmental atelectasis. Signs of significant volume loss are displacement of fissure, ipsilateral mediastinal shift, and elevation of ipsilateral diaphragm.

 Neonates are prone to atelectasis and dystelectasis due to the yet immature pulmonary anatomic architecture; thus, often particularly US or CT/MRI shows surprisingly large a-/dystelectatic dependent lung spaces (e.g. when sedated for an MRI study) without any other cause. Don't overcall these findings—they mostly resolve by itself spontaneously.

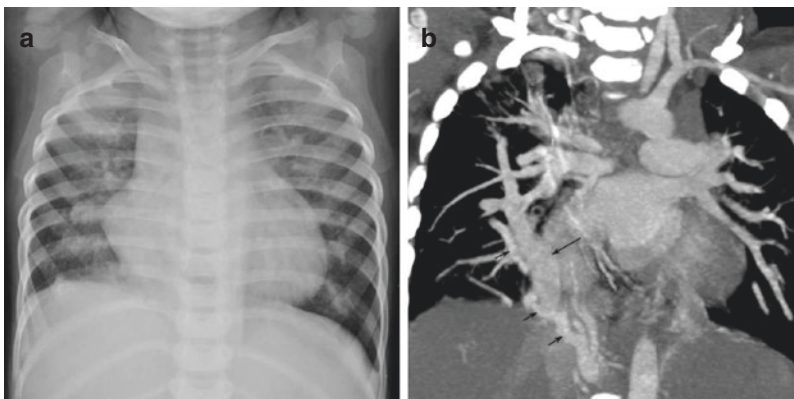


Fig. 10.32 (a, b) Scimitar syndrome. (a) Chest radiograph shows a relatively small-sized right lung with ipsilateral shift of the mediastinum, indicating right pulmonary hypoplasia. Cardiomegaly and pulmonary

congestion are noted. (b) Coronal CTA in MIP reveals a large vertical (scimitar) vein (long arrow) of the right lung draining to inferior vena cava. Right lower lung is partially fed by a branch from celiac artery (short arrows)

10.6 Pleural Abnormalities

10.6.1 Neonatal Pleural Effusion

Neonatal pleural effusions are found in chylothorax, hydrops foetalis, congestive heart failure, as parapneumonic effusion, or as an iatrogenic extravasation from central line placement or dislodgement.

Chest radiographs and/or US are commonly used to detect, assess the amount of, and evaluate for free or loculated pleural effusion, but unable to differentiate whether the effusion is a transudate, an exudate, chyle, or blood. A pleural effusion situates at the dependent posterior part in supine position and causes increased opacity of the ipsilateral hemithorax. Fluid may curve along the lateral and other sides of the hemithorax or insinuate within the fissures. Decubitus views can be used to confirm the presence of a pleural effusion, but US is the method of choice and very sensitive.

- Septations within a pleural effusion can be optimally detected by US and in general do not require a CT scan, which is even less sensitive than US for this particular query.

For follow-up of effusions particularly on US, a standardised patient position is helpful to avoid redistribution of the fluid then mimicking pseudo-improvement or pseudo-deterioration.

10.6.2 Other Pleural Pathologies

Pleural thickening or a pleural mass, either caused by infection/inflammation or tumour, is frequently associated with a pleural effusion, and better revealed by US than by chest radiographs. If the thickening is irregular, nodular, or bulky, a pleural tumour should be considered, even it is very rare in neonates and infants.

Pleural masses in paediatrics are mostly secondary from either mediastinal or chest wall malignancies with direct pleural invasion or distant metastasis (such as from Wilms

tumour, neuroblastoma, sarcoma, etc.). Primary paediatric pleural tumours are very rare (e.g. lipoma, mesothelioma, teratoma). CT or MRI should be the next investigation after US detection/verification of any unexplained pleural mass.

10.7 Air Leaks

10.7.1 Pulmonary Interstitial Emphysema (PIE)

Pulmonary interstitial emphysema is the presence of air in the pulmonary interstitium. It occurs from rupture of respiratory epithelium, mostly by barotrauma, and may lead to pneumothorax, pneumomediastinum, or pneumopericardium.

Pulmonary interstitial emphysema on chest radiographs typically show multiple small round bubbles in both lungs (Fig. 10.3a), or may have linear, non-branching lucent structures that do not conform to the shape of air bronchogram.

- Occasionally, PIE can be unilateral, unilobar, or localised (Figs. 10.4c and 10.24).
- When PIE is localised, it can look like CPAM.
 - Prior chest radiographs of not having cystic pulmonary lesion (either lucent or opaque) and/or decrease in size when follow-up suggest the correct diagnosis of localised PIE; however, some localised PIE may persist for months.

Most cases of PIE are found in preterm neonates with (I)RDS having mechanical ventilation. The lung after surfactant therapy may have bronchiolar distension that mimics findings of PIE. In such cases, the clinical scenario of improvement of respiratory distress after surfactant therapy opposes the diagnosis of PIE as these patients usually have a deteriorating clinical condition. Another differential diagnosis of PIE is bronchopulmonary dysplasia (BPD) which may have small cystic changes, but this usually occurs later (beyond 10 days of life/treatment) while PIE usually occurs within the first week of life.

10.7.2 Pneumothorax

Pneumothorax in neonates has a significant morbidity and mortality. It is frequently the result of barotrauma. Diseases or conditions with increased risk of developing a pneumothorax are (I)RDS, MAS, pulmonary hypoplasia, and infants who need resuscitation at birth.

Chest radiography is the most commonly used modality to diagnose or confirm pneumothorax in neonates; however, sometimes findings of pneumothorax are not obvious when the pleural line is imperceptible and thus the chest film cannot “rule out” a (small) pneumothorax.



Pneumothorax locates anteriorly to the lung in supine position and causes increased radiolucency on that side, which may be mimicked on a radiograph taken in an oblique patient position.

- The costophrenic sulcus may be more lucent giving the “deep sulcus” sign (Fig. 10.33a).
- Predominant medial (Fig. 10.33a, b) or basal (Fig. 10.33c) pneumothorax is not uncommon in neonatal period, showing as a lucent band with relatively sharper mediastinal or diaphragmatic border.
- The pressure effects from pneumothorax may cause an ipsilateral compressive atelectasis and downward displacement of the diaphragm, and a contralateral mediastinal shift.
- The depiction of the anterior junctional line in neonates indicates bilateral pneumothoraces [35].

There has been increasing use of LUS for the diagnosis of pneumothorax in paediatrics including the neonatal period as a bedside modality—mostly performed by clinicians. Lung US is proven to have very high sensitivity and specificity, even better than chest X-ray.

- The US findings of pneumothorax are absent “lung sliding”, absence of “B-lines”, and the presence of the “lung point” sign on real-time B-mode (Table 10.2).
- In M-mode US, the “stratosphere (or barcode)” sign is present as well as the “lung point” sign (Fig. 10.34).

10.7.3 Pneumomediastinum

A pneumomediastinum in neonates occurs more commonly with assisted ventilation, however, it may occur spontaneously or rarely from trauma of the trachea or oesophagus; the clinical symptoms are very variable.

A pneumomediastinum on a neonatal chest radiograph shows the characteristic elevation of the thymus from the heart (Fig. 10.35a), named “angel wing” or “spinnaker” sign.

A pneumomediastinum in the lower aspect of the mediastinum produces the “continuous diaphragm” sign (Fig. 10.35b). The mediastinal line is usually not perceptible.

Mediastinal air may track upwards to the neck or downwards to the abdominal intra- or retroperitoneum.

In rare occasion, pneumomediastinum can be under tension and then requires drainage.

10.7.4 Pneumopericardium

The pericardial space is the least likely location of air leak. When detected, it is usually in the postoperative period after cardiac surgery; however, it can be found in non-surgical neonates receiving pressure ventilation support.



On chest radiographs, air surrounds the cardiac shadow with the pericardial recess being the upper limit at level of the ascending aorta and the pulmonary trunk (Fig. 10.36).

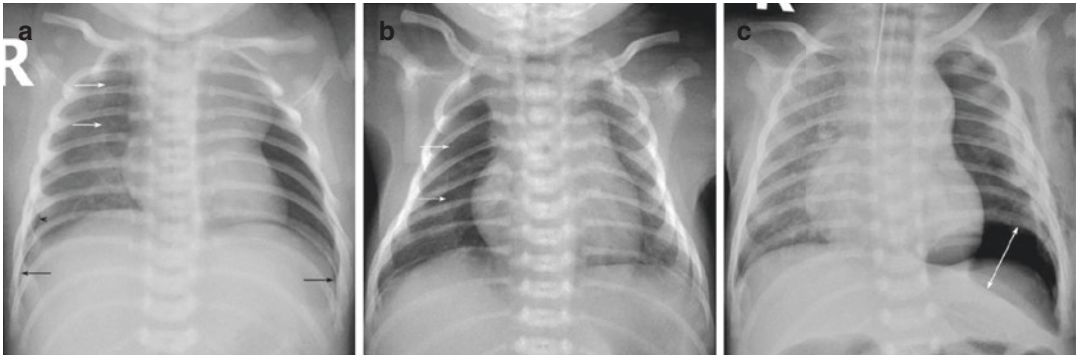


Fig. 10.33 (a–c) Pneumothorax. (a) Left pneumothorax with hyperlucent left lung with “deep sulcus” sign (black arrow). Right pneumothorax with deep sulcus sign (black arrow), displacement of pleural line (arrowhead), and medial

pneumothorax (white arrows). (b) Right medial pneumothorax (arrows). (c) Left basal pneumothorax (double-headed arrow), status post left lateral thoracotomy for PDA ligation

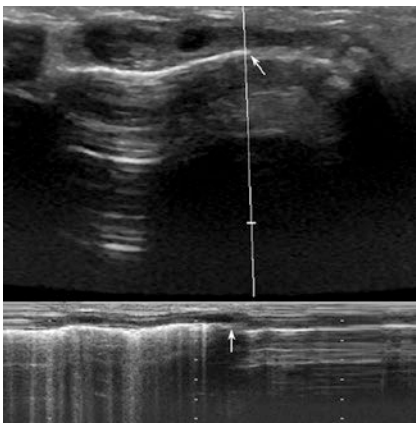


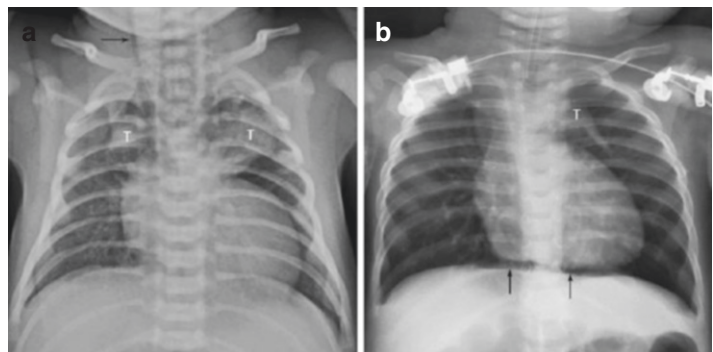
Fig. 10.34 “Lung point” sign in pneumothorax. Motion-mode image is obtained at the site of “lung point” in B-mode (upper arrow). The ventilated lung is firstly detected on the M-mode graph showing seashore sign of the pleural line with alveolo-interstitial lung pattern from moving of B-line. Then there is a sudden change of the graph (lower arrow) to a more barcode pattern of pneumothorax

10.8 Tracheal Abnormalities

Tracheal lesions in neonates include abnormal tracheobronchial branching, compromised tracheal lumen, and tracheo-oesophageal fistula (TOEF). Imaging depends on the clinical symptoms and potentially associated finding.

Imaging of stridor usually starts with both an AP and a lateral view of the chest and the neck, sometimes these are taken with a contrast filled oesophagus to depict oesophageal impressions caused by a potential vascular ring. In these situations, US can provide information of the large vessels using a mediastinal approach. Neonates with suspected tracheal narrowing usually require further investigation by oesophagogram, airway fluoroscopy, tracheoscopy, CT, or MRI. Isolated TOEF (or H-type TOEF) is diagnosed by oesophagography, where a meticulous technique is of

Fig. 10.35 (a, b) Pneumomediastinum. (a) “Angel wing” or “spinnaker” sign. Air density is noted between elevated thymic lobes (T) and cardiac shadow. Note also upward extension of air into right side of the neck (arrow). (b) “Continuous diaphragm” sign. Air is noted between the heart and the diaphragm (arrows). Atrophic left thymic lobe (T) is elevated



utmost importance (tube in oesophagus, strict lateral and oblique views, full distension of oesophagus by the contrast bolus, possibly in prone position ...).

- A frontal radiograph of the large airway with high kV and filtered technique provides a better delineation of the pharynx, larynx, trachea, and the main bronchi.
- An oesophagogram is useful in suspicion of a H-type TOEF or a vascular ring and sling.
- Thoracic CT shows tracheobronchial and vascular abnormalities on multiplanar reformation (MPR), minimal and maximal intensity projection (minIP and MIP), 3D volume rendering technique (VRT), and virtual bronchography, including detection of mediastinal and/or pulmonary lesion.



Fig. 10.36 Pneumopericardium. Air is noted in pericardial space with visible line of pericardium plus mediastinal pleura (arrows). The upper limit is at the level of ascending aorta and the pulmonary trunk. Right and left thymic lobes (T) are elevated

- Thoracic MRI has a definite role in characterising a vascular ring or a pulmonary sling.
- Fluoroscopy, cine CT, and respiratory-gated MRI allow visualisation of caliber change of tracheobronchial tree during respiration.

10.8.1 Abnormal Tracheobronchial Branching

Abnormalities of tracheobronchial branching may be a normal variation or part of complex congenital anomaly (Fig. 10.37).

- A **tracheal bronchus** is an anatomic variant with a bronchus to the upper lobe arising from the trachea, predominantly on the right side. It can be a lobar or segmental bronchus, and a displaced or supernumerary one. A few patients with this condition present with recurrent upper lobe pneumonia; however, most patients are asymptomatic and the tracheal bronchus is detected incidentally (Fig. 10.38a, b).
- Symmetrical bronchial branching with a **bilateral epi-arterial** or **hypo-arterial bronchus** is observed in situs ambiguous. In right isomerism, patients have bilateral tri-lobed lungs with bronchi to both upper lobes arising early and above the pulmonary arteries (epi-arterial bronchus). In left isomerism, both lungs have two lobes with the upper lobe bronchi arising later and below pulmonary arteries (hypo-arterial bronchus) (Fig. 10.38c, d).
- A **bridging bronchus** is an aberrant bronchial branching of the right lower lobe or intermedi-

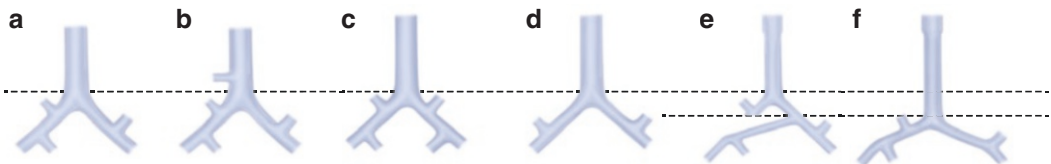


Fig. 10.37 (a–f) Diagram of normal and abnormal bronchial branching patterns. (a) Normal bronchial branching pattern. (b) Tracheal bronchus. (c) Bilateral epi-arterial bronchus, pattern of bilateral tri-lobed lung. (d) Bilateral hypo-arterial bronchus, pattern of bilateral bi-lobed lung. (e) Bridging bronchus type A, having two carina—the

upper carina at T4–5 level and the lower one at T5–6 level with wide lower carinal angle, and association with long tracheobronchial stenosis. (f) Bridging bronchus type B, having a single low carina at T5–6 level, and associated with long tracheobronchial stenosis

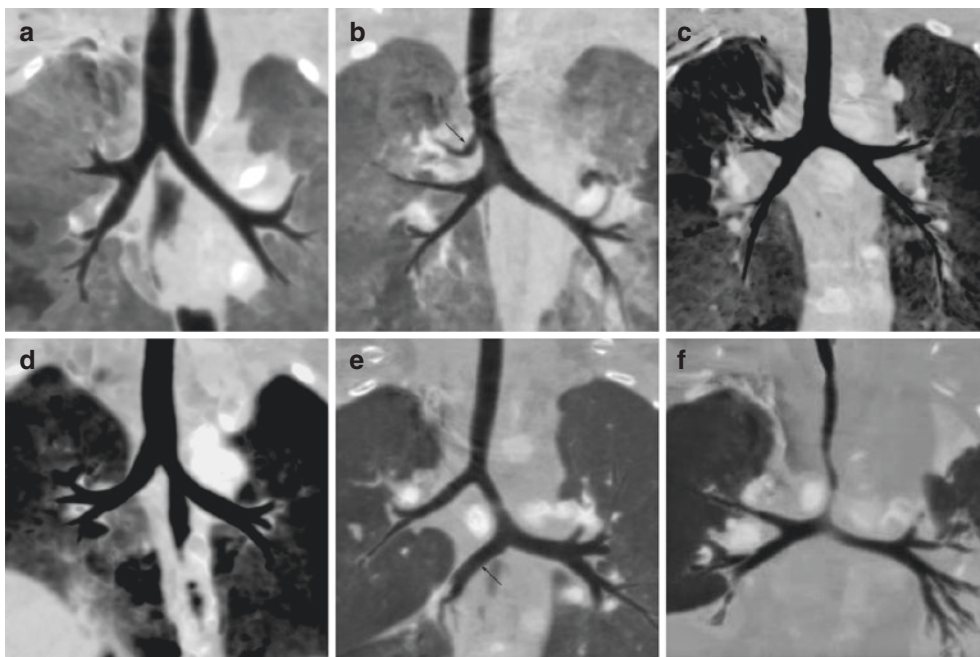


Fig. 10.38 (a–f) Computed tomography images of tracheobronchial branching. (a) Normal tracheobronchial branching pattern. (b) Right tracheal bronchus (arrow), specifically a displaced apical segmental bronchus of right upper lobe. (c) Bilateral epi-arterial bronchus. Symmetrical early branching of right and left upper lobe bronchi found in bilateral tri-lobed lungs. (d) Bilateral hypo-arterial bronchus. Symmetrical late branching of

right and left upper lobe bronchi found in bilateral bi-lobed lungs. (e) Bridging bronchus, type A. Aberrant right lower bronchus (arrow) arising from left main bronchus creating the second lower carina with wide carinal angle. (f) Bridging bronchus type B. A single low carina with wide carinal angle, and long narrowing segment of the trachea

ate or right main bronchus arising from left main bronchus, giving the appearance of a low and inverted-T shaped (pseudo)carina which locates at about T6 level (Fig. 10.38e, f) (normal carinal level is at T4–5). A bridging bronchus usually has a long segment luminal narrowing from having complete cartilaginous rings, and usually is associated with a pulmonary sling—so they are called “ring-sling complex”.

10.8.2 Tracheal Lesions with Luminal Compromise

Airway compromise from tracheal narrowing in neonates can be found in several diseases, including tracheal atresia, tracheal stenosis, tracheomalacia, or extrinsic compression on the trachea by a vascular ring or a mediastinal mass; rarely

intratracheal masses cause the lumen compromise (Fig. 10.39).

- **Tracheal atresia** is characterised by an absence of a tracheal segment. Most cases have a distal trachea-oesophageal fistula, and prompt diagnosis is required for early oesophageal ventilation in the delivery room for saving life. A CT examination is the modality of choice to demonstrate the absence of a tracheal air column, measure the length of the atretic part, identify the carina and identify the fistula, and to classify the type of the anomaly for surgical planning (Fig. 10.40).
- **Congenital tracheal stenosis** is characterised by a complete tracheal cartilaginous ring with absence of the membranous part, producing a fixed luminal narrowing. It can affect either a short or long segment of the trachea or even

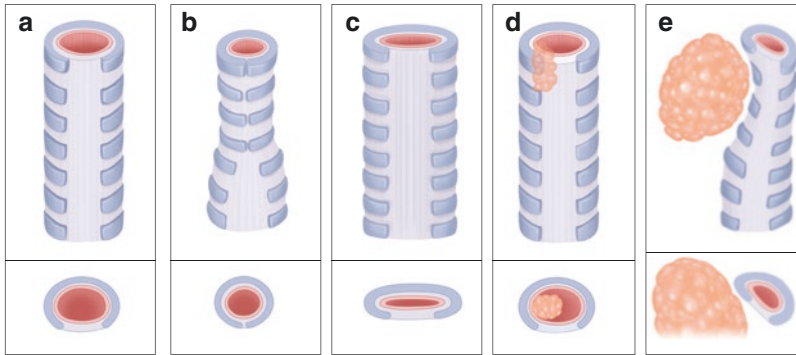


Fig. 10.39 (a–e) Diagram of tracheal luminal narrowing. Upper row—posterior view, lower row—axial view. (a) Normal C-shaped cartilaginous tracheal ring with posterior membranous wall. (b) Complete cartilaginous tra-

cheal ring, resulting in round-shape luminal narrowing. (c) Tracheomalacia, collapsed AP diameter of tracheal lumen during expiration. (d) Intraluminal tracheal lesion. (e) Mediastinal mass compressing the trachea




Fig. 10.40 Tracheal atresia with oesophagobronchial fistula. Thick-slab miniIP of chest CT in coronal plane of a 4-month-old infant with oesophageal intubation reveals a narrow fistula (black arrow) from oesophagus (white arrow) to proximal right main bronchus. Tracheal bifurcation is at about T6 level with a wide carinal angle

involve bronchi (tracheobronchial stenosis). It may be an isolated finding or associated with a bridging bronchus and a pulmonary sling (Fig. 10.38f). Chest CT is commonly used to identify the location, the degree, and the length of the tracheal and bronchus narrowing, also helpful for planning management.

- **Tracheomalacia** is defined by (excessive) expiratory collapse of the trachea, diagnosed when more than 50% of tracheal diameter reduction is noted on an expiration radiograph in symptomatic patients. Modalities to identify this tracheobronchial collapse are tracheobronchoscopy, lateral radiograph of trachea in inspiratory and

expiratory phase, lateral view fluoroscopy during respiration, cine CT, and respiratory-gated MRI. Imaging is skipped if tracheobronchoscopy has been or is going to be performed.

- A **complete vascular ring** and **pulmonary sling** can compress the trachea and the oesophagus. The more severe the airway obstruction, the earlier the lesions manifest.
 - Complete vascular rings include double aortic arch, and right aortic arch with aberrant left subclavian artery and left ductus arteriosus (or ligamentum arteriosum) with or without diverticulum of Kommerell.

 Chest radiographs may show tracheal narrowing and a right sided aortic arch on frontal view (Fig. 10.41a), and also tracheal narrowing on lateral view with indentation on anterior wall. If an oesophagography is performed, it shows a prominent indentation on the posterior wall of the oesophagus (Fig. 10.41b). The oesophagram is skipped if bronchoscopy is undertaken earlier and detected a pulsatile indentation on tracheal wall. Chest CTA or MRI provides vascular anatomy information for surgical planning (Fig. 10.41c) and excludes mediastinal masses or cysts.

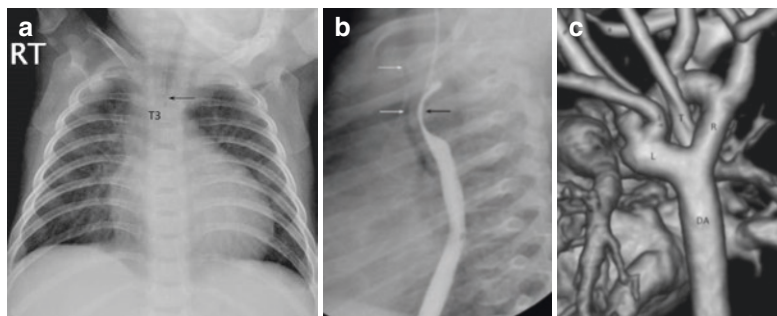
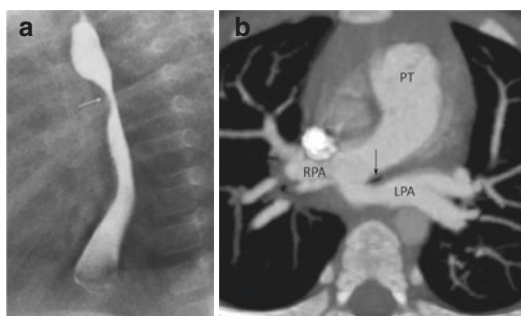


Fig. 10.41 (a–c) Double aortic arch. (a) Chest radiograph shows tapering tracheal air column (arrow) and not seen its distal part from T3 level. (b) Oesophagogram in lateral view detects a large extrinsic indentation on posterior oesophageal wall (black arrow) and a narrowing seg-

ment of trachea (white arrows) at a slightly higher level. (c) Thoracic CTA with volume rendering image in oblique posterior view shows double aortic arch. DA descending aorta, L left arch, R right arch, T feeding tube in oesophagus

Fig. 10.42 (a, b) Pulmonary sling. (a) Oesophagogram in lateral view demonstrates an indentation on anterior oesophageal wall (arrow). (b) Thoracic CTA with thick-slab MIP in axial plane provides the diagnosis of pulmonary sling with left pulmonary artery (LPA) coursing behind the trachea (arrow). PT pulmonary trunk, RPA right pulmonary artery



- The pulmonary sling, also known as aberrant left pulmonary artery arising from right pulmonary artery, has its course interposed between trachea and oesophagus to left pulmonary hilum.

It is detected on lateral oesophagograms as an oval-shaped soft tissue mass posterior to the distal trachea with indentation on the anterior oesophageal wall (Fig. 10.42a). Differential diagnosis of this finding is a bronchogenic cyst.

Chest CTA is the imaging of choice for the diagnosis of pulmonary sling (Fig. 10.42b) and can reveal the associated bronchial abnormality of a bridging bronchus and tracheobronchial stenosis. Non-enhanced MRA can be an alternative option to demonstrate the vascular anatomy.

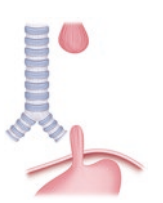
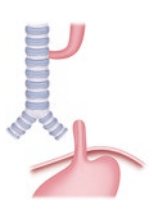
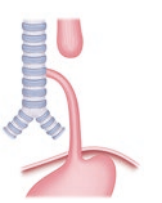
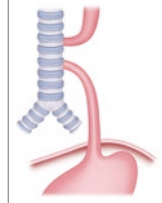
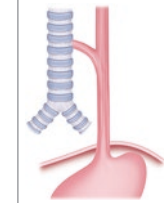
10.9 Oesophageal Abnormalities

Congenital abnormalities of the oesophagus in neonates include oesophageal atresia, trachea- or broncho-oesophageal fistula, and the congenital short oesophagus.

10.9.1 Oesophageal Atresia (OEA) and/or Trachea-Oesophageal Fistula (TOEF)

These two entities are closely related and mostly present together. It occurs in the early embryonic development when the laryngotracheal tube fails to split properly into the oesophagus and trachea, providing a variety of atresia and/or fistula. According to the Gross classification, these are classified together into five types (A, B, C, D, and

Table 10.7 Classification of oesophageal atresia and trachea-oesophageal fistula (adapted from [36])

Classification					
Gross 1953	Type A	Type B	Type C	Type D	Type E
Vogt 1929	Type II	Type IIIa	Type IIIb	Type IIIc	Type IV
Incidence	7–8%	1–4%	82–85%	3–4%	3–4%
Air in GI tract	No	No	Yes	Yes	Yes

Classification of OEA and TOEF according to Gross and Vogt with the incidence. Vogt type I which is oesophageal agenesis is not included in this illustration

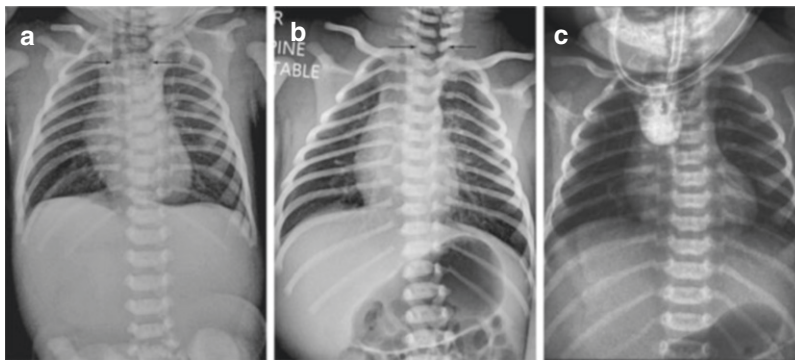


Fig. 10.43 (a–c) Oesophageal atresia. (a) Oesophageal atresia, Gross type A or Vogt type II. There is dilatation of proximal oesophageal blind pouch (between arrows) and no air in gastrointestinal tract. Air is injected into the feeding tube during taking the image to better detection of the proximal pouch. (b) Oesophageal atresia, Gross type C or Vogt type IIIb. Curling feeding tube (arrows) is noted in

dilated proximal oesophageal blind pouch while there is air in the stomach and bowel loops. (c) Oesophageal atresia, Gross type C or Vogt type IIIb. Tube oesophagography with iodinated contrast agent to outline the proximal pouch could be obtained, but should be done under fluoroscopy to prevent the risk of overfilling and aspiration

E). The most common type, about 85%, is type C which is OEA with proximal oesophageal blind pouch and distal trachea-oesophageal fistula (Table 10.7). There also is another classification—the Vogt classification, which is more commonly used in Europe (types I; II; IIIa,b,c; IV).

10.9.1.1 Diagnosis of OEA and/or TOEF and Preoperative Imaging

- Prenatal US may identify OEA, but with a high false positive rate, while amniotic fluid analysis and foetal MRI have a better accuracy [37].
- Postnatal signs and symptoms are excessive salivation, coughing or choking after oral

feeding, and respiratory distress. The diagnosis can be made when the passage of the feeding tube fails.

- Finding the tip of the feeding tube ending or coiling in proximal oesophageal pouch on a chest radiograph confirms the diagnosis. The dilated proximal blind pouch (found in type C and A) is better seen after injection of air via the feeding tube during/briefly before the exposure (no need to inject contrast agents) (Fig. 10.43).
- Presence of abdominal bowel gas in OEA indicates a distal fistula (type C or D/type III b or IIIc) which occurs in most of the cases.

The left or right aortic arch should also be assessed because it may affect the side of thoracotomy or thoracoscopy for OEA repair, as the descending aorta may obscure the oesophageal pouch and cause technical difficulties during surgery.

About a half of patients with OEA have a VACTERL anomaly [vertebral (V), anorectal (A), cardiac (C), tracheal (T), oesophageal (E), renal (R), and limb (L) anomaly].

When OEA without a distal fistula (type A or B/ type II or IIIa) is detected, more extensive imaging requirement is needed because it commonly has a long oesophageal gap. Accurate measurement of the gap length is important for surgical decision.

Demonstration of distal oesophageal blind pouch is usually done under fluoroscopy in infants with gastrostomy. If the gap length is longer than 2 vertebral bodies, primary anastomosis is not recommended [38].

The diagnosis of an isolated H-type fistula (type E/IV) is a challenge, it requires a high index of suspicion from both clinicians and radiologists.

Radiographic findings of aspiration pneumonia, air in the lower oesophagus, and increased air in gastrointestinal tract may give a hint towards a H-type fistula in infants with a history of recurrent pneumonia and severe choking related to feeding.

Oesophagography, preferred with a recorded and stored cine-loop, is the investigation of choice for diagnosing a H-type fistula. The majority of H-type fistulae are located above T2 level with an oblique course, more alike the letter N than H, from the cephalic trachea caudal to the oesophagus (Fig. 10.44). Thus positioning the patient in a lateral or oblique prone position is recommended. Tube oesophagography facilitates more oesophageal distension than normal swallowing and tube injection should be done at several levels because a fistula at the lower cervical oesophagus can occur. This must be performed with caution, having resuscitation facilities ready as there is an increased risk of aspiration. The fistula may not be identifiable on the first oesophagogram, so repeated studies may become necessary and increase the chance of diagnosis.



Fig. 10.44 H-type TOEF. Tube oesophagography in lateral position reveals an anterior upward course of fistula tract (arrow) from anterior wall of oesophagus (OE) to posterior wall of the trachea (T)

10.9.1.2 Postoperative Imaging


Oesophagography is used to detect postoperative complications (anastomotic leakage, anastomotic stricture, and recurrent TOEF), but it may not be necessary in asymptomatic postoperative, as its result does not change further management [39]. Patients with these conditions are usually exposed to a significant radiation dose already for diagnosis, treatment planning, and follow-ups, with reported cumulative effective dose of 17.4 mSv within the first 3 years of life and 70% of which are from diagnostic fluoroscopy that includes radiosensitive regions, such as the thyroid gland and the breast area, thus every dispensable investigation should be avoided [40].

- Common long-term problems are oesophageal dysmotility, gastro-oesophageal reflux, and oesophageal stricture.

10.9.2 Congenital Broncho-Oesophageal Fistula

Congenital broncho-oesophageal fistula is a very rare disease, characterised by an aberrant bronchus arising from the oesophagus instead of the tracheo-bronchial tree (Fig. 10.10). The affected bronchus may be main, lobar, or segmental bronchus.

Recurrent pneumonia of the affected lung, lobe, or segment occurs.

 As on bronchoscopy this aberrant main or lobar bronchus is often not identified, an oesophagogram is used to verify the diagnosis.

10.9.3 Congenital Short Oesophagus

A congenital short oesophagus is rare. Then the whole or a part of the stomach locates up in the posterior mediastinum (Fig. 10.45).

Complications of this condition are gastro-oesophageal reflux and gastric obstruction.

The chest radiograph may show an air-filled or soft tissue opacity lesion in the retrocardiac area or occupies a large portion of either side of the thorax [41].

Surgically, this condition is more difficult to manage than the usual hiatal hernia with a normal length of the oesophagus.

10.10 Mediastinal Abnormalities

10.10.1 Normal Thymus Mimicking Pathologies

Imaging findings of normal neonatal thymus on chest radiograph, US, CT, and MRI have been

mentioned in Sect. 10.4. As there is a wide variance in size and shape of the normal thymus, it is occasionally disturbing when mimicking some pathologies.

- Normal thymus may descend caudally to reach the diaphragm on either or both sides, giving a false impression of wider transverse cardiac diameter.
- An unusual more lateral extension of thymic “sail” can mimic a right upper lobe consolidation.

When facing an unusual size or shape of the thymus, US nearly always suffices to dispel the doubt (Fig. 10.46).

10.10.2 Mediastinal Masses

Mediastinal masses, either solid or cystic, are rare in neonates. They may be radiologically suspected when there is displacement or narrowing of the trachea or a main bronchus (differential diagnosis with vascular ring), the presence of calcifications, or a paraspinal mass with or without a congenital abnormality of the spine.

Ultrasound is the first step to approach the radiographically suspected formation (provided an adequate acoustic window is available, don't forget a potential dorsal access!)

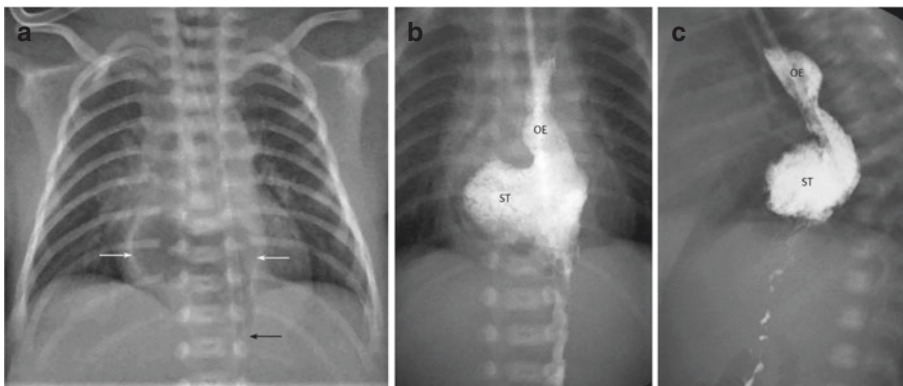


Fig. 10.45 (a–c) Hiatal hernia with short oesophagus and dysplastic stomach. (a) Chest radiograph shows a pocket of air (between white arrows) superimposed on cardiac shadow with an inferior beak (black arrow). The course of the feeding tube passes the left side of this air

pocket. (b, c) Tube gastrography in AP and lateral views demonstrate dysplastic intrathoracic stomach, persistent wide-open oesophago-gastric junction, gastrooesophageal reflux, and short oesophagus with dilated distal part. *OE* oesophagus, *ST* stomach

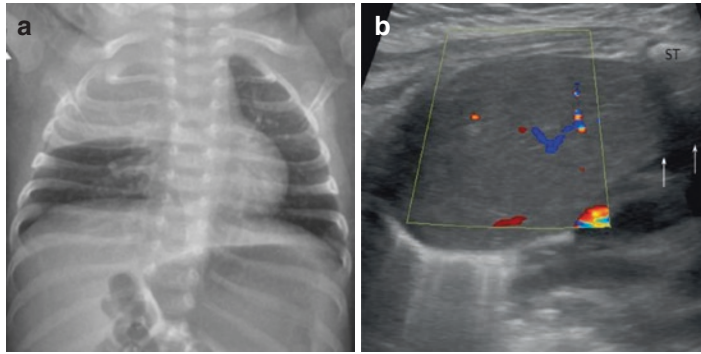


Fig. 10.46 (a, b) Thymic shadow resembling RUL consolidation. (a) Chest radiograph of a 6-week-old infant incidentally detects a consolidative-like lesion in the area of right upper lobe. (b) Chest US in transverse plane at right upper chest provides the diagnosis of normal thymic

tissue extended from substernal area (arrows) to the right latera chest wall. To differentiate from consolidation, normal thymus has a few internal vascular flows that are not along with pulmonary vascular distribution and an absence of air bronchogram. *ST* sternum

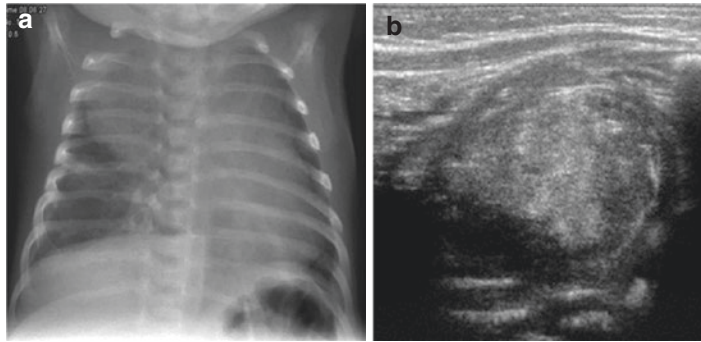


Fig. 10.47 (a, b) Mediastinal neuroblastoma. (a) Chest radiograph shows a widened right side of superior mediastinum with sharp convex lateral margin. (b) Chest US

reveals a solid mediastinal mass with heterogeneous echogenicity extending from the anterior chest wall to the spine

and often will allow a confirmation and even a diagnosis.

However, often thereafter, CT or MRI is indicated for the work-up and/or staging—maybe postponed until after renal maturation, provided US allows a reliable diagnosis and demonstrates a non-urgent condition. Chest CT or MRI then provides information on the solid versus cystic or vascular nature, and they better define the location and extension of the lesion. Chest MRI has advantages in evaluation of intraspinal abnormalities and/or communication/extension into the spinal canal (e.g. of a posterior mediastinal cyst

into the intrathecal CSF, of a neuroblastoma into the spinal canal) and comes free of radiation. Chest CT has benefits in evaluating the lung and its rapid speed. If the lesion is air-filled, an upper GI study is used to diagnose/differentiate a hiatal hernia or an oesophageal duplication.

Possible entities to consider:

- Reported neonatal solid mediastinal masses are teratomas, neurogenic tumours (neuroblastoma, ganglioneuroblastoma, and plexiform neurofibroma) (Fig. 10.47), cardiac tumours (rhabdomyoma), and pericardial

extralobar sequestrations. However, a mature cystic teratoma may present as a predominant cystic lesion without fat or calcification.

- Cystic mediastinal lesions in neonates include bronchogenic cyst, enteric cyst, neurenteric cyst, pericardial cyst, thymic cyst, lymphatic malformation, and anterior or lateral meningocele (and the mature cystic teratoma). An air containing lesion in the posterior mediastinum is likely from a hiatal hernia or a (communicating) oesophageal duplication.
- Aneurysm of ductus arteriosus is, though rarely, reported in neonates.

The location of a mediastinal lesion, its density and pattern of contrast enhancement, including associated vertebral anomalies are helpful for providing the diagnosis or narrowing the differential diagnoses (Table 10.8).

10.10.3 The Aortic Arch and Other Mediastinal Vessels

It is important to assess whether the aortic arch is left or right sided. When the aortic arch is obscured by the thymic shadow, find the slight displacement of distal trachea to the opposite site or the side of descending aorta. Operations such as a modified Blalock-Taussig shunt or reconstruction of oesophageal atresias or fistulas are usually approached from the contralateral side of the aortic arch.

A right aortic arch (Fig. 10.48) is found with following conditions:

- As a normal variant of a right aortic arch with an aberrant left subclavian artery.
- As a right aortic arch with mirror image branching in congenital heart disease, particular the cyanotic ones.
- As a component of a true vascular ring.

Other vascular shadows in the mediastinal shadow should also be evaluated on a chest radiograph. A persistent left SVC can be diagnosed when observing the left course of the central line

in superior mediastinum (Fig. 10.49). If the thymus is atrophic, the pulmonary curve can be assessed along with pulmonary vasculature in cases of congenital heart disease. Other anomalies of the pulmonary circulation (Fig. 10.50) can be addressed by US or echocardiography and may require further investigation with CT or MR angiography, such as pulmonary sling, interruption of proximal right/left main pulmonary artery, aortopulmonary collateral arteries, intra-pulmonary AV-shunts, and anomalous pulmonary venous return—details of which can be found in Chap. 11.

10.11 Diaphragmatic Abnormalities

10.11.1 Congenital Diaphragmatic Hernia (CDH)

Congenital diaphragmatic hernia is characterised by having a developmental diaphragmatic defect and herniation of abdominal contents into the chest. In addition, many of the affected patients have the consequence of pulmonary hypoplasia and persistent pulmonary hypertension. There are associated syndromes, structural or chromosomal abnormalities in 30–50% of the cases.

Based on the anatomic location, CDH is classified into posterolateral (Bochdalek), anteromedial (Morgagni), and central tendon hernia. Bochdalek hernia is the most common type, occurred in 90% of CDH, followed by Morgagni (9–12%), while central tendon hernia is very rare.

More than half of the patients with CDH are detected by US antenatally. Liver herniation and foetal lung volume are important prognostic indicators that are better assessed by MRI. Cardiac malformations are an important associated finding.

The imaging findings on a postnatal chest radiograph depend on the type and side of a CDH, the herniated contents, and timing of the imaging.

- When the chest radiograph is performed early, the herniated gastrointestinal loops are fluid-filled, providing opacity in the chest. When air

Table 10.8 Mediastinal masses in neonates

Mass	Location in the mediastinum		Typical character	Vertebral anomaly
	Typical location	Uncommon location		
Teratoma	Prevascular	Paraspinal Pericardium	Heterogeneity with solid, cystic, fatty, and calcific components	
Neurogenic tumour	Paraspinal		Probable with posterior rib erosion	Probable with intraspinal extension
Cardiac rhabdomyoma	Cardiac		Associated with tuberous sclerosis	
Bronchogenic cyst	Carinal Paratracheal Para-oesophageal	Lung Hilum Prevascular Pleura Diaphragm	Unilocular, thin-walled cyst with variable density of fluid content	
Enteric cyst	Para-oesophageal, close contact with oesophagus	Not in close contact with oesophagus	Same as bronchogenic cyst, probable with ectopic gastric mucosa or pancreatic tissue	
Neurenteric cyst	Paraspinal Para-oesophageal		Same as bronchogenic cyst, probable with ectopic gastric mucosa or pancreatic tissue	Midline vertebral defect Spinal segmentation anomaly
Thymic cyst	Prevascular		Unilocular or multilocular, thin-walled cyst with variable density of fluid content	
Pericardial cyst	Anterior cardiophrenic angle	Pericardial recess at proximal aorta or pulmonary artery	Unilocular, thin-walled cyst with water density of fluid content	
Lymphatic malformation	Prevascular	Pericardium	Multilocular septate cystic lesion	
Thoracic meningocele	Paraspinal Perispinal		Unilocular, thin-walled cyst communication with CSF	Spinal segmentation anomaly Widened intervertebral foramina Scoliosis
Ductus arteriosus aneurysm	Aorticopulmonary window		Contrast filled in arterial phase	

Mediastinal masses in neonates are assessed of their solid or cystic nature, location, typical character, and associated vertebral anomaly to suggest the (differential) diagnosis

has replaced the fluid, the typical air-filled stomach and intestinal tract structures at that location will be identified—then producing a unilateral large hyperlucent hemithorax with multiple cystic lesions.

- Less bowel loops in the scaphoid abdomen, a poorly identifiable diaphragmatic border, defining a traversing bowel loop between chest and abdomen or the stomach (with a feeding tube) in the chest help to differentiate

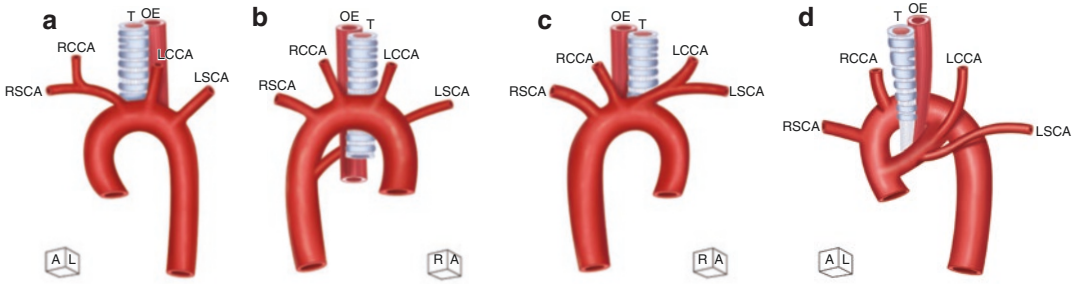


Fig. 10.48 (a–d) Right aortic arch and its branching patterns. (a) Left aortic arch for comparison. From proximal to distal—innominate artery giving rise to right subclavian artery (RSCA) and right common carotid artery (RCCA), left common carotid artery (LCCA), and left

subclavian artery (LSCA). *T* trachea, *OE* oesophagus. (b) Right aortic arch with aberrant left subclavian artery. (c) Right aortic arch with mirror image branching. (d) Double aortic arch with common carotid and subclavian arteries from each arch

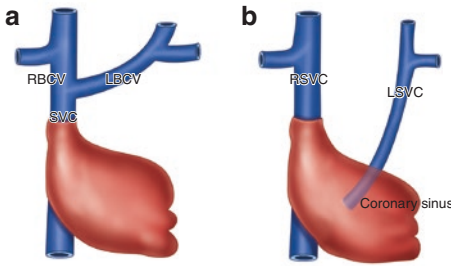


Fig. 10.49 (a, b) Superior vena cava (SVC) and its variation. (a) Normal SVC at the right side, arising from joining of right and left brachiocephalic veins (RBCV and LBCV). (b) Bilateral SVC. The persistent left SVC draining into coronary sinus of right atrium

between congenital diaphragmatic hernia and other entities.

- When herniated content is solid, such as the liver or the omentum, it is usually shown on chest radiograph as a focal lobulation of the diaphragm.

10.11.1.1 Bochdalek Hernia

The Bochdalek hernia usually presents at birth, in 80% it occurs on the left side.

Most of the herniated content in *left Bochdalek hernia* are bowel loops.

Left Bochdalek hernia provides typical imaging findings of multiple air-filled cysts in the left hemithorax, mediastinal shift to the right, undistinguishable left hemidiaphragm, and less bowel loops in the abdomen (Fig. 10.51a). The stomach

may be in the abdomen or herniate into the chest together with bowel loops. Curving of the feeding tube upward with its tip in the left chest suggests herniation of the stomach. Occasionally, the stomach is the only herniated organ with the radiographic appearance of a solitary lung cyst (Fig. 10.51b).

- Pulmonary hypoplasia, the result of lung growth disturbance from significant herniated abdominal contents in utero, is related to a higher risk of pneumothorax during ventilator support in either the pre- or the postoperative period.
- When pneumothorax occurs after diaphragmatic repair, it is suggested to wait for spontaneous resorption, because rapid drainage may cause mediastinal rotation with obstruction of the inferior vena cava.

Right Bochdalek hernia is less frequent. When the herniated contents are bowel loops, the diagnosis can be made on chest radiograph with the same criteria as used for the left side.

- When the herniated content is the liver or the omentum, the chest radiograph may show focal or diffuse (pseudo-)elevation of the affected hemidiaphragm.
- Further investigations mostly by US are usually required—some request a CT or MRI, which normally is not necessary. Ultrasound is quite reliable in assessing these conditions.

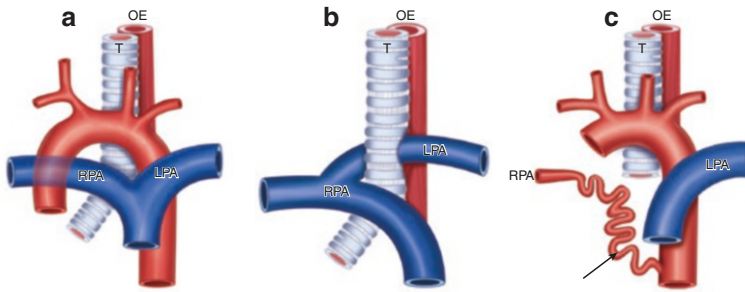
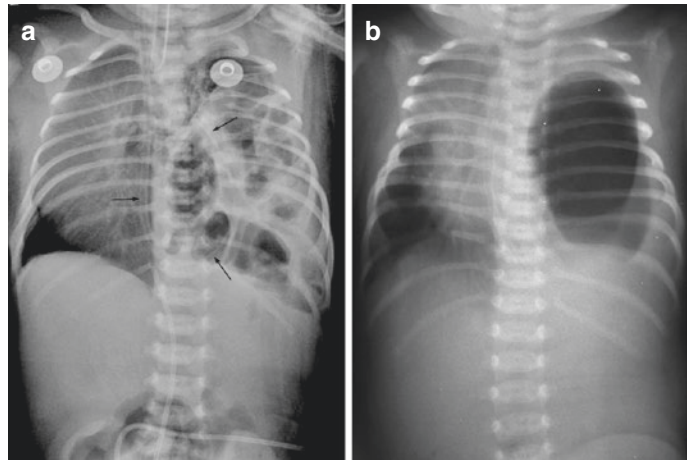


Fig. 10.50 (a–c) Developmental anomalies of pulmonary artery. (a) Normal pulmonary trunk dividing into right and left pulmonary arteries (RPA and LPA). *T* trachea, *OE* oesophagus. (b) Pulmonary sling or aberrant

LPA arising from RPA, then coursing between trachea and oesophagus to left pulmonary hilum. (c) Interrupted proximal RPA with aorto-pulmonary collateral artery (arrow) to reconstitute the more distal RPA

Fig. 10.51 (a, b) Left Bochdalek hernia. (a) Chest radiograph shows upward herniation of the stomach and bowel loops with contralateral mediastinal shift, unidentified left diaphragm, and less bowel loops in the abdomen. The feeding tube curves upward into the left chest (arrows). (b) Another newborn has upward herniation of only the stomach with gastric outlet obstruction, producing a large cyst in the left chest with contralateral mediastinal shift. There is no air in the abdomen and the left diaphragm cannot be outlined



- Presence of hepatic waist with acute angle and muscle folding at the edge of the diaphragmatic defect [42] is used to differentiate diaphragmatic hernia from focal eventration of diaphragm—something also easy to assess by US.
- There is a relationship between a delayed right diaphragmatic hernia and neonatal pneumonia caused by group B streptococcal pneumonia—the hernia rarely but may develop or manifest after improvement of pneumonia and discontinuing ventilatory support within the first 1–2 months of age [43].
- Imaging findings of a right diaphragmatic hernia with significant liver herniation but ipsilat-

eral or no mediastinal shift are reported in hepatopulmonary fusion [44] (Fig. 10.52).

10.11.1.2 Anteromedial Diaphragmatic Hernia

The diaphragmatic defect in a Morgagni hernia is at the paramedian retrosternal location, mostly (90%) on the right side. It may be detected in neonatal age, but the majority presents in older children or adults.

- The diagnosis can be made by depiction of herniated air-filled bowel loops or solid organ at the right anterior pericardiac area.
- When the herniated content is liver, spleen, or omentum, US can be useful (Fig. 10.53).

- Intrapericardial herniation of liver or bowel loops through an anterior diaphragmatic defect is considered a rare form of Morgagni hernia and often associated with a massive pericardial effusion [45] (Fig. 10.54).

Another more complex form of anterior diaphragmatic defect is the Pentalogy of Cantrell malformation. Beside anterior diaphragmatic defect, there are also defects of diaphragmatic pericardium, lower sternum, the mid upper

abdominal wall and in the heart. Herniation through these defects results in omphalocele and ectopia cordis or intrapericardial herniation of bowel loops (Fig. 10.55).

10.11.1.3 Central Tendon Hernia

The central tendinous part of the diaphragm lies between the heart and the liver. When there is a defect of the central tendon with pericardial defect, the herniated content (liver, stomach, or colon) can reach the pericardial space. This hernia is very rarely congenital, it occurs

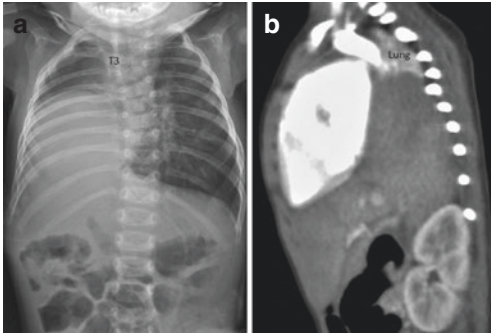


Fig. 10.52 (a, b) Right Bochdalek hernia with hepatopulmonary fusion (surgical diagnosis). (a) Chest radiograph in frontal view shows markedly upward herniation of the liver but there is ipsilateral cardiac shift. Note right hemivertebra of T3. (b) Arterial phase of chest and abdominal CT in right parasagittal reformatted image confirms upward liver herniation posterior to the heart. The atelectatic hypoplastic right lung is noted above the herniated liver



Fig. 10.54 Right anterior diaphragmatic hernia with pericardial effusion. Chest CT is requested for evaluation of intrapericardial mass with massive pericardial effusion detected on echocardiography, status post drainage. Coronal reformatted CT shows intrapericardial herniation of the liver at the anteromedial aspect through the right diaphragm. Note the hepatic “waist” sign (black arrow) and pericardial effusion (white arrows). Decreased density of the herniated liver indicates restriction of blood flow

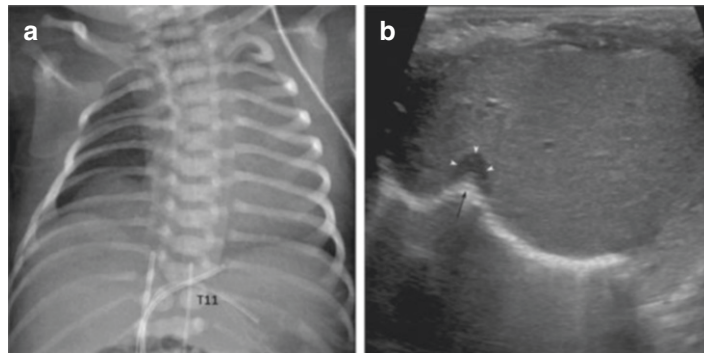


Fig. 10.53 (a, b) Right Morgagni hernia with herniated liver. (a) Chest radiograph shows focal elevation of right hemidiaphragm at medial part. Note butterfly vertebra of T11. (b) Abdominal ultrasound at right parasagittal plane

demonstrates superior extension of the liver at anteromedial part with hepatic waist (arrow) and muscle folding (arrowheads) at the edge of right diaphragmatic defect

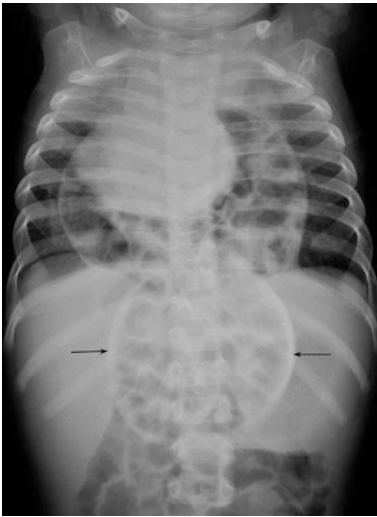


Fig. 10.55 Pentalogy of Cantrell. Chest radiograph in frontal view shows herniation of bowel loops into pericardial space with elevation and rotation of cardiac shadow indicating anterior diaphragmatic and pericardial defects. Note the omphalocele (arrows) at midline upper abdomen. Lower sternal defect is detected during surgery

mostly in adults after trauma or iatrogenic interventions.

10.11.2 Congenital Hiatal Hernia

A hiatal hernia is a protrusion of the stomach through or adjacent to the oesophageal hiatus into the mediastinum and uncommon in infants—most of hiatal hernias manifest later in life.

- The hiatal hernia is classified according to the location of the oesophago-gastric junction and the oesophageal length into three types,
 - (1) sliding hernia with a high oesophago-gastric junction and a normal oesophageal length,
 - (2) para-oesophageal hernia with normal position of the oesophago-gastric junction and a normal oesophageal length, and
 - (3) congenital short oesophagus with high oesophago-gastric junction.
- Gastric herniation in hiatal hernia, particular in the para-oesophageal hernia, may

twist (gastric volvulus) and cause serious complications.

- The chest radiograph in a hiatal hernia may show a retrocardiac, either solid/fluid or air-filled cystic mass (Fig. 10.45). In case of short oesophagus with intrathoracic stomach, the stomach may have a large size and occupy a large portion of a hemithorax or may be hypoplastic. The course of the feeding tube within the lesion may help in suggesting of hiatal hernia.
- The diagnosis is then confirmed by upper GI study, or by US after filling the stomach with some sort of fluid (saline, tea, milk or formula, diluted US-contrast agent).

10.11.3 Elevation of the Diaphragm

Elevation of the diaphragm may be unilateral or bilateral, and focal or diffuse. The elevated part usually exhibits dysmotility—either with decreased or no movement, or even paradox motion. Dynamic diaphragmatic movement can be assessed by fluoroscopy, but radiation-free US is preferred; real-time B-mode with cine-loop documentation and M-mode are used to observe and record and document the motion of the diaphragm during respiration (Fig. 10.56); some also advocate free breathing MRI with cine sequences in a feed and wrap technique.

- Diffuse elevation of one hemidiaphragm in neonates with contralateral mediastinal shift can result from either phrenic nerve paralysis (e.g. due to birth trauma) or diffuse deficiency of the diaphragmatic muscle (diffuse type of diaphragmatic eventration). As diaphragmatic paralysis from birth trauma is usually transient, a wait-and-see strategy is advocated. Only without improvement over time, surgical plication of the diaphragm may become indicated.
- Focal, either small or large, elevation of the diaphragm can be found in focal diaphragmatic eventration (Fig. 10.57) or CDH

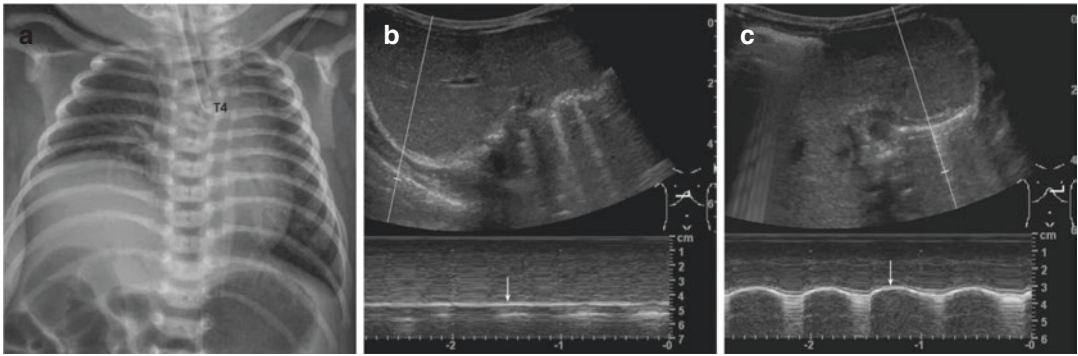
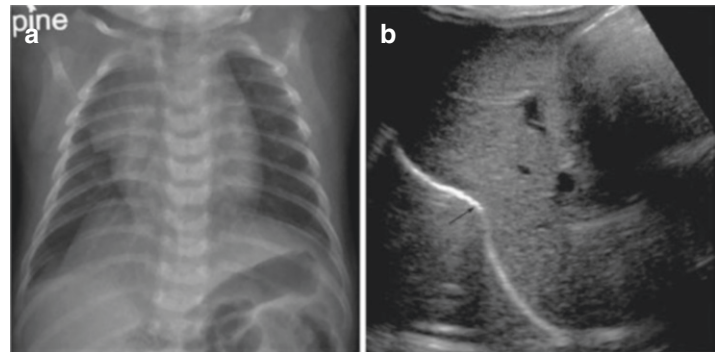


Fig. 10.56 (a–c) Diffuse eventration of right diaphragm (surgical diagnosis). (a) Chest radiograph reveals diffuse elevation of right diaphragm with contralateral mediastinal shift and left hemivertebra of T4. (b) Motion-mode US of right diaphragm shows a linear diaphragmatic-

pleural line (arrow) indicating no right diaphragmatic movement during respiration. (c) Motion-mode US of left diaphragm shows an undulated wave (arrow) indicating left diaphragmatic movement (arrow)

Fig. 10.57 (a, b) Focal diaphragmatic eventration. (a) Chest radiograph reveals lobulation of right hemidiaphragm at its medial two-third parts. (b) Ultrasound of right diaphragm in sagittal plane shows upward elevation of anterior part of the right diaphragm with an obtuse angle (arrow) and no muscle folding at the edge. Compare the difference from congenital diaphragmatic hernia in Fig. 10.53b



(Fig. 10.53), and when posteriorly located, it may be associated with thoracic kidney (Fig. 10.58).

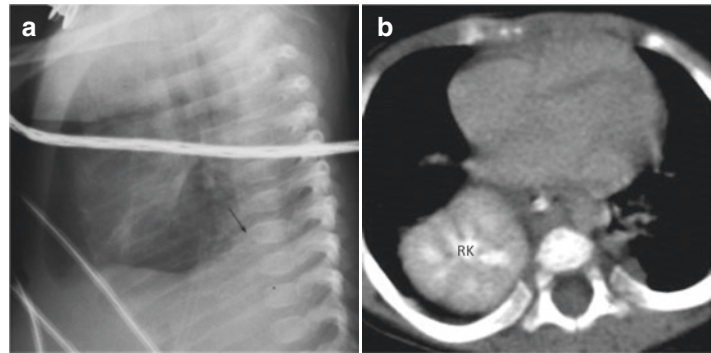
Surgery is not indicated in asymptomatic diaphragmatic eventration, but indicated in CDH—even a small asymptomatic CDH is operated to prevent further herniation and future complications of mass effect or ischaemia. As already mentioned earlier, further investigations for suspected diaphragmatic her-

nia with herniation of solid organ require US, sometimes also CT or MRI.

Other diaphragmatic lesions or variations related to developmental anomalies are rare, including accessory diaphragm and intradiaphragmatic sequestration.

An accessory diaphragm, or duplication of the diaphragm, is a fibromuscular membrane dividing a hemithorax into two compartments, mostly on the right side. Minority of the cases are detected in neonatal life during investigation of

Fig. 10.58 (a, b) Right thoracic kidney. (a) Chest radiograph in lateral view shows a lobulated posterior part (arrow) of the diaphragm. (b) Chest CT (for other indication) reveals high position of the right kidney (RK)



other associated pulmonary, cardiovascular, or diaphragmatic malformations. Chest radiograph may show a linear or curvilinear density in frontal or lateral view, difficult to differentiate from subsegmental atelectasis.

10.12 Chest Wall Abnormalities

Chest wall lesions in neonates usually require chest radiographs when there are suspected birth-related fractures, a suspected skeletal dysplasia, or a bone tumour. For assessing the soft tissue or cystic masses of the chest wall as well as the cartilaginous parts of the ribs and sternum, US and (if necessary) MRI are preferred.

10.12.1 Birth-Related Injury of the Chest Wall

Birth-related injury of the chest wall can occur in difficult delivery or even in a clinical uneventful delivery.

Direct evidence of injury detected on a chest radiograph is a fracture of the clavicle or humerus. Posterior rib fractures related to birth may occur but are rare.


Elevation of a hemidiaphragm is an indirect evidence of ipsilateral phrenic nerve injury, but has to differentiate from diffuse diaphragmatic eventration. Diaphragmatic palsy from phrenic nerve injury is transient, but may take several weeks or even months for complete recovery.

10.12.2 Skeletal Dysplasias

Severe chest wall abnormalities will occur mostly in skeletal dysplasias of the lethal types—usually producing a constricted thoracic cage from short ribs causing severe respiratory insufficiency and respiratory failure, e.g. thanatophoric dysplasia, asphyxiating thoracic dysplasia, achondrogenesis.

- Beside a narrow thorax with short ribs, *thanatophoric dysplasia* has the characteristic platyspondyly and a curved femur with telephone-receiver appearance.
- The *asphyxiating thoracic dysplasia* (also called Jeune syndrome) has a hypoplastic scapula, polydactyly, and cystic renal dysplasia.
- *Achondrogenesis* lacks mineralisation of most vertebral bodies, ischium, and pubic bones.
- The perinatal form of *osteogenesis imperfecta* is another lethal skeletal dysplasia, characterised by osteoporosis, narrow thorax, and multiple fractures with deformed bone shape.
- Rare, less endangering conditions exist, too—such as the agenesis of a clavicle or rib variations.

Imaging is a part of the overall assessment—in addition to a detailed family-history, a thorough physical examination, and molecular laboratory findings to diagnose the specific type of skeletal dysplasia for family counselling.


 Postnatal imaging with skeletal survey includes both AP and lateral views of the skull, spine, and AP view of the extremities, including hands and feet.

- Ribs and pelvis are included in the AP view of the spine.
- Ultrasound may be used to complete the work-up or for assessing soft tissue, cartilaginous, or muscle pathology.

10.12.3 Chest Wall Deformities

These can be detected prenatally by US or are clinically diagnosed at birth. Chest wall deformities include sternal depression (pectus excavatum), chest wall protrusion (pectus carinatum), unilateral missing pectoralis muscle and ribs with syndactyly (Poland syndrome), and cleft sternum with exposed heart (ectopia cordis).

- Ultrasound can be used in suspected Poland syndrome to confirm the absence of pectoralis muscle.

 Chest films often are disappointing in neonates with respect to osseous chest wall pathology—due to the mostly yet cartilaginous nature of these structures, thus US is used for these queries.

10.12.4 Chest Wall Masses

Chest wall masses are infrequent in prenatal or neonatal life—with a variety of diseases including developmental malformations, or benign and malignant tumours (e.g. lymphatic or arteriovenous malformation, cutaneous bronchogenic cyst, congenital haemangioma, hamartoma of the rib, lipoblastoma/-tosis, and rhabdomyosarcoma) or, e.g. from breast conditions (e.g. a breast abscess).

Chest wall hamartoma typically affects multiple contiguous ribs seen on chest radiographs, with often large expansive lesions and varying soft tissue component.

- Ultrasound can be initially used to evaluate solid, cystic, or fat components, including its vascularisation, from which lymphatic malformation, congenital haemangioma, and lipoblastoma or an inflammatory condition may be suggested.
- The further work-up will often need an MRI to demonstrate the full extent, to give the necessary preoperative anatomic-topographic information, or for staging.

10.13 Summary and Conclusions: Take Away

The chest is one of the most often imaged regions in neonates, not only in emergencies or at the NICU, but also for many other reasons such as inflammatory condition (pneumonia, bronchiolitis) or, e.g. a suspected aspiration. Thus it is important to know the normal imaging appearance in neonates, and to understand the options and restrictions of the various imaging methods in this particularly radiosensitive age group. This will lead to a more thoughtful indication of particularly studies using radiation, possibly shifting from chest radiographs to US for some conditions. And the knowledge of common conditions and diseases or queries in this age group which significantly differs from older patient groups explains why, e.g. a CT is far less frequently indicated than in an adult population, where CT is the mainstay of chest imaging.

Radiologists should be equipped with imaging knowledge (typical, atypical, and overlapping imaging features of neonatal chest diseases), added with enough pre- and postnatal information that may provide a more accurate interpretation (e.g. gestational age, prenatal US diagnosis, some specific maternal conditions, premature rupture of amniotic membrane, thick meconium-stained amniotic fluid, clinical sepsis, drooling, stridor, treatment provided, co-morbid conditions, clinical evolution). Approaching of chest

radiography usually includes anatomic location (lung, pleura, mediastinum, chest wall, diaphragm), disease laterality (uni- or bilateral), lung density and volume, and image evolution when follow-up (with or without treatment).

The development of lung, airway, and vascular structures are closely correlated, so that a continuum of abnormalities or combination of more than one conditions (such as the hybrid lesion of CPAM and sequestration, bronchial atresia sequence) can take place. Presurgical evaluation with chest CT requires an arterial phase when there is a concern of systemic arterial supply, such as when the developmental lung lesion locates in medial part of lower lobe. Besides the lung, other important developmental diseases in the chest are tracheal and oesophageal anomalies, and the diaphragmatic defects, which also have several types and different manifestations that require different imaging tools. Oesophageal atresia with TOEF is diagnosed by failure of passing a feeding through the oesophagus, probable with air injection into the feeding tube during radiation exposure to better identify the dilated proximal oesophageal pouch. Diagnosis of H-type TOEF requires a meticulous oesophagography. Most CDHs are diagnosed by chest radiographs alone because most of them have typically air-filled herniated bowel loops. Few CDHs with herniated solid organ can be evaluated by US.

Acknowledgement Acknowledgment to Dr. Atchara Mahayosond, Dr. Teerasak Phewplung, and Dr. Nattinee Leelakanok from Department of Radiology, Faculty of Medicine, Chulalongkorn University for image contribution.

References

1. European Commission. European guidelines on quality criteria for diagnostic radiographic images in pediatrics. 1996. <https://www.sprmn.pt/pdf/EuropeanGuidelinesEur16261.pdf>. Accessed 3 Oct 2021.
2. Don S, Macdougall R, Strauss K, Moore QT, Goske MJ, Cohen M, et al. Image gently campaign back to basics initiative: ten steps to help manage radiation dose in pediatric digital radiography. *AJR Am J Roentgenol*. 2013;200(5):W431–6. <https://doi.org/10.2214/AJR.12.9895>.
3. European Commission. European guidelines on DRLs for pediatric imaging. 2016. http://www.euro-safeimaging.org/wp-content/uploads/2014/02/European-Guidelines-on-DRLs-for-Paediatric-Imaging_Revised_18-July-2016_clean.pdf. Accessed 3 Oct 2021.
4. Mothiram U, Brennan PC, Lewis SJ, Moran B, Robinson J. Digital radiography exposure indices: a review. *J Med Radiat Sci*. 2014;61(2):112–8. <https://doi.org/10.1002/jmrs.49>.
5. Riccabona M. Ultrasound of the chest. In: Riccabona M, editor. *Pediatric ultrasound*. 2nd ed. New York: Springer International Publishing; 2020. p. 231–61.
6. Nagy E, Tschauner S, Marterer R, Riedl R, Sorantin E. Chest CTA in children younger than two years - a retrospective comparison of three contrast injection protocols. *Sci Rep*. 2019;9(1):18109. <https://doi.org/10.1038/s41598-019-54498-z>.
7. Hirsch FW, Sorge I, Vogel-Claussen J, Roth C, Gräfe D, Päts A, et al. The current status and further prospects for lung magnetic resonance imaging in pediatric radiology. *Pediatr Radiol*. 2020;50(5):734–49. <https://doi.org/10.1007/s00247-019-04594-z>.
8. Rehman S, Bacha D. *Embryology, pulmonary*. Treasure Island, FL: StatPearls Publishing; 2020.
9. Blank DA, Kamlin COF, Rogerson SR, Fox LM, Lorenz L, Kane SC, et al. Lung ultrasound immediately after birth to describe normal neonatal transition: an observational study. *Arch Dis Child Fetal Neonatal Ed*. 2018;103(2):F157–62. <https://doi.org/10.1136/archdischild-2017-312818>.
10. Sklair-Levy M, Agid R, Sella T, Strauss-Liviatan N, Bar-Ziv J. Age-related changes in CT attenuation of the thymus in children. *Pediatr Radiol*. 2000;30(8):566–9. <https://doi.org/10.1007/s002470000245>.
11. Edwards DK. The newborn infant with respiratory distress from medical causes. In: Hilton SW, Edwards DK, editors. *Practical pediatric radiology*. 3rd ed. Philadelphia, PA: Saunders Elsevier; 2006. p. 99–124.
12. Avni EF, Braude P, Pardou A, Matos C. Hyaline membrane disease in the newborn: diagnosis by ultrasound. *Pediatr Radiol*. 1990;20(3):143–6. <https://doi.org/10.1007/BF02012957>.
13. Brat R, Yousef N, Klifa R, Reynaud S, Shankar Aguilera S, De Luca D. Lung ultrasonography score to evaluate oxygenation and surfactant need in neonates treated with continuous positive airway pressure. *JAMA Pediatr*. 2015;169(8):e151797. <https://doi.org/10.1001/jamapediatrics.2015.1797>.
14. Odita JC. The significance of recurrent lung opacities in neonates on surfactant treatment for respiratory distress syndrome. *Pediatr Radiol*. 2001;31(2):87–91. <https://doi.org/10.1007/s002470000377>.
15. Dice JE, Bhatia J. Patent ductus arteriosus: an overview. *J Pediatr Pharmacol Ther*. 2007;12(3):138–46. <https://doi.org/10.5863/1551-6776-12.3.138>.
16. Stoll BJ, Hansen NI, Bell EF, Walsh MC, Carlo WA, Shankaran S, et al; Eunice Kennedy Shriver National Institute of Child Health and Human Development Neonatal Research Network. Trends in care practices, morbidity, and mortality of extremely preterm neo-

- nates, 1993–2012. *JAMA* 2015;314(10):1039–1051. doi: <https://doi.org/10.1001/jama.2015.10244>.
17. Northway WH Jr, Rosan RC, Porter DY. Pulmonary disease following respiratory therapy of hyaline-membrane disease. Bronchopulmonary dysplasia. *N Engl J Med*. 1967;276(7):357–68. <https://doi.org/10.1056/NEJM196702162760701>.
 18. Agrons GA, Courtney SE, Stocker JT, Markowitz RI. From the archives of the AFIP: lung disease in premature neonates: radiologic-pathologic correlation. *Radiographics*. 2005;25(4):1047–73. <https://doi.org/10.1148/rg.254055019>.
 19. Alonso-Ojembarrena A, Lubián-López SP. Lung ultrasound score as early predictor of bronchopulmonary dysplasia in very low birth weight infants. *Pediatr Pulmonol*. 2019;54(9):1404–9. <https://doi.org/10.1002/ppul.24410>.
 20. Riskin A, Abend-Weinger M, Riskin-Mashiah S, Kugelman A, Bader D. Cesarean section, gestational age, and transient tachypnea of the newborn: timing is the key. *Am J Perinatol*. 2005;22(7):377–82. <https://doi.org/10.1055/s-2005-872594>.
 21. Raju U, Sondhi V, Patnaik SK. Meconium aspiration syndrome: an insight. *Med J Armed Forces India*. 2010;66(2):152–7. [https://doi.org/10.1016/S0377-1237\(10\)80131-5](https://doi.org/10.1016/S0377-1237(10)80131-5).
 22. Mathur NB, Garg K, Kumar S. Respiratory distress in neonates with special reference to pneumonia. *Indian Pediatr*. 2002;39(6):529–37. PMID: 12084946
 23. Manson D. Diagnostic imaging of neonatal pneumonia. *Radiol Imaging Neonatal Chest*. 2010;18:99–111. https://doi.org/10.1007/978-3-540-33749-2_7.
 24. Pramanik AK, Rangaswamy N, Gates T. Neonatal respiratory distress: a practical approach to its diagnosis and management. *Pediatr Clin N Am*. 2015;62(2):453–69. <https://doi.org/10.1016/j.pcl.2014.11.008>.
 25. Demir OF, Hangul M, Kose M. Congenital lobar emphysema: diagnosis and treatment options. *Int J Chron Obstruct Pulmon Dis*. 2019;14:921–8. <https://doi.org/10.2147/COPD.S170581>.
 26. Stocker JT. Cystic lung disease in infants and children. *Fetal Pediatr Pathol*. 2009;28(4):155–84. <https://doi.org/10.1080/15513810902984095>.
 27. Pogoriler J, Swarr D, Kreiger P, Adzick NS, Peranteau W. Congenital cystic lung lesions: redefining the natural distribution of subtypes and assessing the risk of malignancy. *Am J Surg Pathol*. 2019;43(1):47–55. <https://doi.org/10.1097/PAS.0000000000000992>.
 28. Wu H, Tian J, Li H, Lu L, Chen X, Xu W. Computed tomography features can distinguish type 4 congenital pulmonary airway malformation from other cystic congenital pulmonary airway malformations. *Eur J Radiol*. 2020;126:108964. <https://doi.org/10.1016/j.ejrad.2020.108964>.
 29. Waeltli SL, Garel L, Soglio DD, Rypens F, Messerli M, Dubois J. Neonatal congenital lung tumors - the importance of mid-second-trimester ultrasound as a diagnostic clue. *Pediatr Radiol*. 2017;47(13):1766–75. <https://doi.org/10.1007/s00247-017-3953-3>.
 30. Kapralik J, Wayne C, Chan E, Nasr A. Surgical versus conservative management of congenital pulmonary airway malformation in children: a systematic review and meta-analysis. *J Pediatr Surg*. 2016;51(3):508–12. <https://doi.org/10.1016/j.jpedsurg.2015.11.022>.
 31. Zhang N, Zeng Q, Chen C, Yu J, Zhang X. Distribution, diagnosis, and treatment of pulmonary sequestration: report of 208 cases. *J Pediatr Surg*. 2019;54(7):1286–92. <https://doi.org/10.1016/j.jpedsurg.2018.08.054>.
 32. Panicek DM, Heitzman ER, Randall PA, Groskin SA, Chew FS, Lane EJ Jr, et al. The continuum of pulmonary developmental anomalies. *Radiographics*. 1987;7(4):747–72. <https://doi.org/10.1148/radiographics.7.4.3448653>.
 33. Lichtenberger JP III, Biko DM, Carter BW, Pavio MA, Huppmann AR, Chung EM. Primary lung tumors in children: radiologic-pathologic correlation from the radiologic pathology archives. *Radiographics*. 2018;38(7):2151–72. <https://doi.org/10.1148/rg.2018180192>.
 34. Brock KE, Wall J, Esquivel M, Newman B, Marina N, Albanese C, et al. Congenital peribronchial myofibroblastic tumor: case report of an asymptomatic infant with a rapidly enlarging pulmonary mass and review of the literature. *Ann Clin Lab Sci*. 2015;45(1):83–9.
 35. Markowitz RI. The anterior junction line: a radiographic sign of bilateral pneumothorax in neonates. *Radiology*. 1988;167(3):717–9. <https://doi.org/10.1148/radiology.167.3.3363127>.
 36. van Lennep M, Singendonk MMJ, Dall'Oglio L, Gottrand F, Krishnan U, Terheggen-Lagro SWJ, et al. Oesophageal atresia. *Nat Rev Dis Primers*. 2019;5(1):26. <https://doi.org/10.1038/s41572-019-0077-0>.
 37. Pardy C, D'Antonio F, Khalil A, Giuliani S. Prenatal detection of esophageal atresia: a systematic review and meta-analysis. *Acta Obstet Gynecol Scand*. 2019;98(6):689–99. <https://doi.org/10.1111/aogs.13536>.
 38. Lee S. Basic knowledge of tracheoesophageal fistula and esophageal atresia. *Adv Neonatal Care*. 2018;18(1):14–21. <https://doi.org/10.1097/ANC.0000000000000464>.
 39. Golden J, Demeter NE, Lim JC, Ford HR, Upperman JS, Gayer CP. Routine post-operative esophagogram is not necessary after repair of esophageal atresia. *Am J Surg*. 2017;213(4):640–4. <https://doi.org/10.1016/j.amjsurg.2016.12.020>.
 40. Zamiara P, Thomas KE, Connolly BL, Lane H, Marcon MA, Chiu PP. Long-term burden of care and radiation exposure in survivors of esophageal atresia. *J Pediatr Surg*. 2015;50(10):1686–90. <https://doi.org/10.1016/j.jpedsurg.2015.05.006>.
 41. Leung AW, Lam HS, Chu WC, Lee KH, Tam YH, Ng PC. Congenital intrathoracic stomach: short esophagus or hiatal hernia? *Neonatology*. 2008;93(3):178–81. <https://doi.org/10.1159/000108927>.
 42. Karmazyn B, Shold AJ, Delaney LR, Brown BP, Marine MB, Jennings SG, et al. Ultrasound evaluation of right diaphragmatic eventration and hernia. *Pediatr*

- Radiol. 2019;49(8):1010–7. <https://doi.org/10.1007/s00247-019-04417-1>.
43. Rescorla FJ, Yoder MC, West KW, Grosfeld JL. Delayed presentation of a right-sided diaphragmatic hernia and group B streptococcal sepsis. Two case reports and a review of the literature. *Arch Surg.* 1989;124(9):1083–6. <https://doi.org/10.1001/archsurg.1989.01410090093021>.
44. Jain V, Yadav DK, Kandasamy D, Gupta DK. Hepatopulmonary fusion: a rare and potentially lethal association with right congenital diaphragmatic hernia. *BMJ Case Rep.* 2017;2017:bcr2016218227. <https://doi.org/10.1136/bcr-2016-218227>.
45. Zamprakou A, Berg C, Strizek B, Müller A, Heydweiller A, Gembruch U, et al. Morgagni hernia presenting with massive pericardial effusion and ascites: prenatal management by thoraco-amniotic shunting and fetal endoscopic tracheal occlusion (FETO) and review of the literature. *Arch Gynecol Obstet.* 2016;294(5):953–8. <https://doi.org/10.1007/s00404-016-4103-0>.

Further Reading

- Abrams ME, Ackerman VL, Engle WA. Primary unilateral pulmonary hypoplasia: neonate through early childhood—case report, radiographic diagnosis and review of the literature. *J Perinatol.* 2004;24(10):667–70. <https://doi.org/10.1038/sj.jp.7211156>.
- Alamo L, Vial Y, Gengler C, Meuli R. Imaging findings of bronchial atresia in fetuses, neonates and infants. *Pediatr Radiol.* 2016;46(3):383–90. <https://doi.org/10.1007/s00247-015-3487-5>.
- Al-Salem AH, Mohaidly MA, Al-Buainain HM, Al-Jadaan S, Raboei E. Congenital H-type tracheoesophageal fistula: a national multicenter study. *Pediatr Surg Int.* 2016;32(5):487–91. <https://doi.org/10.1007/s00383-016-3873-6>.
- Becmeur F, Horta P, Donato L, Christmann D, Sauvage P. Accessory diaphragm—review of 31 cases in the literature. *Eur J Pediatr Surg.* 1995;5(1):43–7. <https://doi.org/10.1055/s-2008-1066162>.
- Bellini C, Boccardo F, Campisi C, Bonioli E. Congenital pulmonary lymphangiectasia. *Orphanet J Rare Dis.* 2006;1:43. <https://doi.org/10.1186/1750-W1172-1-43>.
- Berrocal T, Madrid C, Novo S, Gutiérrez J, Arjonilla A, Gómez-León N. Congenital anomalies of the tracheobronchial tree, lung, and mediastinum: embryology, radiology, and pathology. *Radiographics.* 2004;24(1):e17. <https://doi.org/10.1148/rg.e17>.
- Brcic L, Fakler F, Eidenhammer S, Thueringer A, Kashofer K, Kulka J, et al. Pleuropulmonary blastoma type I might arise in congenital pulmonary airway malformation type 4 by acquiring a Dicer 1 mutation. *Virchows Arch.* 2020;477(3):375–82. <https://doi.org/10.1007/s00428-020-02789-6>.
- Calkovska A, Mokra D, Calkovsky V, Matasova K, Zibolen M. Clinical considerations when treating neonatal aspiration syndromes. *Expert Rev Respir Med.* 2019;13(2):193–203. <https://doi.org/10.1080/17476348.2019.1562340>.
- Copetti R, Cattarossi L. The ‘double lung point’: an ultrasound sign diagnostic of transient tachypnea of the newborn. *Neonatology.* 2007;91(3):203–9. <https://doi.org/10.1159/000097454>.
- Cotten CM. Pulmonary hypoplasia. *Semin Fetal Neonatal Med.* 2017;22(4):250–5. <https://doi.org/10.1016/j.siny.2017.06.004>.
- Cristallo Lacalamita M, Fau S, Bornand A, Vidal I, Martino A, Eperon I, et al. Tracheal agenesis: optimization of computed tomography diagnosis by airway ventilation. *Pediatr Radiol.* 2018;48(3):427–32. <https://doi.org/10.1007/s00247-017-4024-5>.
- Desir A, Ghaye B. Congenital abnormalities of intrathoracic airways. *Radiol Clin N Am.* 2009;47(2):203–25. <https://doi.org/10.1016/j.rcl.2008.11.009>.
- Donoghue V, editor. *Radiological imaging of the neonatal chest. Medical radiology (diagnostic imaging).* Berlin: Springer; 2008.
- Gabelloni M, Faggioni L, Accogli S, Aringhieri G, Neri E. Pulmonary sequestration: what the radiologist should know. *Clin Imaging.* 2021;73:61–72. <https://doi.org/10.1016/j.clinimag.2020.11.040>.
- Gordon E, South M, McDougall PN, Dargaville PA. Blood aspiration syndrome as a cause of respiratory distress in the newborn infant. *J Pediatr.* 2003;142(2):200–2. <https://doi.org/10.1067/mpd.2003.36>.
- Gunn C, O’Brien K, Fosså K, Tonkopi E, Lanca L, Martins CT, et al. A multi institutional comparison of imaging dose and technique protocols for neonatal chest radiography. *Radiography (Lond).* 2020;26(2):e66–72. <https://doi.org/10.1016/j.radi.2019.10.013>.
- Hedlund GL, Griscom NT, Cleaveland RH, Kirks DR. Respiratory system. In: Kirks DR, Griscom NT, editors. *Practical pediatric imaging diagnostic radiology of infants and children.* 3rd ed. Philadelphia, PA: Lippincott-Raven; 1998. p. 619–819.
- Jasinovic T, Thamboo A, Osiovič H, Scheepers L, Robinson A, Ludemann JP. Best management of ultra-small tracheobronchial foreign bodies in neonates. *Int J Pediatr Otorhinolaryngol.* 2013;77(3):434–8. <https://doi.org/10.1016/j.ijporl.2012.12.004>.
- Jiang X, Baad M, Reiser I, Feinstein KA, Lu Z. Effect of comfort pads and incubator design on neonatal radiography. *Pediatr Radiol.* 2016;46(1):112–8. <https://doi.org/10.1007/s00247-015-3450-5>.
- Katz C, Bentur L, Elias N. Clinical implication of lung fluid balance in the perinatal period. *J Perinatol.* 2011;31(4):230–5. <https://doi.org/10.1038/jp.2010.134>.
- Körner M, Weber CH, Wirth S, Pfeifer KJ, Reiser MF, Treitl M. Advances in digital radiography: physical principles and system overview. *Radiographics.* 2007;27(3):675–86. <https://doi.org/10.1148/rg.273065075>.

- Leblanc C, Baron M, Desselas E, Phan MH, Rybak A, Thouvenin G, et al. Congenital pulmonary airway malformations: state-of-the-art review for pediatrician's use. *Eur J Pediatr*. 2017;176(12):1559–71. <https://doi.org/10.1007/s00431-017-3032-7>.
- Leekunmerdthai C, Trinavarat P, Sosothikul D, Leelakanok N. Imaging findings of spontaneous thymic hemorrhage in infancy: case report and literature review. *ASEAN J Radiol*. 2020;21(2):44–57. <https://www.asean-journal-radiology.org/index.php/ajr/article/view/71>.
- Limaïem F, Ayadi-Kaddour A, Djilani H, Kilani T, El Mezni F. Pulmonary and mediastinal bronchogenic cysts: a clinicopathologic study of 33 cases. *Lung*. 2008;186(1):55–61. <https://doi.org/10.1007/s00408-007-9056-4>.
- Lincoln JC, Stark J, Subramanian S, Aberdeen E, Bonham-Carter RE, Berry CL, et al. Congenital lobar emphysema. *Ann Surg*. 1971;173(1):55–62. <https://doi.org/10.1097/0000658-197101000-00008>.
- Liu J. Lung ultrasonography for the diagnosis of neonatal lung disease. *J Matern Fetal Neonatal Med*. 2014;27(8):856–61. <https://doi.org/10.3109/14767058.2013.844125>.
- Liu J, Cao HY, Fu W. Lung ultrasonography to diagnose meconium aspiration syndrome of the newborn. *J Int Med Res*. 2016;44(6):1534–42. <https://doi.org/10.1177/0300060516663954>.
- Mani H, Suarez E, Stocker JT. The morphologic spectrum of infantile lobar emphysema: a study of 33 cases. *Paediatr Respir Rev*. 2004;5(Suppl A):S313–20. [https://doi.org/10.1016/s1526-0542\(04\)90056-5](https://doi.org/10.1016/s1526-0542(04)90056-5).
- Miller KE, Edwards DK, Hilton S, Collins D, Lynch F, Williams R. Acquired lobar emphysema in premature infants with bronchopulmonary dysplasia: an iatrogenic disease? *Radiology*. 1981;138(3):589–92. <https://doi.org/10.1148/radiology.138.3.7465834>.
- Morini F, Zani A, Conforti A, van Heurn E, Eaton S, Puri P, et al. Current management of congenital pulmonary airway malformations: a “European Pediatric Surgeons’ Association” Survey. *Eur J Pediatr Surg*. 2018;28(1):1–5. <https://doi.org/10.1055/s-0037-1604020>.
- National Organization for Rare Disorders. Congenital pulmonary lymphangiectasia. <https://rarediseases.org/rare-diseases/congenital-pulmonary-lymphangiectasia/>. Accessed 3 Oct 2021a.
- National Organization for Rare Disorders. Pentalogy of Cantrell. <https://rarediseases.org/rare-diseases/pentalogy-of-cantrell/>. Accessed 3 Oct 2021b.
- Ng J, Antao B, Bartram J, Raghavan A, Shawis R. Diagnostic difficulties in the management of H-type tracheoesophageal fistula. *Acta Radiol*. 2006;47(8):801–5. <https://doi.org/10.1080/02841850600854902>.
- Nickoloff EL, Berdon WE, Lu ZF, Ruzal-Shapiro CB, So JC, Dutta AK. Pediatric high KV/filtered airway radiographs: comparison of CR and film-screen systems. *Pediatr Radiol*. 2002;32(7):476–84. <https://doi.org/10.1007/s00247-002-0689-4>.
- Ohno Y, Koyama H, Lee HY, Miura S, Yoshikawa T, Sugimura K. Contrast-enhanced CT- and MRI-based perfusion assessment for pulmonary diseases: basics and clinical applications. *Diagn Interv Radiol*. 2016;22(5):407–21. <https://doi.org/10.5152/dir.2016.16123>.
- Owens CM. Meconium aspiration. In: Donoghue V, editor. *Radiological imaging of the neonatal chest. Medical radiology (diagnostic imaging)*. Berlin: Springer; 2008. p. 85–97. https://doi.org/10.1007/978-3-540-33749-2_6.
- Peng W, Yang J, Liu E. Analysis of 170 cases of congenital TB reported in the literature between 1946 and 2009. *Pediatr Pulmonol*. 2011;46(12):1215–24. <https://doi.org/10.1002/ppul.21490>.
- Perea L, Blinman T, Piccione J, Laje P. Bilateral congenital lobar emphysema: staged management. *J Pediatr Surg*. 2017;52(9):1442–5. <https://doi.org/10.1016/j.jpedsurg.2017.01.056>.
- Raman SP, Pipavath SN, Raghu G, Schmidt RA, Godwin JD. Imaging of thoracic lymphatic diseases. *AJR Am J Roentgenol*. 2009;193(6):1504–13. <https://doi.org/10.2214/AJR.09.2532>.
- Raol N, Schrepfer T, Hartnick C. Aspiration and dysphagia in the neonatal patient. *Clin Perinatol*. 2018;45(4):645–60. <https://doi.org/10.1016/j.clp.2018.07.005>.
- Riedlinger WF, Vargas SO, Jennings RW, Estroff JA, Barnewolt CE, Lillehei CW, et al. Bronchial atresia is common to extralobar sequestration, intralobar sequestration, congenital cystic adenomatoid malformation, and lobar emphysema. *Pediatr Dev Pathol*. 2006;9(5):361–73. <https://doi.org/10.2350/06-01-0023.1>.
- Sarper A, Ayten A, Golbasi I, Demircan A, Isin E. Bronchogenic cyst. *Tex Heart Inst J*. 2003;30(2):105–8.
- Schneider K. The normal child: growth and development of the infant and child; frequent and important normal variants. In: Daldrup-Link HE, Gooding CA, editors. *Essentials of pediatric radiology: a multimodality approach*. New York: Cambridge University Press; 2010. p. 1–18.
- Seibert JA, Morin RL. The standardized exposure index for digital radiography: an opportunity for optimization of radiation dose to the pediatric population. *Pediatr Radiol*. 2011;41(5):573–81. <https://doi.org/10.1007/s00247-010-1954-6>.
- Sharma D, Farahbakhsh N. Role of chest ultrasound in neonatal lung disease: a review of current evidences. *J Matern Fetal Neonatal Med*. 2019;32(2):310–6. <https://doi.org/10.1080/14767058.2017.1376317>.
- Smet MH, Breysem L, Mussen E, Bosmans H, Marshall NW, Cockmartin L. Visual grading analysis of digital neonatal chest phantom X-ray images: impact of detector type, dose and image processing on image quality. *Eur Radiol*. 2018;28(7):2951–9. <https://doi.org/10.1007/s00330-017-5301-2>.

- Smith MM, Huang A, Labbé M, Lubov J, Nguyen LHP. Clinical presentation and airway management of tracheal atresia: a systematic review. *Int J Pediatr Otorhinolaryngol.* 2017;101:57–64. <https://doi.org/10.1016/j.ijporl.2017.07.028>.
- Soldati G, Demi M, Inchingolo R, Smargiassi A, Demi L. On the physical basis of pulmonary sonographic interstitial syndrome. *J Ultrasound Med.* 2016;35(10):2075–86. <https://doi.org/10.7863/ultra.15.08023>.
- Sorantin E. Soft-copy display and reading: what the radiologist should know in the digital era. *Pediatr Radiol.* 2008;38(12):1276–84. <https://doi.org/10.1007/s00247-008-0898-6>.
- Swischuk LE. *Imaging of the newborn, infant and young child.* 5th ed. Philadelphia, PA: Lippincott Williams & Wilkins; 2004. p. 1–170.
- Thacker PG, Rao AG, Hill JG, Lee EY. Congenital lung anomalies in children and adults: current concepts and imaging findings. *Radiol Clin N Am.* 2014;52(1):155–81. <https://doi.org/10.1016/j.rcl.2013.09.001>.
- Thakkar HS, Durell J, Chakraborty S, Tingle BL, Choi A, Fowler DJ, et al. Antenatally detected congenital pulmonary airway malformations: the Oxford experience. *Eur J Pediatr Surg.* 2017;27(4):324–9. <https://doi.org/10.1055/s-0036-1593379>.
- Walker CM, Wu CC, Gilman MD, Godwin JD II, Shepard JA, Abbott GF. The imaging spectrum of bronchopulmonary sequestration. *Curr Probl Diagn Radiol.* 2014;43(3):100–14. <https://doi.org/10.1067/j.cpradiol.2014.01.005>.
- Woodring JH, Howard TA, Kanga JF. Congenital pulmonary venolobar syndrome revisited. *Radiographics.* 1994;14(2):349–69. <https://doi.org/10.1148/radiographics.14.2.8190958>.
- Yeh SH, Ni YH, Hsu WM, Chen HL, Wu JF, Chang MH. Use of retrograde esophagoscopy in delayed primary esophageal anastomosis for isolated esophageal atresia. *Eur J Pediatr Surg.* 2010;20(1):40–4. <https://doi.org/10.1055/s-0029-1234117>.
- Zarfati A, Voglino V, Tomà P, Cutrera R, Frediani S, Inserra A. Conservative management of congenital bronchial atresia: the Bambino Gesù children's hospital experience. *Pediatr Pulmonol.* 2021;56(7):2164–8. <https://doi.org/10.1002/ppul.25385>.
- Zirpoli S, Munari AM, Primolevo A, Scarabello M, Costanzo S, Farolfi A, et al. Agreement between magnetic resonance imaging and computed tomography in the postnatal evaluation of congenital lung malformations: a pilot study. *Eur Radiol.* 2019;29(9):4544–54. <https://doi.org/10.1007/s00330-019-06042-w>.



Imaging the Neonatal Heart and Large Vessels

11

Erich Sorantin, M. Koestenberger,
and S. Tschauerer

Abbreviations

Ao	Aorta	PS	Pulmonary stenosis
AS	Aortic stenosis	PV	Pulmonary vein
ASD	Atrial septal defect	PW-Doppler	Pulsed wave Doppler
AVSD	Atrioventricular septum defect	RA	Right atrium
CDH	Congenital diaphragmatic hernia	RV	Right ventricle
CMP	Cardiomyopathy	S/D	Systolic to diastolic duration ratio
CoA	Coarctation of the aorta	TAPSE	Tricuspid annular plane systolic excursion
CW-Doppler	Continuous wave Doppler	TAPVR	Total anomalous pulmonary venous return
DORV	Double outlet right ventricle	TGA	Transposition of the great arteries
HC	Hypertrophic cardiomyopathy	TOF	Tetralogy of Fallot
IAS	Interatrial septum	UVH	Univentricular heart
IVS	Interventricular septum	VSD	Ventricular septum defect
LA	Left atrium		
LV	Left ventricle		
LVEF	Left ventricular ejection fraction		
PA	Pulmonary arterial		
PAP	Pulmonary arterial pressure		
PDA	Patent ductus arteriosus		
PFC	Persistent foetal circulation		
PH	Pulmonary hypertension		
PPHN	Persistent pulmonary hypertension of the newborn		

E. Sorantin (✉) · S. Tschauerer
Division of Pediatric Radiology, Department of
Radiology, Medical University Graz, Graz, Austria
e-mail: erich.sorantin@medunigraz.at

M. Koestenberger
Division of Pediatric Cardiology, Department of
Pediatrics and Adolescent Medicine, Medical
University Graz, Graz, Austria

11.1 Introduction

Neonates represent a special challenge for imaging due to their varying body masses from less than 500 g to more than 4000 g as well as their habitats like incubators, warming beds, and more. For the cardiovascular system, echocardiography as a starter, and chest radiographs (CXR) are the most frequent imaging procedures. Diagnosis can be established using these two modalities in the majority of cases. Other imaging procedures like Magnetic Resonance Imaging (MRI) or Computed Tomography (CT), as well as their angiography variants and cardiac catheterisation

(CC), are only needed in situations where, e.g. surgical interventions are necessary in this age group.

All imaging procedures have one challenge in common: any investigation must be adapted to the special needs of this age group—starting with keeping homeostasis (e.g. body temperature) within age dependent normal limits as well as adequate equipment. The increased metabolism of these patients, as compared to adults, demands two times more oxygen thus leading to an increased respiration and heart rate—interestingly enough, two times higher than in adults [1, 2]. Therefore, imaging modalities need more temporal resolution as well as, due to the small body size, geometric resolution. The mentioned factors can be summarised as “the smallest children need the most powerful machines”. Moreover, it has to be considered that sensitivity to radiation exposure is highest in neonatal period during the entire lifetime. This is caused by the high metabolism and cell turnover within the first year of life [2].

This chapter will be structured as follows: embryology of the heart, followed by a general discussion of imaging procedures, and their application in selected, frequent malformations including typical imaging findings.

11.2 Embryology and Development

11.2.1 Basics of Foetal Development of the Heart

In the course of foetal development, the cardiovascular system is the first functional system of the embryo, which starts working as early as in the third week of pregnancy. The embryonic heart activity can be demonstrated by ultrasound (US) from the sixth week of pregnancy.

Disturbances in the different stages of heart development can lead to numerous malformations.

For example, the ventricular septum can have various defects. In addition to the isolated ventricular septal defects (VSD), so-called combined

defects can occur too. This includes, for example, the clinically more relevant picture of a Fallot tetralogy (TOF). TOF consists of a high VSD, an aorta “riding” over the ventricular septum, and a pulmonary stenosis combined with right heart hypertrophy.

If there is no spiral subdivision by the aortico-pulmonary septum, the large vessels are transposed resulting in a heart defect called transposition of the great arteries (TGA). Characteristics of TGA are that the aorta originates from the right ventricle and the pulmonary trunk from the left ventricle. This development is only compatible with life as long as blood exchange between the large (systemic) and small (pulmonic) circulation is possible, e.g. via an additional VSD or a persistent ductus arteriosus (PDA).

11.2.2 Foetal Circulation

The normal foetal circulation is illustrated in Fig. 11.1.

Adaptation from the foetal to the postnatal circulation

In the foetus, the relatively well-oxygenated blood from the placenta is delivered via the umbilical cord and ductus venos (DV). This DV blood enters the right atrium (RA) from the inferior vena cava (IVC) and is directed preferentially to the left atrium (LA) by the foramen ovale (FO) and subsequently delivered preferentially to the brain and the coronary circulation by the foetal left ventricle (LV). The right ventricle (RV) is the predominant ventricle in the foetus, and most of the RV output goes to the descending aorta via the ductus arteriosus (DA) since very little blood enters the pulmonary circulation due to high pulmonary vascular resistance. At birth and removal of the low resistance placenta as well as falling pulmonary vascular resistance, blood flow increases to the pulmonary circulation. Shortly after birth and with a normal postnatal oxygenation, functional closure of DA starts.

The normal oxygen saturation of foetal blood in the left atrium is about 65%. After

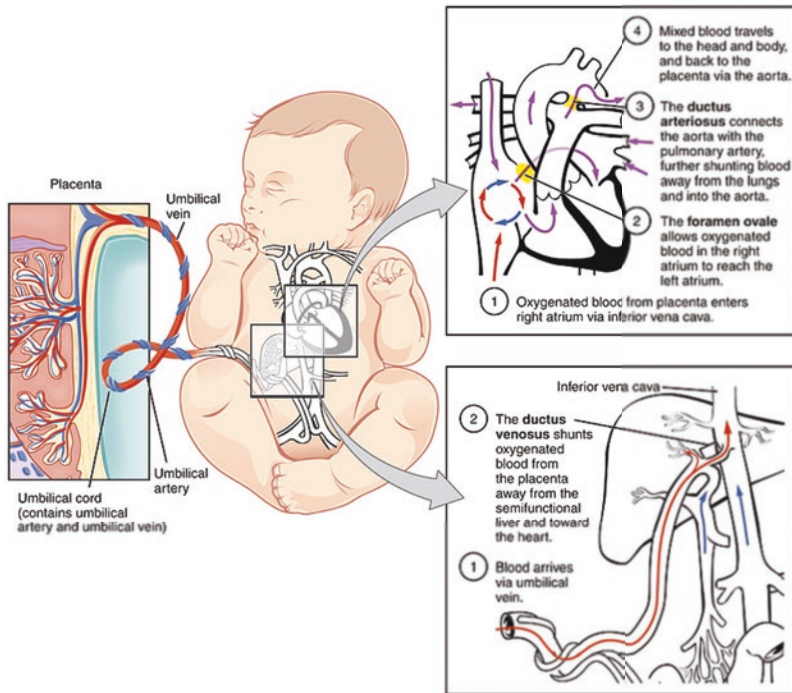


Fig. 11.1 Drawing to explain and illustrate the respective anatomy. *Abbreviations:* DA ductus arteriosus, DV ductus venosus, FO foramen ovale, ICV inferior vena cava, LA left atrium, LV left ventricle, RA right atrium, RV right

ventricle, PA pulmonary artery, Pt portal vein, PV pulmonary veins, Ao aorta ascendens, SVC superior vena cava. (Adapted from: SC Jordan, O Scott: *Heart Disease in Pediatrics*)

birth, the pre-ductal saturation in normal term infants increases to about 90% at 5 min of age [3]. This knowledge is important to avoid unnecessary administration of oxygen during resuscitation.

11.2.3 Important and Common Cardiac and Vascular Malformations

Most frequent malformations can be found in Table 11.1. On top of the list there are structural defects with shunts (like atrial septal and ventricular septal defects), followed by coarctation of the aorta (CoA), pulmonary stenosis, and aortic stenosis. Tetralogy of Fallot and its variants (e.g. pulmonary atresia) represent the most frequent cyanotic structural heart defect. Transposition of the great arteries and other defects like abnormal pulmonary venous return including scimitar vein

Table 11.1 Types and frequency of congenital heart defects

Type	Frequency (%)
VSD	30
ASD	10
PDA	10
Coarctation	7
Pulmonary stenosis	7
Aortic stenosis	6
Tetralogy of Fallot (TOF)	6
Transposition of great arteries	4

are rarer. Atresia of intrahepatic inferior cava vein (azygos continuum) or persistent left upper cava vein usually do not cause circulation problems in the neonatal period. Functional problems within the early postnatal period, like persistent foetal circulation with right to left shunt due to a pulmonary hypertension (part of persistent pulmonary hypertension of newborns—PPHN), should be mentioned too.



Knowledge of cardiac embryology enables understanding of congenital heart defects. After delivery, every neonate has to undergo a complex cardiovascular transition from intrauterine to extra-uterine life in a very short time. Any delay or problem causes functional, potential life threatening conditions.

11.3 Clinical Indications for Imaging the Neonatal Heart

There are several scenarios where the heart and the large vessels need to be assessed by primary imaging modalities like echocardiography and CXR:

- Neonates with murmur.
- Neonates with cyanosis.
- Neonates with palpable pulse difference or measured blood pressure differences between the extremities.
- Neonates on NICU with suspicious radiographic or Doppler US findings.
- Neonates with foetally detected or suspected heart anomalies and conditions where a heart malformation may be part of the spectrum.
- Neonates in whom medical history, clinical inspection as well as results of biomedical monitoring and laboratory checks (e.g. blood gas analysis) reveal alarming symptoms or findings which prompt for further imaging.

11.4 Imaging Modalities

11.4.1 Echocardiography

11.4.1.1 Basics, Transducers, How to Do

Transducers

8–10–12 MHz transducers are needed for good near-field resolution in premature/newborn

infants. Linear transducers can be used in this age group too.

Standard Techniques

Standard techniques are, e.g. M-Mode, two-Dimensional Ultrasound (2DUS), and also include the various Doppler techniques: Continuous Wave Doppler (CW-Doppler), Pulsed Wave Doppler (PW-Doppler), and Colour Doppler Sonography (CDS).

Patient Position

Ideally transthoracic echocardiography is performed in reclined position with patient lying left side down—to avoid interference from lung tissue (especially in older children). A supporting pillow is helpful. For suprasternal views, neck should be hyperextended to gain access. However, such positioning may be cumbersome in very sick neonates; furthermore, the thymus often offers a good window in newborns making such positioning manoeuvres less important.

11.4.1.2 Standard Planes and Standardised Course of Examination

There are four basic planes:

- Long-axis plane parallel to the major axis of the left ventricle (main target: LV).
- Short-axis plane orthogonal to the major axis of the LV (main target: RV).
- Coronal plane through the cardiac apex (main target: four-chamber view).
- Suprasternal view (main target: aortic arch).

The transducer is positioned to four echocardiographic windows to obtain these planes (Fig. 11.2):

1. The parasternal area close to the sternum in the second, third, or fourth intercostal space.
2. The region of the cardiac apex.
3. The subcostal region.
4. The suprasternal notch.

Long- or short-axis planes can be generated in each of these areas. Additional views are obtained by tilting the transducer from right to left, from superior to inferior, or rotating it clockwise and counterclockwise.

Ideally, every examination should follow a standardised protocol: define the visceral situs; describe the relationship between the descending aorta and IVC, specify position and morphology of the atria, describe the systemic and the pulmonary venous return, hepatic veins, the continuity of the IVC, and the interatrial septum (IAS). Then assess the atrioventricular junction to depict the atrioventricular valves and interventricular septum (IVS). Finally evaluate the ventriculo-

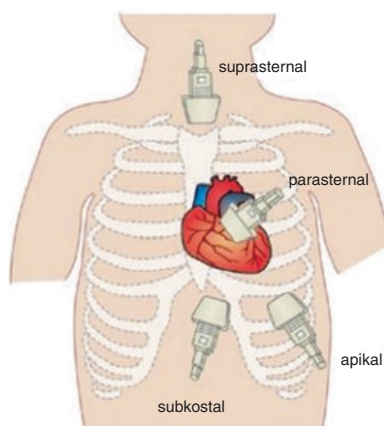


Fig. 11.2 Transducer positioning for acquiring the suprasternal, parasternal, apical, and subcostal windows is shown in this schematic drawing, including typical transducer orientation

arterial junction to describe the origin and course of the great vessels.

11.4.1.3 Standardised Views

Parasternal Long-Axis View (Fig. 11.3)

Applying the transducer between the second and fourth intercostal space can identify an orienting plane along the major axis of heart—from left hip to right shoulder with the RV and LV outflow tract. In infants, the thymus is usually seen between the thoracic wall and heart, and improves visualisation and enlarges the sonographic window.

Next structures: The IVS, the LV, and LA; inflow portion of the LV with the mitral valve, outflow portion with the aortic valve and the ascending aorta (Ao)—visualised in the same plane.

Parasternal Short-Axis Views (Fig. 11.4)

Obtained by rotating the transducer 90° clockwise from a long-axis view. Several short-axis planes can be generated by tilting the transducer from the apical region inferiorly to the base of the heart superiorly. Doing this, a cross section of LV and a part of the RV are seen at different anatomic levels: cardiac apex, papillary muscles, mitral valve, and heart base with origin of the great vessels.

Leftward angulation of the transducer: The RV outflow tract and the main pulmonary artery (PA) with its bifurcation visualised. At

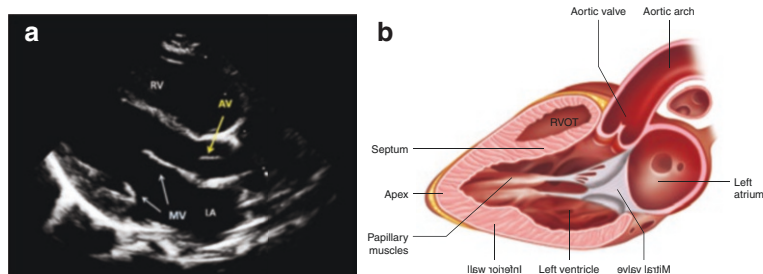


Fig. 11.3 (a) An echocardiogram (in a left parasternal left long-axis view) with a part of the RV seen behind chest wall. The inflow tract of the LV with the MV as well as the outflow tract of the LV with the aortic valve is depicted, too.

For a better anatomical orientation, a respective schematic drawing is added (b). (From: <https://en.wikipedia.org/wiki/File:LeftParasternalLongAxis.gif>). Abbreviations: LV left ventricle, MV mitral valve, RV right ventricle

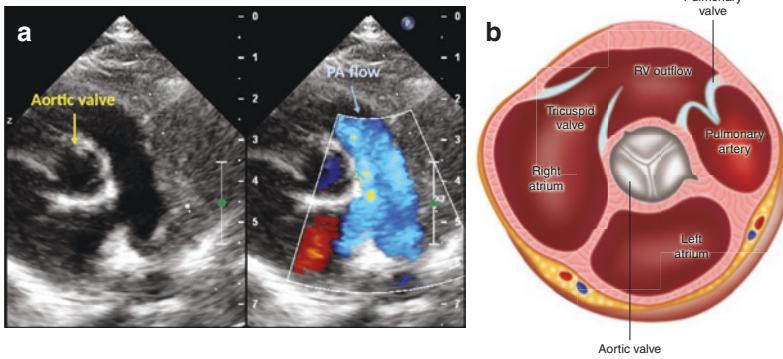


Fig. 11.4 Echocardiography, parasternal short-axis view at the base of the heart: (a) Basic grey scale echocardiography, parasternal short-axis view at the base of the heart. The Ao is visualised in cross section, the PA with its bifur-

cation seen left to the Ao. For a better anatomical orientation, a respective schematic drawing is added (b). (From: https://en.wikipedia.org/wiki/File:Aortic_valve_sa.png). *Abbreviations:* Ao aorta, PA pulmonary artery

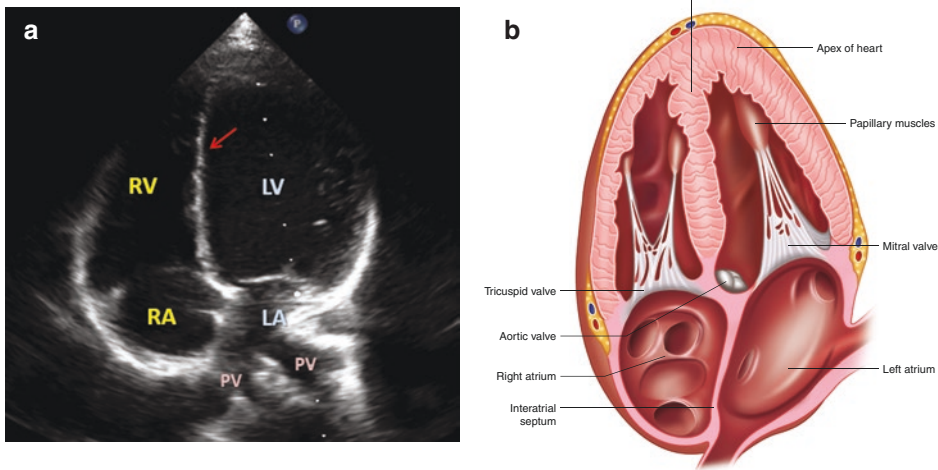


Fig. 11.5 Echocardiography, apical four-chamber view (a). Depicted are all four chambers of the heart. The inter-ventricular and interatrial septum is depicted. For a better anatomical orientation, a respective schematic drawing is

added (b). (From: https://en.wikipedia.org/wiki/File:Apical_4_chamber_view.png). *Abbreviations:* LA left atrium, LV left ventricle, RA right atrium, RV right ventricle

base of the heart: origin of the coronary arteries.

Apical Views

Apical Four-Chamber View (Fig. 11.5)

Standard apical four-chamber view: the transducer is applied to the cardiac apex, the plane

oriented perpendicular to the atrial and ventricular septum.

All four cardiac chambers, the mitral and tricuspid valve, the IAS, and the IVS are best imaged with anterior angulation of the transducer: LV outflow tract and ascending aorta visualised too (“five-chamber view”).

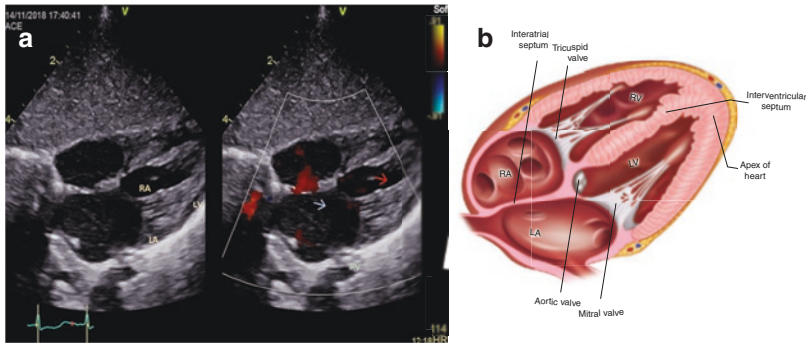


Fig. 11.6 Echocardiography, subcostal view (a). The interventricular and interatrial septum is depicted. For a better anatomical orientation, a respective schematic drawing is added (b). (From: <https://en.wikipedia.org/wiki/>

[File:Subcostal.gif](#)). *Abbreviations:* LA left atrium, LV left ventricle, MV mitral valve, RA right atrium, RV right ventricle, TV tricuspid valve

Subcostal Sagittal and Four-Chamber View (Fig. 11.6)

The transducer is placed subcostal in a sagittal plane; the descending aorta is visualised left to the IV. The transducer is applied to the subcostal region, the plane tilted superiorly: all four cardiac chambers can be imaged similar to the apical four-chamber view; especially in newborns and infants the interatrial septum is visualised especially well; also the drainage of the pulmonary veins (PV) can be demonstrated.

Suprasternal View (Fig. 11.7)

The transducer is placed at the suprasternal notch with an overextended neck (if feasible): the entire aortic arch with the arising supra-aortic vessels can be visualised. The right PA is imaged in a cross section beneath the aortic arch.

- This view is particularly helpful for differentiating between left and right aortic arch and for assessing the supra-aortic great vessels.

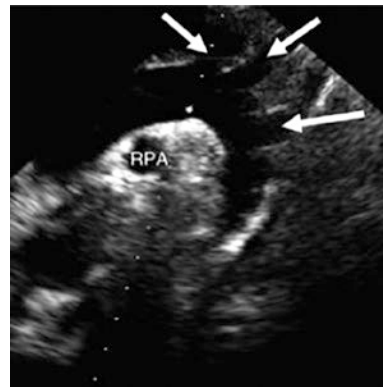


Fig. 11.7 This echocardiographic suprasternal view depicts the entire aortic arch, with the origin of the supra-aortic vessels (white arrows); the right pulmonary artery (RPA) is seen in cross section beneath the aortic arch

- Always include the apical four-chamber view and a view at the IVC entrance to the RA.
- Include an orienting apical view of the heart in every scan at the emergency room (e.g. for pericardial effusion, poor contractility, volume deficit ...).

11.4.1.4 POCUS of the Neonatal Heart

Particularly in newborns and infants in emergencies or at the NICU (e.g. differential diagnosis of a cyanotic newborn), cardiac point-of-care US (POCUS) of the critically ill neonate should be performed.

The typical course of an orienting investigation and the minimal requirements for an orienting assessment of the heart are: Start with an apical and/or subcostal four-chamber view, continue with a parasternal long- and short-axis view, and end with a suprasternal view of the aorta.

11.4.1.5 Echocardiographic Methods

M (Motion)-Mode Echocardiography

M-Mode—this was the first US application in cardiac imaging based on a 1D view of the heart. Today, M-Mode is generated from 2DUS, the respective imaging plane is used to position the M-Mode beam.

Applications of M-Mode in paediatric echocardiography are: the measurement of the cardiac chambers, vessels, and the cardiac septa; assessment of the LV systolic function (shortening fraction and ejection fraction); and the study of valve motion and the interventricular septum.

Transesophageal Echocardiography (TEE)

TEE is a semi-invasive procedure (the transducer introduced into the oesophagus) and not commonly used in neonates. Major indications to perform a TEE in neonates are intra- or peri-operative echocardiography, the evaluation of morphology of ventricular septal defects and of the cardiac valves, and guidance of interventional procedures during cardiac catheterisation.

Tissue Doppler Imaging (TDI)

This is a new technique using Doppler principles to measure velocity of myocardial motion. The most important applications are measurement of the LV and RV systolic and diastolic function. It enables the physician to estimate RV/LV diastolic and systolic function in more detail. As for several other parameters, neonatal normative values differ from those in older children and adults.

11.4.1.6 Doppler Sonography in the NICU

Colour Doppler Sonography

It demonstrates various aspects of blood flow inside the heart and the great vessels and demonstrates flow direction colour encoded as towards or away from the transducer. It also allows assessment of the direction of intra- and

extracardiac shunts, valvular stenosis, and regurgitations.

PW- and CW-Doppler

These techniques are used in combination with 2DUS and CDS to measure direction and velocity of blood flow in the cardiac chambers, the great vessels or across intra- and extracardiac shunts.

The advantage of PW-D is that it samples blood flow in small specific and well-defined area

- The restriction of PW-D is that there is an upper limit of maximum detectable velocity, which can be measured (Nyquist border or limit).

Therefore, CW-Doppler is used in very high flow velocities such as for quantification of, e.g. severe stenosis. Furthermore, try to take flow measurements whenever possible at sections where the flow direction is nearly parallel to the US beam direction and thus with a low Doppler angle ($<20^\circ$)—otherwise angle corrections would have to be applied to avoid wrong measurements, and these corrections may be cumbersome to properly define.

11.4.1.7 Assessment of LV and RV Function

This is often used for assessing heart function, usually incorporated into the device with some cardiac quantification software based on equations:

- Assessment of the LV systolic function:
- LV shortening fraction (LVFS): an older M-Mode index ($FS = \text{LV internal diameter in diastole} - \text{LV internal diameter in systole} / \text{LV diameter in diastole}$).

LV ejection fraction (LVEF) on 2D-Echocardiography: $\text{end-diastolic LV volume} - \text{end-systolic LV volume} / \text{end-diastolic LV volume}$.

Assessment of RV systolic function: Tricuspid annular plane systolic excursion [TAPSE]

TAPSE is an M-Mode index of the displacement of the RV base between systole and diastole. TAPSE measures the longitudinal systolic RV function; currently this is the most objective estimation of RV function in adults and in children in echocardiography [4, 5].

11.4.1.8 Normal Neonatal and Paediatric Values

For the LVEF and the LV fraction shortening (FS), the neonatal and paediatric normative values are similar to adult values. Normal values for functional parameters can be found in Table 11.2.

For the Doppler flow/rate values, the neonatal and paediatric normative values differ from those in adults. Normal values of peak Doppler flow rates are given in Table 11.3.

Most other normal values, especially of the dimensions of the cardiac chambers, vary with age and body surface area. Details can be found at <http://parameterz.blogspot.com/2008/09/z-scores-of-cardiac-structures.html>. As an example, the differences between neonatal, paediatric, and adult values were shown for the RV systolic function parameter, e.g. TAPSE [5].

11.4.2 Chest Radiography

11.4.2.1 Hardware

Currently used needle-ip detectors will be soon not any more available and then only flat panel

Table 11.2 Normal values for functional parameters

Shortening fraction (SF)	28–44%
Ejection fraction (EF)	58–75%

Table 11.3 Normal values of peak Doppler flow rates

Ascending aorta	1.2–1.8 m/s
Descending aorta	0.9–1.1 m/s
Pulmonary artery	0.7–1.1 m/s
Tricuspid valve	E-wave: 0.6 m/s, A-wave: 0.4 m/s
Mitral valve	E-wave: 0.9 m/s, A-wave 0.5 m/s
Vena cava	0.7 m/s

From Snider AR, Serwer GA, (1997) *Echocardiography in pediatric heart disease*. Mosby, St. Louis: Year Book, Inc

detectors can be used. Care has to be taken that the selected system has adequate properties (e.g. Signal to Noise Ratio, Modular Transfer Function, geometric resolution ...) especially in the kV range as used for chest radiographs (CXR) in neonates.

11.4.2.2 Image Acquisition

Body proportions of neonates with a big head, a short neck and chest, as well as a large abdomen demand exact positioning of the imaging plate as well as a meticulous use of manual shutter in order to limit radiation exposure to the requested region. Therefore, CXR within the incubator needs experienced radiographers. Placing the detector within the X-ray drawer of incubators should be avoided, since the increased focus object implies higher radiation exposition, as does the attenuation of patient's couch. Another complexity is added by the weight differences in this age group, e.g. 10% body weight increase after cardiac surgery, augmented by artificial oxygenation or extracorporeal membranous oxygenation. The incubator top itself also leads to attenuation of the X-ray beam hence higher exposure settings are needed as compared to CXR outside, e.g. baby warming devices. Thus, a correct exposure setting is a difficult topic. A good way to solve this and to grant constant good quality at lowest achievable radiation burden is to have exposure tables available at the X-ray machine allowing for proper dose management; those tables will furthermore help to prevent calculation errors when in stress.

11.4.2.3 Image Post-processing

Image post-processing must be adapted to the body composition of neonates and is different to older children. Unfortunately, due to the heterogeneity of mobile equipment and post-processing algorithms, it is impossible to give general recommendations.

11.4.2.4 Image Optimisation

In order to optimise protocols, a simply phantom has proved to be a valuable tool (Fig. 11.8). It consists of three to four 1.0 cm thick acrylic glass plates simulating the respective mass. On top of those plates gaze, skin friendly plasters

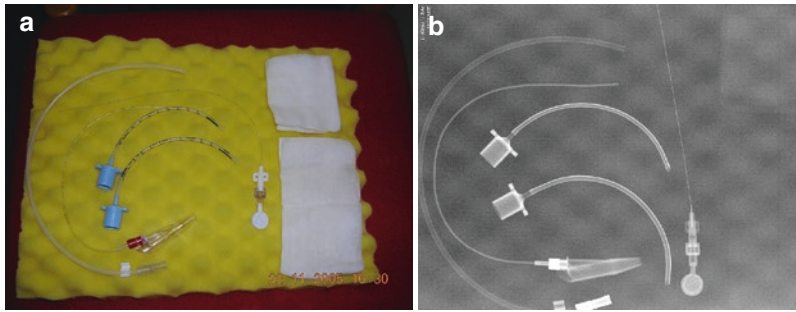


Fig. 11.8 (a) A simple phantom for checking and optimising CXR image quality. Three to four layers of acrylic glass which simulate the mass. Additionally, plasters, endotracheal tubes, findings tube, gaze laying on foam are positioned to produce various densities. By generating radiographs with different exposure values and varying post-processing parameters, determination of optimal set-

tings in a user friendly semi-quantitative way becomes possible. (b) Example of a radiograph after phantom exposure: tubes can be detected easily, but low contrast objects cannot be detected. Therefore, this setting is sub-optimal. Foam gives a chessboard like pattern, which only can be detected if there is no baby lying on it. In a clinical setting, this pattern will not be detectable

as well as endotracheal tubes (as typically used in neonatology) are placed. Afterwards radiographs with varying exposure and post-processing settings are taken and visually analysed. Commercially available phantoms allow to determine the geometric resolution expressed line pairs. Additionally low contrast level can be checked by inserts of different densities. Using digital image processing for analysis represents a more quantitative approach. An overview on quality standards in paediatric CXR (released by the European Commission) as well as its modification can be found in [6, 7].

11.4.2.5 Image Evaluation/Analysis

The best approach is to do it systematically—always in the same sequence, thus providing always the same performance 24/7. Start with installations like an endotracheal tube (tip should be in projection of the sternoclavicular joint), a venous access catheter (tip should be in projection of superior cava vein near to the heart), some chest tubes (all tube holes inside the chest), electrodes from pacemakers (which additionally must be differentiated from skin ECT electrodes). Artefacts can occur from, e.g. holes in the incubator in order to get tubes and electric lines within this habitat. Sometimes lines mimicking pneumothorax can be detected—usually they represent air in skin

folds and are not limited to the lung, but extend into the soft tissue. It is more frequently found in babies with recent weight loss before delivery (since their skin is too big for their present weight).

The next step in image analysis is to assess in which direction the heart apex is pointing. Dextroposition (heart is shifted to the right, but the apex points leftwards) has to be differentiated from dextrocardia (heart apex points to the right—usually caused by situs inversus or dextroversion)—a scheme and examples can be found in Fig. 11.9.

The cardiothorax ratio can be up to 70%, but this is not due to a bigger heart (normalised stroke volume is the same as later in life), but it just appears bigger [8]. The reason is that these patients do not obey breath-hold commands and since during the respiratory cycle the expiratory phase is longer than the inspiratory phase, it is more likely to catch a CXR during expiration than in inspiration. The scheme in Fig. 11.10 demonstrates the pattern how to assess the enlargement of atria and ventricles. Please keep in mind that atrial dilatation occurs fast, whereas ventricular dilatation takes time.

Lung perfusion can be easily assessed by looking for vascular markings. Pulmonary vessels should be visible to at least 50% of chest width, since the vessels are smaller than later in life and the resolution of the detector not much

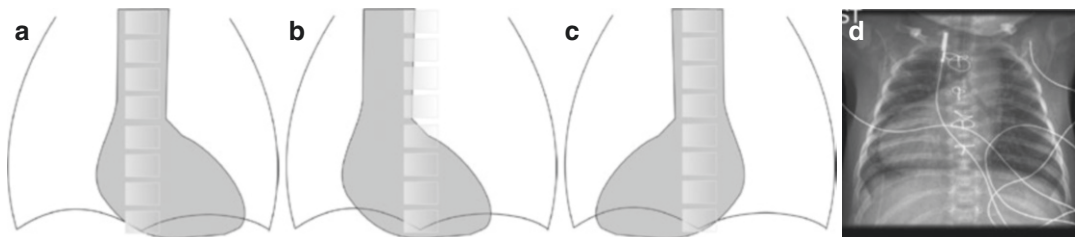


Fig. 11.9 Scheme and radiographs for differentiating dextroposition from dextrocardia. (a) Normal situs—heart apex points to the left. (b) Dextroposition: the cardiac silhouette is moved to the right for any reason, but the heart apex still points to left. (c) Dextrocardia—the heart apex points to right patient side, either due to situs inversus or cardiac dextroversion. (d) Chest radiograph of a patient with dextrocardia with a single left double outlet ventricle, with TGA position of great arteries, and an abdominal situs inversus with polysplenia. The patient underwent already cardiac surgery and the second lowest sternum cerclage is broken. The cardiac apex points to patient's right side and due to the abdominal situs inversus, the gastric tube points to the right patient side too

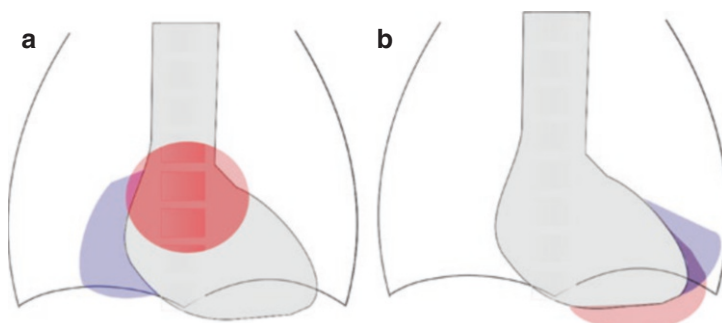


Fig. 11.10 Scheme for cardiac enlargement analysis in chest radiographs. (a) Red structure demonstrates the increase size of left atrium—the heart shadow gets “two ears” and usually the bifurcation angle is getting more obtuse. The blue structures indicate right atrial enlargement, which should usually not be wider than half of the

thoracic vertebra. (b) In red a big, enlarged left ventricle is shown—the heart apex “dives” into the diaphragm. In contrary, right ventricular dilatation/hypertrophy rotates the cardiac apex counter-clockwise so that it points upward and therefore “fingers” can be virtually put between the cardiac apex and the diaphragm on the image

better. Visible vessels in the outer third of the chest width represent hyperperfusion (e.g. left-to-right shunts, left ventricular insufficiency, increased intravascular volume due to renal insufficiency), whereas vessels visible within the medial third represent hypoperfusion (e.g. airway obstruction leading to hypoxic vaso-constriction, pulmonary hypertension) (Fig. 11.11). Active hyperperfusion can be distinguished from passive. In active hyperperfusion, there is enlargement of the pulmonary arteries (e.g. due to a left-to-right shunt in ventricular septum defect VSD), whereas in passive hyperperfusion there is enlargement of the pulmonary veins (e.g. in volume overload). Nevertheless, in severe cases both can exist simultaneously (as, e.g. in decompensating VSD).

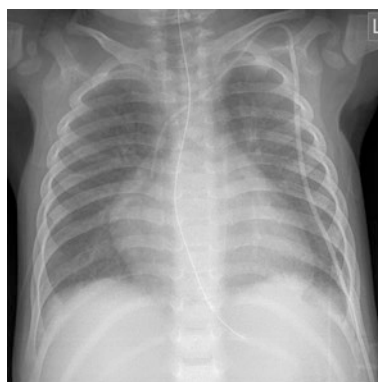


Fig. 11.11 Chest radiograph in a septic neonate with cardiac decompensation. Cardiac silhouette is enlarged, the apex dives into the diaphragm, and the tracheal bifurcation angle is increased due to increased size of the left atrium. Additionally note increased lung perfusion and basal pleural effusions

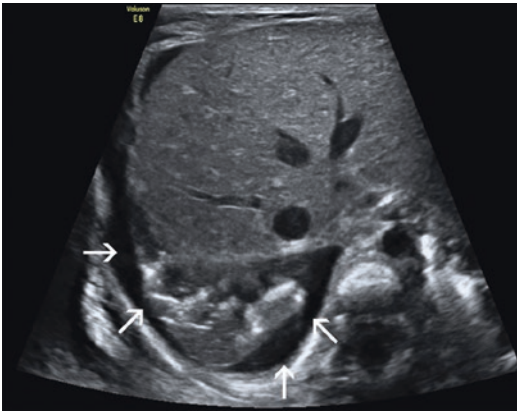



Fig. 11.12 Ultrasound (US), subcostal view. US image demonstrates an almost axial cross section of right thoraco-abdominal region. White arrows point to pleural effusion surrounding the collapsed lung, white lines within the collapsed lung correspond to air filled bronchi

Furthermore, search for pleural effusion, which nevertheless can be best detected by US (Fig. 11.12). Increased fluid load of the lung makes them stiffer and therefore the reduced compliance is demonstrated by less inspiration depth. Interstitial lung oedema makes vessel borders appear fuzzy, whereas alveolar lung oedema can be easily diagnosed by the typical butterfly appearance (which is caused by “more/thicker” lung tissue in the central parts as compared to the periphery). Interstitial and alveolar interstitial lung oedema can partially be distinguished by lung US (Fig. 11.13).

 CXR is one of the most frequently used imaging modality in neonates. Besides all other features, CXR additionally allows for an orienting assessment of the cardiovascular situation.

11.4.3 Cardiac CT

While echocardiography remains the first-line imaging modality for assessing congenital cardiac and vascular abnormalities, not always all relevant details can be assessed sonographically.

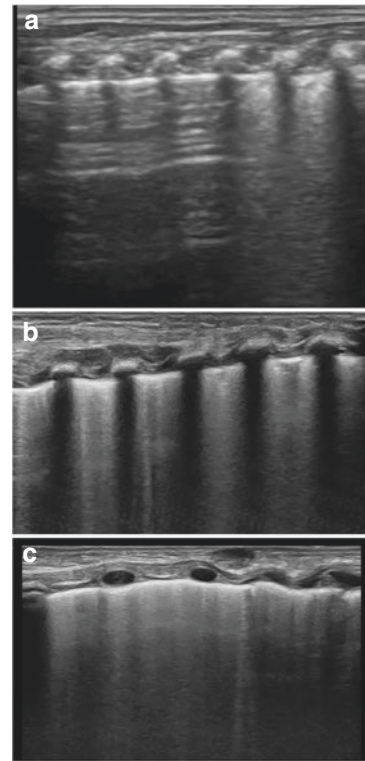


Fig. 11.13 Lung ultrasound (LUS), intercostal view. (a) Normal findings—A-lines generation by reverberation echoes can be detected. (b) B-lines pattern: A-lines are replaced by an echogenic, diffuse pattern, only rib shadows are spared. B-lines correspond to interstitial oedema. (c) Compact B-lines: the whole lung reveals an echogenic pattern erasing even rib shadows—indicating alveolar-interstitial oedema. (See also Chap. 10—chest imaging/lung ultrasound)

Additionally, complications following cardiac surgery such as vessel leakage and haematoma formation need emergency imaging—most often done using CT Angiography (CTA).

Therefore, CT is the modality of choice in second line for imaging of suspected abnormalities of great vessels and their malformations in all details. Moreover, lung malformations and their vascular supply (e.g. sequestration) as well as parenchymal lung disease can be assessed simultaneously including work-up of PH/PPHN. Due to the high cardiac output of neonates and therefore their fast heart rate, they should be investigated on the best CT machine available—preferably

a volume scanner with rotations times well below 0.5 s, best around 0.3 s [1, 9].

In order to minimise radiation exposure, all aspects of a CT investigation should be optimised—starting with tube down during tomogram/scout view as well as adapted kV and mAs settings, where usually 80 kV are sufficient. For automated exposure control setting, set the lower limit to lowest possible value [2, 10].

Intravenous contrast agent (CA) injection for CTA represents another challenge in this age group due to increased heart rate and blood flow velocity, as compared to adults. Moreover, small sized intravenous cannula limit blood flow. Using usual “automated bolus tracking” (ABT) methods commonly only either the aorta or the pulmonary vessels can be imaged. Due to septal defects or surgically created shunts, it is almost impossible to predict the optimal time window.

The so-called Micro-bolus Technique represents a way to image all great vessels and veins simultaneously in one run with the advantage of lower dose as well as less injected CA volume—thus lowering invasiveness considerably [11]. How does this work? First, one part of the intravenous CA with an iodine content of 300 mg/mL is diluted with two parts of physiologic saline in order to minimise beam-hardening artefacts caused by iodine. The region of interest (ROI) is placed within the descending aorta and the mixture of CA and physiologic saline is injected as long as the desired threshold value is reached with an injection rate of 1.0–2.0 mL/s. For choosing the appropriate ABT threshold, it must be considered if the CTA scan is started at the position of the monitoring scan or if the tube needs re-positioning, which takes usually approximately 3–4 s. As a rule of the thumb for CTA, starting at the monitor scan level an ABT threshold of absolute 400 HU (Hounsfield units) at 80 kV can be recommended. In case where the gantry must be repositioned, lower ABT absolute threshold values of approximately 250–300 HU should be used at 80 kV.

In some CT, ABT threshold has to be set as an increase from the native HU of the monitoring

ROI thus about 60–70 HU must be subtracted from the above given absolute values.

Extracardiac structures including the lungs can be assessed too. In neonates typical indications for cardiac CT are the assessment of great vessel malformations as well as the extracardiac structures especially those which are not explorable by echocardiography. Another indication is imaging of complications following cardiac surgery.

Quantitative cardiac CT, e.g. for assessment of the ejection fraction, should be avoided due to the respective high radiation exposure.



CT provides morphologic and functional information including 3D reconstructions, offers excellent information about extracardiac structures including the lungs, but CT(A) is not a first-line diagnostics in neonates due to high radiation exposure.

11.4.4 Cardiac MRI (cMRI)

Cardiac MRI provides morphologic and functional information. It allows determination of cardiac stroke volumes, performance markers such as the ejection fraction, as well as two-dimensional velocity encoded phase contrast measurements to estimate the forward and backward volumes—thus enabling quantification of shunt volumes and regurgitation fraction.

By using newer techniques such as 4D-flow with one measurement, flow and thus volumes of vessels can be assessed simultaneously. However, it has to be kept in mind that current acquisitions take 5–6 min and any movement during that time will disable all measurements. In neonates, injection of gadolinium is rarely needed and should generally be avoided in this age group. Gadolinium-free respiration-triggered MR-angiography (MRA) techniques enable the visualisation of the great vessels with sufficient quality in this age group, whereas MR(A) is getting less accurate within the supra-aortal branches. The long duration of the respective

examinations represents one of the disadvantages in neonatal cMRI/MRA. “Feed & Wrap” techniques, where sleeping neonates and babies up to 3 months are examined after feeding are helpful tools in order to avoid general anaesthesia in stable patients.



cMRI enables to obtain morphology as well functional information (e.g. stroke/shunt/regurgitation volumes, ejection fraction). In neonates, gadolinium application should be avoided since gadolinium-free MRA techniques provide valuable and often diagnostically sufficient alternatives. In stable patients, the “Feed & Wrap” approach allows high quality cMRI investigations avoiding general anaesthesia.

11.4.5 Cardiac Catheterisation and Catheter Angiography

Diagnostic cardiac catheterisation with angiography is rarely used in the neonatal age group. A cardiac catheterisation may be indicated if an exact haemodynamic evaluation is deemed essential (shunt volume, pulmonary artery pressure/pulmonary vascular resistance) and is needed for management in neonates with congenital heart disease. Today the role of cardiac catheterisation has changed: about 50% of cardiac catheterisations in children are therapeutic interventional procedures, such as in congenital aortic or pulmonary stenosis as well as in order to perform a Rashkind procedure.



In neonates, cardiac catheterisation is rarely needed since usual echocardiography and radiographs are sufficient for diagnosis and management decisions. In neonates, the main indications for cardiac catheterisation are emergency interventional procedures in instable patients suffering, e.g. from severe congenital aortic or pulmonary stenosis.

11.5 Pathologic Findings

11.5.1 Congenital Heart Defects with Left-to-Right Shunt

11.5.1.1 Atrial Septal Defect (ASD)

ASD causes a left-to-right shunt within the atria, and several types are known. The septum secundum type can remain undetected until young adulthood and maybe detected in case of a paradox embolism. Septum primum ASD can be associated with an incomplete atrio-ventricular channel (e.g. in Down syndrome patients). In sinus venosus defects, partial anomalous pulmonary venous return can be present too (scheme in Fig. 11.14a).

- **Haemodynamics:** Due to the left-to-right shunt via the ASD, there is an increased lung perfusion with consecutive reduced systemic perfusion. Therefore, all these patients exhibit a reduced aortic diameter. In long term, the increased pulmonary perfusion may lead to pulmonary hypertension.
- **Echocardiography:** The interatrial septum (IAS) is assessed best from subcostal and apical four-chamber views. Depending on location of defect, the viewing plane has to be angulated superiorly or inferiorly from the standard four-chamber view.

The IAS is thin, particularly at the fossa ovalis and therefore it may be difficult to distinguish true defects from artefacts. True defects usually show echogenic margins (“T artefact”). CDS and PW-Doppler demonstrate an interatrial left-to-right shunt.

Haemodynamic relevance of ASD can be assessed by demonstrating RV volume overloads thus causing RA and RV enlargement as well as dilatation of the PA. TEE is helpful in doubtful cases. The most common type of ASD (~70%) is located in the mid portion of the IAS, sometimes multiple defects are present (“multi-fenestrated IAS”). In neonates and infants, a patent foramen ovale (PFO) is a small, flap-like opening with left-to-right shunt in mid portion of the IAS (overlap of septum primum with septum secundum). An example is

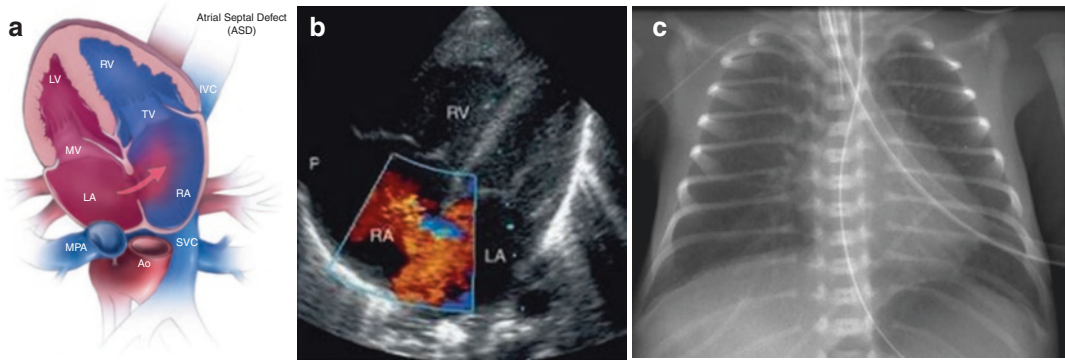


Fig. 11.14 (a) Scheme of ASD II (from https://en.wikipedia.org/wiki/Atrial_septal_defect#/media/File:Asd-web.jpg). (b) Echocardiography, apical four-chamber view. Colour Doppler demonstrates an interatrial left-to-right shunt by red colour signals crossing the interatrial septum. An enlarged RA and RV with a straight course of the interventricular septum indicates volume overload. (c) Chest radiograph of a patient with ASD II—there is an obtuse tracheobronchial angle indicating left atrial dilatation also causing the cardiac bay to be lateral convex

shaped. Due to active hyperperfusion, the hili are not comma shaped and the pulmonary vasculature can be depicted even in the outer third of the hemithorax. Additionally, there is a peripherally inserted venous catheter coming from the right, the tip lies in projection on the brachiocephalic vein, an endotracheal tube is in the correct position, as well as a feeding tube. *Abbreviations:* ASD atrial septal defect, LA left atrium, RA right atrium, RV right ventricle

depicted in Fig. 11.14b. Without RA and RV enlargement as well as PA dilatation, it is considered nearly physiological and needs no further attention. In doubtful cases, echocardiographic follow is recommended.

- **Chest radiography:** An increased size of both atria can be recognised as well an enlarged right ventricle. Due to the thymus, the small aortic shadow cannot be precepted in neonates with the exception of thymus stress atrophy or thymus a-/hypoplasia. Moreover, the most striking finding is the pulmonary hyperperfusion (Fig. 11.14c).
- **Other imaging modalities:** Usually not necessary for management of ASD II patients within the neonatal period.



A simple ASD II does not cause problems in the neonatal period, as long as left-to-right shunts volumes are small and not associated with other structural defects. In most ASD cases, radiographs and echocardiography are the solely imaging modalities necessary for clinical management.

11.5.1.2 Ventricular Septal Defects (VSD)

VSD is the most common congenital heart defect. The interventricular septum (IVS) is divided into a small upper membranous septum and a larger muscular septum. The muscular septum consists of an inlet, a trabecular, and an outlet-(infundibular) portion. Most VSDs are located in the membranous part, often the adjacent muscular septum is involved (“peri-membranous”). Muscular and infundibular VSDs are less common (see scheme in Fig. 11.15a).

- **Haemodynamics:** There is a left-to-right shunt on the ventricular level. Consecutive volume overload leads to increased size of the left atrium, the left ventricle, and later also to right ventricular hypertrophy.
- **Echocardiography:** CDS improves detection of small or multiple VSDs, and shows direction of the shunt across defect. CW-Doppler allows indirect estimation of RV systolic pressure using the modified Bernoulli equation (systolic blood pressure minus peak pressure gradient between LV and RV = systolic RV pressure).

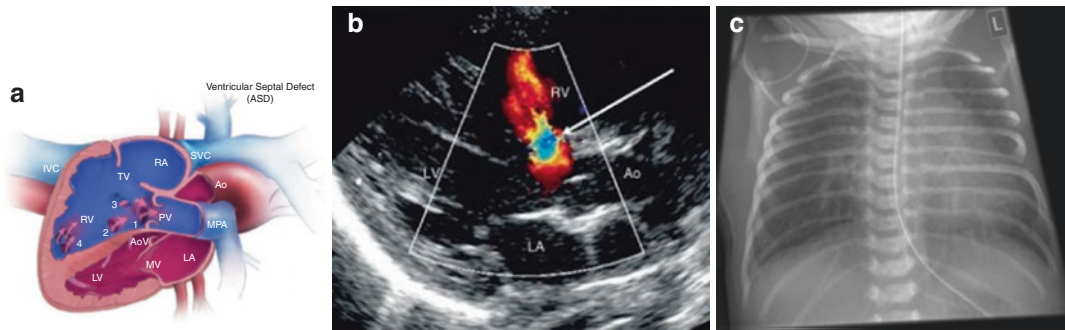


Fig. 11.15 Ventricular septum defect (VSD) (a) Scheme of VSD (from https://en.wikipedia.org/wiki/Ventricular_septal_defect#/media/File:Vsd_simple-1g.jpg). (b) Echocardiography, parasternal long-axis view. A perimembranous VSD is depicted. Colour Doppler demonstrates a left-to-right shunt (white arrow) beneath the

aortic valve through the VSD. (c) Chest radiograph: similar to ASD II there is left atrial dilatation as well as active pulmonary hyperperfusion, but in VSD there is left ventricular dilatation. *Abbreviations:* ASD atrial septal defect, VSD ventricular septal defect

- *Membranous VSDs:* On parasternal long- and short-axis views and in a modified four-chamber view, the defect is seen beneath the aortic valve, sometimes associated with a ventricular septal pseudo-aneurysm.
- *Muscular VSD:* It is seen in the parasternal long-axis view in middle third of the IVS (mid muscular) or inferiorly (apical), and in the parasternal short-axis views at different levels.

The apical four-chamber view shows the inlet VSD in the upper third, the mid muscular VSD in the middle of the IVS, and the apical VSD in the most distal part of the IVS.

The infundibular VSD can be found in the standard long-axis view beneath the aortic valve and in the parasternal short-axis view beneath the pulmonary valve. It is often associated with aortic valve regurgitation due to prolapse of the aortic valve (Fig. 11.15).

- **Chest radiography:** The enlargement of the left atrium and the left ventricle can be detected, as well as pulmonary hyperperfusion. As already mentioned previously, due to the left-to-right shunt, the aortic shadow can be small. Signs of LV failure such as Kerley lines, pleural effusions, and even alveolar lung oedema indicate the need for urgent surgical therapy.
- **Other imaging modalities:** In neonates, there is no need for CT and MRI with the excep-

tion of complications after urgent surgery such as vascular leaks or large haematoma.

Preoperative cardiac catheterisation is usually only indicated in patients with very large VSDs to preoperatively determine the pulmonary artery pressure and therefore to minimise possible intraoperative complications such as pulmonary arterial crisis.



A VSD can lead to considerable left-to-right shunts thus leading to active pulmonary hyperperfusion. In most VSD cases, radiographs and echocardiography are the only imaging modalities necessary for clinical management.

11.5.1.3 Atrioventricular Septal Defects (AVSD)

The AVSD is characterised by one common atrioventricular (AV) valve with one common or two separate orifices. Characteristically leaflets of the common AV-valve insert at the same level into the ventricles (normally the insertion of the tricuspid valve is more apical than the position of the mitral valve).

Partial AVSD (Ostium Primum ASD) The defect is situated only in the lowest part of the IAS near the AV-valve in a subcostal and the apical four-chamber view. It has a left-to-right shunt

only at the atrial level and a variable degree of mitral valve regurgitation.

Complete AVSD It consists of a defect of the ostium primum ASD and an inlet-VSD in the apical and subcostal four-chamber view. It has an interatrial, an interventricular and a LV-RA shunt and a common AV-valve, usually with mitral and tricuspid valve regurgitation. This defect occurs frequently in Trisomy 21 patients. Other maternal risk factors are bad diabetes control as well as alcohol consumption during pregnancy and some drugs.

- **Haemodynamics:** It exhibits AV-valve regurgitation of different degrees at the commissures between the leaflets (“clefts”) of a common AV-valve. As this is always present it leads to volume overload.
- **Echocardiography:** The size of interatrial and interventricular communications and the ventricles as well as the morphology of the common AV-valve are best evaluated in subcostal and apical four-chamber views and in the parasternal short-axis view. The degree of the AV-valve regurgitation and shunt is best assessed by CDS and CW-Doppler.
- **Chest radiography:** Depending on the amount of AV regurgitation, an enlarged cardiac silhouette and signs of pulmonary hyperperfusion can be found.
- **Other imaging methods:** Cardiac catheterisation, CT, and cMRI may be needed for assessment of concomitant malformations as well as in complications.



Atrioventricular septal defects represent a complex cardiac malformation and early surgery may be needed in non-manageable cardiac decompensation. Radiographs and echocardiography are the most commonly used imaging modalities. Cardiac catheterisation is usually used to determine the pulmonary arterial pressure to avoid perioperative complications. CT and cMRI are reserved for assessment of concomitant malformations and complications.

11.5.1.4 Patent Ductus Arteriosus of Botalli (PDA)

The patency of ductus arteriosus occurs in preterm infants, but also as an isolated defect or associated with other congenital heart defects.

- **Haemodynamics:** PDA results in shunting, and the direction depends on pressure differences between lung and systemic perfusion. Right-to-left shunt occurs in pulmonary hypertension (e.g. persistent foetal circulation, severe surfactant deficiency syndrome)—thus resulting in right heart pressure and overload. Opposite—left-to-right shunt is caused if pressure in systemic circulation is higher than the pulmonary pressure, and then volume overload of the pulmonary vessels and the left heart may occur. It has to be noted that shunt direction may change, e.g. being initially right to left in severe surfactant deficiency, followed by left-to-right direction after successful surfactant replacement therapy with consecutive return of the pulmonary pressure to normal values.
- **Echocardiography:** A PDA best seen in the parasternal short axis or high left parasternal views (“ductus view”)—where three vessels arise from the main PA: the right and the left PA and the PDA, the latter connecting to the descending aorta.

Large PDAs results in LA and LV enlargement due to increased pulmonary blood flow. CDS and CW-Doppler demonstrate the direction of the shunt: in cases of pulmonary hypertension, a bidirectional or right-to-left shunt is found at the PDA level (Fig. 11.16).
- **Chest radiography:** In right-to-left shunts, an enlargement of the right heart compartments can be found, as well as, depending on duration, signs of right ventricular hypertrophy. Usually, the pulmonary perfusion is reduced thus leading to hyperlucent lungs. Vice versa, in left-to-right shunts an increased size of the left heart can be found as well as pulmonary hyperperfusion.
- **Other imaging modalities:** Usually not needed; only in older patients an interven-

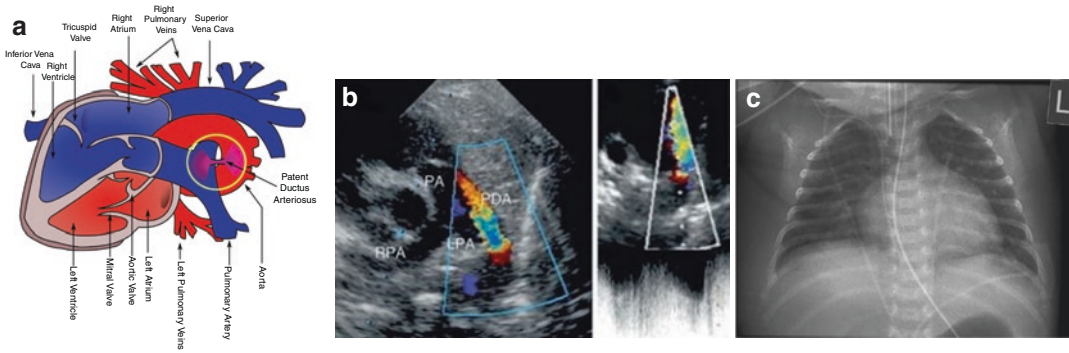



Fig. 11.16 Patent ductus arteriosus (PDA) (a) PDA scheme (from: https://en.wikipedia.org/wiki/Patent_ductus_arteriosus#/media/File:Patent_ductus_arteriosus.svg). (b) Echocardiography, parasternal short-axis view. Left-to-right shunting via the PDA is depicted by Colour Doppler sonography. (c) Chest radiograph: massive enlargement of LA and LV as well as pulmonary hyperperfusion indicating a left-to-right shunt—together with

the typical “train in tunnel” murmur and hyper-pulsatile femoral arteries this suggests a haemodynamic relevant PDA. Additionally, there is an endotracheal tube in correct position and a central line from the right side—the tip is seen in projection of the VCI entrance in RA. *Abbreviations:* LA left atrium, LV left ventricle, PDA patent ductus arteriosus, RA right atrium, RV right ventricle, VCI vena cava inferior

tional closure of a patent PDA by cardiac catheterisation may be an option.

 A PDA can be isolated or in combination with other cardiac malformations. Shunt direction maybe right to left or left to right—depending on pressure differences between the pulmonary and the systemic circulation. Radiographs and echocardiography are usually sufficient for clinical management decisions.

11.5.2 Obstructions of Left Ventricular Outflow

11.5.2.1 Aortic Valve Stenosis (AS)

This congenital heart defect causes pressure overload of the LV and can be associated with other malformations like endocardial fibroelastosis. The “Critical AS of newborns” represents the most severe form and is the most common indication for emergency CC in this age group.

- **Haemodynamics:** A jet stream due to the stenosis causes post-stenotic dilatation of the


ascending aorta. In more advanced cases, pressure overload of the ventricle causes hypertrophy of the LV. A reduced contractility can be observed in ventricular dilatation.

- **Echocardiography:** The parasternal long-axis view enables measurement of valve diameter, and shows the restricted opening of the thickened cusps resulting in a dome shape of the valve during systole. Colour Doppler sonography shows a high-velocity jet into the ascending aorta. Measurements of peak and mean Doppler pressure gradients using different views (suprasternal, subcostal) allow estimation of its severity.

In the “Critical AS of newborn”, the LV cavity and the aortic annulus are small, with an echogenic-thickened endocardium presenting additional endocardial fibroelastosis.

- **Chest radiography:** Depending on severity of the disease, non-specific signs of left ventricular hypertrophy can be detected. In patients after interventional (balloon-) dilatation, aortic insufficiency and pulmonary hyperperfusion can be detected.
- **Cardiac catheterisation:** In the critical AS of newborns, cardiac catheterisation is mandatory for valve dilatation with the consequence of a certain degree of aortic insufficiency.

- **Other imaging modalities:** CTA and MRI are only needed in more complex cases, e.g. if the AS is part of a complex cardiovascular malformation.

 The “Critical AS of newborns” represents the most common indication for “emergency cardiac catheterisation”. The AS-related jet stream causes post-stenotic dilatation of the ascending aorta. Pressure overload of LV leads to muscular hypertrophy, reduced contractility occurs in case of ventricular decompensation and endocardial fibroelastosis. Aortic insufficiency can occur after interventional aortic valve dilatation.

11.5.2.2 Aortic Coarctation (CoA)

Coarctation is one of the “more frequent” cardiovascular malformations (scheme in Fig. 11.17a)—as long as it is an isolated malformation, patients are non-cyanotic. Three types of aortic coarctation exist:

- **Preductal coarctation:** The narrowing is proximal to the (P)DA. Blood flow to the aorta that is distal to the narrowing is dependent on the DA. Preductal coarctation results when an intracardiac anomaly during foetal life decreases blood flow through the left side of the heart, leading to development of a hypoplastic aorta.

- **Ductal coarctation:** The narrowing occurs at the insertion of the DA. This kind usually manifests clinically when the DA closes after few days of life.
- **Postductal coarctation:** The narrowing is distal to the insertion of the (P)DA. Even with an open DA, blood flow to the lower body can be impaired. This type is most common in adults. The triad of hypoplastic left heart, AS, and CoA represents the “Shone complex”.

- **Haemodynamics:** CoA leads to pressure overload of the LV, and in severe causes of CoA the left ventricular function can be depressed considerably—thus these neonates have a PDA dependent systemic perfusion. Increased blood pressure in pre-ductal intercostal arteries causes not only blood pressure differences between upper and lower extremities, but also activation of osteoclasts with the consequence of rib notches, which usually occur after the neonatal period. It has to be kept in mind that there are several other reasons for rib notches.
- **Echocardiography:** CoA is best evaluated from the suprasternal notch in supine position with a hyperextended neck (Fig. 11.17b). The suprasternal long-axis view is used for imaging the entire aortic arch and must be entertained because occasionally also other parts of the aortic arch may be hypoplastic—particularly in neonates. CDS shows a high-velocity jet distal to CoA (Fig. 11.17b). CW-Doppler measurements reveal an increased flow velocity

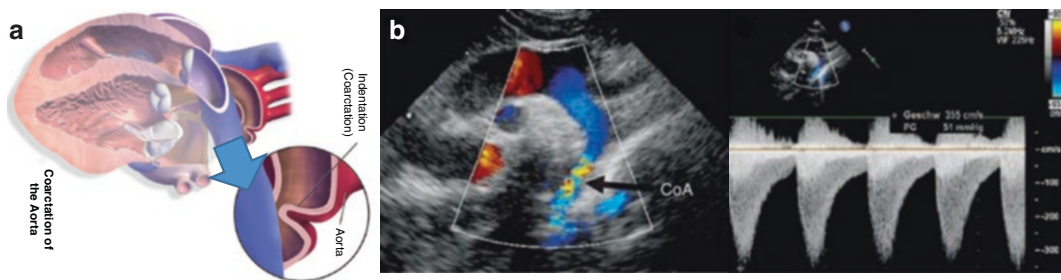


Fig. 11.17 (a) CoA scheme (from: https://en.wikipedia.org/wiki/Coarctation_of_the_aorta). (b) Echocardiography, suprasternal view. The hypoplastic isthmus region with turbulent flow on CDS is marked with black arrow. CW-Doppler measurement shows an

increased flow velocity with a typical flow pattern that obviously extends into the diastole. *Abbreviations:* Ao aorta, CoA coarctation of the aorta, CDS colour Doppler sonography

ity extended into diastole and distal to the CoA that allows calculation of pressure gradients. The LV may be hypertrophied, depending on severity of the CoA.

- **Chest radiography:** In the neonatal period, CXR is usually insensitive, as within the neonatal period the typical findings are usually masked by the thymus. Later in life or with decompensation, the typical the “3 sign” can be seen, which is caused by the pre-stenotic aortic dilatation, the narrowing due to the stenosis, and the post-stenotic aortic dilatation. Moreover, LV hypertrophy can be detected. In cases of an impaired left ventricular function signs of pulmonary hyperperfusion can be detected.
- **Other imaging modalities:** MRI and CTA (Fig. 11.17c) are used for further imaging, especially in the pre-therapeutic setting which usually consist of either catheter interventions or surgery. It has to be kept in mind that cross-sectional imaging has to start well above the aortic arch to include the proximal parts of the supra-aortic vessels. Otherwise, it will not be possible to reliably distinguish between a left or a right aortic arch.



Coarctation is one of the more frequent, non-cyanotic cardiovascular malformations. Echocardiography including assessment of the aortic arch and the supra-aortal vessels allows sufficient assessment in neonates. Further imaging by MRI/MRA or CTA is reserved for complex cases and in the pre-therapeutic setting.

11.5.3 Obstructions of the Right Ventricular Outflow

11.5.3.1 Pulmonary Valve Stenosis (PS)

The diagnosis of PS is made by echocardiography. In infancy, auscultation of the heart usually reveals a systolic murmur.

Some other conditions in which to contemplate the diagnosis of PS are infundibular stenosis and supravulvular pulmonary stenosis.

- **Haemodynamics:** In PS, the opening is too narrow, leading to reduction of blood flow to the lungs. In cases with significant PS, RV hypertrophy can occur later in the course of the condition.
- **Echocardiography:** In the parasternal short-axis pulmonary valve diameter, valvular cusps thickness (with restricted opening and systolic doming, and usually post-stenotic dilatation of main PA in severe PS) can be measured. The RV is usually of normal size and function and may be hypertrophic at the infundibulum in severe PS.

Neonates with a critical PS have a hypoplastic pulmonary valve annulus with usually a reduced RV cavity size; pulmonary blood supply may be dependent on an open PDA (therefore prostaglandins are given to keep it open!). Colour Doppler sonography demonstrates a high-velocity jet distal to the pulmonary valve and CW-Doppler measurements enable estimation of the RV/PA pressure gradient.

- **Cardiac catheterisation:** In critical PS of newborn, cardiac catheterisation is useful for valve dilatation burdened by the risk of a certain degree of pulmonary valve insufficiency.
- **Chest radiography:** The reduced pulmonary perfusion is due to the reduced flow through the pulmonary valve. Furthermore, signs of RV hypertrophy can be detected. Differential diagnosis to Tetralogy of Fallot can be made clinically if patient is not cyanotic.
- **Other imaging modalities:** In neonates, no other imaging is needed for management.



Pulmonary stenosis leads to RV pressure overload and reduced pulmonary perfusion; this can be detected in all imaging modalities. Neonates with a critical PS need an open PDA for lung perfusion.

11.5.3.2 Tetralogy of Fallot (TOF)

Tetralogy of Fallot is the most common cyanotic congenital heart defect. It is characterised by a RV outflow tract obstruction thus causing RV

hypertrophy, a large VSD with overriding aorta (as it gets blood from both ventricles). Pulmonary valve annulus, main PA and PA branches are hypoplastic (various degree), and pulmonary valve leaflets are thickened with systolic doming. A special type is *pulmonary atresia with VSD*—the “so called” *extreme type of TOF*. In this malformation, pulmonary blood supply to the peripheral PA branches is provided only via the PDA or by multiple aortopulmonary collateral arteries arising from the aorta or aortic branches, making this defect PDA dependent. Moreover, in 25% of TOF patients, a right descending aorta can be found (Fig. 11.18).

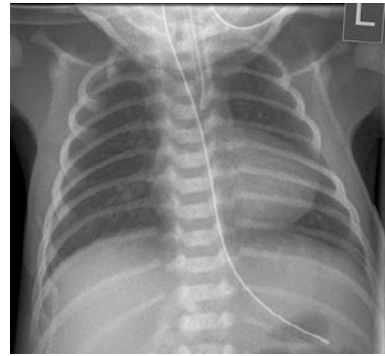


Fig. 11.18 Chest radiograph of a TOF patient. “Fingers” can be virtually placed over the space between the heart apex and the diaphragm—due to counter-clockwise heart rotation, indicating RV hypertrophy. Pulmonary perfusion is reduced. Together with the referring diagnosis of a cyanotic baby, the most likely diagnosis is TOF. Additionally, there is an endotracheal tube in projection of trachea, the tip just above the carina—thus a dangerously low position. Correct positioned naso-gastric tube. *Abbreviations:* LV left ventricle, RV right ventricle, TOF Tetralogy of Fallot

- **Haemodynamics:** Depending on the shunt direction at the VSD level, children may be asymptomatic at birth (so-called Pink Fallot) or present with many severe symptoms. Later in infancy in cases with significant PS, there are typically episodes of bluish colour to the skin due to *cyanosis*. Additionally, when affected babies cry or have stress, they may turn cyanotic.
- **Echocardiography:** The parasternal short axis and suprasternal views demonstrate the PA bifurcation, the size of PA branches, and the PDA, occasionally the right aortic arch. The subaortic VSD with the overriding aorta is best imaged in the parasternal long-axis view.

Additionally, a subvalvular fibromuscular stenosis at the infundibulum may be seen—best visualised in the subcostal four-chamber view or the subcostal long-axis view of the RV.


CDS may show a high-velocity jet in the RV outflow tract—usually beginning below the pulmonary valve (infundibulum) with a predominant right-to-left shunt via the VSD level.

CW-Doppler sonography estimates the pressure gradient across the RV outflow tract.

- **Chest radiography:** Classically TOF presents with a “boot shaped heart”. More important is the recognition of RV hypertrophy with an elevated apex as well as a reduced lung perfusion. Detection of the potentially existing

right descending aorta is often handicapped by the thymus shadow.

- **Other imaging modalities:** Usually not needed in neonatal period.

 Tetralogy of Fallot is the most common cyanotic heart disease, in 25% with a right descending aorta. Echocardiography is needed for detailed assessment. On radiographs, a boot shaped heart, the RV hypertrophy, and a reduced pulmonary perfusion are the clue to the diagnosis in a cyanotic neonate.

11.5.4 Miscellaneous Other Congenital Heart Defects

11.5.4.1 Transposition of Great Arteries (TGA)

Two main types can be distinguished:

- In d-TGA there is a ventriculoarterial discordance. The aorta arises anteriorly from the RV, the PA posteriorly from the LV. In contrast to

the normal heart (with the usual “crossing of great arteries”), the great arteries exit from heart in parallel course.

- In l-TGA also the ventricles are switched—which leads also to the term “congenital corrected TGA (ccTGA)”. Due to the switch, systemic veins drain via the anatomic LV to the PA, whereas pulmonary veins enter the left atrium. The aorta originates from the anatomic RV. Therefore, a “normal” circulation is provided and does usually not cause problems in the neonatal period. Later in life, these patients are getting symptomatic since the anatomical RV is not able to consistently take-over the function of the normal LV.

The main aspect to consider in this condition are:

- **Haemodynamics:** In neonates with TGA, the first symptom is usually the reduced oxygen saturation in combination with no signs of respiratory distress!
- **Echocardiography:** Systemic and pulmonary circulation are connected in parallel; survival depends on communications between those circulations (commonly PDA, PFO/ASD in patients with an intact IVS or VSD) in d-TGA. The parallel course of the great arteries is best demonstrated in the parasternal short and long axis, the parasternal long axis, and in suprasternal views, there both arteries are seen in longitudinal section. The aorta and the aortic arch branches lay anteriorly to the PA. In parasternal short-axis view, the great arteries are seen in a cross-section as double circles.
- **Chest radiography:** The heart is typically “egg shaped”. Due to the parallel course of the great arteries, the mediastinal shadow appears small—but this may be obscured by the thymus shadow.
- **Other imaging modalities:** Depending on the clinical status and the saturation, an urgent “Rashkind Procedure” using CC for creating a shunt between those two circulations by rupturing the atrial septum with a balloon may be necessary to ensure adequate oxygen saturation and save life.



There are two types of TGA—at birth only the d-TGA is getting symptomatic. Clinically, TGA presents with decreased oxygen saturation without respiratory distress. Echocardiography enables a detailed assessment; radiographs are most often not helpful for diagnosis. Emergency catheter intervention may become necessary in unstable patients (Rashkind procedure).

11.5.4.2 Total Anomalous Pulmonary Venous Return (TAPVR)

Different forms of TAPVR exist:

- The cardiac type: all pulmonary veins (PVs) drain directly (or via the coronary sinus) into the RA.
- The supracardiac type: all PVs form a pulmonary venous confluence draining into the SVC via the left innominate vein. The PV confluence is visualised posteriorly to the LA without direct communication.
- The infracardiac type: all PVs drain into the IVC, portal vein, the hepatic vein(s), or the ductus venosus—usually one large vessel is passing downwards to below the diaphragm with venous flow away from heart/chest on CDS.


The most important aspects to consider are:

- **Haemodynamics:** In cases with a small PFO and therefore insufficient “mixing” and thus with severe desaturation, the IAS is bulged to left and only a minimal shunt can be seen via the PFO. An ASD or PFO with right-to-left shunt is mandatory for survival of these neonates. In all forms there is pulmonary hyperperfusion.
- **Echocardiography:** A TAPVR is best demonstrated in parasternal short- and long-axis view, an apical four-chamber view, and suprasternal views. The RV, the RA, and the main PA are usually enlarged, whereas the LA and the LV are normal or even small. Abnormal draining vein can be detected too.

- **Chest radiography:** RV enlargement and pulmonary hyperperfusion are the main findings. Due to the reduced oxygen saturation, respiration is increased and therefore chest films show deeper inspiration—often mimicking an obstructive pattern.
- **CC or other imaging modalities:** In cases with strong suspicion of TAPVR which cannot be ruled out by echocardiography and CXR, the next step should be CTA or eventually native MRA.
- **Other imaging modalities:** Usually not needed.



HCMP symptoms vary depending on LV function, and maybe even completely missing—echocardiography enables a definite diagnosis. Chest radiographs may show an enlarged left heart silhouette.

-  Several types of TAPVR exist—all of them lead to a varying degree of reduced oxygen saturation.
- Echocardiography depicts pulmonary veins inflow to left atrium and can imagine the abnormal draining vein.
- On CXR pulmonary hyperperfusion is present.
- CTA and eventual native MRA are the “problem solvers” in doubtful cases.

11.5.5 Cardiomyopathies (CMP)

11.5.5.1 Hypertrophic CMP

Hypertrophic cardiomyopathy (HCMP) is a condition in which the *heart becomes thickened* without an obvious cause. The interventricular septum and the ventricles are most commonly affected.

- **Haemodynamics:** In patients with HCMP, the cardiac function (e.g. the measured LVEF) is usually normal or increased. In the absence of an obstruction, the patient’s activity is usually not limited.
- **Echocardiography:** Impressive thickening in particular of the IVS and, to a lesser degree, of the LV posterior wall is the dominant finding. The end-diastolic LV diameter is usually normal, but the end-systolic LV diameter is reduced.
- **Radiographic findings:** Depending on the degree of HCMP, the heart silhouette shows a left dominant configuration. As long as the LV function is normal, there is no pulmonary hyperperfusion.

11.5.5.2 Dilated (Congestive) CMP

Dilated cardiomyopathy (DCMP) is a condition in which the *heart is enlarged* and cannot pump *blood effectively*. Symptoms vary from none to feeling tired, *leg swelling*, and *shortness of breath*. Complications can include *heart failure* or an *irregular heartbeat*.

- **Haemodynamics:** In patients with DCMP the cardiac function (i.e. the LVEF) is usually decreased. The patient’s activity is usually moderate to severely limited.
- **Echocardiography:** The LV and the LA are dilated—with a significantly decreased systolic LV function. Mitral regurgitation is common due to the dilatation of the mitral valve annulus. Occasionally, a thrombus is visible in the LA and/or LV. Sometimes, endocardial fibroelastosis is present, particularly in slightly older infants.
- **Chest radiographs:** These usually depict an enlargement of all cardiac compartments and (depending on LV failure) pulmonary hyperperfusion, together with other signs of cardiac decompensation such as Kerley lines, interstitial and/or alveolar lung oedema or pleural effusions.
- **Other imaging modalities:** Usually not needed.




Dilated CMP patients usually present with symptoms caused by cardiac failure. On echocardiography and chest radiographs, all cardiac compartments are enlarged, and CXR may show signs of cardiac decompensation.

11.5.5.3 Diabetic Foetopathy

As the name indicates, neonates of diabetic mothers are affected. These babies are “Large for Gestational Age (LGA)” and their organomegaly affects the heart too, whereas the extent is depending on the maternal diabetic control.

Features of cardiac involvement in diabetic foetopathy represent variations of HCP and resolve spontaneously over weeks.

- **Haemodynamics:** The severity of the cardiomyopathy can vary from an incidental finding to an infant with severe symptoms of congestive heart failure. This kind of HCP is usually benign and manifests with a systolic murmur and transient cardiomegaly.
- **Echocardiography:** Echocardiographic features of hypertrophic subaortic stenosis are seen in severe cases. The natural history of the diabetic HCP is benign, with resolution of symptoms within 2–4 weeks, and resolution of septal hypertrophy during the first 2–12 months of life.
- **Chest radiograph:** Depending on the extent, an enlarged cardiac silhouette can be found as well as signs of cardiac decompensation.
- **Other imaging modalities:** Usually not needed.

 Organomegaly in diabetic foetopathy affects the heart too and resolves spontaneously over time. On imaging cardiac diabetic foetopathy is similar to HCMP. The clinical picture depends on the amount of cardiac function disturbance.

11.5.6 Pericardial Effusion (PE)

Pericardial effusions are due to various clinical reasons. Differential diagnosis must include thoracic duct malformations as well as its surgical injuries (e.g. after cardiac surgery).

- **Haemodynamics:** Compression of the RA and the RV wall (more rarely also the LA and LV) indicates beginning pericardial tamponade—with impaired cardiac output and thus low cardiac output.
- **Echocardiography:** This condition is sonographically characterised by an anechoic space surrounding the heart (and possibly compressing—then this is a real emergency). Heart movements are sometimes called “swinging heart” because these movements resemble the rhythm of swing music (Fig. 11.19b).

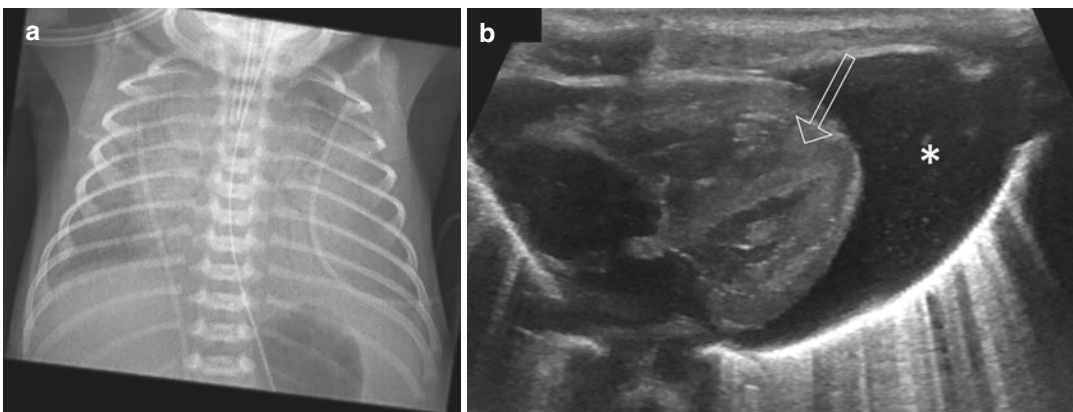


Fig. 11.19 Pericardial effusion and thickened myocardium. **(a)** A chest radiographs shows an enlarged heart with hazy margins, not explainable by a large thymus. Also note some diffuse grainy opacification pattern of the lung without a clear pleural effusion, the endotracheal

tube and a feeding tube. **(b)** Cardiac US demonstrates the huge pericardial effusion (asterisks) and a thickened myocardium (arrow); the adjacent lung shows sonographic signs of a alveolo-interstitial syndrom

- **Chest radiography:** One may recognise a triangular shaped heart shadow with loss of all curvatures—but the diagnosis in small amounts of PE is nearly impossible and can be only suspected in correlation with patients' history (Fig. 11.19a).
- **Other imaging modalities:** Sometimes—depending on aetiology—cardiac MRI can be helpful.



Pericardial effusions can be caused by numerous diseases including thoracic duct malformations and surgical injuries. It is best imaged by US/echocardiography.

11.5.7 Intracardiac Thrombi and Cardiac Tumours

In neonates, intracardiac thrombi are mainly associated with intravascular catheters, or a dilated CMP. For differential diagnosis, thrombus-like impressions of (mostly atrial) walls or tumours such as rhabdomyoma have to be considered.

- **Haemodynamics:** Evaluation of haemodynamic consequences (e.g. congestive heart failure or valve obstruction) is of paramount importance.
- **Echocardiography:** Primary tumours of heart are rare in infants and most of them are benign:

Rhabdomyoma are seen as homogenous, echo-bright mass(es) in both ventricles and associated with tuberous sclerosis.

Fibroma are predominantly single intramuscular tumours of the LV. When a tumour is found, an exact evaluation of the entire heart is necessary to rule out multiple lesions (Fig. 11.20).

- **Chest radiography:** Findings are usually non-specific, in case of haemodynamic impairment there are signs of heart failure.
- **Other imaging modalities:** Besides echocardiography, cardiac MRI is the modality of choice.

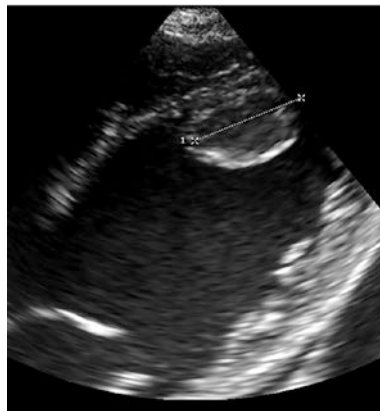


Fig. 11.20 Intracardiac thrombus (+...+) in decompensated dilating cardiomyopathy on an apical US view



Intracardiac thrombi and tumours are rare in neonates. Echocardiography and cardiac MRI are best suited for imaging.

11.6 Typical Clinical Conditions in Newborns with Cardiologic Presentation

11.6.1 Persistent Pulmonary Hypertension of the Newborn (PPHN)

Persistent pulmonary hypertension of the newborn is quite frequent and a “difficult to treat” problem in neonates, especially in preterm babies with an underlying severe sickness including failure of physiologic postnatal adaption of the lungs and the cardiovascular system (Persistent foetal circulation—PFC).

Echocardiography should be performed initially. In infants treated for acute PPHN or undergoing weaning from PPHN, echocardiography should be pursued twice a week [12]. Features to determine the degree of PPHN are available (Table 11.4) [13, 14]. In infants with broncho-pulmonary dysplasia (BPD) after hospital's discharge, echocardiography should be

Table 11.4 Echocardiographic investigations in suspected or confirmed paediatric PH

Echocardiographic variables	Interpretation	At diagnosis	Follow-up
PASP (mmHg)	TR velocity used to estimate RV systolic pressure (\approx PASP)	Yes	Yes
	PASP >50 mmHg at rest, makes PAH highly likely in adults		
Mean PAP (mmHg)	Estimated mPAP = maximum PI velocity plus mean RAP	Yes	Yes
	Def. paediatric PH: Mean PAP >25 mmHg and PVRi >3.0 WU m ²		
Diastolic PAP (mmHg)	DPAP = minimal (end-diastolic) PI velocity plus mean RAP	Yes	Yes
TR peak velocity (m/s)	RVSP = maximum instantaneous TR gradient across tricuspid valve—If TR velocity >3.4 m/s, PH is likely (see PASP)	Yes	Yes
TAPSE (mm)	Decreased in advanced PH with systolic RVD in children and adults	Yes	Yes
S/D Ratio	Increased S/D duration ratio >1.4 inversely correlates with survival in children with PH; indicator of PH severity	Yes	Probable
S' i in RV TDI (cm/s)	Decreased in advanced PH with systolic RV dysfunction; an impaired S' i predicts adverse outcome	Yes	Yes
RV/LV Ratio	RV/LV Ratio >1 indicates increased risk for adverse events in paediatric PH	Yes	Yes
PA acceleration time (ms)	PAAT of less than 100 ms—high probability of PH in adults (HR dependent)	Yes	Yes
LVEF (%; LV systolic function)	LVEF (Simpson's method) may be decreased in severe RV-LV-interaction	Yes	Yes

Modified from: Koestenberger M, et al. *Heart* 2016; 102, Suppl 2: ii14–22. Abbreviations as detailed in text, S' i = maximum systolic peak velocity

performed (a) every 3 months in infants in need of oxygen supply or (b) those at strong risk for PH.

- **Haemodynamics:** Due to pulmonary hypertension a right to left shunt occurs—through the foramen ovale and the PDA—thus reducing oxygenation.
- **Echocardiography:** Patients present with an enlarged RV and with a small LV. The tricuspid valve may be insufficient with a regurgitation jet detectable in the RA indicating PPHN [14]. Left side structures, although small, are not hypoplastic or stenotic (DD: hypoplastic left heart syndrome, HLH). The pulmonary artery is usually enlarged, and pulmonary blood flow is impaired with a

pathologic flow profile (i.e. “notching” of the PA flow).

- **Chest radiography:** RV dilation can be recognised as well as some reduced lung perfusion. Additionally, thoracic soft tissue swelling can be present secondary to RV failure.
- **Other imaging modalities:** Usually not needed.



PPHN can be diagnosed non-invasively only by echocardiography. On CXR, the RV enlargement and a reduced lung pulmonary perfusion are the most common findings.

11.6.2 Congenital Diaphragmatic Hernia (CDH)

In CDH, lung hypoplasia with consequently reduced diffusion area, an abnormal vasoreactivity secondary to hypoxic episodes, and a RV diastolic dysfunction result in changes of the pulmonary vascular resistance and pressure as well as blood flow and lead to PH. The different and varying contribution of the between various factors for PH development in CDH often complicates the decision on the best preoperative and surgical management in the most severe forms of CDH. Likewise, postoperative PH in CDH requires careful evaluation of all known variables affecting pulmonary vascular resistance as well as pulmonary and systemic blood flow in these infants.

- **Haemodynamics:** Pulmonary hypertension is caused by higher pulmonal vascular resistance together with the RV diastolic dysfunction.
- **Imaging:** The same methods, approaches, and findings as in PPHN apply. Additionally this condition is extensively described and addressed both in Chaps. 10 and 13.

11.7 Summary

In neonates, echocardiography and chest radiography are the most common used imaging modalities for cardiovascular assessment. Both modalities can be of limited use in extracardiac malformations and postsurgery complications—thus prompting for further imaging like CT and MR and their angiographic variants. CC is reserved for emergency interventions like critical aortic/pulmonary valve stenosis or in order to perform a Rashkind procedure. For more information, textbooks like [15] are suggested.

References

1. Sorantin E, Coradello H, Wiltgen M. Computer-assisted mechanical ventilation of newborns. *Anaesthesist*. 1992;41(6):342–5.
2. Sorantin E, Weissensteiner S, Hasenburger G, Riccabona M. CT in children - dose protection and general considerations when planning a CT in a child. *Eur J Radiol*. 2013;82(7):1043–9. <http://www.ncbi.nlm.nih.gov/pubmed/22227258>
3. Dawson JA, Kamlin COF, Vento M, Wong C, Cole TJ, Donath SM, et al. Defining the reference range for oxygen saturation for infants after birth. *Pediatrics*. 2010;125(6) <https://pubmed.ncbi.nlm.nih.gov/20439604/>
4. Koestenberger M, Nagel B, Ravekes W, Everett AD, Stueger HP, Heinzl B, et al. Systolic right ventricular function in pediatric and adolescent patients with tetralogy of Fallot: echocardiography versus magnetic resonance imaging. *J Am Soc Echocardiogr*. 2011;24(1):45–52.
5. Koestenberger M, Ravekes W, Everett AD, Stueger HP, Heinzl B, Gamillscheg A, et al. Right ventricular function in infants, children and adolescents: reference values of the tricuspid annular plane systolic excursion (TAPSE) in 640 healthy patients and calculation of z score values. *J Am Soc Echocardiogr*. 2009;22(6):715–9. <https://pubmed.ncbi.nlm.nih.gov/19423286/>
6. European Commission. European Guidelines on quality criteria for diagnostic radiographic images in paediatrics. Eur 16261. 1996;1–71. <ftp://ftp.cordis.lu/pub/fp5-euratom/docs/eur16261.pdf>
7. Tschauner S, Marterer R, Gübitz M, Kalmar PI, Talakic E, Weissensteiner S, et al. European Guidelines for AP/PA chest X-rays: routinely satisfiable in a paediatric radiology division? *Eur Radiol*. 2016;26(2):495–505.
8. Pees C, Glagau E, Hauser J, Michel-Behnke I. Reference values of aortic flow velocity integral in 1193 healthy infants, children, and adolescents to quickly estimate cardiac stroke volume. *Pediatr Cardiol*. 2013;34(5):1194–200.
9. Tschauner S, Zellner M, Pistorius S, Gnannt R, Schraner T, Kellenberger CJ. Ultra-low-dose lung multidetector computed tomography in children – approaching 0.2 millisievert. *Eur J Radiol*. 2021;139:109699.
10. Sorantin E, Riccabona M, Stücklschweiger G, Guss H, Fotter R. Experience with volumetric (320 rows) pediatric CT. *Eur J Radiol*. 2012;82(7):1091–7. <http://www.ncbi.nlm.nih.gov/pubmed/22227261>
11. Nagy E, Tschauner S, Marterer R, Riedl R, Sorantin E. Chest CTA in children younger than two years – a retrospective comparison of three contrast injection protocols. *Sci Rep*. 2019;9(1):18109.
12. Hilgendorff A, Apitz C, Bonnet D, Hansmann G. Pulmonary hypertension associated with acute or chronic lung diseases in the preterm and term neonate and infant. The European Paediatric Pulmonary Vascular Disease Network, endorsed by ISHLT and DGPK. *Heart*. 2016;102(Suppl 2):ii49–56.
13. Abman SH. Pulmonary hypertension: the hidden danger for newborns. *Neonatology*. 2021;118(2):211–7. <https://pubmed.ncbi.nlm.nih.gov/33951650/>

14. Hansmann G, Koestenberger M, Alastalo TP, Aplitz C, Austin ED, Bonnet D, et al. 2019 Updated consensus statement on the diagnosis and treatment of pediatric pulmonary hypertension: The European Pediatric Pulmonary Vascular Disease Network (EPPVDN), endorsed by AEPC, ESPR and ISHLT. *J Heart Lung Transplant.* 2019;38(9):879–901. <https://pubmed.ncbi.nlm.nih.gov/31495407/>
15. Wyman WL, Mertens LL, Cohen MS, Geva T. *Echocardiography in pediatric and congenital heart disease: from fetus to adult.* 3rd ed. Hoboken, NJ: Wiley Blackwell; 2021.



Imaging the Neonatal Urogenital Tract

12

Michael Riccabona

12.1 Introduction

The urogenital tract (UGT) is one of the most frequently imaged part in the neonates. This is because of prenatal imaging that often reveals some, usually mild, changes that induce anxiety in parents and referring physicians hence need confirmation, workup, and/or follow-up after birth. Therefore, there is quite some pressure to investigate the neonatal UGT early, although most often there is no real urgency, and actually more obvious findings do not always benefit from very early imaging. The risk of early imaging is, that due to the immature kidney with the physiologic postnatal dehydration, the reduced urinary output causes less distension of the collecting system than, for example observed in utero and therefore findings may be missed or underestimated. After this first early study, a follow-up in a couple of weeks, when the kidney has matured, is often recommended.

However, there are significant pathologies that do benefit from early diagnosis and treatment such as posterior urethral valve (PUV) or high-grade vesico-ureteric reflux (VUR) and bilateral high-grade dilatation of the urinary tract that may impair renal function. These, as well as acute conditions, such as renal vein thrombosis or acute renal fail-

ure, as well as rare neonatal or congenital renal and adrenal tumours, need to be imaged and diagnosed and/or confirmed early to timely impose treatment, to prevent further deterioration and preserve as much renal function as possible, and to allow for future renal growth and development.

The other group where renal imaging usually is performed early is the group of cystic kidney diseases (CDK)—particularly in early manifestation of bilateral severe disease that may early impair renal function, or impose a mass effect, such as autosomal recessive polycystic kidney disease (ARPKD) and its' differential diagnosis (e.g. neonatal glomerulonephritis and the Finnish type neonatal nephrotic syndrome).

Neonatal urinary tract infection (UTI) does occur as well and often is caused by haematogenous spread, not so often by ascending infection via the urinary tract. There is only a weak association with congenital malformations in UTI in neonates. However, when UTI occurs in neonates, coexisting congenital malformations lead to a higher risk of associated renal damage and scarring endangering renal growth and development, and poses a risk to sufficient renal function in adulthood. Therefore, ultrasound (US) is widely and early used in these patients, and evaluation of a possible VUR by contrast-enhanced voiding urosonography (ce-VUS) or fluoroscopic voiding cystourethrography (VCUG) is recommended when UTI occurs in this age group.

Genital malformations usually are no emergency except for vaginal atresia with a (hae-

M. Riccabona (✉)
Medical University Graz, Graz, Austria
e-mail: michael.riccabona@medunigraz.at

mato-)metrocolpos or conditions that are part of the anorectal and cloacal malformation spectrum. However, often it is much easier to assess and image the neonatal genitalia early (before physiological involution of the neonatal internal genital structures) making visualisation, evaluation, and differentiation much easier. Sometimes, anatomical information that possibly help to define a gender (if possible) is required in the neonatal period, both for medical and for psychological and social reasons.

If in some instances more invasive imaging is necessary, non-invasive procedures (such as MRI that can often be performed in a feed-and-wrap approach) are preferred, whereas other procedures such as nephrostomies or biopsies need proper analog-sedation or even anaesthesia.

A final aspect is the use of intravenous contrast agents (CA): here the neonates pose a specific risk and challenge because of the renal immaturity (effecting both intravenous radiopaque CA and MR-CA) and iodine uptake by the thyroid gland if iodinated CA are given. Therefore, unless urgently necessary, contrast application is usually postponed to the time after the neonatal period, i.e. 4–6 weeks of life; functional studies of the urinary tract and the renal parenchymal better till even the end of the third month (e.g. renal scintigraphy). Ultrasound CA (UCA) can be applied intravenously—though

presently “off label”; but they lack one specific and important feature that hinders their generous use in the urogenital tract: UCA are not excreted by the kidney and are a purely intravascular agent. Thus, pharmacodynamics and distribution cannot be completely compared to iodinated radiopaque or gadolinium-based CA, simply because of their physiologic elimination, which is not via the kidney and urinary tract. Intracavitarily, UCA can be and are used for filling whichever lumen needs to be investigated—such as the bladder (for evaluation of VUR or urethral pathologies, which is the only approved use of UCA in neonates), the vagina (e.g. for US-genitography), or the upper urinary tract (e.g. placement of and follow-up after percutaneous nephrostomies) and in cloacal malformations (see respective other chapters).

In the following, the typical conditions and queries in the neonatal UGT will be presented, imaging algorithms will be discussed, and typical findings will be illustrated. Imaging interpretation and understanding of respective findings particularly concerning malformations heavily rely on a deep understanding of the urogenital tract embryology, thus being acquainted with the major steps in this development is very useful (Fig. 12.1). Further details on interventions, CAs, and the respective methods can be found in the dedicated chapters (i.e. Chaps. 3 and 7).

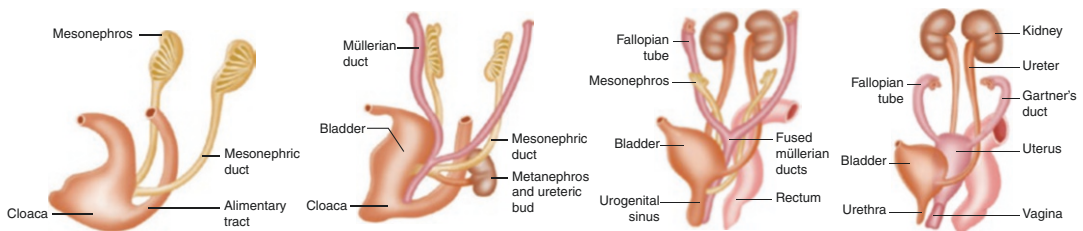


Fig. 12.1 Embryology of the female genitalia (Adapted from Schweigman et al., *Female Genital Anomalies and Important Ovarian Conditions*. In Riccabona M. (ed) *Pediatric Urogenital Radiology*, 3rd edition. Springer 2019). Schematic drawings illustrating the development of the female genitourinary tract: initially, the mesonephric (Wolffian) ducts connect the mesonephros to the cloaca. Later, at approximately 5 weeks of gestation, the ureteric bud originates from the Wolffian duct and then eventually reaches the metanephros, inducing the differ-

entiation into the kidney—the mesonephros degenerates. The Müllerian ducts fuse at about 7–9 weeks in the midline forming the uterovaginal canal. At 8 weeks, the uterovaginal canal reaches the urogenital sinus at the Müllerian tubercle. The sinus results from separation of the cloaca into the urogenital sinus and the rectum. Then the vagina becomes patent at approximately 22 weeks, and the Wolffian ducts are resorbed—remnants are called Gartner’s duct structures

12.2 Imaging Modalities Used in the Neonatal UGT

Most exiting imaging modalities can be applied, but there are specific aspects concerning the use and application of the various imaging modalities in neonates that need to be considered to prudently apply imaging in newborns.

12.2.1 Urogenital Sonography in Neonates

First of all, some considerations regarding ultrasonography (US): as detailed in Chap. 3, high-resolution linear transducers are most useful. Micro-curved transducers may pose a problem if you need too much pressure to properly connect the entire transducer surface. Sector transducers are hardly ever necessary. The frequency range is from 5 to 18 MHz depending on the size and the depths of the imaged structure. Harmonic imaging is often quite useful as it intrinsically offers a high resolution at less image noise and thus allows for a

clear discrimination of the collecting system, Doppler facilities are nearly mandatory for some questions. The setting and environment for the investigation should be made as comfortable as possible for everybody involved (proper seating, proper table height, warm environment, pacifier and glucose drops, pre-warmed gel, etc.). One should start with the urinary bladder (as babies tend to void as soon as you touch them with the transducer) to be able to view the bladder, the ureters, and the ostia as well as the retro-/paravesical space, in particular the uterus and the ovaries. If you realise that the baby is about to void, you may move the transducer down to either trans-symphysically or trans-perineally observe the urethra during voiding. Thereafter, it is a good time to check the inguinal canal and the scrotum (in boys)—before moving the transducer upwards to the kidneys. Evaluate the kidneys in both axial and longitudinal sections from the upper to the lowest border, assess the parenchymal structure and echogenicity, observe if there are cysts, check the collecting system, and define its configuration using one of the existing grading systems (Table 12.1).

Table 12.1 Grading of urinary tract dilatation: (a) ESPR PCD system; (b) American UTD classification

Section (a)					
PCD 0	PCD I	PCD II	PCD III	PCD IV	PCD V
PCD 0 = collecting system not or hardly visible—considered normal					
PCD I = just renal pelvis clearly visible, calices not depictable, axial plevic diameter					
PCD II = axial renal pelvis diameter <10 mm, calices visible, but with normal forniceal and papillar shape/configuration					
PCD III = marked dilatation of calices and pelvis, pelvic axial width usually >10 mm with flattened papilla and rounded fornices, but without parenchymal narrowing—considered pathologically					
PCD IV = gross dilatation of entire collecting system + narrowing of renal parenchyma—considered pathologically (PCD V = used in some places for extreme PCD IV° with only thin, membrane-like residual renal parenchymal rim)					
Modified from the ESPR “Hydronephrosis” grading [23]—based on Hofmann’s US grading, and the SFU classification (Fernbach et al. 1993). Adapted from Riccabona M. et al., <i>Pediatr Radiol</i> 2017;47:1369–1380 (updated version)					

Table 12.1 (continued)

Section (b)		
(b) American urinary tract dilatation (UTD) classification, prenatal and postnatal application		
Criteria for defining risks pre- and post-natally		
Antenatal	A1 = Low risk	A2–3 = Increased risk
APRPD		
16–27 weeks	4–6.9 mm	≥7 mm
≥28 weeks	7–9.9 mm	≥10 mm
Calyces	Central calyceal dilation	Peripheral calyceal dilation
Ureter	Normal	Dilated
Parenchymal thickness	Normal	Abnormal
Parenchymal appearance	Normal	<ul style="list-style-type: none"> • Abnormal echogenicity • CM differentiation • Cortical cysts
Bladder	Normal	<ul style="list-style-type: none"> • Wall thickening • Ureterocele • Posterior urethral dilation
Oligohydramnios	No	Present

Risk based management, prenatal diagnosis

UTD A1 = low risk	UTD A2–3 = increased risk
<i>Prenatal period</i>	
One additional US >32 week	Initially in 4–6 weeks ^a
<i>After birth</i>	
Two additional US	US
1. >48 h–1 month	t >48 h–1 month of age ^a
2. 1–6 months later	Earlier in suspected PUV or bilateral severe UTD etc
<i>Other</i>	
Aneuploidy risk modification if indicated	Specialist consulting (e.g. nephrology, urology)

^a Certain situations (e.g. PUV, bilateral severe UTD) may require more expedient follow-up

Risk based management, postnatal diagnosis

UTD P1 = low risk	UTD = P2 intermediate risk	UTD = P3 high risk
<i>Follow-up US</i>		
1–6 months	1–3 months	1 month
<i>VCUG^a</i>		
Discretion of clinician	Discretion of clinician	Recommended
<i>Antibiotics^a</i>		
Discretion of clinician	Discretion of clinician	Recommended
<i>Functional scan</i>		
Not recommended	Discretion of clinician	Recommended

^a The choice to utilise prophylactic antibiotics or perform VCUG will depend on the suspected underlying pathology

The European and the American grading system for dilated neonatal urinary tract and pelvi-caliceal system. The European system only descriptively refers to the present situation of the pelvi-caliceal system, whereas the American classification tries to integrate foetal findings, other aspects such as the ureter, and then tries to deduct a risk stratification, although the consequence very often is “at the discretion of the referring physician/clinician”

According to Nguyen HT, Benson CC, Bromley B, Campell JB, Chow J et al. (2014) Multidisciplinary consensus on the classification of prenatal and postnatal urinary tract dilation (UTD classification system). *J Pediatr Urol*, 10:982–998

Also observe the pararenal space and particularly the adrenal glands. After checking both kidneys, one might think of turning the baby into prone position and assess the kidneys from dorsally, particularly if the kidneys were not sufficiently seen by the ventro-lateral approach. Take measurements in standardised fashion both of the dilatation of the collecting system (usually measured in an axial plane) and of the renal size, where volume calculations are better than pure length measurements because of the more spherical shape of the neonatal kidney; also note that the normal neonatal kidney looks different from the normal adult appearance (Fig. 12.2). There are procedural rec-

ommendations how to do urinary tract US in childhood as well as how to sonographically image the neonatal genitalia, e.g. by the ESPR abdominal imaging task force (Riccabona et al., *Pediatr Radiol*).

More advanced US imaging will use additional methods: possibly perform voiding urosonography (VUS), and use additional features summarised in the “extended criteria” such as a thickening of the urothelium (Table 12.2).

- Colour Doppler Sonography (CDS) is helpful for assessing the ureteric inflow jet into the bladder and for assessing the vascular anat-

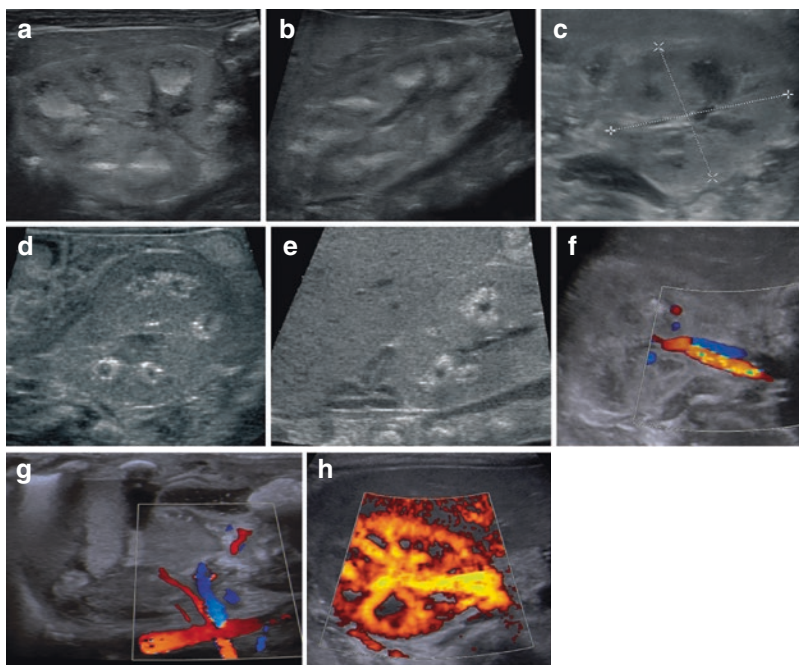


Fig. 12.2 The normal neonatal kidney—Ultrasound appearance and measurements. (a, b) On US, the neonatal kidney is more spherical (a) and exhibits a slightly higher echogenicity of the cortex than later in life with a clear differentiation to a rather hypoechoic medulla (b). Centrally and at the papilla transient echogenic deposits may be seen as a physiological phenomenon. (c) Measurements of axial diameters (and length) should be performed, volume calculation is performed by the equation $\text{length} \times \text{width} \times \text{depth} \times 0.523$ (provided the kidney has an ellipsoid shape). (d, e) Nephrocalcinosis in an axial (d) and coronal (e) view: rare in neonates, unless a

severe underlying condition (as also nephrolithiasis)—do not confuse this or papillary calcifications with the physiological medullo-papillary echogenicity. Typically, nephrocalcinosis and urolithiasis manifest later. The difference is that the echogenicities are peripherally in the medulla and in the papilla whereas the central medulla appears nearly normal. (f, g) This axial view of the kidney shows the normal central vessels on CDS (e), a coronal view from the flank demonstrates the renal artery with the two renal veins draining into the inferior cava vein (e). (h) Shows the normal peripheral architecture on Power Doppler

Table 12.2 Extended criteria for sonographical evaluation of the neonatal urogenital tract

Structure	Findings that indicate pathology
Bladder	Thick bladder wall, trabeculation, diverticula, open bladder neck
Ureter	Dilatation, thick wall, atypical ostium position/configuration, hyper-/hypoperistalsis, duplex ureter, ureterocele
Renal parenchyma	Cysts, dysplasia, altered echogenicity (usually to high), parenchymal narrowing, altered corticomedullary differentiation, small/large, hypovascularity, scars
Urothelium	“Urothelial sign” : thickened urothelium of ureter and/or pelvicalyceal system

Findings that indicate pathology and justify further imaging and/or follow-up, additional to the dilation as defined by the respective grading/classification system

omy and patency (e.g. multiple renal arteries, renal vein thrombosis, retro-aortal left renal vein).

- Power Doppler may be useful for depicting focal renal lesions such as segmental pyelonephritis or assessing vascularisation in impaired kidneys with renal insufficiency or renal tumours.
- Contrast-enhanced ultrasound (ce-US) has become an accepted standard for assessment of VUR (by contrast-enhanced voiding urosonography = ce-VUS). After instillation of diluted UCA into the urinary bladder (0.2–0.5% saline solution in plastic containers—filled by infusion drip, or bolus instillation of the respective amount of UCA into the prefilled urinary bladder via catheter according to the manufacturers advice), the bladder, the ureters (as far as visible), and alternating both collecting systems are observed for possible contrast reflux into the upper urinary tract; also assess for a potential intrarenal reflux. Particularly in neonates a cyclic filling (like for the fluoroscopic examination) is recommended, and one filling should be dedicated to properly visualise the urethra; also a post-void assessment of the collecting system and the urinary bladder should be attempted. Procedural recommendations exist (e.g. Riccabona et al. *Pediatr Radiol*).

Intravenous application of UCA is hardly ever necessary in neonates, however, for differentiation of complicated renal cysts, better delineation of abscesses or necrotic areas, or better delineation of unaffected renal tissue in tumourous conditions and similar applications ce-US can also be performed in neonates as an

off-label application, as the UCA can be used even without mature and proper renal function (after an informed consent has been retrieved) (Klugsevits et al. *Pediatr Radiol* 2021).

- US-elastography at present is not established in the neonatal urinary tract. Some reports exist on its potential use for renal vein thrombosis or renal tumours but by now is not an established procedure.

Finally, it is important to know the normal appearance of a neonatal kidney and the genitalia. The more spherically shaped neonatal kidney exhibits a slightly echogenic cortex. The echogenicity decreases with gestational age—from a slightly more echogenic cortex in very preterm babies to a slightly lower cortical echogenicity as the adjacent liver in term neonates. The corticomedullary differentiation is accentuated, and the distension of the collecting system could vary due to its high elasticity particularly of the extra-renal part, including possible variations of pelvic width depending on position and bladder filling. Furthermore, the distal medulla and papilla may be transiently hyperechogenic for some days to some weeks (“transient echogenicity of the neonatal medulla”) (see Fig. 12.2). This should not be confused with nephrocalcinosis or papillary calcification which is rare in neonates. This is a secondary phenomenon—either due to medication (e.g. vitamin D overdose) to treatment (dehydration and furosemide or antibiotics) or a consequence of a severe kidney condition (e.g. distal tubular acidosis, Barter Syndrome, papillary necrosis). The sonographic difference is that in nephrocalcinosis the echogenicities start at the corticome-

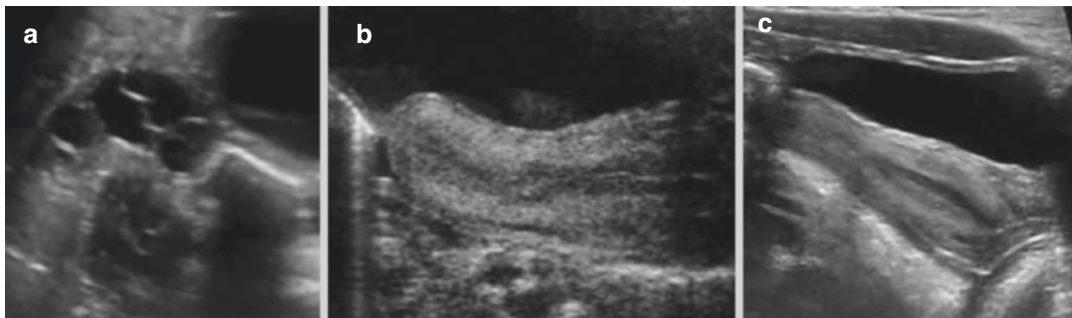


Fig. 12.3 The normal neonatal uterus and ovary on ultrasound. (a) Normal prominent neonatal ovary with multiple follicles. (b, c) Typical neonatal uterus visible in a

sagittal midline section of the lower abdomen behind the full urinary bladder; note the prominent long cervix, whereas the corpus is relatively small

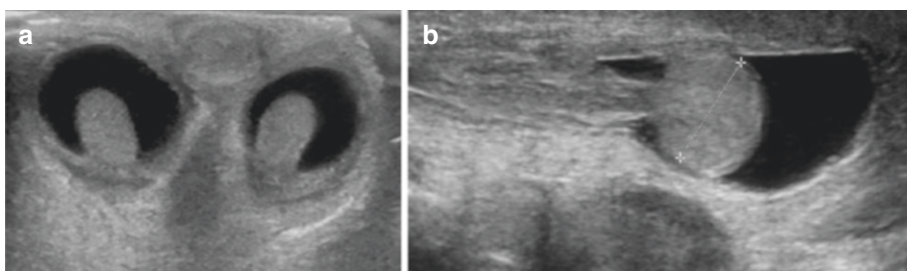


Fig. 12.4 Neonatally physiological hydrocele. (a, b) Axial (a) and longitudinal (b) section of a neonatal scrotum reveals some clear (“non-complex”) fluid in the scro-

tum surrounding the testicles (b, +++++); this physiologic hydrocele usually diminishes and eventually spontaneously vanishes over time

dullary border, whereas the centre of the medulla at least initially (stage I–II) remains normal; the papilla may contain echogenicities. Another typical finding in neonates are follicular “cysts” in the prominent ovaries, which can be quite impressive but do only rarely represent pathology and will mostly decrease and vanish spontaneously. In the neonate, the ovaries are not necessarily located in the pelvis where usually seen in older children or adults—they can physiologically be found throughout the entire abdominal cavity and are very mobile. The neonatal uterus is quite prominent due to maternal hormonal influences—with a long cervix and a small corpus (Fig. 12.3). In boys quite the inguinal canal is often open with some motility of the testis and some amount of hydro-/funiculocele is seen physiologically in the first weeks (Fig. 12.4).

12.2.2 Radiography and IVU

Radiography plays no role in imaging the neonatal UGT as such but sometimes radiographs are taken for assessing associated malformations such as chest or spine radiographs, e.g. of the spine for vertebral malformations, or needed for diagnosing and monitoring secondary disease (e.g. lung immaturity and hypoplasia in oligohydramnios due to a PUV).

Intravenous urography (IVU) is completely outdated in neonates and yields very little information in this age group—in part due to the superb potential of modern US, and in part also explained by the poor contrast concentration in the urinary tract caused by the physiological renal immaturity and therefore reduced ability to concentrate the contrasted urine in the first weeks of life.

12.2.3 Fluoroscopy

Fluoroscopy has some, though relatively rare indications in this age group—either for studying the anatomy (e.g. in cloacal or genital malformations, pathology of the urethra) or for VUR assessment, achievable by voiding cystourethrography (VCUG), retrograde urethrography, or genitography. For all these procedures, recommendations (e.g. by the ESPR abdominal imaging task force) exist on how to prudently perform these studies. Some more basic considerations are discussed in Chap. 3, such as applying low frame rate intermittent pulsed screening and last-image-hold documentation, low CA concentration, and only selected spot exposures (e.g. lateral view of the urethra during voiding in boys with urethral valves) as well as possibly of the kidney in refluxing units to depict intrarenal reflux (Fig. 12.5). A special aspect of these investigations in neonates is that due to the renal immaturity, urine concentration and production are still restricted, and therefore having patients fasted for an investigation or measures to ensure good diuresis such as diuretic stress are less valuable and usually not applicable in this age group. Nevertheless, having a bottle of formula or

milk is often very helpful for feeding and pacifying the baby during an investigation.

The other way of using fluoroscopy in the neonatal UGT is for guiding or monitoring interventions such as for percutaneous nephrostomy, which often is performed by an initial US-guided puncture and then completed by a fluoroscopic overview. The latter helps to retrieve functional information (degree and speed of drainage), assess complications (e.g. perforation, extravasation, and urinoma), or allow for a conspicuous overall demonstration of the entire, then contrast-filled anatomy of the collecting system and ureter (see also Chap. 7).

12.2.4 CT

CT is practically never used in the neonatal UGT, except for some rare tumour conditions where preoperative imaging and staging may become necessary in patients when MRI is contraindicated or when MRI is not available.

If performed, protocols must be adapted, and multiphase acquisitions are obsolete. Thus, individual adaptation of CA dose (≈ 2.5 mL/kg, max. 250 mg Iodine/mL) and timing (arterial delay ≈ 8 s, parenchymal phase 25 s) according

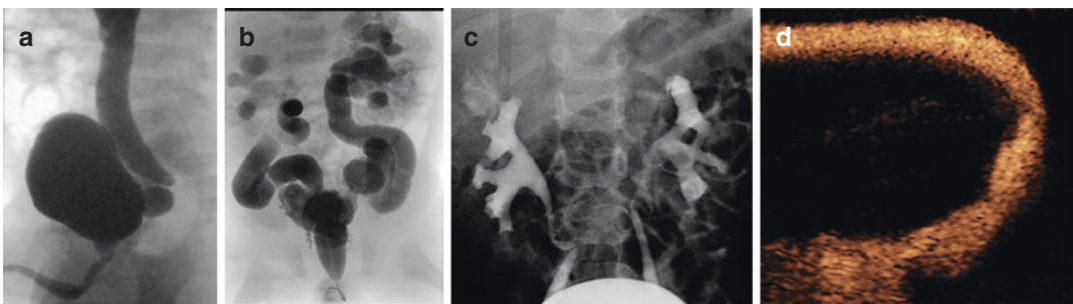


Fig. 12.5 Voiding cystourethrography (VCUG). (a) Lateral view of the normal male urethra during voiding (note the normal indentations of the male urethra—do not confuse those with valves) demonstrating also a Hutch diverticulum and VUR. (b) The last-image-hold view demonstrates gross VUR into both kidneys in a baby boy with PUV. The intrarenal reflux is poorly visible on the left kidney (right side); furthermore, the delayed clearance of the refluxed CA can be assessed indicating also an

obstructive component at the ureterovesical junction (caused by the thickened bladder wall). (c) Focused spot exposure of the kidneys at the maximum of the reflux activity conspicuously demonstrates the intrarenal contrast reflux at the upper calix of the right kidney (left side of the image) for intrarenal reflux. (d) Normal urethra during voiding on contrast-enhanced perineal US—this demonstrates that the urethra is nicely seen also by US and not always a VCUG is necessary

to the essential questions is mandatory; split bolus acquisitions could be a solution but are very cumbersome and difficult in neonates and therefore different and individually tailored approaches need to be entertained.

12.2.5 MRI

MRI of the urogenital tract (MR-urography = MRU) is rarely performed in neonates. Only in some cases with very difficult and unusual anatomy, mostly for anatomical assessment. For this purpose, application of gadolinium-based CA can be avoided and an approach using the “water” MRU (i.e. heavily T2-weighted sequences with fat suppression to visualise the pelvicalyceal system and the ureters) is sufficient in nearly all cases (Fig. 12.6). For imaging genital structures or complex anorectal/cloacal malformations, one may consider using saline instillation via catheters or drains to distend and delineate the individual anatomic hollow structure. In such cases a 1:100 gadolinium solution can be applied to allow a better discrimination of different hollow structures and to depict possible fistulae, as no gadolinium is resorbed if given intra-cavitarily (see Fig. 12.6).

12.2.6 Scintigraphy

Scintigraphy is hardly used in the neonatal UGT. Some centres still perform radionuclide cystography for VUR screening though this is being replaced by ce-VUS-if still considered, indicated and justified at all.

The other technique usually applied to the UGT is renography (Tc^{99m} DMSA static renal scintigraphy or Tc^{99m} MAG3 diuretic-dynamic renography). However, this approach is also less valuable in neonates, as these methods need a mature and sufficiently well-functioning renal tissue (more than 20% split renal function) and a low background activity (less than 10%) to deliver good and reliable information on split renal function and urine drainage. This is not yet granted in neonates because of the physiological renal immaturity and the higher circulating blood volume with delayed clearance of the radioactivity from the body. In some instances, a rough global assessment of the renal function by static renography may be requested, e.g. for deciding if a (or which) kidney should be preserved, or if there is a renal function at all (e.g. query multicystic dysplastic kidney).

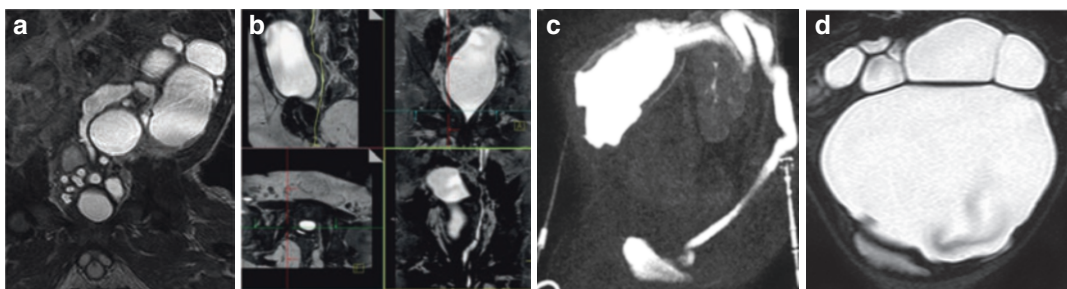


Fig. 12.6 Anatomic (“water”) MR-urography (MRU). (a) A heavily T2-weighted coronal MRU sequence demonstrates a multicystic dysplastic kidney and some fluid filled upper ureteric remnants as well as cystic structures behind the urinary bladder (cystic dysplasia of the seminal vesicles). (b) Shows a multiplanar curved reconstruction in a neonate allowing to follow the narrow normal ureter curving downwards and passing behind and draining into the urethra below the bladder (ectopic insertion). (c) This

neonate with a triple kidney had three megaureters filling the entire abdomen, so early surgery was required for decompensation. To preoperatively be able to understand the complex coarse anatomy, one of the three systems was punctured and filled with diluted gadolinium to outline the course of this ureter using a T1-weighted fat suppressed coronal MRU sequence. Note some gadolinium in the contralateral normal kidney which has refluxed from the bladder

12.3 Imaging in Emergencies of the Neonatal Urogenital Tract

A few but important entities need urgent imaging for deciding on further management and to prevent serious sequelae.

12.3.1 Acute Renal Failure/Kidney Injury

Acute renal failure without known origin requires early US to help distinguish between pre-, intra- and post-renal causes—as this will decide on treatment measures.

- *Prerenal causes* are systemic conditions, most often of cardio-circulatory origin such as some malformations, persistent arterial duct of Botalli with high shunt volume and thus insufficient renal perfusion, severe aortic coarctation or post-hypoxic ischaemic after severe asphyxia or shock. Ultrasound usually shows bilaterally enlarged kidneys with increased echogenicity, sometimes with less pronounced corticomedullary differentiation. Usually no distension of the collecting system is seen (unless there is the polyuric phase). The diagnosis is made by Doppler US showing the reduced particularly diastolic perfusion with elevated resistive indices and reduced vascularity in the renal periphery (Fig. 12.7). No further imaging is needed,

except for assessing the underlying, for example cardiac condition.

- *Intra-parenchymal and renal causes* are rare and often already depicted prenatally such as a nephrotic syndrome of the Finnish type, a neonatal glomerulonephritis, or an infantile recessive polycystic kidney disease.

All these conditions are assessed sonographically and have enlarged kidneys with increased echogenicity (Fig. 12.8); except for the polycystic kidney disease, the corticomedullary differentiation may be preserved. An important contribution of US is the morphologic description pointing at the cause, which usually—together with clinical and anamnestic data—allows to define the diagnoses; Doppler US may help to assess the severity of the situation. However, Doppler findings reflect more the renal function than the underlying condition, and are heavily influenced by systemic factors. Again, no further imaging is usually needed.

- *Post-renal origin* of renal failure consists of some sort of high degree obstruction of the urinary tract such as posterior urethral valve (PUV) or bilateral pelvi-ureteric junction obstruction (PUJO); unilateral PUJO or ureterovesical junction obstruction (UVJO) with a megaureter usually does not cause acute renal failure and is more likely to present either with chronic problems or infections. However, a (functional) single kidney with impaired drainage may cause acutely deteriorating renal failure soon after birth.

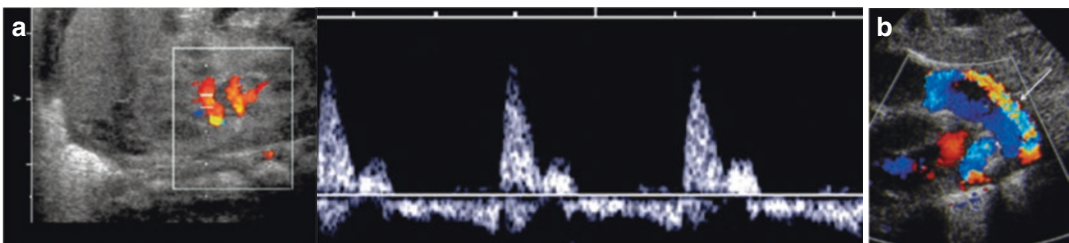


Fig. 12.7 Doppler sonography in pre-renal origin of renal failure. (a, b) Colour Doppler sonography with spectral flow trace of a rather echogenic, slightly swollen neonatal kidney with preserved corticomedullary differentiation

exhibits a reduced (negative) diastolic flow (Resistive Index >100%) (a); the causative persistent ductus arteriosus which also caused the renal failure is easily confirmed by CDS of the heart (b, arrow)

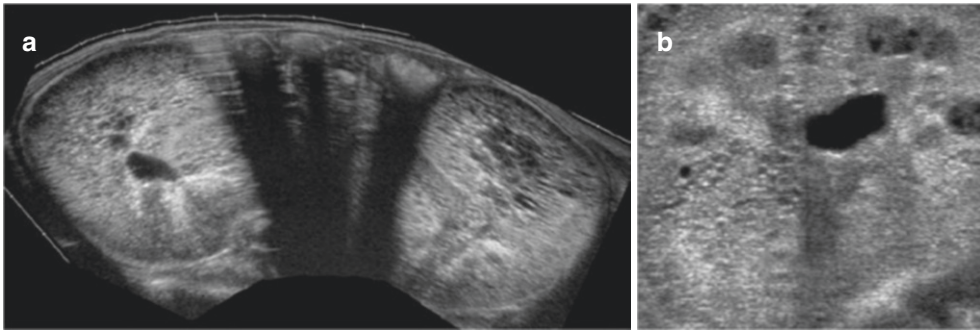


Fig. 12.8 Ultrasound in neonatal polycystic kidney disease. **(a)** Extended view US image (axial section) of the two huge kidneys in a neonate with autosomal recessive polycystic kidney disease. Note the numerous small cysts

throughout the entire kidneys. **(b)** Enlarged and magnified view showing small cysts and dysplastic parenchyma as well as some distention of the central pelvicalyceal system

Again, US is the imaging modality of choice and will depict the dilated system and help with differentiating upper versus lower or even infra-vesical obstruction, thus guiding further management. Only for PUV, a complementing VCUG or ce-VUS may be needed to confirm the diagnosis, even if perineal US usually nicely demonstrates the valve. There usually is no role for MRI or scintigraphy in the acute setting and in the first weeks of life—these methods play a major role in the further workup and management after the neonatal period. The most important measure is to enable sufficient urinary drainage either by bladder catheterisation (suprapubic or trans-urethral) or by percutaneous nephrostomy which again is done with image guidance (usually sonographically guided puncture and fluoroscopically monitored drain placement); for checking on proper drainage, UCA can be installed via the tube as an alternative to radiopaque CA with fluoroscopy.

12.3.2 Renal Vein Thrombosis/Acute Haematuria and Hypertension

Renal vein thrombosis usually presents with haematuria and hypertension.

Ultrasound as the initial and usually only imaging of choice will show an enlarged echogenic kidney often with a disrupted corticomedullary

differentiation and echogenic stripes with either represent haemorrhage and/or remnants of the echogenic pre-papillary medullae; the collecting system usually is not seen (Fig. 12.9a). As these thromboses mostly start in the periphery, the central vein may be still patent in the early phase, eventually no venous flow will be depictable by CDS and sometimes the thrombus in the renal vein can be depicted—potentially reaching into the IVC. The most striking and diagnostic finding is the arterial Doppler wave form, where the spike-like high resistance systolic inflow (sometimes with a delayed systolic upstroke) is followed by a negative diastolic phase, where more or less all of the blood which has been pressed into the kidney during systole is reversed due to the occluded venous drainage (Fig. 12.9b). Additionally, on Power Doppler a marked reduction of peripheral vascularity with a patchy pattern can be seen.

Imaging in neonatal hypertension is not addressed in detail—however, checking the kidneys is always requested if no other obvious reason is known and may reveal renal vein thrombosis or other severe nephropathies.

12.3.3 Miscellaneous Other Conditions

- *Neonatal glomerulonephritis* is rare, usually caused by congenital infections, systemic disease, or transfer of maternal antibodies target-

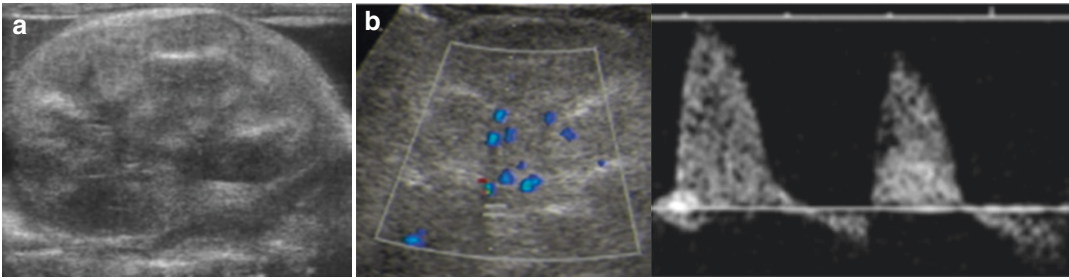


Fig. 12.9 Renal vein thrombosis. (a) Swollen and echogenic neonatal kidney with even more echogenic bands (in part due to blood products from haemorrhagic infarction, in part as residual physiologic echogenicities of the neonatal medullae). (b) Doppler sonography shows a high

resistance arterial flow pattern with inverted diastolic flow, as the arterial inflow is reversed and cannot pass the thrombosed vein; in some aspects also prominent tubuli can be imagined

ing renal proteins. It presents as nephritic syndrome with renal failure, may be progressive and associated with severe morbidity and mortality.

On US the findings are nonspecific—one observes enlarged, often hyperechogenic kidneys with possibly a patchy pattern (mostly in mesangial sclerosis), often an accentuated corticomedullary differentiation (typically in the classical glomerulonephritis) (Fig. 12.10); in segmental hyalinosis and minimal-change glomerular disease (that clinically manifest less severe) the US findings may be very subtle or even normal.

Congenital/neonatal nephrotic syndrome of the Finnish type is a genetic familial disease that usually rapidly progresses to end-stage renal failure. It is an autosomal recessive transmitted condition without any effective therapy—only renal transplantation will eventually cure the patient.

US does not reveal any findings different from the neonatal glomerulonephritis spectrum.

- Bilateral severe *renal involvement in urinary tract infection* may also cause renal failure, particularly if associated with other endangering pre-existing conditions or renal damage such as high-grade VUR or PUV (see below) and renal dysplasia, or bilateral severe obstruction (see also below).

Imaging consists of US and will reveal enlarged kidneys with altered parenchymal echotexture and possibly urothelial thickening; if there is a problem with urine transport

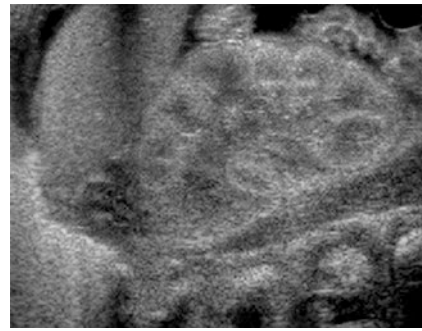


Fig. 12.10 Ultrasound in neonatal glomerulonephritis. Swollen neonatal kidney with echogenic cortex in a newborn with neonatal glomerulonephritis. Note the ascites as a consequence of renal failure

(obstruction or dysplastic distention or high-grade VUR) respective dilatation of the pelvicalyceal system and/or the ureter can be seen.

- *Ovarian or testicular torsion*, although rare and usually occurred prenatally and thus without viable tissue, may be another cause for urgent imaging trying to find out if there is viable tissue; some will go for urgent surgery in any way—particularly if there is suspected bilateral involvement on an emergency US study. Further details are given below.

12.3.4 Potter Syndrome/Bilateral Renal Agenesis

Today, due to foetal imaging, bilateral renal agenesis is hardly ever encountered postnatally.

However, there are cases where this has not been picked up prenatally and thus in every case of no urine output an urgent US should be done to assure presence of a functioning and perfused kidney.



Imaging in neonatal UGT emergencies such as renal failure, renal vein thrombosis, or PUV heavily relies on US. Doppler US is often essential to differentiate between the various entities, and US is sufficient for establishing the diagnosis in most cases.

12.4 Obstructive Uropathy

There are several forms of obstruction, which can be at various levels—from infra-vesical (PUV) to intravesical (clot, tumour) to ureterovesical (functional or morphologic disturbance at the ureterovesical junction, causing a megaureter and a pelvicalyceal dilatation) to ureteral (e.g. ureterocele, ureteric valves/stenosis, possible with secondary kink at the pelvi-ureteric junction) or PUJO. The rare calyceal neck obstruction is usually not a problem of the neonate.

Usually, these conditions are already depicted prenatally by seeing a urinary tract dilatation; additional findings particularly in severe conditions are oligohydramnios and lung immaturity, sometimes even urinary ascites caused by pop-off urinomas or urachus rupture.

12.4.1 Postnatal Imaging in the Dilated Urinary Tract: General Considerations

The role of postnatal US which is usually the first and most important imaging tool is to confirm the suspicion, help with grading, and potentially guide treatment by insuring sufficient drainage, for example via a percutaneous nephrostomy. However, only a few conditions need early and emergent imaging (only if they cause renal failure

such as a PUV or a bilateral obstructive uropathy). Most less severe conditions can be imaged and treated later—particularly as even sometimes impressively neonatal pelvicalyceal distension can improve over time and eventually be treated conservatively without deterioration for many years. Another aspect to consider is the risk to underestimate the severity of the dilatation in the first days after birth—due to the yet physiologically immature kidney and the perinatal transient dehydration, which will cause reduced urinary output and production and thus mimic a far less distended collecting system suggesting a lower degree of obstruction. This is the reason why in moderate or mild dilatation the initial US study can be and should be postponed to 7–10 days after birth. As these conditions have been present in the baby for many months there also is no risk of causing additional acute renal harm even in high-grade unilateral obstruction, as the elastic ureters and renal pelvis will prevent too high intrarenal pressures which might cause parenchymal damage (water-hammer effect, as postulated in early foetal development).

Several algorithms and proposal exist for when to image whom and how—all based on US using established grading systems (UTD grading system by the American societies, or PCD classification of the ESPR) (see Table 12.1). They use standardised sections of the kidney and measurements of the axial diameter of the calyceal dilation, the intra- and extra-renal axial pelvis diameter, the ureteral diameter, but also renal size/volume and parenchymal narrowing. Additionally, the renal parenchyma (e.g. corticomedullary differentiation? dysplastic cystic components? increased echogenicity?) and the shape of the calices (flattened papilla and fornices?) as well as the ureteric diameter and peristalsis should be noted (Fig. 12.11). Furthermore, size and shape of the urinary bladder, the bladder wall (thickness? contour?), possible trabeculation and diverticula, anatomy of the ostium (e.g. ureterocele? gapping?) need to be assessed and if possible also the urethra (best seen during voiding by a trans-symphysial or perineal approach). All these findings (“extended criteria”—see Table 12.2) should then be compared



Fig. 12.11 Ultrasound in a dilated ureter. US (oblique parasagittal section in the lower abdomen) shows a dilated ureter behind the urinary bladder; the peristalsis is documented by M-mode at the site of the dotted line (lower section of the image)

to prenatal findings (if available)—to then decide on further management and imaging.

- The latter then often consists of a follow-up US.
- In suspicion of VUR, a reflux study (ce-VUS or VCUG) is indicated.
- Early MRU or renal scintigraphy is performed only in rare conditions for therapeutical decision making, e.g. with severe bilateral disease and need for early (surgical) intervention in the neonatal period.
- An orienting static DMSA renal scintigraphy may be requested to get a rough impression on (split) renal function.

However, often these investigations are postponed, as, for example even high-grade neonatal VUR may vanish spontaneously, no routine antibiotic prophylaxis is administrated (unless there is a urinary tract infection), and therefore no immediate therapeutic impact derives from these studies. Even high-grade dilations in PUJO or UVJO usually are followed conservatively (unless there is deterioration with decompensation and renal failure, e.g. in a single kidney or a bilateral obstruction) delaying further imaging, and surgery is preferably performed later too, some even state not in the first year of life.

The intravenous urography, which decades ago was one of the major imaging tools for assessing the urinary tract and suspected obstruction, is completely outdated and not performed any longer, particularly not in the neonatal age.

12.4.2 Imaging in Neonates with Suspected Posterior Urethral Valve (PUV)

A PUV is a neonatal emergency, as every deterioration of the renal function must be avoided and an infection can have disastrous effects. Therefore, in all neonatal boys with a clinical or prenatal suspicion of a PUV, early imaging in the first 24–48 h after birth should be performed.

Imaging starts with US of the abdomen and in particular the urinary tract, completed by a perineal or trans-symphysis scan during voiding attempts to visualise the urethra. Typical findings are a massively thickened urinary bladder wall with trabeculation, an open bladder neck, dilated ureters (in part obstructive secondary to the thick bladder wall, in part refluxive), and bladder diverticulae; the PUV itself is only visible during voiding (Fig. 12.12). The kidneys usually exhibit some dilatation, and signs of dysplasia (such as echogenic non-differentiated tissue, parenchymal narrowing, cysts) may show vessel rarefaction on CDS and Power Doppler as a sign of impaired renal function, and some exhibit perirenal (“pop-off”) urinoma (Fig. 12.12). Some urinary ascites may be present, either from a ruptured urinoma or from a persisting urachus. Often the diagnosis is then confirmed by VCUG using either a transurethral or suprapubic access allowing for a nice detailed anatomic assessment and overview (Fig. 12.13); this drain/catheter is left in place to ensure sufficient urinary drainage from the bladder. If dilatation of the upper system persists in spite of bladder relief, an additional drainage of the affected collecting system by PCN will become necessary, as well as for treating persisting urinoma (do not drain the urinoma itself!).

Assessment of renal function is usually performed later by DMSA scintigraphy, after the

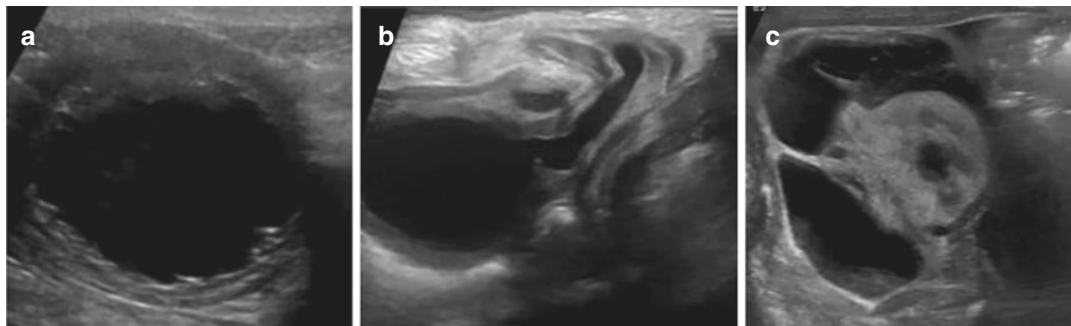


Fig. 12.12 Ultrasound in posterior urethral valve (PUV). (a) Axial US section: thickened bladder wall with trabeculation and high tension in a neonate with PUV. (b) During voiding, perineal US conspicuously delineates the typical configuration of the posterior urethra in PUV (image taken as a still frame from a video loop). (c) The right

axial flank view shows the echogenic dysplastic kidney with a septated urinoma surrounding the kidney due to rupture of a calix and the respective parenchyma by the high backward pressure (called “pop-of urinoma”). Also note the urinary ascites and some distention of the pelvicalyceal system

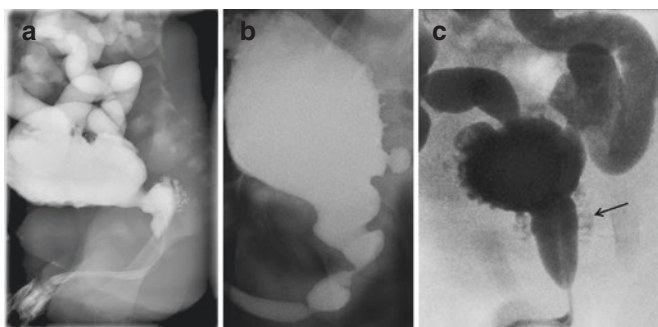


Fig. 12.13 Voiding cystourethrography (VCUG) in posterior urethral valve (PUV). (a–c) Three typical images of a PUV on VCUG: (a, b) are lateral exposures additionally demonstrates gross VUR (a) as well as trabeculae and

(pseudo-)diverticulae (b). Image (c) is a frontal view in last-image-hold technique at the end of micturition checking for CA drainage and residual volume. Note the contrast extravasation into the prostate (arrow)

valve has been surgically resected. Seldom a MAG3 renography or MRU becomes therapeutically necessary in the early period of life.

12.4.3 Imaging in Newborns with Suspected Pelvi-Ureteric Junction Obstruction (PUJO) (and Cystic Dysplastic Kidney/ Multicystic Dysplastic Kidneys)

Relevant PUJOs are often detected prenatally as they exhibit a significantly dilated pelvicalyceal system. The PUJO has usually been in place for

many months and thus there is no need for urgent imaging or treatment except for severe bilateral forms.

Imaging consists of US, best performed at the age of 5–10 days after birth, and shows dilatation of the collecting system with rounded calices and possibly parenchymal narrowing, sometimes even signs of dysplasia such as cysts and/or echogenic, non-differentiated parenchyma (Fig. 12.14). Often there is a sudden narrowing at the PUJ, the proximal ureter may even not be depictable. An accessory renal artery may run in the region of the PUJ possibly causing the obstruction (Fig. 12.14b)—more often some sort of kinking may cause the obstruction which

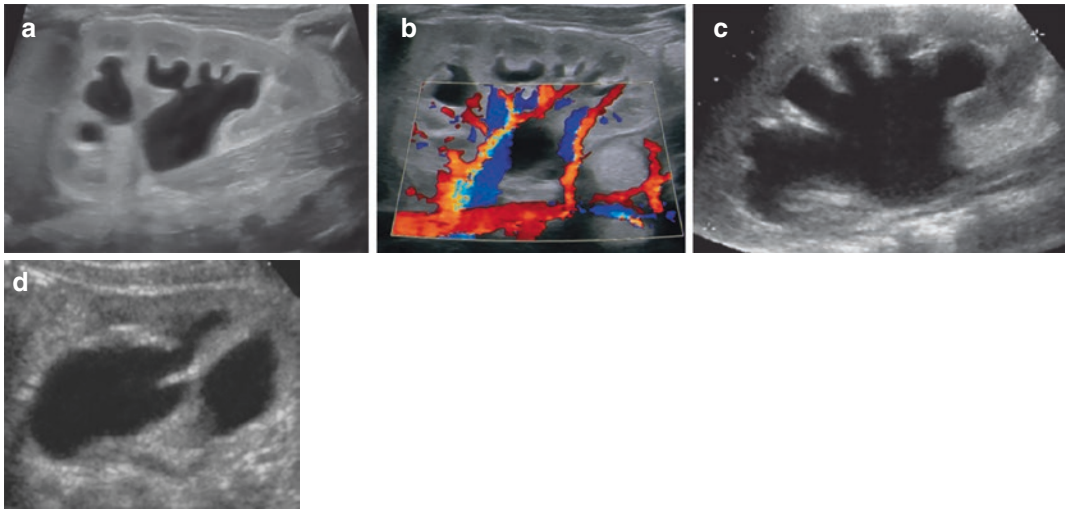


Fig. 12.14 Ultrasound in pelvi-ureteric junction obstruction (PUJO). (a) Lateral sagittal/coronal flank US view shows a left kidney with distended calices, flattened (but perceived) papilla and rounded fornices without severe narrowing of the parenchyma with preserved corticomedullary differentiation, but minor urothelial thickening. (b) CDS shows an additional renal artery (including the respective renal vein) to the lower third of the kidney crossing the pelvi-ureteric junction. In such findings, we tend to monitor these babies more thoroughly even if they initially exhibit only mild dilatation, as there might be a higher risk for deterioration or even decompensation due

to the anatomic situation, with the accessory renal vessel possibly causing an increasing anatomical obstruction during growth. (c, d) Sagittal/coronal (c) and axial (d) view of a neonatal kidney exhibiting more severe dilatation with parenchymal narrowing and loss of corticomedullary differentiation of the echogenic parenchyma (3 weeks after birth). On the first day after birth the “screening US” scan had shown only mild dilatation (PCD grade II), probably due to the physiologically low diuresis in the first days of life. The follow-up scan at 3 weeks had been indicated because of the high-grade PCD on foetal scans

can vary with bladder filling and diuresis as well as position. A “mega-ureter” can also cause such a kink, with secondary obstruction at the PUJ. Doppler US can reveal asymmetrically elevated RI values and even vessel rarefaction on amplitude coded Doppler sonography (aCDS = Power Doppler) in severe forms. Note that in neonates the RI values are physiologically higher than in children (due to possibly a small PDA, hyperviscosity, anaemia, etc.)—thus only the asymmetry can indicate that the obstruction is high and possibly deteriorating/decompensating; naturally, this can also be misleading in bilateral PUJO. Diuretic stress cannot be applied in the first weeks of life for differentiation of dilatation versus obstruction—due to the physiological immature renal function. And also note that dilatation does not equal obstruction—dysplastic or clubbed calices may not be obstructed, whereas a decompensated kidney or

an insufficiently hydrated patient may have reduced urine output and thus may exhibit less distension despite the obstruction.

There are different definitions of obstruction, based on the pathophysiology or the method used: Whitaker described obstruction as *any stenosis that impairs urinary drainage from the pelvicalyceal system and leads to increased pressure and reduced urine flow rate ...* [35]; also in 1982, Koff SA suggested that obstruction is *any restriction to urine flow, that left untreated will cause progressive renal deterioration*. The presently most accepted definition is the one introduced by Peters CA in 1985, who suggested to define obstruction as *any condition that, left untreated, endangers renal functional and growth potential*. Also, clinical symptoms such as haematuria, pain and colic, infection, or hypertension need to be considered and by itself are accepted as indication for surgery. However, looking at these definitions and criteria, it is obvious that

it is quite difficult if not impossible to reliably judge the individual development and to foresee the future, thus at present no definite a-priori pro-futura judgement is possible. Furthermore all these aspects and decisions usually affect older infants and not neonates, particularly as functional imaging is not reliably achievable in the first weeks of life. Therefore, MRU or renal scintigraphy is postponed and usually not performed in neonates unless there is a severe bilateral PUJO with renal insufficiency where early surgery is necessary and all further information on which kidney to operate first is essential.

Assessment of VUR in neonates with PUJO is under discussion; particularly if no infection and no ureteric dilatation is noted, no routine VUR-test is suggested. Some—nevertheless—perform VCUG preoperatively.

If a PUJO is infected, conservative treatment may be insufficient and then percutaneous nephrostomy (PCN) is performed, usually followed by pyeloplasty after the infection is cured before removal of the drain.

The most severe form of PUJO (or ureteric obstruction) is the cystic dysplasia and the multicystic dysplastic kidney (MCDK) which originate from an early high-grade obstruction or even ureteric atresia (e.g. after a vascular insult) during foetal life. On US these exhibit a variable number of differently sized cysts in an echogenic non-structured parenchyma; remnants of the collecting system may be visible (Fig. 12.15); differentiation between cysts and collecting system is achievable by either depicting an obvious connection between those cystic cavities or by observing the residual parenchyma: if there is a parenchymal rest centrally within the surrounding cysts, these hardly ever are remnants of the pelvicalyceal system. As a MCDK can shrink and practically vanish even already during pregnancy, sometimes only a single kidney is visible at birth (but then usually with a normal shaped adrenal gland at the site of the “renal agenesis”). Particularly in these conditions, a thorough assessment of the (female) inner genitalia is mandatory, as due to the joined intrauterine development of the urinary and genital tracts, mal-

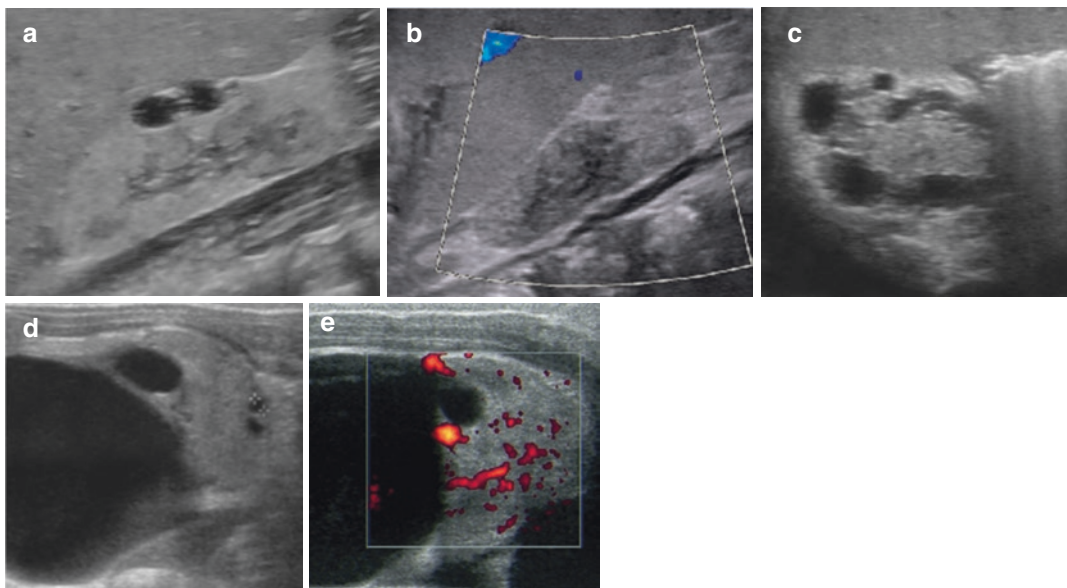


Fig. 12.15 Ultrasound in (hypo-)dysplastic kidneys. (a, b) Sagittal/coronal view of hypodysplastic kidneys—(a) with peripheral cysts, (b) without depictable vascularity on CDS in this small and atypically structured kidney. (c–e) This cystic dysplastic kidney with echogenic non-structured parenchyma exhibits no depictable collecting

system, whereas the centrally positioned collecting system is hugely enlarged due to severe early foetal PUJO inducing dysplasia of the peripheral parenchyma with tiny cortical cysts (+•••+) and severe functional impairment indicated by the reduced vascularity on (a) CDS (e). Note some sedimented sludge in d

formations of the ipsilateral inner genitalia are common and need to be detected (e.g. atretic vagina, uterus duplications, cystic dysplastic seminal vesical). This should be done during the neonatal period, as the inner genitalia is still large and stimulated by maternal hormones and thus easily and reliably assessable.



Urinary tract obstruction is a relatively common phenomenon in neonates usually picked up by prenatal US screening. The obstruction can be at different levels, only a PUV or a high-grade bilateral PCD (or in a single kidney) indicates early imaging, usually achieved by a comprehensive US study, complemented by a reflux test.

12.4.4 Imaging in Neonates with Megaureter, Ureterovesical Junction Obstruction (UVJO) and its Differential Diagnosis (i.e. VUR)

A “megaureter” is a dilated ureter—the reported cut-off values vary, between 4 and 6 mm width, without specifying whether this is measured as the maximum width during the peristaltic wave

or the minimum width. Ureteric width may also vary with hydration and bladder filling. There are different causes for ureteric dilatation: a UVJO or thickened bladder wall or an ureterocele, a dysplastic non-peristaltic segment, or a dilating VUR; also, ureteric valves can cause sectional widening of the ureter with some degree of obstruction of urine flow. The relevance of such a finding will usually only declare later in infancy, only those neonates with a dilated collecting system or clinical symptoms or dysplastic renal parenchyma need early further investigations.

Again, US is the mainstay of imaging and is performed similarly to PUJO (see above). Often the entire course of these dilated ureters can be assessed, and special attention should be paid to differentiate the various forms of UVJO. It is important to avoid a nearly empty bladder during the examination not to miss a ureterocele. Also document the peristalsis by M-mode or video-clip, search for valves, and observe a possible kink at the PUJ (Fig. 12.16; see also Fig. 12.11). Particularly in boys, visualisation of the urethra (best during voiding) and a detailed analysis of the bladder are necessary (wall thickening or trabeculation? open bladder neck? PUV? ...). The kidney is examined for possible dilatation and signs of obstruction or dysplasia, and an orienting abdominal survey is recommended.

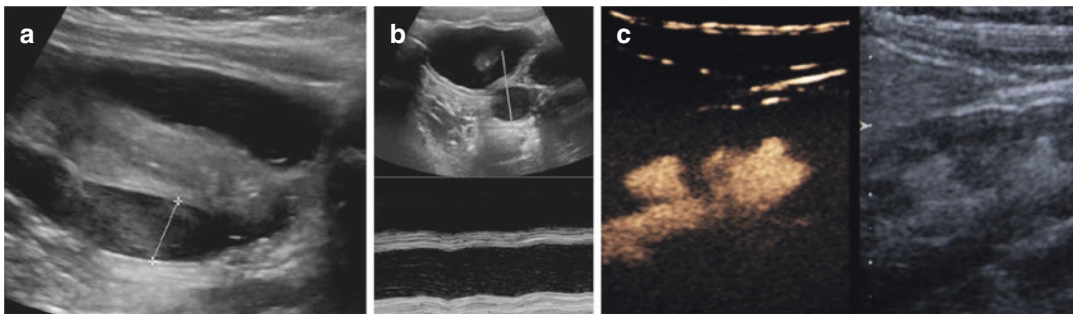


Fig. 12.16 Megaureter. (a) A dilated ureter is depicted in this oblique sagittal view behind the bladder, with plenty echoes in the lumen (+...+; note this does not necessarily equal infection, it can also derive from the physiologic medullary deposits that are cleared from the kidney by improving diuresis). (b) Axial view through urinary bladder depicts a megaureter. M-mode (lower section of the

image) documents the lack of peristalsis. (c) Dilated ureters can be obstructive or refluxing or even both—therefore some VUR test is often advisable. Here contrast-enhanced voiding urosonography (ce-VUS) proved high-grade VUR (ce-VUS is preferred in dilated systems/ureters, as even a few bubbles can be depicted without dilution effect as sometimes observed on fluoroscopic VCUG)

Commonly, to differentiate a refluxive versus an obstructive megaureter, some kind of VUR test is then indicated, particularly if secondary signs for a VUR such as grossly changing dilatation before and after voiding, bladder wall thickening and trabeculation, or thickening of the pelvic wall (= renal urothelial sign) are observed. This can be achieved by VUCG or ce-VUS, but particularly in dilated systems, ce-VUS is superior in VUR detection, as it will depict even a few refluxing bubbles, whereas on fluoroscopy dilution effects may hinder sufficient opacification of the megaureter and thus mask an existing VUR; furthermore, grading of the VUR may be difficult.

Usually, no other imaging is necessary. Scintigraphy, if necessary at all, is delayed into infancy, only sometimes a non-enhanced “anatomic” MRU (heavily T2-weighted sequences, possibly a thick slice cine-sequence to evaluate and document ureteric peristalsis) is performed to give an overview of the entire anatomy of the dilated system in complicated malformations, which in neonates can easily be performed in feed-and wrap approach avoiding anaesthesia or sedation.



A dilated ureter can have different causes; in neonates imaging consists of US. No other imaging is needed except for possibly a reflux test - unless there are clinical symptoms such as a urinary tract infection or high-grade PCD and/or renal parenchymal dysplasia.

12.5 Duplication and Other or Associated Malformations of the Urinary Tract

There are a number of variations, anomalies, and malformations affecting the kidney and the collecting system itself or its position, possible fusion of kidneys, as well as a single kidney. These are summarised by the term congenital anomalies of the kidneys and the urinary tract (CAKUT).

12.5.1 Renal Duplication

A *duplex kidney* in itself is not a malformation or a pathology—if not associated with VUR or obstruction it is rather considered a variation, which does not need neither imaging nor follow-up. Nevertheless, duplications (as well as rare triplications, see Fig. 12.6) can be associated with VUR and/or obstruction, also ectopic ureteric orifices (intra- or even extra-vesically, e.g. into the vagina) are more common, as are orifice pathology such as an *ureterocele* (Fig. 12.17).

On US, a complete duplication is identified by either visualising an additional ostium in the bladder or observing a doubled ureteric inflow jet, although this in neonates is a bit more cumbersome to detect than in older infants (Fig. 12.18). Furthermore, one will find a parenchymal bridge diving the kidney in a usually smaller upper and larger lower part, with two different collecting systems often with disproportional size and configuration. Try to see if there are two different PUJ and two separate proximal ureters—sometimes one is successful in also visualising a ureter fissus as in incomplete duplication. In dilated PCDs, the upper pole ureter, draining more distally in the bladder, usually is obstructed, whereas the ureter of the lower system inserts more cranio-laterally into the bladder and thus is prone to reflux (Meyer-Weigert Rule). In an upper pole obstruction, this can be quite impressive, sometimes with only a cyst-like remnant of the upper moiety with a thin dysplastic echogenic parenchymal rim; these parts usually have a significantly reduced renal function, thus a possibly earlier existing megaureter might be masked and challenging to find (Fig. 12.19). If the lower system exhibits parenchymal damage or changing dilatation, it usually is refluxive—in these systems, the probability of spontaneous regression is lower than in normal single systems. Nevertheless, also low moiety obstruction or mixed obstructive-refluxive systems exist. Note that duplex kidneys may have additional renal arteries and veins which are important features for the surgeon—thus always search for it using CDS, and try to assess the perfusion of the different moieties. Often the upper dysplastic moiety

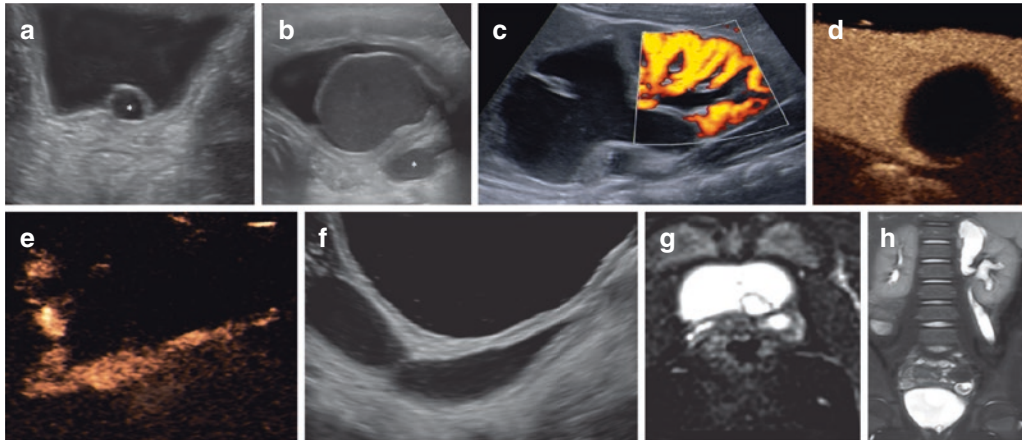


Fig. 12.17 Ureterocele. (a) Axial US of the urinary bladder: a small ureterocele protruding into the bladder is seen (asterisk). (b) A large ureterocele nearly filling up the urinary bladder and obstructing the bladder outlet; additionally, the respective megaureter (asterisk) can be seen behind the bladder, as well as sludge in the ureterocele and the megaureter. (c) The respective kidney with a huge dilatation of the upper moiety system, and a normal parenchyma as well as vascular architecture (on Power Doppler) of the lower moiety which has only a minor dilatation. Again note the layered sludge in the dilated upper moiety's system. (d, e) ce-VUS demonstrates the non-contrasted and thus non-refluxing ureterocele (d), but

VUR into the system of the lower moiety collecting system of the lower moiety of the respective duplex kidney (e). (f, g) Ultrasound shows a dilated ureter running behind the bladder obviously not draining into the urinary bladder (f)—thus an ectopic insertion was to be suspected. The axial T2-weighted MRI shows the very low ectopic insertion with a small ureterocele (g). (h) Coronal T2-weighted "water" MR-urography (MRU) image shows the dysplastic and dilated upper moiety of the ectopically draining system and the small ureterocele at the bladder neck, in parts the megaureter is also visible; the collecting system of the lower moiety has less dilatation

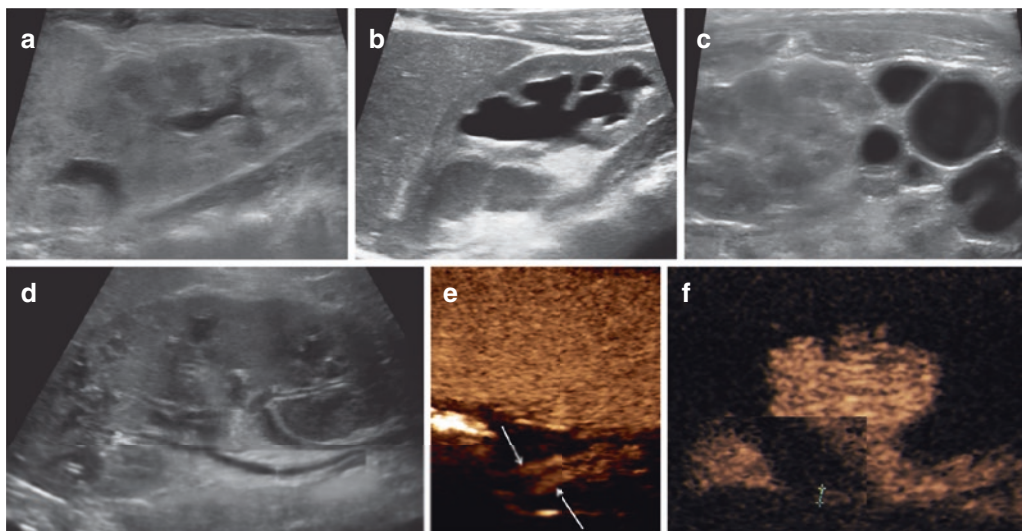


Fig. 12.18 Duplex kidney. (a) An uncomplicated duplex kidney with some mild dilatation of the upper and the lower system; however, the upper moiety exhibits a slightly dysplastic appearance of the parenchyma. (b) A duplex kidney with sludge and echoes in the upper pole system (in this case is caused by urinary tract infection). (c) A duplex kidney with a multicystic dysplasia (MCDK) of the lower moiety, but a normal parenchyma without dilatation of the collecting system of the upper moiety. No contralateral kidney was seen, hence this lower moiety

might present a cross-fused contralateral kidney with MCDK. (d) A duplex kidney with obvious cystic dysplastic parenchyma particularly of the upper moiety. In this assembled image, both ureters can be seen too (+...+ = upper pole ureter). (e, f) ce-VUS of the same system as shown in image d depicts two refluxing non-dilated ureters close to the single ostium behind the bladder (e, ureter fissus, arrows), with reflux into both, also the upper (+...+) pelvicalyceal systems on this assembled image (f)

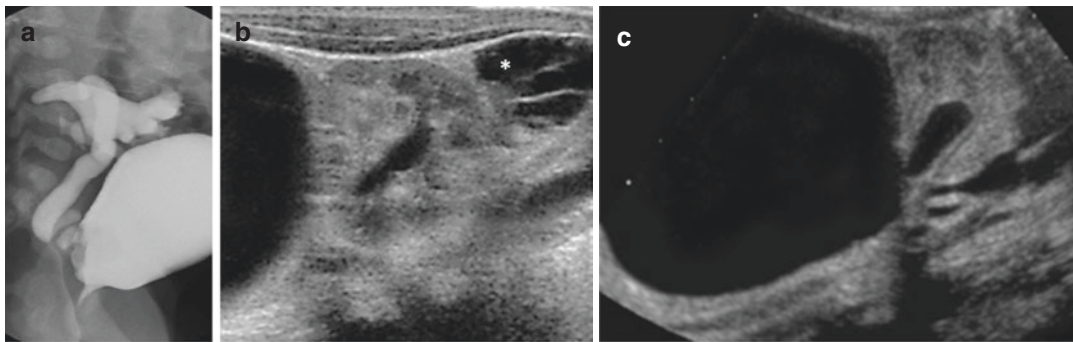


Fig. 12.19 Voiding cystourethrography (VCUG) in a duplex system. (a) VCUG (oblique spot exposure for viewing the ureteral insertion) shows the “dropping lily sign” of the refluxing lower moiety’s collecting system;

(b, c) On US one can see this relatively normal moiety’s parenchyma with parts of the megaureter visible at the lower pole of the kidney (asterisk, b) and the huge cystiform dilatation of the upper system (c)

will exhibit severe vessel rarefaction on aCDS thus indicating poor function of this system.

When image assessment of duplex systems is indicated, usually some kind of VUR test is performed—either ce-VUS or VCUG. If there is refluxing lower system, the respective PC-system appears like a “dropping flower” on VCUG. If there has been ureterocele that has been unroofed, VUR into this upper pole megaureter can occur. Note that a large ureterocele cannot only cause ureteric obstruction, but by herniating into the bladder neck it can also cause bladder outlet obstruction. Ureteroceles can furthermore evert and become diverticula during voiding then also becoming refluxive (Fig. 12.19).

In neonates, no other imaging is performed except for very confusing situations with a need for early correction. Later in infancy, particularly pre-operatively, MRU may become indicated for detailed anatomical assessment also with respect to additional renal arteries, and for defining the respective relative function of the moieties. Scintigraphy is also still used for this query, but is less reliable, as it may be difficult to differentiate the clear border between the upper and the lower moiety to assess.

12.5.2 Other Common Renal Migration, Position, and Fusion Anomalies

The most common alternate renal positional malformation is a *horseshoe kidney*—besides

renal ectopia (usually in pelvis and more medially, with some abnormal rotation). It is defined as a fusion of the lower poles ventrally to the large retroperitoneal vessels easily depictable by US if searched for also using graded compression; consequently, the kidneys tend to be slightly malrotated and caudally tilted to the midline, with an altered renal axis (Fig. 12.20). Often some distention of the renal pelvis, sometimes also the calices is noted, but all these systems are not necessarily obstructive. They also often exhibit variations in vasculature and feeding/draining vessels. In order not to miss such an entity, it is essential to really always sonographically follow the kidney to the lowest pole in an axial section assuring that the kidney borders are always seen—or the respective bridge to the contralateral kidney is noted.

Other (fusion) anomalies are *pancake kidneys*, *cross-fused ectopia*, simple *ectopic kidney* or *single kidneys/renal agenesis*, also *renal hypo(dys)plasia*. The names are self-explanatory—the respective presentation is usually easily seen on US. For differentiation, e.g. of a pancake kidney or a cross-fused kidney, the ureteric orifices need to be visualised (both on same side versus one on each side). Note these variations are often associated with a somewhat dysplastic collecting system with megacalycosis (not obstructive), rotation anomalies, as well as parenchymal dysplasia and variations in vasculature.

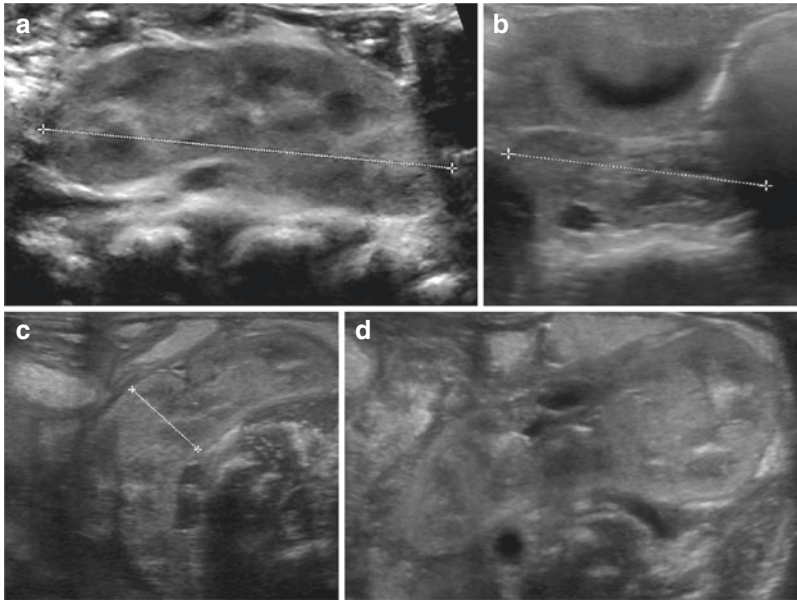


Fig. 12.20 Kidney position anomalies. (a) A pelvic ectopic kidney (+...+) is seen behind the sufficiently filled urinary bladder, positioned nearly in the midline. (b) Another pelvic ectopic kidney (+...+) sitting sagittally practically in the midline in front of the lumbo-sacral spine distal to the aortic bifurcation, with some signs of parenchymal dysplasia. (c, d). An axial midline abdomi-

nal US just below the umbilicus demonstrates the parenchymal bridge of a horseshoe kidney connecting the larger left with the smaller right kidney (+...+, c). This may easily be missed because of poor access and overlying obscuring gas, thus often some gentle graded compression is necessary to really visualise the connection between the two lower kidney poles which may appear asymmetric (d)

12.5.3 Miscellaneous Other Conditions

- **Prune belly syndrome** is a congenital malformation that present following three main symptoms: aplasia of the abdominal wall muscles (that's why the belly looks like a dried prune and what gave the disease its name), bilateral cryptorchidism (usually bilateral intra-abdominal testes), and malformations of the urogenital tract (usually hypoplastic and narrow urethra and megaureter with renal dysplasia). There are associations with other malformations such as clubfoot or gastroschisis.

Mainstay of imaging is US that may visualise all these findings, complemented by VCUg (assessment of the urethra and for VUR) as well as sometimes renal scintigraphy (assessing renal function, usually later in life).

- **Calyceal diverticula** need to be mentioned too, to complete the list (see also Ddx of renal cysts and renal dysplasia).

Imaging in neonates is achieved by US, if necessary, MRU can be performed after renal maturation (e.g. after a minimum of 6 weeks of life) if necessary for treatment decisions.

- **Bladder diverticula** usually occur secondary to bladder outflow obstruction and manifest later, except for PUV where these can already be present at birth. Note that an ureterocele may evert and thus become a diverticulum during voiding (i.e. increased intravesical pressure) then changing from an obstructive to a refluxive system.
- **A persisting urachus** is a common query in a wetting umbilicus. There are different forms of urachal remnants: a true entire persisting channel (e.g. associated with bladder outlet obstruction), parts of the urachus (e.g. distally, subumbilical), or a central cystic remnant with or without connection to the bladder. Besides investigating the subumbilical area with a high-resolution linear transducer to visualise the tiny midline structure (Fig. 12.21), a good bladder filling and sometimes contrast instillation (via

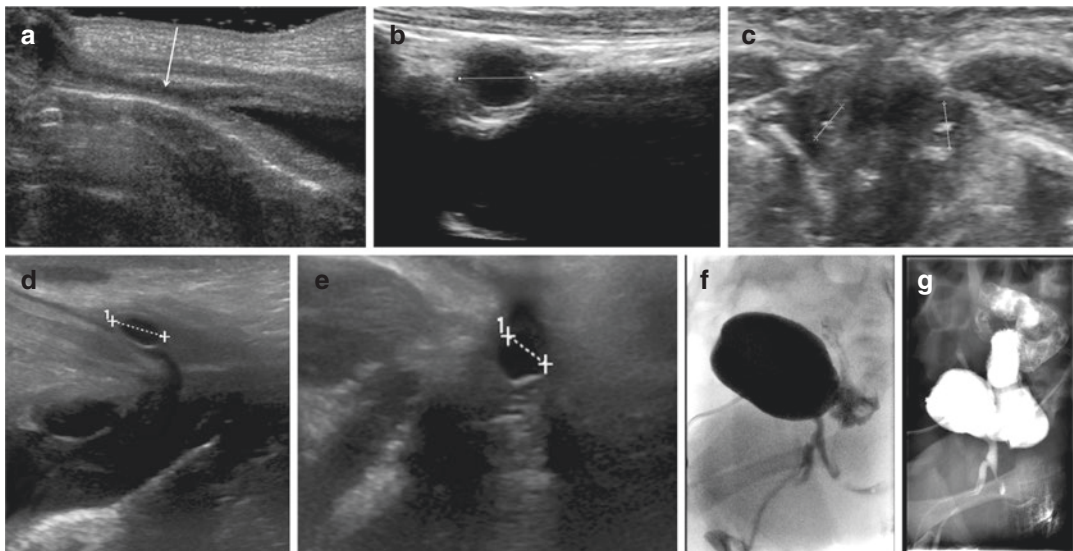


Fig. 12.21 Urethral pathology and urachus. (a) Sagittal midline US view depicts a tubular structure running from the bladder roof to the umbilicus (arrow), consistent with a persisting urachus. (b) Urachus cyst: a cyst is seen in an axial midline US view in the course of the urachus close to the abdominal wall (+····+) just below the umbilicus. (c) Perineal US depicts a utriculus cyst. (d) Perineal US depicts a cystic urethral duplication/diverticulum (d, 1+····+), or a cyst behind the posterior urethra. (e) Perineal US depicts an utriculus cyst. (f, g) VCUG in a urethral duplication with fistula to the anal canal

umbilicus in an axial US view—these are remnants of the umbilical artery and not a urachus remnant—as these can be followed laterally to each side of the bladder. (d) Perineal US depicts a cystic urethral duplication/diverticulum (d, 1+····+), or a cyst behind the posterior urethra. (e) Perineal US depicts an utriculus cyst. (f, g) VCUG in a urethral duplication with fistula to the anal canal

the umbilicus or by filling the bladder) may become necessary to prove the patency of this persisting urachus (if of therapeutic relevance). A quite common minimal remnant of the urachus is a regional swelling of the bladder wall at the top of the bladder. Don't confuse this with a bladder tumour (Fig. 12.21). Note that remnants of the umbilical artery can mimic a persisting urachus appearing as low echogenic bands also coursing downwards from the umbilicus—but they usually are paired and have a slightly lateral course to each side of the bladder (Fig. 12.21). Similarly, a persisting omphaloenteric duct will course to the side and can be recognised by this different course without connection to the bladder.

- **Urethral and bladder duplication** are extremely rare and usually part of a spectrum of other malformations (e.g. ARM-spectrum).

Imaging is best performed by US for the bladder and fluoroscopy (VCUG or urethrography) for the urethra, sometimes also ce-VUS or sonographic urethrography may provide the diagnosis (Fig. 12.21).

- **Urethral fistulas** connecting to the urinary bladder, the vagina, the rectum, or the perineum are part of the cloaca spectrum, and addressed in Chap. 13.

For imaging note that for detecting and contrasting such a fistula applying CA is necessary and the filling always should be attempted from the high-pressure system (usually the urinary bladder/voiding) to the system with the lower pressure. Thus a VCUG or a ce-VUS are the method of choice, or an urethrography; sometimes a genitography is needed as an add-on.


- **Neurogenic bladder** (e.g. in dysraphism or myelomeningocele) usually manifests only later and is difficult to diagnose in neonates—thus not further addressed.
- The **epispadias-exstrophy complex** is a spectrum of malformations ranging from epispadias to cloacal exstrophy. The anterior abdominal wall is open as is the anterior bladder wall including the bladder neck and the urethra. Anomalies of the upper urinary tract are infrequent, but secondary VUR will



Fig. 12.22 Pelvic radiograph in bladder exstrophy. Note the atypical shape of the pelvis and the split symphysis

practically always be present after surgical repair. Additionally, there is a split symphysis with shortened pubic bones and rotated iliac bones, and vertebral body anomalies may be associated (Fig. 12.22). Other existing forms are a covered exstrophy of the bladder, a pseudo-exstrophy and the various forms of cloacal exstrophies—to discuss all those entities in detail is beyond the scope of this chapter.

Considering the above-mentioned features, imaging always includes a radiograph of the pelvis and the lumbar spine, an US of the spinal canal and the urinary tract as well as the brain, a chest radiograph for preoperative workup, and postoperatively VUR assessment as well as repeated US of the UGT during follow-up.

 Duplications and other variations of kidney position, rotation, and fusion may in itself not have any sequelae. However, they carry a higher risk of dysplasia, VUR, or obstruction and thus at least a follow-up monitoring later in infancy is reasonable. A meticulous initial diagnostic workup of asymptomatic neonates with such conditions usually discovered incidentally without other imaging defined risk factors (“extended criteria”) is not necessary.

12.6 Cystic Kidney Disease

Cystic kidney disease (CDK) is a part of the CAKUT spectrum, in part they are also predetermined genetically—particularly a large number of those CDKs that are important in neonates are inherited or at least genetic. Many of these are now seen as ciliopathies (affecting also other organs with hairy cilia) or uromodulin defects, some are part of syndromes.

Diagnosis is usually made by presentation and family history (and genetics). The US examination may give a clue, too: bilateral large echogenic kidneys (due to numerous microcysts) in a neonate practically always are autosomal recessive polycystic kidney disease (ARPKD), whereas a neonatal unilateral manifestation (of some cysts, possibly of different size) is seen in autosomal dominant polycystic kidney disease (ADPKD) or in dysplasia and MCDK (Fig. 12.23, see also Fig. 12.8). Another hint may be involvement of other organs (e.g. hepatic fibrosis in ARPKD, aneurysm of the large arteries in ADPKD, cerebellar vermis hypo/aplasia with the “molar tooth sign” in nephronophthisis). Some CDK only manifest beyond neonatal age—thus a normal neonatal US of the kidney does not rule out an inherited CDK. There are many other entities such as nephronophthisis complex, medullary cystic kidney disease, glomerulocystic kidney disease, diabetes with renal cysts-syndrome, cysts in tuberous sclerosis, and other syndromes (Table 12.3 and Fig. 12.24). And finally, also renal tumours may manifest as a complicated renal cyst with haemorrhage, septations, nodular wall components (e.g. in a cystic Wilms’ tumour or a cystic mesoblastic nephroma—see below). Except for the latter no additional imaging and also no MRI are performed in neonates, sometimes (e.g. when searching for the cause of a cystic dysplastic kidney) a reflux test may be come indicated.

Note that a single simple renal cyst in a newborn should not be handled like in adults, where such a cyst is no reason for concern—in neonates it mostly is a manifestation of an underlying CDK and thus needs at least follow-up and a thorough family history.

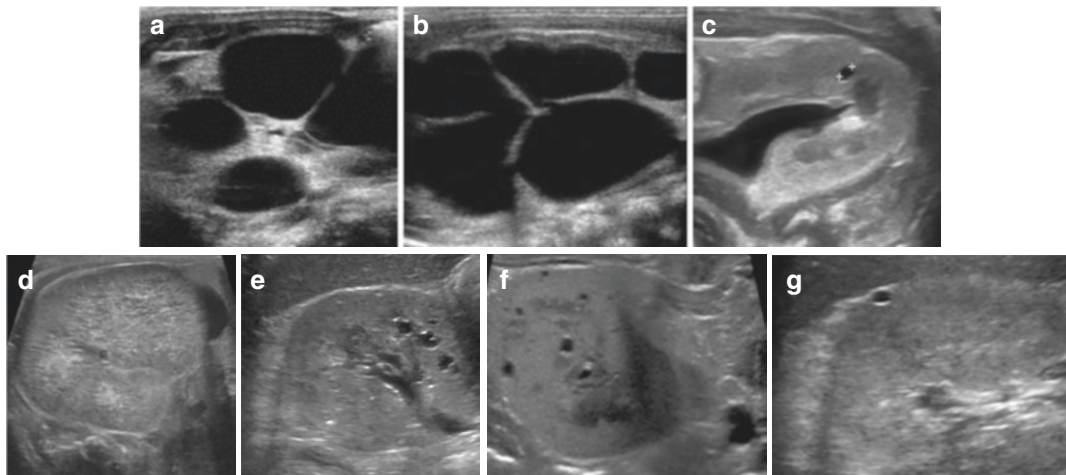


Fig. 12.23 Ultrasound in cystic kidney disease (CDK). (a, b) Multicystic dysplastic kidney: note the central echogenic dysplastic parenchymal remnants and the peripherally located multiple large varying size (a)—in opposite to a severely dilated collecting system in high-grade PUJO with a rim-like peripheral parenchyma (b), which can be the clue for making the diagnosis. (c) A neonate with a small single “simple” renal cyst (+...+)—which turned out to be a syndromal cyst. (d) An enlarged neonatal kidney with irregular appearance of the entire parenchyma (of both kidneys) due to numerous small microcysts in autosomal recessive polycystic kidney disease. (e)

Multiple small slightly complex cysts at the corticomedullary junction zone in a 1-month-old baby with known familial autosomal dominant polycystic kidney disease. (f) Different sized cysts at different kidney locations (small cortical and larger medullary cyst) in this axial view of the neonatal kidney in a baby who eventually was diagnosed with Alport syndrome. (g) A simple small peripheral sub-capsular cyst in a slightly dysplastic looking neonatal kidney with VUR; this child also suffered from tuberous sclerosis, so the aetiology of this cysts (dysplastic in connection with VUR, or syndromal as manifestation of tuberous sclerosis) remains unclear

Table 12.3 Cystic kidney disease and kidney cysts in childhood and in neonates

Non-genetic/hereditary entities with renal cysts	Genetically determined CDK
(Cystic) hypodysplasia	Autosomal Dominant
Multicystic dysplastic kidney (MCDK)	Autosomal dominant polycystic kidney disease (ADPKD)
Localised cystic disease of the kidney	Tuberous sclerosis (TC)
Multilocular cyst	Medullary cystic kidney disease (MCKD)
Cystic nephroma	Glomerulocystic kidney disease (GCKD)
Segmental MCDK	Autosomal Recessive
Parapelvic cyst	Autosomal recessive polycystic kidney disease (ARPKD)
Calyceal cyst (calyceal diverticulum)	Juvenile nephronophthisis
Medullary sponge kidney	Cysts associated with syndromes
Acquired cystic kidney disease	Various chromosomal disorders
In chronic renal failure, not in neonates	Renal cysts with diabetes syndrome
Cystic malignant renal tumours	Various autosomal recessive syndromes
Cystic mesoblastic nephroma	Mitochondrial syndromes
Cystic (Wilms) tumour	X-linked syndromes, e.g. Alport's syndrome
Simple cysts (extremely rare in neonates)	

List of cystic kidney diseases—the neonatally important entities are marked blue

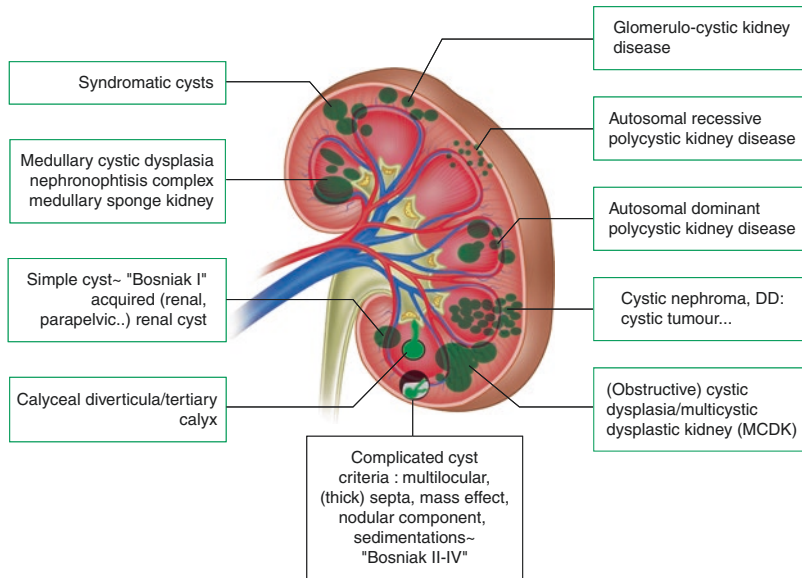


Fig. 12.24 Schematic drawing of typical location and appearance of various renal cysts and cystic kidney disease. Schematic drawing with respective US images and histology samples in typical CDK entities and respective differential diagnosis. (Adapted from “Riccabona M.

Imaging in renal agenesis, dysplasia, hypoplasia and cystic diseases of the kidney”. In Riccabona M. (ed) *Pediatric Urogenital Radiology*; 3rd edition, Springer 2018; p:560. ISBN 978-3-319-39200-4)

12.6.1 Differential Diagnosis in CKD

For differential diagnosis, the congenital/neonatal glomerulonephritis and the nephrotic syndrome of the Finnish type need to be considered, also other entities who present with either a renal cysts or echogenic large kidneys such as cystic dysplasia or (bilateral) renal vein thrombosis or shock kidneys (on US also large and echogenic). But usually these can either be differentiated by the clinical history and presentation, sometimes also the Doppler US information is helpful—but note that reduced particularly diastolic perfusion and flow velocities can be seen also in severely affected kidneys with CDK or other renal conditions, as it reflects more the renal function and systemic influences than the underlying renal disease. Cystic renal tumours may manifest as a complicated renal cyst, another cause of a complicated renal cyst may be an abscess or an infected calyceal diverticulum.

Except for the tumour-queries (and unclear abscesses), no additional imaging beyond US is performed in neonates.

Further imaging, follow-up, as well as management of these patients is important after the neonatal

age. These studies are performed more or less regularly during childhood but not in newborns and thus not listed here. But there is a very informative recent consensus statement by Gimpel et al. (*Radiology* [6]) addressing all these issues on how to image and follow-up whom with whichever CDK, which can be recommended for further reading.



Cystic kidney diseases comprise many entities that can be diagnostically challenging particularly in the neonate. The diagnosis is based on clinical presentation, family history, and appearance on US also evaluating for extra-renal manifestations. Eventually molecular genetic testing will provide the final diagnosis particularly in all familial forms such as ciliopathies and uromodulin defects, and is indicated in unclear situations, as an accurate diagnosis is essential for not only patient management, but also with respect to future genetic counselling of the patients and their families and for planning follow-up.

12.7 Urinary Tract Infection in the Newborn

Neonatal urinary tract infection (UTI) is not so common as in infancy and usually is of haematogenous origin, although there is an association with (severe) urinary tract malformation such as megaureter, PUJO and PUV, or gross high-grade VUR. Clinical symptoms may be very unspecific, often only septicaemia is noted and the involvement of the urinary tract is found thereafter during septic workup. Neonates with UTI may not have fever, and cannot articulate dysuric complaints. Diagnosis is established by catheter urine sampling (or urine from suprapubic puncture) with elevated number of microorganisms (bacteria count higher than 10^4); leukocyturia or a positive nitrite test may be misleading and may even not be present. Treatment consists of (often intravenous) antibiotics and general symptomatic management.

Imaging consists primarily of US and should in neonates be performed early, within 24–48 h. One will assess for associated urinary tract malformations that pose a risk for complications, and signs of (usually diffuse or multifocal) renal involvement or pyonephrosis which might impact aggressiveness of treatment. Renal involvement is indicated by an increased size of the swollen kidney with altered parenchymal echogenicity; a thickened bladder, ureteric or pelvic wall is also seen but is unspecific (also seen in obstruction or VUR) (Fig. 12.25). Power Doppler may reveal patchy perfusion defects. If pathology is detected or if there is no adequate response to treatment, another US examination is performed and may reveal puss in a dilated collecting system seen as floating echoes within the collecting system. Note that these echoes can also derive from physiological medullary deposits that are rinsed out, and that some dilatation of the collecting system and ureter may be due to hypotonia caused by bacterial toxins and does not necessarily indicate an obstruction or VUR. Sometimes also an inflammatory

“lobar nephronia”, necrosis and abscess formation is found. On US these appear as pseudo-tumorous focal swelling, focal disruption of parenchymal echotexture, eventually becoming a complex liquid cyst-like structure with some sort of outer membrane (Fig. 12.25).

DMSA scintigraphy or MRI is hardly ever indicated, particularly as it does not impact treatment, even if diffusion-weighted sequences are very sensitive (though not always specific) for depicting renal involvement. Only if there is a suspicion of a tumour, MRI may sometimes be helpful and indicated.

When/after the UTI is treated, VUR assessment (by VCUG or ce-VUS) is essential, as well as a follow-up US for assessing potential scarring (not earlier than 4–6 weeks after the infection). DMSA scintigraphy (or MRI) is also used for depicting scarring, but these studies should not be done earlier than 4–6 months after the infection to be decisive.

There is another though rare inflammatory condition in neonates: fungus infection, usually secondary to fungal septicaemia with, e.g. candida. Particularly in preterm neonates with some dilatation of the collecting system fungus balls (on US appearing as echogenic intraluminal foci with or without shadowing) may develop and cause secondary stone formation with also obstructive symptoms—one of the rare incidences of urolithiasis in neonates with secondary obstruction; alternate causes for nephrolithiasis in neonates may be metabolic disease or long-term intensive care treatment with phases of restricted urine production, antibiotics, and diuretic treatment.



Every neonate with UTI (and unknown urinary tract anatomy) should early be investigated by US—to assess for possible associated urinary tract malformations posing a risk for complications and scarring.

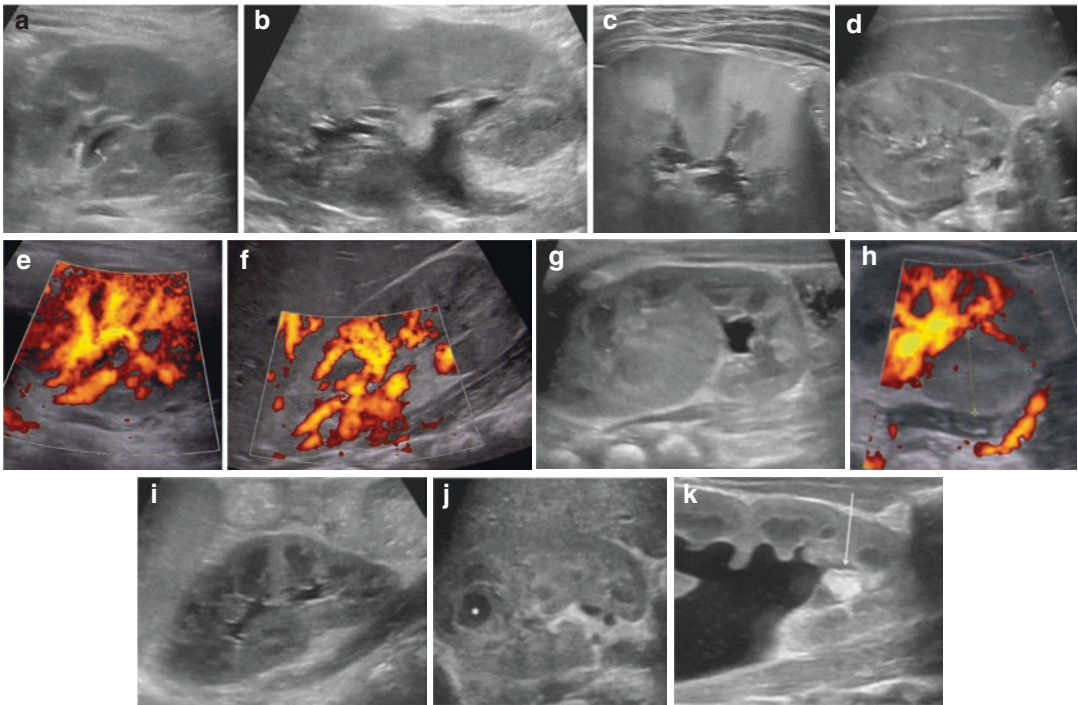


Fig. 12.25 Ultrasound in neonatal urinary tract infection (UTI). (a–k) US in UTI may reveal thickened urothelium (a, ++++), a swollen kidney with echogenic peripelvic tissue and regional disrupted echotexture as well as scarring (b, at the upper slightly clubbed calix in this 6-week-old girl), focally altered renal parenchyma (c, d), patchy per-

fusion defects on Power Doppler (e, f), and a pseudotumorous swelling (i.e. lobar nephronia) with regional perfusion defect on Power Doppler (g, h) which vanished under antibiotic therapy (i). Other findings may be abscess formation (asterisk, j) or an echogenic fungus ball (k, in the lower calix of this dilated collecting system, arrow)

12.8 The Neonatal Female Genitalia

In the neonate, there are a number of conditions of the female genitalia that may benefit of or need imaging. Inflammation is rare; most often ovarian cysts, but also ovarian torsion and genital malformations indicate US, which is the mainstay of genital imaging in this age group.

It is important to remember that—stimulated by maternal hormones—the neonatal uterus is large and has a prominent cervix, the ovaries often are large too (less in very preterm infants or after some time in the neonatal intensive care unit (NICU)), exhibit follicles and follicular cysts, not to be mistaken as pathology (see Fig. 12.3). These findings nearly always regress spontaneously without need for imaging follow-up or therapeutic

action. However, this gives imaging an ideal chance to evaluate the female genitalia in detail; therefore, all imaging queries that address possible genital malformations should be investigated in the neonatal period to make optimal use of this unique diagnostic window. A full urinary bladder is often necessary. Sometimes also filing of the bladder and in some conditions even of the urethra and the rectum/colon may be indicated. Also note that the neonatal ovaries are very mobile and can be found nearly everywhere in the abdominal cavity or even in the inguinal canal and the labia majora, thus a thorough search (also sometimes using gentle “graded compression”) is important when trying to find them on US. MRI is usually not necessary for assessment of the neonatal genitalia, except for tumour conditions either for staging or for preoperative anatomic assessment.

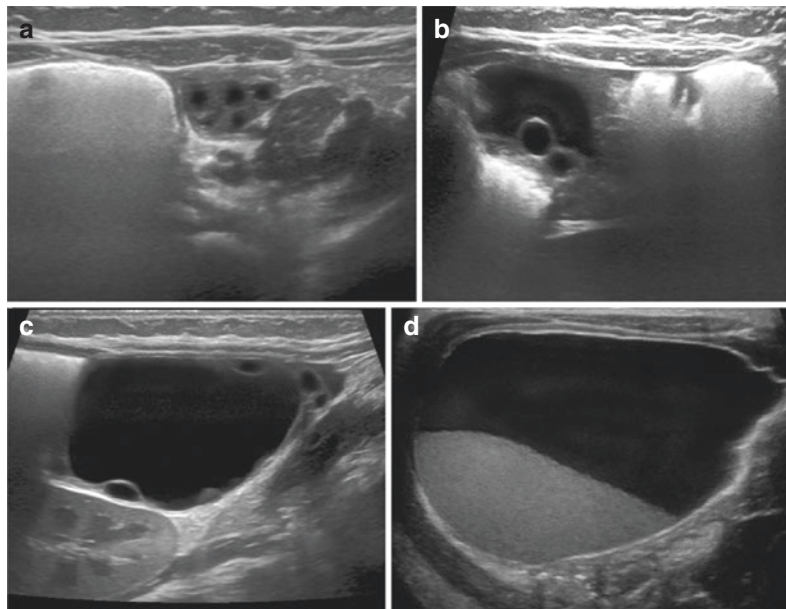


Fig. 12.26 Neonatal ovarian cysts. (a) A typical neonatal ovary located close to the abdominal wall with multiple normal follicular “cysts”—graded compression was used to remove the overlying and obscuring bowel gas. (b) A larger ovarian cyst with “daughter follicles” inside. (c) A

large ovarian cyst sitting in the mid abdomen reaching up to the kidney—again with a daughter cyst and depictable ovarian parenchyma at the cyst’s wall. (d) A huge ovarian cyst with sedimented debris after haemorrhage

12.8.1 Neonatal Ovarian Cysts

The most common findings in newborn girls are stimulated ovaries with sometimes huge, sometimes even haemorrhagic cysts. If these are very large, they are prone to torsion. Therefore, large cysts (diameter larger than 4 cm) are followed and reported, also to make the clinician aware of such a possible event to then enable prompt surgical response. Some promote US-guided cyst puncture if these cysts are reaching 6 cm or above, do not regress or even grow, or get haemorrhagic.

US is the imaging of choice (see above) when an ovarian cyst is suspected. To differentiate ovarian cysts from other intra-abdominal cysts like intestinal duplications, mesenteric cysts, or even choledochal cysts, features such as a daughter cyst as well as identification of ovarian parenchyma are important. Ovarian perfusion (e.g. when it is herniated into the inguinal canal) and a normal contralateral ovary must be included in

the examination. If one finds tissue such as calcifications or nodular components or fat in the cyst, one may suggest a cystic teratoma, though definite differentiation is difficult. Sometimes debris-fluid levels from haemorrhage may mimic a duplication cyst (Fig. 12.26)—thus carefully observe the cyst wall (is there a “gut signature”?) and its relation to the adjacent bowel loops (move and shift against? follow peristaltic movement? receive vessels from the bowel or mesentery).

12.8.2 Malformations/Congenital Anomalies of the Female Genital Tract

These anomalies result from developmental disturbance of the Müllerian duct and/or urogenital sinus. There are two major types of errors: lateral (mostly uterine) or vertical (vaginal and hymen disorders) fusion defects, agenesis or hypoplasia and caudal defects (e.g. Mayer Rokitansky

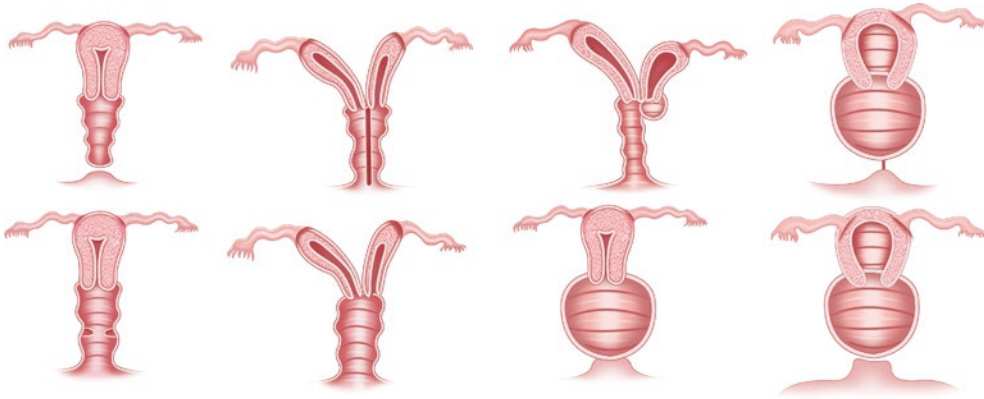


Fig. 12.27 Variations and options in vaginal anomalies. Schematic drawings illustrating some of the various vaginal anomalies with or without obstruction. (Adapted from Schweigman et al., *Female Genital Anomalies and*

Important Ovarian Conditions. In Riccabona M. (ed) *Pediatric Urogenital Radiology*, 3rd edition. Springer 2019)

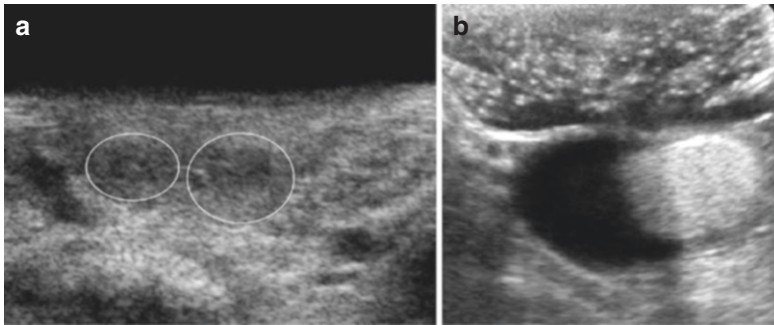


Fig. 12.28 Neonatal uterus and vaginal duplication on ultrasound. (a) Two uterine horns are depicted behind the sufficiently filled urinary bladder (circles) on an axial US view of the lower pelvis. (b) US-genitography in a duplex vagina, axial view lower pelvis: echogenic UCA instilled via a small tube outlines the contrast-filled right-sided







vagina, whereas the second vagina to the left (patient right side) remains filled with anechoic fluid indicating that there is no connection between these two structures. Note the echoes in the urinary bladder residual after the initial ce-VUS (the UCA starts to dissolve)

Küster Hauser Syndrome) as well as combined malformations (also involving the urinary tract or anorectal malformations) (Figs. 12.27 and 12.28). For understanding these anomalies, some knowledge about embryology is helpful (see Fig. 12.1), for classification of particularly uterine variations, the system of the American Society of Reproductive Medicine is commonly used (Table 12.4).

There is another group of newborns where genital imaging is always requested—the group of disorders in sexual development (DSD), mostly based on the clinical suspicion (ambiguous genitalia, syndromes, and complex

malformations), sometimes as an incidental finding. It is defined as a congenital condition in which of chromosomal, gonadal, or anatomical gender is atypical. To discuss all these entities is beyond the scope of this chapter, however, this is a very important and very sensitive issue and needs to be addressed; to account for this the old terms such “intersex” have been changed to a new nomenclature (Table 12.5)! Note that not all entities have ambiguous external genitalia (e.g. Turner syndrome or Klinefelter syndrome). What is the aim of assessment? To determine sex and anatomy, to detect malformations that may lead to

Table 12.4 Classification of Müllerian duct anomalies

Class I	Vaginal/cervical, fundal, combined, or tubal Müllerian agenesis/hypoplasia	
Class II	Variation of unicornuate uterus (communicating, non-communicating, no cavity, no horn)	
Class III	Uterus didelphis	
Class IV	Variation of bicornuate uterus (complete versus incomplete/partial)	
Class V	Septate uterus (complete, partial)	
Class VI	Arcuate uterus	

List of Mullerian duct anomalies with schematic drawings illustrating some of the various uterine—oriented towards the American Society of Reproductive Medicine most recent proposal (adapted from Schweigman et al., Female Genital Anomalies and Important Ovarian Conditions. In Riccabona M. (ed) Pediatric Urogenital Radiology, 3rd edition. Springer 2019)

Table 12.5 Classification of DSD (according to Hughes IA et al. Arch Dis. Child 2006; 91:554–563)

Old terminology	New terminology
Intersex	Disorder of sex development (DSD)
Male pseudohermaphrodite Undervirilisation of XY male	46,XY DSD
Female pseudohermaphrodite Overvirilisation of XX female	46,XX DSD
True hermaphrodite	Ovotesticular DSD
XX male or XX sex reversal	46,XX testicular DSD
XY sex reversal	46,XY complete gonadal dysgenesis

medical problems or as part of the workup of syndromes, to prevent future medical or surgical problems, and to lay the base for a developing and establishing a long-term plan. And for this, in addition to genetic testing and hormonal evaluation, early imaging plays a major role. And therefore, imaging aims at identifying gonadal (testis? ovaries, ovotestis? streak gonads?) (Fig. 12.29) and genital (uterine and vaginal malformations) structures, to classify them, to assess potentially associated findings such as adrenal gland hyperplasia, and to evaluate for potentially associated malformations particularly of the urinary tract. It is primarily and in neonates practically uniquely performed by US of the inner and outer genital structures

and the entire urinary tract using high-resolution (linear) transducers and also entertaining a perineal approach. It can be completed by US-genitography after filling bladder and vagina possibly also using UCA (Fig. 12.30). Fluoroscopic genitography may become necessary in some instances, but often this is only performed after the neonatal age or before surgery if necessary. Note that this poses a considerable radiation burden and thus the fluoroscopy technique is of utmost importance. The technique includes low concentration contrast agent drip, pulsed fluoroscopy with low pulse rates, last-image-hold and only carefully selected exposures (Fig. 12.31). MRI is also usually performed only after the neonatal age,

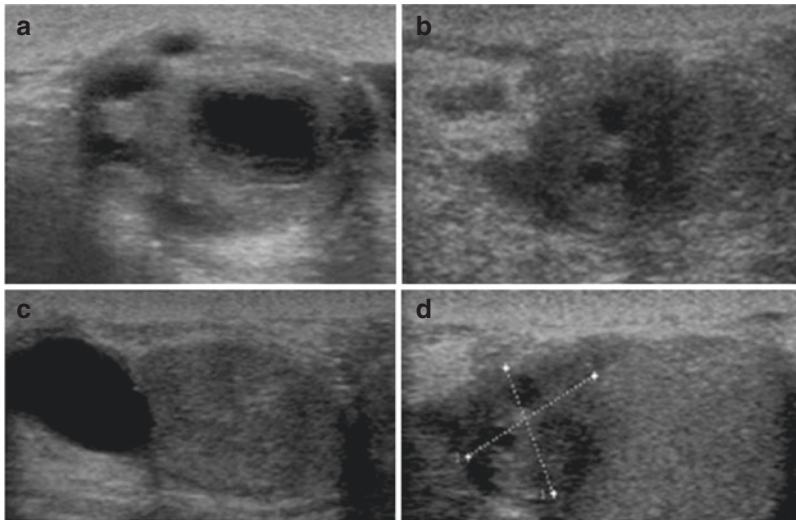


Fig. 12.29 Streak gonads/ovotestis. For different US different examples of ovotestis (as confirmed by histology) showing either a parenchyma that looks like a testicle with follicle-like cysts (**a**, **b**), or cystic component(s) adjacent to a gonad which looks like a testicle (**c**, **d**, +...+).

(Courtesy of C. Asavaoia, Cluj-Napoka, Romania). These—just like small undifferentiated streak gonads—can be found anywhere in the pelvis, the scrotum, the labia, or the inguinal canal

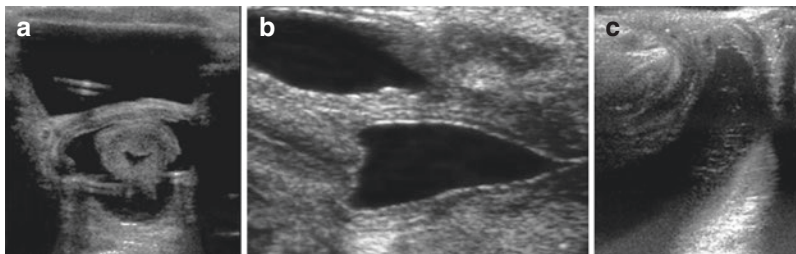


Fig. 12.30 Perineal ultrasound for vaginal queries after vaginal filling (“Sonogenitography”). (**a**) Sonogenitography: the vagina (and preferably also the urinary bladder, to grant access to the inner genitalia) is filled with a NaCl drip infusion via small catheters (visible in the bladder and the vagina); thus, the slightly fluid

filled cervix is seen in this transabdominal axial view of the lower pelvis. (**b**) Sagittal transabdominal view of the cervix outlined by the saline-filled vagina (can also be seen similarly in urethro-vaginal reflux). (**c**) Perineal view—the urethra, the filled vagina and the anal canal can be identified

e.g. in complex malformations or if US is equivocal. If neuroimaging is needed, MRI of the pelvis can be added. As this is a rare and difficult but immensely important task, these investigations are often performed in dedicated centres, and recommendations on how to perform these studies as well as on imaging algorithms exist (e.g. by the ESPR abdominal imaging task force).

A particular scenario which may pose an urgent query in a neonate is a hymen or vaginal

atresia with *hydrometrocolpos*, possibly associated with urinary tract malformations (e.g. MCDK) and uterine as well as vaginal duplications. The hugely enlarged vagina is seen as a cyst- or bladder-like structure filled with usually complex fluid; the level of the atresia/obstruction can be seen best perineally (Fig. 12.32). The uterus can be involved too, although this may more commonly be seen in pubertal girls. The other common neonatal and possibly acutely deteriorating situation is congenital

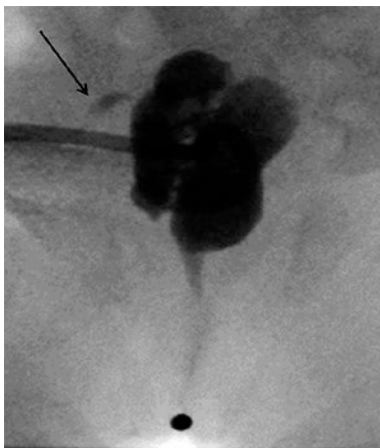


Fig. 12.31 Fluoroscopic genitography. Last-image hold picture during fluoroscopic genitography outlining a vertical septum differentiating the two contrast-filled vaginas. The contrast was originally instilled into the urinary bladder via suprapubic catheter in a neonatal girl with cloacal malformation—after voiding the contrast remained in the two vaginal cavities. The metallic marker defines the single external orifice. Also note some subtle contrast in the right ovarian tube (arrow). (Courtesy of LS. Ordning-Müller, Oslo, Norway)

adrenal hyperplasia, which is an autosomal recessive disorder causing cortisol deficiency and hyperstimulation of the adrenal gland with salt-losing symptoms as well as genital virilisation or anomalies by excessive androgen synthesis of variable degree (e.g. enlarged clitoris, urogenital sinus ...) (Fig. 12.33).

12.8.3 Ovarian Torsion in the Neonate

Ovarian torsion results from partial or complete twisting of the ovarian pedicle on its axis, and can happen even antenatally or neonatally. Symptoms are not always present or they may present as unspecific symptoms such as fever, vomiting, leukocytosis, or irritability. Initially there is a compromised lymphatic drainage causing ovarian swelling, followed by venous obstruction and haemorrhagic infarction. Eventually also the arterial blood supply is

Fig. 12.32 Hydrometrocolpos. Sagittal (a) and axial (b) transabdominal view showing a dilated vagina with clot and debris; note the relatively thick wall, particularly of the dilated fluid filled cervix

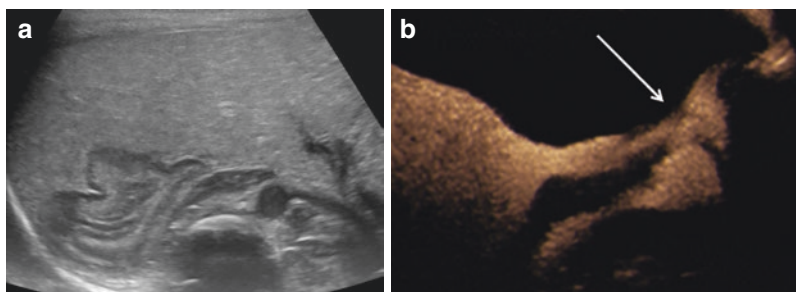
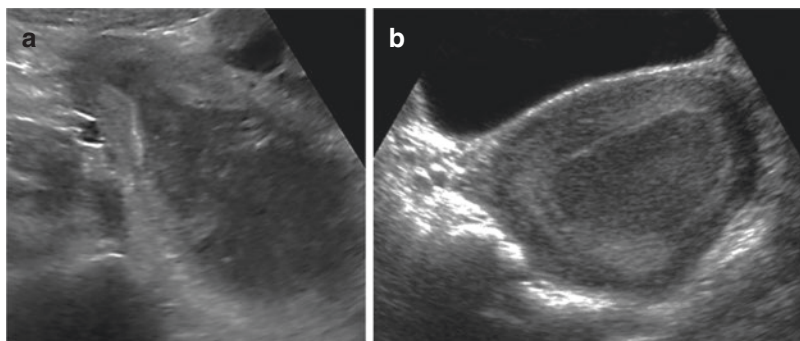


Fig. 12.33 Adreno-genital syndrome/congenital adrenal hyperplasia. (a) Cerebelliform configuration of the enlarged adrenal gland as typically seen in congenital adrenal hyperplasia. (b) US-genitography/ce-VUS depicts

a distal urogenital sinus tract (arrow) with a single common orifice of the urethra and vagina during voiding (sagittal section transabdominal/trans-symphyseal view)

interrupted resulting in necrosis, possibly gangrene or infection, with the risk of peritonitis and subsequent sequelae.

Imaging is indicated in every girl with unspecific and not-defined abdominal pain and tenderness and is achieved by urgent US, as this is an emergency condition that threatens the ovary and fertility. It will show a hugely enlarged, usually hyperechogenic ovary. The homogeneity and echogenicity depend on the duration and possible necrosis as well as potential underlying predisposing conditions, e.g. a large or haemorrhagic cyst or cystic teratoma. There may be partial or intermittent torsion. Typically, multiple peripheral small follicles with blood-fluid layers as a consequence of the haemorrhagic infarction can be seen on a meticulous study with high-resolution transducers. Another very specific finding is the “whirl-pool” or “target” sign of the vascular pedicle similar as in intestinal volvulus, but is seen not so frequently in part because of the restricted accessibility of the respective region. Doppler is less useful in the ovaries and particularly in neonates, as it may be difficult to find blood flow even in a normal ovary, and a maintained blood flow does not rule out (intermittent/partial) torsion due to the dual blood supply of the ovary. Thus, in every suspicion, an urgent laparoscopy may become indicated to save the ovary, as early untwisting and detorsion leads often to a successful reperfusion.

12.8.4 Tumours of the Neonatal Female Genital Tract

Neonatal or even congenital tumours of the female genitalia exist, though rare, as most mass lesion of the neonatal ovary are ovarian cysts. Neonatal ovarian masses are most often serous cyst adenomas and more infrequently germ cell tumours and teratomas. If a mass is seen in the vagina or uterus and the pelvic floor, rhabdomyosarcoma and neurofibroma should be considered. US is helpful in detecting those tumours, MRI can help with narrowing down the differential diagnosis by observing tissue specific signal behaviour, but eventually histology will define

the diagnosis; even tumour markers and biochemistry may be undecisive.



Female genital tract imaging is in neonates achieved mostly by US, whichever condition—malformations and variations, torsion, or tumours. Knowledge of embryology is essential for understanding sexual anomalies and proper assessment, as well as knowledge of the normal US appearance of the neonatal uterus and the ovaries. Doppler US is less valuable in the neonatal female genitalia, even in suspected torsion.

12.9 Problems in the Male Neonatal Genitalia

When parents see some abnormalities of the outer genitalia this often is a major concern—may it be a small scrotum, and unusual size or shape of the penis, a dislocated external urethral orifice, or when observing a micturition. There are a number of abnormalities, which usually do not pose a major or urgent query in neonates; however, some need urgent attention such as neonatal testicular torsion or urethral pathology with bladder outlet obstruction and UTI.

12.9.1 Penis and Urethra Pathology

- *Micro- or macro-penis* is seen easily on clinical inspection—further imaging aims at assuring a normal urethra and the absence of other genital anomalies, other variations of sexual development or hormonal (or even genetic) disturbances. Mainstay of imaging is US and VCUG or urethrography (in specific rare queries such as urethral duplication or fistulae).

Other penile anomalies such as phimosis, paraphimosis, and inconspicuous penis are diagnosed clinically and need no imaging except for assessment of the hypothalamic–

pituitary axis by MRI (usually a question later in childhood).

- **Aphallia** and an entrapped penis or penile duplications are extremely rare, and may need US and MRI for confirmation (absence of corpora cavernosa and corpus spongiosum), classification and further detailed assessment—particularly of the then often associated other (UGT and spinal) malformations such as a bladder duplication in penis duplication.
- The most common finding is **hypospadias** in itself particularly in mild forms not an urgency; only severe forms need correction and then usually also delayed until after the neonatal age. It is a malformation of the penis and the urethra, which is too short and incomplete and causes voiding disturbance; it may be associated with a meatal stenosis or a penis curvatum, and with an undescended testis.

As there is no strong correlation with other genitourinary anomalies, no standard US screening of the urogenital tract is recommended by most guidelines, however, for parental reassurance one may think of doing such a scan.

- **Epispadias** is even rarer and describes a urethral meatus on the dorsum of the penis; three types are known: balanitis, penile, and peno-pubic. There is also a female sub-symphyseal type with a split bifid clitoris and abnormally separated labia. As there is a strong association with VUR due to lateralisation of the ostia and an abnormal bladder trigone, some sort of VUR-test is recommended, as well as an US of the entire UGT. A radiograph of the pelvis is taken to assess for skeletal anomalies.
- **Neonatal priapism** may occur during the first few days of life and can persist for 2–10 days. It is a very different condition compared to adults and it is a relatively benign phenomenon. Reasons can be polycythaemia, blood transfusion, drugs, and recently described hypothermia. Besides laboratory workup, US with an attempt of Doppler US to differentiate ischaemic from non-ischaemic high-flow subtypes can be performed; however, in neo-

nates US and CDS usually are normal, and management consist of careful observation till resolution.

12.9.2 Scrotal and Testicular Pathology

- **Scrotal anomalies** exist, though rare—such as penoscrotal transposition, ectopic or accessory scrotum, bifid scrotum, scrotal hypoplasia, or scrotal agenesis. This condition however does not imply the need for imaging except for assessment of associated urogenital malformations and assurance of a present functioning testis.

There are a few relevant entities; the most common is an *undescended or mobile testis and cryptorchidism*. This per se is in a neonate not a matter of real concern unless there are other stigmata indicating a more complex genital malformation, or it is a bilateral undescended testis.

The need for imaging which primarily consists of US using high-resolution linear probes is under discussion. If US is performed, it may show the testicle often next to the entrance or in the inguinal canal (Fig. 12.34)—any other position is possible, even splenogonadal fusion or a testicle close to the kidney may be seen.

In bilateral undescended testicles, a search for intra-abdominal testes or other genital

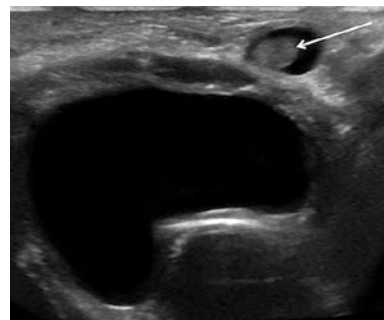


Fig. 12.34 Ultrasound in cryptorchism/undescended testis. Axial view of the urinary bladder—the small left testicle (arrow) is seen at the entrance to the inguinal canal surrounded by some fluid (funiculocoele or abdominal ascites in the inguinal canal)

anomalies may be considered; MRI is not recommended for this query in neonates.

Note that US tends to misjudge the location of the testis, as with activating the cremasteric reflex during the investigation the testis is even pulled up higher into the abdominal cavity. If a testicle is undescended, it may be small and hypodysplastic, then difficult to clearly differentiate from other nodes.

- The other important entity is **testicular torsion**; though rare, it happens in neonates too and is considered an emergency, even if most of the time it is an old intrauterine torsion where the testicular tissue cannot be rescued. Nevertheless, particularly in bilateral or acute fresh symptoms US is often performed and recommended as an option in some recommendations and imaging algorithms.

Ultrasound in these cases will reveal a small hypoechoic testicular remnant with calcification and lack of perfusion. Perinatal torsion may occur during birth—this type of torsion is extravaginal and has a poor salvage rate. Scrotal US will show an enlarged testicle with altered, asymmetric intra-parenchymal perfusion and varying echogenicity (depending on duration and degree of torsion) (Fig. 12.35). Early postnatal torsion will show the same US appearance. However, the usefulness of US in a definite clinical suspicion is doubtful, as no delay in surgical exploration (and treatment) should be caused, particularly in bilateral torsion.

Torsion of the testicular appendages is rare in neonates and usually occurs in pre-pubertal boys, but an important differential diagnosis with a similar clinical appearance. On US the torsed swollen para-testicular structure may exhibit any echogenicity and will cause a reactive hydrocele and reactive inflammatory hyperaemia of the testis and epididymis.

- **Malformation of the testis** include *multiple testicles* or agenesis of a testis. Furthermore, there is the rare *cystic dysplasia of the rete testis*, and *adreno-gonadal fusion/adrenal rest* in the testis, which should not be confused with a testicular tumour.
- **Epididymitis and orchitis** are extremely rare in neonates—the imaging features are the same as in older children; however, (a)CDS may be cumbersome in these small patients and thus one may not be able to depict intratesticular arterial flow even in a healthy testicle.
- **Hydroceles** are quite common and a small amount of fluid is considered nearly physiologic in newborns, particularly preterm.

Usually no imaging is needed, as the clinical exam with a transluminescent scrotum is diagnostic and the condition will resolve spontaneously within the first year of life. In unclear situations or if they are large, US is performed and one will see the uncomplicated fluid in the scrotum (possibly also in the inguinal canal then called *funiculocele*). Mostly they are picked up during an exam for other

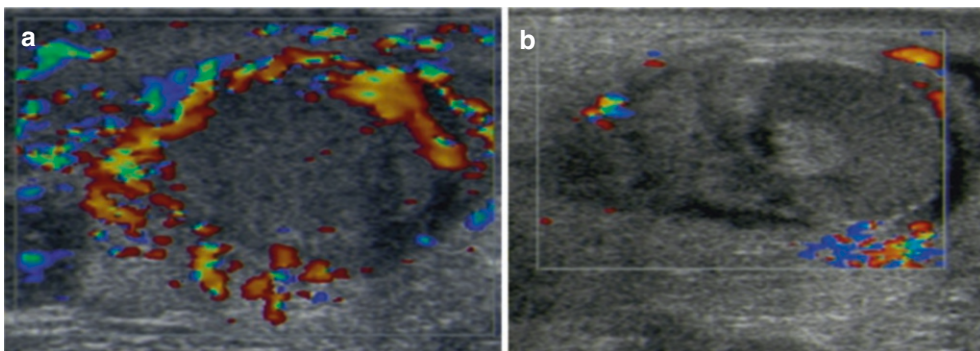


Fig. 12.35 Neonatal testicular torsion. (a) A 2-week-old baby boy without intratesticular perfusion on CDS of the asymmetrically swollen testis with slightly inhomogeneous echogenicity as the torsion was sub-acute. (b) Old

torsion in a neonate with very inhomogeneous non-perfused testicle due to a prenatal torsion; there also is some hydrocele and beginning central calcification or residual haemorrhage of/into the necrotic tissue

reasons (see Fig. 12.4). If the fluid contains echoes and thus appears “complicated”, other causes such as infection or haemorrhage must be considered.

Note that a huge hydrocele (or a large, possibly incarcerated) inguinal hernia can cause impairment of blood supply to the testicles, which can happen also postoperatively by a large haematoma.

A specific entity is *meconium periorchitis*—the sterile inflammation is caused by meconium from an (intrauterine) perforation with meconium peritonitis, where small stippled or clot like calcifications can be seen around the testis within the sometimes slightly complicated hydrocele—sometimes only as remnants of former episodes without any need for acute intervention.

- A rare entity is the *cystic dysplasia of the rete testis*; this should not be confused with a tumour or a lymphatic/vascular malformation.
- **Testicular masses** are rare, but exist; mostly these are benign and cysts, teratomas, haemangiomas or vascular malformations, and

other germ cell tumours, juvenile granulosa cell tumour being the most frequent.

Imaging consists of US and shows a possibly partially cystic mass, with possibly some regional perfusion alteration (Fig. 12.36). Ultrasound is unspecific in terms of defining the entity; however, if after a biopsy a watchful waiting strategy is entertained as the only therapy approach, a standardised measurement and volumetry is important—though sometimes the repeatable measurement planes are difficult to define. MRI is only indicated for staging in malignant tumours usually occurring beyond the neonatal age.

Testicular *microlithiasis*, though sometimes associated with tumours is no issue in neonates.

12.9.3 Anomalies of the Inner Male Genitalia

Practically the only relevant condition is the *cystic dysplasia of the seminal vesicles*; sometimes an ectopic ureter may drain into these vesicles,

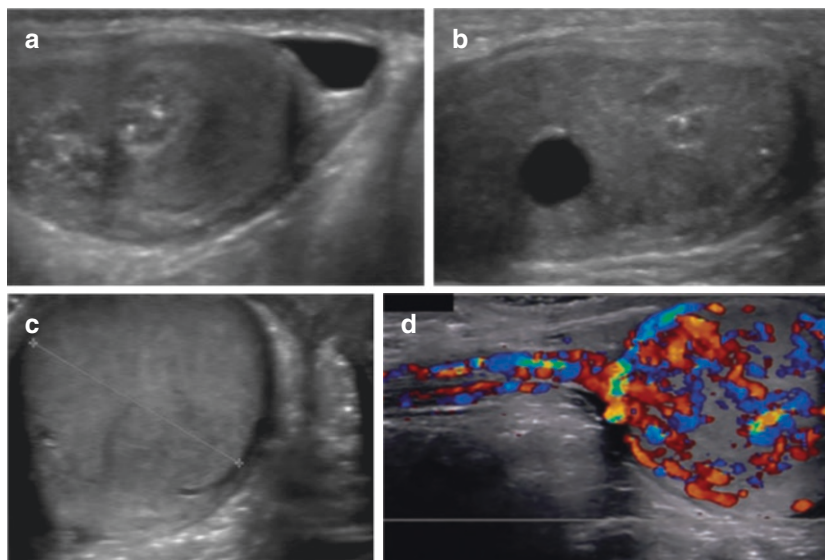



Fig. 12.36 Ultrasound of neonatal testicular masses. (a, b) Scrotal US depicts a multicentric intratesticular mass (a), which turned out to be a granulosa cell tumour; over time it developed a cystic component during the watch and wait surveillance (b), which would make differentia-

tion against a partially cystic teratoma difficult. (c, d) Large neonatal testicular tumour (+...+, c) with vivid hypervascularity and normal course of the supplying vessels on CDS (d)

too. Note that as in females, these malformations are usually associated with other urinary tract malformation and thus a full and detailed study of the entire urinary tract is important. Rarely an ectopic ureteral insertion into the seminal vesicle may be observed mimicking such a cystic dysplasia, as the urine filled seminal vesicle may appear cyst-like and enlarged, but then usually associated with a severely hypoplastic and poorly- or non-functioning corresponding kidney.

 Male genital tract imaging in neonates achieved by US, whichever condition—the most common queries are mostly cryptorchism, torsion, or tumours. Doppler US is helpful both in torsion and in tumour conditions provided that the respective US equipment is capable of detecting intratesticular parenchymal vessels (check in the contralateral normal testis first).

12.10 Neonatal Urogenital Tumours

There are a few even congenital tumours one may encounter the neonatal UGT. The most common tumour is neuroblastoma, the most common neonatal renal tumour is mesoblastic nephroma also called Bolande's tumour (although also in neonates Wilms' tumour do occur). Renal metastasis

and UGT carcinoma practically do not exist in neonates, but there are exceptions—I encountered even a very aggressive neonatal adrenal carcinoma. Nephroblastomatosis is hardly ever seen (or just not recognised, due to restriction of imaging in detecting those in this age possibly very small remnants of embryonic renal tissue) in neonates.

Even in the genital tract, there are neonatal tumours such as teratoma and germ cell tumours (see above).

In the bladder (and the vagina or prostate and the pelvic floor) rhabdomyosarcoma may occur—although typically these manifest later in infancy or childhood.

And of course, there can be involvement in systemic (haematologic) diseases such as leukaemia.

Other neonatally rare benign tumours are hamartoma, ossifying renal tumour of infancy, multilocular cystic nephroma, teratoma, and angiomyolipoma (e.g. in tuberous sclerosis)—though usually these as well as neurofibroma manifest later in infancy.

The initial imaging is by US; for workup, defining extent and staging MRI is used—particularly if a malignant tumour is suspected. US findings are less specific than the age defined tumour probability—e.g. in older children most renal tumours are Wilms' tumour, whereas in neonates typically the benign *mesoblastic nephroma* occurs, even if cystic neonatal Wilms' tumour exists too (Fig. 12.37).

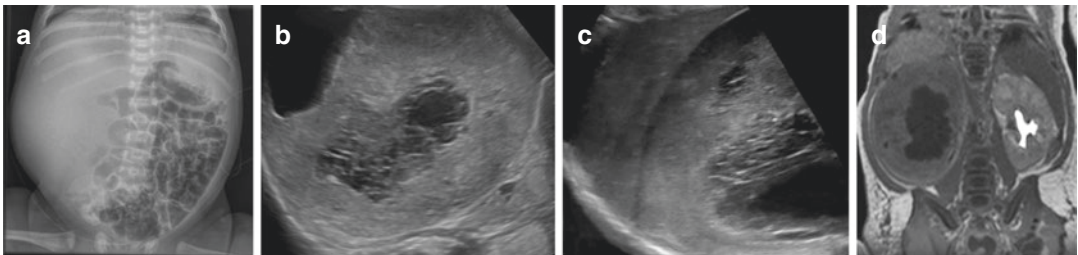


Fig. 12.37 Mesoblastic nephroma. (a) A neonate had an impressively extended abdomen—the radiograph showed a soft tissue mass on the right side. (b, c) US then depicted a centrally multicystic intrarenal mass (b), with peripheral rim-like residual renal parenchyma best visible using a high-resolution linear high frequency transducer (c). (d)

The preoperative MRI (coronal view, T1-weighted gadolinium enhanced MRU image) confirmed the findings, also showing no contrast excretion into the cystic tumour components of this mesoblastic nephroma. Note that imaging cannot differentiate particularly such a complex mass from a neonatal Wilms' tumour

For differential diagnosis of renal tumours, the typical entities such a lobar nephronia or a granulomatous pyelonephritis are very uncommon in neonates; sometimes malformations with an atypical parenchymal bridge or a complex-cystic mass may pose a problem such as a segmental MCDK. If very large, differentiation against a neuroblastoma may be challenging, as not all neuroblastoma exhibit calcifications, whereas Wilms' tumour may also have calcifications—this is discussed in the respective chapter. In the bladder (and urethra), fibromatous polyps may mimic a malignant tumour. In the testis, ectopic adrenal tissue rests (adreno-gonadal fusion) may be mistaken for a tumour, or a vascular malformation or a congenital dysplasia of the rete testis may be confusing.

One entity that needs to be mentioned in this age group—though not strictly a urogenital tumour—is a *pre-sacral mass*, particularly teratomas, which are the most common solid tumour in neonates. These mostly non-familial lesions occur more frequently in girls, and are classified according to the amount of intrapelvic or extrapelvic involvement. They are attached to the sacrum and/or coccyges and may have solid internal components.

Often they are congenital and detected on prenatal imaging (US and MRI); postnatally, one may try US. But usually preoperatively the best assessment of its entire anatomy and internal components is achieved by MRI—in particular using coronal and sagittal sequences. This will also help in differentiating these masses from an anterior sacral meningocele or neuroenteric cyst, or the rarer neuroblastoma or ganglioneuroma.



Tumours of the neonatal urogenital tract are very rare; mostly besides some benign tumours it is mesoblastic nephroma. Ultrasound will usually suffice for diagnosis, and—as it is a benign condition—no other imaging is required, except there are doubts and thus additional information and staging is needed.

12.11 The Neonatal Adrenal Gland

There are three major entities that need to be considered in the neonatal adrenal gland: variation in size and shape, adrenal gland haemorrhage, and neuroblastoma.

One also needs to know that the adrenal gland in newborn looks quite different and impressively large (length 10–12 mm), with a typical appearance of an outer hypoechoic rim and a smaller central hyperechoic band (Fig. 12.38). This is in part due to the physiological different activity of the cortex and the medulla which is prominent in neonates.

12.11.1 Variations in Size and Shape of the Adrenal Gland

Typically, the adrenal gland has a Y- or V-shape riding on top of the kidney, but there are variations such fused or horseshoe glands and more. The most common alteration in shape is if associated with a missing or ectopic kidney—then it appears stretched and band-like (Fig. 12.38). Furthermore, there may be hypoplasia or aplasia, associated with severe hormonal deficits if bilateral. Hypertrophy or hyperplasia is difficult to define sonographically, usually only achievable in combination with clinical symptoms or syndromes (such as congenital adrenal hyperplasia = adreno-genital syndrome) and hormonal findings; a hint towards the diagnosis may be a cerebriiform shape and contour of the large gland. Dysontogenetic cysts exist, too.

12.11.2 Adrenal Gland Haemorrhage

Neonatal haemorrhage of the adrenal gland occurs typically after asphyxia or birth trauma, but also with septicaemia and some systemic conditions. It may occur already foetally and can be bilateral too. Usually these bleeds are quite large and thus cause displacement of surrounding structures—particularly the kidney with the risk of impaired renal venous drainage and renal vein thrombosis.

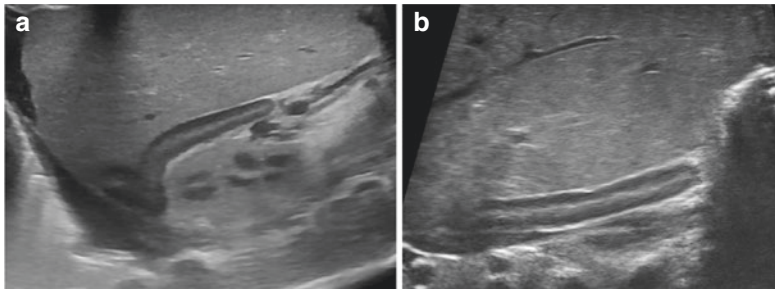


Fig. 12.38 Normal neonatal adrenal gland and its variations. (a) Sagittal/coronal flank view slightly oblique oriented through the liver shows the normal prominent neonatal adrenal gland sitting on top of the right kidney.

(b) Unusual shape of the band-like adrenal gland in a neonate with an ectopic kidney in the pelvis (instead of the normal kidney position, thus explaining the unusual shape of this adrenal gland)

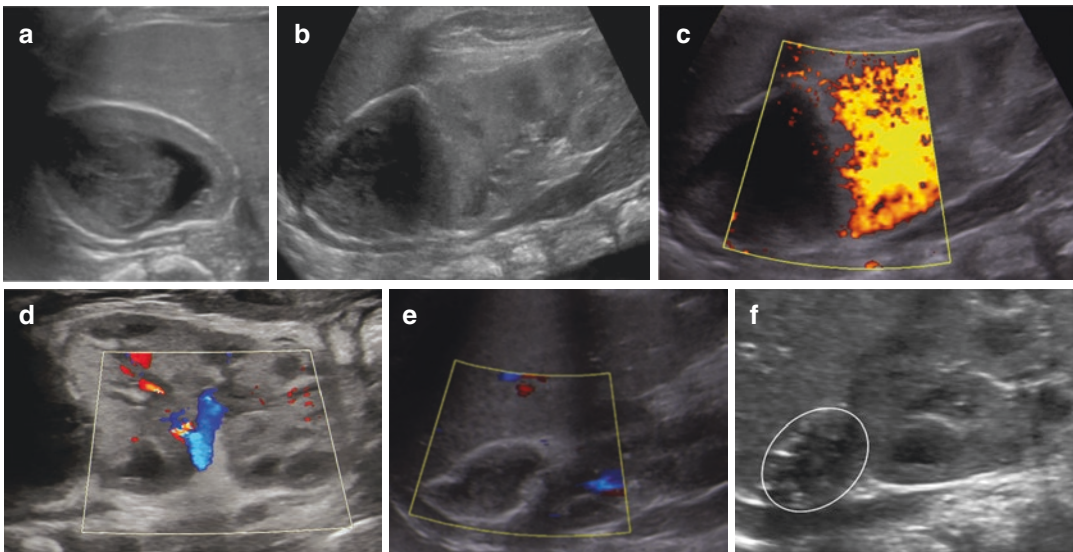


Fig. 12.39 Adrenal gland haemorrhage. (a, b) US (axial view right upper abdomen) shows a complex fluid filled mass on top of the right kidney in a neonate, impressing the upper pole of the displaced, but otherwise normal kidney (b). (c, d) Power and Colour Doppler was performed to assure unimpaired renal perfusion, particularly there

was no sign for a renal vein thrombosis. (e) Over time the “complex” fluid developed a clot like aspect and shrunk, no central vascularity was depictable on CDS also in this stage. (f) Eventually only small residual changes and some minor calcifications were left (circle)

Imaging is done by US—no other imaging is helpful. In the hyper-acute stage, one will see a relatively hyperechoic enlarged gland which very soon turns into a less echogenic complex-cystic mass. Over time the clot organises and eventually is resolved, often showing calcifications as a remnant of an old adrenal gland haemorrhage (Fig. 12.39). Note that every exam should include a CDS of the ipsilateral adjacent kidney to assess for a potentially associated renal vein thrombosis.

For differential diagnosis, one has to consider a haemorrhaged neuroblastoma although rare it is indistinguishable on imaging. A haemorrhagic cyst (extremely rare), or a complex haemorrhagic or infected renal cyst, sometimes even a huge dilated upper moiety of a duplex kidney with internal echoes may be also challenging to differentiate from adrenal haemorrhage if large. Follow-up is essential in these situations to monitor the further development and evolution, particularly as it always is the

worry of these patients' parents and physicians. In the initial (or even prenatal) examination, the size and the presence of solid portions or septations do not allow for a clear differentiation between the two groups of cystic adrenal lesions. However, tiny calcifications and flow signals on CDS favour a neuroblastoma. And on US follow-up, the cystic neuroblastomas become more complex solid and cystic masses and usually do not disappear, whereas haemorrhagic cysts either disappear completely or evolve to calcified remnants. And even if it is a neonatal neuroblastoma grade 1 which spontaneously regresses this would not impact further management. Nevertheless—if any doubt, besides biochemical testing for tumour markers and an MRI should be initiated.

12.11.3 Neuroblastoma and Related Issues

The most common tumour of the adrenal gland in infants is neuroblastoma which may exist already neonatally or even prenatally, whereas adenoma

or pheochromocytoma is a rarity in neonates, also adrenal gland carcinoma—although they exist. Low-grade tumours may spontaneously regress, particularly if small. Neuroblastoma and ganglioneuro(blasto)ma, occurring at any location of the neurogenic crest and the paravertebral ganglia, are nearly always associated with elevated catecholamines in urine.

Imaging starts usually with US, complemented by MRI (for staging and detailed anatomic assessment) and chest films, CT (for pulmonary metastasis), and I^{123} MIBG nuclear medicine scans (radioactive iodine labelled metaiodobenzylguanidine). There are no specific US features that allow differentiation from other tumours, except one depicts invasion into the spinal canal through the neuroforamina. Stippled calcifications are typically present in the sometimes inhomogeneous low-echogenicity mass with relatively sharp borders, but there are atypical tumours without calcifications, or with haemorrhage or necrosis (Fig. 12.40). If these tumours are very large, they may pose a challenge to differentiate it from exophytic renal or hepatic masses.

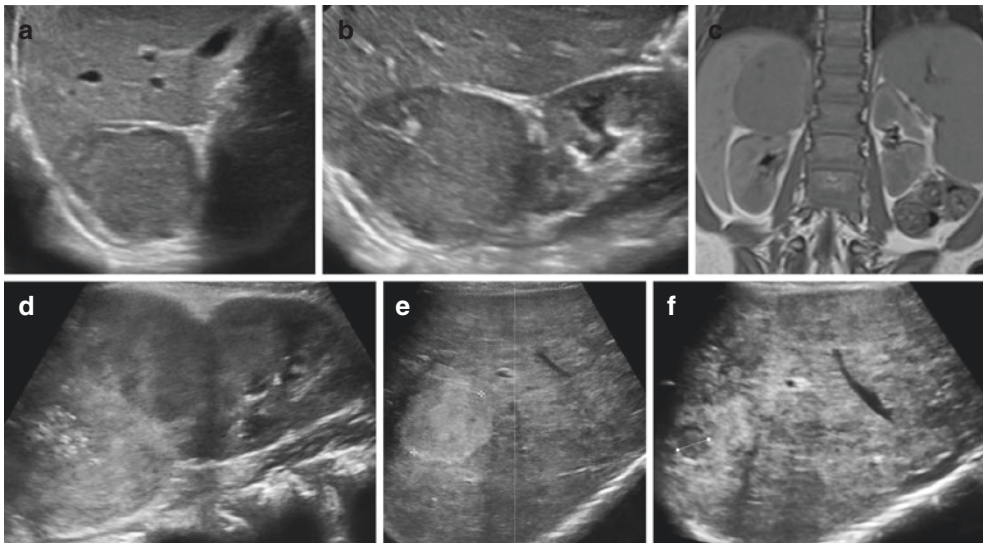


Fig. 12.40 Neonatal neuroblastoma. (a, b) These US images show a 3-week-old neonate with a mass in the adrenal gland location (a), with a small calcification (b)—no metastasis was found and the tumour markers were indicative of a neuroblastoma (in this age in this setting a watch and wait surveillance was decided). (c) The respective coronal image of the MRI study which was performed

for staging. (d–f) There is a congenital adrenal tumour with stippled calcification but a somewhat inhomogeneous echotexture in a coronal/sagittal view (d)—also confirmed to be a neuroblastoma, but with obvious liver metastasis (++); some were echogenic (e), most of them hypoechoic (f). Complete workup including bone marrow analysis made this a stage Ms (old term IVs)

Besides depicting the tumour and describing its extent staging using the International Neuroblastoma Risk Group Staging System (INRGSS) criteria (Table 12.6) using imaging defined risk factors (Table 12.7) is essential. As local lymph nodes as well as the liver may be involved a thorough investigation of all these

areas is mandatory. Note there is a specific neonatal form called stage MS (former name “4s”) which is often a small primary tumour with metastasis confined to skin, liver, and/or bone marrow—this as well as some neonatal stage L1 tumours may regress spontaneously and thus are treated only by active surveillance. Of course, biochemistry with tumour markers (e.g. ferritin, vanillylmandelic acid, homovanillic acid, neurone-specific enolase, or lactate dehydrogenase) is also essential for diagnosis, differential diagnosis, and tumour monitoring.

Table 12.6 INRGSS definition (Monclair T, Brodeur GM, Ambros PF, Brisse H, Cecchetto G, Holmes K, Kaneko M, London WB, Matthay KK, Nuchtern JG, von Schweinitz D, Cohn SL, and Pearson ADJ for the INRG Task Force. The International Neuroblastoma Risk Group (INRG) Staging System. *J. Clin. Oncol.*, 27:298–303, 2009)

Stage L1	Locoregional tumour without IDRFs
Stage L2	Locoregional tumour with one or more IDRFs
Stage M	Distant metastatic disease (except Ms)
Stage Ms	INRG Stage L1 or L2, with metastatic disease confined to skin and/or liver and/or bone marrow

Note that neither the midline nor the lymph node status is included in the staging criteria. However, stage MS is only applicable in infants less than 18 months of age


 The normal neonatal adrenal gland is—unlike in older children and adults—nicely visible on US. The most common conditions one can encounter are adrenal gland haemorrhage (imaged sufficiently by US) and neuroblastoma (where an additional MRI, possibly also a CT and scintigraphy is recommended).

Table 12.7 Imaging defined risk factors (Monclair T, Brodeur GM, Ambros PF, Brisse H, Cecchetto G, Holmes K, Kaneko M, London WB, Matthay KK, Nuchtern JG, von Schweinitz D, Cohn SL, and Pearson ADJ for the INRG Task Force. The International Neuroblastoma Risk Group (INRG) Staging System. *J. Clin. Oncol.*, 27:298–303, 2009)

Ipsilateral extension within 2 compartments	Neck-chest, chest-abdomen, abdomen-pelvis
Neck	Tumour encasing carotid and/or vertebral artery and/or jugular vein Extending to skull base Compressing trachea
Cervico-thoracic junction	Tumour encasing brachial plexus roots Encasing subclavian vessels and/or vertebral and/or carotid artery Compressing trachea
Thorax	Tumour encasing aorta and/or major branches Compressing trachea and/or principal bronchi Lower mediastinal tumour Infiltrating the costovertebral junction between T9 and T12
Thoraco-abdominal	Tumour encasing aorta and/or vena cava
Abdomen and pelvis	Tumour infiltrating porta hepatis and/or hepatoduodenal ligament Encasing branches of superior mesenteric artery at mesenteric root Encasing origin of coeliac axis and/or superior mesenteric artery Invading one or both renal pedicles Encasing aorta and/or vena cava or iliac vessels Pelvic tumour crossing sciatic notch
Infiltration of adjacent organs or structures	Pericardium, diaphragm, kidney, liver, duodeno-pancreatic block and mesentery

Note that there are other aspects that need to be recorded but are not considered risk factors such as multifocal primary tumours, intraspinal tumour with or without symptoms, and pleural effusion or ascites

12.12 Summary

Imaging of the urogenital tract is one of the most common indications for imaging in neonates. To a large extent, this is due to foetal screening for urinary tract dilatation which frequently depicts pelvicalyceal dilatation, indicating postnatal assessment and follow-up. Only a few of these patients have underlying conditions that need urgent treatment in the neonatal period such as PUV or severe (bilateral) PUJO or high-grade VUR. Other neonatal conditions which need prompt diagnosis and treatment include acute renal failure, renal vein thrombosis, neonatal UTI, neonatal/congenital urogenital tract tumours, and ovarian or testicular torsion. Ultrasound is always the first and most often the only modality needed to answer the clinical queries in suspected neonatal urogenital pathology, complemented by fluoroscopy or MRI in selected cases, whereas CT or nuclear medicine studies are rarely indicated in the neonate.

Acknowledgement I sincerely want to thank Dr. Lil-Sofie Ording-Müller from Oslo/Norway for editing and revising this chapter.

References

- Avni FE, Garel C, Cassart M, D'Haene N, Hall M, Riccabona M. Imaging and classification of congenital cystic renal diseases. *AJR Am J Roentgenol.* 2012;198:1004–13.
- Avni FE, Lerisson H, Lobo ML, Cartigny M, Napolitano M, Menzel HJ, Riccabona M, Wozniak M, Kljucsevsek D, Augdal TA, Bruno C, Ibe D, Darge D, Stafrace S, Petit P, Ording Muller LS. Disorders of sex development in neonates: plea for a standardized imaging approach: plea for a standardized imaging approach. *Pediatr Radiol.* 2019;49:1240–7.
- Chow JS, Bellah RD, Darge K, Ntoulia A, Phelps A, Riccabona M, Back SJ. Contrast-enhanced genitotomography (ceGS) and colosonography (ceCS): emerging alternatives to fluoroscopy. *Pediatr Radiol.* 2021;51:2387–95.
- Darge K, Grattan-Smith D, Riccabona M. Pediatric uroradiology: state of the art. *Pediatr Radiol.* 2011;41:82–91.
- Eo H, Kim JH, Jang KM, Yoo SY, Lim GY, Kim MJ, Kim OK. Comparison of clinico-radiological features between congenital cystic neuroblastoma and neonatal adrenal haemorrhagic pseudocyst. *Korean J Radiol.* 2012;12:52–8.
- Fernbach SK, Maizels M, Conway JJ. Ultrasound grading of hydronephrosis: Introduction to the system used by the society for fetal urology. *Pediatr Radiol.* 1993; 23: 478–80.
- Gimpel C, Avni FE, Breyssem L, Burgmaier K, Caroli A, Cetiner M, Haffner D, Hartung EA, Franke D, König J, Liebau MC, Mekahli D, Ong ACM, Pape L, Titieni A, Torra R, Winyard PDJ, Schaefer F. Imaging of kidney cysts and cystic kidney diseases in children: an International Working Group Consensus Statement. *Radiology.* 2019;290:769–82.
- Gordon I, Riccabona M. Investigating the newborn kidney – update on imaging techniques. *Semin Neonatol.* 2003;8:269–78.
- Hildebrandt F, Benzing T, Katsanis N. Ciliopathies. *N Engl J Med.* 2011;364:1533–43.
- Hugs IA, Houk C, Ahmede SFG, Lee PA. Consensus statement on management of intersex disorders. *Arch Dis Child.* 2006;91:554–63.
- Kjucsevsek D, Riccabona M, Petit P, Avni EF, Bruno C, Damasio MB, Darge K, Littooj A, Lobo ML, Mentzel JH, Napolitano M, Wozniak M, Ording Müller LS. Intracavitary contrast-enhanced Ultrasound in children: a review, with clinical applications and procedural recommendations from the ESPR Abdominal Task Force Group. *Pediatr Radiol.* 2020;50:596–606.
- Koff SA. Ureteropelvic junction obstruction: role of newer diagnostic methods. *J Urol.* 1982;5:898–901.
- Koff SA, Shore RM. Diuretic radionuclide urography. *Urol Radiol.* 1983;5:189–95.
- Koff SA. Determinants of progression and equilibrium in hydronephrosis. *Urology.* 1983;215:496–500.
- Nguyen HT, Benson CC, Bromley B, Campell JB, Chow J, et al. Multidisciplinary consensus on the classification of prenatal and postnatal urinary tract dilation (UTD classification system). *J Pediatr Urol.* 2014;10:982–98.
- Peters CA. Urinary tract obstruction in children. *J Urol.* 1995;154:1874–84.
- Pfeifer SM, Attaran M, Goldstein J, Lindheim SR, Petrozza JC, Rackow BW, Siegelman E, Troiano R, Winter T, Zuckerman A, Ramaiah SD, editors. ASRM Müllerian anomalies classification 2021. *Fertil Steril.* 2021;116:1238–52.
- Riccabona M, Ring E, Fueger G, Villits P, Petritsch P. Dopplersonography in congenital ureteropelvic junction obstruction and congenital multicystic kidney disease. *Paediatr Radiol.* 1993;23:502–5.
- Riccabona M, Sorrantin E, Fotter R. Application of functional m-mode sonography in pediatric patients. *Eur Radiol.* 1998;8:1457–61.
- Riccabona M, Simbrunner J, Ring E, Ebner F, Fotter R. Feasibility of MR-urography in neonates and infants with anomalies of the upper urinary tract. *Eur Radiol.* 2002;12:1442–50.

21. Riccabona M. Imaging of renal tumours in infancy and childhood. *Eur Radiol.* 2003;13:L116–29.
22. Riccabona M. (Acute) renal Failure in neonates, infants, and children - the role of ultrasound, with respect to other imaging options. *Ultrasound Clin.* 2006a;1:457–69.
23. Riccabona M. Imaging of the neonatal genitourinary tract. *Eur J Radiol.* 2006b;60:187–98.
24. Riccabona M, Avni FE, Blickman JG, Darge K, Dacher JN, Lobo LM, Willi U. Imaging recommendations in paediatric urology: minutes of the ESPR workgroup session on urinary tract infection, foetal hydronephrosis, urinary tract ultrasonography and voiding cysto-urethrography. ESPR-Meeting, Barcelona/Spain, June 2007. ESUR Paediatric guideline subcommittee and ESPR Paediatric Uroradiology Work Group. *Pediatr Radiol.* 2008;38:138–45.
25. Riccabona M, Avni FE, Blickman JG, Dacher JN, Darge K, Lobo ML, Willi U, (Members of the ESUR Paediatric Paediatric Recommendation Work Group and ESPR Paediatric Uroradiology Work Group). Imaging recommendations in paediatric urology, Part II: Urolithiasis and haematuria in children, paediatric obstructive uropathy, and postnatal work-up of foetally diagnosed high grade hydronephrosis. Minutes of a mini-symposium at the ESPR Annual Meeting, Edinburg, June. *Pediatr Radiol.* 2009;39:891–8.
26. Riccabona M. Obstructive diseases of the urinary tract in children: lessons from the last 15 years. *Pediatr Radiol.* 2010;40:947–55.
27. Riccabona M, Avni F, Damasio B, Ordning-Mueller LS, Lobo ML, Darge K, Papadopoulou F, Wil-li U, Blickmann J, Vivier PH. ESPR Uroradiology Task Force and ESUR Paediatric Working Group - Imaging recommendations in Paediatric Uroradiology, Part V: Childhood cystic kidney disease, childhood renal transplantation, and contrast-enhanced ultrasound in children. *Pediatr Radiol.* 2012;42:1275–83.
28. Riccabona M. Basics, principles, techniques and modern methods in paediatric ultrasonography. *Eur J Radiol.* 2014;83:1487–94.
29. Riccabona M, Lobo ML, Willi U, Avni F, Blickmann J, Damasio B, Ordning-Mueller LS, Darge K, Papadopoulou F, Vivier PH. ESPR Uroradiology Task Force and ESUR Paediatric Working Group - Imaging recommendations in Paediatric Uroradiology, Part VI: Childhood renal biopsy and imaging of neonatal and infant genital tract. *Pediatr Radiol.* 2014;44:496–502.
30. Riccabona M, Darge K, Lobo ML, Ordning-Mueller LS, Augdal TA, Avni FE, Blickman J, Damasio BM, Ntoulia A, Papadopoulou F, Vivier PH, Willi U. ESPR Uroradiology Task Force – Imaging Recommendations in Paediatric Uroradiology - Part VIII: Retrograde urethrography, imaging in disorders of sexual development, and imaging in childhood testicular torsion. Report on the mini-symposium at the ESPR Meeting in Amsterdam, June 2014. *Pediatr Radiol.* 2015;45:2023–8.
31. Riccabona M, Lobo ML, Ordning-Mueller LS, Augdal TA, Avni FE, Blickman J, Bruno C, Damasio B, Darge K, Ntoulia A, Papadopoulou F, Vivier PH. ESPR Abdominal (GU and GI) Imaging Task Force – Imaging Recommendations in Paediatric Uroradiology, Part IX: Imaging in anorectal and cloacal malformation, imaging in childhood ovarian torsion, and efforts in standardising pediatric urology terminology. Report on the mini-symposium at the ESPR Meeting in Graz, June 2015. *Pediatr Radiol.* 2017;47:1369–80.
32. Schöllnast H, Lindbichler F, Riccabona M. Ultrasound (US) of the urethra in infants: comparison US versus VCUG. *JUM.* 2004;23:769–76.
33. Sorantin E, Fötter R, Aigner R, Ring E, Riccabona M. The sonographically thickened wall of the upper urinary tract: correlation with other imaging methods. *Pediatr Radiol.* 1997;27:667–71.
34. Whitaker RH. Equivocal upper tract obstruction. In: Whitaker RH, editor. *Current perspectives in pediatric urology. Clinical practice in urology.* London: Springer; 1989. p. 61–8.
35. Whitaker RH, Buxton-Thomas MS. A comparison of pressure flow studies and renography in equivocal upper urinary tract obstruction. *J Urol* 1984;131:446–9. [https://doi.org/10.1016/s0022-5347\(17\)50442-5](https://doi.org/10.1016/s0022-5347(17)50442-5).
36. Woolf AS, Hillman KA. Unilateral renal agenesis and the congenital solitary functioning kidney: developmental, genetic and clinical perspectives. *BJU Int.* 2007;99:17–21.

Further reading

- Gimpel C, Avni FE, Breyssem L, Burgmaier K, Caroli A, Cetiner M, Haffner D, Hartung EA, Franke D, König J, Liebau MC, Mekahli D, Ong ACM, Pape L, Titieni A, Torra R, Winyard PJD, Schaefer F. Imaging of kidney cysts and cystic kidney diseases in children. An International Working Group consensus statement. *Radiology.* 2019;290:769–82.
- Riccabona M, Guest Editor. Paediatric uroradiology. Special pediatric edition. *Eur J Radiol.* 2002;43.
- Riccabona M, Guest Editor. Imaging neonates. Special pediatric edition. *Eur J Radiol.* 2006;60.
- Riccabona M. The pediatric kidney. In: Quaia E, editor. *Radiological imaging of the kidneys.* 2nd ed. Berlin: Springer; 2010. p. 675–714. ISBN 978-3-540-87596-3.
- Riccabona M. Pediatric uroradiology. In: Riccabona M, editor. *Pediatric imaging essentials.* Stuttgart, New York: Thieme; 2014. p. 163–209. ISBN 978-3-13-166191-3.

- Riccabona M. Contrast media use in pediatrics: safety issues. Chapter 17. In: Thomson HS, Webb AW, editors. Contrast media: safety issues and ESUR guidelines. 3rd ed. Berlin: Springer; 2014. p. 245–51. ISBN 978-3-642-36723-6.
- Riccabona M, Guest Editor. Pediatric ultrasound. Special pediatric edition. Eur J Radiol. 2014;83.
- Riccabona M, editor. Pediatric urogenital radiology. 3rd ed. Heidelberg: Springer; 2018. ISBN 978-3-319-3900-4
- Riccabona M. Pediatric ultrasound – requisites and applications. 2nd revised ed. Berlin: Springer; 2020. ISBN 978-3-642-39155-2



Imaging the Neonatal GI Tract, Also Including Liver, Spleen, Pancreas, Retroperitoneum and Mesentery

Maria Luisa Lobo, Samuel Stafrace,
and Michael Riccabona

13.1 Introduction

After the brain, the chest and the urogenital system, the gastrointestinal (GI) system is one of the most commonly imaged organ systems in neonates. Congenital conditions need pre- and often postoperative imaging. A number of acquired conditions occur in neonates, some of which can be life threatening, such as volvulus or necrotizing enterocolitis (NEC) and their diagnosis as well as treatment and outcome heavily relies on rapid emergent imaging.

Imaging usually consists of a combination of radiographs and ultrasound (US), complemented by fluoroscopy. An MRI may sometimes be necessary (e.g. for the liver and the biliary tract as well as for tumourous conditions). A specific aspect in imaging of the GI tract is the need of use of oral or rectal contrast agents (CA) with the respective implications from iodine absorption and potential systemic sequelae (e.g. hypothyroidism); these aspects will be addressed in a

dedicated section. Knowledge and understanding of embryology as well as foetal development and neonatal adaptation is essential when imaging the abdomen. As some conditions of the upper GI tract have an overlap with thoracic imaging (e.g. diaphragmatic hernias or oesophageal atresia), there is some overlap with Chap. 10. Some of the conditions are therefore discussed less extensively in this chapter, and further details can be found in the other respective sections of this book.

A rather specific problem in this age group, in particular in relation to preterm neonates, is the motility problem of the immature gut (e.g. “meconium plug”). Special feeding measures have been developed to prevent and treat this condition, and sometimes radiopaque CA are added to the food or installed into the stomach via gastric tube, sometimes even rectally, attempting to dilute the stiff and sticky meconium. This is often followed by a number of subsequent radiographs. There is indeed an area where imaging and therapy overlap. This overlap is also well demonstrated with image-guided therapies such as US- or fluoroscopically guided treatment of meconium ileus, meconium plugs or intussusceptions.

In the first section of this chapter, the main imaging techniques will be discussed focusing on the respective applications and details specific to the neonatal period. Thereafter, typical entities encountered in this age group spanning from congenital malformations to acquired conditions

M. L. Lobo (✉)

Serviço Imagiologia Geral, Centro Hospitalar
Universitário Lisboa Norte—CHULN, Lisbon,
Portugal

S. Stafrace

Pediatric Radiology, McMaster University and
McMaster Children's Hospital, Ontario, Canada

M. Riccabona

Medical University Graz, Graz, Austria

including tumours will be addressed, with description of their respective imaging needs and typical imaging findings including respective differential diagnoses.

13.2 Imaging Methods, Needs and Restrictions as Applicable to the Neonatal GI Tract

13.2.1 Ultrasonography (US)

Ultrasound is the mainstay of abdominal and particularly GI imaging in neonates. The parenchymal organs such as the liver, the spleen and the pancreas can be exquisite. The assessment of the bowel has also become a routine indication in neonatal US.

For adequate imaging, one requires the use of high-resolution linear transducers. The use of high frame rates is helpful due to the physiologically high respiration motion. For increasing numbers of indications, Colour Doppler Sonography (CDS) has also become a mandatory requisite.

Unlike the recent developments in other organ systems, neonatal US of the abdomen is often not performed as a point-of-care non-radiologist investigation but as a much more extensive assessment by the specialised radiology team. This, in view of the fact, that when a neonatal abdominal US is requested rarely addresses a single question but a much more extensive specialised broad study is necessitated. It is not technically easy to depict various, sometimes subtle, findings in neonates (e.g. pneumatosis, free air, gut wall pathology ...) which often are the concern of the clinicians; hence, it is important to have dedicated specialised staff who can perform such studies.

When evaluating the bowel filling techniques are often helpful and sometimes even mandatory. Such filling can be performed orally or by a gastric tube (e.g. the instillation of saline or tea) as well as rectally (instillation by rectal tube, usually using warm saline). This filling helps to

replace air and gas allowing a better visualisation of the gut and its lumen. It also improves the ability to follow structures and identify their exact anatomical position (e.g. the duodenal course) as it enables better distension of the bowel allowing for the reliable identification of some conditions (such as a small left colon). Ultrasound-CA (UCA) can also be used particularly in difficult areas (e.g. for visualisation of fistulas in cloacal or anorectal malformations or for a conspicuous delineation of the duodenal course ...). The intraluminal (oral or rectal) UCA is added to the saline creating a solution, similar to contrast-enhanced voiding urosonography (ce-VUS) (1–5% suspension in NaCl). The details depend on the region imaged, the specific equipment and the transducer used (Fig. 13.1). These UCA can also be applied intravenously to study vessels or contrast dynamics improving detection and classification of lesions and often increasing conspicuity of the respective findings. However, at present, this method is an off-label application that will need a justifying indication and adequate informed consent.

Some other important aspects and scanning techniques when evaluating the neonatal abdomen and GI tract that deserve special mention include:

- Graded compression—this can be applied also in the neonate phase, albeit gently. When applying this technique, it is helpful to slowly and gradually compress (gently massage) and not to lift the transducer too early as otherwise gas will rapidly come back into the imaged loops and the manoeuvre will prove unsuccessful (Fig. 13.2).
- The perineal approach particularly for looking at the anorectal area (Fig. 13.3). Note that measurements on perineal scans (e.g. distance between anal dimple and rectal pouch) may differ from those taken from traditional Columbia radiographs.
- Finally, the use of positioning manoeuvres in neonates and the utility of unconventional scanning windows. Examples include using the flank to access the abdominal aorta and

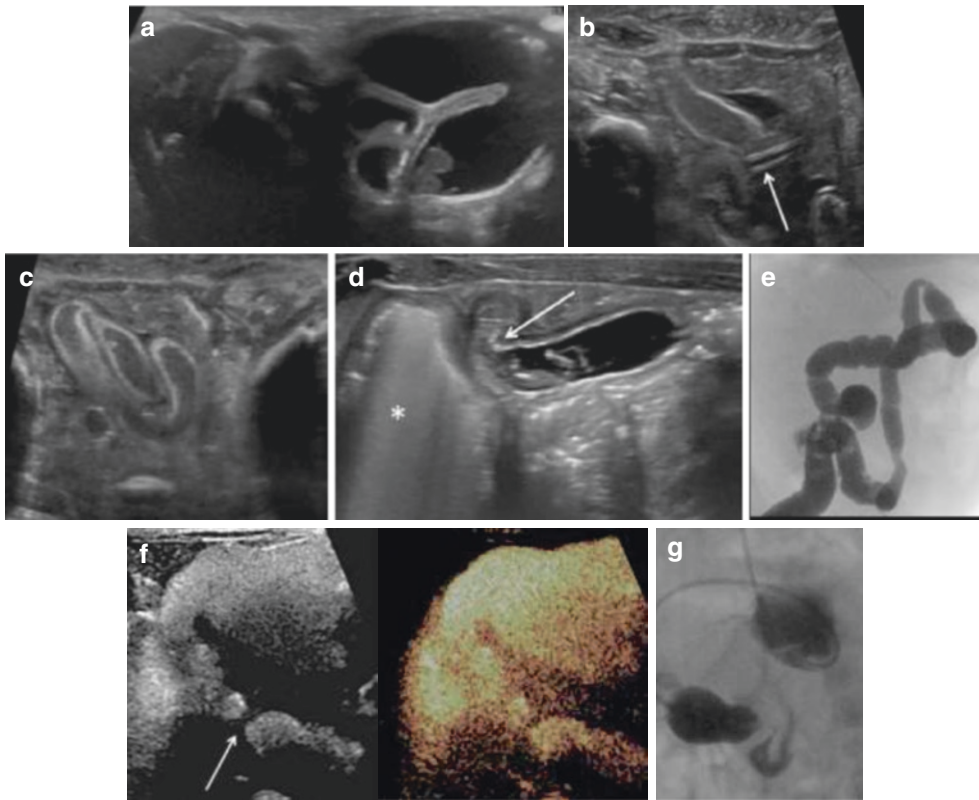


Fig. 13.1 Hydrocolon and other filling techniques. (a–d) Hydrocolon: US demonstration of fluid filled bowel loops after saline enema which are well distended (a). In (b, c) the fluid-filled loops are much less distended (note the feeding tube used to instil the saline = arrow in (b)). (d, e) In (d) the descending left colon is distended by a rectal saline enema. US depicts a sudden change in calibre with a non-distensible thick-walled bowel segment (arrow) indicating a (post-inflammatory) stenosis in a neonate after conservative treated necrotizing enterocolitis. Note the dilated air-filled oral pre-stenotic loop (asterisk). The fluoroscopic enema with CA (“irrigoscopy”) confirms the US findings with a short segment narrow stenosis of the left colon near the left flexure (e). (f, g) A neonate with a

suspected duodenal stenosis that only became manifest after surgical correction of an additional oesophageal atresia. In order to confirm the suspicions a bedside sonography was performed with filling of the stomach with saline. This did not reliably confirm the diagnosis. As it was difficult to transport the child to the fluoroscopy suite a contrast-enhanced US study was performed (after informed consent was obtained) and the stomach was filled with a saline UCA solution. This conspicuously outlined the short narrow duodenal stenosis (arrow). (g) Some days later, after stabilisation of the neonate, traditional fluoroscopic confirmation was done based on the pre-operative request of the surgeons (g)

inferior cava (can be very helpful), turning the baby into the right decubitus position to enable the visualisation of passage of gastric contents through the pyloric canal, or turning the baby onto their left side which may provoke gastro-oesophageal reflux allowing depicting or exposing a sliding hiatal hernia (Fig. 13.4, see also Fig. 13.34).

13.2.2 Radiography

An abdominal radiograph is often the first imaging step when assessing suspected abdominal or bowel obstruction. Usually, this is performed in a supine position, complemented by an upright or a lateral cross table view for assessing free air and air gas levels. Dedicated techniques and expo-

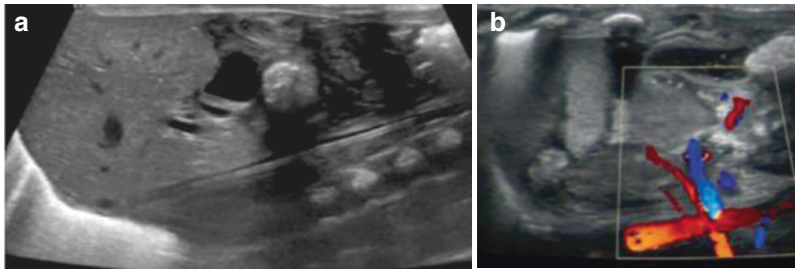


Fig. 13.2 Example for useful graded compression in neonates. (a) After graded compression the central line in the inferior cava vein coming from the lower extremity can be

nically depicted. If this method does not work, an unconventional coronal view from the flank may sometimes allow for better visualisation of those major abdominal vessels (b)

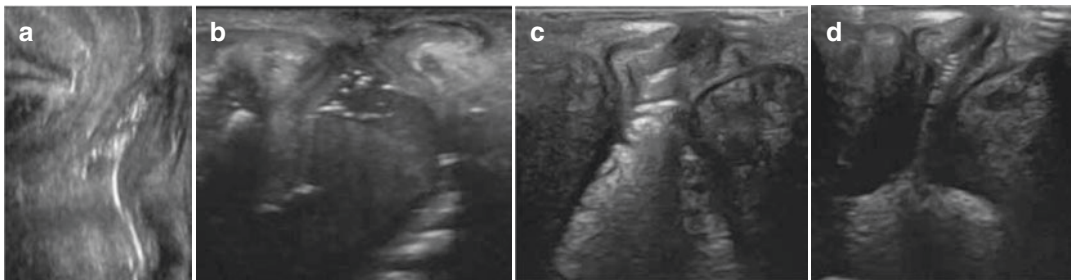


Fig. 13.3 Perineal US for assessing the anorectal anatomy. (a) Ultrasound: normal view in a midline sagittal section imaged from dorso-inferior through the non-ossified coccyx demonstrates the rectum and anal canal (image rotated in a somewhat anatomic presentation). (b) Transperineal US: this image shows the anal canal which is opened during defaecation (normal orientation as on the US display). (c, d) Both transperineal US images in a mid-

line sagittal view from the same patient taken from a video loop at different points in time: a perfect example of a perineal US in a neonate with imperforate anus (and a perineal fistula), but with preserved peristalsis of the anal canal—also demonstrating why measurements on perineal scans may be varying and can differ from those obtained of a Columbia radiograph

asures are essential, details about this can be found in Chap. 3 on general remarks and imaging methods. Note that the use of radioprotective devices does not often make a difference. On the contrary, proper collimation (not just using the electronic shutters in a retrospective way) is essential for providing high quality low dose images.

In some conditions (e.g. in oesophageal atresia or when imaging umbilical line catheters ...) a so-called torsogram (or sometimes incorrectly called “babygram”—one exposure covering both the chest and abdomen, Fig. 13.5) is performed. This allows the ability to see the conti-

nunity of structures (such as an umbilical line) but also reduces manipulation of vulnerable pre-term babies. These radiographs are also used for assessing the spine and possible skeletal abnormalities with windowing. In such indications (using the same exposure and data set) one can alter the reconstruction algorithm for better bony detail without having to take a further exposure. Working closely with the technologists/radiographers is vital in sharing the clinical concerns allowing them to present the best image possible to answer the relevant clinical questions.

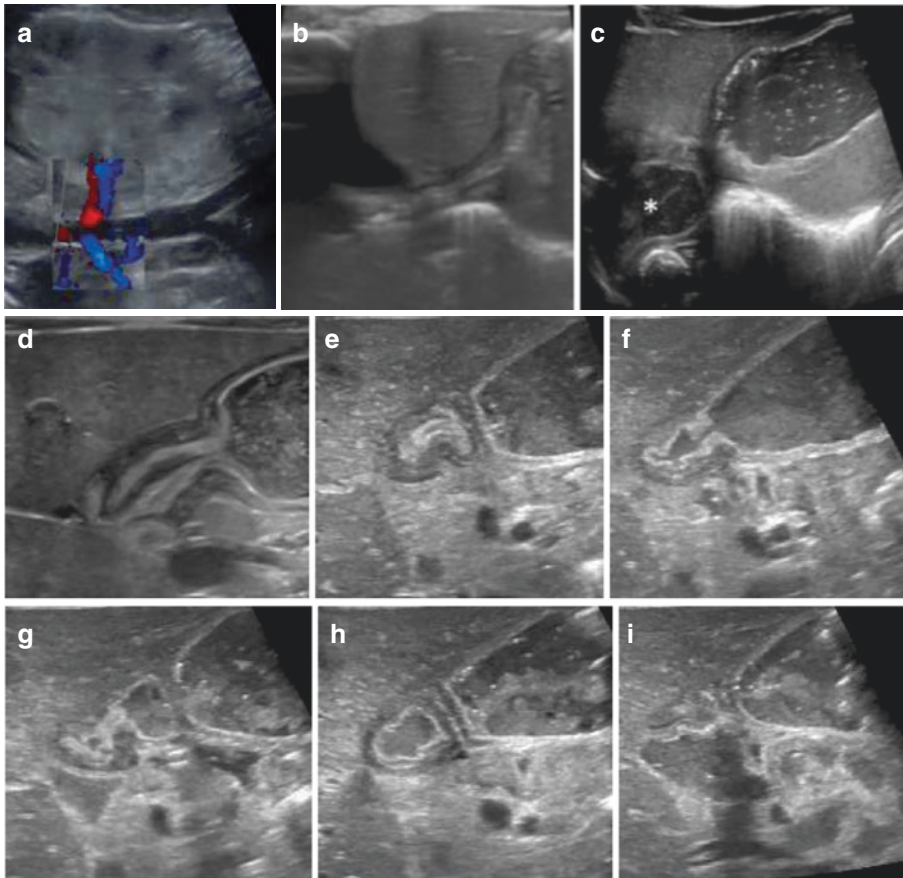


Fig. 13.4 Positioning manoeuvres and unconventional access. (a) Coronal abdominal US image with superimposed CDS (composed image): the abdominal aorta including the aortic bifurcation is nicely visualised, with CDS demonstrating the renal vessels (one renal artery blue/respectively, the other in red next to the blue encoded ipsilateral renal vein). (b, c) Ultrasound of the gastro-oesophageal junction and positing/filling manoeuvres: non-distended normal gastro-oesophageal junction (b). After filling the stomach with tea both the fluid filled stomach and a second fluid filled pocket in the thorax in

continuity with the “oesophagus is depicted”—consistent with a hiatal hernia (c, asterisk). (d–i) Pylorus on US: the initial image shows a prominent pylorus with a fluid filled stomach but a nearly occluded pyloric canal (d). With positioning (turning the baby into a right oblique position) the pylorus first is shortened (e), then opens and allows for passage of gastric content (f–h)—with eventually good distention of the fluid filled duodenal bulb (i)—thus “ruling out” a significant gastric outlet obstruction such as manifest hypertrophic pyloric stenosis

The lateral decubitus cross table projection is used for depicting free air or air-fluid levels to avoid lifting the baby into an upright position (Fig. 13.5f).

A special radiograph still performed is the so-called “Columbia view”, where the infant is posi-

tioned prone and their bottom upright—this allows analysis of the length of the anal canal useful in concerns of congenital anorectal anomalies and for measuring the distance from the blind-ended pouch to the expected position of the missing anus/the anal dimple indicated by a metallic

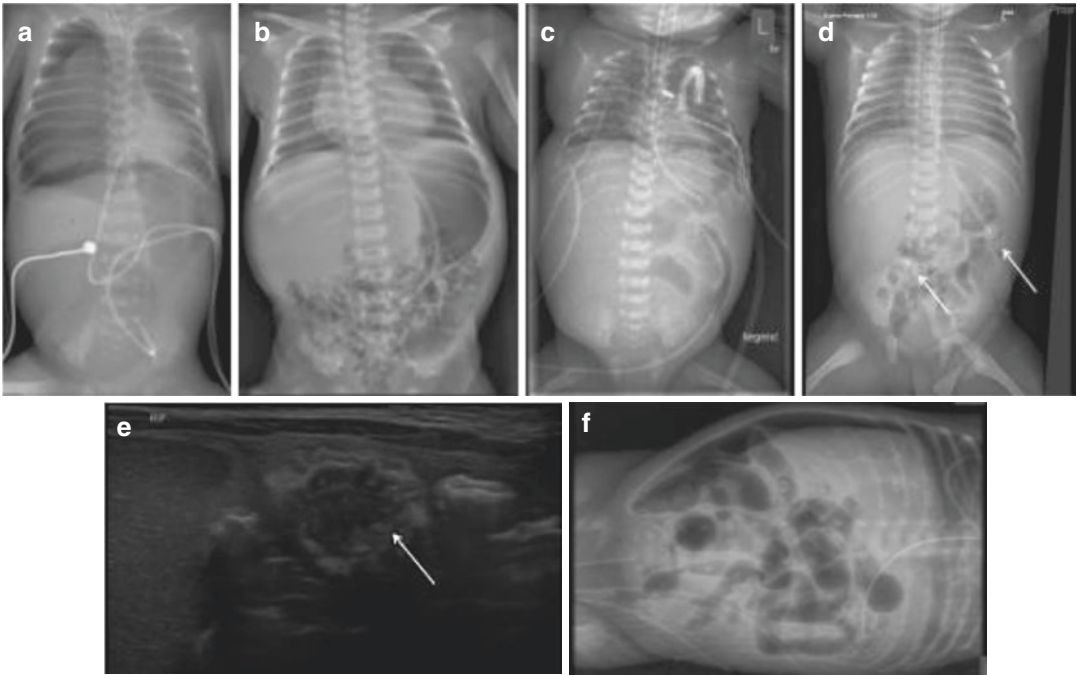


Fig. 13.5 Torsogram. **(a)** Torsogram of a neonate with an obvious right pneumothorax with mediastinal shift to the left and a rather high ending tracheal tube taken after placement of umbilical lines. The venous line just reaches the right atrium, whereas the arterial line courses downwards and end in the left iliac artery. **(b)** Neonatal torsogram showing a soft tissue mass in the right upper quadrant displacing the bowel and something that appears like two gastric tubes, but is only one that has curved upward with tip in the pharynx. Neonate with a background of polymalformation syndrome, hepatomegaly and cardiomegaly. **(c)** Postoperative torsogram in a neonate. The tracheal tube is in proper position as is the gastric tube. External ECG lines are noted. There is a chest tube on the left side after bedside surgery for PDA ligation with the respective clip in the mediastinum. Central ending peripheral line (the tip pro-

jected at the level of the superior vena cava) coming from the left arm. Note also the structural changes of the lung (early onset bronchopulmonary dysplasia) and some post-operative emphysema in the left chest wall. Note the unusual abdominal gas distribution; the baby also had an ileal stenosis. **(d, e)** Meconium peritonitis with pseudocyst formation: the torsogram **(d)** on the first day of life demonstrates subtle calcifications (arrows) in the abdomen in keeping with antenatal perforation with meconium peritonitis. The US examination **(e)** in another 1-day-old newborn demonstrates an oval cystiform structure with mixed echoes and scattered irregular mural calcification (arrow) in the right upper quadrant. **(f)** Lateral decubitus radiograph demonstrating clearly depictable free air, due to perforation in a neonate with necrotizing enterocolitis, along the right flank and above the liver

marker (Fig. 13.6). This study is often paired with US assessment of the region which is complementary.

13.2.3 Fluoroscopy

Fluoroscopy plays many roles in neonatal imaging including but not only, the assessment for malrotation or its complication midgut volvulus (in many centres now done after an ini-

tial US examination), the assessment of the colon looking for congenital distal bowel conditions and for assessing anorectal and cloacal malformations. Fluoroscopy is also helpful in the evaluation of post-inflammatory or post-operative stenosis/strictures of the gut (see Fig. 13.1e, g).

Fluoroscopy may also additionally play a therapeutic effect in conditions like small left colon, distal atresias or stenosis, and in meconium plug/ileus—the latter can also be relieved

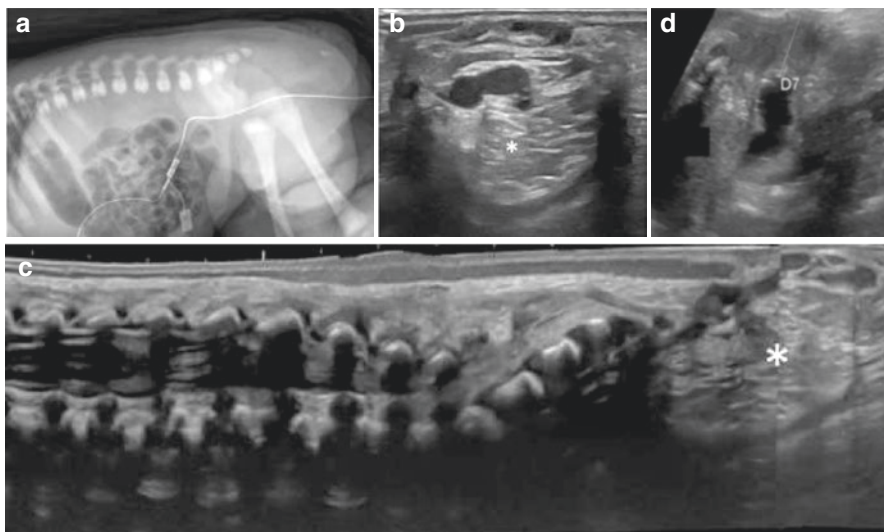


Fig. 13.6 Columbia view and perineal US. (a) Abdominal radiograph (bottom-up prone position in a lateral cross table projection) demonstrating a soft tissue mass. (b) The complementing US image (axial section, acquired dorsally through the mass) demonstrates a complex partially cystic, partially solid mass (asterisk) which was a prena-

tally diagnosed sacrococcygeal teratoma Type II. (c) The complementing sagittal US of the spine and spinal canal (extended/panoramic view) demonstrates the sacrococcygeal mass (asterisk) with a short cartilaginous coccyx and a normal position of the conus. (d) Perineal view of the anal canal which can be nicely measured (D7, 1.5 cm) after filling of the rectum with a saline enema

by rinsing the meconium with diluted CA under fluoroscopic guidance or even under US surveillance using a “hydrocolon technique” (see above). Methods used often depend on experience of the operators in the neonatal centres.

Water-soluble iso- or hypo-osmolar CA are the routine contrast agents of choice. For some indications, instillation of air can also be sufficient. Hyperosmolar-ionic CA may be dangerous because these agents may cause catastrophic fluid and electrolyte imbalances. Some centres have indeed moved away from using these agents completely due to these associated risks. If used in the well-hydrated infants, for example in the treatment of meconium plug or ileus, the agents should be diluted (e.g. in NaCl, with a 1:3 dilution).

More details on the respective exposure settings and handling for fluoroscopic examinations of neonates can be found in Chap. 3 of this book.

13.2.4 MRI (CT)

Very rarely an MRI and only exceptionally a CT may become indicated in imaging the neonatal abdomen.

MRI is used for imaging the parenchymal organs, particularly the liver (e.g. choledochal cyst with cholestatic dilated intrahepatic bile ducts) or other gross pathology if US is equivocal. MRI can also be helpful preoperatively (Fig. 13.7). The detail and resolution of US are often under-appreciated by the referring clinical colleagues and in the majority of neonatal conditions US does indeed suffice.

The other field for performing abdominal MRI in neonates is in the assessment of congenital tumours and their differential diagnostic work-up and staging.

Unless considered absolutely necessary, contrast-enhanced MR with MR-CA should be avoided due to the immaturity of the kidneys and the increased risk of gadolinium deposits in the

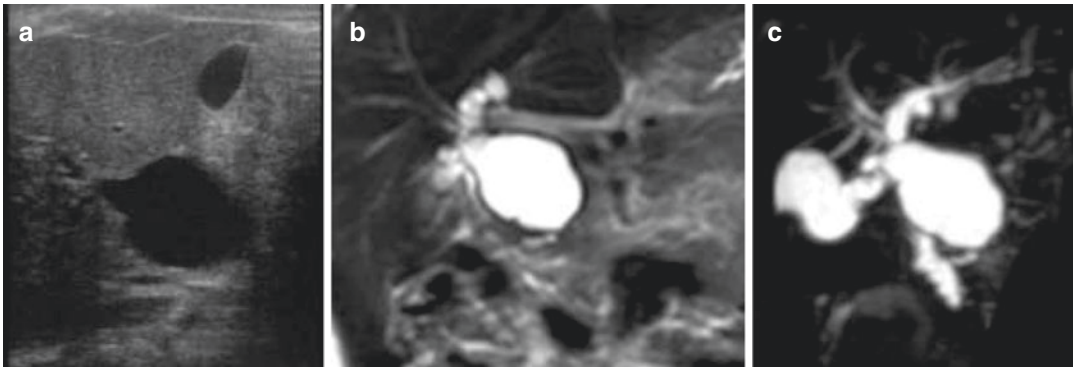


Fig. 13.7 MRI for neonatal abdominal queries. (a–c) Choledochal cyst: US depicts a cystic structure in the liver hilum in continuity with the slightly dilated hepatic duct (a). The respective MRI (b, T2-weighted coronal image) and MRCP (c, 3D MIP image) confirm the large choledochal cyst

Table 13.1 Contrast rules for abdominal investigations in neonates

Fluoroscopy: as detailed in the text	<ul style="list-style-type: none"> • Non- or hypo-osmolar water solvable CA at a concentration of 100–150 mg/mL are mostly used, sometimes even further diluted • Gastrografin should be used with caution and always diluted (1:3 or 1:4 solution in NaCl) • Barium-based CA can be used if there are no recognised contraindications (such as perforation, risk of aspiration)
US contrast agent	<ul style="list-style-type: none"> • Intravenous application = 0.1–0.2 mL/kg • Intracavitary applications (stomach, bowel ...)—as for ce-VUS (1–5% suspension in NaCl)
CT	<ul style="list-style-type: none"> • Intravenous CA administration: 2.5–3 mL/kg, hypo- or iso-osmolar CA, concentration 150–200 mg/I/mL • Bowel opacification: 2% solution of iso-osmolar CA 200 mL I/kg, up to 100 mL peroral (if tolerated)
MRI	<ul style="list-style-type: none"> • Intravenous gadolinium application: only macrocyclic agents, 0.05–0.1 mmol/kg • Bowel opacification: 1:100 dilution, or simply utilise water or blackberry juice administered orally

body. If used, special care must be taken when this is drawn-up as the actual volumes are very small.

CT is hardly ever used to image the neonatal abdomen unless there is no MR availability or in emergency conditions such as in trauma with gross intra-abdominal haemorrhage. In abdominal tumour staging, a chest CT may be needed (often performed at same sitting of the MRI). In these conditions iodinated CA is required, sometimes even contrasting of the bowel may be necessary but one should avoid performing a CT-CA and an MR-CA in close proximity (24–48 h delay between injection of different CA is recommended particularly in preterm and newborn babies).

13.2.5 Contrast Agent Aspects

As previously mentioned, the immaturity of the organs, in particular in preterm neonates, may cause restrictions in CA utilisation. The renal elimination of the CA is delayed due to the renal immaturity. Sometimes contrast can be noted to be excreted through the gut or the bile with opacification of the bowel and/or gallbladder appreciable on radiographs after intravenous contrast injection.

Because of the higher relative circulating blood volume in neonates (90 mL/kg versus 60 mL/kg), the dose of intravenous CA often is relatively higher than that used in older children and the iodine concentration lower (Table 13.1).

Timing and delay times are also different. For radiopaque CA, the impact of iodine (even if administered orally or rectally) needs to be considered as this may cause neonatal hypothyroidism (checking of thyroid hormones and follow-up may be indicated, particularly if high doses are applied).

Ultrasound-CA (UCA) can also be used in neonates. This has the added advantage that it is not excreted by the kidney and thus renal function does not restrict use. However, except for ce-VUS (and liver imaging in the USA), the use of UCA in neonates (and children) is not approved and the particularly intravenous applications are off-label needing detailed informed consent. This does not mean the use of UCA is forbidden—this is the same with many drugs used in perinatal and neonatal medicine which are also not approved for neonatal use. Further details on all these aspects including dose can be reviewed in Chap. 3 in the respective dedicated section on CA in neonates.

13.2.6 Specific Appearances of Neonatal Abdominal Organs

There are a few aspects that need to be considered when investigating neonatal abdominal organs, which may appear different than later in life.

- The left liver lobe is larger in neonates; only after closure of the ductus venosus (venous duct of Arantius) does the left lobe regress. Eventually it becomes smaller than the right liver lobe (after a few months of life).
- The ductus venosus may be physiologically open up to approximately 3 weeks after birth. This can be easily assessed using Doppler techniques (Fig. 13.8). It should not be mistaken for an abnormal shunt. It can calcify after closure; again, this normal finding should not be misinterpreted.

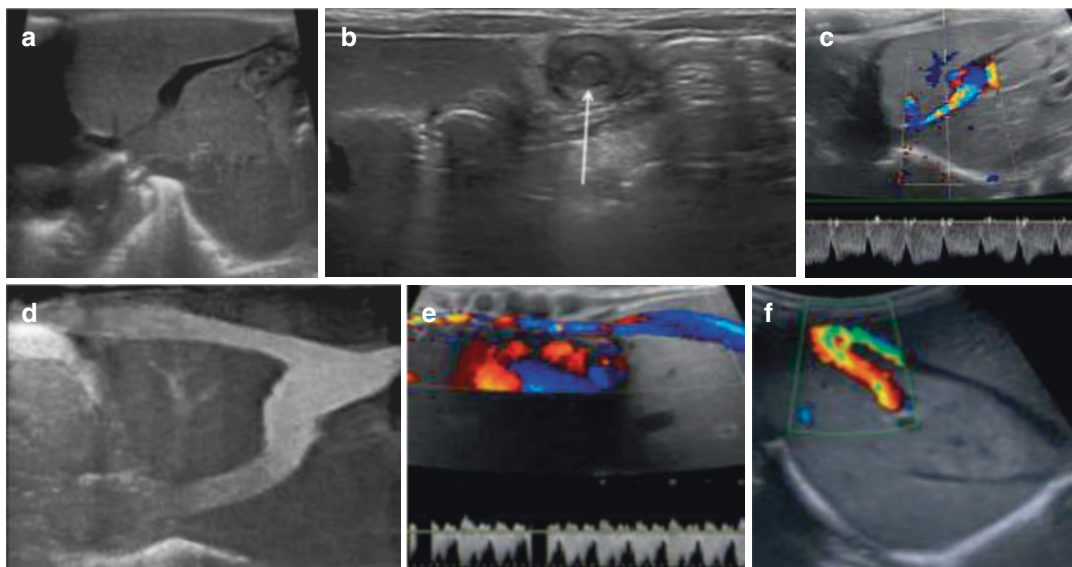


Fig. 13.8 Persisting venous duct, portocaval shunts and vascular variations. **(a)** Midline sagittal US (phased high-resolution linear transducer) of the upper abdomen demonstrates the physiologically persisting umbilical vein. **(b)** Axial section in same location as **(a)** in a different patient showing a thrombus in the umbilical vein (arrow). **(c)** Midline sagittal CDS with spectral trace of the colour encoded, physiologically persisting venous duct; the shunt flow with atrial modulation is confirmed by the spectral analysis. **(d, e)** B-flow depicts an abnormal

venous vessel coursing from the chest to the venous sinus and then shunting into the right atrium via a large persisting venous duct **(d)**. The flow comes from the chest into the liver with a flow spectrum as a pulmonary vein is shown in **(e)**. **(f)** A porto-venous shunt nicely shown by CDS. Note that the draining vein (with high velocity turbulent flow) is much larger than the other liver veins, as is the feeding branch of the portal vein (encoded in red). The additionally present hepatic haemangiomas are not so well perceived in this image

- The umbilical veins thrombose and can sometimes appear generous in size as they extend from the umbilicus along the falciform ligament to the umbilical sinus of the liver (Fig. 13.8). This feature becomes less evident over the first few weeks of life. The latter should not be misinterpreted as pathology.
- Liver parenchymal echogenicity in very preterm infants may be lower than or equal to renal cortical echogenicity in the neonatal phase.
- The spleen is positioned more obliquely (likely related to the generous size of the left lobe of the liver)—thus landmarks such as the relation with the left kidney as used in older children for roughly estimating kidney and/or spleen size are less reliable.
- Kidneys often appear to have a slightly brighter (cortical) parenchyma in the early weeks of life. Foetal renal lobulation of the kidneys is more obvious.
- The adrenals are larger in neonates.
- Haustrae of the colon are not developed—particularly in preterm infants, making differentiation of colon from ileum very difficult or impossible.
- The torsogram, which is often taken with this clinical suspicion, reveals a high-ending feeding tube with or without air in the stomach and the intestines; depending on whether there is a connecting lower fistula. Usually, no further imaging is needed preoperatively. It is very difficult, if not impossible, to preoperatively delineate the length of the atretic oesophageal segment. Even contrast studies will not reveal this information. Therefore, no contrast administration via tube is necessary. This can only be achieved in neonates with a gastrotomy after CA administration under fluoroscopy.
- If one needs to confirm the atresia very often installation of air in the high-ending feeding tube is sufficient to outline the upper distended and occluded oesophageal segment. Two major grading systems are established (Vogt and Gross—see Sect. 10.9). Only the H-type fistula, which usually is diagnosed much later due to aspiration symptoms, needs a contrast study of the oesophagus.
- Oesophageal atresia can be associated with other malformations, such as an additional lower atresia, cardiac malformations, vertebral malformations, etc. Therefore, at latest after surgery, a thorough work-up for other malformations is recommended. This usually entails an US of the entire abdomen, an US of the spine, an echocardiogram and a chest radiograph (latter likely already done preoperatively) (Fig. 13.9).

13.3 Congenital Malformations of the Stomach and the Bowel

13.3.1 Atresia and Associated Findings

13.3.1.1 Oesophageal Atresia

This entity has been extensively addressed in Chap. 10. Some important take away points are listed here:

- Oesophageal atresia is often diagnosed foetally.
- If not known prenatally, the failure to pass a gastric tube usually raises the clinical suspicion postpartum.

13.3.1.2 Gastric Outlet and Duodenal (Small Bowel) Stenosis/Atresia

These entities are often identified prenatally. Postnatally, they present with vomiting after feeding attempts on the first day(s) of life. Depending on the level of obstruction, this may be bilious or non-bilious. The abdomen is usually sunken. Aetiologically, there can be the classic type atresia or webs and less commonly the presence of a stenosis or a web with a central perfora-

tion. The latter causes incomplete occlusion and can sometimes be confusing on imaging, as air can pass distally through the stenosis.

- Imaging wise the abdominal radiograph shows either only a distended air-filled stomach (*gastric outlet obstruction*) or the so-called double bubble pattern with an air-filled dilated proximal duodenum (in *duodenal atresia*), the latter is often associated with an annular pancreas (Figs. 13.9 and 13.10). Clinically, a hiatal hernia may pose a differential diagnosis.

- Preoperatively, often no other imaging is necessary. However, if one needs to confirm the suspicion of such pathology, a number of imaging options are available. One can perform an US study with filling of the stomach with saline and/or (to assess and differentiate against a duodenal stenosis) potentially adding UCA to allow for proper visualisation of the non-occluded section of the duodenum as well as for depiction of a possible connection to the more distal bowel—seen by passage of UCA beyond the stenosis (Fig. 13.10).

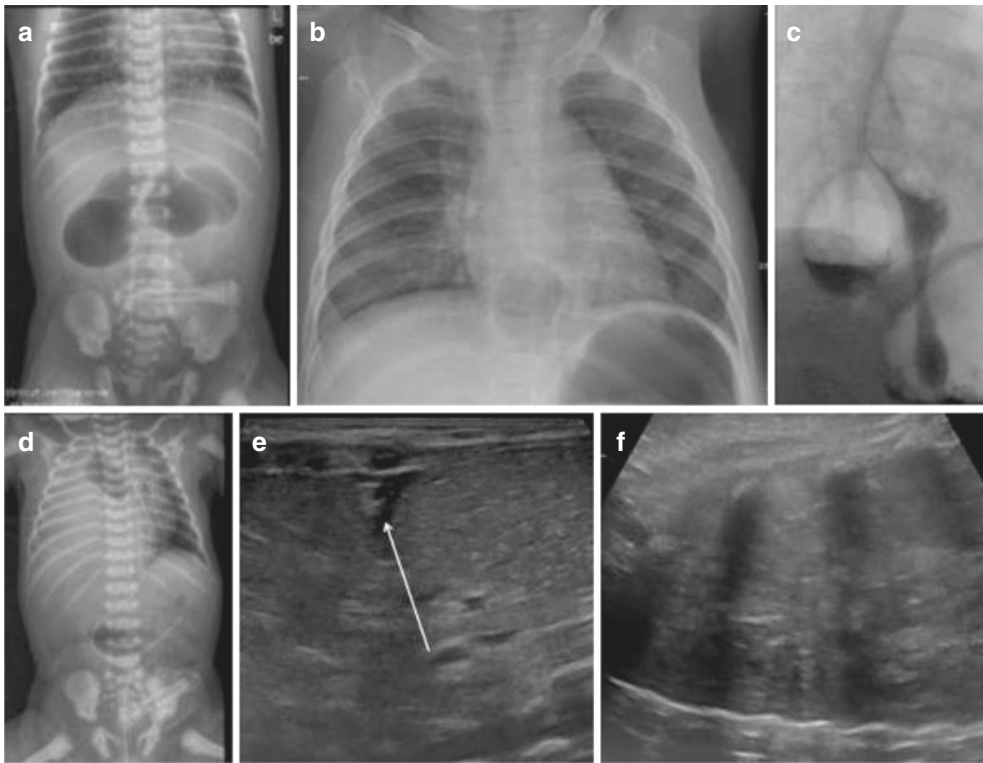


Fig. 13.9 Radiographs: Double bubble and other upper abdominal pathology. (a) Abdominal radiograph in a 1-day-old newborn showing the typical double bubble (i.e. two air filled structures in the upper abdomen) indicative of duodenal atresia. (b, c) A chest radiograph of a newborn depicts an air-filled structure in the area of the distal oesophagus, suspicious of a hiatal hernia (b). The corresponding fluoroscopy (c) confirms the continuity of the structure with the contrast filled stomach separated from the contrasted and partially air-filled distal oesophagus, establishing the diagnosis of a para-axial hiatal her-

nia. (d–f) Torsogram (d) of a newborn with right sided diaphragmatic hernia; note the deep ending gastric tube confirming that the stomach is down intraabdominally, and a high ending tracheal tube as well as a deep ending venous line from the right leg (right common iliac vein); additionally, an umbilical clasp and a bladder catheter are in place. US confirms the intrathoracic position of the liver (e) with a small ventral muscular remnant of the diaphragm (arrow, e) and compressed atelectatic adjacent lung (identifiable by the air bronchogram, f)

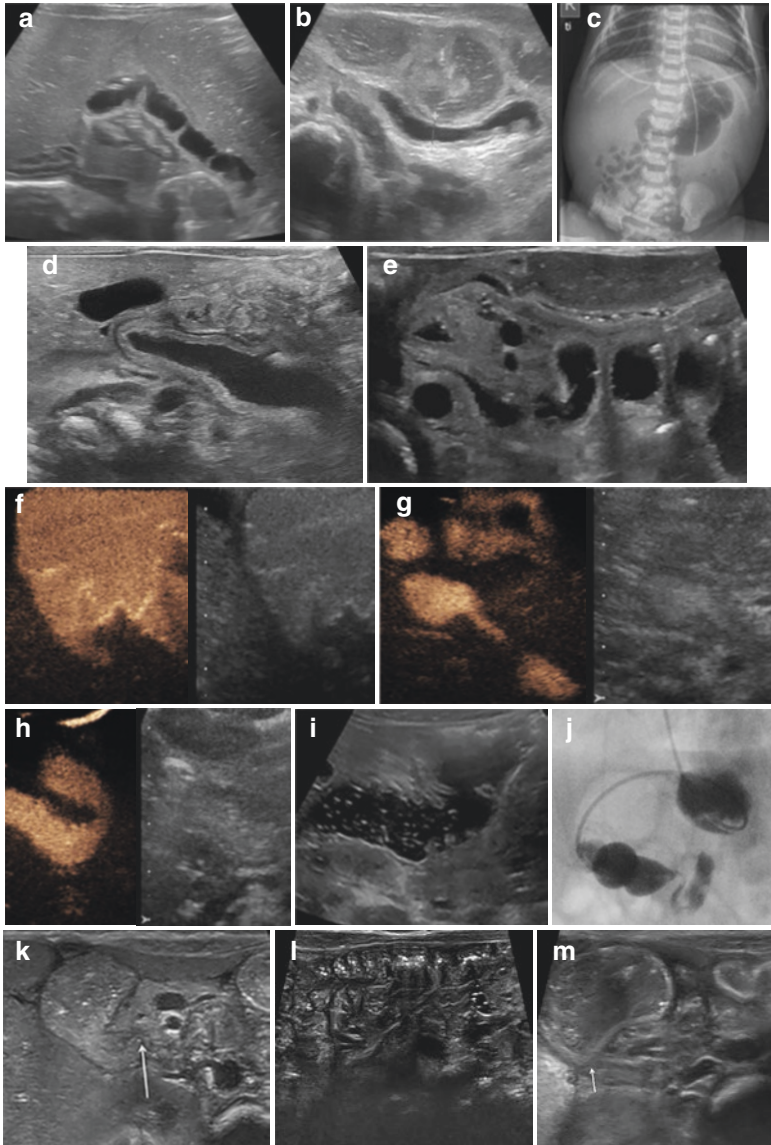


Fig. 13.10 (Distal/proximal) Duodenal/small bowel stenosis and annular pancreas. **(a, b)** Ultrasound of the fluid filled duodenum—its course can be nicely appreciated. **(c–e)** The duodenum and jejunum appear distended on the abdominal radiograph **(c)**, with only small loops more distally, suspicious for a small bowel stenosis. US after filling the stomach and the duodenum/jejunum with tea via a gastric tube (to avoid interfering air content) shows a normal course of the duodenum **(d)** and well distended large proximal small bowel loops **(e)**, whereas the distal loops remained nearly collapsed (not shown), confirming the suspicion (as did surgery). **(f–i)** A neonate referred for an abdominal US study under the suspicion of malrotation; US did not show a volvulus, but it was difficult to analyse and follow the course of the duodenum. Therefore, diluted UCA was instilled via a gastric tube filling the stomach, the pylorus **(f)** and then the duodenum. One can nicely appreci-

ate the normal course of the duodenum with quite some narrowing in the mid portion **(g)**. The duodeno-jejunal flexure was normal and nicely distensible **(h)**. The distal bowel was sonographically normal and well distensible in the hydrocolon after a rectal saline enema **(i)**. Eventually surgery performed for clinical reasons revealed an annular pancreas which was not appreciable by US. **(j)** Fluoroscopy in a neonate after repair of an oesophageal atresia with persisting vomiting and feeding problems reveals a duodenal stenosis. **(k–m)** An upper abdominal US reveals a dilated proximal duodenum **(k)** and collapsed distal small bowel loops **(l)** in a neonate with annular pancreas which in itself could not be depicted, but these indirect signs with a sudden narrowing of the duodenum **(k, m)**, arrows) at the head of the pancreas after instillation of some saline into the stomach together with the clinical symptoms indicated surgery that confirmed the suspicion

- If no UCA is available, this can be assessed with an upper GI fluoroscopic study using non-ionic iso-osmolar water-soluble CA (avoiding barium in such indications because of the aspiration risk and the fact that the thicker barium could obscure a small central hole in a web) (see also Fig. 13.1).
- Commonly, a thorough sonographic search for associated malformations is conducted either pre- or postoperatively. Note that an annular pancreas can be very difficult to depict (or “rule out”) by US. However, indirect signs may indicate this rare condition (see Fig. 13.10).

Other stenosis of the short bowel are much rarer and one more commonly encounters them in the (distal) ileum. Only some of them are depicted prenatally. Some may have caused intra-uterine perforation with meconium peritonitis—seen by peritoneal calcification both on abdominal radiographs and on US (see Figs. 13.5 and 13.36). A special rare type of small bowel atresia is the *apple-peel intestinal atresia* (type IIIb or “Christmas tree” intestinal atresia), where the duodenum or proximal jejunum ends in a blind pouch. The distal small bowel wraps around the mesenteric root in a spiral resembling an apple peel. Often a long small bowel segment is absent, and it may be associated with malrotation.

A common helpful finding in more distal atresias is the “unused” or “small left colon”, often perceived as the diagnostic key finding. On US one may observe distended, meconium-filled proximal bowel loops with collapsed distal loops and a narrow (left) colon; the latter only occurs in more distal stenosis, when not sufficient meconium is produced to distend the colon during foetal life.

- This “small left colon” can sonographically be confirmed by a saline enema (“hydrocolon”) where one can demonstrate the very narrow lumen and the lack of distensibility of the left colon and often also the recto-sigmoid

(Fig. 13.11). By the constant drip-infusion technique one often is able to delineate the entire colon up to the ileocecal valve or to the level of the obstruction, helping to differentiate an atresia from a meconium ileus or meconium plug.

In equivocal clinical and sonographic findings and where the US expertise is not available fluoroscopy studies are performed; a contrast-enema may be performed that may be complemented by a follow-through study. Note that if both contrast studies are done the enema should be performed prior to the follow-through in order to avoid superimposition of small bowel contrast remnants obscuring the colon, whereas the CA in the colon from the first study can be easily rinsed out after the study. Relevant differential diagnostic entities such as malrotation need to be assessed either sonographically or by the early phases of the fluoroscopic upper GI study.

Other causes of obstruction such as an internal hernia, Ladd’s bands and similar anatomic conditions and the presence of a duplication cyst (sonographically easily identifiable by the so-called gut signature of the thick, multi-layered wall of the respective cystic structure) must be also be considered in such clinical scenarios.

13.3.1.3 Atresia of the Colon and Differential Diagnosis (e.g. Hirschsprung’s Disease)

Colonic atresia manifests similarly to the distal ileal stenosis or atresia. This may already be appreciated on prenatal imaging. It typically manifests clinically later than higher stenosis through failure to pass meconium and the presence of a distended abdomen.

- Diagnosis is made by an enema, which can be performed sonographically using saline or fluoroscopically using radiopaque CA (see

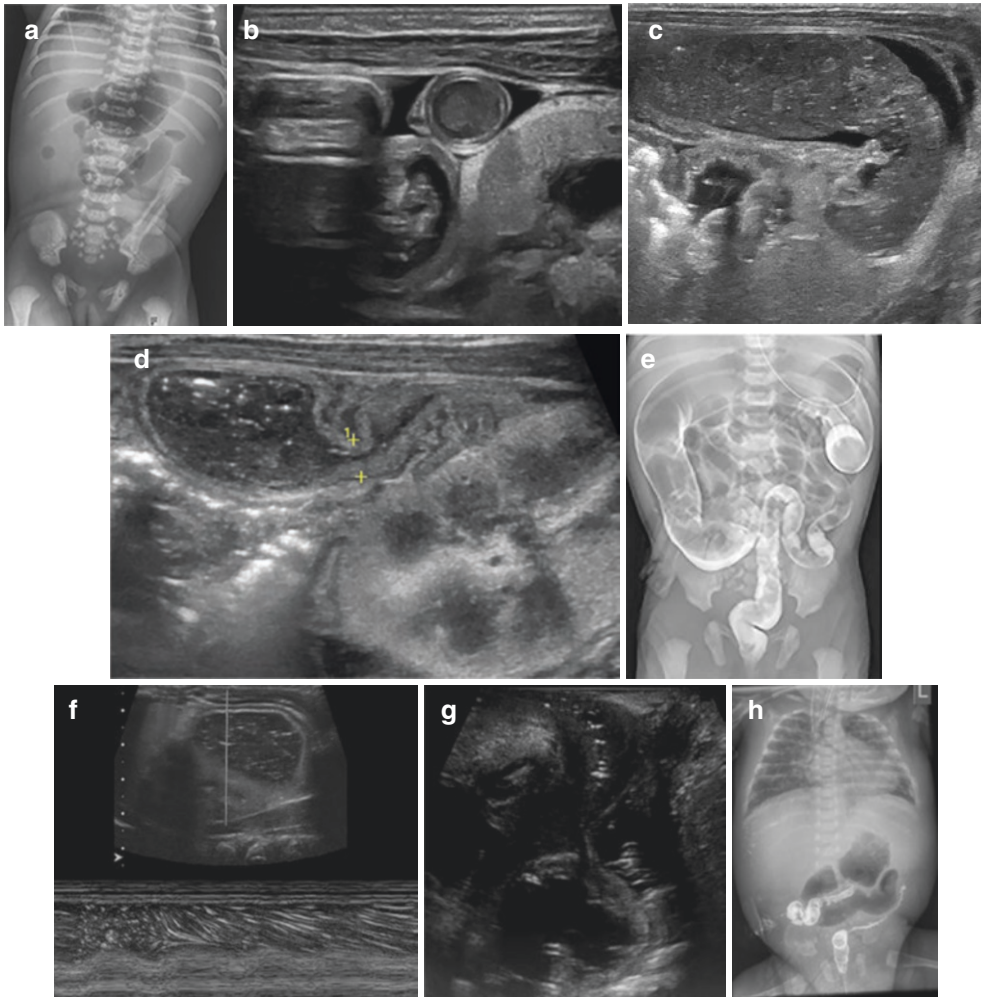


Fig. 13.11 Unused small left colon—fluoroscopy and hydrocolon (neonatal congenital colonic stenosis). **(a)** Abdominal radiograph in a 2-day-old neonate shows distended proximal small bowel loops but paucity of air in the distal bowel—suspicious of an ileal stenosis, which was subsequently confirmed at surgery. **(b–d)** A neonate presenting with clinical intestinal sub-occlusion at 30 h of life (previous small amount of meconium passage had been noted). US revealed dilated bowel loops **(b)**, small bowel and colon proximal to splenic flexure) with a “small” appearing left colon; the transition zone was noted at the splenic flexure **(c)**. A hydrocolon was then performed using a diluted contrast solution (in order to obtain an abdominal film afterward) was performed and confirmed the colonic stenosis **(d)** which clinically

resolved conservatively (aetiology probably related to maternal anti-hypertensive drugs). **(e)** Corresponding radiograph after the hydrocolon with the diluted contrast as detailed above. **(f–h)** Similar findings can be observed in another neonate with colonic stenosis who became severely symptomatic 14 days after birth. US revealed a dilated proximal colon with stenotic hyperperistalsis documented also using m-mode **(f)**; only the very small appearing left colon could not be properly visualised (not shown). Perineal US-defaecography shows a normal opening of the anal canal and a normal shape and contour of the rectum **(g)**. The bedside torsogram after a contrast enema **(h)** shows a long-distance colonic stenosis with a normal rectum and proximal colon

Fig. 13.12). Distal colonic atresia may be confused with Hirschsprung's disease which is an aganglionic colon segment causing absence of adequate peristalsis. Different degrees of Hirschsprung's disease are known, starting from an ultrashort rectal segment to long segment disease that may affect the entire colon or rarely even the distal ileum. In Hirschsprung's disease, imaging typically reveals distended loops (on radiographs) and lack of peristalsis (on US or fluoroscopy), and on defaecography (usually is performed fluoroscopically) the pathologic behaviour of the sphincter mechanism can be seen (Fig. 13.12). Note that studies done too early may miss short segment disease, and no special preparation such as cleansing enemas should be performed prior to

the study to enable the visualisation of the transition zone from the affected narrow to the unaffected dilated bowel.

- In some centres, defaecography is performed by US after a saline enema using a perineal approach but this is technically challenging ("US defaecography"). In older children, an MR-defaecography is an alternative option.

Radiology may not appreciate Hirschsprung's disease and when it does the change in calibre seen on radiological investigations is also poorly correlated with the eventual transition zone demonstrated histologically after surgery. Diagnosis is usually confirmed by suction biopsy of the bowel wall proving the absence of the neuronal plaque and helping to differentiate Hirschsprung's

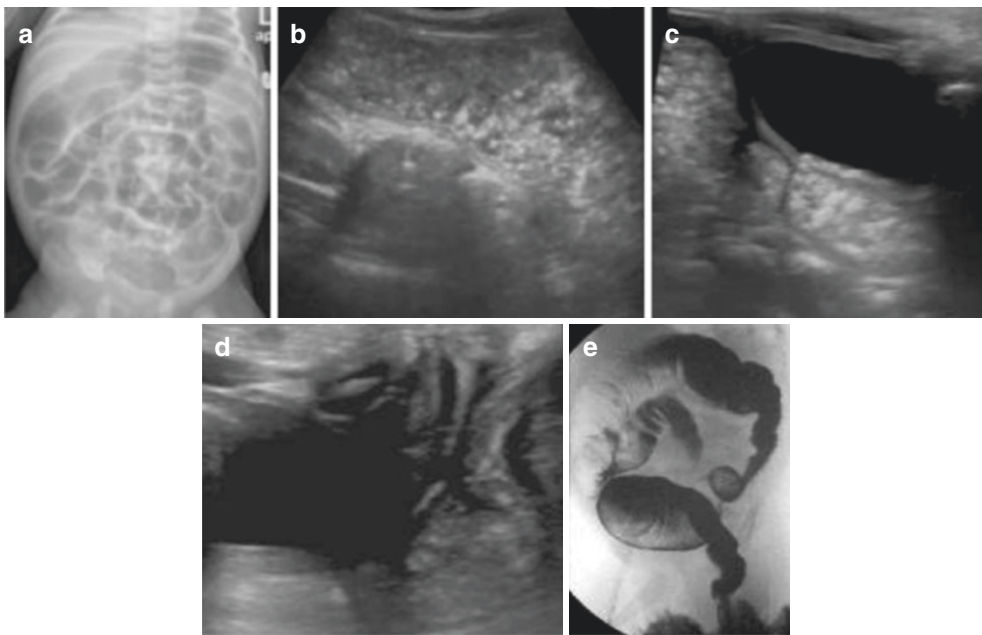


Fig. 13.12 Hirschsprung's disease. (a–d) Abdominal radiograph (a) from an 18-day-old neonate with severe constipation since birth demonstrating a distended abdomen and distal bowel obstruction pattern. On US, the sigmoid colon is massively distended and filled with stools (b). On transabdominal US the transition zone is seen at the rectosigmoid (c), perineal US reveals a normal anal canal (d). An urgent colostomy was performed and

Hirschsprung's diagnosis was confirmed on biopsy. (e) Fluoroscopic image during defaecography for radiographic evaluation of suspected Hirschsprung's disease. Note that if too much CA is instilled the visualisation may be difficult. Also if colorectal cleansing has been performed, the transition zone may be difficult to depict or even missed. Due to technical restrictions, ultrashort segments can also not be appreciated

disease from neuro-intestinal dysplasia (NID, which contains neurons, but also presents with constipation symptoms).

In *colonic atresia* an enema (sonographic or fluoroscopic) demonstrates a small/narrow recto-sigmoid and distal colon with a stop in progression of CA or NaCl (or air) to the proximal colonic sections at the level of the atresia. The pre-stenotic bowel appears distended and meconium-filled and does not get opacified by the contrast medium.

13.3.1.4 Anorectal and Cloacal Malformations

This is a large spectrum of congenital malformations related to the distal rectum and anus

ranging from a simple anal stenosis or a ventrally positioned anus to a full cloacal malformation with fistulous connections between the gut, the vagina and the bladder, draining by common cloaca. The latter is only seen in females, whereas purely anorectal malformations have a male predominance. These less severe forms of anorectal malformations (ARMs) include anal stenosis, ventral anus position, anal atresia of different length and possible fistula tracts—connecting to the perineum, the urethra, the vagina, but also to urinary bladder. Besides the standard international classification, the most commonly used classification is the Krickenbeck classification (Table 13.2). There is a high probability of

Table 13.2 The international (a) and the Krickenbeck (b) classifications (2005) of anorectal malformations

(a)					
Type		Male		Female	
High (Supra-levator)	Anorectal agenesis	Without fistula		Without fistula	
		With fistula	Rectovesical Rectourethral	With fistula	Rectovesical Rectocloacal Rectovaginal
	Rectal atresia				
Intermediate	Anal agenesis	Without fistula		Without fistula	
		With fistula	Rectobulbar	With fistula	Rectovaginal—low Rectovestibular
Low (Trans-levator)	At normal site	Covered anus—complete Anal stenosis			
	At perineal site	Anterior perineal anus Anocutaneous fistula—covered anus (incomplete)			
	At vulvar site			Vulvar anus Anovulvar fistula Anovestibular fistula	

(b)	
Major clinical groups	Rare/regional variants
Perineal/cutaneous fistula	Pouch colon atresia/stenosis
Recto-urethral fistula/atresia/stenosis	Rectal atresia/stenosis (and imperforate anus)
Bulbar fistula	Recto-vaginal fistula
Prostatic fistula	H-type fistula
Recto-vesical fistula	others
Vestibular fistula	
Cloaca	
Anorectal malformations with no fistula	
Anal stenosis	

The two tables show the two most used classifications—table (a) grading ARMs into low, intermediate and high anal atresias, addressing also fistulas and different appearances in boys and girls, whereas table (b) (the Krickenbeck classification) lists the relevant clinical groups of anorectal malformations

associated malformations, which needs to also be addressed with an extensive imaging work-up.

The imaging work-up is guided after clinical inspection, which can sometimes already classify the abnormality with relative high certainty. Different imaging pathways depend on the treatment decision needs. Occasionally only a detailed surgical investigation under anaesthesia is performed without extensive imaging (e.g. in a ventrally positioned anus or in the presence of an imperforate anus). No imaging is usually needed for anal stenosis. There are extensive published recommendations discussing the imaging algorithms for neonates with ARM with references at the end of this chapter.

- In *anal atresia*, a perineal US during the first 48 h of life is recommended (Fig. 13.13). In some centres, the prone bottom-up cross table Columbia radiograph (“invertogram”) is still performed. This should not be performed earlier than 24(–48) h after birth allowing enough time

for passage of air to the more distal rectum better outlining the distal end of the rectal pouch and thus enabling measurements of the atretic segment differentiating low from intermediate and high atresia (see Fig. 13.6). This differentiation is essential for further management, as low atresias are primarily operated by some kind of perineal pull-through procedure, whereas high atresias (the atretic segment is longer than 1.5–2 cm) initially get an entero-/colostomy. The corrective surgery for the atresia is performed later in childhood after complementing fluoroscopic studies outlining the recto-sigmoid and interrogating for possible fistulae (+/- MRI of the pelvic floor). If there is a perineal or para-anal fistula, dilatation of this fistula tract may help as a bridging option until the definitive surgical correction is performed.

- A thorough search for associated spinal malformations is recommended; associations include hypoplastic sacrum or coccyx as well as a low-ending conus or a hypo-

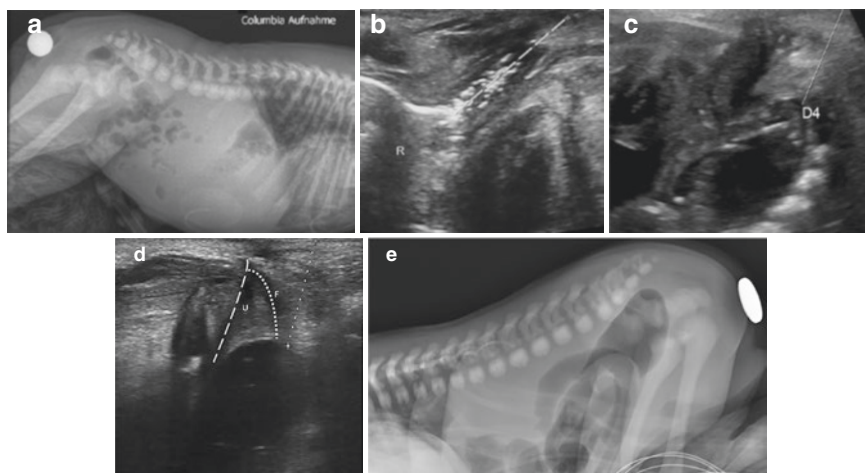


Fig. 13.13 Perineal Ultrasound anal atresia. (a) Columbia radiograph in a neonate with clinical anal atresia appearing like an intermediate to long atresia; the poor distention of the rectal pouch is somewhat unusual. (b) A corresponding perineal US with the respective measurement (+...+) confirms the long distance between the anal dimple and the air filled rectal pouch (R), however demonstrating air echoes in the anal canal supporting a low stenosis. (c) A second perineal US example shows a long

distance (D4) between the, in this case, fluid filled rectum and the anal dimple in an intermediate to high atresia (in contrary to the case depicted above). (d, e) Perineal US in anal atresia (d) allows not only measurement of the distance between the anal dimple and, in this case, the fluid filled rectal pouch (dotted line), but also demonstrates a fistula tract (F) towards the distal urethra (U). Corresponding Columbia radiograph in the same neonate (e)

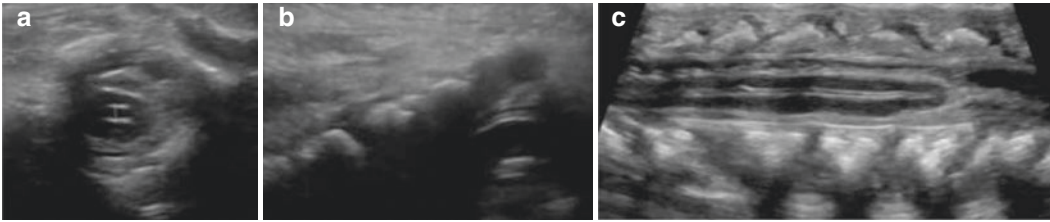



Fig. 13.14 Ultrasound in cord pathology potentially associated with anorectal malformations. (a) A neonate with VACTERL syndrome: a dorsal cross section of the upper lumbar spinal canal and the cord demonstrating associated dilated central canal (+...+, hydromyelia). (b) Sagittal dorsal section of the sacrum and the hypoplastic

coccyx in a neonate with Currarino triad. (c) Sagittal dorsal US image of the spinal cord: minimal variant of cord pathology as potentially associated with anorectal malformations: slightly hypoplastic cord with round shaped conus in a rather low position

plastic high-ending conus. This is achieved by US and radiographs (Fig. 13.14).

- Note that the Columbia projection has some restrictions (e.g. inspissated distal meconium in the distal rectum obscuring the real height of the rectal pouch, or by peristalsis of the recto-anal structures thus showing a varying picture—see Fig. 13.3).
- If a fistula is suspected, then contrast studies are recommended, e.g. a VCUG or a ce-VUS, or instillation of UCA into the recto-sigmoid (“colostogram”)/the vagina or the cloaca; such investigations are usually performed at 1–3 months of age.
- *Cloacal malformations* are very complex and a different topic, which should be investigated and managed at specialised centres with a multi-specialty team in view of the long-term implications and high associated morbidity. Recommendations on how to proceed in such scenarios are available in terms of consensus and expert statements based on reviewing of the available literature from such centres (see references) (Fig. 13.15). These neonates require extensive radiological investigations including US, spine radio-

graphs, contrast-enhanced studies (usually fluoroscopy and VCUG) and MRI (often performed delayed).

 For imaging in neonatal GI tract atresias and stenosis, radiographs and US (also using filling techniques) are often sufficient for establishing the diagnosis, sometimes supplemented by fluoroscopy. The number of dilated loops in the radiograph should guide if this is likely to be an upper/proximal obstruction (small number of distended loops) vs. a lower/distal obstruction (larger number of loops; difficult to count). Lower/distal obstruction would necessitate the imaging algorithm to start with distal contrast/US examinations first.

13.3.2 Malrotation and Volvulus

During foetal development, the gut undergoes an anticlockwise 270° rotation around the superior mesenteric vessels (Fig. 13.16). Any disturbance in this normal process will cause a malposition of

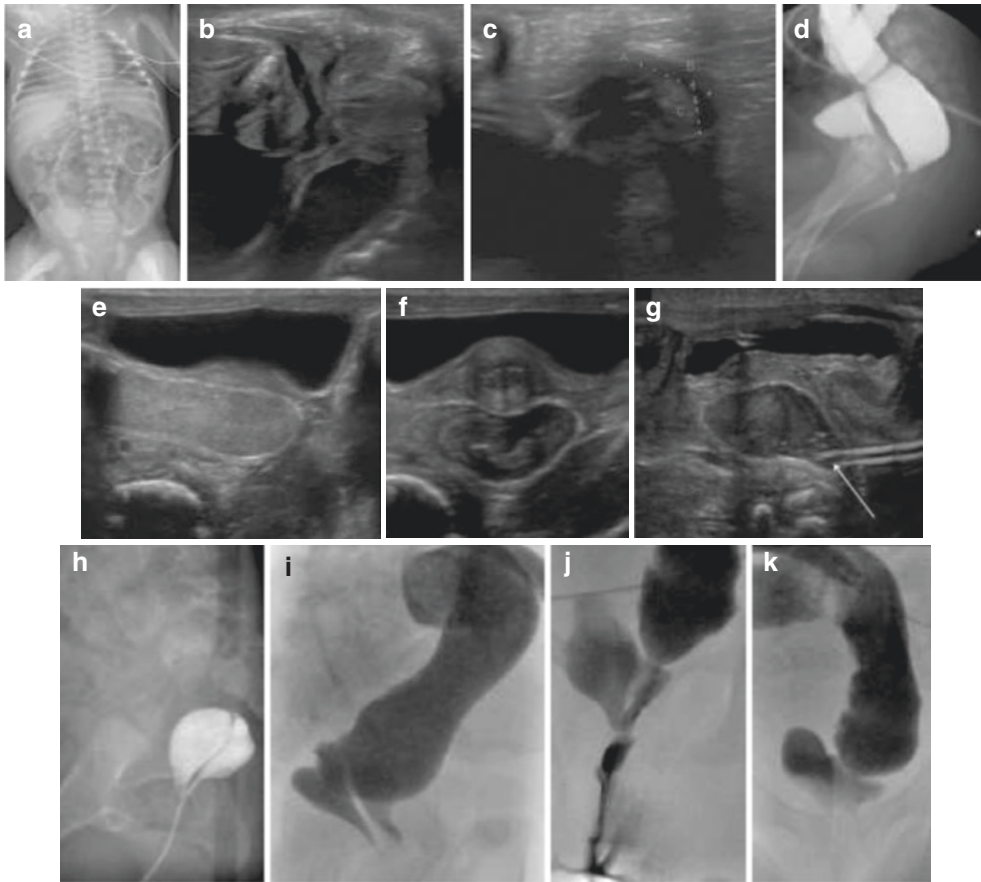


Fig. 13.15 Imaging in anorectal and cloacal malformations. (a) Male newborn with anorectal malformation and congenital cardiopathy. The torsogram also demonstrates vertebral anomalies. Emergency colostomy was performed on day 1. (b, c) Perineal US at day 7 during US colostogram (filling of colon from the colostomy with saline to outline the respective pathology) shows the high anal atresia with the well filled rectal pouch (b) and in (c) a fistula (A) from the remnant of the anal canal (B) to the urethra (C). (d) Corresponding lateral view of the fluoroscopic colostogram at the age of 3 months confirming the US diagnosis. (e–k) A neonatal girl with cloacal malformation: US shows the distended urinary bladder and rec-

tum in an oblique view (e) and an axial transabdominal section (f). After insertion of a small tube via the single orifice (arrow), the vagina and the rectum are filled, a second small catheter could be advanced into the urinary bladder (arrowhead, g). With the catheters in place an initial genitography and VCUG were performed showing the two filled structures (urinary bladder and vagina, both draining through the same canal), without contrast reflux into the rectum or the ureters (h). After colostomy a fluoroscopic colostogram shows the respective anatomy of the rectosigmoid with retrograde filling of the vagina and the urinary bladder as well as the narrow single outlet canal (i–k)

the bowel with shortening of the small bowel mesentery and secondarily a non-fixation of the gut making it more prone to twisting and volvulus.

- *Malrotation*, which refers to this abnormal lie of the bowel, can manifest early or later in life and may be also seen as an incidental finding.

Malrotation is a spectrum. The jejunum may lay in an obvious abnormal position in the right abdomen or lower but still in the left abdomen. In severe forms even the colon may be inverted, with the caecum (and the appendix) on the left side and the recto-sigmoid and the anatomically “left colon” on the right that is referred to as *non-rotation*. It is important

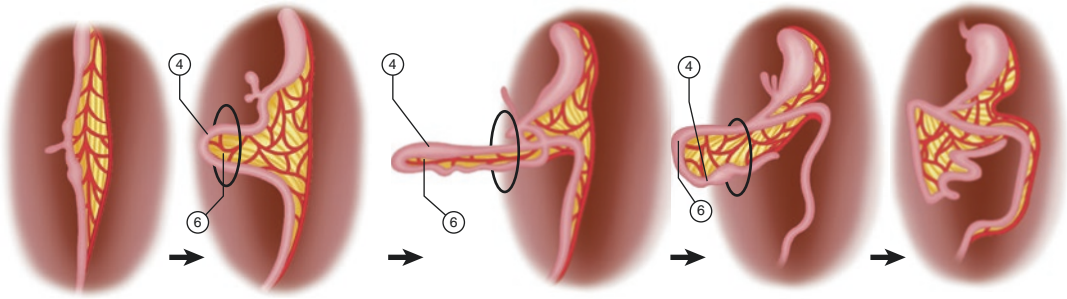


Fig. 13.16 Schematic drawing physiological rotation of bowel during development. Schematic drawing illustrating the foetal development and rotation of the bowel. (Adapted from “Human embryology, Organogenesis”,

chapter 19, digestion tract, (www.embryology.ch/ last visited January 2022)—An online course in embryology for medicine students. Developed by the universities of Fribourg, Lausanne and Bern)

not to confuse such an abnormal lie with an elongated recto-sigmoid, which is quite common in neonates and preterms and may ascend impressively high on the paramedian right side before then coursing to the left. In preterms a physiologically very mobile caecum can also be positioned quite high up in the right abdomen.

- Sonographically, it can be diagnosed by following the course of the duodenum that should pass retro-mesenterial from the right to the left upper quadrant then ascending to the duodeno-jejunal flexure, where the bowel is adherent and fixed; this course can be difficult to see due to overlying gas. Graded compression and filling of the duodenum by saline or diluted UCA may help outline the (normal or abnormal) course (Fig. 13.17). Furthermore, when using these filling techniques, one can easily observe that the small bowel loops in the left upper abdominal quadrant will fill first and with more distal bowel loops in the right side of the abdomen will be filled later with fluid. Expertise is required for such an approach.
- In many centres, fluoroscopy is still used to demonstrate the respective duodenal anatomy by an “upper GI study”. A limited amount of CA is instilled into the stomach and the passage of contrast through the

pylorus into the duodenum and proximal jejunum can be appreciated real time. The normal duodenum is C-shaped, coursing from the right upper abdomen to the left and then ascends to the same level as the pylorus to the duodeno-jejunal junction (Fig. 13.17). Technique for this fluoroscopic study is paramount and based on anatomical landmarks. This duodenal course can only be properly viewed if there is not too much CA superimposition from the stomach. In the acute scenario, an NG tube may help initially aspirate the stomach (as a too filled stomach may push down the duodeno-jejunal flexure and also obscure the third part of the duodenum), and also to control the amount of contrast instilled. Imaging of the duodenum should be performed in straight AP and also in the lateral/slightly oblique position (hence appreciating the descending and ascending limbs of the duodenum just anterior to the spine).

- An acute *volvulus* (complicating a Malrotation) is an emergency situation and must be quickly diagnosed and treated to avoid possible long distance bowel necrosis with catastrophic outcomes and severe long-term morbidity due to “short bowel syndrome” in turn leading to lifelong nutritional problems, growth retardation, liver problems and more. Acute volvulus

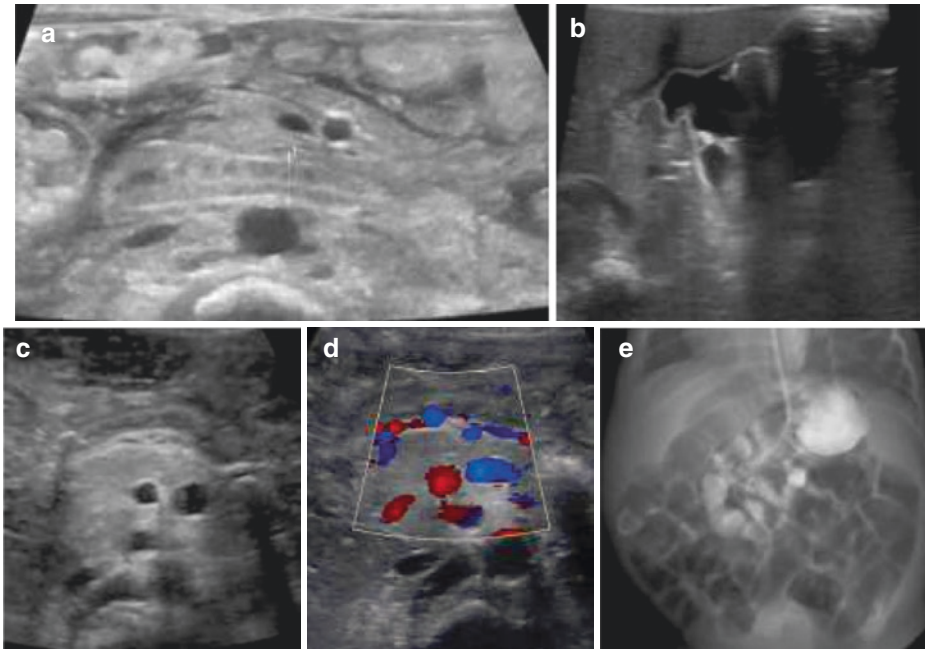


Fig. 13.17 Imaging in malrotation. (a) Axial view of the upper mid abdomen: the normal course of the duodenum (collapsed in this case due to gentle graded compression to gain access for viewing this anatomy) crossing from right to left behind the mesenteric vessels (1+...+) is demonstrated, thus ruling out malrotation. (b) Fluid filled stomach with distended proximal duodenum which cannot be followed further, but seems to take an abnormal course (due to malrotation). (c, d) Inverted position of mesenteric vessels in an axial view of the upper abdo-

men—the mesenteric vein is left in front of the aorta, whereas the mesenteric artery is right in front of the inferior cava vein (c). Colour Doppler sonography (d) helps to identify the vessels, but note that the artery is not always red and the vein not always blue; this depends on transducer angulation and scale settings (inverted or not). (e) A corresponding fluoroscopic upper GI study shows the abnormal course of the slightly opacified duodenum and jejunum (same patient as in b)

typically presents with acute onset bilious vomiting and acute abdomen which may be distended.

- The radiograph of the abdomen may show signs of a high obstruction.
- Ultrasound classically reveals the so-called “spiral sign” or “whirlpool sign”, where the mesenteric vessels twist like a whirlpool around the mesenteric root. This leads to initial venous congestion and eventually arterial vascular compromise with secondary necrosis of the small bowel. The bowel itself is twisted around the mesenteric root within this corkscrew also resulting in a mechanical high-level proximal obstruction. Particularly after gastric instillation of some saline via a feeding tube, the dilated upper obstructed duodenum can easily be

seen by US. Colour Doppler sonography will facilitate the depiction of the dilated vessels curling around the mesenteric artery (Fig. 13.18). Secondary findings such as the identification of necrotic and non-perfused bowel or ascites depend on the duration of the condition—the more secondary signs one will find, the worse is the prognosis in terms of amount of viable gut. If one has a clear diagnosis with the respective findings on radiography and US (with CDS), there should be no delay in treatment which is emergency surgery based on these investigations.

- Fluoroscopy, through an upper GI study using oral CA administration, will reveal either a complete cut off at the level of the

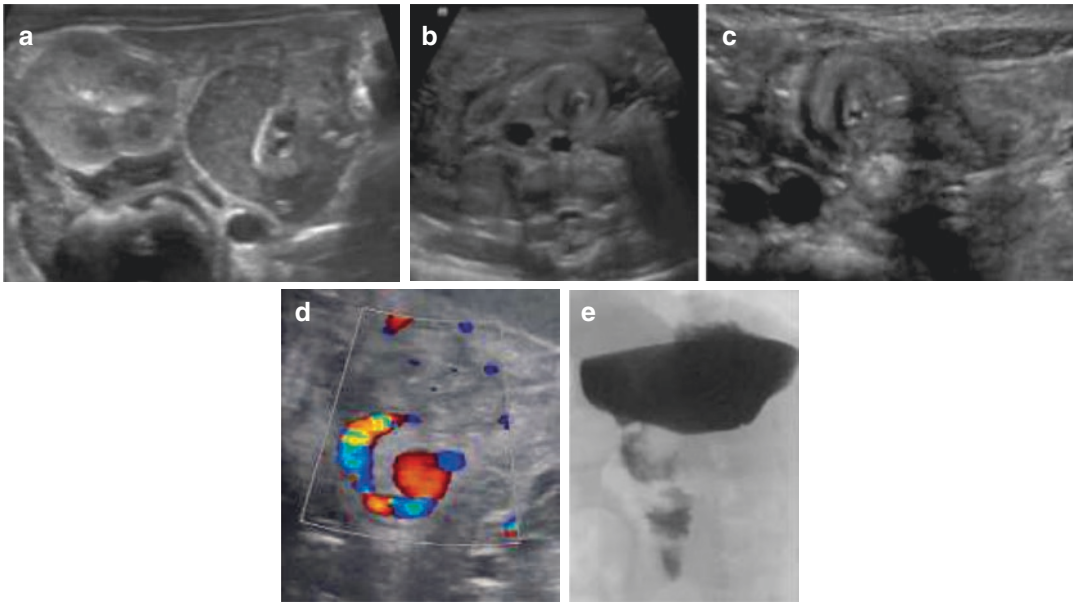


Fig. 13.18 Volvulus: Radiograph, Ultrasound and colour Doppler sonography and Fluoroscopy. (a–c) Neonate with acute onset vomiting and a tense abdomen. The distended fluid filled proximal duodenum is visualised in the right upper quadrant (a). When following this structure, one ends up in a pseudotumorous structure that has a spiral-like pattern consisting of the collapsed small bowel twisted around a central vessel (b). Slightly further inferior to this, other curling dilated vessels can be appreci-

ated resembling a “whirl-pool” appearance (c). These findings are diagnostic for an acute volvulus. (d) Colour Doppler sonography helps to convincingly demonstrate the course of the twisted vessels in this neonate with volvulus. (e) Corresponding image of the fluoroscopic upper GI study showing the course of the opacified small bowel and the typical whirl-pool like appearance of the proximal small bowel curling around the mesenteric root/vessels

third part of the duodenum (where the resulting proximal obstruction is complete) or a corkscrew appearance as the contrast passes through the narrowed twisted spiral of bowel loops (Fig. 13.18).

ation and disarrangement of bowel causing obstruction, inner hernias or even volvulus like situations.



Imaging in malrotation and volvulus consists of abdominal radiographs and US (including Doppler US) which may be supplemented by fluoroscopy. As volvulus is a real emergency, if the classical signs are demonstrated already with US, then immediate surgery is indicated without further delay caused by additional studies such as fluoroscopy.

Ladd's bands, fibrous peritoneal structures associated with malrotation, may cause malfix-

13.3.3 Duplication (Cyst), Meckel's Diverticulum and Persisting Omphaloenteric Duct

Gastrointestinal duplications are rare; the most common manifestation is a duplication cyst that can occur anywhere in the entire GI tract. These cysts exhibit the typical bowel wall structure and mucosa. They can have a connection with the gut resulting in changing of the size depending on the respective filling. Depending on size and location, they can cause obstruction and respective clinical symptoms. Bleeding can occur into duplication cysts and they can also present with bleeding per rectum.

The *omphaloenteric duct* is a remnant of foetal anatomy and connects the bowel to the umbilicus. Usually it obliterates and vanishes. Sometimes the duct persists and can cause symptoms depending on the residual structure. For example: when positioned at the umbilicus, it can cause inflammation and discharge; when situated at the gut end, it causes (Meckel-) diverticula which can inflame and present similar to an appendicitis or present with bleeding.

The congenital *Meckel's diverticulum* is the most common GI tract malformation and is a remnant of the omphalomesenteric duct (also called the vitelline duct or yolk stalk). It is rarely symptomatic in neonates, maybe detected incidentally, but may cause painless rectal bleeding if the diverticulum contains gastric or pancreatic mucosa.

- Imaging of these abnormalities is mainly through US. Duplication cysts are easily

identified. They are recognisable by the so-called “gut wall signature” exhibiting a multi-layered wall around the cyst (Fig. 13.19); there may be peristalsis associated with the peristalsis of the gut. The other aspects depend on its size and whether there is a luminal connection or not. If there is a connection with the bowel lumen, filling techniques can be helpful to prove the connection and visualise the change in size, e.g. during/after feeding.

The omphaloenteric duct is practically only visible in its distal section close to the umbilicus below the abdominal wall (Fig. 13.20)—the other sections cannot usually be clearly depicted by US nor by other modalities.

- The abdominal radiograph is sometimes performed as the initial examination in an unclear

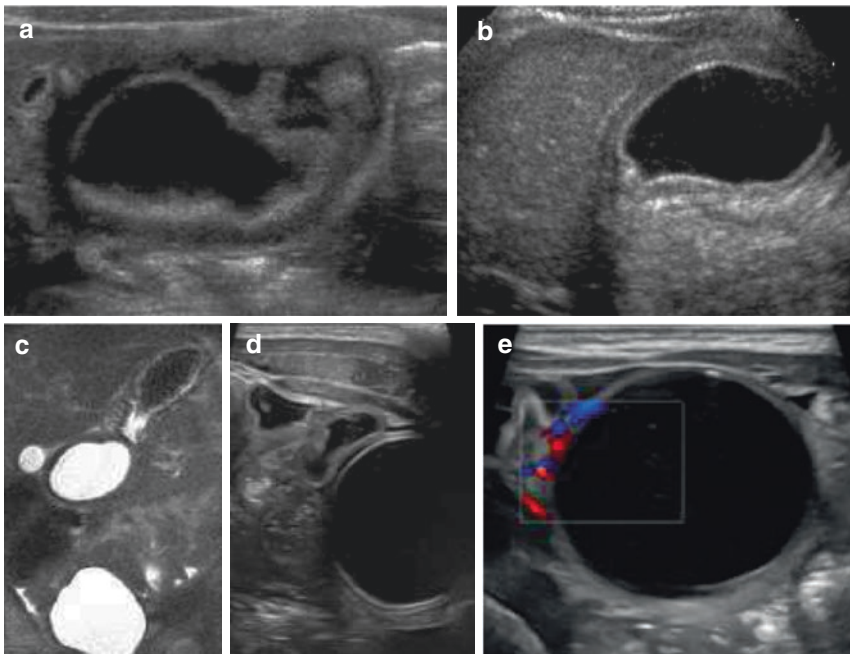


Fig. 13.19 Duplication cyst. (a–c) A neonate with vomiting after feeding with imaging depicting a thick walled cyst in the vicinity to the stomach (a); it appears to change in size, but does not contain neither air nor debris (b). The wall exhibits a gut like signature in keeping with an intestinal (gastric) duplication cyst with secondary gastric outlet obstruction. Fluoroscopically and on contrast-enhanced US no connection with the GI tract was appreciable. (c) An

MRI (feed and wrap, no contrast given) was performed (coronal T2-weighted sequence). It confirms a gastric cyst with a bowel-like wall; surgery confirmed the non-communicating gastric duplication cyst. (d, e) A huge cyst with “gut signature” of its wall obviously connected to the wall of the adjacent bowel loop (d); CDS also demonstrates the origin of its vasculature from the mesenteric bowel vessels (e) again consistent with an intestinal duplication cyst

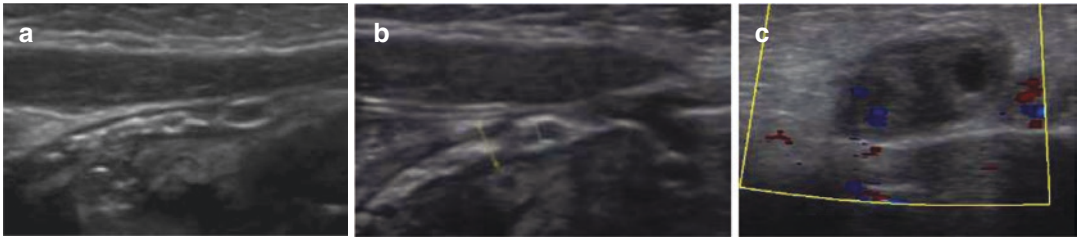


Fig. 13.20 Omphaloenteric duct remnant. (a, b) Parasagittal paramedian, slightly oblique US view near the umbilicus which was clinically inflamed: a duct-like tubular structure which contains air situated just below to the abdominal wall (but obviously inside the abdominal cavity) is demonstrated through the use of a high-resolution linear transducer (a). This is seen extending from the umbilicus to the right lower quadrant with some sort of a lumen (+...+, b). The end cannot be depicted, but probably leading towards a distal ileum loop in keeping

with a remnant of the omphaloenteric duct. (c) An axial US view (magnified high-resolution image) from another neonate. This demonstrates two symmetric tubular structures suggestive of vessels in the same location with no flow depicted on CDS. When following these paired structures, they course inferiorly to each side of the urinary bladder before diving into deeper compartments representing remnants of the paired umbilical arteries. Such findings should not be confused with a persisting urachus or a persisting omphaloenteric duct

equivocal abdominal condition that may show opacification or signs of obstruction.

- Other imaging modalities such as fluoroscopy or MRI are rarely performed—a CT for such indications is hardly ever of use and not justifiable given the radiation dose implications.

A Meckel diverticulum can sometimes be picked-up sonographically with a similar appearance of a duplication cyst in the respective location and, particularly in cases of bleeding, may demonstrate inhomogeneous layered content. However, small and deeply positioned diverticula are easily missed. The lumen may be connected to the bowel or occluded; visibility on US depends on size, content and overlaying interfering intestinal gas.

- The typical diagnostic method is Tc^{99m} pertechnetate scintigraphy (Meckel scan). However, this is only useful if the diverticulum contains gastric mucosa. As such it has a low sensitivity and specificity, and is rarely performed in neonates.

- MRI or CT is hardly ever necessary or indicated for this query in the neonatal age group.

13.3.4 Hernias: Hiatal and Diaphragmatic Hernia, Inguinal/Umbilical/and Internal Hernia

Hernias related to different structures/orifices can present with obstruction in neonates. The most commonly seen (particularly in preterm infants) are *inguinal hernias* where abdominal contents herniate into the inguinal canal due to physiological immaturity and weakness.

Another commonly appreciated hernia is the *umbilical hernia*, which, although rarely causes obstruction, they can be impressively large. This is a clinically obvious finding.

Various other *internal hernias* can occur (e.g. in connection with Ladd's bands in malrotation). These rarely present in the neonatal stages but usually posing problems only later in life.

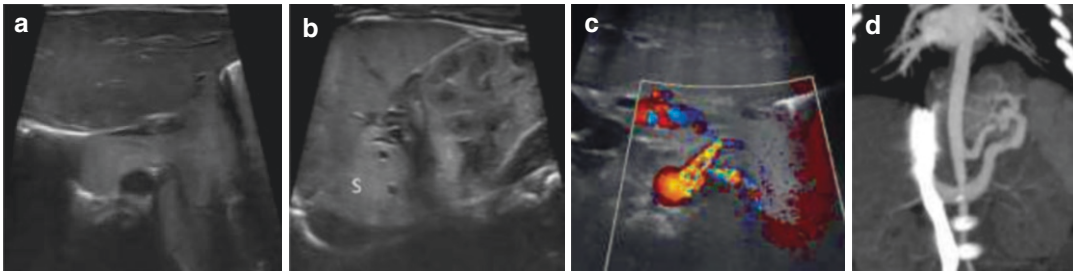


Fig. 13.21 Sequestration. (a–d) A neonate referred for postnatal evaluation of a prenatally diagnosed intra-abdominal sequestration. The postnatal US shows a thoracic and an abdominal component (a, b). CDS demonstrates the aortic origin of the feeding artery, thus

confirming a sequestration (S, c). This was then confirmed by contrast-enhanced CT (d) showing the main systemic artery arising from the abdominal aorta and the venous drainage into the left renal vein then the IVC

Diaphragmatic hernias have extensively been addressed in Chap. 10—only a few major take-away points are listed here (Figs. 13.21 and 13.22).

- Most large diaphragmatic hernias are depicted prenatally; only small defects with little clinical implications are missed prenatally or neonatally and manifest later in life (e.g. hiatal hernia with the complication of a gastric volvulus ...).
- The severity and clinical consequences depend on the size, position (mostly left sided, some right sided, rarely bilateral hernias) as well as the herniated contents (e.g. if the hernia contains the liver or stomach). These can severely impact foetal lung development and the survival chances of the neonate (related to lung hypoplasia and pulmonary hypertension).
- There is a spectrum of associated malformations (e.g. heart, spine, sequestration ...) which need to be considered and assessed (see Fig. 13.14).
- Initial imaging consists of a “torsogram” (chest and abdomen radiograph) which reveals the herniated and displaced intestines (only appreciable if filled with air) and outline of the tubes and lines, and an US of the chest and abdomen (Fig. 13.22). Further studies such as an MRI (or

rarely even a CT) are hardly ever necessary as rarely add more information, but sometimes may be helpful, confirmative or in complex cases necessary preoperatively (see Fig. 13.21).

- Further imaging depends on the associated malformations and on the pre- and postoperative course (see Chap. 6). Surgery is only performed after the satisfactory respiratory stabilisation of the neonate.

Inguinal and umbilical hernia Whereas the umbilical hernia does not pose a clinical diagnostic challenge, inguinal hernias can be a bit trickier—particularly in severely diseased neonates with generally oedematous soft tissues. The differentiation of the content (testis or in girls ovaries versus mesentery and/or bowel) will prompt an US investigation—in part to decide on the urgency of treatment/surgery. Putting it simply, a hernia containing a structure that could be vascularly compromised and that cannot be reduced needs urgent surgery. Other reasons for inguinal swelling are hydrocele/funiculocele, an undescended testis, and sometimes inguinal lymph nodes.

- Imaging by US is straightforward using high-resolution linear probes easily showing the contents. Colour Doppler sonography allows assessment of perfusion (of the bowel wall,

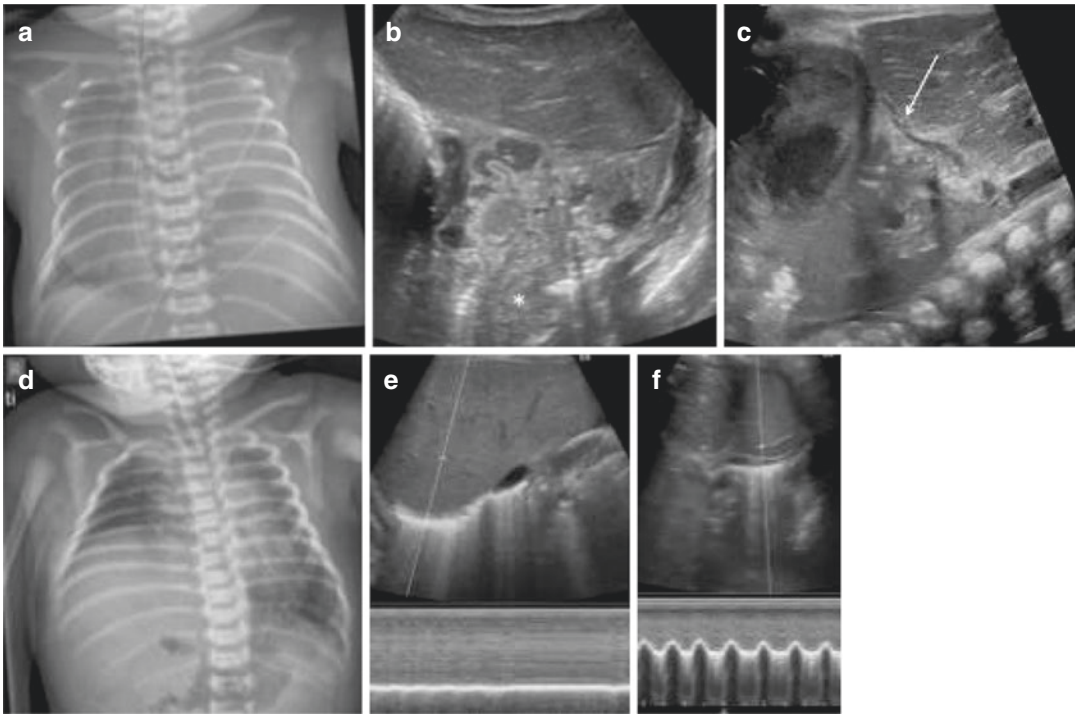



Fig. 13.22 Diaphragmatic hernia and diaphragmatic palsy. (a–c) A neonate with a prenatally recognised left side diaphragmatic hernia. This is confirmed by the initial postnatal chest radiograph (a, note the gastric tube up in the left hemithorax). The corresponding US images show that the stomach, bowel loops and also the spleen to be herniated upwards (asterisk, b). The liver is intra-abdominal (c). Remnants of the thin diaphragm are also appreciable (arrow). (d–f) Another neonate presenting with minor respiratory distress several days after birth needing CPAP support with a relatively high PEEP and high air/oxygen flow. The chest radiograph shows a high position of the right diaphragm, but no signs of a sequestration or a diaphragmatic hernia, with good (nearly over-

inflated) although asymmetric lungs (d). US reveals a high lying liver without respiratory motion of the elevated right hemi diaphragm (also documented on m-mode (e)) and without any other pathology (the inhomogeneous ventilation of the lung is normal at that age). There was a normal diaphragmatic respiratory excursion on the left side (f). All this is in keeping with a diaphragmatic palsy. Note that on the radiograph there is a high ending gastric tube but no tracheal tube demonstrating the infant is not invasively and actively ventilated. The latter support could possibly obscure the insufficient diaphragmatic motion and thus hinder the sonographic diagnosis of a diaphragmatic paralysis

the ovary, or the testis). This can be challenging particularly in preterm babies (Fig. 13.23). No other imaging is needed. Sometimes an abdominal radiograph is performed to assess for ileus may show air-filled bowel loops running into the inguinal canal a finding that should not be missed.

 Imaging of hernias consists of radiographs and more commonly US, which often (if necessary at all) is all that is required for clinicians to be able to make a management plan.

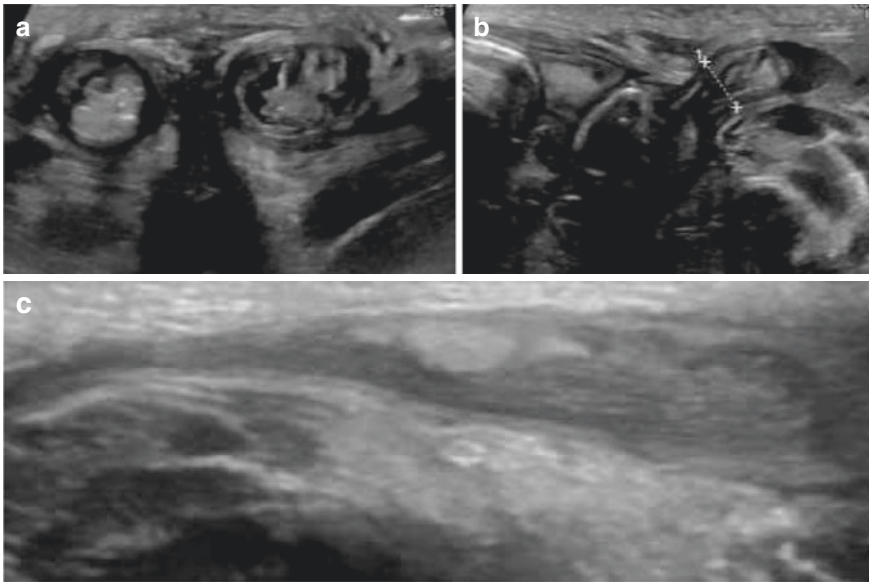


Fig. 13.23 Inguinal hernia. (a, b) An axial US view using a high frequency high-resolution phased linear transducer of both inguinal canals shows enlarged canals with typical content (bowel, ascites) on both sides consistent with bilateral inguinal hernias in this preterm infant. The oblique parasagittal view tilted into the longitudinal direction of the left inguinal canal more convincingly demonstrates not only the herniation (1+...+), but also its

intra-abdominal origin and connection (b). (c) It is important not to confuse echogenic content in the scrotum or inguinal canal that derives from a foetal meconium peritonitis with a hernia, as shown in this high frequency high-resolution phased linear transducer oblique parasagittal US view tilted into the longitudinal direction from another neonate

13.4 Congenital Malformations of Abdominal Parenchymal Organs, the Retroperitoneum and the Mesentery

13.4.1 Biliary Atresia and Its Differential Diagnosis (Neonatal Hepatitis Syndrome)

Biliary atresia presents with obstructive jaundice and acholic stools. The obstructive cholangiopathy causes progressive periportal fibrosis due to obliteration of extra and/or intrahepatic bile ducts with cholestasis, eventually resulting in biliary cirrhosis. The Davenport classification divides intra- and extrahepatic and mixed forms of this condition (see Fig. 13.24). The prevalence varies with geographical regions with the highest inci-

dence being reported in Asia. Aetiology is unknown; viral infection, genetic factors and toxins are all possible contributors. In the syndromic form (“biliary atresia splenic malformation syndrome”), it is associated with polysplenia, intestinal malrotation, pre-duodenal portal vein, absent inferior vena cava, aberrant hepatic artery and abdominal heterotaxia. Early diagnosis is essential for long-term morbidity. Early surgery (Kasai procedure), performed in the first months of life, is the only option to prevent or at least postpone liver transplantation.

Different forms and subtypes exist depending on the extent of fibrosis and involvement of intra- and/or extrahepatic bile ducts. Sometimes a cystic remnant of the duct may be present. Other conditions such as parenteral nutrition associated cholestasis, cystic fibrosis, neonatal hepatitis, or alpha-1 antitrypsin deficiency may mimic biliary atresia and its histology. Biopsy specimens from

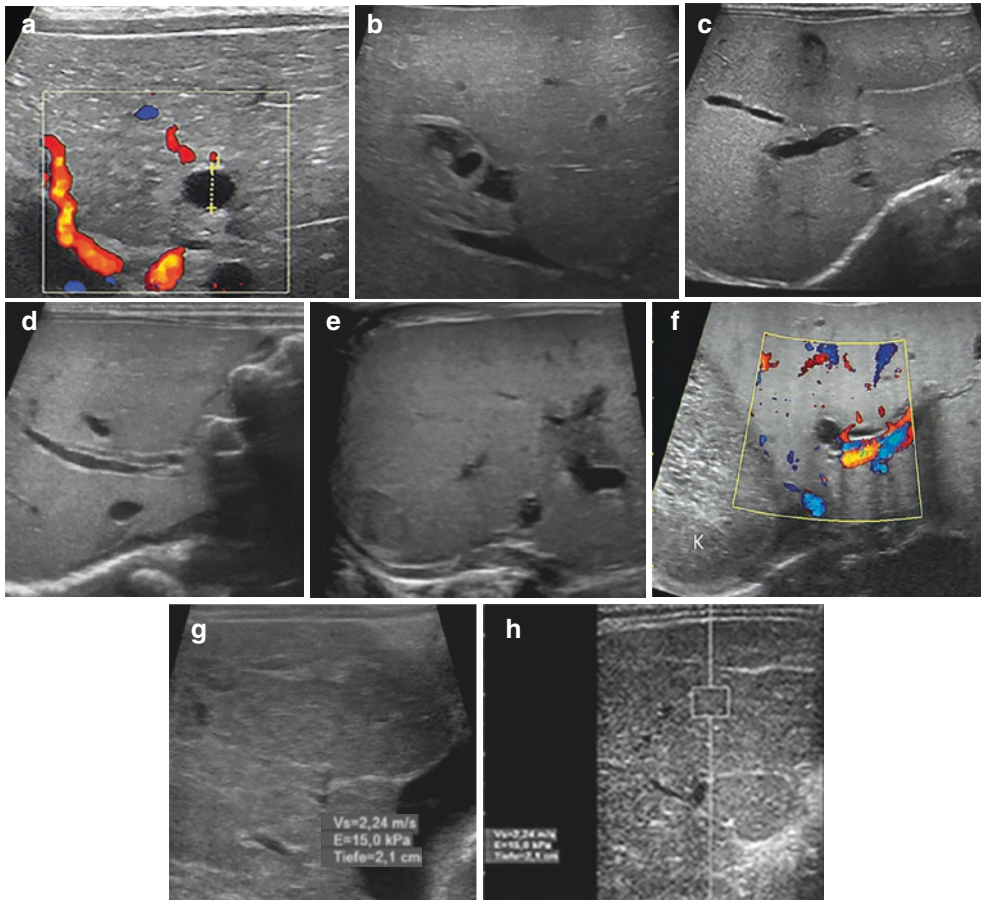


Fig. 13.24 Biliary atresia and its relevant differential diagnosis. (a) Ultrasound depicts a central cystic bile duct (or gallbladder, +····+) remnant in a neonate with eventually proven biliary atresia—no flow was appreciable on CDS within this. (b–d) Biliary atresia (US performed at 10 days of life): US depicts a small irregular gallbladder (b), an echogenic stripe anterior to right portal vein of 2.5 mm thickness (1+····+, borderline triangle cord sign) (c); an enlarged hepatic artery (d) with intraluminal echoes from movement artefact. There are no biliary ducts visible at the hilum (difficult to assure in small babies). The liver echogenicity is diffusely increased. (e–h)

Differential diagnosis in neonatal jaundice/cholestasis: (e) shows a liver with a somewhat diffusely increased echogenicity together with some periportal oedema and a hypoechoic nodule (an incidental small liver haemangioma). On biopsy these findings were proven to represent neonatal giant cell hepatitis. Other differentials include congenital liver fibrosis/liver manifestation in ARPKD (f). Of note the typical appearances of the right kidney which is also in part included on the image (K) and (g) neonatal cirrhosis (as in this neonate with tyrosinosis) with pathologic findings and markedly increased liver stiffness seen on US-elastography (h)

infants younger than 6 weeks can be indistinguishable from neonatal hepatitis and inconclusive.

- Imaging wise, US is the initial method of investigation. It may show a cyst in the area of the hepatic porta or the so-called “triangular

cord sign” (echogenic triangular structure at the porta hepatis). In advanced stages, all signs of biliary cirrhosis may be present. A small (ghost) or non-existing gallbladder can be a clue to the diagnosis—although there may be an agenesis of the gallbladder without intrahepatic or extrahepatic bile duct pathol-

ogy. Even the presence of a relatively normal appearing gallbladder does not rule out biliary atresia. Features are progressive and an inconclusive scan early in life may become more suggestive a few weeks later. Other imaging methods such as MR or CT are less useful.

- Hepatobiliary scintigraphy (applying Tc^{99m} labelled iminodiacetic acid) demonstrating the lack of bile excretion into the intestines can be supportive. However, this finding can also be present in other conditions without sufficient bile production or drainage.
- Direct visualisation of the bile ducts and the respective bile system after opacification is now considered the most reliable test for biliary atresia. Therefore, (percutaneous or intraoperative) cholecysto-cholangiography with liver biopsy is the diagnostic reference standard.
- Prenatal US and foetal MRI may reveal suggestive findings. However, this diagnosis is challenging particularly keeping in mind that a normal US study does not entirely rule out biliary atresia.

A decision making flow chart/algorithm has recently been published by the ESPR Abdominal Task Force: where there is a clinical suspicion of biliary atresia in infants with conjugated hyperbilirubinemia and acholic stools, an US should be performed examining for typical signs. If dilated bile ducts are seen, biliary atresia is ruled out and other causes for the dilatation must be considered such as biliary obstruction or an abnormality on the choledochal cyst spectrum. If US shows suggestive findings, surgery with intraoperative liver biopsy and cholangiography are recommended. If US findings are normal and one has a low clinical suspicion, weekly US (and some laboratory follow-up) should be performed. Whenever clinical signs or imaging findings persist, are equivocal or remain suspicious, a liver biopsy and an endoscopic retrograde cholangio-pancreatography/percutaneous transhepatic cholecysto-cholangiography should be performed (which usually only becomes relevant after the neonatal period) [1, 2].

Another differential diagnosis is a condition causing *neonatal liver fibrosis* named congenital hepatic fibrosis. This rare entity is part of the

spectrum of ciliopathies (hepato-renal fibrocystic disease), usually associated with polycystic kidney disease (see respective Chap. 12); the liver manifestation may even precede the renal cystic or clinical findings.

- Imaging is performed by US showing prominent echogenic periportal changes (Fig. 13.24). Early signs of portal hypertension with splenomegaly and ascites are commonly appreciable possibly also the associated renal (micro-) cystic findings. Diagnosis is confirmed by molecular genetic testing (if at all necessary) and rarely through a liver biopsy. If MRI is performed, it may show broadened periportal field with some contrast enhancement. However, CA and enhancement is usually not needed and contrast injection should be avoided wherever possible in neonates for reasons discussed above.



The investigation of biliary atresia is difficult and US does not completely exclude this pathology. The gold standard remains the contrast opacification of the biliary tree. In neonates with persisting jaundice early imaging is essential and other entities that may cause a similar clinical scenario need to be considered.

13.4.2 Choledochal Cysts and Their Differential Diagnosis

Choledochal cysts are congenital abnormal dilatations of the bile ducts. The aetiology is in part associated with ciliopathies (which are a systemic disease with different manifestations often affecting the kidneys—see respective Chap. 12). Another recognised cause for choledochal cysts are focal ectasias due to wall structure defects as well as probably effects from pancreatic secretion into the biliary system caused by a long common channel. These often worsen during infancy; however, many of them can be depicted neonatally. Large cysts particularly in the extrahepatic

portion can also rupture and can cause biliary peritonitis. As choledochal cysts interfere with bile passage and drainage, they cause a chronic inflammatory reaction and biliary fibrosis eventually leading to cirrhosis; furthermore, these infants are prone to infections such as ascending cholangitis. The most commonly used classification is the Todani classification, which classifies the types of choledochal cysts depending on the anatomical distribution (Table 13.3; Fig. 13.25). Central choledochal cysts may be mistaken for the “cyst-sign” in biliary atresia

(where the bile ducts are occluded), and that choledochal cysts may coexist with biliary atresia or biliary hypoplasia. For a thorough differential diagnosis, all other forms of biliary obstruction and dilatation need to be considered, though rare in neonates.

- Imaging heavily relies on US. The appearance varies with the type and size. One will find varying bile duct dilatation with sometimes a fusiform shape or a more defined cystic-ectatic portion (Fig. 13.26). The wall may be thickened and echogenic (particularly in older infants), and the cystic dilated parts may exhibit sludge and sedimentations within them. As the normal peripheral intrahepatic bile ducts are not routinely visible by US (or by MRI), subtle manifestations with minimal dilatation may be missed in a neonate. Additionally, the common bile duct may be obscured by overlying gas from the duodenum and the colon and can be hard to visualise. Graded compression techniques may be helpful—although they bare the risk of compression of the dilated portion of the duct and therefore obscuring the diagnosis. The presence of a common channel between the pancreatic and choledochal duct before entering the sphincter mechanism (often an underlying and/or associated condition) is usually not depicted by US. Nevertheless, a

Table 13.3 Contrast rules for abdominal investigations in neonates

Type I	Dilatation of common hepatic duct
Type II	True diverticulum of common bile duct
Type III	Choledochocele (cystic dilatation of the intrapancreatic portion of common duct, pancreatic duct drains into it)
Type IV	Type I and multiple cysts (A = intrahepatic and extrahepatic, B = only extrahepatic)
Type V	Caroli disease: segmental non-obstructive dilatation of the hepato-choledochal duct and multiple purely intrahepatic peripheral cysts arising from and connected to peripheral bile ducts (ciliopathy)

Features of choledochal cysts according to the Todani classification. Note that cystically dilated (common) bile duct representing the fibrotic type usually presents with jaundice and has a lower amylase activity in the bile, whereas the fusiform-cylindrical type (glandular type) of dilatation is usually associated with abdominal pain and higher amylase activity in the bile.

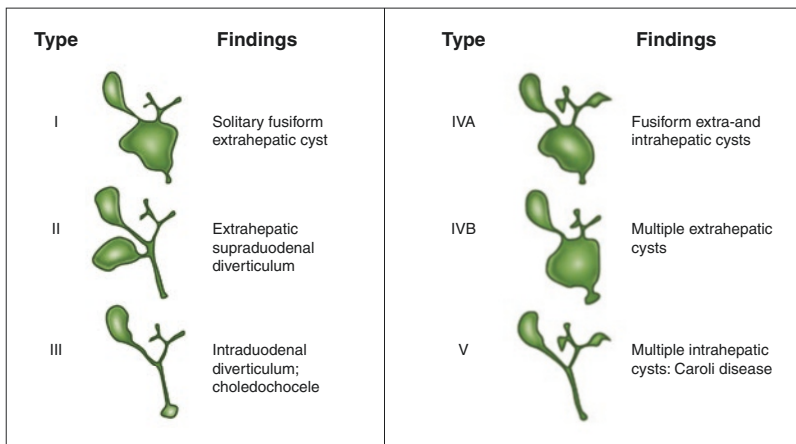


Fig. 13.25 Schematic drawing of different forms of choledochal cysts. Todani classification of choledochal cysts—the different forms and distributions are schematically shown

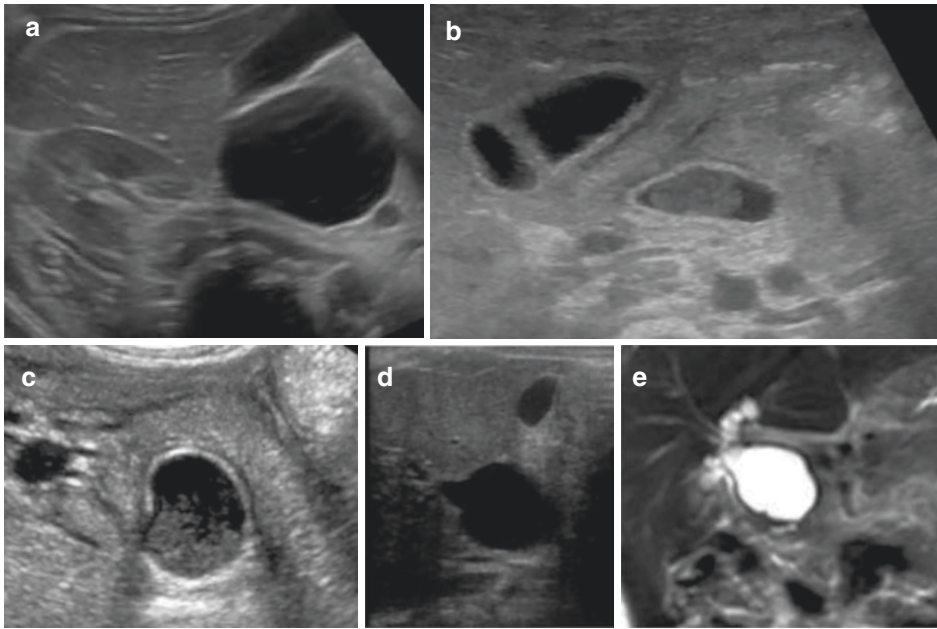


Fig. 13.26 Choledochal cysts—Ultrasound and MRI (see also Fig. 13.7). (a) US demonstrates a large cyst in the liver hilum in this neonate with jaundice. There is no dilation of the intra- or extrahepatic bile ducts. Appearances are consistent with a huge extrahepatic supra-duodenal diverticulum (Todani type II). (b, c) Sludge in a fusiform (b) or cystiform (c) dilated choledochal duct in jaundiced neonates with choledochal cysts

type I (in such cases it may be difficult to differentiate from secondary dilatation from intraluminal obstruction by inspissated sludge balls). (d, e) Ultrasound in a neonate with the foetal diagnosis of an abdominal cyst. This shows a cystic dilatation of the common bile duct and some slight irregular dilatation of hilar intrahepatic ducts. Consecutive MR-cholangiography confirms a choledochal cyst type IVa (Todani)—see also Fig. 13.7

detailed liver US is recommended in any case of (persisting) neonatal hyperbilirubinemia, in clinical jaundice of unknown origin or in the assessment of an unclear abdominal cystic structure, for example, known from foetal studies. The second modality used is MRI which nicely depicts all cystic structures and gives a great general overview. However, due to resolution limitations in neonates, small cysts and minor dilatation can be missed. In neonates it is even more challenging to visualise the pancreatic duct or the common channel. The use of biliary specific CA is not approved in neonates; other gadolinium-based CA do not increase the specificity. As the classic complications such as stone disease, infection with abscess formation or pancreatitis typically occur after the neonatal period, imaging of these aspects is not neces-

sary in this age group and therefore not addressed.

- The final diagnosis is eventually established by endoscopic retrograde cholangiopancreatography which is technically challenging, in particular, in preterms and small neonate. Often such investigation is postponed until the babies have grown a bit and the procedure easier, given that surgery is often also delayed unless this becomes clinically urgent, such as in the rare complication of choledochal cyst rupture.

Intrahepatic abscesses usually occur as a complication of a misplaced umbilical line (Fig. 13.27). Rarely other causes of neonatal hepatic abscesses occur, e.g. in fungal septicemia. If clinically suspected US, again, is the modality of choice demonstrating a complex cystic mass lesion with, more or

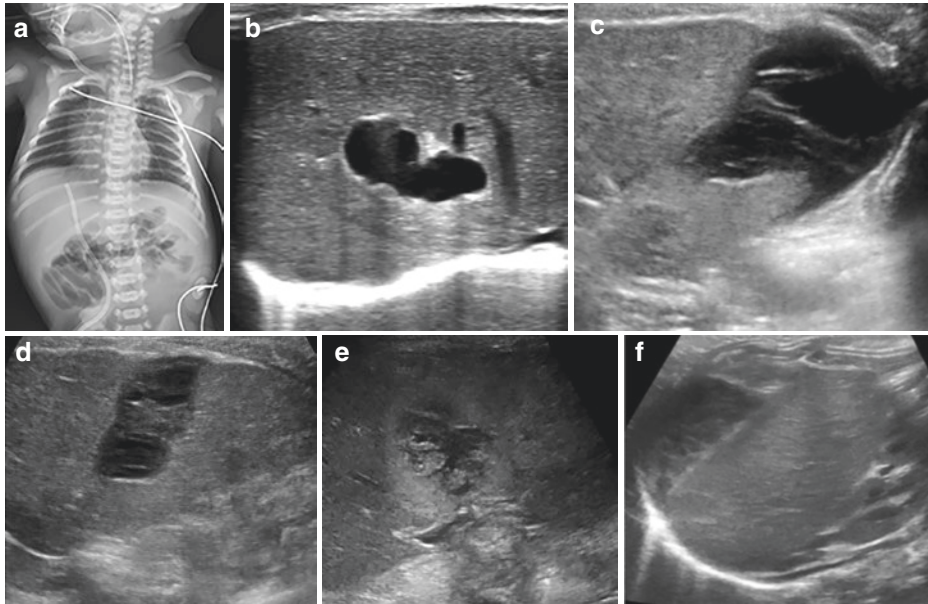


Fig. 13.27 Intrahepatic collections or abscesses and their differential diagnosis. (a, b) A neonatal torsogram reveals a wrong position of the tip of an umbilical catheter (a). The corresponding US (b) demonstrates a regional complex fluid formation. (c) Regional septate cystic formation in a neonate after a complicated Kasai operation suspicious for either a haematoma or a biloma (aspiration showed that this was a mixture of both these entities). (d) Regional septate complex fluid collection in the vicinity of the umbilical vein remnants without mass effect in a neonate after umbilical catheterisation in keeping with

focal necrosis (probably after unrecognised umbilical catheter dislocation and subsequent misplacement). (e) Intrahepatic heterogeneous fluid collection surrounded by echogenic liver parenchyma in another neonate with liver abscess/necrosis after umbilical line misplacement. (f) A neonate with some ascites and anaemia. The coronal right flank US projection depicts a complex fluid subcapsular collection in the right liver lobe, suspicious of a subcapsular haematoma (probably from birth trauma, possibly with some underlying cause such as a haemangioma, as no coagulopathy was found).

less, a membrane-like outline, no vascularisation in the necrotic centre and, sometimes, hypervascularity surrounding the abscess on CDS. In small abscesses or in fungal aetiology, this condition may only appear as small hypoechoic nodules and can then be difficult to differentiate from other focal nodular lesions seen in other systemic diseases (e.g. neonatal leukaemia, haemato-phagocytotic syndrome or septic granulomatosis). Cystic hamartoma or haemorrhagic liver cysts are also a differential diagnosis but usually not a real clinical problem. Hydatid cysts are a rarity in neonates.

Alternate aetiology for *neonatal jaundice* may be a neonatal gallstone, or the inspissated bile syndrome, particularly after antibiotic treatment or intensive care periods with fluid restriction. Rarely, a neonatal liver tumour may cause obstruction (see below).

- US will easily demonstrate the often echogenic small foci (in cholelithiasis). These, sometimes, do not demonstrate posterior acoustic shadowing. Biliary sludge is more homogenous, often less echogenic, and larger with dilatation of the bile duct if obstructive (Fig. 13.28).

Portal vein thrombosis in neonates is often asymptomatic and incidentally recognised by US performed for other indications. This is most commonly a complication related to the use of umbilical venous catheters. The thrombosis can be partial or completely occlusive and it often involves primarily the left intrahepatic portal vein initiating at the umbilical venous sinus. Grey scale US demonstrates echogenic content in the portal vein, sometimes difficult to depict with no flow on CDS

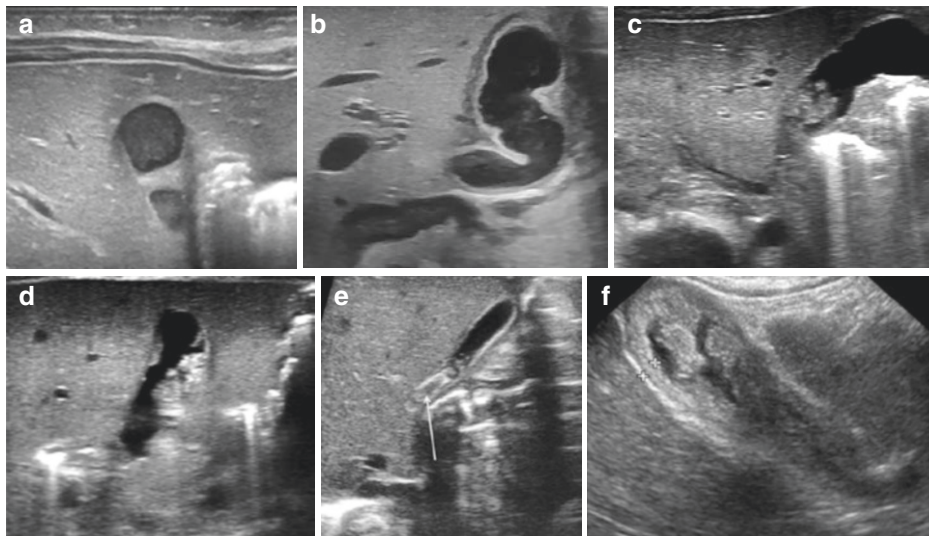


Fig. 13.28 Cholelithiasis and sludge. (a) Axial US image in the right upper quadrant displaying the gallbladder in a neonate: the gallbladder is nearly entirely filled with echoes (sludge). (b) This US image shows a similar phenomenon with a slightly thickened gallbladder wall in the NICU after resuscitation. The sludge is located in the more central parts of the gallbladder in this parasagittal oblique US view. (c, d) A neonate with Trisomy 21 and jaundice on day 3 of life: US reveals sludge balls in the gallbladder with an enlarged, thin-walled gallbladder in terms of inspissated bile syndrome. Note that some antibi-

otics as well as longer term administration of parenteral nutrition and dehydration, etc. can also cause sludge and bile stone formation. (e) A neonatal bile stone: the longitudinal high-resolution US image of the gallbladder demonstrates a single, only marginally calcified gallstone in the neck of the gallbladder (arrow). The gallbladder is partially distended with no features of cholecystitis. The biliary tree was not dilated in this neonate. (f) US image of a thick-walled gallbladder (+...+) with multiple polyps in a slightly older infant, practically pathognomonic for adrenoleukodystrophy

(Fig. 13.29). Where in doubt short interval repeat US is recommended, other flow-sensitive techniques such as B-flow or SMI can be applied, or intravenous ce-US can be performed to establish the diagnosis. However, in neonates it mostly resolves under appropriate treatment. This process needs to be monitored by regular US follow-up investigations.



US is the mainstream diagnostic tool in all hepatic conditions in the neonate where sometimes this needs to be repeated at short interval for better assessment and evidence of any progression of subtle signs. Other modalities, namely MRI or molecular imaging can help according to the specific condition suspected in line with the imaging algorithms described in the above paragraphs.

13.4.3 Splenic and Pancreatic Conditions Important in the Neonatal Period

There are a number of conditions of the *spleen* that may occur in the neonate which one has to be aware of. These rarely have serious implications. Typical entities that encountered include:

- The asplenia/polysplenia syndrome, which is commonly associated with other malformations or seen with situs inversus with the splenic tissue to the right and the liver to the left side. Where characterisation/localisation is difficult to establish the splenic tissue (one spleen or multiple splenunculi) typically lies posterior to the stomach, so localising the stomach (e.g. by filling) aids locating splenic tissue.
- Splenic cysts—often of congenital aetiology in the neonatal period.

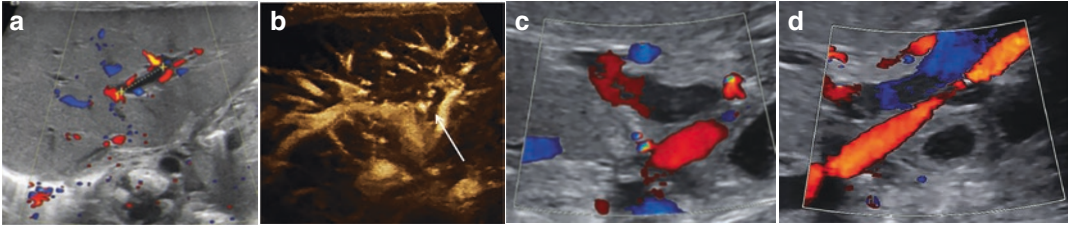


Fig. 13.29 Portal vein thrombosis. (a) Colour Doppler sonography depicts missing flow signals in the main branch of the left portal vein (a, +...+) in a neonate after removal of an umbilical venous catheter, suspicious of a partial portal vein thrombosis. (b) On contrast-enhanced US (after iv. administration of Sonovue®/Bracco, Italy) the thrombosis is confirmed evidenced as lack of any enhancement in the respective vessel segment (arrow).

Note the vivid contrasting of the adjacent left hepatic artery. (c, d) Another neonate with echogenic luminal content and missing flow signals on CDS in the portal vein consistent with portal vein thrombosis (c). Also note residual peripheral flow seen also proximal to the portovenous clot in (d) possibly a sign of the beginning of cavernous transformation, or the thrombosis causes only partial/subtotal obstruction

Table 13.4 Normal splenic size (based on US measurements) in centimetres (cm) in preterm neonates (longitudinal axis/length)—according to “Normal values. In van Rijn, Rick R. et al.: 2011, pp 636, and Kahramaner Z et al. *Pediatr Radiol* [3, 4]”

GA (weeks)	Mean length (cm)	Minimum–maximum (cm)
24–31	2.4	1.6–2
32–35	2.8	1.7–4.0
36–37	3.3	2.6–4.2
38–41	3.4	2.4–4.9
Term—3 months	4.5	3.3–5.8

- Hamartomas (rarer).
- Focal lesions such as infiltration in systemic diseases or fungal infection (e.g. candida septicemia). These typically are multiple and more appreciable with higher frequency probes.
- A splenunculus with the differential diagnosis of splenogonadal fusion; the latter condition needs to be mentioned but is extremely rare.
- Splenic infarcts; these are rare in neonates even in infants with coagulopathies. Sometimes these are seen after surgery or in association with cardiac malformations.
- Lymphangiomatosis in Gorham Stout disease. The splenic manifestations of this conditions do not usually manifest in the neonatal period.

The spleen is usually imaged by US, rarely an MRI is necessary. Splenic size in the neonate is typically measured by its maximal longitudinal diameter, volume calculations may be cumbersome and very much depend on the shape (therefore less useful in daily practice). The spleen in neonates is tilted obliquely making measurements in the sagittal/coronal section as oriented

to the body may be misleading. In term neonates (up to 3 months of age), the long axis diameter should range between 3.3 and 5.8 cm (median = 4.5 cm) (Table 13.4). Typical US findings in the various entities are:

- In uncomplicated splenic cysts (usually epithelial cysts) anechoic contents with thin, sharp margins (dysontogenetic, possibly as part of a systemic cystic disease) (Fig. 13.30).
- Hamartomas may be cystic or solid tumour-like lesions (Fig. 13.30).
- Focal nodular lesions have different appearances on US, usually hypoechoic (Fig. 13.30)—(echogenic angiomyolipoma or haemangioma occur beyond the neonatal age).
- Polysplenia demonstrates multiple nodular small abutting spleens, often closely grouped together (Fig. 13.30).
- A splenunculus is an additional small spheric spleen next to the normal main organ, exhibiting the same echogenicity as the spleen and thus usually easily differentiated from lymph nodes or other masses such as an infra-

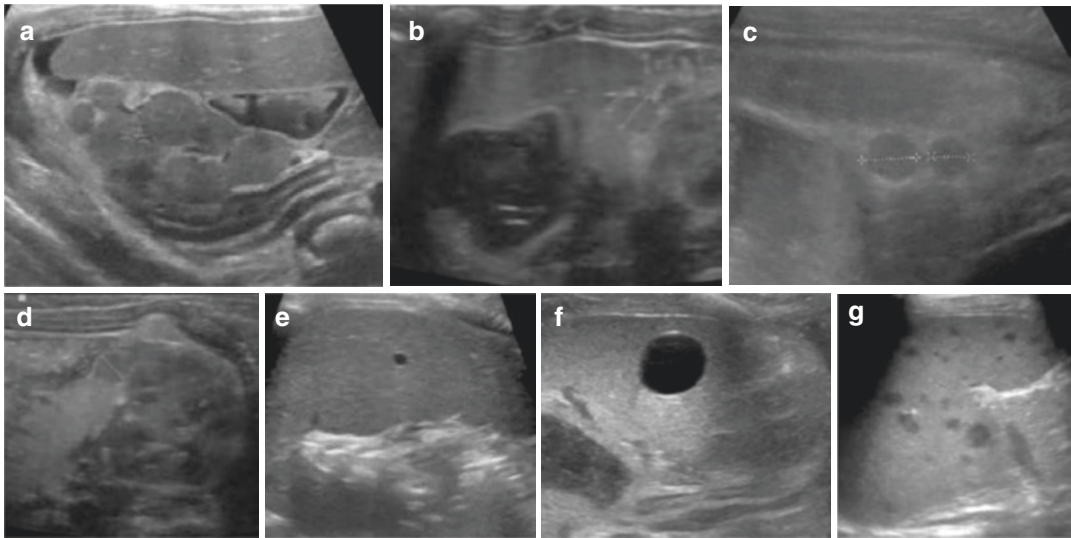


Fig. 13.30 Splenic pathology in neonates. (a) US of the right upper quadrant, axial section in a neonate with situs inversus: below the spleen (and some ascites) multiple nodules are detected that exhibit an echogenicity as splenic tissue, consistent with polysplenia. Also note the neonatally physiological large adrenal gland. (b–d) Ultrasound images of splenunculi (accessory spleens, +...+) in different locations adjacent to a normal spleen. (e, f) Incidental US finding: US depicts a tiny (e) and a

larger (f) splenic cyst in two neonates imaged for other reasons. (g) A longitudinal US image of the spleen depicts scattered mixed echogenic mainly hypoechoic lesions in an immunosuppressed infant which progressed over the course of days—in keeping with disseminated infection with splenic (micro-)abscesses. These typically are secondary to fungal infection and often calcify with later stages of healing

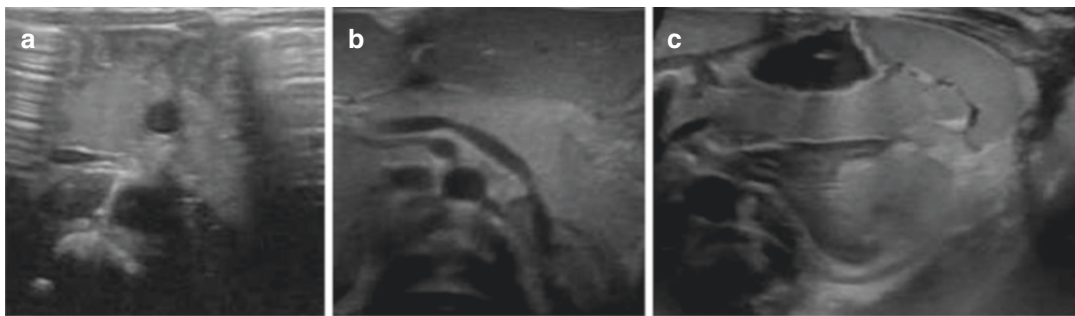


Fig. 13.31 The neonatal pancreas. (a–c) The normal neonatal pancreas: initially, due to overlying gas, only parts of the pancreatic head and body can be visualised (a) in spite of graded compression. After distention of the

stomach (b) a good sonographic window is provided allowing the visualisation of the entire pancreas (b, c). Note that the spleen can be used as a window to access the pancreatic tail (c)


diaphragmatic sequestration (Fig. 13.30). This is an extremely common finding.

- Splenogonadal fusion, though extremely rare, can cause diagnostic challenges on US; in these cases a feed-and-wrap unenhanced MRI study exhibiting the typical testicular signal may prove helpful.

The *pancreas* is a rare imaging concern in neonates. On US it appears as a rather homogenous slightly echogenic organ (Fig. 13.31). In newborns the AP diameter varies between 0.5 and 1 cm.

Relevant conditions that the imager should be aware of are:

- *Annular pancreas*: incorporation of the duodenum within the pancreas during fusion of the pancreatic elements—usually missed in the neonatal age as hardly depictable by US imaging due to duodenal gas. Indirect signs such as a diameter change of the orally distended duodenum with tapering at the pancreatic head may suggest this diagnosis (see Fig. 13.10).
- *Pancreas divisum*: here one finds separate ventral and dorsal pancreatic components secondary of non-fusion of these elements that develop separately. This results in two different draining ducts that drain into the papilla major and minor, respectively. On imaging (US or MRI) two plate-like bars of typical pancreatic tissue separated by an anechoic plate-like layer may be depictable. In the neonatal period, this condition, as well as the spectrum of anatomical variations of the pancreatic duct system, is not reliably assessable by US or MRI although these modalities can be complementary.
- *Pancreatitis*: this is rare in neonates, hardly ever necrotic or haemorrhagic. On US, the findings may be completely unremarkable, often changes in echotexture manifest in a delayed fashion and sometimes only appreciable in retrospect.
- *Pancreatic cysts*: are rare and usually uncomplicated. If localised in the pancreatic head, a choledochal cyst should be considered.
- *Pancreatic tumours*—see below in the respective section.

 US is the main diagnostic tool for imaging the neonatal pancreas and spleen, sometimes complemented by MRI. Usually only minor or irrelevant findings such as dysontogenetic or epithelial cysts or an accessory spleen are encountered.

13.4.4 Vascular Variations/ Pathology, Retroperitoneal Anomalies and Miscellaneous Other Conditions

Many of the abdominal *arteriovenous malformations* (AVMs) manifesting in the liver in neonates show heart failure, anaemia, hepatomegaly and portal hypertension. AVMs have no neoplastic tissue, no growth potential and do not regress.

- Imaging features may be quite similar as haemangiomas but often show only poor demarcation and a cluster of enlarged, tortuous vessels without the appreciation of a focal parenchymal mass. On Doppler sonography they exhibit high-velocity arteries and veins with low arterial resistance.
- Contrast dynamics (both on ce-US and on dynamic ce-MRI) are different from haemangiomas—with rapid arterial enhancement, quick wash-out of the nidus and early hepatic venous drainage (no progressive enhancement and CA retention). The differentiation against *congenital arterio-portal fistulae* (an intrahepatic connection between the hepatic artery and portal venous system) is achieved, as the latter generally exhibits only solitary connections (see Fig. 13.8).

In *portosystemic shunts* blood is shunted to the systemic circulation from the portal system without circulating through the liver veins; it can be intra- or extrahepatic; congenital or acquired.

These portosystemic shunts derive from aberrant development of the foetal abdominal vasculature, with persisting foetal connections and/or abnormal closure of the usual normal vessels or agenesis of some vessels.

The *Abernethy malformation* (an extrahepatic portosystemic shunt) is a congenital malformation

of the splanchnic circulation caused by persisting embryonic vessels with the portal vein draining pre-hepatically into the IVC or another vessel of the systemic circulation with a resulting lack in hepatic normal porto-venous perfusion. This impacts liver metabolism possibly causing hepatic encephalopathy and in the liver it may be associated with focal nodular hyperplasia, hepatoblastoma and eventually also hepatocellular carcinoma although these serious sequelae manifest later on in life. Other reported associated anomalies are biliary atresia, cardiac malformations and polysplenia.

These shunts or AVMs need to be differentiated from vascular anomalies where, e.g. pulmonary veins connect with the portal vein, and a *persisting venous duct* (ductus venosus—which is normal in the first weeks of life but could persist secondary to an underlying liver disease. Rarely this persists secondary an abnormal wall of the venous duct preventing its closure) (see Fig. 13.9).

- On imaging, particularly the type 2 extrahepatic portosystemic shunts pose a challenge on US. In the scenario of a neonate with liver disease, a small portal vein of a decreasingly small liver with poor visibility of the intrahepatic portal vein branches and with increased hepatic arterial flow should be suggestive. The intrahepatic portosystemic shunts are seen as single or multiple enlarged, tortuous vessels forming aberrant connections to the hepatic veins. They show turbulent biphasic or triphasic waveforms on spectral Doppler even in the portal vein (due to the impact of the hepatic venous flow with cardiac pulsations).
- The detailed anatomy of these intra- and extrahepatic shunts is best imaged by contrast-enhanced studies (ce-MRI, ce-CT, ce-US).

A *pre-duodenal portal vein* is a rare congenital vascular disorder originating from an incorrect formation of the foetal vitelline veins. This may be associated with heterotaxy or polysplenia syndromes, duodenal atresia, biliary atresia and annular pancreas.

A *persisting left IVC* is rare and may only be in part a duplication (“double IVC”). These often drain at the level of the renal vein into a normal single upper retroperitoneal IVC. In *azygos con-*

tinuation, the hepatic portion of the normal IVC is usually atretic and the blood drained upwards through an enlarged persisting azygos or hemiazygos vein. All these conditions may be part of a more complex vascular malformation or even a syndrome, some of which are explained by early embryonal insults to some vessel portions with establishment of an alternate circulation. In *situs inversus*, the location of the main vessels will appear abnormal; the aorta to the right side of the patient midline and the IVC to the left.

Another entity is a narrowed (or *retro-aortic* course) *left renal vein* possibly with consecutive venous drainage obstruction from kidney or the left ovary—these conditions are addressed in Chap. 12.

Mid-aortic syndrome represents a narrowed, stenotic abdominal aorta (= abdominal aortic coarctation) which could also potentially demonstrate some tortuosity. Histologically, one finds intimal and sub-intimal fibrosis and fragmentation of the elastic media. Consecutively, there may be perfusion deficits of the affected organs and dependent body areas as well as hypertension. Tapering of the abdominal aorta may also be caused by steal phenomena (e.g. in arteriovenous shunts, liver haemangiomas or large liver tumours). These must be actively searched for and US assessment should include a full Doppler spectral analysis to further support the correct diagnosis by demonstrating typical pre-, intra- and post-stenotic Doppler wave forms in the aorta and the dependent organs and compartments.

In neonates most of these entities are identified sonographically either because of a suspicion on prenatal examinations, or found incidentally, e.g. when imaging for elevated liver enzymes, for neonatal cholestasis or when performing a baseline study in a syndromic patient. Occasionally, postnatal clinical symptoms such as jaundice, ascites, elevated blood pressure or obstruction necessitate imaging.

- Ultrasound with CDS (possibly enhanced by UCA = CEUS) should characterise the anatomy and may also help with sub-classifying the type of malformation (e.g. in Abernethy malformation there is a type I, which is an

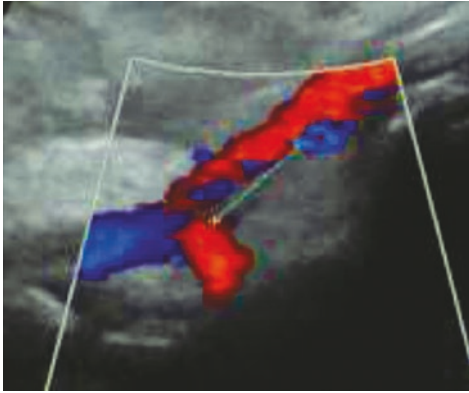


Fig. 13.32 Iliac vein thrombus. Colour Doppler image of an iliac vein thrombosis after femoral peripheral venous catheter in a 10-day-old preterm neonate (+...+)


end-to-side shunt where the splenic vein and the superior mesenteric vein drain separately into the IVC, and a type 2 where there is a common single shunt trunk connecting these vessels).

- To extensively visualise the entire vascular anatomy, MRI or CT angiography can be performed. This is often postponed to the post-neonatal period if not of urgent relevance for active management decisions.

The *manifestations of systemic diseases* in abdominal organs (e.g. tyrosinosis causing liver cirrhosis, glycogenosis and other storage or metabolic diseases) are discussed in the respective dedicated chapter.

Variations in vessel course and number (such as accessory hepatic artery, or a hepatic artery or branch originating from the mesenteric artery) are too numerous and beyond the scope of this chapter.

Rarely other, mostly acquired, vascular pathologies need to be evaluated. Occlusion or thrombosis of large vessels, which occur mostly after either a venous catheter or an interventional procedure/heart catheterisation (Fig. 13.32) are of particular importance.

 Ultrasound is the mainstream modality in evaluating vascular anomalies in the abdomen. This may be augmented by cross-sectional angiography as guided by the US findings if of acute relevance. Otherwise, assessment by other modalities can be postponed to a later age. For fully understanding vascular malformations and anomalies an in-depth knowledge of the complex foetal development of the abdominal vessels is essential.

13.5 Acquired Conditions in the Neonatal Abdomen

13.5.1 Hypertrophic Pyloric Stenosis and Pylorospasm with Respective Differential Diagnosis

Hypertrophic pyloric stenosis (HPS) can occasionally present in the neonatal period though this entity typically manifests itself slightly later at around 4–6 weeks postpartum. It is more common in males. Neonates presenting with non-bilious projectile vomiting suspicious of hypertrophic pylorus stenosis will need imaging.

- Imaging consists of US, which reveals a thickened and elongated pyloric structure with a thickened circumferential muscle and a narrowed lumen. Particularly in preterm infants, the classic full measurement criteria of pylorus thickness and length/diameter may not be achieved (length of 15 mm on longitudinal view, single wall thickness of 3 mm and full wall thickness of 10 mm on transverse view) simply because of the shorter duration of the disease and the actual smaller size of the infant. The morphology of the pylorus will still appear typical with a thickened wall and diagnosis can be made by observing real-time gastric empty-

ing after filling the stomach with fluid (tea or saline in some centres). Visualisation and actual gastric emptying can be helped by positioning the neonate to the right side. Real-time observation is also helpful for differentiation of HPS from *pylorospasm* which will show relaxation and opening of the pyloric canal and the smooth passage of gastric contents through the pylorus after some time of observation. In pylorospasm, the canal is not usually elongated but during the spastic period exhibits muscular thickening (Fig. 13.33).

If the scan excludes HPS, the study must be completed by assessing for other conditions with similar symptoms including the gastro-oesophageal junction for hiatal hernia as well as the relationship of the mesenteric vessels and, as best, the appearances and course of the duode-

num for congenital duodenal anomalies or malrotation. Other rarer pathologies presenting with vomiting in the upper GI tract such as a duplication cyst should also be detected. Sometimes, a complementary fluoroscopic examination may become necessary.

Another cause for thickening of the pylorus and sometimes also the gastric wall is the administration of the drug Indomethacin typically given as a treatment for patent ductus arteriosus. This thickening tends to spontaneously vanish as soon as the medication is withdrawn. Sonomorphologically no significant differences from the above-mentioned conditions can be seen.

Besides pylorospasm, *gastro-oesophageal reflux* is the most common differential diagnosis for early vomiting. This can only be diagnosed if the stomach is filled and by observing the gastro-oesophageal junction after feeding. Some provo-

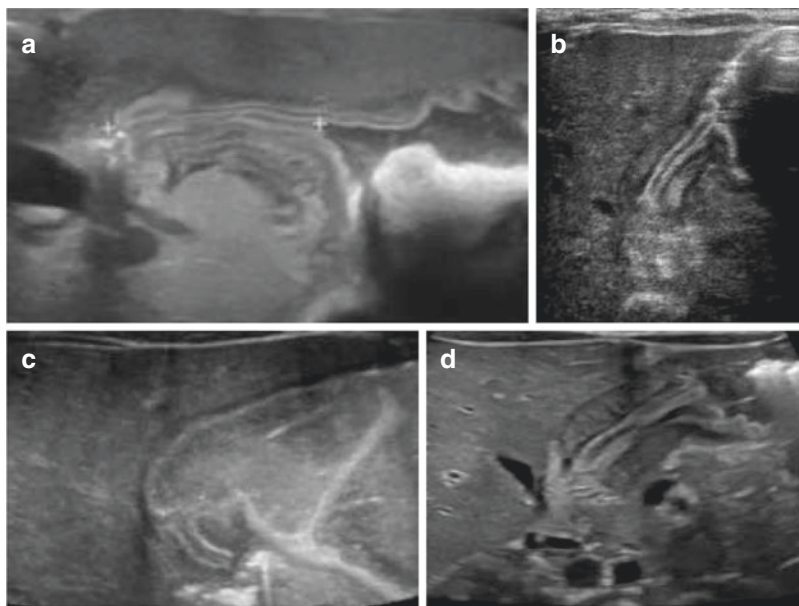


Fig. 13.33 Neonatal hypertrophic pyloric stenosis (HPS). (a) Longitudinal US image of the pylorus with a high-resolution linear transducer in a preterm infant shows an elongated pyloric canal (+ +) but without wall thickening or “pyloric shoulder” in a poorly filled and non-distended stomach. This is not to be confused with hypertrophic pyloric stenosis. (b, c) Longitudinal US image of the pylorus with a linear transducer (b) demonstrating some thickening of the pyloric wall and an elongated pyloric canal. Measurements, however, may not reach the cut off values

for hypertrophic pyloric stenosis in young neonate. After filling of the stomach and positioning manoeuvres one can observe only little opening and shortening of the canal without sufficient passage of gastric content into the duodenum (c), thus indicating a manifest hypertrophic pyloric stenosis considered in an early stage. (d) Longitudinal image of a “full blown” hypertrophic pyloric stenosis with marked wall thickening and an empty duodenal bulb. Note the normal position of the mesenteric vessels seen just deeper to the thickened pylorus

cation manoeuvres are also helpful. Gastro-oesophageal reflux, as long as not resulting in failure to thrive or malnutrition, is not necessarily considered disease but more often considered some kind of immaturity. This is handled by supportive measures without the need for further studies or aggressive treatment. Therefore, additional imaging will usually become indicated only after the neonatal period (e.g. ph-metrie, fluoroscopy/barium swallow) when the above measures are not enough. The combination of

gastro-oesophageal reflux with hypertrophic pyloric stenosis is known as “Roviralta syndrome” and particularly occurs in infants with neurological impairments.

- On sonography this entity appears as flow of the gastric content in an inverted direction into the more or less dilated distal oesophagus. Depending on the duration, clearance and distension, some objective grading is achievable (mild, moderate, severe) (Fig. 13.34). If the

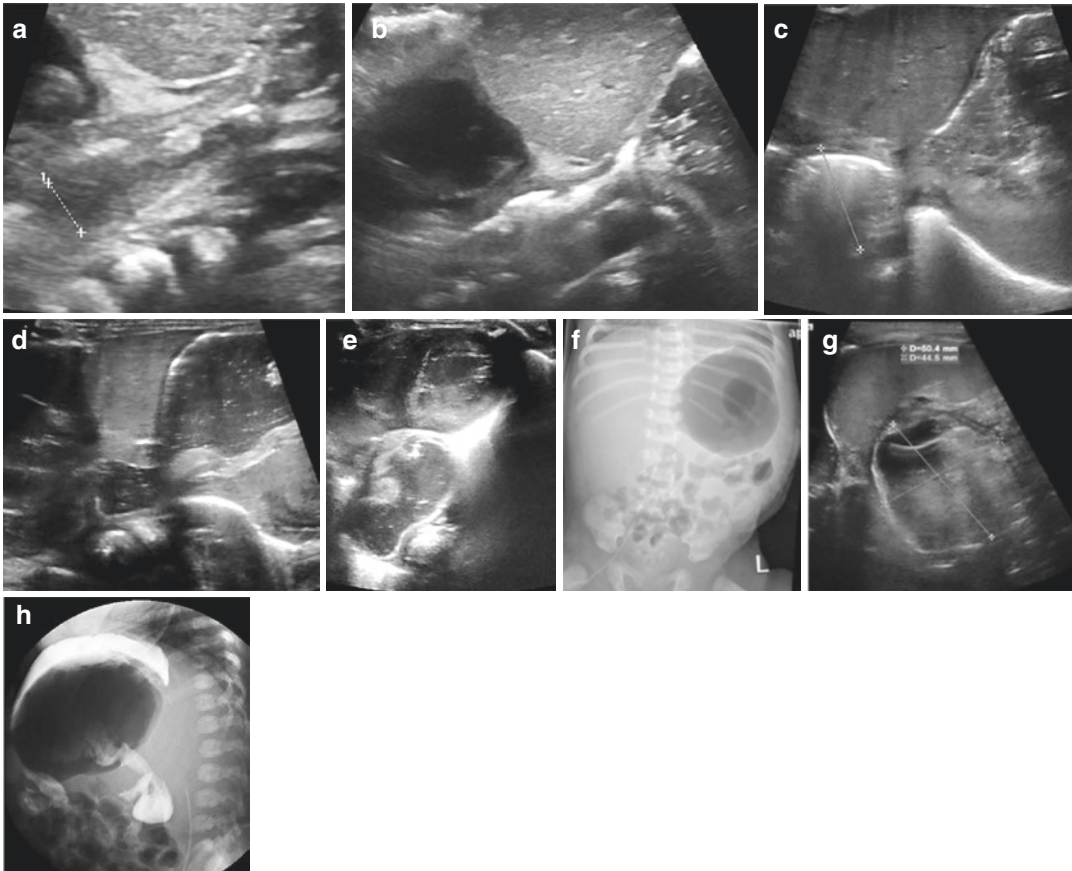



Fig. 13.34 Gastro-oesophageal reflux, hiatal hernia and gastric outlet obstruction. (a, b) Paramedian, slightly oblique, sagittal US view through the gastro-oesophageal junction in a neonate with vomiting after feeding demonstrating dilatation and fluid content of the distal oesophagus (+...+) proving gastro-oesophageal reflux (a). Briefly afterwards only some air is visualised and the oesophagus is emptied again in keeping with a short lasting refluxing episode. Note that the stomach is well filled and the gastro-oesophageal junction is short and relatively straight. (c–e) Another neonate with severe vomiting and

feeding problems: initially US depicts an air-filled formation (+...+) at the gastro-oesophageal junction (c). After additional feeding with tea the gastro-oesophageal junction is more clearly outlined (d) with an increasing fluid filled cyst-like thick-walled formation intrathoracically above the stomach consistent with a hiatal hernia (e). (f–h) Gastric duplication cyst in a neonate: the respective radiograph (f) and US image (g) exhibit a large cystic structure (which on US is not the stomach, + +). The corresponding fluoroscopy (oblique projection) confirms a communicating gastric duplication cyst (h)

dilatation is severe, a sliding hiatal hernia should be considered and meticulously observed for. Cine-clips are helpful in demonstrating this and also very useful for the conspicuous documentation of the reflux itself.

Achalasia can also be appreciated on US although this is difficult. Traditional fluoroscopy (a barium meal/upper GI study) can be helpful and usually is the method of choice in this clinical suspicion.

 Hypertrophic pyloric stenosis is not commonly seen in the first 3 weeks of life but can still happen. The commonest reason for vomiting in the first few months of life is gastro-oesophageal reflux. Ultrasound is the imaging modality of choice if such conditions need to be assessed and sometimes immensely benefits from filling techniques also allowing for functional assessment (e.g. gastric emptying) or the depiction of hiatal hernias.

13.5.2 Necrotizing Enterocolitis (Including Pneumatosis and Perforation), Neonatal Colitis and Respective Differential Diagnosis

Necrotizing enterocolitis (NEC) is a severe abdominal inflammation which typically affects the preterm cohort. This is also seen in other specific risk groups such as term newborns with asphyxia or in infants with congenital heart disease. Aetiology is multifactorial and quite complex and thought to include a combination of the presence of immature mucosa (with reduced bowel peristalsis possibly with distension), hypoperfusion, the immune response to innate commensal bacteria and the ease of translocation of bacteria resulting in inflammation of the bowel wall. The mucosa can become gangrenous, cause necrotic bowel loops and lead to perforation with peritonitis. The condition can quickly progress to

systemic infection, multiorgan failure and death. The clinical manifestations are nonspecific particularly in the early phases of the disease. Laboratory assessments show an inflammatory picture, feeding is not tolerated, the abdomen appears distended and meconium passage can be delayed.

- Imaging normally starts with an abdominal radiograph which can demonstrate thickened bowel walls or fixed dilated loops. More specific findings include mural gas (intestinal pneumatosis) appearing as linear or round small gas bubbles in the thickened bowel wall (Fig. 13.35) and the presence of portal venous gas over the liver. In case of a perforation, free peritoneal air can be depicted in a supine projection with classical findings such as the “football sign” if this is severe. Small volumes of air can be better detected by a cross-table view or a radiograph in the lateral decubitus position, although the latter necessitates turning an unstable sick neonate that is not ideal (Fig. 13.35). If the bowel is only fluid filled, these signs may be lacking as only fluid and meconium are spilled into the peritoneal cavity at the site of the perforation.
- The other major imaging modality that can assist with assessing the bowel is US. Targeted bowel imaging should always be complemented by a full abdominal survey. In the early phases of the disease US may show bowel wall thickening, sometimes accompanied by the loss of appreciation of stratification of the bowel wall (dependent on the transducer availability and frequency), some ascites, and on CDS hyperaemia of the bowel wall and the mesenteric vessels (Fig. 13.35). With progression, the perfusion may be reduced and eventually becoming absent in necrotic segments (Fig. 13.35). Bowel wall gas (intestinal pneumatosis) can be visualised as small echogenic bubbles within the bowel wall (Fig. 13.35). One would need to magnify and use the highest possible resolution to differentiate intramural from intraluminal gas which can be challenging. Gas bubbles should be actively looked for in the

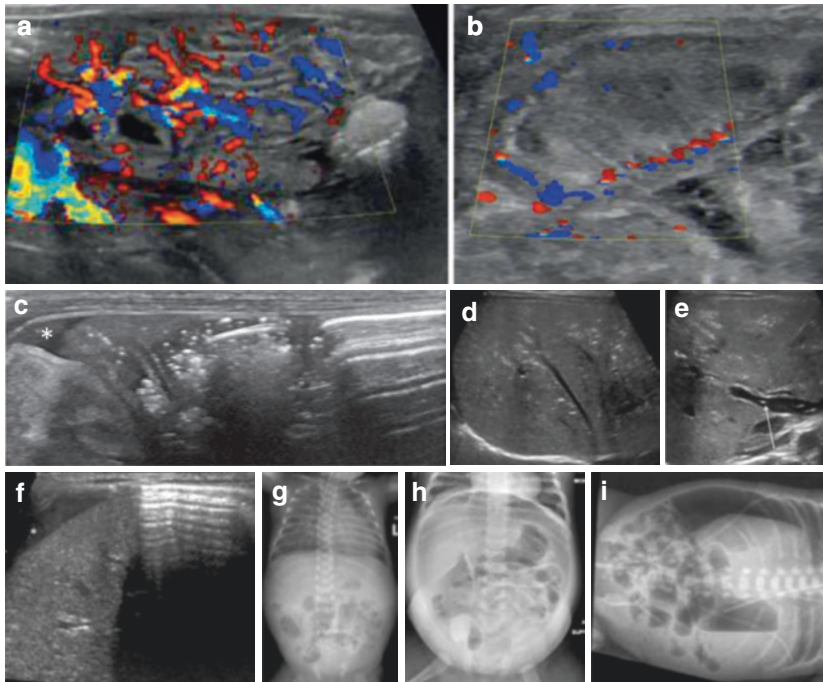


Fig. 13.35 Necrotizing enterocolitis (NEC), pneumatosis and perforation/free air. (a) Colour Doppler sonography in a preterm neonate with suspected NEC shows vivid hypervascularity of the gut wall often seen in early stages of NEC. (b) With time the bowel gets distended, the wall oedematous and hazy, and the vascularity decreases—as a sign of progression of the inflammation (referred to as “segment at risk”). (c) Preterm neonate with NEC: this high-resolution linear transducer US image shows echogenic pixels in the bowel wall consistent with intestinal pneumatosis. Note that US is often more sensitive towards early findings than radiographs. Also note the small amount of complex ascites near the right flank (asterisk). (d, e) Echogenic dots in the liver parenchyma (d) and some floating echogenic dots in the central portal vein (e) at the liver hilum (arrow) in keeping with porto-venous and hepatic pneumatosis (i.e. when the intramural air

bubbles arrive from the bowel wall at the liver). To prove that this is really gas/air, spectral Doppler can be applied which then shows the typical gas spikes. (f) “Curtain phenomenon” on US: air reverberation echoes are depicted in front of the liver without any other containing structure, which disappear with transducer pressure—consistent with free peritoneal air after perforation. Again note the complex ascites in front of the liver. (g–i) Typical abdominal radiographs in NEC and perforation: Pneumatosis of the bowel wall as well as portal venous gas is seen in this 4-day-old neonate with NEC (g). A supine radiograph demonstrates diffuse pneumoperitoneum (football sign) with hyperlucency of the whole abdomen, appreciation of the falciform ligament and the continuous diaphragm sign in gross perforation (h). A lateral decubitus cross table radiograph clearly shows free abdominal air, used for confirmation in equivocal cases (i)

dependent segment of the bowel although, gas trapped in inspissated meconium, can be difficult to differentiate from mural gas. Mural gas bubbles are then transported by the mesenteric veins into the portal vein and the liver causing portal venous pneumatosis (Fig. 13.35). This is quite striking on US; the liver appears full of echogenic dots and stripes in the non-dependent superficial areas. If one can track the bubbles in the portal vein (best documented by

spectral Doppler showing the typical air and gas spikes in the spectrum) this can be differentiated from aerobilia (caused for example by an intestinal obstruction). Pneumatosis is not specific for necrotizing enterocolitis as it can occur in a number of conditions ranging from neonatal colitis, rotavirus infection, enteritis, any kind of mucosal damage (such as in oncology conditions) that allow passage of gas into the bowel wall, in distension or obstruction.

Sometimes it's idiopathic with no clear cause identified. However, in the right clinical setting, it is a very helpful sign in diagnosing NEC.

- In cases of perforation, as in other conditions causing this, complex ascites can be visualised sonographically. Sometimes the actual necrotic bowel segment can also be localised. Free peritoneal air is depictable by US exhibiting the “curtain sign” where the reverberation echoes from the free peritoneal air disappear under graded compression (see Fig. 13.35). Free air could be mistaken for gas from distended loops limiting the study unless considered a possible entity during the examination. To be well appreciated, the US settings should be set to a probe with high frequency (reducing the depth) and the abdomen examined without too much transducer pressure. Containment of gas within a (bowel) structure, as defined by the other bowel wall, should be actively considered.
- Other entities in the differential diagnosis of a neonate with a distended abdomen are atresias and meconium plug/ileus. These other causes for perforation have to also be considered (Fig. 13.36).
- One of the differential diagnoses in terms of the clinical manifestation of NEC is *neonatal colitis* which often exhibits some blood content in the stool. Usually this is a typical clinical presentation and diagnosis. US may reveal thickening and inflammatory changes of the colonic wall, but appearances remain quite nonspecific (see Fig. 13.37).
- The abdominal radiograph is completely nonspecific and only used for depiction of other entities that may cause a similar clinical appearance.

After an episode of NEC neonates may develop stenosis and strictures (seen both in neonates treated either conservatively or surgically). If this occurs in the colon, strictures can be nicely depicted by US using the hydrocolon technique; this distending the colon and enabling depiction of stenotic areas (see Fig. 13.1). US assessment has the added benefit of visualising the colonic

wall and differentiating ongoing inflammation versus a fibrotic stenosis, thus helping treatment decisions. Alternatively, more classically, these pathologies are addressed under fluoroscopy by enema or a follow-through study. Since strictures are typically colonic, an enema should be the first study. An upper GI follow-through study could also help if the latter is not diagnostic.

In neonates with NEC who required emergency surgical management a stoma is typically left at surgery during the acute course. The patency and absence of strictures in the respective distal bowel segments need to be assessed before repair and closure through a loopogram performed at a later stage. In the right setting and expertise, this can be performed by US using filling techniques or more traditionally in fluoroscopy through a distal loopogram.



NEC is a common condition seen in every neonatal unit and one has to be comfortable with the clinical course and imaging requirements. The role of US keeps growing in the diagnosis and later management of these infants replacing fluoroscopy where the radiological expertise is available.

13.5.3 Meconium Plug and Neonatal Meconium Ileus

These two quite similar entities describe a distal obstruction by inspissated meconium; usually localised at the level of the distal ileum or in the proximal colon. Whereas normal preterm neonates with immature gut peristalsis suffer from the “meconium plug” which sometimes can be managed even without imaging by nutritional measurements and enemas, “meconium ileus” typically presents in older and term neonates classically associated with mucoviscidosis/cystic fibrosis.

- The imaging approach is quite similar in both entities. This routinely starts with an abdomi-

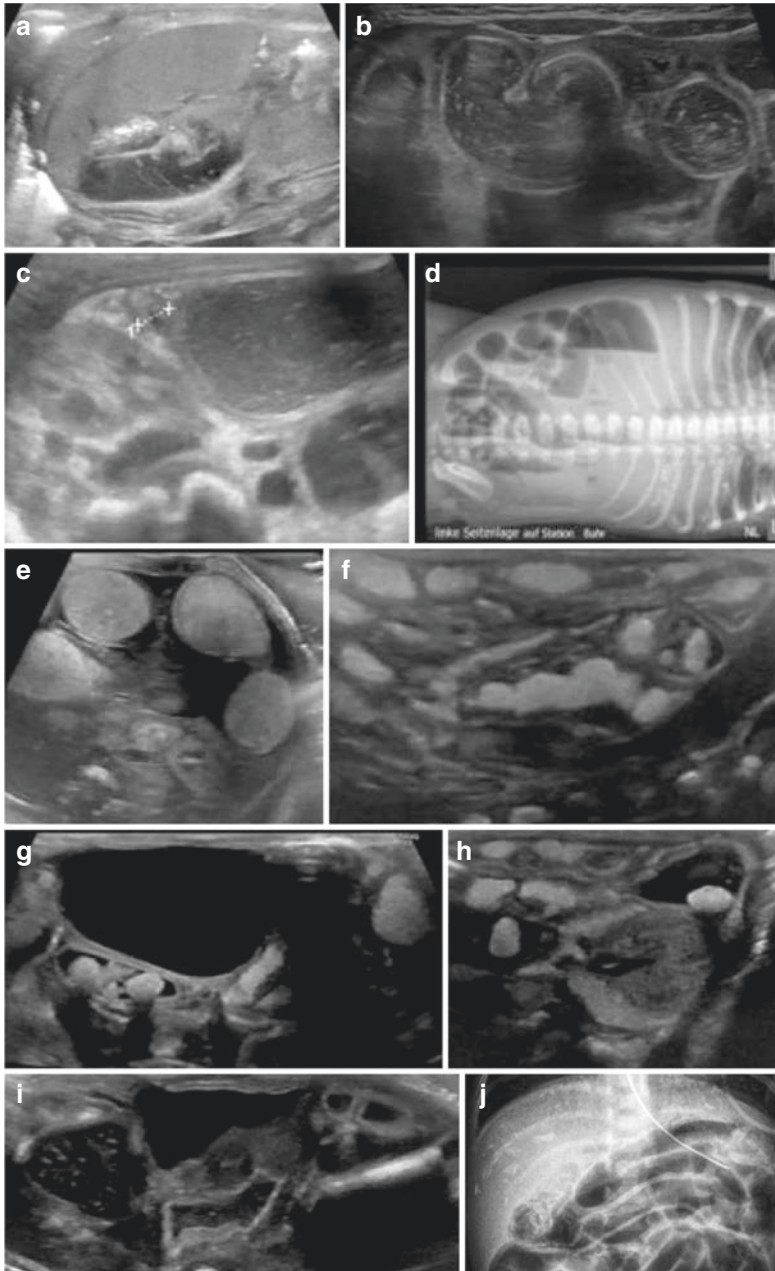


Fig. 13.36 Meconium ileus, intrauterine perforation, meconium peritonitis and ileum stenosis. (a) Ultrasound of left upper quadrant depicts stippled peritoneal calcifications particularly along the splenic and hepatic surfaces in keeping with intrauterine perforation and meconium peritonitis. (b, c) US depicts dilated (small) bowel loops (b) and some ascites as well as a small collapsed right colon (c, +++) raising suspicious of ileal obstruction (differential diagnosis atresia/stenosis versus meconium plug/ileus). (d) A cross table abdominal radiograph in lateral position clearly shows the ileus, but no signs of perforation or free air (note: if the small bowel is fluid filled at the site of the perforation this does not rule

out the condition). Additionally note the intra-abdominal calcifications (same neonate as a) proving intrauterine meconium peritonitis and ileum stenosis/atresia. (e–i) A preterm neonate with meconium ileus: echogenic ball-like content of the small bowel and parts of the colon (e). The hydrocolon technique reveals a relatively normal sized colon (f) and allows reaching the meconium balls with the irrigation saline (g, h), eventually mobilising the obstruction and thus reducing the ileus (i). (j) Radiograph in another preterm neonate; enlarged view of the upper abdomen: the calcifications after foetal meconium peritonitis are obvious. Also note the presence of pneumatosis of the bowel

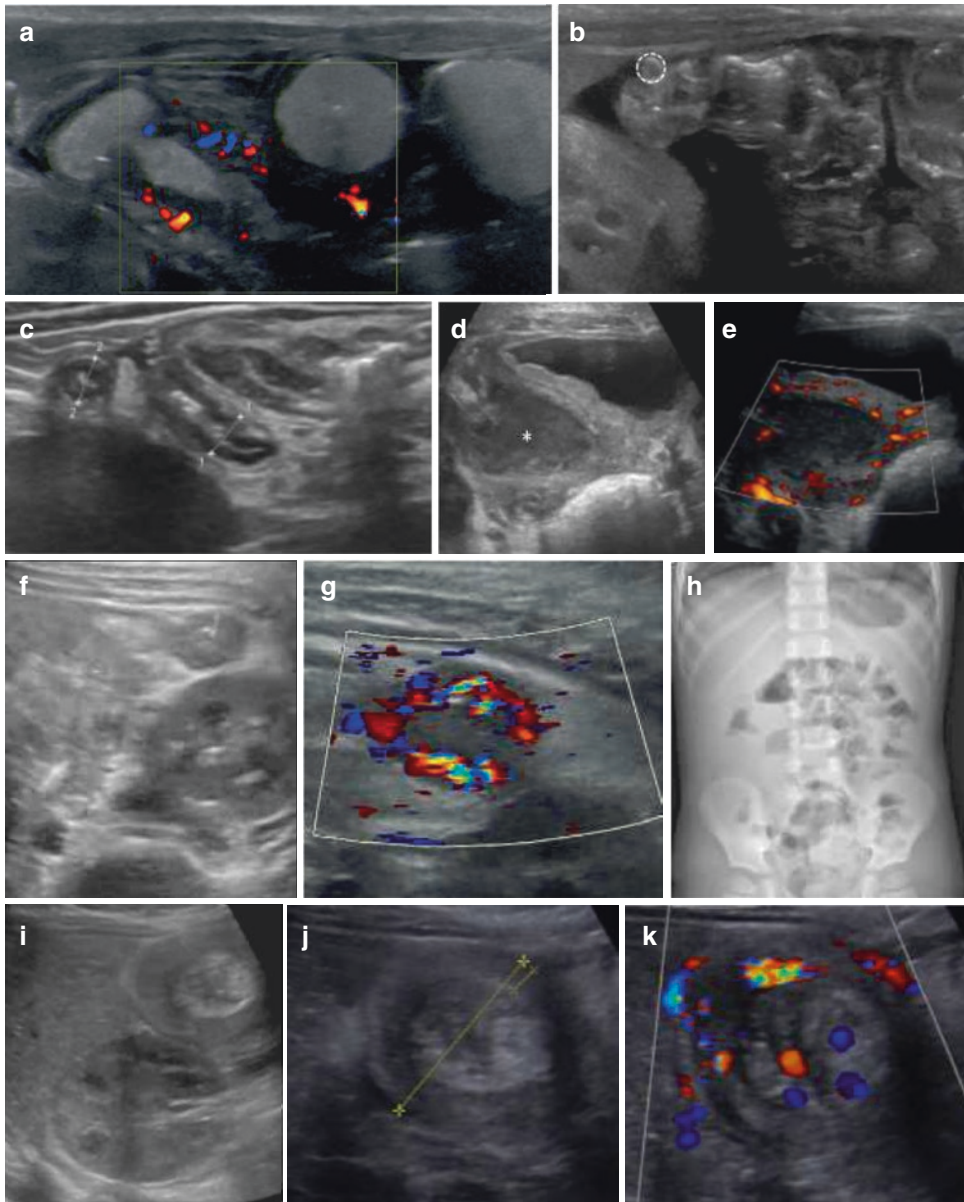


Fig. 13.37 Other colon and bowel conditions in neonates. (a, b) A preterm neonate with abdominal complaints. US reveals dilated meconium filled bowel loops and ascites, with a normal transition of the ileum into the caecum and only a few vessels in the thickened and poorly stratified bowel wall on CDS (a); the appendix is visible and appears normal (b, dotted circle). (c–e) Neonatal appendicitis: The normal neonatal appendix can be visible and resembles the appearance of older children. It can be elongated and quite kinked as well as it can be found lying in unusual locations as in this example (c, magnified view 1, 2+...+). Appendicitis in neonates is often clinically non-specific. Most cases will be detected at a later stage, usually already perforated with an abscess formation

(asterisk, d) and an inhomogeneously vascularized abscess wall (Power Doppler, e). (f, g) US of the left abdomen depicts the thickened wall (+...+) of the left colon with a narrow lumen (f) and hypervascularity on CDS (g) in a neonate with haematochezia consistent with a neonatal colitis. (h–k) Intussusception: another infant with an acute abdomen and bloody stools. The radiograph (h) shows signs of an ileus with an area of soft tissue density without bowel gas in the right lower quadrant. The subsequent US then reveals the typical findings of intussusception (i, axial section) with the doughnut sign (j, +...+) and clearly delineating a thickened outer intussusciens wall (x...x). Colour Doppler also confirms viability of the intussusceptum small bowel loop and mesentery (k)

nal radiograph allowing assessment of the extent of bowel distension and the distribution which guide as to the level of obstruction. Clinicians typically would like to know: is the bowel obstructed? Where is it obstructed, and by what? Radiographs can often only partially answer these questions.

- US can visualise the dilated proximal bowel loops distended by echogenic meconium and the collapsed bowel loops distal to the plug or the ileus. The small left colon (as described above in Sect. 13.3.1) can be nicely visualised on US by the hydrocolon technique (Fig. 13.36). Alternatively, a fluoroscopic enema will also well demonstrate the small unused left colon. The benefit of such a diagnostic enema is that one may potentially pass the contrast retrogradely to the level of the obstruction thus enabling differentiation of an atresia (unable to reach the distended more proximal loops and its contents) from a meconium ileus. Furthermore, the same technique rinses the colon from the inspissated meconium reducing the obstruction. This can be also performed sonographically, avoiding the radiation burden and, in such a case, performable at the bedside in the NICU.

Occasionally, in cases of foetal bowel perforation, one will find meconium in the abdominal cavity. This manifests with scattered calcifications as postnatal remnants of the so-called *meconium peritonitis* (Fig. 13.36). Not all these children manifest clinically and when such appearances are noted incidentally, as long as there are no signs of obstruction, these infants need no further bowel imaging as they will need no further treatment.

13.5.4 Miscellaneous Other (Rare) Conditions (Neonatal Appendicitis, Intussusception, Bile Stone ...)

There are other rare acquired diseases in neonates that need to be mentioned and considered.

Rarely, even neonates can present with acute **appendicitis**. The clinical symptoms are very nonspecific and do not differ from any other acute neonatal distal bowel conditions. These are mostly identified late and often already demonstrating abscess formation. This needs to be differentiated from an inflamed duplication cyst or a Meckel diverticulum. An infected urachal cyst is usually in a different location (centrally between the umbilicus and the bladder) and thus easily differentiable anatomically from remnants of the omphaloenteric duct.

- The imaging modality of choice is US and will exhibit similar findings as in older infants. The diameter of a suspicious appendix is naturally slightly smaller (but no definite cut-off values are defined for this age group) (Fig. 13.37). Given the young age and absence of intra-abdominal fat, the younger the infant, the less likely the presence of a fatty mesenteric reaction. This could also explain why in this age group appendicitis progresses rapidly and often presents with diffuse peritonitis or abscesses.

Ileocecal intussusception is usually a disease of older infants and young children but has been described in neonates particularly in the presence of a pathologic lead point. Neonates are less likely to have a lymph node as a lead point as they tend to get less reactive lymph nodes than older children. Some small duplication cyst or similar congenital entities are hence more likely the provoking cause in a neonate. Presentation is similar, though more nonspecific; sometimes even nearly asymptomatic.

- Imaging shows the same findings as in older children. On US one can appreciate the “pseudo-kidney sign” or “donut-sign” as well as the “target-sign” in cross section images of the affected bowel loops. As the gut in the neonate is very mobile, the position of the intussusception can vary widely. Besides showing the recipient loop and the intussuscepted ileum within this together with the adjacent mesentery, the vascularisation should

also be assessed by CDS (Fig. 13.37). Ascites may also be present. Differentiation against ileal- or jejuno-ileal intussusception can be a bit trickier. In doubtful cases, a diagnostic hydrocolon will allow assessment of the unaffected colon and thus confirm the suspicion. This sonographic technique can also be used to reduce the intussusception with the respective precautions and handling provided (fluid balance, analgesia/sedation, etc....).

- Commonly, as in many neonates with nonspecific abdominal symptoms, an abdominal radiograph is taken for an overview of the distended bowel distribution and detection of free peritoneal air, possibly complemented by a hanging or lateral decubitus cross table view.
- Therapeutically, as in older infants, a hydrostatic sonographic reduction or a fluoroscopic reduction is performed. The same rules apply for the procedure depending on the centre and available expertise (analgesia/sedation, fluid balance, observation, etc.). Reflux of air or fluid (depending on the technique) into the terminal ileum is the radiological success criterion.

Enteritis also occurs in neonates although this is less common. It does not pose an imaging problem; however, it may be associated with complications such as pneumatosis or intussusception.

Polyps are extremely rare and thus not addressed here. If one needs to assess for a suspected polyp, filling and distending the bowel by a hydrocolon or fluoroscopically is nearly mandatory to properly visualise and define the respective anatomy.

Ascites is a very common finding in severely diseased neonates. It may either be secondary to renal failure, to systemic problems, to cardiac conditions or more specifically to abdominal disease, such as portal hypertension, intestinal inflammation and peritonitis.

- Ultrasound will visualise the fluid and enable the differentiation between clear and uncomplicated fluid or more complicated turbid fluid with echoes and sedimentations. Sometimes even meconium balls can be seen within the peritoneal fluid (Fig. 13.38). The latter spectrum would support a surgical cause.

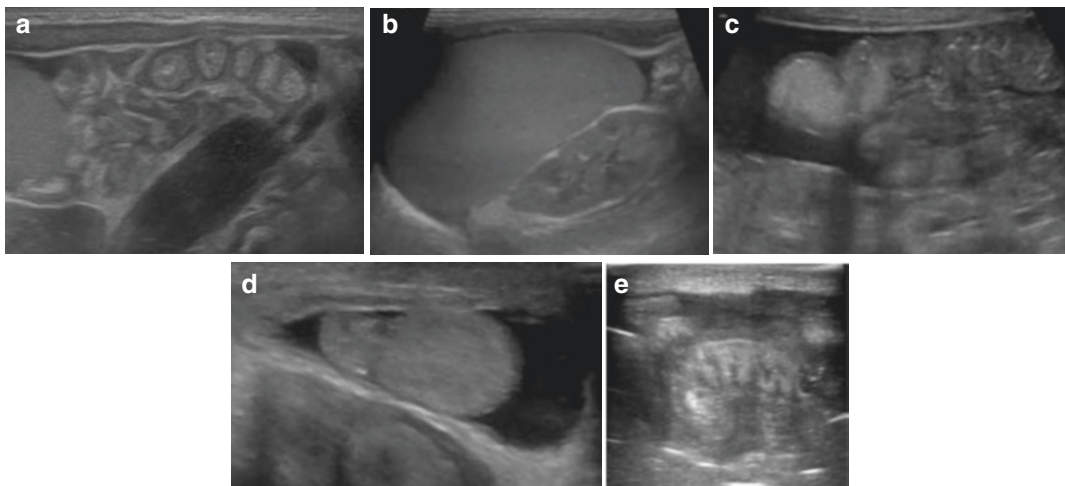


Fig. 13.38 Ascites. (a–c) Different locations and amount of uncomplicated simple ascites; i.e. free peritoneal fluid without echoes (adjacent to bowel, a and c; lower pole of liver or spleen b). It may change with positioning and graded compression and does not always imply severe pathology. (d) Ascites can also be found in the scrotum, as

long as the inguinal canal is open and should not be confused with a hydrocele. (e) Once the free peritoneal fluid becomes more echogenic and contains particles it is much more concerning as this is usually associated with bacterial inflammation, perforation or haemorrhage

Omphalitis is usually simply a clinical problem. Sometimes the query of a sub-umbilical abscess of the abdominal wall arises and then US of the abdominal wall can be helpful to define the position and extent as well as the size of the fluid component if an abscess is indeed present. The same may also occur after surgery at the site of the abdominal wall incision with US, again, being very helpful in such scenarios.

Another rare significant acquired abdominal condition in neonates are **bile stones or the inspissated bile syndrome** (latter seen after treatment with some antibiotics, and in pre-existing biliary conditions with cholestasis).

- On US these bile stones are usually less echogenic than they tend to be in older children and sometimes (particularly in an under-distended gallbladder) may be difficult to differentiate from polyps (see Fig. 13.28). One rare condition worth mentioning here is adrenoleukodystrophy that may present with multiple gallbladder polyps which is practically pathognomonic.

Traumatic injuries are addressed in a separate chapter of this book.



Common conditions in older children such as appendicitis and ileo-colic intussusception can still occur in neonates and although rare should still be a clinical consideration.

13.6 Abdominal Tumourous Conditions in Neonates (Except in the Urogenital Tract)

Congenital benign or malignant tumours are rarely seen in the neonate. The following is a short overview of the most relevant conditions and their differential diagnosis. Imaging is often nonspecific in terms of defining the exact entity in question. Other biochemical tests (e.g. tumour markers) and

laboratory tests help narrow down the differential diagnosis in combination with the history and imaging appearances. Biopsy and histology will eventually establish the diagnosis and imaging can help target the lesion (or best part of the lesion) for obtaining such a specimen.

US is nearly always the first modality. Further imaging, particularly in suspected malignant lesions, will be obtained through cross-sectional modalities (mostly by MRI) for better anatomical definition (pre-surgical) and also for staging. MRI may also become necessary in syndromes and systemic conditions with focal lesions allowing evaluation of the broader systemic manifestations in such syndromes.

13.6.1 Abdominal Cysts and How to Approach Them

Abdominal cysts are a relatively frequent finding and are often detected antenatally. In females these mostly originate from the ovaries (this is addressed in Chap. 12). Differentials include mesenteric cysts, cysts from the omphaloenteric duct or the urachus, as well as duplication cysts from the gastrointestinal tract. More rarely, cystic tumours (mostly teratomas) may be encountered in either region. Intraparenchymal cysts may occur, mostly cysts of the spleen or the liver, which are frequently dysontogenetic and do not pose neither a clinical nor an imaging problem. The exception would be when these are very large thus displacing or compressing adjacent anatomical structures.

- Imaging usually is limited to US. Sometimes an abdominal radiograph may offer additional valuable information, for example in the depiction of calcifications in a mature teratoma. US will not only visualise the cyst but can often define the origin narrowing down the differential diagnosis. US can beautifully assess the wall of the cysts (thin, smooth, regular versus thick, irregular with/without parenchymal nodular components, calcifications, mural stratification, etc....) as well as the content (i.e. no echoes in an uncomplicated cyst; echoes, septations and nodules in complicated cysts)

(Fig. 13.39). Not all cysts that appear complicated are malignant. Haemorrhage can be seen in an ovarian cyst, a cystic lymphangioma or in a Meckel diverticulum. Epithelial debris and mucus (and sometimes haemorrhage) can be seen in duplication cysts and stones and sedimentations can be seen in choledochal cysts, all benign conditions.

- Very rarely MRI (or contrast-enhanced CT) is used as an add-on modality trying to further characterise the entity and to demonstrate the exact extent and anatomy, for example pre-surgically in large hamartomatous lesions.

13.6.2 Hamartoma and Other Benign Tumours

Hamartomas are benign entities that do not grow invasively and do not cause metastasis. However, they can be huge and cause clinical problems due

to mass effect. Hamartomas can be solid, cystic or mixed, sometimes multi-cystic and can occur in all the parenchymal organs particularly within the liver (Fig. 13.39).

- They usually are detected and defined by US. The larger and the less conspicuous these appear on US, the higher is the need of additional imaging, usually achieved by MRI. Characterising is difficult and diagnosis is often made on specimen.

Pancreatic insulinomas or *nesidioblastosis* can rarely present in neonates. Nesidioblastosis is the diffuse form and is difficult to depict on imaging often only showing diffuse enlargement of the pancreas. Suspicion arises clinically based with hyperinsulinaemic hypoglycaemia. Focal insulinomas may be easily missed by US as are often quite small and hypo- to iso-echogenic to the neonatal pancreatic tissue.

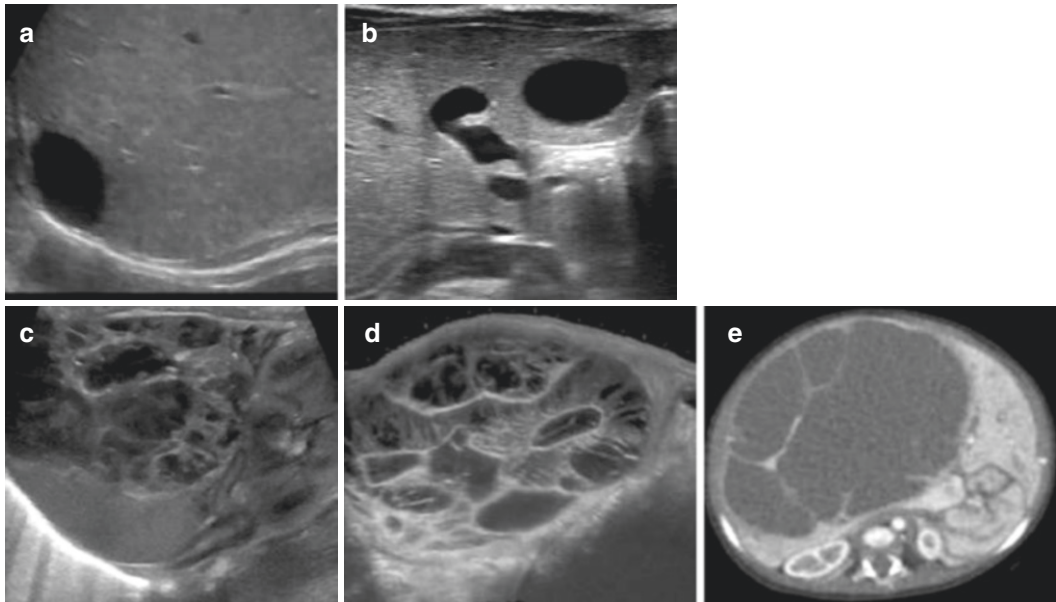


Fig. 13.39 Liver cysts. (a, b) Two examples of simple congenital liver cysts—one subcapsular (a) (or possibly a congenital mesothelial cyst given the location) and another central one in the left liver lobe (b). (c, d) A huge multicystic liver tumour in a neonate with hepatomegaly detected sonographically. Its full extent can only be

assessed using either curved array probes (c), sacrificing resolution, or panoramic imaging techniques (d). (e) Contrast-enhanced CT is performed preoperatively to visualise all important relationships of this multicystic congenital liver hamartoma

- **Contrast-enhanced** studies improve US potential as these hypervascular tumours usually have a strong arterial enhancement with wash-out in the parenchymal phase.
- Other imaging techniques are often required. Dynamic contrast-enhanced MRI and PET-CT/MRI are often performed in these scenarios after the baseline US study.
- Alternatively, a Ga⁶⁸ Dotatate nuclear medicine scan may be a further option.

Neonatal teratomas are usually benign and solitary tumours. These may occur anywhere in the body. In the abdomen they most often occur in the sacrococcygeal area. The imaging appearance depends on their composition. They are most often cystic lesions, which can be impressively large (see Fig. 13.6). They may also exhibit nodular soft tissue components, fatty tissue or even ossification and calcifications. They are often already detected prenatally.

- Postnatally, US is used to confirm the suspicion, possibly a radiograph is acquired to see possible bony pathology.
- If pre-surgically additional anatomic information is needed or there are doubts on the entity, other sectional imaging (MRI or CT) is performed.

13.6.3 Congenital and Infantile Abdominal Haemangioma

Neonatal haemangiomas are classified as vascular neoplasms which may occur in all organs.

In neonates, most of these are seen in the liver, practically mostly as congenital (hepatic) haemangiomas (CHH). They are benign hepatic tumours of infancy and are considered true vascular neoplasms. Infantile hepatic haemangioma (IHH) occurs after birth usually within the first 6 month of life. These type of haemangiomas are different from the adult-type haemangiomas, which are venous malformations.

Congenital haemangiomas are present at birth, usually manifesting as a solitary large mass with either rapid or partial involution. Less com-

mon types occur, namely, *rapidly spontaneously involuting congenital hepatic haemangiomas* (RICH) (regress by the end of the first year) and *non-involuting congenital haemangiomas* (NICH). The latter do not regress but may grow in proportion to the child's growth.

Such haemangiomas can manifest as an abdominal mass lesion with mass effect, secondary consumptive coagulopathy or high-output cardiac failure due to the large shunt flow. These may need treatment, for example by embolisation as typical congenital haemangiomas are not very responsive to propranolol treatment.

The *infantile hepatic haemangiomas* are different to CHH. These appear within the first few weeks of life and can be single, multiple or even diffuse. They undergo proliferation during the next few months and gradually involute over time. They show good response to propranolol as medical treatment. They usually are asymptomatic and are detected incidentally by screening.

In large haemangiomas, hepatomegaly, mass effect and rarely high-output cardiac failure may still occur; some can be associated with secondary hypothyroidism.

The old terms haemangioendothelioma or haemangioendotheliomatosis should be avoided unless there is a real tumourous epithelioid haemangioendothelioma, which is a different entity. Multiple or diffuse hypervascular liver lesions are now called diffuse or multifocal infantile hepatic haemangioma.

- Imaging for all types of haemangiomas is the same: unlike adult-type haemangiomas, which are usually echogenic, neonatal haemangiomas usually present as hypoechoic lesions of different sizes on US. Echogenicity is variable as well as is the vascularisation appreciable on CDS.
- Congenital hepatic haemangiomas tend to be large and well circumscribed with a somewhat heterogeneous echotexture. These may exhibit haemorrhage, necrosis, fibrosis or even calcifications. If there is a diffuse or multinodular haemangioma, they may sometimes be difficult to distinguish from the normal liver parenchyma (Fig. 13.40). As these

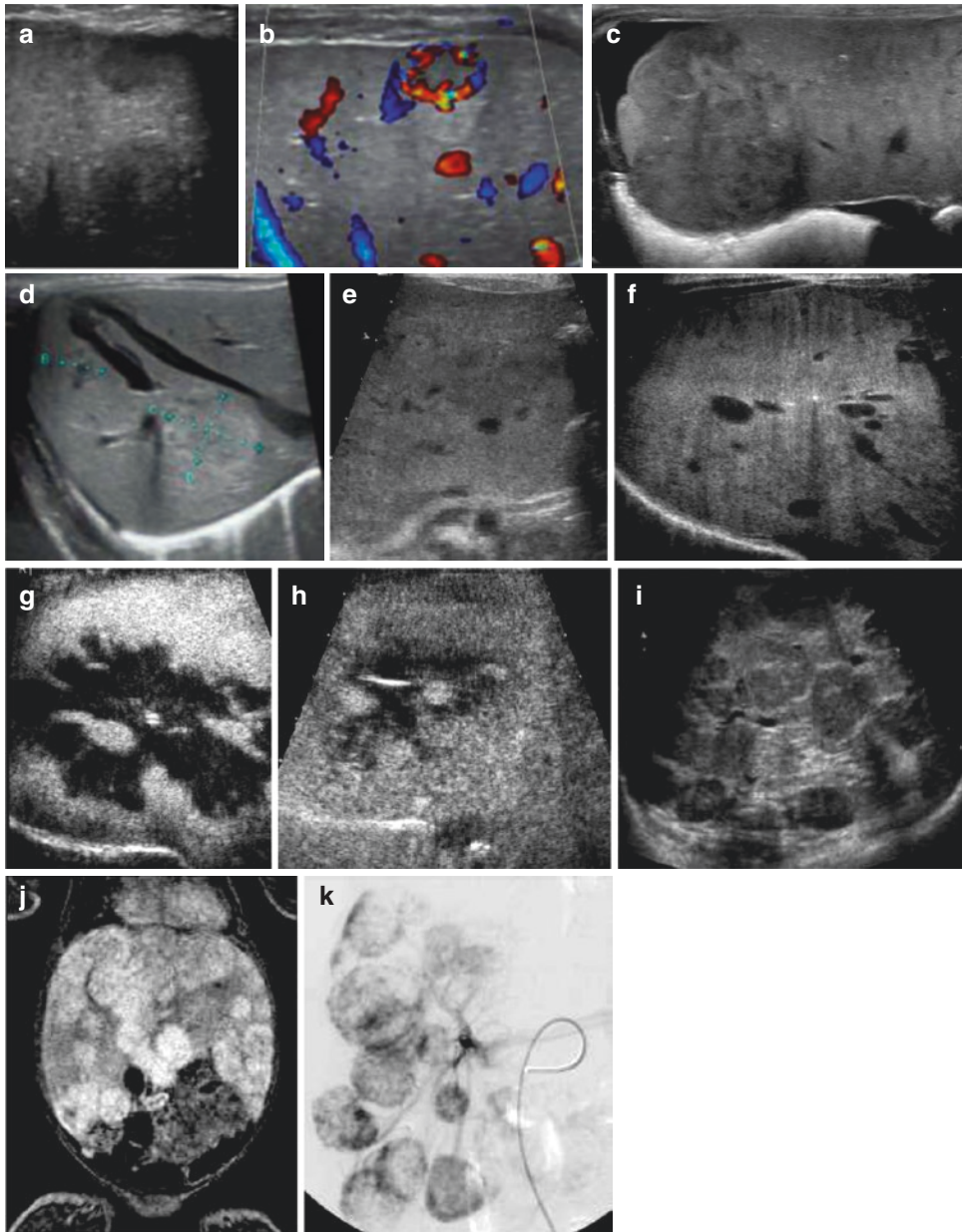


Fig. 13.40 Haemangioma. (a, b) Neonatal haemangioma: a small superficial hypoechoic nodule is depicted using a linear transducer (a), CDS assessment shows peripheral vessels (b). (c) A large multinodular, somewhat inhomogeneous hypoechoic mass is seen in the right liver lobe of a neonate with some specks of calcification proven to represent a large neonatal haemangioma. Note the adjacent free peritoneal fluid (remnant from perinatal rupture and haemorrhage). (d) Another neonate where US depicts two nodular masses (+...+) appearing inhomogeneous and quite easy to be missed. Also note the intrahepatic porto-systemic shunt (see also Fig. 13.8f). (e-h) A neonate with cardiac insufficiency and hepatomegaly was referred to rule out a liver haemangioma. The initial US image shows an inhomogeneous texture (e), the high-res-

olution image depicts some tiny calcifications (also an enlarged hepatic artery with high flow as well as high flow in the respective hepatic vein was seen—not shown). To properly delineate the extent of the suspected mass and to define its entity, a contrast-enhanced US was performed. The early phase (g) shows vivid peripheral enhancement with early filling of a central vein (indicating shunting) and in the late phase (h) a centripetal fill-in (“Iris phenomenon”) typical for haemangiomas. (i-k) This neonatal liver US demonstrates multiple hypoechoic nodular lesions in keeping with the clinical picture of cardiac decompensation from high shunt flow highly suspicious of liver “haemangiomatosis” (= multifocal liver haemangiomas) which was then also confirmed by dynamic contrast-enhanced MRI (j) and subsequently embolised (k)

may contain large vascular channels, they may be radiologically mistaken for arteriovenous malformations. Contrast-enhanced US will show strong early peripheral enhancement, progressively becoming confluent with sometimes early venous filling if there are large vascular channels. If there is high shunt flow, a large feeding artery and tapering of the abdominal aorta distally to the exit of the feeding vessel can be observed. Increased diastolic and systolic flow velocities and possibly some turbulence can be seen on spectral Doppler sonography. Differentiation from other hepatic tumours can be supported clinically by the lack of elevated alpha-fetoprotein levels which is helpful particularly in heterogeneous liver lesions with calcifications.

If US is equivocal, dynamic ce-MRI (or even sometimes CT) may be used demonstrating the same perfusion and enhancement pattern as described above. These methods will give a better overview, particularly in multiple or larger lesions.

13.6.4 Mesenteric and Intestinal Lymphatic/Vascular/Arteriovenous Malformation and Respective Differential Diagnosis

Besides the hepatic *vascular malformations* (described above), vascular malformations may also occur in other abdominal organs. For example, this is rarely seen in the spleen. They can also be encountered in the bowel or in the mesentery. Symptoms vary depending on the histological entity, size and shunt presence. Lesions can be completely asymptomatic in the neonatal age and are often detected incidentally.

Cystic lymphatic malformations of the mesentery, sometimes large, may pose a challenge in differentiating from mesenteric cysts or entrapped pockets of ascites (Fig. 13.41). These and large *arteriovenous malformations of the bowel* can affect long bowel lengths. US of the latter demonstrates an inhomogeneously thickened bowel wall with multiple vessels even when studied at the neonatal stage.

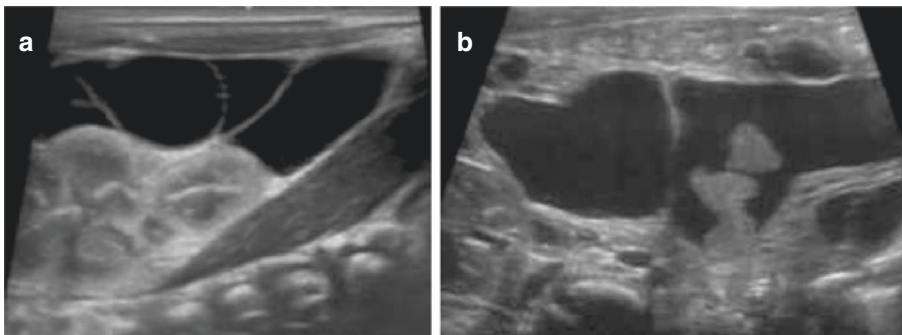


Fig. 13.41 Neonatal abdominal lymphatic malformation. (a) Neonatal US in an infant with distended abdomen shows a large septated cystic structure in front of the kidney extending up to the liver and into the left abdominal compartments in keeping with a mesenteric lymphatic malformation. (b) A similar case with a prenatally recog-

nised abdominal cyst classified as a suspected ovarian cyst. Postnatal US shows a large multicystic mass with clot-like internal echoes which turned out to be a haemorrhagic lymphatic malformation. For another similar example see Fig. 5.10 (“prenatally recognised abdominal cyst”)

- Imaging usually starts with US, sometimes through an incidental finding on an US scan performed for other reasons. Nevertheless, for these latter rarer queries, other sectional contrast-enhanced imaging (mostly performed by MRI) could be performed. Sometimes such a lesion is picked-up incidentally in a CT angiography performed for other reasons (Fig. 13.42).

Cystic teratomas are another differential diagnosis to be considered with cystic lesions in the mesentery or retroperitoneum. The imaging features of this entity do not differ from teratomas in other body areas.

13.6.5 Malignant Abdominal Tumours

Besides the urogenital tumours (neuroblastoma, teratoma, renal tumours) hepatoblastoma and



Fig. 13.42 Neonatal CT-Angiography (CTA) depicting an intestinal AVM. Contrast-enhanced CTA in a 2-week-old neonate (small for dates) performed for other reasons (complex vascularized sequestration, not shown). The abdomen was included not to miss an abdominal origin of the feeding artery, and furthermore due to the babies' size the volume acquisition could not be coned down smaller without huge increase in dose (and quality loss with the equipment available at that time). Note the arteriovenous vascular malformation at the mesenteric artery (magnified view and dedicated reconstruction of the abdomen) which in retrospect was also appreciable (though poorly) on US

embryogenic sarcomas of the liver are the most common tumours encountered in the neonatal abdomen.

Hepatoblastoma is usually large at presentation. They may show haemorrhage and calcifications, signs of rupture as well as early metastasis to the lungs. Serum alpha-fetoprotein is normally elevated. Normal values for neonates are different and unless very high, in very early manifestations of congenital hepatoblastoma, it can still be challenging to differentiate from other pathology based on tumour markers.

- The first modality of choice is again US. Hepatoblastomas are often inhomogeneous, may exhibit calcifications and have relatively well-defined borders with possibly necrotic or haemorrhagic central areas. Usually the tumours are solitary, but they may be multifocal and even invade or compress hepatic vasculature, the IVC or the bile ducts. Differentiation of the various alternate entities such as the embryonic sarcoma on imaging is not possible (Fig. 13.43).
- MRI is done to complete the work-up and for staging purposes. Signal behaviour depends on the histologic subtype. Comprehensive imaging by MRI is crucial, not only for characterisation of the mass depicted on US, e.g. from an atypical haemangioma (by depicting vascular invasion and other hepatoblastoma features), but also for exact determination of the pre-treatment extent of disease system (through PRETEXT) which guides immediate management and surgical planning.

Other neonatal liver, spleen or pancreatic (semi-)malignant masses are rare. However, metastatic disease (e.g. in neuroblastoma) or focal infiltration in leukaemia or haemophagocytosis syndromes need to be considered (Fig. 13.43).

A few other tumours worth mentioning in the neonate include:

- Germ cell tumours—these are also associated with elevated alpha-fetoprotein levels.
- Rhabdomyosarcoma of the liver.

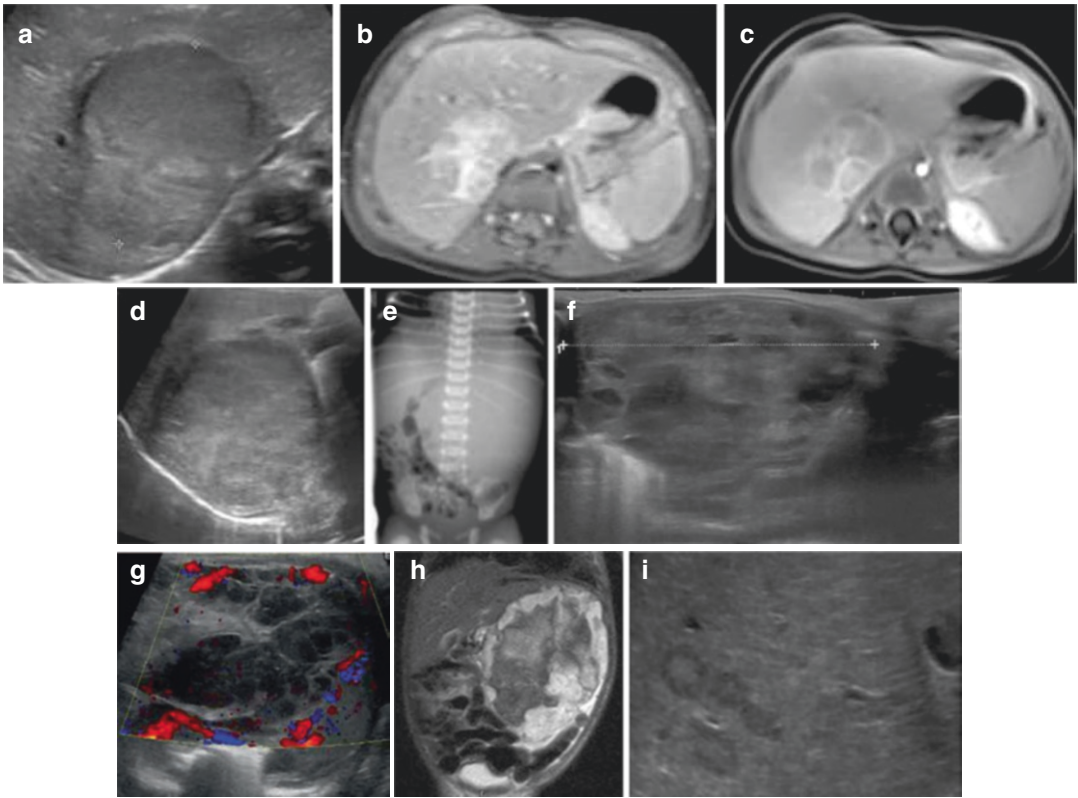



Fig. 13.43 Neonatal liver tumours. (a–d) Neonatal hepatoblastoma: a neonate referred for an abdominal US for elevated liver enzymes. US revealed a relatively homogeneous liver tumour (a, +····+) with a nearly halo-like outline and mostly smooth margins. Together with biochemistry a hepatoblastoma was suspected. In spite of the young age contrast-enhanced MRI (axial sections shown) was performed for further assessment and staging (b, c). The tumour showed some inhomogeneity and dorsal penetration of the liver surface in the follow-up study in spite of initiated chemotherapy (d). (e–i) A neonate investigated for a hugely distended abdomen. The radiograph demon-

strates a soft tissue mass in the left side of the abdomen (e). The subsequent US study delineates a complex, partially cystic, large tumour originating from the liver only entirely measurable using panoramic techniques (+····+, f). This was associated with mostly peripheral vivid vascularity (g) and some contrast enhancement of the solid appearing sections on ce-US (not shown). An embryonic liver sarcoma was suspected. MRI then confirmed these radiological findings (h). Histology confirmed the suspected sarcoma aetiology. (i) A liver US study in a neonate with neuroblastoma shows multiple intrahepatic small nodular masses in keeping with liver metastasis (magnified view)

- Pancreaticoblastoma or pseudopapillary neoplasm. These usually occur in older infants and later in childhood, except for the cystic type of pancreaticoblastoma which can occur in neonates with Beckwith-Wiedemann syndrome.
- Metastatic disease such as from neuroblastoma or leukaemia. These can also manifest as

solitary pseudo-tumours such as in Burkitt lymphoma.

No specific imaging features can be described. Usually they are first addressed by US before proceeding to MRI (or CT) and/or biopsy or surgery as per other tumour masses.

 Abdominal cysts have a broad differential diagnosis with quite typical clues on US often resulting in a specific diagnosis and rarely needing further imaging. Solid tumours in neonates, on the contrary, can be challenging to differentiate on US and often require further imaging for characterisation and staging.

A special entity in neonates is congenital hepatic haemangioma and its differential diagnosis. In this case US and contrast dynamics are essential for confirming the diagnosis and defining further work-up, treatment and follow-up.

13.7 Summary

Neonatal abdominal imaging covers a broad spectrum of congenital and acquired conditions of the bowel and the solid organs of the gastrointestinal tract. In the large majority of infants with such issues, radiographs and US are the mainstay of imaging with fluoroscopy and cross-sectional imaging playing specific roles depending on the shorter differential diagnosis guided by the initial evaluations. Imaging also plays a pivotal role in the therapy of a number of neonatal conditions as outlined in the chapter.

Like many subspecialties in medicine there are choices on how best to image these children and such choices should focus on the imaging modalities available and the in-house expertise of the radiology team always focusing on what is best for the specific patient in question.

References

1. Napolitano M, Franchi-Abella S, Damasio BM, Augdal TA, Avni FE, Bruno C, Darge K, Ključevšek D, Littooi AS, Lobo ML, Mentzel HJ, Riccabona M, Stafrace S, Toso S, Woźniak MM, DiLeo G, Sardanelli F, Ording Müller LS, Petit P. Practical approach to imaging diagnosis of biliary atresia, Part 1: Prenatal ultrasound and magnetic resonance imaging, and

postnatal ultrasound. *Pediatr Radiol.* 2021b;51:314–31. <https://doi.org/10.1007/s00247-020-04840-9>.

2. Napolitano M, Franchi-Abella S, Damasio MB, Augdal TA, Avni FE, Bruno C, Darge K, Ključevšek D, Littooi AS, Lobo ML, Mentzel HJ, Riccabona M, Stafrace S, Toso S, Woźniak MM, Di Leo G, Sardanelli F, Ording Müller LS, Petit P. Practical approach for the diagnosis of biliary atresia on imaging: an up-date and guidelines from the ESPR. Part 2: MRCP, Hepatobiliary scintigraphy, percutaneous cholecysto-cholangiography, ERCP, percutaneous liver biopsy, risk scores and decisional flow chart. *Pediatr Radiol.* 2021a;51:1545–54. <https://doi.org/10.1007/s00247-021-05034-7>.
3. van Rijn RR, Robben SGF. Normal values. In: van Rijn RR, Blickman JG, editors. *Differential diagnosis in pediatric imaging*. New York: Thieme; 2011. p. 636. <https://doi.org/10.1055/b-0034-87961>.
4. Kahramaner Z, Erdemir A, Cicek E, Cosar H, Turkoglu E, Sutcouglu S, Özer E. Reference ranges for sonographic dimensions of the liver and spleen in preterm infants. *Pediatr Radiol.* 2013;43(11):1464–74. <https://doi.org/10.1007/s00247-013-2729-7>.

Literature

- Buonpane C, Lautz TB, Hu YY. Should we look for Hirschsprung disease in all children with meconium plug syndrome? *J Pediatr Surg.* 2019;54:1164–7. <https://doi.org/10.1016/j.jpedsurg.2019.02.036>.
- Davenport M. Biliary atresia: clinical aspects. *Semin Pediatr Surg.* 2012;21:175–84.
- Fotter R. Imaging of constipation in infants and children. *Eur Radiol.* 1998;8:248–58. <https://doi.org/10.1007/s003300050373>.
- Ključevšek D, Riccabona M, Petit P, Avni EF, Bruno C, Damasio MB, Darge K, Littooi AS, Lobo ML, Mentzel HJ, Napolitano M, Wozniak M, Ording Müller LS. Intracavitary contrast-enhanced ultrasound in children: a review, with clinical applications and procedural recommendations from the ESPR Abdominal Task Force Group. *Pediatr Radiol.* 2020;50:596–606. <https://doi.org/10.1007/s00247-019-04611-1>.
- Nagy E, Riccabona M. Sonographic enema (“hydrocolon”) as a diagnostic option for assessing colonic pathology: case series to demonstrate feasibility and diagnostic value in neonates and infants. *Pediatr Radiol.* 2019;47S (abstract).
- Riccabona M, Lobo ML, Augdal TA, Avni F, Blickman J, Bruno C, Damasio MB, Darge K, Mentzel HJ, Napolitano M, Ntoulia A, Papadopoulou F, Petit P, Woźniak MM, Ording-Müller LS. European Society of Paediatric Radiology Abdominal Imaging Task Force recommendations in paediatric urology, Part X: How to perform paediatric gastrointestinal ultrasonography, use gadolinium as a contrast agent in children, follow up paediatric testicular microlithiasis,

- and an update on paediatric contrast-enhanced ultrasound. *Pediatr Radiol*. 2018;48:1528–36.
- Riccabona M, Lobo ML, Ording-Muller LS, Augdal TA, Avni FE, Blickman J, Bruno C, Damasio B, Darge K, Ntoulia A, Papadopoulou F, Vivier PH. ESPR Abdominal (GU and GI) Imaging Task Force – imaging recommendations in paediatric uro-radiology, Part IX: Imaging in ano-rectal and cloacal malformation, imaging in childhood ovarian torsion, and efforts in standardising paediatric uro-radiology terminology. Report on the mini-symposium at the ESPR meeting in Graz, June 2015. *Pediatr Radiol*. 2017;47:1369–80. <https://doi.org/10.1007/s00247-017-3837-6>.
- Riccabona M, Maurer U, Lackner H, Uray E, Ring E. The role of sonography in the evaluation of gastroesophageal reflux - correlation to pH-metry. *Eur J Paediatr*. 1992;151:655–7.
- Riccabona M. US of the gastrointestinal (GI) tract. In: Riccabona M, editor. *Pediatric ultrasound, requisites and applications*. New York: Springer; 2020. p. 335–74. https://doi.org/10.1007/978-3-030-47910-7_14.
- Shamir SB, Kurian J, Kogan-Libermann D, Tragin HB. Hepatic imaging in neonates and young infants: state of the art. *Radiology*. 2017;285:763–77. <https://doi.org/10.1148/radiol.2017170305>.
- Sinzig M. Imaging of the pediatric gastrointestinal tract. In: Riccabona M, editor. *Pediatric imaging trainer. Radiography, ultrasound, CT, and MRI in neonates and children*. New York: Thieme; 2014. p. 82–120.
- Stafrace S, Lobo LM, Augdal TA, Avni FE, Bruno C, Damasio MB, Darge K, Franchi-Abella S, Ključevšek D, Littooj AS, Lobo ML, Napolitano M, Mentzel HJ, Riccabona M, Stafrace S, Toso S, Woźniak MM, Di Leo G, Sardanelli F, Ording Müller LS, Petit P, Riccabona M. Imaging of anorectal malformations: where are we now? *Pediatr Radiol*. 2022;52(9):1802–9.
- Thaker VV, Leung AM, Braverman LE, Brown RS, Levine B. Iodine induced hypothyroidism in full-term infants with congenital heart disease: more common than currently appreciated? *J Clin Endocrinol Metab*. 2014;99:3521–6. <https://doi.org/10.1210/jc.2014-1956>.

Imaging of the Neonatal Musculoskeletal Tract

14

Janina M. Patsch

14.1 Normal Prenatal Development of the Skeleton

During foetal life, the skeleton develops through endochondral or desmal ossification. In endochondral ossification, cartilaginous anlagen serve as scaffolds for bone formation. In desmal ossification, bone develops directly from mesenchymal tissue without cartilaginous scaffolds. Desmal ossification occurs at the calvaria (= neurocranium), and the majority of the face (= viscerocranium), except the mandible (which grows from Meckel's cartilage). The rest of the skeleton including the skull base (= chondrocranium) ossifies from cartilaginous precursors (= endochondral).

14.2 Normal Skeletal Imaging Features of Term and Preterm Neonates

At birth, the diaphyses and metaphyses of all tubular bones are ossified and are thus visible on radiographs (Fig. 14.1). The epiphyses and physes are

cartilaginous structures and thus remain invisible on neonatal radiographs with some regional exceptions: First, secondary (epiphyseal) ossification centres (SOC) are present at the knee (i.e. distal femoral epiphysis and proximal tibial epiphyses). These should not be confused with the patella, which remains cartilaginous until later infancy (3–6 years). Second, a secondary ossification centre might be visible in the humeral head of term infants. At the hand, the carpus is still cartilaginous without radiographically visible ossification centres. While the calcaneus and talus are physiologically ossified in a term neonate, the midfoot structures are still invisible on radiographs. The cuboid shows a variable degree of ossification and can be ossified in full-term babies. Please note that secondary ossification of the epiphyses is a continuous, long-term process expressing skeletal growth and maturity. Thus, please be reminded, that physiologic epiphyseal ossification is always partial in neonates (at the knee, hindfoot, and proximal humerus).

The vertebral bodies are ossified but have a distinct morphology; they are ovoid in shape with prominent anterior vascular (nutrient) channels. There are two physiologic cartilaginous “gaps” between the vertebral bodies and the two vertebral hemiarches (= neurocentral synchondrosis). The neurocentral synchondroses can be seen on lateral and oblique radiographs; they must not be confused with pathologic vertebral clefts, especially coronal clefts (Fig. 14.25). Likewise, the two osseous hemiarches are connected by carti-

J. M. Patsch (✉)
Division of General and Pediatric Radiology,
Department of Biomedical Imaging and
Image-Guided Therapy, Medical University
of Vienna, Vienna, Austria

Vienna Bone and Growth Center, Medical University
of Vienna, Vienna, Austria
e-mail: Janina.patsch@meduniwien.ac.at

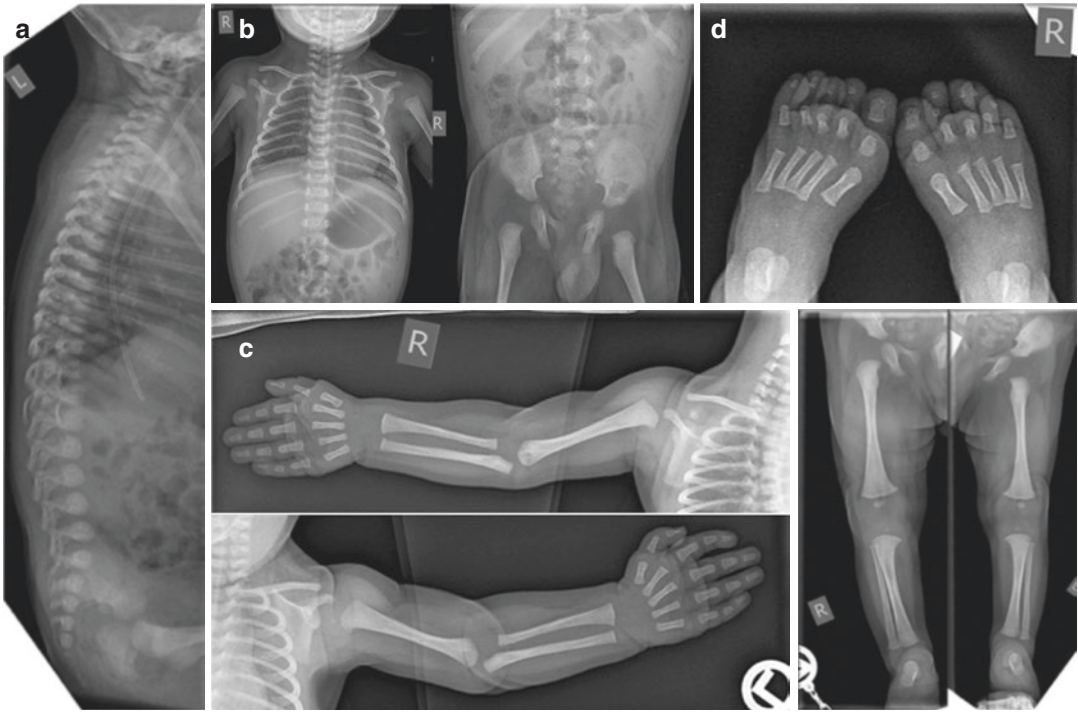


Fig. 14.1 (a–d) Normal radiographic appearance of a neonatal skeleton (a) spine, (b) thorax and pelvis, (c) upper extremities, and (d) lower extremities



Fig. 14.2 Physiologic posterior synchondrosis of vertebral hemiarcs in a neonate. Maximum intensity projection (MIP) reconstruction of computed tomography data. The hemiarcs fuse during the first years of life

lage which facilitates spinal sonography in newborns. This posterior midline “gap” should also not be mistaken for dysraphism or a sagittal cleft (“butterfly vertebrae”) on frontal radiographs (Fig. 14.2).

Please also note that the anterior arch of the atlas (C1) only ossifies during the first year of life. At birth, all sacral segments should be ossified and visible, again there is a large cartilaginous proportion of the sacrum which ossifies later in life. The coccyx is mostly cartilaginous with focal segmental ossifications.

Importantly, ultrasound (US) and magnetic resonance imaging (MRI) can be used to depict all cartilaginous anlagen which remain otherwise invisible on radiographs unless secondary ossification has started.

14.3 Abnormal Shape and Ossification Defects of the Skull

14.3.1 Craniosynostosis

The fontanelles and all sutures of the newborn should be patent at birth. The premature closure of a suture

Fig. 14.3 Craniosynostosis. Schematic drawings demonstrate common types and associated pathologic head shape

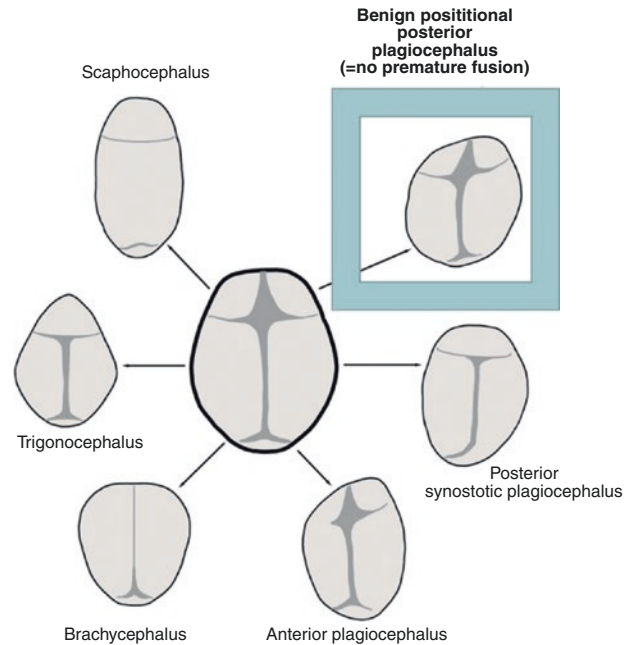


Table 14.1 Craniosynostosis: terminologies and affected sutures

Fused suture(s)	Terminology
Sagittal suture	Scaphocephalus
Metopic suture	Trigenocephalus
Both coronal sutures	Brachycephalus; can also lead to Turricephalus
Single coronal suture	Anterior plagiocephalus
Single lambdoid suture	Posterior synostotic plagiocephalus

(= craniosynostosis) leads to an abnormal head shape with specific shape pathologies being linked to specific suture pathologies (Fig. 14.3; Table 14.1).

In the case of clinical suspicion of craniosynostosis, US offers a quick and patient-friendly option for diagnosis.

How to Performed US of Cranial Sutures to “Rule Out” Craniosynostosis

Before the scan is started, the head shape needs to be inspected thoroughly.

It is advised to perform skull and suture palpation. The subsequent scan needs to be approached systematically, suture by suture:

Specifically, the sagittal, metopic, both coronal, and both lambdoid sutures are to be scanned and documented accordingly.

The transducer (a hockey stick or at a least high-resolution linear transducer) is placed at a 90° angle to the course of the suture, the entire suture must be followed and checked for patency.

- A patent suture can be recognised by a sharply delineated, echo-free gap between two skull bones (Fig. 14.4a—right image).
- In premature fusion, the gap is absent and a characteristic ridge formation can be seen (Fig. 14.4a—left image).

For detailed surgical planning, computed tomography (CT) is the method of choice due to excellent bone contrast and the option of 3D-reconstructions. Conventional radiographs are of limited relevance: sensitivity and specificity are clearly inferior to US and CT. If they are done, a tilted oblique view in two planes is recommended to properly be able to visualise and assess all the relevant sutures (Fig. 14.5).

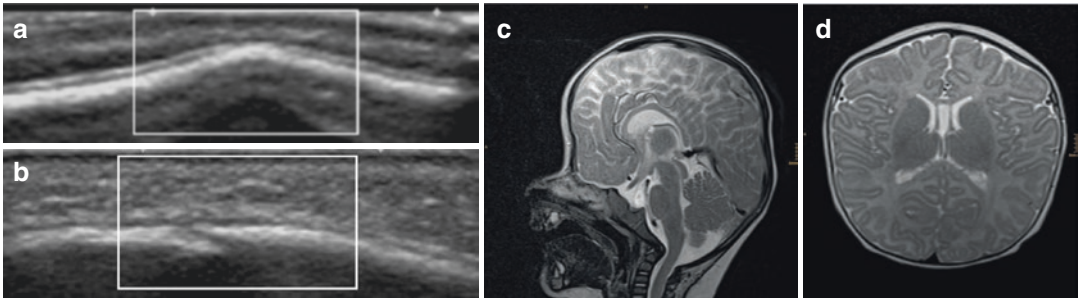


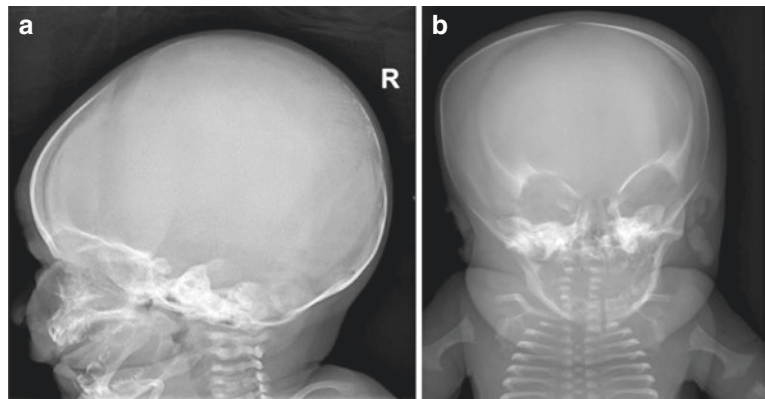
Fig. 14.4 (a–d) Craniostynosis: Ultrasound and MR. (a) Ultrasound demonstrates ridge formation (highlighted by box) in premature suture fusion (left image); right image shows patent suture with normal appearance. (b)

Sagittal T2-weighted MR image showing brachy-/turri-cephalus in bilateral coronal synostosis. (c) Axial T2-weighted MR image of same child

Fig. 14.5 Lateral radiograph in Craniostynosis (Scaphocephalus). Lateral radiograph with elongation of the skull due to premature fusion of the sagittal suture



Fig. 14.6 (a, b) Mineralisation/ossification defects of the skull. (a) Significant calvarial ossification defects in a neonate with hypophosphatasia (b) Complete absence of skull ossification in a perinatally lethal skeletal dysplasia. Please note severe rhizomelia and thoracic hypoplasia



14.3.2 Abnormal Mineralisation/ Ossification of the Skull

In full-term infants, the skull, the skull base, and the face including the mandible should be ossified. However, the neonatal mandible is still cartilaginous in the midline (= symphysis menti). In neonates, the paranasal sinuses are just slit-like structures and are barely visible on

radiographs. Teeth eruption starts 6 months after birth. In a neonatal skull radiograph, dental crypts and initial calcifications of the dental crowns should be visible. Absence of crown calcifications/crypts can be observed in certain skeletal dysplasias (e.g. chondroectodermal dysplasia).

Global and focal ossification defects of the skull (Fig. 14.6) can be noted in skeletal dysplasias, some

syndromes, chromosomal anomalies, and major disorder of bone metabolism (e.g. osteogenesis imperfecta; neonatal hypophosphatasia; Menkes disease). Parietal foramina are considered a normal variant. In osteogenesis imperfecta or other congenital systemic bone disease, “Wormian bones” can be seen; they are small bones, located within a suture, typically within the lambdoid suture. The bone density of the skull should also be considered and rated as normal, increased (e.g. in osteopetrosis) or decreased (e.g. in major disorders of bone metabolism).

14.4 Visible or Palpable Lesions of the Paediatric Head and Neck

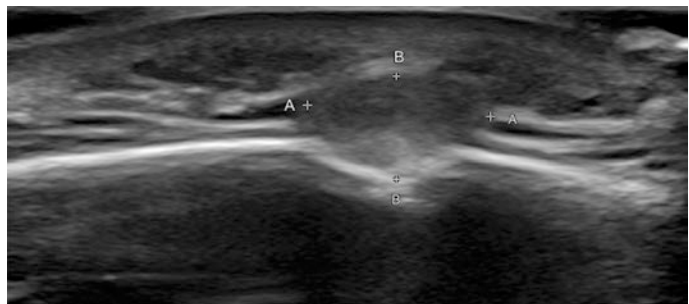
Visible and/or palpable head and neck lesions are common in neonates. These are mostly benign lesions, but they often cause significant anxiety among parents. Here, the use of US is ideal to differentiate typical benign lesions from rarer entities including those suspicious for malignancy. In addition to a characteristic US imaging appearance, many lesions have typical localisations and palpatory findings.

14.4.1 (Epi)-Dermoid Cysts

- Congenital, benign lesion (= inclusion cyst)
 - Epidermoid cyst: ectodermal elements
 - Dermoid cyst: ectodermal elements + skin elements

(US imaging) Features (Fig. 14.7):

Fig. 14.7 (Epi)-dermoid cyst. Congenital palpable skull lesion with suture association and osseous scalloping. The echogenicity depends on content of the inclusion cyst



- Sharply marginated
- Filled with sebaceous material, thus often not echo-free but of intermediate US signal. Small hyperechogenic foci (fat; Ca²⁺) possible
- No vascular signals within the mass on Colour Doppler sonography (CDS)
- Almost always have a relation to sutures or the midline
- Sutures are often “scalloped”

14.4.2 Haemangioma

- Congenital or infantile (mostly appear during first few weeks of life)
- True but benign neoplasm (= not a vascular malformation)
- Visual aspect: mass, often with bluish colour (depending on the location and depth of the lesion)

(US imaging) Features (Fig. 14.8):

- Mostly of increased echogenicity
- Imaging appearance depends on biological phase of activity (in neonates typically in proliferation vs. involution; effects of therapy) and possibly complications (e.g. bleeding)
- High vascularity on CDS
- Arterial and venous Doppler signals on pulse-waved Doppler
- In addition to defining exact localisation and depth, US can also detect changes in the internal vascular signals (in response to potential therapy with beta-blockers)
- For large lesions and to properly assess size and extent/depth, MRI may become necessary

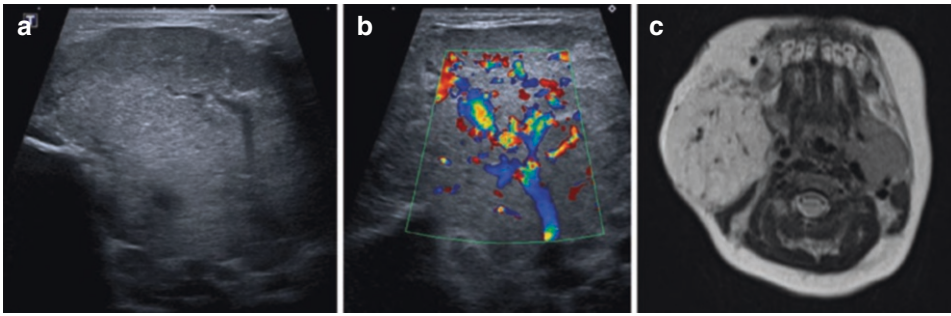


Fig. 14.8 (a–c) Parotid haemangioma in a neonate (= in proliferation). (a) Grey-scale US demonstrates right-sided mass with (b) high vascularity on CDS; (c): Large mass

was confirmed by MRI (T2 TSE; axial plane). Multiple flow voids correspond to high vascularity

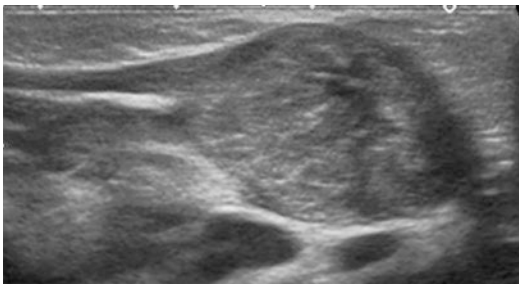


Fig. 14.9 Fibromatosis colli. Ultrasound: Lateral longitudinal view (using a high-resolution linear transducer) demonstrates swelling of the sternocleidomastoid muscle; respecting anatomical boundaries

14.4.3 Fibromatosis Colli

- Mass along the course of the sternocleidomastoid muscle, mostly after prolonged/difficult birth or intrauterine packing/foetal malposition
- Several causes are discussed (haematoma versus muscle injury versus consecutive fibrotic changes or a mix of these factors)
- Torticollis often not pronounced in neonates, develops later if untreated (by physiotherapy)
- Develops during first weeks of life
- Visual aspect

(US imaging) features (Fig. 14.9):

- Focal swelling of the sternocleidomastoid muscle (! compare to other side!)
- Heterogenous echogenicity possible
- Increased flow/vessel signals on CDS possible

14.4.4 Lymphatic Malformations

- Congenital (if large, mostly known antenatally by prenatal US and/or foetal MRI)
- (Imaging) features (Fig. 14.10):
- Septate/multicystic lesion on US—can depict even very small cysts
- Echogenicity very low, unless there is intracystic haemorrhage
- Solid components may be seen
- Sedimentation and motion of small particles within cystic spaces can be seen
- Role of US is less important in large lesions spanning multiple anatomic compartments
- In large lymphatic malformations, MRI is particularly important because of
 - Reproducible assessment of size and location of the malformation (including individual cysts size) and anatomical relationship of the malformation to surrounding structures
 - Airway narrowing can be well documented and quantified
 - MRI = operator-independent 3D imaging

14.4.5 Cervical (Lymph)-Adenitis

- Palpable lymph nodes can cause a lot of uncertainty in (new) parents
- (US imaging) features (Fig. 14.11):
 - Hypoechoic signal, oval shape, and sharp margins (short-axis to long-axis ratio of less than 0.5).

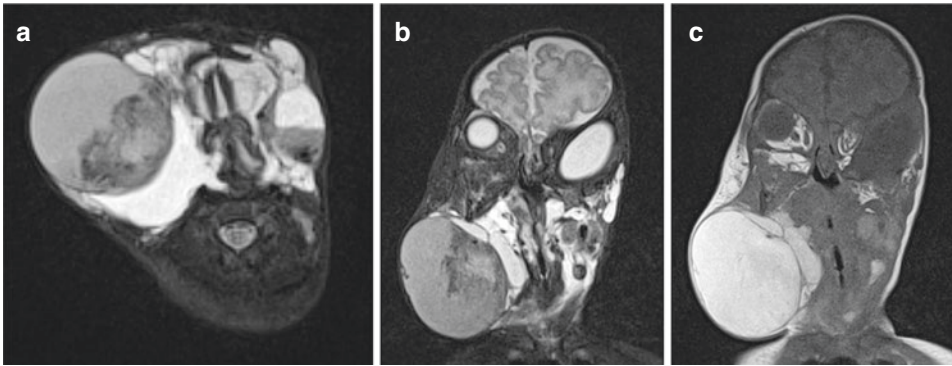


Fig. 14.10 (a–c) Lymphatic malformation in a neonate. Magnetic resonance imaging (MRI) shows large, multi-cystic neck mass. (a) Axial STIR. Note haemorrhage in several large cysts (hypointense on T2). (b) Coronal STIR

highlights extension into multiple anatomic neck spaces, also visible in axial plane (a). (c) Intralesional haemorrhagic components are hyperintense on T1-weighted TSE

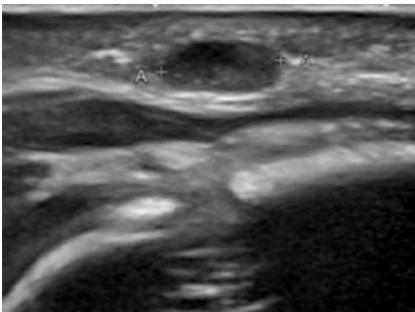


Fig. 14.11 Reactive lymph node in a newborn. Ultrasound image from oblique view of the occiput, using a high frequency linear transducer Ovoid shape (short-axis to long-axis ratio < 0.5). No connection to bone or underlying bone or suture

- Hilar structures can be depicted (fat/vessels).
- Note that hilar vascularisation cannot always be visualised due to the small size of the structures and patient motion.
- Complication = suppuration + neck abscess.

14.4.6 Malignant Neck Masses in Neonates (Please See Also Chap. 16)

- In general, exceedingly rare
- Important differential diagnosis are:
 - **Neuroblastoma**

– Rhabdomyosarcoma

– Pathologic lymphadenitis

“Tip of the iceberg in underlying malignancy”

Round in shape (short-axis to long-axis ratio > 0.5)

Hilar anatomy is disturbed; parenchymal changes

Vascularity often altered on CDS

14.5 Neonatal Osteomyelitis

Osteomyelitis is an infection of bone and bone marrow. Neonatal osteomyelitis differs significantly from infections in older children and adults. A key difference is based on the rich vascularity of the epiphyses, physes (= growth plates per se), and metaphyses in young infants (including neonates). There is a triple vascular supply through metaphyseal, epiphyseal, and perichondral/intrinsic vessels crossing the physis.

Of importance, in neonates the crossing vessels are particularly strong and prominent.

As a result, any infection that seeds in the metaphysis can easily spread towards the epiphysis and the joint, leading to secondary septic arthritis (or the other way round). Epiphyseal cartilage is very vulnerable to the (acidic) microenvironment of inflammation/infection, with disastrous sequelae including joint destruction (Fig. 14.12).

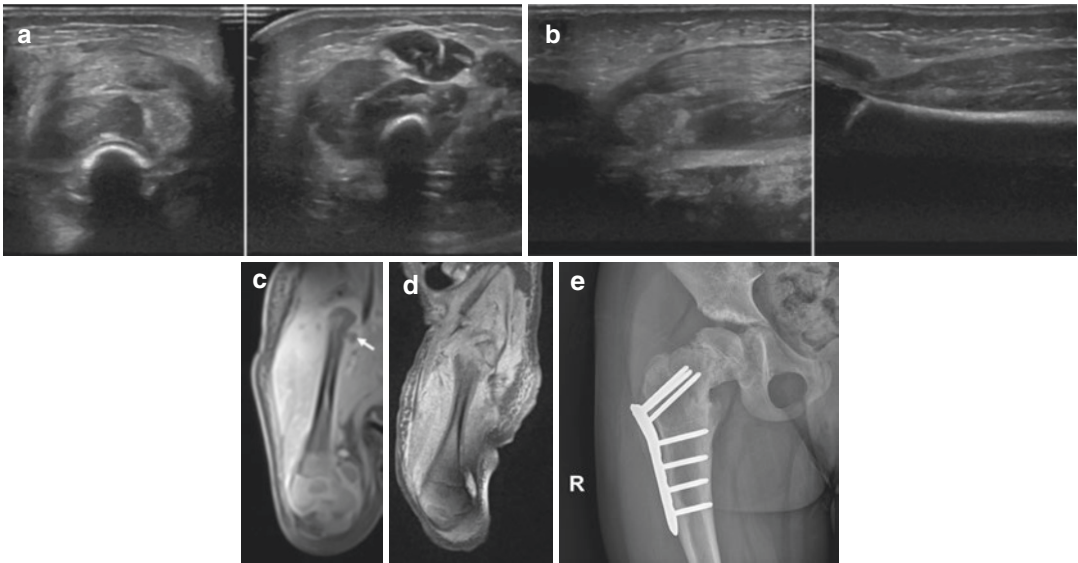


Fig. 14.12 Imaging findings in neonatal osteomyelitis. (a) US demonstrates subcutaneous and intramuscular oedema on axial view of the right thigh. There is a subperiosteal fluid collection; unaffected left side is shown for comparison. (b) Sagittal view of affected right thigh

and left normal side for comparison. (c) MR image demonstrates soft tissue abscess (T1-weighted; Gadolinium-enhanced; coronal plane). (d) Sagittal MR image (T2-weighted) at 8 weeks with (post-infectious) epiphysiolysis. (e) Long-term sequelae at the age of 6 years

Importantly, neonatal osteomyelitis is lacking early and specific clinical symptoms.

- Infants present themselves with
 - General malaise
 - Reluctance to drink
 - Limited mobility of the affected extremity (= pseudo-paralysis)
 - Local hypersensitivity to touch
- Soft tissue swelling can be difficult to be detected in neonates and young infants (due to significant amounts of subcutaneous fat)
- Expression of pain is equivocal
- Fever is an inconsistent sign in neonates

Ultrasound is of major diagnostic importance because soft tissue changes (= edema), subperiosteal abscess formations, joint effusion, and local hyperemia can be detected.

Magnetic resonance tomography is essential in order to determine the intraosseous extent of the infection (which cannot be seen by US unless there is a large cortical defect) and the spread to different anatomical compartments. The adminis-

tration of gadolinium-based contrast agents is indicated. Abscess formations can also be detected using diffusion-weighted imaging/ADC maps.

14.6 The Floppy Infant, Suspected Myopathy/Muscle Disease

Congenital myopathies are rare diseases with a wide clinical spectrum of onset and severity. With neonatal onset, children present with low postnatal muscle tonus (= “floppy infant”). In primary myopathies, structural muscle genes or pathways important for muscle metabolism are affected. Based on the predominant findings in the muscle biopsy, five main sub-groups of congenital myopathies are defined:

- Core myopathies (e.g. RYR1).
- Nemaline myopathies (e.g. ACTA1).
- Centronuclear myopathies (e.g. MTM1).
- Congenital fibre type disproportion myopathy.
- Myosin storage myopathy.

The vast majority of muscle disorders present after the newborn period, however, in some cases early hypotonia (= “floppy infant”) can be observed (e.g. Duchenne’s). Spinal muscle atrophy Type 1 (Werdnig-Hoffmann) presents between birth and the age of 6 months with hypotonia, poor head control, feedings difficulties, and fasciculations of the tongue. Genetic testing and muscle biopsy are key for finding the right diagnosis in suspected muscle disease.

Further, myopathy can co-exist in a multitude of inborn-errors of metabolism (e.g. mitochondrial disease, storage diseases [e.g. Pompe’s] or complex genetic syndromes).

The prevalence of additional orthopaedic problems such as developmental dysplasia of the hip with dislocation or clubfeet is increased in children with muscle diseases.

Neonatal myo-sonography can be helpful in documenting pathologic appearance of skeletal muscle, thereby narrowing down the wide spectrum of differential diagnoses for low muscle tone, and possibly defining a promising muscle tissue for a diagnostically useful biopsy.

How to Perform Muscle US in a Newborn

Myo-sonography should be performed according to a structured acquisition protocol.

The following five regions should be scanned bilaterally (in the axial plane):

- Rectus femoris muscle
- Tibialis anterior muscle

- Gastrocnemius muscle (Fig. 14.13a)
- Biceps brachii muscle (Fig. 14.13b)
- Triceps brachii muscle

Images have to be documented in b-mode with correct labelling of region and side. Additional video loops are recommended.

Imaging features of pathologic muscle

By US, myopathic musculature has high echogenicity due to oedema and fatty infiltration. MRI can quantify these pathological changes (oedema; fatty infiltration/atrophy) in a more operator-independent manner.

14.7 Medical Devices and the Neonatal Skeleton: Intraosseous Needles

In neonatal medical emergencies, the establishment of vascular access poses a significant challenge. In such situations, the placement of an intraosseous needle can offer a quick and safe alternative solution for drug administration.

Typically, an intraosseous needle is placed in the anterior proximal tibia with safety distance to the growth plate (Fig. 14.14). Depending on the product, other sites for placement are possible (e.g. medullary cavity of other long bones including femur and humerus). As important complications, bleeding, iatrogenic injury of the posterior proximal tibia (or other bone depending on site), and secondary infections can occur.

Fig. 14.13 Ultrasound of the gastrocnemius muscle (a) and biceps brachii (b). Note severe atrophy and increased echogenicity of muscle compared to surrounding subcutaneous fat in a 4-month-old boy with RYR1-myopathy

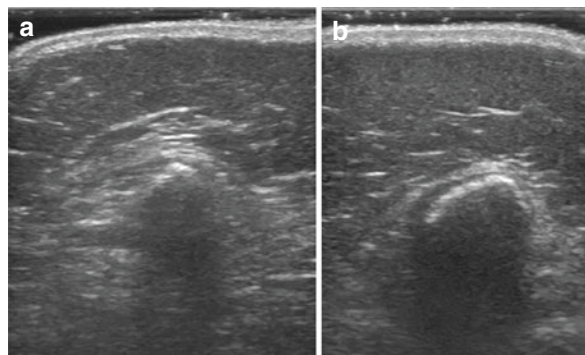




Fig. 14.14 Intraosseous needle in a neonate. Radiograph demonstrates correct placement of an intraosseous needle in the anterior proximal tibia

14.8 Insufficiency Fractures in Hospitalised Neonates and Preterm Babies

Rib fractures are occasionally observed in preterm neonates, children with long ICU stays, and those with severe congenital chronic diseases (e.g. hepatopathy). Genetic or metabolic bone diseases (e.g. osteogenesis imperfecta) can also present with fractures at other locations (e.g. long bones).

From a diagnostic point of view, insufficiency fractures are often identified as incidental findings. Rib fractures incidentally detected on chest radiographs are the most common types. Newborns tend to have strong callus formation which must not be mistaken for a bone neoplasm. Fractures and callus can also be confirmed by US, but in the majority of the cases the radiographic changes are diagnostic and no further imaging is required.

Importantly, whenever a fracture is discovered by diagnostic imaging, the cause for the fracture needs to be clarified to make sure cases of abuse are not missed (Please also see Chap. 17 on non-accidental injury and birth trauma).

14.9 Congenital Anomalies of the Musculoskeletal Tract: A First Aid Kit

From a systematic point of view, congenital musculoskeletal anomalies can be either isolated (i.e. a local pathology only) or associated with other

malformations or phenotypic traits (e.g. in syndromes).

This chapter does not intend to provide a full list of paediatric orthopaedic conditions but to review those of importance. Likewise, the reader is referred to comprehensive reference books (e.g. Taybi & Lachmann's) with regard to the radiology of syndromes. Nevertheless, this chapter aims to serve as a radiologic "first aid kit" when dealing with congenital malformations of the musculoskeletal tract. Furthermore, please use the references and recommended books attached.

14.9.1 Lower Extremity: Congenital Femoral Deficiency (CFD)

The term congenital femoral deficiency contains several types of longitudinal femoral malformations (Fig. 14.15). While several classifications exist, the Paley classification is most widely used to describe the exact extent of the defect and to plan surgery: Defects with small but otherwise intact femur (Type 1) are differentiated from mobile pseudo-arthroses (Type 2) and major diaphyseal defects (Type 3). If the knee joint has structural deficiencies, a type 4 CFD is diagnosed.

With the femoral head being physiologically not ossified at birth, radiographs need to be inter-



Fig. 14.15 Congenital femoral deficiency (CFD). Radiograph shows short, dysmorphic left femur (later classified as Paley type 1b). (Image courtesy Orthopedic Hospital Speising (Rudolf Ganger, MD PhD))

preted with caution and regard to patient age. The presence of unossified cartilaginous structures relevant for Paley classification (i.e. the femoral head and neck) can be directly assessed by MRI and US. Fluoroscopic arthrograms are an alternative

but are invasive and require ionising radiation. Mild forms of femoral hypoplasia are typically diagnosed much later in life once the discrepancy in limb length becomes clinically more evident.



Fig. 14.16 Bilateral tibial hemimelia with complete absence of the left tibia. Radiograph of both lower extremities: Right tibia is hypoplastic, left tibia is missing. Please note associated severe bilateral foot abnormalities. (Image courtesy Orthopedic Hospital Speising (Rudolf Ganger, MD PhD))

14.9.2 Lower Extremity: Tibial Hemimelia

Longitudinal defects of the tibia (tibial hemimelia) present with significant lower leg shortening and deformity after birth, if not known from prenatal US and/or MRI.

They are also classified according to Paley.

Type 1 is a hypoplastic nondeficient tibia, in Type 2 the proximal and distal tibia epiphysis are present with a dysplastic ankle, in Type 3 the distal tibial plafond is absent with tibiofibular diastasis, in Type 4 there is distal tibial aplasia, and in Type 5 there is complete tibial aplasia. In addition, absent structures or duplications should be recorded for the entire extremity (specifically toes, metatarsals, tarsals, femur, fibula, distal tibial remnants, or femoral condyles). Tibial hemimelia is typically associated with multiple other congenital malformations including cardiac defects, CFD, and other orthopaedic conditions. It can be bilateral (Figs. 14.16 and 14.17). Other

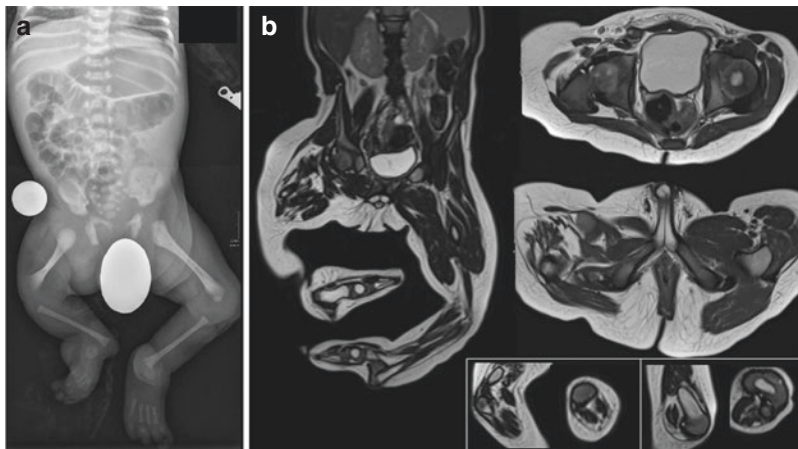


Fig. 14.17 (a, b) Complex malformation of both lower extremities. (a) Radiograph shows congenital femoral deficiency on the right. Bilateral tibial aplasia. Associated ray defects on both feet. (b) MR: All images are T2 TSE (1.5 T). Coronal and axial views highlight severe associ-

ated muscle hypoplasia. MR confirms the presence of a relatively normal femoral head with signs of delayed ossification/maturation. The white box shows absence of patella on the right and the contralateral knee for normal comparison

(= older) classifications are from Kalamchi & Dawe, Weber, and Jones.

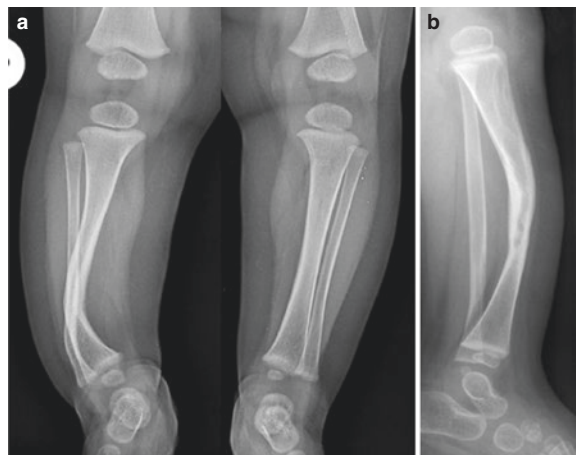
14.9.3 Lower Extremity: Fibular Hemimelia

Although fibular hemimelia is more frequent than tibial hemimelia, it is often diagnosed later than in the neonatal period (Fig. 14.18). Clinical signs are limb shortening and associated foot deformities. The Paley classification for fibular hemimelia describes the following main types: Type 1 stable ankle, Type 2 dynamic valgus ankle, Type 3 fixed equino-valgus ankle, Type 4 fixed equinovarus ankle. The cruciate ligaments can be absent as



Fig. 14.18 Fibular hemimelia in a 2 year old. Radiograph of both lower limbs. The right fibula is hypoplastic, there is associated dysmorphia and shortening of the right tibia. (Image courtesy Orthopedic Hospital Speising (Rudolf Ganger, MD PhD))

Fig. 14.19 Congenital (pre-) pseudoarthrosis of the tibia (CPT) with anterolateral bowing. (a) Radiographs show pathologic right (antero-)lateral bowing and normal left side. Patient age is 9 months. (b) Lateral radiograph in another patient (1.5 years) demonstrating pronounced anterior bowing and pathologic bone morphology as fracture precursor



well. Congenital femoral deficiency and congenital abnormalities of the feet are highly associated with fibular hemimelia. Other classifications date back to Achtermann/Kalamchi, and Birch.

14.9.4 Lower Extremity: Anterolateral Bowing of the tibia (= Congenital (Pre)-Pseudoarthrosis of the Tibia; CPT)

In anterolateral bowing of the tibia, a congenital local disorder of periosteal soft tissue and bone formation leads to altered biomechanical properties of the affected bone with consecutive local deformity and fracture with pseudoarthrosis (Fig. 14.19). The deformity is typically noted during the first year of life with increased tibial curvature (i.e. anterolateral bowing). Rarely it is seen right after birth.

Tibial dysplasia has a strong association with neurofibromatosis Type 1 (NF 1), but can also occur in an isolated pattern.

14.9.5 Lower Extremity: Posteromedial Bowing (Crus Valgum Recurvatum)

This rare congenital deformity presents with posteromedial bowing of the tibia and associated ankle deformities (Fig. 14.20). (Partial) spontaneous improvement of osseous bowing is possible.

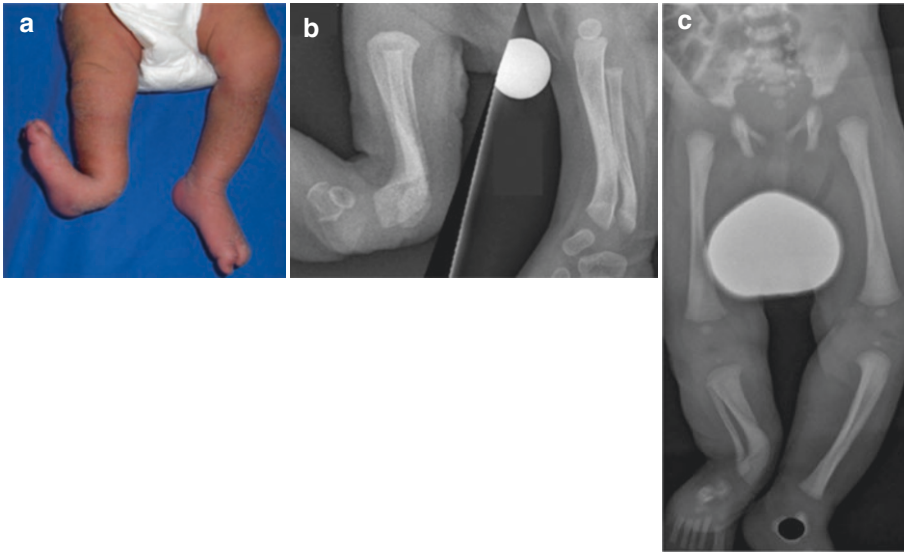


Fig. 14.20 Postero-medial bowing (*Crus valgum recurvatum*). (a) Radiographs and clinical photography demonstrating major bowing deformity. (b) Radiographs in another case of postero-medial bowing after birth (left image) and significant improvement at follow-up

(7 months; right image). (c) Radiographs demonstrating major bowing deformity in the same child as in Fig. 14.20a (Image courtesy Orthopedic Hospital Speising (Rudolf Ganger, MD PhD))

14.9.6 Lower Extremity: Selected Congenital Abnormalities of Feet

Clinical examination is key to the diagnosis in congenital foot anomalies in neonates.

If—after clinical examination—radiographs are still needed in suspected alignment disorders, weight-bearing should be simulated in neonates. The weight-bearing simulation can/should be omitted in full skeletal surveys (to rule out dysplasia), in cases of suspected abuse (to rule out old or new fractures), and in cases of suspected bone fragility (e.g. osteogenesis imperfecta).

Disorders of foot alignment with relevance for neonates

- **Metatarsus adductus:**
 - Very common alignment disorder, mostly likely due to intrauterine packing (not seen in prematurity)
 - Does not require imaging
 - If imaging is done:
 - Normal talocalcaneal angle + adducted forefoot

Check for rigidity (= fixed deformity?)

Other abnormalities?

- **Clubfoot (*Talipes equinovarus*)**
 - Often known from prenatal ultrasound and/or MRI, especially in complex malformations with associated clubfeet (e.g. meningomyelocele, ...)
 - Combination of
 - Increased tibio-calcaneal angle ($>90^\circ$ on lateral views)
 - Hindfoot and forefoot varus (AP)
 - Additional views in maximum dorsiflexion: changes in tibio-calcaneal angle and/or talocalcaneal angle?
- **Congenital vertical talus (*Rocker bottom foot*)**
 - Severe congenital rigid flatfoot with convex planta pedis (\rightarrow name)
 - Equinus + hindfoot valgus + severe plantarflexion at the talus
 - Additional view: maximum plantarflexion (persistence of high cuboid position relative to talus?)
 - See Fig. 14.21

Other congenital abnormalities of the feet include those related to failure of formation (ray defects, e.g. associated with hemimelia), abnormal differentiation (synostosis, syndactyly), duplications (pre-/postaxial polydactyly), overgrowth (macroductyly), undergrowth (e.g. brachymetatarsia). Like in the hand, congenital constriction bands syndrome can cause deformities ranging from mere cosmetic problems to amputations along with secondary fusion abnormalities. The feet always have to be examined clinically in generalised skeletal anomalies (e.g. dysplasias and complex syndromes), radiographs can be used thereafter to confirm or rule out the suspected changes. Associated foot anomalies are very common in longitudinal malformations of the lower extremities (e.g. CFD, tibial hemimelia, fibular hemimelia).



Fig. 14.21 Congenital vertical talus (rocker bottom foot). Lateral radiograph shows convexity of planta pedis giving rise to the term “rocker bottom foot”. There is a combination of pes equinus, severe plantarflexion of the talus, and hind-foot valgus. The cuboid has high position relative to talus

14.9.7 Upper Extremity: Selected Congenital Abnormalities of Hands

Congenital malformations of the hand can occur as isolated defects or in conjunction with complex syndromes (Fig. 14.22). The IFSSH classification differentiates seven major groups of defects (Table 14.2).

The sole indication for neonatal surgical management of hand malformations are cases of suspected ischaemia in children with amniotic bands. All other defects are managed at a later timepoint, mostly by multiple consecutive surgeries.

14.9.8 Congenital Joint Dislocations and Contractures

Congenital joint dislocations can occur in children with connective tissue disorders (e.g. Larsen syndrome). Besides the hip, large joints such as the knee and the shoulder are typically affected (Fig. 14.23).

The term “arthrogryposis” describes a clinical pattern of multiple joint contractures but the underlying spectrum of diseases is wide and heterogeneous.

14.9.9 Congenital Malformations of Vertebrae

Severe congenital spinal malformations are often known prenatal US and/or foetal MRI, especially if they are associated with complex defects (e.g.

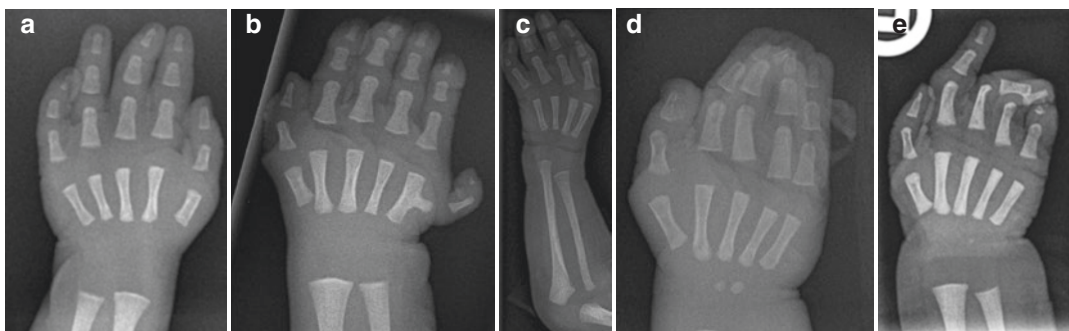
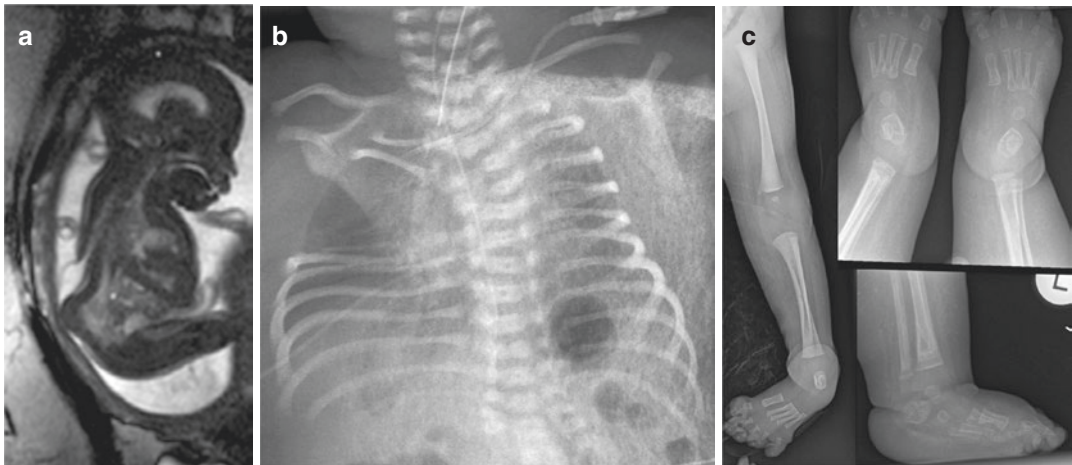
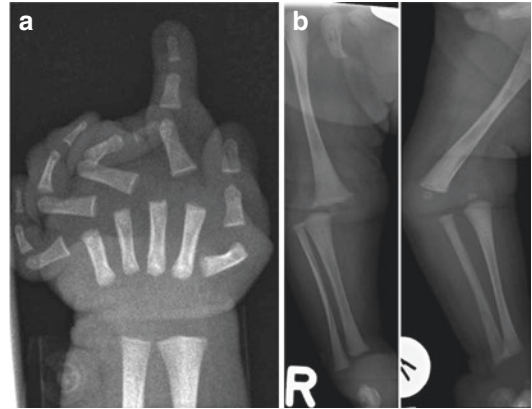


Fig. 14.22 (a–e) Congenital abnormalities of the hand. Radiographs show (a) a normal neonatal hand, (b) postaxial polydactyly, (c) radial ray defect with aplasia of the thumb

and first metacarpal; short radius, (d) syndactyly with a non-osseous postaxial appendage, and (e) constriction bands syndrome (amputations combined with syndactyly)

Table 14.2 Congenital malformation of the hand—IFSSH classification

Category	Example/context
Failure of formation	Longitudinal defects (e.g. Radial ray deficiency) Transverse defect (e.g. Symbrachydactyly)
Failure of differentiation	Radioulnar synostosis
Duplication	Pre/postaxial polydactyly
Overgrowth	Macroductyly
Undergrowth	Brachydactyly
Congenital constriction bands syndrome	Amniotic bands
Generalised skeletal anomalies	Hand malformations in complex syndromes (e.g. Apert)

Fig. 14.23 Multiple congenital joint dislocations in a connective tissue disorder. (a) Hand radiograph shows multiple dislocated metacarpophalangeal and interphalangeal joints. (b) Lower extremity radiographs show dislocated knee joint (left = anteroposterior; right = lateral view)**Fig. 14.24** Complex defect (thoracic meningocele, vertebral malformation, abnormal ribs, clubfeet). (a) Foetal MRI (Image courtesy Department of Neuroradiology and Musculoskeletal Radiology, Medical University of

Vienna (Gregor Kasprian, MD)) shows open dysraphism with thoracic meningocele. (b) Chest radiograph demonstrating right-sided major rib anomalies. (c) Lower limb/foot radiographs show bilateral club feet

dysraphism, myelomeningocele) or lead to severe congenital scoliosis (Fig. 14.24a).

However, in the majority of cases vertebral malformations often remain undetected unless

incidentally captured on radiographs of the chest or the abdomen. In general, as scoliosis only develops over time, vertebral anomalies cannot be detected by clinical examination alone; some

are picked up on chest radiographs (Fig. 14.24b). Only in few specific scenarios, dedicated neonatal spine radiographs are actually indicated (e.g. to rule out/quantify sacral dysgenesis in anorectal malformations or as part of skeletal surveys in neonates with suspected skeletal dysplasia). Vertebral malformations are easily depicted by cross-sectional imaging techniques. However, they must not be overlooked on cross-sectional studies which are acquired for non-spinal indications (e.g. cardiac CT). In neonates with suspected or confirmed complex syndromes, the probability of associated spinal malformations is increased (e.g. VACTERL, Alagille syndrome...), and other associated skeletal pathology must be kept in mind (Fig. 14.24c).

In vertebral malformations, specific terms should be used for reporting specific anomalies:

- **Formation disorders:**
 - **Hemivertebrae**
Half (or more) of the vertebral body is missing
AP/coronal view: wedged appearance
 - **Butterfly vertebrae**
Two half vertebrae are separated by a sagittal cleft (seen on AP/coronal views)
Figure 14.25c, d

- **Segmentation disorders**
 - **Fused vertebrae** (complete vs. partial)
 - **Unsegmented bars** lead to significant scoliosis over time but are often not detected until scoliosis develops in infancy

14.10 The Neonate with Suspected Skeletal Dysplasia: A Radiologic Approach

The suspicion of skeletal dysplasia is mostly raised by prenatal US detecting proportionate or disproportionate short stature/limbs, facial dysmorphism (e.g. midface hypoplasia, flat nasal bridge, cleft palate, ...) and/or other skeletal abnormalities (e.g. fractures, bowing of long bones, ...). Unless a clear prenatal diagnosis is made, the majority of the diagnostic workup starts after birth, sometimes even later in infancy. In spite of the availability and major importance of genetic testing, the skeletal survey has a significant role to play in such a clinical scenario. In fact, the establishment of a correct genetic/syndromic diagnosis relies on a three-pillar approach based on diligent clinical workup, diagnostic imaging, and genetic testing. Of note, there is a wide spectrum of phenotypic morphology even within similar genetic

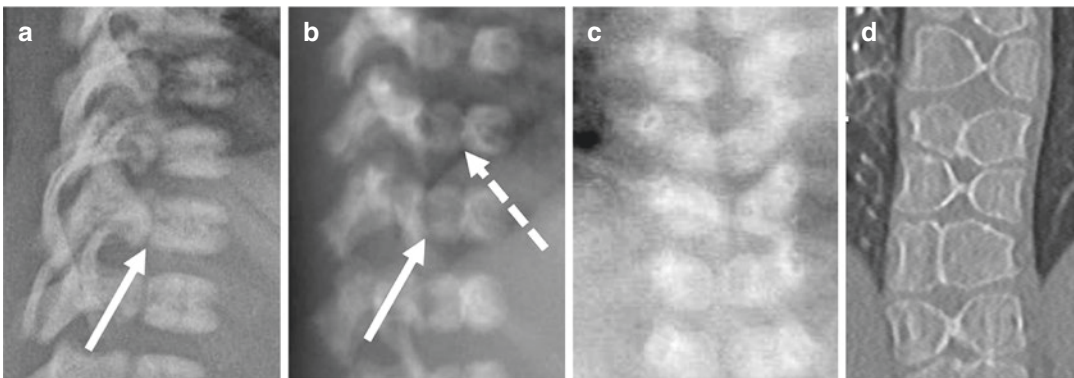


Fig. 14.25 Neonatal normal and abnormal vertebral bodies: Physiologic and pathologic appearance on imaging. (a) Lateral radiograph demonstrating normal shape and morphology of neonatal vertebrae with neurocentral synchondrosis (white arrow). (b) Coronal clefts (= pathologic, dotted arrow) in a child with skeletal dysplasia. White arrow highlights normal neurocentral synchondro-

sis. (c) AP view (zoom on chest radiograph) demonstrating multiple butterfly vertebrae (= sagittal clefts). (d) Coronal reformation of computed tomography (CT) demonstrating butterfly vertebrae; same child as in Fig. 14.25c, 5 years later (CT was done for planning of cardiac surgery)

disease background (e.g. different family members are affected to a different extent), thus a diligent description of radiologic findings is essential.

Unfortunately, radiographic signs are often reported with imprecise terminology, even among radiologists. Another challenge is that reference images in books or publications are not necessarily age-matched for the unsolved case you are currently dealing with. Often figures are too small to show the relevant radiographic features in sufficient resolution. Finally, a significant number of research publications on skeletal dysplasias is done without imaging experts and is simply reporting the presence of wrong features again triggering a vicious circle of misreporting.

In Chap. 16 of this book, a step-by-step approach on how to read a skeletal survey in suspected skeletal dysplasias is provided. A list and description of terms/features that are useful in the workup of a neonatal skeletal survey is also given.

14.10.1 Which Views/Planes Should Be Included in a Neonatal Skeletal Survey?

To some degree, skeletal surveys vary from centre to centre or from country to country, mainly in terms of included views. Watson et al. have reviewed this issue from a UK, European (European Dysplasia Network; ESDN), and U.S. standpoint (American College of radiology; ACR/International Skeletal Dysplasia Registry—Cedars-Sinai Medical Centre). The recommendations vary to a certain extent with main differences being on whether (1) to include both upper and lower limbs, (2) to acquire whole body films in neonates, (3) to include a lateral view of the knee (which does not apply to neonatal surveys), and (4) to include the skull to the routine protocol (Watson et al. 2015).

At our centre, we have adapted and expanded the U.K. version (Offiah and Hall 2023) as follows:

- Spine (lateral; cervico-thoraco-lumbar)
- Chest (AP; to include both clavicles and the cervical spine)
- Pelvis + lumbar spine (AP)
- Both lower extremities (AP)
- Both upper extremities (AP)
 - Please check carefully whether all fingers and toes (!) are completely depicted, if not, then add both hands AP and both feet AP

At our centre, additional views (e.g. skull, lateral knee) are acquired for specific indications.

Summary and Takeaway Message

Although the majority of congenital skeletal disorders are rare and require referral to tertiary centres of expertise, the general (paediatric) radiologist may encounter a wide variety of paediatric bone and joint pathologies in neonates. The use of diagnostic imaging has to be coordinated with treatment plans to avoid unnecessary exams and radiation. Along those lines, imaging of “lumps and bumps” and suspected musculoskeletal infections should always start with ultrasound.

Acknowledgement I would like to thank Rudolf Ganger, MD PhD (Orthopedic Hospital Speising, Vienna, Austria; for providing me with clinical photographs and radiographs of congenital malformations of the lower extremities), Lukas Schmölz (for research assistance) and Valentin Patsch (for figure design and creation). Thanks to my family for giving me the time to write both Chaps. 14 and 16 of this book.

Further Reading

- Adam A, Dixon A, Gillard J, Schaefer-Prokop C. Grainger & Allison's diagnostic radiology. 7th ed. Amsterdam: Elsevier; 2020.
- Bansal AG, Oudsema R, Masseaux JA, Rosenberg HK. US of pediatric superficial masses of the head and neck. *Radiographics*. 2018;38(4):1239–63.
- Claeys KG. Congenital myopathies: an update. *Dev Med Child Neurol*. 2020;62(3):297–302.
- Freyschmidt J. 'Koehler/Zimmer'. *Borderlands of normal and early pathological findings in skeletal radiography*. 5th ed. New York: Thieme; 2003.
- Fuller CB, Lichtblau CH, Paley D. Rotationplasty for severe congenital femoral deficiency. *Children* (Basel). 2021;8(6):462.

- Glass RB, Fernbach SK, Norton KI, Choi PS, Naidich TP. The infant skull: a vault of information. *Radiographics*. 2004;24(2):507–22.
- Jaramillo D, Dormans JP, Delgado J, Laor T, St Geme JW III. Hematogenous osteomyelitis in infants and children: imaging of a changing disease. *Radiology*. 2017;283(3):629–43.
- Lachmann RS, editor. *Taybi and Lachmann's radiology of syndromes, metabolic disorders and skeletal dysplasias*. 5th ed. Amsterdam: Elsevier; 2007.
- Monroe EJ. Brief description of ISSVA classification for radiologists. *Tech Vasc Interv Radiol*. 2019;22(4):100628.
- Offiah AC, Hall CM. Observational study of skeletal surveys in suspected non-accidental injury. *Clin Radiol*. 2023;58(9):702–5. [https://doi.org/10.1016/s0009-9260\(03\)00226-5](https://doi.org/10.1016/s0009-9260(03)00226-5). PMID: 12943642.
- Paley D. Surgical reconstruction for fibular hemimelia. *J Child Orthop*. 2016a;10(6):557–83.
- Paley D. Tibial hemimelia: new classification and reconstructive options. *J Child Orthop*. 2016b;10(6):529–55.
- Raimann A, Haberler C, Patsch J, Ertl DA, Sadeghi K, Freilinger M, Lang S, Schmoock M, Plecko B, Haeusler G. Lethal encephalopathy in an infant with hypophosphatasia despite enzyme-replacement therapy. *Horm Res Paediatr*. 2021;94(9–10):390–8.
- Scrivens A, Reynolds PR, Emery FE, Roberts CT, WPolglase GR, Hooper SB, Roehr CC. Use of intraosseous needles in neonates: a systematic review. *Neonatology*. 2019;116(4):305–14.
- Tal L. Evaluation of Pediatric foot radiographs. 2012. <https://www.pedrad.org/Portals/5/Events/2012/Laor-Foot.pdf>
- Walleczek NK, Förster K, Seyr M, Kadroska N, Kolar J, Wasinger-Brandweiner V, Vodopiutz J. Rare skeletal disorders: a multidisciplinary postnatal approach to diagnosis and management. *Wien Med Wochenschr*. 2021;171(5–6):94–101.
- Watson SG, Calder AD, Offiah AC, Negus S. A review of imaging protocols for suspected skeletal dysplasia and a proposal for standardisation. *Pediatr Radiol*. 2015;45(12):1733–7. <https://doi.org/10.1007/s00247-015-3381-1>. Epub 2015; Jun 17. PMID: 26081673
- Review.

Imaging the Neonatal (and Paediatric) Hip

15

Gerolf Schweintzger and Michael Riccabona

15.1 Introduction and General Remark

Since the first report of “the diagnosis of congenital hip joint dislocation by ultrasound compound treatment” in 1980 by the Austrian orthopaedic surgeon Reinhard Graf, various methods on how to perform hip ultrasound (US) are described. They differ in their systematic approach.

Ultrasound has become the study of choice for evaluating paediatric musculoskeletal disorders and is today well established. It is superior to radiography in neonates and young infants because it can demonstrate the cartilaginous and soft tissue components of the hip joint in addition to the bony structures, which in this age is of tremendous importance.

The methods used for hip US around the world are described and the respective findings are illustrated. Additionally, other applications of US in paediatric hip conditions such as assessing hip effusion are discussed.

The two main queries for performing US of the hip need different examination techniques:

1. In neonates and infants, the goal is to assess developmental dysplasia of the hip (DDH). In this scenario, US is indicated either based on
 - (a) A clinical suspicion such as typical hip instability, clicks, foetal malposition, impaired mobility, neurological impairment, etc.
 - (b) Or as a general screening, particularly in regions or countries with high incidence or endemic DDH.
 - (c) Finally, in some countries and instances a selective screening is preferred, where the indication for a hip US examination is based on risk factors such as familial risk, breach presentation, endemic dysplasia, infants with risk factors, preterm infants, and so forth.
2. The aims of assessment throughout childhood are evaluation for hip joint effusion, capsular thickening, inflammation, or other pathology such as epiphysiolysis and Perthes disease.

15.1.1 Technical Requisites

High-resolution linear array transducers are recommended with a wide frequency range, from as high as 24 MHz, more commonly 18/15 MHz to 5 MHz (potentially “trapezoid/convex mode”—phased linear mode) depending on the age, the size of the infant, and the available equipment.

G. Schweintzger (✉)
Abteilung für Kinder- und Jugendheilkunde, LKH
Hochsteiermark, Leoben, Austria
e-mail: gerolf.schweintzger@kages.at

M. Riccabona
Medical University Graz, Graz, Austria

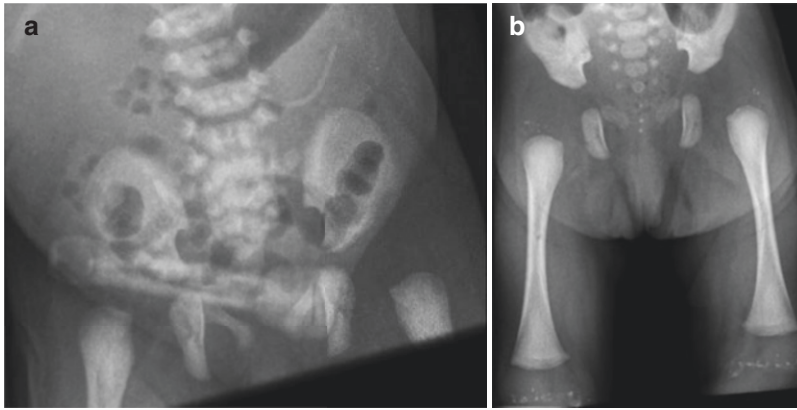


Fig. 15.1 Incidental findings in the neonatal hip on radiographs. **(a)** A neonatal pelvic radiograph taken for other reasons shows a split pelvis, sacrococcygeal hypoplasia (in caudal regression syndrome) and incidentally a hip dislocation on the left side. Superimposed is the

umbilical clamp. **(b)** A leg radiograph shows bilateral stippled calcifications in the hip and knee epiphysis in a neonate with chondrodysplasia punctata—although this might be picked on US, the radiograph displays the findings much more convincingly

15.1.2 Other Requisites

Documentation facilities are essential, special positioning devices are helpful in some techniques—particularly the Graf method. Take care to provide a proper environment, swaddling facilities, diapers, and pacifiers. Sometimes charts and material helping to explain findings to parents may be useful.

Furthermore, knowledge and education of the investigator are essential—not only concerning the US technique but also its implications on management with respect to the consequences of over-diagnosis/treatment or, even worse, missing a significant finding.

15.1.3 What About Imaging Techniques Other than US?

For hip queries in neonates, rarely other imaging techniques such as radiographs of the hip, leg, or pelvis are indicated; however, one may find hip pathology in abdominal, pelvis, or leg radiographs performed for other indications (Fig. 15.1a, b). Nevertheless, in older infants and children, a radiograph is sometimes part of the diagnostic work up and irreplaceable.

CT is practically never indicated in neonatal hip queries (except for acute trauma mostly in older infants), and in neonates MRI for hip queries also is a rarity. Only in older infants, MRI may become indicated, e.g. for assessing Perthes disease or a septic hip. Additionally, in these situations (also for tumour queries) and in older infants or children, a scintigraphic study may be an imaging option. These modalities and findings, however, will not be discussed in detail here—it is addressed in Chap. 14.

15.2 Developmental Dysplasia of the Hip (DDH)

Early diagnosis and treatment of DDH are important and irreplaceable for a normal development of the hip joint. The main goal is to prevent and avoid long-term sequelae. Advances in US technology allow for better visualisation and differentiation of osseous and especially non-osseous structures. This led to better understanding of the basics of the pathophysiology for what is now termed “developmental dysplasia of the hip”.

Usually, DDH is a result of a combination of both structural and ligamentous laxity leading to an abnormal incongruent hip. Structural causes

are related to primary dysplasia. It has been suggested that only 2% of cases of DDH result from the early phase of joint development within the first trimester of pregnancy. The remaining 98% of cases are caused by changes to a normal hip during the last weeks of pregnancy due to ligamentous laxity related to exposure to maternal hormones, frank breech presentation, oligohydramnios, etc. Postnatal factors are also discussed to play a role in DDH, such as tight swaddling or cradle boards which force the legs into extension and adduction and press the femoral head cephalad. This increased pressure in combination with shearing stress leads to a deformation of the hyaline cartilaginous roof and inhibits the maturation of the bony roof. If treatment is necessary, the age of the infant at the onset of therapy has to be taken into account, and the classification or stage of the DDH must be considered.

Generally, treatment follows a stepwise approach: Sometimes a preparation phase is necessary in late onset treatment before a reduction is possible. After the reduction, the hip joint is still unstable, therefore it is mandatory that a retention phase has to follow for stabilisation—before the final maturation phase can be started. During these stages, the femoral head should be constrained in a secure fixation in squatting position—also known as “human position”—to avoid excessive pressure on the cartilaginous roof, allowing remodelling of the bony roof. Excessive abduction has to be avoided to minimise the risk of avascular necrosis (AVN). Early DDH diagnosis by using US allows early treatment with faster remodelling and maturation of the poorly formed bony roof. Thus, the time of treatment can be considerably shortened.



Pressure on the cartilaginous roof inhibits the growth and maturation of the bony roof.

The US approach according to Graf's technique is most commonly and widely used, especially in Europe, partially with the Rosendahl

modification. It is also used in the Asian and South American region. It is based on the work of Graf and continuously adapted and optimised from 1980 until now. An alternative—particularly in France—is the femoral head coverage (the Morin and modified Morin–Terjesen method). While centres in North America also primarily use the Graf technique, they also typically add an assessment of the femoral head movement and its displacement from the acetabulum, known as the Harcke method.

15.3 Hip US According to Graf

The aim of the Graf method is to enable a reproducible, reliable, and standardised assessment of the neonatal hip. It consists of a standardised scanning protocol leading to acquisition of scans in a so-called standard plane. It then classifies the findings into four main types by description and angle measurements. A further subtle subclassification additionally takes the shape of the bony acetabulum in proportion to the stability of the cartilaginous acetabulum into account which reflects the coverage of the femoral head within the socket of the hip joint related to the age of the infant. It is important to know that the US appearance of the infant hip changes in the first few months of life, due to the ossification of the initially preformed cartilaginous structures.

The process for a correct and reproducible sonographic image of the newborn and infant hip according to Graf's criteria follows a stepwise procedure (see below for further details). This acquisition process leads to reproducible images with a high intra- and inter-observer reliability that minimises diagnostic errors.

15.3.1 Standard Plane

Only the defined standard plane must be used for evaluating the hip joint to allow for a reproducible assessment. This necessitates proper imaging of the three following landmarks (Fig. 15.2):

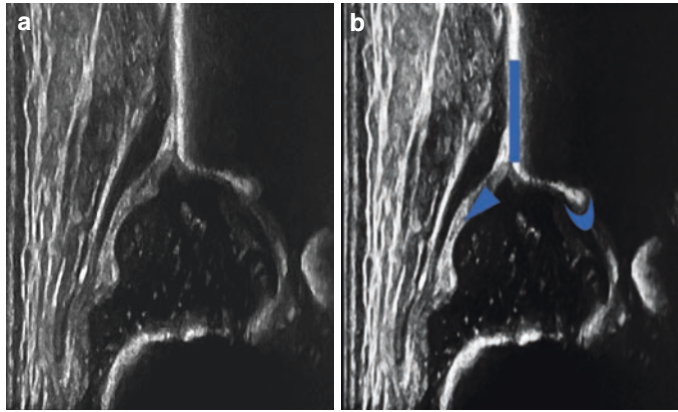


Fig. 15.2 (a) Normal US image of a normal hip according to Graf. (b) Same image with landmarks indicated

- The lower margin (also termed as lower limb) of the bony ilium in the depth of the acetabular fossa, which is the border to the triradiate cartilage. It has to be displayed clearly. For US purposes, the lower margin (limb) of the os ilium is the centre of the acetabulum. If this landmark is not depicted precisely on the US image, the sectional plane does not pass through the centre of the acetabulum and therefore no diagnosis can be made in a centred hip joint without this pivotal point.

“No lower margin (limb), no diagnosis!”

- The middle of the acetabular roof (= the mid-portion of the acetabulum). The shape of the iliac bone is seen as a straight line superior to the acetabular bony roof. This is the weight-bearing section of the hip joint when walking in upright position. The middle section is reached when the plane is rotated around the lower margin (limb) of the os ilium until it leaves the concave contour of the gluteal fossa (see below), representing the posterior plane. Then this can easily be identified as the concavity straightens, with a clear border to the cartilaginous acetabular roof and the labrum.

👁 In the posterior plane or section, the iliac contour is concave and bent, shaped away from the transducer. In the middle section—the standard plane—the iliac silhouette runs straight from the bony rim in cranial direction. “Straight” does not necessarily mean parallel to the edge of the monitor!

- The acetabular labrum. The labrum on the inner side of the joint capsule is triangular in cross section—with a relatively high echogenicity due to the collagenous fibres. It is part of the cartilaginous roof. The base of the labrum is fixed laterally to the hyaline cartilage; the acetabular roof is displayed with low echogenicity.

👁 If any one of these three landmarks is missing or not clearly shown, the US examination is worthless and may not be used for diagnosis and angle measurement! Measuring in an incorrectly acquired US image leads to wrong and useless results. Therefore, it is crucial to pay special attention to the proper sequence of identification of the three landmarks. Only if the lower margin of the os ilium is shown one can proceed to check the sectional plane and lastly the acetabular labrum.

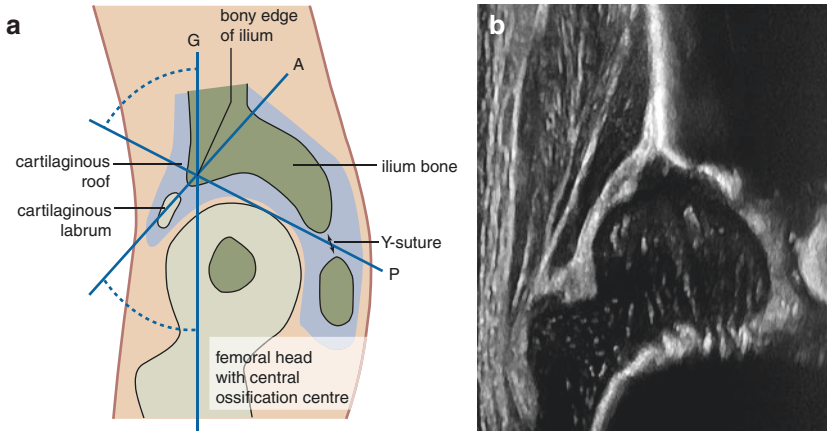


Fig. 15.3 Hip US—Graf standard plane. (a) Schematic drawing of relevant structures, lines, and angles for hip US according to Graf. (b) Typical corresponding US

image (standardised projection—upright position, always projected as right sided). Note the blurred acetabular rim

- Then the hip angle measurement is performed by inserting three lines to define the two angles Alpha (α) and Beta (β) (details see below) (Fig. 15.3).

- Both hips are displayed on the screen in the same way as right sided joint, similar as in radiography. So, for documentation it is necessary to insert a marker or pictogram for side identification.

15.3.2 Device Presets

Images with relatively strong contrast (e.g. hard post-processing with low dynamic range) are preferred. This allows a good discrimination of interfaces and better identification of the anatomic structures. The focus should be positioned at the level of the hip joint; there is no need for a multi-focus scan (this might slow the scan and thus make the investigation more cumbersome).

The image orientation is defined: cranial is on the right side of the monitor image. Some turn the monitor by 90° (up = cranial) as originally introduced to reflect a somewhat anatomic projection similar to a radiograph (as shown in most figures in this chapter).

- Some devices allow for flipping the image on the display into this above-mentioned orientation.
- Rarely (not consistent with general recommendations) the cranial position is defined as in an abdominal US (the left side of the monitor is cranial), for example if the hip scan is performed after an abdominal US.



Make sure that with this orientation the system's angle measurement software is not confused—as it may happen in some US systems; this may also happen if you use the left-right inversion button in some devices!

15.3.3 Examination Technique


15.3.3.1 Positioning the Infant for Sonographic DDH Assessment

When using Graf's technique, the infant is positioned in lateral decubitus position with a slightly bent hip and rotated inward. An extreme extension as well as flexion should be avoided.

Specific devices for placing the infant and stabilising the transducer may be helpful. It is noteworthy that they are recommended by some examiners, but not mandatory. These devices can help to reduce angulation artefacts and can also notably increase the precision of the scan—inde-

pendent from the skill and experience of the examiner.

After the static examination, an additional stress test for dynamic assessment is performed in the same position and maintaining the standard section.

 The stress test is mandatory in all hips which are not within the physiological range or have a clinical abnormality/risk factor.

The French approach for femoral head coverage assessment and the Graf's modified approach according to Rosendahl use a similar examination technique.

For hip US according to Harcke, the infant is placed in supine or lateral decubitus position during the dynamic examination, and the hips are scanned in coronal and transverse planes—with the legs in a neutral position and flexed (details see below).

15.3.3.2 Access from Lateral in Coronal Section

The goal is the acquisition of an image in the reproducible standard plane in the mid portion of the acetabulum according to Graf (Figs. 15.2 and 15.3).

The transducer is placed over the major trochanter in a cranio-caudal coronal direction.

Then the transducer is carefully moved to parallel sections and rotated on the acetabular axis without tilting—thus imaging the standard plane essential for diagnosis and measurement. It is important that the lower margin (lower limb) of the os ilium is clearly seen and identified. Then the transducer is rotated from the bowed concave silhouette of the gluteal fossa until it straightens into the standard plane (Fig. 15.4a, b).

The structures are then identified on an adequate view of the acetabular mid portion and the landmarks are checked.

15.3.3.3 Dynamic Assessment in the Graf Technique

A dynamic assessment is *advisable* even in normal-appearing newborn hips. The femoral head can be mobile due to laxity of the joint capsule after birth induced by maternal hormones. In a normal joint, an elastic whipping of the cartilaginous roof with the labrum may be seen. This may not be confused with the dislocation or provokable dislocation of the femoral head in unstable and decentred hips.

Dynamic assessment is *mandatory* with suspicious clinical examination results or if any suspicious findings in the standard section are noted, also in neonates with other risk factors (see above).

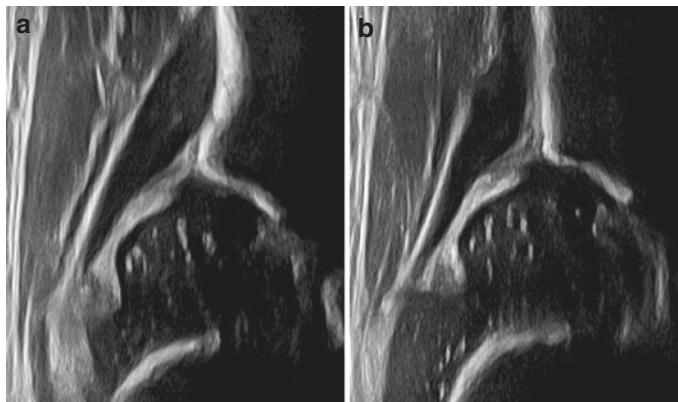


Fig. 15.4 (a) Hip US according to Graf, dorsal plane—gluteal fossa. Note the concave shape of the os ilium bent away from the transducer. (b) Rotation to the standard plane: The contour of the os ilium becomes straight

The technique is rather simple: push the leg softly in cranial and slight dorsal direction for assessment of stability whilst stabilising the back of the infant. If a positioning device is used, the buckles serve as abutment.

In a *stable hip* joint, the femoral head stays well positioned within the socket and the cartilaginous roof exhibits only subtle movements (“whipping”).

In an *instable hip joint*, the displacement of femoral head is seen—out of the dysplastic acetabular fossa superiorly; the acetabular labrum is displaced in cranial direction without losing contact to the femoral head. In dislocated or luxated hips reducibility into a normal human position is checked, paying attention to probable reposition obstacles. This is achieved by a soft pulling and abducting manoeuvre under US surveillance.

15.3.4 Documentation

At least two individually acquired images must be recorded per hip joint; these are taken in the standard plane with a pictogram or any other

clearly evident side identification for documentation. One of these two images must contain the correct measurement lines (see Fig. 15.5).

Recommendations for documentation in unstable hips include a series of images—or better—a video-clip/cine-loop showing all respective changes, particularly also during the stress manoeuvre.

15.3.5 (Normal) US Anatomy of the Newborn and Infant Hip (Fig. 15.5)

To identify all relevant structures in the standard plane, it is helpful to follow a structured and stepwise assessment. This avoids misinterpretation and incorrect findings.

- *Femoral head*: The hyaline cartilaginous femoral head is roundish, with a low echogenicity and scattered internal echoes representing vascular sinusoids. Later the central echogenic ossification centre appears, termed the nucleus. Its size varies depending on age. It is not round nor necessarily in the centre of the femoral head and only its outer border is visible.

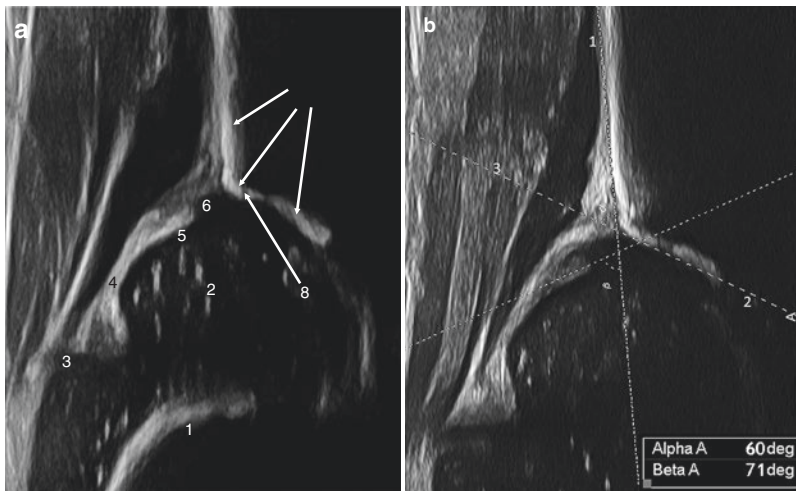




Fig. 15.5 Hip US according to Graf: Relevant structures, one of hip US image according to Graf without (a) and one with (b) angle measurements. Patient identification and side mandatory, (gestational) age helpful. (a) 1 transition zone of osseous to cartilaginous part of femur, 2

femoral head, 3 fold, 4 capsule, 5 cartilaginous labrum, 6 cartilaginous roof, 7 osseous contour of ilium bone, 8 bony rim, 9 lower margin (limb). (b) 1 base line, 2 bony roof line, 3 cartilaginous coverage line, α (between line 1 and 2) 60° , β (between lines 1 and 3) 71°

 On US, the nucleus cannot be used as on radiographs for assessing the position of the femoral head in relation to the acetabulum. It is important to note that the size of the ossified part of the femoral head is the limiting factor for hip US performance, which therefore has no clear age limit. When the ossified nucleus becomes large, it blocks the US beam producing a broad acoustic shadow. This inhibits the visualisation of the lower margin (limb) of the os ilium in the mid portion of the acetabular fossa.

- *Ossified femoral neck*: It is the border zone between the ossified part of the femur and the cartilaginous femoral head termed osseocartilaginous junction.
- *Joint capsule*: The capsule runs from the femoral neck to the acetabulum and inserts into the periosteum of the os ilium.
- *Cartilaginous acetabular roof*: It is composed of two components. The lateral portion is the fibrocartilaginous acetabular labrum, a hyperechoic triangular structure between the joint capsule and the femoral head. The labrum is laterally fixed at the hyaline cartilage roof. This is the second portion, which is normally hypoechoic, with the same echogenicity as the femoral head.
- *The osseous os ilium*: The lateral contour of the iliac bone is seen as a straight line that runs cranially with a clear border to the cartilaginous acetabular roof and allows a good osseous definition. In caudal direction, the bony rim and the osseous roof complete the roof of the femoral head.
- *The socket or acetabular roof* is composed of both the osseous and the cartilaginous roof.

 The strong echoes of the os ilium are produced by total reflection and absorption of parallel US beams with acoustic shadowing, mimicking an outer and inner wall. Only the lateral surface artefact is seen in the US image.

15.3.6 US Criteria in Graf's Technique (Landmarks) (Fig. 15.2)

Only US images taken in the standard plane with the three obligatory landmarks are allowed to be used for diagnosis and measurements. These must contain:


- The lower margin of the bony ilium in the depth of the acetabular fossa representing the physis, the iliac growth plate (as part of the triradiate cartilage).
- The midportion of the acetabular roof with a straight iliac bone line running cranially.
- The triangular acetabular labrum.

If any one of these three points is missing or not clearly shown, the US is inadequate and therefore angle measurements are unreliable and can even worsen the diagnosis.


15.3.7 Findings in DDH

Sonographic criteria vary depending on the method applied (Graf, Harcke, adapted Graf by Rosendahl, femoral head coverage according to Morin and Terjesen, pubo-femoral distance).

Comment There is a general agreement that it is important to diagnose DDH early in order to avoid long-term sequelae with immense health-care costs and even individual morbidity, e.g. by repeated surgery and even early joint replacement. Hence, early detection by US is seen as an advantage allowing for an early start of treatment. Then the treatment duration can be considerably shortened and outcome is improved, also reducing the need for invasive procedures. Nevertheless, the debate on the role of general versus selected US screening (or even only individual US indications based on some sort of clinical screening) is ongoing in the Anglo-American literature, whilst in most of the middle European Countries, a general US screening is established; a similar approach is discussed in some Asian and South American countries.

 Hip US for detection DDH is called a “final” investigation indicating the risk that if one misses an endangered hip, the patient will only come back after years or decades when he/she is symptomatic. Therefore, strict and consistent adherence to all quality criteria is essential. In addition, although clinical investigations and anamnestic data are a mandatory part of every examination, these are not sufficient to detect subtle changes and should not be used as exclusive screening tools particularly in (pre-term) neonates or neonates at risk.

- *Base line*: It is drawn from the most upper portion of the hyaline cartilage as pivot point caudally, tangential to the echo of the os ilium where the proximal perichondrium inserts to the periosteum of the os ilium (Fig. 15.6a).

 The baseline is not necessarily paralleling the near field border of the US image (the transducer).

15.3.8 Angle Measurement: Measured Between the Three Lines

Three lines form the two angles alpha (α) and beta (β):

- *Bony roof line or acetabular roof line*: It is drawn from the inferior margin (lower limb) of the acetabulum as pivot point tangential to the bony roof (Fig. 15.6b). This definition implies the outer border of the os ilium.
- *Cartilage roof line*: It is drawn from the bony rim through the centre of acetabular labrum (Fig. 15.6c). The bony rim is defined as the transition point where the convexity of the osseous acetabulum changes into its concavity

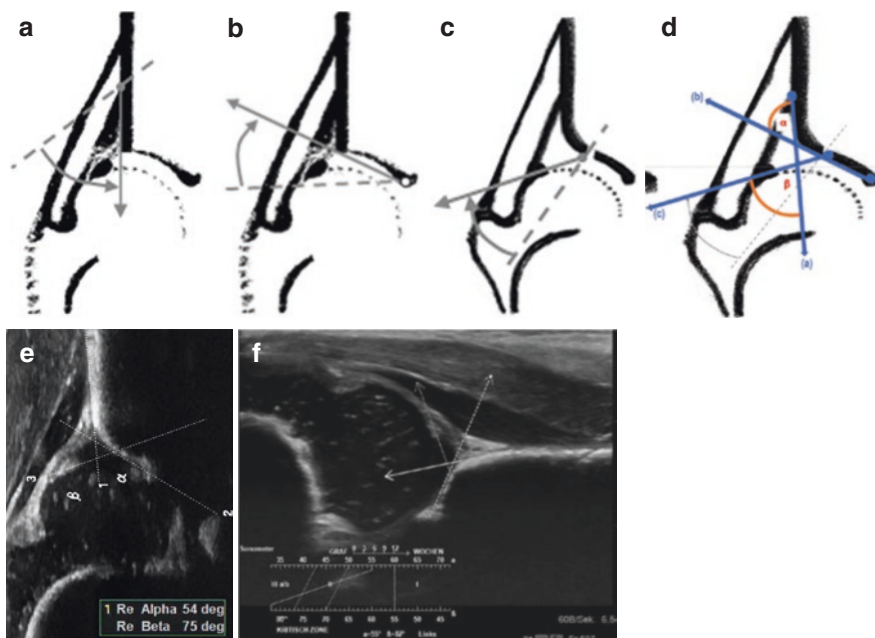



Fig. 15.6 Angle measurements and lines in hip US according to Graf (a–f). (a) How the baseline is defined. (b) Definition of acetabular roof line. (c) Cartilaginous roof line added, (d) with normal angle α and β —upright standard view, increasingly used for practicability and device restrictions; (e) Hip US with integrated calculation software: the software automatically indicates angles (α


54° , $\beta 75^\circ$) (f) not an upright standard view, cranial on this image is displayed on right-hand side: increasingly used for practicability and device restrictions; sonometer software indicates hip type (full line) after manual definition of respective lines (immature type II hip, sufficient or sub-optimal coverage, dynamic assessment shows elastic whipping)

ity. This is the most outer point of the osseous socket.

 These three lines do *not* necessarily intersect in one point!

- *The bony angle alpha (α)* is formed between the base line and the bony roof line (Fig. 15.6d, e); it reflects the osseous coverage and quantifies the bony socket.
- *The cartilage angle beta (β)* is formed between the base line and the cartilaginous roof line (Fig. 15.6d, e); it quantifies the cartilaginous acetabular roof.

With these two angles, the entire socket with its bony and cartilaginous parts can be accurately assigned to a specific hip type. This measurement system is independent of the position of the infant, the projection, and the presence of an ossified centre of the femoral head. Additional measurement lines and calculations were shown not to improve results or precision.

 The angle measurement system is only valid in correctly performed exams (see above). It is used to determine the presence of hip dysplasia and to categorise its severity using the most widely accepted Graf classification. A correct section through the hip joint with sufficient depiction of all three landmarks is mandatory for judging hip maturity and for performing angle measurements—if a section is taken angulated or too ventrally or dorsally (usually recognisable by a bent shape of iliac line or incorrect/missing identification of the bony fossa definition), measurements are always wrong and therefore diagnostically useless. *So NEVER use these images to try to make a diagnosis!*

An α -angle of 60° or greater is considered normal in any age and implies a mature hip joint.


Smaller α -angles indicate poorer coverage and at least immaturity (in infants younger than 3 months) or dysplasia in infants older than 3 months. The soft cartilaginous roof must compensate the ossification deficit and cannot resist the pressure of the femoral head in cranial direction. The β -angle indicates the risk of instability—the higher the angle, the worse the risk.

15.3.9 Classification of the Hip According to Graf

The strict classification not only differentiates between normal hips, dysplasia, and luxation. It also takes into account the age-dependent maturation and thus allows for differentiation between physiologic immaturity and a maturation deficit (Table 15.1).

The US grading correlates with the pathological changes in the hip joint. In cases with dislocation, the femoral head was initially positioned within the socket, but biomechanical factors caused cessation of the normal development and the femoral head started to slide out of the socket thus deforming the acetabulum (developing dislocation of the hip).

The classification is composed by description and measurement.

 Description and measurement must be consistent!

15.3.9.1 Type I: Normal or Mature Hip (Figs. 15.2, 15.4, and 15.5)

This hip type is considered mature at any age and can therefore be present already at birth. Maturation should be completed at the age of 3 months.

The degree of the ossification of the bony acetabular roof is appropriate for a hip joint of an infant at the age of 3 months. The bony socket is well developed with normal position of a well-covered femoral head in the acetabular fossa. The bony rim is angular or slightly blunt, but well defined. The cartilaginous acetabular roof covers

Table 15.1 Sonographic classification according to the Graf method

Type according to Graf	Age	Superior bony rim	Bony roof angle	Cartilaginous roof and β angle
Type I	Any age	Angular/slightly rounded (“blunt”)	$>60^\circ$	Normal mature hip $>50\%$ acetabular roof coverage
Type II+	0–6 weeks	Rounded	$50\text{--}59^\circ$	Covers the femoral head
Type II-	7–12 weeks	Rounded	$50\text{--}59^\circ$	Covers the femoral head
Type IIb	>12 weeks	Rounded	$50\text{--}59^\circ$	Covers the femoral head
Type IIc	Any age	Severely rounded to flattened	$43\text{--}49^\circ$	Still covers the femoral head $\beta < 77^\circ$
Type D	Any age	Severely rounded to flattened	$43\text{--}49^\circ$	Displaced $\beta > 77^\circ$
Type III	Any age	Flattened	$<43^\circ$	Labrum and cartilaginous roof pressed upwards $\beta\text{-angle} > 77^\circ$
Type IV	Any age	flattened	$<43^\circ$	Labrum and cartilaginous roof pressed upward downward

Adapted from: Graf R, Scott S, Lercher K et al (2006) *Hip sonography: diagnosis and management of infant hip dysplasia*. Springer, Berlin

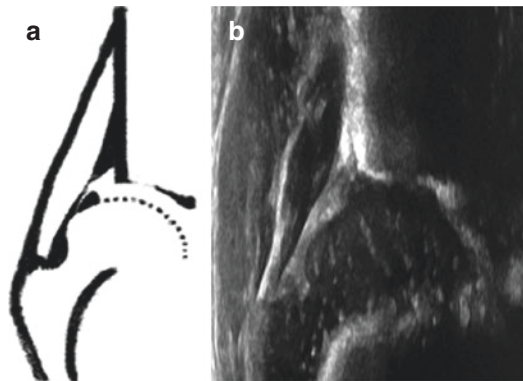



Fig. 15.7 Schematic drawing (a) and US image (b) of hip US according to Graf showing findings in Type I

well the femoral head, holding it firmly in the socket (the cartilage “covers” the head) (Fig. 15.7).

The bony angle (α) between base line and bony roof line is $>60^\circ$.

The cartilaginous angle (β) is $<55^\circ$.

 In newborns, β -angles are shown to be higher, even in static examinations (see Sect. 15.3.3—“Dynamic Assessment in the Graf Technique”).

15.3.9.2 Type II: Immaturity

The physiologic hip maturation of an immature hip tends to be rapid in the first few weeks

(namely 4–6 weeks) after birth, with a normal hip development expected within the first 12 weeks of age. So, these hips are termed as “*physiologically immature*” and are labelled as “*Type IIa*”. These type IIa hips are further sub-classified into hips that show appropriate development at or after the sixth week. This finding is classified as a normal/physiological immature hip joint with favourable outcome and most probably normal maturation to a mature hip joint (*Type IIa+*).

Hips with persistent immaturity after the sixth week are classified as hips with delayed maturation (*Type IIa-*) remaining at higher risk for a maturation/ossification deficit by the time the infant reaches the age of 12 weeks.

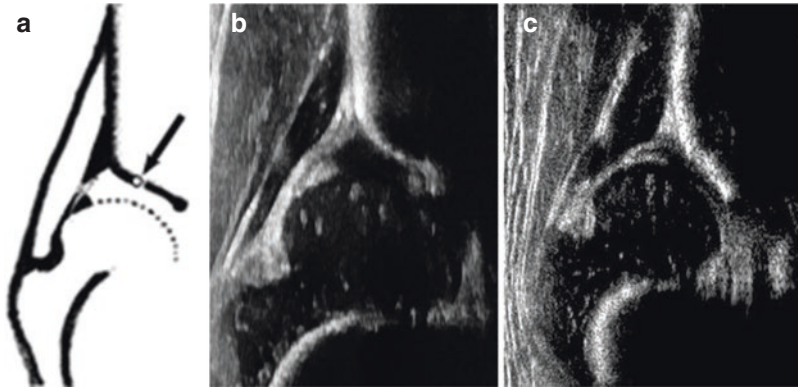



Fig. 15.8 Schematic drawing (a) and US image (b) of hip US according to Graf showing findings in Type II. (c) Image Type D. Note the insufficiently covered fem-

oral head in (c) opposite to (b) where the femoral head is centred. The arrow (in a) indicates the acetabular rim/y-suture

 The age of the infant with physiologic maturation has to be taken into consideration. Depending on the subtype, the rounded bony roof is defined from sufficient (or adequate/satisfactory) to deficient. The cartilaginous acetabular roof still covers more than half of the femoral head, but appears much wider than the osseous acetabulum due to poorer ossification.

- Subtypes of hip Type II:
 - IIa+: physiologic immaturity. Spontaneous maturation is expected
 - IIa–: maturation deficit within the first 3 months of life. Follow-up exams are recommended because of the risk of potentially delayed ossification (Fig. 15.8).

15.3.9.3 Type IIb: Ossification Deficit

After the age of 3 months, a Type II hip is described as Type IIb and classified to have an ossification deficit and be dysplastic. In Type IIb hips, the labelling “b” underlines the importance

to state the age. Hips with ossification deficits are at risk for residual dysplasia.

Follow-up examinations and eventually treatment are recommended.

Measurements in Type IIa and Type IIb hips:

α -angle ranges between 50° and 59° , β -angle is $>77^\circ$ (exception: newborns have higher β -angles).

15.3.9.4 Type IIc

This hip type is termed “critical hip” or “hip at risk”. It describes a developmentally dysplastic hip that is definitely endangered for residual dysplasia and even decentration. This type needs treatment.

On US, it exhibits a very rounded bony rim which is severely deficient, with a cartilaginous roof that still covers the femoral head. In some hips, the cartilaginous roof can be displaced upwards during the mandatory dynamic stress manoeuvre (this allows the discrimination between Type IIc = stable, and an unstable hip).

Measurements in Type IIc hips:

α -angle = 43° – 49° , $\beta < 77^\circ$ (stable in the stress test).

α -angle = 43° – 49° , $\beta > 77^\circ$ (unstable in the stress test).

15.3.9.5 Decentred Hips

Type D (Formerly IIId)

This type defines an unstable hip with beginning decentration. On US it exhibits a very rounded bony rim with already initially displaced cartilaginous acetabulum that is pressed upwards by the femoral head.

Treatment with fixation of the femoral head in the socket is recommended.

Measurements in Type D hips:

$$\alpha \text{ angle} = 43^\circ\text{--}49^\circ, \beta > 77^\circ.$$

Type III: Decentred Hip

This type shows an insufficient osseous containment with a flat bony rim. The bony as well as cartilaginous coverage is poor. The femoral head is decentred, and the cartilaginous acetabulum is displaced upwards because the femoral head has pushed the cartilaginous acetabular roof in cranial and dorsal direction.

This type needs treatment by repositioning and secure fixation.

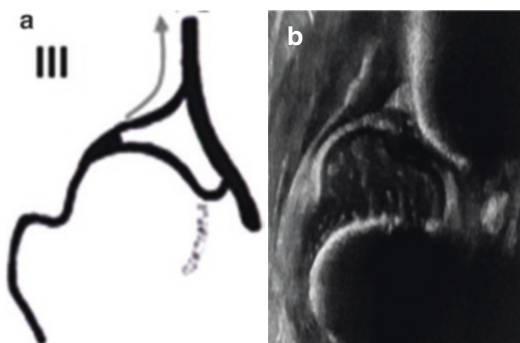


Fig. 15.9 Schematic drawing (a) and US image (b) of hip US according to Graf showing findings in Type III. The arrow in (a) demonstrates the displacement of the cartilaginous roof and the contour of the joint capsule running cephalad

On US, the following features are seen:

- Type IIIa: The cephalad displaced hyaline cartilage is hypoechoic.
- Type IIIb: Due to a long-standing pressure of the femoral head on the cartilaginous acetabulum, structural anomalies occur and the echogenicity increases and becomes higher than the cartilage of the femoral head. This is a sign of severe damage with poor outcome of the joint and occurs only in untreated hips which have been dislocated for a long time or in neglected cases (very uncommon in middle Europe) (Fig. 15.9).

Measurements in Type III hips:

$$\alpha \text{ angle} = <43^\circ, \beta > 77^\circ.$$

Type IV: Luxated Hip (Fig. 15.10)

In this most severe form of DDH, the femoral head is displaced from the joint space and luxated into a cranial and dorsal position. The cartilaginous acetabulum is herniated, displaced caudally, and compressed between the femoral head and the iliac bone.

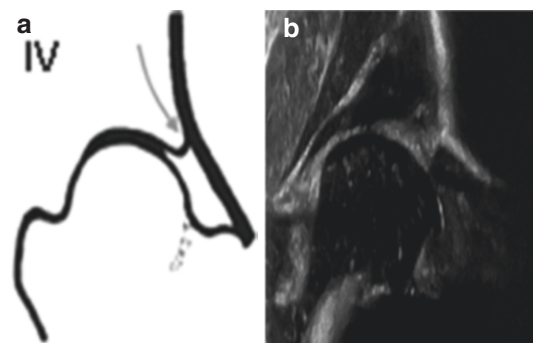




Fig. 15.10 Schematic drawing (a) and US image (b) in hip US according to Graf showing findings in Type IV. Note the shape of the joint capsule arrow in (a) demonstrates the contour of the caudally pressed joint capsule

 In decentred hips, measurements are not necessarily required and often impossible, because the displaced femoral head has left the standard plane when moving in cranio-dorsal direction, out of the dysplastic socket. This is why the bony rim is often not displayed on the US image.

The dynamic assessment helps to evaluate for reducibility and to rule out reposition obstacles, such as, for example some intraarticular fibro-fatty tissue (pulvinar), constriction of the elongated joint capsule, or a tight iliopsoas tendon.

 **Also note that** wrong angulation will cause wrong results—dedicated devices are available to reduce the probability of this common pitfall (Fig. 15.11).

The discussion about the necessity of follow-up US exams in immature hips is still ongoing. In the

Anglo-American countries, the costs to the health care system are strongly taken into account. The screening policies also differ in different countries, because multicentre prospective randomised controlled trials are lacking. There is consensus that these studies are judged to be unfeasible from the ethical point of view. To stratify newborns or infants to the control group without follow-up or even treatment might cause unpredictable harm to this group of study members. Furthermore, if properly done the study must be performed over decades to determine late sequelae of a missed dysplasia, whilst there is consensus that a missed and untreated displacement of the hip is deleterious to the joint (Fig. 15.12a, b).

There is consensus that a radiograph should be performed in infants with treated hips after the onset of walking. So-called residual dysplasias and missed dysplasias as a result of maturation deficit are not detectable solely by clinical examination. Children with residual and late dysplasias are at higher risk for earlier and prolonged orthopaedic problems, even resulting in hip replacement. Furthermore, secondary hip dislocation may occur in, e.g. neurologically impaired infants and children then necessitating a radiograph.

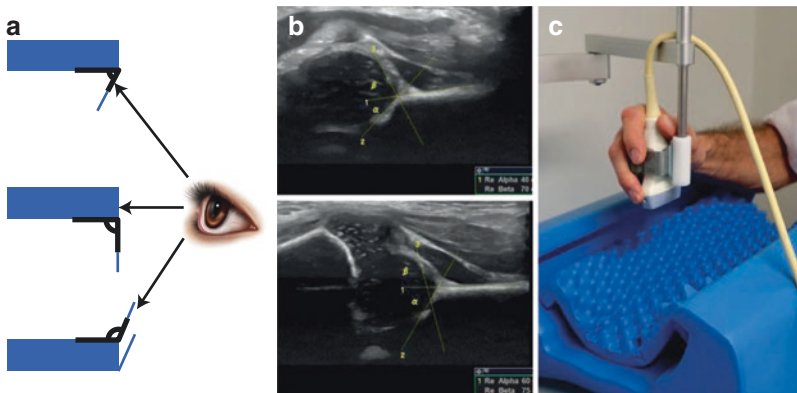


Fig. 15.11 (a–c) Common pitfall in hips US: wrong angulation with respective implication on angle measurements in the Graf and modified Rosendahl method: As demonstrated in schematic drawing of a table corner, the angle will appear different depending on the viewing angle and perspective (a), influencing angle measurements on US (b)—where the correct angle measurement is only given on the lower hip US image, whereas the

upper image exhibits wrong angle measurements; the malposition is recognisable by missing femoral structures (e.g. osseocartilaginous junction) on the respective upper hip US image. Note that the measurement lines do not have to cross in one point to be correct. (c) shows a technical device that may help to avoid accidental tilting of the transducer

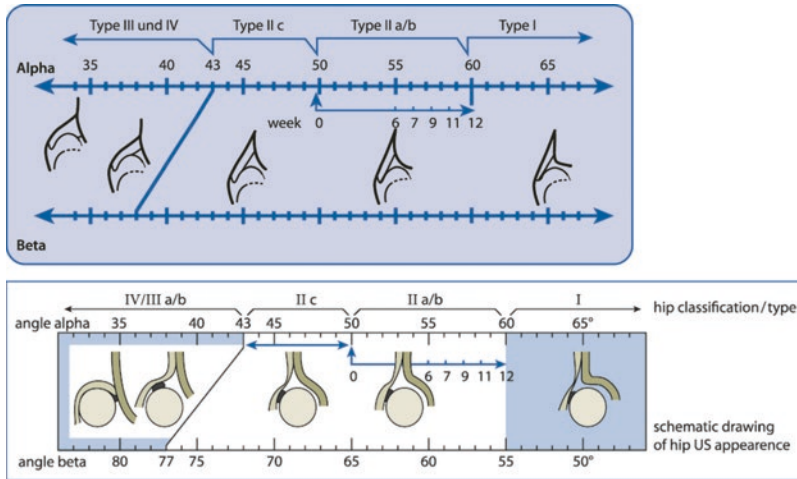


Fig. 15.12 Schematic drawing of the different hip types with angle measurement helpful for classification (“Sonometer”)

Comment on “How to perform hip US according to Graf’s technique”: There is consensus that the examination should be performed by appropriately trained health professionals. The training should be offered in standardised and approved training programmes and taught by certified and approved trainers and instructors—with accreditation by organisations that guarantee and survey the quality of the content of the training programme. A learning by doing, e.g. as by bedside teaching only, was proven not to be sufficient. An ongoing quality assurance programme with respective audits is valuable to ensure persisting quality even after years.

stability for discrimination hips are classified as stable, dislocatable, or dislocated, thus it classifies hip morphology and stability separately and offers a simpler and less subtle grading. The age of the infant is not taken into account, but the system is more easily and consistently applicable—although with a lower fine-tuning.

- **Technique:** The hip morphology (α -angle) is assessed in standard coronal view (Graf) with a centred femoral head. If the hip is decentering, eccentric, or dislocated (Graf types 2c, D, 3, 4), an attempt is made to relocate the femoral head by mild traction, and thereafter hip morphology is reassessed. If the hip is irreducible, the morphology is assessed with dislocated femoral head.

15.4 Modified Graf Classification (Rosendahl)

In the imaging approach, there is no essential difference from the Graf technique, but with addition of a compulsory stress test (similar to Graf’s “dynamic examination”). But this classification further aims at simplifying the grading. According to the morphology (using Graf’s angle discrimination), one categorises hips into immature, mildly dysplastic, or severely dysplastic. Using

Always an additional Barlow manoeuvre is performed to assess for coexisting instability even in morphologically normal hips. The stability is classified as above.

15.5 Hip US According to Harcke

In North America, hip US with the dynamic manoeuvre according to Harcke has become widely used. The exact study protocol varies

among institutions and it relies on the sonographer's skill in performing the examination and interpreting the result of the images without angle measurements.

This technique parallels the clinical manoeuvres of Barlow and Ortolani during the physical examination of the hip. It attempts also to detect a subtle instability, which eluded the clinical examination. Thus, the objective is to classify hip stability.

15.5.1 Technique

The infant is placed in supine or lateral decubitus position, and the transducer is positioned over the lateral or posterolateral aspect of the hip. The position of the femoral head at rest is noted in a neutral position. Then the stability of the hip is assessed with motion and gentle stress by pushing the femoral head posteriorly as in Barlow's manoeuvre. Then the development and configuration of both the bony and cartilaginous acetabulum are assessed.

Usually the examination has four steps:

- Coronal images with the hip in neutral position (similar to Graf's method).
- Coronal images with the hip in flexion, plus a posterior lip view.
- Then transducer is rotated to obtain transverse images with the hip flexed, with passive abduction and adduction.

- This is finally followed by transverse images in neutral position and with posterior stress—to evaluate hip stability.

15.5.2 Normal Findings During Harcke Investigation

On coronal extension and flexion views, the cartilaginous femoral head is contained within the acetabulum defined by the triradiate cartilage centrally and the posterior ischium, with the femoral metaphysis seen anteriorly. Approximately half of the diameter of the femoral head lies on either side of the ilium. On the transverse extension view, the femoral head is seated in the centre of a V-shaped acetabulum formed by the ischium posteriorly, the pubic bone anteriorly, and the triradiate cartilage centrally.

When the Barlow manoeuvre is performed, no displacement is seen with stress and the image remains the same, with the head centred in fossa (see Fig. 15.13a).

15.5.3 DDH According to Harcke

The position and stability of the femoral head at rest and with stress are reported as normal, subluxatable with stress, subluxed or dislocated (see Fig. 15.14b). With the abduction manoeuvres the

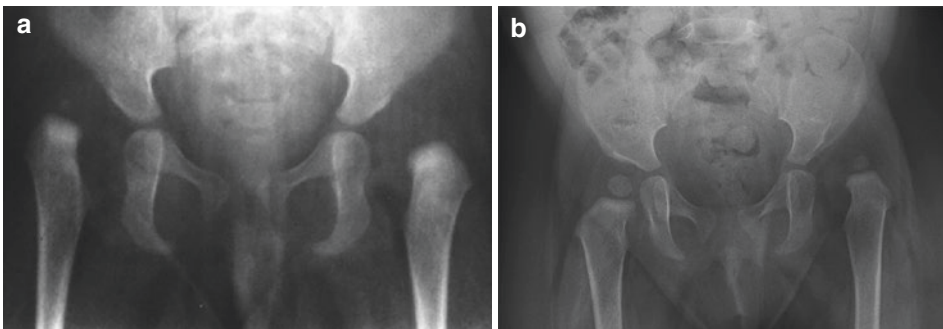


Fig. 15.13 (a) Obvious dislocation of both hips on a pelvic radiograph in an infant—this imaging however is not the standard first step when assessing hip dislocation or

DHD, (b) Dislocation of the left hip. Note the severe defect of the bony rim, the smaller centre of the femoral head that is displaced cephalad

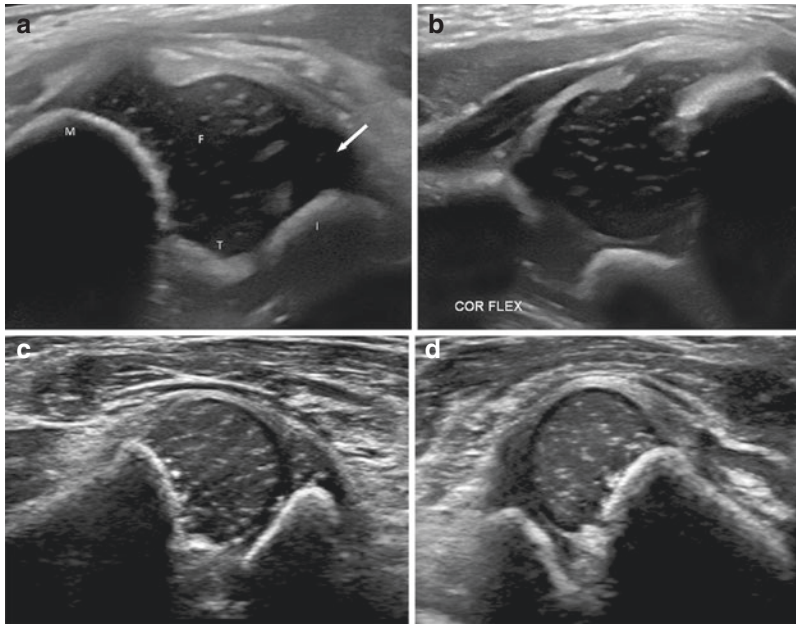


Fig. 15.14 Harcke hip US (a) Normal hip: normal position of the femoral head on this transverse flexion view. Note the cup-like appearance formed by the metaphysis and the ischium. No change with stress manoeuvre. (b) Coronal flexion view. (c, d) Abnormal hip: transverse view of the hip with stress showing subluxation of the

femoral head from its normal position and disruption of its cup-like configuration. This hip was reducible. *Abbreviations: F* femoral head, *M* femoral metaphysis, *I* ischium, *T* triradiate cartilage. Arrow: cartilaginous labrum. (Courtesy of Dr. B. Coley, Cincinnati/Ohio, USA)

formerly displaced femoral head with no contact or coverage to the acetabulum is shown to return to the acetabulum. The coronal neutral image has traditionally been used to evaluate the degree of femoral head coverage and the acetabular shape. Respective images must document all findings and need to be labelled appropriately (Fig. 15.14a).

In abnormal decentred hips, either Harcke's or Graf's method can be applied additionally for treatment decisions.

A similar approach is used for the "femoral head coverage" assessment (French approach).



The method is more subjective, but it also includes description of hip stability. Neither accuracy nor population-based rates of pathological hips have been published based on this technique.

15.6 Femoral Head Coverage According to Morin (and Modified Morin = Terjesen, Also Called the French approach)

This method assesses the degree of lateralisation of the femoral head based on Graf's standard plane or Harcke's coronal flexion view—with the child placed in supine position. The Graf standard plane is recommended, but not mandatory.

A modified Graf's baseline is drawn through the lateral bony rim of the acetabulum parallel to the long axis of the transducer. Then two additional lines parallel to this iliac line are added—one indicates the lateral border of the femoral head in the near field of the transducer and the other the medial part (i.e. the junction of the femoral head in the depth of the acetabular fossa).

The distance between medial and iliac line (a) and between medial and lateral line (b) is measured.

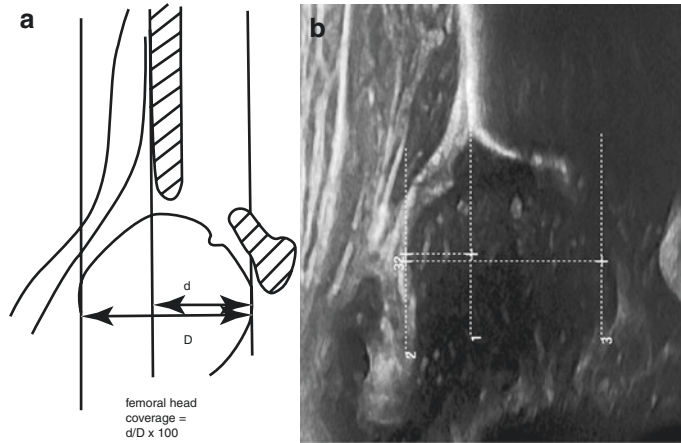


Fig. 15.15 Femoral head coverage (a) Scheme (b) modified Graf standard plane. Child placed in supine position

The ratio is multiplied by 100 which gives the coverage degree as a percentage of the femoral head covered by the bony acetabulum (Fig. 15.15).

15.6.1 Modified Morin (Terjesen)

The hip is assessed in Graf’s standard plane, but instead of the baseline according to Graf a line through the lateral bony rim of the acetabulum parallel to the long axis of the transducer is drawn. Then the “bony rim percentage”, later named “femoral head coverage” is assessed as above.

- Anatomic landmarks and normal limits for measuring the femoral head coverage:
 The lateral part of femoral head, the contour of the bony os ilium, and the medial junction of the head in the acetabular fossa are used, additionally if required the pubic bone.

15.6.2 Hip Assessment Based on Femoral Head Coverage

All results outside of the accepted limits (see below) reflect DDH. But this classification has less potential for grading, and can only be used as an initial screening tool to assess for normal or abnormal hips. Further grading (if necessary

for treatment decisions) is then often performed using Graf’s or the modified Graf method.

• *Coverage degree*

Normal:	>55%
Lower normal limits: Male	-47%
Female	-45%
Undetermined:	45–54%
Altered:	<45%

15.6.3 Pubo-Femoral Distance

This parameter is sometimes also assessed. For being able to achieve this, the centre of the pubic bone needs to be displayed as a roundish hyper-echoic cup on the US image.

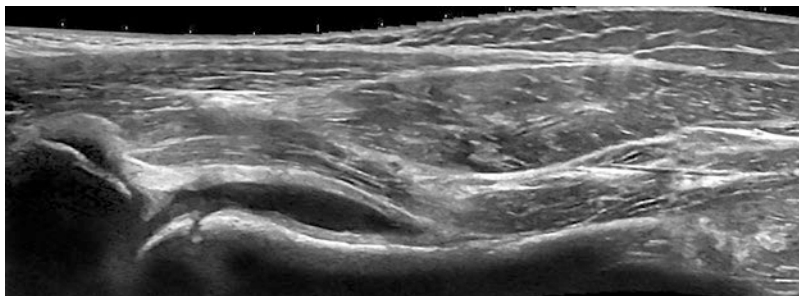
The distance between the medial border of the femoral head and the ossified portion of the pubic bone is measured.

Distances ≤6 mm or a difference of less than 0.15 cm between both sides are considered normal.

15.7 Three-Dimensional US (3DUS) for DDH Assessment

Several attempts have been made to use (semi-) automated 3DUS reconstruction algorithms for presenting the hip in a standardised fashion after

Fig. 15.16 Hip US in simple hip effusion (transient synovitis, extended field of view): echo-free fluid in widened joint space, thickened capsule



3DUS acquisitions (usually using the Graf or Rosendahl approach) and for automated angle measurements. However, 3DUS is currently not introduced into daily clinical practice—in part also because of the equipment (and cost) implications and its restricted availability.

There are some potential advantages: possibly 3DUS may offer a better standardisation if the acquisition is done properly, particularly less dependent on possible angling and tilting errors.

Disadvantages are that 3DUS has a higher risk of motion artefacts during acquisition. Furthermore, no dynamic scanning is possible at present (so-called real time 4DUS) for this application, particularly visualisation of these changes in rendered views is difficult. And the available linear or curved-array 3DUS transducers are rather clumsy—the much smaller and handier available 3DUS sector transducers should not be used for hip US, as these may impair measurement accuracy.

15.8 Ultrasound and Imaging of Other Hip Conditions

There are a number of conditions which more commonly affect older infants and children. However, some may also occur in neonates and as such are briefly addressed. A more detailed description of all other applicable imaging methods with illustration of respective findings can be found in the respective chapters of the books such as Chap. 14 on imaging the neonatal musculoskeletal system or Chap. 17 on imaging in neonatal trauma.

The queries for these other sonographic hip assessments throughout childhood are a painful hip mainly caused by hip effusion, which may be

accompanied by capsular thickening (Fig. 15.16). Others, but much rarer aspects depictable by US are irregularity of bony structures and other pathologic features like disruption of the osseous contour.

15.8.1 Indications and Technique

The sonographically targeted features are joint effusion, capsular thickening in inflammatory conditions, a slipped (capital femoral) epiphysis, proximal femoral deficiency, and others such as rare tumours or Perthes disease, trauma, or other joint haemorrhage.

For all these queries, the US approach is different from the classical DDH scanning technique: Ultrasound should be performed in a supine position leaving the leg in a resting position, which is typically slightly flexed and externally rotated (important also for pain relief). Manipulation can cause discomfort and stress induced defense with a restless child, leading to prolonged examination time and poorer result. A support under the popliteal fossa may be helpful to relax the leg and make the examination less painful.



It is highly recommended to start the examination with the contralateral, not affected, healthy side. This is also helpful for intraindividual comparison to become familiar with the individual normal anatomy. This approach is recommended for every musculoskeletal examination performed on the extremities.

The use of a linear transducer is preferred. A trapezoid or virtual convex mode widens the view and may allow for a better overview. Sometime a panoramic mode (e.g. extended-field-of-view) is useful to demonstrate large soft tissue masses or longer segments of bony structures. The range of the chosen beam frequency depends on the age and size of the infant; the selection of the transducers varies—one may also need lower frequencies in older children or for deep structures (frequency range 14/10–3 MHz); also curved arrays may be used in such situations. Sometimes the split-screen/dual image function may be helpful for direct comparison of affected and unaffected side.

The transducer is positioned longitudinally on the groin—anteriorly along the femoral neck, usually slightly lateral to the course of the femoral vessels. By this sagittal and parasagittal sections are acquired. Cross sectional/axial views are rarely helpful, but can be acquired in selected cases.

15.8.2 The Normal Hip Joint

Typical US findings in normal hip joints performed in longitudinal sections with a frontal sagittal view show the ossified femoral head, the femoral neck connected by non-ossified physis (= an anechoic line). The visible con-

tours of the acetabulum and the femoral head and neck appear continuous, without disruption, smooth and with a clearly defined non-interrupted surface (Fig. 15.17b). Osseous defects can also be seen. The anterior part of the joint capsule parallels the anterior cortex of the femoral neck and has a concave shape. The fibrous joint capsule is normally displayed with two small layers, separated by the small apposed synovial lining—producing an acoustic artefact presenting as a linear echogenic reflection or a small amount of anechoic fluid within the joint space that separates the two capsule layers.

15.8.3 Arthritis and Inflammation of Hip Joint

The most common cause in neonate is (septic) coxitis, in the older infant transient synovitis of hip (toxic synovitis, parainfectious synovitis, “coxitis fugax”).

The irritable hip is a common disorder in childhood characterised by acute onset with refusal to walk. In most cases, the medical history and the physical examination completed with basic laboratory testing (e.g. full blood count, CRP) together with US usually establish the diagnosis. Normally, the clinical symptoms and the joint effusion improve and resolve within a few days. A prolonged or even persisting clini-

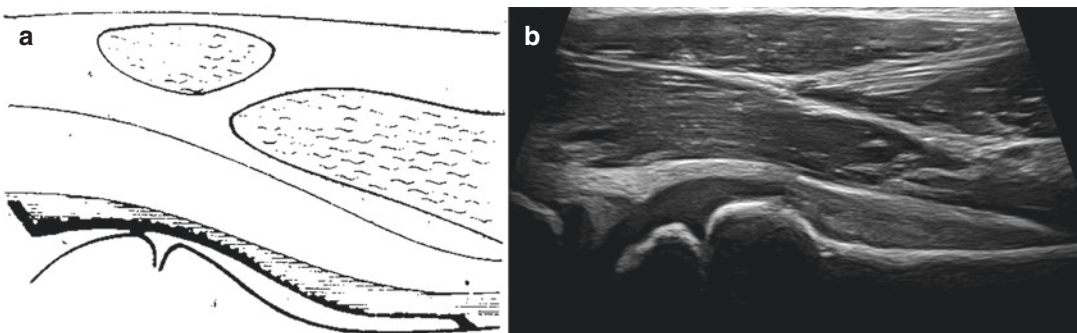


Fig. 15.17 (a, b) Normal longitudinal hip US in an older child: normal joint capsule (synovium) appears prominent, parallels the anterior cortex of the femoral neck and

has concave shape as both layers are collapsed schematic drawing (a) and US image (b)

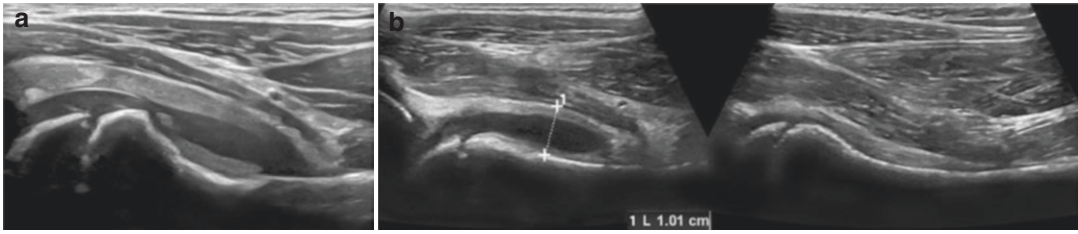



Fig. 15.18 Transient synovitis (a) Thickened synovial capsule and anechoic joint effusion (b) Split image. Note: Measurement perpendicular to the femoral neck includes outer layer of the joint capsule

cal course and effusion have to attract attention to important differential diagnoses, particularly Perthes disease, Lyme arthritis, or diseases within the rheumatic spectrum. Therefore, it is important to assess and monitor the development of the disease.

A joint effusion leads to accumulation of fluid in the anterior recess of the capsule and consecutive widening of joint capsule (Fig. 15.18). Fluid within the joint will elevate the anterior part of capsule with bulging and widening of the joint space. Thus, the shape of the capsular margin becomes convex. One additionally needs to pay attention at the contour of the femoral head and the congruence between femoral head and neck—not to miss fragmentation or irregularities as seen in Perthes Disease, or step-off formation as in a slipped epiphysis (epiphysiolysis).

- In *simple, uncomplicated cases*, a hypo-anechoic clear and uncomplicated effusion is present. The distance between femoral neck and the outer layer of the joint capsule exceeds 5 mm in children under 4 years and 7 mm over 8 years. Measurement should be taken perpendicular to the femoral neck at the vertex of the concavity. An intraindividual difference of >3 mm is judged as abnormal (Fig. 15.18a, b). It is notable that with high-resolution transducers a swelling and thickening of the synovial capsule can be depicted, but grading of the capsular thickness was shown as relatively little helpful. Furthermore, no obvious thicken-

ing needs to be present in such an inflammation and the capsule as well as the effusion itself can have varying echogenicity. The appearance is not specific and depends on the kind of inflammation, the age, the duration, the transducer used, etc.

 The measurement of joint distention and thus for quantification of the effusion is taken perpendicular to the femoral neck and includes the outer layer of the joint capsule. Particularly in persisting complaints, a hip radiograph is mandatory; however, it is often already taken at the first visit at the initial presentation of the patient.

- In *complicated cases*, one may observe a hyperechoic joint effusion with echogenic particles—in a febrile and severely ill infant this is highly suspicious for septic/bacterial arthritis/coxitis (Figs. 15.18 and 15.19). The synovial reaction is highly sensitive, but lacks specificity. It may also reflect a haematoma/a haemarthros (e.g. in haemophilia, after trauma or in rheumatic conditions). The medical history (and laboratory biochemistry) is crucial and absolutely essential for differentiation. Colour Doppler sonography (CDS) may sometimes show hypervascularity of the potentially significant thickened synovial capsule layer (Fig. 15.19). If increased vascu-

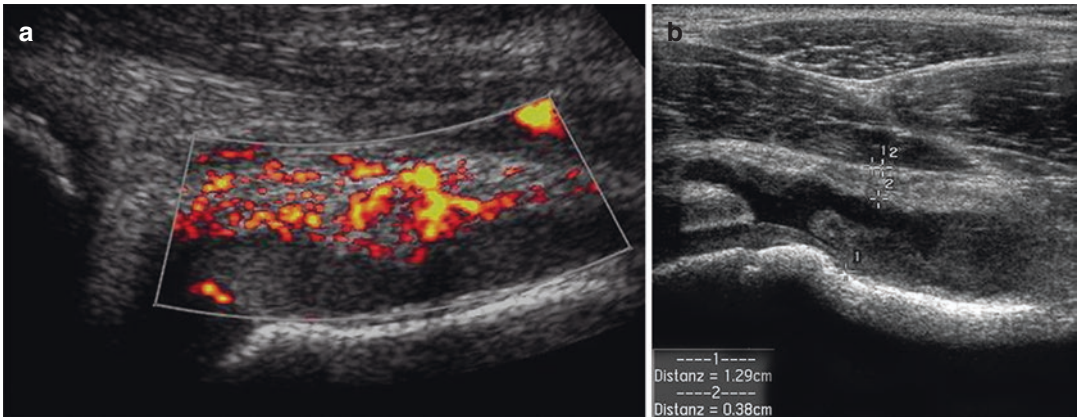




Fig. 15.19 (a) Power Doppler in septic arthritis: Note impressive hypervascularity of the thickened synovium, complex fluid in the widened joint space (b) massive

synovial reaction, measurement (+...+) *not* useful in establishing diagnosis. Note: this is a sensitive, but unspecific sign

 The assessment of capsule-to-bone distance and the echogenicity of the intraarticular effusion do not permit a differentiation between viral, bacterial/septic, or even rheumatoid arthritis. That means simple effusion does not rule out bacterial/septic arthritis, and complicated effusion does not proof septic arthritis! Establishing a diagnosis solely by US is impossible and may bear the risk of incorrect results and thus delayed start of appropriate therapy. If there is any doubt, further examinations to rule out especially septic arthritis are required. This is usually achieved by clinical data, (possibly US-guided) arthrocentesis, and for some MRI.

 In particularly septic osteoarthritis of young infants, there may be distention and subsequent luxation and osseous defects. Luxation can be identified by applying DDH US techniques (e.g. using Graf's criteria)—search for it!

larity is depicted, spectral analysis may show diastolic hyperaemia unless joint pressure increases and diastolic perfusion is impaired. Particularly after long-standing and bacterial

arthritis, defects may remain—with poor ossification of the femoral neck and defects in the convexity of the femoral head.

15.8.4 (Femoral Head) Epiphysiolysis/Slipped (Capital Femoral) Epiphysis

This is a rare condition. In infants US is judged to be superior to plain radiographs due to its higher sensitivity in detecting disruption of the neck-head continuity and without the restriction of poor ossification of the cartilaginous femoral head in infants, thus improving assessment. The same approach accounts for all other joints with a cartilaginous epiphysis (e.g. shoulder and elbow, namely in/after birth trauma) (Fig. 15.20). Nevertheless, a radiograph is compulsory in the initial assessment and for long-term follow-up.

The US scanning is performed from the anterior approach in a sagittal plane, with the probe parallel to the femur. By this, longitudinal images of the joint should be obtained. In birth trauma, the displacement may occur in any direction, therefore US access from different directions and positions is recommended. Typical US findings are:

The continuity of the bone margin is disrupted at the level of the physis and produces a step-off phenomenon of the femoral head (or the epiphysis in other joints). The anechoic cartilage of the femoral head or the epiphysis (with or without a

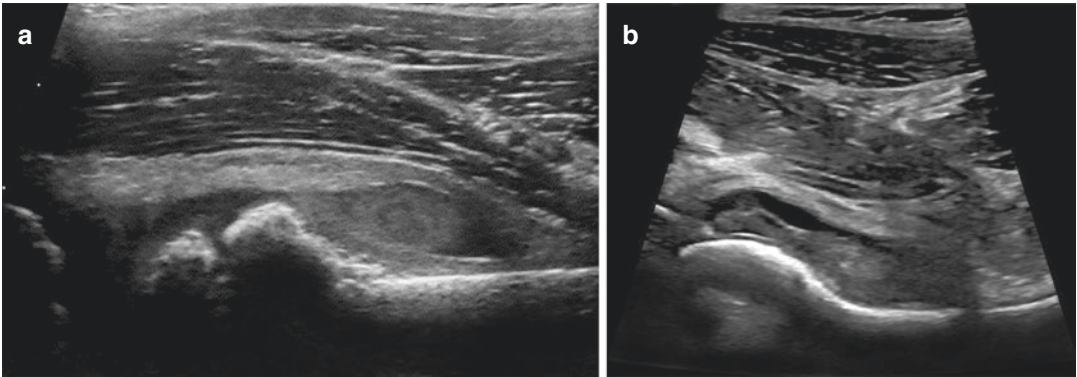


Fig. 15.20 (a) Ultrasound in haemarthrosis in a child with haemophilia. Note complex fluid representing acute haemorrhage. (b) Hip US in patient with juvenile rheuma-

toid arthritis. Proliferation of the synovial capsule, only sparse effusion

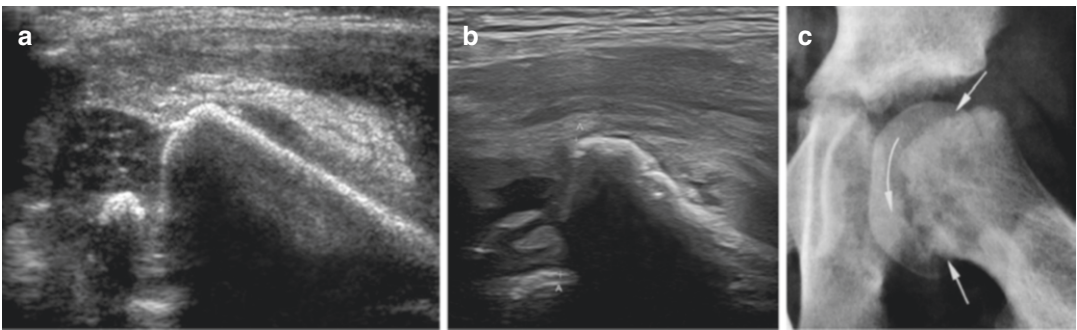


Fig. 15.21 (a–b) Ultrasound in epiphysiolysis in a newborn after birth trauma. Note the discontinuity between ossified bone and hypoechoic cartilaginous epiphysis indi-

cating dislocation of epiphysis. (c) Radiograph of a left hip with slipped capital femoral epiphysis; note the displacement of the epiphysis in relation to the femoral head

depictable ossification centre) is slipped off and displaced backwards. One millimetre displacement on US equals approximately 5° displacement on an axial radiograph.

- Particularly in acute epiphysiolysis the complex joint fluid represents haemorrhagic components in the early phase. The surrounding soft tissues may show nonspecific secondary changes like oedema and subperiosteal bleeding—with elevation of the periosteum.
- In the chronic form (epiphysiolysis capitis femoris lenta) less joint effusion is seen, which is usually hypoechoic, and often a thickened joint capsule is observed. Periosteal reaction can be noted only in the late stage.

US-guided reposition may be feasible in the neonate. If tolerated, dynamic assessment may

reveal pathologic motion at the physis. The same criteria apply to epiphysiolysis of any other joint in neonates and infants (Fig. 15.21).

15.8.5 Perthes Disease

This condition is defined as an avascular necrosis of the femoral head of unclear aetiology and unknown origin. Twenty percent of affected children have a history of a transient synovitis of hip.



In suspicion of Perthes Disease based on a persisting joint effusion, radiographs and (dynamic contrast-enhanced) MRI must be performed.

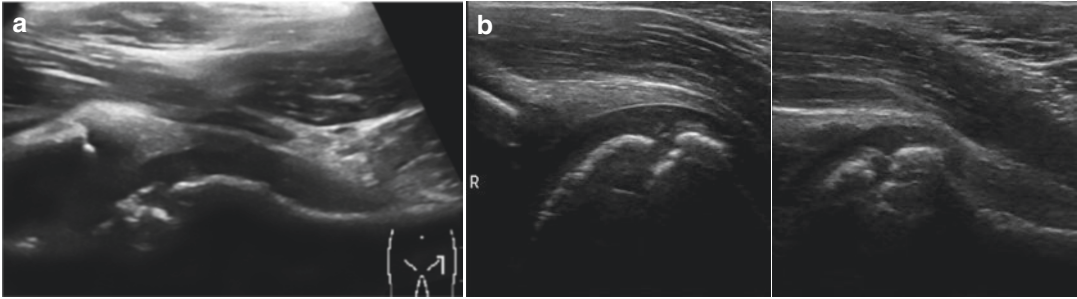


Fig. 15.22 Ultrasound in Perthes disease. (a) Scattered epiphysis of femoral head in early Perthes disease (stage II). (b) Both hips imaged for comparison (split image technique)

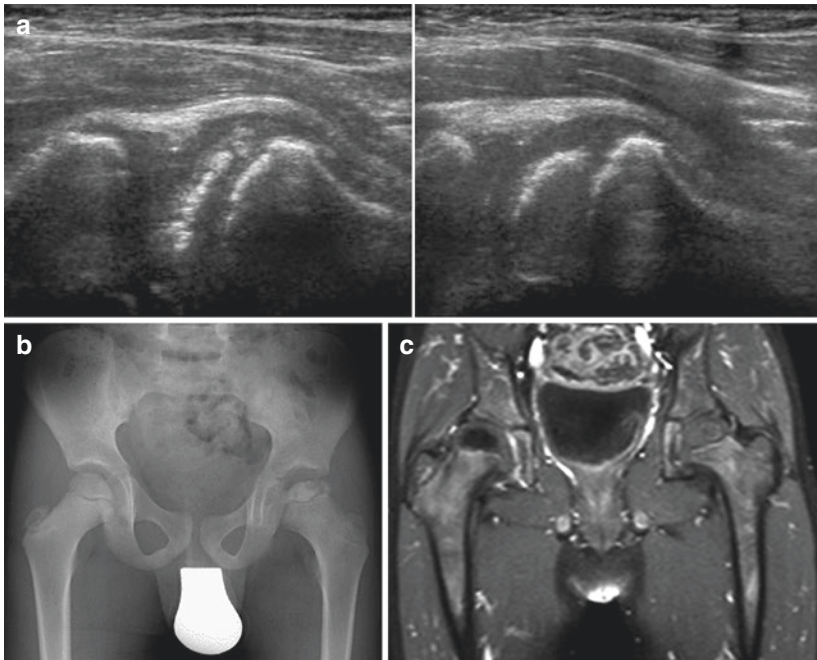


Fig. 15.23 (a) Ultrasound in Perthes disease. Scattered epiphysis of femoral head in early Perthes disease (stage IV). Both hips imaged for comparison (split image technique). Note the reduced height of affected left femoral head (Grade IV—US appearance varies with stage); additional imaging compulsory (radiograph and MRI). (b) Radiograph of the

pelvis and hip in a patient with Perthes disease: note the condensed left femoral head, which however is still centred. (c) Contrast-enhanced MRI of the hips (coronal T1-weighted view with fat suppression after gadolinium application) in a patient with Perthes disease: note the asymmetric contrast uptake of the femoral head (different patients)

US Findings and Staging

- Grade I: Potentially only some joint effusion is seen—the contour of the femoral head is maintained. A slight asymmetric reduction of the height of the epiphysis as well as the femoral head on the affected side may be perceivable. These changes are subtle and not always seen on US.

- Grade II (Fig. 15.22): Sonographically, an irregular disruption of the outer contour of the bony femoral head indicates fragmentation. There may be secondary effusion and capsular thickening.
- Grade III and IV (Fig. 15.23): Due to reparative mechanisms, the femoral head becomes increasingly homogeneous, with significantly reduced femoral head height.

15.9 Summary and Take Away Message

It has become important for all physicians caring of newborns and infants to have at least basic knowledge about the essentials of US examinations—not only for early diagnosis of musculoskeletal problems, but also for optimising treatment and to help to avoid unnecessary (radiation) burden to the patient. If done properly, US can support decision making in daily clinical setting and is therefore irreplaceable in daily routine. Therefore, it should be part in every education programme and integrated in the medical curriculum of health care professionals.

With respect to hip US, one needs to state that it has become the mainstay for DDH assessment, with different techniques throughout the world—in Europe the Graf method including dynamic assessment (or the modified Graf technique according to Rosendahl) is most often used, whereas in North America, the Harcke technique is also used. The indication varies too—some only perform US as a selected screening in risk patients, other countries have a well-established general screening programme. This is recommended particularly in regions with high DDH incidence. Whichever approach is chosen, one needs to remember that this US for DDH is a so-called final investigation: if one misses pathology, the patient will only come back after years or even decades with severe complaints and high morbidity, also causing high health care costs. As a missed pathology will have potentially disastrous implications, proper scanning technique and the skillful and prudent performance are mandatory by appropriately trained health professionals. The training should be offered in standardised and approved training programmes and taught by certified and approved trainers and instructors to avoid pitfalls and misinterpretation.

The absence of evidence does not necessarily mean the evidence of absence of benefit for the patient, even multicentre prospective double-blinded randomised controlled studies are lacking—therefore the author favours the general US screening approach even if some contradict.

Additionally, US has a high value in the early diagnosis of hip joint effusion and can help to differentiate the most common other pathologies in infants and children such as haemarthrosis, slipped capital epiphysis, and (traumatic) epiphysiolysis or septic coxitis.

This chapter guides through different US techniques in performing US of the hip, mainly focusing on DDH and the method according to Graf. It should help to understand the principles of hip US, address its importance particularly in endemic regions, discuss the indications, illustrate the respective findings, and briefly touch on pitfalls, therapeutic and prognostic implications, but does not replace studying textbooks and consulting current medical literature.

Acknowledgement I would like to express my gratitude to my friend and academic teacher Prof. Dr. Reinhard Graf, Stolzalpe, Austria, for the permission to use schematic drawings from his manual, as well as text citations.

I furthermore like to thank Dr. Brian Coley, Cincinnati, Ohio, very much for editing the text and providing some images.

Further Reading

- American Institute of Ultrasound in Medicine. AIUM practice guideline for the performance of an ultrasound examination for detection and assessment of developmental dysplasia of the hip. *J Ultrasound Med.* 2013;32:1307–17, update 2018. <https://onlinelibrary.wiley.com/doi/10.1002/jum.14829>
- Barrera CA, Cohen SA, Sankar WN, et al. Imaging of developmental dysplasia of the hip: ultrasound, radiography and magnetic resonance imaging. *Pediatr Radiol.* 2019;49:1652–68.
- Biedermann R, Eastwood DM. Universal or selective ultrasound screening for developmental dysplasia of the hip? A discussion of the key issues. *J Child Orthop.* 2018;12:296–301.
- De Bruyn R. The musculoskeletal system. In: de Bruyn R, editor. *Pediatric ultrasound how, why and when.* 2nd ed. Amsterdam: Elsevier; 2010. p. 319–39.
- Fröhlich S, Mittelmeier W. Hüftsonografie. In: Robel-Tillig E, editor. *Pädiatrische Ultraschalldiagnostik.* Ecomed-Storck GmbH; 2021. (In German).
- Graf R. The diagnosis of congenital hip joint dislocation by ultrasound compound treatment. *Arch Orthop Trauma Surg.* 1980;97:117–33.
- Graf R. Hip sonography: background; technique and common mistakes; results; debate and politics; challenges. *Hip Int.* 2017;27(3):215–9.

- Graf R, Spiess T. Säuglingshüfte. In: Deeg K-H, Hofmann V, Hoyer PF, editors. *Ultraschalldiagnostik in Pädiatrie und Kinderchirurgie*. 4th ed; 2014. p. 1076–106. (In German).
- Graf R, Lercher K, Baumgartner F, et al. *Sonografie der Säuglingshüfte und therapeutische Konsequenzen* (In German). 6th ed; 2010.
- Graf R, Scott S, Farkas P, et al. *Essentials of infant hip sonography according to Graf. Stolzalpe: Edition Stolzalpe Sonocenter*; 2014.
- Harcke HT. Hip ultrasonography in clinical practice. *Pediatr Radiol*. 2017;47:1155–9.
- Hefti F. *Kinderorthopädie*. 3rd ed; 2015. p. 216–54; 301–9. (In German).
- Morrow AC. *Diagnostic imaging pediatrics*. 3rd ed; 2017. p. 932–43.
- O’Beirne JG, Chlapoutakis K, Alshryda S, et al. International Interdisciplinary Consensus Meeting on the evaluation of developmental dysplasia of the hip. *Ultraschall Med*. 2019;40:454–64.
- OEGUM/DEGUM recommendation: www.OEGUM.at/content/view/506/210 download “Standarddokumentation der Sonografie der Neugeborenen- und Säuglingshüfte” (in German).
- Riccabona M, Coley B, Schweintzger G. Small part and hip ultrasound. In: Riccabona M, editor. *Pediatric ultrasound*. 3rd ed; 2014. p. 397–414.
- Rosendahl K, Toma P. Ultrasound in the diagnosis of developmental dysplasia of the hip in newborns. The European approach. A review of methods, accuracy and clinical validity. *Eur Radiol*. 2007;17:1960–7.
- Schwarz Doria A, Babyn P. Arthritis and differential inflammatory joint disorders. In: Coley BD, editor. *Caffey’s pediatric diagnostic imaging*. 12th ed; 2013. p. 1444–88.
- Schweintzger G. Hüftsonografie. In: Feldkamp A, Rech A, editors. *Pädiatrische Ultraschalldiagnostik*; 2010. (In German).
- Schweintzger G. Hüftgelenkdysplasie und postnatales Hüftscreening. In: Hoffman G, Lentze MJ, Spranger J, et al., editors. *Pädiatrie*. 5th ed; 2020. p. 119–25. (In German).
- Servaes S, et al. Developmental dysplasia of the hip. In: Coley BD, editor. *Caffey’s pediatric diagnostic imaging*. 12th ed; 2013. p. 1437–43.
- Siegel MJ. Musculoskeletal system and vascular imaging. In: Siegel MJ, editor. *Pediatric sonography*. 4th ed; 2011. p. 602–46.
- Teixeira SR, Dalto VF, Maranhão DA, et al. Comparison between Graf method and pubo-femoral distance in neutral and flexion positions to diagnose developmental dysplasia of the hip. *Eur J Radiol*. 2015;84:301–6.
- Thallinger C, Pospischill R, Ganger R, et al. Long term results of a nationwide general ultrasound screening system for developmental disorders of the hip: the Austrian hip screening Program. *J Child Orthop*. 2014;8:3–10.
- Treguier C, Chapuis M, Branger B, et al. Pubo-femoral distance: an easy sonographic screening test to avoid late diagnosis of developmental dysplasia of the hip. *Eur Radiol*. 2013;23:836–44.
- Tschauner C, Fürntrath F, Saba Y. Developmental dysplasia of the hip: impact of sonographic newborn hip screening on the outcome of early treated decentered hip joints—a single center retrospective comparative cohort study based on Graf’s method of hip ultrasonography. *J Child Orthop*. 2011;5:415–24.
- von Kries R, Ihme N, Oberle D, et al. Effect of ultrasound screening on the rate of first operative procedures for developmental hip dysplasia in Germany. *Lancet*. 2003;362(9399):1883–7.
- Waibel P, Maurer K. The pediatric musculoskeletal system. In: Riccabona M, editor. *Pediatric imaging essentials*. 1st ed; 2014. p. 229–68.
- Yeh RW, Valsdottir LR, Yeh MW, et al. Parachute use to prevent death and major trauma when jumping from aircraft: randomized controlled trial. *BMJ*. 2018;363:k5094. <https://doi.org/10.1136/bmj.k5094>.

Neonatal Imaging in Thyroid Disease, Inherited Disease, Syndromes, and Oncology

Janina M. Patsch

16.1 The Normal Neonatal Thyroid Gland: Imaging Appearance and Reference Values

The thyroid gland originates and *descends* from a primordial bud located at the posterior aspect of the tongue (= later foramen caecum). The path of this descent corresponds to the *thyroglossal duct* (= anterior to the hyoid and the laryngeal cartilages). Normally, the duct obliterates. If obliteration does not occur, remnants can give rise to thyroglossal duct cysts. Likewise ectopic thyroid tissue can be found anywhere along the duct's path.

Thyroid imaging is indicated in neonates with suspected thyroid disease (e.g. hypothyroidism found in neonatal blood spot test from heel prick; neonatal thyrotoxicosis). Ultrasound is the modality of choice. It should be kept in mind that thyroid volumetry requires axial and parasagittal views of both lobes and the isthmus which can be challenging in neonates (Table 16.1). Alternatively, width and depth can be measured

Table 16.1 Normative values for thyroid size and volume in neonates

		Mean (± 2 SD)
Width (cm)	Right lobe	0.7 (0.6–0.9)
	Left lobe	0.7 (0.6–0.9)
Depth (cm)	Right lobe	0.7 (0.4–1.0)
	Left lobe	0.7 (0.4–1.0)
Length (cm)	Right lobe	2.0 (1.8–2.3)
	Left lobe	2.0 (1.8–2.2)
Total volume (mL)	Both lobes	1.0 (0.6–1.5)

Data from Mikolaiczak 2015

Volume per lobe was calculated as follows: length \times depth \times width $\times \pi/6$ (0.52). Total thyroid volume = sum of the volume of the individual lobes (disregarding the volume of the isthmus which is negligible in normal neonates)

in the axial plane. Perfusion assessed by colour Doppler sonography (CDS) should always be documented.

16.1.1 Neonatal Thyroid Disease

The thyroid gland can be fully or partially absent (= *agenesis/hemi-agenesis*). Thyroid hormones are needed for normal foetal/neonatal brain development, metabolism, and growth. Because *congenital hypothyroidism* leads to *cretinism* if untreated with thyroid hormone replacement therapy, the heel prick test screens for this curable condition.

Neonatal hypothyroidism can also be caused by transplacental passage of thioamides (= anti-

J. M. Patsch (✉)
Division of General and Pediatric Radiology,
Department of Biomedical Imaging and Image-Guided Therapy, Medical University of Vienna,
Vienna, Austria

Vienna Bone and Growth Center, Medical University of Vienna, Vienna, Austria
e-mail: Janina.patsch@meduniwien.ac.at

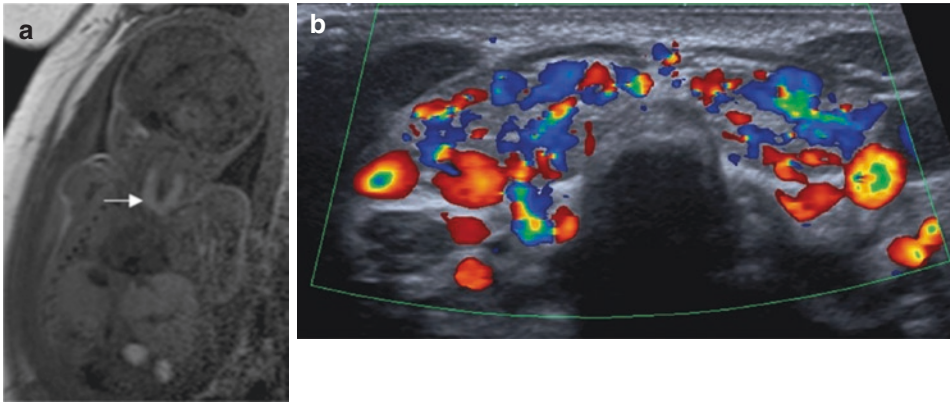


Fig. 16.1 Neonatal thyrotoxicosis. (a) Foetal MR (1.5 T, coronal plane, T1-w) increased thyroid size. Note the foetal thyroid gland has physiologically a bright T1-signal on MR-imaging (Image Courtesy Prof. Gregor Kasprian, Department of Neuroradiology and Musculoskeletal

Radiology, Medical University of Vienna). (b) Postnatal ultrasound demonstrates enlarged and hypervascular thyroid gland. In this case, neonatal thyrotoxicosis was caused by transplacental passage of stimulating TSH-receptor antibodies

thyroid drugs used to treat *maternal hyperthyroidism, e.g. Graves' disease*). Likewise, thyroid inhibitory antibodies can cross the placenta in *maternal Hashimoto's disease*. Moreover, maternal iodine deficiency, maternal diabetes mellitus, and lithium therapy can lead to neonatal hypothyroidism. Babies born with Down's syndrome have an increased risk for hypothyroidism. Of practical importance, there is a possible risk for developing hypothyroidism in infants with exposure to iodine-containing contrast agents. Neonatal hypothyroidism can be associated with epiphyseal stippling (as, e.g. in chondrodysplasia punctata types or in cases with maternal warfarin use).

The most severe—even life-threatening—manifestation of *neonatal hyperthyroidism* is *neonatal thyrotoxicosis* (Fig. 16.1). The most frequent cause is *maternal Graves' disease* with stimulating antibodies crossing the placenta. Very rarely, a similar pathophysiologic mechanism can occur in babies with *maternal Hashimoto's disease*. The majority of cases with neonatal hyperthyroidism are transient, but persistent forms exist with activating mutations of the TSH-receptor or in McCune-Albright Syndrome.

16.2 Selected Chromosomal Disorders, Syndromes, and Multi-system Associations

16.2.1 Chromosomal Disorders

Human cells contain 46 chromosomes (diploid set of 23 pairs = 44 autosomes; 2 sex chromosomes X + Y). Chromosomal aberrations can be *numeric or structural*. Typically, *trisomies* (= triplet of a certain chromosome instead of a pair) or *monosomies* (= singlet instead of a pair) are based on erroneous cell division with a non-disjunction during maternal or paternal meiosis. They also be due to a *Robertsonian translocation* in a carrier parent. It is also possible that only some cells of the body carry the defects if the non-disjunction occurs during embryonic mitosis (= *mosaicism* with variable clinical phenotype). In cases of chromosomal breakage, the fragment can fuse to other chromosomes with and without the loss of “relevant” genetic material (= unbalanced vs. balanced translocations). Structural aberrations include *partial deletions* and *microdeletions*.

The following sections will address a selection of the most common and most important conditions.

16.2.2 Trisomy 21

Children born with trisomy 21 (= *Down's* syndrome; Fig. 16.2) have characteristic facial features (including up-slanting palpebral fissures, medial epicanthus, flat face) and hypotonia. Certain cardiac defects (especially endocardial cushion defects = atrioventricular septal defects/AVSD and ventricular septum defect/VSD) are increased (Fig. 16.2a). The risk for duodenal atresia/stenosis, Hirschsprung's disease, intestinal malrotation, and anorectal anomalies is also higher than in the rest of the population (Fig. 16.2e). Pulmonary cysts might

be seen in peri-operative cross-sectional imaging of the chest. On neonatal radiographs, epiphyseal stippling can sometimes be found (Fig. 16.2c). The risk for acute lymphatic leukaemia is increased.

16.2.3 Trisomy 18 and 13

Other than children with trisomy 21, those with trisomy 18 or 13 have a high postnatal mortality. Rarely, they survive the first year of life. There are also partial or mosaic forms of trisomy 18 and 13.

Children born with *trisomy 13* (= Patau syndrome) have a wide spectrum of severe malformations and major congenital defects. Characteristic facial dysmorphism with cleft palate and micrognathia, midline defects including

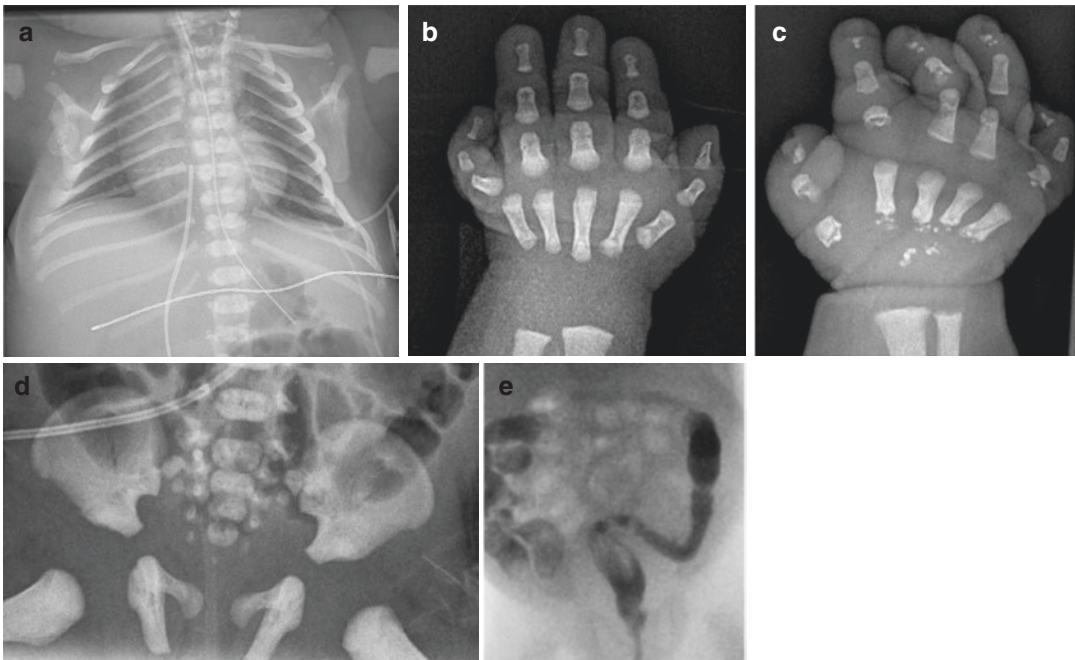


Fig. 16.2 Trisomy 21 (*Down's* Syndrome). (a) Chest radiograph demonstrates bell-shaped chest and cardiomegaly due to congenital heart defect. (b) Hand radiograph shows short 5th finger with inward bending (clinodactyly). (c) Hand radiograph with cartilaginous stippling (= "stippled epiphyses"). (d) Radiograph with abnormal shape and

morphology of pelvis with wide acetabulum with "mickey-mouse ears" configuration of iliac wings. (e) Fluoroscopic enema depicts Hirschsprung's disease associated with trisomy 21. Long aganglionic segment (= with narrow diameter) and transition zone (= funnel-shaped widening of colonic diameter) at the descending colon

severe brain malformations (such as holoprosencephaly), cardiac defects, polycystic kidneys, and various skeletal changes (e.g. post-axial polydactyly, rocker bottom feet).

Children born with *trisomy 18* (= Edwards' syndrome) have characteristic facial features, microcephaly with prominent occiput, hypotonia, and a multitude of severe congenital pathologies including the brain, heart, lungs, urogenital, gastrointestinal, and musculoskeletal system.

16.2.4 Turner's Syndrome (45 XO)

Neonates with Turner's syndrome often have peripheral oedema and a webbed neck. The chest is shield-like and the nipples are wide-spaced. There is an increased rate of renal anomalies, in particular horseshoe kidneys (Fig. 16.3). Genital anomalies include hypoplastic or absent uterus and streak gonads. In the cardiovascular system, aortic coarctation is relevant in the neonatal period.

16.2.5 VACTERL

While many congenital disorders are based on specific chromosomal aberrations or specific genetic defects, multi-system associations are

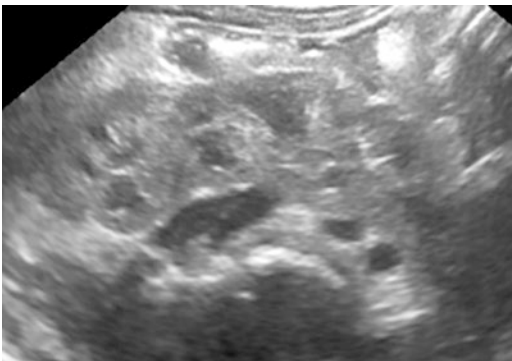


Fig. 16.3 Horseshoe kidney in a girl with Turner's syndrome. Axial view by ultrasound shows transverse continuity of renal parenchyma ventral to the vascular axis (= fused/non-separated lower renal poles)

conditions without (yet) known underlying genetic cause.

In cases with the VACTERL association/spectrum disorder, vertebral anomalies, ano-rectal malformations, cardiovascular malformations, oesophageal atresia with/without tracheoesophageal fistula, renal anomalies, and limb defects can co-occur (Fig. 16.4). For more details on these individual sub-entities, please be referred to respective chapters in this book.

16.2.6 CHARGE Syndrome

Coloboma, heart defects (Fig. 16.5b–d), choanal atresia, genital and ear anomalies (→ acronym = CHARGE) are associated with an underlying defect in the CHD7 gene (chromodomain helicase DNA-binding protein).

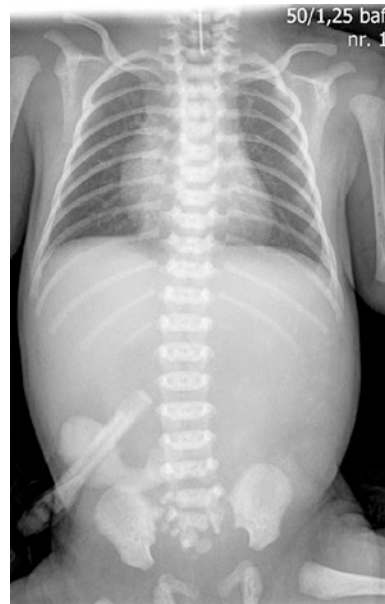


Fig. 16.4 VACTERL association. Radiograph (= torso-gram) shows co-occurrence of oesophageal atresia without fistula (= gastric tube fails to reach stomach; no intraluminal gas in the abdomen), sacral dysgenesis, unilateral hypoplasia of the 12th rib (left) and cardiomegaly. The co-existing cloacal malformation and renal dysgenesis are not visible on radiographs and require other imaging modalities for diagnosis (e.g. renal dysgenesis: ultrasound, cloacal malformation: US/MR-genitography)

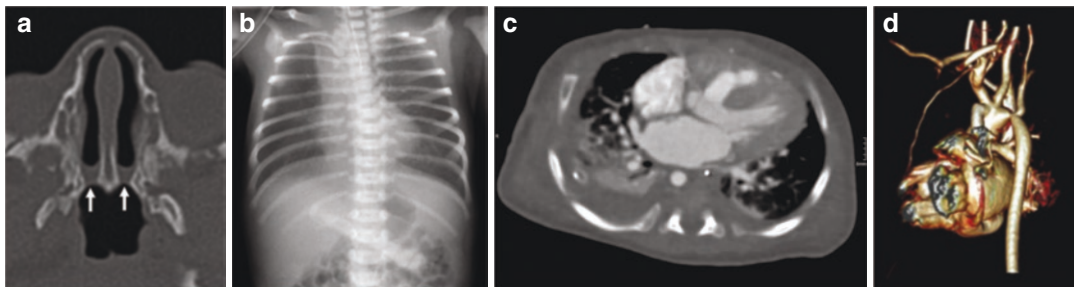


Fig. 16.5 CHARGE syndrome. (a) Bilateral non-osseous choanal atresia on CT. Fluid levels result from obstructing choanal membranes (white arrows). (b) Radiograph demonstrates oesophageal atresia (i.e. tip of gastric tube is located at proximal end of atretic oesophagus) with fistula (= intraluminal gas present in gastrointestinal tract). Heart is boot-shaped, indicative of tetralogy of Fallot. (c) Cardiac

CT (contrast-enhanced) of same patient with tetralogy of Fallot. Features visible on this CT-image are ventricular septal defect (VSD) with overriding aorta and right ventricular hypertrophy. There is a right-descending aorta. Please note gastric tube in lower oesophagus after surgical correction of oesophageal atresia. (d) 3D reconstruction of cardiac CT (as shown in c) demonstrates aortic coarctation

From a neonatal imaging perspective, cross-sectional imaging plays a central role in diagnosing the regional pathologies (e.g. MRI/CT for inner ear malformations; pre-operative cardiac imaging for complex cardiac malformations). With choanal atresia being potentially life-threatening to neonates, airway management is crucial in clinical management. CT and MRI can differentiate between osseous and membranous forms of choanal atresia and determine unilaterality vs. bilaterality (Fig. 16.5a). There are characteristic facial and external ear features (“CHARGE ear”). In addition, various congenital skeletal abnormalities can be found, predominantly of the spine and the limbs. Cleft palates and brain malformations are frequent. The incidence of oesophageal atresia is increased in neonates born with CHARGE syndrome (Fig. 16.5b).

16.2.7 Beckwith-Wiedemann Syndrome

The prenatal co-occurrence of macrosomia, abdominal wall defects (especially omphalocele; Fig. 16.6a), and placental mesenchymal dysmorphism (Fig. 16.6c) should raise the suspicion for Beckwith-Wiedemann syndrome. Postnatally, macroglossia (Fig. 16.6b), hemihypertrophy, and hypoglycaemia (caused by hyperinsulinism) can

be part of the clinical spectrum. Children with Beckwith-Wiedemann syndrome have a predisposition to cancer—which is of major practical relevance for paediatric imaging, as it requires continuous paediatric-oncologic monitoring including regular abdominal ultrasound scans. By ultrasound, general organomegaly is often found.

16.2.8 Metabolic Disease Presenting in the Neonatal Period: Implications for Imaging

Since the 1960s, many countries perform nationwide neonatal screening (“heel-prick-test”) for certain congenital disease (Table 16.2; with the list being continuously expanded). For these (mostly but not exclusively metabolic) diseases, an adequate diet or therapy can improve the natural course significantly. Thus neonatal screening has a direct impact on improved health and well-being of affected children and families.

For these diseases (Table 16.2), the role of neonatal imaging is limited but the importance of diagnostic imaging grows with patient age and clinical course (e.g. CF). Certainly, when imaging is performed in affected babies (e.g. CAH), distinct imaging findings can be observed (e.g. cerebriform hypertrophy of the adrenal glands).

On the contrary, a multitude of inborn errors of metabolism (not included in neonatal screening;

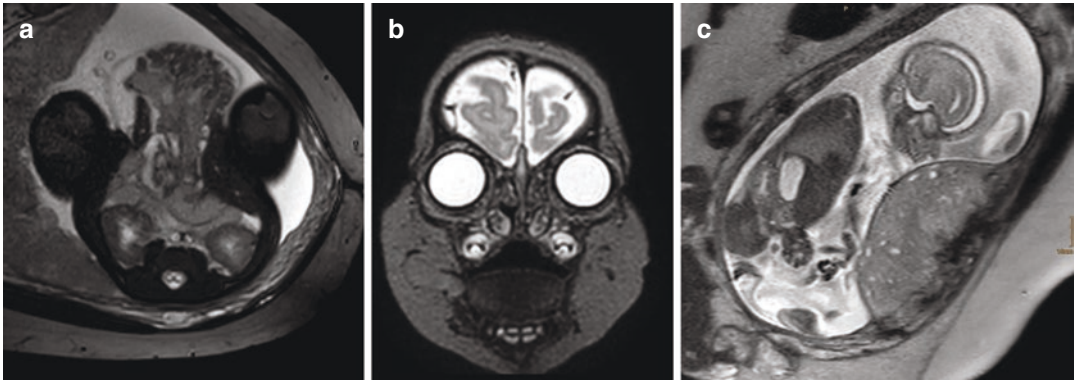


Fig. 16.6 Beckwith-Wiedemann syndrome. (a) Foetal-MR (T2-weighted; axial) demonstrates abdominal wall defect (= omphalocele) (Image Courtesy: Prof. Gregor Kasprian, Division of Neuroradiology and Musculoskeletal Radiology, Department of Biomedical Imaging and Image-guided Therapy, Medical University of Vienna). (b) Macroglossia in Beckwith-Wiedemann syndrome: Postnatal MRI (1.5 T, T2-weighted; coronal

plane; same child as in a). (c) Foetal MRI in another case of Beckwith-Wiedemann syndrome: Placental mesenchymal dysmorphia (= cysts and pathologic signal) and omphalocele (Image courtesy: Prof. Gregor Kasprian, Division of Neuroradiology and Musculoskeletal Radiology, Department of Biomedical Imaging and Image-guided Therapy, Medical University of Vienna)

Table 16.2 Congenital diseases detectable by neonatal blood screening (“heel-prick-test”)

Endocrine disorders	Congenital adrenal hyperplasia (CAH) Hypothyroidism
Aminoacidopathies and urea cycle disorders	Phenylketonuria (PKU)/Hyperphenylalaninaemia Tyrosinemia type I Maple Syrup Disease (Leucinosi)s Arginine succinate lyase (ASL) deficiency Homocystinuria (HCY)/hypermethioninaemia Citrullinaemia
Organoacidopathies	Methylmalonic acidemia Propionic acidemia Isovaleric acidemia Glutaric aciduria type I (GA1) Glutaric aciduria type II (GA2)/Multiple acyl-CoA-dehydrogenase-deficiency (MADD)
Fatty acid β -oxidation disorders (FAODs)	Medium-chain-acyl-CoA-dehydrogenase-deficiency (MCADD) Very-long-chain-acyl-CoA-dehydrogenase-deficiency (VLCDD) Long-chain-acyl-CoA-dehydrogenase-deficiency Trifunctional protein (TFP) deficiency
Carnitine cycle defects	Carnitine palmitoyltransferase (CPT) I deficiency Carnitine palmitoyltransferase (CPT) II deficiency Carnitine transporter deficiency (CTD) Carnitine-Acylcarnitine translocase (CACT) deficiency
Biotinidase deficiency	
Galactosemia	
Cystic fibrosis (CF)	
Severe congenital Immune Defects	
Spinal muscle atrophy (SMA)	

Table 16.3 Categories of inborn errors of metabolism (according to the International classification of inherited metabolic disorders; J Inherit Metab Dis. 2021 Jan;44(1):164–177)

1. Disorders of amino acid metabolism
2. Disorders of peptide and amine metabolism
3. Disorders of carbohydrate metabolism
4. Disorders of fatty acid and ketone body metabolism
5. Disorders of energy substrate metabolism (e.g. mitochondrial disease)
6. Mitochondrial DNA-related disorders
7. Nuclear-encoded disorders of oxidative phosphorylation
8. Disorders of mitochondrial cofactor biosynthesis
9. Disorders of mitochondrial DNA maintenance and replication
10. Disorders of mitochondrial gene expression
11. Other disorders of mitochondrial function
12. Disorders of metabolite repair/proofreading
13. Miscellaneous disorders of intermediary metabolism
14. Disorders of lipid metabolism
15. Disorders of lipoprotein metabolism
16. Disorders of nucleobase, nucleotide, and nucleic acid metabolism
17. Disorders of tetrapyrrole metabolism
18. Congenital disorders of glycosylation
19. Disorders of organelle biogenesis, dynamics, and interaction
20. Disorders of complex molecule degradation
21. Disorders of vitamin and cofactor metabolism
22. Disorders of trace elements and metals
23. Neurotransmitter disorders
24. Endocrine metabolic disorders

overview of categories according to international classification of inherited metabolic disorders (ICIMD) given in Table 16.3) might manifest at birth or in the neonatal period with the acute need for hospitalisation due to hypotonia, neurologic deficits/seizures (e.g. mitochondrial disease), fever, hepatosplenomegaly, infections, haemorrhages, hypercoagulability, or extramedullary haematopoiesis. In these clinically sick neonates, there is major importance of radiologic imaging to rule out other differential diagnosis presenting with similar symptoms and to facilitate and accelerate clinical decision making and other diagnostic steps. (e.g. brain imaging by US and MRI in a baby with seizures).

16.3 Skeletal Dysplasias

16.3.1 Introduction and Basic Concepts

Skeletal dysplasias are rare diseases which typically manifest with *short stature and other signs of dysmorphism* caused by inborn pathologic

changes in bone and cartilage physiology. The clinical spectrum ranges from severe (= perinatally lethal) to very mild forms with premature onset of osteoarthritis in (early) adulthood. While *genetic testing* has revolutionised the field, *clinical and radiologic assessment* are still essential to provide optimal results (= *three-pillar approach*). To date, 461 different genetic skeletal disorders have been defined, with the classification being continuously revised and expanded. The latest classification has been issued by the Nosology Committee of the International Skeletal Dysplasia Society in 2019. Currently, 42 distinct subgroups (i.e. disease families) are listed. These subgroups (listed in Table 16.4) are mainly based on common pathophysiology and genetic pathways leading to common clinical and radiologic features. As I am considering it important for radiologists to be introduced to the concept of disease groups/families, I am listing the 42 disease groups in a separate table. For a full list of diseases included in these 42 groups, please be referred to Mortier et al. (2019) and more in-depth resources (e.g. Taybi and Lachmann's Radiology of Syndromes, metabolic disorders

Table 16.4 Disease groups/families according to the Nosology and Classification of Genetic Skeletal Disorders tenth revision (2019)

Disease group/family (<i>n</i> = 42)	Example(s) with (possible) neonatal presentation (selected from 461 diseases included in the 2019 Nosology)
1. FGFR3 chondrodysplasia group	Achondroplasia Thanatophoric dysplasia
2. Type 2 collagen group	Spondyloepiphyseal dysplasia congenita (SEDC) Kniest dysplasia
3. Type 11 collagen group	Otospondylomegapiphyseal dysplasia (OSMED)
4. Sulphation disorder group	Diastrophic dysplasia
5. Perlecan group	Dyssegmental dysplasia (Rolland-Desbuquois type)
6. Aggrecan group	Short stature and advanced bone age (ACAN mutation)
7. Filamin group and related disorders	Larsen syndrome
8. TRPV4 group	Metatropic dysplasia
9. Ciliopathies with major skeletal involvement	Ellis-van-Creveld Jeune syndrome (Asphyxiating thoracic dysplasia)
10. Multiple epiphyseal dysplasia and pseudoachondroplasia group	Later presentation than neonatal period (e.g. Pseudoachondroplasia)
11. Metaphyseal dysplasias	Cartilage–hair hypoplasia
12. Spondylometaphyseal dysplasias	
13. Spondylo-epi-(meta)-physeal dysplasias (S(M)DC)	
14. Severe spondylodysplastic dysplasias	Opsismodysplasia
15. Acromelic dysplasias	
16. Acromesomelic dysplasias	Grebe Dysplasia
17. Mesomelic and rhizo-mesomelic dysplasias	Omodysplasia
18. Bent bone dysplasias group	Campomelic dysplasia
19. Primordial dwarfism and slender bones group	3M-Syndrome
20. Dysplasia smit multiple joint dislocations	Desbuquois dysplasia
21. Chondrodysplasia punctata (CPD) group	Rhizomelic chondrodysplasia punctata
22. Neonatal osteosclerotic dysplasias	Caffey disease
23. Osteopetrosis and related disorders	Osteopetrosis, severe neonatal or infantile forms
24. Other sclerosing bone disorders	Lenz-Majewski hyperostotic dysplasia
25. Osteogenesis imperfecta and decreased bone density group	Osteogenesis imperfecta (Type 3)
26. Abnormal mineralisation group	Hypophosphatasia (infantile form)
27. Lysosomal Storage Diseases with Skeletal Involvement (Dysostosis multiplex group)	I-cell disease (Mucopolipidosis II)
28. Osteolysis group	Hutchinson-Gilford progeria
29. Disorganised development of skeletal components group	Multiple hereditary exostoses (MHE), Neurofibromatosis type 1 (NF1)
30. Overgrowth (tall stature) syndromes with skeletal involvement	CLOVES, Marfan syndrome
31. Genetic inflammatory/rheumatoid-like osteoarthropathies	Later presentation than neonatal period
32. Cleidocranial dysplasia and related disorders	Cleidocranial dysplasia
33. Craniosynostosis syndromes	Apert syndrome, Pfeiffer syndrome

Table 16.4 (continued)

Disease group/family (<i>n</i> = 42)	Example(s) with (possible) neonatal presentation (selected from 461 diseases included in the 2019 Nosology)
34. Dysostosis with predominant craniofacial involvement	Treacher Collins syndrome
35. Dysostoses with predominant vertebral and costal involvement	Klippel-Feil syndrome, Spondylocostal dysostosis, Cerebrocostomandibular syndrome (Rib gap syndrome)
36. Patellar dysostoses	Later (radiographic) presentation than neonatal period
37. Brachydactylies (without extraskeletal involvement)	Brachydactyly type A1, A2, B, B2, C, D, E
38. Brachydactylies (with extraskeletal involvement)	Rubinstein-Taybi syndrome
39. Limb hypoplasia—reduction defects group	Cornelia de Lange syndrome; Fanconi anaemia; Thrombocytopenia-absent radius (TAR), Holt-Oram syndrome, Tibial hemimelia, Poland syndrome
40. Ectrodactyly with and without other manifestations	Split hand-foot malformation
41. Polydactyly–Syndactyly–Triphalangism group	Greig syndrome, Pallister-Hall syndrome
42. Defects in joint formation and synostoses	Multiple synostoses syndrome

and Skeletal Dysplasias. Spranger’s book “*Bone Dysplasias – An Atlas of Genetic Disorders of Skeletal Development*”).

In many cases, skeletal disorders are suspected and/or detected by prenatal ultrasound and thereafter confirmed by genetic testing. Prenatal parental counselling is aiming to address severity and expected prognosis of the individual child. Nevertheless, it has to be kept in mind that termination of pregnancy is subject to a multitude of factors including personal choice, ethical, and legal considerations (which certainly differ on a regional and national base).

In children born with suspected or confirmed skeletal disorders, skeletal imaging is typically performed by a predefined set of conventional radiographs (= *skeletal survey*) in the first few weeks of life. For more details on skeletal surveys in neonates, please be referred to the last sections of Chap. 14 (neonatal MSK imaging).

The *challenge of early (= neonatal) imaging* is to combine adequate radiation protection following the ALARA (= as low as reasonably achievable) principle, excellent practical skills in the acquisition of neonatal radiographs, and correct radiologic interpretation of the images.

Normal and pathologic radiographic features have a distinct morphology in neonates. Key features might be transient or only evolve after time. In neonates, dysplastic epiphyseal and metaphyseal changes are almost invisible due to the physiologic absence of secondary ossification in most epiphyses. Likewise, pathologies of other unossified structures (e.g. the patella) are not applicable to neonatal radiographs. In general, relevant imaging findings can be very subtle and tend to evade the human eye if not looked for specifically. Thus, structured assessment is essential to avoid missed or wrong diagnoses. ***In suspected genetic skeletal disorders, the main task for radiologists is to translate the image to appropriate wording*** which complements clinical assessment and genetic analysis. (i.e. to report the presence or absence of specific radiographic features). Because there is ***considerable feature overlap between individual groups/diseases and major variability of disease/feature severity***, it is preferable to refrain from “attempting” to provide a specific diagnosis from skeletal surveys (unless the diagnosis is very clear and/or the reader is an expert). The literature is limited with respect to neonatal imaging phenotypes of genetic skeletal disor-

ders. Therefore, I would like to explicitly mention the excellent atlas “Fetal and Perinatal Skeletal Dysplasias” by Hall et al. (full reference given at the end of this chapter).

Due to the abundance of genetic bone diseases, it is not possible to present a full comprehensive review in this chapter. Instead, I have prepared the following sections as a guide for radiologists at centres with neonatal units (and only occasional need for survey reporting), but without tertiary centre experience for skeletal dysplasia.

16.3.2 Structured Assessment of a (Neonatal) Skeletal Survey (Adapted from Hall’s Atlas)

- **Determine presence of all (long) bones.**
- Compare **length of long bones** to known standards (Table 16.3).
- Assess skeletal **maturity/bone age** (in particular in hands, feet, knees), **ossification** (in particular pelvis, spine, skull, hands, feet), **and bone density.**
- Determine/assess **morphology of individual bones/skeletal regions** (using a gamut list = rule out/confirm the presence or absence of specific radiographic features).
- In addition, pay particular attention to **detect and describe**
 - **Missing or supernumerary bones**
 - **Fractures (+/– callus)**
 - **Signs of rickets**
 - **Punctate calcifications**

Clinical signs, stigmata, and other information invisible on radiographs (e.g. certain soft tissue and/or skin features) should be provided by the referring paediatricians.

16.3.3 Selected Normative Values for Assessment of Bone Size and Proportions

In order to define shortening or disproportion on radiographs, normative values need to be used as reference (Tables 16.5, 16.6 and 16.7). The vast majority of these reference values data back to

Table 16.5 Normal radiographic length of neonatal long bones

	Median (± 2 SD)
Humerus (mm)	64 (56–73)
Radius (mm)	53 (48–59)
Ulna (mm)	60 (54–67)
Femur (mm)	76 (69–85)
Tibia (mm)	64 (56–73)
Fibula (mm)	60 (54–68)

Data from Maresh and Deming (1939)
Median and ± 2 standard deviations (2 SD)

Table 16.6 Normal measures of the neonatal spine

	Median (± 2 SD)
Intervertebral disc height (cm)	0.23 (0.18–0.28)
Vertebral body height (cm)	0.63 (0.51–0.69)
Intervertebral disc (space)/vertebral ratio	0.365 (0.36–0.37)

Data from Ponrartana 2015 (based on magnetic resonance imaging)

Median and ± 2 standard deviations (2 SD)

Table 16.7 Normal measures of the neonatal skull

	Median (± 2 SD)
Cephalic length (mm)	136.9 (123.5–150.3)
Cephalic width (mm)	102.3 (91.3–113.3)

Data from Waitzman et al. 1992. The data are based on computed tomography (CT) but can also be applied to AP or lateral radiographs

Median and ± 2 standard deviations (2 SD)

U.S. data from the 1930 to 1950s. At that time, several institutions focused on radiographic definition of normative paediatric data (e.g. The Brush foundation at the Western Reserve University; The long-term Denver Child Research Council Study). The Greulich and Pyle atlas—which is still used as gold standard for radiographic bone age definition—dates back to these times and is based on images from the Brush Foundation. Of importance, these “old” reference data are also lacking racial and ethnic diversity, they are only based on Caucasian children.

Reporting the presence or absence of these features is key to truly support the three-pillar approach and should be given top priority when reading skeletal dysplasias. Gamut lists in reference literature will give more details on potential differential diagnosis for specific features.

Table 16.8 is a strongly condensed version of major skeletal key gamuts applicable to neonates. It is aimed at linking key terms with radiographic morphology. Table 16.8 is based on key literature including Taybi & Lachmann's lexikon and Christine Hall's foetal and perinatal book. Due to the rare nature of certain conditions, a small number of figures linked to Table 16.8 demonstrate features in older children. In these cases, the morphology shown is representative (Figs. 16.7, 16.8, 16.9, 16.10, 16.11, 16.12, 16.13, 16.14, 16.15, 16.16, 16.17, 16.18, 16.19, 16.20, 16.21, 16.22, 16.23, 16.24, 16.25, 16.26, 16.27, 16.28, 16.29, 16.30, 16.31, 16.32, 16.33, 16.34, 16.35, 16.36, 16.37, 16.38, 16.39, 16.40, 16.41, 16.42, 16.43, and 16.44).

Table 16.8 Condensed version of major skeletal key gamuts applicable to neonates

Region	Subregion/parameter	Pathologic features/terms	Corresponding figure
Limbs—long and short tubular bones	Number/size/shape	Duplications	Figure 14.21 Figure 16.10
		Proximal femoral deficiency	Figure 14.15
		Ulna/Ulnar ray aplasia/hypoplasia	
		Radius/radial ray aplasia/hypoplasia	Figure 14.21
		Fibular ray defect (aplasia, hypoplasia, shortness)	Figure 14.17
		Absent tibia/hypoplasia	Figure 14.16
	Proportions	Rhizomelic shortening	Figure 14.6 Figure 16.7
	Epiphyses	Advanced ossification or advanced bone age	Figure 14.1 (normal) Figure 16.16 (advanced)
		Stippling	Figure 16.17 Figure 16.22
	Metaphyses	Flared or broad	Figure 16.7 Figure 16.9 Figure 16.21
		Irregular and/or sclerotic	Figure 16.15
		Cupped	Figure 16.15
	Diaphyses	Slender	Figure 16.31
		Concertina-like	Figure 16.24
	Bowed or angulated	Figure 16.8 Figure 16.23 Figure 16.24	
	Dumbbell-shaped	Figure 16.7 Figure 16.9	
Limbs—hands and feet	Number	Pre-axial polydactyly	Figure 16.10
		Post-axial polydactyly	Figure 14.21
		Amputation/reduction defect	Figure 14.21 Figure 16.13
		Digital defects (adactyly, oligodactyly, monodactyly)	Figure 14.21
	Morphology/proportions/shape	Trident hand	Figure 16.19
		Mitten hand	Figure 16.14
		Ectrodactyly = split hand/foot = lobster claw hand/foot	Figure 16.12
		Syndactyly	Figure 14.21
		Symphalangism	Figure 16.14

Table 16.8 (continued)

Region	Subregion/parameter	Pathologic features/terms	Corresponding figure	
		Brachydactyly	Figure 16.19	
		Short, hypoplastic, or absent thumb	Figure 14.21	
		Triphalangeal thumb	Figure 16.34	
Limbs—joints	Alignment	Dislocation/subluxation	Figure 14.22	
		Hand contractures/claw hand	Figure 16.11	
		Congenital vertical talus = Rocker bottom feet	Figure 14.20	
		Talipes	Figure 14.23	
Spine	Number/formation/segmentation	Agenesis/dysgenesis/malsegmentation	Figure 14.24	
		Coronal clefts	Figure 14.24	
		Sagittal clefts	Figure 14.24	
		Platyspondyly	Figure 16.18	
	Height of vertebral bodies			
	Shape of vertebral bodies	Anterior beaking (beyond the neonatal norm)	Figure 16.18	
Thorax	Shape	Small/narrow/thoracic dysplasia	Figure 16.20	
		Bell-shaped	Figure 16.2	
	Ribs	Short	Figure 16.20 Figure 16.23 Figure 16.25	
		Missing	Figure 16.23	
		Beaded	Figure 16.25	
			Coat-hanger	See Al-Mudares and Fernandes N Engl J Med 2020; 382:1257
			Flaring, anterior-end cupping	Figure 16.20 Figure 16.26
			Gaps	See Watson TA et al., Skeletal Radiolol. 2014; 43:263–6
			Slender, thin, or twisted	Figure 16.23
	Clavicles		Absent/hypoplastic/dysplastic	Figure 16.32
Hooked/handle-bar			Figure 16.33	
Non-ossification/delayed			Figure 16.9 Figure 16.23 Figure 16.24	
		Abnormal iliac wings (round; flared) Small acetabular angle	Figure 16.2 Figure 16.19 Figure 16.20 Figure 16.21	
Pelvis	Ossification of pubic and ischial bones	Horizontal iliac wings	Figure 16.21	
	Ilium	“Trident acetabulum”	Figure 16.20 Figure 16.21	
		Small sciatic notch	Figure 16.21	
		Microcephaly	Figure 16.29	
		Macrocephaly	Figure 16.27	
Skull	Size	Ossification defects	Figure 14.6	
		Hyperostosis/osteopetrosis	Figure 16.30	
		Craniosynostosis shape	Figure 14.3 Figure 14.4 Figure 14.5	
	Mineralisation and thickness		Cloverleaf skull	Figure 16.27

Table 16.8 (continued)

Region	Subregion/parameter	Pathologic features/terms	Corresponding figure
		Premature closure	Figure 14.3 Figure 14.3 Figure 14.4 Figure 14.5
	Shape/morphology	Wormian bones	Figure 16.23
		Facial hypoplasia	Figure 16.10
	Sutures	Depressed/small nose	Figure 16.10
Face	Proportions	Frontal bossing	Figure 16.10
	Shape/morphology	Micrognathia/mandibular dysgenesis/agenesis	Figure 16.29

Fig. 16.7 Rhizomelia. The radiograph shows severe shortening of the proximal segment of the upper extremities (= humerus). The humerus is dumb-bell shaped



Fig. 16.8 Bowed long bones. Post-mortem foetal radiograph (“babygram”) in a case of thanatophoric dysplasia



Fig. 16.9 Dumb-bell shaped femur. Left radiograph shows over-tubulated, shortened femur with wide metaphyses and reduced ossification of the pelvis in a neonate with a type 2 collagen disorder. Right radiograph is normal for comparison. Please note that left image is zoomed to fit



Fig. 16.10 Bilateral pre-axial polydactyly. Duplication of both great toes and the first metatarsals



Fig. 16.11 Arthrogryposis multiplex congenita. (a) Radiograph demonstrates a “claw hand”. (b) Foot radiograph shows clubfoot (same child as in a)

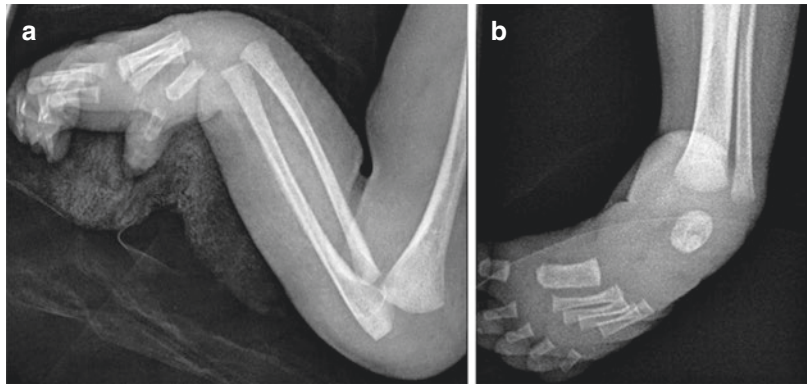


Fig. 16.12 Split-foot and split-hand malformation (= ectrodactyly). (a) Anteroposterior radiograph of both feet. (b) Anteroposterior hand radiograph. Colloquial term “lobster claw hand” should be avoided

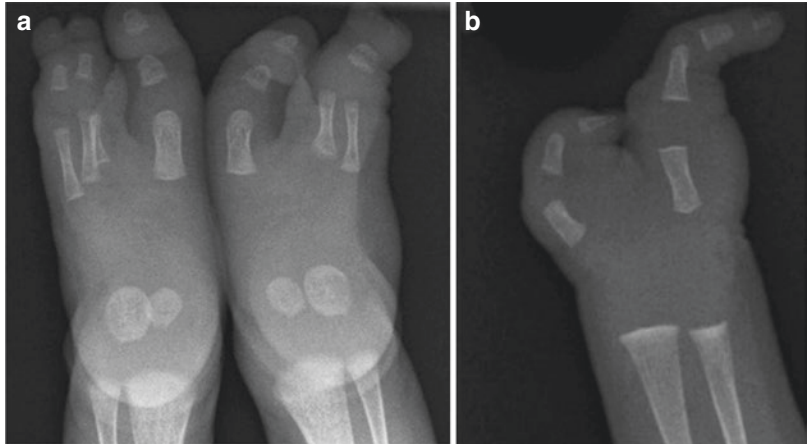




Fig. 16.13 Unilateral amputation defect (= transverse defect). Radiograph with shortened radius and ulna. The hand is missing

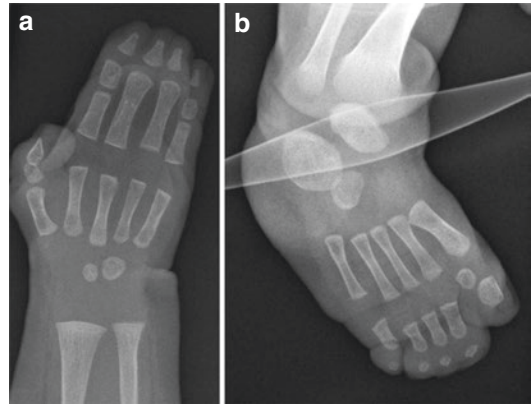


Fig. 16.14 Apert syndrome. (a) Radiograph demonstrates “mitten hand” with non-osseous syndactyly and symphalangism (of the third and fourth digit at the proximal interphalangeal joint level). Middle phalanges of second and fifth ray are abnormally short and under-tubulated/stubby. (b) Non-osseous syndactyly of the foot (same child as in a)



Fig. 16.15 Rickets. Frayed and cupped metaphyses in a boy with pre-term birth and postnatal diagnosis of Gaucher’s disease. The child died at the age of 4 months from multi-organ failure



Fig. 16.16 Advanced bone age in the newborn period. In this boy with a skeletal dysplasia, the hamate and capitate have started to ossify. At birth, the carpus should be purely cartilaginous



Fig. 16.17 Stippling of epiphyses and cartilaginous anlagen. The feature is characteristic in chondrodysplasia punctata (subtypes). It can also be observed in neonates with trisomy 21, congenital hypothyroidism, or foetal warfarin exposition. Of importance, this feature is transient and disappears over time



Fig. 16.18 Normal vertebral height (left) versus platyspondyly (right). This child with platyspondyly suffers from a skeletal dysplasia (Type 2 collagen disease group)

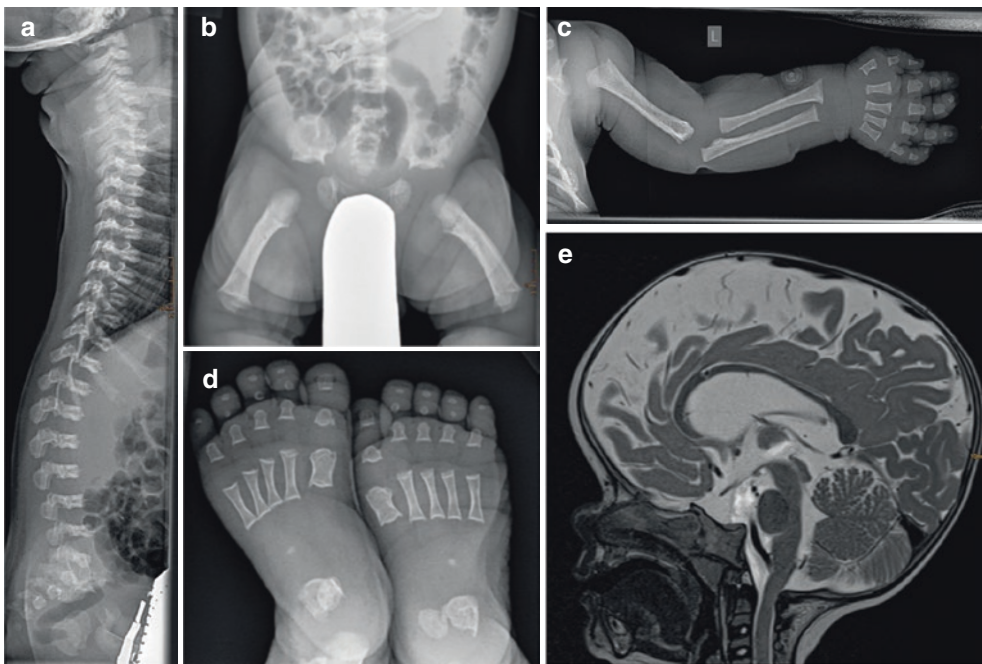


Fig. 16.19 Achondroplasia: a skeletal dysplasia from the FGFR3 chondrodysplasia group (Adapted from Patsch JM, Mehany SN. Wien Med Wochenschr 2021—with permission). **(a)** Platyspondyly with anterior beaking, flaring of anterior ribs. Note the increased height of intervertebral spaces. **(b)** Round iliac wings, horizontal acetabular roofs with trident

shape. Small sciatic notch. **(c)** Trident hand, mild rhizomelia. **(d)** Feet with short toes, especially short big toes. Short metatarsals. **(e)** MRI of the brain and the craniocervical junction in a child with achondroplasia. Sagittal T2-TSE image shows (relative) macrocephaly with frontal bossing, midface hypoplasia, and flat nasal bridge. Narrowing of foramen magnum

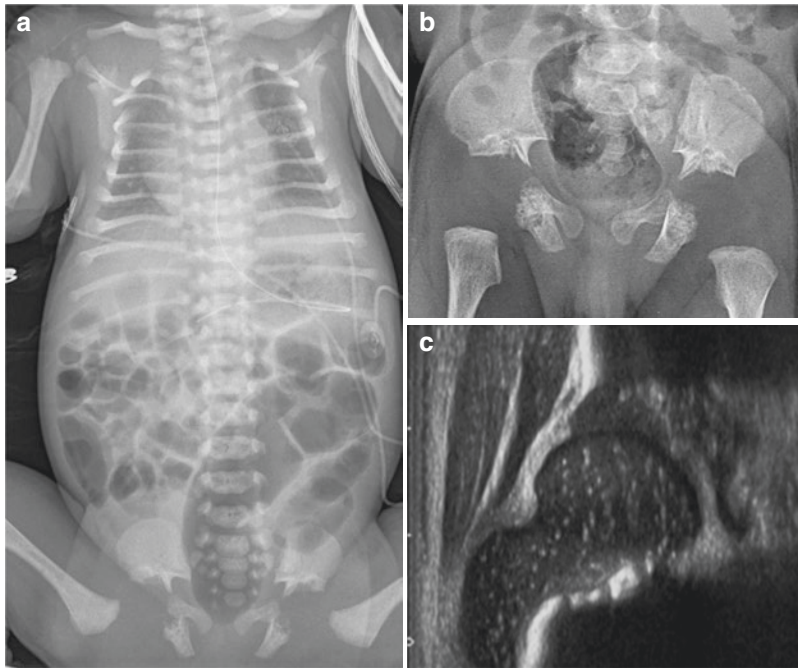


Fig. 16.20 Jeune syndrome (= asphyxiating thoracic dysplasia): A ciliopathy with major skeletal involvement. **(a)** Hypoplastic thorax with short ribs with anterior end flaring. Please note that thoracic hypoplasia can be easily missed on chest radiographs. **(b)** Pelvic radiograph demonstrating broad iliac wings, and a horizontal acetabulum (= small

acetabular angle) with trident appearance (“medial spike”). **(c)** Neonatal hip ultrasound underlines abnormal morphology (same child as in **a**, **b**). Structured hip assessment (= screening to rule out hip dysplasia, e.g. according to the Graf method) is impossible due to the absence of the required anatomical landmarks of the ilium/acetabulum



Fig. 16.21 Achondroplasia: Pelvis and femur. Horizontal acetabulum (= small acetabular angle), small sciatic notch, and medial spike (“trident acetabulum”). Iliac wings are

round and lack normal flaring. Characteristic oval “radiolucent” area at proximal femoral metaphysis/diaphysis (due to metaphyseal widening and radiographic projection effect)

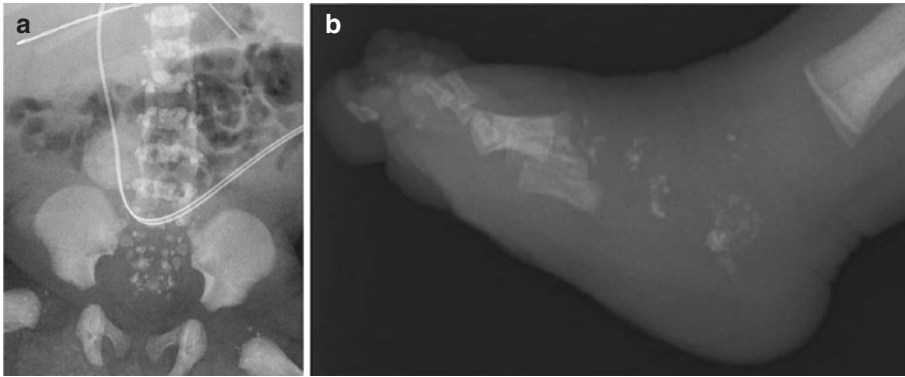


Fig. 16.22 Stippling of epiphyses and cartilaginous anlagen (e.g. chondrodysplasia punctata). (a) Radiograph demonstrates stippled epiphyses at both proximal femurs

and spine (including sacrum). Note umbilical venous catheter (partially depicted). (b) Lateral foot radiograph shows stippling at the midfoot and hindfoot

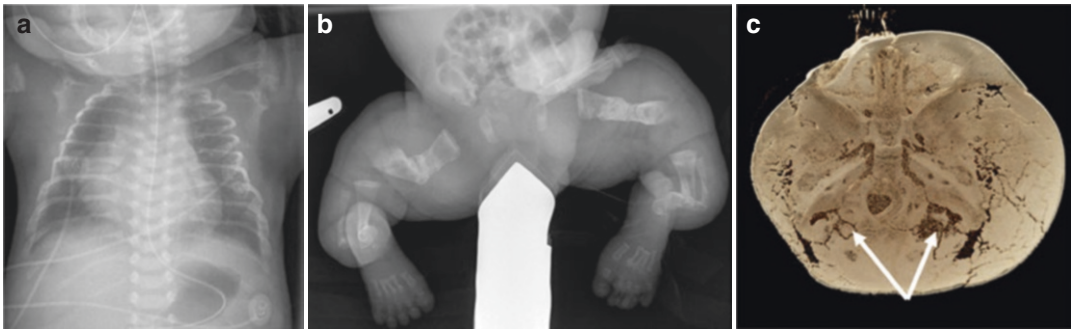


Fig. 16.23 Osteogenesis imperfecta: A skeletal dysplasia with severely decreased bone density (Figure adapted from Patsch JM, Mehany SN. Wien Med Wochenschr 2021—with permission). (a) Thoracic hypoplasia, thin ribs. (b) Congenital bowing and angulation deformity of

long bones (due to intrauterine fractures). Reduced by ossification pubic and ischial bones. (c) 3D-view on skull base and posterior fossa (by computed tomography). Arrows show Wormian (= intra-sutural) bones



Fig. 16.24 Concertina-like femur. Severe deformity of long bones due to multiple intrauterine fractures in osteogenesis imperfecta (type 3). Femoral diaphysis is “pushed-together” resembling the musical instrument (concertina). Also note: large right-sided inguinal hernia

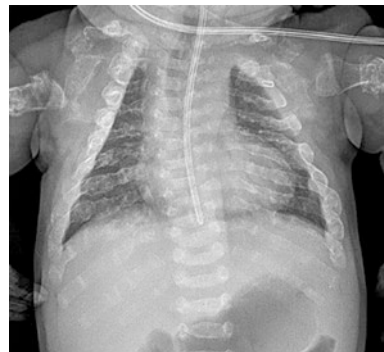


Fig. 16.25 Beaded ribs in osteogenesis imperfecta. Multiple congenital fractures and callus formation lead to beaded appearance of ribs

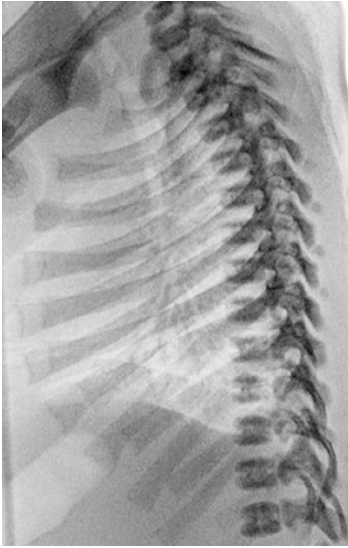


Fig. 16.26 Increased anterior end flaring/cupping of ribs. Lateral view. Please note that a certain degree of flaring is physiologic

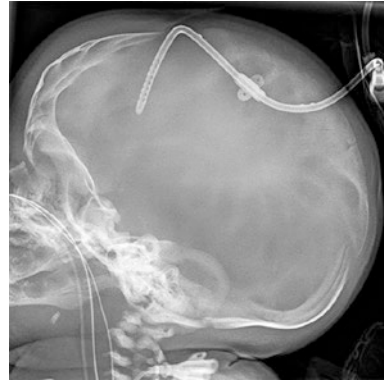


Fig. 16.28 Macrocephaly in a boy with meningocele (Chiari Type 2) and hydrocephalus. Early postnatal shunting was required. Skull has partial ossification defects and copper-beaten appearance

Fig. 16.27 Clover leaf skull. Premature closure of all major sutures (coronal, sagittal, and lambdoid) given rise to “trilobar” appearance of the skull in a child with Saethre-Chotzen syndrome



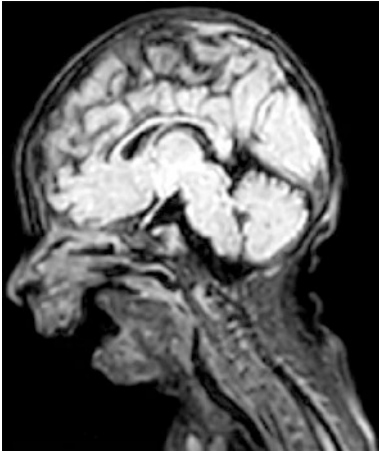


Fig. 16.29 Micrognathia and microcephaly in Treacher-Collins syndrome. MRI (sagittal 3D FLAIR; 3 T)



Fig. 16.32 Hypoplastic clavicles. A 15-month-old boy with cleidocranial dysplasia



Fig. 16.30 Osteopetrosis. Bone mineral density is diffusely increased. Note: This radiograph is not from a neonate, but a 15-year-old-girl



Fig. 16.33 Hooked clavicles (“handle-bar”). Neonate with thanatophoric dysplasia who died at 2 days of age due to cardio-respiratory failure



Fig. 16.31 Slender tubular bones as a distinct feature of certain skeletal dysplasias. (a) A 2-year-old boy with 3M syndrome. (b) An 11-year-old with Cockayne syndrome (a type of progeria)



Fig. 16.34 Triphalangeal thumb

Fig. 16.35 Normal MR-morphology of neonatal bone marrow on T1-weighted images (humerus). Imaging was performed due to a thoracic lymphatic malformation (on the left)

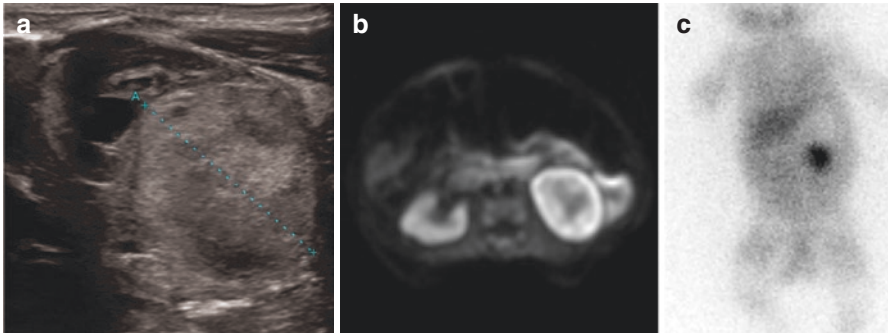
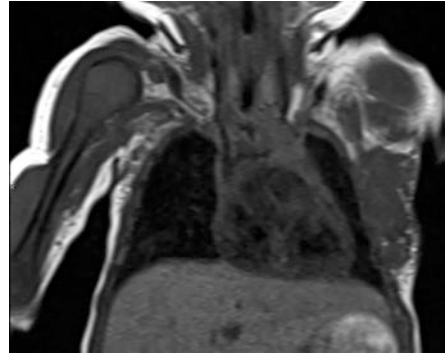


Fig. 16.36 Congenital neuroblastoma. (a) Ultrasound demonstrates echogenic mass with proximity to left kidney. Differential diagnosis included Wilms tumour. (b) Axial MR image (diffusion-weighted image; $b = 800$)

shows restricted diffusion within the left-sided mass, displacing the kidney. (c) Iodine 123-MIBG-Scan confirmed left-sided localised neuroblastoma

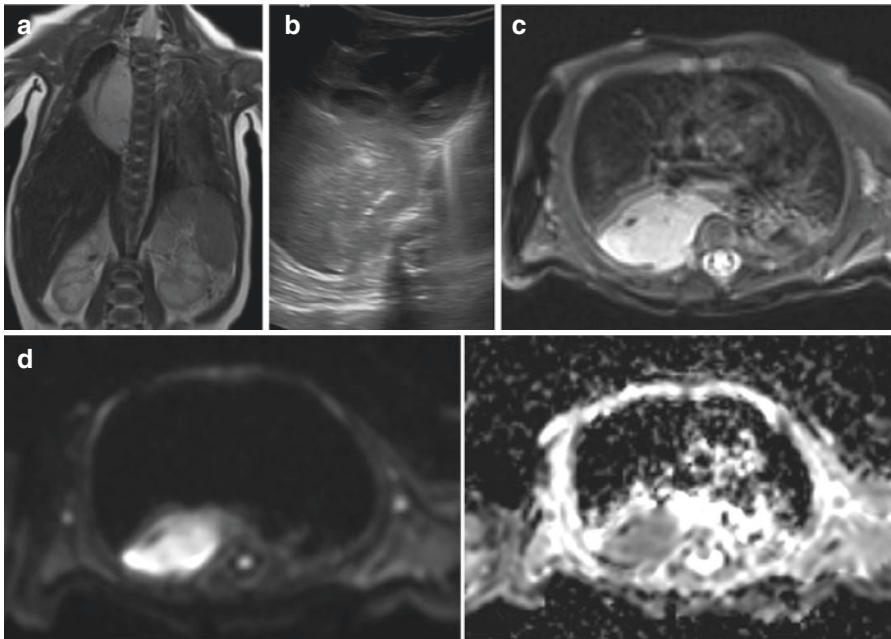


Fig. 16.37 Congenital thoracic neuroblastoma. (a) Coronal T2-weighted MR image demonstrates large right-sided paravertebral mass. (b) Chest ultrasound shows a thoracic mass with internal speckled calcifications. (c) Axial

T2-weighted MR image with fat saturation shows extension into right-sided neuroforamen. (d) Axial diffusion-weighted MR images ($b = 800$) image (left) and ADC-map (right) show restricted diffusion within the tumour

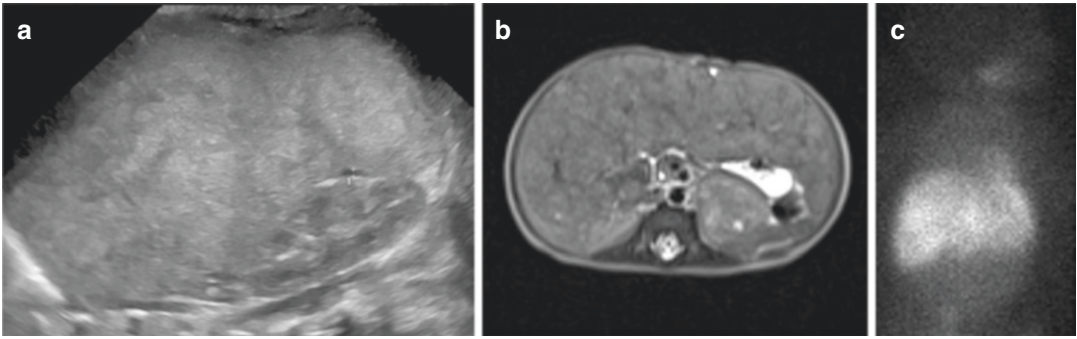


Fig. 16.38 Metastasized congenital neuroblastoma. (a) Ultrasound demonstrates a diffusely enlarged liver with pathologic echogenicity and nodular pattern. (b) Axial T2-TSE MR image confirms diffuse liver metastases

from left-sided congenital neuroblastoma. (c) 123-MIBG scan with diffuse tracer uptake of liver (concordant with a, b)

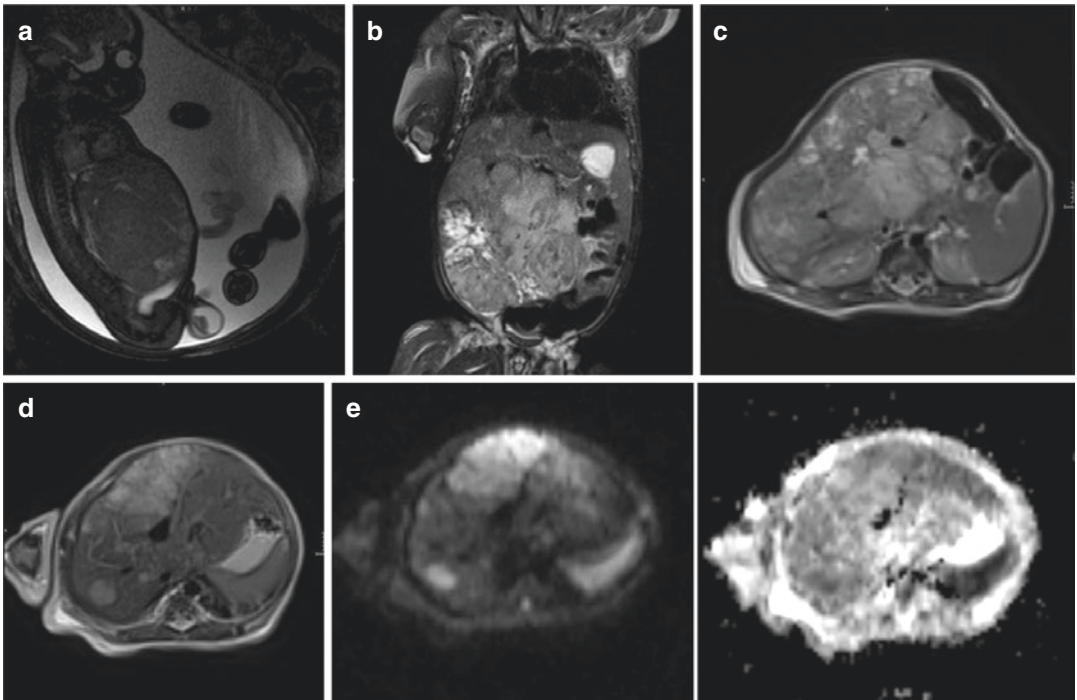


Fig. 16.39 Congenital Hepatoblastoma. (a) Foetal MR (T2-weighted) image shows a large liver mass (Image Courtesy: Prof. Gregor Kasprian, Division of Neuroradiology and Musculoskeletal Radiology, Department of Biomedical Imaging and Image-guided Therapy, Medical University of Vienna). (b) Postnatal coronal MR image (T2-weighted with fat saturation) of

same patient. (c) Postnatal axial MR image (T2-weighted). (d) Postnatal axial MR image (T2-weighted) with multiple satellite lesions. (e) Axial MR images (right: diffusion-weighted with $b = 800$; left: ADC map) show restricted diffusion of tumour and intrahepatic metastases

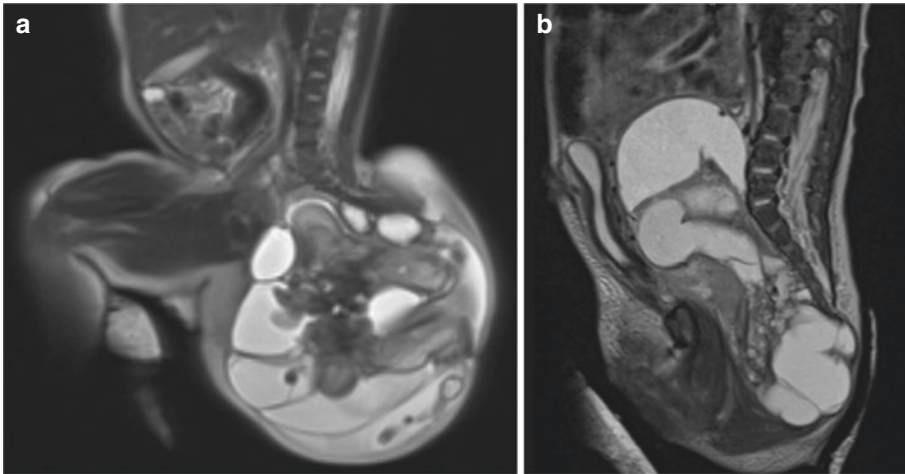


Fig. 16.40 Sacro-coccygeal teratoma. (a) MR image (sagittal T2-weighted) shows large complex-cystic mass with solid components. There is no intra-abdominal extension of the tumour. (b) MR image (sagittal T2-weighted) of another neonate with sacro-coccygeal teratoma and wide intra-abdominal extension

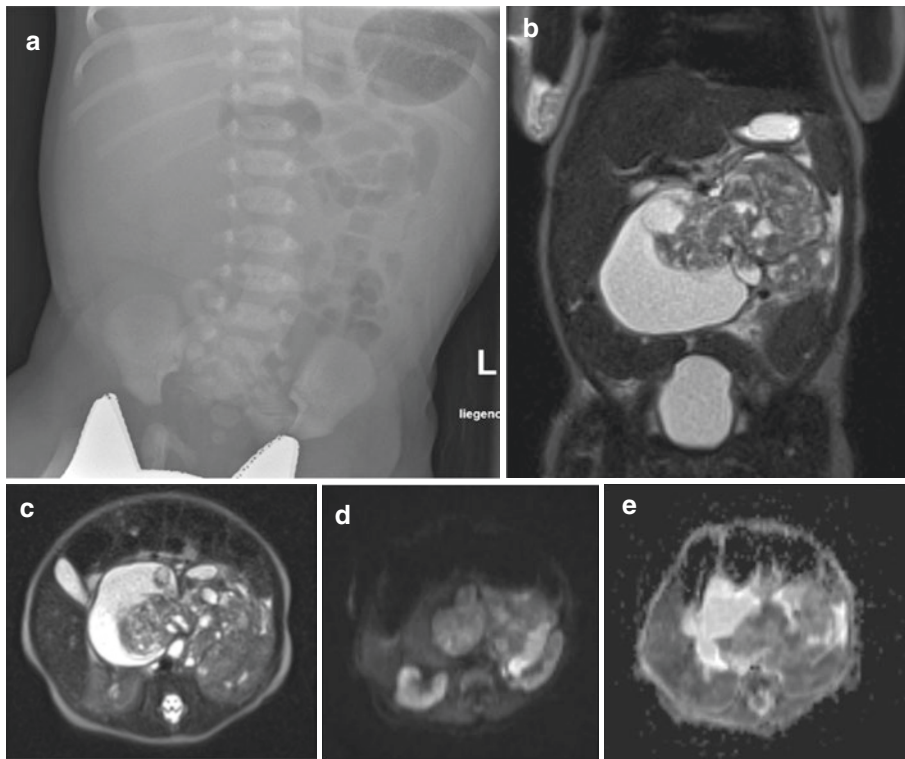


Fig. 16.41 Retroperitoneal teratoma. (a) Abdominal radiograph shows large mass displacing bowel loops. (b) Coronal MR image (T2-weighted) shows large complex-cystic mass with solid components. (c) Axial MR image (T2-weighted) shows retroperitoneal location of the tumour. (d) Axial diffusion-weighted MR image (e) with ADC-map. Histology confirmed an immature teratoma

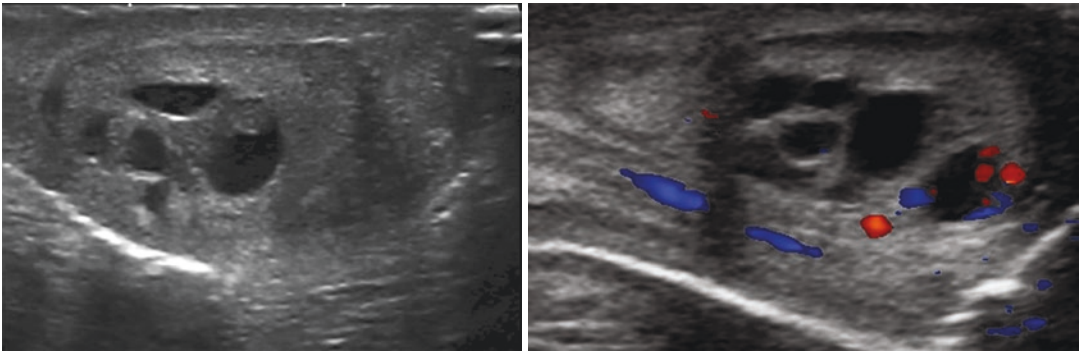


Fig. 16.42 Juvenile granulosa cell tumour presenting as congenital scrotal mass. Ultrasound confirmed a multi-cystic mass

Fig. 16.43 Congenital/infantile fibrosarcoma in a patient with extensive myolipofibromatosis of right lower extremity. **(a)** Radiograph shows large soft tissue mass with osseous destruction of the fibula and partial involvement of the tibia. **(b)** Sagittal MR image (T2-weighted) shows intralesional haemorrhage and tumour vessels (flow voids)

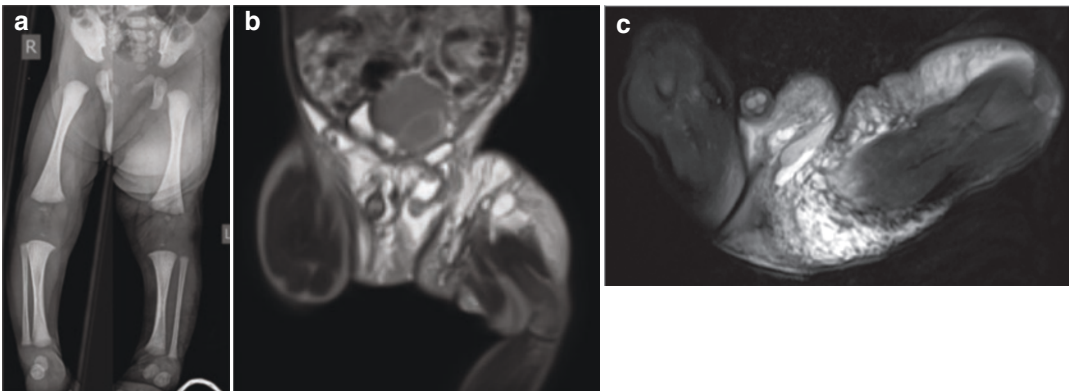
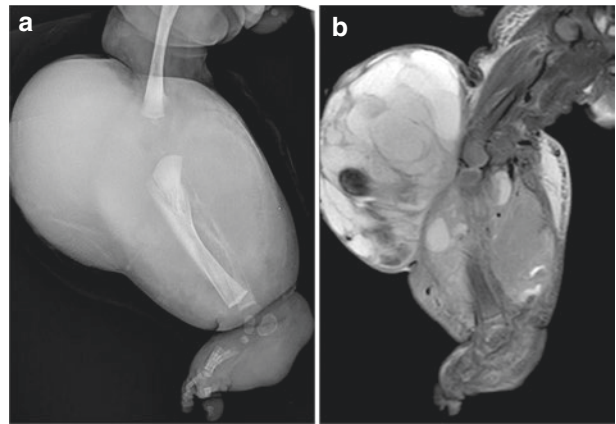


Fig. 16.44 Large lymphatic malformation involving pelvis and left lower extremity. **(a)** Radiograph shows normal skeletal features and left-sided soft tissue mass. **(b)** Coronal MR image (T2-weighted) demonstrates anatomic

location and multi-cystic character of the malformation. Assessment of cyst size is relevant for treatment planning. **(c)** Axial MR image (T2-weighted with fat saturation) of same patient as in **a, b**

16.4 Neonatal Oncology

16.4.1 Clinical Key Concepts: Made Easy for Radiologists

There is a wide spectrum of benign and malignant neonatal tumours, and some have unique presentations and behaviour in this age group.

For example, stage IVS neuroblastoma has a good prognosis in older children, but may be fatal in newborns and therefore constitutes oncological emergency. Other tumours are less aggressive such as neuroblastoma grade I or the “semi-malignant” mesoblastic nephroma and should not be over-treated. Other neonatal oncologic conditions are brain tumours (often supratentorial, e.g. teratoma, astrocytoma, primitive neuroectodermal tumours, and choroid plexus tumour), retinoblastoma, rhabdomyo(-sarco-)ma, teratoma, arterio-venous tumours, or malformations (such as “haemangioma” or “lymphangioma”) and, as a systemic condition, neonatal leukaemia. Even liver tumours (hamartoma, haemangioendothelioma, embryonal sarcoma, hepatoblastoma) or neonatal Wilms tumours or liver metastasis (e.g. from neuroblastoma or other, sometimes rare entities such as endodermal sinus tumour and choriocarcinoma) exist. Not to forget about more common lesions such as inflammatory pseudo-tumours, some tumour mimics such as an intraabdominal sequestration, or congenital haemangioma and other masses (e.g. cardiac angiomyolipoma ...) which may in the individual case pose a challenge for initial differential diagnosis.

Congenital tumours are now increasingly detected by prenatal screening—with new opportunities in understanding their (patho-)physiology, but also new challenges in management and treatment. Particularly, the latter requires in-depth knowledge of the neonatal biology (i.e. how the immature organism can handle drugs with its increased potential for toxicity) and, last but not least, consideration of the impact of treatment on organ function and growth with respective long-term morbidity from chemotherapy and radiation therapy.

For diagnosis, imaging and particularly ultrasonography (US) play a key role, especially as tumour markers such as are often unspecific and physiologically elevated in newborns (e.g. NSE, AFP ...). Characterisation as well as staging is then usually performed by MRI, although US has a larger potential in newborns than in older children, and contrast-enhanced US may help with tumour characterisation (although off-label, which nevertheless applies to most drugs for treating these infants). Imaging is indispensable not only for initial diagnosis and work-up but also for monitoring of treatment effects and in the assessment of complications.

16.4.2 Normal and Abnormal Neonatal Bone Marrow: Imaging Appearance

In neonates, red bone marrow predominates in all parts of the skeleton. The knowledge of age-specific bone marrow properties is important for the correct interpretation of normal findings and suspected focal or disseminated disease.

Acknowledgement I would like to thank Lukas Schmözl (for research assistance) and Valentin Patsch (for figure design and creation).

Thanks to my family for giving me the time to write both Chaps. 14 and 16 of this book.

Further Reading

- Adam A, Dixon A, Gillard J, Schaefer-Prokop C, Grainger & Allison's diagnostic radiology. 7th ed. Amsterdam: Elsevier; 2020.
- Al-Mudares F, Fernandes CJ. “Coat Hanger” appearance of the ribs. *N Engl J Med.* 2020;382:1257.
- Birkemeier KL. Imaging of solid congenital abdominal masses: a review of the literature and practical approach to image interpretation. *Pediatr Radiol.* 2020;50(13):1907–20.
- Daldrup-Link HE, Gooding CA, editors. *Essentials of pediatric radiology – a multimodality approach.* Cambridge: Cambridge University Press; 2010.
- Ferreira CR, Rahman S, Keller M, Zschocke J, ICIMD Advisory Group. An international classification of

- inherited metabolic disorders (ICIMD). *J Inherit Metab Dis.* 2021;44(1):164–77.
- Hall CM, Offiah AC, Forzano F, Lituania M, Fink M, Krakow D. Fetal and perinatal skeletal dysplasias: an atlas of multimodality imaging. London: Radcliffe Publishing; 2012.
- Handa A, Nishimura G, Zhan MX, Bennett DL, El-Khoury GY. A primer on skeletal dysplasias. *Jpn J Radiol.* 2021; <https://doi.org/10.1007/s11604-021-01206-5>.
- Kiefer FW, Klebermass-Schrehof K, Steiner M, Worda C, Kasprian G, Diana T, Kahaly GJ, Gessl A. Fetal/neonatal thyrotoxicosis in a newborn from a hypothyroid woman with Hashimoto thyroiditis. *J Clin Endocrinol Metab.* 2017;102(1):6–9.
- Lachmann RS, editor. Taybi and Lachmann's radiology of syndromes, metabolic disorders and skeletal dysplasias. 5th ed. Philadelphia, PA: Mosby; 2006.
- Loeber JG, Platis D, Zetterström RH, Almashanu S, Boemer F, Bonham JR, Borde P, Brincat I, Cheillan D, Dekkers E, Dimitrov D, Fingerhut R, Franzson L, Groselj U, Hougaard D, Knapkova M, Kocova M, Kotori V, Kozich V, Kremezna A, Kurkijärvi R, La Marca G, Mikelsaar R, Milenkovic T, Mitkin V, Moldovanu F, Ceglarek U, O'Grady L, Oltarzewski M, Pettersen RD, Ramadza D, Salimbayeva D, Samardzic M, Shamsiddinova M, Songailienė J, Szatmari I, Tabatadze N, Tezel B, Toromanovic A, Tovmasyan I, Usurelu N, Vevere P, Vilarinho L, Vogazianos M, Yahyaoui R, Zeyda M, Schielen PCJI. Neonatal screening in Europe revisited: an ISNS perspective on the current state and developments since 2010. *Int J Neonatal Screen.* 2021;7(1):15.
- Maresh MM, Deming J. The growth of the long bones in 80 infants. Roentgenograms versus anthropometry. *Child Dev.* 1939;10(2):91–106. www.jstor.org/stable/1125472
- Mehany SN, Patsch JM. Imaging of pediatric bone and growth disorders: of diagnostic workhorses and new horizons. *Wien Med Wochenschr.* 2021;171(5–6):102–10.
- Mikołajczak A, Borszewska-Kornacka MK, Bokiniec R. Sonographic reference ranges for the thyroid gland in euthyroid term newborns. *Am J Perinatol.* 2015;32(13):1257–62.
- Mortier GR, Cohn DH, Cormier-Daire V, Hall C, Krakow D, Mundlos S, Nishimura G, Robertson S, Sangiorgi L, Savarirayan R, Sillence D, Superti-Furga A, Unger S, Warman ML. Nosology and classification of genetic skeletal disorders: 2019 revision. *Am J Med Genet A.* 2019;179(12):2393–419.
- Ogilvy-Stuart AL. Neonatal thyroid disorders. *Arch Dis Child Fetal Neonatal Ed.* 2002;87:F165–71.
- Ponrartana S, Aggabao PC, Dharmavaram NL, Fisher CL, Friedlich P, Devaskar SU, Gilsanz V. Sexual dimorphism in newborn vertebrae and its potential implications. *J Pediatr.* 2015;167(2):416–21.
- Prayer D, editor. Fetal MRI. New York: Springer; 2011.
- Raimann A, Haberler C, Patsch J, Ertl DA, Sadeghi K, Freilinger M, Lang S, Schmoock M, Plecko B, Haeusler G. Lethal encephalopathy in an infant with hypophosphatasia despite enzyme-replacement therapy. *Horm Res Paediatr.* 2021;94(9–10):390–8.
- Spranger JW, Brill PW, Hall C, Nishimura G, Superti-Furga A, Unger S. Bone dysplasias – an atlas of genetic disorders of skeletal development. 4th ed. Oxford: Oxford University Press; 2018.
- Tsai A, Stamoulis C, Barber I, Kleinman PK. Infant lower extremity long bone growth rates: comparison of contemporary with early 20th century data using mixed effect models. *Am J Hum Biol.* 2017;29(1).
- Walleczek NK, Förster K, Seyr M, Kadrnoska N, Kolar J, Wasinger-Brandweiner V, Vodopiutz J. Rare skeletal disorders: a multidisciplinary postnatal approach to diagnosis and management. *Wien Med Wochenschr.* 2021;171(5–6):94–101.
- Watson TA, Arthurs OJ, Muthialu N, Calder AD. Multi-detector thoracic CT findings in cerebro-costo-mandibular syndrome: rib gaps and failure of costo-vertebral separation. *Skelet Radiol.* 2014;43(2):263–6.



Imaging After Birth Trauma and in Suspected Non-accidental or Inflicted Injury

17

Sebastian Tschauner and Erich Sorantin

17.1 Introduction

Giving birth can be traumatic for both the mother and the newborn. The two main sources of birth injuries for the yet unborn are related to either biomechanical or hypoxic processes, which might show overlaps to a certain degree. This is not generally different between spontaneous and assisted deliveries. However, assisted deliveries typically bear a higher risk for mechanical damage. Infants delivered vaginally suffer from different types of birth-related injuries compared to caesarean section—the number of major birth traumata decrease when more caesarean sections were performed.

The main differential diagnosis to birth trauma is accidental and non-accidental trauma. The most important factor differentiating between the causes of trauma is anamnesis, history, and imaging. The radiologist might play a central role in helping to reveal the correct cause of an injury in a neonate. The patterns of injury might favour the either or the other option. The presence of multiloculate or different-aged injuries might raise the suspicion for child abuse, and must be communicated to the paediatricians. Note that even in neonates, other rare traumata occur such as involvement in traffic accident or injuries from

falling out of the bed or during resuscitation, e.g. after a prolonged apnoea.

The chapter tries to summarise the respective injuries and their imaging appearance, and lists the imaging modalities used as well as suggested imaging algorithms for typical scenarios.

17.2 Clinical Indications for Imaging Birth Trauma, Accidents, and Suspected Inflicted Trauma

Imaging is indicated in every case of suspected birth-related, accidental or non-accidental trauma in the neonatal period. Its main goal should be the detection of a treatable pathology. Radiology is often confronted with further types on indications like medico-legal questions or the documentation of the natural course of a disease. Especially in these cases, radiology should avoid inflicting additional damage by radiation or invasiveness. The radiologists, together with the clinical team, have to choose the proper imaging method from the entire arsenal of available modalities. The proper method depends on the kind of clinical symptoms and the kind of trauma and history, including the type of suspected or evident trauma or presented injury patterns.

The detection of child abuse has always been a challenge for all professional groups involved in childcare. Radiology plays a central role, as it is able to reveal typical injury patterns and

S. Tschauner (✉) · E. Sorantin
Division of Pediatric Radiology, Department of
Radiology, Medical University of Graz, Graz, Austria
e-mail: Sebastian.tschauner@medunigraz.at

incidental findings, which might potentially prevent fatal consequences for the child. One major mechanism of injury results from an adult holding the neonatal chest and shaking, known as “shaken baby syndrome”. In this context, a radiologist can often diagnose paravertebral rib fractures, and intracranial or retinal haemorrhage. Further injuries can occur when the baby is thrown away after the shaking event. Moreover, injuries can result from physical torture like beating, or by pulling or shaking the extremities, leading to atypical extremity fractures. It is obvious to anyone involved in paediatric care that injuries are common during childhood and adolescence, and the distinction between accidental and non-accidental causes is regularly limited. Therefore, it is essential to know potential imaging hints in terms of more specific trauma locations and patterns.

17.2.1 Injury Patterns

17.2.1.1 Bruises

Intra- and subcutaneous haematomas are routinely attributable to birth trauma in the first days of life. They are also indicative for previous episodes of violence after the perinatal period, and are seen in the majority of children affected by abusive trauma. Haematomas in newborns in any location require proper explanation. As newborns are not yet learning to walk, typical predilection sites like the shins are not existing yet, and all haematomas not related to birth trauma are suspicious for inflicted injuries. The shape of the bruises can also give clues about the type of force acting (handprint, strangle mark, rope or stick imprints, bite marks).

17.2.1.2 Fractures

Fractures of a newborn are known to occur during labour. The other two causes of neonatal fractures are accidents like falls from the changing table, and non-accidental inflicted injuries in cases of child abuse. Clinical history, fracture patterns, and fracture healing, as well as other injuries might help in discriminating between the possible causes.

Metaphyseal “corner fractures” or “chip fractures” are suggested more specific for child abuse, so are rib and skull fractures. Other fractures are not so specific for non-accidental trauma and need further workup.

Kemp et al. analysed the different kinds of fractures in children under the age of 18 months. They found indicators for child abuse in terms that


- Multiple fractures are more likely caused by abuse.
- Rib fractures are in 70% caused by abuse.
- A child with femoral fracture is abused 1 in 3 to 4 times.
- A child with humerus fracture is abused 1 in 2 times.
- Mid-shaft humerus fractures are more common due to abuse.
- Non-accidental trauma is more common in a child not yet walking.
- Skull fractures are caused by abuse in 1 of 3 cases.
- Skull fractures are present in child abuse and accidents.

However, the mentioned patterns are not valid for the neonatal period, especially not in the days after birth. Overall, the interpretability is more limited in newborns.


Fracture Healing

In childhood, fractures are only caused by excessive external force to the skeleton. Exceptions are osteochondrodysplasias and metabolic disorders that weaken the paediatric bones. In healthy individuals, fracture healing follows an age-dependent distinctive pattern. Neonatal bone healing is known to be more rapid than in later life.

Despite the availability of some scientific evidence, the literature lacks large-scale studies on fractures and their normal healing. The individual studies show significant discrepancies in terms of methodology, sample demographics, terminology, and fracture healing times. Thus, estimations of fracture age should be done with great caution.

 Imaging can raise suspicion of child abuse when there are fractures in multiple locations, especially involving the ribs, and fractures of different age; fracture healing is difficult to judge in the newborn and thus estimation of timing of an insult is difficult.

rhages (PPV 71%), and rib fractures (PPV 73%) were the most significant indicators for AHT.

 The “shaken baby syndrome” is a potentially lethal form of child abuse due to intracranial injuries. It is extremely rare in newborns, but more common in infancy.

17.2.1.3 Shaken Baby Syndrome

The so-called shaken baby syndrome occurs with an annual incidence of about 25 per 100,000 newborns and infants. It should be noted that the incidence in newborns might be substantially lower. Infants in the so-called physiological “main crying age” between 1 and 4 months are particularly affected.

As injury mechanism, the adult grabs the baby by the upper arms or the chest and shakes violently back and forth, causing an acceleration–deceleration trauma. Rotational and shear forces cause the tearing of the bridging veins between the white meninges and the brain surface with the result of intracranial haemorrhage. Nerve connections at the transition between white and grey brain matter could be sheared off leading to a diffuse axonal trauma that causes permanent damage to the axons of the brain. This damage, combined with impaired cerebral blood flow and oxygen supply, also results in diffuse brain oedema. The development of retinal haemorrhages and vitreous haemorrhages can also be attributed to the effects of shear and rotational forces within the eyeball and an increase in intracranial pressure.

17.2.1.4 Intracranial Injuries

The central nervous system is commonly involved in cases of non-accidental trauma. The rate of abusive head trauma below the age of 1 year is approximately 1 in 4000 infants. Abusive head trauma has been described to lead to the victim dying in one out of four cases. In patients not dying, permanent disabilities can often occur. Data from the literature indicate that apnoea (positive predictors (PPV) 93%), retinal haemor-


17.3 Imaging Methods

17.3.1 Ultrasound (US)

Ultrasound (US) will be the initial method of choice in the vast majority of cases, especially if the head or trunk is injured. Different types of probes, like sector-, curved-, or linear-transducers enable the skilled examiner to investigate nearly all body regions of a neonate. High-resolution probes enable also high-detail scans of the more superficially located areas of interest, and offer a convincing documentation of relevant findings.

Ultrasound is suited to diagnose conditions like extra- or intracranial haemorrhage, cerebral hypoxia, neonatal chest pathology including effusions or pneumothorax, spinal cord and plexus trauma, abdominal injuries, or extremity fractures.

It should not go unnoted that US is a versatile modality that needs extensive and ongoing training to allow for high sensitivity and specificity. In the context of birth trauma, the most common indication for US is brain scanning. The high number of requested studies in many hospitals give trainees the possibility to quickly gain knowledge. Other indications, like musculoskeletal or neuronal trauma, are far less commonly encountered in diagnostic US in newborns and need a more experienced examiner, possibly supplemented by MRI or radiographs.

 Neonates with suspected (non-accidental) trauma should receive initial imaging by US, because it usually offers high sensitivity and can be performed bedside, especially in the neonatal period.

17.3.2 Radiography

Extremity injuries indicate the acquisition of radiographs. The neonatal period differs only regarding the smaller body part size, in part also because of the non-ossified parts of the skeleton restricting radiographic potential. Otherwise, radiological technologists also need to acquire images in two orthogonally oriented planes as standard in older infants.

Whole body radiographs in terms of so-called babygram are not recommended, but a skeletal survey of the entire body can be useful when searching fractures. This skeletal survey is a systematic series of radiographs to cover the whole skeleton. A standard skeletal scan comprises bilateral anteroposterior (AP) and posteroanterior (PA) projections of the hands, forearms, humerus, foot, leg, femur, pelvis, spine, and skull. Bilateral AP/PA images of the wrist, elbow, shoulder, ankle, knee, hip, and sacroiliac joints are included in a joint survey. Additionally performed lateral projections often help to identify lesions. Skeletal surveys are also helpful in cases of diffuse skeletal abnormalities like osteochondrodysplasias, or might reveal other anatomic variations that may occur in babies and children.

17.3.3 Computed Tomography (CT)

CT indications are sparse during the neonatal period, mainly involving life-threatening cerebral and polytrauma situations.

Head CT is the preferred method for assessing significant traumatic brain damage. The main indication for cranial CT are neurological abnormalities and signs of abusive head trauma. CT scans times are in subsecond on modern scanners and often do not need anaesthesia, though some immobilisation or subtle sedation may be helpful. CT helps to demonstrate cerebral acute haemorrhages, mass effects, or skull fractures, and acts as a decision-making tool in emergency cases of necessary urgent neurosurgical intervention. It is also important to perform state-of-the-art post-processing in terms of multiplanar

reconstructions, reconstructions with different kernels, and 3D visualisations.

It is debatable whether all children with hints of abuse but without neurological deficit should undergo a routine head CT. Some authors recommend cranial CT scans for any child under the age of 1 year in all cases of suspected abuse. The American College of Radiology recommends that children with a higher risk (“...e.g., rib fractures, multiple fractures, facial injuries, or age <6 mo...”) should have a head CT, even if they have no neurological symptoms. Substantial amounts of radiation exposure and impaired sensitivity for smaller parenchymal lesions are the drawbacks of CT, thus often an initial US or an MRI is used if available in the acute setting.

17.3.4 Magnetic Resonance Imaging (MRI)

MRI is mainly indicated for cerebral imaging, being able to visualise any kind of cerebral injury and intra- or extracranial haemorrhage. MRI is more sensitive than CT in detecting even smaller or older cerebral haemorrhages and other parenchymal damage—as in patients with abnormalities on first CT scans, MRI showed additional findings including subdural haemorrhage, subarachnoid haemorrhage, ischaemic injuries, ischaemia, and shear injuries in a relevant number of cases. But MRI is routinely performed only a few days after first presentation, when the patient is more stable.

A typical MRI protocol comprises T1- and T2-weighted sequences, as well as FLAIR, gradient echo or other susceptibility weighted sequences, and diffusion weighted images (DWI). Advanced MRI sequences include spectroscopy or native perfusion like arterial spin labelling (ASL), which may add prognostic information.

The “feed-and-wrap” technique allows scanning the paediatric head while the patient is sleeping. Preparation for “feed-and-wrap” scanning includes (breast) feeding and comforting as well as some sort of immobilisation, as well as

close timing in coordination with the MRI personnel to avoid motion artefacts.

Real-time ultrafast cranial MRI might establish as a viable alternative to “feed and wrap” scanning in neonates small children, then becoming also a method for the peracute event.

17.3.5 Nuclear Medicine

Nuclear medicine in terms of a body bone scan is rarely performed in neonates in the context of birth injuries, accidental or suspected non-accidental trauma—it is more often used in older children as a general screening tool to then only take focused radiographs of suspicious regions.



US is often the initial imaging in trauma, radiographs are acquired for suspected skeletal injuries. CT is associated with a substantial amount of ionising radiation, but is still the method of choice in the acute cranial injury. MRI has become the mainstay of neuroimaging in neonates with inflicted or birth injuries.

17.4 Cranial Injuries

17.4.1 Superficial Bruising, Grazes, and Lacerations

Superficial cranial injuries of any kind, including facial petechial bleedings, usually do not require radiological imaging in the initial setting or in follow-up.

17.4.2 Skull Fractures

The neonatal skull is more flexible to resist the occurrence of fractures during labour. A certain amount of overlap in the parietal bones may be palpable after birth, although imaging is only

required in rare cases. Occasionally, dystocic birth and use of extraction devices can result in skull fractures. They can also happen because of blunt trauma after birth, especially in the context of falls. Neonatal skull fractures are classified into linear fractures, depression fractures, or osteodiastasis. Linear skull fractures are most commonly found in the parietal area and are most commonly caused by head compression during delivery. When there is a depression of the skull, these fractures are often referred to as “ping pong skull fractures”. A small percentage of skull fractures are caused by birth, while the majority are related to accidents.

Simple fractures of the roof of the skull, usually in the parietal region, happen from minor incidents such as falling from a bed, sofa, or changing table. A lower fall does usually not generate extensive, multi-fragmentary, or branching fractures. This is also true for occipital depression fractures and severe brain injuries. Serious violence should be suspected in these cases, and might be due to abusive trauma.

Leptomeningeal cysts, also known as expanding or “growing” fractures, are a rare occurrence in infants, in which fractures enlarge over time due to cerebrospinal fluid pulsations from leptomeninges entrapped in the skull defect.

Radiography is not a reliable method to diagnose skull fractures, where especially depressed ones might stay occult. It also needs to be considered that skull radiographs are rarely acquired. Therefore, the real incidence of perinatal skull fractures remains unknown.

Ultrasound is widely available and well suited to detect all kinds of skull fractures. It needs training in that specific task to enable proper differentiation between sutures, normal-variants of accessory sutures, and fractures. Additional ultrasound windows, like temporal or nuchal, enable to see all parts of the skull in neonates. Imaging features of such a skull fracture on US are cortical fissures, gaps or steps that can cross normal sutures (Fig. 17.1). US can also depict accompanying injuries like swelling, oedema, or haematomas.

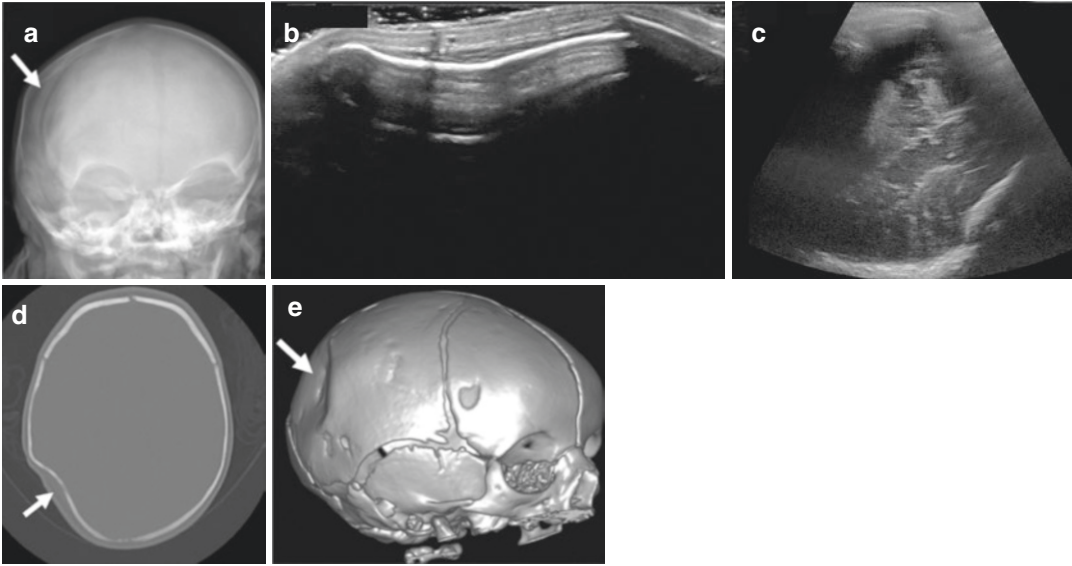


Fig. 17.1 Ping-pong type skull fracture. An 18-day-old female newborn after fall on the head. (a) Initially, a skull radiograph was requested. The AP projection shows a slight translucency in the right parietal area—such a subtle radiographic abnormality can easily be missed. (b) US was performed to assess the suspected fracture. It demonstrates an impression of the calvaria in the parietal region on the right side. The intracranial conditions cannot be seen through the calvaria from this position. (c) US from

the left nuchal sonographic window is able to depict the fracture, including the cerebral structures. No intracranial bleeding was obvious. (d) Because of suspected neurological deficits, a CT was performed on the next day. There were no intracranial haemorrhages, but the images depict the already-known parietal skull fracture. (e) The 3D-rendering of the CT clearly and more conspicuously visualises the fracture

In the acute setting, CT and MRI are more commonly performed today, both being able to detect the relevant injuries with high accuracy. While there has been progress regarding “black bone” MRI sequences, CT can be still considered superior in the depiction of bones and fracture fragments, but is only indicated in cases with neurologic symptoms.

An important differential diagnosis to skull fractures is physiologically open or accessory sutures. A commonly misinterpreted structure is the metopic suture that is normally present in newborns; it separates the halves of the frontal bones and extends into the large fontanel (Fig. 17.2).



Skull fractures occur in neonates, but can unspecifically occur in situations of birth trauma, accidental and non-accidental injury.

17.4.3 Extracranial Haemorrhage

Imaging might be indicated based on the clinical history and presentation, but is overall rarely needed for isolated extracranial haematomas. The common types of extra- and intracranial bleedings are given in Fig. 17.3.

17.4.3.1 Caput Succedaneum

Caput succedaneum represents subcutaneous serous and haemorrhagic fluid collections, externally to the galea aponeurosis outside the periosteum (Fig. 17.4). The extension classically exceeds sutures and the midline. It is a kind of classic birth trauma. All modalities are able to depict caput succedaneum, while it is commonly visualised as secondary finding, especially on ultrasound or MRI studies done for other indications. Most cases lack clinical relevance and resolve shortly after birth.

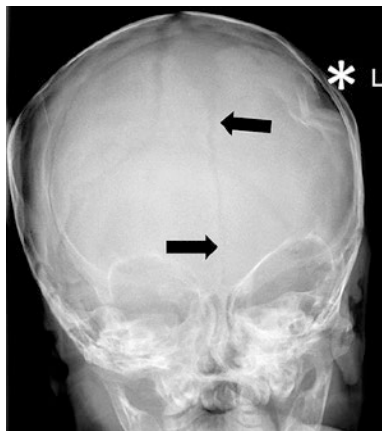


Fig. 17.2 Metopic suture in a newborn. A 3-week-old girl after fall from the swaddling table. There is a frontoparietal skull fracture on the left side (asterisk) in the AP skull radiograph. Sometimes, additional sutures are mistaken for fractures. One of these sutures is the metopic suture that arises from the fontanel anteriorly and separates the frontal bones (black arrows). It is typically open in the neonatal period

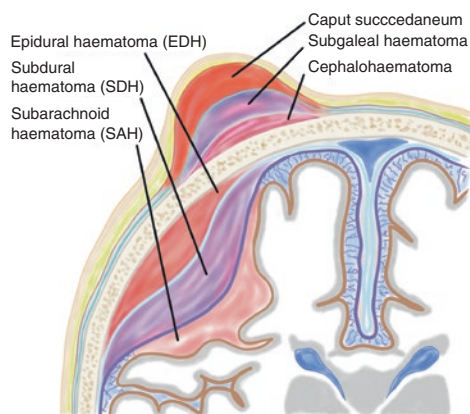


Fig. 17.3 Types of extracranial and intracranial haematomas. Schematic display of the different types of extra- and intracranial haematomas. The extracranial haemorrhages include caput succedaneum, subgaleal haematoma, and cephalohaematoma. The intracranial bleedings can be in an epidural, subdural, and subarachnoid location, as well as intraparenchymatous or intraventricular (not shown in this scheme)

17.4.3.2 Subgaleal Haematoma

Extracranial haematomas located between the periosteum and the galea aponeurosis are considered subgaleal haemorrhages, originating from ruptured emissary veins. An incidence of

1.7–59 per 10,000 live births has been reported. Subgaleal haematomas can possibly be an emergency as haemorrhagic shock may occur. Without strict volume replacement therapy, the outcome might be lethal in some cases. Onset of the haematoma can be as early as 1 h after delivery, but an occurrence up to 4 days post-partum has been described. Potential superinfection is a known complication, as well as calcifications. These types of haematomas cross sutures and can be located anywhere around the skull. They may even extend to the neck. It is often associated with vacuum extraction or use of forceps during labour. Other causes of subgaleal haematoma can be head trauma or even spontaneous.

Imaging should focus on differentiating between other types of extracranial haematoma, abscess, or tumour. Ultrasound is well suited to depict the changes seen in subgaleal haematomas. The haematomas can be of different echogenicity, mainly depending on clotting and onset/duration (Fig. 17.4). Sonopalpation can confirm the liquid nature of the lesion, and rule out a series of other differential diagnoses. It is important to report the size of the haematoma, preferably with estimated volume. Ultrasound can also depict an underlying skull fracture with high accuracy.

17.4.3.3 Cephalohaematoma

A cephalohaematoma is defined as haemorrhage between the external skull surface and the pericranium, often caused by the rupture of vessels between skull bones and periosteum. The extension of the haemorrhage can be severe, possibly leading to anaemia and hypotension in certain cases. It is limited to the cranial sutures. The cephalohaematoma can infect and cause meningitis or osteomyelitis in rare cases. Linear skull fractures are associated with this kind of haematoma only in minority of cases. Over the course of weeks to months, the cephalohaematoma resorbs entirely, leaving no abnormalities on the skull.

Cephalohaematomas appear as crescent-shaped fluid formations adjacent to the external

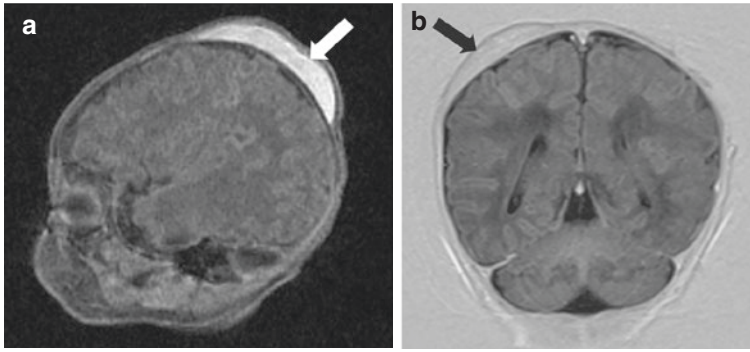


Fig. 17.4 Caput succedaneum in MRI. (a) An 8-day-old newborn with suspected intracranial haemorrhage. MRI demonstrates no intracranial pathologies, but a caput succedaneum in the right parietal location on a

T1-weighted image (white arrow). (b) This T1-weighted inversion recovery MRI image shows the caput succedaneum as a mildly hyperintense extra-cranial swelling (black arrow)

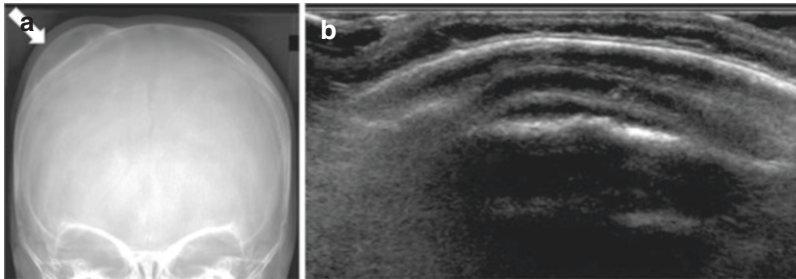


Fig. 17.5 Calcified cephalohaematoma. A 9-month-old boy with a history of a cephalohaematoma after birth. Now there is still a tough swelling of the parietal region. (a) The radiograph in AP projection shows a calcified

haematoma in the right parietal region (arrow). (b) The corresponding US shows a sharply delineated hyper-echoic convex structure with subsequent reverberation artefacts

table of the skull on US, CT, and MRI. The haematoma may vary in echogenicity, density, or signal intensity based on the age and potential complications. Imaging, however, is rarely needed or indicated.

When a cephalohaematoma is not absorbed during the first few weeks of manifestation, it can ossify, potentially growing over time. This kind of complication occurs in about 5% of the cases, and is subdivided into two types with surgical relevance: without and with depression of the inner lamella.

X-rays might show a “double skull sign” (Fig. 17.5). Otherwise, they are not very helpful in diagnosing or classifying calcified cephalohaematomas. CT and MRI are suitable to display the relevant changes and guide the operative management.



Subgaleal extracranial haematomas can cross sutures and can be potentially lethal. US as the imaging modality of choice is able to estimate nature and size of the lesion, and can image underlying skull fractures. Cephalohaematomas might ossify and might show a “double skull sign”. CT or MRI is needed only prior to surgical reconstruction.

17.4.4 Intracranial Haemorrhage

Intracranial haemorrhage can be caused by the forces of labour and delivery and instrument-assisted birth. The types of intracranial haemato-

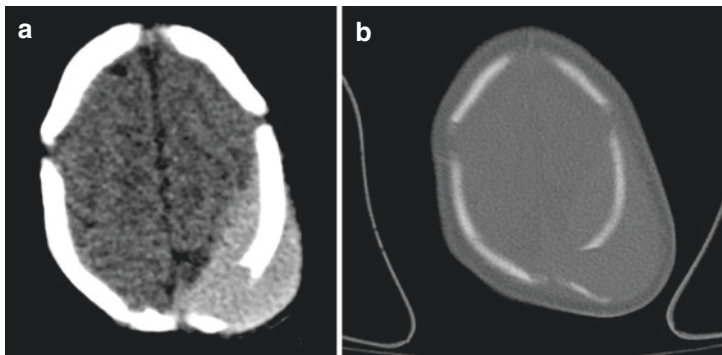


Fig. 17.6 Epidural and cephalohaematoma in a case of NAI. (a) Newborn girl (6 days old) with swelling after trauma to the head. CT in axial orientation demonstrates a combination of epidural haemorrhage and cephalohaema-

toma in the left parieto-occipital region. (b) Axial CT image, bone window in the corresponding section: it shows a dehiscent bone fragment. The injuries were confirmed to be of non-accidental origin

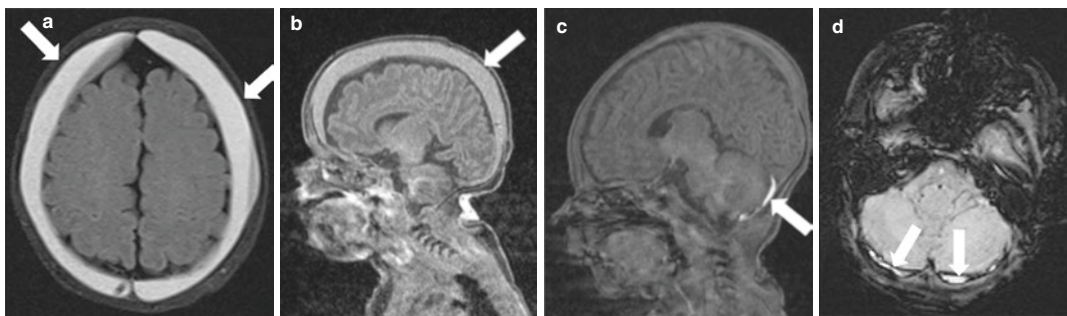


Fig. 17.7 Subdural haematoma MRI. (a) MRI in a 20-day-old patient with subacute bilateral subdural haematomas (axial section, FLAIR sequence, arrows) known since birth. Note that the signal intensity may vary depending on the contents and age of the haematoma. (b) MRI, sagittal section T1-weighted image in the same patient: it shows a mildly hyperintense subdural haemor-

rhages (arrow). (c) MRI, sagittal T1-weighted gradient-echo section. A hyperintense subdural haemorrhage (arrows) in the posterior fossa without mass effect is shown, which can often be seen as an “incidental” finding after birth. (d) The bilateral haemorrhage can also be seen in the axial MRI section of the posterior fossa in an SWI sequence (arrows)

mas are well known to any doctor and do not principally differ from intracranial bleedings seen at other periods of life. A schematic overview of intracranial haematomas is given in Fig. 17.3.

17.4.4.1 Epidural Haemorrhage

Epidural haemorrhage occurs in the physiologically not present space between the internal skull surface and the dura mater. It usually presents with a bi-convex shape and is typically associated with skull fractures (Fig. 17.6). All imaging modalities can be used to image epidural haematomas, with CT and MRI being the most sensitive ones.

17.4.4.2 Subdural Haemorrhage


A subdural haemorrhage (SDH) is an accumulation of blood between the dura and arachnoid. Subdural haemorrhage can distribute freely throughout the cerebral cavity, not bound to cranial sutures, resulting in the usual crescentic form (Fig. 17.7). Subdural bleedings often occur in children suffering from abusive head trauma. Subdural bleeding is seen in up to 90% of AHT autopsies. It is usually a thin blood film covering the cerebral convexities, typically bilaterally. Subdural bleeding commonly spreads into the posterior interhemispheric fissure.

Ultrasound can detect subdural bleedings, and should be used as initial imaging in stable condi-

tions. However, sensitivity and reproducibility are both restricted compared to CT and MRI, which is critical in situations where “hard” (i.e., reliable) medico-legal documentation is required.

CT scans may detect a modest quantity of interhemispheric subdural bleeding that would be overlooked at autopsy. Due to beam hardening artefacts and partial volume effects of the interior table of the skull, CT is less sensitive than autopsy in identifying minor convexity subdural haemorrhages.

MRI should be used in conjunction with CT to identify blood products, tiny regions of ischaemia, and diffuse axonal damage. Conventional MRI may identify damage in brain areas that seem normal, boosting diagnostic certainty and providing extra prognostic information in children with less severe lesions. MRI might also be able to differentiate between subdural hygroma that contain cerebrospinal fluid, and acute or chronic haematoma containing blood products.

 Subdural haematomas are often noted as kind of birth injury, typically located along the tentorium.

17.4.4.3 Subarachnoid Haemorrhage

Most AHT-related autopsies show subarachnoid haemorrhage. However, subarachnoid bleedings are unspecific and can be either caused by accidents, birth trauma, or abusive head trauma. Figure 17.3 gives a schematic overview about different types of extra- and intracranial haematomas.

17.4.4.4 Subpial Haemorrhage

Subpial haematomas are bleedings located between the pia mater and the surface of the cortex. They are rare occurrences and typically difficult to distinguish from other types of haemorrhage, especially subarachnoid haematomas. Figure 17.8 gives an

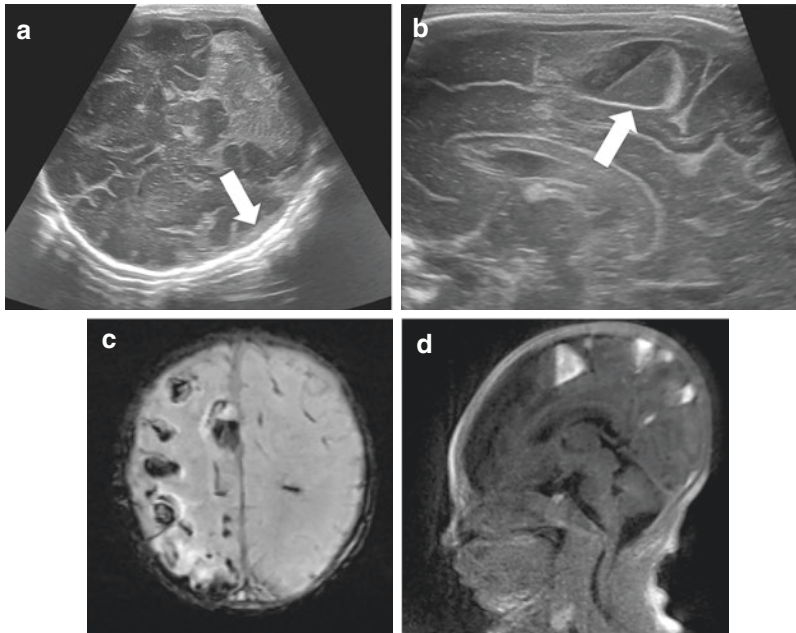


Fig. 17.8 Subpial bleedings as cerebral birth injury. A 3-day-old male newborn with a history of dystocic birth and requirement for acute Caesarean section. Known trauma to the right side of the head during labour. (a) US view with a left nuchal window demonstrates a subarachnoid haemorrhage on the right parietal side (arrow). (b) Parasagittal right side US section shows a fluid collection

along the cortical borders with fluid-level, suggestive of subpial haematoma (arrow). (c) MRI SWI section in axial orientation shows intracranial haemorrhages, predominantly on the right side. (d) T1-weighted right sagittal view shows bleedings along the cortex, subarachnoid, and subpial in location. The fluid-level described in (b) is also visible in the parietal region

example of mixed subarachnoid and subpial haemorrhages due to birth trauma.

17.4.4.5 Intracerebral Haemorrhage, Contusions, and Diffuse Axonal Injury

Intracerebral haemorrhage due to birth trauma is a rare occurrence particularly in preterm babies, which why it needs to raise suspicion for non-accidental origin or another underlying pathology like vascular lesions or hypertension or a haemorrhagic infarction. Cerebral contusion areas or shear injuries should trigger the radiologist to actively inform the referring physician of potential child abuse.

Ultrasound is suited to image larger contusions or intracerebral haematomas. Like in other types of intracerebral bleedings, CT is a sensitive method to diagnose macroscopic intracerebral haemorrhage. However, US and CT can have restrictions detecting diffuse axonal injuries (DAI). MRI is able to effectively detect (DAI), which are infrequent findings. Diffuse injuries along the grey-white matter junction and the brainstem may be noted. Like in adults, DAI in a newborn has a bad prognosis.

17.4.4.6 Hypoxic Ischaemic Brain Injuries

Hypoxic ischaemic brain injuries (HIE) occur in neonates and can display two main patterns of

distribution based on the underlying source. The first pattern, following a complete asphyxia or anoxia, includes grey matter and brain stem damage, including cerebral oedema. The second pattern occurs after partial asphyxia or prolonged hypoxia, resulting in damage to the paracentral regions in terms of watershed lesions.

Primary imaging for suspected hypoxic brain injuries is US that can be performed bedside in patient with suspected HIE. B-mode images might feature a loss of grey-white matter differentiation, Doppler is more sensitive and may also allow for grading of the severity of injury in association with an increased intracranial pressure (see also Chap. 8).

CT can be used to image suspected HIE, but the sensitivity is limited. Strengths of CT encompass visualisation of haemorrhages.

MR imaging is increasingly used in evaluating infants with HIE. In HIE, neonatal brain MRI offers prognostic information, but does not add therapeutic value—except for prognostic assessment helping to decide on discontinuation of treatment. MRI can directly visualise areas of ischaemia with the help of diffusion weighted imaging (DWI), and haemorrhagic transformation with gradient echo sequences or susceptibility weighted imaging (SWI) (Fig. 17.9). Advanced MRI in HIE relies on proton MR spectroscopy (1H-MRS) of the basal ganglia and thalami in HIE, primarily

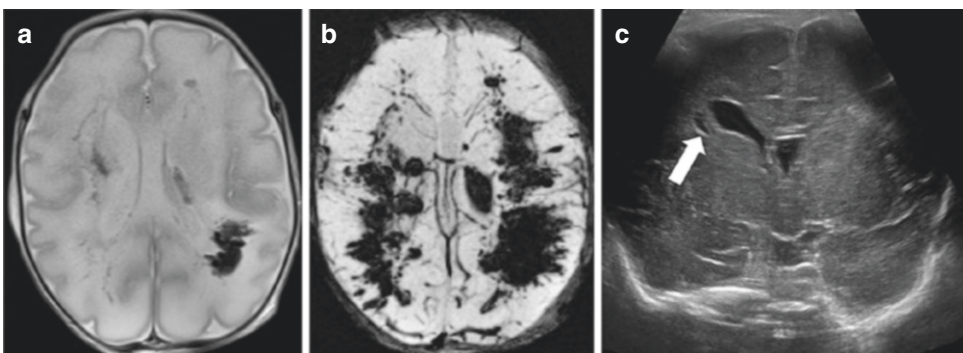


Fig. 17.9 Perinatal hypoxia and haemorrhagic transformation. A 4-day-old female neonate with severe perinatal hypoxia. US had shown diffuse brain swelling scattered with mixed-echogenic white matter abnormalities. MRI of the brain was performed. (a) This axial T2-weighted MRI image at the level of the lateral ventricles demonstrates oedematous brain changes and signs of haemor-

rhage, especially in the left parieto-occipital region. (b) A corresponding axial SWI section shows massive haemorrhagic transformation, predominately in the white matter of both hemispheres. (c) US in coronal plane showed small cystic changes in the periventricular regions, left-dominant swelling in the central portions, as well as a loss of grey-white matter differentiation

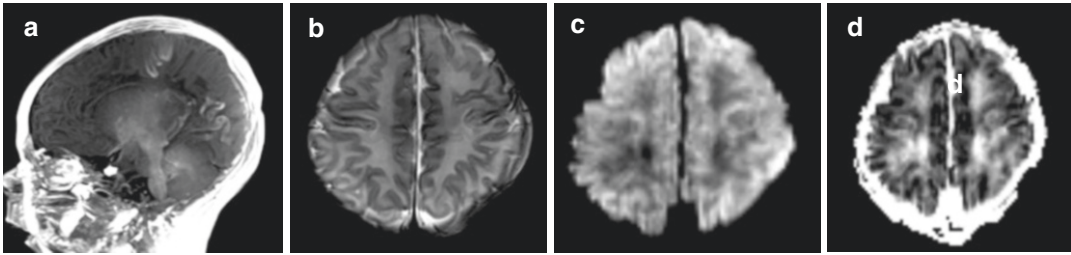


Fig. 17.10 Cortical laminar necrosis. A 6-day-old patient with a history of peripartal hypoxia. Feed-and-wrap MRI of the brain was performed to assess potential hypoxic brain injuries. (a) Curvilinear T1 signal intensities are noted in the parietal and occipital region in the parasagittal plane. These findings are suggestive of cortical

laminar necrosis. (b) The corresponding axial T2-weighted MR image demonstrates cortical and subcortical oedema in the affected regions. (c, d) DWI (c) and ADC (d) confirm the hypoxic oedema in the regions of the cortical laminar necrosis

aimed to predict outcome. 1H-MRS is one of the most powerful predictors in HIE, and metabolic disturbances may persist for weeks. Arterial spin labelling (ASL) is a type of native (without intravenous contrast) perfusion of the brain which might add further prognostic information. Hydrogen protons are inverted while passing through the brain-supplying arteries in the neck, followed by acquisition of labelled images of the brain. Hyperperfusion of basal ganglia and thalamus was described as an indicator for poor neurodevelopmental outcomes in newborns with HIE. Note that this approach implies a methodically intrinsic risk—heating of the brain which is treated by cooling, thus limiting the use to a slightly delayed stage of the disease.



While US with Doppler techniques still is the routine bedside imaging method, MRI is becoming the method of choice in neonates with suspected hypoxic ischaemic encephalopathy, but offers limited influence on the outcome.

17.4.4.7 Cortical Laminar Necrosis

Cortical laminar necrosis refers to a type of ischaemic brain injury that involves regions of the cerebral cortex partially or completely. The animal model has revealed the possibility of perinatally acquired cortical laminar necrosis.

MRI is very sensitive in revealing changes of cortical laminar necrosis, whereas CT and US cannot reliably depict or even less rule out such a condition. T1 hyperintensities of the cortex are the most specific sign that can remain visible for months, believed to be caused by denaturated proteins (Fig. 17.10). DWI can depict increased signal intensities of the affected cortex with corresponding hypointensities in the ADC maps in the acute period. Susceptibility imaging might also show signal changes. Cortical laminar necrosis has been associated with ischaemic events, meningoencephalitis, child abuse, and in metabolic disorders, thus, can be considered an unspecific finding.

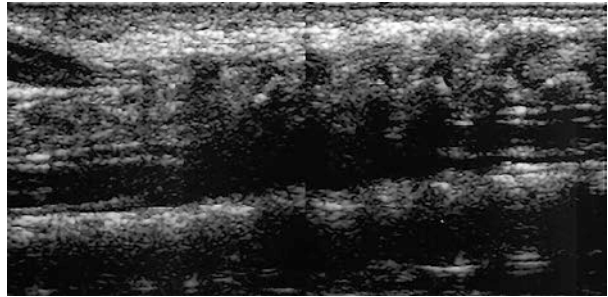
17.5 Spinal Cord and Spine Injuries

17.5.1 Spinal Cord Injuries

Birth damage to the spinal cord is uncommon, and specialists involved in childcare rarely see them. Awareness to prevent non-physiological pressures, especially longitudinal stretching, torsion, and severe neck hyperextension during delivery has reduced the risk of birth-related spinal cord damage.


Intrauterine foetal malpositions such as brow, face, or breech presentations are risk factors for spinal injuries during labour. Vaginal birth in the breech position with significant hyperextension

Fig. 17.11 Spinal cord injury. A 2-day-old neonate after complicated vaginal delivery and birth trauma with high paraplegia: sagittal (dorsal) US of the lower spinal canal shows cord disruption with adjacent haematoma. (Courtesy Riccabona M, *Pediatric Ultrasound*, 2nd edition, Springer 2020. p 176, Fig. 9.7b)



of the head is another risk factor. Caesarean section has also been linked to similar injuries. Spinal cord injuries are considerably less frequent after cephalic birth.

If there is any suspicion of spinal cord injuries, spinal US of the entire cord should be done immediately. Swelling and altered echogenicity or even disruption of the damaged portion may be seen (Fig. 17.11). Spinal US can be complemented by plain films, followed by MRI. CT scanning should be used if additional information regarding the bone component of the cervical spine is required. Diaphragmatic excursions and potential phrenic palsy are easily assessed by US. Documentation can be performed by storing para-axial cine clips through both diaphragms and m-mode trace, which demonstrate the amount and synchronicity of the diaphragmatic movements (also see Chap. 10).

 US can easily detect and document suspected phrenic palsy by acquiring para-axial cine clips through both diaphragms.

17.5.2 Vertebral Fractures

Vertebral fractures can occur during delivery, both in the cervical and the thoracic spine. They most frequently occur in terms of spinal fracture-dislocations, without actual bone damage. They are significantly associated with forceps delivery.

X-ray imaging is of limited use in the neonatal period. CT will pick up fractures, but the rec-

ommended imaging modality is MRI, which might help to guide therapy as far as possible, as MRI is able to depict the different types of haematomas, vertebral alignment, and myeloma pathologies. Even severe pathology might be associated with different degrees of recovery.

17.5.3 Brachial Plexus Injuries

The brachial plexus consists of ventral and dorsal rootlets, ranging from the fifth cervical segment to the first thoracic segment. In foetuses delivered with cephalic or shoulder position, lateral neck strain is the most common cause of brachial plexopathy. Brachial plexopathy can be classified into

- Erb palsy, involving the fifth and sixth cervical nerve root
- Klumpke's palsy, involving the eighth cervical and first thoracic nerve root

Macrosomia (birth weights more than 4000 g) and instrumental delivery are other risk factors. The majority of patients (up to 80%) might recover spontaneously. Additionally, associated traumatic lesions such as shoulder luxation or humerus epiphysiolysis as well as clavicular fractures can be detected.

Ultrasound represents an excellent modality for imaging the entire neonatal spinal cord. However, the proper detection of nerve root lesions including nerve root avulsions and accompanying pseudo-meningoceles requires extensive knowledge and training. Radiography and CT are of limited use. High-resolution MRI is a suitable method,

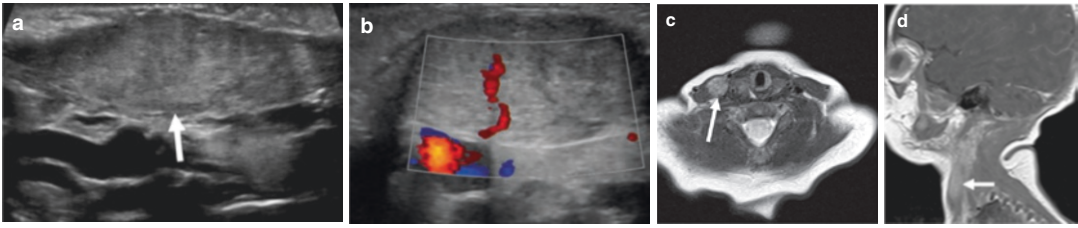


Fig. 17.12 Fibromatosis colli. An 8-day-old female patient with swelling on the right side of the neck. (a) Fusiform thickening (arrow) of the right sternocleidomastoid muscle is seen on B-mode US (oblique parasagittal orientation). (b) Colour Doppler sonography may show prominent vessels as seen in this example. (c) T2-weighted axial MRI image reveals a hyperintense lesion in the right

sternocleidomastoid muscle. Note that the examination was not performed to detect fibromatosis colli, but for assessment of a potential hypoxic brain injury. Therefore, the finding can be considered “incidental” in this situation. (d) Note that the fibromatosis colli might show varying signal intensity and might also be hyperintense on MRI, as in this T1-weighted sagittal image (arrow)

and is able to directly visualise the cervical nerve roots and potential lesions.

MR neurography (MRN) relies on dedicated high-resolution MRI sequences to improve the visibility of neuronal tissues oriented in the plane of the plexus tract. These sequences include 3D STIR (short tau inversion-recovery) and 3D PSIF (reversed fast imaging in steady state precession). Studies found MRN as viable method imaging birth trauma-related plexopathy.



Brachial plexopathy can be imaged by US or MRI, which both offer high sensitivity, with MRI being more robust if performed properly in skilled hands.

17.5.4 Fibromatosis Colli

Fibromatosis colli is most commonly associated with birth trauma (e.g. forceps delivery and dystocic birth) or breech position and clinically presenting in terms of torticollis due to a hard unilateral neck tumour.

The preferred imaging method is US, if necessary at all—usually the history and the clinical findings are already diagnostic. If required, it is mostly performed to differentiate it from other cervical mass lesions. The sternocleidomastoid muscle is usually unilaterally diffusely expanded,

the muscular body is primarily affected in terms of a fusiform or ovaloid thickening (Fig. 17.12). The echogenicity of the affected fibrotic areas may vary. Sometimes a high resistance waveform in sometimes very impressive vessels may be seen on spectral Doppler. In the late phase, previous haemorrhagic parts are indicated by the presence of hyperechoic calcific foci. Radiographs might be of use in cases, where other skeletal deformities need to be assessed. CT and MRI are hardly ever indicated, as US has a sensitivity of up to 100%.

17.6 Thoracic Injuries

17.6.1 Pneumothorax

Pneumothorax can develop after delivery. Intubation and mechanical ventilation, pre-existing abnormalities (e.g. cysts, pulmonary malformations), insertion of central venous lines, and many other factors can cause air leakage, including interstitial emphysema, pneumothorax, and pneumopericardium increase the risk of developing a pneumothorax. The prevalence of pneumothorax was found to be 0.3% in neonates with a birth weight above, and 2.5% in newborns with a birth weight below 2.5 kg.

Lung US is a well-suited method to detect and follow-up neonatal pneumothorax. The accuracy of lung US detecting pneumothorax is believed to be comparable or superior to chest



Fig. 17.13 Pneumothorax. A 1-day old boy, chest radiograph of this intubated neonate for respiratory distress: it shows a huge tension pneumothorax on the left side with mediastinal shift to the right compressing the right lung. The tracheal tube and the central line are also shifted to the right, the gastric tube therefore tends to end too high—at the gastro-oesophageal junction. Note the chest wall emphysema on the left side

X-ray (Fig. 17.13). Still, chest radiography is not obsolete in critically ill neonates. Done correctly, radiation doses are low and additional diagnostic information might be revealed by X-ray.

17.6.2 Rib Fractures

Rib fractures are known to be associated with dystocic birth, and they are closely related to clavicular fractures. More commonly, and also more typically, rib fractures are a result of abusive trauma. About 50% of all fractures attributed to child abuse involve the ribs. The characteristic serial rib fractures occur because of torturer's hands almost fully encircle and squeeze the little child's thorax. The transverse processes of the thoracic vertebrae function as a hypermochlion, and paravertebral rib fractures occur. Radiographs are the initial imaging performed in patients with suspected child abuse. The radiologist needs to consider that only a minority (about one third) of rib fractures are visible in skeletal survey radio-

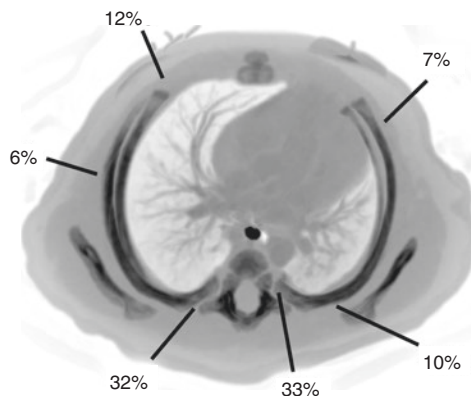


Fig. 17.14 Rib fracture locations caused by NAI. Schematic illustration of a paediatric chest in axial orientation. Distribution of rib fracture locations as a consequence of non-accidental trauma is given in percentages, modified according to Kleinman et al.

graphs. Therefore, it is necessary to perform high-detail radiographs in suspected cases of child abuse (Fig. 17.14). Still, radiography will not be able to detect all rib fractures.

CT has a higher sensitivity than radiography detecting rib fractures. According to current guidelines, chest CT may be appropriate in cases of uncertainty or multi-trauma situations. If child abuse is likely but the skeletal survey is negative, a CT scan of the chest may be useful, possibly revealing fractures of the ribs, shoulder girdle, or spine.



Rib fractures are usually associated with child abuse, and do typically involve the dorsal parts of the ribs.

17.7 Abdominal Injuries

Abdominal birth trauma is rare. Authors reported cases of splenic ruptures during delivery. Hepatic haematoma may arise with an underlying disease such a congenital haemangioma with a typically subcapsular location in neonates. Other aetiologies of liver haematoma include iatrogenic umbilical venous catheter perforation, coagulopathy in sepsis, hypoxia, and direct (birth) trauma. Haematomas may develop from tumour haemor-

rhage or vascular abnormalities. There exist rare reports of abdominal trauma cases due to an underlying foetal abdominal tumour. Adrenal bleeding may occur in addition to traumatic lesions of the parenchymal abdominal organs. It's worth noting that bleeding may happen in adrenal neuroblastomas as well. Small haematomas are clinically quiet; big haematomas may burst and cause death.

Ultrasonography should be the first imaging procedure to detect free peritoneal fluid or parenchymal upper abdominal organ damage. A hyper-echogenic wall may simulate an abscess on US in the early stages of parenchymal bleeding. If child abuse is suspected, a subsequent CT scan (using contrast) of the abdomen is the gold standard, but only necessary in rare occasions.

17.8 Musculoskeletal

Delivery-related fracture rate is about 3 in 1000 live births. Birth trauma together with accidents is believed to be the leading cause of neonatal fractures. It is critical to determine whether a fracture happened during or after birth. Helpful clues can be the estimation of fracture age based onto calcifications and reparation processes observed. Study results indicate that missing signs of fracture healing after 11 days of life can be suspicious of child abuse.

17.8.1 Clavicle Fractures

Delivery may cause fractures of the clavicles, especially in circumstances of dystocia or the necessity to use assistive equipment like forceps. Literature reports an incidence of 2.7–5.7 cases per 1000 live births. Clavicular fracture may be seen as isolated injuries or in conjunction with humeral fractures or brachial plexus injuries. Clavicle fracture can be linked to impaired neonatal-to-maternal anthropometry as well as delivery difficulties in approximately 9 of 10 cases. In severely ill neonates, it usually is depicted incidentally on radiographs performed for other reasons (Fig. 17.15).

An important differential diagnosis to acute fractures are pseudoarthroses of the clavicles, which can occur uni- or bilaterally and might be present at

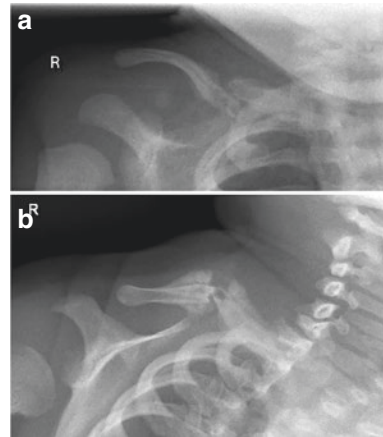


Fig. 17.15 Clavicle fracture. Radiographs in fractures of the right clavicle. (a) The radiograph demonstrates a clavicular fracture with shortening and dislocation in a 4-day-old neonate. (b) The oblique radiograph shows a clavicular fracture in a 7-day-old newborn. It shows dislocation and (as also in Fig a) periosteal reaction, indicating a subacute process. Both fractures could be attributed to birth trauma



Fig. 17.16 Clavicular pseudoarthrosis. An 28-day-old female newborn with slight deformity in the right clavicular region. The radiograph of the right clavicle in AP projection shows a discontinuity and displacement of the right clavicular shaft with rounded borders. There is no periosteal reaction or callus

birth. Congenital clavicular pseudoarthrosis is the failed fusion of the clavicle's medial and lateral ossification centres. In the absence of trauma, anteroposterior radiographs of the clavicle might reveal a rounded sclerotic bone at the location of the site of the pseudoarthrosis (Fig. 17.16), however, distinction to clavicular fractures might be difficult.



Clavicle fractures are a typical birth injury and might be associated with brachial plexopathy. They are rarely caused by abusive trauma.

Fig. 17.17 Humerus fracture. A 5-day-old newborn with crying episodes. The clinical examination revealed a deformity of the painful left upper arm. (a) An AP radiograph of the left humerus depicts a mid-shaft fracture, moderately dislocated. (b) The lateral projection also shows a deviation of the humerus shaft fracture. Note that there are hardly any signs of regenerative processes, indicating an acute injury

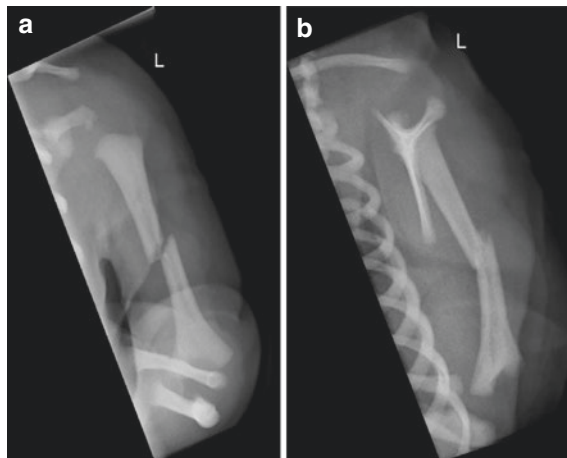
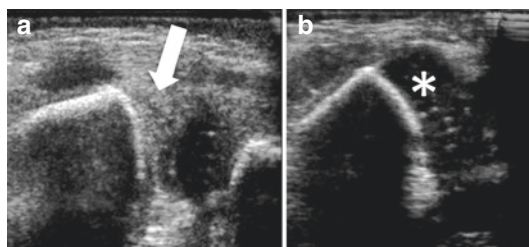


Fig. 17.18 Humerus epiphysiolysis. Boy with 2 weeks of age and swelling of the left elbow after trauma. Bilateral para-coronal US sections in both distal upper arms. (a) A coronal US section through the injured left distal humerus shows a missing cartilage signal at the expected site the distal humerus epiphysis (arrow), in keeping with an epiphysiolysis with dislocation. (b) There is a normal epiphysis on the contralateral side (asterisk) for comparison



17.8.1.1 Humerus Fractures

Humeral fractures usually affect the humeral shaft or the proximal or distal epiphyseal regions. Excessive traction on the upper extremity like in dystocic delivery may result in chondroepiphyseal separation of the distal humerus in terms of a Salter-Harris type 1 injury. Clinically, swelling and signs of pain in the neonate's elbow including restriction of movement can help distinguishing it from brachial plexus palsy's hypomobility.

Radiography is a proper method to assess presence, alignment, and healing of humeral shaft fractures (Fig. 17.17). Because unossified cartilage cannot be detected radiographically, US is a suitable way to assess epiphyseal injuries in a bedside manner (Fig. 17.18). Alternatively, MR may detect these injuries, but is rarely needed.

17.8.2 Femur Fractures

Femur fractures account for approximately 1 in 10,000 live births, and can, therefore, be consid-

ered rare. The typical fracture site is the femur shaft with oblique or spiral fracture lines. Moreover, there exist reports about transphyseal distal femur fractures. A main risk factor is operative birth and the tight spaces available when performing caesarean sections. Presentation might be delayed for a few days, but radiography should be able to make the diagnosis. Another though rare cause is physiotherapy in babies with prematurity associated osteopenia.

Radiologists need to be aware of the phenomenon of subperiosteal new bone formation (SPNBF), pseudo periosteal reactions, or pseudoperiostitis, which can be visible in long bones of infants. This physiological reaction mimics periosteal reaction, commonly along the femur or tibia shafts and makes it considerably more difficult to judge the cause. However, SPNBF is not known to occur in the neonatal period but between 1 and 4 months of life.

Imaging is performed by radiographs, sometimes US (performed, e.g. because of unclear



Fig. 17.19 Femur shaft fracture on the right side. A 4-day-old boy with swelling of the right proximal thigh. The upper leg radiograph of the pelvico-femoral region in AP projection shows a subacute fracture of the proximal right femur. This injury was caused by birth trauma

swelling, suspicion of venous thrombosis, or suspected septic coxitis and similar conditions) will reveal the fracture particularly if its dislocated (Fig. 17.19).



Periosteal-like reactions known as subperiosteal new bone formation should not be observed in the neonatal period, but thereafter.

17.8.3 Tibia Fractures

Fractures of the tibia and the lower legs have been reported with a low rate of occurrence. Typical metaphyseal corner fractures of the tibia linked to delivery are rarities. These fracture types are more likely caused by non-accidental trauma and seen on radiographs (Fig. 17.20).

17.8.4 Congenital Pseudoarthroses

Congenital pseudoarthroses represent a range of pathological bowing or non-union of long bones in children. The amount of bowing can be so severe to resemble a false joint. Cases of congenital pseudoarthroses are usually diagnosed in newborn age, and rarely after 2 years. An associ-



Fig. 17.20 Metaphyseal corner fracture. A 9-day-old girl after suspected non-accidental trauma. Skeletal survey radiographs revealed multiple fractures, including a metaphyseal corner fracture (arrow) of the distal radius, demonstrated in this lateral projection of the distal forearm. Note that there is also a buckle fracture of the distal ulna

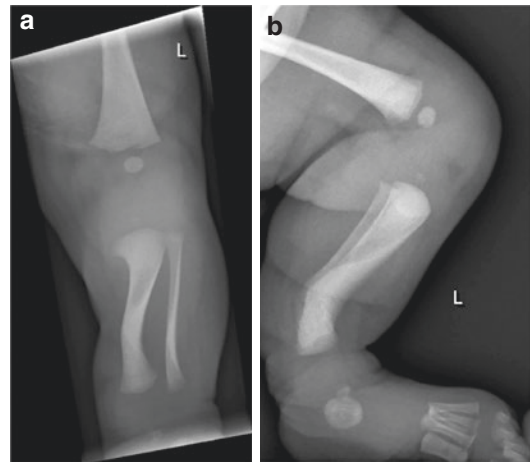


Fig. 17.21 Tibia and fibula pseudoarthrosis. A 10-day-old male newborn with clinically obvious bowing of the left lower leg. (a) The AP radiograph of the lower leg shows a lateral deviation and increased sclerosis of the tibia and fibula. (b) The lateral projection demonstrates a deviation of both tibia and fibula anteriorly at the junction of the mid-distal lower leg bones. Tibia pseudoarthrosis can be classified into four types after Paley. This case would be Paley type 1

ation with neurofibromatosis (NF) type 1 has been postulated. The most common site is the tibia, whereas pseudoarthroses of the fibula, radius, and ulna are less frequently observed and usually imaged by radiographs (Fig. 17.21). Congenital pseudoarthrosis of the tibia can be



Fig. 17.22 Fractures in Osteogenesis imperfecta. Male newborn (15 days old) with relatively short arms and legs. The AP radiograph of the pelvis demonstrates a generalised osteopenic bone texture, and pathologic fractures of the proximal femora with regenerative bone formation on the right side. The diagnosis in this case is osteogenesis imperfecta

classified by severity into four types (ranging from 1 to 4) after Paley. Further information on this topic is also available in Chap. 14.

17.8.5 Differential Diagnosis

Overdiagnosis of non-accidental trauma is tragic for the child, who may be taken away from his parents, and for the family, who may face the loss of a family member together with the “social stigma” that comes along with it. On the other hand, an incorrect diagnosis of osteogenesis imperfecta (Fig. 17.22) or other osteochondrodysplasias or metabolic bone diseases may endanger a neonate’s life. These conditions and their imaging features are described in more detail in Chap. 14. It should also be noted that birth trauma may not be obvious immediately after birth, which reduces the potential to distinguish it from non-accidental injuries in a newborn. This is specifically true in undisplaced fractures where healing processes (e.g. callus, periosteal reaction, fracture gap demineralisation) did not yet cause visible changes.

Another phenomenon to consider is the osteopenia of prematurity—preterm newborns have a higher rate of demineralisation after delivery which can be imaged with X-rays, e.g. of the wrist to demonstrate cupping, fraying, or splaying of the metaphyses. There might be other characteristic radiography sign like “rosary beads” of rickets at the anterior rib ends in chest X-rays.

17.9 Summary

Trauma is a common issue in the neonatal period, possibly involving every part of a newborn’s body. The causes of neonatal trauma include birth-related injuries as well as accidental and non-accidental trauma. A proper anamnesis is able to categorise the origin of an injury in many cases correctly. Radiologically, many findings are non-specific. However, there are injuries that must raise suspicion for child abuse, especially in cases of rib fractures, fractures in different locations and of different age, as well as intracranial haemorrhage.

Bibliography

1. Abbott R, Abbott M, Alzate J, Lefton D. Magnetic resonance imaging of obstetrical brachial plexus injuries. *Childs Nerv Syst.* 2004;20:720–5.
2. Abzug JM, Kozin SH. Evaluation and management of brachial plexus birth palsy. *Orthop Clin North Am.* 2014;45:225–32.
3. Adamsbaum C, Barr M. Imaging in abusive head trauma: an in-depth look at current issues. *Pediatr Radiol.* 2014;44(Suppl 4):S535–6.
4. Adamsbaum C, Morel B, Ducot B, Antoni G, Rey-Salmon C. Dating the abusive head trauma episode and perpetrator statements: key points for imaging. *Pediatr Radiol.* 2014;44(Suppl 4):S578–88.
5. Aly H, Massaro A, Acun C, Ozen M. Pneumothorax in the newborn: clinical presentation, risk factors and outcomes. *J Matern Fetal Neonatal Med.* 2014;27:402–6.
6. Alzahrani NM, Jeanes A, Paddock M, Shuweihi F, Offiah AC. The diagnostic performance of chest computed tomography in the detection of rib fractures in children investigated for suspected physical abuse: a systematic review and meta-analysis. *Eur Radiol.* 2021;31:7088–97.
7. Amar AP, Aryan HE, Meltzer HS, Levy ML. Neonatal subgaleal hematoma causing brain compression: report of two cases and review of the literature. *Neurosurgery.* 2003;52:1470–4; discussion 1474.
8. Section on Radiology; American Academy of Pediatrics. Diagnostic imaging of child abuse. *Pediatrics.* 2000;105:1345–8.
9. Amir J, Katz K, Grunebaum M, Yosipovich Z, Wielunsky E, Reisner SH. Fractures in premature infants. *J Pediatr Orthop.* 1988;8:41–4.
10. Ammirabile A, Buonsenso D, Di Mauro A. Lung ultrasound in pediatrics and neonatology: an update. *Healthcare (Basel).* 2021;9(8):1015.

11. Andresen F, Zieger B, Wurtemberger U, Kunze M, Hentschel R. [The neonatal subgaleal hematoma - a neonatal emergency]. *Z Geburtshilfe Neonatol.* 2021;225(6):529–33.
12. Antonov NK, Ruzal-Shapiro CB, Morel KD, Millar WS, Kashyap S, Lauren CT, Garzon MC. Feed and wrap MRI technique in infants. *Clin Pediatr (Phila).* 2017;56:1095–103.
13. Arroba Basanta ML, De La Rubia Fernandez LR, Del Castillo Martin F. Neonatal pathologic fracture and neurofibromatosis. *An Esp Pediatr.* 1986;25:491–2.
14. Babyn PS, Chuang SH, Daneman A, Davidson GS. Sonographic evaluation of spinal cord birth trauma with pathologic correlation. *AJR Am J Roentgenol.* 1988;151:763–6.
15. Barber I, Kleinman PK. Imaging of skeletal injuries associated with abusive head trauma. *Pediatr Radiol.* 2014;44(Suppl 4):S613–20.
16. Barkovich AJ. MR and CT evaluation of profound neonatal and infantile asphyxia. *AJNR Am J Neuroradiol.* 1992;13:959–72; discussion 973–5.
17. Barlow KM, Minns RA. Annual incidence of shaken impact syndrome in young children. *Lancet.* 2000;356:1571–2.
18. Basagaoglu B, St Cyr G, Dempsey RF, Dauser RC, Lam S, Maricevich RS. Chicken or the egg: a case report of endoscopic-assisted treatment of concomitant sagittal craniosynostosis with calcified cephalohematoma. *J Craniofac Surg.* 2020;31:e130–3.
19. Beals RK, Sauser DD. Nontraumatic disorders of the clavicle. *J Am Acad Orthop Surg.* 2006;14:205–14.
20. Berdon WE, Feldman KW. A modest proposal: thoracic CT for rib fracture diagnosis in child abuse. *Child Abuse Negl.* 2012;36:200–1.
21. Biousse V, Suh DY, Newman NJ, Davis PC, Mapstone T, Lambert SR. Diffusion-weighted magnetic resonance imaging in Shaken Baby Syndrome. *Am J Ophthalmol.* 2002;133:249–55.
22. Birchansky S, Altman N. Imaging the brachial plexus and peripheral nerves in infants and children. *Semin Pediatr Neurol.* 2000;7:15–25.
23. Blumfield E. Pearls and pitfalls in imaging of abusive head trauma. *Semin Ultrasound CT MR.* 2020;41:411–20.
24. Bode-Janisch S, Bultmann E, Hartmann H, Schroeder G, Zajaczek JE, Debertin AS. Serious head injury in young children: birth trauma versus non-accidental head injury. *Forensic Sci Int.* 2012;214:e34–8.
25. Bresnan MJ, Abroms IF. Neonatal spinal cord transection secondary to intrauterine hyperextension of the neck in breech presentation. *J Pediatr.* 1974;84:734–7.
26. Brittain C, Muthukumar P, Job S, Sanka S. ‘Ping pong’ fracture in a term infant. *BMJ Case Rep.* 2012;2012:bcr0120125631.
27. Bulloch B, Schubert CJ, Brophy PD, Johnson N, Reed MH, Shapiro RA. Cause and clinical characteristics of rib fractures in infants. *Pediatrics.* 2000;105:E48.
28. Caffey J. Some traumatic lesions in growing bones other than fractures and dislocations: clinical and radiological features: The Mackenzie Davidson Memorial Lecture. *Br J Radiol.* 1957;30:225–38.
29. Cannella R, Sparacia G, Lo REV, Oddo E, Mamone G, Miraglia R. Advanced magnetic resonance imaging of cortical laminar necrosis in patients with stroke. *Neuroradiol J.* 2019;32:431–7.
30. Cartocci G, Fineschi V, Padovano M, Scopetti M, Rossi-Espagnet MC, Gianni C. Shaken Baby Syndrome: magnetic resonance imaging features in abusive head trauma. *Brain Sci.* 2021;11(2):179.
31. Catena N, Senes FM. Obstetrical chondro-epiphyseal separation of the distal humerus: a case report and review of literature. *J Perinat Med.* 2009;37:418–9.
32. Cattarossi L, Copetti R, Brusa G, Pintaldi S. Lung ultrasound diagnostic accuracy in neonatal pneumothorax. *Can Respir J.* 2016;2016:6515069.
33. Chacham S, Pasi R, Chegondi M, Ahmad N, Mohanty SB. Metabolic bone disease in premature neonates: an unmet challenge. *J Clin Res Pediatr Endocrinol.* 2020;12:332–9.
34. Chalfant JS, Sanchez TR. Congenital clavicular pseudoarthrosis-how to differentiate it from the more common clavicular fractures. *Pediatr Emerg Care.* 2019;35:e37–9.
35. Chang HY, Cheng KS, Liu YP, Hung HF, Fu HW. Neonatal infected subgaleal hematoma: an unusual complication of early-onset E. coli sepsis. *Pediatr Neonatol.* 2015;56:126–8.
36. Chapman S, Hall CM. Non-accidental injury or brittle bones. *Pediatr Radiol.* 1997;27:106–10.
37. Chaturvedi A, Chaturvedi A, Stanescu AL, Blickman JG, Meyers SP. Mechanical birth-related trauma to the neonate: an imaging perspective. *Insights Imaging.* 2018;9:103–18.
38. Choudhary AK, Ishak R, Zacharia TT, Dias MS. Imaging of spinal injury in abusive head trauma: a retrospective study. *Pediatr Radiol.* 2014;44:1130–40.
39. Choudhary AK, Servaes S, Slovis TL, Palusci VJ, Hedlund GL, Narang SK, Moreno JA, Dias MS, Christian CW, Nelson MD Jr, Silvera VM, Palasis S, Raissaki M, Rossi A, Offiah AC. Consensus statement on abusive head trauma in infants and young children. *Pediatr Radiol.* 2018;48:1048–65.
40. Christophe C, Ziereisen F, Damry N, Guissard G, Fonteyne C, Dan B. Brain MR imaging in shaken-baby syndrome: how? when and why? *Arch Pediatr.* 2006;13:733–5.
41. Clarke TA, Edwards DK, Merritt A, Young LW. Radiological case of the month. Neonatal fracture of the femur: iatrogenic? *Am J Dis Child.* 1982;136:69–70.
42. Cowan F, Rutherford M, Groenendaal F, Eken P, Mercuri E, Bydder GM, Meiners LC, Dubowitz LM, De Vries LS. Origin and timing of brain lesions in term infants with neonatal encephalopathy. *Lancet.* 2003;361:736–42.

43. Cramer JA, Rassner UA, Hedlund GL. Limitations of T2*-gradient recalled-echo and susceptibility-weighted imaging in characterising chronic subdural hemorrhage in infant survivors of abusive head trauma. *AJNR Am J Neuroradiol.* 2016;37:1752–6.
44. Crim J, Ingalls K. Accuracy of MR neurography in the diagnosis of brachial plexopathy. *Eur J Radiol.* 2017;95:24–7.
45. Cumming WA. Neonatal skeletal fractures. Birth trauma or child abuse? *J Can Assoc Radiol.* 1979;30:30–3.
46. Dabezies EJ, Warren PD. Fractures in very low birth weight infants with rickets. *Clin Orthop Relat Res.* 1997;(335):233–9.
47. Davidge KM, Clarke HM, Borschel GH. Nerve transfers in birth related brachial plexus injuries: where do we stand? *Hand Clin.* 2016;32:175–90.
48. De Silva P, Evans-Jones G, Wright A, Henderson R. Physiological periostitis; a potential pitfall. *Arch Dis Child.* 2003;88:1124–5.
49. De Vis JB, Hendrikse J, Petersen ET, De Vries LS, Van Bel F, Alderliesten T, Negro S, Groenendaal F, Benders MJ. Arterial spin-labelling perfusion MRI and outcome in neonates with hypoxic-ischemic encephalopathy. *Eur Radiol.* 2015;25:113–21.
50. De Vries E, Robben SG, Van Den Anker JN. Radiologic imaging of severe cervical spinal cord birth trauma. *Eur J Pediatr.* 1995;154:230–2.
51. Demaerel P. MR imaging in inflicted brain injury. *Magn Reson Imaging Clin N Am.* 2012;20:35–44.
52. Deng BY, Li N, Wu WS, He XG, Li JF, Huang TL, Li YC, Jiang SL. Use of neonatal lung ultrasound for the early detection of pneumothorax. *Am J Perinatol.* 2020;37:907–13.
53. Dremmen MHG, Wagner MW, Bosemani T, Tekes A, Agostino D, Day E, Soares BP, Huisman T. Does the addition of a “black bone” sequence to a fast multisequence trauma MR protocol allow MRI to replace CT after traumatic brain injury in children? *AJNR Am J Neuroradiol.* 2017;38:2187–92.
54. Drury A, Cunningham C. Determining when a fracture occurred: does the method matter? Analysis of the similarity of three different methods for estimating time since fracture of juvenile long bones. *J Forensic Legal Med.* 2018;53:97–105.
55. Du R, Augustine KI, Chin CT, Engstrom JW, Weinstein PR. Magnetic resonance neurography for the evaluation of peripheral nerve, brachial plexus, and nerve root disorders. *J Neurosurg.* 2010;112:362–71.
56. Dudink J, Jeanne Steggerda S, Horsch S, eurUS. brain group. State-of-the-art neonatal cerebral ultrasound: technique and reporting. *Pediatr Res.* 2020;87:3–12.
57. Duhaime AC, Christian C, Moss E, Seidl T. Long-term outcome in infants with the shaking-impact syndrome. *Pediatr Neurosurg.* 1996;24:292–8.
58. Duhaime AC, Gennarelli TA, Thibault LE, Bruce DA, Margulies SS, Wisner R. The shaken baby syndrome. A clinical, pathological, and biomechanical study. *J Neurosurg.* 1987;66:409–15.
59. Eisenberg D, Kirchner SG, Perrin EC. Neonatal skull depression unassociated with birth trauma. *AJR Am J Roentgenol.* 1984;143:1063–4.
60. Eley KA, Watt-Smith SR, Golding SJ. “Black bone” MRI: a potential alternative to CT when imaging the head and neck: report of eight clinical cases and review of the Oxford experience. *Br J Radiol.* 2012;85:1457–64.
61. Expert Panel on Pediatric Imaging, Wootton-Gorges SL, Soares BP, Alazraki AL, Anupindi SA, Blount JP, Booth TN, Dempsey ME, Falcone RA Jr, Hayes LL, Kulkarni AV, Partap S, Rigsby CK, Ryan ME, Safdar NM, Trout AT, Widmann RF, Karmazyn BK, Palasis S. ACR Appropriateness Criteria(R) suspected physical abuse-child. *J Am Coll Radiol.* 2017;14:S338–49.
62. Fadell M, Miller A, Trefan L, Weinman J, Stewart J, Hayes K, Maguire S. Radiological features of healing in newborn clavicular fractures. *Eur Radiol.* 2017;27:2180–7.
63. Feldman KW, Weinberger E, Milstein JM, Fligner CL. Cervical spine MRI in abused infants. *Child Abuse Negl.* 1997;21:199–205.
64. Flodmark O, Becker LE, Harwood-Nash DC, Fitzhardinge PM, Fitz CR, Chuang SH. Correlation between computed tomography and autopsy in premature and full-term neonates that have suffered perinatal asphyxia. *Radiology.* 1980;137:93–103.
65. Fötter R, Sorantin E, Schneider U, Ranner G, Fast C, Schober P. Ultrasound diagnosis of birth-related spinal cord trauma: neonatal diagnosis and follow-up and correlation with MRI. *Pediatr Radiol.* 1994;24:241–4.
66. Franco A, Chaturvedi A. Neonatal distal femoral physeal injury secondary to mechanical trauma of birth: a case report. *Clin Imaging.* 2018;51:65–7.
67. Gencturk M, Tore HG, Nascene DR, Zhang L, Koxsel Y, McKinney AM. Various cranial and orbital imaging findings in pediatric abusive and non-abusive head trauma, and relation to outcomes. *Clin Neuroradiol.* 2019;29:253–61.
68. Genssler W, Menzel K. [Skull fractures in neonatal age (author’s transl)]. *Radiol Diagn (Berl).* 1976;17:181–4.
69. Gibson DA, Carroll N. Congenital pseudarthrosis of the clavicle. *J Bone Joint Surg Br.* 1970;52:629–43.
70. Gigante C, Kini SG, Origo C, Volpin A. Transphyseal separation of the distal humerus in newborns. *Chin J Traumatol.* 2017;20:183–6.
71. Gkiatas I, Papadopoulos D, Korompilias A, Vekris M, Beris A, Kostas-Agnantis I. Traumatic upper plexus palsy: is the exploration of brachial plexus necessary? *Eur J Orthop Surg Traumatol.* 2019;29:255–62.
72. Glaser K. Double contour, cupping and spurring in roentgenograms of long bones in infants. *Am J Roentgenol Radium Ther.* 1949;61:482–92.

73. Goetz E. Neonatal spinal cord injury after an uncomplicated vaginal delivery. *Pediatr Neurol.* 2010;42:69–71.
74. Grahn P, Poyhia T, Sommarhem A, Nietosvaara Y. Clinical significance of cervical MRI in brachial plexus birth injury. *Acta Orthop.* 2019;90:111–8.
75. Groenendaal F, De Vries LS. Fifty years of brain imaging in neonatal encephalopathy following perinatal asphyxia. *Pediatr Res.* 2017;81:150–5.
76. Gudinchet F, Maeder P, Oberson JC, Schnyder P. Magnetic resonance imaging of the shoulder in children with brachial plexus birth palsy. *Pediatr Radiol.* 1995;25(Suppl 1):S125–8.
77. Gunda D, Cornwell BO, Dahmouh HM, Jazbeh S, Alleman AM. Pediatric central nervous system imaging of nonaccidental trauma: beyond subdural hematomas. *Radiographics.* 2019;39:213–28.
78. Gunes A, Bulut E, Uzumcugil A, Oguz KK. Brachial plexus ultrasound and MRI in children with brachial plexus birth injury. *AJNR Am J Neuroradiol.* 2018;39:1745–50.
79. Hahnemann ML, Kinner S, Schweiger B, Bajanowski T, Karger B, Pfeiffer H, Wittschieber D. Imaging of bridging vein thrombosis in infants with abusive head trauma: the “Tadpole Sign”. *Eur Radiol.* 2015;25:299–305.
80. Halliday KE, Broderick NJ, Somers JM, Hawkes R. Dating fractures in infants. *Clin Radiol.* 2011;66:1049–54.
81. Hamilcikan S, Yilmaz K, Can E. Humeral diaphysis fracture in a neonate after vaginal delivery. *Sisli Etfal Hastan Tip Bul.* 2018;52:51–3.
82. Hanrahan JD, Cox IJ, Edwards AD, Cowan FM, Sargentoni J, Bell JD, Bryant DJ, Rutherford MA, Azzopardi D. Persistent increases in cerebral lactate concentration after birth asphyxia. *Pediatr Res.* 1998;44:304–11.
83. Harper NS, Eddleman S, Shukla K, Narcise MV, Padhye LJ, Peterson LJ, Murati MA, George CLS. Radiologic assessment of skull fracture healing in young children. *Pediatr Emerg Care.* 2021;37:213–7.
84. Henry MK, Wood JN. Advanced cervical spine imaging in abusive head trauma: an update on recent literature and future directions. *Acad Pediatr.* 2018;18:733–5.
85. Hickey K, Mckenna P. Skull fracture caused by vacuum extraction. *Obstet Gynecol.* 1996;88:671–3.
86. Hogberg U, Andersson J, Hogberg G, Thiblin I. Metabolic bone disease risk factors strongly contributing to long bone and rib fractures during early infancy: a population register study. *PLoS One.* 2018;13:e0208033.
87. Hogberg U, Fellman V, Thiblin I, Karlsson R, Wester K. Difficult birth is the main contributor to birth-related fracture and accidents to other neonatal fractures. *Acta Paediatr.* 2020;109:2040–8.
88. Hong TS, Reyes JA, Moineddin R, Chiasson DA, Berdon WE, Babyn PS. Value of postmortem thoracic CT over radiography in imaging of pediatric rib fractures. *Pediatr Radiol.* 2011;41:736–48.
89. Horsman A, Ryan SW, Congdon PJ, Truscott JG, James JR. Osteopenia in extremely low birthweight infants. *Arch Dis Child.* 1989;64:485–8.
90. Hosokawa T, Yamada Y, Sato Y, Tanami Y, Oguma E. Subperiosteal new bone and callus formations in neonates with femoral shaft fracture at birth. *Emerg Radiol.* 2017;24:143–8.
91. Hughes CA, Harley EH, Milmo G, Bala R, Martorella A. Birth trauma in the head and neck. *Arch Otolaryngol Head Neck Surg.* 1999;125:193–9.
92. Huisman TAGM, Phelps T, Bosemani T, Tekes A, Poretti A. Parturitional injury of the head and neck. *J Neuroimaging.* 2015;25:151–66.
93. Ichor RN, Naim M, Pollock AN, Nance ML, Margulies SS, Christian CW. Hypoxic-ischemic injury complicates inflicted and accidental traumatic brain injury in young children: the role of diffusion-weighted imaging. *J Neurotrauma.* 2007;24:106–18.
94. Islam O, Soboleski D, Symons S, Davidson LK, Ashworth MA, Babyn P. Development and duration of radiographic signs of bone healing in children. *AJR Am J Roentgenol.* 2000;175:75–8.
95. Jacobsen S, Hansson G, Nathorst-Westfelt J. Traumatic separation of the distal epiphysis of the humerus sustained at birth. *J Bone Joint Surg Br.* 2009;91:797–802.
96. Jain R, Bielski RJ. Fracture of lower femoral epiphysis in an infant at birth: a rare obstetrical injury. *J Perinatol.* 2001;21:550–2.
97. Jones JCW, Feldman KW, Bruckner JD. Child abuse in infants with proximal physical injuries of the femur. *Pediatr Emerg Care.* 2004;20:157–61.
98. Joseph JR, Dipietro MA, Somashekar D, Parmar HA, Yang LJ. Ultrasonography for neonatal brachial plexus palsy. *J Neurosurg Pediatr.* 2014;14:527–31.
99. Kalagiri RR, Govande V, Hemingway M, Beeram MR. Bilateral congenital pseudoarthrosis of the clavicles in a newborn. *Proc (Bayl Univ Med Cent).* 2016;29:387–8.
100. Kanai Y, Honda Y, Honda T, Sanpei M. Delayed birth-related femur fracture after cesarean section: a case report. *AJP Rep.* 2018;8:e158–60.
101. Kancherla R, Sankineani SR, Naranje S, Rijal L, Kumar R, Ansari T, Trikha V. Birth-related femoral fracture in newborns: risk factors and management. *J Child Orthop.* 2012;6:177–80.
102. Kaufman HH, Hochberg J, Anderson RP, Schochet SS Jr, Simmons GM Jr. Treatment of calcified cephalohematoma. *Neurosurgery.* 1993;32:1037–9; discussion 1039–40.
103. Kay M, Simpkins C, Shipman P, Whitewood C. Diagnosing neonatal transphyseal fractures of the distal humerus. *J Med Imaging Radiat Oncol.* 2017;61:494–9.
104. Kemp AM, Dunstan F, Harrison S, Morris S, Mann M, Rolfe K, Datta S, Thomas DP, Sibert JR, Maguire S. Patterns of skeletal fractures in child abuse: systematic review. *BMJ.* 2008;337:a1518.

105. Kemp AM, Rajaram S, Mann M, Tempest V, Farewell D, Gawne-Cain ML, Jaspán T, Maguire S, Welsh Child Protection Systematic Review Group. What neuroimaging should be performed in children in whom inflicted brain injury (iBI) is suspected? A systematic review. *Clin Radiol*. 2009;64:473–83.
106. Kesavadas C, Santhosh K, Thomas B, Gupta AK, Kapilamoorthy TR, Bodhey N, Pendharker H, Patro S. Signal changes in cortical laminar necrosis-evidence from susceptibility-weighted magnetic resonance imaging. *Neuroradiology*. 2009;51:293–8.
107. Kilani RA, Wetmore J. Neonatal subgaleal hematoma: presentation and outcome—radiological findings and factors associated with mortality. *Am J Perinatol*. 2006;23:41–8.
108. King J, Diefendorf D, Apthorp J, Negrete VF, Carlson M. Analysis of 429 fractures in 189 battered children. *J Pediatr Orthop*. 1988;8:585–9.
109. King SJ, Boothroyd AE. Cranial trauma following birth in term infants. *Br J Radiol*. 1998;71:233–8.
110. Kingsley D, Till K, Hoare R. Growing fractures of the skull. *J Neurol Neurosurg Psychiatry*. 1978;41:312–8.
111. Kleinman PK. Diagnostic imaging in infant abuse. *AJR Am J Roentgenol*. 1990;155:703–12.
112. Kleinman PK. *Diagnostic imaging of child abuse*. Cambridge: Cambridge University Press; 2015.
113. Kleinman PK, Marks SC Jr, Nimkin K, Rayder SM, Kessler SC. Rib fractures in 31 abused infants: post-mortem radiologic-histopathologic study. *Radiology*. 1996;200:807–10.
114. Kleinman PK, Marks SC Jr, Richmond JM, Blackbourne BD. Inflicted skeletal injury: a post-mortem radiologic-histopathologic study in 31 infants. *AJR Am J Roentgenol*. 1995;165:647–50.
115. Koo WW, Sherman R, Succop P, Krug-Wispé S, Tsang RC, Steichen JJ, Crawford AH, Oestreich AE. Fractures and rickets in very low birth weight infants: conservative management and outcome. *J Pediatr Orthop*. 1989;9:326–30.
116. Kortesis BG, Pyle JW, Sanger C, Knowles M, Glazier SS, David LR. Surgical treatment for scaphocephaly and a calcified cephalohematoma. *J Craniofac Surg*. 2009;20:410–3.
117. Kozin SH, Chafetz RS, Barus D, Filipone L. Magnetic resonance imaging and clinical findings before and after tendon transfers about the shoulder in children with residual brachial plexus birth palsy. *J Shoulder Elb Surg*. 2006;15:554–61.
118. Kozin SH, Chafetz RS, Shaffer A, Soldado F, Filipone L. Magnetic resonance imaging and clinical findings before and after tendon transfers about the shoulder in children with residual brachial plexus birth palsy: a 3-year follow-up study. *J Pediatr Orthop*. 2010;30:154–60.
119. Kulshrestha R, Chowdhury JR, Lalam RK, Kiely NT. Spinal cord infarction in a sick neonate from predominant haemorrhagic aetiology: a case report. *Spinal Cord Ser Cases*. 2017;3:17038.
120. Kwazneski DR, Iyer RC, Panthaki Z, Armstrong MB. Controversies in the diagnosis and treatment of pediatric brachial plexus injuries. *J Craniofac Surg*. 2009;20:1036–8.
121. Kwon DS, Spevak MR, Fletcher K, Kleinman PK. Physiologic subperiosteal new bone formation: prevalence, distribution, and thickness in neonates and infants. *AJR Am J Roentgenol*. 2002;179:985–8.
122. Lanska MJ, Roessmann U, Wiznitzer M. Magnetic resonance imaging in cervical cord birth injury. *Pediatrics*. 1990;85:760–4.
123. Le Fanu JR, Neary R, Bartlett D. Patterns of skeletal fractures in child abuse. “Unexplained” fractures. *BMJ*. 2008;337:a2279.
124. Lee CC, Chou IJ, Chang YJ, Chiang MC. Unusual presentations of birth related cervical spinal cord injury. *Front Pediatr*. 2020;8:514.
125. Lee GS, Methratta ST, Frasier LD. Classic metaphyseal lesion of distal tibia following footling breech delivery. *Pediatr Radiol*. 2019;49:1840–2.
126. Lee Y, Lee KS, Hwang DH, Lee IJ, Kim HB, Lee JY. MR imaging of shaken baby syndrome manifested as chronic subdural hematoma. *Korean J Radiol*. 2001;2:171–4.
127. Levin AV, Magnusson MR, Rafto SE, Zimmerman RA. Shaken baby syndrome diagnosed by magnetic resonance imaging. *Pediatr Emerg Care*. 1989;5:181–6.
128. Liao KD, Yu YH, Li YG, Chen L, Peng C, Liu P, Chen CL, Chen RY, Zhong M, Wang Y. Three-dimensional magnetic resonance pelvimetry: a new technique for evaluating the female pelvis in pregnancy. *Eur J Radiol*. 2018;102:208–12.
129. Lindaman LM. Bone healing in children. *Clin Podiatr Med Surg*. 2001;18:97–108.
130. Liu J. Lung ultrasonography for the diagnosis of neonatal lung disease. *J Matern Fetal Neonatal Med*. 2014;27:856–61.
131. Loeser JD, Kilburn HL, Jolley T. Management of depressed skull fracture in the newborn. *J Neurosurg*. 1976;44:62–4.
132. Lopez J, Chen J, Purvis T, Reategui A, Khavanin N, Iyer R, Manson PN, Dorafshar AH, Cohen AR, Redett RJ. Pediatric skull fracture characteristics associated with the development of leptomeningeal cysts in young children after trauma: a single institution’s experience. *Plast Reconstr Surg*. 2020;145:953e–62e.
133. Lyon AJ, Mcintosh N, Wheeler K, Williams JE. Radiological rickets in extremely low birth-weight infants. *Pediatr Radiol*. 1987;17:56–8.
134. Mahapatra SK, Jangira V, Kalra M. Neonatal radial nerve palsy associated with humerus fracture: is the fracture to be blamed? *Orthop Surg*. 2014;6:162–4.
135. Maharaj D. Assessing cephalopelvic disproportion: back to the basics. *Obstet Gynecol Surv*. 2010;65:387–95.
136. Malesky MJ, Pondaag W. Obstetric brachial plexus injuries. *Neurosurg Clin N Am*. 2009;20:1–14, v.

137. Malik S, Khopkar SR, Korday CS, Jadhav SS, Bhaskar AR. Transphyseal injury of distal humerus: a commonly missed diagnosis in neonates. *J Clin Diagn Res.* 2015;9:SD01-2.
138. Malone CA, Sauer NJ, Fenton TW. A radiographic assessment of pediatric fracture healing and time since injury. *J Forensic Sci.* 2011;56:1123–30.
139. Mazal AT, Faramarzian A, Samet JD, Gill K, Cheng J, Chhabra A. MR neurography of the brachial plexus in adult and pediatric age groups: evolution, recent advances, and future directions. *Expert Rev Med Devices.* 2020;17:111–22.
140. McKinney AM, Teksam M, Felice R, Casey SO, Cranford R, Truwit CL, Kieffer S. Diffusion-weighted imaging in the setting of diffuse cortical laminar necrosis and hypoxic-ischemic encephalopathy. *AJNR Am J Neuroradiol.* 2004;25:1659–65.
141. Medina LS, Yaylali I, Zurakowski D, Ruiz J, Altman NR, Grossman JA. Diagnostic performance of MRI and MR myelography in infants with a brachial plexus birth injury. *Pediatr Radiol.* 2006;36:1295–9.
142. Medlock MD, Hanigan WC. Neurologic birth trauma. Intracranial, spinal cord, and brachial plexus injury. *Clin Perinatol.* 1997;24:845–57.
143. Melchert F, Wischnik A, Nalepa E. The prevention of mechanical birth trauma by means of computer aided simulation of delivery by means of nuclear magnetic resonance imaging and finite element analysis. *J Obstet Gynaecol (Tokyo 1995).* 1995;21:195–207.
144. Merhar SL, Kline-Fath BM, Nathan AT, Melton KR, Bierbrauer KS. Identification and management of neonatal skull fractures. *J Perinatol.* 2016;36:640–2.
145. Messer DL, Adler BH, Brink FW, Xiang H, Agnew AM. Radiographic timelines for pediatric healing fractures: a systematic review. *Pediatr Radiol.* 2020;50:1041–8.
146. Meyer JS, Gunderman R, Coley BD, Bulas D, Garber M, Karmazyn B, Keller MS, Kulkarni AV, Milla SS, Myseros JS, Paidas C, Pizzutillo PD, Podberesky DJ, Prince JS, Ragheb J, American College of Radiology. ACR Appropriateness Criteria((R)) on suspected physical abuse-child. *J Am Coll Radiol.* 2011;8:87–94.
147. Minns RA, Jones PA, Tandon A, Fleck BW, Mulvihill AO, Elton RA. Prediction of inflicted brain injury in infants and children using retinal imaging. *Pediatrics.* 2012;130:e1227–34.
148. Miranda P, Vila M, Alvarez-Garijo JA, Perez-Nunez A. Birth trauma and development of growing fracture after coronal suture disruption. *Childs Nerv Syst.* 2007;23:355–8.
149. Moczygemba CK, Paramsothy P, Meikle S, Kourtis AP, Barfield WD, Kuklina E, Posner SF, Whiteman MK, Jamieson DJ. Route of delivery and neonatal birth trauma. *Am J Obstet Gynecol.* 2010;202:361.e1–6.
150. Morin LR, Fossey FP, Besselièvre A, Loisel JC, Edwards JN. Congenital pseudarthrosis of the clavicle. *Acta Obstet Gynecol Scand.* 1993;72:120–1.
151. Moss SD, Walker ML, Ostergard S, Golembeski D. Intrauterine growing skull fracture. *Childs Nerv Syst.* 1990;6:468–70.
152. Naik P. Remodelling in children's fractures and limits of acceptability. *Indian J Orthop.* 2021;55:549–59.
153. Najada AS, Habashneh MS, Khader M. The frequency of nutritional rickets among hospitalized infants and its relation to respiratory diseases. *J Trop Pediatr.* 2004;50:364–8.
154. Neiger R, Sacks LM. An unusual neonatal case presentation. Cephalohematoma with underlying skull fracture in a neonate delivered by cesarean section. *J Perinatol.* 1988;8:160–2.
155. Nguyen DC, Patel KB, Woo AS, Kane AA, Smyth MD. Endoscopic-assisted treatment of sagittal craniosynostosis and calcified cephalohematoma. *J Craniofac Surg.* 2014;25:2127–9.
156. Nikam RM, Yue X, Kandula VV, Paudyal B, Langhans SA, Averill LW, Choudhary AK. Unravelling neuroinflammation in abusive head trauma with radiotracer imaging. *Pediatr Radiol.* 2021;51:966–70.
157. Niwa T, Aida N, Shishikura A, Fujita K, Inoue T. Susceptibility-weighted imaging findings of cortical laminar necrosis in pediatric patients. *AJNR Am J Neuroradiol.* 2008;29:1795–8.
158. Ogden JA, Lee KE, Rudicel SA, Pelker RR. Proximal femoral epiphysiolysis in the neonate. *J Pediatr Orthop.* 1984;4:285–92.
159. Ono S, Fujimoto H, Kawamoto Y. A rare full-term newborn case of rib osteomyelitis with suspected preceding fracture. *AJP Rep.* 2016;6:e104–7.
160. Paine CW, Fakeye O, Christian CW, Wood JN. Prevalence of abuse among young children with rib fractures: a systematic review. *Pediatr Emerg Care.* 2019;35:96–103.
161. Paley D. Congenital pseudarthrosis of the tibia: biological and biomechanical considerations to achieve union and prevent refracture. *J Child Orthop.* 2019;13:120–33.
162. Parchi P, Andreani L, Piolanti N, Niccolai F, Cervi V, Lisanti M. Effect of vitamin D in fracture healing in a child: case report. *Arch Osteoporos.* 2014;9:170.
163. Patra S, Narayana Kurup JK, Acharya AM, Bhat AK. Birth brachial plexus palsy: a race against time. *BMJ Case Rep.* 2016;2016:bcr2016215996.
164. Paul SP, Channer HL, James JA. Delayed presentation of a neonatal clavicle fracture: a management challenge. *Br J Hosp Med (Lond).* 2019;80:410–1.
165. Perez-Martinez A, Bento-Bravo L, Martinez-Bermejo MA, Conde-Cortes J, Lezaun R, Egues J. Fracture and intracardiac migration of a neonatal venous catheter—extraction via the umbilical pathway. *Pediatr Radiol.* 2002;32:211.
166. Pham CB, Kratz JR, Jelin AC, Gelfand AA. Child neurology: brachial plexus birth injury: what every neurologist needs to know. *Neurology.* 2011;77:695–7.
167. Piatt JH Jr. Birth injuries of the brachial plexus. *Pediatr Clin N Am.* 2004;51:421–40.

168. Piatt JH Jr. Birth injuries of the brachial plexus. *Clin Perinatol.* 2005;32:39–59, v–vi.
169. Pollak L, Razieli A, Arieli S, Schiffer J. Revival of non-surgical management of neonatal depressed skull fractures. *J Paediatr Child Health.* 1999;35:96–7.
170. Princic J, Tonin M, Ales A. [Birth trauma as the cause of fracture of the distal epiphysis of the humerus. A case report]. *Unfallchirurg.* 1995;98:487–8.
171. Prosser I, Lawson Z, Evans A, Harrison S, Morris S, Maguire S, Kemp AM. A timetable for the radiologic features of fracture healing in young children. *AJR Am J Roentgenol.* 2012;198:1014–20.
172. Prosser I, Maguire S, Harrison SK, Mann M, Sibert JR, Kemp AM. How old is this fracture? Radiologic dating of fractures in children: a systematic review. *AJR Am J Roentgenol.* 2005;184:1282–6.
173. Puza S, Roth N, Macones GA, Mennuti MT, Morgan MA. Does cesarean section decrease the incidence of major birth trauma? *J Perinatol.* 1998;18:9–12.
174. Quinlan WR, Brady PG, Regan BF. Congenital pseudarthrosis of the clavicle. *Acta Orthop Scand.* 1980;51:489–92.
175. Rabbitt AL, Kelly TG, Yan K, Zhang J, Bretl DA, Quijano CV. Characteristics associated with spine injury on magnetic resonance imaging in children evaluated for abusive head trauma. *Pediatr Radiol.* 2020;50:83–97.
176. Rehm A, Promod P, Ogilvy-Stuart A. Neonatal birth fractures: a retrospective tertiary maternity hospital review. *J Obstet Gynaecol.* 2020;40:485–90.
177. Reiners CH, Souid AK, Oliphant M, Newman N. Palpable spongy mass over the clavicle, an underutilized sign of clavicular fracture in the newborn. *Clin Pediatr (Phila).* 2000;39:695–8.
178. Riebel T, Nasir R. [Ultrasound of extremity lesions caused by birth trauma]. *Ultraschall Med.* 1995;16:196–9.
179. Riethmuller D, Schaeffer M, Forey PL, Chevallier M, Berthet C, Equy V, Hoffmann P. Skull fracture during instrumental delivery using spatulas: a case report with CT-scan imaging. *J Gynecol Obstet Hum Reprod.* 2021;50:102108.
180. Ryan ME. Rapid magnetic resonance imaging screening for abusive head trauma. *Pediatr Radiol.* 2020;50:13–4.
181. Saarikko A, Mellanen E, Kuusela L, Leikola J, Karpainen A, Autti T, Virtanen P, Brandstack N. Comparison of Black Bone MRI and 3D-CT in the preoperative evaluation of patients with craniosynostosis. *J Plast Reconstr Aesthet Surg.* 2020;73:723–31.
182. Sanchez Fernandez I, Morales-Quezada JL, Law S, Kim P. Prognostic value of brain magnetic resonance imaging in neonatal hypoxic-ischemic encephalopathy: a meta-analysis. *J Child Neurol.* 2017;32:1065–73.
183. Sanchez TR, Lee JS, Coulter KP, Seibert JA, Stein-Wexler R. CT of the chest in suspected child abuse using submillisievert radiation dose. *Pediatr Radiol.* 2015;45:1072–6.
184. Sanchez TR, Nguyen H, Palacios W, Doherty M, Coulter K. Retrospective evaluation and dating of non-accidental rib fractures in infants. *Clin Radiol.* 2013;68:e467–71.
185. Schwarz D, Kele H, Kronlage M, Godel T, Hilgenfeld T, Bendszus M, Baumer P. Diagnostic value of magnetic resonance neurography in cervical radiculopathy: plexus patterns and peripheral nerve lesions. *Investig Radiol.* 2018;53:158–66.
186. Section on Radiology & American Academy of Pediatrics. Diagnostic imaging of child abuse. *Pediatrics.* 2009;123:1430–5.
187. Shamir SB, Kurian J, Kogan-Liberman D, Taragin BH. Hepatic imaging in neonates and young infants: state of the art. *Radiology.* 2017;285:763–77.
188. Sheil AT, Collins KA. Fatal birth trauma due to an undiagnosed abdominal teratoma: case report and review of the literature. *Am J Forensic Med Pathol.* 2007;28:121–7.
189. Shelmerdine SC, Langan D, Hutchinson JC, Hickson M, Pawley K, Suich J, Palm L, Sebire NJ, Wade A, Arthurs OJ, DRIFT Study Research Group. Chest radiographs versus CT for the detection of rib fractures in children (DRIFT): a diagnostic accuracy observational study. *Lancet Child Adolesc Health.* 2018;2:802–11.
190. Sherk HH, Probst C. Fractures of the proximal humeral epiphysis. *Orthop Clin North Am.* 1975;6:401–13.
191. Sherr-Lurie N, Bialik GM, Ganel A, Schindler A, Givon U. Fractures of the humerus in the neonatal period. *Isr Med Assoc J.* 2011;13:363–5.
192. Shopfner CE. Periosteal bone growth in normal infants. A preliminary report. *Am J Roentgenol Radium Therapy Nucl Med.* 1966;97:154–63.
193. Sieswerda-Hoogendoorn T, Boos S, Spivack B, Bilo RA, Van Rijn RR. Abusive head trauma Part II: Radiological aspects. *Eur J Pediatr.* 2012;171:617–23.
194. Smith AB, Gupta N, Strober J, Chin C. Magnetic resonance neurography in children with birth-related brachial plexus injury. *Pediatr Radiol.* 2008;38:159–63.
195. Smith NC, Rowan P, Benson LJ, Ezaki M, Carter PR. Neonatal brachial plexus palsy. Outcome of absent biceps function at three months of age. *J Bone Joint Surg Am.* 2004;86:2163–70.
196. Smith WR, Kozin SH, Zlotolow DA. Delayed treatment of a neonatal type-I Monteggia fracture-dislocation: a case report. *J Pediatr Orthop B.* 2018;27:142–6.
197. Sorantin E, Brader P, Thimary F. Neonatal trauma. *Eur J Radiol.* 2006;60:199–207.
198. Sorantin E, Lindbichler F. [Nontraumatic injury (battered child)]. *Radiologe.* 2002;42:210–6.
199. Sorge I, Hirsch FW, Voit D, Frahm J, Krause M, Roth C, Zimmermann P, Grafe D. Decreased need for anesthesia during ultra-fast cranial MRI in young children: one-year summary. *Rof. 2021;194(2):192–8.*

200. Stover B. [Diagnostic imaging in child abuse]. *Radiologe*. 2007;47:1037–48; quiz 1049.
201. Sugar NF. Diagnosing child abuse. *BMJ*. 2008;337:a1398.
202. Sung TH, Man EM, Chan AT, Lee WK. Congenital pseudarthrosis of the clavicle: a rare and challenging diagnosis. *Hong Kong Med J*. 2013;19:265–7.
203. Swanson AE, Veldman A, Wallace EM, Malhotra A. Subgaleal hemorrhage: risk factors and outcomes. *Acta Obstet Gynecol Scand*. 2012;91:260–3.
204. Takeda R, Kobayashi S, Kamioka N, Hamajima N, Muramatsu K, Suzuki S. Post-traumatic west syndrome due to abusive head trauma in two infants with different brain imaging findings. *Tohoku J Exp Med*. 2020;250:167–71.
205. Teixeira SR, Goncalves FG, Servin CA, Mankad K, Zuccoli G. Ocular and intracranial MR imaging findings in abusive head trauma. *Top Magn Reson Imaging*. 2018;27:503–14.
206. Thamburaj K, Soni A, Frasier LD, Tun KN, Weber SR, Dias MS. Susceptibility-weighted imaging of retinal hemorrhages in abusive head trauma. *Pediatr Radiol*. 2019;49:210–6.
207. Thayyil S, Chandrasekaran M, Taylor A, Bainbridge A, Cady EB, Chong WK, Murad S, Omar RZ, Robertson NJ. Cerebral magnetic resonance biomarkers in neonatal encephalopathy: a meta-analysis. *Pediatrics*. 2010;125:e382–95.
208. Thomas SA, Rosenfield NS, Leventhal JM, Markowitz RI. Long-bone fractures in young children: distinguishing accidental injuries from child abuse. *Pediatrics*. 1991;88:471–6.
209. Thompson KA, Satin AJ, Gherman RB. Spiral fracture of the radius: an unusual case of shoulder dystocia-associated morbidity. *Obstet Gynecol*. 2003;102:36–8.
210. Tokuriki S, Igarashi A, Okuno T, Ohta G, Kosaka T, Ohshima Y. Postnatal changes in humerus cortical bone thickness reflect the development of metabolic bone disease in preterm infants. *Dis Markers*. 2016;2016:2176594.
211. Tortora D, Severino M, Rossi A. Arterial spin labeling perfusion in neonates. *Semin Fetal Neonatal Med*. 2020;25:101130.
212. Towbin A. Spinal cord and brain stem injury at birth. *Arch Pathol*. 1964;77:620–32.
213. Troger J, Stegen P. [Child abuse. Important findings in diagnostic imaging]. *Radiologe*. 1995;35:401–5.
214. Tsai A, Connolly SA, Ecklund K, Johnston PR, Kleinman PK. Subperiosteal new bone formation with the distal tibial classic metaphyseal lesion: prevalence on radiographic skeletal surveys. *Pediatr Radiol*. 2019;49:551–8.
215. Ulma RM, Sacks G, Rodoni BM, Duncan A, Buchman AT, Buchman BC, Vercler CJ, Kasten SJ, Muraszko KM, Buchman SR. Management of calcified cephalohematoma of infancy: The University of Michigan 25-year experience. *Plast Reconstr Surg*. 2021;148:409–17.
216. Van Rijn RR, Spevak MR. Imaging of neonatal child abuse with an emphasis on abusive head trauma. *Magn Reson Imaging Clin N Am*. 2011;19:791–812; viii.
217. Vazquez E, Delgado I, Sanchez-Montanez A, Fabrega A, Cano P, Martin N. Imaging abusive head trauma: why use both computed tomography and magnetic resonance imaging? *Pediatr Radiol*. 2014;44(Suppl 4):S589–603.
218. Verhees RA, Besselaar AT, Van Aken MH, Jansen FH, Pelleboer RA. [A neonatal supracondylar humeral fracture resembling a plexus injury]. *Ned Tijdschr Geneeskd*. 2016;160:A9427.
219. Vialle R, Pietin-Vialle C, Ilharberorde B, Dager S, Vinchon M, Glorion C. Spinal cord injuries at birth: a multicenter review of nine cases. *J Matern Fetal Neonatal Med*. 2007;20:435–40.
220. Viehl L, Kelly BA, Mcalister W, Anadkat J, Julian S. Monteggia fracture in an extremely preterm infant with biochemical rickets: a case report. *JBJS Case Connect*. 2020;10:e0454.
221. Vigo V, Battaglia DI, Frassanito P, Tamburrini G, Caldarelli M, Massimi L. Calcified cephalohematoma as an unusual cause of EEG anomalies: case report. *J Neurosurg Pediatr*. 2017;19:46–50.
222. Viswanathan S, Khasawneh W, McNelis K, Dykstra C, Amstadt R, Super DM, Groh-Wargo S, Kumar D. Metabolic bone disease: a continued challenge in extremely low birth weight infants. *JPEN J Parenter Enteral Nutr*. 2014;38:982–90.
223. Von Heideken J, Thiblin I, Hogberg U. The epidemiology of infant shaft fractures of femur or humerus by incidence, birth, accidents, and other causes. *BMC Musculoskelet Disord*. 2020;21:840.
224. Wall JJ. Congenital pseudarthrosis of the clavicle. *J Bone Joint Surg Am*. 1970;52:1003–9.
225. Walters MM, Forbes PW, Buonomo C, Kleinman PK. Healing patterns of clavicular birth injuries as a guide to fracture dating in cases of possible infant abuse. *Pediatr Radiol*. 2014;44:1224–9.
226. Wang L, Niu Y, Kong X, Yu Q, Kong X, Lv Y, Shi H, Li C, Wu W, Wang B, Liu D. The application of paramagnetic contrast-based T2 effect to 3D heavily T2W high-resolution MR imaging of the brachial plexus and its branches. *Eur J Radiol*. 2016;85:578–84.
227. Warner C, Maguire S, Trefan L, Miller A, Weinman J, Fadell M. A study of radiological features of healing in long bone fractures among infants less than a year. *Skelet Radiol*. 2017;46:333–41.
228. Waters PM. Update on management of pediatric brachial plexus palsy. *J Pediatr Orthop*. 2005;25:116–26.
229. Weinberg B, Seife B, Alonso P. The apical oblique view of the clavicle: its usefulness in neonatal and childhood trauma. *Skelet Radiol*. 1991;20:201–3.
230. Wells C. An early case of birth injury. Multiple abnormalities in a Romano-British skeleton. *Dev Med Child Neurol*. 1964;6:397–402.
231. Weng W, Reid A, Thompson A, Kuthubutheen J. Evaluating the success of a newly introduced Feed

- and Wrap protocol in magnetic resonance imaging scanning of the temporal bone for the evaluation of congenital sensorineural hearing loss. *Int J Pediatr Otorhinolaryngol.* 2020;132:109910.
232. Wilcox AL, Calise DV, Chapman SE, Edwards JF, Storts RW. Hypoxic/ischemic encephalopathy associated with placental insufficiency in a cloned foal. *Vet Pathol.* 2009;46:75–9.
 233. Wilkins KE. Principles of fracture remodeling in children. *Injury.* 2005;36(Suppl 1):A3–11.
 234. Williams CE, Gunn AJ, Synek B, Gluckman PD. Delayed seizures occurring with hypoxic-ischemic encephalopathy in the fetal sheep. *Pediatr Res.* 1990;27:561–5.
 235. Windle WF. Neurological and psychological deficits from asphyxia neonatorum. *Public Health Rep.* 1957;72:646–50.
 236. Wintermark P. Injury and repair in perinatal brain injury: insights from non-invasive MR perfusion imaging. *Semin Perinatol.* 2015;39:124–9.
 237. Wischnik A, Nalepa E, Lehmann KJ, Wentz KU, Georgi M, Melchert F. [Prevention of human birth trauma I. Computer-assisted simulation of delivery using magnetic resonance tomography and finite element analysis]. *Geburtshilfe Frauenheilkd.* 1993;53:35–41.
 238. Wong AM, Yeh CH, Liu HL, Wu TW, Lin KL, Wang HS, Toh CH. Arterial spin-labeling perfusion imaging of children with subdural hemorrhage: perfusion abnormalities in abusive head trauma. *J Neuroradiol.* 2017;44:281–7.
 239. Wong CH, Foo CL, Seow WT. Calcified cephalohematoma: classification, indications for surgery and techniques. *J Craniofac Surg.* 2006;17:970–9.
 240. Wootton-Gorges SL, Stein-Wexler R, Walton JW, Rosas AJ, Coulter KP, Rogers KK. Comparison of computed tomography and chest radiography in the detection of rib fractures in abused infants. *Child Abuse Negl.* 2008;32:659–63.
 241. Worlock P, Stower M, Barbor P. Patterns of fractures in accidental and non-accidental injury in children: a comparative study. *Br Med J (Clin Res Ed).* 1986;293:100–2.
 242. Xu Z, Zhang T, Chen J, Liu Z, Wang T, Hu Y, Zhang J, Xue F. Combine contrast-enhanced 3D T2-weighted short inversion time inversion recovery MR neurography with MR angiography at 1.5 T in the assessment of brachial plexopathy. *MAGMA.* 2021;34:229–39.
 243. Yaginuma K, Watanabe M, Suzuki Y, Suyama K, Hashimoto K, Hosoya M. Cortical laminar necrosis in an infant with influenza A virus infection. *Clin Case Rep.* 2020;8:1843–4.
 244. Yamataka A, Fujiwara T, Tsuchioka T, Kurosu Y, Sunagawa M. Heterotopic splenic autotransplantation in a neonate with splenic rupture, leading to normal splenic function. *J Pediatr Surg.* 1996;31:239–40.
 245. Yeo LI, Reed MH. Staging of healing of femoral fractures in children. *Can Assoc Radiol J.* 1994;45:16–9.
 246. Yilmaz U, Korner H, Meyer S, Reith W. Multifocal signal loss at bridging veins on susceptibility-weighted imaging in abusive head trauma. *Clin Neuroradiol.* 2015;25:181–5.
 247. Yusuf IH, Barnes JK, Fung TH, Elston JS, Patel CK, Medscape. Non-contact ultra-widefield retinal imaging of infants with suspected abusive head trauma. *Eye (Lond).* 2017;31:353–63.
 248. Zeck W, Haas J, Rossegger H, Bjelic V, Scholl W. Does a change in obstetric management influence the incidence of traumatic birth lesions in mature, otherwise healthy newborn infants? *J Obstet Gynaecol Res.* 2007;33:475–9.
 249. Zenger MN, Kabatas S, Zenger S, Cakmakci H. The value of power Doppler ultrasonography in the differential diagnosis of intracranial extraaxial fluid collections. *Diagn Interv Radiol.* 2007;13:61–3.
 250. Zhou L, Yousem DM, Chaudhry V. Role of magnetic resonance neurography in brachial plexus lesions. *Muscle Nerve.* 2004;30:305–9.
 251. Zuccoli G, Panigrahy A, Haldipur A, Willaman D, Squires J, Wolford J, Sylvester C, Mitchell E, Lope LA, Nischal KK, Berger RP. Susceptibility weighted imaging depicts retinal hemorrhages in abusive head trauma. *Neuroradiology.* 2013;55:889–93.

Further Reading

- Kleinman PK. *Diagnostic imaging of child abuse.* Cambridge: Cambridge University Press; 2015.
- Oestreich AE, Caré MM. *Recognizing child abuse in radiology.* New York: Springer International Publishing; 2017.
- Vlasyuk V. *Birth trauma and perinatal brain damage.* New York: Springer International Publishing; 2019.